

UNIVERSIDAD DE MURCIA

Departamento de Bioquímica y Biología Molecular-A
Universidad de Murcia

Caracterización cinética de la catálisis, inactivación suicida e inhibición irreversible de tirosinasa.

JOSE LUIS MUÑOZ MUÑOZ

2012

UNIVERSIDAD DE
MURCIA

D. Francisco García Cánovas, Catedrático de Universidad del Área de Bioquímica y Biología Molecular en el Departamento de Bioquímica y Biología Molecular A, AUTORIZA:

La presentación de la Tesis Doctoral titulada "Caracterización cinética de la catálisis, inactivación suicida e inhibición irreversible de tirosinasa", realizada por D. Jose Luis Muñoz Muñoz, bajo mi inmediata dirección y supervisión, y que presenta para la obtención del grado de Doctor por la Universidad de Murcia.

En Murcia, a 30 de Abril de 2012

UNIVERSIDAD DE
MURCIA

D. Jose Neptuno Rodríguez López, Catedrático de Universidad del Área de Bioquímica y Biología Molecular en el Departamento de Bioquímica y Biología Molecular A, AUTORIZA:

La presentación de la Tesis Doctoral titulada "Caracterización cinética de la catálisis, inactivación suicida e inhibición irreversible de tirosinasa", realizada por D. Jose Luis Muñoz Muñoz, bajo mi inmediata dirección y supervisión, y que presenta para la obtención del grado de Doctor por la Universidad de Murcia.

En Murcia, a 30 de Abril de 2012

UNIVERSIDAD DE
MURCIA

D. José Bautista Tudela Serrano, Catedrático de Universidad del Área de Bioquímica y Biología Molecular en el Departamento de Bioquímica y Biología Molecular A, AUTORIZA:

La presentación de la Tesis Doctoral titulada "Caracterización cinética de la catálisis, inactivación suicida e inhibición irreversible de tirosinasa", realizada por D. Jose Luis Muñoz Muñoz, bajo mi inmediata dirección y supervisión, y que presenta para la obtención del grado de Doctor por la Universidad de Murcia.

En Murcia, a 30 de Abril de 2012

UNIVERSIDAD DE
MURCIA

D. José Tudela Serrano, Catedrático de Universidad del Área de Bioquímica y **Director del Departamento*** Bioquímica y Biología Molecular A, INFORMA:

Que una vez evaluado, de conformidad con el procedimiento establecido en el artículo 21 del Reglamento de doctorado de la Universidad de Murcia, el expediente completo de la tesis doctoral titulada "Caracterización cinética de la catálisis, inactivación suicida e inhibición irreversible de tirosinasa", realizada por D. Jose Luis Muñoz Muñoz, bajo la inmediata dirección y supervisión de D. Francisco García Cánovas, Jose Neptuno Rodríguez López y José Tudela Serrano, este Consejo de Departamento, en sesión celebrada en fecha 18 de Mayo de 2012, ha dado su autorización para su presentación ante la Comisión General de Doctorado.

Murcia, a 18 de Mayo de 2012

Doctorando: D. Jose Luis Muñoz Muñoz

*Informe del Departamento para alumnos del RD 778/1998.

*Informe de La Comisión Académica del Programa para alumnos del RD 56/2005 y RD 1393/2007.

Los estudios realizados en esta Memoria han sido parcialmente financiados por las subvenciones correspondientes a los siguientes Proyectos de Investigación (de los cuales del 1 al 6 he sido colaborador):

1. *Aplicaciones bioanalíticas y biocatalíticas de polifenoloxidasas y peroxidasas de alcachofa* (CICYT RTA AGL2002-01255 ALI). Investigador Principal: **Dr. Francisco García Cánovas.** 2003-2005.
2. *Producción y aplicaciones biocatalíticas de polifenoloxidasas de residuos agroindustriales de alcachofa* (Fundación Séneca, 00672/PI/04, CARM, Murcia). Investigador Principal: **Dr. José Tudela Serrano**. 2005-2007.
3. *Aplicaciones biotecnológicas de nuevas polifenoloxidasas comerciales* (Ministerio de Educación y Ciencia, Programa Nacional de Biotecnología, Proyecto BIO2006-15363). Investigador Principal: **Dr. José Tudela Serrano.** 2007-2009.
4. *Biocatálisis enzimática con nuevos sistemas polifenoloxidasas-mediadores* (Programa Sectorial de Biotecnología BioCARM, BIO-BMC 06/01-0004, Consejería de Educación, CARM, Murcia, España). Investigador Principal: **Dr. José Tudela Serrano.** 2007-2009.
5. *Nuevas polifenoloxidasas con aplicaciones bioanalíticas de alto rendimiento* (Fundación Séneca, 08856/PI/08, CARM, Murcia, España). Investigador Principal: **Dr. José Tudela Serrano.** 2009-2011.
6. *Polifenoloxidasas y mediadores para el análisis enzimático de sustancias con interés biotecnológico* (Ministerio de Educación y Ciencia, Programa Nacional de Biotecnología, Proyecto BIO2009-12956). Investigador Principal: **Dr. José Tudela Serrano.** 2010-2012.

El autor de esta Memoria ha disfrutado de las siguientes ayudas:

1. Beca de Postgrado de Formación de Profesorado Universitario. Programa Nacional de Formación del Personal Investigador, Ministerio de Educación y Ciencia. Referencia AP2005-4721. Periodo 2006-2010.
2. Beca Predoctoral de la Fundación Caja Murcia. Periodo 2010-Actualidad.

En Murcia, a 2 de Mayo de 2012

Fdo. **Dr. Francisco García Cánovas**
Catedrático de Universidad en el área de
Bioquímica y Biología Molecular
Universidad de Murcia

Fdo. **Dr. Jose Neptuno Rodríguez López**
Catedrático de Universidad en el área de
Bioquímica y Biología Molecular
Universidad de Murcia

Fdo. **Dr. José Tudela Serrano**
Catedrático de Universidad en el área de
Bioquímica y Biología Molecular
Universidad de Murcia

Fdo. **Jose Luis Muñoz Muñoz**
Alumno de Doctorado
Departamento de Bioquímica y
Biología Molecular-A
Universidad de Murcia

Quisiera expresar mi más sincero agradecimiento a todas aquellas personas que de alguna manera han sido partícipes en el desarrollo de la presente Memoria:

A los doctores: ***Francisco García Cánovas****,* ***Jose Neptuno Rodríguez López*** *y* ***José Tudela Serrano****, todos ellos directores de esta Tesis Doctoral, por su generosidad, disponibilidad y por todo el apoyo que me han prestado.*

Al ***Dr. Ramón Varón Castellanos****, por sus modelos y expresiones matemáticas que, sin ellos, nos hubiera sido posible poder desarrollar los mecanismos cinéticos de la enzima, además de por su continuo ánimo y moral.*

Al ***Dr. Pedro Antonio García Ruiz*** *del Departamento de Química Orgánica, por su continua colaboración con su profundo conocimiento de la Química Orgánica.*

Al ***Dr. Jose Berna Cánovas*** *del Departamento de Química Orgánica por sus ayudas en la síntesis de compuestos orgánicos que, sin ellos, no habrían sido posible muchos de los resultados de esta Tesis Doctoral.*

A ***Francisco García Molina****, con el que compartí y, por ahora, comparto laboratorio, por los buenos momentos que compartimos y por las saludables discusiones que tuvimos y, espero que durante muchos años, sigamos teniendo.*

*Al resto de compañeros del laboratorio: los de la nueva sala del té (****Magda****,* ***Jesús****,* ***Vanesa****,* ***Alejandro*** *y* ***Xavi****), los chicos de al lado (****María****,* ***Magalí****,* ***Sole****,* ***Fernanda*** *y* ***Luis****) y a las nuevas incorporaciones del laboratorio (****Mar*** *y* ***Juan Diego****) y, en especial, a* ***María del Mar****, que empezamos a compartir espectrofotómetros y oxigrafos y que, esperemos, continúe con el legado del estudio de las famosas "*k*".*

A todos los miembros del Departamento de Bioquímica y Biología Molecular-A de la Universidad de Murcia, en especial a ***Juana****,* ***Encarna****,* ***Mercedes*** *y* ***Pepa*** *por su cariño y por saber llevar mi inexperiencia en las prácticas.*

A mi ***Madre****, por estar siempre cuando se le necesita, a mi* ***hermana****, por ser como es ella, y al resto de mi* ***familia*** *por soportarme, en todos estos años, de las dichosas enzimas y las "cosas raras" que les cuento.*

A mi mujer y compañera, ***Alicia****, por soportarme y estar ahí en estos años de laboratorio y no dejarme de animar y escuchar siempre tanto en los buenos como en los malos momentos.*

A mi ***Paulita****, por ser como es y darme una sonrisa cuando más se necesita.*

Contenido

CONTENIDO

Publicaciones	**X**
Índice	
1. Introducción	1
2. Objetivos	135
3. Materiales y Métodos	139
4. Resultados y Discusión	153
5. Conclusiones	533
6. Bibliografía	543

Publicaciones

PUBLICACIONES*

El contenido de esta Tesis Doctoral ha originado la publicación de los siguientes artículos de investigación y comunicaciones en congresos científicos.

Artículos de Investigación

1. **Muñoz, J.L.;** García-Molina, F.; Varón, R.; Rodriguez-Lopez, J.N.; García-Cánovas, F. y Tudela, J. (2006) Calculating molar absortivities for quinones. Application to the measurement of tyrosinase activity. *Analytical Biochemistry* **351**, 128-138, Factor de Impacto: 2.670, Categoría: Chemistry, Analytical, posición: 13 de 70 (Tercio I).

2. **Muñoz, J.L.;** García-Molina, F.; Varón, R; Rodriguez-López, J.N; Garcia-Ruiz, P.A.; García-Cánovas, F. y Tudela, J. (2007) Kinetic characterisation of the oxidation of chlorogenic acid by polyphenoloxidase and peroxidase. Characteristics of the *o*-quinone. *Journal of Agricultural and Food Chemistry* **55**, 920-928, Factor de Impacto: 2.322, Categoría: Agriculture, Multidisciplinary, posición: 1 de 45 (Tercio I).

3. **Muñoz-Muñoz, J.L.;** García-Molina, F.; Varón, R; Rodriguez-López, J.N; García-Cánovas, F. y Tudela, J. (2007) Kinetic characterization of the oxidation of esculetin by polyphenol oxidase and peroxidase. *Bioscience, Biotechnology and Biochemistry* **71**, 390-396, Factor de Impacto: 1.256, Categoría: Food Science and Technology, posición: 29 de 96 (Tercio II).

4. **Muñoz-Muñoz, J.L.;** García-Molina, F.; Molina-Alarcon, M.; Tudela, J.; García-Cánovas, F. y Rodriguez-López, J.N. (2008) Kinetic characterization of the enzymatic and chemical oxidation of the catechins in the green tea. *Journal of Agricultural and Food Chemistry* **56**, 9215-9224, Factor de Impacto: 2.532, Categoría: Agriculture, Multidisciplinary, posición: 1 de 35 (Tercio I).

5. **Muñoz-Muñoz, J.L.;** García-Molina, F.; Garcia-Ruiz, P.A.; Molina-Alarcon, M.; Tudela, J.; García-Cánovas, F. y Rodriguez-López, J.N. (2008) Phenolic substrates and suicide inactivation of tyrosinase: kinetics and mechanism. *Biochemical Journal* **416**, 431-440, Factor de Impacto: 4.009, Categoría: Biochemistry and Molecular Biology, posición: 67 de 263 (Tercio I).

6. **Muñoz-Muñoz, J.L.;** García-Molina, F.; Arribas, E.; Garcia-Ruiz, P.A.; Tudela, J.; García-Cánovas, F. y Rodriguez-López, J.N. (2009) Enzymatic and chemical oxidation of trihydroxylated phenols. *Food Chemistry* **113**, 435-444, Factor de Impacto: 2.696, Categoría: Food Science and Technology, posición: 9 de 107 (Tercio I).

7. **Muñoz-Muñoz, J.L.;** García-Molina, F.;Garcia-Ruiz, P.A.; Varon, R.; Tudela, J.; García-Cánovas, F. y Rodriguez-López, J.N. (2009) Stereospecific inactivation of tyrosinase by L-and D-ascorbic acid. *Biochimica et Biophysica Acta - Protein and Proteomics* **1794**, 244-253, Factor de Impacto: 2.233, Categoría: Biochemistry and Molecular Biology, posición: 165 de 275 (Tercio II).

8. **Muñoz-Muñoz, J.L.;** García-Molina, F.; Garcia-Molina, M.; Tudela, J.; García-Cánovas, F. y Rodriguez-López, J.N. (2009) Ellagic acid: characterization as

substrate of polyphenol oxidase. *IUBMB Life* **61**, 171-177, Factor de Impacto: 3.578, Categoría: Biochemistry and Molecular Biology, posición: 89 de 283 (Tercio I).

9. **Muñoz-Muñoz, J.L.;** García-Molina, F.; Garcia-Molina, M.; Tudela, J.; García-Cánovas, F. y Rodriguez-López, J.N. (2009) Kinetic characterization of the oxidation of carbidopa and benserazide by polyphenol oxidase and peroxidase. *Bioscience, Biotechnology and Biochemistry* **73**, 1308-1313, Factor de Impacto: 1.390, Categoría: Food Science and Technology, posición: 38 de 107 (Tercio II).

10. **Muñoz-Muñoz, J.L.;** García-Molina, F.; Varon, R.; Tudela, J.; García-Cánovas, F. y Rodriguez-López, J.N. (2009) Generation of hydrogen peroxide in the melanin biosynthesis pathway. *Biochimica et Biophysica Acta - Protein and Proteomics* **1794**, 1017-1029, Factor de Impacto: 2.233, Categoría: Biochemistry and Molecular Biology, posición: 165 de 275 (Tercio II).

11. **Muñoz-Muñoz, J.L.;** García-Molina, F.; Garcia-Ruiz, P.A.; Varon, R.; Tudela, J.; García-Cánovas, F. y Rodriguez-López, J.N. (2010) Some kinetic properties of deoxytyrosinase. *Journal of Molecular Catalysis B: Enzymatic* **62**, 173-182, Factor de Impacto: 2.400, Categoría: Chemistry, Physical, posición: 47 de 121 (Tercio II).

12. **Muñoz-Muñoz, J.L.;** Garcia-Molina, F.; Varon, R.; Tudela, J.; García-Cánovas, F. y Rodriguez-López, J.N. (2010) Quantification of the antioxidant capacity of different molecules and their kinetic antioxidant efficiency. *Journal of Agricultural and Food Chemistry* **58**, 2062-2070, Factor de Impacto: 2.469, Categoría: Agriculture, Multidisciplinary, posición: 2 de 45 (Tercio I).

13. **Muñoz-Muñoz, J.L.;** Acosta-Motos, J.R.; Garcia-Molina, F.; Varon, R.; Garcia-Ruiz, P.A.; Tudela, J.; García-Cánovas, F. y Rodriguez-López, J.N. (2010) Tyrosinase inactivation in its action on dopa. *Biochimica et Biophysica Acta - Proteins and Proteomics* **1804**, 1467-1475, Factor de Impacto: 2.480, Categoría: Biochemistry and Molecular Biology, posición: 153 de 283 (Tercio II).

14. **Muñoz-Muñoz, J.L.;** Garcia-Molina, F.; Varon, R.; Tudela, J.; García-Cánovas, F. y Rodriguez-López, J.N. (2010) New features of the steady-state rate related with the initial concentration of substrate in the diphenolase and monophenolase activities of tyrosinase. *Journal of Mathematical Chemistry* **48**, 347-362, Factor de Impacto: 1.381, Categoría: Mathematics, Interdisplinary Applications, posición: 23 de 80 (Tercio I).

15. **Muñoz-Muñoz, J.L.;** Garcia-Molina, F.; Varon, R.; Garcia-Ruiz, P.A.; Tudela, J.; García-Cánovas, F. y Rodriguez-López, J.N. (2010) Suicide inactivation of the diphenolase and monophenolase activities of tyrosinase. *IUBMB Life* **62**, 539-547, Factor de Impacto: 3.578, Categoría: Biochemistry and Molecular Biology, posición: 89 de 283 (Tercio I).

16. **Muñoz-Muñoz, J.L.;** Garcia-Molina, F.; Arribas, E.; Garcia-Ruiz, P.A.; Tudela, J.; García-Cánovas, F. y Rodriguez-López, J.N. (2011) Suicide inactivation of tyrosinase in its action on tetrahydropterines. *Journal of Enzyme Inhibition and Medicinal Chemistry* **26**, 728-733, Factor de Impacto: 1.574, Categoría: Chemistry, Medicinal, posición: 29 de 54 (Tercio II).

17. **Muñoz-Muñoz, J.L.;** Garcia-Molina, F.; Varon, R.; Tudela, J.; García-Cánovas, F. y Rodriguez-López, J.N. (2011) Kinetic cooperativity of tyrosinase. A general

mechanism. *Acta Biochimica Polonica* **58**, 303-311, Factor de Impacto: 1.234, Categoría: Biochemistry and Molecular Biology, posición: 245 de 286 (Tercio III).

18. **Muñoz-Muñoz, J.L.;** García-Molina, F.; García-Ruiz, P.A.; Varón, R.; Tudela, J.; Rodríguez-López, J.N. y García-Canovas, F. (2011) Catalytic oxidation of aminophenol and aromatic amines by mushroom tyrosinase. *Biochimica et Biophysica Acta - Proteins and Proteomics* **1814**, 1974-1983, Factor de Impacto: 2.773, Categoría: Biochemistry and Molecular Biology, posición: 145 de 286 (Tercio II).

19. **Muñoz-Muñoz, J.L.;** Garcia-Molina, F.; Acosta-Motos, J.R.; Varon, R.; Garcia-Ruiz, P.A.; Tudela, J.; García-Cánovas, F. y Rodriguez-López, J.N. (2011) Indirect inactivation of tyrosinase in its action on tyrosine. *Acta Biochimica Polonica* **58**, 477-488, Factor de Impacto: 1.234, Categoría: Biochemistry and Molecular Biology, posición: 245 de 286 (Tercio III).

20. **Muñoz-Muñoz, J.L.;** Berna, J.; Garcia-Molina, F.; Garcia-Ruiz, P.A.; Tudela, J.; Rodriguez-López, J.N. y García-Cánovas, F. (2012) Unravelling the suicide inactivation of tyrosinase: a discrimination between mechanisms. *Journal of Molecular Catalysis B: Enzymatic* **75**, 11-19, Factor de Impacto: 2.330, Categoría: Chemistry, Physical, posición: 57 de 127 (Tercio II).

21. **Muñoz-Muñoz, J.L.;** Garcia-Molina, F.; Berna, J.; Garcia-Ruiz, P.A.; Varon, R.; Tudela, J.; Rodriguez-López, J.N. y García-Cánovas, F. (2012) Kinetic characterization of *o*-aminophenols and aromatic *o*-diamines as suicide substrates of tyrosinase. *Biochimica et Biophysica Acta - Proteins and Proteomics* **1824**, 647-655, Factor de Impacto: 2.773, Categoría: Biochemistry and Molecular Biology, posición: 145 de 286 (Tercio II).

22. **Muñoz-Muñoz, J.L.;** Garcia-Molina, F.; Ros, E.; Tudela, J.; García-Cánovas, F. y Rodriguez-López, J.N. (2012) Prooxidant and antioxidant activities of rosmarinic acid. *Journal of Food Biochemistry* (**En prensa**), Factor de Impacto: 0.625, Categoría: Food Science and Technology, posición: 81 de 126 (Tercio II).

*Presentación del proyecto de Tesis en 2007.

Otros artículos de investigación relacionados con esta Tesis Doctoral:

1. García-Molina, F.; **Muñoz, J.L.;** Varón, R.; Rodriguez-López, J.N.; García-Cánovas, F. y Tudela, J. (2007) A further step in the kinetic characterisation of the tyrosinase enzymatic system. *Journal of Mathematical Chemistry* **41**, 393-406, Factor de Impacto: 0.965, Categoría: Mathematics, Interdisplinary Applications, posición: 25 de 65 (Tercio I).

2. García-Molina, F.; **Muñoz, J.L.;** Varón, R.; Rodriguez-López, J.N.; García-Cánovas, F. y Tudela, J. (2007) Effect of tetrahydropteridines on the monophenolase and diphenolase activities of tyrosinase*. Journal of Enzyme Inhibition and Medicinal Chemistry* **22**, 383-394, Factor de Impacto: 1.636, Categoría: Chemistry, Medicinal, posición: 18 de 35 (Tercio II).

3. García-Molina, F.; **Muñoz, J.L.;** Varón, R.; Rodriguez-López, J.N.; García-Cánovas, F. y Tudela, J. (2007) An approximate analytical solution to the lag period of monophenolase activity of tyrosinase. *International Journal of Biochemistry and Cell Biology* **39**, 238-252, Factor de Impacto: 4.804, Categoría: Biochemistry and Molecular Biology, posición: 56 de 262 (Tercio I).

4. García-Molina, F.; **Muñoz, J.L.;** Varón, R.; Rodriguez-López, J.N; García-Cánovas, F. y Tudela, J. (2007) A review on spectrophotometric methods for measuring the monophenolase and diphenolase activities of tyrosinase. *Journal of Agricultural and Food Chemistry* **55**, 9739-9749, Factor de Impacto: 2.322, Categoría: Agriculture, Multidisciplinary, posición: 1 de 45 (Tercio I).

5. García-Molina, F.; **Muñoz-Muñoz, J.L.;** Garcia-Molina, M.; Molina-Alarcon, M.; Garcia-Ruiz, P.A.; Tudela, J. y Rodriguez-López, J.N. (2009) Determination and applications of the molar absorptivities of phenolic adducts with captopril and mesna. *Journal of Agricultural and Food Chemistry* **57**, 1143-1150, Factor de Impacto: 2.562, Categoría: Agriculture, Multidisciplinary, posición: 2 de 35 (Tercio I).

6. García-Molina, F.; **Muñoz-Muñoz, J.L.;** Acosta, J.R.; Garcia-Ruiz, P.A.; Varon, R.; Tudela, J.; García-Cánovas, F. y Rodriguez-López, J.N. (2009) Melanogensis inhibition by tetrahydropterines. *Biochimica et Biophysica Acta - Protein and Proteomics* **1794**, 1766-1774, Factor de Impacto: 2.480, Categoría: Biochemistry and Molecular Biology, posición: 153 de 283 (Tercio II).

7. Garcia-Molina, F.; **Muñoz-Muñoz, J.L.;** Martinez-Ortiz, F.; Tudela, J.; García-Cánovas, F. y Rodriguez-López, J.N. (2010) Effect of tetrahydropterines on the generation of quinones catalyzed by tyrosinase. *Bioscience, Biotechnology and Biochemistry* **74**, 1108-1109, Factor de Impacto: 1.326, Categoría: Food Science and Technology, posición: 44 de 118 (Tercio II).

8. García-Molina, F.; **Muñoz-Muñoz, J.L.;** García-Molina, M.; Garcia-Ruiz, P.A.; Tudela, J.; García-Cánovas, F. y Rodriguez-López, J.N. (2010) Melanogensis inhibition by NADH. *Bioscience, Biotechnology and Biochemistry* **74**, 1777-1787, Factor de Impacto: 1.326, Categoría: Food Science and Technology, posición: 44 de 118 (Tercio II).

9. García-Molina, F.; **Muñoz-Muñoz, J.L.;** Martinez-Ortiz, F.; Garcia-Ruiz, P.A.; Tudela, J.; García-Cánovas, F. y Rodriguez-López, J.N. (2011) Tetrahydrofolic acid as a potent suicide substrate of mushroom tyrosinase. *Journal of Agricultural and Food Chemistry* **59**, 1383-1391, Factor de Impacto: 2.816, Categoría: Agriculture, Multidisciplinary, posición: 2 de 55 (Tercio I).

Comunicaciones en Congresos Internacionales

1. García-Molina, F.; **Muñoz, J.L.;** Peñalver, M.J.; Varón, R.; Rodríguez-López, J.N.; García-Cánovas, F. y Tudela, J. (2006) *Tyrosinase is not inhibited by an excess of monophenol.* 20th IUBMB International Congress of Biochemistry and Molecular Biology and 11th FAOBMB Congress. Kyoto (Japón).

2. **Muñoz Munoz, J.L.;** García-Molina, F.; Peñalver, M.J.; Varón, R.; Rodríguez-López, J.N.; García-Cánovas, F. y Tudela, J. (2006) *A further step in the kinetic characterization of the tyrosinase enzymatic system.* 20th IUBMB International Congress of Biochemistry and Molecular Biology and 11th FAOBMB Congress. Kyoto (Japón).

3. **Muñoz-Muñoz, J.L.;** García-Molina, F.; Acosta-Motos, J.R.; Garcia-Molina, M.; Tudela, J.; García-Cánovas, F. y Rodríguez-López, J.N. (2009) *Generation of*

hydrogen peroxide in the melanin biosynthesis pathway. 34th FEBS Congress. Praga (República Checa).

4. Acosta-Motos, J.R.; **Muñoz-Muñoz, J.L.;** García-Molina, F.; Garcia-Molina, M.; Tudela, J.; García-Cánova,s F. y Rodríguez-López, J.N. (2009) *Stereospecificity of the suicide inactivation of tyrosinase. A kinetic study.* 34th FEBS Congress. Praga (República Checa).

5. **Muñoz-Muñoz, J.L.;** García-Molina, F.; Varon, R.; Tudela, J.; García-Cánovas, F. y Rodríguez-López, J.N. (2010) *Quantification of the primary antioxidant capacity of different molecules.* 35th FEBS Congress. Goteborg (Suecia).

6. García-Molina, F.; **Muñoz-Muñoz, J.L.;** Varon, R.; Tudela, J.; García-Cánovas, F. y Rodríguez-López, J.N. (2010) *Quantification of the secondary antioxidant capacity of different molecules.* 35th FEBS Congress. Goteborg (Suecia).

7. **Muñoz-Muñoz, J.L.;** García-Molina, F.; Garcia-Molina, M.; Ros, E.; Varon, R.; Tudela, J.; García-Cánovas, F. y Rodríguez-López, J.N. (2010) *Rosmarinic acid oxidation and its antioxidant capacity.* OzBio 2010. 12th IUBMB Congress. Melbourne (Australia).

8. García-Molina, F.; **Muñoz-Muñoz, J.L.;** Martínez-Ortiz, F.; Varón, R.; Tudela, J.; García-Cánovas, F. y Rodríguez-López, J.N. (2010) *Oxidation of tetrahydropterines by quinones.* OzBio 2010. 12th IUBMB Congress. Melbourne (Australia).

9. **Muñoz-Muñoz, J.L.;** García-Molina, F.; García-Molina, M.; Garcia-Ruiz, P.A.; Varón, R.; Tudela, J.; García-Cánovas, F. y Rodríguez-López, J.N. (2010) *Some kinetic properties of deoxytyrosinase.* 3rd EuCheMS Congress. Nuremberg (Alemania).

10. García-Molina, F.; **Muñoz-Muñoz, J.L.;** García-Molina, M.; Varón, R.; Tudela, J.; García-Cánovas, F. y Rodríguez-López, J.N. (2010) *A new features of the steady-state rate related with the initial concentration of substrate in the diphenolase and monophenolase activities of tyrosinase.* 3rd EuCheMS Congress. Nuremberg (Alemania).

Comunicaciones en Congresos Nacionales

1. **Muñoz, J.L.;** García-Molina, F.; Peñalver, M.J.; Varón, R.; Rodríguez-López, J.N.; García-Cánovas F. y Tudela J. (2005) *Cálculo de las absortividades molares de las quinonas. Aplicación a la medida de la actividad de tirosinasa.* Congreso de Bioquímica y Biología Molecular de la SEBBM. Fecha: 12-15 Septiembre. Zaragoza (España).

2. García-Molina, F.; Peñalver, M.J.; **Muñoz, J.L.;** Rodríguez-López, J.N.; Tudela, J. y García-Cánovas F. (2005) *Método cronométrico para la determinación de Polifenol oxidasa para la determinación de cisteína y N-Acetilcisteína.* Congreso de Bioquímica y Biología Molecular de la SEBBM. Fecha: 12-15 Septiembre. Zaragoza (España).

3. **Muñoz, J.L.;** García-Molina, F.; Peñalver, M.J.; Varón, R.; Rodríguez-López, J.N.; García-Cánovas F. y Tudela J. (2005) *Cálculo de las absortividades molares de las*

quinonas generadas a partir de difenoles, trifenoles y flavonoides. Acto de celebración del aniversario del nacimiento de Severo Ochoa. FECYT. Fecha: 16-Noviembre. Madrid (España).

4. García-Molina, F.; **Muñoz, J.L.;** Hiner, A.; García Ruiz, P.A.; Varón, R.; Rodríguez-López, J.N.; García-Cánovas F. y Tudela J. (2005) *Caracterización de la actividad catalasa de tirosinasa: Implicaciones fisiológicas.* Acto de celebración del aniversario del nacimiento de Severo Ochoa. FECYT. Fecha: 16-Noviembre. Madrid (España).

5. **Muñoz, J.L.;** García-Molina, F.; Peñalver, M.J.; Varón, R.; Rodríguez-López, J.N.; García-Cánovas F. y Tudela J. (2006) *Caracterización cinética de la oxidación de ácido clorogénico por polifenoloxidasa y peroxidasa. Características de la o-quinona.* Congreso de la Sociedad Española de Bioquímica y Biología Molecular SEBBM. Fecha: 7-10 de Septiembre. Elche (España).

6. García-Molina, F.; **Muñoz, J.L.;** Peñalver, M.J.; Varón, R.; Rodríguez-López, J.N.; García-Cánovas F. y Tudela J. (2006) *Métodos espectrofotométricos de medida de las actividades monofenolasa y difenolasa de tirosinasa.* Congreso de la Sociedad Española de Bioquímica y Biología Molecular SEBBM. Fecha: 7-10 de Septiembre. Elche (España).

7. García-Molina, F.; **Muñoz, J.L.;** Peñalver, M.J.; Varón, R.; Rodríguez-López, J.N.; García-Cánovas F. y Tudela J. (2006) *Efecto de tetrahidrobiopterinas sobre las actividades monofenolasa y difenolasa de tirosinasa.* Congreso de la Sociedad Española de Bioquímica y Biología Molecular SEBBM. Fecha: 7-10 de Septiembre. Elche (España).

8. **Muñoz-Muñoz, J.L.;** García-Molina, F.; Varón, R.; Rodríguez-López, J.N.; García-Cánovas F. y Tudela J. (2007) *Caracterización cinética de la oxidación de las catequinas del té verde por polifenol oxidasa y peroxidasa.* Congreso de la Sociedad Española de Bioquímica y Biología Molecular SEBBM. Fecha: 12-15 de Septiembre. Málaga (España).

9. García-Molina, F.; **Muñoz-Muñoz, J.L.;** Varón, R.; Rodríguez-López, J.N.; García-Cánovas F. y Tudela J. (2007) *Estudio de los aductos de captopril y Mesna con o-quinonas.* Congreso de la Sociedad Española de Bioquímica y Biología Molecular SEBBM. Fecha: 12-15 de Septiembre. Málaga (España).

10. **Muñoz-Muñoz, J.L.;** García-Molina, F.; Garcia-Molina, M.; Garcia-Ruiz, P.A.; García-Cánovas, F.; Rodríguez-López J.N. y Tudela J. (2008) *Sustratos fenólicos e inactivación suicida de tirosinasa: cinética y mecanismo.* Congreso de la Sociedad Española de Bioquímica y Biología Molecular SEBBM. Fecha: 10-13 de Septiembre. Bilbao (España).

11. García-Molina, F.; **Muñoz-Muñoz, J.L.;** Garcia-Molina, M.; Garcia-Ruiz, P.A.; García-Cánovas, F.; Rodríguez-López J.N. y Tudela J. (2008) *Oxidación enzimática y química de compuestos trihidroxilados.* Congreso de la Sociedad Española de Bioquímica y Biología Molecular SEBBM. Fecha: 10-13 de Septiembre. Bilbao (España).

12. García-Molina, F.; **Muñoz-Muñoz, J.L.;** Garcia-Molina, M.; Tudela, J.; García-Cánovas F. y Rodríguez-López J.N. (2009) *Inhibición de la melanogénesis por tetrahidropterinas.* Congreso de la Sociedad Española de Bioquímica y Biología Molecular SEBBM. Fecha: 23-26 de Septiembre. Oviedo (España).

13. **Muñoz-Muñoz, J.L.;** García-Molina, F.; Garcia-Molina, M.; Tudela, J.; García-Cánovas F. y Rodríguez-López J.N. (2009) *Inhibición de la melanogénesis por NADH y NADPH.* Congreso de la Sociedad Española de Bioquímica y Biología Molecular SEBBM. Fecha: 23-26 de Septiembre. Oviedo (España).

14. **Muñoz-Muñoz, J.L.;** García-Molina, F.; Garcia-Molina, M.; Varón, R.; Tudela, J.; Rodríguez-López J.N. y García-Cánovas F. (2011) *Cooperatividad cinética de tirosinasa. Un mecanismo general.* Congreso de la Sociedad Española de Bioquímica y Biología Molecular SEBBM. Fecha: 5-8 de Septiembre. Barcelona (España).

15. García-Molina, F.; **Muñoz-Muñoz, J.L.;** Garcia-Molina, M.; Varón, R.; Garcia-Ruiz, P.A.; Tudela, J.; Rodríguez-López J.N. y García-Cánovas F. (2011) *Inactivación indirecta de tirosinasa en su acción sobre tirosina.* Congreso de la Sociedad Española de Bioquímica y Biología Molecular SEBBM. Fecha: 5-8 de Septiembre. Barcelona (España).

Índice

INDICE

1. INTRODUCCIÓN……1.
1.1. Tirosinasa: aspectos generales
1.1.1. Tirosinasa de bacterias.
1.1.2. Tirosinasa de plantas y hongos.
1.1.3. Tirosinasa de artrópodos.
1.1.4. Tirosinasa de mamíferos.
1.2. Tirosinasa: funciones fisiológicas
1.2.1. Tirosinasa de bacterias.
1.2.2. Tirosinasa de plantas y hongos.
1.2.3. Tirosinasa de artrópodos.
1.2.4. Tirosinasa de mamíferos.
1.2.4.1. Melanocitos e histología de la melanogénesis.
1.2.4.2. Tipos de melaninas y su formación.
1.2.4.3. Regulación de la melanogenesis.
1.3. Tirosinasa: estructura
1.3.1. Propiedades moleculares.
1.3.2. Estructura tridimensional.
1.3.2.1. Tirosinasa de bacterias.
1.3.2.2. Tirosinasa de plantas y hongos.
1.3.2.3. Tirosinasa de artrópodos.
1.3.2.4. Tirosinasa de mamíferos.
1.3.3. Sitio activo.
1.3.3.1. Metatirosinasa.
1.3.3.2. Oxitirosinasa.
1.3.3.3. Desoxitirosinasa.
1.4. Tirosinasa: actividades catalíticas
1.4.1. Actividad difenolasa.
1.4.2. Actividad monofenolasa.
1.4.3. Estereoespeficidad.
1.4.4. Actividad ascorbato oxidasa
1.4.5. Actividad catalasa
1.4.6. Actividad tetrahidropterina oxidasa
1.4.7. Actividad NADH oxidasa
1.4.8. Actividad tetrahidrofolico oxidasa
1.4.9. Actividad *o*-aminofenol, aminas aromáticas oxidasa
1.5. Tirosinasa: regulación enzimática
1.5.1. Inhibidores.
1.5.1.1. Polifenoles.
1.5.1.2. Derivados del benzaldehido y benzoatos.
1.5.1.3. Lipidos (triacilglicéridos) de cadena larga y esteroides.
1.5.1.4. Agentes hipopigmentantes.
1.5.2. Inactivadores.
1.5.2.1. Inactivadores irreversibles.
1.5.2.2. Inactivadores suicidas.
1.5.3. Diseño de inhibidores de tirosinasa.
1.5.4. Aplicaciones de los inhibidores.
1.5.5. Activadores
1.6. Tirosinasa: alteraciones de la pigmentación y diseño de fármacos
1.6.1. Hipopigmentación.

1.6.2. Hiperpigmentación.
1.6.3. Melanoma maligno.
1.7. Tirosinasa: aplicaciones biotecnológicas
1.7.1. Producción de biopolímeros entrecruzados.
1.7.2. Detección y cuantificación de compuestos fenólicos.
1.7.3. Eliminación de compuestos fenólicos y bioremediación.
1.7.4. Producción de *o*-difenoles a partir de monofenoles con tirosinasa de *Agaricus bisporus*.
1.7.5. Avances en bioingeniería.
1.7.6. Otras aplicaciones de tirosinasa.

2. OBJETIVOS
2.1. Objetivo general
2.2. Objetivos específicos

3. MATERIALES Y MÉTODOS
3.1. Reactivos y materiales
3.1.1. Reactivos.
3.1.2. Preparación de tirosinasa de champiñón.
3.1.3. Determinación de proteínas.
3.1.4. Generación de oxitirosinasa y desoxitirosinasa.
3.1.5. Generación de metatirosinasa.
3.1.6. Evaluación de las especies enzimáticas oxitirosinasa, metatirosinasa y desoxitirosinasa en una preparación enzimática de tirosinasa.
3.2. Equipos y métodos
3.2.1. Ensayos oximétricos.
3.2.2. Ensayos espectrofotométricos.
3.2.3. Ensayos de RMN.
3.2.4. Síntesis orgánica del 3,6-difluorocatecol.
3.2.5. Espectrofotometría de masas.
3.2.6. Análisis de regresión.
3.2.6.1. Regresión no lineal.
3.2.6.2. Regresión lineal.
3.2.7. Simulación numérica.
3.2.7.1. Integración numérica de ecuaciones diferenciales.
3.2.7.2. Métodos de paso variable.
3.2.7.3. Implementación.
3.2.7.4. Condiciones de simulación.

4. RESULTADOS Y DISCUSIÓN
4.1. NUEVOS AVANCES DEL COMPORTAMIENTO CINÉTICO DE LAS ACTIVIDADES MONOFENOLASA Y DIFENOLASA DE TIROSINASA.
4.2. COOPERATIVIDAD CINETICA DE TIROSINASA.
4.3. ALGUNAS PROPIEDADES CINÉTICAS DE DESOXITIROSINASA.
4.4. GENERACIÓN DE PERÓXIDO DE HIDRÓGENO EN LA RUTA DE BIOSÍNTESIS DE MELANINAS.
4.5. CÁLCULO DE LAS ABSORTIVIDADES MOLARES DE QUINONAS.
4.6. CARACTERIZACIÓN CINÉTICA DE LA OXIDACIÓN DE ESCULETINA.
4.7. CARACTERIZACIÓN CINÉTICA DE LA OXIDACIÓN DE CARBIDOPA Y BENSERAZIDA.

4.8. CARACTERIZACIÓN CINÉTICA DE LA OXIDACIÓN DEL ÁCIDO CLOROGÉNICO.
4.9. CARACTERIZACIÓN CINÉTICA DE LA OXIDACIÓN ENZIMÁTICA Y QUÍMICA DE LAS CATEQUINAS DEL TÉ VERDE.
4.10. OXIDACIÓN ENZIMÁTICA Y QUÍMICA DE FENOLES TRIDROXILADOS.
4.11. ÁCIDO ELÁGICO: CARACTERIZACIÓN COMO SUSTRATO DE POLIFENOL OXIDASA.
4.12. ACTIVIDADES PROOXIDANTES Y ANTIOXIDANTES DEL ÁCIDO ROSMARÍNICO.
4.13. CUANTIFICACIÓN DE LA CAPACIDAD ANTIOXIDANTE DE DIFERENTES MOLÉCULAS.
4.14. OXIDACIÓN CATALÍTICA DE *o*-AMINOFENOLES Y AMINAS AROMÁTICAS.
4.15. SUSTRATOS FENÓLICOS E INACTIVACIÓN SUICIDA DE TIROSINASA.
4.16. INACTIVACIÓN DE TIROSINASA EN SU ACCIÓN SOBRE DOPA.
4.17. INACTIVACIÓN INDIRECTA DE TIROSINASA EN SU ACCIÓN SOBRE TIROSINA.
4.18. INACTIVACIÓN DE TIROSINASA POR ÁCIDO L- Y D-ASCÓRBICO.
4.19. INACTIVACIÓN SUICIDA DE TIROSINASA EN SU ACCIÓN SOBRE TETRAHIDROPTERINAS.
4.20. CARACTERIZACIÓN CINÉTICA DE *o*-AMINOFENOLES Y *o*-DIAMINAS AROMÁTICAS COMO SUSTRATOS SUICIDAS.
4.21. INACTIVACIÓN SUICIDA DE LAS ACTIVIDADES DIFENOLASA Y MONOFENOLASA DE TIROSINASA.
4.22. DESVELANDO LA INACTIVACIÓN SUICIDA DE TIROSINASA: UNA DISCRIMINACIÓN ENTRE MECANISMOS.

5. CONCLUSIONES
5.1. Conclusiones específicas
5.2. Conclusiones generales

6. BIBLIOGRAFÍA

Anexo I: Documentos acreditativos factores de impacto

Introducción

1. INTRODUCCIÓN

1.1 Tirosinasa: aspectos generales

Las proteínas son biopolímeros responsables de una amplia variedad de funciones dentro y fuera de la célula: unas transportan y almacenan moléculas pequeñas; otras constituyen gran parte de la organización estructural de las células y los tejidos, otras están implicadas en la motilidad celular. Quizás las más importantes de todas las proteínas sean las enzimas, catalizadores que llevan a cabo la enorme variedad de reacciones químicas que canalizan el metabolismo en rutas esenciales. Cada tipo celular, en todos los organismos, posee varios miles de clases de proteínas para cumplir esta diversidad de funciones. La totalidad de estas proteínas de una célula viviente se denomina “proteoma”. Aunque toda la información genética, que es la responsable de codificar el proteoma, está almacenada en forma de ADN en la célula, es el propio proteoma el que determina qué proteínas son expresadas, y a qué nivel de expresión, en un tipo celular y bajo unas condiciones muy concretas.

Se ha estimado que alrededor de un tercio de todas las proteínas del proteoma necesitan enlazar a uno o varios iones metálicos en su sitio activo como grupos prostéticos. Muchas de estas proteínas enlazan metales como magnesio o calcio que juegan un papel muy importante en la estabilización estructural de la proteína. Una parte muy importante de todas estas metaloproteínas, contienen metales de transición en su sitio activo como puede ser hierro, níquel, cobre, vanadio, etc. (Holm et al., 1996). Muchos de estos metales de transición se encuentran en varios estados de oxidación estables con lo que intervienen activamente en las reacciones redox de la célula (ejemplos de estos metales son cobre o el hierro). Las proteínas que contienen estos iones están implicadas, mayoritariamente, en reacciones de transferencia electrónica.

Los metales están unidos a la matriz proteica a través de interacciones entre residuos aminoacídicos como histidina, cisteína, ácido aspártico, asparragina y metionína. Esta matriz proteica juega un papel esencial en el reconocimiento entre dos proteínas, por ejemplo, en la transferencia electrónica o entre un sustrato y una enzima para que se produzca el reconocimiento y la catálisis. Las propiedades del metal coordinado pueden ser moduladas por la matriz proteica gracias a la unión de moléculas señalizadoras o gracias a un cambio en las condiciones del medio (pH).

Las metaloproteínas que contienen cobre en su sitio activo se denominan cuproproteinas. Cumplen cuatro funciones básicas: (1) almacenaje, transporte y consumo de este ión metálico, (2) transferencia electrónica, (3) almacenaje, transporte y consumo del oxigeno molecular y (4) catálisis. La presencia de cobre en estas proteínas, da lugar a diferentes características espectroscópicas. Gracias a estas características, las cuproproteínas han sido clasificadas históricamente en 3 tipos (tipo 1, 2 y 3). Sin embargo, el descubrimiento de nuevas estructuras proteicas, han llevado a determinar nuevas clases de cuproproteinas. Así, hoy en día, se incluyen en siete clases diferentes (Solomon et al., 1996; Bubacco et al., 1999).

- Tipo I: las cuproproteínas tipo I corresponden a proteínas de transferencia electrónica como son la plastocianina o la azulina. Tienen un color azul intenso debido al Cu^{2+} oxidado de su sitio activo. Por esto, también se llaman "cuproproteínas azules". La esfera de coordinación del cobre está formada por dos átomos de nitrógeno (generalmente histidinas) y un átomo de azufre (de una cisteína).
- Tipo II: Los centros de cobre de estas cuproproteínas están ligados a cuatro nitrógenos u oxígenos. Su espectro EPR es muy diferente del de las cuproproteínas de tipo I. En esta clase se encuentran enzimas como la galactosa oxidasa o la Cu-Zn superóxido dismutasa.
- Tipo III: El sitio activo de estas proteínas consiste en dos átomos de cobre coordinados cada uno con tres residuos de histidina. Proteínas de este tipo están implicadas en el transporte y la activación del oxigeno en el organismo. Así, tenemos como ejemplos a hemocianina, catecol oxidasa y tirosinasa.
- Tipo IV: Este tipo de cuproproteínas son consideradas como una mezcla de las tipo II y las tipo III ya que poseen una agrupación trinuclear de cobre. Entre este tipo de proteínas se encuentran la lacasa, la ascorbato oxidasa o la ceruloplasmina, donde los cobres están enlazados a ocho residuos de histidina.
- CuA: En este tipo de cuproteínas, el sitio del CuA es dinuclear, estando estos dos átomos de cobre unidos por residuos de azufre de cisteínas. Este sitio activo presenta un espectro EPR muy característico produciendo un color púrpura a la enzima.
- CuB: El sitio del CuB está próximo a un hierro hemo y está presente en la citocromo C oxidasa (COX) que es la enzima que cataliza la reducción, por cuatro electrones, del O_2 a agua.

- CuZ: El sitio activo de este tipo de cuproteínas está formado por cuatro iones de cobre unidos a siete residuos de histidina. Este tipo de sitios activos se encuentra en enzimas como la oxido nitroso reductasa que reduce el N_2O a N_2.

La enzima tirosinasa o polifenol oxidasa (TYR) (monofenol, *o*-difenol: oxígeno óxido-reductasa, EC 1.14.18.1) se encuentra ampliamente distribuida en toda la escala filogenética. Esta cuproproteína cataliza dos tipos de reacciones acopladas en las que interviene oxígeno molecular, (a) hidroxilación de monofenoles a *o*-difenoles (actividad monofenolasa) y (b) oxidación de *o*-difenoles a *o*-quinonas (actividad difenolasa). La gran variedad de posibles sustratos y la elevada reactividad de las *o*-quinonas generadas por tirosinasa determinan la participación de esta enzima en procesos fisiológicos tan diversos como la biosíntesis de ligninas, la esclerotización de la cutícula de artrópodos y la biosíntesis de melaninas (Mason, 1955; Vámos-Vigyázó, 1981; Robb, 1984; Lozano y Solano, 1989; Sugumaran, 2001; 2010; Claus y Decker, 2006).

En los organismos aeróbicos, la mayor parte del oxígeno consumido es reducido a agua en la oxidasa terminal de la cadena respiratoria. Sin embargo, también se utiliza una cantidad significativa del mismo en reacciones catalizadas por una clase de enzimas denominadas oxigenasas (Hayaishi, 1962). Es conocido que estas enzimas incorporan uno o dos átomos de oxígeno por mol de sustrato, por lo que se dividen en monooxigenasas y dioxigenasas, respectivamente (Hayaishi, 1974). Las monooxigenasas, llamadas también oxidasas de función mixta, catalizan la reducción de un átomo de oxígeno a agua, mientras que el otro es transferido al sustrato. Estas enzimas pueden presentar cuatro tipos distintos de grupos prostéticos: cobre, hierro “no hemo”, hierro “hemo” y flavinas. Aquellas monooxigenasas que contienen cobre como cofactor representan un grupo bastante reducido en comparación con las otras tres clases. Una de las monooxigenasas más importantes y extensamente estudiadas, con cobre como cofactor, como ya se ha indicado anteriormente, es la tirosinasa o polifenol oxidasa.

A continuación, se desarrollaran las principales características de tirosinasas de diferentes organismos según su naturaleza.

1.1.1. Tirosinasa de bacterias

Aunque la melanina es un pigmento comúnmente asociado con mamíferos, especialmente humanos (Hearing, 2005), este pigmento también se encuentra

presente en muchos microorganismos como levaduras o bacterias. La producción de este pigmento, como ya hemos indicado, se produce gracias a las cuproproteinas, principalmente tirosinasa pero, en algunos casos, también a lacasa. Además del efecto fotoprotector, la función que tienen las melaninas en los microorganismos no está totalmente definida, pero parece claro que juegan un papel clave en la protección del microorganismo contra la radiación, o en la propia virulencia de este. También se han descrito otras funciones para tirosinasa como son la eliminación, en bacterias simbióticas, de fenoles defensivos de plantas, la producción de pigmentos como betalaínas, síntesis de antibióticos basados en aminoácidos como lincomicina, etc. (Fairhead y Thony-Meyer, 2012). Las tirosinasas bacterianas más extensamente estudiadas son las gel género *Streptomyces*. Sin embargo, actualmente se han caracterizado, tanto cinética como estructuralmente, otras muchas tirosinasas bacterianas (*Bacillus*, *Marinomonas*, etc.) (Sendovski et al., 2011; Sanchez-Amat et al., 2010).

Las tirosinasas bacterianas se dividen en 5 tipos principales como se muestra en la Figura 1. La primera clase de tirosinasa bacteriana (Figura 1A-I) se caracteriza por ser el producto del operón *melC* (Lerch y Ettinger, 1972), con lo que también se denominan tirosinasa *melC*. Este tipo de tirosinasas son secretadas por las bacterias del genero *Streptomyces* usando la vía de señalización TAT y son producidas en forma de heterodímero (Schaerlaekens et al., 2001; Chen et al., 1993). Este dímero consiste en una apotirosinasa que está unido a una proteína auxiliar, que es el producto del gen *melC1* (el operón que codifica este gen se esquematiza en la Figura 2). Esta proteína auxiliar o proteína “caddie” (CP) tiene muchas funciones como ser la responsable de secreción, de incorporar el cobre al sitio activo de la enzima en su ensamblamiento, etc. (Chen et al., 1993). Ejemplos de este tipo de tirosinasas pueden ser *Streptomyces castaneoglobisporus* (de la que recientemente se ha obtenido su estructura cristalina) (Matoba et al., 2006), o *Marimonas mediterránea* (López-Serrano et al., 2004).

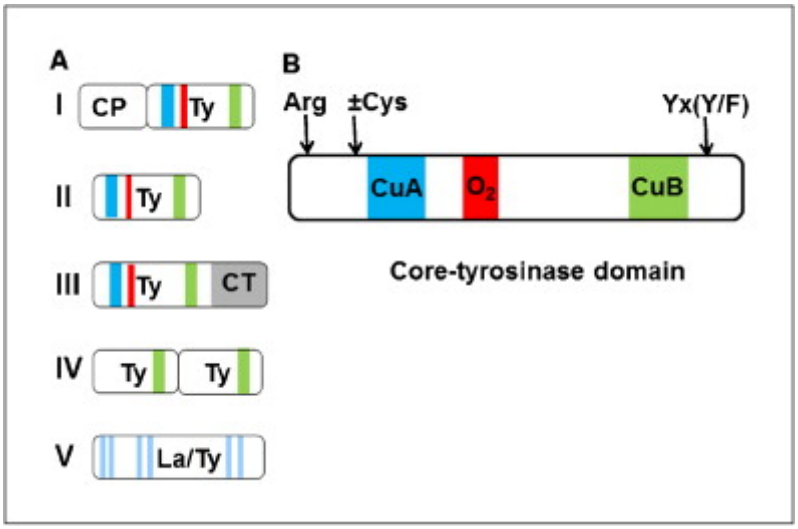

Figura 1. Distintos tipos de tirosinasas bacterianas (Fairhead y Thony-Meyer, 2012).

El segundo tipo de tirosinasa bacteriana (Figura 1A-II), no requiere proteína auxiliar para incorporar el cobre al sitio activo. Un ejemplo es la tirosinasa de *Bacillus megaterium*, la cual tiene una similitud estructural muy grande con las tirosinasas de tipo I (Sendovski et al., 2011). Además, esta tirosinasa de *Bacillus megaterium* tiene aplicaciones biotecnológicas muy grandes ya que es capaz de aguantar concentraciones altas de disolventes orgánicos en el medio, por ejemplo una concentración de etanol, acetona o dimetilsulfóxido superior al 50% (Shuster y Fishman, 2009).

Las tipo III (Figura 1A-III), son similares a las tirosinasas fúngicas y se caracterizan por tener un extremo C-terminal que actúa de una forma similar a como lo hace la proteína caddie pero que no interviene tampoco en la incorporación del cobre a la enzima (Fairhead y Thony-Meyer, 2010). Un ejemplo es la tirosinasa de *Verrucomicrobium spinosum*.

Las tipo IV (Figura 1A-IV) son más pequeñas que el resto de tirosinasas bacterianas y solo son activas como homodímeros (es un homodímero de 14 kDa inducible por el calor). Como principal ejemplo se encuentra la tirosinasa de *Bacillus turingiensis* (Liu et al., 2004).

La tirosinasa de tipo V (Figura 1A-V) ha sido bien caracterizada pero hoy en día hay mucha discusión acerca de si es en realidad una tirosinasa o, por el contrario, es una enzima que posee actividad similar a tirosinasa (Sánchez-Amat et al., 2001). Parece ser que esta enzima tiene más similaridad estructural a la lacasa (Sakuray y

Kataoka, 2007). Además, no tiene el motivo de unión del cobre A y B característico de las tirosinasas ni el motivo de unión del oxigeno, pero sin embargo es capaz de oxidar monofenoles (Sakuray y Kataoka, 2007). Un ejemplo es la enzima producida por *Aeromonas media*.



Figura 2. Esquema del operón *melC* de *Streptomyces antibioticus*. Las cajas representan las regiones codificantes, los círculos abiertos simbolizan las regiones promotoras, los círculos cerrados son los sitios de unión del ribosoma y la flecha es el sitio del comienzo de la transcripción (Claus y Decker, 2006).

La primera tirosinasa de bacterias purificada fue a partir de extractos celulares de *Streptomyces nigrifaciens* (Nambudiri y Bhat, 1972) y *Streptomyces glaucescens* (Lerch y Ettinger, 1972) Las tirosinasas procedentes de organismos procariotas han sido utilizadas como modelo para el estudio y el conocimiento de tirosinasas de otras fuentes ya que los procariotas presentan ciertas ventajas frente a los eucariotas: 1) se cultivan rápidamente; 2) las tirosinasas son excretadas al medio extracelular, donde están implicadas en la producción de melanina extracelular; 3) la forma activa más probable es monomérica. En el caso de *Streptomyces glaucescens*, la enzima es monomérica y tiene una masa molecular de 29 kDa. La más pequeña de todas ha sido aislada de *Bacillus thuringiensis*, con sólo 14 kDa (Liu et al., 2004; Fairhead y Thony-Meyer, 2012), actualmente es la que posee una masa molecular más pequeña de las estudiadas hasta la fecha y, además, se cree que la forma activa es un dímero al contrario que las tirosinasas del género *Streptomyces*; 4) la proteína no es modificada post-traduccionalmente. Por todo ello, han sido caracterizadas genética, espectroscópica y cinéticamente lo que ha llevado a profundizar en la comprensión del mecanismo de acción cinético y estructural de tirosinasa, ya que las tirosinasas de eucariotas son difíciles de aislar en cantidad y pureza suficiente para su estudio estructural.

Las tirosinasas de *Streptomyces nigrifaciens*, *Streptomyces glaucescens*, *Bacillus thuringiensis* y *Pseudomonas putida* F_6 (Claus y Decker, 2006; McMahon et al., 2007) son monómeros, mientras que las de *Vibrio tirosinaticus* y *Thermomicrobium roseum* son dímeros (Kong et al., 2000; Liu et al., 2004).

Los estudios con tirosinasa de *Streptomyces* han sido impulsados en los últimos años. Así se ha sobre-expresado y purificado la tirosinasa de *Streptomyces castaneoglobisporus* (Kohashi et al., 2004) llegando a obtener la estructura cristalina de la enzima de esta bacteria. Como acabamos de indicar, se ha cristalizado esta enzima, formando un complejo con ORF378 (open reading frame; marco de lectura abierto), que es una proteína transportadora de cobre al sitio activo de tirosinasa (Matoba et al., 2006), los estudios cristalográficos realizados por estos autores muestran evidencia de que el sitio activo, formado por el cobre dinuclear, es flexible durante la catálisis y proponen que la histidina 54 (His^{54}), unida al cobre A, se libera del sitio activo al aceptar un protón del sustrato durante la catálisis, y lo vuelve a liberar para unirse de nuevo al cobre A.

Recientemente, se ha aislado y caracterizado a tirosinasa de *Bacillus megaterium*, sobreexpresándola en *Escherichia coli* (Shuster y Fishman, 2009). Esta tirosinasa tiene una excepcional elevada actividad en disolventes orgánicos miscibles en agua, lo cual le reporta futuras aplicaciones en el campo de la química orgánica, y no necesita la proteína caddie para su actividad. Además, se ha obtenido el cristal de esta tirosinasa con una resolución máxima de 2 Å, y se ha purificado como un monómero compuesto por 297 aminoácidos y una masa molecular de 31 kDa (Sendovski et al., 2010; 2011). Gracias a la estructura cristalina de tirosinasa, se ha demostrado que las actividades normales de tirosinasa necesitan de posiciones móviles en la unión de los iones de cobre en el sitio activo (Sendovski et al., 2011).

1.1.2. Tirosinasa de hongos y plantas

La tirosinasa más estudiada es la producida por *Agaricus bisporus* ya que es la enzima utilizada como modelo para extrapolar resultados a otros tipos de tirosinasas. Igualmente, la enzima del ascomiceto *Neurospora crassa,* ha sido también muy estudiada tanto desde el punto de vista estructural, como molecular y cinético (Lerch, 1981; Robb, 1984; Gerritsen et al., 1994; Sánchez-Ferrer et al., 1995; van Gelder et al., 1997; Espín et al., 1997; Fan y Flurkey, 2004; Marusek et al., 2006; Selinheimo et al., 2007).

Tirosinasa ha sido extraída y purificada de muchos tejidos vegetales, entre ellos, manzana (Nicolas et al., 1994; Espín et al., 1995), aguacate (Weemaes et al., 1998; Gómez-López, 2002), champiñón (*Agaricus bisporus*, Espín et al., 1999a; Fan y Flurkey, 2004; Ismaya et al., 2011a), pera (Espín et al., 1996), menta (*Mentha piperita*, Kavrayan y Aydemir, 2001), tabaco (*Nicotiana tabacum*, Shi et al., 2002), látex de

Hevea brasilensis (Wititsuwannakul et al., 2002), patata (*Solanum tuberosum*, Marri et al., 2003), café (*Coffea arabica*, Goulart et al., 2003), álamo (*Populus trichocarpa P. deltoides*, Wang y Constabel, 2003), caqui (*Diospyros kaki*, Núñez-Delicado et al., 2003), mora (*Morus alba L*., Arslan et al., 2004), remolacha (*Beta vulgaris L*., Gandía-Herrero et al., 2004) y melocotón (*Prunus persica L.*, Cabanes et al., 2007). Se trata de una enzima intracelular localizada en el cloroplasto, mitocondria, microsoma, peroxisoma y citoplasma (Mayer y Harel, 1979; Zawistowski et al., 1991; Mayer, 2006), aunque suele localizarse fundamentalmente ligada a la membrana tilacoidal en el cloroplasto. El nivel y localización predominante de tirosinasa en la célula, en plantas, depende de la especie, variedad, madurez y edad (Vámos-Vigyázó, 1981).

A pesar de haber sido extraída de multitud de tejidos vegetales, solo en unos pocos casos se ha logrado purificar hasta homogeneidad (Zawistowski et al., 1991). Con técnicas como electroforesis en gel, isoelectroenfoque, análisis inmunológico o filtración en gel, se ha deducido que en los extractos de tirosinasa existen fenómenos de asociación-disociación de unidades similares y/o diferentes, modificación post-traduccional *in vivo* incluyendo proteolisis limitada, polimerización de compuestos fenólicos o glicosidación (Vámos-Vigyázó, 1981; Kupper et al., 1989; Chazarra et al., 2001). Estas formas pueden ser interconvertibles y difieren en su especificidad de sustrato, pH óptimo, estabilidad térmica etc.

En muchos frutos y vegetales, tirosinasa es responsable del pardeamiento enzimático, después del daño causado a la célula (van Gelder et al., 1997). Debido a la dificultad de extracción y purificación se han propuesto distintas formas enzimáticas para tirosinasa de hongos y plantas superiores. Así, tirosinasa de champiñón se ha descrito con una estructura tetramérica (Strothkamp et al., 1976). Pero más recientemente se obtuvieron dos isoenzimas monoméricas de *Agaricus bisporus* (Wichers et al., 2003).

Una característica frecuente de tirosinasa de hongos y plantas es que, en estado nativo, existe como una enzima latente, la cual tiene que ser activada. Se ha descrito activación *in vivo* por proteasas (Rathjen y Robinson, 1992). Por otra parte*, in vitro* se ha demostrado activación proteolítica (Laveda et al., 2001), activación por detergentes, SDS (Laveda et al., 2000), o por poliaminas (Jimenez-Atienzar et al., 1991).

Recientemente se han clonado, expresado y caracterizado dos cADNs de tirosinasa a partir de *Agaricus bisporus* (Wichers et al., 2003; Wu et al., 2010).

Los sustratos fisiológicos de tirosinasa más importantes encontrados en frutas y hortalizas, según especies y variedades, son: las catequinas (catequina, epicatequina, galocatequinas, etc.), derivados del ácido cinámico (ácido clorogénico, ácido *p*-cumárico, ácido cafeico, etc.), catecoles y derivados, derivados del ácido benzoico (ácidos protocatéquico, vaníllico, siríngico, etc.), flavonas, flavonoides, antocianidinas, etc. (Vámos-Vigyázó, 1981). Debido a esta inespecificidad, las tirosinasas también pueden actuar sobre otros tipos de sustratos sintéticos no naturales.

Hoy en día se ha impulsado mucho la investigación sobre tirosinasas de hongos y plantas debido a sus posibles aplicaciones biotecnológicas en la industria de la alimentación, farmacéutica y medio ambiental (Halaouli et al., 2006).

1.1.3. Tirosinasa de artrópodos

En condiciones fisiológicas, la tirosinasa de insectos, también llamada phenoloxidasa (PO) está soluble en la hemolinfa y por lo tanto en contacto con sus sustratos. Para evitar reacciones no deseadas, PO se encuentra en forma de proenzima y se activa cuando se requiere por mecanismos regulados como son la proteolisis limitada (Söderhäll et al., 1990; Hall et al., 1995; Asano y Ashida, 2001). La presencia de pro-tirosinasa fue sugerida hace mucho tiempo pero no ha sido purificada hasta ahora. Recientemente se ha cristalizado la pro-fenoloxidasa (ProPO) de *Manduca sexta* a una resolución de 1.97 Å. Es un heterodímero consistente en dos polipéptidos homólogos, cada uno con un sitio activo tipo III (Li et al., 2009). En un extracto de cutículas del gusano de seda *Bombyx mori*, se ha demostrado la existencia de dos isoformas de pro-tirosinasa, las cuales presentan pequeñas variaciones en cuanto a su movilidad electroforética (Asano y Ashida, 2001).

La biosíntesis de melaninas en insectos y otros artrópodos es un proceso importante para la vida de estos organismos. La ruta es diferente a la de mamíferos ya que posee diferentes enzimas, en insectos tirosinasa se denomina fenoloxidasa (PO) y existe una dopacromo isomerasa (decarboxilante) en lugar de la dopacromo tautomerasa, además se utilizan diferentes sustratos (Sugumaran, 2002; 2010). Con respecto a los sustratos, PO utiliza fundamentalmente dopamina y N-acetildopamina (Sugumaran, 2002), necesarias para los procesos de esclerotización. Por otra parte, las melaninas de insectos son polímeros de 5,6-dihidroxiindol (DHI) y las de mamíferos son mezclas de DHI y de ácido 5,6-dihidroxiindol-2-carboxílico (DHICA). La

polimerización a través de DHI es mejor y más rápida. Así, la formación de DHI en el sitio de infección da lugar a una mejor encapsulación del agente invasor.

Por otra parte, el estudio del origen filogenético de las enzimas implicadas en la ruta de biosíntesis de melaninas en mamíferos y en insectos parece indicar por las secuencias, que tirosinasa vendría de la hemociacina de moluscos y que PO podría derivar de hemocianina de artrópodos (Fujimoto et al., 1995). Las dos enzimas se diferencian también en el tamaño, PO es mayor que tirosinasa de mamíferos y además PO no lleva péptido señal y se encuentra soluble en la hemolinfa de insectos.

La importancia de las melaninas en insectos es amplia y está relacionada con procesos de camuflaje, la esclerotización de la cutícula, la respuesta inmune y la curación de las heridas (Sugumaran, 2002).

1.1.4. Tirosinasa de mamíferos

Las tirosinasas de mamíferos actúan sobre sus sustratos fisiológicos L-tirosina y L-dopa (Hearing y Eckel, 1976; Hearing et al., 1981). Las moléculas de esta enzima son glicoproteínas a las que se unen diversos azúcares en residuos de asparragina. El procesado de tirosinasa se produce en los polirribosomas y, en primer lugar, se produce la síntesis de la parte proteica de la molécula. A continuación, la enzima se traslada al retículo endoplasmático y al aparato de Golgi donde sufre diferentes modificaciones estructurales. Así, en este procesado, se incorpora una molécula de ácido siálico y cuatro azúcares (manosa, glucosamina, galactosa y fructosa) por cada molécula de tirosinasa (Ferrini et al., 1987). Con este procesado post-traduccional, tirosinasa pasa de tener 55000 daltons y un punto isoeléctrico (pI) de 4.2, a ser una molécula de 70000 daltons y con un pI de 3.3 (Burnett, 1971; Hearing et al., 1981; Laskin y Piccinini, 1986). Una vez se produce este procesado, y la enzima ya está madura, se transporta por medio de vesículas a los melanosomas donde permanece unida a la membrana de estos, desde donde participa en la ruta de biosíntesis de melaninas (Hearing y Jiménez, 1987).

La tirosinasa es la responsable de la conversión de L-tirosina en L-dopa y éste en *o*-dopaquinona. Esta *o*-dopaquinona formada se transforma, por medio de una serie de reacciones espontáneas no enzimáticas, en diferentes tipos de melaninas. Mutaciones en el gen que codifica a tirosinasa dan lugar a que se detenga la ruta de biosíntesis de melaninas (Camand et al., 2001) produciendo albinismo (Oetting, 2000). Se ha aislado y caracterizado el gen de tirosinasa en niños afectados por albinismo oculocutáneo, en los que no se detectaba actividad tirosinasa. El análisis secuencial

mostró una simple inserción en el exón 2, lo que producía una señal de terminación prematura, que daba lugar a una molécula de tirosinasa inactiva (Tomita et al., 1989).

En organismos inferiores y en plantas, tirosinasa es el único enzima que controla la síntesis de melaninas. Sin embargo, en animales, la duplicación del gen de tirosinasa da dos genes que codifican las proteínas relacionadas con tirosinasa (TRPs), con una gran similitud con tirosinasa como se muestra en la Figura 3 (Jackson, 1994; Olivares y Solano, 2009), aunque con diferentes funciones y capacidades catalíticas (Hearing y Tsukamoto, 1991; del Marmol y Beermann, 1996).

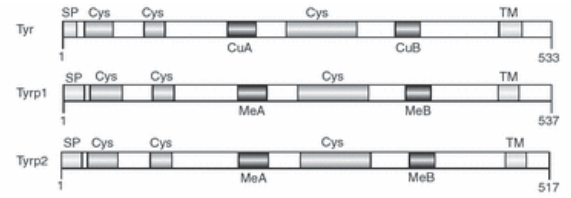

Figura 3. Representación del gen codificante para tirosinasa (Tyr), proteína relacionada con tirosinasa-1 (Tyrp1) y proteína relacionada con tirosinasa-2 (Tyrp-2).

Estas proteínas dirigen los intermedios quinónicos a un polímero más ordenado y estructuralmente diverso. TRP-2, también llamada dopacromo tautomerasa, cataliza el reagrupamiento no descarboxilativo de dopacromo a ácido 5,6-dihidroxiindol-2-carboxílico (DHICA) (Aroca et al., 1990; Olivares y Solano, 2009). Sin embargo TRP-1 tiene una función que está sujeta a controversia pero se ha descrito que esta enzima es importante para el tráfico de tirosinasa hacia el melanosoma (Jimbow et al., 1997). Las funciones de las tres enzimas están relacionadas con el cofactor metálico que utilizan: tirosinasa (cobre), TRP-2 (dopacromo tautomerasa) (zinc) y, probablemente, TRP-1 (cobre) (Olivares y Solano, 2009).

1.2. Tirosinasa: funciones fisiológicas

1.2.1. Tirosinasa de bacterias

Aunque la enzima modelo utilizada en la mayoría de experimentos relacionados con melanogénesis es la tirosinasa de champiñón, hay algunos ejemplos de tirosinasas de bacterias que se encuentran muy bien caracterizadas tanto estructural como cinéticamente. Así, las primeras descritas fueron las tirosinasas del género *Streptomyces* (Lerch y Ettlinger, 1972), pero actualmente hay otros muchos ejemplos como las enzimas de *Pseudomonas melanogenum*, *Marinomonas mediterránea*, *Thermomicrobium roseum* o *Bacillus megaterium* (Liu et al., 2004; Ruan et al., 2004; Sánchez-Amat, 2001; 2010; Claus y Decker, 2006). Se ha descrito una tirosinasa de *Ralstonia solanaceum* que posee una relación entre las actividades monofenolasa/difenolasa muy elevada (Hernández-Romero et al., 2006). La primera tirosinasa de la que se obtuvo su estructura cristalina fue la de *Streptomyces castaneoglobisporus* (Matoba et al., 2006), se propuso que el sitio activo de dicha enzima es flexible durante la catálisis. Recientemente, se ha aislado, clonado y caracterizado una tirosinasa de *Bacillus megaterium* que tiene una gran actividad en medios orgánicos (Shuster y Fishman, 2009). Se ha obtenido el cristal de esta tirosinasa de *Bacillus megaterium* con una resolución de 2-2.3 Å (Sendovski et al., 2011).

La principal función encontrada para la tirosinasa de bacterias ha sido la de protección del microorganismo y de sus esporas frente a la radiación UV gracias a la formación de melaninas, las cuales son pigmentos oscuros de diferente composición (Ruan et al., 2004). Además, estas melaninas son capaces de unir metales pesados, que de otra forma serían muy tóxicos para la célula bacteriana. Por otra parte, las melaninas protegen a la célula bacteriana frente a oxidantes, calor o componentes antimicrobianos, lo que contribuye a aumentar la patogenésis microbiana (Nosanchuk y Casadevall, 2003). En ambientes terrestres, la tirosinasa extracelular también está implicada en la polimerización y detoxificación de componentes fenólicos de plantas y en la formación de materia húmica.

1.2.2. Tirosinasa de plantas y hongos

La función de tirosinasa en plantas y hongos es confusa y objeto de controversia (Sommer et al., 1994; Joy et al., 1995; Onsa et al., 2000), a este hecho se atribuyen varias características propias del sistema enzimático, como pueden ser su doble actividad (monofenolasa y difenolasa) y la complejidad en su extracción y

purificación (Robb, 1984; Zhang et al., 1999; Nagai y Suzuki, 2001). Todo esto hizo que, en 1979, Mayer definiera a tirosinasa como "una enzima en busca de función" (Mayer y Harel, 1979; Mayer, 2006). Aún así, se han sugerido para ella diferentes funciones, basadas casi todas en la capacidad de la enzima de formar *o*-quinonas:

(a) Su acción se ha relacionado con la síntesis de *o*-difenoles y con la vía de síntesis de fenilpropanoides (Azcón-Bieto y Talón, 1993). Sin embargo, no se han obtenido resultados concluyentes que apoyen esta teoría (Vaughn y Duke, 1984), ya que la única evidencia de participación de esta enzima es un proceso biosintético es la demostración de que de que tirosinasa de champiñón participa en la síntesis de 2-hidroxi-4-iminoquimina, una quinona metabólicamente activa (Boekelheide et al., 1980). Gandia-Herrero (2005) sugiere que tirosinasa puede hidroxilar tiramina a dopamina, la cual, en presencia del ácido betalámico, podría rendir dopamina-xantina y ésta, a través de su oxidación, podría originar 2-descarboxibetanidina. Sin embargo, como indican los propios autores, se necesitan evidencias más convincentes de esta ruta biosintética. El grupo de Nakayama (Nakayama et al., 2000; 2001) ha descubierto una enzima, que tiene una gran similaridad estructural con tirosinasa, que es capaz de catalizar la formación oxidativa de auresidina. Esta enzima, llamada auresidina sintasa, también contiene una agrupación dinuclear de cobre pero, en cambio, tiene muy baja afinidad por los sustratos L-tirosina y L-dopa.

(b) Se ha sugerido que tirosinasa podría actuar como transportador electrónico debido a que las *o*-quinonas que produce poseen un alto poder oxidante (Mayer y Halel, 1979; Mayer 2006). Además, se cree que tirosinasa está asociada con los fotosistemas I y II y se especula con su posible participación en la producción de ATP y la regulación del oxigeno (Lax y Vaughn, 1991). En este sentido, recientemente (Fujieda et al., 2012), se ha demostrado que la tirosinasa *melB* de *Aspergillus oryzae* funciona como un transportador de oxigeno. Así, como se muestra en Figura 4, la forma inicial de tirosinasa (Pro-forma o forma inactiva) une reversiblemente el oxigeno y, gracias a una rotura proteolítica con tripsina, se transforma en una forma activada.

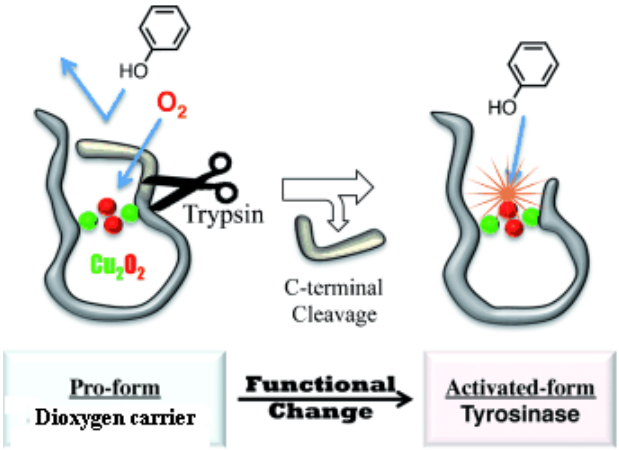

Figura 4. Representación esquemática de la activación de *melB* tirosinasa de *Aspergillus oryzae*.

(c) La implicación de tirosinasa en la regulación del crecimiento de las plantas se ha postulado en muchas ocasiones. Se ha demostrado que las *o*-quinonas interaccionan con el triptófano, generando finalmente ácido indol acético. También se ha observado que tirosinasa es inducida durante la fase de maduración de ciertas frutas (Joy et al., 1995).

La función más frecuentemente asociada a tirosinasa de hongos y plantas es la defensa. Así, un corte, daño o infección en un tejido produce la mezcla de la enzima con sus sustratos, que hasta el momento han estado confinados en otros compartimentos celulares, dando lugar a la formación de *o*-quinonas. Estas *o*-quinonas pueden unirse a proteínas inactivándolas o bien pueden polimerizar formando melaninas. Estas melaninas poseen un elevado poder bacteriostático (Pierpoint et al., 1977) a la vez que protegen a diversas plantas frente a insectos y microorganismos, catalizando la formación de una capa de melanina frente al ataque (Kowalski et al., 1992). Además, parece claro que la función de tirosinasa en hongos radica en la formación de melaninas durante el desarrollo de cuerpos fructíferos y esporas (Bell y Wheeler, 1986) ya que incrementa la resistencia de las paredes celulares de las esporas frente a las enzimas hidrolíticas de las bacterias como son gluconasas o quitinasas (Kuo y Alexander, 1967). Igualmente, se ha detectado una respuesta de plantas de patata (*Solanum tuberosum*) aumentando la actividad de tirosinasa frente al ataque por el escarabajo Colorado de patata (Kruzmane et al., 2002; Mayer, 2006). Un esquema de la conexión entre los niveles de expresión de tirosinasa y alguna de sus funciones se muestra en la Figura 5.

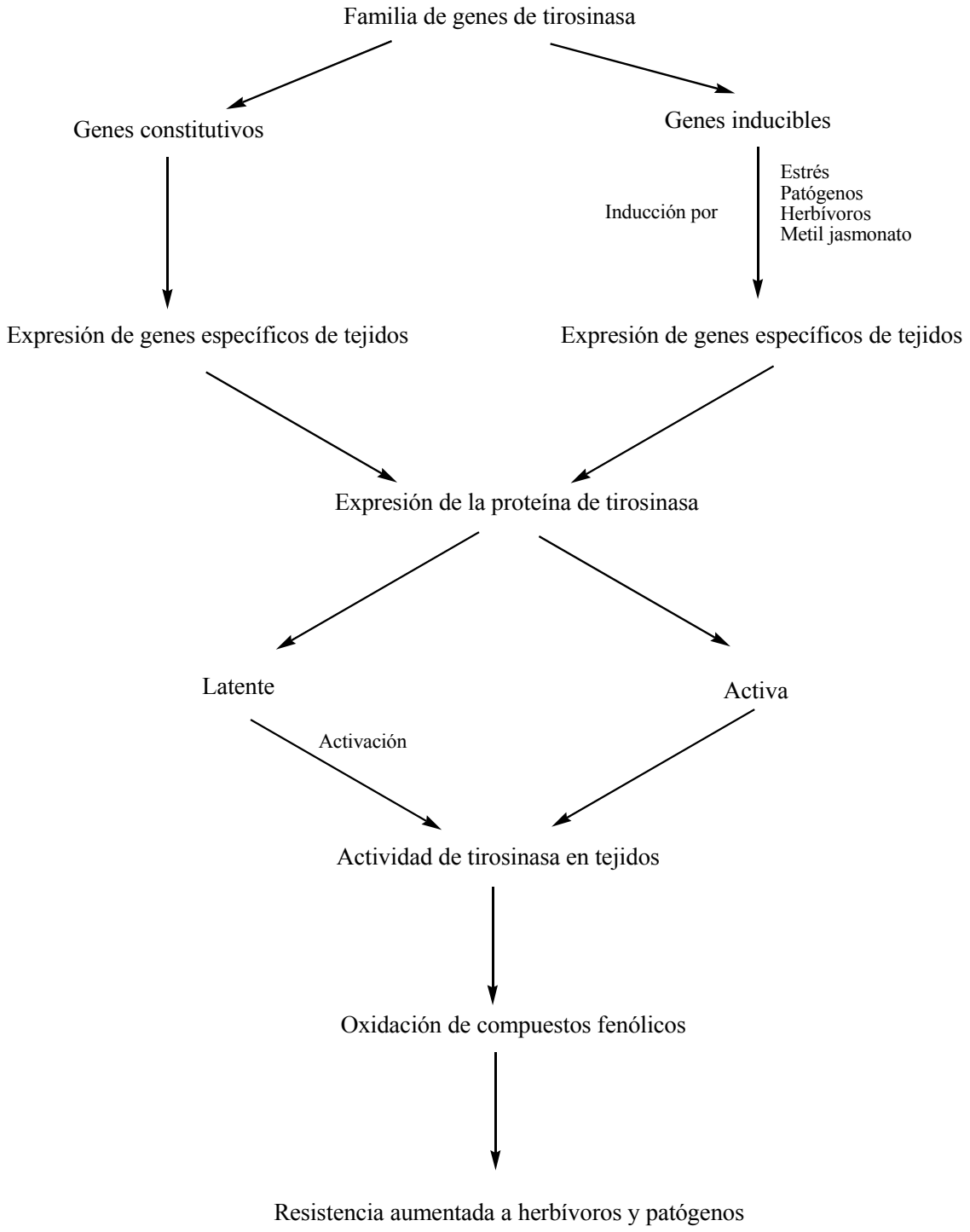

Figura 5. Representación entre los niveles variables de la actividad de tirosinasa y algunas de sus funciones.

Pardeamiento de frutas y hortalizas

El pardeamiento de los alimentos abarca reacciones de aminoácidos, proteínas, glúcidos o lípidos y es el responsable del deterioro que sufren los mismos

en su almacenamiento y procesamiento. Esta pérdida de calidad alimentaria se debe principalmente a la eliminación de aminoácidos esenciales, inhibición de enzimas proteolíticas, interacción con cationes metálicos y formación de sustancias tóxicas. Este pardeamiento se clasifica en dos tipos: enzimático y no enzimático (Figura 6).

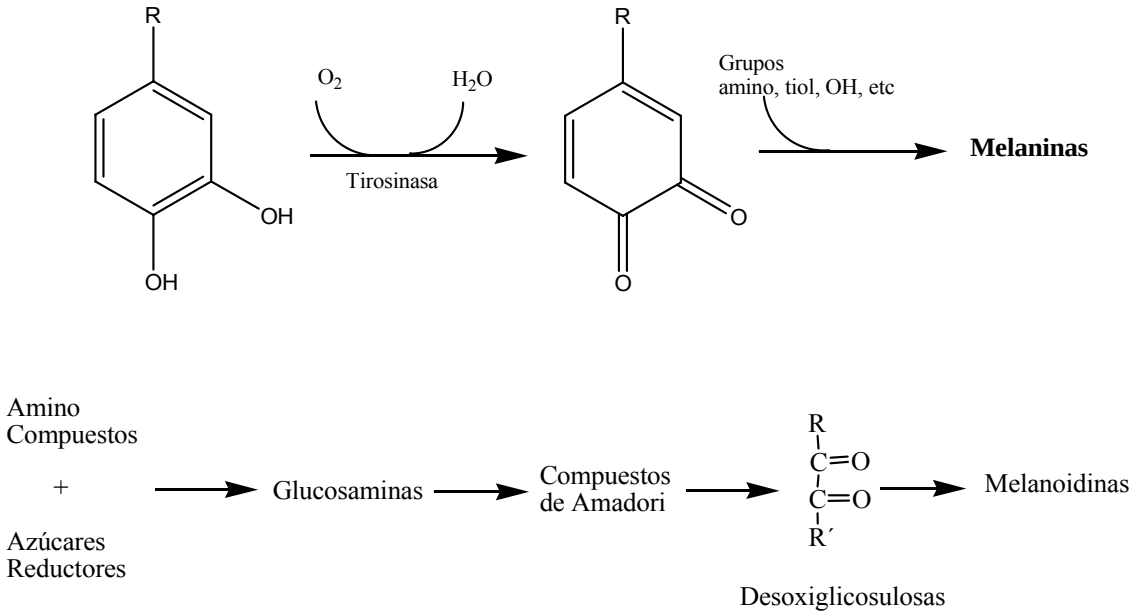

Figura. 6. Reacciones de pardeamiento enzimático y no enzimático de frutas y hortalizas.

Las reacciones del pardeamiento no enzimático son reacciones entre aminas, péptidos o proteínas con azúcares reductores en lo que comúnmente se denominan reacciones de Maillard.

El pardeamiento enzimático es debido en gran parte a tirosinasa. Sin embargo, otras enzimas como lacasas o peroxidasas también intervienen en el proceso (Vámos-Vigyázó, 1981). En el champiñón (de donde es la tirosinasa modelo), el pardeamiento no enzimático prácticamente no interviene en comparación con el enzimático. El champiñón recolectado sufre un oscurecimiento que se incrementa con el tiempo transcurrido desde la cosecha, la iluminación, la ventilación o el calentamiento ambiental, especialmente cuando los carpóforos sufren algún daño o corte (Burton et al., 1993; Alique y de la Plaza et al., 1995). El pardeamiento también ocasiona una pérdida de aroma y sabor de las frutas y hortalizas lo que conlleva grandes pérdidas económicas en el sector alimentario, al reducir la vida útil del producto (Noble y

Burton, 1993). Así, numerosas estrategias han sido desarrolladas para disminuir o eliminar el pardeamiento tanto enzimático como no enzimático (Nicolas et al., 1994).

1.2.3. Tirosinasa de artrópodos

El éxito de los insectos como animales terrestres es debido, en gran parte, a la formación de su exoesqueleto, el cual les protege de la desecación y las toxinas y que les permite conservar su forma, sirviendo como punto de anclaje para músculos y órganos. Este exoesqueleto o cutícula tienen que mudarlo cada cierto tiempo, para permitir el crecimiento del animal. El exoesqueleto recién formado es suave y claro pero, en seguida, se oscurece y endurece, gracias a los procesos de esclerotización y melanización, procesos que ocurren simultáneamente e independientemente uno del otro.

Durante el proceso de esclerotización, N-acetildopamina (NADA) y N-β-alanildopamina son activados por enzimas cuticulares a intermedios activos, los cuales interaccionan con proteínas y polímeros de quitina (Sugumaran, 2001; 2002). Los primeros estudios llevados a cabo sobre este proceso, concluyeron que las *o*-quinonas generadas por tirosinasa eran las principales desencadenantes de la esclerotización (Pryor, 1940). Así pues, la ruta propuesta implica que el aminoácido L-tirosina es hidroxilado a L-dopa, el cual sufre una descarboxilación para dar dopamina, que al reaccionar con acetil-CoA conduce a la formación de N-acetildopamina (NADA) para, posteriormente, convertirse en NADA-quinona (NADAQ) de nuevo gracias a la acción de tirosinasa (Figura 7). Esta *o*-quinona no puede sufrir una adición intramolecular, por lo que reacciona con sitios puntuales de las cadenas de proteínas (intermoleculares). Al reaccionar con los grupos ε-amino de lisinas, produce un difenol sustituido que es oxidado, no enzimáticamente, por NADQ a la forma quinónica. La sustitución posterior con otro residuo de la cadena de proteína da lugar a la formación de una molécula proteica entrecruzada, denominada esclerotina.

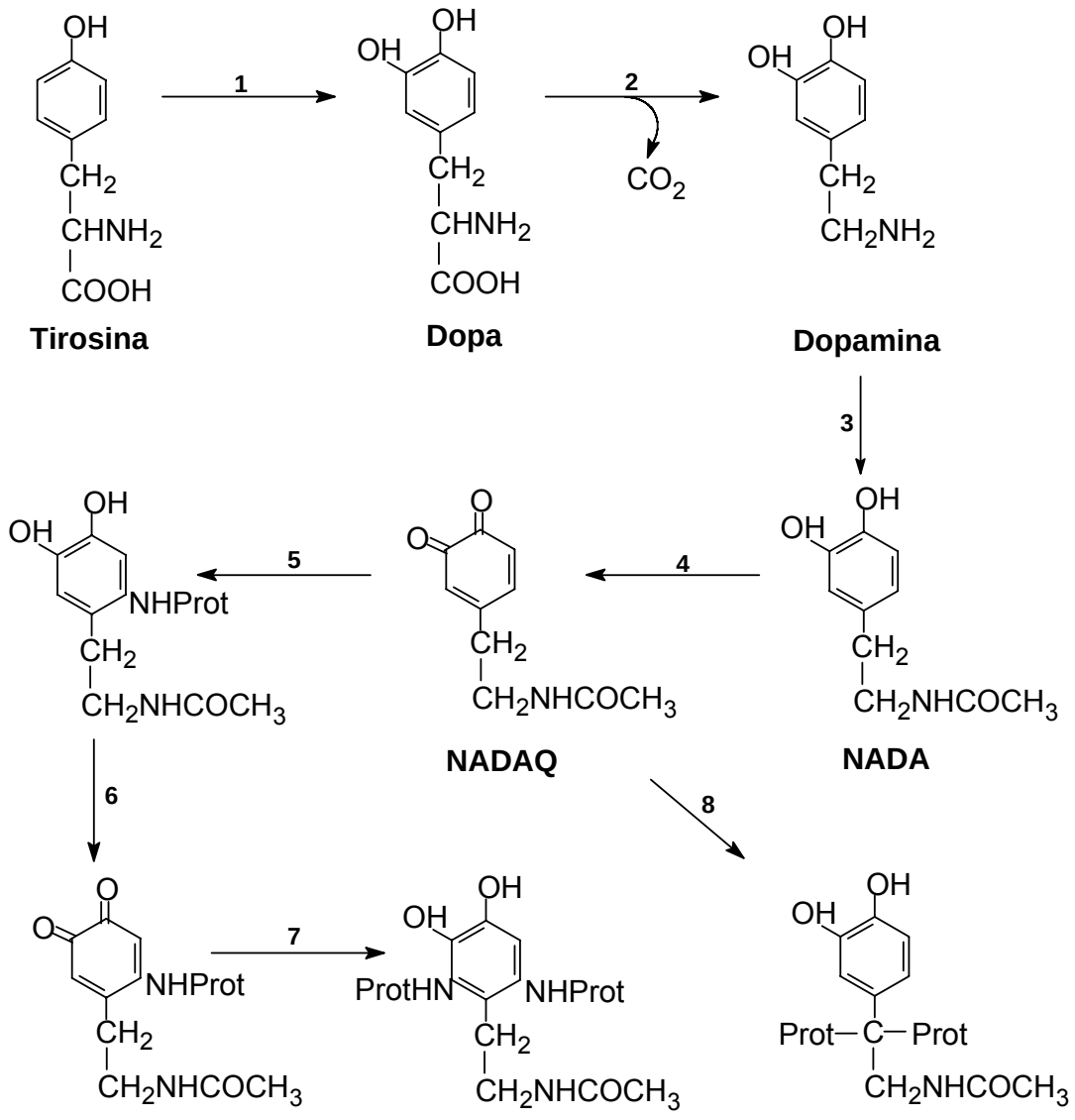

Figura 7. Ruta propuesta para la intervención de tirosinasa en el proceso de esclerotización (Pryor, 1940). Los pasos 1-4 están catalizados enzimáticamente, pudiendo estar implicada tirosinasa.

Un tipo diferente de esclerotización fue descrito por Andersen (2010) y por Sugumaran y sus colaboradores (Abede et al., 2010). Estos autores encontraron que NADA sufría la desaturación de su cadena lateral. El compuesto resultante, dehidro-NADA, es oxidado a su correspondiente quinona, la cual actúa como factor desencadenante de la esclerotización. Este proceso se denominó β-esclerotización y sugería la existencia de una NADA desaturasa como enzima clave en la esclerotización de insectos. Posteriormente, fue descubierta una tercera vía de

esclerotización (Sugumaran y Lipke, 1983), donde la 2-hidroxi-4-alquilidenquinona (tautómero de la 4-alquilquinona), actúa como unidad entrecruzante (esclerotización quinona metide).

Otros estudios han conducido a la solubilización y caracterización de diversas enzimas implicadas en esa ruta metabólica (Saul y Sugumaran, 1989; 1990), pudiéndose unificar las tres vías descritas en una ruta general de esclerotización (Figura 8).

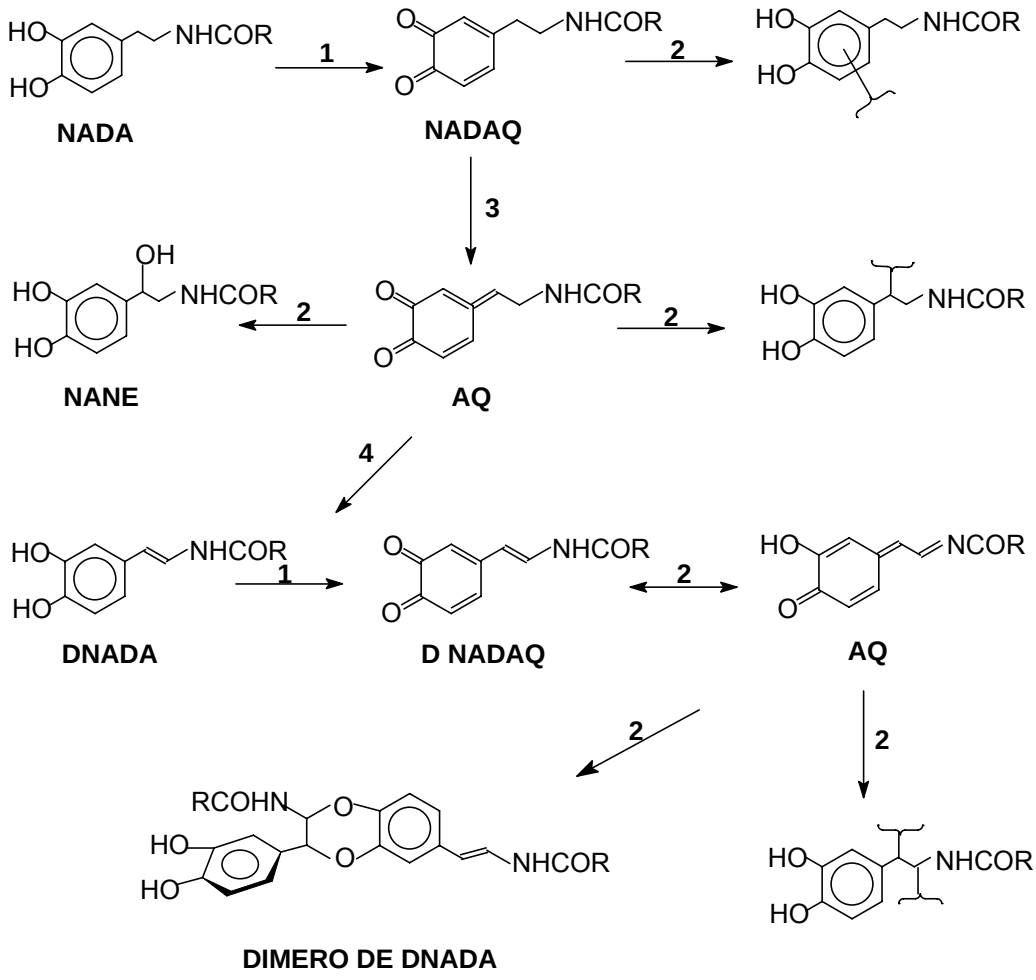

Figura 8. Ruta para la esclerotización de la cutícula de artrópodos (Sugumaran, 1991). Abreviaturas: NADA = N-acetildopamina; NADAQ = N-acetil-*o*-dopaminoquinona; NANE = N-acetilnorepinefrina; DNADA = dehidro-NADA; DNADAQ = dehidro-NADAQ; AQ = intermedios alquilidenquinónicos. Las etapas catalizadas enzimáticamente son: (1) PPO o tirosinasa; (3) quinona isomerasa y (4) alquilidenquiona isomerasa. Las etapas (2) transcurren mediante reacciones no catalizadas enzimáticamente.

1.2.4. Tirosinasa de mamíferos

1.2.4.1. Melanocitos e histología de la melanogénesis

La piel es el órgano más extenso del hombre (entre 2 y 2.5 m^2), que recubre y protege toda la superficie del cuerpo. Su función principal es la protección de los tejidos subyacentes contra los agentes externos, aunque su metabolismo es activo y no debe considerarse una simple barrera física. Está formada por tejido conjuntivo (dermis) y un tejido epitelial (epidermis). Ambas capas están separadas por una membrana basal (Figura 9).

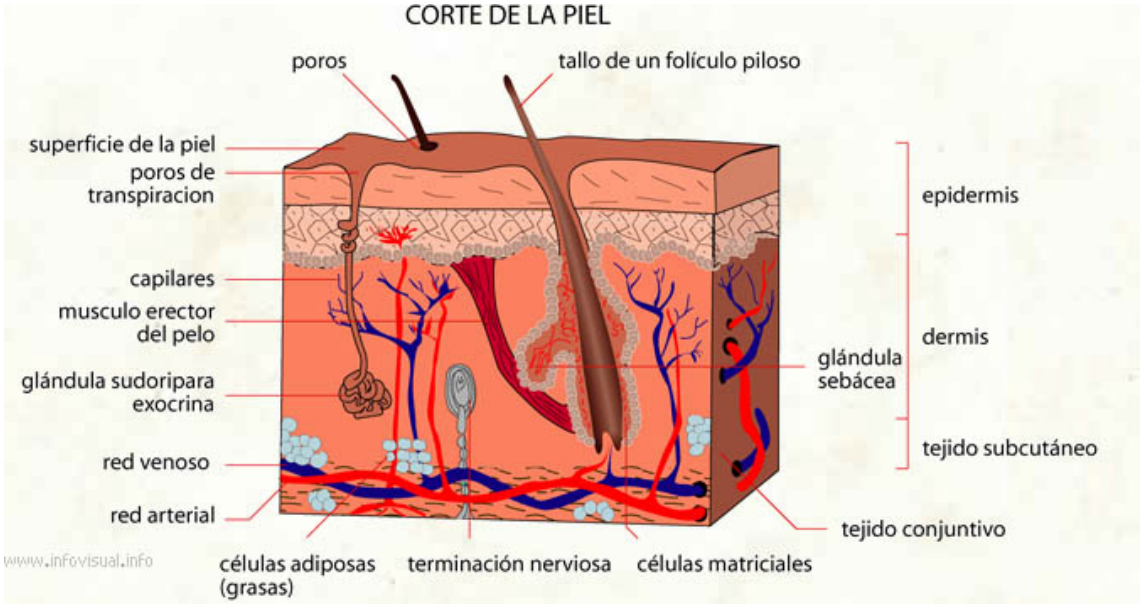

Figura 9. Corte transversal de la piel.

La dermis está constituida principalmente por fibroblastos mientras que la epidermis es un epitelio con multitud de tipos celulares entre las que destacan los queratinocitos, las células de Merkel, las células dendríticas y los melanocitos, que son células muy especializadas localizadas a nivel de la membrana basal de la epidermis y cuya función principal es la formación de los pigmentos polifenólicos, las melaninas. Un corte de la epidermis puede verse en la Figura 10.

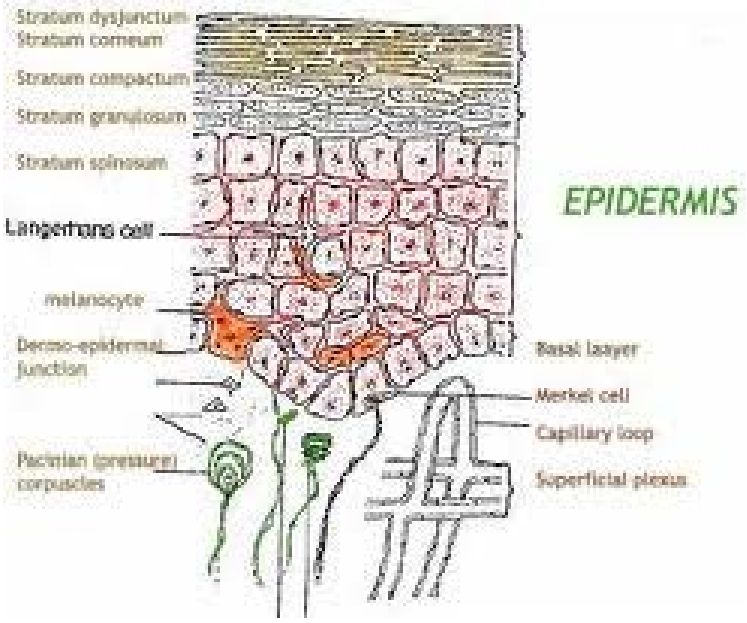

Figura 10. Detalle de la epidermis con sus diferentes tipos celulares.

La melanina se sintetiza, como se describió anteriormente, en los melanocitos. Las células precursoras de los melanocitos son los melanoblastos, que tiene un origen neuroectodérmico y migran a la epidermis durante el desarrollo embrionario, distribuyéndose entre las capas basales. El melanocito tiene un tamaño pequeño y posee unas prolongaciones dendríticas, cargadas de gránulos de melanina, donde se encuentra confinada la enzima tirosinasa (Figura 11). Esta célula posee además un núcleo pequeño y una estructura llamada complejo de GERL, en el que participan el complejo de Golgi, el retículo endoplasmático y los lisosomas (Novikoff et al., 1971).

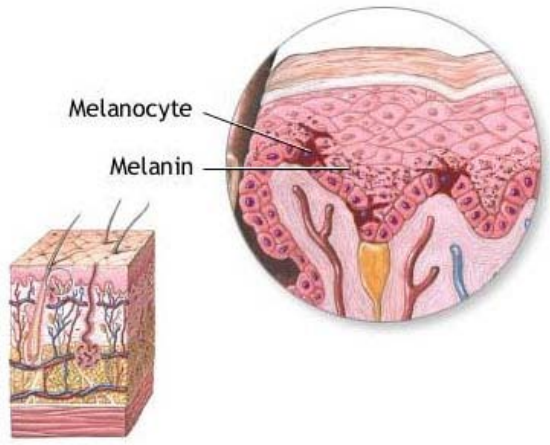

Figura 11. Detalle de la capa basal de la epidermis donde se encuentran los melanocitos y donde se confinan los pigmentos de melanina.

La verdadera fábrica de melanina es el melanosoma. Este orgánulo tiene una gran importancia ya que mantiene en su interior a los diferentes intermedios de la melanogénesis que son compuestos altamente reactivos y citotóxicos (Pawelek y Lerner, 1978). La biogénesis de melanosomas comienza en el GERL. En este proceso se pueden definir varias etapas:

(1) En la primera etapa, se observa solo una vesícula esférica delimitada por membrana, sin una estructura interior definida, aunque contiene ya tirosinasa activa.

(2) En la segunda etapa, se distingue un orgánulo ovoidal dotado de estructura lamelar visible al cual se le conoce como premelanosoma. Aún no se observa depósito de pigmento.

(3) En la tercera etapa, el melanosoma presenta zonas densas y oscuras en su interior debido a la melanina, que se ha depositado de forma ordenada sobre el esqueleto lamelar.

(4) En la última etapa, el melanosoma ha degenerado y presenta un tono opaco debido al elevado contenido de melanina. Este orgánulo va a migrar al extremo de las dendritas para pasar, finalmente, a los queratinocitos circundantes.

Es interesante recalcar que el número de melanocitos es prácticamente igual en todas las razas humanas, así que las diferencias en el color de la piel se debe, principalmente, a la cantidad de pigmento que estos melanocitos producen y transfieren a los queratinocitos circundantes (Toda et al., 1973; Hearing, 1999).

En el proceso de la melanogénesis, como ya ha sido indicado en el capitulo 1.1.3., están involucradas tres enzimas específicas situadas en los melanosomas: tirosinasa y las proteínas relacionadas con tirosinasa, TRP-1 y TRP-2 (también llamada dopacromo tautomerasa) (Prota et al., 1998; Olivares et al., 2001). Tirosinasa ejerce su función de biosíntesis de melaninas en el interior del melanosoma. Se han descrito varios factores que pueden favorecer esta compartimentación:

(a) Disponibilidad de cobre.

(b) Afinidad de las isoenzimas por los sustratos. Las distintas isoenzimas presentan diferente afinidad por sus sustratos. Así, de las tres isoenzimas descritas, la microsómica, la soluble y la melanosómica, es esta última la que presenta más afinidad y mejor eficacia catalítica por sus sustratos (Hearing y Jimenez, 1987).

(c) Presencia de inhibidores citosólicos. Se han descrito varios inhibidores citosólicos que se unen al sitio activo de tirosinasa, inactivándola (Vijayan et al., 1982; Chakraborty et al., 1989).

(d) Disponibilidad de L-dopa. Como se describirá más adelante, tirosinasa necesita cantidades catalíticas de L-dopa cuando actúa sobre monofenoles como L-tirosina (Ros et al., 1994).

(e) Efecto del pH. La posible existencia de un pH ligeramente ácido en el interior del melanosoma, ha sido muy discutido desde hace años (Oikawa et al., 1987). Diversos estudios han demostrado la existencia de un pH de 5.5 en el interior de los lisosomas que son orgánulos, al igual que los melanosomas, que están delimitados por membrana. El pH puede actuar como un factor regulador de la ruta biosintética de melaninas hacia melanógenos di- o trihidroxilados (García-Carmona et al., 1982; Rodríguez-López et al., 1991). Estos compuestos van a tener diferentes capacidades citotóxicas.

1.2.4.2. Tipos de melaninas y su formación

Las melaninas son polímeros polifenólicos heterogéneos con colores que van desde el amarillo hasta el negro. Estos compuestos están ampliamente distribuidos en la naturaleza y pueden ser encontrados en toda la escala filogenética, desde la bacteria hasta el hombre.

El estudio de las propiedades físicas y químicas de las melaninas, integras o degradadas, ha llevado al descubrimiento de tres tipos de melaninas (Prota, 1988; Lamoreaux et al., 2001):

(1) Las eumelaninas, pigmentos insolubles de color marrón a negro, con una estructura polimérica nitrogenada formada a partir de unidades indólicas.

(2) Las feomelaninas, pigmentos solubles en bases fuertes, de color amarillo a pardo-rojizo, caracterizados por su alto contenido en azufre.

(3) Los tricocromos, pigmentos fenólicos de bajo peso molecular solubles en álcalis, que contienen el cromóforo Δ-bi-(1,4-benzotiazina), dimérico (Figura 12).

(4) Mezclas. Muchas de las melaninas de mamíferos son mezclas de eumelaninas y feomelaninas en diferente proporción.

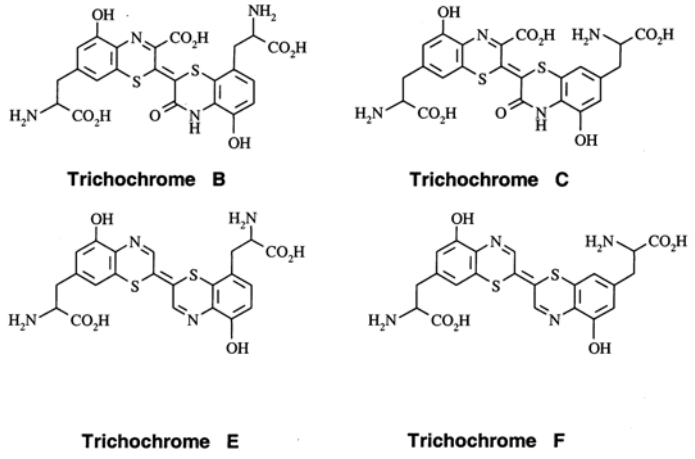

Figura 12. Estructuras químicas de tricocromos (Prota, 2000).

Numerosos estudios han contribuido de manera significativa a la identificación de las rutas de biosíntesis de melaninas correspondientes a diversos tipos de precursores fenólicos (Raper, 1928; Mason, 1948; 1956; Robb, 1984, Prota, 1988; 2000). Se ha comprobado la participación de tirosinasa en la formación de *o*-difenoles y *o*-quinonas y se ha estudiado si la evolución de estas *o*-quinonas transcurre exclusivamente mediante reacciones no enzimáticas (Prota, 1988; 2000) o con la posible ayuda de otras enzimas llamadas distales (Figura 13), la disponibilidad de compuestos tiólicos es básica para la formación proporcionada de eumelaninas, feomelaninas o tricocromos.

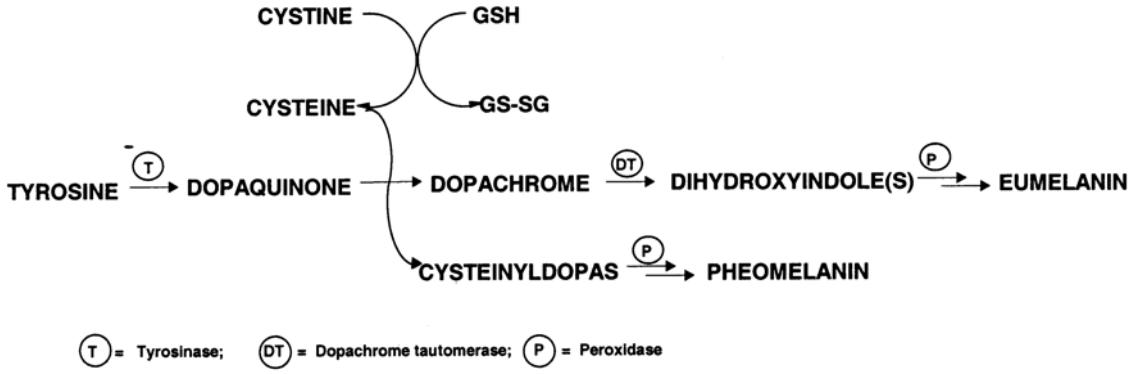

Figura 13. Ruta simplificada de la melanogénesis (Prota, 2000). Como se puede observar, cisteína y glutatión intervienen en la ruta clásica de Raper-Mason.

La melanogénesis (Figura 14) comienza con la hidroxilación, por oxigeno molecular, de monofenoles (L-tirosina) y la oxidación de *o*-difenoles (L-dopa) originando las correspondientes *o*-quinonas. Esta *o*-quinonas evolucionan hacia la formación de melaninas a través de reacciones no enzimáticas (Robb, 1984). Son el

intermedio clave de la ruta melanogénica, y han sido descritas tres rutas de evolución diferentes:

(a) Ciclación de *o*-dopaquinona a leucodopacromo, oxidación de este a dopacromo y generación posterior de eumelaninas.

(b) Adición de compuestos tiólicos a *o*-dopaquinona, formándose feomelaninas y tricocromos.

(c) Adición de agua al anillo de las *o*-quinonas, generándose compuestos trihidroxilados, los cuales serán oxidados posteriormente y evolucionan hasta polímeros.

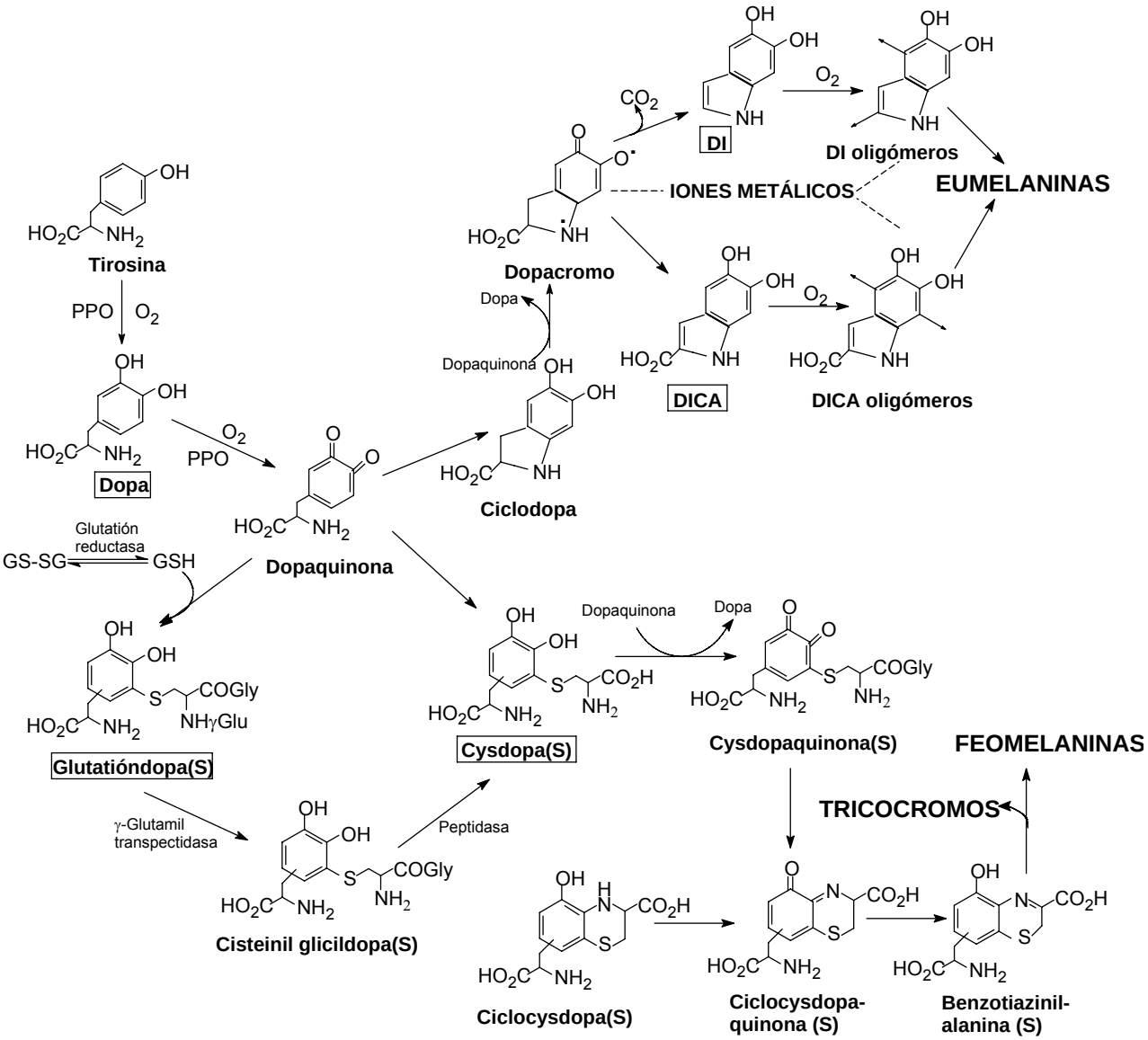

Figura 14. Principales rutas de biosíntesis de melaninas (Prota, 1988). Las sustancias incluidas en recuadros son productos de excreción del metabolismo.

La ruta de biosíntesis de melaninas descrita inicialmente por Raper (1928) y Mason (1948), proponía una serie de intermedios, algunos de ellos no fueron correctamente caracterizados (Graham y Jeffs, 1977; Pawelek et al., 1980). Esta ruta inicial fue modificada posteriormente por Lerner y Fitzpatrick (1950). Recientemente se le han introducido algunas modificaciones descritas por Lozano y Solano (1989), Hearing y Tsukamoto (1991) y Jimenez-Cervantes et al. (1994). Nuestro grupo de investigación también introdujo algunas modificaciones en la ruta ya que estudió el efecto del pH en ella (García-Canovas et al., 1982) (Figura 15).

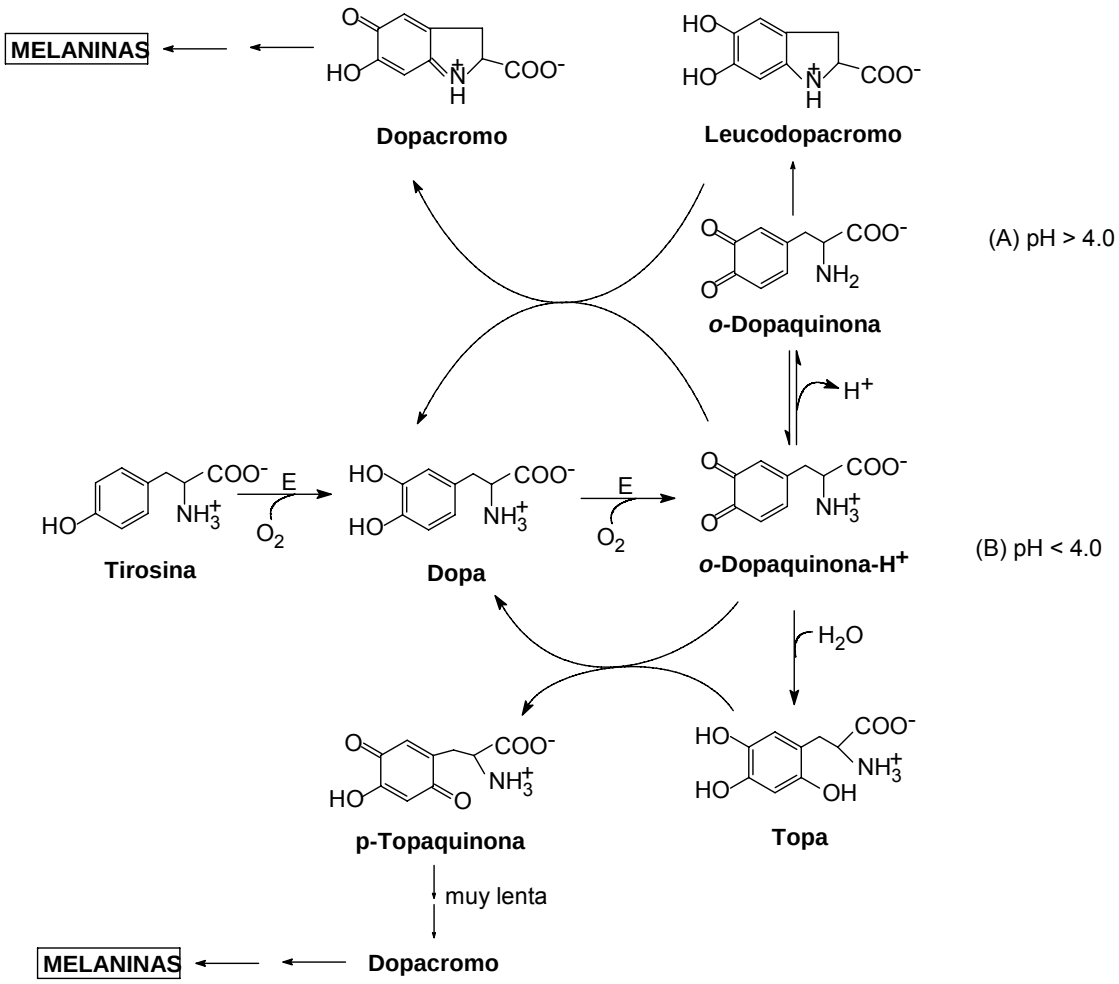

Figura 15. Rutas propuestas para la oxidación de dopa hasta dopacromo catalizada por tirosinasa a diferentes valores de pH (García-Cánovas et al., 1982). E = tirosinasa. A valores de pH > 4,0 predomina la contribución de la ruta de ciclación (A), mientras que a valores de pH < 4,0 participan significativamente las rutas de ciclación y de hidroxilación (A y B).

Biosíntesis de eumelaninas

La biosíntesis de eumelaninas, que fue propuesta en 1928 por Raper-Mason, se muestra en la Figura 15. En la síntesis de eumelaninas, la *o*-dopaquinona, formada a partir de L-tirosina o L-dopa por tirosinasa, sufre una ciclación espontánea, previa desprotonación del grupo amino, para generar ácido 5,6-dihidroxiindolil-2-carboxílico (leucodopacromo). A continuación, hay una reacción redox, espontánea y muy rápida, entre leucodopacromo y *o*-dopaquinona, que origina dopacromo y regenera L-dopa (Lerner y Fitzpatrick, 1950; García-Cánovas et al., 1982) (Figura 15).

El dopacromo formado se transforma lenta y espontáneamente en 5,6-dihidroxiindol (DHI) que se oxida a 5,6-indolquinona (IQ) en una reacción donde podría intervenir tirosinasa (Korner y Pawelek, 1980; 1982) o TRP-1 (García-Borrón y Solano, 2002). La IQ es un compuesto muy reactivo que puede reaccionar con diferentes intermedios de la ruta, sobre todo con DHI (Lambert et al., 1989) para dar lugar a un proceso polimerizante que conlleva la formación de eumelaninas (Figura 16).

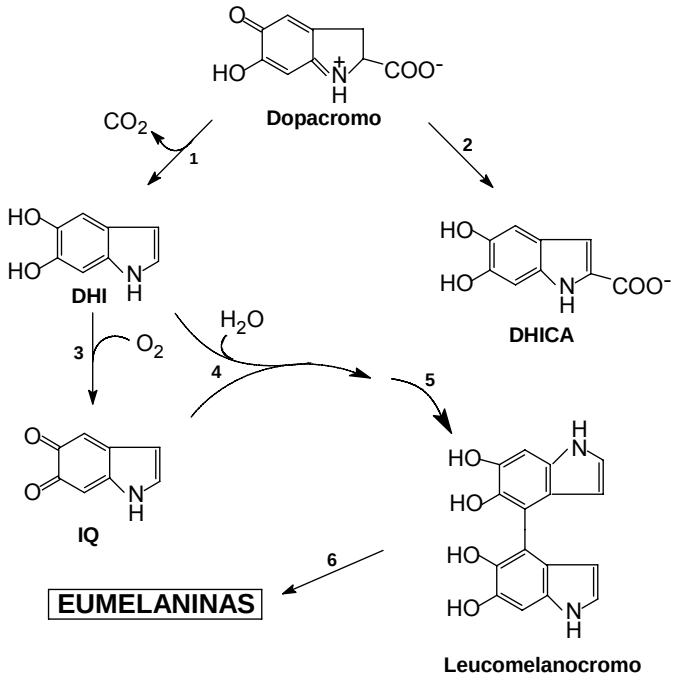

Figura 16. Rutas de evolución de dopacromo (Lambert et al., 1989). Las etapas 1, 4, 5 y 6 son espontáneas, mientras que las 2 y 3 podrían estar catalizadas enzimáticamente. En la etapa 2, la enzima implicada sería la dopacromo tauomerasa (Barber et al., 1984; Jiménez-Cervantes et al., 1994), mientras que en la 3 sería tirosinasa (Korner y Pawelek, 1982).

Dopacromo tautomerasa (TRP-2) cataliza la reacción 2 y tiene dos funciones en la ruta de biosíntesis de melaninas: (a) aceleración de la ruta (Jiménez-Cervantes et al., 1994, 2001) y (b) distintas propiedades del pigmento melánico. Así, el incremento de grupos carboxílicos, produce melaninas de menor tamaño y con una mayor capacidad complejante de cationes (Orlow et al., 1992; Kushimoto et al., 2001).

La desviación de la ruta hacia la formación de DHICA, evita la generación de compuestos citotóxicos, como puede ser DHI, que debido a su semejanza con las bases púricas, adenina y guanina, puede incorporarse en el ADN provocando mutaciones puntuales (Miranda et al., 1987; Olivares et al., 2001).

Biosíntesis de feomelaninas

Si en el medio de reacción, existen compuestos con grupos tiólicos, tales como glutatión o cisteína, la ruta de biosíntesis de melaninas se desvía desde *o*-dopaquinona hacia feomelaninas (Prota, 1988; Kondo y Hearing, 2011). La primera etapa de la ruta biosintética de feomelaninas es la adición reductiva de cisteína a *o*-dopaquinona para producir dos isómeros de cisteinildopa (CD), 5-cisteinildopa y 2-cisteinildopa, aunque la posición más favorable es la 5. La segunda etapa es una reacción redox entre CD y *o*-dopaquinona que origina cisteinildopaquinonas y dopa. La tercera etapa es la ciclación de estas cisteinildopaquinonas y posterior deshidratación para originar *o*-quinonaiminas (Napolitano et al., 2000). Estas *o*-quinoneiminas se reagrupan con o sin descarboxilación para formar intermedios de 1,4-benzotiazinas las cuales, finalmente, polimerizan para dar las feomelaninas (Wakamatsu et al., 2009; Greco et al., 2009) (Figura 17).

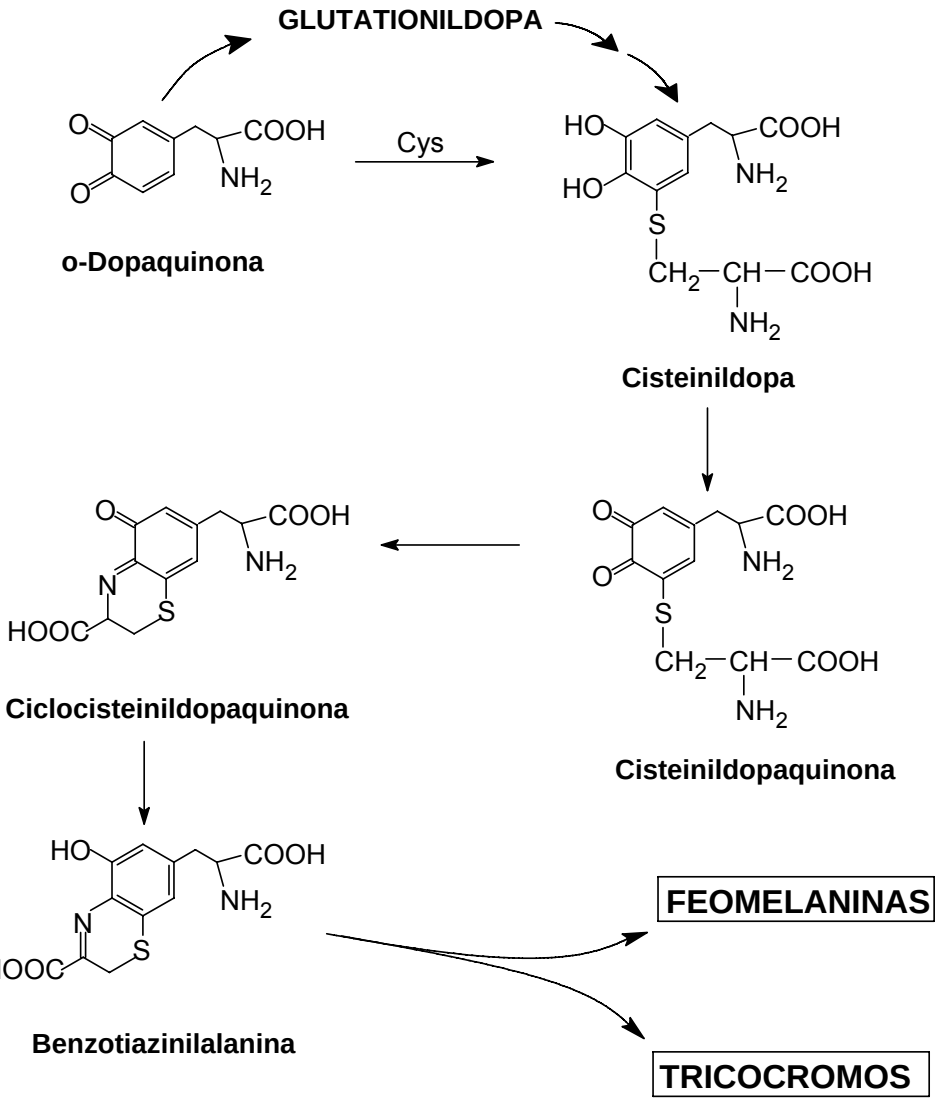

Figura 17. Ruta de formación de feomelaninas (Prota, 1980).

Como se muestra en la Figura 18, la *o*-dopaquinona juega un papel muy importante en producir eumelaninas o feomelaninas. En la Figura 16 también se describe que, en la biosíntesis de eumelaninas, están implicadas tirosinasa, TRP-1 y TRP-2 mientras que, en la de feomelaninas, solo interviene tirosinasa en el proceso.

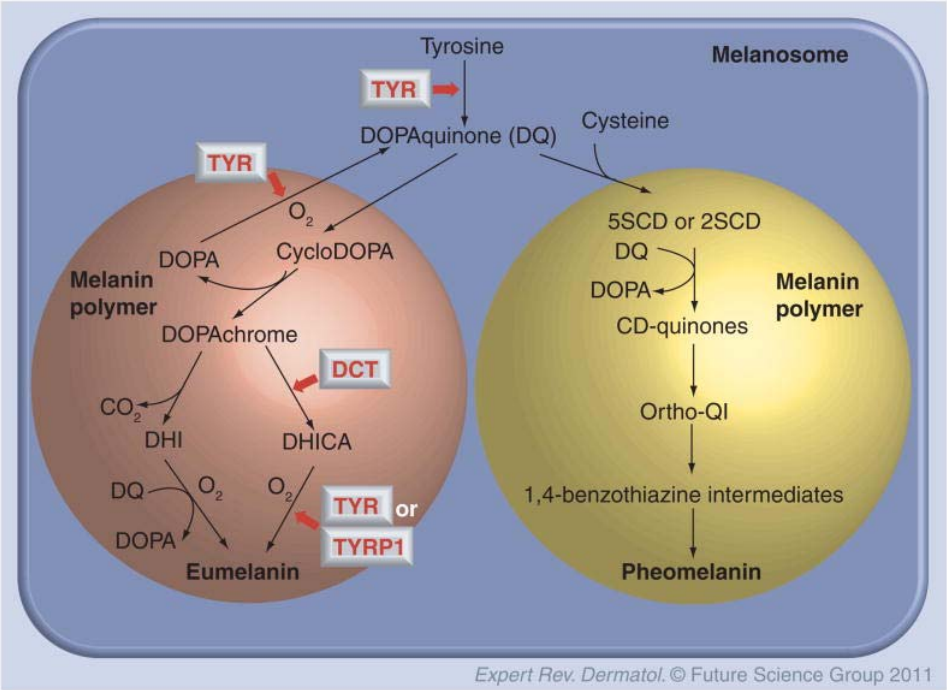

Figura 18. Vías biosintéticas de formación de eumelaninas y feomelaninas.

Biosíntesis de melaninas mezclas

Los melanocitos producen mezclas de eumelaninas y feomelaninas, con lo cual, la melanogénesis debería ser considerada como una melanogénesis mezcla. Ito y Wakamatsu, (2008) describieron que esta melanogénesis mezcla es una vía de tres etapas donde la cantidad total de melaninas producidas es proporcional a la producción de *o*-dopaquinona, la cual a su vez es proporcional a la actividad de tirosinasa. La primera etapa es la producción de los isómeros de cisteinildopa hasta que la concentración de cisteína en el melanocito sea mayor de 0.13 μM. La segunda etapa es la oxidación de estos cisteinildopa hasta feomelaninas, proceso que ocurre hasta que la concentración de cisteinildopa sea mayor de 9 μM. La última etapa es la producción de eumelaninas, la cual comienza cuando la cisteína celular y la concentración de cisteinildopa son prácticamente nulas. Por tanto, la ratio de eumelaninas y feomelaninas es determinada por la actividad de tirosinasa y por la disponibilidad de tirosina y cisteína en el melanosoma (Land et al., 2003).

Formación de compuestos trihidroxilados

Dawson y Tarpley (1963) pusieron de manifiesto la necesidad de considerar, como un paso obligatorio en la síntesis de catecolaminas, un ataque nucleofílico del agua sobre la *o*-benzoquinona, dando lugar al trihidroxibenceno. La reacción posterior

de éste con la *o*-benzoquinona, produce la regeneración de catecol y la formación de hidroxibenzoquinona (Figura 19). La polimerización de esta quinona conduce a la formación de catecolmelanina.

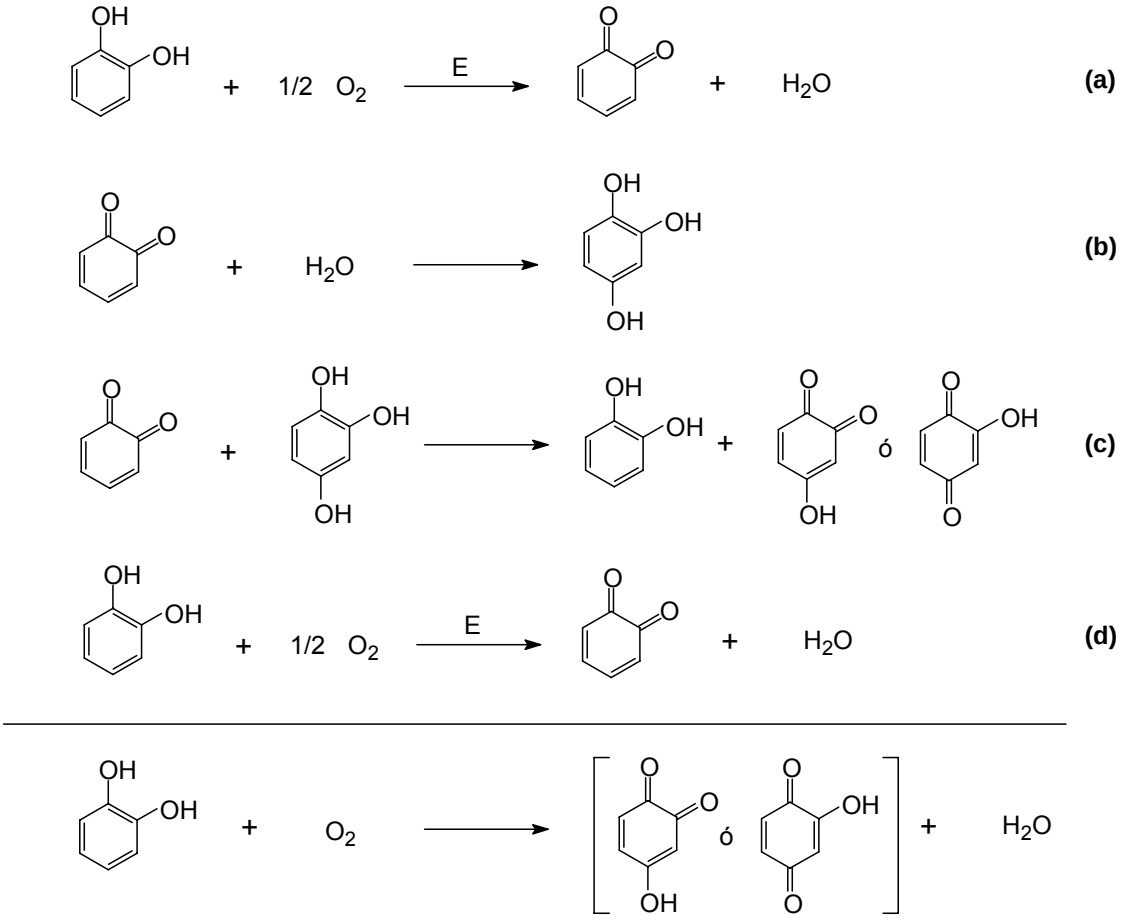

Figura 19. Mecanismo de reacción de adición de agua (Dawson y Tarpley, 1963). La reacción (a) es rápida, aunque la velocidad va a venir determinada por la cantidad de tirosinasa (E) presente en la reacción. La velocidad de la reacción (b) viene determinada por el pH, (c) es probablemente espontánea mientras que (d) es una reacción idéntica a (a).

1.2.4.3. Regulación de la melanogénesis

A. Papel de las radiaciones ultravioleta en la melanogénesis.

Está muy documentado el incremento de la síntesis de melaninas gracias a repetidas exposiciones a radiación ultravioleta (Miyamura et al., 2007).

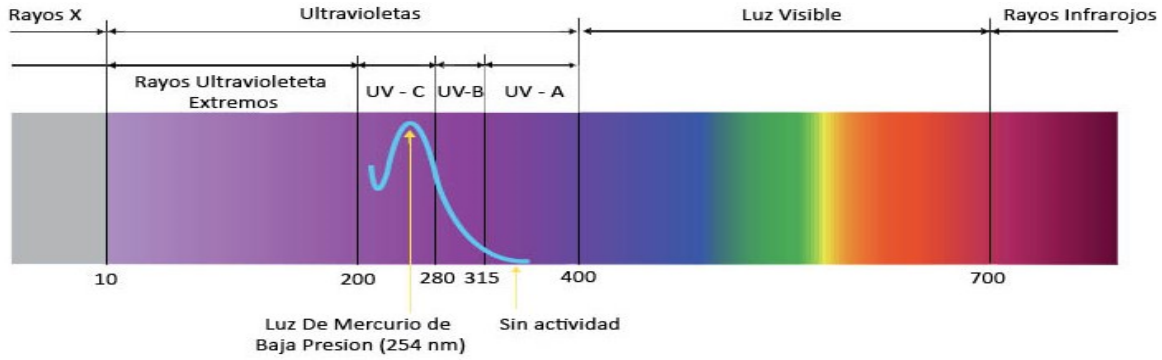

Figura 20. Espectro electromagnético y detalle del espectro de luz ultravioleta.

La radiación ultravioleta (UV) pertenece a la franja del espectro electromagnético con longitudes de onda entre 100 y 400 nm aproximadamente (Figura 20). Se extiende desde la parte violeta del espectro visible hasta la zona de rayos X blandos, aunque ambos límites son arbitrarios. La luz UV se subdivide en tres subclases: (a) UV-A (320-400 nm), (b) UV-B (290-320 nm) y (c) UV-C (200-290 nm). El nivel de energía es mayor cuanto menor sea la longitud de onda, con lo que la luz UV-C va a ser la que posee una mayor energía de irradiación. Sin embargo, la luz UV-C se dispersa cuando atraviesa la capa atmosférica con lo que su concentración es prácticamente nula a nivel del mar. Por otra parte, la capacidad de penetración de la luz ultravioleta es inversamente proporcional a la energía que posee, con lo que la luz UV-A es la que penetra más fácilmente en la piel humana. Esta radiación UV-A produce una pigmentación muy rápida debido a la traslocación del melanosoma desde el área perinuclear al área de las dendritas. Las radiaciones UV-B tienen un efecto más lento incrementando el número de melanocitos y el número de melanosomas en estos melanocitos y queratinocitos.

La radiación UV-B es absorbida directamente por el ADN celular dando lugar, sobre todo, a dímeros de timina (Hearing y Jiménez, 1987; Miyamura et al., 2007).

La proteína supresora de tumores p53 también participa en la activación de la melanogénesis después de una exposición de la piel a luz UV y actúa mediante dos mecanismos:

(a) Estimula la expresión de proopiomelanocortina (POMC) en los queratinocitos epidérmicos, activando a los melanocitos vecinos vía receptor de melanocortina 1 (MC1R).

(b) Estimula directamente la expresión de los genes que codifican para tirosinasa y la proteína relacionada con tirosinasa (TRP-1) en melanocitos (Kondo y Hearing, 2011).

Los niveles de ARNm de tirosinasa aumentan a través de un mecanismo dependiente de p53 cuando son irradiadas con luz UV células de melanoma en cultivo (Khlgatian et al., 2002; Kondo y Hearing, 2011).

B. PKC-β y activación de tirosinasa.

PKC-β es una proteína quinasa implicada en la regulación de la biosíntesis de melaninas ya que regula a tirosinasa gracias a la fosforilación de residuos de serina de su dominio citoplasmático (Park et al., 1993; 1999). PKC-β activada está asociada con la membrana melanosomal y se encuentra solo en los melanocitos, no en queratinocitos epidérmicos o fibroblastos (Park et al., 1999) (Figura 21).

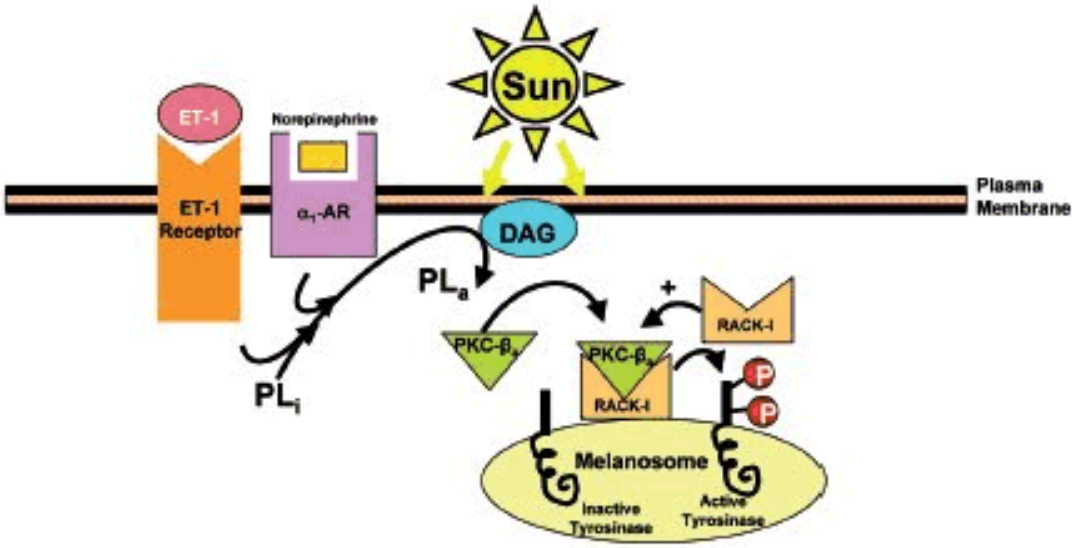

Figura 21. Activación de tirosinasa por PKC-β. La radiación UV, así como receptores de superficie tras la unión de sus respectivos ligandos (Endotelina/Receptor de endotelina 1 y Norepinefrina/α_1-adrenoreceptor) (Park et al., 2009).

La activación de DAG (diacilglicerol), activa a PKC-β gracias a que fosfolipasa inactiva se transforma en activa (PL_i a PL_a). PKC-β se une al receptor de la C-quinasa I (RACK-I) (Mochly-Rosen, 1995) y este complejo se trasloca a la membrana del melanosoma fosforilando a tirosinasa en residuos de serina (Park et al., 2004). La fosforilación de tirosinasa parece conducir a la formación de complejos entre tirosinasa y TRP-1 (Wu y Park, 2003). Esto provoca que tirosinasa se hace más estable y que, por tanto, aumente su actividad enzimática (Kobayashi et al., 1998a). Los melanocitos

expresan tanto receptores β_2 como α_1 adrenérgicos (Gillbro et al., 2004; Grando et al., 2006). El receptor α_1 interactúa con norepinefrina derivada del melanocito e incrementa el nivel de DAG (Kauser et al., 2003; Grando et al., 2006), por lo que se induce la melanogénesis dependiente de la PKC-β. Los queratinocitos producen epinefrina que se une a los receptores β_2 de los melanocitos y aumentan los niveles de AMPc conduciendo a la síntesis de melaninas (Grando et al., 2006).

C. Proteínas reguladoras de la melanogénesis.

El factor de transcripción asociado con Microftalmia (MITF) es un regulador clave de la pigmentación de mamíferos y es regulado por factores ambientales, como la luz UV, y por factores secretados por queratinocitos, fibroblastos y otras células (Figuras 22 y 23) (Yamaguchi et al., 2007; Kondo y Hearing, 2011). Las tres enzimas implicadas en la melanogénesis (tirosinasa y TRP1 y TRP-2) están reguladas transcripcionalmente por MITF, al igual que otras proteínas específicas del melanocito.

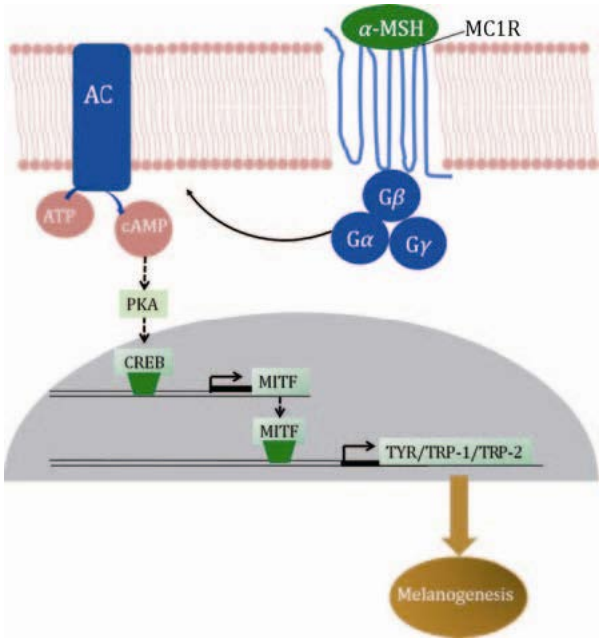

Figura 22. Ruta de señalización de melanocortina. α-MSH se une a su receptor (MC1R) y se activa la proteína G acoplada al MC1R. Esto lleva consigo la activación de la adenilato ciclasa, formándose AMPc que activa la proteína quinasa A (PKA), la cual sufre activación y se trasloca al núcleo donde fosforila la familia de factores de transcripción CREB y estos al factor de transcripción MITF que se une al promotor de los genes de tirosinasa, TRP-1 y TRP-2 (Gillbro y Olsson, 2011).

La isoforma M de MITF es la proteína encargada de regular la transcripción de tirosinasa y PKC-β en melanocitos (Fuse et al., 1996; Du et al., 2003; Park et al., 2006). Además, la actividad y la estabilidad de MITF están controladas por su estado de fosforilación.

La melanogénesis está regulada hormonalmente por la hormona estimulante de melanocitos α-MSH y su receptor MC1R a través de la cascada señalizadora AMPc/PKA (Figuras 22 y 23). Estos receptores constan de cinco proteínas relacionadas, cada una con siete dominios transmembrana, que pertenecen a la superfamilia del receptor de proteínas G acopladas (Mountjoy et al., 1992). El gen de POMC (propiomelanocortina) codifica un precursor que es procesado para formar α-MSH, hormona adrenocorticotrópica (ACTH) y β-endorfina (Suzuki et al., 1996; Kadekaro et al., 2003; Rouzaud et al., 2005). La estimulación hormonal por α-MSH a través de MC1R resulta en un incremento de los niveles de AMPc intracelular, gracias a adenilato ciclasa, lo que conlleva a una activación de PKA. Esta vía de señalización hormonal tiene consecuencias específicas en melanocitos ya que PKA fosforila a proteínas CREB (cAMP responsive element binding protein) que se unen a un elemento CRE que posee el promotor MITF activando su transcripción. Este factor de transcripción MITF se une a los promotores de los genes de tirosinasa, TRP-1 y TRP-2, estimulando la melanogénesis (Rouzaud et al., 2005; Yamaguchi et al., 2007; Yamaguchi y Hearing, 2009; Gillbro y Olsson, 2011;Kondo y Hearing, 2011). Recientemente, se ha demostrado que α-MSH es capaz de controlar la melanogénesis independientemente de MC1R, posiblemente actuando directamente sobre los melanosomas (Schallreuter et al., 2008).

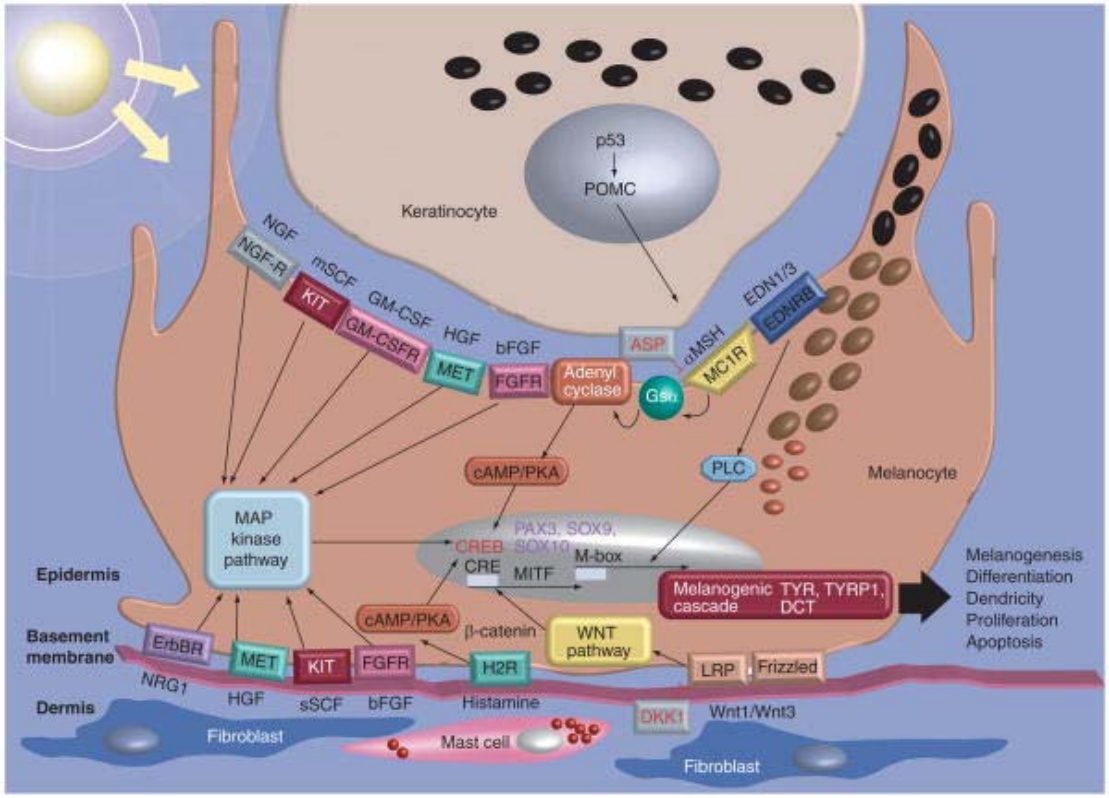

Figura 23. Rutas de señalización que regulan la melanogénesis. La radiación ultravioleta incrementa los niveles de α-MSH, ACTH y su receptor el MC1R para estimular la producción de AMPc. El AMPc también puede aumentar por la unión de epinefrina a su receptor. El agonista de c-Kit actúa fosforilando a MITF por medio de las MAPK quinasas (Park et al., 2009; Kondo y Hearing, 2011).

La gran variedad en el color de piel y pelo entre diferentes grupos étnicos es debido, en gran parte, al polimorfismo en el gen MC1R (Ha et al., 2003).

La regulación hormonal que sufre el melanocito también provoca un cambio en la formación del tipo de pigmento de la piel. Así, la señalización de α-MSH, a través de MC1R, es inhibida por la proteína señalizadora *Agouti* (ASP, ASIP en humanos) (Lu et al., 1994; Ollmann et al., 1997; Siegrist et al., 1997). Esta proteína compite con α-MSH en la unión a MC1R inhibiendo la adenilato ciclasa (Figura 24). Altas expresiones de ASP están asociadas con la formación de pigmentos amarillos en el pelo de ratón (Kondo y Hearing, 2011). MC1R y sus ligandos, α-MSH y ASIP, regulan el cambio en la síntesis de eumelaninas y feomelaninas en los melanocitos (Hida et al., 2009). En perros existe la β-defensina (K^B), esta proteína se une a MC1R en los melanocitos e

incrementa la producción de eumelanina, dando pigmentación oscura (Candille et al., 2007), se desconoce el papel de la β-defensina en la pigmentación humana.

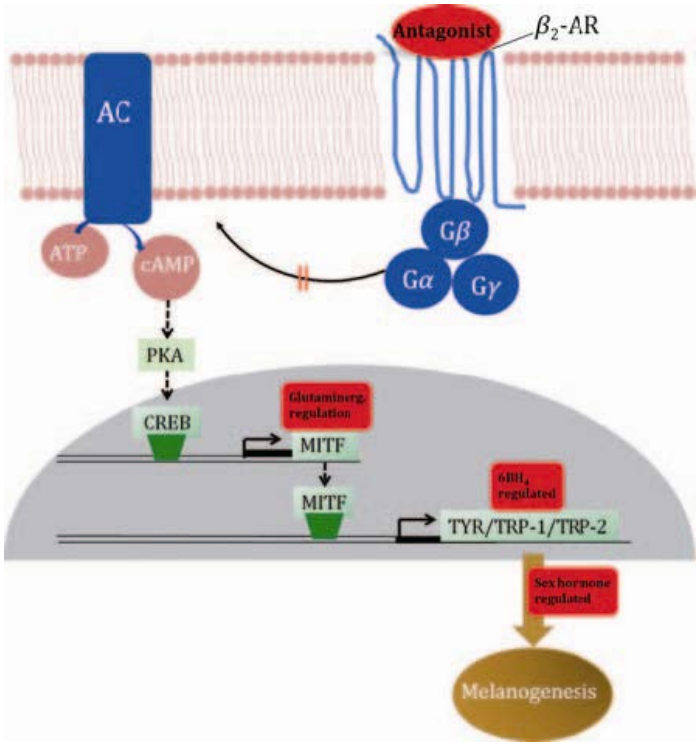

Figura 24. Nuevas etapas potenciales de transducción para reducir la pigmentación cutánea. Efecto de antagonistas del receptor β_2-adrenérgico, MITF, a través de regulación glutaminérgica, regulación de $6BH_4$ y control por hormonas sexuales (Gillbro y Olsson, 2011).

Como ya hemos indicado, α-MSH y ACTH son estimuladores potentes de la melanogénesis. En queratinocitos, la exposición a luz UV-B induce la expresión de POMC vía p53, lo cual conlleva a una secreción de α-MSH y, por tanto, una regulación de la melanogénesis vía MC1R (Figura 23). α-MSH también aumenta la síntesis de melanina por otro mecanismo distinto de la activación del MC1R, el cual consiste en la unión a 6-R-L-eritro-5,6,7,8-tetrahidrobiopterina ($6BH_4$), inhibidor de tirosinasa, impidiendo su acción (Schallreuter et al., 1994; Schallreuter, 1999).

El gen que codifica para MC1R es polimórfico con lo que, al ser un factor importante en la pigmentación y fototipo, es una importante diana para el riesgo de melanoma. Se han identificado variantes del MCR1 humano en pacientes con melanoma (Pérez-Oliva et al., 2009) demostrándose que MCR1 es N-glicosilado en los

residuos Asn15 y Asn29, con cadenas de glicanos estructural y funcionalmente diferentes. Esta N-glicosilación no es imprescindible para aumentar la afinidad del receptor pero es importante ya que aumenta la disponibilidad de los receptores MC1R en la membrana plasmática, mejorando por tanto el tráfico (Herráiz et al., 2011a).

Otros factores desarrollados por queratinocitos que regulan a los melanocitos pueden ser (Figura 25):

(a) Stem cell factor (SCF: Factor de células totipotenciales). Este factor es un factor de crecimiento derivado de queratinocitos y se une al melanocito a través del receptor tirosina quinasa c-KIT. Esta unión provoca la autofosforilación y activación de la quinasa de proteínas activadas por mitógenos (MAP-quinasa). MAP-quinasa fosforilada (activa) estimula la transcripción de las tres enzimas melanogénicas (tirosinasa, TRP-1 y TRP-2) por medio de la fosforilación del MITF. Además el SCF participa en la pigmentación inducida por irradiación UV (Slominski et al., 2004; Yamaguchi y Hearing, 2009). El receptor c-KIT es una proteína transmembrana (glicoproteína) de 145 KDa. Funciona como un receptor con actividad tirosina quinasa. El receptor posee un dominio extracelular con cinco regiones de tipo Ig, una única región transmembrana y un dominio citoplasmático con actividad tirosina quinasa (Heinrich et al., 2002; Herráiz et al., 2011b). El ligando para c-Kit es el SCF. La activación del receptor se produce como consecuencia de un proceso de homodimerización. Este proceso provoca una serie de cambios estructurales en el receptor que determinan una activación del dominio con actividad quinasa de Kit y esto lleva consigo la fosforilación de proteínas. La perdida de expresión del receptor c-Kit está asociada con la progresión del melanoma a su forma metastásica (Lassam y Bickford, 1992; Zakut et al., 1993).

(b) Endotelina-1 (ET-1). Es un péptido de 21 aminoácidos involucrado en la homeostasis vascular que regula la melanogénesis, activando tirosinasa y aumentando los niveles de TRP-1 (Yada et al., 1991; Imokawa et al., 1992). También estimula la proliferación de melanocitos y la formación de dendritas (Hara et al., 1995). Los queratinocitos sintetizan y secretan ET-1 y la radiación UV estimula dicha producción por los queratinocitos (Imokawa et al., 1992; Hara et al., 1995). ET-1 aumenta los niveles de MC1R e incrementa la afinidad de este por α-MSH (Funasaka et al., 1998; Tada et al., 1998).

(c) Neurotrofinas (NTS). Factor de crecimiento nervioso (NGF), neurotrofina 3 (NT-3), neurotrofina 4 (NT-4), factor de crecimiento derivado del cerebro (BDNF),

(Levi-Montalcini, 1987; Hohn et al., 1990). Los melanocitos expresan el receptor de baja afinidad de 75 kDa común a todas las neurotrofinas $p75^{NTR}$ (Peacocke et al., 1988), así como los de alta afinidad para NGF y NT-3 (TrkA y TrkC; de la familia de los receptores de tirosina quinasa) (Yaar et al., 1991; Botchkarev et al., 2006). El NGF derivado de queratinocitos es quimiotáctico para melanocitos e induce su dendricidad (Yaar et al., 1991). Suplementos de NGF aumentan los niveles de proteína Bcl-2 (B-cell lymphoma 2) reduciendo la muerte celular apoptósica de melanocitos (Zhai et al., 1996; Stefanato et al., 2003).

(d) Mediadores Inflamatorios. Varios mediadores inflamatorios pueden afectar a la pigmentación de la piel. Los melanocitos expresan receptores de PG (PGE_2 y $PGF_{2\alpha}$). La radiación UV regula positivamente los niveles de receptores para PG en melanocitos (Scott et al., 2004; 2005). Igualmente, los leucotrienos B_4 y C_4 incrementan la síntesis de melaninas y estimulan la proliferación de melanocitos y su motilidad (Norris et al., 1998). Los melanocitos responden también a histamina, que es liberada por mastocitos durante la inflamación cutánea, la cual produce dendricidad y regulación positiva de los niveles de tirosinasa (Gantz et al., 1991; Yoshida et al., 2000).

(e) Otros estimuladores: bFGF (basic Fibroblastic Growth Factor; Factor de crecimiento fibroblástico básico). Es un mitógeno de melanocitos (Halaban et al., 1987; 1988), producido por queratinocitos, que afecta a los melanocitos a través del contacto célula-célula. El factor de crecimiento de queratinocitos, otro miembro de la familia de proteínas FGF, promueve la transferencia de melanosomas desde los melanocitos a los queratinocitos (Cardinali et al., 2005). El NO (oxido nítrico) es producido por melanocitos y queratinocitos en respuesta a las citoquinas antiinflamatorias (Heck et al., 1992; Bécherel et al., 1994; Joshi et al., 1996; Fecker et al., 2002) y la radiación ultravioleta (Romero-Graillet et al., 1997). El óxido nítrico aumenta la actividad tirosinasa en la melanogénesis (Romero-Graillet et al., 1997).

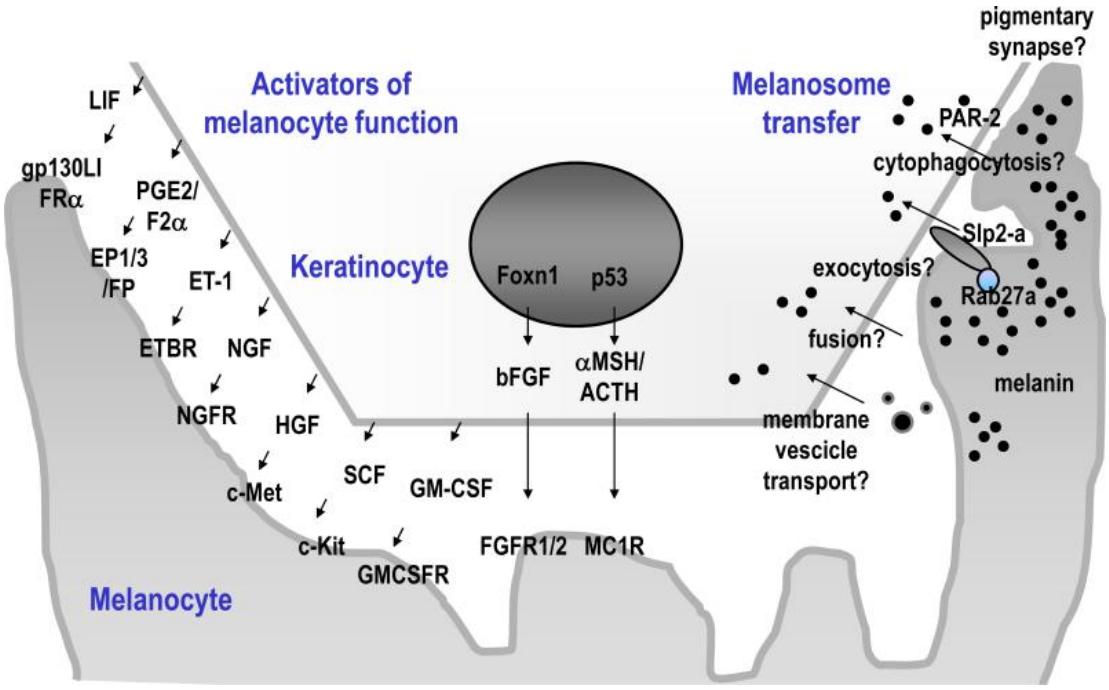

Figura 25. Factores derivados de queratinocitos que regulan la pigmentación en el melanocito.

D. Potenciadores de la pigmentación de la piel.

Cremas protectoras solares. Es una forma de añadir artificialmente protección a la piel ya que protegen frente a las quemaduras del sol (Pathak y Fitzpatrick, 1993). Sin embargo, esta prevención no existe en realidad ya que se alarga mucho la exposición al sol lo que provoca que el resultado sea contrario al pretendido inicialmente (Westerdahl et al., 1995; Autier et al., 1997). Ya que estos protectores solares protegen frente a un amplio rango de longitudes de onda, se ha propuesto usarlos en combinación con agentes que inducen al bronceado. Este bronceado es un proceso natural que se caracteriza por aumentar el número de melanocitos en la capa basal de la epidermis. También aumenta el tamaño y número de melanosomas, la dendricidad de los melanocitos, el transporte de los melanosomas de los melanocitos a los queratinocitos o la proliferación de los queratinocitos (Jimbow et al., 1991; 1993).

Los melanosomas se depositan sobre el núcleo, en los queratinocitos, resultando en la formación de “tapas supranucleares” que son características de la piel bronceada por el sol y de la pigmentación endógena (Gates y Zimmermann, 1953; Kobayashi et al., 1998b). Estas “tapas supranucleares” proporcionan protección frente a la exposición a radiación ultravioleta, absorbiendo los radicales libres generados en las células y produciendo una dispersión de la luz entrante. El grosor del estrato

córneo también contribuye a la protección (Young, et al., 1988). Como ya se ha indicado anteriormente, en la melanogénesis se forman eumelaninas o feomelaninas. Las eumelaninas son más fotoprotectoras que las feomelaninas con un aumento de la fotoprotección en proporción directa con el grado de pigmentación eumelánica (Pathak y Fitzpatrick, 1993).

Dentro de las cremas protectoras solares, existen sustancias que simulan la pigmentación natural y sustancias que estimulan dicha pigmentación. Entre las primeras, destacan la dihidroxiacetona y las melaninas tópicas. La dihidroxiacetona (DHA) no induce una verdadera respuesta melanogénica sino que se une covalentemente a grupos amino libres en proteínas, seguidos por una reacción de polimerización (Levy, 2000). DHA protege frente UVA en animales y humanos (Fusaro y Johnson, 1975; Levy, 2000). Co-adyuva en el tratamiento de la psoriasis con PUVA (terapia con psoraleno y radiación ultravioleta de longitud de onda A). Se ha sugerido que el bronceado producido por el DHA en conjunción con los protectores puede reducir la incidencia de melanoma maligno (Fusaro y Lynch, 2000). Las melaninas tópicas no producen una verdadera respuesta de bronceado, pero protegen absorbiendo la radiación UV y neutralizando los radicales libres (Orlow et al., 1992; Kalka et al., 2000; Levy, 2000).

En cuanto a las sustancias que estimulan la pigmentación natural destacan los psoralenos y UV-A (PUVA), el dimetilsulfóxido, la L-tirosina, el L-dopa y los derivados fosforilados de éste, los agentes lisosomotrópicos, los diacilgliceroles o las metilxantinas. A continuación, se describen algunos de ellos:

Los psoralenos estimulan la pigmentación en presencia de luz UVA. Estos psoralenos, además, tienen la capacidad de generar puentes cruzados y monoaductos del ADN (Averbeck, 1989). Existe evidencia que sugiere que la inducción de la melanogénesis por PUVA puede ir unido a p53 (Zhao et al., 1999).

La L-tirosina es el sustrato fisiológico de tirosinasa. Un incremento de L-tirosina en el medio aumenta la actividad de la enzima y el contenido de melaninas de melanocitos epidérmicos humanos que se co-cultivan con queratinocitos (Slominski et al., 1988).

El L-dopa y sus derivados fosforilados actúan como sustratos y como “cofactores” de tirosinasa (Lerner y Fitzpatrick, 1949). En células de melanoma producen un aumento de la producción de feomelaninas y una disminución de eumelaninas y de tirosinasa en los melanosomas, indicando un potencial efecto inhibitorio (Sato et al., 1987).

Aunque los productos de oxidación de L-dopa son tóxicos para las células, durante la melanogénesis, los melanocitos no sufren esta toxicidad por el hecho de que la melanogénesis se encuentra compartimentada en los melanosomas (Schachtschabel et al., 1978; 1988). El L-dopa se usa en el tratamiento de la enfermedad de Parkinson, observándose múltiples efectos secundarios como alteraciones psíquicas, fluctuaciones motoras, etc. (King, 1999).

En cuanto a los agentes lisosomotrópicos, existe evidencia de que los melanosomas de los caucasianos y los individuos de piel negra tienen los mismos niveles de tirosinasa, pero en los primeros está inhibida por su pH más ácido (Lozumi et al., 1993). El tratamiento de los melanocitos de los caucasianos con el agente lisosomotrópico cloruro de amonio aumenta la actividad de tirosinasa por el incremento en el pH del melanosoma (Fuller et al., 1990).

Los diacilgliceroles (DAG) (Figura 19) estimulan la PKC-β. La estimulación de la PKC-β se ha asociado con proliferación y diferenciación de melanocitos (Abdel-Malek et al., 1992). Varios estímulos, incluyendo la radiación UV, incrementan los niveles de DAG y activan la PKC-β (Matsui et al., 1994). Sin embargo, existen evidencias de que el tratamiento con ciertos DAG puede resultar en inflamación (Allan et al., 1995).

Las metilxantinas, incluyendo cafeína o teofilina son inhibidores de la fosfodiesterasa (Perchellet y Boutwell, 1981; Hoganson et al., 1989). La 3-isobutil-1-metilxantina (IBMX) es un potente estimulador de la melanogénesis, por lo que se usa como control positivo en los estudios de melanogénesis (Brown et al., 1998). El tratamiento de las células de melanoma con IBMX aumenta el contenido de melanina y la actividad tirosinasa en un orden de magnitud (Fuller et al., 1990; Eller, et al., 1994; Pedeux, et al., 1998).

E. Regulación redox en melanocitos humanos y melanoma.

Existen diferentes estrategias en la regulación redox en melanocitos. A continuación desarrollamos algunas de ellas:

(a) Síntesis de melaninas, glutatión y cisteína. La interacción del glutatión y la cisteína con la ruta de síntesis de melaninas es compleja. Ambos están involucrados en uno de los pasos iniciales de la síntesis de feomelaninas en su conjugación con dopaquinona (DQ) para formar cisteinildopa o glutationildopa (Figura 18), así como en la eliminación del peróxido de hidrógeno producido durante la síntesis de eumelaninas

y feomelaninas, vía peroxidasa dependiente de GSH o glutatión peroxidasa. Se ha descrito que, cuando la concentración de cisteína es mayor de 0.13 μM, se produce la síntesis de feomelaninas. Cuando la concentración de cisteinildopa o glutationildopa es menor de 9 μM, comienza la síntesis de la eumelaninas.

(b) Interrupción del metabolismo del glutatión y citotoxicidad para células de melanoma. La glutatión peroxidasa es el primer paso para convertir peróxido de hidrógeno en agua, pero si la utilización de estas moléculas lleva consigo el agotamiento de glutatión, se acumula peróxido de hidrógeno formándose un ciclo citotóxico. Butionina sulfoximina (BSO) es un inhibidor selectivo e irreversible de γ-glutamil sintetasa (GGS), enzima involucrada en el primer paso de la síntesis de glutatión (Griffith y Meister, 1979; Griffith, 1982). El uso de BSO resulta en un aumento del estrés oxidativo, que proporciona una posible estrategia terapéutica en el tratamiento del melanoma.

(c) Melaninas como anti-oxidantes. Existen numerosos trabajos donde se estudia la interacción de las melaninas con oxígeno, radical hidroxilo y anión superóxido (Sarna et al., 1993). Se ha documentado bastante bien la capacidad de las melaninas para neutralizar especies reactivas del oxigeno (ROS). La fuente de esta reactividad anti-oxidante es la transformación redox quinol/quinona de monómeros de 5,6-dihidroxiindol (DHI). Así, benzoquinol, el simple dihidroxibenzeno sustituido en posición *para*, puede reducir aniones superóxido vía reacciones de transferencia de electrones (Misra y Fridovich, 1972), actuando así como una superóxido dismutasa (SOD). Una actividad SOD similar se ha comprobado para melaninas aisladas (Bustamante et al., 1993).

(d) Melaninas como pro-oxidantes celulares. Durante la formación de melaninas se generan ROS (Nappi et al., 1995; Nappi y Vass, 1996; Muñoz-Muñoz et al., 2009b), cuyas implicaciones no se sabe todavía cuales pueden llegar a ser. Cuando se inhibe la feomelanogénesis, se estimula la eumelanogénesis y se produce dos veces más de peróxido de hidrógeno, el cuál es tóxico, por lo que controlando la melanogénesis se controla la toxicidad celular (Nappi et al., 1995; Nappi y Vass, 1996).

(e) Niveles anti-oxidantes y formación de melanoma. Casi todos los tumores malignos tienen algún desequilibrio en sus niveles anti-oxidantes comparados con la célula control (Oberley y Oberley, 1997). Los niveles de enzimas anti-oxidantes como catalasa, MnSOD, y glutatión peroxidasa están normalmente disminuidos, así

como los niveles de moléculas anti-oxidantes de bajo peso molecular como glutatión o vitaminas C y A (Yohn et al., 1991).

1.3. Tirosinasa: estructura

1.3.1. Propiedades moleculares

Se han descrito alrededor de veinte secuencias de tirosinasa (Van Gelder et al., 1997), desde genes procedentes de procariotas hasta los propios genes humanos. Aunque existen muchas diferencias taxonómicas, se han identificado muchos dominios que se repiten a lo largo de todas las secuencias de tirosinasas. Así, en las tirosinasas de plantas, se ha mostrado una secuencia común que posee péptidos de transito y dirigen el post-traslado de la proteína al interior de los cloroplastos, para el subsiguiente procesado y transporte. En las plantas más evolucionadas, la enzima está mayoritariamente unida a la membrana, mientras que en frutas la enzima puede llegar a estar soluble, aunque igualmente se han descrito tirosinasas unidas a membrana. La tirosinasa de mamíferos está unida a la membrana del melanosoma. La tirosinasa de *Agaricus bisporus* y la de *Neurospora crassa* son citosólicas, mientras que las de la especie bacteriana *Streptomyces* son secretadas fuera de la célula.

Muchas tirosinasas de plantas, hongos e invertebrados se encuentran en forma latente en la célula y tienen que ser activadas para cumplir su función. Este mecanismo de activación *in vivo* todavía es bastante desconocido, pero parece que interviene una proteasa endógena cortando un péptido protector. Esto se esquematiza en la Figura 4. Sin embargo, tirosinasa puede ser activada *in vitro* por una amplia variedad de sustancias, desde detergentes hasta acidificación.

Las enzimas mejor caracterizadas son las del género bacteriano *Streptomyces* (*Streptomyces glaucescens*), la de champiñón (*Agaricus bisporus*) y la del ascomiceto *Neurospora crassa*. Los primeros estudios de relación estructura/reactividad con tirosinasa de champiñón, mostraron la existencia de cuatro isoenzimas α, β, γ y δ, las cuales mostraban diferente actividad sobre monofenoles y *o*-difenoles (Bouchilloux et al., 1963). Posteriormente, utilizando técnicas de electroforesis en gel de poliacrilamida con SDS, demostraron que tirosinasa de champiñón estaba formada por dos tipos de cadenas polipeptídicas, una pesada (H), cuyo peso molecular era de 43 KDa, y otra ligera (L), de 13.4 KDa (Strothkamp et al., 1976). Estas subunidades se asocian formando un heterotetrámero con un peso molecular de 120 KDa, lo que corresponde a una agrupación de subunidades H_2L_2 (Strothkamp et al., 1976). Por otro lado, Gutteridge y Robb identificaron (Gutteridge y Robb, 1975) dos tipos de cadenas pesadas, que denominaron H^{α} y H^{β}. Esto llevó a proponer que la isoenzima α se trataba el tetrámero $H_2^{\alpha}L_2$, mientras que la isoenzima β, era $H_2^{\beta}L_2$.

La tirosinasa de *Neurospora crassa* se sintetiza en el curso de la diferenciación sexual, pero no durante el crecimiento vegetativo. Sin embargo, su cultivo en presencia de antimetabolitos e inhibidores de síntesis proteica, condujo a la expresión de esta enzima en grandes cantidades. Esto permitió el aislamiento y la caracterización de dos formas alélicas diferentes, denominadas termolábil (TL) y termoestable (TE). Ambas isoenzimas se asocian reversiblemente en un rango de pesos moleculares entre 35 y 120 KDa (Prota, 1988). Konrad Lerch, en 1982, determinó la secuencia de aminoácidos de la forma TL demostrando que es una cadena polipeptídica de 407 aminoácidos con un peso molecular de 46 KDa. La enzima tiene el grupo amino terminal bloqueado y se ha descrito que solo existe un residuo de azufre (Cys^{94}), el cual no está libre, se encuentra unido a la His^{96} mediante un enlace tioéter. Mediante un proceso post-traduccional, se postula que este enlace se rompe activándose la enzima, que hasta entonces estaba inactiva.

1.3.2. Estructura tridimensional

Hasta hace muy poco tiempo, solamente se había cristalizado y determinado la estructura tridimensional de catecol oxidasa de *Ipomea batatas*, enlazada con el inhibidor feniltiourea (Klabunde et al., 1998; Gerdemann et al., 2002). Sin embargo, recientemente se ha avanzado mucho en este campo de la cristalografía, y en la determinación de la estructura de proteínas, lo que ha llevado a la cristalización de multitud de tirosinasas, ya sea de bacterias (*Streptomyces castaneoglobisporus* y *Bacillus megaterium*), hongos y plantas (*Ipomea batatas*, *Vitis vinífera, Agaricus bisporus* y *Aspergillus oryzae*) o artrópodos (*Manduca sexta*). También se han descrito algunas características estructurales de la enzima de mamíferos. A continuación, se detallan las estructuras tridimensionales de algunas de ellas:

1.3.2.1. Tirosinasa de bacterias

Las tirosinasas bacterianas más estudiadas y, por tanto, mejor caracterizadas son las del género *Streptomyces*. Así, se ha determinado la estructura cristalina de tirosinasa de *Streptomyces castaneoglobisporus* (Matoba et al., 2006; Matoba et al., 2011). También se ha cristalizado y determinado la estructura tridimensional de tirosinasa de *Bacillus megaterium* (Sendovski et al., 2010; Sendovski et al., 2011) y, recientemente, se ha conseguido cristalizar la catecol oxidasa de *Aspergillus oryzae* (Kaljunen et al., 2011).

La primera tirosinasa que pudo ser cristalizada fue la de *Streptomyces castaneoglobisporus*. Matoba y colaboradores (2006) obtuvieron cristales de la enzima con la ayuda de la proteína "*caddie"* ORF378 con una resolución de 1.2-1.8 Å. El complejo de tirosinasa con la proteína ORF378 tiene una forma elipsoidal con unas dimensiones de 40 x 55 x 60 Å (Figura 26).

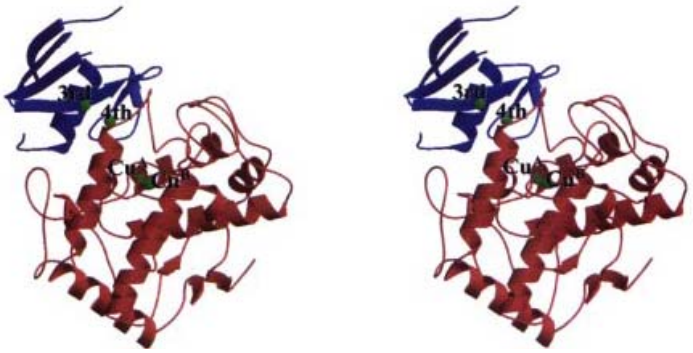

Figura 26. Estructura general de tirosinasa unida a la proteína ORF378. Tirosinasa y ORF378 son dibujadas en rojo y azul, respectivamente. Los iones de cobre se indican en verde.

El sitio activo de la enzima (compuesto por la agrupación dinuclear de cobre) está formado por un haz de cuatro hélices α (α_2, α_3, α_6 y α_7). Cada uno de los iones cobre está coordinado por tres residuos de histidina, las cuales se encuentran en el haz de cuatro hélices α, excepto la His^{54}. Un ión cobre (designado como CuA) es coordinado por His^{38}, His^{54} e His^{63}. His^{38} e His^{63} están localizadas en medio de las hélices α_2 y α_3, respectivamente. El segundo ión de cobre (CuB) está coordinado por las histidinas His^{190}, His^{194} e His^{216}. Los residuos His^{190} e His^{194} están al principio y en medio de la hélice α_6 respectivamente, mientras que His^{216} se encuentra en medio de la α_7. Esta agrupación dinuclear de cobre está localizada en el fondo de una larga concavidad, que funciona como un bolsillo para la unión de sustratos. Este bolsillo está formado por residuos hidrofóbicos. Además de la estructura de hélices α, tirosinasa tiene también algunas láminas β. Así, los extremos N- y C-terminal forman una estructura en lámina β (Figura 27).

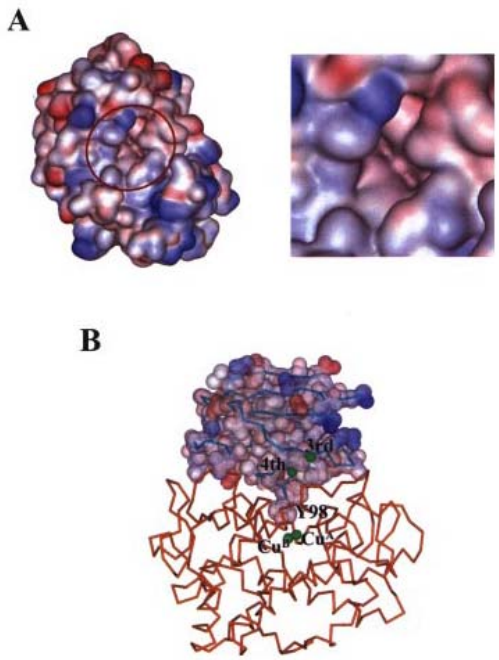

Figura 27. Superficie molecular de tirosinasa (A) y de la proteína *caddie* (B).

La proteína *caddie* ORF378 (Figura 27B), se encuentra en la superficie de tirosinasa e impide la entrada del sustrato al sitio activo de la enzima. Esta proteína está formada por seis láminas β, muy retorcidas en la lámina β_4, y una hélice α, la cual está rodeada por una lámina β retorcida. ORF378 no tiene similaridad en cuanto a su secuencia con las proteínas determinadas estructuralmente hasta la fecha. Esta proteína *caddie* se ha mostrado como una proteína que ayuda al transporte de iones Cu(II) al sitio activo de apotirosinasa (tirosinasa sin cobres en el sitio activo).

La determinación de la estructura tridimensional de tirosinasa de *Streptomyces castaneoglobisporus*, ha demostrado que la His^{54}, que está unida al CuA del sitio activo de la enzima, es flexible durante la catálisis. Los autores de este trabajo postulan que puede ser esta histidina, la que acepte el segundo protón del *o*-difenol que se une a la enzima.

Posteriormente a la cristalización de la enzima de *Streptomyces castaneoglobisporus*, se ha discutido la posición de las histidinas axiales del sitio activo de la enzima y su implicación en la catálisis (Decker et al., 2006). En estos estudios, se postula que la histidina axial unida al CuA, no es la His^{54} sino la His^{63}. Además, se indica que las dos histidinas axiales unidas a los cobre (A y B) están en posición *cis* al contrario de la posición *trans* que propusieron Matoba et al. (2006).

Recientemente, se ha descrito el mecanismo molecular por el cual se transporta el cobre, al sitio activo de tirosinasa. Este transporte está favorecido por la proteína *caddie* ORF378, a la cual denominan metalochaperona (Matoba et al., 2011).

Otra tirosinasa bacteriana cristalizada (Figura 28) a la que se ha determinado su estructura tridimensional (Figura 29), es la de la bacteria *Bacillus megaterium* (Sendovski et al., 2010; Sendovski et al., 2011). Esta tirosinasa de *Bacillus megaterium* se ha descrito como una enzima con una alta actividad en disolventes orgánicos, y no requiere la presencia de ninguna proteína *caddie* para su actividad (Shuster y Fishman, 2009). La estructura de esta tirosinasa ha sido determinada con una resolución de 2.0-2.3 Å. La estructura determinada es un dímero con forma elipsoidal, y con unas dimensiones de 45 x 25 x 80 Å (Figura 29). El sitio activo está formado, al igual que ocurría con la enzima de *Streptomyces castaneoglobisporus*, por un haz de cuatro hélices α (α_2, α_3, α_7 y α_8). Cada ión también está coordinado por tres residuos de histidina. El CuA está coordinado por la His^{41} (α_2), la His^{69} (α_3) y la His^{60} (se localiza en un gran lazo entre dos hélices α). El CuB está coordinado por las histidinas His^{204}, His^{208} (ambas en α_7) y la His^{231} (α_8).

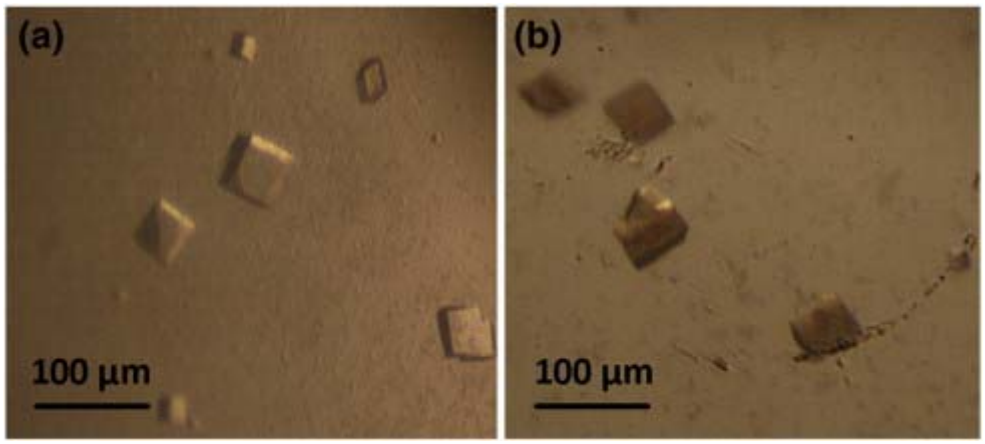

Figura 28. Cristales de tirosinasa de *Bacillus megaterium*. (A) en ausencia de L-tirosina. (B) en presencia de L-tirosina con la consiguiente formación de melaninas.

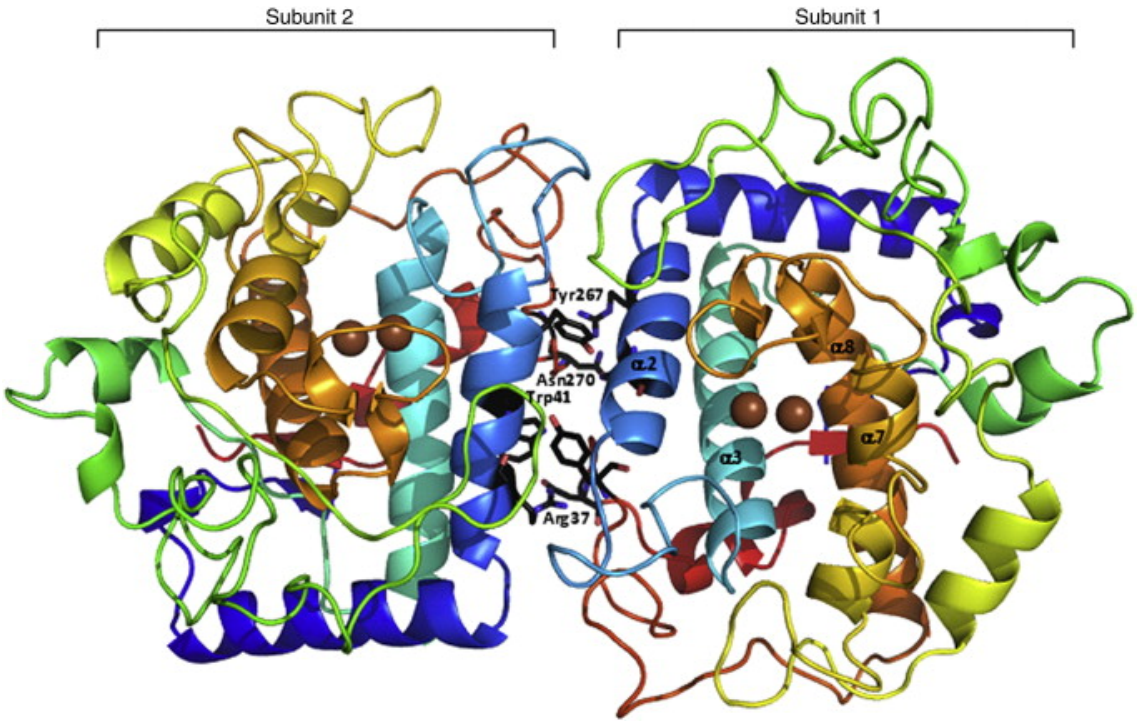

Figura 29. Estructura dimérica tridimensional de tirosinasa de *Bacillus megaterium*. Los iones cobre se muestran en color marrón. Las interacciones entre ambas subunidades se representan en color negro. Las cuatro hélices α principales del sitio activo de la enzima se muestran en color azul oscuro (α_2), azul claro (α_3), amarillo fuerte (α_7) y naranja (α_8).

Esta tirosinasa ha sido cristalizada en forma de dímero como se muestra en la Figura 29. En dicha estructura dimérica se observan distintas interacciones entre ambas subunidades, por ejemplo, entre la tirosina 267 de un monómero, con la arginina 270 del otro monómero.

Aunque haya sido cristalizada la forma dimérica, en disolución la enzima se encuentra en forma monomérica. Mediante cromatrografía de exclusión molecular de alta resolución, se ha comprobado que, en disolución, existen las dos formas (monomérica y dimérica), y que al aumentar la concentración de enzima, el equilibrio se desplaza transformándose toda la enzima en dimérica.

En este estudio de la cristalización de tirosinasa de *Bacillus megaterium*, también se demostrado la plasticidad que existe en el modo de unión de los iones cobre al sitio activo de la enzima. Como se muestra en la Figura 30(b), se pudo cristalizar la enzima solo con el CuA en el sitio activo, perdiéndose el CuB. Por tanto,

el CuB parece ser lábil en su unión, mientras que el CuA estuvo presente en todas las estructuras cristalinas encontradas, lo que indica que su unión es más fuerte.

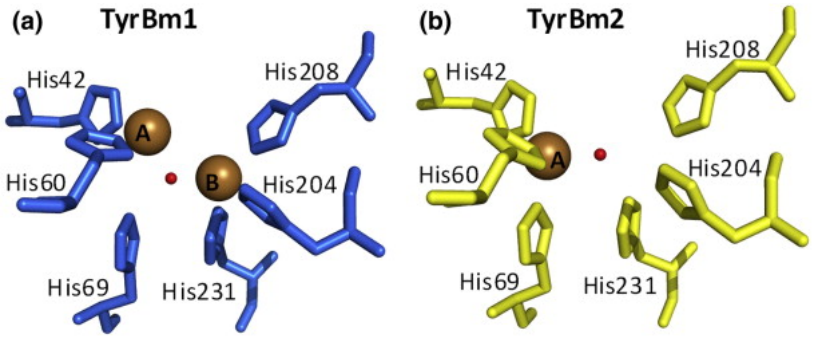

Figura 30. Diferentes estructuras cristalinas encontradas en tirosinasa de *Bacillus megaterium*. Se muestran las diferentes posibilidades en las posiciones de ocupación del cobre. (a) Sitio activo de tirosinasa con los átomos de cobre en el mismo. (b) Sitio activo con un solo átomo de cobre (CuA).

Por último, los autores demuestran las implicaciones que tiene esta plasticidad del sitio activo, en el mecanismo catalítico de la enzima. Así, se ha discutido mucho acerca de si la unión del sustrato (monofenol u *o*-difenol) es al CuA o al CuB. Se propone que el monofenol es orientado hacia el CuA. En cambio, parece que el *o*-difenol se une al CuB. Además, se postula que una Arginina (Arg^{209}) está próxima al CuB y es flexible durante la catálisis.

1.3.2.2. Tirosinasa de hongos y plantas

La primera tirosinasa de plantas cristalizada (*Ipomea batatas*) no es considerada una tirosinasa como tal ya que no posee actividad monofenolasa. Por tanto, es una catecol oxidasa (Klabunde et al., 1998; Gerdemann et al., 2002).

Como se observa en la Figura 31, la catecol oxidasa de *Ipomea batatas* es una enzima monomérica, con un peso molecular de 39 KDa y con una forma elipsoidal de 55 x 45 x 45 Å (Klabunde et al., 1998). El sitio activo está formado por un haz de cuatro hélices α (α_2, α_3, α_6 y α_7). Este haz de cuatro hélices está apoyado por dos hélices α más (α_1 y α_4) y por láminas β cortas. Cada uno de los átomos de cobre está coordinado, al igual que en bacterias, por tres residuos de histidina. El CuA está coordinado por His^{88}, His^{109} e His^{118}. His^{88} se encuentra en medio de la hélice α_2 mientras que His^{109} e His^{118} están al comienzo y en medio de la hélice α_3. El CuB se

encuentra coordinado por His^{240}, His^{244} e His^{274}, las cuales se encuentran las tres en la mitad de las hélices α_6 y α_7.

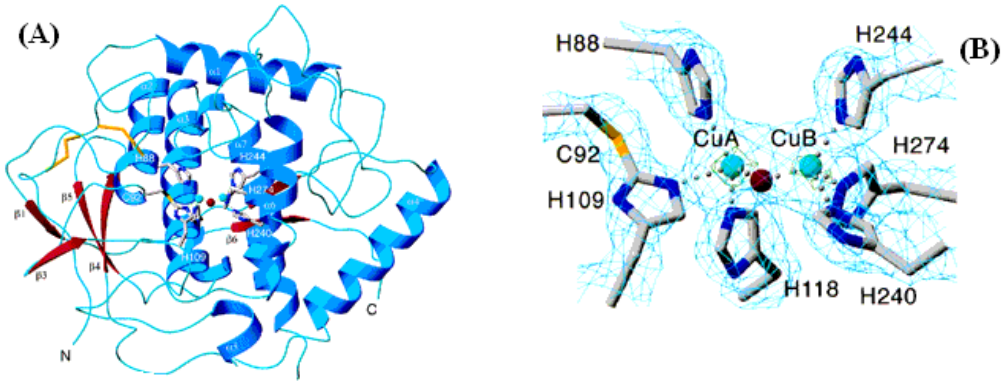

Figura 31. (A) Estructura tridimensional de catecol oxidasa de *Ipomea batatas*. (B) Detalle del sitio activo de la enzima con la densidad electrónica de cada átomo de cobre.

En la determinación de esta estructura de catecol oxidasa, los autores demostraron un puente tioéter entre las His^{109} y la Cys^{92} en el CuA. Se ha visto que el CuA tiene una Phe^{261} que es capaz de rotar su cadena lateral, y así permite la entrada del *o*-difenol al sitio activo. Esto explicaría que la catecol oxidasa no tenga actividad monofenolasa, ya que la Phe^{261} no permitiría entrar al monofenol al sitio activo.

A tirosinasa también se la denomina normalmente, en plantas, polifenol oxidasa y, en este sentido, se obtuvo la estructura tridimensional de polifenol oxidasa de uva (*Vitis vinifera*) en 2010 (Virador et al., 2010a; 2010b). La estructura de esta polifenol oxidasa es un monómero de 38.4 KDa con forma elipsoidal, y con unas dimensiones de 56.7 x 48.0 x 48.3 Å (Figuras 32 y 33). Al igual que el resto de tirosinasas descritas hasta ahora, la enzima de uva tiene un sitio activo formado por un haz de cuatro hélices α (α_4, α_5, α_{12} y α_{14}). Los residuos de histidina unidos a los átomos de cobre son His^{243} (α_{12}), His^{272} (α_{12}) e His^{239} (α_{14}) para el CuB, mientras que His^{87} (α_4), His^{117} (α_5) e His^{108} (α_5) para el CuA. La His^{108} es encuentra unida a un residuo de cisteína (Cys^{91}) de forma análoga a como ocurre en la catecol oxidasa de *Ipomea batatas.*

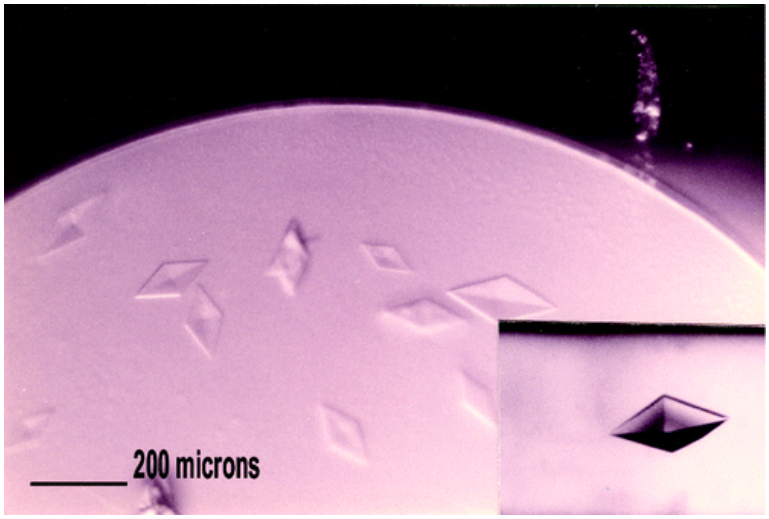

Figura 32. Cristales obtenidos de polifenol oxidasa de *Vitis vinifera* y su detalle en el inserto para observar su dimensión.

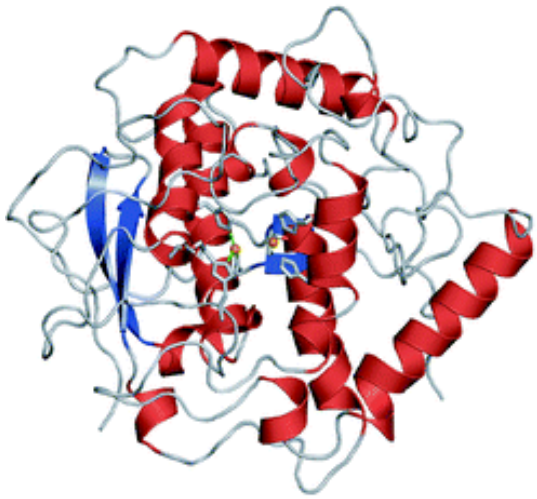

Figura 33. Estructura tridimensional de la polifenol oxidasa de uva vista en el modelo estructural de cintas.

Al igual que ocurría con la catecol oxidasa de *Ipomea batatas*, en la polifenol oxidasa de *Vitis vinifera* existe un puente tioéter entre Cys^{91}-His^{108}, que provoca que el CuA tenga muchos impedimentos estéricos. Por tanto, la enzima de uva tampoco presenta actividad monofenolasa, probablemente debido a que el CuA, que es el átomo de cobre al cual se une el monofenol, tiene el acceso al monofenol bloqueado y no deja acceder a éste (Virador et al., 2010a).

En cuanto a la determinación estructural de tirosinasas de hongos, la enzima mas estudiada ha sido la de champiñón (*Agaricus bisporus*), por ser la tirosinasa modelo disponible comercialmente. Recientemente, se ha conseguido cristalizar y determinar la estructura tridimensional (Figura 34) de la estructura de esta tirosinasa (Ismaya et al., 2011a; Ismaya et al., 2011b).

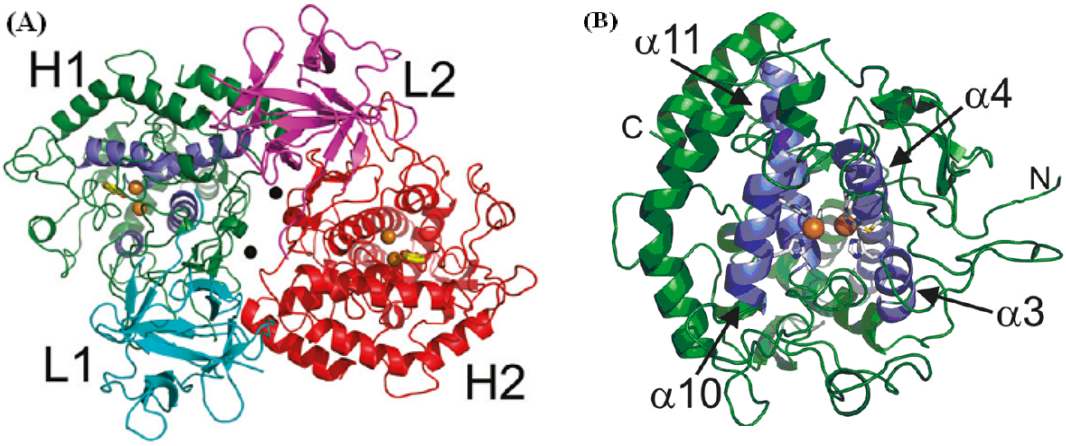

Figura 34. Estructura tridimensional de tirosinasa de *Agaricus bisporus*. (A) Estructura tretramérica compuesta por H_2L_2. (B) Estructura monomérica con detalle del sitio activo de la enzima. En marrón se muestran los dos átomos de cobre del sitio activo mientras que en azul se muestran las hélices α que forman la cavidad del sitio activo.

La estructura cristalina de tirosinasa de *Agaricus bisporus* está formada por un tetrámero H_2L_2, como ya se ha descrito anteriormente (Strothkamp et al., 1976). Se unen dos heterodímeros HL para formar el tetrámero. Ambas subunidades HL están interconectadas mediante multitud de uniones como puentes salinos (His^{76}-Glu^{139} y Glu^{317}-His^{56}), y puentes de hidrógeno (Val^{332}-Ile^{55}, Gln^{331}-Asn^{57}, Ser^{337}-Asn^{57}) (Figura 35).

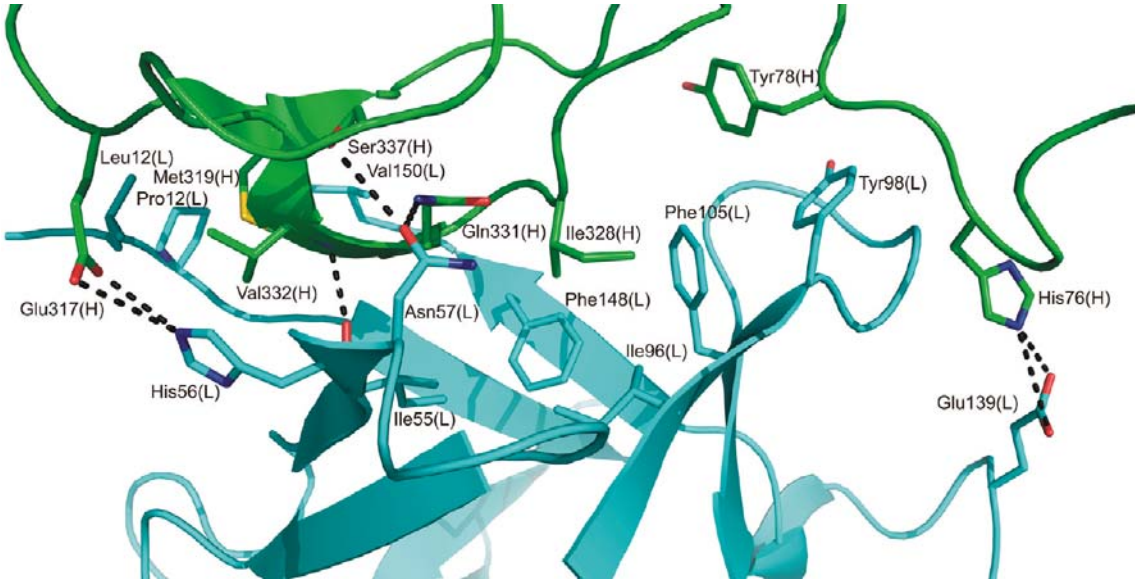

Figura 35. Detalle de las interacciones entre las subunidades H y L en la estructura tridimensional de tirosinasa de champiñón (*Agaricus bisporus*).

La subunidad H de esta enzima contiene la agrupación dinuclear de cobre, donde cada cobre está coordinado por tres residuos de histidina (Figura 36). El sitio activo está localizado en el centro de dos parejas de hélices α (α_3/α_4 y α_{10}/α_{11}), que están enfrentadas una a otra en 90º. El CuA está coordinado por His^{61} (α_3), His^{85} (entre la α_3 y la α_4) y por His^{94} (α_4), mientras que el CuB lo está por His^{259}, His^{263} (ambas en α_{10}) y por His^{296} (α_{11}). Además, puede verse un puente tioéter entre la His^{85} del CuA y la Cys^{83}, que se encuentra próxima a este cobre. Este sitio activo se encuentra localizado en el fondo de una cavidad hidrofóbica superficial de la enzima. Por tanto, esta cavidad está accesible al sustrato y al disolvente.

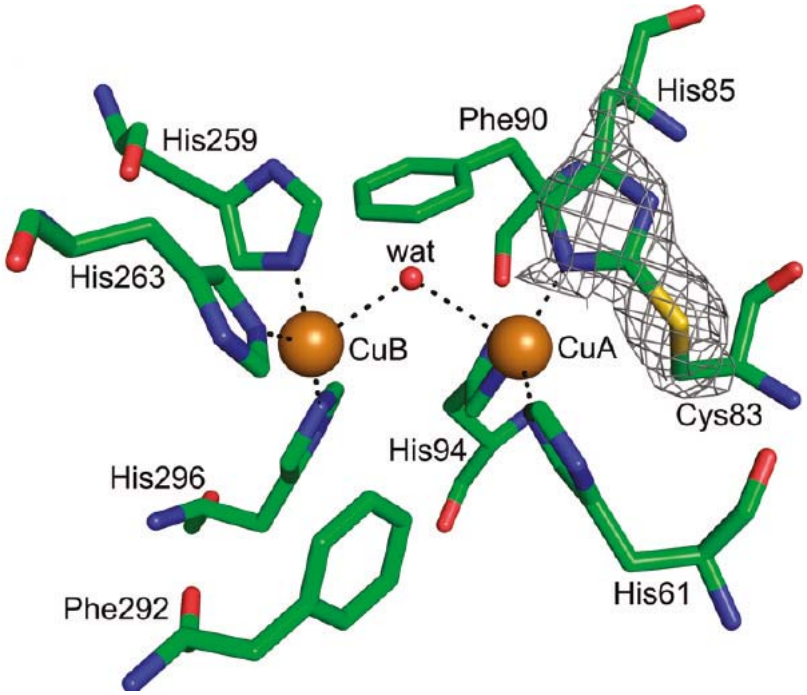

Figura 36. Geometría de coordinación de la agrupación dinuclear de cobre. Los átomos de cobre están coloreados en marrón.

Recientemente, gracias a la purificación de cuatro isoenzimas de tirosinasa de *Agaricus bisporus*, y a su cristalización, se ha comparado la estructura de todas ellas por modelado molecular (Inlow, 2012). Gracias a estos modelos, se han podido realizar predicciones de cómo se procesa post-traduccionalmente la enzima, para que pase de un estado latente (inactiva) a uno activo. Sin embargo, esto solo proporciona una hipótesis a partir de la estructura, y debe comprobarse experimentalmente en futuros estudios.

La última catecol oxidasa de hongos que ha sido recientemente cristalizada, es la del ascomiceto *Aspergillus oryzae* (Kaljunen et al., 2011). Se ha obtenido la estructura cristalina de la enzima, y se determinó su peso molecular de 40.5 KDa.

1.3.2.3. Tirosinasa de artrópodos

La enzima tirosinasa, también llamada fenoloxidasa en artrópodos, posee ambas actividades de tirosinasa: monofenolasa y difenolasa. En 2009, se cristalizó la primera fenoloxidasa de artrópodos (*Manduca sexta*), y se determinó su estructura tridimensional (Li et al., 2009). La estructura de esta enzima es un dímero (Figura 37A). El primer monómero de la enzima tiene 685 aminoácidos, mientras que el segundo presenta 695. La estructura final tiene una resolución de 1.97 Å.

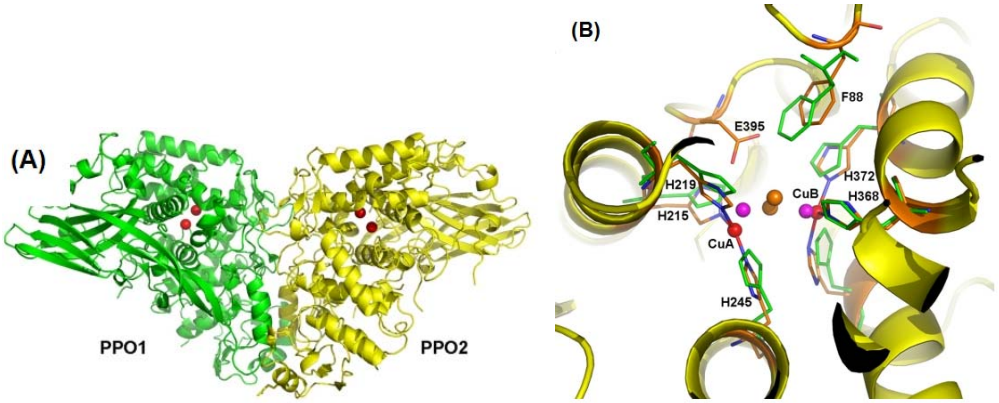

Figura 37. (A) Estructura tridimensional de fenoloxidasa de *Manduca sexta* con sus dímeros. (B) Detalle del sitio activo de la enzima con las histidinas que coordinan a ambos átomos de cobre.

El sitio activo de la enzima contiene dos átomos de cobre (CuA y CuB), y cada uno está coordinado por tres residuos de histidina (Figura 37B). En esta enzima, el sitio activo está ocluido en el centro de la enzima, y no está expuesto al exterior como ocurría, por ejemplo, con la tirosinasa de *Agaricus bisporus*. En el primer monómero (PPO1), el CuA está coordinado por las His^{209}, His^{213} y His^{239}, mientras que el CuB lo está por His^{366}, His^{370} e His^{406}. El segundo monómero (PPO2) tiene también otra agrupación dinuclear de cobre, donde el CuA está coordinado por His^{215}, His^{219} e His^{245}, mientras que CuB lo está por His^{368}, His^{372} e His^{408}.

Estos autores proponen que existe un residuo de ácido glutámico (Glu^{395}), que se encuentra libre y próximo al CuA, que podría ser el encargado de aceptar el protón proveniente del sustrato fenólico, y coordinar la unión del fenolato al CuA, lo cual es fundamental para la *orto*-hidroxilación. Esto explicaría por qué sólo el monómero PPO2 tiene actividad monofenolasa, ya que el Glu^{395} sólo se encuentra en este monómero.

1.3.2.4. Tirosinasa de mamíferos

Poco se ha descrito acerca de la estructura tridimensional de tirosinasa de mamíferos. Los pocos estudios realizados, se han llevado a cabo por la alta homología de secuencias de aminoácidos entre las distintas tirosinasas, como se demuestra en la Figura 38.

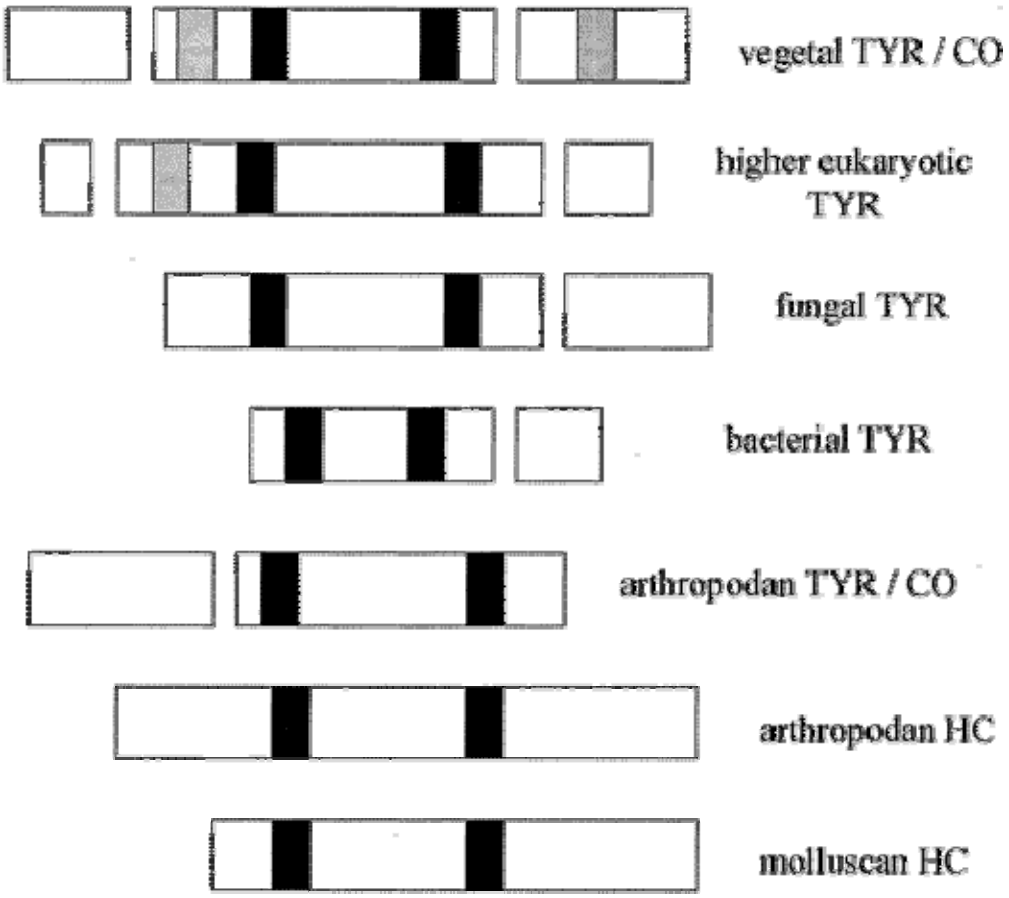

Figura 38. Estructura primaria de proteínas con cobre tipo III. Las longitudes de los segmentos son proporcionales al número de residuos de aminoácidos. Regiones ricas en histidinas de las uniones a cobre se muestran en negro, regiones ricas en cisteína en color gris (Gerdemann et al., 2002).

Basándose en estas similitudes, García-Borrón y Solano (2002) propusieron un modelo del sitio activo de tirosinasa de mamíferos, y las posibles interacciones dentro de éste (Figura 39).

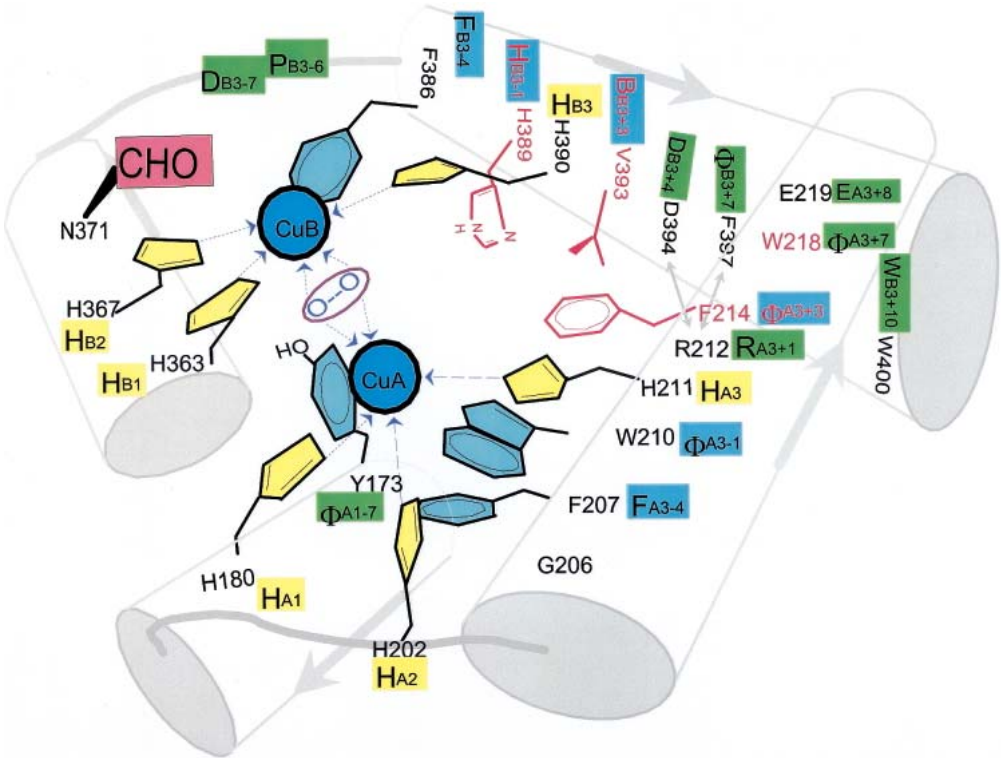

Figura 39. Modelo propuesto para el sitio activo de tirosinasa de mamíferos, mostrándose el haz de cuatro hélices α del sitio activo, y las posibles interacciones existentes dentro de éste (García-Borrón y Solano, 2002).

El sitio activo de la tirosinasa de mamíferos podría consistir en un bolsillo hidrofóbico, dentro de un haz de cuatro hélices α. Dos regiones ricas en histidina, llamadas CuA y CuB, serían las encargadas de la unión de los átomos de cobre. Ambas regiones contendrían tres residuos de histidina, muy conservadas en toda la escala filogenética. El CuA tiene el motivo His-x(n)-His-x(8)-His, y el CuB tiene el motivo His-x(3)-His-x(n)-His, donde n es un número variable de residuos. La segunda histidina del CuA sería la única flexible, ya que se encontraría en un lazo en la estructura, mientras que las otras cinco histidinas estarían localizadas en fragmentos de hélice α adyacentes (García-Borrón y Solano, 2002; Inoue et al., 2008; Olivares y Solano, 2009).

Además de las regiones ricas en histidinas (CuA y CuB), la estructura de todas las tirosinasas de mamíferos muestran un péptido señal N-terminal, que es importante en el tráfico y procesado, unos dominios ricos en cisteínas, un segmento de transmembrana hidrofóbico C-terminal y una cola citoplasmática corta (Olivares y

Solano, 2009). La cola citoplasmática y el segmento transmembranal, son necesarios para dirigir la enzima al melanosoma.

1.3.3. Sitio activo

Como ya hemos indicado en esta Memoria, el sitio activo de tirosinasa o polifenol oxidasa, esta formado por dos átomos de cobre, denominados CuA y CuB, unidos cada uno a tres residuos de histidina. El estado del cobre del sitio activo ha sido objeto de mucha discusión, desde que se le descubriera como el cofactor de la enzima (Kubowitz, 1938). Kertesz y Zito (1962), propusieron que siempre se encontraba en estado de Cu^{+}, basándose en los resultados obtenidos por técnicas de resonancia de espín electrónico, y en el descubrimiento de que tirosinasa contenía un átomo de cobre por mol (Fling et al., 1963). Hoy día se acepta, en general, que el sitio activo de tirosinasa presenta un par de átomos de cobre en estado de oxidación dos, como lo demuestra la razón 1:2 encontrada en las reacciones Co:Cu, benzoato:Cu (Duckworth y Coleman, 1970) y H_2O_2:Cu (Jolley et al., 1974).

Actualmente, está aceptado que el sitio activo de tirosinasa puede presentarse en tres formas enzimáticas, dependiendo del estado de oxidación del cobre: metatirosinasa, oxitirosinasa y desoxitirosinasa.

1.3.3.1. Metatirosinasa

Según la fuente biológica y el procedimiento de separación, se observaron cantidades variables (2-30 %) de oxitirosinasa intrínseca en la enzima nativa (Jolley et al., 1974; Gutteridge y Robb, 1975; Lerch, 1976). Se utilizó el término metatirosinasa para indicar la naturaleza bicúprica de la forma completamente libre de oxígeno, por analogía con metahemocianina (Figuras 40 y 41).

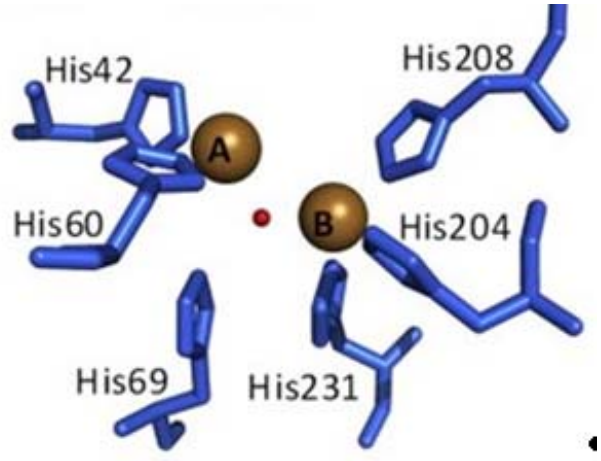

Figura 40. Sitio activo en la forma meta de tirosinasa de *Bacillus megaterium* (Sendovski et al., 2011).

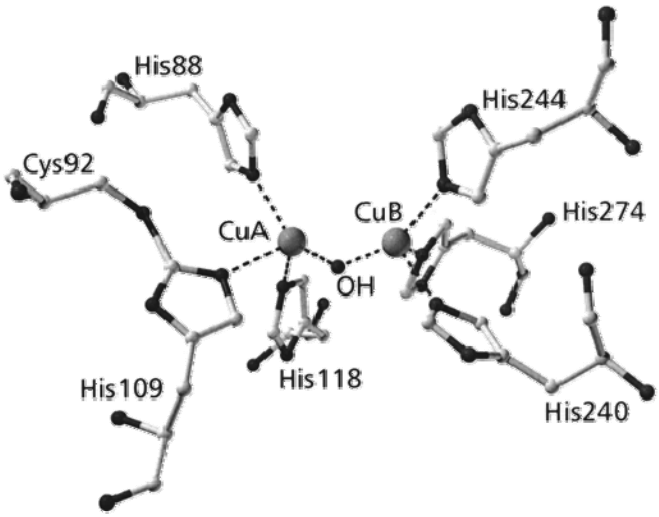

Figura 41. Sitio activo de la forma meta de catecol oxidasa de *Ipomea batatas* (Gerdemann et al., 2002).

En las Figuras 40 y 41 se puede observar la similitud estructural de la forma meta de tirosinasa de una bacteria (*Bacillus megaterium*) y de una planta (*Ipomea batatas*).

Mediante estudios de susceptibilidad magnética y valoraciones de oxidación-reducción, se demostró (Makino et al., 1974) que la forma metatirosinasa es

completamente diamagnética, y que el cobre se encuentra en estado de oxidación Cu^{2+}. La liberación de iones Cu^{2+}, cuando la enzima se desnaturaliza en condiciones anaeróbias (Makino et al., 1974), apoya estos resultados.

Al contrario que las formas apo- y desoxitirosinasa, metatirosinasa presenta absorción en la región visible del espectro y dicroísmo circular. Estas características espectrales son diferentes a las de las oxidasas con varios átomos de cobre en el sitio activo, como son catecol oxidasa, lacasa, ascorbato oxidasa y ceruloplasmina (Messerschmidt y Huber, 1990; Klabunde et al., 1998; Eicken et al., 1999). Por analogía con metahemocianina (Solomon et al., 1996), el modelo estructural propuesto para metatirosinasa se puede describir como dos iones Cu^{2+} tetragonales, unidos por un puente endógeno de proteína.

1.3.3.2. Oxitirosinasa

Esta forma presenta un máximo de absorción a 345 nm, que desaparece en presencia de sustratos monofenólicos y *o*-difenólicos, indicando que oxitirosinasa es un intermedio catalítico. Se conoce desde hace tiempo (Makino et al., 1974) el espectro de absorción UV/VIS de oxihemocianina y oxitirosinasa, los cuales son muy similares, presentan un máximo de absorción a 345 nm y una banda ancha más débil a 640 nm, Figura 42. Oxitirosinasa se puede obtener a partir de las otras formas enzimáticas mediante la adición de peróxido de hidrógeno a la forma metatirosinasa, o mediante la unión reversible de una molécula de oxígeno a la forma desoxitirosinasa. El modelo estructural propuesto para oxitirosinasa se muestra en la Figura 43 (Gerdemann et al., 2002).

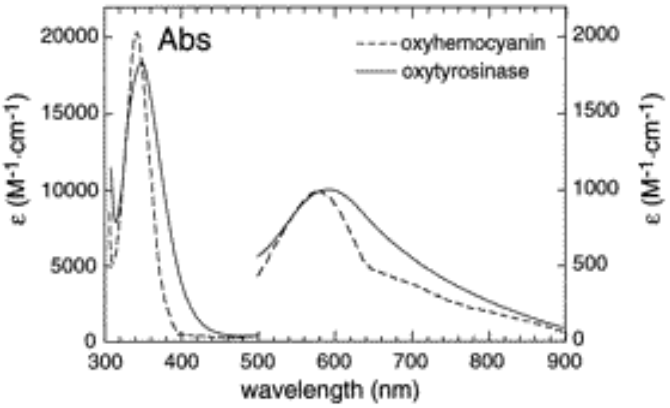

Figura 42. Espectro de absorción UV/VIS del estado oxigenado de hemocianina y tirosinasa (Solomon et al., 1996). Nótese la similitud entre ambos espectros.

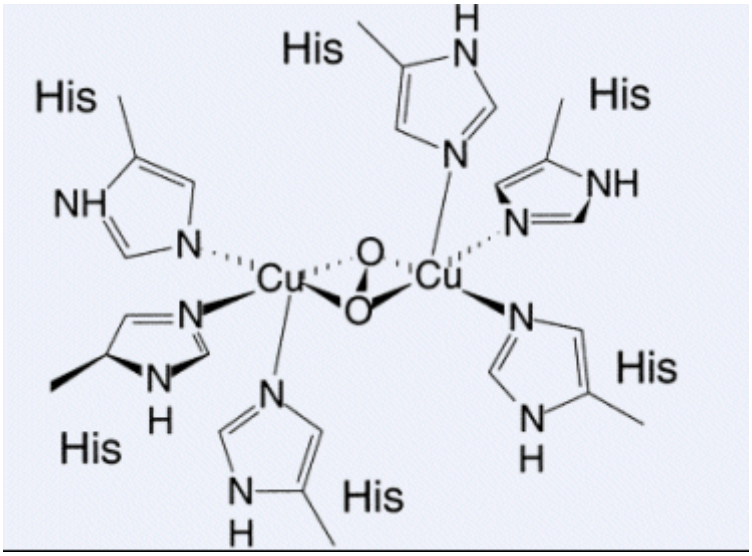

Figura 43. Sitio activo de la forma oxi de catecol oxidasa de *Ipomea batatas* (Gerdemann et al., 2002).

Recientemente, se han descrito algunas propiedades del sitio activo de tirosinasa en su forma oxi, mediante modelado molecular con ordenador (Deeth y Diedrich, 2010).

1.3.3.3. Desoxitirosinasa

La unión del oxigeno a las proteínas de cobre tipo III ha sido extensamente estudiado en desoxihemocianina (Beltramini et al., 1992; Metz y Solomon, 2001; Solomon et al., 2001; Chen y Solomon, 2004; Ronda et al., 2007 y Erker et al., 2008). En cambio, solo se han estudiado algunas propiedades de la forma desoxi de tirosinasa de *Streptomyces glaucescens* y de *Neurospora crassa* (Sorrell et al., 1998).

Se ha estudiado el enlace de oxígeno en el caso de tirosinasa de *Streptomyces antibioticus* (Hirota et al., 2005) y *Agaricus bisporus* (Della Longa et al., 1996). Por otra parte, se han hecho estudios comparativos de las tres tipos de proteínas tipo III, hemocianina, catecol oxidasa y tirosinasa (Decker y Tuczek, 2000; Bubacco et al., 2004; Chen y Solomon, 2004; Rosenzweig y Sazinsky, 2006; Decker et al., 2007). Se ha demostrado la actividad difenolasa de hemocianina sobre *o*-difenoles (Salvato et al., 1998; Decker et al., 2001; Decker y Jaenicke, 2004; Jaenicke y Decker, 2004; Baird et al., 2007; Nillius et al., 2008), y su actividad monofenolasa sobre monofenoles

(Suzuki et al., 2008). En un esfuerzo por conseguir la reacción de hidroxilación sobre monofenoles, se han diseñado complejos de cobre que enlazan oxígeno y muestran actividad monofenolasa y difenolasa (Mirica et al., 2006; Sander et al., 2008; Rolff et al., 2010; Rolff et al., 2011).

Recientemente, nuestro grupo ha publicado un estudio donde pone de manifiesto algunas propiedades de la desoxitirosinasa, obtenida en condiciones anaerobias (Muñoz-Muñoz et al., 2010a). Se demostró experimentalmente la existencia de una transición lenta, desde una desoxitirosinasa relajada hasta una forma tensa donde, probablemente debido a la repulsión de cargas, hay una separación de los iones cobre desde 3.5 Å existente en la forma relajada, hasta 4.6 Å en la forma tensa, por analogía con desoxihemocianina (Metz y Solomon, 2001). Así, en tirosinasa de *Agaricus bisporus*, se ha propuesto que ocurre una transición similar, como se indica en la Figura 44.

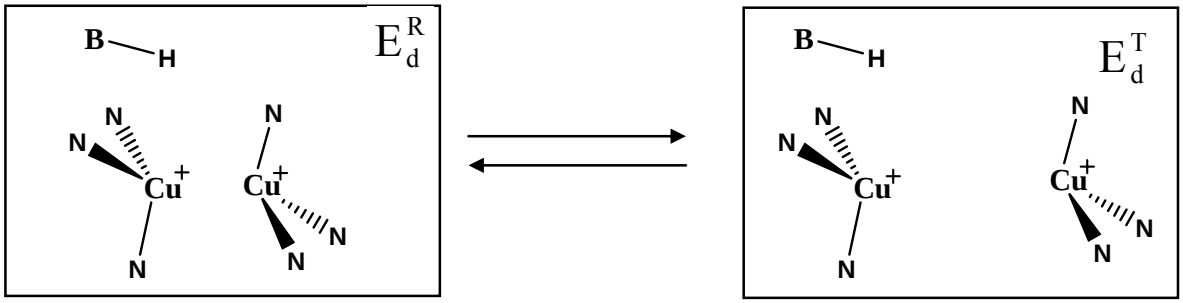

Figura 44. Transición entre la forma desoxi relajada y la forma desoxi tensa. Nótese la diferente distancia entre los iones Cu(I) al pasar de una forma a otra.

1.4. Tirosinasa: actividades catalíticas.

Una vez cristalizada la tirosinasa de *Agaricus bisporus*, se observó que el sitio activo se encuentra en un lugar superficial en la proteína y, además, es una cavidad amplia, lo que facilita que puedan entrar a la enzima una amplia variedad de moléculas (Ismaya et al., 2011). Esta poca especificidad de sustratos ha sido ampliamente descrita para tirosinasa (Zawistowski et al., 1991). Existen grandes diferencias en cuanto a las constantes cinéticas que caracterizan a la enzima de diferentes fuentes biológicas, éstas varían según el modo de extracción, la variedad o el método de medida (Zawistowski et al., 1991; García-Molina et al., 2007a). Es importante resaltar la descripción de numerosos estudios donde se demuestra la inexistencia de actividad monofenolasa en diferentes tirosinasas de fuentes vegetales (Rivas y Whitaker, 1973; Vámos-Vigyázó, 1981; Wesche-Ebeling y Montgomery, 1990a; 1990b; Leoni et al., 1990). Esto llevó a la conclusión errónea de que son catecol oxidasas (EC 1.10.3.2) en lugar de auténticas polifenol oxidasas (EC 1.14.18.1). La detección y cuantificación de la actividad monofenolasa requiere un profundo conocimiento del mecanismo de reacción de tirosinasa y se abordará más adelante (sección 1.4.2.). Los estudios cinéticos de nuestro grupo de investigación han permitido identificar y caracterizar correctamente, por primera vez, la actividad monofenolasa de diferentes frutas y hortalizas (Espin et al., 1995; 1996; 1998a; 1998b).

Por otra parte, como ya hemos indicado, tirosinasa muestra actividad enzimática sobre una gran variedad de sustratos con estructura química diferente a la estructura fenólica natural. Así, se ha demostrado que la enzima puede oxidar a ácido ascórbico (Ros et al., 1995; 1996; Espín et al., 2000a; Munoz-Munoz et al., 2009a), descomponer peróxido de hidrógeno (García-Molina et al., 2005; Yamazaki et al., 2004) y oxidar a tetrahidropterinas (García-Molina et al., 2009), NADH (García-Molina et al., 2010b) o al ácido tetrahidrofólico (García-Molina et al., 2011). La determinación de estas actividades catalíticas ha sido dificultosa debido a la alta inestabilidad que tiene el producto de reacción quinónico de cada sustrato. Esta caracterización se ha podido llevar a cabo gracias a la puesta a punto de distintos métodos de medida para cada tipo de producto quinónico (García-Molina et al., 2007a). A continuación se profundizará en cada tipo de actividad catalítica de tirosinasa: difenolasa, monofenolasa, ascorbato oxidasa, catalasa, tetrahidropterina oxidasa, NADH oxidasa y tetrahidrofólico oxidasa.

1.4.1. Actividad difenolasa

La actividad difenolasa consiste en la oxidación de dos moléculas de *o*-difenol a *o*-quinonas gracias al oxigeno molecular formándose dos moléculas de agua. El ciclo catalítico de la oxidación de una molécula de *o*-difenol por tirosinasa comienza con la forma metatirosinasa (Esquema 1 para el mecanismo cinético y Esquema 2 para el mecanismo estructural). Se ha demostrado que durante el ciclo catalítico de la enzima no se forman intermedios semiquinónicos como se propuso inicialmente (Mason et al., 1961).

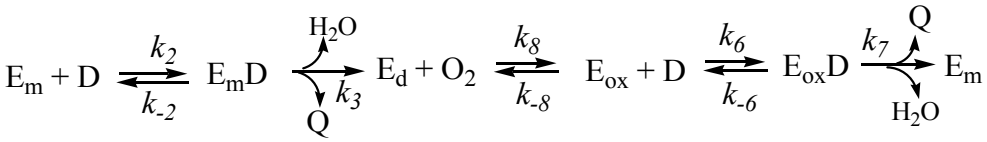

Esquema 1. Mecanismo cinético para explicar la actividad difenolasa de tirosinasa. E_m = metatirosinasa, E_d = desoxitirosinasa, E_{ox} = oxitirosinasa.

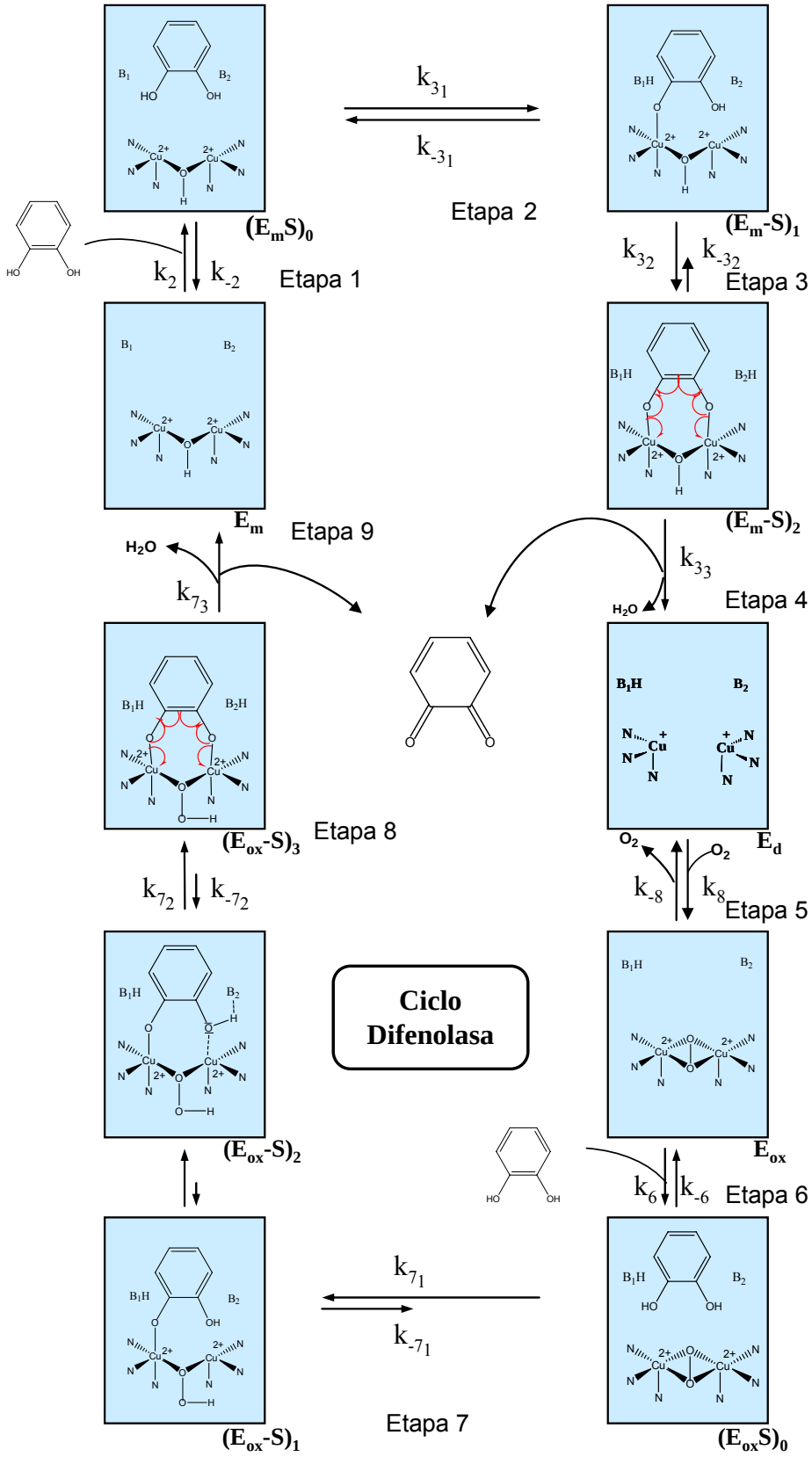

Esquema 2. Mecanismo estructural propuesto para la actividad difenolasa de tirosinasa de *Agaricus bisporus* (Muñoz-Muñoz et al., 2012).

La forma metatirosinasa une el *o*-difenol y el cobre del sitio activo se reduce, pasando de un estado de oxidación 2+ a 1+, oxidándose el *o*-difenol a *o*-quinona. Esta oxidación tiene lugar en un proceso en el que están implicados dos electrones. En la etapa siguiente, desoxitirosinasa reacciona reversible con oxigeno molecular y forma oxitirosinasa, con lo que los cobres del sitio activo vuelven al estado de oxidación 2+. Posteriormente, oxitirosinasa une otra molécula de *o*-difenol, reduciéndose el peróxido de hidrógeno del sitio activo a agua y generando metatirosinasa y *o*-quinona, cerrándose, así, el ciclo catalítico (Esquema 1).

La etapa determinante del ciclo catalítico es la etapa controlada por k_7, como se ha demostrado por estudios de efecto isotópico (Peñalver et al., 2003; Fenoll et al., 2004). La mayor rapidez de catálisis debida a la mayor potencia nucleofílica de los *o*-difenoles respecto a los monofenoles, convierte a aquellos en mejores sustratos de tirosinasa. La afinidad de la unión de los sustratos comprende, en cambio, etapas de enlace y transformación.

La mayoría de los estudios de la actividad difenolasa de tirosinasa se han realizado mediante experimentos de estado estacionario (Duckworth y Coleman, 1970; Gutteridge y Robb, 1975), que han conducido al establecimiento para esta enzima de un mecanismo trisustrato con dos sustratos y dos productos iguales entre sí (Galindo et al., 1983) denominado Uni Uni Bi Uni Ping Pong. También, se han realizado estudios de flujo detenido (Stopped-flow), en los que se demuestra que oxitirosinasa es un intermedio del ciclo catalítico (Makino y Mason, 1973; Rodríguez-López et al., 2000).

En la unión de los *o*-difenoles a tirosinasa posiblemente están involucrados una serie de procesos moleculares que incluyen la difusión de los sustratos hasta el sitio activo, la orientación de estos en dicho sitio y la coordinación del oxígeno fenólico a uno de los átomos de cobre. Estas reacciones están facilitadas o dificultadas por interacciones con diferentes cadenas de aminoácidos que se encuentran en el sitio activo o en sus proximidades. La importancia del impedimento estérico en el acceso del *o*-difenol al sitio activo de oxitirosinasa se pone de manifiesto a partir del cálculo de los valores de la constante de unión k_6 (Rodríguez-López et al., 2000).

Los datos obtenidos mediante estudios de estado estacionario y fase de transición muestran que los *o*-difenoles se unen con mayor rapidez a metatirosinasa que a oxitirosinasa ($k_2 >> k_6$) (Esquema 2). Muchos de los mecanismos propuestos

para explicar la actividad de tirosinasa sobre *o*-difenoles, proponen que el sustrato se une a un átomo de cobre del sitio activo (Wilcox et al., 1985). Este mecanismo supone que la desprotonación del grupo hidroxilo ocurre simultáneamente con la unión del sustrato, y está catalizada probablemente por la cadena lateral básica de un residuo próximo. Esto se ha justificado con datos cinéticos y de difracción de rayos X de la catecol oxidasa de *Ipomea batatas*. Además, se ha postulado que en esta catecol oxidasa existe un residuo Glu^{236} que actuaría como un catalizador ácido-base en la unión del sustrato al sitio activo de la enzima. También se ha comprobado que existe, en la fenol oxidasa de *Manduca sexta* y en la polifenol oxidasa de *Vitis vinifera*, un ácido glutámico como catalizador ácido-base (Li et al., 2009; Virador et al., 2010a). Las diferencias en la velocidad de unión de *o*-difenoles a metatirosinasa y oxitirosinasa posiblemente puedan ser debidas a la existencia en la forma meta de una base, mientras que en la forma oxi esta base estaría protonada y, por lo tanto el protón del grupo hidroxilo del *o*-difenol, debe de transferirse al grupo peróxido del sitio activo de la enzima (Tyeklar y Karlin, 1989; Casella et al., 1996; Karlin et al., 1998; Klabunde et al., 1998; Rodríguez-López et al., 2000; Mirica et al., 2002; Peñalver et al., 2003; Piquemal et al., 2003; Fenoll et al., 2004). Además, los átomos de cobre de metatirosinasa tienen un estado de oxidación 2+ y, por lo tanto, el ataque del fenolato está más favorecido que en la forma oxi donde los iones cobre tienen menos carga positiva debido a la unión del grupo peróxido (Etapas 2 y 7 del Esquema 2).

Una vez producida la unión del *o*-difenol, tirosinasa cataliza su oxidación produciendo *o*-quinonas. Estos *o*-difenoles se coordinan como fenolatos en una posición axial en el centro bicúprico tetragonal, probablemente por el desplazamiento de una molécula de agua (Etapas 2 y 3). El hecho de que solo los *o*-difenoles puedan ser oxidados por tirosinasa, cosa que no ocurre con *p*-difenoles, pone de manifiesto que exista una coordinación bidentada entre el *o*-difenol y los átomos de cobre, como se muestra en el Esquema 2. Sin embargo, este aspecto es objeto de discusión, ya que existen grupos de investigación que proponen una coordinación monodentada del sustrato (Klabunde et al., 1998; Eicken et al., 1999).

Por otra parte, se ha postulado, prácticamente hasta el día de hoy, que la coordinación del segundo grupo hidroxilo del sustrato al sitio activo puede llevar asociado el desplazamiento de un residuo de histidina del CuA de la enzima (Matoba et al., 2006). Sin embargo, gracias a los datos cristalográficos de las estructuras de tirosinasa de diferentes fuentes (Decker et al., 2006; Deeth y Diedrich, 2010; Sendovski et al., 2011), se ha demostrado que las histidinas axiales se encuentran en

posición *cis*, al contrario de lo que postulaba Matoba et al. (2006), que las representaba en posición *trans*. Estos estudios demuestran que las histidinas unidas a los cobres del sitio activo son rígidas y su enlace no se rompe en la catálisis. Por lo tanto, se postula la existencia de dos bases en el sitio activo de la enzima capaces de aceptar los dos protones de los grupos hidroxilos del *o*-difenol (Etapas 3 y 8 del Esquema 2). Estudios recientes también han demostrado la existencia de dos pKas cinéticamente significativos en el sitio activo de la enzima que apoyan esta hipótesis (Muñoz-Muñoz et al., 2010a; Muñoz-Muñoz et al., 2012).

En el mecanismo descrito en el Esquema 2, dos electrones, procedentes de una molécula de sustrato, son transferidos al sitio activo de metatirosinasa y el mismo proceso ocurre con otra molécula de sustrato al grupo peróxido de oxitirosinasa. Esto implica que los sustratos con alta densidad electrónica en los átomos de carbono que soportan los grupos hidroxilos, C3 y C4 (Duckworth y Coleman, 1970), serán buenos sustratos y, por lo tanto, tendrán una alta constante catalítica k_{cat}. Sin embargo, se ha comprobado que sustratos que poseen unos valores de desplazamiento químico similar (δ), como es el caso de L-dopa o pirocatecol (valores de δ_3 y δ_4 de 146.59 p.p.m. en ambos casos para el pirocatecol y de 146.92 y 146.06 p.p.m. para el L-dopa), eran oxidados por tirosinasa con valores muy diferentes para su k_{cat} (878 ± 50 s^{-1} para el pirocatecol y 108 ± 9 s^{-1} para el L-dopa) (Rodríguez-López et al., 2000). También se ha observado que los sustratos sin cadena lateral, como pirogalol o pirocatecol, presentan los valores de k_{cat} más elevados para tirosinasa, seguidos por los sustratos con una cadena lateral hidrofóbica y, finalmente, los que tienen una cadena polar presentan valores de k_{cat} más bajos. Con todo esto, se llega a la conclusión de que la k_{cat} de tirosinasa se encuentra modulada no solo por factores electrónicos sino también por factores estéricos y polares de los sustratos, como ya había sido sugerido anteriormente (Solomon et al., 1996; Espín et al., 2000b; Rodríguez-López et al., 2000).

El Esquema 2 muestra el mecanismo estructural propuesto por nuestro grupo de investigación. En este Esquema, el *o*-difenol se une a la forma meta (E_m), en la Etapa 1, posiblemente formando un enlace por puente de hidrógeno con la base B_1. Posteriormente, el sustrato se une en posición axial a uno de los átomos de cobre de la forma E_m, quizás CuB (Etapa 2). Esta coordinación va acompañada de la transferencia del protón a un residuo proteico B_1 (posiblemente una histidina) (Etapa

2). La coordinación bidentada del *o*-difenol (Etapa 3) está acompañada de una segunda transferencia de protón, probablemente a una segunda base B_2 próxima al CuA. La transferencia electrónica a partir del *o*-difenol conduce a la formación de la *o*-quinona y a la especie desoxitirosinasa (E_d), (Etapa 4). A continuación, tiene lugar la unión del oxígeno en el plano ecuatorial de los cobres (Etapa 5), generando la forma oxitirosinasa, en la cual el peróxido está coordinado a los dos iones de cobre oxidados, Cu^{2+}. En la reacción de la forma oxi (E_{ox}) con una segunda molécula de *o*-difenol (Etapa 6), la coordinación de *o*-difenol a uno de los iones de cobre del sitio activo está acompañada por la transferencia de un protón al grupo peróxido (Etapa 7), lo que está de acuerdo con trabajos anteriores (Tyeklar y Karlin, 1989; Casella et al., 1996; Karlin et al., 1998; Klabunde et al., 1998; Rodríguez-López et al., 2000; Mirica et al., 2002; Peñalver et al., 2003; Piquemal et al., 2003; Fenoll et al., 2004). La coordinación del *o*-difenol se ha propuesto que se realiza diaxialmente, ya que el plano ecuatorial estaría ocupado por el peróxido (Etapa 8). Para la coordinación bidentada del *o*-difenol se transfiere un segundo protón, probablemente al igual que en la forma meta, por transferencia a una segunda base B_2 próxima al CuA, lo que está de acuerdo con la flexibilidad descrita para el sitio activo de tirosinasa (Matoba et al., 2006; Sendovski et al., 2011; Ismaya et al., 2011) y con la existencia de dos pKas en la enzima (Muñoz-Muñoz et al., 2010a; Muñoz-Muñoz et al., 2012). La transferencia electrónica del *o*-difenol al grupo peróxido origina la ruptura del enlace oxígeno-oxígeno y la formación de una molécula de agua y la correspondiente *o*-quinona, regenerándose metatirosinasa (Etapa 9). En esta última etapa, los residuos proteicos B_1 y B_2 actúan como ácidos proporcionando los protones necesarios para la liberación de la molécula de agua.

1.4.2. Actividad monofenolasa

El mecanismo de la actividad monofenolasa ha sido ampliamente estudiado (Mason, 1956; Osaki, 1963; Cabanes et al., 1987a; Naish-Byfield y Riley, 1992; Rodríguez-López et al., 1992a; Ros et al., 1994). Algunos estudios de estado estacionario de la ruta, describen inhibición por exceso de tirosina (Devi et al., 1987; 1989; Tripathi et al., 1988). Sin embargo, las características más ampliamente descritas de la actividad monofenolasa son:

(a) En tirosinasa y polifenol oxidasa, la actividad monofenolasa siempre se expresa junto a la actividad difenolasa, puesto que el producto de la primera actividad, el *o*-difenol, es el sustrato de la actividad difenolasa.

(b) La expresión de la actividad monofenolasa abarca las mismas etapas no enzimáticas que las encontradas en la actividad difenolasa desde *o*-quinona hasta aminocromo.

(c) La actividad monofenolasa se caracteriza por mostrar un periodo de retardo característico antes de que el sistema llegue al estado estacionario. Este periodo de retardo tiene una duración muy variable, dependiendo de la naturaleza de la enzima. Para eliminar el periodo de retardo, se añaden pequeñas cantidades de L-dopa (Pomerantz, 1966), lo que llevó a la hipótesis de la existencia de un sitio activador en la enzima para el L-dopa y a evaluar su constante de activación para la actividad monofenolasa (Duckworth y Coleman, 1970). Sin embargo, nuestro grupo de investigación ha llegado a una interpretación cinética del periodo de retardo y, por otra parte, ha obtenido una expresión analítica aproximada para este periodo de retardo (Rodríguez-López et al., 1992a; Fenoll et al., 2001; Molina et al., 2007). En el Esquema 3 se muestra el mecanismo cinético propuesto para la actividad conjunta difenolasa y monofenolasa de tirosinasa.

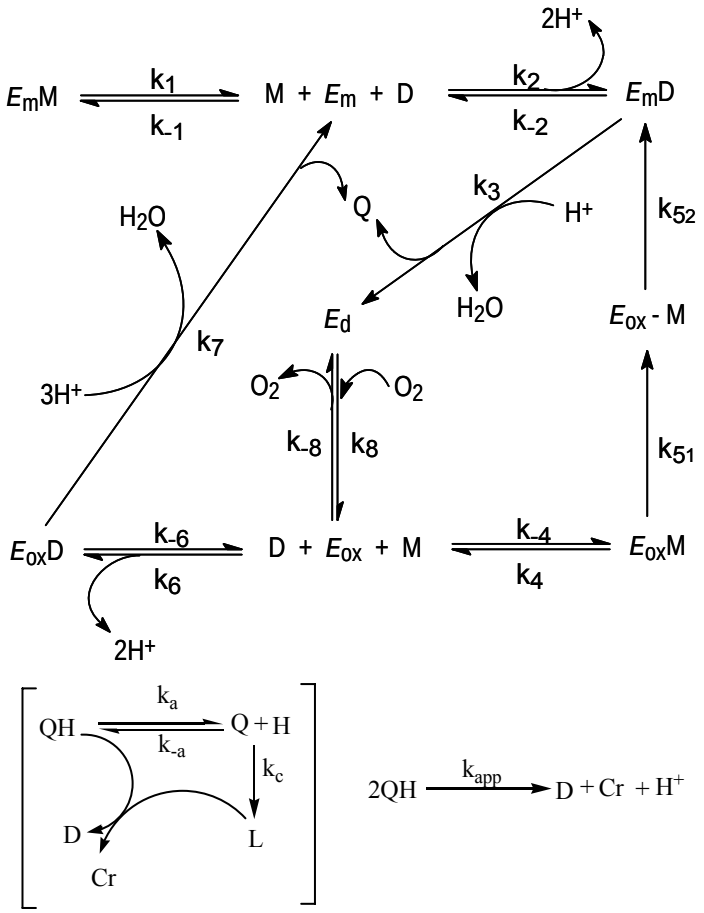

Esquema 3. Detalle del mecanismo cinético propuesto para la actividad mono- y difenolasa de tirosinasa de *Agaricus bisporus*. La terminología es la misma que en el Esquema 1 y además M = monofenol, $E_{ox}\mathrm{M}$ = complejo oxitirosinasa/monofenol. $E_m\mathrm{M}$ = complejo metatirosinasa/monofenol.

Según este mecanismo, oxitirosinasa reacciona con el monofenol y forma un complejo ternario que conduce a la hidroxilación del sustrato, originándose el *o*-difenol. En este momento, este *o*-difenol puede ser liberado del sitio activo de la enzima o puede ser oxidado a su *o*-quinona correspondiente. Si es oxidado, se forma E_d, la cual se une rápidamente a O_2 y produce de nuevo E_{ox}. Si es liberado, se origina E_m, que reacciona con otra molécula de *o*-difenol, lo oxida a *o*-quinona y la enzima se transforma en E_d y esta, al reaccionar con el oxigeno, origina E_{ox}. Esta secuencia de reacciones coincide con la primera mitad del ciclo difenolasa, lo que demuestra la fuerte relación que existe entre ambas actividades (monofenolasa y difenolasa) (Mason, 1956; Fenoll et al., 2001). La necesidad de mantener un nivel adecuado de *o*-

difenol en el estado estacionario de la actividad monofenolasa para poder realizar la hidroxilación, hace pensar que el *o*-difenol actúa como un cosustrato en lugar de como un activador (Cabanes et al., 1987a; Rodríguez-López et al., 1992a; Ros et al., 1994). Cuando la enzima actúa sobre monofenoles, necesita acumular una cantidad determinada del *o*-difenol correspondiente, de tal forma que debe cumplirse la relación $R = [D]_{ss} / [M]_{ss}$ (Rodríguez-López et al., 1992a; Ros et al., 1993a; 1993b; 1994; Rodríguez-López et al., 2001). En esta situación, la enzima realiza dos ciclos en la ruta monofenolasa por uno en la difenolasa, de tal manera que la concentración de *o*-difenol no varía (Fenoll et al., 2001).

En el Esquema 4 se muestra el mecanismo estructural propuesto para explicar la acción de tirosinasa sobre monofenoles y *o*-difenoles. Se incluyen las etapas del ciclo difenolasa del Esquema 2 y las etapas correspondientes al ciclo monofenolasa.

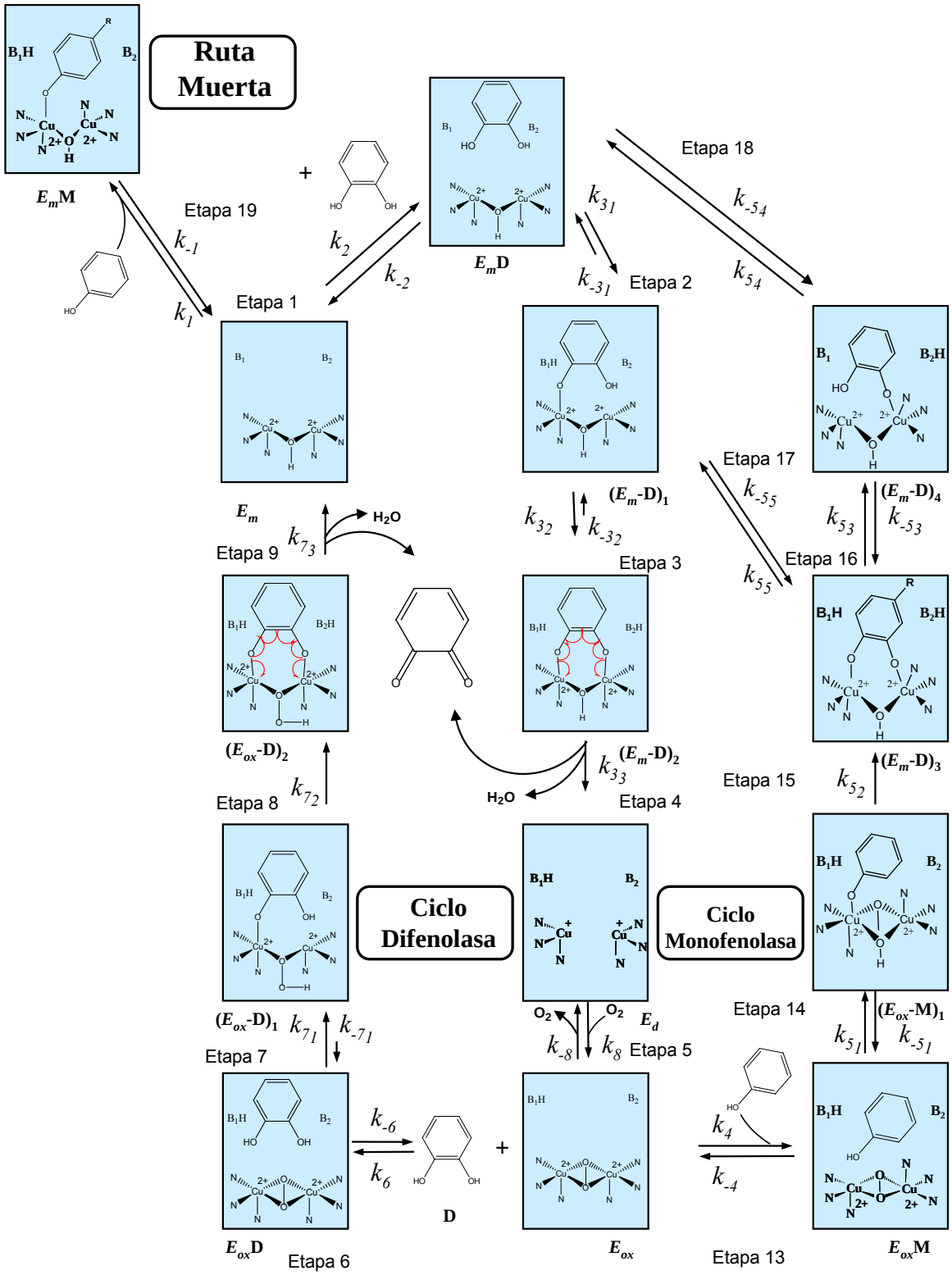

Esquema 4. Mecanismo estructural propuesto para explicar la hidroxilación de sustratos monofenólicos y la oxidación de *o*-difenoles a *o*-quinonas catalizada por tirosinasa de *Agaricus bisporus* en presencia de oxigeno (Muñoz-Muñoz et al., 2012).

En la etapa 13, el monofenol se enlaza a la forma E_{ox}. Posteriormente, el monofenol podría transferir el protón del grupo hidroxilo de C-4 al peróxido, mediante la Etapa 14 uniéndose en axial al CuA. En la Etapa 15, un ataque electrofílico por parte del oxígeno del grupo peróxido al anillo en C-3, origina un intermedio ($E_m - D$)$_3$, en el cual el *o*-difenol formado está unido en posición axial/equatorial. De este modo, ya que los orbitales no son coplanares, entre los iones de cobre y los carbonos en posiciones 3 y 4 no puede ocurrir la oxidación/reducción concertada y el *o*-difenol puede romper el enlace con el ión CuB (Etapa 16) originando la especie ($E_m - D$)$_4$, y, a través de la Etapa 18, se puede originar la especie ($E_m D$), intermedio que también se encuentra en el Esquema 2. A su vez, la especie ($E_m - D$)$_3$ puede romper el enlace con el CuA mediante la Etapa 17, originando el intermedio ($E_m - D$)$_1$, que conecta con el ciclo difenolasa (Esquemas 2 y 4). Nótese que a partir del intermedio $E_m D$ se puede liberar *o*-difenol al medio (Etapa 1).

Periodo de retardo. Una de las principales características de la actividad monofenolasa es el periodo de retardo o lag que consiste en la aparición de una fase de transición hasta que el sistema llega al estado estacionario. El estudio de esta fase de transición da lugar a la determinación de un periodo de inducción o periodo de retardo, cuando se extrapola la acumulación lineal de producto con el tiempo (Rodríguez-López et al., 1992a; Ros et al., 1994). Este periodo de retardo puede ser eliminado en presencia de *o*-difenoles y de otros agentes reductores como ácido ascórbico (Ros et al., 1993a), tetrahidropterinas (García-Molina et al., 2007b; 2009; 2010a), NADH (García-Molina et al., 2010b) o con ácido tetrahidrofólico (García-Molina et al., 2011).

Los estudios cinéticos realizados por el nuestro grupo de investigación (GENZ) han demostrado que el lag es el tiempo necesario para que una concentración determinada de enzima, actuando con L-tirosina como sustrato, acumule en el medio una concentración determinada de L-dopa, de tal forma que la relación $R=[D]_{ss}/[M]_{ss}$ alcance un valor constante (Rodríguez-López et al., 1992a; Ros et al., 1994; Fenoll et al., 2001).

El análisis cinético del periodo de retardo no permite obtener una solución analítica rigurosa. Sin embargo, bajo la aproximación del estado estacionario, y

teniendo en cuenta el balance de materia para el sistema (tirosinasa actuando sobre L-tirosina), es posible obtener una solución analítica aproximada que cumple con los resultados experimentales, a saber: a) cuando la concentración de sustrato es constante, el lag disminuye al aumentar la concentración de enzima (antes se acumula el *o*-difenol necesario para cumplir la relación constante, R, indicada anteriormente), b) cuando la concentración de enzima se mantiene constante, al aumentar la concentración de sustrato aumenta el periodo de retardo (hay que acumular cada vez más *o*-difenol y por lo tanto el periodo de retardo aumenta) (Molina et al., 2007).

1.4.3. Estereoespecificidad

Como hemos indicado en la sección de estructura de tirosinasa, la enzima presenta un sitio activo con átomos de cobre altamente conservados en toda la escala filogenética. Como se ha expuesto anteriormente en los Esquemas 2 y 4, los sustratos fisiológicos de la enzima (monofenoles y *o*-difenoles) deben unirse a los átomos de cobre y, posteriormente, sufrir las reacciones correspondientes: hidroxilación (monofenoles) y oxidación (*o*-difenoles) (Fenoll et al., 2001). Se ha demostrado que tirosinasa es esteroespecífica en lo que respecta a la afinidad por el sustrato ($1/K_m$). Sin embargo, puesto que la velocidad máxima (V_{max}) depende de la potencia nucleofílica de los oxígenos de los grupos hidroxilos de los monofenoles y *o*-difenoles, ésta no varia para los distintos estereoisómeros ya que su potencia nucleofílica es la misma.

Experimentalmente, se ha descrito la esteroespecificidad de la enzima de champiñón (Espín et al., 1998b), pera y fresa (Espín et al., 1998a). En todas las tirosinasas estudiadas, se ha podido demostrar que las enzimas tienen mas afinidad por el estereoisómero L de los sustratos que por el D y, por otra parte, la misma velocidad máxima para ambos estereoisómeros.

Cuando se estudia la inactivación suicida de la enzima, la estereoespecificidad se vuelve a poner de manifiesto. Así, en estudios de la inactivación suicida de tirosinasa en su acción sobre el ácido ascórbico, la enzima mostró más afinidad por ácido L-ascórbico que por el ácido D-ascórbico, pero la rapidez de inactivación fue la misma para ambos isómeros, una situación similar se encuentra al estudiar los isómeros del dopa (Muñoz-Muñoz et al., 2009a; 2010b).

1.4.4. Actividad ascorbato oxidasa.

Nuestro grupo de investigación demostró la actividad ascorbato oxidasa de tirosinasa de champiñón (Ros et al., 1995). Como ya se ha indicado en la sección 1.3.2.2., el sitio activo de la enzima se encuentra superficialmente en la molécula y, además, es una cavidad amplia, lo que posibilita la entrada de un gran número de sustratos muy diferentes entre sí (Ismaya et al., 2011).

En el Esquema 5 se representa el mecanismo estructural propuesto para la oxidación del ácido ascórbico por tirosinasa. En él se recogen los hallazgos estructurales recientes de la enzima como la existencia de dos bases claves de acuerdo con los dos pKas cinéticamente significativos en la enzima, la situación de las histidinas axiales del sitio activo de la enzima en posición *cis* o la rigidez estructural de las histidinas unidas a los átomos de cobre. En este mecanismo, la forma E_m se une al sustrato (ácido ascórbico) formando el complejo E_mS (Etapa 1). Después, se produce el ataque del oxigeno del grupo hidroxilo del sustrato probablemente al CuB de la enzima ayudado por la base B_1, que acepta el protón de este grupo (Etapa 2). Posteriormente, en la Etapa 3, se transfiere el segundo protón del sustrato a la segunda base del sitio activo (B_2) uniéndose de forma bidentada el sustrato con los átomos de cobre. Ahora, mediante la Etapa 4, se produce la oxidación/reducción concertada liberándose el ácido dehidroascórbico y generando E_d. Después ocurre la unión del oxigeno molecular para formar E_{ox} (Etapa 5), esta forma enzimática une otra molécula de sustrato originando el complejo $E_{ox}S$ (Etapa 6). En el paso siguiente, el sustrato transfiere un protón del primer grupo hidroxilo al grupo peróxido de la enzima ya que la base B_1 se encuentra protonada (Etapa 7). A continuación, el sustrato le transfiere un segundo protón a la base B_2 (que está desprotonada) y, posteriormente, se une a la forma oxi de forma bidentada (Etapa 8). Por último, se produce la oxidación/reducción concertada regenerando E_m y liberando ácido dehidroascórbico (Etapa 9).

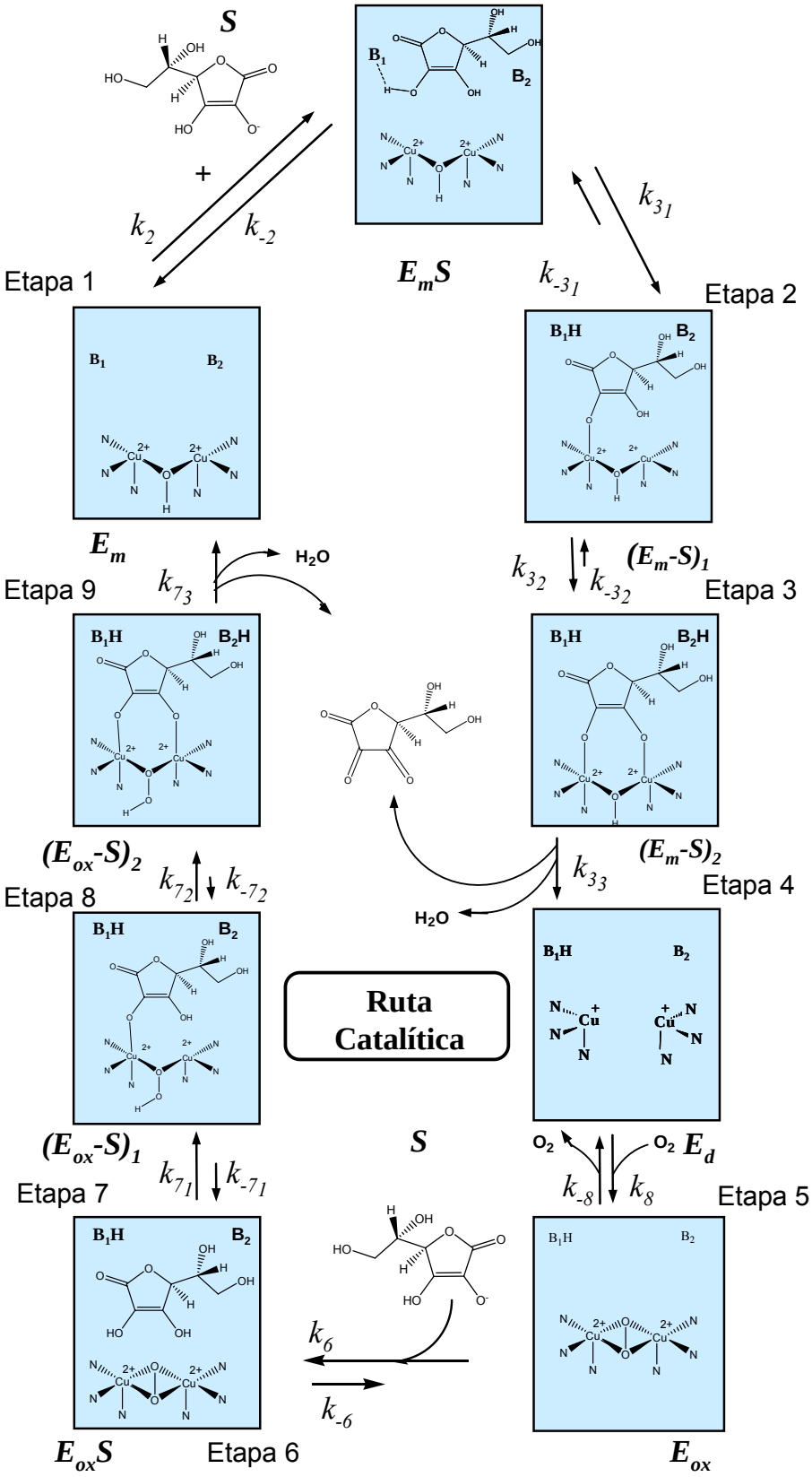

Esquema 5. Mecanismo estructural propuesto para la oxidación del ácido ascórbico por tirosinasa de *Agaricus bisporus* (Munoz-Munoz et al., 2009a).

1.4.5. Actividad catalasa

Recientemente, García-Molina et al. (2005) demostraron que tirosinasa de *Agaricus bisporus* también muestra actividad catalítica cuando el H_2O_2 es el único sustrato. Esta propiedad de descomposición del H_2O_2 (actividad catalasa) ha sido descrita por otros autores (Yamazaki et al., 2004). Esta actividad se estudia en condiciones anaerobias midiendo la formación de O_2. Así, partiendo de E_m, cuando existe peróxido de hidrogeno en el medio, éste entra al sitio activo de la enzima (Etapa 1) y forma oxitirosinasa (E_{ox}). A continuación, esta forma E_{ox} se transforma en E_d liberando oxigeno y los átomos de cobre pasan a Cu^{1+} (Etapa 3). Ya en la forma E_d, el ataque de otra molécula de H_2O_2 al sitio activo (Etapa 4), origina el complejo E_dS, la oxidación de los átomos de cobre a Cu^{2+} (Etapa 5), regenera la forma E_m y libera H_2O (Etapa 6).

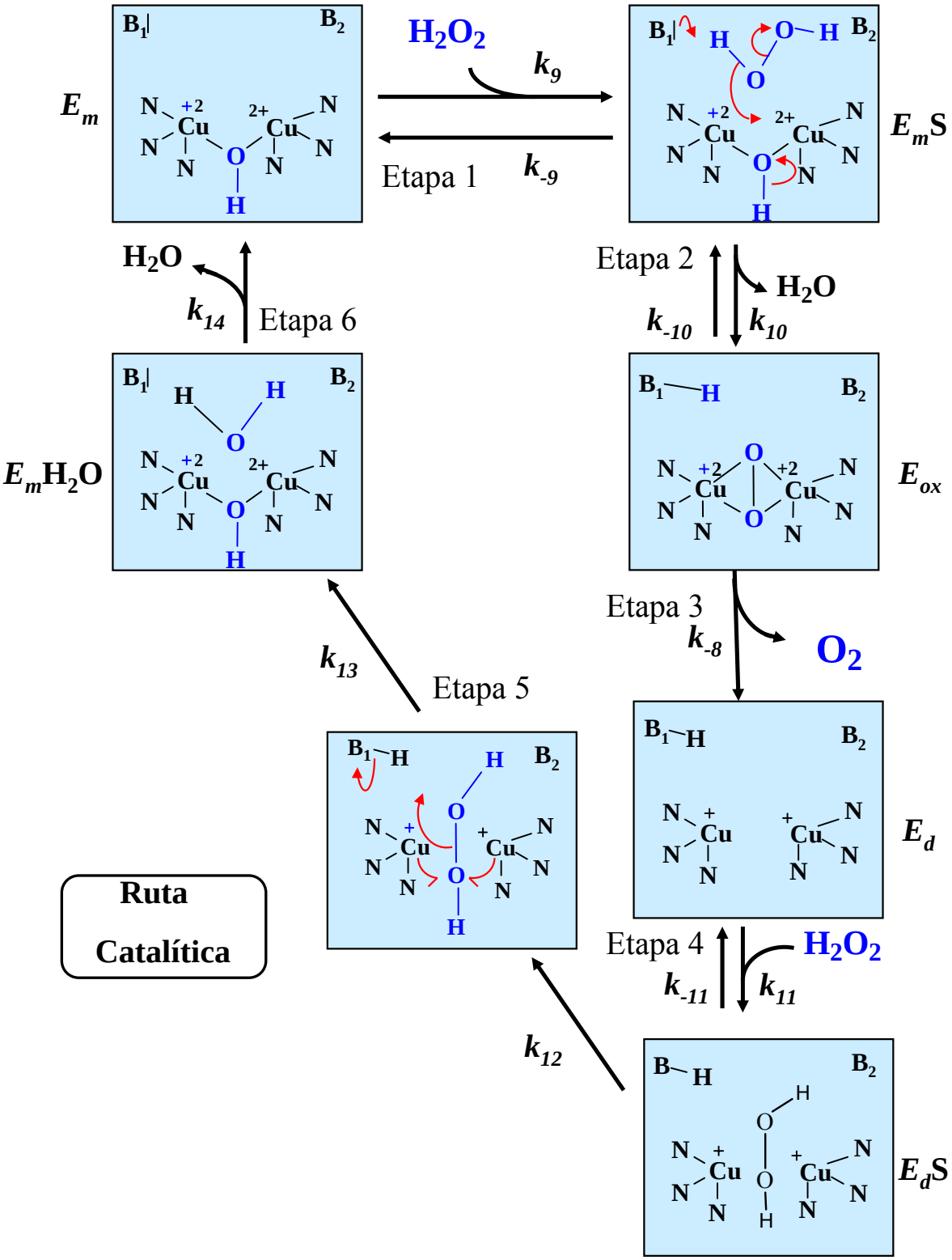

Esquema 6. Mecanismo estructural descrito para la descomposición del H_2O_2 por tirosinasa de *Agaricus bisporus* gracias a su actividad catalasa (García-Molina et al., 2005).

1.4.6. Actividad tetrahidropterina oxidasa

Nuestro grupo de investigación ha demostrado la actividad tetrahidropterina oxidasa de tirosinasa de *Agaricus bisporus* cuando la enzima actúa sobre este cofactor y sus derivados (García-Molina et al., 2007b; 2009; 2010a). En concreto, se demostró la oxidación del cofactor natural 5,6,7,8-tetrahidrobiopterina y sus derivados metilados 6-metil-5,6,7,8-tetrahidropterina y 6,7-dimetil-5,6,7,8-tetrahidropterina (Esquema 7). El mecanismo catalítico comienza de nuevo con la forma metatirosinasa. La unión no se produce por los dos grupos hidroxilos, sino por dos heteroátomos (un nitrógeno y un carbono). El mecanismo estructural recoge de nuevo los avances en la estructura de la enzima. Como puede comprobarse, un protón es transferido desde un nitrógeno a la base B_1 mientras que el otro protón es transferido desde un átomo de carbono a la base B_2. En la forma E_{ox}, el primer protón lo cede el sustrato al peróxido del sitio activo mientras que el segundo protón lo cede a la base B_2. Cuando se producen ambas transferencias, se lleva a cabo la oxidación/reducción concertada y se regenera la forma E_m.

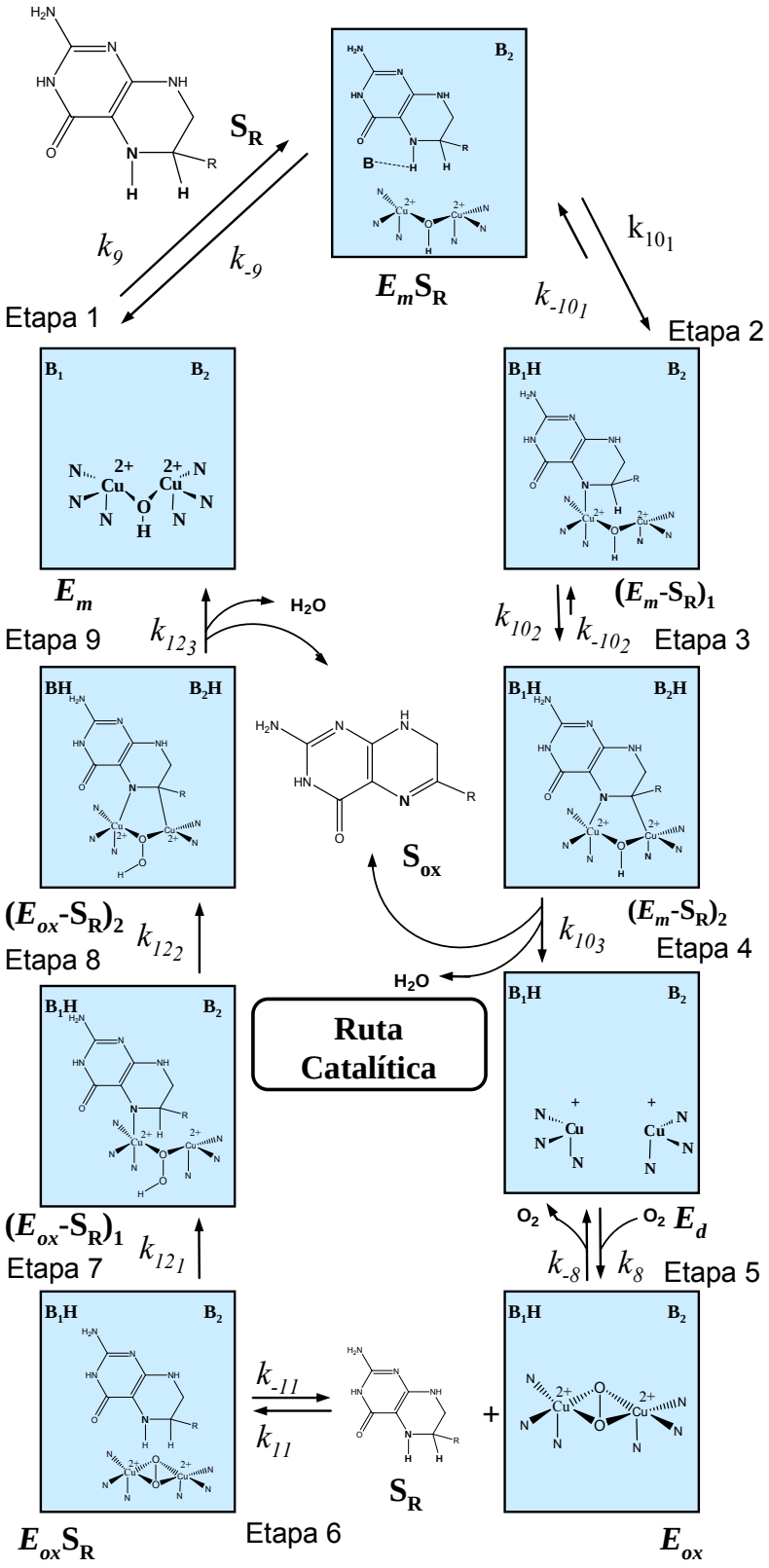

Esquema 7. Mecanismo estructural propuesto para la oxidación de las tetrahidropterinas por tirosinasa de *Agaricus bisporus* (Muñoz-Muñoz et al., 2011a).

1.4.7. Actividad NADH oxidasa

Recientemente, nuestro grupo demostró la actividad NADH oxidasa de tirosinasa de *Agaricus bisporus* (García-Molina et al., 2010b). En este estudio se propone un mecanismo cinético y estructural donde se libera una histidina del CuA de la enzima, como ya se propuso anteriormente (Matoba et al., 2006). Sin embargo, en el Esquema 8 se plantea el mismo mecanismo estructural para la oxidación del NADH pero adjuntando los recientes hallazgos en la cristalografía de la enzima. Por tanto, la transferencia del protón no se propone a las histidinas unidas a los átomos de cobre, así, la transferencia debe ser del segundo protón del NADH a la base B_2 del sitio activo de la enzima, que es la que se encuentra próxima al CuA. Otra particularidad es que, a partir del estudio del efecto del pH, el sustrato debe entrar protonado al sitio activo de la enzima, como se muestra en el Esquema 8.

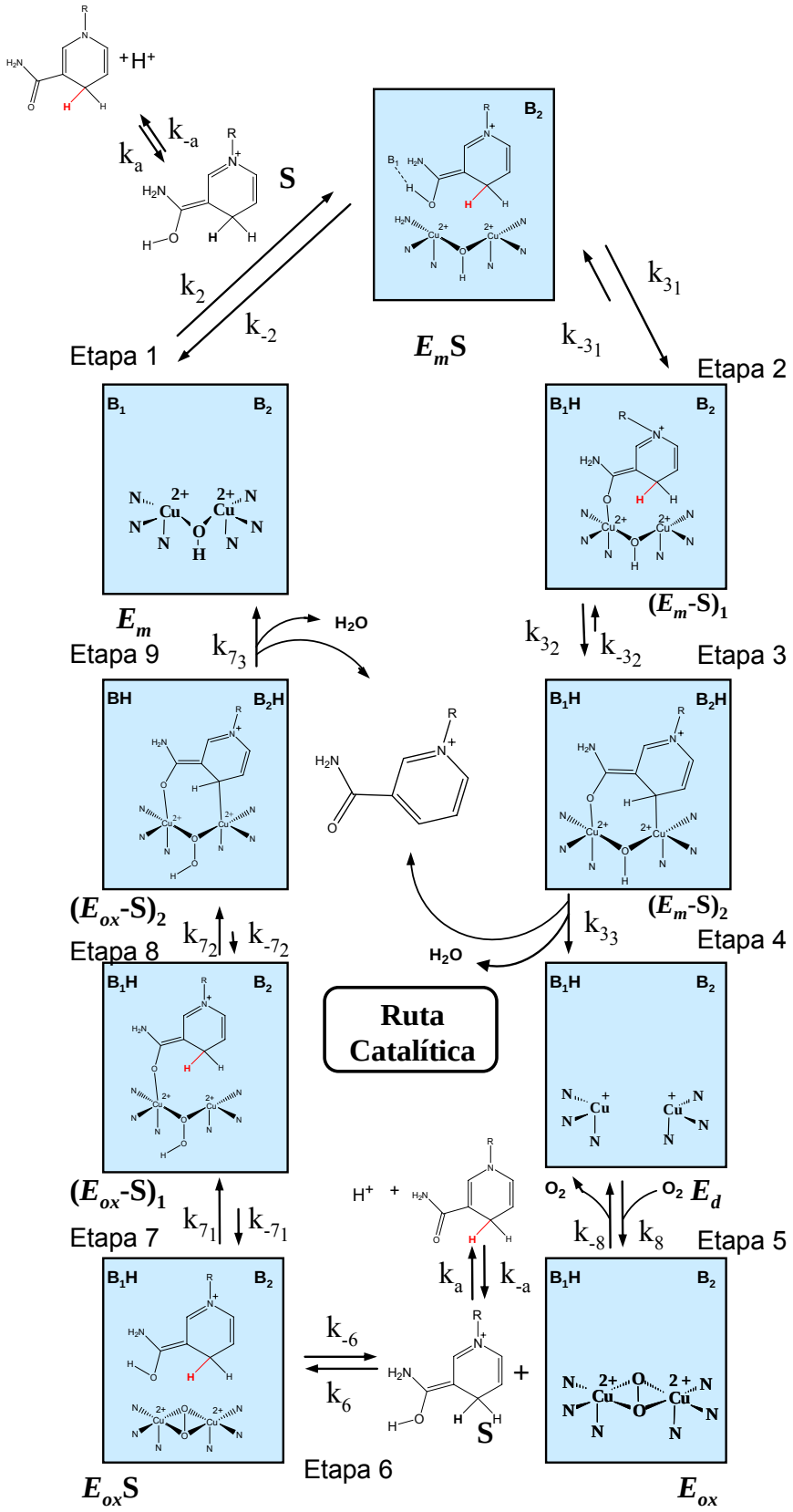

Esquema 8. Mecanismo estructural propuesto para la oxidación del NADH por tirosinasa de *Agaricus bisporus* (García-Molina et al., 2010b).

1.4.8. Actividad tetrahidrofólico oxidasa

Al igual que el resto de actividades catalíticas distintas de las fisiológicas de la enzima, se ha descrito la oxidación del ácido tetrahidrofólico por tirosinasa de *Agaricus bisporus* (García-Molina et al., 2011). En el Esquema 9 se describe el mecanismo estructural propuesto para explicar la oxidación del ácido tetrahidrofólico por tirosinasa. Al igual que ocurría con las tetrahidropterinas, en la oxidación del ácido tetrahidrofólico (THF) intervienen un átomo de nitrógeno protonado y un grupo hidroxilo como los grupos responsables de ceder los dos protones en el sitio activo de la enzima. En cambio, la constante catalítica es mayor en las tetrahidropterinas que en el caso de THF. Como en el caso del NADH, el THF debe estar protonado para entrar al sitio activo de la enzima y producirse la oxidación/reducción concertada.

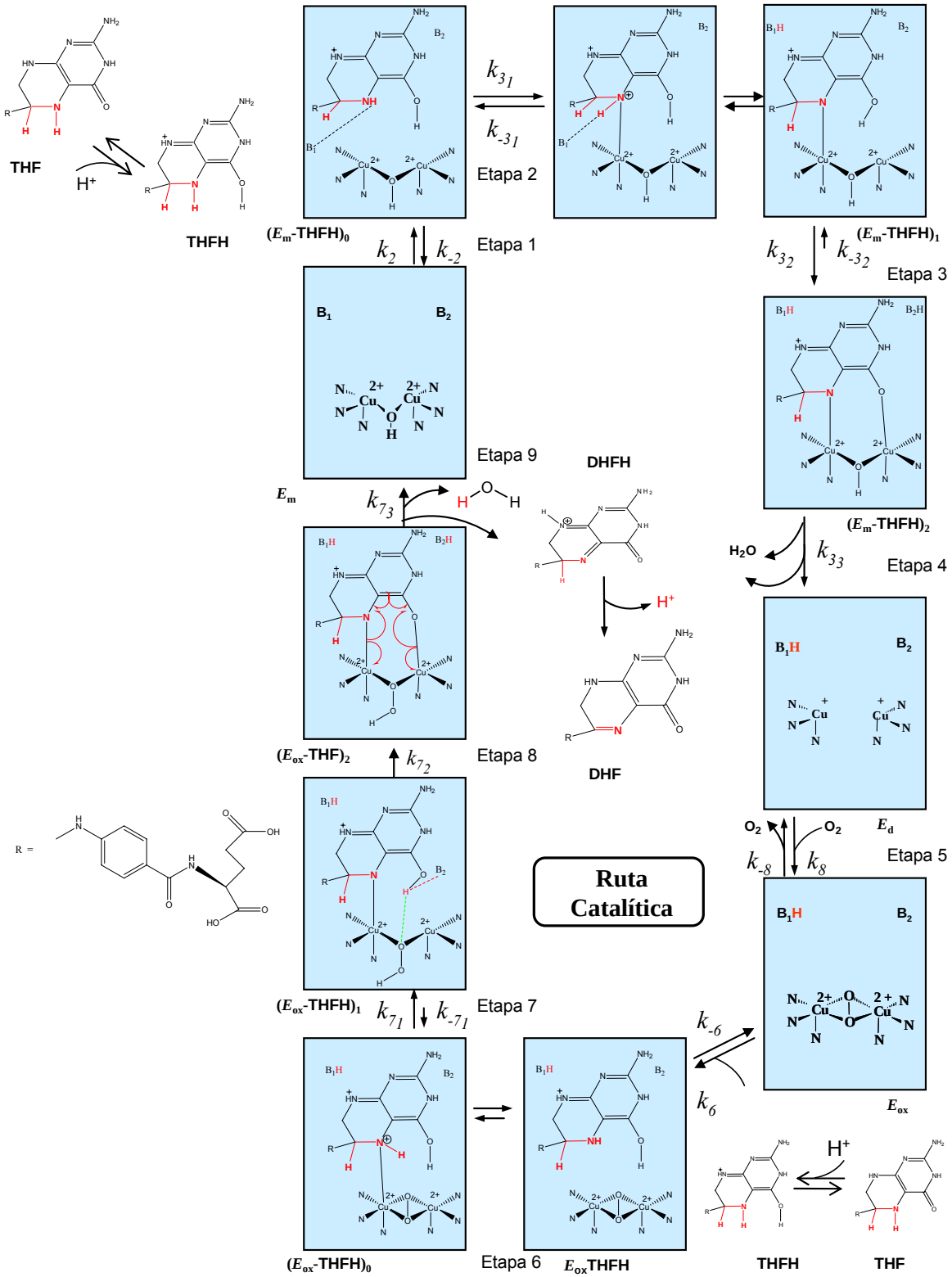

Esquema 9. Mecanismo estructural propuesto para la oxidación del ácido tetrahidrofólico por tirosinasa de *Agaricus bisporus* (García-Molina et al., 2011).

1.4.9. Oxidación de *o*-aminofenoles y aminas aromáticas

Las últimas actividades catalíticas caracterizadas cinéticamente para las que se ha propuesto un posible mecanismo cinético y estructural, son la hidroxilación y oxidación de monoaminas aromáticas y la oxidación de *o*-aminofenoles y *o*-diaminas aromáticas. Parte de estas actividades se demostraron hace muchos años (Toussaint y Lerch, 1987) y, más recientemente, se han caracterizado cinéticamente la oxidación de varios compuestos (Rescigno et al., 1998; Sanjust et al., 2003; Gasowska et al., 2004; Rescigno et al., 2011). Un estudio sistemático de estas reacciones únicamente se ha llevado a cabo en esta Memoria (Muñoz-Muñoz et al., 2011b).

El Esquema 10 muestra el mecanismo estructural propuesto para explicar la hidroxilación de monoaminas aromáticas y la oxidación de *o*-aminofenoles, mientras que en el Esquema 11 se muestra el mecanismo estructural propuesto para explicar la oxidación de *o*-diaminas aromáticas. En ambos esquemas se propone la existencia de dos bases en el sitio activo de la enzima y la rigidez de las uniones de las histidinas unidas a los átomos de cobre. En el caso de los *o*-aminofenoles, el primer protón a transferir será el del grupo amino a la base B_1 (en el caso de E_m) y el grupo hidroxilo transferirá el protón a las base B_2 (Etapas 2 y 3 respectivamente). En el caso de la forma E_{ox}, la base B_1 se encuentra protonada. El grupo amino es más nucleófilo que el hidroxilo con lo que siempre atacará primero sobre el átomo de cobre del CuB (Etapa 6). Sin embargo, probablemente una vez unido, no le transfiere el protón al grupo peróxido de la enzima como ocurría en el resto de actividades catalíticas de tirosinasa, proponemos que el grupo hidroxilo sea el que le ceda el protón a la base B_2 primero (Etapa 7) y, a continuación, es el grupo amino el que se lo cede al peróxido (Etapa 8). Esto provoca que la constante catalítica de estos compuestos (*o*-aminofenoles) sea mas baja que sus correspondientes *o*-difenoles. En la reacción de hidroxilación de monoaminas aromáticas (Esquema 10), la unión del grupo amino al CuA del sitio activo de la enzima se produce rápidamente porque es un grupo muy nucleófilo. Sin embargo, la transferencia del protón al peróxido del sitio activo está muy dificultada porque es un grupo que no cede el protón fácilmente (Etapa 11). Esto provoca que las constantes catalíticas de las monoaminas aromáticas sean mucho más bajas en comparación con sus monofenoles correspondientes. En cambio, las constantes de Michaelis de estas monoaminas son, generalmente, más bajas (con lo que la enzima tiene más afinidad por ellas) que las de sus monofenoles.

En el caso de las *o*-diaminas aromáticas (Esquema 11), el mecanismo estructural es similar que para el caso de los *o*-aminofenoles. Sin embargo, en este

caso son dos grupos NH_2 los que tienen que transferir los protones a las bases del sitio activo de la enzima. Esto provoca que las constantes catalíticas sean todavía más bajas en el caso de las *o*-diaminas aromáticas que en el caso de los *o*-aminofenoles y, al mismo tiempo, que en el caso de sus *o*-difenoles correspondientes.

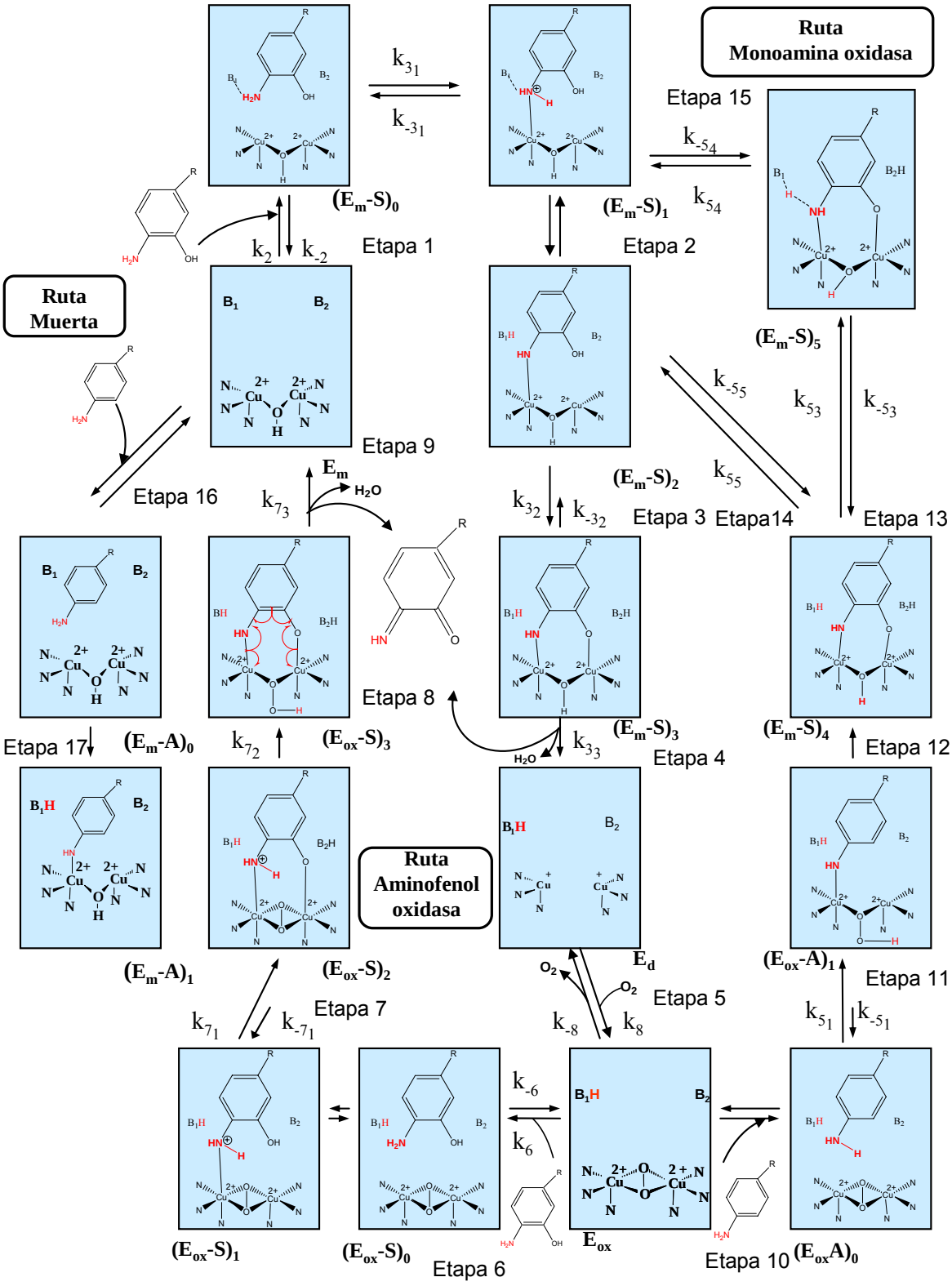

Esquema 10. Mecanismo estructural propuesto para la hidroxilación y oxidación de monoaminas aromáticas y *o*-aminofenoles respectivamente por tirosinasa de *Agaricus bisporus*.

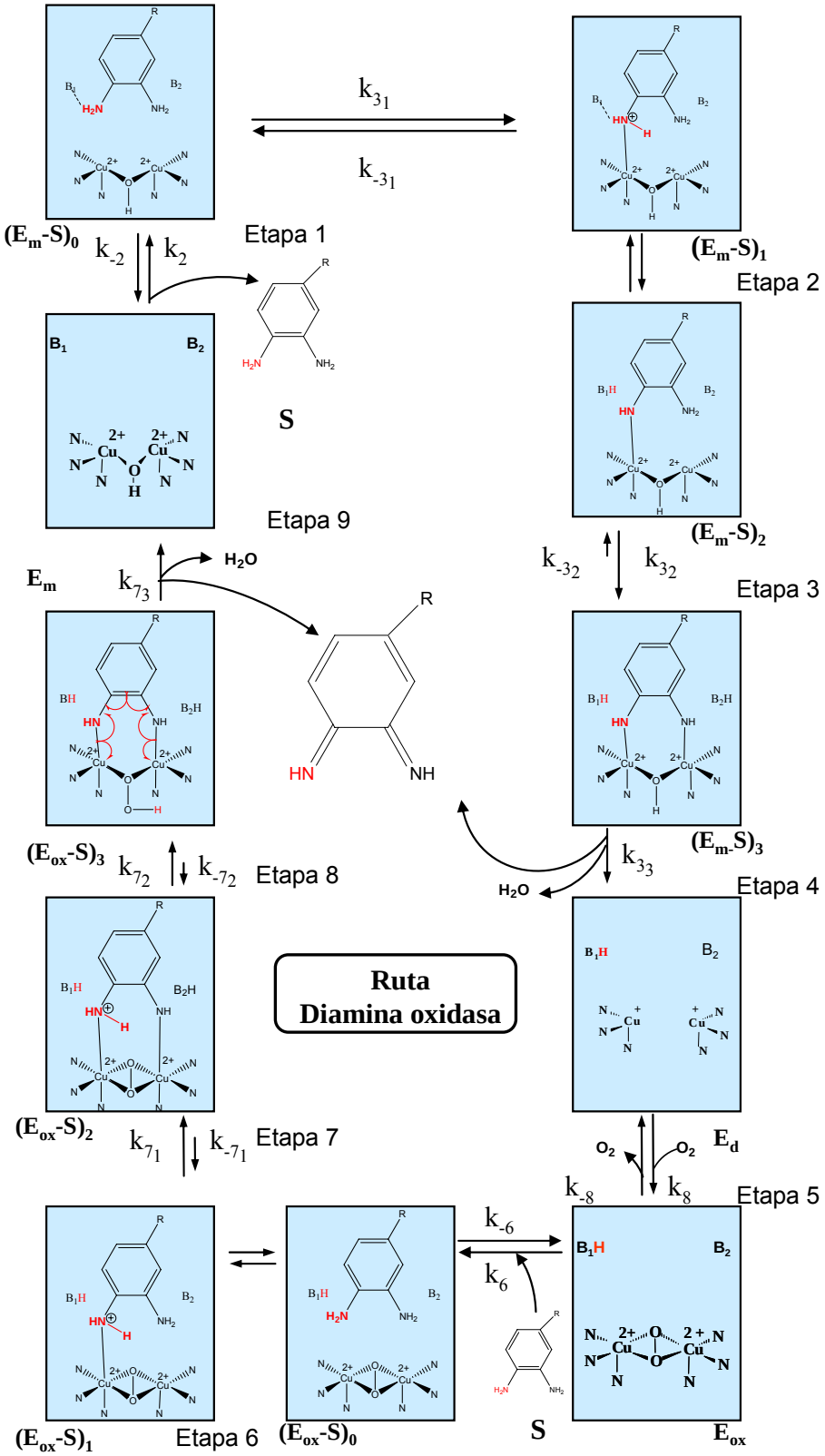

Esquema 11. Mecanismo estructural propuesto para la oxidación de *o*-diaminas aromáticas por tirosinasa de *Agaricus bisporus*.

1.5. Tirosinasa: regulación enzimática

En este capitulo se describen los diferentes tipos de regulación que presenta tirosinasa, tanto externamente, con la acción de inhibidores o inactivadores, como internamente mediante una inactivación particular de esta enzima (inactivación suicida).

1.5.1. Inhibidores

Se han aislado e identificado un gran número de inhibidores tanto de fuentes naturales (Parvez et al., 2007) como sintéticos (Rescigno et al., 2002; Solano et al., 2006; Chang, 2009). Sin embargo, la definición de inhibidor de tirosinasa es a veces confusa, ya que algunos autores usan este término para definir como inhibidores aquellas moléculas que de una forma u otra desvían la ruta de biosíntesis de melaninas, por generar otras *o*-quinonas distintas a *o*-dopaquinona en lugar de que ocurra una interacción inhibidor/enzima directa. Muchos de estos inhibidores se estudian utilizando tirosina/dopa como sustratos y la actividad enzimática se sigue midiendo la formación de dopacromo. Así pues, la inhibición de tirosinasa puede ser clasificada, desde un punto de vista experimental, en diferentes tipos:

1. Agentes reductores que producen la reducción de *o*-dopaquinona a L-dopa. En este tipo se encuentran inhibidores clásicos como ácido ascórbico, que se utiliza como inhibidor de la melanogénesis ya que, al reducir la *o*-dopaquinona, impide la formación de dopacromo y, por tanto, la formación de melaninas.
2. Eliminadores de *o*-dopaquinona, que reaccionan también con esta y forman compuestos coloreados. En este tipo destacan los compuestos tiólicos como la cisteína que forma un aducto con la *o*-quinona y ralentiza el proceso de formación de eumelaninas hasta que el compuesto tiólico es consumido.
3. Sustratos enzimáticos alternativos. En este tipo se encuentran compuestos fenólicos cuyo producto quinónico absorbe en una longitud de onda del espectro electromagnético diferente a la del dopacromo. Cuando la enzima tiene una buena afinidad por estos compuestos, la formación de dopacromo disminuye y, por tanto, son clasificados erróneamente como inhibidores de la enzima.

4. Inactivadores enzimáticos no específicos. En este tipo se encuadran los ácidos y bases, los cuales inespecíficamente desnaturalizan a la enzima inactivándola.
5. Inactivadores específicos de tirosinasa. Estos son los inhibidores basados en el mecanismo de la enzima, entre los que destacan los sustratos suicidas. Inactivan irreversiblemente a la enzima induciéndole una inactivación suicida.
6. Inhibidores específicos de tirosinasa. Son aquellos inhibidores que se unen reversiblemente a la enzima reduciendo su actividad catalítica.

De todas estas clases, solo la 5 y la 6 se pueden considerar como verdaderos inhibidores ya que son los que se unen a la enzima e inhiben su actividad. Estos verdaderos inhibidores se pueden clasificar en cuatro subtipos: (a) inhibidores competitivos, (b) inhibidores acompetitivos, (c) inhibidores mezcla y (d) inhibidores no competitivos. En cualquier caso, debido a la inespecificidad de tirosinasa, el grado de inhibición de la enzima por cualquier inhibidor nuevo se compara con el ácido kójico, que es el inhibidor clásico de tirosinasa (Cabanes et al., 1994; Chen et al., 1991) (Figura 45). Recientemente, se han identificado y caracterizado los genes implicados en la síntesis de las enzimas que catalizan la biosíntesis del ácido kójico a partir de glucosa en *Aspergillus oryzae* (Terabayashi et al., 2010).

Otros inhibidores clásicos de referencia para tirosinasa son tropolona (Espín y Wichers, 1999b) y L-mimosina (Cabanes et al., 1987b) (Figura 45).

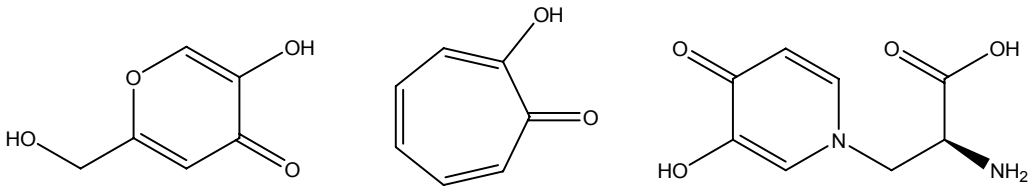

Figura 45. Estructuras químicas de los inhibidores de referencia de tirosinasa, ácido kójico, tropolona y L-mimosina.

Los inhibidores de tirosinasa pueden clasificarse en 5 clases principales, (a) polifenoles, (b) derivados del benzaldehido y del benzoato, (c) lípidos (triacilglicéridos) de cadena larga y esteroides, (d) Agentes hipopigmentantes y (e) inactivadotes, donde se encuadrarían los inactivadores suicidas y los inhibidores irreversibles.

1.5.1.1. Polifenoles

Los polifenoles representan un grupo muy diverso con múltiples funcionalidades y están ampliamente distribuidos en toda la escala filogenética. Además, probablemente sean el grupo más numeroso de compuestos inhibidores de tirosinasa, descritos hasta la fecha. Dependiendo en que posición en la molécula están los grupos hidroxilos, los polifenoles son considerados sustratos de tirosinasa o inhibidores de ella. Los flavonoides son los polifenoles más numerosos aislados y estudiados como sustratos/inhibidores de tirosinasa. Están ampliamente distribuidos en las hojas, raíces, semillas y flores de plantas. Se han descrito más de 4000 flavonoides en plantas. En ellas, se ha postulado que los flavonoides les confieren protección frente a radicación UV, patógenos o frente a herbívoros (Harbone y Williams, 2000). Los flavonoides se dividen en siete grandes grupos; flavonoles, flavonas, flavanonas, flavanoles, isoflavonoides, chalconas y cumarinas (Chang, 2009).

Flavonoles: Muchos flavonoles se han aislado de plantas y algunos de ellos se han descrito como inhibidores de tirosinasa. Sin embargo, son inhibidores muy débiles de la enzima por lo que son poco usados en cosmética o en la inhibición del pardeamiento.

Flavonas, flavanonas y flavanoles: La piel de los cítricos contiene una gran cantidad de flavonoides. Algunos de ellos se han estudiado como inhibidores de tirosinasa. Destacan la nobiletina (5,6,7,8,3´,4´-hexametoxiflavona), naringina (5,7,4´-trihidroxiflavanona), y la neohesperidina (5,7,3´-trihidroxi-4´-metoxiflavona). Sin embargo, estos inhibidores, comparados con la inhibición producida por el ácido kójico sobre tirosinasa, muestran una inhibición débil.

Además de la piel de los cítricos, los extractos de las especies de *Morus*, tienen una alta concentración de polifenoles y son potentes inhibidores de tirosinasa. Así, el mulberrósido F tiene una actividad inhibitoria de tirosinasa 4.5 veces más potente que el ácido kójico. Además, la norartocarpetina (Figura 46) es 40 veces mas potente que el ácido kójico con un modo de inhibición competitivo (K_I = 1.35 μM) (Ryu et al., 2008). La estreptogenina (flavanona, Figura 46) tiene una estructura muy similar a la norartocarpetina (flavona) con los mismos cuatro grupos hidroxilos. Esta flavanona muestra una inhibición muy similar a la norartocarpetina y el mismo mecanismo de inhibición competitivo.

Por otro lado, es importante tener en cuenta que las sustituciones en la estructura del flavonoide puede ocasionar una perdida de actividad inhibitoria. Así, se

ha demostrado que la metoxilación de un grupo hidroxilo en la posición C7 del esqueleto de la flavona ocasiona una 100 veces menos de inhibición que el compuesto sin el grupo metoxilo. Esto se ha demostrado al comparar artocarpetina (Figura 46) y norartocarpetina. Además, se ha sugerido que la mitad 3-hidroxi-4-ceto en el flavonoide es fundamental para la unión con los átomos de cobre del sitio activo de tirosinasa. Por último, los resultados sugieren que el número y la posición de los grupos hidroxilos son claves en el grado y modo de inhibición.

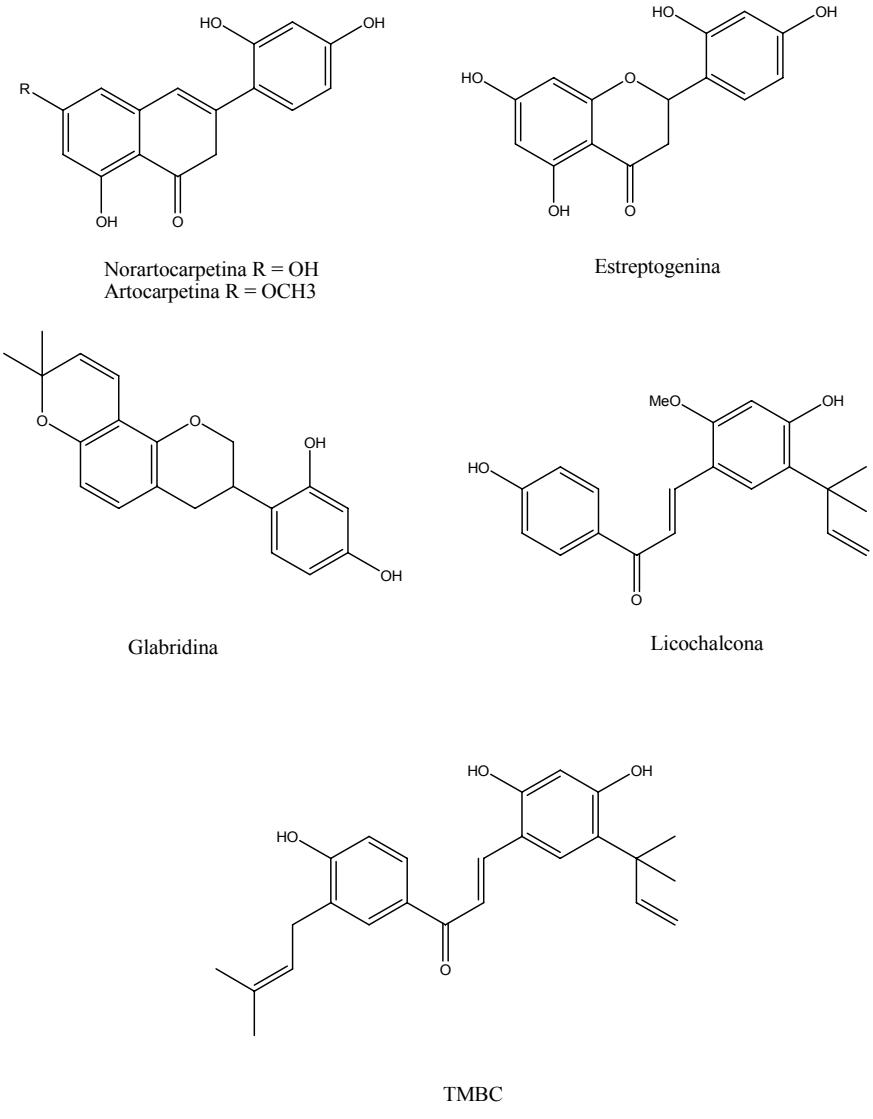

Figura 46. Estructuras químicas de los principales flavonoides inhibidores de tirosinasa. Se muestran algunos ejemplos de las subclases de flavonoides: flavonas (artocarpetina y norartocarpetina), flavanonas (estreptogenina), isoflavanos (glabridina) o chalconas (licochalcona y TMBC).

Isoflavonoide: Los extractos de las raíces de *Glycyrrhiza* (*Leguminoseae*) han sido muy estudiados como agentes despigmentantes en los países asiáticos. La glabridina (Figura 46) fue el primer compuesto estudiado y caracterizado como inhibidor de tirosinasa. Mostró una potencia inhibitoria 15 veces mayor que el ácido kójico mostrando un modo de inhibición no competitiva (Yokota et al., 1998).

Se ha demostrado la relación estructura/actividad en estos isoflavonoides donde se ha visto, que la posición y el número de grupos hidroxilos en el anillo A de la isoflavona afectan a la potencia y al modo de inhibición del compuesto. Así, una isoflavona con grupos hidroxilos en C6 y C7 del anillo A (6,7,4´-trihidroxiisoflavona) incrementa unas diez veces su grado de inhibición y la afinidad de la enzima por ella. Además, cuando los grupos hidroxilos se encuentran en las posiciones C7 y C8 del anillo A (7,8,4´-trihidroxiisoflavona y 5,7,8,4´-tetrahidroxiisoflavona), se cambia el modo de inhibición del compuesto de competitivo reversible a inactivación suicida irreversible (Chang, 2009).

Chalconas: Estructuralmente, las chalconas tienen dos anillos aromáticos en configuración *trans*, separados por tres átomos de carbono de los cuales dos están unidos por doble enlace y el tercero es un grupo carbonilo. Se han aislado tres derivados de chalconas (licurasida, isoquiritina y licochalcona; Figura 46) de raíces de *Glycyrrhiza*. Se comportan como inhibidores competitivos de la actividad monofenolasa de tirosinasa de *Agaricus bisporus*. La última de ellas, la licochalcona, tiene una potencia 5.4 veces más fuerte que el ácido kójico (Fu et al., 2005). Recientemente, se ha aislado la 2,4,2´,4´-tetrahidroxi-3-(3-metil-2-butenil)-chalcona (TMBC; Figura 46) de *Morus nigra*, este compuesto mostró un grado de inhibición 26 veces mayor que el ácido kójico respecto a la actividad difenolasa de tirosinasa (K_I = 1-1.5 μM) (Zhang et al., 2009). Nerya et al. (2004) han descrito que el grupo hidroxilo en C4 del anillo B en el esqueleto de la chalcona, es muy importante en el modo y grado de inhibición de ésta, probablemente debido a que la estructura resultante es muy similar a la del sustrato natural de la enzima, L-tirosina. Una acción similar ocurre cuando se encuentra el grupo N-benzilbenzamida en el esqueleto de la chalcona.

Estilbenos: Un estilbeno consiste en un eteno con un doble enlace sustituido con un anillo bencilo sobre los átomos de carbono del doble enlace. Oxiresveratrol (2,4,3´,5´-tetrahidroxi-*trans*-estilbeno; Figura 47) se aisló inicialmente de *Morus alba* y mostró 32 veces más inhibición hacia tirosinasa que el ácido kójico, actuando como inhibidor no competitivo sobre las actividades monofenolasa y difenolasa de la enzima (Shin et al., 1998). Como se muestra en la Figura 47, el oxiresveratrol también muestra

la estructura 4-resorcinol en el anillo B y la 5-resorcinol en el anillo A. Esto hace que el oxyresveratrol tenga 50 veces más poder inhibitorio que su análogo resveratrol (2,3´,5´-trihidroxi-*trans*-estilbeno).

Otros estilbenos que han sido aislados y caracterizados como fuertes inhibidores de tirosinasa son el gnetol (2,6,3´,5´-tetrahidroxi-*trans*-estilbeno; Figura 47) aislado de *Gnetum gnemom*, que mostró unas 30 veces más inhibición que el ácido kójico sobre la actividad difenolasa de tirosinasa (Ohguchi et al., 2003), o el piceatanol (3,5,3´,4´-tetrahidroxi-*trans*-estilbeno; Figura 47) aislado del vino tinto y que mostró unas 32.7 veces más de inhibición que el ácido kójico hacia la actividad monofenolasa de tirosinasa de *Agaricus bisporus* (Yokozawa y Kim, 2007).

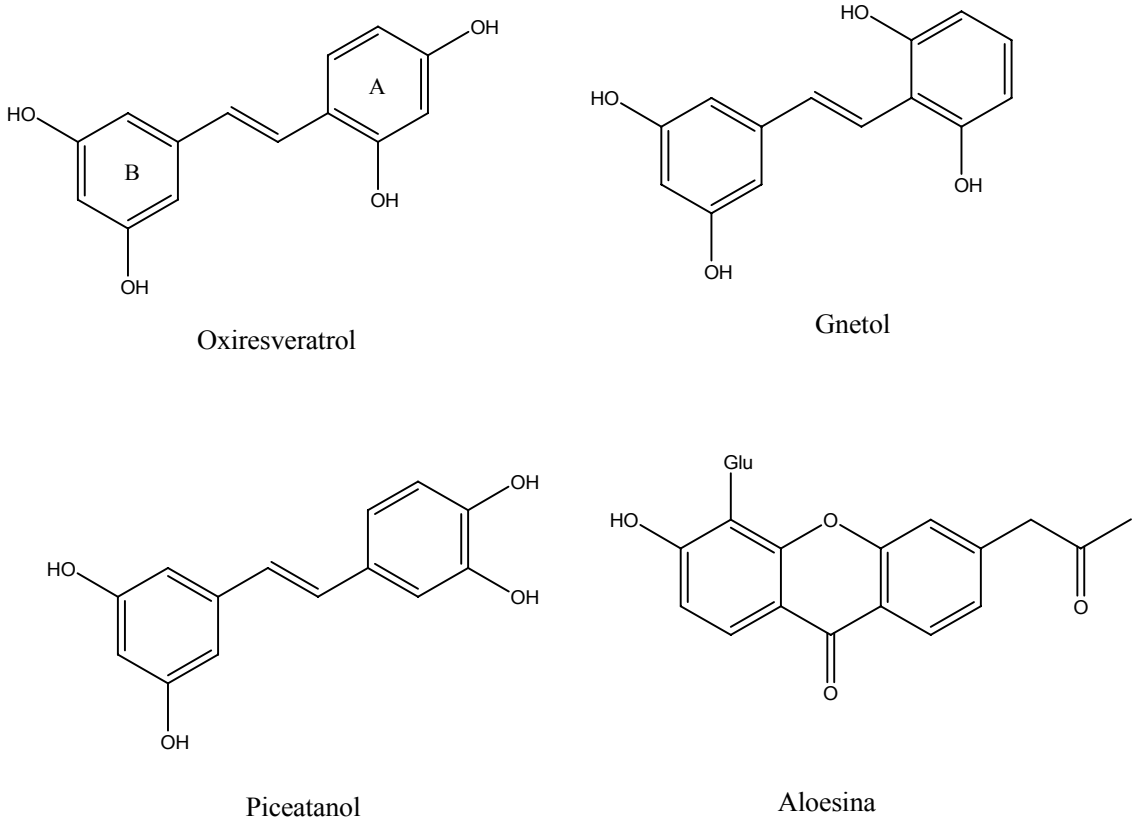

Figura 47. Estructuras químicas de los principales estilbenos y cumarinas inhibidores de tirosinasa.

Cumarinas: Las cumarinas son lactonas del ácido fenilpropanoico con un núcleo *H*-bezopiranona. Destaca la aloesina (Figura 47) que es una hidroxicumarina glucósido natural aislada del *Aloe vera*. Se utiliza en cremas en cosmética debido a su origen natural.

1.5.1.2. Derivados del benzaldehido y benzoatos

Se han descrito un amplio número de derivados del benzaldehido y del ácido benzoico como el propio ácido benzoico, benzaldehido, ácido anísico, anisaldehido, ácido cinámico o el ácido metoxicinámico (Figura 48) (Lee, 2002). El grupo aldehído es conocido que reacciona con grupos nucleofílicos importantes biológicamente como grupos sulfidrilos, amino o hidroxilos. Probablemente, el mecanismo de inhibición de estos tipos de inhibidores derivados del benzaldehído se produce por su capacidad de formar bases de Schiff con un grupo amino primario en la enzima (Kubo et al., 2000). Los derivados del ácido benzoico inhiben a tirosinasa uniéndose a los átomos de cobre del sitio activo de la enzima (Conrad et al., 1994).

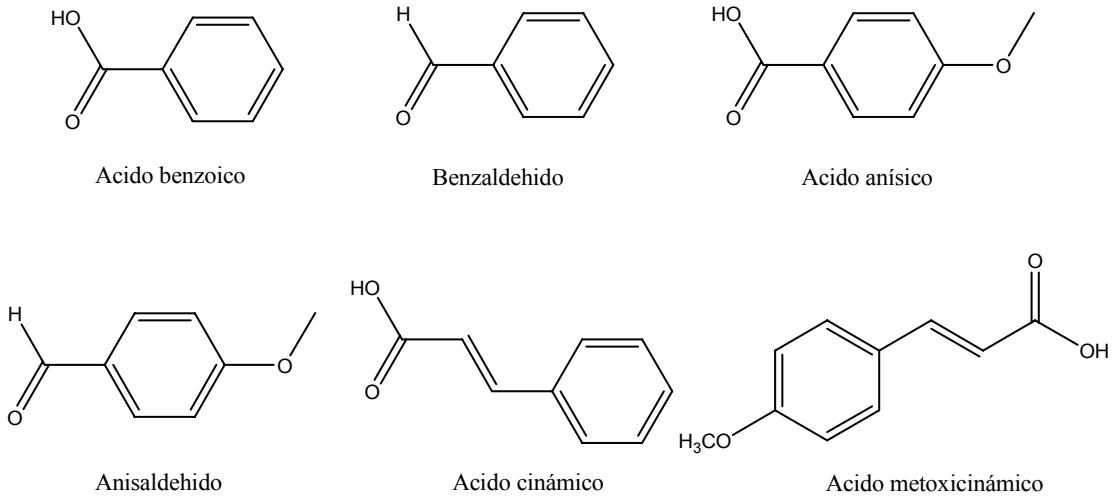

Figura 48. Estructuras químicas de los derivados del benzaldehído y del ácido benzoico como inhibidores de tirosinasa.

1.5.1.3. Lípidos (triacilglicéridos) de cadena larga y esteroides

Recientemente se han purificado numerosos lípidos de fuentes naturales que muestran actividad inhibitoria de tirosinasa. Un triacilglicerol del ácido linoleico (trilinoleína; Figura 49) se purificó de los subproductos de la producción del sake y se mostró igual de potente que el ácido kójico en la inhibición de la actividad difenolasa de tirosinasa de *Agaricus bisporus* (Jeon et al., 2006). El mecanismo de inhibición propuesto fue el de unirse a algunos sitios de tirosinasa, exceptuando el sitio activo de la enzima. Además, el ácido *trans*-geránico (Figura 49) ha sido recientemente purificado y caracterizado como inhibidor de tirosinasa con una potencia similar a la del ácido kójico (Masuda et al., 2008).

De la misma forma que los lípidos, los esteroides han mostrado inhibición de tirosinasa de forma bastante potente. En este sentido, destacan el estigmast-5-en-3β,26-diol (Figura 49) y el 2β(2*S*)-hidroxi-7(*E*)-tritriacontenoato que mostraron 7 y 12.3 veces mayor inhibición que el ácido kójico (Khan et al., 2005).

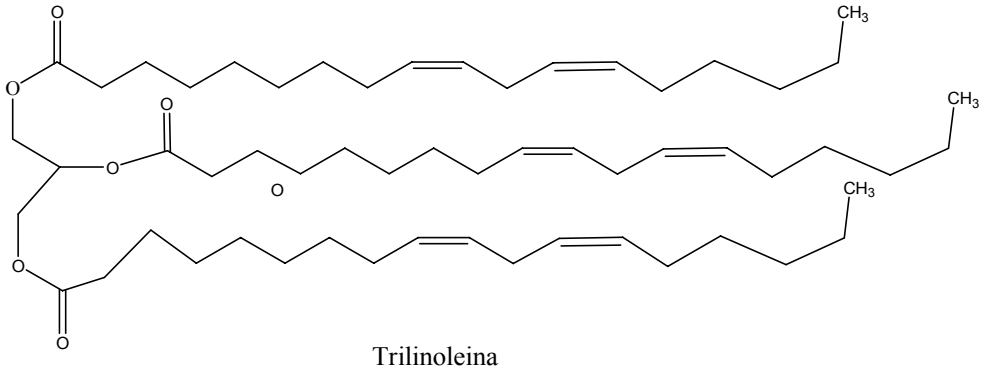

Trilinoleina

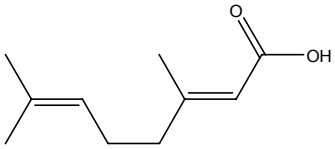

Acido geránico

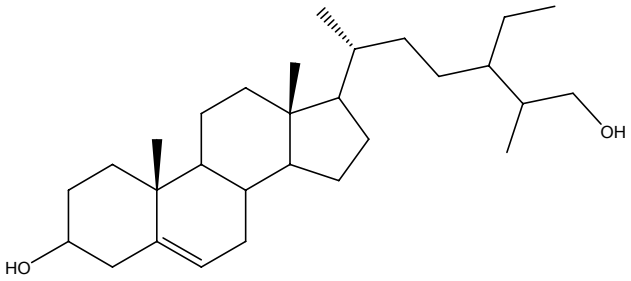

Estigmast-5-en-3β,26-diol

Figura 49. Estructuras químicas de algunos lípidos de cadena larga y esteroides que actúan como inhibidores de tirosinasa.

1.5.1.4. Agentes hipopigmentantes

En este apartado se muestran diferentes mecanismos de acción de agentes hipopigmentantes sobre la piel humana. Así, se pueden hacer diferentes enfoques:

(a) Inhibición de la maduración y aumento de la degradación de tirosinasa.
(b) Inhibición del factor de inducción de la transcripción asociado a microftalmia (MITF).
(c) Inhibición del receptor de melanocortina 1 (MC1R).
(d) Interferencia con la transferencia y maduración de melanosomas.
(e) Pérdida de melanocitos.

La principal aproximación es la inhibición de tirosinasa ya que ésta es la enzima clave en la regulación de la melanogénesis. Otros parámetros de estos agentes hipopigmentantes a considerar son la toxicidad, solubilidad, absorción cutánea, penetración y estabilidad. Para hacer los test de inhibición se recomendó

realizar los ensayos con piel humana o, al menos, con co-cultivos de melanocitos y queratinocitos (Solano et al., 2006).

1.5.2. Inactivadores

1.5.2.1. Inactivadores irreversibles

Este grupo de inhibidores irreversibles se caracterizan por formar enlaces covalentes con la enzima, induciendo su inactivación permanente. Estos compuestos actúan, normalmente, en el sitio activo de la enzima. Entre estos inhibidores destacan el captopril (Figura 50), el anión 3,5-dihidroxifenil decanoato o el cardol trieno (Figura 50). El captopril es un antihipertensivo que forma un complejo cobre-captopril a través de su grupo tiol libre lo que provoca la quelación del cobre y la inactivación de la enzima (Espín y Wichers, 2001). Recientemente (Zhuang et al., 2010), ha mostrado al cardol trieno como inhibidor competitivo irreversible de la enzima con una IC_{50} de 8 μM.

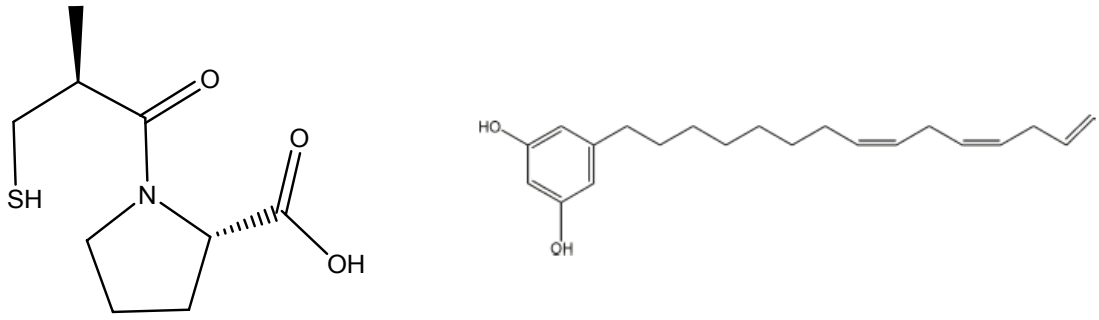

Captopril Cardol trieno

Figura 50. Estructuras químicas del captopril y del cardol trieno como ejemplos de inactivadores irreversibles de tirosinasa de *Agaricus bisporus*.

1.5.2.2. Inactivadores suicidas

Tirosinasa sufre un proceso de inactivación cuando reacciona con sus sustratos, un fenómeno que ha sido muy estudiado y caracterizado en la enzima de una gran variedad de fuentes naturales como hongos, plantas y animales (Ingraham et al., 1952; Lerch, 1983). El estudio de la inactivación por sustratos suicidas, también llamados inhibidores basados en el mecanismo, ha aumentado recientemente gracias a las aplicaciones farmacológicas que pueden tener y esto ha llevado al diseño de nuevos inhibidores de tirosinasa (Silverman, 1995; Zhong y Groutas, 2004; Ghanbari et al., 2006). Por ejemplo, se han diseñado inactivadores irreversibles (insecticidas) contra acetilcolinesterasa o sustratos suicidas de β-lactamasas (ácido clavulánico) que

ayudan a la acción de antibióticos (Walsh, 1984) El refinamiento de los métodos espectrofotométricos ha permitido el estudio sistemático de la cinética de inactivación suicida de la enzima por *o*-difenoles o trifenoles (García-Molina et al., 2007a).

La cinética de inactivación suicida de tirosinasa se describe por una serie de parámetros que caracterizan al sustrato suicida: λ_{max} (constante aparente de inactivación máxima), r (razón de partición o número de turnovers que realiza un mol de enzima antes de su inactivación), K_m^S (constante de Michaelis para el sustrato) y k_{cat} (constante catalítica).

Hasta la fecha de hoy, se han propuesto tres tipos de mecanismos para explicar el proceso de inactivación suicida en tirosinasa:

1. Un ataque del producto de la reacción, *o*-quinona, sobre un grupo del sitio activo (Ingraham et al., 1952).
2. Un ataque mediante radicales libres sobre el sitio activo de la enzima. Este ataque, por ROS (especies reactivas del oxigeno), se generarían durante el ciclo catalítico de la enzima (Seiji et al., 1978).
3. La presentación y oxidación de un *o*-difenol como si fuera un monofenol (presentación tipo cresolasa) (Land et al., 2007; Land et al., 2008; Ramsden et al., 2009).

Los dos primeros tipos de mecanismos actualmente se encuentran descartados ya que esta inactivación también ocurre incluso en presencia de NADH o ácido ascórbico lo que provoca que se reduzcan las *o*-quinonas a los *o*-difenoles iniciales. Además, al proteger a la enzima con eliminadores de radicales libres, la inactivación suicida también seguía ocurriendo (Dietler y Lerch, 1982).

Con respecto al tercer mecanismo, el cual implica la hidroxilación de un *o*-difenol como si fuera un monofenol (presentación tipo cresolasa), los autores sugieren que se origina un producto intermedio de la reacción que provoca una desprotonación y una eliminación reductiva en el mecanismo de la enzima (Land et al., 2007; Land et al., 2008; Ramsden et al., 2009; Ramsden y Riley 2010a; Ramsden y Riley, 2010b) (Esquema 12).

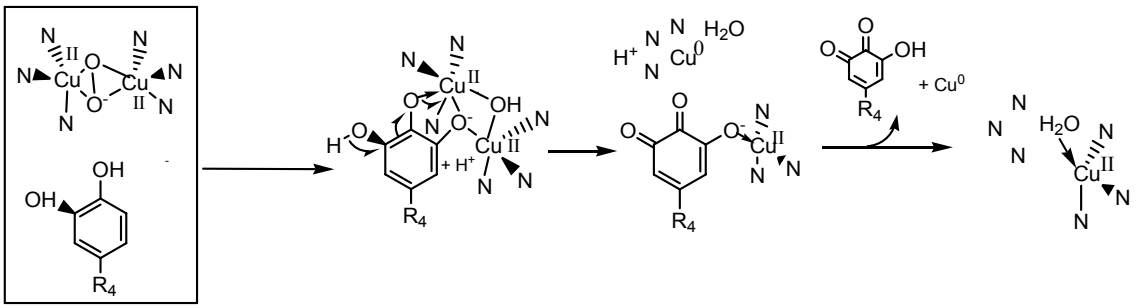

Esquema 12. Mecanismo propuesto para explicar la inactivación suicida de tirosinasa durante su actividad monofenolasa cuando actúa sobre *o*-difenoles (Land et al., 2007).

El mecanismo descrito en el Esquema 12 resalta la importancia de la estructura química de los sustratos en el mecanismo de inactivación suicida de tirosinasa. Según este mecanismo, cuando el sustrato es un trihidroxibenceno (por ejemplo pirogalol), la enzima no sufriría inactivación suicida, al igual que ocurre en el caso de los sustratos que tuvieran sustituyentes en C3 y C6 del anillo fenólico. Por último, este mecanismo propuesto en el Esquema 12 tampoco explicaría la inactivación suicida ocasionada por otras moléculas no fenólicas. Así, no explica la inactivación suicida de tirosinasa cuando actúa sobre el peróxido de hidrógeno (García-Molina et al., 2005), sobre el ácido ascórbico (Munoz-Munoz et al., 2009a), sobre el NADH (García-Molina et al., 2010b), sobre las tetrahidropterinas (Muñoz-Muñoz et al., 2011a) o sobre el ácido tetrahidrofólico (García-Molina et al., 2011).

Nuestro grupo de investigación GENZ ha realizado numerosos estudios sobre el mecanismo de inactivación suicida de tirosinasa de *Agaricus bisporus* (García-Canovas et al., 1987), de epidermis de rana (Tudela et al., 1987; 1988), y sobre peroxidasa de diferentes fuentes biológicas (Arnao et al., 1990; Hiner et al., 1996). Además, hemos estudiado la inactivación suicida de una enzima que puede ser medida a través de reacciones acopladas (Escribano et al., 1989) y hemos publicado un diseño experimental válido para caracterizar de forma sistemática la inactivación suicida de una enzima (García-Cánovas et al., 1989).

Recientemente, se ha avanzado mucho en el estudio y la comprensión del mecanismo de inactivación suicida de tirosinasa. Se han identificado potentes inactivadores suicidas de la enzima ya que son sustratos con un bajo valor de r y un alto valor de λ_{max}. Entre estos destacan una serie de isoflavonas: 6,7,4´-trihidroxyisoflavona, 7,8,4´-trihidroxiisoflavona, 5,7,8,4´-tetrahidroxiisoflavona y 8-

hidroxinaringenina (Chang et al., 2005; Chang, 2007; Chang et al., 2010). Estos compuestos han dado lugar recientemente a una patente como sustratos suicidas de la enzima (Chang y Wu, 2008).

Gracias a los numerosos estudios publicados sobre cinética enzimática de tirosinasa, nuestro grupo ha publicado recientemente un mecanismo cinético y estructural que explica la inactivación suicida de tirosinasa cuando actúa sobre todos sus sustratos, ya sean fenólicos o no. También se tienen en cuenta los nuevos avances en la estructura de la enzima, en la rigidez de las uniones de las histidinas del sitio activo y la existencia de dos pKas cinéticamente significativos en el mecanismo (Muñoz-Muñoz et al., 2010a; Muñoz-Muñoz et al., 2012). El mecanismo cinético se describe en el Esquema 13.

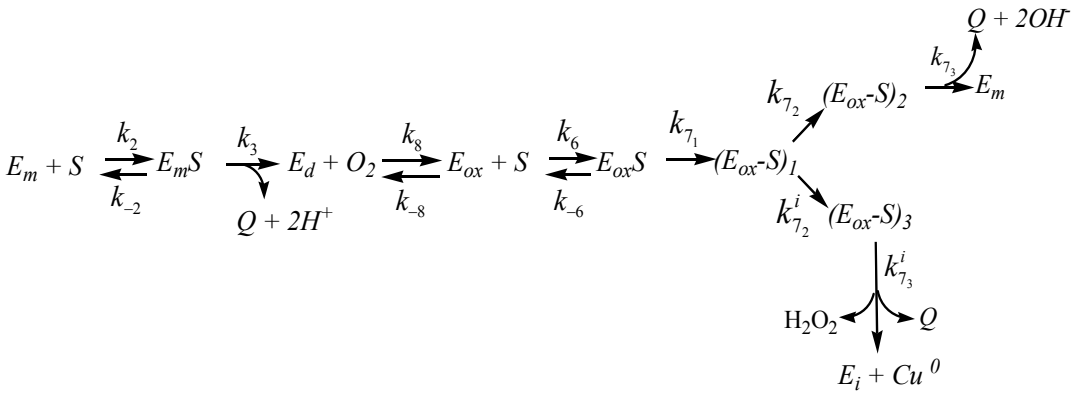

Esquema 13. Mecanismo cinético para explicar la ruta catalítica y la de inactivación suicida de tirosinasa de *Agaricus bisporus*. E_m = metatirosinasa, E_d = desoxitirosinasa, E_{ox} = oxitirosinasa, S = sustrato.

El mecanismo estructural se describe en el Esquema 14 cuando se trata de *o*-difenoles (Munoz-Munoz et al., 2012). Nótese como este mecanismo recoge la inactivación suicida provocada por los *o*-difenoles sustituidos en C3 y C6 del anillo fenólico. El mecanismo comienza con la bifurcación entre la ruta catalítica y la ruta de inactivación suicida a partir del complejo enzima-sustrato ($E_{ox}-\mathrm{S})_1$ que es el complejo donde el sustrato se encuentra unido a un átomo de cobre del sitio activo de la enzima (CuB). A continuación, se pueden producir dos posibilidades: (i) que el segundo protón del sustrato se transfiera a la base B_2 produciéndose la ruta difenolasa de la enzima

(Etapas 8 y 9 del Esquema 14) o (*ii*) que este protón sea transferido de nuevo al grupo peróxido y se produzca la inactivación suicida (Etapas 10 y 11). Como se observa en el Esquema 14, la inactivación suicida provoca que se libere Cu^0 del sitio activo de la enzima y se genere H_2O_2.

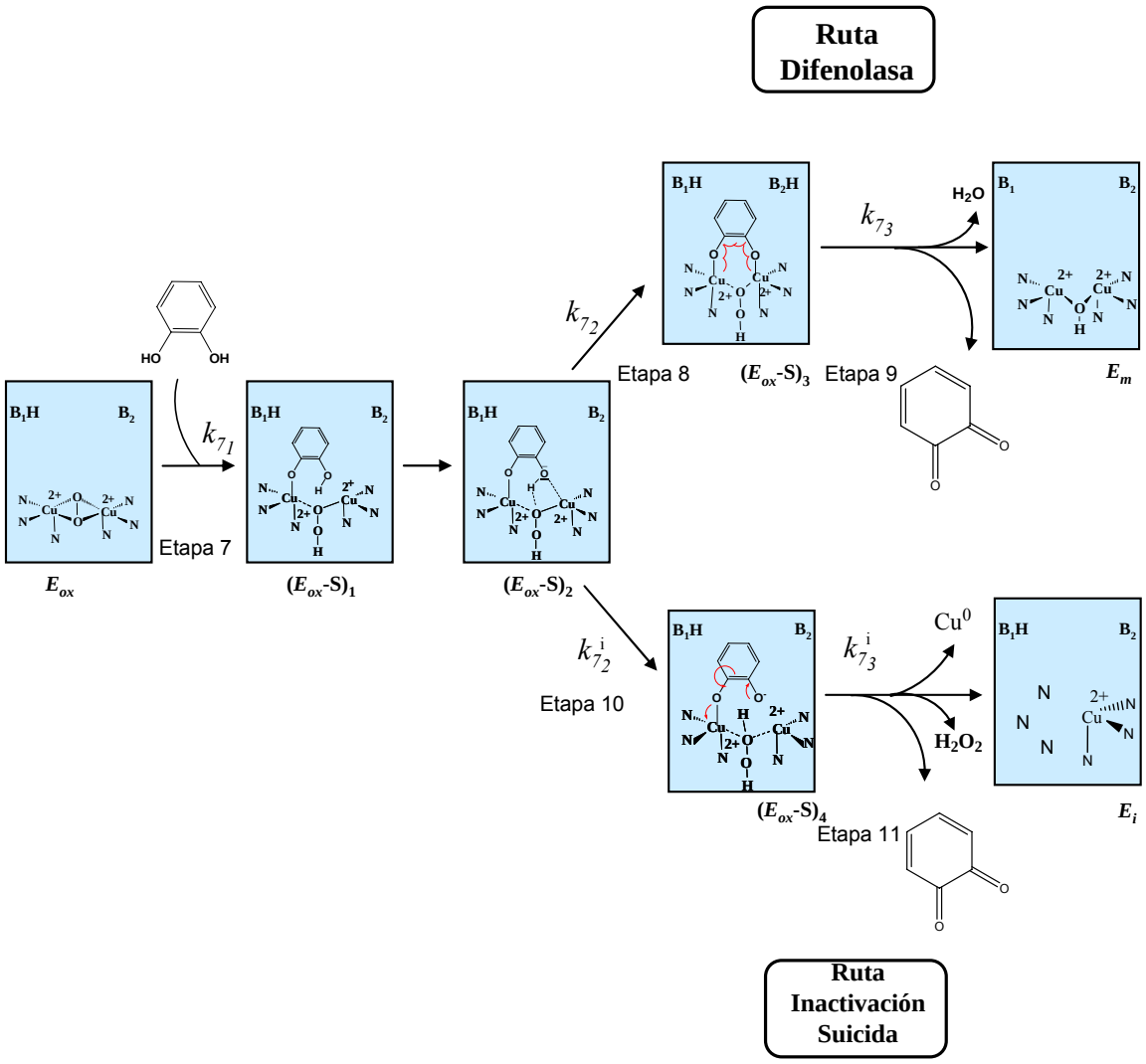

Esquema 14. Mecanismo estructural propuesto para explicar la inactivación suicida de tirosinasa de *Agaricus bisporus*.

A partir de este mecanismo se han caracterizado otras moléculas no fenólicas como sustratos suicidas de tirosinasa. Así, se ha caracterizado al peróxido de hidrogeno como sustrato suicida (García-Molina et al., 2005), al ácido ascórbico (Munoz-Munoz et al., 2009a), al NADH (García-Molina et al., 2010b), al ácido tetrahidrofólico (THF) (García-Molina et al., 2011), o a las tetrahidropterinas (Muñoz-Muñoz et al., 2011a) como sustratos suicidas de la enzima. El mecanismo estructural que describe este proceso de inactivación por H_2O_2 se muestra en el Esquema 15, en

el Esquema 16 para el caso del NADH y en el Esquema 17 para el THF. Este último sustrato se ha mostrado como uno de los sustratos suicidas más potentes descritos en la bibliografía.

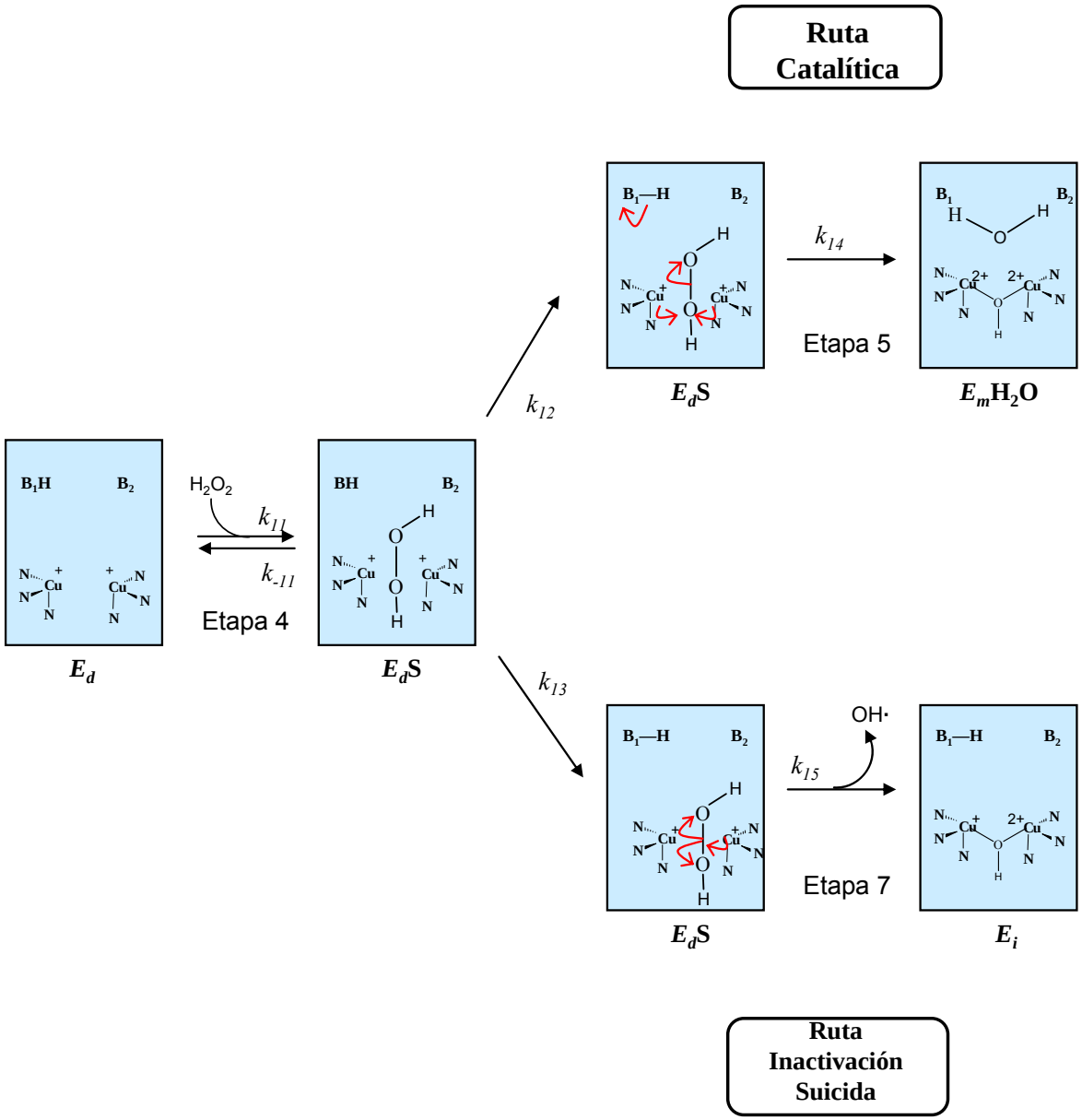

Esquema 15. Mecanismo estructural propuesto para explicar la inactivación suicida de tirosinasa de *Agaricus bisporus* al actuar sobre H_2O_2.

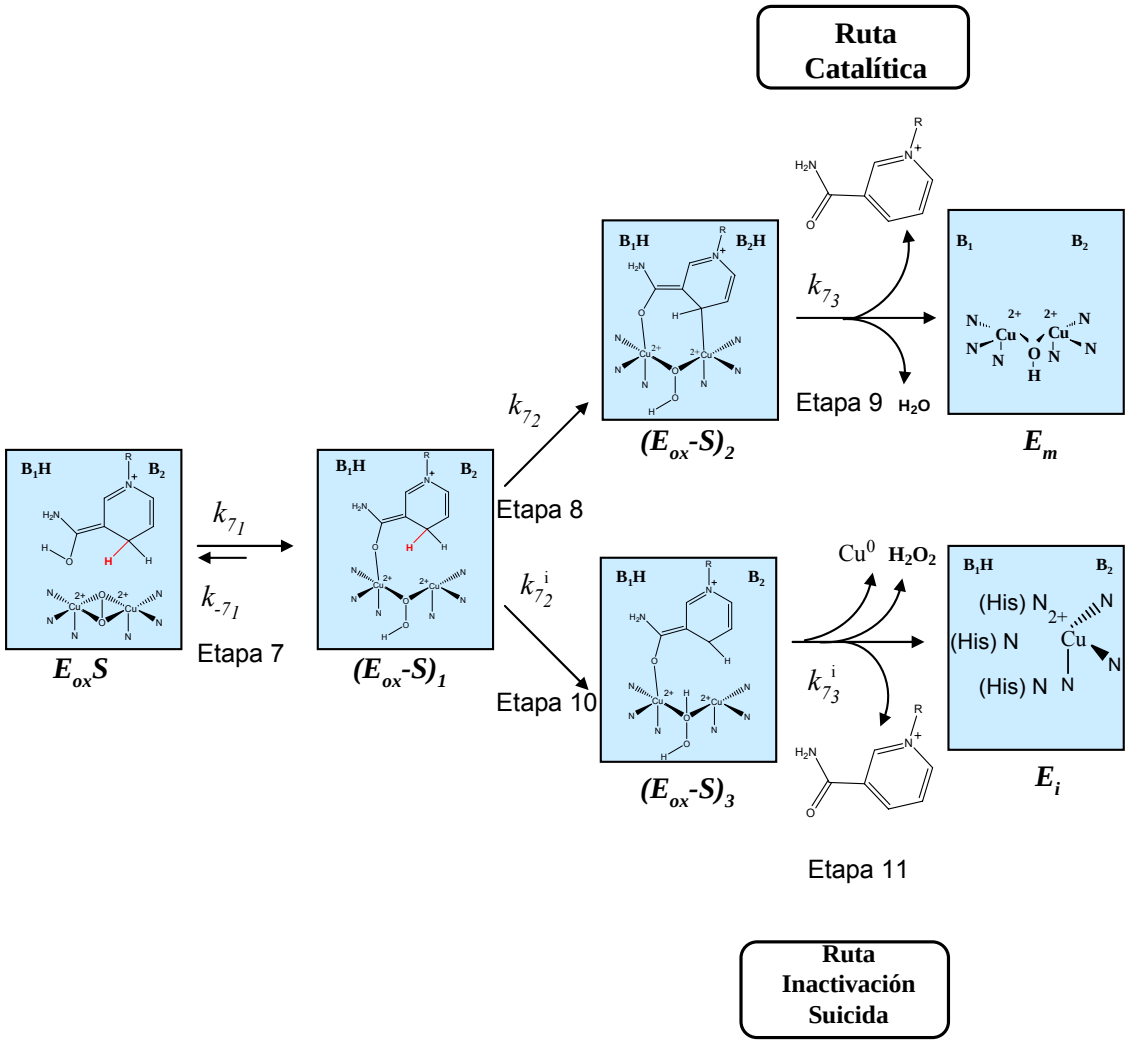

Esquema 16. Mecanismo estructural propuesto para explicar la inactivación suicida de tirosinasa de *Agaricus bisporus* al actuar sobre NADH.

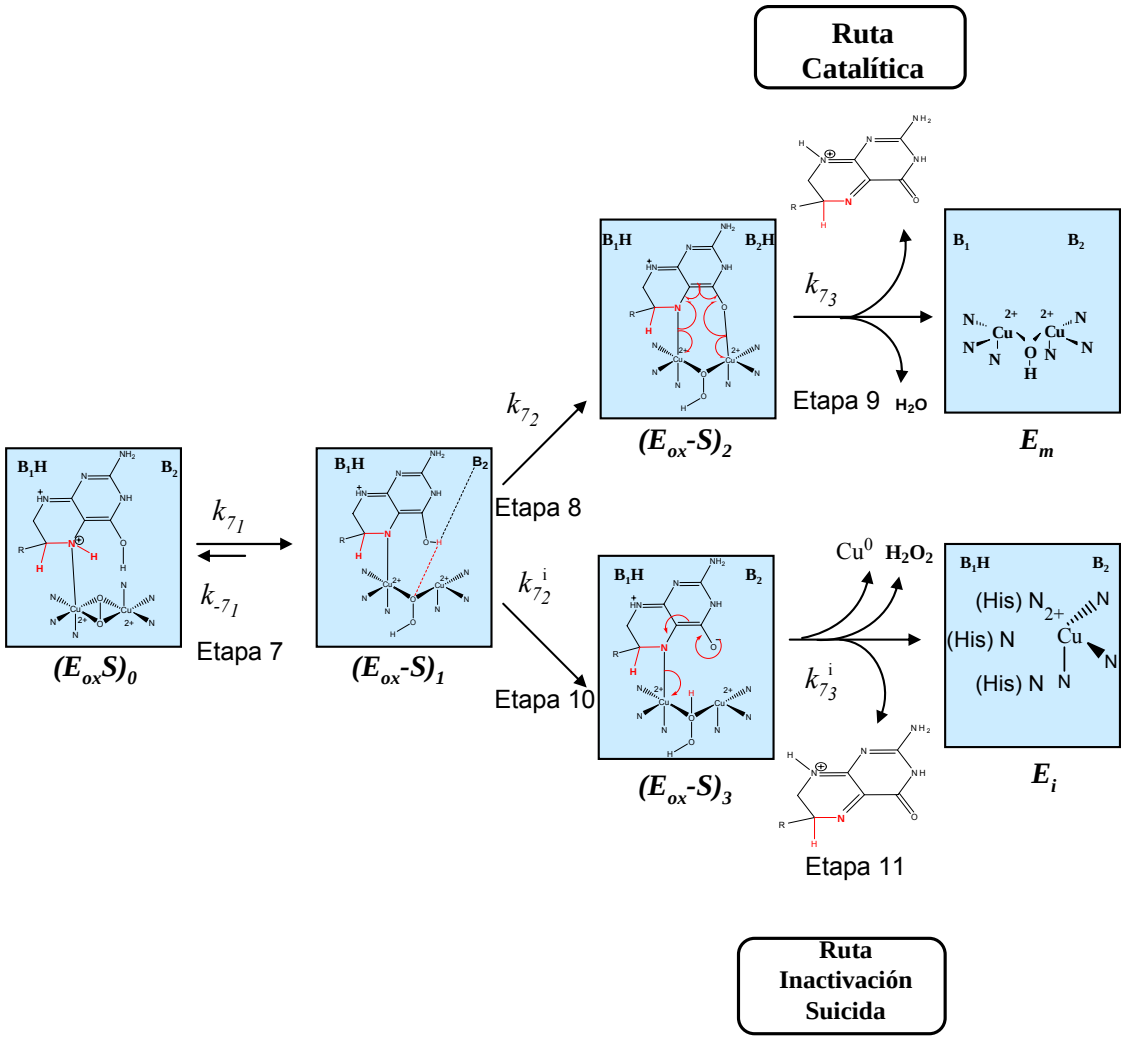

Esquema 17. Mecanismo estructural propuesto para explicar la inactivación suicida de tirosinasa de *Agaricus bisporus* al actuar sobre THF.

1.5.3. Diseño de inhibidores de tirosinasa

Como ya hemos indicado anteriormente, tirosinasa es la enzima clave en la regulación de la melanogénesis por lo que su inhibición ha atraído mucha atención, tanto desde el punto de vista biomédico como en cosmética, y sobre todo en relación al tratamiento de la hiperpigmentación (Kubo et al., 2000). Hasta la fecha se han identificado numerosos tipos de inhibidores de tirosinasa (ya sean naturales o sintéticos) (Kim y Uyama, 2005), pero solo unos pocos han mostrado eficacia en la reducción de la biosíntesis de melaninas (Briganti et al., 2003). Por lo tanto, el descubrimiento de nuevos inhibidores mucho más potentes que los actuales puede ser de importancia para las industrias farmacéutica y cosmética.

Actualmente, con la ayuda de métodos de simulación por ordenador, se ha estudiado la relación existente entre la estructura/actividad de numerosos compuestos y se ha ensayado los más prometedores a nivel experimental (Xue et al., 2008; Casañola-Martín et al., 2008; 2010; Marrero-Ponce et al., 2010). Además, recientemente se están diseñando compuestos sintéticos con estructura química similar a derivados bifenilos (Bao et al., 2010), a derivados de las vanillinas (Rescigno et al., 2011) y a derivados del ácido benzoico (Ha et al., 2012a; 2012b) (Esquema 18) gracias a los avances de la química orgánica. Por último, se han llevado a cabo estudios comparativos entre los distintos métodos de simulación por ordenador para la síntesis de nuevos inhibidores de tirosinasa (Le-Thi-Thu et al., 2011).

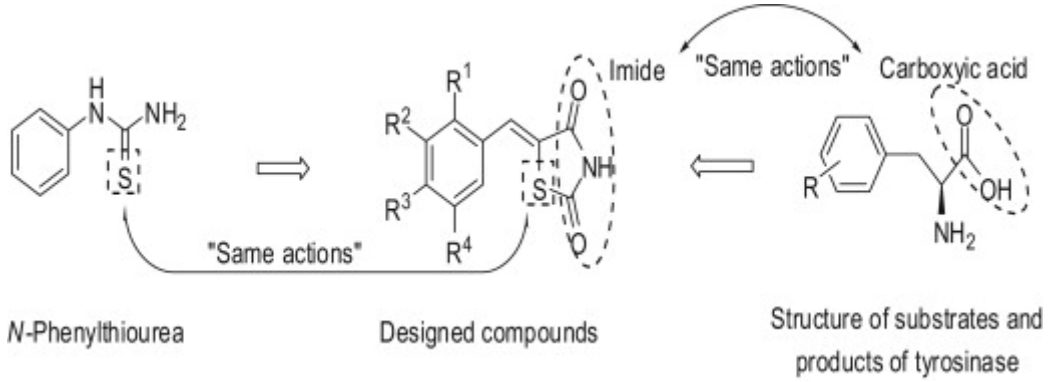

Esquema 18. Diseño de inhibidores de tirosinasa basados en el ácido benzoico.

1.5.4. Aplicaciones de los inhibidores

La inhibición de tirosinasa puede ser aplicada en varios campos entre los que destacan la agricultura e industria alimentaria, la industria de la cosmética y desde un punto de vista médico.

Agricultura e industria alimentaria: El pardeamiento de frutas y hortalizas es un problema de gran interés ya que produce unas pérdidas económicas muy elevadas anualmente. La velocidad del pardeamiento enzimático depende de la concentración de tirosinasa y compuestos fenólicos, de la disponibilidad de oxigeno, del pH y de las condiciones de temperatura del tejido (Martínez y Whitaker, 1995). Las técnicas convencionales actuales para disminuir el pardeamiento incluyen el uso del autoclave y el blanqueado, pero estos procesos causan importantes pérdidas de peso y nutrientes en el producto (Konanayakam y Sastry, 1988). Otro método utilizado es el uso de microondas pero tiene el inconveniente de que se forma un gradiente de temperatura en el producto (Decareau, 1985), lo que causa que, en las regiones más

calientes, hay inactivación de enzimas pero, en las regiones más frías, estas enzimas no están completamente inactivas.

Otra posible técnica es el uso de reactivos químicos como son las sales de haluros, ácidos aromáticos carboxílicos (Rouet-Mayer y Philipson, 1986) y otros compuestos que actúan como reductores como el ácido cítrico, ácido ascórbico y sus derivados (Santerre et al., 1988; Hsu et al., 1988) y compuestos tiólicos como la cisteína (Dudley y Hotchkiss, 1989). Actualmente, se suele utilizar 4-hexilresorcinol como inhibidor de tirosinasa ya que no tiene efectos secundarios perjudiciales para la salud descritos hasta la fecha (McEvily et al., 1991), además de que es muy efectivo en el control del pardeamiento enzimático (Frankos et al., 1991). Sin embargo, la seguridad alimentaria requiere una búsqueda continua de nuevos reactivos químicos menos perjudiciales y más potentes.

La regulación de tirosinasa también abarca el uso de altas temperaturas, elevada acidez, eliminación de sustratos fenólicos dentro del producto o la eliminación de oxigeno en éste. La eliminación de sustratos fenólicos se realiza con absorbentes como carragenatos, ciclodextrinas o quitosanos mientras que la eliminación del oxigeno en el producto es inaplicable experimentalmente ya que, en tejidos vivos, el riesgo de desviaciones metabólicas causadas por las condiciones anaerobias es muy alto. Una alternativa es la limitación de su disponibilidad con tecnologías post-cosecha basadas en atmósferas controladas o modificadas.

Industria cosmética: El uso de inhibidores de tirosinasa tiene un creciente interés en la industria cosmética debido a los efectos de prevención y de blanqueamiento de la piel que ocasionan. De todos los inhibidores de tirosinasa descritos hasta hoy, solo unos cuantos han sido utilizados como agentes despigmentantes principalmente debido a riesgos de toxicidad para uso humano. Entre estos agentes destacan el ácido linoleico, el hinokitiol, el ácido kójico, la arbutina o la hidroquinona que inhiben eficazmente a tirosinasa. Sin embargo, la hidroquinona también ha mostrado efectos secundarios (Maeda y Fukuda, 1991: Parvez et al., 2007). Actualmente, se utilizan la arbutina y la aloesina en cosmética. Estos compuestos se usan conjuntamente ya que se ha comprobado que el co-tratamiento con arbutina y aloesina produce una inhibición sinérgica de tirosinasa (Jin et al., 1999). La aloesina actúa mediante una inhibición no-competitiva mientras que la arbutina se comporta como inhibidor competitivo.

Desde el punto de vista médico, también se utilizan los inhibidores de tirosinasa en ensayos clínicos. Por ejemplo, recientemente se ha investigado el efecto de 8-

hidroxidaidzeina como sustrato suicida de la enzima, en células de melanoma B16 y en voluntarios humanos (Tai et al., 2009). Estos estudios mostraron que este sustrato suicida es 10 veces más potente que el ácido kójico al actuar tanto sobre células de melanoma y directamente, como crema despigmentante, sobre la piel humana.

1.5.5. Activadores

Se han realizado pocos estudios acerca de la acción de activadores sobre tirosinasa. Se ha discutido mucho acerca de la acción de iones metálicos divalentes sobre la enzima como Fe^{2+}, Cu^{2+}, Mn^{2+}, Ni^{2+}, Zn^{2+}, Co^{2+} o Cd^{2+} (Palumbo et al., 1985). El Co^{2+}, el Zn^{2+}, Cu^{2+} y el Ni^{2+} se han descrito como activadores (Gheibi et al., 2006; 2011).

Además, recientemente se ha evaluado los efectos de diferentes compuestos con la misma estructura aurona sobre las actividades monofenolasa y difenolasa de tirosinasa de *Agaricus bisporus* (Dubois et al., 2012). En estos estudios se propone que dependiendo donde se encuentre el grupo hidroxilo en el anillo B de la aurona, estos compuestos actuarán como activadores (Figura 51, moléculas A y B) o como sustratos (Figura 51, moléculas C y D) de la enzima.

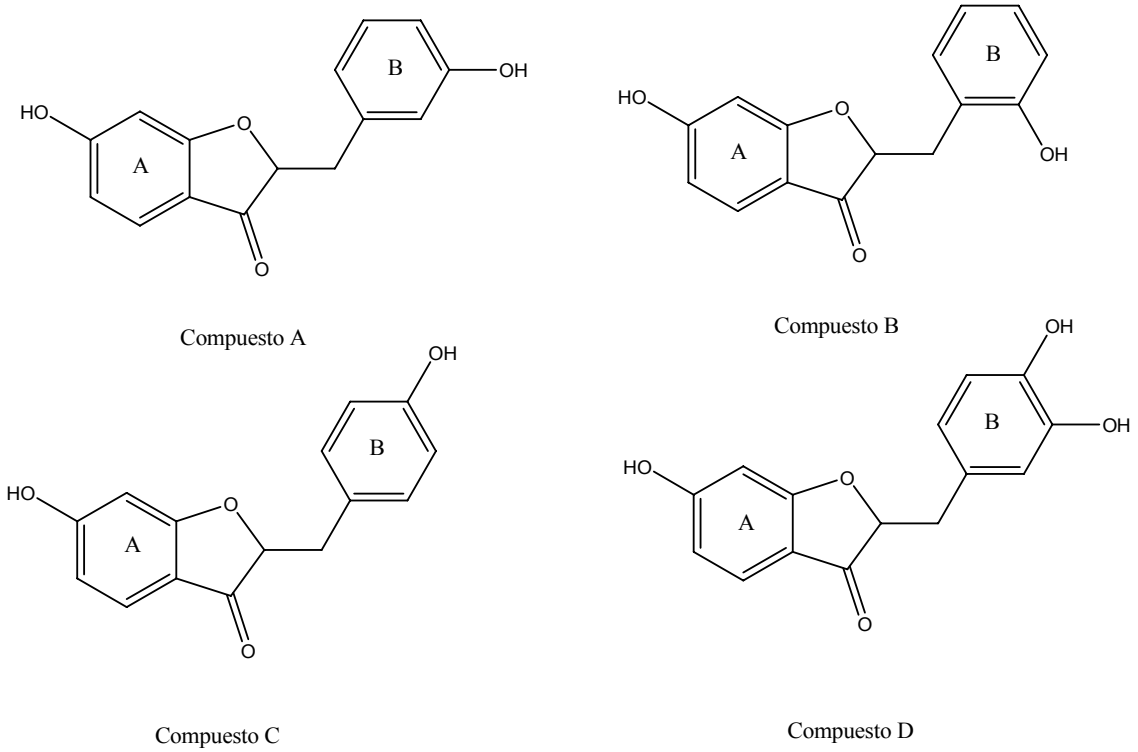

Figura 51. Estructuras químicas de las auronas descritas como activadores (A y B) o como sustratos (C y D) de tirosinasa de *Agaricus bisporus* (Dubois et al., 2012).

1.6. Tirosinasa: alteracciones de la pigmentación y diseño de fármacos

Las variaciones en el color de la piel en humanos vienen determinadas por la madurez de los melanosomas y no por el número de melanocitos. La relación de melanocitos/células basales es de 1:4 a 1:9 dependiendo de la región del cuerpo pero no de la raza. La hipopigmentación resulta de la reducción del número de melanocitos y/o melanosomas maduros y de la transferencia anormal de los melanosomas a los queratinocitos vecinos. La hiperpigmentación es debida a un incremento en la producción de pigmento melánico, originado por incremento de melanocitos y/o de la actividad de tirosinasa y por el recambio de melanina (Fistarol e Itin, 2010).

A continuación se tratarán los principales desordenes pigmentarios que pueden ser hipopigmentarios e hiperpigmentarios. Por último, debido a su incidencia creciente trataremos el cáncer de piel o melanoma maligno.

1.6.1. Hipopigmentación

Se han descrito múltiples desórdenes hipopigmentarios entre los que destacan el vitiligo, el albinismo oculocutáneo y los síndromes de Hermansky-Pudlak, Chediak-Higashi y Griscelli.

Vitiligo: El vitiligo es una enfermedad autoinmune, caracterizada por una hipopigmentación del pelo y por una eliminación total de los melanocitos en la capa basal de la epidermis (Figura 52). Suele manifestarse sobre todo en extremidades tanto superiores como inferiores. Se ha comprobado que tirosinasa, además de ser la enzima clave en la melanogénesis, es un autoantígeno en varios desórdenes pigmentarios. Mediante ensayos de ELISA, se han encontrado anticuerpos antitirosinasa en el suero de pacientes de vitiligo. Estos anticuerpos pueden servir como marcadores para esta enfermedad (Baharav et al., 1996).



Figura 52. Mano y piel afectadas por vitiligo.

Albinismo oculocutáneo (OCA): El albinismo oculocutáneo es un desorden hereditario autosómico recesivo, caracterizado por hipopigmentación en piel, pelo y ojos (Figura 53) acompañado normalmente por fotofobia (Kondo y Hearing, 2011). Los defectos en la biosíntesis de melaninas o en el transporte provocan que los pacientes con OCA tengan deficiencia o ausencia total de melanina. Esta enfermedad puede ser subdividida en seis subclases: OCA1A, OCA1B, OCA1-TS (ésta es sensible a la temperatura), OCA2, OCA3 y OCA4 (Dessinioti et al., 2009).



Figura 53. Albinismo oculocutáneo (OCA).

El subtipo más importante por el número de casos que se producen, es el OCA1A cuyos pacientes presentan una pérdida total de actividad tirosinasa debido a

una mutación en su gen codificante (Boissy y Nordlund, 1997). No se forma melanina durante toda la vida del paciente con lo que el fenotipo característico de éste es la piel y el pelo completamente blancos y pupilas rojas (Figura 53) (Giebel et al., 1991).

Síndrome Hermansky-Pudlak: El síndrome de Hermansky-Pudlak es un grupo genéticamente heterogéneo de desordenes autosómicos recesivos descritos en humanos. Hay ocho genes en humanos que producen este síndrome lo que da lugar a ocho subtipos. Defectos en las proteínas que codifican estos genes pueden afectar a la biogénesis y/o función de melanocitos y células epiteliales de la retina. El síndrome de Hermansky-Pudlak se caracteriza por presentar un fenotipo muy similar al de OCA pero estos pacientes pueden presentar desde una reducción mínima a una ausencia total en la producción de melanina.

Síndrome Chediak-Higashi: Este síndrome es un desorden raro autosómico recesivo que se caracteriza por la hipopigmentación en pelo y piel, por discapacidades neurológicas y por deficiencia inmune severa debido a la pérdida de la función de muerte celular natural.

Síndrome Griscelli: Es un extraño desorden autosómico recesivo caracterizado por el pelo y la piel blancos y acumulación de grandes y anormales melanosomas de última etapa en el centro de los melanocitos (Spritz et al., 2003). Se subdivide en tres tipos: GS1 que manifiesta discapacidades neurológicas y retraso mental, GS2 asociado con defectos inmunológicos letales y GS3 que solo tiene manifestaciones dermatológicas.

1.6.2. Hiperpigmentación

La hiperpigmentación se caracteriza por un aumento en la cantidad de melanina. El principal desorden con hiperpigmentación es el melasma que es un proceso que ocurre en mujeres jóvenes de piel canela asociado a cambios hormonales en los estrógenos y la progesterona (Figura 54). Esta alteración de la pigmentación se subdivide en epidérmico y dérmico. En el epidérmico, hay un incremento de la deposición de melanina en los estratos basal y suprabasal de la epidermis mientras que, en el dérmico, la melanina se deposita en macrófagos perivasculares de los plexos vasculares. Recientemente, se ha publicado una revisión sobre agentes hipopigmentantes donde se describen sus mecanismos de acción sobre desordenes como el melasma (Kim et al., 2012).



Figura 54. Mujer con melasma tipo epidérmico.

1.6.3. Melanoma

El melanoma es el nombre genérico de los tumores melánicos o pigmentados. Se trata de un tumor generalmente cutáneo, pero también del intestino y el ojo (melanoma uveal) y muy invasivo ya que es capaz de generar metástasis. Se diagnostican cada año cerca de 160.000 casos nuevos de melanoma en el mundo y resultan más frecuentes en hombres y personas de raza blanca que habitan en regiones con climas soleados. De acuerdo con la Organización Mundial de la Salud, hay cerca de 48000 muertes cada año relacionadas con el melanoma. Además, cerca del 75% de las muertes asociadas al cáncer de piel se relacionan con el melanoma maligno. Por lo general, el riesgo de un individuo de contraer un melanoma depende de dos grupos de factores: genéticos y ambientales. Los genéticos incluyen la historia familiar y el genotipo heredado, mientras que los ambientales incluyen la exposición a la luz solar. Existen diferentes tipos y morfologías de melanoma entre los que destacan el melanoma de diseminación superficial que representa el 70% del total de melanomas (Figura 55) y el melanoma nodular (15% del total) (Figura 56).

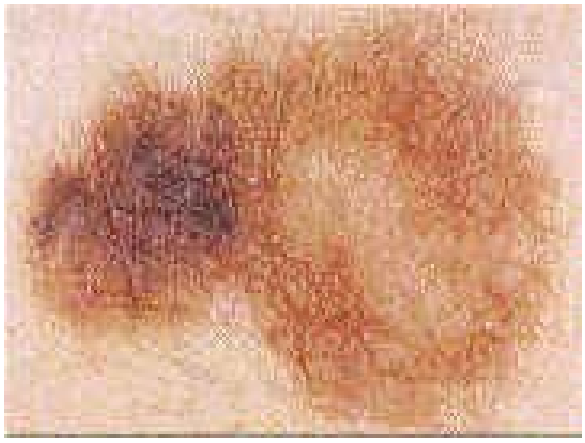

Figura 55. Melanoma de diseminación superficial.



Figura 56. Melanoma nodular.

Melanogénesis en el diagnóstico de melanoma. La capacidad de sintetizar melanina que tienen los melanomas se utiliza para hacer el diagnóstico diferencial con otros tipos de tumores. La melanina puede detectarse por las tinciones histológicas estándares o con métodos específicos como el de Fontana-Masson. La concentración y el tipo de melanina (eumelanina o feomelanina) puede ser determinada por resonancia de espín electrónico (Sealy et al., 1982). La detección y cuantificación de melaninas proporcionan información útil acerca de las opciones terapéuticas y más todavía, la melanina puede atenuar el efecto de la radioterapia, fototerapia o quimioterapia (Slominski et al., 1998).

Inmunohistoquímica. Se han establecido marcadores de diferenciación melanocítica que son muy útiles en el diagnóstico del melanoma. El marcador más sensible para el diagnóstico de melanoma dermoplásico es el S100B (proteína enlazante de calcio de la familia S100 tipo B) (Ohsie et al., 2008).

Existen otro tipo de marcadores, los de proliferación. Tienen dos aplicaciones clínicas: a) diagnóstico de la diferenciación de nevus benignos a melanoma maligno, b) establecimiento de un pronóstico clínico para pacientes con melanoma maligno. Las ciclinas A, B, D1 y D3 son marcadores que se visualizan raramente en nevus benignos y frecuentemente en melanomas.

Como ya hemos indicado anteriormente, el melanoma maligno es la mayor causa de muerte relacionada con cáncer de piel en el mundo. Se piensa que la transformación melanocítica ocurre por acumulación secuencial de alteraciones genéticas y moleculares (Miller y Mihm, 2006; Wolchok y Saenger, 2007). Se han encontrado varias rutas involucradas en las alteraciones clonales primarias, incluyendo la proliferación celular (ruta proliferativa) o la superación de la senescencia celular (ruta senescente) y la disminución de la apoptosis, requerida para el desarrollo del melanoma avanzado (ruta apoptósica). El 90 % de los melanomas son esporádicos y de ellos el 50 % sufren mutaciones BRAF (Miembro de la familia RAF: Familia de genes que codifican quinasas de serina y treonina) y un 25 % sufre mutaciones NRAS (RAS (RAt Sarcoma: Proteínas de membrana unidas a proteínas G) (Gray-Schopfer et al., 2007)). Es difícil encontrar ambas mutaciones juntas.

Tanto BRAF como NRAS pertenecen a la ruta de transducción de señales MAPK (Mitogen-activated protein kinase). La señalización MAPK se inicia en la membrana celular, tanto por la unión de un ligando o por adhesión de integrinas al receptor de tirosina quinasa (RTKs), lo cual transmite señales de activación por medio de la RAS-GTPasa de la superficie interna de la membrana celular. El GTP unido a RAS, puede unirse a proteínas efectoras como RAF o fosfatidilinositol 3 kinasa (PI3K) (Campbell y Der, 2004; Giehl, 2005) (Figura 57).

El gen BRAF, por sustitución simple puede ser activado. Mutaciones de este gen se ven en muchos cánceres como los de ovario, tiroides (Kimura et al., 2003), etc., pero en el melanoma es donde el nivel de mutaciones BRAF encontradas ha sido mayor (Palmieri et al., 2007). La activación del BRAF induce constitutivamente la señalización MEK-ERK (Extracelular signal regulated kinase) en células (Wan et al., 2004). La activación de BRAF conduce a la inducción de la expresión del MITF, reconocido como el mayor regulador de los melanocitos. El BRAF activado participa en el control de la progresión del ciclo celular (Carreira et al., 2005) (Figura 57).

La presencia de mutaciones BRAF en los nevus sugiere que dichas mutaciones son necesarias pero no son suficientes para el desarrollo del melanoma

(Patton et al., 2005). En conclusión, el BRAF activado induce proliferación celular y supervivencia celular, lo que representa dos hechos biológicos que ocurren en la expansión melanocítica de los nevus y en la progresión maligna desde enfermedad superficial a invasiva (Pollock et al., 2003).

Como ya hemos indicado en el capitulo 1.2.4.3., en ratones, MC1R es estimulado por α-MSH y activa la vía de las MAPK quinasas (ERK1/ERK2) por medio del AMPc. En humanos, sin embargo, las variantes de MC1R asociadas con pelo rojo y piel clara, que cursan con un incremento de cáncer de piel, MC1R activa el ERKs de forma independiente al AMPc. Esta activación del ERK por α-MSH resulta de la fosforilación mediada por la tirosina quinasa del c-KIT (receptor del stem cell factor), receptor tirosina quinasa esencial para la proliferación y supervivencia de los precursores de los melanocitos (Herraiz et al., 2011b).

El gen CDKN2A (Cyclin-Dependent Kinase Inhibitor 2A), también llamado supresor multi-tumor (MTS1) es el mayor gen involucrado en la patogénesis del melanoma y la predisposición al mismo (Stone et al., 1995), y codifica las proteínas $p16^{CDKN2A}$ y $p14^{CDKN2A}$ que son supresoras de tumores. La inactivación del CDNK2A puede ser por deleción, mutación o silenciamiento del promotor. La $p16^{CDKN2A}$ inhibe la actividad de CDK4 (cyclin D-1-cyclin-dependent-kinase 4), encargada de fosforilar la proteína del retinoblastoma. Esta proteína fosforilada libera el factor de transcripción E2F que se une al ADN, estimula la síntesis de proteínas necesarias para la transcripción y promueve la progresión del ciclo celular (Pacificio y Leone, 2007). La $p14^{CDKN2A}$ estabiliza p53 interactuando con la proteína MDM2 (Murine Double Minute-2) que promueve la degradación del producto del gen supresor de tumores p53 por el proteosoma, ubiquitinizándolo (Stott et al., 1998; Fang et al., 2000) (Figura 57).

El gen PTEN (phosphatase and tensin homolog deleted on chromosome 10), se encuentra mutado en una gran cantidad de melanomas. La proteína codificada por el PTEN es un importante supresor de tumores que controla la división celular, la migración y la apoptosis, preservando a las células de un crecimiento y división demasiado rápido e incontrolado (Tamura et al., 1998).

MITF (Microphtalmia-associated transcriptor factor). Es el factor regulador de melanocitos por excelencia. En humanos las mutaciones en el MITF producen el síndrome de Waardenburg IIa, que cursa con pelo blanco y sordera (Hughes et al., 1994). Altos niveles de MITF exhiben actividad anti-proliferativa en células con melanoma (Wellbrock y Marais, 2005). Se han encontrado bajos niveles de MITF en células invasivas de melanoma (Hoek et al., 2008) y se han asociado con peor

pronóstico clínico de la enfermedad (Salti et al., 2000), especulándose que el MITF puede ser un factor pronóstico. En melanomas, el MITF tiene como diana un gran número de genes con comportamientos antagonistas, (McGill et al., 2002; Du et al., 2004; Loercher et al., 2005). Además, MITF está al final de dos rutas antiapoptósicas, la del ERK y la del PTEN, sugiriendo que MITF puede integrar las señales extracelulares pro-supervivencia. La expresión y funcionamiento del MITF puede ser regulada por un abanico de factores de transcripción cooperantes: Pax3, CREB, Sox10, Lef1, Brn-2 (Thomson et al., 1995; Goding, 2000) y miembros del MAPK y cAMP (Bertolotto et al., 1996; Bertolotto et al., 1998; Hemesath et al., 1998).

En el 90% de melanomas se encuentra hiperfosforilación de ERK, con mutaciones de BRAF, (50-70%), (Libra et al., 2005) y NRAS, (15-25%) (Dahl y Guldberg, 2007). Se puede encontrar una predisposición familiar en el 10% de los individuos diagnosticados de melanoma (Platz et al., 2000). Las dos alteraciones más frecuentes son mutaciones y deleciones del CDKN2A, y mutaciones puntuales en CDK4 (Palmieri et al., 2009).

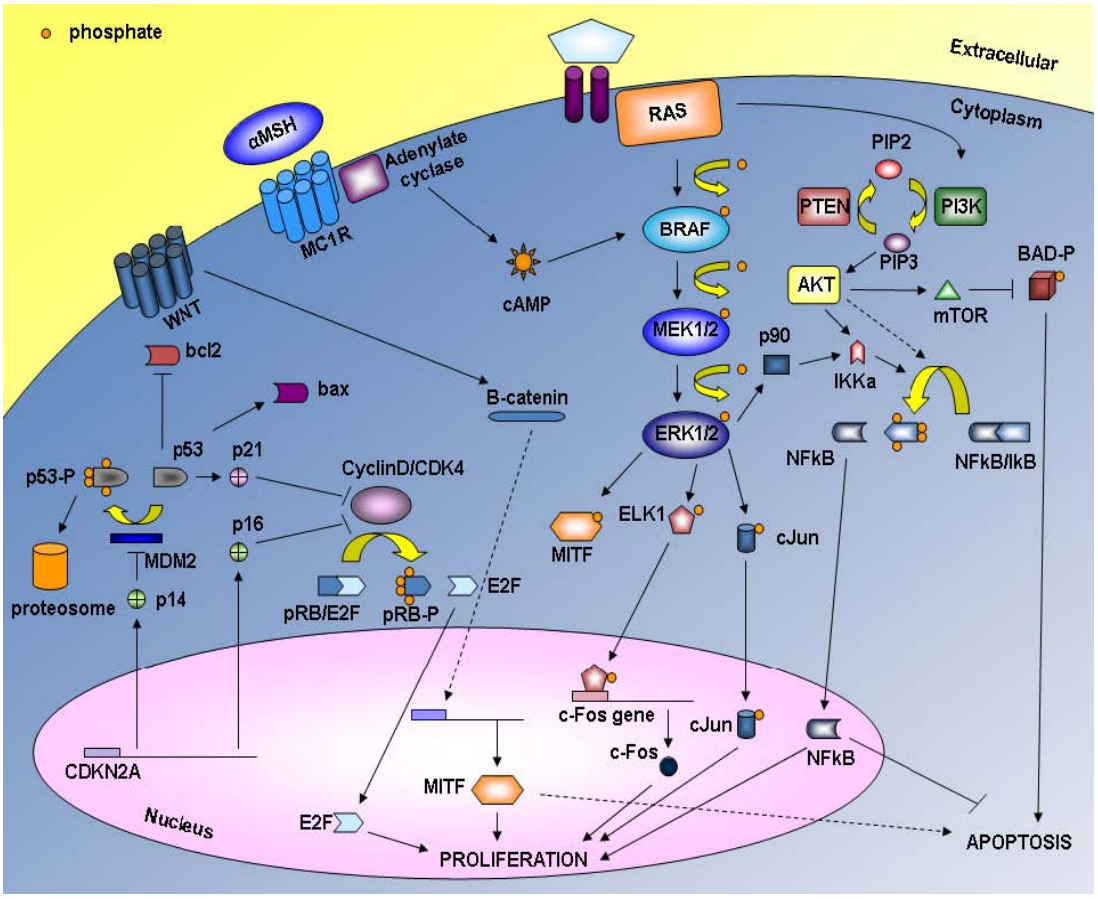

Figura 57. Principales rutas involucradas en el melanoma. Rutas asociadas con N-RAS, BRAF, MAPK (mitogen-activated proteín kinase), CDKN2A y MITF. Las flechas indican señales activadoras, mientras que las líneas cortadas quieren decir señales inhibidoras. Las abreviaturas usadas fueron: BAD, BCL-2 antagonist of cell death; cAMP, cyclic AMP; CDK4, Cyclin-dependent kinase 4; CDKN2A, Cyclin-dependent kinase inhibitor of kinase 2A; ERK 1/2, Extracellular-related kinase 1 or 2; IkB, inhibitor of kB protein; IKK, Inhibitor of kB-protein kinase; MCIR, melanocortin-l-receptor; MITF, Microphtalmia-associated transcription factor; MEK1/2, Mitogen activated protein kinase-extracellular related kinase I/2; PI3K, Phosphatidylinositol 3 kinase; PIP2, Phosphatidylinositol biphosphate; PIP3, Phosphatidylinositol triphosphate; PTEN, Phosphate and tensin homologue (Palmieri et al., 2009).

En cuanto al tratamiento del melanoma, actualmente se siguen tres estrategias:

1. Cirugía.
2. Tratamiento adyuvante como radioterapia o quimioterapia.
3. MEDPT: Como una estrategia dirigida a la terapia del melanoma maligno se ha diseñado la técnica denominada MDEPT (Melanocyte-Directed Enzyme Prodrug Therapy) (Jordan et al., 1999; 2001). En este tipo de estrategias, el compuesto o droga tiene que ser un sustrato de tirosinasa dirigido hacia el

tratamiento del melanoma. La liberación del fármaco activo se produce al actuar la enzima sobre el sustrato con lo que éste debe tener una parte fenólica en su estructura para que la enzima pueda oxidarlo y, así, favorecer la liberación del fármaco. Otro requerimiento que deben cumplir estos compuestos es que el fármaco debe ser estable hasta que ocurra su liberación. Un esquema de este tipo de estrategias se representa en la Figura 58.

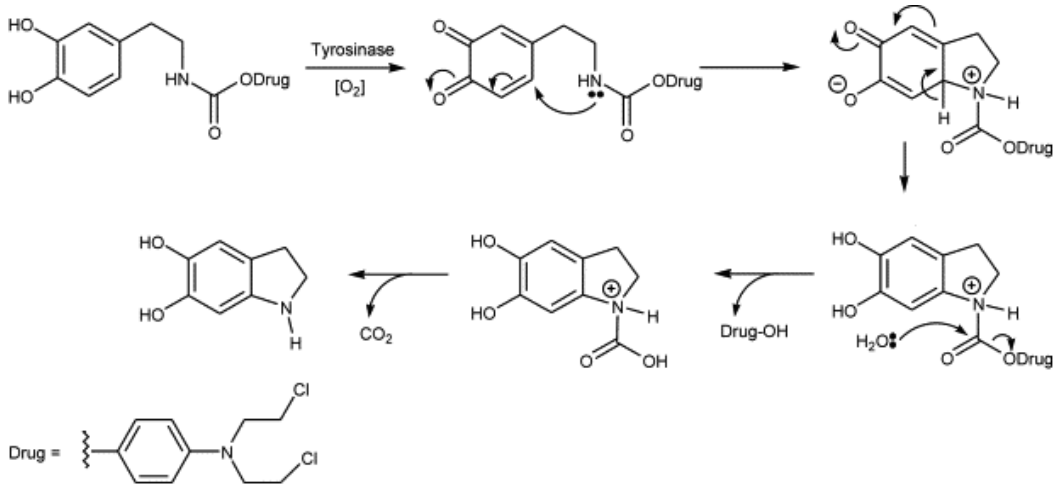

Figura 58. Esquema de liberación de pro-fármacos gracias a la acción de tirosinasa.

Recientemente, han sido propuestas nuevas rutas de liberación de pro-fármaco para sustratos tipo 6-aminodopamina y 4-aminofenol (Knaggs et al., 2005) y para compuestos derivados de tiramina (Perry et al., 2009). Un ejemplo de estos últimos compuestos como pro-fármacos se muestra en la Figura 59.

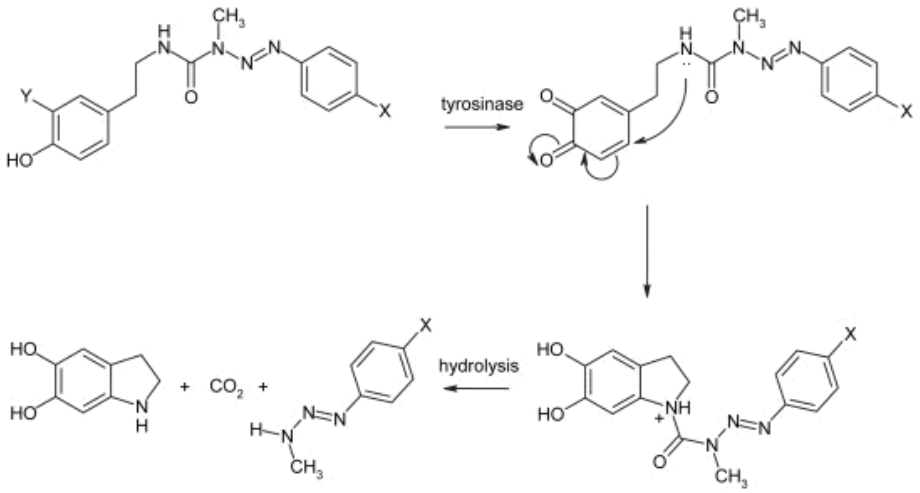

Figura 59. Vía de liberación para los triazenos basados en la activación de la tiramina por tirosinasa.

Gracias al éxito que tiene este tipo de estrategias en el tratamiento del cáncer de piel o melanoma, se están diseñando otras estrategias de activación, catalizada por enzimas, de pro-fármacos anticancerígenos (Rooseboom et al., 2004). En estas estrategias se usan otras enzimas como aldehído oxidasa, amino ácido oxidasa, citocromo P450 reductasa, DT-diaforasa o citocromo P450.

1.7. Tirosinasa: aplicaciones biotecnológicas

Hasta la última década, los estudios con tirosinasa se han realizado con la enzima comercial de *Agaricus bisporus*, como modelo de la investigación sobre la melanogénesis y el pardeamiento enzimático de frutas y hortalizas (Jolivet et al., 1998). Hoy en día, hay un interés creciente en la utilización de tirosinasas de otros organismos para diferentes aplicaciones biotecnológicas y medioambientales. Algunas de estas aplicaciones se detallan a continuación (Otávio de Faria et al., 2007).

1.7.1. Producción de biopolímeros entrecruzados

Existe un creciente interés en el desarrollo de nuevos biopolímeros para su uso como emulsionantes o en alimentos con bajo contenido en calorías y grasas. El mecanismo de formación es multietapa: tirosinasa convierte monofenoles y *o*-difenoles en *o*-quinonas. Éstas son muy reactivas y producen biopolímeros al reaccionar con varios nucleófilos, mediante reacciones no enzimáticas. En este sentido, se ha utilizado tirosinasa para producir conjugados de sericina, que es un péptido encontrado en las aguas de desecho de la industria textil de la seda (Anghileri et al., 2007).

Por otra parte, tirosinasa se ha utilizado para introducir residuos fenólicos (Lenhart et al., 1998) y protéicos (Aberg et al., 2004) en quitosano, un polisacárido obtenido principalmente de los exoesqueletos de crustáceos (Figura 60). Como ya se ha indicado anteriormente, tirosinasa cataliza la oxidación de *o*-difenoles a *o*-quinonas electrofílicas, que difunden y se unen covalentemente a las aminas nucleofílicas de los quitosanos. Los biopolímeros de quitosanos tienen gran interés, ya que de ellos se obtienen: (*i*) hidrogeles como sustitutivos de la piel (Kane et al., 1996), (*ii*) adhesivos (Peppas y Shalin, 1996) y (*iii*) matrices para la liberación de fármacos e ingeniería de tejidos (Lee y Mooney, 2001; Mallapragada y Narasimhan, 2008).

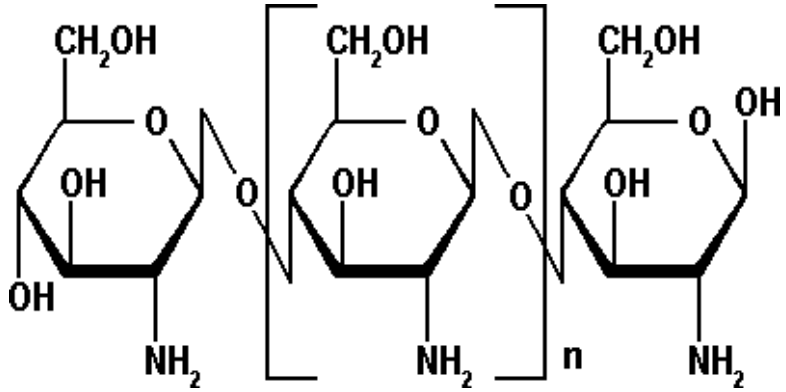

Figura 60. Estructura química del quitosano.

Por otra parte, se ha descrito el entrecruzamiento, catalizado por tirosinasa, de un biopolímero (polisacárido-proteína) obtenido con gelatina y quitosano (Chen et al., 2002). En este biopolímero, tirosinasa oxida a residuos de L-tirosina de la gelatina y estos residuos reaccionan con grupos amino del quitosano. Las propiedades de este gel gelatina-quitosano son diferentes de las de la gelatina original.

Por último, se ha mostrado la capacidad de tirosinasas de hongos de polimerizar varias proteínas como lisozima y ribonucleasa (Leatham et al., 1980), caseína (Hurrell et al., 1982) o α-lactoalbúmina y β-lactoalbúmina (Thalmann y Loetzbeyer, 2002), en presencia de polifenoles entrecruzantes de baja masa molecular como ácidos clorogénico y cafeico. Es decir, el fenol actúa como sustrato para el proceso de entrecruzamiento, facilitando la interconexión entre las proteínas (Matheis y Whitaker, 1984).

1.7.2. Detección y cuantificación de compuestos fenólicos

Las aguas residuales pueden contener residuos fenólicos procedentes de las industrias papelera, textil, petroquímica, etc. (Lee et al., 1996; Yamada et al., 2005). Para detectar y cuantificar estos residuos fenólicos, actualmente se están desarrollando diferentes técnicas como electroforesis capilar, inmunoensayos y biosensores enzimáticos, frente a los métodos tradicionales espectrofotométricos y cromatográficos (Yamada et al., 2005). En el campo de los biosensores, se está utilizando tirosinasa inmovilizada como biosensor enzimático, debido a su capacidad de oxidar fenoles (Sima et al., 2011; Yuan et al., 2011; Wang et al., 2012). Así, se mide el consumo de oxigeno producido por la enzima o la reducción electroquímica de la *o*-quinona liberada por la enzima (Tembe et al., 2006). La principal ventaja del biosensor de tirosinasa inmovilizada, es la posibilidad de determinar compuestos fenólicos *in situ*. La inmovilización de tirosinasa tiene una segunda aplicación analítica, ya que se utiliza en la determinación de compuestos organofosforados y triazinas, debido a la capacidad de estos compuestos de inhibir a la enzima (Andreescu et al., 2002; Sigolaeva et al., 2010).

1.7.3. Eliminación de compuestos fenólicos y bioremediación

La presencia de compuestos fenólicos en el agua residual supone un problema ambiental muy grave. En los últimos años, se han desarrollado nuevos métodos para eliminar estos fenoles de dichas aguas, como la oxidación química y extracción con disolventes, o la adsorción con carbón activo (Lee et al., 2002). Sin embargo, estos

métodos son muy caros y laboriosos. Algunos de ellos no solo no eliminan totalmente los fenoles de las aguas (Loh y Tan, 2000) sino que además generan otros compuestos más tóxicos (Toscano et al., 2003). Para resolver estos problemas, se han desarrollado métodos microbianos y enzimáticos. Los métodos enzimáticos no necesitan periodo de aclimatación y son muy específicos, no generando productos de desecho (Bevilaqua et al., 2002). Estos métodos enzimáticos utilizan enzimas oxidativas como peroxidasas, lacasas o tirosinasas (Durán y Espósito, 2000). Las peroxidasas y las lacasas tienen el inconveniente de que necesitan cofactores químicos muy costosos como manganeso, malonato o H_2O_2 (Paice et al., 1995), mientras que las tirosinasas solo necesitan O_2 como cosustrato, lo que reduce drásticamente los costes de transformación (Burton et al., 2003).

1.7.4. Producción de *o*-difenoles a partir de monofenoles con tirosinasa de *Agaricus bisporus*

Desde hace décadas, la terapia de elección para el tratamiento del Parkinson es el L-dopa. Por este motivo, se calcula que se consumen cada año cerca de 250 toneladas de L-dopa. El L-dopa, mayoritariamente, se genera mediante síntesis química a partir de vanillina e hidantoína y en un proceso de ocho pasos consecutivos (Reinhold et al., 1987). Por otra parte, se han investigado las rutas de producción de L-dopa en *Escherichia coli* (Lee et al., 1996). Sin embargo, las actividades específicas de estos procesos son relativamente bajas y el sustrato y el producto (L-tirosina y L-dopa) sufren reacciones acopladas que producen otros metabolitos secundarios. Por lo tanto, existe un gran interés en el desarrollo de sistemas generadores de L-dopa que estén exentos de células. Otra alternativa es la obtención de L-dopa utilizando tirosinasa inmovilizada que presenta una baja productividad de 1.44 a 54 mg/l/h (Pialis et al., 1996; Carvalho et al., 2000; Ho et al., 2003; Ates et al., 2007). Este bajo rendimiento se atribuye principalmente a dos factores:

1. La conversión de L-tirosina en L-dopa es incompleta (menos del 30% es consumida durante el proceso).
2. En este sistema de producción, parte del L-dopa producido vuelve a reaccionar con tirosinasa y produce *o*-dopaquinona. Esta dopaquinona cicla espontáneamente a leucodopacromo el cual, mediante una reacción de oxidación/reducción con una segunda molécula de dopaquinona, regenera una molécula de L-dopa pero también genera una molécula de dopacromo, el cual evoluciona hacia melaninas (Figura 15).

Para evitar la producción de melaninas, se puede añadir ácido ascórbico al medio, el cual reduce *o*-dopaquinona a L-dopa en una reacción no enzimática instantánea (Figuras 61 y 62). Por otra parte, altas concentraciones de ácido ascórbico inhiben la actividad monofenolasa y difenolasa de tirosinasa y, además, inactivan irreversiblemente a la enzima (Ros et al., 1993a; 1995; Muñoz-Muñoz et al., 2009a). El problema de la acumulación de *o*-difenol en el medio, se puede eliminar añadiendo un complejante de este metabolito como es el borato sódico, el cual forma un complejo con el L-dopa (Yamazaki e Itoh, 2003) (Figura 63). Este enfoque se ha utilizado para conseguir rendimientos más altos en la síntesis de *o*-difenoles, mediante el uso de tirosinasa inmovilizada (Figura 64) (Marín-Zamora et al., 2009). Siguiendo la metodología anterior, se han sintetizado *o*-difenoles de diferentes características y cargas como 4-*terc*-butilcatecol, 4-metilcatecol, 4-metoxicatecol, ácido 3,4-dihidroxifenilpropiónico o ácido 3,4-dihidroxifenilacético, a partir de sus monofenoles correspondientes (4-t*erc*-butilfenol, 4-metilfenol, 4-metoxifenol, ácido *p*-hidroxifenilpropiónico y el ácido *p*-hidroxifenilacético). Con esta metodología de trabajo patentada (García-Ruiz et al., 2008; Marín-Zamora et al., 2009), se consiguieron rendimientos de 88-96%, ya que el borato forma un complejo con el *o*-difenol formado en el medio. Para la formación de este complejo se necesita un pH muy básico en el medio de ensayo (pH 9.0) y una concentración muy alta de borato (0.5 M). Además, se necesita hidroxilamina y acido ascórbico en el medio, la primera para transformar la forma metatirosinasa en desoxitirosinasa (cerrando así el ciclo catalítico), y el ácido ascórbico para reducir la *o*-quinona a *o*-difenol. Este ácido ascórbico no inactiva prácticamente a la enzima (Muñoz-Muñoz et al., 2009a), porque forma a su vez un complejo con el borato.

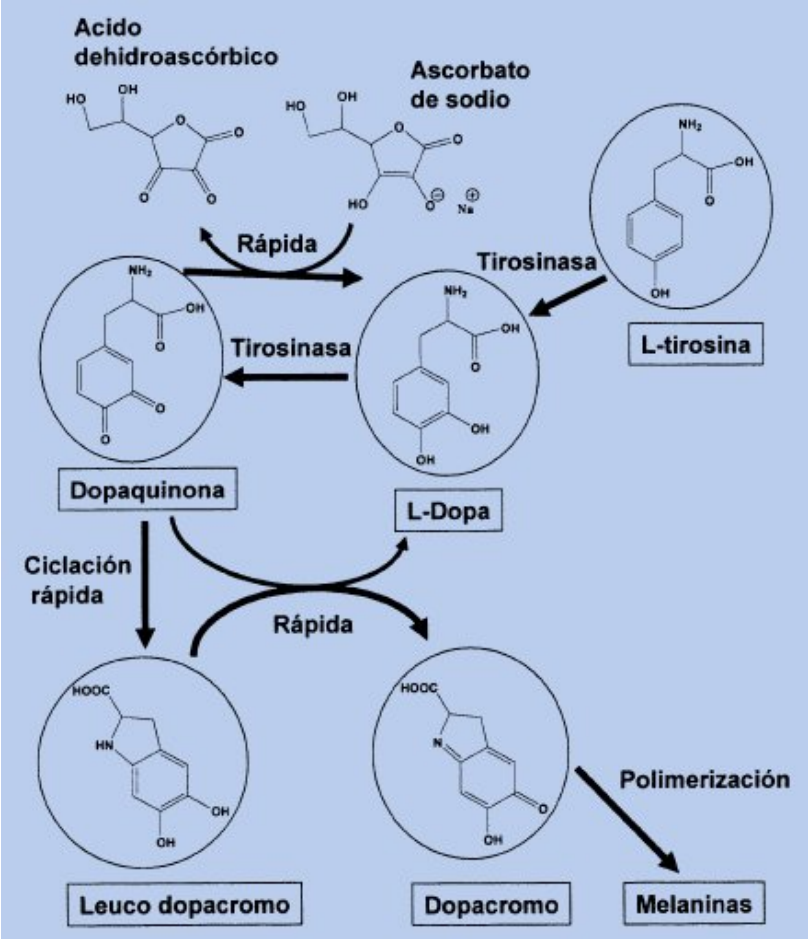

Figura 61. Esquema simplificado de la acción de tirosinasa sobre L-tirosina y L-dopa en presencia de ácido ascórbico.

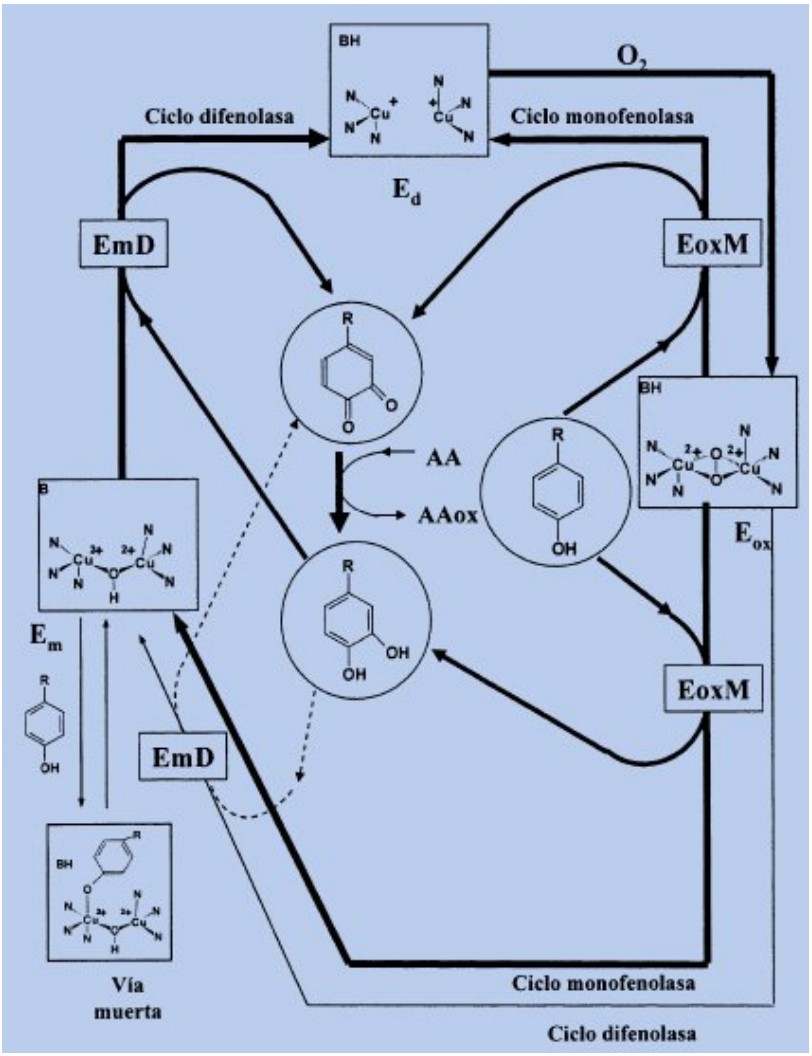

Figura 62. Detalles en el esquema de reacción de tirosinasa sobre monofenoles y *o*-difenoles en presencia de ácido ascórbico (AA).

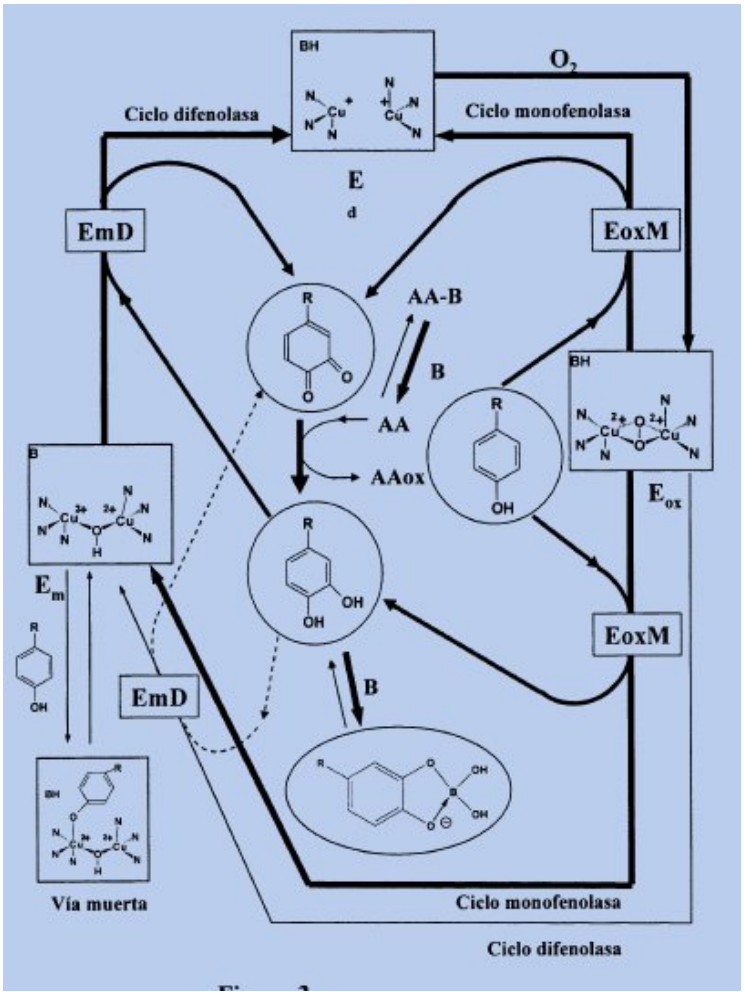

Figura 63. Esquema simplificado de la acción de tirosinasa sobre monofenoles y *o*-difenoles en presencia de ácido ascórbico (AA) y borato sódico (B).

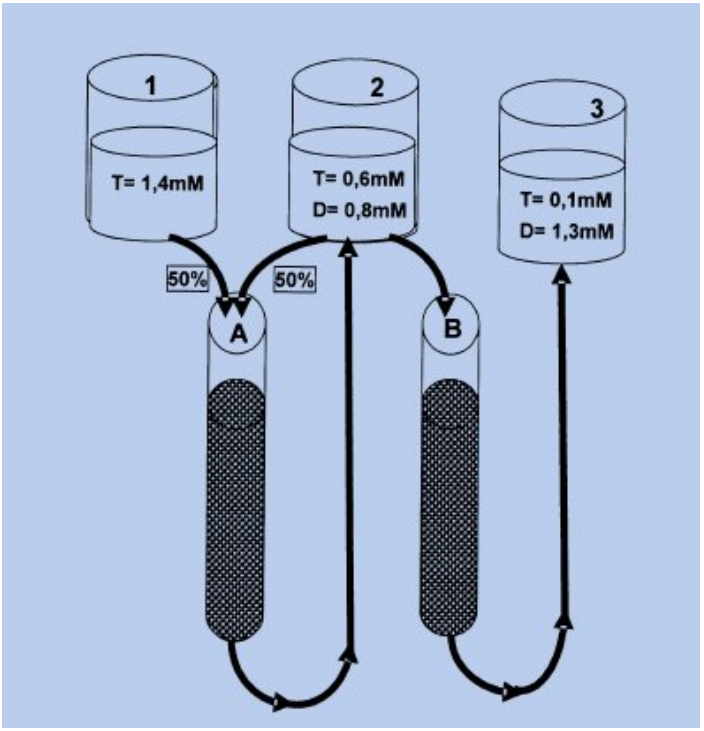

Figura 64. Esquema de la obtención de L-dopa (D) a partir de L-tirosina (T), en flujo continúo y dos reactores con tirosinasa inmovilizada.

Entre las aplicaciones derivadas de la síntesis de *o*-difenoles, a partir de sus respectivos monofenoles, destaca la obtención de antioxidantes potentes como son el ácido cafeico y el hidroxitirosol. La producción de ácido cafeico a partir de su monofenol (ácido *p*-cumárico) y utilizando tirosinasa de *Agaricus bisporus* como enzima catalizadora, fue descrita por Sato en 1969 (Sato, 1969). El hidroxitirosinol es un fuerte antioxidante que se encuentra en el aceite de oliva y en diferentes frutas, pero que no está disponible comercialmente. Recientemente, se está utilizando tirosinasa de *Agaricus bisporus* y de *Pycnoporus sanguineus* (Halaouli et al., 2005) para producir hidroxitirosol a partir de tirosol.

Recientemente se ha publicado la síntesis de L-dopa mediante una técnica electroenzimática, donde se utiliza tirosinasa de *Agaricus bisporus* inmovilizada y reduciendo la *o*-dopaquinona a L-dopa (Min et al., 2010). También se ha publicado recientemente un nuevo método de inmovilización de tirosinasa en resinas epoxi Eupergit® C250L (Figura 65) (Guazzaroni et al., 2012a). Con esta inmovilización, se ha conseguido sintetizar eficazmente una serie de difenoles con rendimientos en torno al 97%.

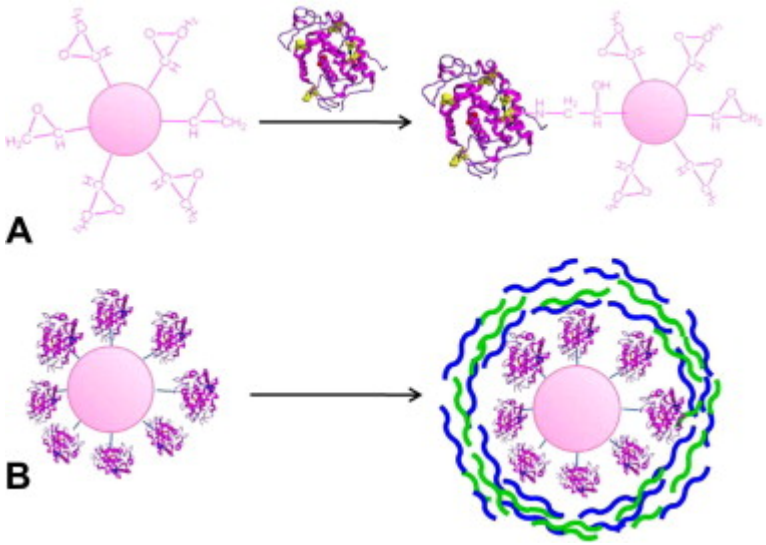

Figura 65. Representación esquemática de tirosinasa con una resina (A) e inmovilizada con las dos resinas (B) (Guazzaroni et al., 2012a).

Utilizando esta técnica de inmovilización, los mismos autores (Guazzaroni et al., 2012b) han conseguido inmovilizar a la enzima y sintetizar difenoles en medio orgánico, demostrando que tirosinasa es más activa en medio orgánico que en medio acuoso.

1.7.5. Avances en bioingeniería

Las tirosinasas de hongos son intracelulares y, además, se producen en baja concentración. Debido a esto, existen una serie de problemas para su uso en futuras aplicaciones: (*i*) Formación de pigmentos melánicos durante el aislamiento y la purificación. Se han propuesto varios métodos para mejorar la purificación de tirosinasa de *Agaricus bisporus*, como la adición de ácido ascórbico al medio (Rescigno et al., 1997). (*ii*) Baja estabilidad de tirosinasa y nula reutilización de éstas. Durán y colaboradores (2002) publicaron una revisión acerca de los soportes utilizados para inmovilizar a tirosinasa, mientras que Seo et al., (2003) estudiaron el desarrollo de biosensores con tirosinasa de *Agaricus bisporus* inmovilizada, permitiendo la cuantificación de fenoles y la eliminación de compuestos relacionados en muestras de agua y tierra. Actualmente, se utiliza un biosensor de tirosinasa para seguir la actividad fosfatasa alcalina (Serra et al., 2005). Recientemente, se ha mejorado la estabilidad de tirosinasa de *Agaricus bisporus* atrapándola en diferentes matrices (Jahangiri et al., 2012). (*iii*) Se necesitan sistemas de expresión de tirosinasa adecuados para la producción de ésta a gran escala. Hasta ahora se han descrito muy pocos promotores

válidos de tirosinasa (Ishida et al., 2001) y, además, la regulación de la expresión de tirosinasas de hongos no es muy conocida. Solamente trabajando con *Aspergillus niger*, se han obtenido rendimientos altos en la expresión de esta enzima (Halouli et al., 2005; 2006).

1.7.6. Otras aplicaciones de tirosinasa

Aplicaciones sanitarias: Tirosinasa se utiliza como marcador en el vitiligo, que como ya se ha indicado, es una enfermedad autoinmune donde la enzima se reconoce como un autoantígeno y, como resultado, conduce a un desorden hipopigmentario. La administración oral de tirosinasa de *Agaricus bisporus* en animales modelo de vitiligo, supone una disminución de la respuesta inmunitaria (Zehtab et al., 2001).

Por otro lado, el papel que tiene tirosinasa en los procesos tumorales es contradictorio. Así, hay autores que sugieren que esta enzima es supresora de tumores, mientras que otros afirman que tiene un papel importante en la mutagenicidad, ya que produce compuestos fenólicos y *o*-quinonas reactivas (Papaparaskeva-Petrides et al., 1993).

Industria cosmética: Los inhibidores de tirosinasa se utilizan en este tipo de industrias debido a su acción despigmentante sobre la piel. De todos los inhibidores descritos, ya sean naturales o sintéticos, solo algunos de ellos, como el ácido kójico, se utilizan realmente como agentes despigmentantes debido a sus posibles efectos secundarios (Maeda y Fukuda, 1991; Chang, 2009).

Industria de la alimentación: Se ha propuesto la fabricación de varios biopolímeros con bajo contenido en calorías y grasas (Otávio de Faria et al., 2007). La inactivación de tirosinasa es una operación muy común para evitar el pardeamiento enzimático, durante la elaboración en conserva de frutas y hortalizas (Sanchez-Hernández et al., 1999).

Objetivos

2. OBJETIVOS

2.1. OBJETIVO GENERAL

El objetivo fundamental de esta Memoria consiste en profundizar en el mecanismo de actuación de tirosinasa, principalmente en los procesos de inactivación suicida y de inhibición irreversible. Como una aplicación del estudio del mecanismo, se caracterizan cinéticamente una amplia gama de sustratos y se profundiza en las propiedades prooxidantes y antioxidantes de estas moléculas.

2.2. OBJETIVOS ESPECÍFICOS

- Profundizar en el mecanismo cinético de actuación de la enzima en sus actividades monofenolasa y difenolasa.
- Estudiar la especie enzimática del ciclo catalítico menos conocida, desoxitirosinasa.
- Investigar el origen del peróxido de hidrógeno en la ruta de biosíntesis de melaninas.
- Establecer un método rápido para la caracterización de las *o*-quinonas, producto de la reacción enzimática.
- Caracterizar cinéticamente un conjunto de sustratos fisiológicos vegetales cuyas *o*-quinonas son muy inestables y poder establecer sus propiedades prooxidantes y antioxidantes.
- Proponer un método para caracterizar el poder antioxidante de una molécula, monofenol, difenol o flavonoide.
- Establecer un parámetro que permita comparar el poder antioxidante de distintas moléculas.
- Estudiar la inactivación de tirosinasa bajo distintas condiciones.
- Intentar clarificar en presencia de oxigeno el mecanismo de inactivación suicida.
- Abordar la inhibición irreversible en ausencia de oxigeno de las especies enzimáticas: metatirosinasa y en las formas relajada y tensa de desoxitirosinasa.

- Aplicar la amplia especificidad de sustrato de la enzima a la eliminación de aminas aromáticas y *o*-aminofenoles, estudiando previamente su catálisis e inactivación.

Material y Métodos

3. MATERIALES Y MÉTODOS

3.1. REACTIVOS Y MATERIALES

3.1.1. Reactivos

Todos los compuestos usados en la preparación de esta Memoria se obtuvieron de Sigma (Madrid, España), Fluka (Madrid, España), Aldrich (Madrid, España), Merck (Darmstadt, Alemania) o Acros (Geel, Belgica). Todos los sustratos fenólicos utilizados se prepararon en ácido fosfórico diluido (150 μM) para prevenir su autooxidación. En todos los ensayos se utilizó agua purificada tipo I (18 MΩ/cm) gracias a un sistema de ósmosis inversa, electrodiálisis y, por último, desionización por resinas de intercambio iónico con un sistema Milli-RX + Milli-Q Reference (Millipore Corp., Bedford, USA).

3.1.2. Preparación de tirosinasa de champiñón

La enzima modelo usada fue la tirosinasa de champiñón ya que es la que se encuentra disponible comercialmente. Tirosinasa de champiñón fue suministrada por Sigma (Madrid, España) y purificada siguiendo el método propuesto por Duckworth y Coleman (1970) pero con dos etapas cromatográficas adicionales. Se disolvieron 0.5 g de la enzima de Sigma de partida (5% de pureza) (Robb, 1984), en 25 ml de tampón fosfato sódico 0.1 M pH 7.0 y la mezcla se mantuvo en agitación a 4ºC durante 1 hora. A continuación, se realizó la purificación de tirosinasa por precipitación con sulfato amónico neutralizado a pH 7.0.

En primer lugar, se llevó el extracto hasta una concentración de sulfato amónico de 36% y se mantuvo durante 1 hora a 4 ºC. Tras la hora, el extracto se centrifugó a 55000 g durante 1 hora y se separó el precipitado desechándose ya que no mostró ninguna actividad enzimática. El sobrenadante se precipitó otra vez con sulfato amónico al 55% (pH 7.0) y el extracto se dejó durante 1 hora a 4 ºC tras lo cual se volvió a realizar otra centrifugación como la descrita anteriormente. El precipitado, que contenía el 90% de unidades enzimáticas de tirosinasa de partida, se disolvió en 4 ml de tampón fosfato sódico 0.1 M, pH 7.0.

La disolución de tirosinasa de champiñón mostró una coloración marrón oscura debida, en parte, a la formación de melaninas. Para eliminar estos pigmentos del

extracto, éste se sometió a varios procesos. En primer lugar, se filtró por una columna de fosfato cálcico (Sigma, España) (80 mg/ml, pH 6.4) lo que llevó a una clarificación de la disolución sin apenas perder concentración enzimática. A continuación, la disolución se pasó por una columna de Sephadex G-100 (2.0 x 30 cm) (Pharmacia, Upsala, Suecia) equilibrada con tampón fosfato 0.01 M, pH 7.0.

Las fracciones que mostraron actividad tirosinasa fueron después purificadas por FLPC gracias a una columna de intercambio aniónico Mono-Q HR 5/5 (Pharmacia, Upsala, Suecia) equilibrada con tampón fosfato 0.01 M, pH 7.0 y desplazada con un gradiente de NaCl (0-0.5 M). Por último, a la enzima purificada se le eliminaron sales gracias a otra columna G-25 (Pharmacia, Upsala, Suecia) en agua ultrapura desionizada y se almacenó en nitrógeno liquido. La concentración enzimática se determinó utilizando el valor de peso molecular de 120000 Dalton asignado a tirosinasa de champiñón en la bibliografía (Jolley et al., 1974).

3.1.3. Determinación de proteínas

La cuantificación de las distintas proteínas se llevó a cabo mediante el método de Bradford (1976) el cual utiliza el kit comercial de Bio-Rad® y albúmina de suero bovino como estándar. El método de Bradford mejora al usado por Lowry (Lowry et al., 1951), uno de los más extendidos, en que utiliza solo 1 reactivo y solo necesita 5 minutos para cada ensayo mientras que el de Lowry necesita 3 reactivos y de 30 a 40 minutos en cada ensayo. Además, el método de Bradford no tiene la mayoría de interferentes que posee el de Lowry.

Este método de Bradford se basa en que, cuando una disolución ácida de azul Coomassie G-250 se une a una proteína, cambia la longitud de onda en su absorción desde 465 nm hasta 595 nm. La muestra se deja incubar 5 minutos con el azul Coomassie y se lee la absorbancia a 595 nm. El resultado se introduce en la recta de calibrado previamente realizada con la albúmina de suero bovino. Así, se determinó la concentración proteica que tenemos en cada fracción. Este ensayo se hace por cuadruplicado a tres concentraciones de proteína diferentes manteniéndose la linealidad. Así, se eliminó el error típico en las medidas y reflejando valores sin desviaciones significativas en las repeticiones.

3.1.4. Generación de oxitirosinasa y desoxitirosinasa

La forma oxi de tirosinasa (E_{ox}) se generó añadiendo 2 μM de H_2O_2 a la enzima nativa. En esta enzima nativa, la forma metatirosinasa (E_m) se transforma en E_{ox}. Una vez generada toda la E_{ox}, se pasó una corriente de nitrógeno a la disolución

y así se convirtió toda la enzima a desoxitirosinasa (E_d), ya que se desplaza el equilibrio $E_{ox} \rightleftarrows E_d + O_2$ hacia la derecha al desplazar el nitrógeno el O_2 del medio (Jolley et al., 1974; Jackman et al., 1992; Muñoz-Muñoz et al., 2010a).

3.1.5. Generación de metatirosinasa

La forma meta de tirosinasa se generó a partir de la enzima nativa mediante 2 métodos:

a) Añadir una concentración de catalasa (2 μM). Así, el equilibrio $E_{ox} \rightleftarrows E_m + H_2O_2$ se desplaza hacia la derecha ya que elimina el H_2O_2 del medio gracias a la reacción $2H_2O_2 + \text{catalasa} \rightarrow O_2 + 2H_2O$. Con esto, en la disolución de enzima nativa, E_{ox} se transforma en E_m.

b) Añadir 2 μM de H_2O_2 a la enzima nativa, de tal manera que la E_m se transforma en E_{ox}. Posteriormente, se añade 2 μM de catalasa al medio y ocurre el mismo paso descrito anteriormente (Jolley et al., 1974; Jackman et al., 1992; Muñoz-Muñoz et al., 2010a).

3.1.6. Evaluación de las especies enzimáticas matatirosinasa, desoxitirosinasa y oxitirosinasa en una preparación enzimática de tirosinasa

Es conocido que en cualquier disolución de tirosinasa de cualquier fuente, existen tres formas enzimáticas, E_{ox}, E_m y E_d (Jackman et al., 1992). Para poder determinar la proporción de cada una de estas formas enzimáticas en una preparación, se propone un método cinético basado en la inactivación que sufre tirosinasa por 2-mercaptoetanol (Aasa et al., 1978). Esta inactivación ocurre en distintas escalas de tiempo puesto que la constante de velocidad de inactivación es diferente para E_{ox}, E_m y E_d (0.014 s^{-1} para E_{ox}, 4 x 10^{-5} s^{-1} para E_m y 1 x 10^{-5} s^{-1} para E_d). Este método es válido ya que las constantes de inactivación para E_{ox} y E_m están muy diferenciadas en el tiempo (tres órdenes de magnitud) (Muñoz-Muñoz, et al., 2009a).

3.2. EQUIPOS Y MÉTODOS

3.2.1. Ensayos oximétricos

Los ensayos oximétricos se realizaron utilizando un oxímetro Hansatech DW (King´s Lynn Norfolk, UK). Este oxímetro se basa en un electrodo tipo Clark, recubierto por una membrana de teflón de 12.5 μM. La muestra se agitó continuamente y la temperatura se mantuvo constante a 25 ºC. Este electrodo está conectado a una unidad amperométrica a su vez controlada por un ordenador PC-compatible. En primer lugar, se ajusta la concentración máxima y mínima de O_2. Para ajustar el máximo, se considera que el agua está saturada de oxigeno con 0.26 mM del mismo. Posteriormente, para ajustar el mínimo, se burbujeó una corriente de N_2 en la cámara de reacción para eliminar el O_2 del agua, llegando en unos minutos al cero de oxigeno. El electrodo fue calibrado "químicamente" mediante el método 4-*tert*-butilcatecol/tirosinasa, basado en la oxidación de 4-*tert*-butilcatecol (TBC) por oxígeno catalizada por tirosinasa (Rodríguez-López et al., 1992b). Tirosinasa requiere una molécula de oxígeno para oxidar dos moléculas de TBC a dos moléculas de *o-tert*-butilquinona (TBCQ), de acuerdo con la estequiometría:

$$2TBC + O_2 \longrightarrow 2TBCQ + 2H_2O$$

Para este tipo de calibración química, se realizaron tres disoluciones de TBC cuantificadas espectrofotométricamente. La calibración se llevó a cabo al oxidar unas concentraciones conocidas de TBC con una alta concentración de enzima, lo cual llevó a consumir todo el TBC en el primer minuto de la reacción. La diferencia entre el trazo inicial y el trazo final (Δ) corresponde a la concentración de oxígeno consumido en la oxidación de TBC por tirosinasa, teniendo en cuenta la estequiometría. Cuando la concentración de TBC es superior a 0.52 mM, este método es válido para conocer el cero de oxígeno, ya que esa concentración estequiométrica de TBC es usada para consumir todo el oxígeno presente en la cámara del oxímetro.

Los ensayos oximétricos se realizaron en la cámara del oxímetro (2 ml) que contenía tampón fosfato sódico 30 mM pH 7.0 como medio de ensayo. El medio fue agitado constantemente. La temperatura se mantuvo constante a 25 ºC utilizando un baño circulante Haake D1G con un termostato y criostato, y se comprobó con un termómetro digital Cole-Parmer con una precisión de $\pm$ 0.1 ºC.

3.2.2. Ensayos espectrofotométricos

Los ensayos espectrofotométricos se llevaron a cabo en un espectrofotómetro Perkin-Elmer Lambda-35 (Walthan, Massachusetts, USA) conectado mediante una interfase RS232C con un ordenador PC-compatible Intel Pentium® (4) a 3 GHz. Este ordenador contuvo el software UV-Winlab suministrado por la casa comercial Perkin-Elmer. La temperatura de los experimentos se mantuvo constante a 25 ºC utilizando un baño circulante Haake D1G con un termostato y criostato, y comprobada esta temperatura con un termómetro digital Cole-Parmer con una precisión de ± 0.1 ºC. Las cubetas de referencia contenían un volumen final de 1 ml. La actividad de la enzima fue determinada con distintos métodos según el sustrato sobre el que actuase (Garcia-Molina et al., 2007).

3.2.3. Ensayos de RMN

Para todos los sustratos estudiados, los espectros de ^{13}C-RMN se obtuvieron en agua deuterada, pH 7.0 (pH óptimo de tirosinasa de champiñón), los cuales proporcionaron los valores de desplazamiento químicos. Los espectros de ^{13}C-RMN se realizaron en un espectrómetro Varian Unity de 400 MHz o en uno de 600 MHz. Los valores de desplazamiento químico (δ) se obtuvieron tomando como referencia el valor para el tetrametilsilano (δ = 0). El máximo grosor de línea aceptado para cada espectro de RMN fue de 0.06 Hz y un error máximo para cada pico de ± 0.03 p.p.m.

La dependencia entre los valores de δ en ^{13}C para un átomo de carbono y su densidad electrónica es conocida (Günther, 1980; Farnun, 1975). Se ha demostrado que existe linealidad entre δ y la constante σ y tal correlación se ha utilizado en los estudios cinéticos y de velocidad de reacción (Levy y Nelson, 1976). Los valores de δ en ^{13}C se han utilizado para verificar o calcular mejor los valores de σ (Marriot y Topsom, 1985). Cuando varios nucleófilos tienen el mismo átomo nucleofílico y similares características estructurales en la proximidad del sitio nucleofílico, las constantes de ataque nucleofílico para el mismo sustrato se correlacionan con la densidad electrónica de los nucleófilos (Hirsch, 1972; Bordell y Hughes, 1984).

Además, la capacidad electrodonadora del átomo de oxígeno de diferentes compuestos fenólicos (poder nucleofílico) ha sido correlacionada con los valores experimentales de δ para el átomo de carbono que contiene el grupo hidroxilo (Tomiyama et al., 1993).

3.2.4 Síntesis del 3,6-difluorocatecol

Para obtener el 3,6-difluorocatecol se llevó a cabo la secuencia sintética que se muestra en el esquema descrito más abajo empleando el 1,2,3,4-tetrafluorobenceno [distribuido por Sigma-Aldrich (Madrid, Spain)] como material de partida. La primera etapa de síntesis implica la sustitución nucleofílica del átomo de fluor en posición 2 del 1,2,3,4-tetrafluorobenceno por uno de los grupos hidroxilo del etilenglicol para producir el 2-(2,3,6-trifluorofenoxy)etanol en un 42% de rendimiento. A continuación, una segunda sustitución nucleofílica, esta vez, de naturaleza intramolecular, conduce a la formación de una difluorobenzodioxina en un 45% de rendimiento. Finalmente, un calentamiento térmico de una disolución de esta benzodioxina en tolueno y en presencia de tricloruro de aluminio rindió el 3,6-difluorocatecol en un 76% de rendimiento (Ladd y Weinstock, 1981).

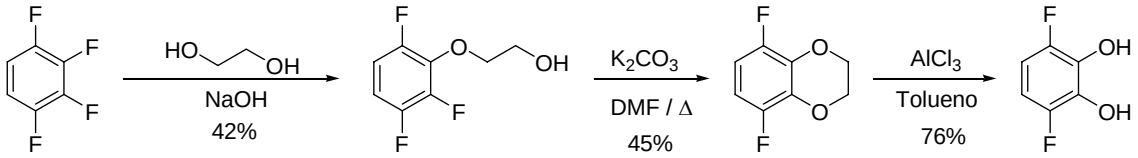

3.2.5 Espectrofotometría de masas

Los espectros de masas se llevaron a cabo usando un espectrómetro Agilent VL. La ionización se realizó utilizando condiciones de electronebulización (ESI) y los datos fueron adquiridos en el modo de ión negativo. La fuente de temperatura fue 350 ºC y el voltaje se ajustó a ± 150 V. Los espectros de masas se registraron de 50 a 700 uma. La muestra se diluyó aproximadamente diez veces en metanol conteniendo ácido fórmico 0.1% e introduciéndola en el espectrómetro de masas usando una microjeringa Hamilton de 0.1 ml de capacidad.

3.2.6 Análisis de regresión

3.2.6.1. Regresión no lineal

Los ajustes por regresión no lineal pueden realizarse a través de los análisis en gradiente y de los algoritmos tipo Gauss-Newton. Los primeros métodos exploran el espacio de los parámetros buscando la dirección en la que tiene lugar la máxima variación de la función, respecto a todos ellos. A continuación, evolucionan en la dirección opuesta a la anterior, mejorando los valores de los parámetros en iteraciones

sucesivas del método. Estos procedimientos no requieren estimaciones iniciales muy próximas a **z**, pero requieren largo tiempo de cálculo, características opuestas a las de los algoritmos tipo Gauss-Newton.

Los algoritmos de Gauss-Newton introducen una aproximación lineal de la función en un entorno próximo a los valores de los parámetros calculados en cada iteración (Watts, 1981). Así, en base a las estimaciones z^i, se calculan los incrementos B^{i+1} que conducen a las estimaciones mejoradas z^{i+1}:

$$z^{i+1}= z^i + B^{i+1}$$

La expresión que define al vector de incrementos de parámetros en cada iteración abarca diversos componentes:

$$B= (V^T W V)^{-1} (V^T W D)= A^{-1} C$$

Así pues, cada iteración requiere una nueva evaluación de los residuos D y de las derivadas V, respecto a las estimaciones en curso de los parámetros z y actualizadas mediante los incrementos B.

La ponderación W asociada a cada dato determina la contribución específica del mismo al ajuste global de todos los valores experimentales. Los factores de ponderación:

$$W_i= 1 / S_i^2$$

están inversamente relacionados con las varianzas respectivas de cada punto, obtenidas a partir de varias repeticiones para cada dato experimental (Endrenyi, 1981).

La fiabilidad del ajuste se realiza mediante la región de confianza correspondiente al nivel de significación α (Wats, 1981):

$$(z-z)^T V^T V(z-z) \leq pS(z) F(p,n-p, \alpha) / (n-p)$$

Esta región es un elipsoide *p*-dimensional en el espacio de los parámetros con centro z, interpretación geométrica asociada al concepto estadístico de matriz de correlación (Endrenyi, 1981). Esta expresión abarca la varianza experimental, S(z)/(n-p), estimada para el número de grados de libertad del ajuste (n-p), así como los valores de la distribución F de Fisher.

Entre los mejores métodos de regresión no lineal, se encuentra un algoritmo de Gauss-Newton que incorpora cierta proporción de búsqueda en gradiente (Marquardt, 1963). La contribución del proceso en gradiente se introduce en la anterior expresión de B a través de la matriz A cuyos elementos diagonales contienen la constante L. A la constante L se le asigna un valor inicial de 10^{-3} (Marquardt, 1963) que puede aumentar o disminuir en factores de diez, durante las sucesivas iteraciones.

3.2.6.2. Regresión lineal

La minimización de la suma de los residuos al cuadrado para una función lineal simple o múltiple, conduce directamente a expresiones algebraicas que definen los parámetros correspondientes (Draper y Smith, 1981; Endrenyi, 1981). Así, a partir de las anteriores expresiones para las matrices z y B se obtiene:

$$z = (x^T W x)^{-1} (x^T W y)$$

Siendo igualmente aplicables los conceptos de ponderación y fiabilidad anteriormente descritos.

3.2.7. Simulación numérica

La finalidad última de la bioquímica consiste en la caracterización de los procesos químicos que tienen lugar en los sistemas biológicos. Dicha caracterización exige un proceso de actuación ordenado y riguroso. La realización de un estudio experimental que permita un conocimiento de las propiedades del sistema, hace posible la construcción de un modelo que intente explicar estos datos experimentales, así como la información bibliográfica existente. Una vez construido el modelo correspondiente, se somete a un proceso de simulación que proporciona una serie de datos teóricos. El contraste de estos datos y la información disponible sobre el sistema real es de utilidad para aceptar, modificar o rechazar el modelo propuesto.

Se obtienen una serie de curvas de progreso, asignando valores concretos a las constantes de velocidad de los mecanismos descritos, y simulando mediante la integración numérica del correspondiente sistema de ecuaciones diferenciales. A estas curvas de progreso se les aplicó el análisis de datos cinético, obteniéndose una serie de constantes cinéticas, que se compararon con las obtenidas en los ensayos experimentales. Además, la simulación ha permitido verificar la relación del análisis cinético. A continuación se procede a describir, brevemente, el concepto de integración numérica, así como los métodos más usados.

3.2.7.1. Integración numérica de ecuaciones diferenciales

El comportamiento cinético de un modelo enzimático puede considerarse, a nivel matemático, como un problema de valor inicial, esto es, un sistema de ecuaciones diferenciales:

$$Y_j^{'} = f_j(X, Y_j)$$

$$Y_j = (X_0) = Y_j^{(0)}$$

cuyas funciones tienen un valor conocido, en un instante de tiempo determinado, usualmente X_0= 0. Cuando el sistema de ecuaciones diferenciales correspondiente tiene estructura no lineal, carece de solución analítica, y debe ser resuelto, de modo aproximado, por métodos numéricos.

Considerando el sistema anterior, en el instante inicial, X_0, se conoce el valor exacto de la variable dependiente, Y_0, y se calcula su derivada $Y'(X_0)$, a través de la ecuación diferencial correspondiente. Después, se avanza un intervalo de tiempo, denominado tamaño de paso, h, a lo largo de dicha derivada, alcanzándose el instante $X_1= X_0 + h$. Esto equivale a la obtención de un nuevo valor de la función, Y_1.

$$Y_1 = Y_0 + hY^{'}(X_0)$$

A continuación se reanuda el proceso tomando como punto de partida Y_1, en el instante X_1, y se realizan sucesivas interacciones hasta completar el rango de tiempo considerado.

$$Y_{n+1} = Y_n + hY^{'}(X_n)$$

Este procedimiento se denomina método de Euler y equivale, a nivel geométrico, a la reproducción de una curva mediante una sucesión de rectas. Existen una gran variedad de métodos alternativos que intentan optimizar la exactitud del cálculo en cada iteración, según se describe posteriormente. Entre estos se encuentran los métodos basados en la serie de Taylor y en los basados en la resolución numérica de integrales.

Existen numerosos métodos de integración basados directa o indirectamente en el desarrollo de Taylor. De entre todos ellos, el más utilizado es el método clásico de Runge-Kutta de cuarto orden, ampliamente referenciado en la bibliografía.

3.2.7.2. Métodos de paso variable

Un tipo de error, característico de los métodos de integración numérica de ecuaciones diferenciales, es el error de truncamiento, tanto menor cuanto mayor es el orden del método considerado. Sin embargo, un aumento indefinido en el orden de un método, origina operaciones más complejas y un tiempo de cálculo excesivo. El error de truncamiento puede reducirse disminuyendo el tamaño de paso de la integración numérica, h, pero un valor excesivamente pequeño de éste, obliga a operar con valores de ordenadas cuya magnitud es muy próxima, ocasionando errores de redondeo (pérdida de cifras significativas), rápidamente propagados en sucesivas iteraciones.

Por tanto, una mejora en los métodos de integración numérica, consiste en el establecimiento de un paso variable, a lo largo del campo de existencia de la función, cuya magnitud permita optimizar la reducción del error de truncamiento y la amplificación del error de redondeo, dentro de límites satisfactorios, para el problema de valor inicial bajo estudio. A tal fin, es necesario disponer de una estimación de ambos tipos de error, estando asociado el error de redondeo, al número de cifras significativas con que opera cada ordenador, habitualmente ocho (precisión simple), dieciséis (precisión doble) o treinta y dos (precisión cuádruple). El método de Fehlberg es eficaz para el cálculo del paso variable acoplado al método de Runge-Kutta de cuarto orden, por lo que se ha utilizado en este trabajo.

3.2.7.3. Implementación

Los ensayos de simulación reproducen el comportamiento de las concentraciones de ligandos y especies enzimáticas involucradas en los mecanismos de reacción propuestos en esta Memoria para tirosinasa. Los respectivos sistemas de ecuaciones diferenciales han sido resueltos numéricamente para casos particulares de valores de constantes de velocidad y concentraciones iniciales de especies para cada mecanismo de reacción (Gálvez y Varón, 1981). La integración numérica está basada en el algoritmo de Runge-Kutta-Fehlberg (Gerald y Wheatley, 1989) con un error máximo de $2{,}22 \times 10^{-6}$ unidades de concentración, implementado en el programa WES (García-Sevilla et al., 2000) compilado en el lenguaje C++ para Windows e instalado en un PC compatible.

3.2.7.4. Condiciones de simulación

El conjunto de ecuaciones diferenciales obtenidas del mecanismo de reacción de tirosinasa, las condiciones iniciales, así como los valores de las constantes, los

cuales se tomaron de forma que cumplieran el valor de las constantes cinéticas determinadas experimentalmente, así como que permitieran simular los distintos supuestos en tiempos razonablemente cortos y asequibles para el ordenador utilizado, se describen en el capítulo de Resultados y Discusión, en las publicaciones adjuntas.

Resultados y Discusión

4.1. NUEVOS AVANCES DEL COMPORTAMIENTO DE LA VELOCIDAD DE ESTADO ESTACIONARIO RESPECTO DE LA CONCENTRACIÓN INICIAL DE SUSTRATO EN LAS ACTIVIDADES MONOFENOLASA Y DIFENOLASA DE TIROSINASA.

Los nuevos avances del comportamiento de la velocidad de estado estacionario respecto de la concentración inicial de sustrato en las actividades monofenolasa y difenolasa de tirosinasa han dado lugar a la siguiente publicación adjunta.

4.1.1. Título

New features of the steady-state rate related with the initial concentration of substrate in the diphenolase and monophenolase activities of tyrosinase.

4.1.2. Autores

Muñoz-Muñoz, J.L.; Garcia-Molina, F.; Varon, R.; Tudela, J.; Garcia-Cánovas, F. y Rodríguez-López, J.N.

4.1.3. Referencia

Journal of Mathematical Chemistry (2010) 48, 347-362.

4.1.4. Resumen

Tirosinasa muestra dos actividades enzimáticas: la hidroxilación de monofenoles a *o*-difenoles (actividad monofenolasa) y la oxidación de *o*-difenoles a *o*-quinonas (actividad difenolasa). La acción sobre *o*-difenoles implica dos sustratos: oxigeno y *o*-difenol. El mecanismo propuesto es un Uni Uni Bi Bi ping-pong. En esta contribución, se demuestra experimentalmente que existe una ruta favorecida cinéticamente, lo que se traduce en la aparición de curvas de velocidad inicial *vs.* la concentración inicial de *o*-difenol con inhibición por exceso de sustrato y sigmoides en la representación de velocidad inicial *vs.* la concentración inicial de oxigeno. Sin embargo, el mecanismo de actuación de la enzima sobre monofenoles, que es más complejo porque implica tres sustratos (monofenol, oxigeno y *o*-difenol), no muestra desviaciones del comportamiento hiperbólico en los datos de velocidad inicial *vs.* la concentración inicial de monofenol, estos resultados pueden explicarse si la etapa limitante en el mecanismo de acción de tirosinasa es la hidroxilación de monofenol a *o*-difenol.

J Math Chem (2010) 48:347–362
DOI 10.1007/s10910-010-9675-5

ORIGINAL PAPER

New features of the steady-state rate related with the initial concentration of substrate in the diphenolase and monophenolase activities of tyrosinase

Jose Luis Muñoz-Muñoz · Francisco Garcia-Molina · Ramón Varon · Jose Tudela · Francisco Garcia-Cánovas · Jose N. Rodríguez-López

Received: 22 February 2010 / Accepted: 23 March 2010 / Published online: 11 April 2010
© Springer Science+Business Media, LLC 2010

Abstract Tyrosinase has two types of enzymatic activities: the hydroxylation of monophenols to *o*-diphenols (monophenolase activity) and oxidation of *o*-diphenols to *o*-quinones (diphenolase activity). The action on *o*-diphenols involves two substrates: oxygen and *o*-diphenol, while the mechanism proposed is a Uni Uni Bi Bi ping-pong. In this contribution, we demonstrate experimentally that there is a kinetically preferred pathway, which translates into the appearance of curves of initial velocity *vs*. initial diphenol concentration shows inhibition by an excess of substrate, while sigmoid curves are obtained when the initial velocity *vs*. initial oxygen concentration are graphed. However, the action mechanism of the enzyme on monophenols, which is more complex because it involves three substrates (monophenol, oxygen and *o*-diphenol), does behave differently from the hyperbolic behaviour as regards the initial velocity *vs*. initial monophenol concentration, results that can be explained if the limiting step in the action of tyrosinase is the hydroxylation of monophenol to *o*-diphenol.

Keywords Tyrosinase · Kinetically preferred pathway · Slow pathway · Diphenolase activity · Monophenolase activity

J. L. Muñoz-Muñoz · F. Garcia-Molina · J. Tudela · F. Garcia-Cánovas (✉) · J. N. Rodríguez-López
GENZ: Grupo de Investigación Enzimología, Departamento de Bioquímica y Biología Molecular-A, Facultad de Biología, Universidad de Murcia, 30100 Espinardo, Murcia, Spain
e-mail: canovasf@um.es

R. Varon
Departamento de Química-Física, Escuela de Ingenieros Industriales de Albacete, Universidad de Castilla la Mancha, Avda. España s/n. Campus Universitario, 02071 Albacete, Spain

1 Introduction

It has long been known that cooperativity is not an exclusive characteristic of oligomeric enzymes, and two models have been proposed to explain the phenomenon: binding equilibrium models and kinetic models [1–3]. The simplest models are kinetic since, in them, a monomer with only one active site is capable of deviating from hyperbolic behaviour and showing sigmoidal behaviour when the concentration of substrate is varied [3]. Among enzymes which have been seen to deviate from the hyperbolic are: phosphofructokinase [4], isocitrate dehydrogenase of yeast [5] and heart malic dehydrogenase [6].

Tyrosinase (TYR: monophenol, *o*-diphenol; oxygen-oxidoreductase; EC 1.14.18.1) has two copper atoms in its active site and is ubiquitously present in biological systems [7]. It catalyzes the oxidation of *o*-diphenols (*o*-diphenolase or catecholase activity) to the corresponding *o*-quinones, through the consumption of molecular oxygen. It may also catalyze the regioselective ortho-hydroxylation of monophenols to catechols (monophenolase or cresolase activity) and their subsequent oxidation to *o*-quinones. The catalytic centre of tyrosinase possesses a binuclear copper similar to that of hemocyanin and catechol oxidase [7]. The catalytic cycle of tyrosinase has three enzymatic forms: E_m (*met*-tyrosinase), with the copper as $Cu^{2+}Cu^{2+}$, E_d (*deoxy*-tyrosinase), with the copper as $Cu^{+}Cu^{+}$ and E_{ox} (*oxy*-tyrosinase) with copper in the form $Cu^{2+}Cu^{2+}O_2^{2-}$ [8]. In the structure of tyrosinase from *Streptomyces castaneoglobisporus* [9], each copper ion is coordinated by three histidines (2 histidines in equatorial position and one in axial position) [9–11].

The action mechanism of tyrosinase on *o*-diphenols and monophenols has been widely studied [7,12]. The mechanism is complex since the enzyme exists in three forms in the catalytic cycle (*met*-tyrosinase, *deoxy*-tyrosinase and *oxy*-tyrosinase), while the reaction product, *o*-quinone, is unstable. The development of suitable methods to measure each of these activities [13] and the characterisation of the kinetic mechanism of the enzyme acting on diphenols and monophenols [7,14] has increased our understanding of the melanin biosynthesis pathway [15,16].

This work uses kinetic studies of the steady-state of both activities (monophenolase and diphenolase), to (1) detect the limiting step of the process, (2) explain the inhibition by an excess of *o*-diphenol in diphenolase activity, (3) explain the generation of a sigmoid curve when the oxygen concentration in diphenolase activity is varied, (4) interpret the absence of inhibition by excess monophenol in the monophenolase activity when the concentration of monophenol is varied and (5) explain the absence of a sigmoid curve when the oxygen concentration in monophenolase activity is varied.

1.1 Abbreviation

For clarity and for the sake of brevity, the following additional notations will be used in the text.

1.1.1 Species and concentrations

D	Diphenol (L- and D-dopa)
M	Monophenol (L- and D-tyrosine)
E	Enzyme (tyrosinase)
$[E]_0$	Initial concentration of enzyme

1.1.2 Kinetic parameters

V_0^D	Initial rate of tyrosinase acting on D
V_0^M	Initial rate of tyrosinase acting on M
$V_{\max}^D$	Maximal rate of tyrosinase for D
$V_{\max}^M$	Maximal rate of tyrosinase for M
k_{cat}^D	Catalytic constant of tyrosinase acting on D
k_{cat}^M	Catalytic constant of tyrosinase acting on M
$K_m^{D(P)}$	Apparent Michaelis constant of tyrosinase for D in the kinetically preferred pathway
$K_m^{M(P)}$	Apparent Michaelis constant of tyrosinase for M in the kinetically preferred pathway
$K_{m,D}^{O_2(P)}$	Apparent Michaelis constant for O_2 in the diphenolase activity in the kinetically preferred pathway
$K_{m,D}^{O_2(S)}$	Apparent Michaelis constant for O_2 in the diphenolase activity in the slow pathway
$K_{m,M}^{O_2(P)}$	Apparent Michaelis constant for O_2 in the monophenolase activity on the kinetically preferred pathway
$K_{m,M}^{O_2(S)}$	Apparent Michaelis constant for O_2 in the monophenolase activity on the slow pathway

2 Experimental

2.1 Reagents

Commercial mushroom tyrosinase (TYR) and the substrates used in this work (L- and D-dopa and L- and D-tyrosine) were purchased by Sigma (Madrid). Other chemicals were of analytical grade and supplied by Merck (Darmstadt, Germany). Stock solutions of the diphenolic and monophenolic substrates were prepared in 0.15 mM phosphoric acid to prevent autooxidation. Milli-Q system (Millipore corp.) ultrapure water was used throughout.

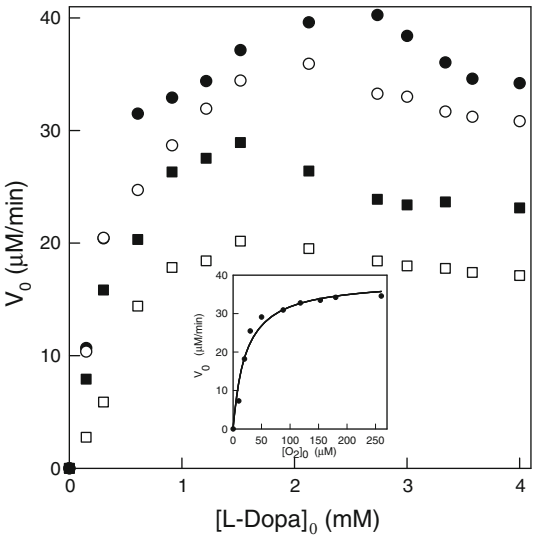

Fig. 1 Representation of the initial velocity values obtained for action of TYR on different initial concentration of *o*-diphenol, at different concentrations of oxygen. The experimental conditions were: 30 mM sodium phosphate buffer (pH 7.0), 25 °C, $[E]_0 = 6$ nM and the initial oxygen concentrations were (μM): (*filled circle*) 260, (*open circle*) 100, (*filled square*) 30 and (*open square*) 20. The L-dopa concentrations (mM) were varied as indicated in the figure. *Inset* Representation of the initial velocity *vs.* initial concentration of O_2, at L-dopa concentration of 4 mM and $[E]_0 = 6$ nM

2.2 Enzyme source

Mushroom tyrosinase was purified by Duckworth and Coleman's procedure but with two additional chromatographic steps [17]. The enzyme solution was passed through a column (2.0 × 30 cm) of Sephadex G-100 (Pharmacia) equilibrated on 0.01 M sodium phosphate buffer (pH 7). Samples showing tyrosinase activity were further purified by FPLC anion-exchange chromatography on a Mono-Q HR 5/5 column (2.0 × 30 cm) (Pharmacia) equilibrated with 0.01 M sodium phosphate (pH 7) and eluted with sodium chloride (0–0.5 M gradient). Purified enzyme was desalted with Sephadex G-25 (Pharmacia) into ultrapure water and stored in liquid nitrogen. Protein concentration was determined by Bradford's method [18], using bovine serum albumin as standard.

2.3 Spectrophotometric assays

These assays were carried out with a Perkin-Elmer Lambda-35 spectrophotometer, on line interfaced to a PC-computer, where the kinetic data were recorded, stored and later analyzed. The product of the enzyme reaction, the *o*-quinone, is not suitable for experimental detection at long assay times due to the instability of the *o*-quinones [19,20], and so the experimental assays were made at short times. The reaction was followed by measuring: (a) the disappearance of NADH at 340 nm with $\varepsilon = 6,230\ \mathrm{M^{-1}\ cm^{-1}}$, (L- and D-dopa) [13] and (b) the appearance dopachrome accumulation at 475 nm with $\varepsilon = 3600\ \mathrm{M^{-1}\ cm^{-1}}$ (L- and D-tyrosine) [21]. The cuvette (final volume 1 ml) contained $[\mathrm{NADH}]_0 = 0.2$ mM for the measurement with *o*-diphenols and 30 mM sodium phosphate buffer (pH 7.0) (monophenols and *o*-diphenols). The initial substrate (monophenol and *o*-diphenol) and oxygen concentrations were varied as indicated in the legends of Figs. 1 and 3. The reaction was started with the addition of enzyme.

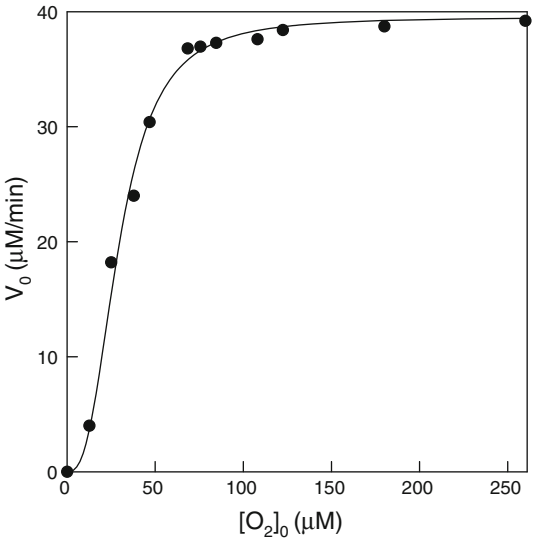

Fig. 2 Representation of the initial velocity values obtained for action of TYR on a fixed concentration of L-dopa (2.8 mM), varying the initial concentration of oxygen. The experimental conditions were: 30 mM sodium phosphate buffer (pH 7.0), 25 °C and $[E]_0 = 6$ nM. The O_2 concentrations (μM) were varied as indicated in the figure

2.4 Oxymetric assays

Measurements of dissolved oxygen concentration were made with a Hansatech (Kings Lynn, Cambs, UK) oxygraph unit controlled by a PC. The oxygraph used a Clark-type silver/platinum electrode with a 12.5 μm Teflon membrane. The sample was continuously stirred during the experiments and its temperature was maintained at 25 °C. The zero oxygen level for calibration and experiments was obtained by bubbling oxygen-free nitrogen through the sample for at least 10 min [22]. The cuvette (final volume 2 ml) contained 30 mM sodium phosphate buffer (pH 7.0) and monophenol and *o*-diphenol at a concentration at which tyrosinase is saturated by them. The initial oxygen concentration was varied as is indicated in the legends of Figs. 2 and 4.

2.5 Kinetic data analysis

V_0-values were calculated from triplicate measurements at each reducing substrate concentration. The fitting was carried out using the Sigma Plot 9.0 program for Windows [23], obtaining $V_{\max}$ and K_m^S by non-linear regression to the Michaelis-Menten equation.

3 Results and discussion

Mushroom tyrosinase (EC 1.14.18.1) is an enzyme that contains copper in its active centre and which catalyzes the hydroxylation of monophenols to *o*-diphenols (monophenolase activity) and the oxidation of *o*-diphenols to their corresponding *o*-quinones (diphenolase activity) in a reaction in which molecular oxygen intervenes [7]. We shall first look at diphenolase activity.

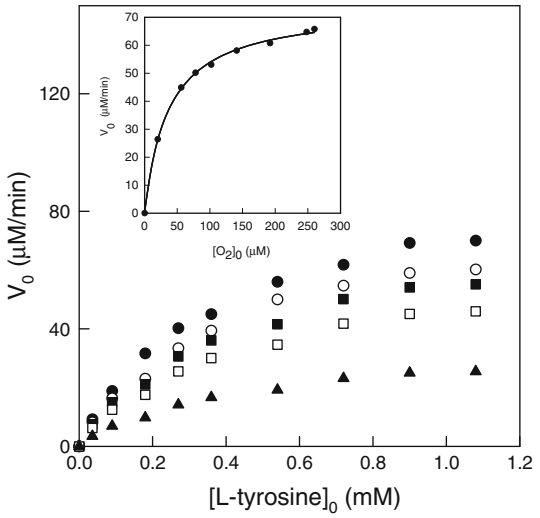

Fig. 3 Representation of the initial velocity values obtained for action of TYR on different initial concentrations of L-tyrosine at different initial concentrations of oxygen. The experimental conditions were: 30 mM sodium phosphate buffer (pH 7.0), 25 °C, $[E]_0 = 145$ nM and the initial oxygen concentrations (μM) were: (*filled circle*) 260, (*open circle*) 200, (*filled square*) 100, (*open square*) 50 and (*open triangle*) 20. The L-tyrosine concentrations (mM) were varied as indicated in the figure. *Inset* Representation of the initial velocity at an initial L-tyrosine concentration of 1.1 mM and different initial concentrations of oxygen. The experimental conditions were the same as in Fig. 3

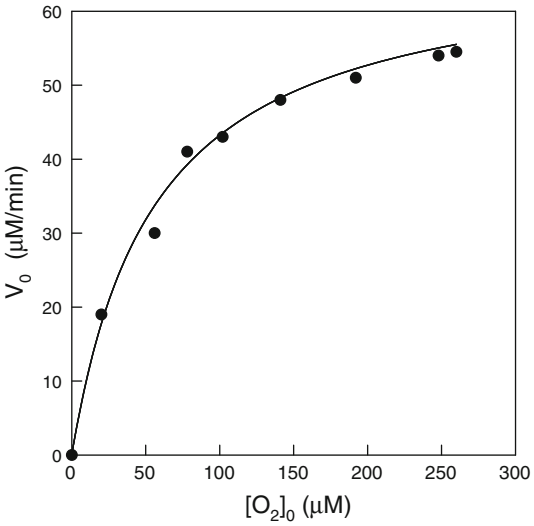

Fig. 4 Representation of the initial velocity values obtained for TYR acting on L-tyrosine (0.54 mM), varying the initial oxygen concentration. The experimental conditions were: 30 mM sodium phosphate buffer (pH 7.0), 25 °C and $[E]_0 = 145$ nM. The O_2 concentrations (μM) were varied as indicated in the figure

3.1 Diphenolase activity

The mechanism proposed to explain diphenolase activity is described in Scheme 1. Enzyme turnover begins with *met*-tyrosinase, which reacts with *o*-diphenol (D) to form the complex *met*-tyrosinase/diphenol. The *o*-diphenol is oxidised to *o*-quinone

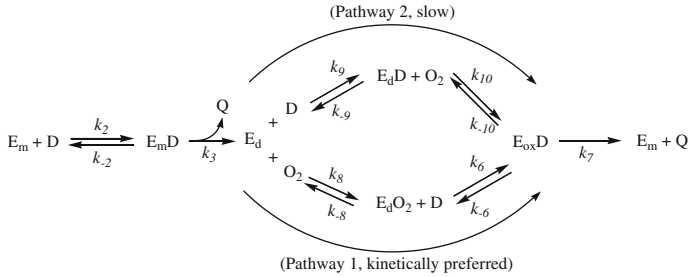

Scheme 1 Kinetic mechanism proposed to explain the action of tyrosinase on *o*-diphenols. E_m, *met*-tyrosinase; E_d, *deoxy*-tyrosinase; E_{ox}, *oxy*-tyrosinase; D, *o*-diphenol; Q, *o*-quinone; $E_m D$, *met*-tyrosinase/*o*-diphenol complex; $E_d D$, *deoxy*-tyrosinase/*o*-diphenol complex; $E_d O_2$; *deoxy*-tyrosinase/oxygen complex; $E_{ox} D$, *oxy*-tyrosinase/*o*-diphenol complex

and the form *deoxy*-tyrosinase is generated. This form, with Cu^+Cu^+, can react with O_2 to give *oxy*-tyrosinase, which, when it reacts with the *o*-diphenol, forms *oxy*-tyrosinase/diphenol, which, in turn, is transformed into *met*-tyrosinase and *o*-quinone. The pathway described (pathway 1) in the mechanism of Scheme 1 is the normal pathway followed by the enzyme. However, at high concentrations of *o*-diphenol, the *deoxy*-tyrosinase form can bind to it before the oxygen to form a *deoxy*-tyrosinase/*o*-diphenol complex, which subsequently binds to the O_2, giving rise to a new form, *oxy*-tyrosinase/*o*-diphenol, which is transformed into *met*-tyrosinase and *o*-quinone (pathway 2, slow).

The experimental data for the initial velocity *vs.* initial *o*-diphenol (substrate) concentration, Fig. 1, shows that the pathways described above differ kinetically, so that pathway 1 should be kinetically preferred and pathway 2 slow. Note that inhibition by excess of substrate occurs earlier at low O_2 concentrations, that is, at the lowest concentrations of *o*-diphenol. Figure 1 Inset shows the initial velocity obtained at a fixed initial concentration of *o*-diphenol (high) and varying the initial concentration of oxygen.

A kinetic study of the kinetically preferred pathway gives the values of $K_m^{D(P)}$, the apparent Michaelis constant for the *o*-diphenol in the kinetically preferred pathway, and k_{cat}^D, the catalytic constant. The analytical expressions according to [14] are:

$$K_m^{D(P)} = k_{\text{cat}}^D / k_6 \tag{1}$$

and

$$k_{\text{cat}}^D = \frac{k_3 k_7}{k_3 + k_7} \tag{2}$$

The Michaelis constant for oxygen is:

$$K_{m,D}^{O_2(P)} = k_{\text{cat}}^D / k_8 \tag{3}$$

Figure 1 Inset shows the initial velocity obtained at a high concentration of *o*-diphenol (and different concentrations of oxygen). From these data, the apparent Michaelis constant for oxygen in the slow pathway can be obtained:

$$K_{m,D}^{O_2(S)} = k_{\text{cat}}^{D}/k_{10} \tag{4}$$

The data showed in Table 1 and Fig. 1 indicate that the mechanism is dependent of the oxygen concentration because the apparent Michaelis constant for oxygen increased from the Eq. (3)-value to the Eq. (4)-value (see Table 1).

Figure 2 shows the values of the initial velocity obtained at a fixed concentration of *o*-diphenol and increasing initial concentrations of oxygen. The sigmoid shape is similar to that obtained with the enzyme phosphofructokinase [24], behaviour which can be explained, according to Scheme 1, if two pathways exist to reach the intermediate *oxy*-tyrosinase/*o*-diphenol, $E_{ox}D$, starting from *deoxy*-tyrosinase, E_d. As indicated by Ferdinand [3], an indicative test for kinetically preferred pathway, in a bisubstrate reaction, includes inhibition by excess of substrate (*o*-diphenol in this case) and sigmoicidity with respect to the other substrate (oxygen in this case).

Therefore, at fixed concentration of oxygen, the velocity increases as the initial concentration of *o*-diphenol increases until it binds to the form *deoxy*-tyrosinase, entering the slow pathway and inhibition through excess substrate occurs (Fig. 1). In the case described in Fig. 2, at low initial concentrations of oxygen and high concentrations of *o*-diphenol, the enzyme follows pathway 2 and, as oxygen is added, it takes the kinetically preferred pathway and a sigmoid curve is obtained. From these experimental results, it can be deduced that the mechanism described in Scheme 1 does not reach rapid equilibrium but passes through a steady-state, since the velocity expression with respect to initial *o*-diphenol concentration and in the case of rapid equilibrium is a hyperbola, Eq. 5 (expressions $\alpha_1 - \alpha_4$ are given in Appendix), is:

$$\frac{V_0}{[E]_0} = \frac{\alpha_1[D]_0[O_2]_0}{\alpha_2 + \alpha_3[O_2]_0 + \alpha_4[D]_0 + [D]_0[O_2]_0} \tag{5}$$

which does not agree with the experimental results. This leads us to conclude that the mechanism reaches a steady-state so that the velocity equation of the mechanism would correspond to Eq. (6). Expressions $\beta_1 - \beta_{11}$ are given in the Appendix.

$$\frac{V_0}{[E]_0} = \frac{\beta_1[D]_0[O_2]_0 + \beta_2[D]_0[O_2]_0^2 + \beta_3[D]_0^2[O_2]_0}{\beta_4 + \beta_5[O_2]_0 + \beta_6[D]_0 + \beta_7[O_2]_0^2 + \beta_8[D]_0[O_2]_0 + \beta_9[D]_0^2 + \beta_{10}[D]_0[O_2]_0^2 + \beta_{11}[D]_0^2[O_2]_0} \tag{6}$$

3.2 Monophenolase activity

The mechanism that describes the monophenolase activity of tyrosinase is described in Scheme 2. In this case, too, the binding of monophenol to de*oxy*-tyrosinase was considered, and the pathway was seen to be slow. However, since the steady-state concentration of *o*-diphenol is low, so that $[D]_0/[M]_0 = R = 0.046$ [25], it is assumed that, in this case, D does not bind to the *deoxy*-tyrosinase. The velocity equation for the

Table 1 Kinetic constants and parameters obtained for action of TYR on isomers of dopa and tyrosine

Substrate	$K_m^{S(P)}$ (mM)	$K_m^{O_2(P)}$ (μM)	$K_m^{O_2(S)}$ (μM)	k_{cat} (s^{-1})	$k_6 \times 10^{-5}$ ($M^{-1}s^{-1}$)	$k_4 \times 10^{-3}$ ($M^{-1}s^{-1}$)	$k_8 \times 10^{-7}$ ($M^{-1}s^{-1}$)	$k_{10} \times 10^{-6}$ ($M^{-1}s^{-1}$)
L-dopa	0.50 ± 0.06	4.78 ± 0.72	28 ± 4	110.0 ± 10.2	2.20 ± 0.32	–	2.3 ± 0.4	3.93 ± 0.88
D-dopa	2.15 ± 0.28	4.57 ± 0.68	31 ± 2	105.3 ± 10.4	0.48 ± 0.08	–	2.3 ± 0.4	3.39 ± 0.66
L-tyrosine	0.27 ± 0.03	0.53 ± 0.07	37 ± 2	8.1 ± 1.4	–	30.0 ± 4.1	2.3 ± 0.4	–
D-tyrosine	1.21 ± 0.16	0.52 ± 0.08	40 ± 4	7.9 ± 1.9	–	6.5 ± 1.2	2.3 ± 0.4	–

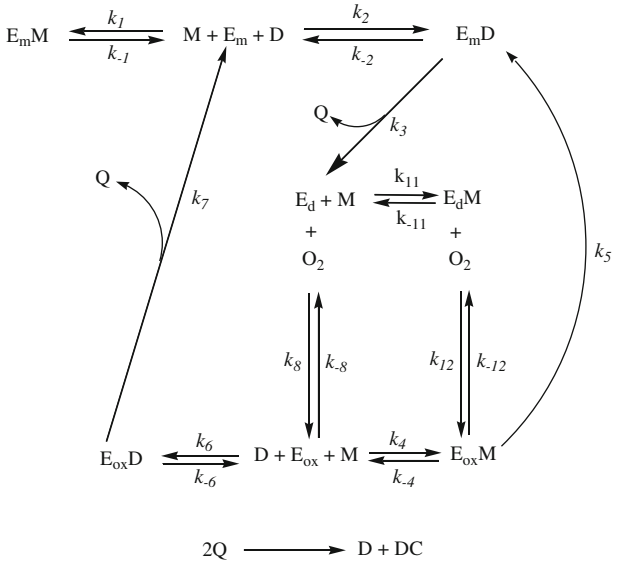

Scheme 2 Kinetic mechanism proposed to explain the action of tyrosinase on monophenols. E_m, *met*-tyrosinase; E_d, *deoxy*-tyrosinase; E_{ox}, *oxy*-tyrosinase; D, *o*-diphenol; Q, *o*-quinone; M, monophenol; $E_m M$, *met*-tyrosinase/monophenol complex; $E_m D$, *met*-tyrosinase/*o*-diphenol complex; $E_d M$, *deoxy*-tyrosinase/monophenol complex; $E_{ox} M$, *oxy*-tyrosinase/monophenol complex; $E_{ox} D$, *oxy*-tyrosinase/*o*-diphenol complex

mechanism of Scheme 2, accepting that the steady-state is reached, is Eq. (7), where a 3:3 ratio exists for the monophenol between the numerator and the denominator. The analytical expressions for $\gamma_1 - \gamma_{21}$ are given in the Appendix.

$$\frac{V_0}{[E]_0} = \frac{\begin{array}{c}\gamma_1[O_2]_0[M]_0^2 + \gamma_2[O_2]_0[D]_0[M]_0 + \gamma_3[O_2]_0[M]_0^3 \\ + \gamma_4[O_2]_0^2[M]_0^2 + \gamma_5[D]_0[O_2]_0[M]_0^2 + \gamma_6[D]_0[O_2]_0^2[M]\end{array}}{\begin{array}{l}\gamma_7[M]_0 + \gamma_8[M]_0^2 + \gamma_9[O_2]_0[M]_0 + \gamma_{10}[D]_0[M]_0 \\ + \gamma_{11}[D]_0[O_2]_0 + \gamma_{12}[M]_0^3 + \gamma_{13}[O_2]_0[M]_0^2 + \gamma_{14}[O_2]_0^2[M]_0 \\ + \gamma_{15}[D]_0[M]_0^2 + \gamma_{16}[D]_0[O_2]_0[M]_0 + \gamma_{17}[D]_0[O_2]_0^2 + \gamma_{18}[O_2]_0[M]_0^3 \\ + \gamma_{19}[O_2]_0^2[M]_0^2 + \gamma_{20}[D]_0[O_2]_0[M]_0^2 + \gamma_{21}[D]_0[O_2]_0^2[M]_0\end{array}} \tag{7}$$

Furthermore, the experimental data for the initial velocity *vs*. substrate concentration (monophenol), Fig. 3, point to a hyperbolic behaviour. From these data, it can be deduced that the mechanism does not follow the steady-state model, but must follow the rapid equilibrium model, meaning that the equation is simpler. If we consider the step governed by k_5 (hydroxylation reaction) as the slow step of the turnover, the velocity equation takes a hyperbolic form, Eq. (8). The expressions for $\varphi_1 - \varphi_9$ are given in the Appendix.

$$\frac{V_0}{[E]_0} = \frac{\varphi_1[D]_0[O_2]_0[M]_0 + \varphi_2[D]_0^2[O_2]_0}{\varphi_3[D]_0 + \varphi_4[O_2]_0[M]_0 + \varphi_5[D]_0[M]_0 + \varphi_6[D]_0[O_2]_0 + \varphi_7[O_2]_0[M]_0^2 + \varphi_8[D]_0[O_2]_0[M]_0 + \varphi_9[D]_0^2[O_2]_0} \tag{8}$$

Since $[D]_0/[M]_0 = R$ [25], $[D]_0$ in Eq. (8) can be substituted by $R[M]_0$ so that the equation simplifies to Eq. (9):

$$\frac{V_0}{[E]_0} = \frac{\left[\varphi_1 R[O_2]_0 + \varphi_2 R^2[O_2]_0\right][M]_0}{\varphi_3 R + \varphi_4[O_2]_0 + \varphi_6[O_2]_0 + \left[\varphi_5 R + \varphi_7[O_2]_0 + \varphi_8 R[O_2]_0 + \varphi_9 R^2[O_2]_0\right][M]_0} \tag{9}$$

The results of the kinetic study with monophenols are shown in Table 1. When the initial concentration of oxygen is saturating, so that only the rapid pathway is followed, the apparent Michaelis constant for the monophenol can be obtained (see Table 1):

$$K_m^{M(P)} = k_{\text{cat}}^M / k_4 \tag{10}$$

and

$$k_{\text{cat}}^M = k_5 \tag{11}$$

The apparent Michaelis constant for oxygen is:

$$K_{m,M}^{O_2(P)} = \frac{3}{2} k_{\text{cat}}^M / k_8 \tag{12}$$

The data showed in Table 1 and Fig. 3 shows that the mechanism is dependent of the oxygen concentration because the apparent Michaelis constant for oxygen increased from the Eq. (12)-value to a more complex expression, which is shown in Eq. (A47) (see Appendix).

Figure 3 Inset shows the values of the initial velocity *vs.* oxygen concentration at very high monophenol concentrations, and from this hyperbola the $K_{m,M}^{O_2(S)}$ can be obtained. When the initial concentration of oxygen is varied and the monophenol concentration is maintained constant, no sigmoid shape is obtained for velocity *vs.* oxygen concentration (Fig. 4). The data for Figs. 3 and 4 agreed with Eqs. (8) and (9) which are obtained taking into account the rapid equilibrium. These results agreed with other isotopic effect studies demonstrated that the limiting step of the monophenolase activity corresponded to the transference of the hydroxyl proton of the monophenol (position 4) to the peroxide of *oxy*-tyrosinase, which correspond to the step controlled by k_5 (Scheme 2) [26,27].

As can be seen in Fig. 1 Inset and Fig. 3 Inset, representing the initial velocity *vs.* initial oxygen concentration provides the Michaelis constant for oxygen in the slow pathway. In the case of monophenols, we obtain $K_{m,M}^{O_2(S)}$, a very complex expression (A47): note the increasing values of the apparent Michaelis constant for oxygen in

the slow pathway compared with that obtained in the kinetically preferred pathway (Table 1).

As regards the stereochemistry, according to the results depicted in Table 1, the values for K_m^S are much higher in the D isomers compared with L, both in *o*-diphenols and monophenols. However, $K_m^{O_2(P)}$ does not vary since k_{cat} is the same, the values of δ_3 and δ_4 being the same for both isomers. The data in Table 1 shows that the values of $K_m^{O_2(S)}$ are practically the same for both isomers, although much higher than those of $K_m^{O_2(P)}$. This difference is due to the oxygen binding constant: in the kinetically preferred pathway oxygen binds to *deoxy*-tyrosinase and in the slow pathway it binds to the intermediate *deoxy*-tyrosinase/*o*-diphenol or *deoxy*-tyrosinase/monophenol.

The experimental results show that tyrosinase expresses kinetic cooperativity when it acts on *o*-diphenols, which can be explained if only one active centre exists. Furthermore, these results indicate that, in the monophenolase activity, the limiting step in the turnover is the hydroxylation of monophenols to *o*-diphenols.

Acknowledgments This paper was partially supported by grants from the Ministerio de Educación y Ciencia (Madrid, Spain) Project BIO2009-12956, from the Fundación Séneca (CARM, Murcia, Spain) Projects 08856/PI/08 and 08595/PI/08, from the Consejería de Educación (CARM, Murcia, Spain) BIO-BMC 06/01-0004 and from FISCAM PI-2007/53 from the Consejería de Salud y Bienestar Social de la Junta de Comunidades de Castilla La Mancha. J.L.M.M. has a fellowship from the Ministerio de Educación y Ciencia (Madrid, Spain) Reference AP2005-4721. F.G.M has a fellowship from Fundación Caja Murcia (Murcia, Spain).

Appendix: Analytical expressions for the equations described in the main text

The expressions of the parameters $\alpha_i (i = 1, 2, 3, 4)$ involved in Eq. (5) are:

$$\alpha_1 = \frac{2k_3k_7}{k_3 + k_7} \tag{A1}$$

$$\alpha_2 = \frac{k_3K_9K_{10}}{k_3 + k_7} \tag{A2}$$

$$\alpha_3 = \frac{k_{-2}k_7 + k_3k_7 + k_2k_3K_6}{k_2(k_3 + k_7)} \tag{A3}$$

$$\alpha_4 = \frac{k_3K_{10}}{k_3 + k_7} \tag{A4}$$

The expressions of the parameters $\beta_i (i = 1, 2, 3, \ldots, 11)$ involved in Eq. (6) are:

$$\beta_1 = k_2k_3k_8k_6k_7k_{-9} + k_2k_3k_9k_{-8}k_7k_{10} + k_2k_3k_8k_6k_7k_{-9} + k_2k_3k_9k_{-8}k_7k_{10} \tag{A5}$$

$$\beta_2 = k_2k_3k_8k_6k_7k_{10} + k_2k_3k_8k_6k_7k_{10} \tag{A6}$$

$$\beta_3 = k_2k_3k_9k_6k_7k_{10} + k_2k_3k_9k_6k_7k_{10} \tag{A7}$$

$$\beta_4 = k_2k_3k_{-8}k_7k_{-9} + k_2k_3k_{-8}k_{-6}k_{-9} + k_2k_3k_{-8}k_{-10}k_{-9} \tag{A8}$$

$$\begin{aligned}\beta_5 = {} & k_{-2}k_8k_6k_7k_{-9} + k_{-2}k_9k_{-8}k_7k_{10} + k_3k_8k_6k_7k_{-9} + k_3k_9k_{-8}k_7k_{10} \\ & + k_2k_3k_{-8}k_7k_{10} + k_2k_3k_{-8}k_{-6}k_{10} + k_2k_3k_8k_7k_{-9} + k_2k_3k_8k_{-6}k_{-9} \\ & + k_2k_3k_8k_{-10}k_{-9}\end{aligned} \tag{A9}$$

$$\beta_6 = k_2k_3k_6k_7k_{-9} + k_2k_3k_6k_{-10}k_{-9} + k_2k_3k_9k_{-8}k_7 + k_2k_3k_9k_{-8}k_{-6} + k_2k_3k_9k_{-8}k_{-10} \quad \text{(A10)}$$

$$\beta_7 = k_{-2}k_8k_6k_7k_{10} + k_3k_8k_6k_7k_{10} + k_2k_3k_8k_7k_{10} + k_2k_3k_8k_{-6}k_{10} \quad \text{(A11)}$$

$$\beta_8 = k_{-2}k_9k_6k_7k_{10} + k_3k_9k_6k_7k_{10} + k_2k_8k_6k_7k_{-9} + k_2k_9k_{-8}k_7k_{10} + k_2k_3k_6k_7k_{10} + k_2k_3k_9k_{-6}k_{10} + k_2k_3k_8k_6k_{-9} + k_2k_3k_9k_{-8}k_{10} + k_2k_3k_8k_6k_{-10} \quad \text{(A12)}$$

$$\beta_9 = k_2k_3k_9k_6k_7 + k_2k_3k_9k_6k_{-10} \quad \text{(A13)}$$

$$\beta_{10} = k_2k_8k_6k_7k_{10} + k_2k_3k_8k_6k_{10} \quad \text{(A14)}$$

$$\beta_{11} = k_2k_9k_6k_7k_{10} + k_2k_3k_9k_6k_{10} \quad \text{(A15)}$$

The expressions of the parameters $\gamma_i (i = 1, 2, 3, \ldots, 20, 21)$ involved in Eq. (7) are:

$$\gamma_1 = k_{-1}k_2k_3k_8k_4k_5k_7k_{-11} + k_{-1}k_2k_3k_8k_4k_5k_{-6}k_{-11} + k_{-1}k_2k_3k_{11}k_{-8}k_5k_7k_{12} + k_{-1}k_2k_3k_{11}k_{-8}k_5k_{-6}k_{12} \quad \text{(A16)}$$

$$\gamma_2 = k_{-1}k_2k_3k_8k_6k_5k_7k_{-11} + k_{-1}k_2k_3k_8k_6k_{-4}k_7k_{-11} + k_{-1}k_2k_3k_8k_6k_{-12}k_7k_{-11} + k_{-1}k_2k_3k_8k_6k_5k_7k_{-11} + k_{-1}k_2k_3k_8k_6k_{-4}k_7k_{-11} + k_{-1}k_2k_3k_8k_6k_{-12}k_7k_{-11} \quad \text{(A17)}$$

$$\gamma_3 = k_{-1}k_2k_3k_{11}k_4k_5k_7k_{12} + k_{-1}k_2k_3k_{11}k_4k_5k_{-6}k_{12} \quad \text{(A18)}$$

$$\gamma_4 = k_{-1}k_2k_3k_8k_4k_5k_7k_{12} + k_{-1}k_2k_3k_8k_4k_5k_{-6}k_{12} \quad \text{(A19)}$$

$$\gamma_5 = k_{-1}k_2k_3k_{11}k_6k_5k_7k_{12} + k_{-1}k_2k_3k_{11}k_6k_{-4}k_7k_{12} + k_{-1}k_2k_3k_{11}k_6k_{-4}k_7k_{12} \quad \text{(A20)}$$

$$\gamma_6 = k_{-1}k_2k_3k_8k_6k_5k_7k_{12} + k_{-1}k_2k_3k_8k_6k_{-4}k_7k_{12} + k_{-1}k_2k_3k_8k_6k_5k_7k_{12} + k_{-1}k_2k_3k_8k_6k_{-4}k_7k_{12} \quad \text{(A21)}$$

$$\gamma_7 = k_{-1}k_2k_3k_{-8}k_5k_7k_{-11} + k_{-1}k_2k_3k_{-8}k_5k_{-6}k_{-11} + k_{-1}k_2k_3k_{-8}k_{-4}k_7k_{-11} + k_{-1}k_2k_3k_{-8}k_{-4}k_{-6}k_{-11} + k_{-1}k_2k_3k_{-8}k_{-12}k_7k_{-11} + k_{-1}k_2k_3k_{-8}k_{-12}k_{-6}k_{-11} \quad \text{(A22)}$$

$$\gamma_8 = k_{-1}k_2k_3k_4k_5k_7k_{-11} + k_{-1}k_2k_3k_4k_5k_{-6}k_{-11} + k_{-1}k_2k_3k_4k_{-12}k_7k_{-11} + k_{-1}k_2k_3k_4k_{-12}k_{-6}k_{-11} + k_{-1}k_2k_3k_{11}k_{-8}k_5k_7 + k_{-1}k_2k_3k_{11}k_{-8}k_5k_{-6} + k_{-1}k_2k_3k_{11}k_{-8}k_{-4}k_7 + k_{-1}k_2k_3k_{11}k_{-8}k_{-4}k_{-6} + k_{-1}k_2k_3k_{11}k_{-8}k_{-12}k_7 + k_{-1}k_2k_3k_{11}k_{-8}k_{-12}k_{-6} \quad \text{(A23)}$$

$$\gamma_9 = k_{-1}k_{-2}k_8k_4k_5k_7k_{-11} + k_{-1}k_{-2}k_8k_4k_5k_{-6}k_{-11} + k_{-1}k_{-2}k_{11}k_{-8}k_5k_7k_{12} + k_{-1}k_{-2}k_{11}k_{-8}k_5k_{-6}k_{12} + k_{-1}k_{-2}k_3k_{-8}k_5k_7k_{12} + k_{-1}k_2k_3k_{-8}k_5k_{-6}k_{12} + k_{-1}k_2k_3k_{-8}k_{-4}k_7k_{12} + k_{-1}k_2k_3k_{-8}k_{-4}k_{-6}k_{12} + k_{-1}k_2k_3k_8k_5k_7k_{-11} + k_{-1}k_2k_3k_8k_5k_{-6}k_{-11} + k_{-1}k_2k_3k_8k_{-4}k_7k_{-11} + k_{-1}k_2k_3k_8k_{-4}k_{-6}k_{-11} + k_{-1}k_2k_3k_8k_{-12}k_7k_{-11} + k_{-1}k_2k_3k_8k_{-12}k_{-6}k_{-11} \quad \text{(A24)}$$

$$\gamma_{10} = k_{-1}k_2k_3k_6k_5k_7k_{-11} + k_{-1}k_2k_3k_6k_{-4}k_7k_{-11} + k_{-1}k_2k_3k_6k_{-12}k_7k_{-11} \quad \text{(A25)}$$

$$\gamma_{11} = k_{-1}k_{-2}k_8k_6k_5k_7k_{-11} + k_{-1}k_{-2}k_8k_6k_{-4}k_7k_{-11} + k_{-1}k_{-2}k_8k_6k_{-12}k_7k_{-11} + k_{-1}k_3k_8k_6k_5k_7k_{-11} + k_{-1}k_3k_8k_6k_{-4}k_7k_{-11} + k_{-1}k_3k_8k_6k_{-12}k_7k_{-11} \tag{A26}$$

$$\gamma_{12} = k_{-1}k_2k_3k_{11}k_4k_5k_7 + k_{-1}k_2k_3k_{11}k_4k_5k_{-6} + k_{-1}k_2k_3k_{11}k_4k_{-12}k_7 + k_{-1}k_2k_3k_{11}k_4k_{-12}k_{-6} \tag{A27}$$

$$\gamma_{13} = k_1k_{-2}k_8k_4k_5k_7k_{-11} + k_1k_{-2}k_8k_4k_5k_{-6}k_{-11} + k_1k_{-2}k_{11}k_{-8}k_5k_7k_{12} + k_1k_{-2}k_{11}k_{-8}k_5k_{-6}k_{12} + k_{-1}k_{-2}k_{11}k_4k_5k_7k_{12} + k_{-1}k_{-2}k_{11}k_4k_5k_{-6}k_{12} + k_{-1}k_2k_8k_4k_5k_7k_{-11} + k_{-1}k_2k_8k_4k_5k_{-6}k_{-11} + k_{-1}k_2k_{11}k_{-8}k_5k_7k_{12} + k_{-1}k_2k_{11}k_{-8}k_5k_{-6}k_{12} + k_{-1}k_2k_3k_4k_5k_7k_{12} + k_{-1}k_2k_3k_4k_5k_{-6}k_{12} + k_{-1}k_2k_3k_{11}k_{-4}k_7k_{12} + k_{-1}k_2k_3k_{11}k_{-4}k_{-6}k_{12} + k_{-1}k_2k_3k_8k_4k_7k_{-11} + k_{-1}k_2k_3k_8k_4k_{-6}k_{-11} + k_{-1}k_2k_3k_{11}k_{-8}k_7k_{12} + k_{-1}k_2k_3k_{11}k_{-8}k_{-6}k_{12} + k_{-1}k_2k_3k_8k_4k_{-12}k_7 + k_{-1}k_2k_3k_8k_4k_{-12}k_{-6} \tag{A28}$$

$$\gamma_{14} = k_{-1}k_{-2}k_8k_4k_5k_7k_{12} + k_{-1}k_{-2}k_8k_4k_5k_{-6}k_{12} + k_{-1}k_2k_3k_8k_5k_7k_{12} + k_{-1}k_2k_3k_8k_5k_{-6}k_{12} + k_{-1}k_2k_3k_8k_{-4}k_7k_{12} + k_{-1}k_2k_3k_8k_{-4}k_{-6}k_{12} \tag{A29}$$

$$\gamma_{15} = k_{-1}k_2k_3k_{11}k_6k_5k_7 + k_{-1}k_2k_3k_{11}k_6k_{-4}k_7 + k_{-1}k_2k_3k_{11}k_6k_{-12}k_7 \tag{A30}$$

$$\gamma_{16} = k_1k_{-2}k_8k_6k_5k_7k_{-11} + k_1k_{-2}k_8k_6k_{-4}k_7k_{-11} + k_1k_{-2}k_8k_6k_{-12}k_7k_{-11} + k_1k_3k_8k_6k_5k_7k_{-11} + k_1k_3k_8k_6k_{-4}k_7k_{-11} + k_1k_3k_8k_6k_{-12}k_7k_{-11} + k_{-1}k_{-2}k_{11}k_6k_5k_7k_{12} + k_{-1}k_{-2}k_{11}k_6k_{-4}k_7k_{12} + k_{-1}k_3k_{11}k_6k_{-4}k_7k_{-12} + k_{-1}k_2k_8k_6k_5k_7k_{-11} + k_{-1}k_2k_8k_6k_{-4}k_7k_{-11} + k_{-1}k_2k_8k_6k_{-12}k_7k_{-11} + k_{-1}k_2k_3k_6k_5k_7k_{12} + k_{-1}k_2k_3k_6k_{-4}k_7k_{12} + k_{-1}k_2k_3k_8k_6k_5k_{-11} + k_{-1}k_2k_3k_8k_6k_{-4}k_{-11} + k_{-1}k_2k_3k_8k_6k_{-12}k_{-11} \tag{A31}$$

$$\gamma_{17} = k_{-1}k_{-2}k_8k_6k_5k_7k_{12} + k_{-1}k_{-2}k_8k_6k_{-4}k_7k_{12} + k_{-1}k_3k_8k_6k_5k_7k_{12} + k_{-1}k_3k_8k_6k_{-4}k_7k_{12} \tag{A32}$$

$$\gamma_{18} = k_1k_{-2}k_{11}k_4k_5k_7k_{12} + k_1k_{-2}k_{11}k_4k_5k_{-6}k_{12} + k_{-1}k_2k_{11}k_4k_5k_7k_{12} + k_{-1}k_2k_{11}k_4k_5k_{-6}k_{12} + k_{-1}k_2k_3k_{11}k_4k_7k_{12} + k_{-1}k_2k_3k_{11}k_4k_{-6}k_{12} \tag{A33}$$

$$\gamma_{19} = k_1k_{-2}k_8k_4k_5k_7k_{12} + k_1k_{-2}k_8k_4k_5k_{-6}k_{12} + k_{-1}k_2k_8k_4k_5k_7k_{12} + k_{-1}k_2k_8k_4k_5k_{-6}k_{12} + k_{-1}k_2k_3k_8k_4k_7k_{12} + k_{-1}k_2k_3k_8k_4k_{-6}k_{12} \tag{A34}$$

$$\gamma_{20} = k_1k_{-2}k_{11}k_6k_5k_7k_{12} + k_1k_{-2}k_{11}k_6k_{-4}k_7k_{12} + k_1k_3k_{11}k_6k_{-4}k_7k_{12} + k_{-1}k_2k_{11}k_6k_5k_7k_{12} + k_{-1}k_2k_{11}k_6k_{-4}k_7k_{12} + k_{-1}k_2k_3k_{11}k_6k_7k_{12} + k_{-1}k_2k_3k_{11}k_6k_{-4}k_{12} \tag{A35}$$

$$\gamma_{21} = k_1k_{-2}k_8k_6k_5k_7k_{12} + k_1k_{-2}k_8k_6k_{-4}k_7k_{12} + k_1k_3k_8k_6k_5k_7k_{12} + k_1k_3k_8k_6k_{-4}k_7k_{12} + k_{-1}k_2k_8k_6k_5k_7k_{12} + k_{-1}k_2k_8k_6k_{-4}k_7k_{12} + k_{-1}k_2k_3k_8k_6k_5k_{12} + k_{-1}k_2k_3k_8k_6k_{-4}k_{12} \tag{A36}$$

The expressions of the parameters $\varphi_i (i = 1, 2, 3 \ldots 9)$ involved in Eq. (8) are:

$$\varphi_1 = K_1 k_2 k_3 k_5 k_7 + K_1 k_2 k_3 k_5 k_{-6} \tag{A37}$$
$$\varphi_2 = K_1 k_2 k_3 k_6 K_4 k_7 + K_1 k_2 k_3 k_6 K_4 k_7 \tag{A38}$$
$$\varphi_3 = K_1 k_2 k_3 K_8 K_4 k_7 + K_1 k_2 k_3 K_8 K_4 k_{-6} \tag{A39}$$
$$\varphi_4 = K_1 k_{-2} k_5 k_7 + K_1 k_{-2} k_5 k_{-6} \tag{A40}$$
$$\varphi_5 = K_1 k_2 k_3 K_{12} k_7 + K_1 k_2 k_3 K_{12} k_{-6} \tag{A41}$$
$$\varphi_6 = K_1 k_{-2} k_6 K_4 k_7 + K_1 k_3 k_6 K_4 k_7 + K_1 k_2 k_3 K_4 k_7 + K_1 k_2 k_3 K_4 k_{-6} \tag{A42}$$
$$\varphi_7 = k_{-2} k_5 k_7 + k_{-2} k_5 k_{-6} \tag{A43}$$
$$\varphi_8 = k_{-2} k_6 K_4 k_7 + k_3 k_6 K_4 k_7 + K_1 k_2 k_5 k_7 + K_1 k_2 k_5 k_{-6} + K_1 k_2 k_3 k_7 + K_1 k_2 k_3 k_{-6} \tag{A44}$$
$$\varphi_9 = K_1 k_2 k_6 K_4 k_7 + K_1 k_2 k_3 k_6 K_4 \tag{A45}$$

The analytical expression for R is:

$$R = \frac{k_{\text{cat}}^{M} K_m^{D(P)}}{2 k_{\text{cat}}^{D} K_m^{M(P)}} = \frac{k_4}{2 k_6} \tag{A46}$$

Taking into account the Eqs. (A46) and Eqs. (A41), (A43), (A44) and (A45), $K_m^{O_2(S)}$ in the monophenolase activity, is:

$$K_m^{O_2(S)} = \frac{\varphi_5 R}{\varphi_7 + \varphi_8 R + \varphi_9 R^2} \tag{A47}$$

References

1. A. Cornish-Bowden, in *Fundamentals of enzyme kinetics*, ed. by A. Cornish-Bowden (Butterworths, London, 1979), pp. 172–175
2. R.B. Silverman, in *Contemporary enzyme kinetics and mechanism*, ed. by D.L. Purich (San Diego, 2009), pp. 246–248
3. W. Ferdinand, in *The enzyme molecule*, ed. by W. Ferdinand (John Wiley and Sons, London, 1976), pp. 139–185
4. D. Atkinson, G.M. Walton, J. Biol. Chem. **240**, 757 (1965)
5. J.A. Hathaway, D.E. Atkinson, J. Biol. Chem. **238**, 2875 (1963)
6. R.G. Wolfe, J.B. Neilands, J. Biol. Chem. **221**, 61 (1956)
7. E.I. Solomon, U.M. Sundaram, T.E. Machonkin, Chem. Rev. **96**, 2563 (1996)
8. R.L. Jolley, L.H. Evans, N. Makino, H.S. Mason, J. Biol. Chem. **249**, 335 (1974)
9. Y. Matoba, T. Kumagai, A. Yamamoto, H. Yoshitsu, M. Sugiyama, J. Biol. Chem. **281**, 8981 (2006)
10. H. Decker, T. Schweikardt, F. Tuczek, Angew. Chem. Int. Ed. **45**, 4546 (2006)
11. R.J. Deeth, C. Diedrich, J. Biol. Inorg. Chem. **15**, 117 (2010)
12. A. Sanchez-Ferrer, J.N. Rodriguez-Lopez, F. Garcia-Canovas, F. Garcia-Carmona, Biochim. Biophys. Acta **1247**, 1 (1995)
13. F. Garcia-Molina, J.L. Munoz, R. Varon, J.N. Rodriguez-Lopez, F. Garcia-Canovas, J. Tudela, J. Agric. Food Chem. **55**, 9739 (2007)
14. L.G. Fenoll, J.N. Rodriguez-Lopez, F. Garcia-Sevilla, P.A. Garcia-Ruiz, R. Varon, F. Garcia-Canovas, J. Tudela, Biochim. Biophys. Acta **1548**, 1 (2001)

15. J.N. Rodriguez-Lopez, J. Tudela, R. Varon, F. Garcia-Carmona, F. Garcia-Canovas, J. Biol. Chem. **267**, 3801 (1992)
16. J.L. Munoz-Munoz, F. Garcia-Molina, R. Varon, J. Tudela, F. Garcia-Canovas, J.N. Rodriguez-Lopez, Biochim. Biophys. Acta **1794**, 1017 (2009)
17. J.N. Rodriguez-Lopez, L.G. Fenoll, P.A. Garcia-Ruiz, R. Varon, J. Tudela, R.N. Thorneley, F. Garcia-Canovas, Biochemistry **39**, 10497 (2000)
18. M.M. Bradford, Anal. Biochem. **72**, 248 (1976)
19. F. Garcia-Carmona, F. Garcia-Canovas, J.L. Iborra, J.A. Lozano, Biochim. Biophys. Acta **717**, 124 (1982)
20. F. Garcia-Canovas, F. Garcia-Carmona, J. Vera-Sanchez, J.L. Iborra, J.A. Lozano, J. Biol. Chem. **257**, 8738 (1982)
21. J.L. Munoz, F. Garcia-Molina, R. Varon, J.N. Rodriguez-Lopez, F. Garcia-Canovas, J. Tudela, Anal. Biochem. **351**, 128 (2006)
22. J.N. Rodriguez-Lopez, J.R. Ros-Martinez, R. Varon, F. Garcia-Canovas, Anal. Biochem. **202**, 356 (1992)
23. Jandel Scientific, Sigma Plot 9.0 for Windows^{TM}; Jandel Scientific: Core Madera (2006)
24. E. Van Schaftingen, M.-F. Jet, L. Hue, H.-G. Hers, Proc. Natl. Acad. Sci. USA **78**, 3483 (1981)
25. J.R. Ros, J.N. Rodriguez-Lopez, F. Garcia-Canovas, Biochim. Biophys. Acta **1204**, 33 (1994)
26. L.G. Fenoll, M.J. Peñalver, J.N. Rodriguez-Lopez, P.A. Garcia-Ruiz, F. Garcia-Canovas, J. Tudela, Biochem. J. **380**, 643 (2004)
27. M.J. Peñalver, J.N. Rodriguez-Lopez, P.A. Garcia-Ruiz, F. Garcia-Canovas, J. Tudela, Biochim. Biophys. Acta **1650**, 128 (2003)

4.2. COOPERATIVIDAD CINETICA DE TIROSINASA: UN MECANISMO GENERAL.

El mecanismo general propuesto para explicar la cooperatividad cinética de tirosinasa ha dado lugar a la siguiente publicación adjunta.

4.2.1. Título

Kinetic cooperativity of tyrosinase. A general mechanism.

4.2.2. Autores

Muñoz-Muñoz, J.L.; Garcia-Molina, F.; Varon, R.; Tudela, J.; Garcia-Cánovas, F. y Rodríguez-López, J.N.

4.2.3. Referencia

Acta Biochimica Polonica (2011) 58, 303-311.

4.2.4. Resumen

Tirosinasa muestra cooperatividad cinética cuando actúa sobre *o*-difenoles, sin embargo esto no ocurre cuando actúa sobre monofenoles, confirmando que la etapa lenta es la hidroxilación de monofenoles a *o*-difenoles. Se generaliza este modelo al estudiar una amplia gama de sustratos. Sustratos tipo S_A, que originan un producto estable mediante la evolución de la *o*-quinona a través de una reacción de primer o pseudo primer orden (α-metil-Dopa, Dopa metil ester, dopamina, ácido 3,4-dihidroxifenilpropionico, ácido 3,4-dihidroxifenilacético, α-metil-tirosina, tirosina metil ester, tiramina, ácido 4-hidroxifenilpropionico y ácido 4-hidroxifenilacético). Sustratos tipo S_B, que comprende aquellos cuya *o*-quinona no evoluciona con una estequiometría definida (catecol, 4-metilcatecol, fenol y *p*-cresol) y, por último, sustratos tipo S_C, aquellos que originan *o*-quinonas estables (4-*terc*-butilcatecol/4-*terc*-butilfenol).

ACTA ABP BIOCHIMICA POLONICA

Vol. 58, No 3/2011
303–311
on-line at: www.actabp.pl

Regular paper

Kinetic cooperativity of tyrosinase. A general mechanism

Jose Luis Muñoz-Muñoz[1], Francisco Garcia-Molina[1], Ramón Varon[2], Jose Tudela[1], Francisco Garcia-Cánovas[1]✉ and Jose N. Rodríguez-López[1]

[1]GENZ: Grupo de Investigación Enzimología, Departamento de Bioquímica y Biología Molecular-A, Facultad de Biología, Universidad de Murcia, Espinardo, Murcia, Spain; [2]Departamento de Química-Física, Escuela de Ingenieros Industriales de Albacete, Universidad de Castilla la Mancha, Avda, España s/n. Campus Universitario, Albacete, Spain

Tyrosinase shows kinetic cooperativity in its action on *o*-diphenols, but not when it acts on monophenols, confirming that the slow step is the hydroxylation of monophenols to *o*-diphenols. This model can be generalised to a wide range of substrates; for example, type S_A substrates, which give rise to a stable product as the *o*-quinone evolves by means of a first or pseudo first order reaction (α-methyl dopa, dopa methyl ester, dopamine, 3,4-dihydroxyphenylpropionic acid, 3,4-dihydroxyphenylacetic acid, α-methyl-tyrosine, tyrosine methyl ester, tyramine, 4-hydroxyphenylpropionic acid and 4-hydroxyphenylacetic acid), type S_B substrates, which include those whose *o*-quinone evolves with no clear stoichiometry (catechol, 4-methylcatechol, phenol and *p*-cresol) and, lastly, type S_C substrates, which give rise to stable *o*-quinones (4-*tert*-butylcatechol/4-*tert*-butylphenol).

Keywords: tyrosinase, *o*-diphenols

Received: 10 November, 2010; revised: 14 March, 2011; accepted: 04 July, 2011; available on-line: 29 August, 2011

INTRODUCTION

Tyrosinase (TYR; monophenol monooxygenase, *o*-diphenol:oxygen oxidoreductase; EC 1.14.18.1) has two copper atoms in its active site and is ubiquitously present in biological systems. It has two physiological activities involving molecular oxygen; (a) the *ortho*-hydroxylation of monophenols to *o*-diphenols and (b) the oxidation of *o*-diphenols to their corresponding *o*-quinones (monophenolase and diphenolase activities, respectively). The active site of TYR takes on three forms in the catalytic cycle: E_m (*met*-TYR, $Cu^{2+}Cu^{2+}$), E_d (*deoxy*-TYR, $Cu^{2+}Cu^{2+}$) and E_{ox} (*oxy*-TYR, $Cu^{2+}Cu^{2+}O^{2-}_2$) (Solomon *et al.*, 1996). In the TYR structure from *Streptomyces castaneoglobisporus* (Matoba *et al.*, 2006), each copper atom of the active site of TYR is coordinated with three histidines (two joined equatorially and the other axially) (Matoba *et al.*, 2006). The E_{ox} form can act both on monophenols and *o*-diphenols, while the E_m form is only active on *o*-diphenols (Sanchez-Ferrer *et al.*, 1995).

The instability of the products formed by the action of TYR on monophenols and *o*-diphenols, the *o*-quinones, is responsible for the formation of H_2O_2 in the melanin biosynthesis pathway (Munoz-Munoz *et al.*, 2009) and, at the same time, hinders the kinetic characterisation of these substrates (Rodriguez-Lopez *et al.*, 2000; Espin *et al.*, 2000). For this reason, and to obtain correct measurements of the initial velocity that would permit quantitative kinetic studies, we used a reductant (NADH or AH_2) to prevent the evolution of these *o*-quinones and so be able to characterize kinetically the action of this enzyme on *o*-diphenols using spectrophotometric methods. Moreover, *o*-quinones can react with nucleophilic reagents such as MBTH or thiols such as L-cysteine (Rodriguez-Lopez *et al.*, 1994; Peñalver *et al.*, 2002), which is useful for directing them towards an adduct with a given stoichiometry. Because oxygen acts as a substrate of the enzyme, an oxymetric method has also been used to measure the enzymatic activity of TYR on some substrates (Rodriguez-Lopez *et al.*, 1992).

Cooperativity is a widely studied process in enzymology (Monod *et al.*, 1965; Koshland *et al.*, 1966). At first it was thought that this phenomenon was exclusive to proteins or oligomeric enzymes such as haemoglobin, and binding equilibrium models were proposed to explain it — first the model proposed by Monod, Wyman and Changeaux and subsequently that of Koshland, Nemethy and Filmer (Monod *et al.*, 1965; Koshland *et al.*, 1966). However, it was subsequently demonstrated that also monomeric enzymes had a sigmoid kinetics — Rabin's model and, later, that proposed by Ferdinand (Rabin, 1967; Ferdinand, 1976). Among enzymes which have been shown to deviate from the hyperbolic kinetics models are phosphofructokinase (Atkinson & Walton, 1965), isocitrate dehydrogenase of yeast (Hathaway & Atkinson, 1963) and heart malate dehydrogenase (Wolfe & Neilands, 1956).

When extracted in a latent form, the TYR of some vegetal sources, such as grapes (*Vitis vinifera cv Airen*) or iceberg lettuce (*Lactuca sativa L.*) (Valero & Garcia-Carmona, 1992; Chazarra *et al.*, 2001), show negative or positive cooperativity when the initial velocity data are represented *vs.* the substrate concentration, deviating from the typical hyperbolic kinetics described for enzymes

✉e-mail: canovasf@um.es

Abbreviations: see Table 1. *Species and concentrations*: $[O_2]_0$, Initial oxygen concentration; D, diphenol; $[D]_0$, initial diphenol concentration; M, monophenol; $[M]_0$, initial monophenol concentration; *E*, enzyme (tyrosinase); $[E]_0$, initial concentration of enzyme; E_{ox}, *oxy*-tyrosinase; E_d, *deoxy*-tyrosinase; E_m, *met*-tyrosinase. *Kinetic parameters*: V_0^D, initial rate of tyrosinase acting on D; $V^M{}_0$, initial rate of tyrosinase acting on M; $V_{max}{}^D$, maximal rate of tyrosinase for D; $V_{max}{}^M$, maximal rate of tyrosinase for M; $k_{cat}{}^D$, catalytic constant of tyrosinase acting on D; $k_{cat}{}^M$, catalytic constant of tyrosinase acting on M; $K_m^{D(P)}$, apparent Michaelis constant of tyrosinase for D in the kinetically preferred pathway; $K_m{}^{M(P)}$, apparent Michaelis constant of tyrosinase for M in the kinetically preferred pathway; $K_{m,D}{}^{O_2(P)}$, apparent Michaelis constant for O_2 in the diphenolase activity on the kinetically preferred pathway; $K_{m,D}{}^{O_2(S)}$, apparent Michaelis constant for O_2 in the diphenolase activity on the slow pathway; $K_{m,M}{}^{O2(P)}$, apparent Michaelis constant for O_2 in the monophenolase activity on the kinetically preferred pathway; $K_{m,M}{}^{O_2(S)}$, apparent Michaelis constant for O_2 in the monophenolase activity on the slow pathway.

type Michaelis–Menten. In a recent work (Munoz-Munoz *et al*., 2010), our group found deviations from hyperbolic kinetics when the steady-state rate was represented *vs*. the concentration of the *o*-diphenolic substrate in the diphenolase activity of mushroom TYR, when working with the physiological substrates L-dopa, and its isomer D-dopa. In light of this, we suggested the existence of a kinetically preferred pathway and a slow pathway in the catalytic mechanism of TYR acting on *o*-diphenols. This translated into the appearance of inhibition by excess substrate when the steady state rate was represented *vs* initial *o*-diphenolic substrate concentration and sigmoid curves when the initial velocity was represented *vs* the concentration of oxygen. These deviations from the classical hyperbolic behaviour shown by TYR when the initial substrate concentration is varied are demonstrated in the diphenolase activity of TYR (Munoz-Munoz *et al*., 2010). However, they do not appear in the monophenolase activity (Munoz-Munoz *et al*., 2010). These findings can be explained kinetically if we accept that, in the case of diphenolase activity, the enzymatic system functions in the steady state, while, in the case of monophenolase activity, the system works in rapid equilibrium.

Recently, in a paper dealing with mushroom tyrosinase, Haghbeen *et al*. (2010), proposed that the enzyme showed a mixed type of cooperativity, that is, positive at low substrate concentrations and negative at high concentrations. This type of cooperativity has also been described in other enzymes such as bovine seminal ribonuclease (Piccoli *et al*., 1988), and requires several substrate binding sites. However, recent studies on the structure of mushroom tyrosinase describe it a monomer (Wichers *et al*., 1996; 2003).

In a previous work, we demonstrated the kinetic cooperativity of tyrosinase acting on the monophenol/*o*-diphenol pair, L-tyrosine/L-dopa, and its isomers D-tyrosine/D-dopa (Munoz-Munoz *et al*., 2010). Because the enzyme has wide substrate specificity, our aim in this work is to extend this kinetic study to different types of tyrosinase substrate in an attempt to generalise the applicable model. The substrates studied are characterised by their different groups in C-1: H in the case of catechol, a hydrophobic group like methyl (4-methylcatechol) or *tert*-butyl (4-*tert*-butylcatechol), a negatively charged group (3,4-dihydroxyphenylacetic acid and 3,4-dihydroxyphenylpropionic acid), a positively charged group (dopamine and dopa methyl ester) and a doubly charged group, such as α-methyldopa and its respective monophenols. Moreover, the studied substrates were classified into three groups (S_A, S_B and S_C), according to the type of *o*-quinone that they generate when oxidised by TYR. The S_A group includes those that give rise to *o*-quinones that stabilise through a first order reaction, or which evolve through the attack of a nucleophile like MBTH in a first order reaction. The S_B group is formed of those that give rise to *o*-quinones that evolve with no clear stoichiometry, and lastly the S_C group comprises those that give rise to stable *o*-quinones. The analysis of the initial velocity data with regard to substrate concentration (monophenol, *o*-diphenol and oxygen) provides a general model that explains the cooperativity of TYR.

Table 1. Structures of substrates used in this work

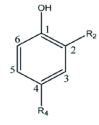

o-Diphenols	R_4	R_2
Catechol (Cat)	H	-OH
4-Methylcatechol (4MeCat)	CH_3	-OH
4-*tert*-Butylcatechol (TBC)	$-C-(CH_3)_3$	-OH
3,4-Dihydroxyphenylacetic acid (DHPAA)	$-CH_2-COO^-$	-OH
3,4-Dihydroxyphenylpropionic acid (DHPPA)	$-CH_2-CH_2-COO^-$	-OH
Dopamine	$-CH_2-CH_2-NH_3^+$	-OH
Dopa methyl ester (DopaMeEster)	$-CH_2-CH(NH_3^+)-COOCH_3$	-OH
α-Methyl DOPA (α-MeDOPA)	$-CH_2-C(CH_3)(NH_3^+)-COO^-$	-OH
Monophenols	R_4	R_2
Phenol	-H	-H
p-Cresol	CH_3	-H
4-*tert*-Butylphenol (TBF)	$-C-(CH_3)_3$	-H
4-Hydroxyphenylacetic acid (PHPAA)	$-CH_2-COO^-$	-H
4-Hydroxyphenylpropionic acid (PHPPA)	$-CH_2-CH_2-COO^-$	-H
L-Tyramine	$-CH_2-CH_2-NH_3^+$	-H
L-Tyrosine methyl ester	$-CH_2-CH(NH_3^+)-COOCH_3$	-H
α-Methyl-L-tyrosine	$-CH_2-C(CH_3)(NH_3^+)-COO^-$	-H

MATERIALS AND METHODS

Reagents. Commercial mushroom tyrosinase (TYR) was purchased from Sigma (Madrid, Spain). The substrates (*o*-diphenols and monophenols) used in this work were: catechol (Cat), 4-*tert*-butylcatechol (TBC), 4-methylcatechol (4-MeCat), α-methyl dopa, dopa methyl ester (DopaMeEster), dopamine, 3,4-dihydroxyphenylpropionic acid (DHPPA), 3,4-dihydroxyphenylacetic acid (DHPAA), phenol, 4-*tert*-butylphenol (TBF), *p*-cresol, α-methyl tyrosine, tyrosine methyl ester, tyramine, 4-hydroxyphenylpropionic acid (PHPPA) and 4-hydroxyphenylacetic acid (PHPAA) and were purchased from Sigma-Aldrich. NADH and L-cysteine were also purchased from Sigma-Aldrich (Madrid, Spain). Other chemicals were of analytical grade and supplied by Merck (Darmstadt, Germany). Stock solutions of the diphenolic and monophenolic substrates were prepared in 0.15 mM phosphoric acid to prevent autooxidation. Milli-Q system (Millipore Corp.) ultrapure water was used throughout.

Spectrophotometric assays. These assays were carried out with a Perkin-Elmer Lambda-35 spectrophotometer, interfaced to a PC-computer, where the kinetic data were recorded, stored and later analyzed. The product of the enzyme reaction, the *o*-quinone, cannot be correctly detected experimentally due to the instability of *o*-quinones (Garcia-Carmona *et al*., 1982; Garcia-Canovas *et al*., 1982). Therefore, the reaction was followed in each case by measuring: (a) the disappearance of NsADH at 340 nm with $\varepsilon = 6230\ M^{-1} \cdot cm^{-1}$, (Cat, 4-MeCat and TBC) (Garcia-Molina *et al*.,

2007), (b) the accumulation of dopachrome at 475 nm with $\varepsilon = 3600\ M^{-1}\cdot cm^{-1}$ (α-methyl dopa, dopa methyl ester, tyrosine methyl ester, α-methyl tyrosine) (Munoz *et al.*, 2006), (c) the appearance of the adduct between L-cysteine and *o*-diphenol at 300 nm with $\varepsilon =$ 2067, 2050 and 2007 $M^{-1}\cdot cm^{-1}$ for dopamine, DHPPA and DHPAA, respectively (Peñalver *et al.*, 2002) and (d) the appearance of the adduct between a nucleophile (MBTH) and the quinoneimine of 4-aminoanisole and 4-aminophenylalanine (Rodriguez-Lopez *et al.* 1994). The cuvette (final volume 1 ml) contained 30 mM sodium phosphate buffer (pH 7.0). The initial substrate (monophenol and *o*-diphenol) and oxygen concentrations were varied as indicated in the figure legends. The reaction was started by adding enzyme.

Oxymetric assays. Measurements of dissolved oxygen concentration were made with a Hansatech (Kings Lynn, Norfolk, UK) oxygraph unit controlled by a PC. The oxygraph used a Clark-type silver/platinum electrode with a 12.5 mm teflon membrane. The sample was continuously stirred during the experiments and its temperature was maintained at 25 °C. The zero oxygen level for calibration and experiments was obtained by bubbling oxygen-free nitrogen through the sample for at least 10 min (Rodriguez-Lopez *et al.*, 1992). The initial concentrations of the monophenols TBF, *p*-cresol, tyramine, PHPPA, PHPAA and oxygen were varied as indicated in the legends of the figures. The initial oxygen concentration was varied as indicated in the legends of figures.

Kinetic data analysis. V^{M}_{0} or V^{D}_{0} values were calculated from triplicate measurements at each oxygen and reducing substrate concentration. The fitting was carried out using the Sigma Plot 9.0 program for Windows (Jandel Scientific, 2006), obtaining V^{M}_{max} or V^{D}_{max}, respectively, and $K^{M(P)}_{m}$ or $K^{D(P)}_{m}$, respectively, by non-linear regression to the Michaelis–Menten equation.

^{13}C-NMR assays. ^{13}C-NMR spectra of several substrates were obtained at pH = 7.0 in a Varian Unity spectrometer at 300 MHz, using $^{2}H_2O$ as solvent for the substrates. Chemical displacement (δ) values were measured relative to those for tetramethylsilane (δ = 0). The maximum line breadth accepted in the ^{13}C-NMR spectra was 0.06 Hz. Therefore, the maximum accepted error for each peak of the spectrum was ± 0.03 p.p.m.

RESULTS AND DISCUSION

Mushroom tyrosinase (EC 1.14.18.1) is an enzyme that catalyses two types of reaction, the hydroxylation of monophenols to *o*-diphenols (monophenolase activity) and the oxidation of *o*-diphenols to *o*-quinones (diphenolase activity) (Solomon *et al.*, 1996).

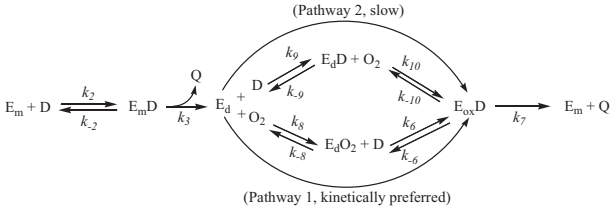

Scheme 1. Kinetic mechanism proposed to explain the action of TYR on *o*-diphenols
E_m, *met*-TYR; E_d, *deoxy*-TYR; E_{ox}, *oxy*-TYR; D, *o*-diphenol; Q, *o*-quinone; E_mD, *met*-TYR/*o*-diphenol complex; E_dD, *deoxy*-TYR/*o*-diphenol complex; E_dO_2; *deoxy*-TYR/oxygen complex; $E_{ox}D$, *oxy*-TYR/*o*-diphenol complex.

The activity on *o*-diphenols is described in Scheme 1, while the more complex activity on monophenols is described in Scheme 2. The product of monophenols and *o*-diphenols are *o*-quinones, which evolve chemically. As regards the evolution of these *o*-quinones, the substrates of the enzyme can be grouped into three types (groups S_A, S_B and S_C). The first group (S_A) corresponds to substrates that originate *o*-quinones, which evolve to a stable product, either spontaneously through a first order reaction (such as L-α-MeDopa, DL-α-MeDopa, DopaMeEster or dopamine) or through attack by a nucleophilic reagent (pseudo first order reaction, as in the case of MBTH) towards a stable chromophore. In both cases an *o*-diphenol is accumulated in the medium. Group S_B comprises those substrates whose *o*-quinones do not evolve through a well defined stoichiometry so that *o*-diphenol is not accumulated quantitatively: for example, Cat/phenol and 4-MeCat/*p*-Cresol. Lastly, group S_C corresponds to those substrates that give rise to a stable *o*-quinone, such as the pair TBC/TBF.

Monophenolase activity

The monophenolase activity is measured by adding the amount of *o*-diphenol at $t = 0$ that leads the system to reach the steady state, with $[D]_0/[M]_0 = R =$ constant (Scheme 2) (Ros *et al.*, 1994).

***S_A* type substrates.** In the case of PHPPA, the chromophore obtained when MBTH reacts with the *o*-quinone was measured spectrophotometrically at the corresponding wavelength (Rodriguez-Lopez *et al.*, 1994). Figure 1 shows the data obtained by varying the initial concentration of PHPPA, $[PHPPA]_0$, and keeping the oxygen concentration fixed. In all cases a hyperbolic behaviour is observed. The only way in which the mechanism of Scheme 2 will behave hyperbolically, Eqn. (1) (Varon-Castellanos *et al.*, 1995), is to assume that the set of reactions occurs through rapid equilibrium, with the step controlled by k_5 being limiting (Munoz-Munoz *et al.*, 2010). The expressions of φ_1–φ_9 and R are shown in the Appendix (at www.actabp.pl).

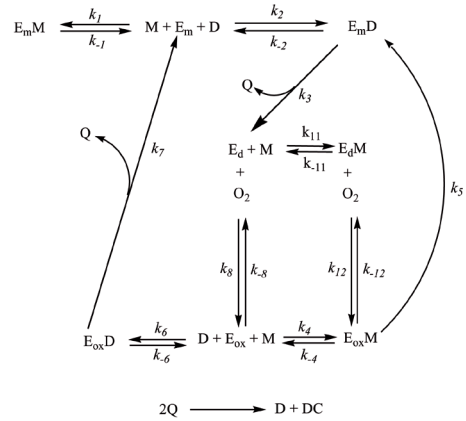

Scheme 2. Kinetic mechanism proposed to explain the action of TYR on monophenols
E_m, *met*-TYR; E_d, *deoxy*-TYR; E_{ox}, *oxy*-TYR; D, *o*-diphenol; Q, *o*-quinone; M, monophenol; E_mM, *met*-TYR/monophenol complex; E_mD, *met*-TYR/*o*-diphenol complex; E_dM, *deoxy*-TYR/monophenol complex; $E_{ox}M$, *oxy*-TYR/monophenol complex; E_dD, *oxy*-TYR/*o*-diphenol complex.

$$\frac{V_0^M}{[E]_0} = \frac{\left[\varphi_1 R[O_2]_0 + \varphi_2 R^2[O_2]_0\right][M]_0}{\varphi_3 R + [\varphi_4 + \varphi_6 R][O_2]_0 + \left[\varphi_5 R + \varphi_7[O_2]_0 + \varphi_8 R[O_2]_0 + \varphi_9 R^2[O_2]_0\right][M]_0} \quad (1)$$

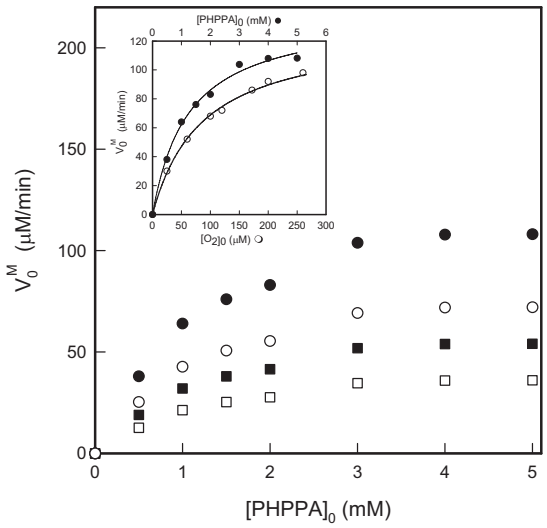

Figure 1. Initial velocities for the action of TYR *versus* different initial concentrations of PHPPA, at different concentrations of oxygen, determined by the appearance of MBTH-quinone adduct at λ = 474 nm.
The experimental conditions were 30 mM sodium phosphate buffer (pH 7.0), 25 °C, $[E]_0$ = 30 nM, the initial concentration of MBTH, $[MBTH]_0$, was 5 mM, $[\text{dimethyl formamide}]_0$ = 2% (v/v) and the initial oxygen concentrations were (mM) (●) 260, (O) 120, (■) 60 and (□) 25. The PHPPA concentrations (mM) were varied as indicated in the figure, always adding a quantity of DHPPA for the DHPPA/PHPPA ratio (R) to remain constant (R = 0.093). Inset. Representation of the initial velocity (V^M_0) *vs.* initial concentration of O_2, $[O_2]_0$, (O) and the initial concentration of PHPPA, $[PHPPA]_0$ (●). $[PHPPA]_0$- and $[O_2]_0$-values were 5 mM (O) and 260 mM (●), respectively. In both cases, the initial enzyme concentration was 30 nM.

Figure 1 Inset shows the values obtained for the initial velocity at different initial concentrations of oxygen, $[O_2]_0$, and at a saturating concentration of monophenol (initial monophenol concentration, $[M]_0 \rightarrow \infty$). The hyperbolic behaviour confirms the rapid equilibrium described in Scheme 2. Non-linear regression analysis of the initial rate *vs.* $[O_2]_0$ according to Eqn. (2), provides the value of $K^{O_2(S)}{}_{m,M}$ (see Table 2).

$$V_0^M = \frac{V_{max}^M [O_2]_0}{K_{m,M}^{O_2(S)} + [O_2]_0} \quad (2)$$

Representation of the initial velocity values obtained at a saturating oxygen concentration *vs.* the concentration of monophenol and fitted to Eqn. (3) is shown in Fig. 1 Inset. Non-linear regression provides the value of $K^{M(P)}{}_m$ (see Table 2).

$$V_0^M = \frac{V_{max}^M [M]_0}{K_m^{M(P)} + [M]_0} \quad (3)$$

The expressions $K^{M(P)}{}_m$ and $k^M{}_{cat}$ were developed in (Munoz-Munoz *et al.*, 2010). From Eqns. (4) and (5), we can obtain k_4 and k_5 (see Table 2).

$$K_m^{M(P)} = k_{cat}^M / k_4 \quad (4)$$

$$k_{cat}^M = k_5 \quad (5)$$

At monophenol concentrations where only the kinetic preferred pathway would be followed, an analytic expression can be obtained for the apparent Michaelis constant for oxygen in this pathway (Rodriguez-Lopez *et al.*, 1993), Eqn. (6). This constant cannot be determined from the experimental results because it is very small (Rodriguez-Lopez *et al.*, 1993), but can be calculated from Eqn. (6). The values obtained for the different monophenols studied in this paper are included in Table 2.

$$K_{m,M}^{O_2(P)} = \frac{3}{2}\frac{k_{cat}^M}{k_8} \quad (6)$$

Another case of an S_A type monophenol, where the accumulated chromophoric product is measured directly, is that of L-tyrosine methyl ester — see Figs 2 and 2 Inset. Once again, the hyperbolic appearance of the initial velocity data represented *versus* the substrate concentration indicates that, kinetically, the mechanism occurs through rapid equilibrium. From these data, it is concluded that the Michaelis constant for oxygen in the slow pathway is greater than the apparent Michaelis constant in the preferred kinetic pathway, which is to be expected because, in the slow pathway, the monophenol binds to E_d before this enzymatic form binds oxygen (Table 2). This behaviour is seen again for the other S_A type substrates studied in this paper: tyramine, α-methyl-L-tyrosine and PHPAA.

***S*$_B$ type substrates.** When this type of substrate is studied experimentally, oxymetric measuring techniques must be used, since the *o*-quinones evolve with no clear stoichiometry. Following the same methodology as de-

Table 2. Kinetic constants and parameters obtained for action of TYR on monophenols

Substrate	$K^{M(P)}{}_m$ (mM)	$K^{O_2(S)}{}_{m,M}$ (μM)	$K^{O_2(P)}{}_m$ (μM)	$k^M{}_{cat}$ (s^{-1})	$k_4 \times 10^{-3}$ ($M^{-1} \cdot s^{-1}$)	$k_8 \times 10^{-7}$ ($M^{-1} \cdot s^{-1}$)	δ_4 (p.p.m.)
Phenol	0.61 ± 0.04	63 ± 5	0.47 ± 0.04	10.8 ± 1.5	17.71 ± 1.95	2.3 ± 0.4	158.15
p-Cresol	0.38 ± 0.05	68 ± 5	0.48 ± 0.04	11.1 ± 1.5	29.21 ± 3.21	2.3 ± 0.4	155.50
TBF	0.05 ± 0.01	69 ± 8	0.55 ± 0.05	8.5 ± 0.9	170.00 ± 17.88	2.3 ± 0.4	156.10
PHPAA	1.72 ± 0.23	90 ± 10	2.03 ± 0.18	46.8 ± 1.8	27.21 ± 3.52	2.3 ± 0.4	156.49
PHPPA	0.41 ± 0.07	74 ± 6	2.74 ± 0.21	63.2 ± 2.3	154.15 ± 17.12	2.3 ± 0.4	156.13
Tyramine	0.62 ± 0.16	45 ± 5	1.18 ± 0.21	27.3 ± 3.2	44.03 ± 4.58	2.3 ± 0.4	157.28
L-Tyrosine methyl ester	0.51 ± 0.11	44 ± 2	0.16 ± 0.02	3.7 ± 0.1	7.25 ± 0.81	2.3 ± 0.4	158.95
α-Methyl-L-tyrosine	1.17 ± 0.19	49 ± 5	0.03 ± 0.01	0.6 ± 0.1	0.51 ± 0.06	2.3 ± 0.4	159.10

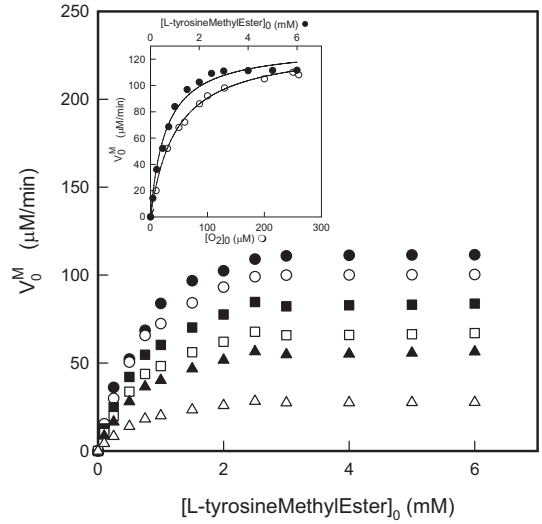

Figure 2. Initial velocities for the action of TYR *versus* different initial concentrations of tyrosine methyl ester, at different concentrations of oxygen, determined by the formation of aminochrome

The experimental conditions were 30 mM sodium phosphate buffer (pH 7.0), 25 °C, λ = 475 nm, $[E]_0$ = 0.55 mM and the initial oxygen concentrations were (mM) (●) 260, (O) 200, (■) 85 (□) 50, (▲) 30 and (Δ) 10. The tyrosine methyl ester concentrations (mM) were varied as indicated in the figure, adding, in each experiment, a concentration of dopa methyl ester, so that $[D]_0/[M]_0 = R = 0.046$. Inset. Representation of V^M_0 *vs* $[O_2]_0$ (O) and the initial concentration of tyrosine methyl ester, [tyrosine methyl ester]$_0$ (●). [tyrosine methyl ester]$_0$- and $[O_2]_0$-values were 6 mM (O) and 260 mM (●), respectively. In both cases, the initial enzyme concentration was 0.55 mM.

scribed above, a quantity of *o*-diphenol proportional to the concentration of monophenol is added at $t = 0$, so that the lag is eliminated and the initial velocity of the steady-state can be measured correctly. In this way, phenol and *p*-cresol can be characterised (Figs. 3 and 3 Inset) (Table 2).

***S*$_C$ type substrates.** Among the different monophenolic substrates of TYR studied, only TBF was found to provide a stable *o*-quinone. This was studied by adding at $t = 0$ a quantity of TBC that enabled the steady state to be reached with no lag period. The values of the kinetic constants are shown in Table 2.

Diphenolase activity

The mechanism of diphenolase activity is straightforward and is described in Scheme 1. The pathway described (pathway 1, kinetically preferred) is the normal pathway followed by the enzyme. However, at high *o*-diphenol concentrations, the *deoxy*-tyrosinase form can bind to it before oxygen does to form a *deoxy*-tyrosinase/*o*-diphenol complex, which subsequently binds O_2, giving rise to a new form, *oxy*-tyrosinase/*o*-diphenol, which is transformed into *met*-tyrosinase and *o*-quinone (pathway 2, slow).

The kinetic characterisation of the *o*-diphenols is easier than in the case of monophenols, and several spectrophotometric methods have been described for the same (Garcia-Molina *et al.*, 2007). Substrate types S_A, S_B and S_C can be studied as indicated in the figures. Figure 4, for example, depicts the study of catechol (type S_B) in the presence of NADH. The experimental results for the initial velocity obtained by varying the concentration of *o*-diphenol at different fixed concentrations of oxygen point to inhibition by excess of *o*-diphenol, suggesting that the system is working in a steady-state (Ferdinand, 1976). Note that the slow pathway begins earlier at low concentrations of oxygen. Figure 4 Inset shows the results obtained when the oxygen concentra-

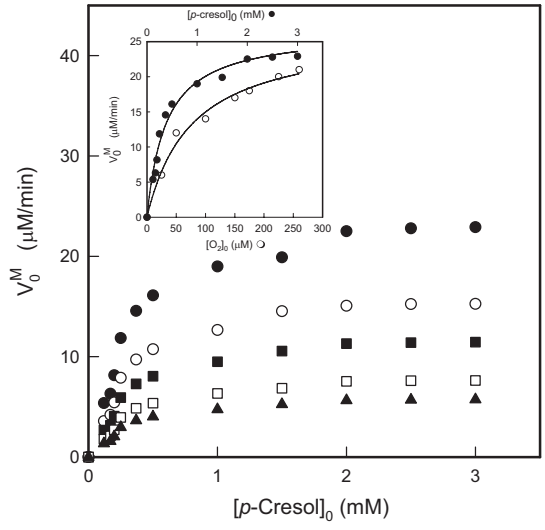

Figure 3. Initial velocities obtained for the action of TYR *versus* different initial concentrations of *p*-cresol, at different concentrations of oxygen, determined by the disappearance of molecular oxygen

The experimental conditions were 30 mM sodium phosphate buffer (pH 7.0), 25 °C, $[E]_0$ = 35 nM and the initial oxygen concentrations were (mM) (●) 260, (O) 225, (■) 50, (□) 25 and (▲) 15. The *p*-cresol concentrations (mM) were varied as indicated in the figure, adding, in each experiment, a concentration of 4-MeCat, so that $[D]_0/[M]_0 = R = 0.003$. Inset. Representation of V^M_0 *vs.* $[O_2]_0$ (O) and the initial concentration of *p*-cresol, [*p*-Cresol]$_0$ (●). [*p*-Cresol]$_0$- and $[O_2]_0$-values were 3 mM (O) and 260 mM (●), respectively. In both cases, the initial enzyme concentration was 35 nM.

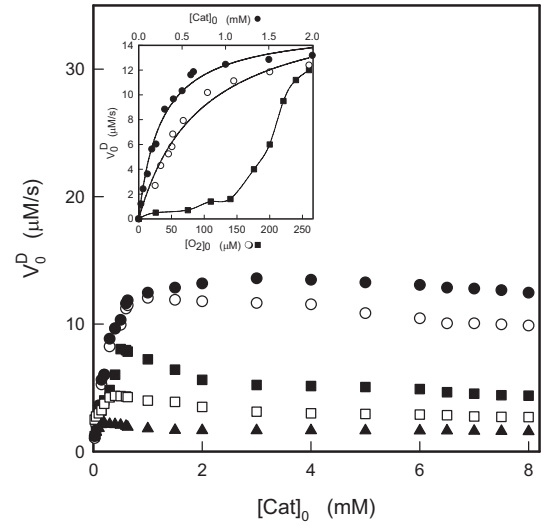

Figure 4. Initial velocities for the action of TYR *versus* different initial concentrations of Cat, at different concentrations of oxygen, determined by the disappearance of NADH

The experimental conditions were 30 mM sodium phosphate buffer (pH 7.0), 25 °C, λ = 340 nm, the initial concentration of NADH was 0.2 mM, $[E]_0$ = 10 nM and the initial oxygen concentrations were (mM) (●) 260, (O) 200, (■) 50, (□) 35 and (▲) 25. The Cat concentrations (mM) were varied as indicated in the figure. Inset. Representation of the initial velocity (V^D_0) *vs.* $[O_2]_0$ (O, ■) and the initial concentration of Cat, $[Cat]_0$ (●). $[Cat]_0$ were 8 mM (O) and 2 mM (■) and $[O_2]_0$ was 260 mM (●). In all cases, the initial enzyme concentration was 10 nM.

$$\frac{V_0^D}{[E]_0} = \frac{\beta_1[D]_0[O_2]_0 + \beta_2[D]_0[O_2]_0^2 + \beta_3[D]_0^2[O_2]_0}{\beta_4 + \beta_5[O_2]_0 + \beta_6[D]_0 + \beta_7[O_2]_0^2 + \beta_8[D]_0[O_2]_0 + \beta_9[D]_0^2 + \beta_{10}[D]_0[O_2]_0^2 + \beta_{11}[D]_0^2[O_2]_0} \quad (7)$$

tion is increased at a low concentration of *o*-diphenol — the sigmoid curve obtained indicates that the enzymatic system must work in the steady state (Ferdinand, 1976). Kinetic analysis of the mechanism described in Scheme l provides the corresponding velocity, Eqn. (7). The expressions of the parameters β_1–β_{11} are described in the Appendix.

The data obtained at a saturating concentration of *o*-diphenol, when the reaction follows the slow pathway and in accordance with Eqn. (8), enables $K^{O2(S)}_{m,D}$ to be obtained (Fig. 4 Inset) (Table 3).

$$V_0^D = \frac{V_{max}^D[O_2]_0}{K_{m,D}^{O_2(S)} + [O_2]_0} \quad (8)$$

with

$$K_{m,D}^{O_2(S)} = k_{cat}^D / k_{10} \quad (9)$$

From $K^{O2(S)}_{m,D}$ and in accordance with Eqn. (9), k_{10} can be calculated. Working at a saturating oxygen concentration, representation of the initial velocity *vs.* *o*-diphenol concentration (before the slow pathway of Scheme 2 is reached) provides $K^{D(P)}_m$ with the help of Eqn. (10) (Fig. 4 Inset).

$$V_0^D = \frac{V_{max}^D[D]_0}{K_m^{D(P)} + [D]_0} \quad (10)$$

with

$$K_m^{D(P)} = k_{cat}^D / k_6 \quad (11)$$

From $K^{D(P)}_m$ and taking into account Eqn. (11), k_6 can be calculated. The value of V^D_{max} obtained with Eqn. (10) must be compared with the value obtained with Eqn. (8) since they should be the same (Figs. 4 Inset, 5 Inset, 6 Inset and 7 Inset).

Since there is no branching in the tyrosinase catalytic pathway (Scheme 1), the mechanism must follow the kinetic preferred pathway and it should be possible to obtain $K^{O2(P)}_{m,D}$, Eqn. (12). From the value of k_8 for the binding of oxygen to the form E_d (Rodriguez-Lopez *et al.*, 2000), it is possible to obtain the values of this apparent constant (Table 3).

$$K_{m,D}^{O_2(P)} = k_{cat}^D / k_8 \quad (12)$$

Similar results were obtained with the rest of the *o*-diphenols studied. Figures 5 and 5 Inset show the results for DHPPA measured through the formation of an adduct with L-cysteine. The results obtained with TBC are depicted in Figs. 6 and 6 Inset, and the results obtained with DopaMeEster measuring the formation of aminochrome (Figs. 7 and 7 Inset).

Slow step in the tyrosinase action mechanism

From the experimental data obtained for the monophenolase activity, Fig. 1–3, and for the diphenolase activity, Figs. 4–7, it can be assumed that the mechanism of Scheme 2 involves a much slower step than the others — the hydroxylation of monophenols to *o*-diphenols governed by k_5 (Eqn. 5). The system works in rapid equilibrium and hyperbolic behaviour is evident in the dependence of the initial velocity on the concentra-

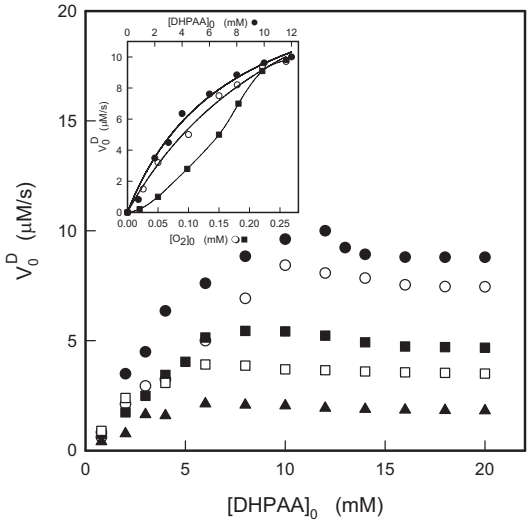

Figure 5. Initial velocities for the action of TYR *versus* different initial concentrations of DHPAA, at different concentrations of oxygen, determined by the formation of adduct between L-Cys and DHPPA

The experimental conditions were 30 mM sodium phosphate buffer (pH 7.0), 25 °C, λ = 300 nm, the initial concentration of L-Cys was 0.2 mM, $[E]_0$ = 0.7 nM and the initial oxygen concentrations were (mM) (●) 260, (O) 220, (■) 100, (□) 75 and (▲) 40. The DHPPA concentrations (mM) were varied as indicated in the figure. Inset. Representation of V^D_0 *vs.* $[O_2]_0$ (O, ■) and the initial concentration of DHPPA, $[DHPPA]_0$ (●). $[DHPPA]_0$ were 20 mM (O) and 12 mM (■) and $[O_2]_0$ was 260 mM (●). In all cases, the initial enzyme concentration was 0.7 nM.

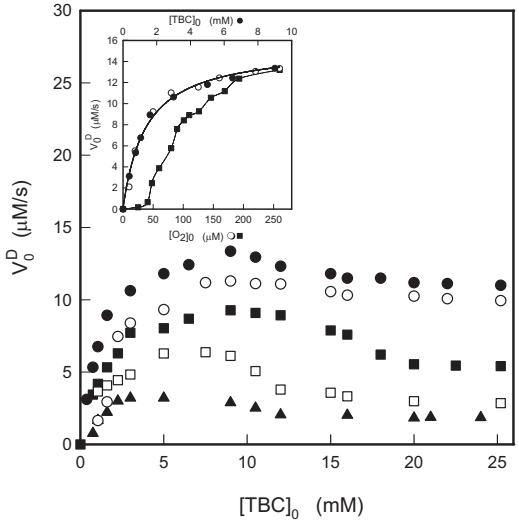

Figure 6. Initial velocities for the action of TYR *versus* different initial concentrations of TBC, at different concentrations of oxygen, determined by the disappearance of NADH

The experimental conditions were 30 mM sodium phosphate buffer (pH 7.0), 25 °C, λ = 340 nm, $[NADH]_0$ = 0.2 mM, $[E]_0$ = 10 nM and the initial oxygen concentrations were (mM) (●) 260, (O) 200, (■) 110, (□) 20 and (▲) 10. The TBC concentrations (mM) were varied as indicated in the figure. Inset. Representation of V^D_0 *vs* $[O_2]_0$ (O, ■) and the initial concentration of TBC, $[TBC]_0$ (●). $[TBC]_0$ were 26 mM (O) and 9 mM (■) and $[O_2]_0$ was 260 mM (●). In all cases, the initial enzyme concentration was 10 nM.

Table 3. Kinetic constants and parameters obtained for action of TYR on *o*-diphenols

Substrate	$K^{D(P)}_m$ (mM)	$K^{O2(S)}_m$ (mM)	$K^{O2(P)}_m$ (mM)	k^D_{cat} (s^{-1})	$k_6\times10^{-5}$ ($M^{-1}\cdot s^{-1}$)	$k_8\times10^{-7}$ ($M^{-1}\cdot s^{-1}$)	$k_{10}\times10^{-6}$ ($M^{-1}\cdot s^{-1}$)	δ_4 (p.p.m.)
Cat	0.15±0.03	54±5	37.82±5.23	870.4±46.1	58.00±4.87	2.3±0.4	16.11±2.59	146.59
4-MeCAT	0.21±0.03	59±8	36.52±5.47	840.2±62.3	40.00±3.56	2.3±0.4	14.24±2.81	144.06
TBC	1.50±0.08	69±7	28.04±4.44	645.3±58.2	4.30±0.52	2.3±0.4	9.98±1.86	144.09
DHPAA	1.41±0.18	100±11	20.35±3.35	468.4±47.4	3.32±0.41	2.3±0.4	4.68±0.85	144.96
DHPPA	0.83±0.06	80±9	27.17±4.48	625.2±63.3	7.53±0.84	2.3±0.4	7.81±1.22	144.61
Dopamine	0.72±0.08	90±8	20.04±3.43	461.1±51.2	6.40±0.69	2.3±0.4	5.02±1.06	145.58
DopaMeEster	0.85±0.11	41±4	19.13±3.25	44.3±4.8	0.52±0.06	2.3±0.4	1.07±0.25	146.18
L-αMeDopa	5.21±0.51	25±3	1.78±0.26	41.2±3.2	0.08±0.01	2.3±0.4	1.64±0.34	146.19
DL-αMeDopa	6.46±0.58	28±3	1.87±0.27	43.1±3.1	0.07±0.01	2.3±0.4	1.53±0.29	146.19

tion of each of the substrates. However, in the diphenolase activity the oxidation of an *o*-diphenol occurs in the steady state, leading to the curves of Figs. 4–7, in agreement with Eqn. (7).

Discussion of the kinetic constants depicted in Tables 2 and 3.

The values of the catalytic constants for the different monophenols (Table 2) are directly related to the power of the nucleophilic attack of the oxygen of the hydroxyl group of C-4, which is, in turn, directly related to the chemical shift δ_4, as described previously (Espin *et al.*, 2000). A similar dependence is seen for the *o*-diphenols, but the nucleophilic power of the hydroxyl group of C-4 on the *o*-diphenols is greater than that of the hydroxyl group of C-4 on the monophenols, since $\delta^D_4 < \delta^M_4$, so $k^D_{cat} > k^M_{cat}$ (see Tables 2 and 3).

The constants that can be obtained from fitting the experimental data of the initial velocity *vs.* substrate concentration are: $K^{O2(S)}_{m,D}$ at saturating concentrations of the substrate (monophenol or *o*-diphenol) and $K^{M(P)}_m$ at saturating concentrations of oxygen (in the case of monophenols). For *o*-diphenols, the concentration of the *o*-diphenolic substrate would vary as long as the slow pathway is reached (zone of practically constant velocity in the curves), as seen from the Insets of Figs. 4–7. In this way, $K^{D(P)}_m$ can be determined. These data are reflected in Tables 2 and 3, from which it can be seen that $K^M_m \leq K^D_m$. It can also be seen that the enzyme, in the E_d form, first binds to the monophenol or *o*-diphenol and then to oxygen, with a similar apparent Michaelis constant, $K^{O2(S)}_{m,M} \approx K^{O2(S)}_{m,D}$.

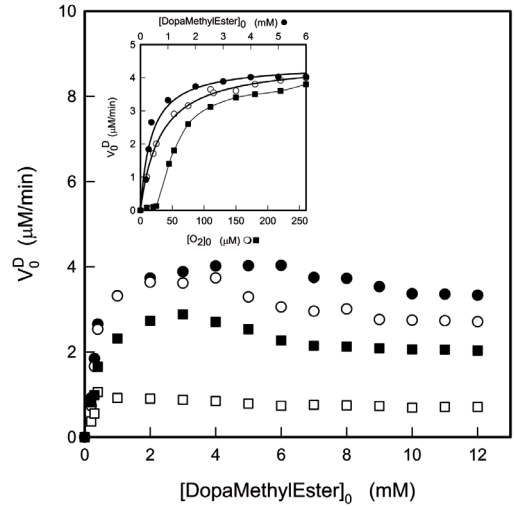

Figure 7. Initial velocities for the action of TYR *versus* different initial concentrations of dopa methyl ester, at different concentrations of oxygen, determined by the formation of dopachrome.
The experimental conditions were: 30 mM sodium phosphate buffer (pH 7.0), 25 °C, λ=475 nm, $[E]_0$=90 nM and the initial oxygen concentrations were (mM): (●) 260, (O) 75, (■) 25 and (□) 10. The dopa methyl ester concentrations (mM) were varied as indicated in the figure. Inset. Representation of V^D_0 *vs* $[O_2]_0$ (O, ■) and the initial concentration of dopa methyl ester, [dopa methyl ester]$_0$ (●). [dopa methyl ester]$_0$ were 12 mM (O) and 5 mM (■) and $[O_2]_0$ was 260 mM (●). In all cases, the initial enzyme concentration was 90 nM.

If we consider that, experimentally, only the kinetically preferred pathway exists, the values of $K^{O2(P)}_{m,M}$ and $K^{O2(P)}_{m,D}$ can be obtained from the analytical expressions described previously, Eqns. (6) and (12) (Rodriguez-Lopez *et al.*, 1993). These kinetic Michaelis constants (Tables 2 and 3) are much lower for monophenols than for *o*-diphenols. Moreover, both constants (for monophenols and *o*-diphenols) are lower than those obtained experimentally for the slow pathway.

The values of the binding constants of the substrates to the E_{ox} form (k_4 for monophenols and k_6 for *o*-diphenols) can be obtained from Eqns. (4) and (11), respectively. The *o*-diphenol binding constants governed by k_6 are greater than those of monophenols governed by k_4, which agrees with the values of δ_4 (Tables 2 and 3).

The binding constants of oxygen to the enzyme could vary from the value of k_8 (binding to E_d form) to the value of k_{10} (binding to E_dD), as can be seen from Tables 2 and 3 ($k_8 > k_{10}$). Note that the value of k_{10} (binding of oxygen to E_dD) depends on the nature of the substrate, and is practically one order of magnitude greater for substrates with no charge, such as Cat, 4-MeCat and TBC.

Recently, allosteric cooperativity and cooperative inhibition have been described in mushroom tyrosinase (Haghbeen *et al.*, 2010), as seen from a kinetic study and data analysis of both activities by means of Eadie-Hofstee graphs, using *p*-coumaric acid and 4-[(4-methylphenyl)azo]-phenol (MePAPh) as substrates for the monophenolase activity and caffeic acid and 4-[(4-methylphenyl)azo]-1,2-benzenediol (MePACat) for the diphenolase activity. The negative cooperativity in both activities observed by those authors was more pronounced in the case of monophenolase activity. The same authors suggest that other reports on the kinetics and inhibition of both activities of tyrosinase (Escribano *et al.*, 1989; Ros *et al.*, 1994; Park *et al.*, 2003; Yamazaki & Itoh, 2003; Fenoll *et al.*, 2004; Garcia-Molina *et al.*, 2005; Xue

et al., 2007) do not uncover the true kinetics due to the indirect methods and limited substrate concentrations used in the experiments (Haghbeen & Tan, 2003) and that a direct method, such as that involving the disappearance of substrate, should contributed to finding the true kinetics of the enzyme.

In a previous work (Garcia-Molina *et al.*, 2007), we made a revision of the spectrophotometric methods used to follow the monophenolase and diphenolase activities of tyrosinase, using numerical integration to demonstrate that the rates of disappearance of substrate and appearance of product are equal when the system reaches the steady-state, even when the product that can be measured experimentally is accumulated after a series of chemical reactions. In the case of monophenolase activity, the system reaches the steady-state when a fixed quantity of *o*-diphenol has accumulated in the medium. In addition, we demonstrated that only the *o*-quinones (originating from the enzymatic conversion of monophenol or *o*-diphenol) that evolve with a given stoichiometry are capable of quantitatively accumulating *o*-diphenol in the medium. We also demonstrated that *o*-quinones are unstable and therefore can only be measured at short times. However, for diphenolase activity, Haghbeen *et al.* (2010) measured the disappearance of substrate over a period of five minutes (30 min in the case of monophenolase activity). We also demonstrated that monophenolase activity should be measured at different times, increasing as the monophenol concentrations increase. However, this was not taken into account by Haghbeen *et al.* (2010), who used a constant 30 min.

When measuring the disappearance of substrate in the ultraviolet region of the spectrum, it must be remembered that there is a danger of saturating the phototube of the spectrophotometer at high substrate concentrations. Although Haghbeen *et al.* (2010) used a 0.5 cm cuvette to be able to increase the substrate concentration, this is not sufficient to saturate the enzyme. Hence, in Fig. 2 (Haghbeen *et al.*, 2010), all the substrates were studied up to 100 mM regardless of the values of K_m described before (Haghbeen & Tan, 2003). The most striking case is the velocity *vs.* substrate concentration graph for *p*-coumaric acid (up to 100 μM), for which the K_m is 97 μM (Haghbeen & Tan, 2003), Later, the same authors increased the concentration to 200 μM (Fig. 3) (Haghbeen *et al.*, 2010). Note that, according to Cleland (1967), substrate concentration should vary from $K_m/5$ to $5K_m$ to allow obtaining of correct parameters (V_{max} and K_m). We must therefore conclude that the measurements made by Haghbeen and Tan (2003) and Haghbeen *et al.* (2010) are probably erroneous, which may be the origin of the deviations observed in monophenolase and diphenolase activities.

A wide variety of phenolic substrates of tyrosinase exist in plants, which explains why the enzyme is known as polyphenol oxidase. For example, the first six *o*-diphenols and their respective monophenols in Table 6 are found in a variety of plants. When the plants are attacked by predators such as bacteria, fungi or insects, the contact between the tyrosinases, their phenolic substrates and oxygen increases and the kinetic cooperativity of tyrosinase foments the formation of *o*-quinones and other melanogenes that are toxic for the predators' cells. Such kinetic cooperativity of tyrosinase therefore triggers an effective defence mechanism of the plants.

The three last substrates (mono- and *o*-diphenols) in Table 1 might be considered potential antitumor agents in the case of melanoma cells. The kinetic cooperativity of tyrosinase would increase the production of *o*-quinones and other melanogenes, and these could exit the melanosomes and interact with proteins and nucleic acids of the tumoral melanocytes, provoking oxidative stress, crosslinking reactions and the destruction of the melanin cells. A similar effect on melanoma cells has been demonstrated experimentally using derivates of *bis*(catechol) as tyrosinase substrates (Bai *et al.*, 2010).

In conclusion, the experimental results obtained with a series of monophenol/*o*-diphenol pairs show that tyrosinase expresses kinetic cooperativity when it acts on *o*-diphenols (steady-state). However, during its action on monophenols, the cooperativity disappears due to the existence of a slow step, the hydroxylation of monophenols (rapid equilibrium).

Acknowledgements

This paper was partially supported by grants from the Ministerio de Educación y Ciencia (Madrid, Spain) Project BIO2009-12956, from the Fundación Séneca (CARM, Murcia, Spain) Projects 08856/PI/08 and 08595/PI/08, from the Consejería de Educación (CARM, Murcia, Spain) BIO-BMC 06/01-0004 and FISCAM PI-2007/53 from the Consejería de Salud y Bienestar Social de la Junta de Comunidades de Castilla La Mancha. F.G.M. and J.L.M.M. have two fellowships from Fundación Caja Murcia (Murcia, Spain).

REFERENCES

Atkinson D, Walton GM (1965) Kinetics of regulatory enzymes. *Escherichia coli* phosphofructokinase. *J Biol Chem* **240:** 757–763.

Bai M, Huang J, Zheng X, Song Z, Tang M, Mao W, Yuan L, Wu J, Weng X, Zou X (2010) Highly selective suppression of melanoma cells by inducible DNA cross-linking agents: bis(catechol) derivatives. *J Am Chem Soc* **132:** 15321–15327.

Canovas FG, Garcia-Carmona F, Sanchez JV, Pastor JL, Teruel JA (1982) The role of pH in the melanin biosynthesis pathway. *J Biol Chem* **257:** 8738–8744.

Chazarra S, Garcia-Carmona F, Cabanes J (2001) Hysteresis and positive cooperativity of Iceberg lettuce polyphenol oxidase. *Biochem Biophys Res Commun* **289:** 769–775.

Cleland WW (1967) The statistical analysis of the enzyme kinetic data. *Adv Enzymol* **29:** 1–32.

Escribano J, Tudela J, Garcia-Carmona F, Garcia-Canovas F (1989) A kinetic-study of the suicide inactivation of an enzyme measured through coupling reactions-application to the suicide inactivation of tyrosinase. *Biochem J* **262:** 595–603.

Espin JC, Varon R, Fenoll LG, Gilabert MA, Garcia-Ruiz PA, Tudela J, Garcia-Canovas F (2000) Kinetic characterization of the substrate specificity and mechanism of mushroom tyrosinase. *Eur J Biochem* **267:** 1270–1279

Ferdinand W (1976) In *The enzyme molecule.* Ferdinand W, ed, pp 139–185. John Wiley and Sons, London.

Garcia-Carmona F, Garcia-Canovas F, Iborra JL, Lozano JA (1982) Kinetic study of the pathway of melanisation between L-dopa and dopachrome. *Biochim Biophys Acta* **717:** 124–131.

Garcia-Molina F, Munoz JL, Varon R, Rodriguez-Lopez JN, Garcia-Canovas F, Tudela J (2007) A review of spectrophotometric methods for measuring the monophenolase and diphenolase activities of tyrosinase. *J Agric Food Chem* **55:** 9739–9749.

Haghbeen K, Tan EW (2003) Direct spectrophotometric assay of monooxygenase and oxidase activities of mushroom tyrosinase in the presence of synthetic and natural substrates. *Anal Biochem* **312:** 23–32.

Haghbeen K, Khalili MB, Nematpour FS, Gheibi N, Fazli M, Alijanianzadeh M, Jahromi SZ, Sariri R (2010) Surveying allosteric cooperativity and cooperative inhibition in mushroom tyrosinase. *J Food Biochem* **34:** 308–328.

Hathaway JA, Atkinson DE (1963) The effect of adenylic acid on yeast nicotinamide adenine dinucleotide isocitrate dehydrogenase, a possible metabolic control mechanism. *J Biol Chem* **238:** 2875–2881.

Jandel Scientific. Sigma Plot 9.0 for Windows™; Jandel Scientific: Core Madera 2006.

Koshland Jr DE, Nemethy G, Filmer D (1966) Comparison of experimental binding data and theoretical models in protein containing subunits. *Biochemistry* **5:** 365–385.

Matoba Y, Kumagai T, Yamamoto A, Yoshitsu H, Sugiyama M (2006) Crystallographic evidence that the dinuclear copper center of tyrosinase is flexible during the catalysis. *J Biol Chem* **281**: 8981–8990.

Monod J, Wyman J, Changeaux JP (1965) On the nature of allosteric transitions: A plausible model. *J Mol Biol* **12:** 88–118.

Munoz JL, Garcia-Molina F, Varon R, Rodriguez-Lopez JN, Garcia-Canovas F, Tudela J (2006) Calculating molar absorptivities for *o*-quinones: application to the measurement of tyrosinase activity. *Anal Biochem* **351:** 128–138.

Munoz-Munoz JL, Garcia-Molina F, Varon R, Tudela J, Garcia-Canovas F, Rodriguez-Lopez JN (2009) Generation of hydrogen peroxide in the melanin biosynthesis pathway. *Biochim Biophys Acta* **1794:** 1017–1029.

Munoz-Munoz JL, Garcia-Molina F, Varon R, Tudela J, Garcia-Canovas F, Rodriguez-Lopez JN (2010) New features of the steady-state rate related with the initial concentration of substrate in the diphenolase and monophenolase activities of tyrosinase. *J Math Chem* **48:** 347–362.

Park Y, Jung J, Kim D, Kim W, Hahn M, Yang J (2003) Kinetic inactivation study of mushroom tyrosinase: Intermediate detection by denaturants. *J Protein Chem* **22:** 463–471.

Peñalver MJ, Rodríguez-Lopez JN, García-Molina F, Garcia-Canovas F, Tudela J (2002) Method for the determination of molar absorptivities of thiol adducts formed from diphenolic substrates of polyphenol oxidase. *Anal Biochem* **309:** 180–185.

Piccoli R, Di Donato A, D'Alessio G (1988) Co-operativity in seminal ribonuclease function. *Biochem J* **253:** 329–336.

Rabin BR (1967) Co-operative effects in enzyme catalysis: A possible kinetic model based on substrate-induced conformation isomerisation. *Biochem J* **102:** 22c–23c.

Rodriguez-Lopez JN, Ros-Martinez JR, Varon R, Garcia-Canovas F (1992) Calibration of a Clark-type electrode by tyrosinase-catalyzed oxidation of 4-tert-butylcatechol. *Anal Biochem* **202:** 356–360.

Rodriguez-Lopez JN, Ros JR, Varon R, Garcia-Canovas F (1993) Oxygen Michaelis constants for tyrosinase. *Biochem J* **293:** 859–866.

Rodriguez-Lopez JN, Escribano J, Garcia-Canovas F (1994) A continuous spectrophotometric method for the determination of monophenolase activity of tyrosinase using 3-methyl-2-benzothiazolinone hydrazone. *Anal Biochem* **216:** 205–212.

Rodriguez-Lopez JN, Fenoll LG, Garcia-Ruiz PA, Varon R, Tudela J, Thorneley RNF, Garcia-Canovas F (2000) Stopped-flow and steady-state study of the diphenolase activity of mushroom tyrosinase. *Biochemistry* **39:** 10497–10506.

Ros JR, Rodriguez-Lopez JN, Garcia-Canovas F (1994) Tyrosinase: kinetic analysis of the transient phase and the steady-state. *Biochim Biophys Acta* **1204:** 33–42.

Sanchez-Ferrer A, Rodriguez-Lopez JN, Garcia-Canovas F, Garcia-Carmona F (1995) Tyrosinase: a comprehensive review of its mechanism. *Biochim Biophys Acta* **1247**: 1–11.

Solomon EI, Sundaram UM, Machonkin TE (1996) Multicopper oxidases and and oxygenases. *Chem Rev* **96**: 2563–2606.

Valero E, Garcia-Carmona F (1992) Hysteresis and cooperative behavior of a latent plant polyphenoloxidase. *Plant Physiol* **98:** 774–776.

Varon-Castellanos R, Garcia-Moreno M, Garcia-Sevilla F, Ruiz-Galea MM, Garcia-Canovas F (1995) *Computerized derivation of the steady-state equations of enzyme reactions*. A5, ed. Albacete, Spain

Wichers HJ, Gerritsen YAM, Chapelon CGJ (1996) Tyrosinase isoforms from the fruit bodies of *Agaricus bisporus*. *Phytochemistry* **43:** 333–337.

Wichers HJ, Recourt K, Hendriks M, Ebbelaar CEM, Biancone G, Hoeberichts FA, Mooibroek H, Soler-Rivas C (2003) Cloning, expression and characterisation of two tyrosinase cDNAs from *Agaricus bisporus*. *Appl Microbiol Biotechnol* **61:** 336–341.

Wolfe RG, Neilands JB (1956) Some molecular kinetic properties of heart malic dehydrogenase. *J Biol Chem* **221:** 61–69.

Xue CB, Wan-Chen L, Lin J, Xiang-Ye X, Ting X, Lei Y (2007) Inhibition kinetics of cabbage butterfly (*Pieris rapae* L.) larvae phenoloxidase activity by 3-hydroxy-4-methoxybenzaldehide thiosemicarbazone. *Appl Biochem Biotechnol* **43:** 101–114.

Yamazaki S, Itoh S (2003) Kinetic evaluation of phenolase activity of tyrosinase using simplified catalytic reaction system. *J Am Chem Soc* **125:** 13034–13035.

APPENDIX. Analytical expressions for the equations described in the main text.

The expressions of the parameters $\varphi_i (i = 1,2,3.....9)$ involved in Eq. (1) are:

$$\varphi_1 = K_1 k_2 k_3 k_5 k_7 + K_1 k_2 k_3 k_5 k_{-6} \quad \text{(A1)}$$

$$\varphi_2 = K_1 k_2 k_3 k_6 K_4 k_7 + K_1 k_2 k_3 k_6 K_4 k_7 \quad \text{(A2)}$$

$$\varphi_3 = K_1 k_2 k_3 K_8 K_4 k_7 + K_1 k_2 k_3 K_8 K_4 k_{-6} \quad \text{(A3)}$$

$$\varphi_4 = K_1 k_{-2} k_5 k_7 + K_1 k_{-2} k_5 k_{-6} \quad \text{(A4)}$$

$$\varphi_5 = K_1 k_2 k_3 K_{12} k_7 + K_1 k_2 k_3 K_{12} k_{-6} \quad \text{(A5)}$$

$$\varphi_6 = K_1 k_{-2} k_6 K_4 k_7 + K_1 k_3 k_6 K_4 k_7 + K_1 k_2 k_3 K_4 k_7 + K_1 k_2 k_3 K_4 k_{-6} \quad \text{(A6)}$$

$$\varphi_7 = k_{-2} k_5 k_7 + k_{-2} k_5 k_{-6} \quad \text{(A7)}$$

$$\varphi_8 = k_{-2} k_6 K_4 k_7 + k_3 k_6 K_4 k_7 + K_1 k_2 k_5 k_7 + K_1 k_2 k_5 k_{-6} + K_1 k_2 k_3 k_7 + K_1 k_2 k_3 k_{-6} \quad \text{(A8)}$$

$$\varphi_9 = K_1 k_2 k_6 K_4 k_7 + K_1 k_2 k_3 k_6 K_4 \quad \text{(A9)}$$

where:

$$K_1 = k_{-1} / k_1 \quad \text{(A10)}$$

$$K_4 = k_{-4} / k_4 \quad \text{(A11)}$$

$$K_8 = k_{-8} / k_8 \quad \text{(A12)}$$

The analytical expression for R is:

$$R = \frac{k_{cat}^{M} K_m^{D(P)}}{2k_{cat}^{D} K_m^{M(P)}} = \frac{k_4}{2k_6} \quad \text{(A13)}$$

The expressions of the parameters $\beta_i (i = 1, 2, 3, ...11)$ involved in Eq. (7) are:

$$\beta_1 = k_2 k_3 k_8 k_6 k_7 k_{-9} + k_2 k_3 k_9 k_{-8} k_7 k_{10} + k_2 k_3 k_8 k_6 k_7 k_{-9} + k_2 k_3 k_9 k_{-8} k_7 k_{10} \quad \text{(A14)}$$

$$\beta_2 = k_2 k_3 k_8 k_6 k_7 k_{10} + k_2 k_3 k_8 k_6 k_7 k_{10} \quad \text{(A15)}$$

$$\beta_3 = k_2 k_3 k_9 k_6 k_7 k_{10} + k_2 k_3 k_9 k_6 k_7 k_{10} \quad \text{(A16)}$$

$$\beta_4 = k_2 k_3 k_{-8} k_7 k_{-9} + k_2 k_3 k_{-8} k_{-6} k_{-9} + k_2 k_3 k_{-8} k_{-10} k_{-9} \quad \text{(A17)}$$

$$\begin{aligned}\beta_5 = {} & k_{-2} k_8 k_6 k_7 k_{-9} + k_{-2} k_9 k_{-8} k_7 k_{10} + k_3 k_8 k_6 k_7 k_{-9} + k_3 k_9 k_{-8} k_7 k_{10} + k_2 k_3 k_{-8} k_7 k_{10} + \\ & + k_2 k_3 k_{-8} k_{-6} k_{10} + k_2 k_3 k_8 k_7 k_{-9} + k_2 k_3 k_8 k_{-6} k_{-9} + k_2 k_3 k_8 k_{-10} k_{-9}\end{aligned} \quad \text{(A18)}$$

$$\beta_6 = k_2 k_3 k_6 k_7 k_{-9} + k_2 k_3 k_6 k_{-10} k_{-9} + k_2 k_3 k_9 k_{-8} k_7 + k_2 k_3 k_9 k_{-8} k_{-6} + k_2 k_3 k_9 k_{-8} k_{-10} \quad \text{(A19)}$$

$$\beta_7 = k_{-2} k_8 k_6 k_7 k_{10} + k_3 k_8 k_6 k_7 k_{10} + k_2 k_3 k_8 k_7 k_{10} + k_2 k_3 k_8 k_{-6} k_{10} \quad \text{(A20)}$$

$$\begin{aligned}\beta_8 = {} & k_{-2} k_9 k_6 k_7 k_{10} + k_3 k_9 k_6 k_7 k_{10} + k_2 k_8 k_6 k_7 k_{-9} + k_2 k_9 k_{-8} k_7 k_{10} + k_2 k_3 k_6 k_7 k_{10} + \\ & + k_2 k_3 k_9 k_{-6} k_{10} + k_2 k_3 k_8 k_6 k_{-9} + k_2 k_3 k_9 k_{-8} k_{10} + k_2 k_3 k_8 k_6 k_{-10}\end{aligned} \quad \text{(A21)}$$

$$\beta_9 = k_2 k_3 k_9 k_6 k_7 + k_2 k_3 k_9 k_6 k_{-10} \quad \text{(A22)}$$

$$\beta_{10} = k_2 k_8 k_6 k_7 k_{10} + k_2 k_3 k_8 k_6 k_{10} \quad \text{(A23)}$$

$$\beta_{11} = k_2 k_9 k_6 k_7 k_{10} + k_2 k_3 k_9 k_6 k_{10} \quad \text{(A24)}$$

4.3. ALGUNAS PROPIEDADES CINÉTICAS DE DESOXITIROSINASA.

El estudio de algunas propiedades cinéticas de la especie enzimática desoxitirosinasa ha dado lugar a la siguiente publicación adjunta.

4.3.1. Título

Some kinetic properties of deoxytyrosinase.

4.3.2. Autores

Muñoz-Muñoz, J.L.; Garcia-Molina, F.; Varon, R.; Tudela, J.; Garcia-Cánovas, F. y Rodríguez-López, J.N.

4.3.3. Referencia

Journal of Molecular Catalysis B: Enzymatic (2010) 62, 173-182.

4.3.4. Resumen

El paso de una corriente de nitrógeno a una preparación de oxi-tirosinasa (E_{ox}), origina la forma desoxitirosinasa, relajada (E_d^R). Esta forma enzimática, bajo condiciones anaerobias, transita lentamente a otra desoxitirosinasa, tensa (E_d^T). En presencia únicamente de oxigeno, la generación de la forma E_{ox} a partir de E_d^R es rápida, mientras que a partir de E_d^T es lenta. Sin embargo, cuando se adicionan los dos substratos (oxigeno/*o*-difenol o bien oxigeno/monofenol) al mismo tiempo, tanto la forma E_d^R como la E_d^T, muestran rápidamente actividad enzimática, indicando un efecto sinérgico entre los dos sustratos en la recuperación de una forma E_{ox} activa. No obstante, la actividad que se obtiene en el caso de E_d^T es menor que la de la enzima nativa, y también es menor que la de la enzima que se puede generar rápidamente preincubando con oxigeno la forma E_d^R recién formada por el paso de la corriente de nitrógeno, o bien respecto a la generada lentamente preincubando la forma E_d^T con oxigeno. Las formas E_d^R y E_d^T tienen distinta afinidad por los sustratos, las constantes de Michaelis para los dos sustratos son mayores para E_d^T con respecto a E_d^R, sin embargo las velocidades máximas son muy similares. Las propiedades cinéticas de E_d^R son similares a las de la enzima nativa. El comportamiento de los monofenoles es semejante al de los *o*-difenoles, sin embargo los últimos inactivan a la enzima en

condiciones anaerobias y los primeros la protegen de la inactivación. El pH influye en la velocidad de la transición de E_d^R a E_d^T, siendo más rápida a pH 6.5, a este pH las propiedades cinéticas de la enzima nativa y E_d^T son similares y la oxigenación de E_d^T para generar E_{ox} es más rápida. A valores de pH superiores e inferiores a 6.5, la transición de E_d^R a E_d^T se hace más lenta. A partir del estudio del efecto del pH sobre las transiciones de E_d^R a E_d^T y de la reoxigenación de E_d^T a E_{ox}, se desprende la posible existencia de dos pK_a´s aparentes con valores aproximados de 6.0 y 6.8. La enzima a valores de pH altos contiene dos grupos ácido/base con carga negativa, lo cual provoca que se repelan (pH > 6.8) o dos cargas positivas (a pH < 6.0) con lo cual también se repelerían, esto podría llevar consigo la separación de los átomos de cobre. Sin embargo, a pH 6.5 existiría una carga positiva y otra negativa e impediría la separación de los átomos de cobre.

Author's personal copy

Journal of Molecular Catalysis B: Enzymatic 62 (2010) 173–182

Contents lists available at ScienceDirect

Journal of Molecular Catalysis B: Enzymatic

journal homepage: www.elsevier.com/locate/molcatb

Some kinetic properties of deoxytyrosinase

J.L. Muñoz-Muñoz[a], F. García-Molina[a], P.A. García-Ruiz[b], R. Varon[c], J. Tudela[a], F. García-Cánovas[a,*], J.N. Rodríguez-López[a]

[a] GENZ: Grupo de Investigación de Enzimología, Departamento de Bioquímica y Biología Molecular-A, Facultad de Biología, Universidad de Murcia, E-30100 Espinardo, Murcia, Spain
[b] QCBA: Grupo de Química de Carbohidratos y Biotecnología de Alimentos, Departamento de Química Orgánica, Facultad de Química, Universidad de Murcia, E-30100 Espinardo, Murcia, Spain
[c] Departamento de Química-Física, Escuela de Ingenieros Industriales de Albacete, Universidad de Castilla la Mancha, Avda, España s/n, Campus Universitario, E-02071 Albacete, Spain

ARTICLE INFO

Article history:
Received 12 June 2009
Received in revised form 7 October 2009
Accepted 21 October 2009
Available online 30 October 2009

Keywords:
Tyrosinase
Hemocyanin
Kinetic mechanism
deoxy-tyrosinase
pH

ABSTRACT

Passing a nitrogen stream over a preparation of *oxy*-tyrosinase (E_{ox}) gives rise to the relaxed *deoxy*-tyrosinase form (E_d^R), which, under anaerobic conditions, slowly transforms into tense *deoxy*-tyrosinase (E_d^T). In the presence of oxygen, regeneration of the form E_{ox} from E_d^R is rapid but from E_d^T it is a slow process. However, when two substrates (oxygen/*o*-diphenol or oxygen/monophenol) are simultaneously added, both the E_d^R and E_d^T forms rapidly revert to the active E_{ox} form, pointing to a synergistic effect of both substrates. However, the activity obtained in the case of E_d^T is less than that of the native enzyme and of the enzyme that can be generated rapidly by pre-incubation with oxygen of the E_d^R recently formed by passage of the nitrogen stream, or that generated slowly by pre-incubating the E_d^T form with oxygen. Although the V_{max} of the forms E_d^R and E_d^T are very similar, the Michaelis constant of the latter is higher. The kinetic properties of E_d^R are similar to those of the native enzyme. The behaviour of the monophenols is similar to that of the *o*-diphenols, although, while the latter inactivate the enzyme under anaerobic conditions, the former protect it from inactivation. The pH affects the transition from E_d^R to E_d^T, which is more rapid at pH 6.5, at which value the kinetic properties of the native enzyme and of E_d^T are similar and the oxygenation step in which E_d^T regenerates E_{ox} is more rapid. At pH values other than 6.5, the transition of E_d^R to E_d^T takes place slowly. From a study of the effect of pH on the transition of E_d^R to E_d^T and of the re-oxygenation of E_d^T to E_{ox}, the possible existence of two apparent pK_as, with approximate values of 6.0 and 6.8, may be surmised. At high pH, the enzyme contains two acid/base groups carrying negative charges, which repel (pH > 6.8) or two positive charges (at pH < 6.0), which also repel, while at ~pH 6.5 one positive and one negative group exists, which prevents the separation of the two copper atoms.

© 2009 Elsevier B.V. All rights reserved.

1. Introduction

Tyrosinase (EC 1.14.18.1) is involved in melanin biosynthesis in bacteria, plants and mammals. The enzyme catalyses the ortho-hydroxylation of monophenols (monophenolase activity) and the oxidation of *o*-diphenols to *o*-quinones (diphenolase activity). The catalytic centre of tyrosinase possesses a binuclear copper similar to that of hemocyanin and catechol oxidase [1,2]. The catalytic cycle of tyrosinase has three enzymatic forms: E_m (*met*-tyrosinase), with the copper as $Cu^{2+}Cu^{2+}$, E_d (*deoxy*-tyrosinase), with the copper as $Cu^{+}Cu^{+}$ and E_{ox} (*oxy*-tyrosinase) with copper in the form $Cu^{2+}Cu^{2+}O_2^{2-}$ [3].

The three proteins with type 3 active copper centres which take part in O_2 binding and activation are hemocyanin, which binds O_2 reversibly, catechol oxidase, which converts catechols to the corresponding *o*-quinones, and tyrosinase, which hydroxylates monophenols and converts catechols to *o*-quinones [1,2]. In the structures of hemocyanin [4], catechol oxidase [5] and tyrosinase from *Streptomyces castaneoglobisporus* [6], each copper ion is coordinated by three histidines. Of the three proteins described, the binding of oxygen to the *deoxy* form has mainly been studied in *deoxy*-hemocyanin [7–12]. Some properties of the *deoxy* form of tyrosinase from *Streptomyces glaucencens* and *Neurospora crassa* have been studied [13], as well as the oxygen binding in tyrosinases from *Streptomyces antibioticus* [14] and *Agaricus bisporus* [15]. Subsequently, comparative studies were made of the three related proteins, hemocyanin, catechol oxidase and tyrosinase [2,10,16–18], while hemocyanin activity on *o*-diphenols [19–26] and on monophenols [27] has been demonstrated. Furthermore, synthetic copper complexes show-

* Corresponding author. Fax: +34 968 364147.
E-mail address: canovasf@um.es (F. García-Cánovas).
URL: http://www.um.es/genz (F. García-Cánovas).

1381-1177/$ – see front matter © 2009 Elsevier B.V. All rights reserved.
doi:10.1016/j.molcatb.2009.10.005

Author's personal copy

ing activity on *o*-diphenols and monophenols have been described [28–30].

In our studies of the kinetic mechanism of tyrosinase [31–34], especially of the suicide inactivation processes with phenolic compounds [35] and with ascorbic acid [36], we proposed an action mechanism on monophenols and *o*-diphenols and worked with tyrosinase in the different forms existing in the catalytic cycle: E_m, *met*-tyrosinase; E_{ox}, *oxy*-tyrosinase and E_d, *deoxy*-tyrosinase [36].

Mason's study of mushroom tyrosinase [3] demonstrated that when a nitrogen stream is passed through a solution of E_{ox}, the typical spectrum of E_{ox} disappears and that when attempts are made to regenerate the enzyme after a certain time, only 50–60% is recovered, suggesting that the enzyme evolves towards a form that is re-oxygenated slowly.

To broaden our knowledge of the different enzymatic forms of tyrosinase, we have made a kinetic study of the evolution of E_d under anaerobic conditions and of the kinetic of the re-oxygenation process. We have further studied the effect of the order in which the substrates (oxygen/*o*-diphenol or oxygen/monophenol) are added to the enzyme, considering the effect of pH on the transition of E_d and on its re-oxygenation, and discussed the possibility that two apparent pK_as may be responsible for its transition. The results are discussed in relation with the process described for the oxygenation of *deoxy*-hemocyanin [8].

2. Experimental

2.1. Materials

Mushroom tyrosinase or polyphenol oxidase (PPO; *o*-diphenol:O_2 oxidoreductase, EC 1.14.18.1, 8300 units/mg), was supplied by Sigma (St. Louis, MO). Tyrosinase was purified as previously described [32]. The protein concentration was determined by Bradford's method [37] and using bovine serum albumin as the standard. The substrates used were: hydrogen peroxide, supplied by Scharlau (Madrid, Spain), 4-*tert*-butylcatechol (TBC) supplied by Acros Co. (Madrid, Spain), and L-tyrosine and L-dopa supplied by Aldrich (Switzerland). Other chemicals were of analytical grade and supplied by Merck (Darmstadt, Germany).

2.2. Methods

2.2.1. Oxymetric assays

Measurements of dissolved oxygen concentration were made with a Hansatech (Kings Lynn, Cambs, UK) oxygraph unit controlled by a PC-computer. The oxygraph used a Clark-type silver/platinum electrode with a 12.5 μm Teflon membrane. The sample was continuously stirred during the experiments and its temperature was maintained at 25 °C. The zero oxygen level for calibration and experiments was obtained by bubbling oxygen-free nitrogen through the sample for at least 10 min. The oxygraph was calibrated as described in [38].

2.2.2. Spectrophotometric assays

When the substrate was TBC, the reaction was followed by monitoring the formation of *o*-*tert*-butylquinone at 410 nm ($\varepsilon = 1200\ M^{-1}\ cm^{-1}$) [39]. When the substrate was L-tyrosine or L-dopa the increase in absorbance at 475 nm ($\varepsilon = 3500\ M^{-1}\ cm^{-1}$) was followed [39].

2.2.3. Generation of E_{ox} and E_d

E_{ox} was generated from the native enzyme, adding micromolar concentrations (5 μM) of H_2O_2 so that the E_m form passed to E_{ox}. E_d was generated by bubbling nitrogen through the E_{ox} solution to transform all the E_{ox} to E_d ($E_{ox} \rightleftarrows E_d + O_2$) [36,40].

2.2.4. Evaluation of enzymatic species E_m, E_d and E_{ox} in an enzymatic preparation of tyrosinase

Regardless of the source, tyrosinase preparations are reported to contain three enzyme forms, namely E_m, E_d and E_{ox} [40]. To evaluate these enzymatic forms in an enzyme sample, we propose a kinetic method [36] based on the fact that the inactivation of these forms by 2-mercaptoethanol [41] occurs over a wide time range: inactivation constants of 0.014, 4×10^{-5} and $1 \times 10^{-5}\ s^{-1}$ for E_{ox}, E_m and E_d, respectively. Under aerobic conditions at oxygen concentrations of 0.26 mM, practically the only forms existing are E_{ox} and E_m [32]. Note that the difference between k_i^{ox} and k_i^m is three orders of magnitude, a difference that can be used to evaluate these enzymatic forms.

The experimental method consists of pre-incubating the enzyme under aerobic conditions with 2-mercaptoethanol at a concentration of 10 μM. Aliquots of the reaction mixture are taken at different incubation times and immediately assayed for residual activity using TBC as the substrate. In this way, at sufficiently long times, a situation is reached in which the activity tends asymptotically to a constant value. The decrease in the initial activity to reach this approximately constant final value would correspond to the concentration of E_{ox} in the medium. In this way, inactivation assays of the enzyme sample previously incubated with different concentrations of H_2O_2 in the μM order are made with 2-mercaptoethanol. This gives rise to different concentrations of E_{ox} and therefore different levels of activity in the linear zone [36].

Analysis by non-linear regression fitting of the experimental data to the uniexponential equation:

$$\frac{A_t}{A_0} = \frac{A_{m_0}}{A_0} + \frac{A_{ox_0}}{A_0} e^{-k_{app}^{ox} t} \quad (1)$$

gives the values of $(A_{m_0}/A_0) \times 100$, which is the percentage of E_m, $(A_{ox_0}/A_0) \times 100$ which is the percentage of E_{ox} and k_{app}^{ox}, the apparent inactivation constant. In Eq. (1), A_t, is the residual activity at time t, A_0 is the initial activity, A_{m_0} is the activity corresponding to E_{m_0} and A_{ox_0} is the activity corresponding to E_{ox_0} [36].

The representation of the decrease in activity (corresponding to E_{ox}) *vs.* instantaneous activities, when $t \to \infty$, (corresponding to E_m) shows a linear variation, which can be used as a calibration straight to determine the percentages of E_{ox} and E_m in an enzymatic preparation of tyrosinase.

2.2.5. Characterisation of the kinetic parameters of the native enzyme, E_d^R and E_d^T

The kinetic parameters V_{max}^D and K_m^D for the diphenolase activity were calculated from the initial velocities, V_0^D, with TBC and O_2 (0.26 mM) as substrates [39]. These values were fitted to the Michaelis equation by non-linear regression [42]. At pH 7.0, since the E_d^R form evolves slowly to E_d^T at 25 °C, the native enzyme (without passing nitrogen) and the forms E_d^R and E_d^T were maintained in an ice bath, while the measurements with E_d^R were made immediately in order to delay the transition. In the same way, at pH 6.5, the native form and E_d^T were analysed for the diphenolase activity on TBC.

The kinetic parameters, V_{max}^M and K_m^M, for the monophenolase activity were calculated from the initial velocities, V_0^M, using L-tyrosine and adding an amount of L-dopa so that $[D]_{ss}/[M]_{ss} = 0.035$ [43] and recording the increase in absorbance at 475 nm. At pH 7.0, using the same methodology as for the diphenolase activity, the native enzyme and the forms E_d^R and E_d^T were characterised. In the same way, at pH 6.5, the native form and E_d^T were analysed using L-tyrosine as substrate.

Author's personal copy

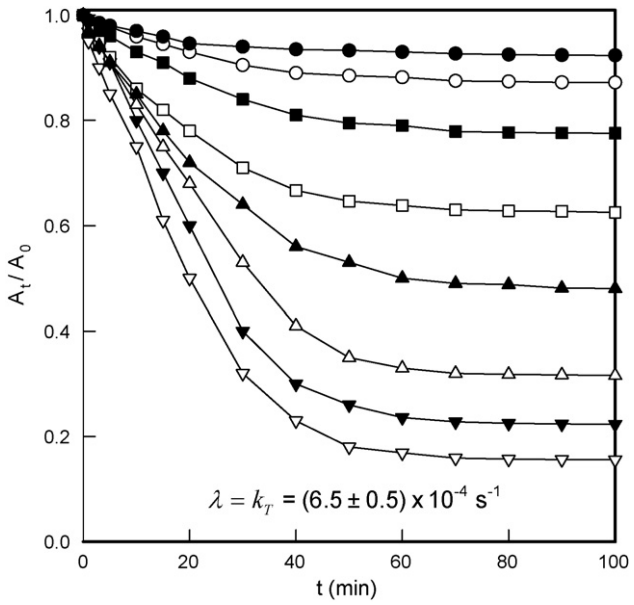

Fig. 1. Variation of the A_t/A_0-values *vs.* time obtained from a kinetic study of transition of E_d^R to E_d^T followed through the diphenolase activity. The experimental conditions were as follows: 30 mM sodium phosphate buffer (pH 7.0), 25 °C. A nitrogen stream was first passed through the buffer and then 10 nM enzyme (previously treated with 5 μM H_2O_2) was added; still passing the nitrogen stream, aliquots were taken at the indicated times and the activity was followed using different concentrations of TBC, measuring the increase in absorbance at λ = 410 nm. TBC concentrations (mM) were: ▽ 0.5, ▼ 1, △ 2, ▲ 4, □ 5, ■ 7, ○ 9 and ● 15.

2.2.6. Kinetic study of the transition of E_d^R to E_d^T

The data of this transition were fitted to the equation (see Appendix A):

$$\frac{A_t}{A_0} = \alpha + \beta e^{-\lambda t} \quad (2)$$

where A_t is the instantaneous activity, A_0 is the instantaneous activity at $t = 0$, and $\lambda = k_T$, the apparent transition constant. The parameters α and β are functions of the substrate concentration (see Appendix A). Fitting the data shown in Fig. 1 to Eq. (2) by non-linear regression provides the value of the transition constant, $k_T = (6.5 \pm 0.5) \times 10^{-4}\ s^{-1}$. Note that when $t \to \infty, A_\infty/A_0 = \alpha$, and the amplitude of the exponential is $(A_0 - A_\infty)/A_0 = 1 - \alpha = \beta$.

2.2.7. Inactivation of E_d^R and E_d^T by o-diphenols

All the native enzyme was converted into E_{ox} by adding H_2O_2 (2 μM). A nitrogen stream was then passed to obtain E_d^R. The form E_d^R was incubated with L-dopa (5–45 μM), and aliquots were taken at different times to measure instantaneous activities using L-dopa.

Once E_d^R had been generated, 90 min were allowed to pass for it to be transformed into E_d^T. This form was then incubated with L-dopa (5–45 μM), and aliquots were taken at different times to measure instantaneous activities using L-dopa.

2.2.8. Effect of monophenols on enzyme inactivation by o-diphenols

The forms E_d^R or E_d^T were pre-incubated with L-tyrosine (20 μM) and in the presence of L-dopa (5–45 μM), while aliquots were taken at different times to measure instantaneous activities using L-dopa.

3. Results and discussion

Tyrosinase, in its native state, basically exists in three forms known as *met*-tyrosinase (E_m), *deoxy*-tyrosinase (E_d) and *oxy*-tyrosinase (E_{ox}) [40]. As described in Section 2, the addition of H_2O_2 (μM) to an aerobic medium transforms the E_m into E_{ox} [3]. Passing a stream of nitrogen transforms E_{ox} into E_d. This E_d, with time, evolves towards another enzyme form with different kinetic properties (higher K_m for substrates and slightly lower V_{max}). This transition, therefore, can be followed from the loss of enzymatic activity with time at a non-saturating substrate concentration. By analogy with the nomenclature used by Solomon for *deoxy*-hemocyanin [8], these enzymatic forms could be regarded as E_d^R and E_d^T, R (relaxed) and T (tense), and, in the case of *deoxy*-hemocyanin, the distances between the copper atoms at the active site are 3.5 Å (R) and 4.6 Å (T), respectively [8].

Table 1
Kinetic constants of the native, E_d^R and E_d^T forms of tyrosinase.

	K_m^D(mM)	V_{max}^D(μM/s)	K_m^M(mM)	V_{max}^M(μM/s)
E_{native}	1.39 ± 0.14[a]	37.11 ± 0.74[a]	0.17 ± 0.02[b]	0.52 ± 0.02[b]
E_d^R	1.80 ± 0.19[a]	36.19 ± 0.96[a]	0.19 ± 0.02[b]	0.48 ± 0.02[b]
E_d^T	3.21 ± 0.38[a]	33.28 ± 0.99[a]	0.40 ± 0.04[b]	0.45 ± 0.01[b]
E_{native}	2.12 ± 0.24[c]	37.21 ± 1.45[c]	0.29 ± 0.01[d]	0.53 ± 0.03[d]
E_d^T	2.21 ± 0.28[c]	37.08 ± 1.92[c]	0.31 ± 0.01[d]	0.54 ± 0.03[d]

K_m^D = Michaelis constant for *o*-diphenol (TBC). V_{max}^D = Maximum rate for *o*-diphenol (TBC). K_m^M = Michaelis constant for monophenol (L-tyrosine). V_{max}^M = Maximum rate for monophenol (L-tyrosine).

[a] Determined in 30 mM sodium phosphate buffer (pH 7.0) and using TBC as substrate. The enzyme concentration was 30 nM.

[b] Determined in 30 mM sodium phosphate buffer (pH 7.0) and using L-tyrosine as substrate and L-dopa with ratio constant of 0.035. The enzyme concentration was 75 nM.

[c] Determined in 30 mM sodium phosphate buffer (pH 6.5) and using TBC as substrate. The enzyme concentration was 30 nM.

[d] Determined in 30 mM sodium phosphate buffer (pH 6.5) and using L-tyrosine as substrate and L-dopa with ratio constant of 0.035. The enzyme concentration was 75 nM.

3.1. Diphenolase activity

3.1.1. Kinetic study of transition of E_d^R to E_d^T

The native enzyme and the forms E_d^R and E_d^T are characterised kinetically by the kinetic constants and parameters shown in Table 1 (see Section 2). The kinetic parameters shown in this table indicate that the enzyme form E_d^T has the highest K_m, that is, a lower affinity for the *o*-diphenol, but, the V_{max} for all these forms are the same. As regards E_d^R, since this form is not totally stable, it may partially evolve towards E_d^T. Note that the kinetic behaviour of these enzymatic forms as regards V_{max} and K_m is similar to that shown by the native enzyme with respect to the Dopa isomers, other enantiomers [44] and, in general, all *o*-diphenols [45]. In all these cases, it can be seen that the catalysis is associated with the nucleophilic power of the oxygen of the OH in *para*-position of the *o*-diphenol. Since, in this work, the *o*-diphenol is always TBC (δ_4- and δ_3-values of 144.09 and 146.24 ppm, respectively [45]), the V_{max}-value might be very similar. Bearing in mind the increase in K_m in the form E_d^T, the difference in the initial velocities at a non-saturating substrate concentration permits us to follow the transition. Fig. 1 shows the relative values of the initial velocities, revealed with TBC with respect to the transition time.

3.1.2. Kinetic of E_d^T re-oxygenation

These experiments study the transformation of E_d^T to E_{ox}, for which the most straightforward kinetic scheme would be (Schemes 1A and 1BSM):

$$E_d^T + O_2 \underset{k_r}{\overset{k_b}{\rightleftharpoons}} E_d^T O_2 \xrightarrow{k^*} (E_d^T O_2)^* \xrightarrow{k_{ox}} E_{ox}$$

Scheme 1A. Kinetic mechanism of the oxygenation of the form E_d^T.

Author's personal copy

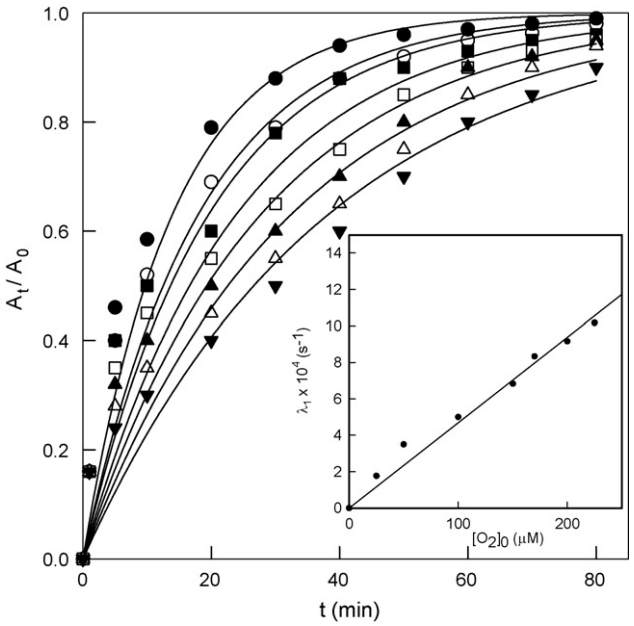

Fig. 2. Dependence of the A_t/A_0-values *vs.* time obtained from a kinetic study of oxygenation of E_d^T. A nitrogen stream was first passed through 30 mM sodium phosphate buffer (pH 7.0), 25 °C. Then, 10 nM of the E_{ox} form was added; still passing the nitrogen stream, the mixture was left for 90 min for the E_d^R to be transformed into E_d^T. The enzyme, in the form of E_d^T, was added to the cell of the oxygraph containing 30 mM sodium phosphate buffer (pH 7.0) at 25 °C, and a sufficient concentration of oxygen so that the final O_2 concentrations (μM) become: ▼ 25, △ 50, ▲ 100, □ 150, ■ 175, ○ 200 and ● 225. At the indicated times, 100 μl of the above mixture was extracted with microsyringe and added to the reaction cell with O_2 (0.26 mM) and TBC (1 mM). Inset: Representation of the apparent transition constant λ_1 *vs.* $[O_2]_0$, the initial oxygen concentration.

The incubation of E_d^T is started at different concentrations of oxygen. Aliquots are taken at different times and the enzymatic activity is revealed with TBC (see Fig. 2). Note the monoexponential behaviour, which depends on the concentration of O_2. The kinetic analysis of the mechanism depicted in Scheme 1A (see Appendix B) indicates that E_{ox} is accumulated with time according to:

$$[E_{ox}] = [E_d^T]_0(1 - e^{-\lambda_1 t}) \quad (3)$$

where λ_1 represents the apparent constant of E_d^T oxygenation and the analytical expression of λ_1 is:

$$\lambda_1 = \frac{k^*[O_2]_0}{K_{O_2}^T + [O_2]_0} \quad (4)$$

with

$$K_{O_2}^T = \frac{k_r}{k_b} \quad (5)$$

Analysis by non-linear regression of the velocities with time, according to Eq. (3), provides the apparent transition constant λ_1. The representation of λ_1 *vs.* $[O_2]_0$, Fig. 2 Inset, does not show a hyperbolic behaviour, indicating that the value of $K_{O_2}^T$ for E_d^T is higher than for the native enzyme, so that E_d^T cannot be saturated at the oxygen concentrations used. There is an apparent contradiction between the initial velocity experiments, which give the results shown in Table 1, and those shown in Fig. 2. In the former, an aliquot of E_d^T shows its activity as soon as it comes into contact with the substrates O_2/*o*-diphenol together, while in Fig. 2, where E_d^T is pre-incubated with oxygen, only a small part of the activity is detected, although at long time intervals, all the activity is revealed (as in the case of the native enzyme). These experiments can be explained by a similar mechanism to that proposed by Solomon [8] (Scheme 1BSM) for the oxygenation of *deoxy*-hemocyanin. According to the mechanism proposed in [8], the substrate (O_2) approaches the binuclear copper (I) site driven by optimizing the metal–ligand overlap, while the binuclear pathway for the binding of O_2 is favoured energetically to the mononuclear pathway and the changes in the charge density of the coppers and oxygens are similar, indicating that this is a simultaneous two electron-transfer process, that is, there is a charge transfer step [8]. Subsequently, the singlet state is preferred to the triplet state [8]. Furthermore, in [8] it is proposed that *deoxy*-hemocyanin in the form T [$d(Cu^A - Cu^B) = 4.6$ Å] is less energetic (15.6 kcal/mol) and therefore more stable than R [$d(Cu^A - Cu^B) = 3.5$ Å] (17.8 kcal/mol); but, whatever the case, the formation of the oxy form is exothermic and for hemocyanin the value of ΔG determined from experimental data is negative, while at the end of the process, all the protein is in the form of *oxy*-hemocyanin [8].

In the case of tyrosinase, the data obtained suggest that a similar process might occur. The diminution in the affinity (increased K_m for *o*-diphenol and oxygen) might be explained by the fact that under anaerobic conditions the $E_d^R \rightarrow E_d^T$ transition would involve separation of the copper atoms and the forms E_d^R and E_d^T would be similar to the forms R and T described for *deoxy*-hemocyanin [8]. Incubation of E_d^T with O_2 triggers the slow process described above (Scheme 1BSM), culminating in the formation of E_{ox}, which has recovered all its activity on *o*-diphenol. In this case, the *o*-diphenol binds in the same way as it does to the native enzyme, transferring the proton of the OH in *para*-position to the peroxide, which acts as a base, while the resulting anion attacks Cu^B of the active site and then the OH in *meta*-position would transfer its proton to the histidine 54 (His^{54}) of the Cu^A [6]. The His^{54} is released, and the *o*-diphenol binds diaxially, leading to a joint oxidation/reduction step as a result of the coplanarity of the orbitals and an activity similar to that of the native enzyme. However, as Fig. 2 shows, once this process has started, only the activity of the E_{ox} generated (Scheme 1BSM) will be detected. But note that the measurements of initial velocity in the presence of O_2 and *o*-diphenol point to a synergic effect, so that the presence of the *o*-diphenol will immediately re-establish the O_2 bond. This form, which is recovered in a way that differs from that described in [8], shows worse kinetic constants (especially K_m) than the native form and also than E_d^R (see Table 1) (Scheme 1CSM). Similarly, the form E_d^R, when brought into contact simultaneously with the *o*-diphenol/O_2, shows immediate enzymatic activity—almost the same as that shown by the native enzyme but greater that that of E_d^T. When both forms E_d^R and E_d^T come into simultaneous contact with the oxygen/*o*-diphenol, the form $E_{ox}D$ may be generated in a different way, especially in the case of E_d^T, when the *o*-diphenol cannot transfer the proton of OH in *para*-position to the peroxide, since it does not exist. In this case, it may first transfer the proton to the His^{54}, the phenolate binding to Cu^A. The copper atoms restructure and bind with the O_2, while the proton of the OH in *meta*-position is transferred to the peroxide, which would act as a base, and the phenolate can now bind to the Cu^B.

This atypical generation of $E_{ox}D$ may reduce the enzymatic activity, as occurs experimentally, and is lower for E_d^T than for E_d^R. Although activity is obtained, the enzyme in the form E_d^T does not recover its native form in a few turnovers, since no lag period appears in the kinetic measurements. However, as described in Schemes 1CSM and 1DSM, the alternative mechanism proposed for E_d^T (Scheme 1CSM) is also possible. The influence of the oxygen concentration during pre-incubation is clear in the results shown in Fig. 3, as the oxygen concentration in the reaction medium increases, so the enzyme activity increases, but note that this effect does not occur at $t \rightarrow 0$, since E_d^R, recently formed, is rapidly oxygenated as it passes to E_{ox} since its $K_m^{O_2}$ is low (Scheme 1DSM).

Author's personal copy

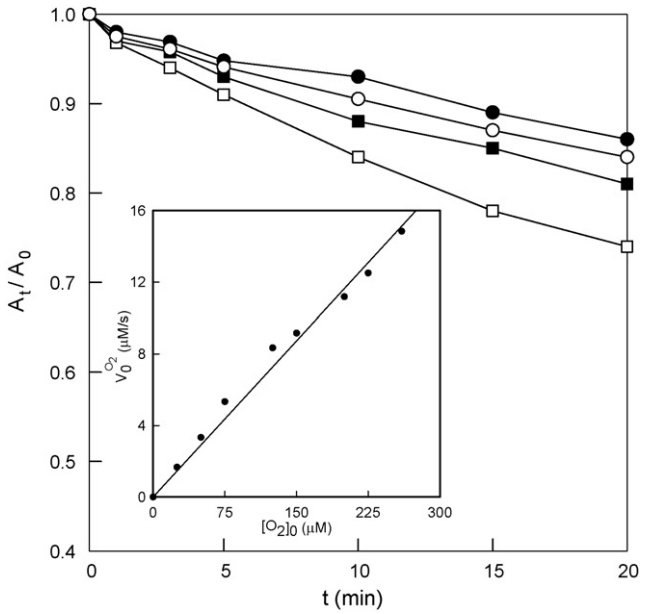

Fig. 3. Effect of oxygen concentration on the A_t/A_0-values in following the transition of E_d^R to E_d^T. The experimental conditions were 30 mM sodium phosphate buffer (pH 7.0), 25 °C (previously de-aired with N_2). The enzyme E_{ox} is transformed into E_d^R under the nitrogen while the transition to E_d^T is studied under a continuous nitrogen stream. Aliquots are revealed in media with TBC (1 mM) and different initial oxygen concentrations (μM): without previous pre-incubation, □ TBC + O_2 (260 μM) at the same time; with previous pre-incubations (1 min) with oxygen at the following initial concentration (μM): ■ 130, ○ 195 and ● 260 and finally the reaction is started with TBC (1 mM). Inset: representation of initial rates of oxygen consumption, $V_0^{O_2}$ *vs.* $[O_2]_0$, the initial oxygen concentration, for the enzymatic form E_d^T.

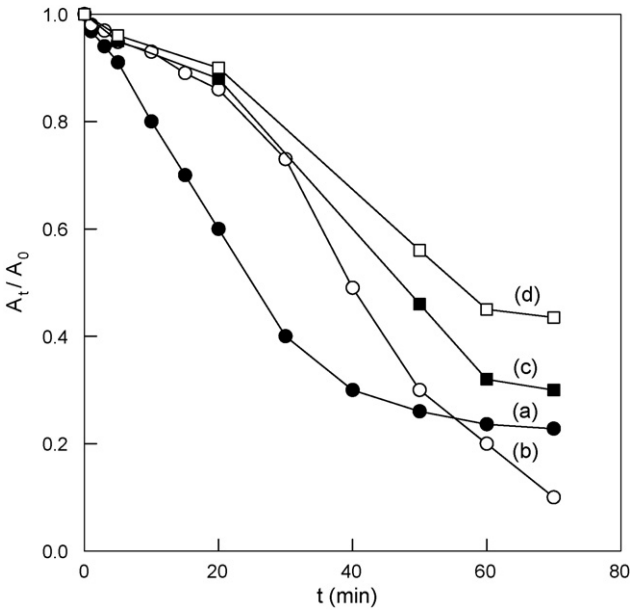

Fig. 4. Variation of the A_t/A_0-values *vs.* time obtained from a kinetic study of the effect of pre-incubation time with oxygen on transition of E_d^R to E_d^T. The experimental conditions were: 30 mM sodium phosphate buffer (pH 7.0), 25 °C de-aired with N_2. The enzyme E_{ox} (10 nM) was then added under a continuous nitrogen stream. At the times indicated in the figure, aliquots were taken and added to the cell containing phosphate buffer pH 7.0 and oxygen. The mixture was left to incubate, starting the reaction with TBC (1 mM) and measuring the initial velocity at λ = 410 nm. ● Without pre-incubation with O_2 [curve (a)]. Pre-incubating with O_2 (260 μM) during; ○ 1 min [curve (b)], ■ 5 min [curve (c)] and □ 15 min [curve (d)].

At longer times, much of the E_d^R has been transformed into E_d^T and this new form has less affinity for oxygen, that is, a higher $K_m^{O_2}$ (Schemes 1BSM and 1CSM). Fig. 3 Inset shows how the enzyme in the form E_d^T, at saturating TBC concentrations, is not saturated by the concentrations of oxygen used.

3.1.3. Study of the transition of E_d^R to E_d^T with the sequential addition of the substrates, O_2 and *o*-diphenol

The effect of the oxygen concentration on the kinetic of the transformation of E_d^T into E_{ox} is shown in Fig. 2 and its effect on the apparent delay in the transition of E_d^R into E_d^T is depicted in Fig. 3. In Fig. 4, we depict the effect of the pre-incubation time of an aliquot of the enzyme at a fixed concentration of oxygen on the transition of E_d^R into E_d^T. As can be seen, the order in which the substrates are added affects this process and this helps confirm the validity of Schemes 1A, 1BSM, 1CSM and 1DSM proposed to explain the transition of E_d^R to E_d^T and E_d^T to E_{ox}.

The experiment consisted of studying the transition of E_d^R to E_d^T under anaerobic conditions, but treating the aliquot obtained of the enzyme with O_2 for different pre-incubation times (0, 1, 5 and 15 min, respectively), and beginning the reaction with *o*-diphenol.

Curve (a) of Fig. 4 corresponds to the transition of E_d^R to E_d^T, determining the activity of the aliquot obtained with the simultaneous addition of the substrates O_2/*o*-diphenol. In this curve one must obviously bear in mind the exact moment at which the aliquot is taken. At short times, for example, the enzyme would be in the form E_d^R and Scheme 1DSM would explain the recovery of the enzymatic activity. However, at long times, the enzyme would be like E_d^T Scheme 1CSM would basically explain the activity. Curves (b), (c) and (d) are obtained by following the transition (E_d^R to E_d^T), treating the aliquot obtained with the same oxygen concentration but pre-incubating for different times. Once again, we must bear in mind the times at which the aliquot is taken and its behaviour. Note that at short times there are practically no differences in the enzymatic activity obtained in any of the cases. Hence, Scheme 1DSM would explain all the cases, the enzyme being practically the same as E_d^R. However, at longer timer of the transition, the effects of the pre-incubation time with oxygen become patent in the transition of E_d^R to E_d^T. At very short pre-incubation times (1 min), Fig. 4 curve (b), the representation of Scheme 1ESM would explain the experimental results: the enzyme is not transformed into E_{ox}, the substrate (*o*-diphenol) has no synergic effect and the enzymatic activity is very low [Fig. 4 curve (b)]. In curves (c) and (d) of Fig. 4, the importance of the pre-incubation time is evident, and can be explained according to Scheme 1BSM. At longer pre-incubation times, there is already some E_{ox} and so more enzymatic activity is obtained [Fig. 4, curves (c) and (d)].

The slow stages proposed in these schemes for the re-oxygenation of E_d^T may explain the experimental results described in [3], in which, after passing a nitrogen stream, the total spectrum of the *oxy*-tyrosinase form is not recovered [3].

3.1.4. Effect of pH on transition of E_d^R to E_d^T

The results of studying the effect of pH on the kinetic of the transition of E_d^R to E_d^T are shown in Fig. 5. The value of the apparent transition constant, k^{app}, remains practically constant at very acidic pH values, reaches a maximum at pH 6.5 and then declines at higher pHs (Fig. 5 Inset). However, the amplitude of the exponential (Fig. 5 Inset) decreases as the pH rises, with a minimum at 6.5 and increasing at higher values. These findings suggest the existence of two significant apparent pK_as for this transition, one corresponding to pH ≈ 6.75 and the other to pH ≈ 6.0. The pH optimum for this transition is 6.5, as seen from Fig. 5 Inset, in which the kinetic properties of E_d^T are very similar to those of the native enzyme (Table 1). A qualitative explanation could be that outlined in the following schemes:

Author's personal copy

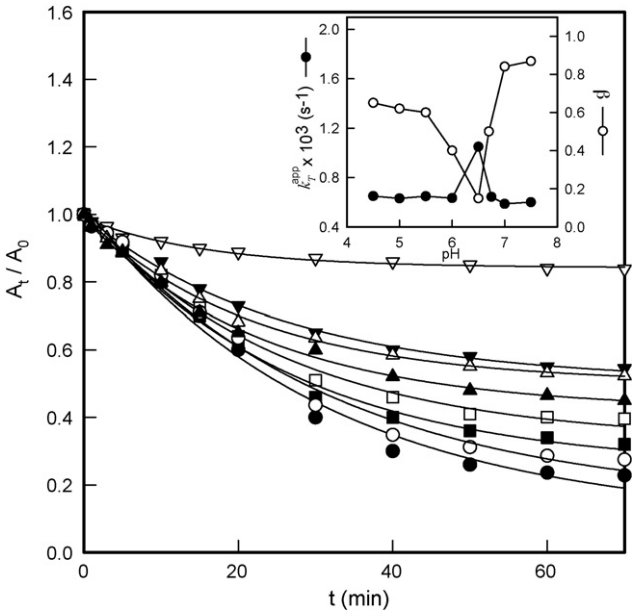

Fig. 5. Dependence of the A_t/A_0-values *vs.* time obtained from a kinetic study of the effect of pH on the transition of E_d^R to E_d^T. The form E_d^R was generated as in Fig. 1 at each pH, and the transition in a nitrogen atmosphere was studied by taking aliquots at the indicated times and revealed with TBC (1 mM). The buffers used (previously de-aired with N_2) were 30 mM sodium acetate buffer (pH 4.0–5.5) and 30 mM sodium phosphate buffer (pH 6.0–7.5), 25 °C. The pH values were: ● 7.5, ○ 7.0, ■ 6.75, ▽ 6.5, □ 6.0, ▲ 5.5, ▼ 5.0 and △ 4.5. Inset: Representation of k_T^{app} *vs.* pH (♦) and β *vs.* pH (◊).

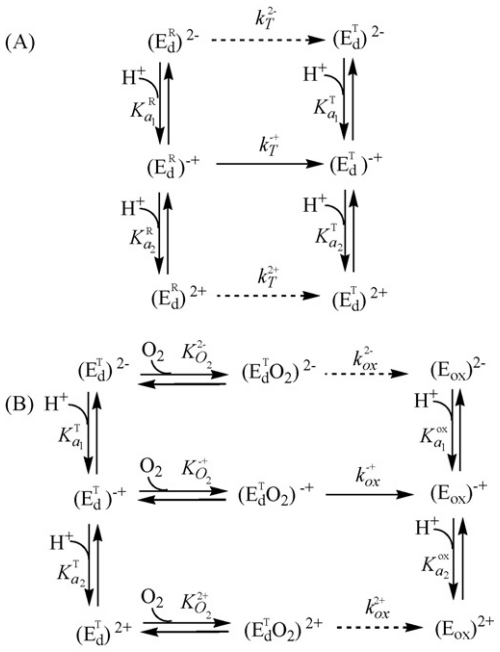

Scheme 2. (A) Effect of pH on the transition of E_d^R to E_d^T, $K_{a_1}^R$, $K_{a_2}^R$, $K_{a_1}^T$ and $K_{a_2}^T$ are the corresponding deprotonation equilibrium constants and k_T^{2-}, k_T^{+-} and k_T^{2+} are the transition constants of the corresponding enzyme forms. (B) Effect of pH on the re-oxygenation of E_d^T. $K_{a_1}^T$ and $K_{a_2}^T$ have the same meaning as in Scheme 2A. $K_{a_1}^{ox}$ and $K_{a_2}^{ox}$ are the corresponding deprotonation constants. $K_{O_2}^{2-}$, $K_{O_2}^{+-}$ and $K_{O_2}^{2+}$ are the dissociation equilibrium constants of $(E_dO_2)^{2-}$, $(E_dO_2)^{+-}$ and $(E_dO_2)^{2+}$, respectively. k_{ox}^{2-}, k_{ox}^{+-} and k_{ox}^{2+} are the rate constants of the indicated transformations.

At pH values > 6.5, the form E_d^R could have two negative charges that repel each other and the enzyme would evolve slowly towards E_d^T, while the two copper atoms of the active site are more separate [8]. At pH values < 6.5, the form E_d^R would have two positive charges that again repel each other as the transition to E_d^T continues. Furthermore, the values of the apparent transition constant are practically identical (Fig. 5 Inset). At pH 6.5, the enzyme would be as described in Scheme 2A, with a positive and negative charge. The attraction between these charges would prevent the transition to E_d^T from being so great, as occurs at both high and low pH values. In this way, the kinetic constants of the different enzymatic forms (native and E_d^T) are practically the same at pH 6.5, that is, the copper atoms hardly separate. This hypothesis could be supported by the findings of the existence of a salt bridge between two helices that is conserved in hemocyanin, catechol oxidase and tyrosinase between Arg(Lys)-Asp, as has been described previously [46].

3.1.5. *Effect of pH on re-oxygenation of E_d^T*

The form E_d^T was generated in 1 mM sodium phosphate buffer pH 7.0 as described in Section 2. The enzyme was then introduced in the oxygraph cell at different values of pH and with a 30 mM buffer. The re-oxygenation process was followed by taking aliquots at different times. As described previously, the oxygenation kinetic of E_d^T at pH 7.0 showed monoexponential behaviour for the re-oxygenation, demonstrating that the enzyme form E_d^T rapidly binds to the oxygen but enters into a slow stage of the mechanism, and only when regenerated as E_{ox} can enzymatic activity be obtained (Schemes 1BSM and 2B). Fig. 6 shows the E_d^T re-oxygenation kinetics and the values of the apparent constant for transition at different pH values (Fig. 6 Inset). Note that at pH 6.5 the apparent constant is much higher, as occurs in the transition of E_d^R to E_d^T (Scheme 2B), which agrees with the explanation proposed in the previous step, indicating that the attraction between charges of opposing sign may contribute to the transition of E_d^T to E_d^R taking place rapidly and on a small scale.

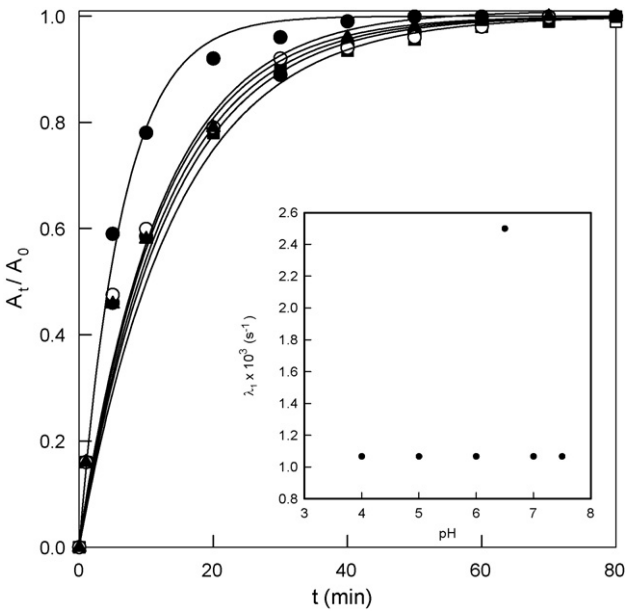

Fig. 6. Variation of the A_t/A_0-values *vs.* time obtained from a kinetic study of the effect of pH on the oxygenation of E_d^T to E_{ox}. The form E_d^T is generated in 1 mM sodium phosphate buffer (pH 7.0) and the oxygenation is studied at different pH values, mixing the enzyme E_d^T on the oxygraph cell with 30 mM buffers. Taking aliquots at the indicated times, activity was determined with TBC (1 mM) and O_2 (0.26 mM). The buffers used were: 30 mM sodium phosphate buffer pH: ● 6.5, ○ 7.5, ■ 7.0, □ 6.0 and 30 mM sodium acetate buffer pH: ▲ 5.0, △ 4.0. Inset: Representation of apparent oxygenation constant λ_1 *vs.* pH.

Author's personal copy

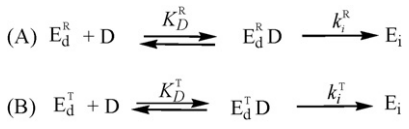

Scheme 3. (A) Kinetic mechanism of inactivation of E_d^R by *o*-diphenol. (B) Kinetic mechanism of inactivation of E_d^T by *o*-diphenol.

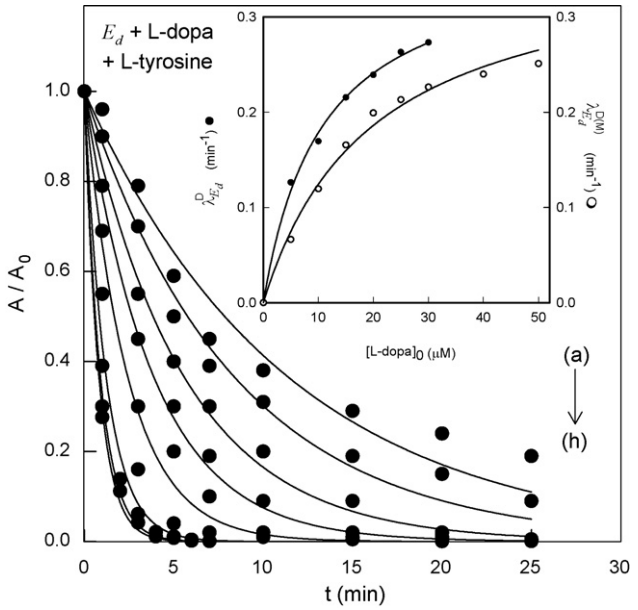

Fig. 7. Inactivation of the E_d^R form of tyrosinase by *o*-diphenols. The form E_d^R was obtained as is described in Section 2 and immediately incubated with *o*-diphenol (L-dopa), taking aliquots at different times to measure the residual activity with 2.5 mM L-dopa (λ = 475 nm). The values obtained were fitted to Eq. (6) and the apparent inactivation constant was obtained at each concentration of *o*-diphenol. The experimental conditions were: 30 mM sodium phosphate buffer (pH 7.0), 25 °C, $[E_d^R]_0 = 10$ nM (see Section 2), $[H_2O_2]_0 = 2$ μM and L-dopa (μM): (a) 5, (b) 10, (c) 15, (d) 20, (e) 25 and (f) 30. Inset. ● Representation of $\lambda^{D}_{E_d^R}$ *vs.* $[L\text{-dopa}]_0$. Fitting of these data to Eq. (8) gives the $K^{D}_{E_d^R}$. ○ Representation of the values of $\lambda^{D(M)}_{E_d^R}$ *vs.* $[L\text{-dopa}]_0$ obtained in the presence of L-tyrosine. Fitting to Eq. (10), gives the parameter $K^{D(M)}_{E_d^R}$ and analysis according to Eq. (12) gives $K^{M}_{E_d^R}$ (Table 2).

3.1.6. Incubations of E_d^R and E_d^T with *o*-diphenol

When the enzyme is pre-incubated with *o*-diphenol under aerobic conditions, both the recently generated E_d^R (Scheme 3A) and E_d^T (Scheme 3B) undergo a process of irreversible inactivation. The form E_d^R shows a lower apparent binding constant (greater affinity) than E_d^T, although its apparent inactivation constant is slightly greater, indicating that its binding to the *o*-diphenol is favoured by the proximity of the copper atoms, which are probably further apart in E_d^T, hindering substrate binding, Fig. 7 and Table 2 (Scheme 3CSM). In the case of E_d^T (Scheme 3B and Scheme 3DSM), inactivation also takes place. An analysis of the data of instantaneous activities *vs.* time, according to the following equations:

$$[E_a] = [E_d^R]_0 e^{-\lambda^{D}_{E_d^R} t} \quad (6)$$

$$[E_a] = [E_d^T]_0 e^{-\lambda^{D}_{E_d^T} t} \quad (7)$$

provides the apparent inactivation constants. A study of the different concentrations of *o*-diphenol and its analysis by Eqs. (8) and (9) give the values of K^{D}_{E}, $k^{R}_{i_D}$ and $k^{T}_{i_D}$ (Table 2).

$$\lambda^{D}_{E_d^R} = \frac{k^{R}_{i_D}[D]_0}{K^{D}_{E_d^R} + [D]_0} \quad (8)$$

$$\lambda^{D}_{E_d^T} = \frac{k^{T}_{i_D}[D]_0}{K^{D}_{E_d^T} + [D]_0} \quad (9)$$

In these cases (Schemes 3CSM and 3DSM), the *o*-diphenol could transfer the proton from the OH in *para*-position to the His^{54} of the Cu^A and the phenolate binds to the Cu^A, while the OH in *meta*-position later transfers its proton to the medium and binds in diaxial position. This binding will facilitate the oxidation/reduction and the enzyme is inactivated. Such a process may be favoured in E_d^R compared with E_d^T because of the proximity of the copper atoms.

The inactivation of the forms E_d^R and E_d^T with *o*-diphenol could have an industrial application in the agro-food industry for juice extraction since rapidly passing a nitrogen stream would lead to the formation of *deoxy*-tyrosinase, which, in the presence of the *o*-diphenols in the extracts (mainly chlorogenic acid), would lead to its inactivation, eliminating the enzymatic browning that normally occurs.

3.2. Monophenolase activity

3.2.1. Initial velocity measurements

From the measurements of initial velocity, it is possible to calculate the kinetic constants of the native enzyme and of the form E_d^R, which are shown in Table 1. When E_d^T is formed, the kinetic properties with respect to L-tyrosine can be studied (see Table 1). Note the increase in K_m^M and slight diminution of V_{max}^M, both of which agree with the results shown for the *o*-diphenols (Table 1). As mentioned above, by analogy with hemocyanin [8], the copper atoms are probably more distant in the form E_d^T than in E_d^R so that its affinity for the monophenol would be lower, despite the synergic effect observed between the substrates (O_2/L-tyrosine) as in the case of *o*-diphenols. The enzyme shows its characteristic lag, τ, in these measurements.

3.2.2. Study of the transition of E_d^R to E_d^T by following the monophenolase activity with L-tyrosine

Under anaerobic conditions, E_d^R is transformed into E_d^T, the enzymatic activity detected with L-tyrosine shows identical behaviour to that observed with the *o*-diphenol, TBC, and so the binding of the enzyme with the pair O_2/monophenol shows the same synergic effect as with the *o*-diphenol, Fig. 8. The values of the

Table 2
Equilibrium and kinetic constants for the inactivation of E_d^T and E_d^R by *o*-diphenols and its protection by monophenols.

Enzymatic form	Substrate	K_E^{Da} (μM)	$k^R_{i_D} \times 10^3$ (min^{-1})	$k^T_{i_D} \times 10^3$ (min^{-1})	K_E^{Ma} (μM)
E_d^T	L-dopa	19.24 ± 2.12	–	0.25 ± 0.01	–
	L-tyrosine	–	–	–	22.32 ± 3.96
E_d^R	L-dopa	10.77 ± 1.12	0.37 ± 0.01	–	–
	L-tyrosine	–	–	–	23.95 ± 2.99

[a] In K_E^D and K_E^M, E corresponds to the enzymatic forms E_d^T or E_d^R.

Author's personal copy

apparent transition constant are the same as those of Fig. 1 [$k_T = (6.5 \pm 0.5) \times 10^{-4}\ s^{-1}$]. The effect of pH (results not shown) is similar to that depicted in Fig. 5.

3.2.3. Re-oxygenation of E_d^T and detection with monophenol

The form E_d^T was generated and pre-incubated with oxygen. The kinetics was followed and the monophenolase activity was detected with L-tyrosine (Scheme 4ASM). Generation of the complex $E_{ox}M$ can follow the normal pathway, whereby the monophenol transfers the proton from OH in *para*-position to the peroxide, which acts as base, and the phenolate makes a nucleophilic attack on the Cu^B. This is followed by an electrophilic attack of the peroxide in the *meta*-position of the ring. This axial-equatorial bond must readjust before the concerted oxidation/reduction process can take place, as described in [47]. Fig. 8 Inset shows the results of this transition. Note that the apparent transition constant is the same as that obtained with *o*-diphenol [$\lambda_1 = (1.15 \pm 0.1) \times 10^{-3}\ s^{-1}$]. The effect of pH is similar to that depicted in Fig. 6 (results not shown). When the substrates (oxygen/monophenol) are added at the same time, enzymatic activity is generated, although to a lesser extent than for the native enzyme (Scheme 4BSM for E_d^R and Scheme 4CSM for E_d^T). In this case, generation of the complex $E_{ox}M$ may partly follow any of the paths described in the corresponding schemes. Note that, as in the case of the *o*-diphenol (Scheme 1CSM), an atypical pathway of $E_{ox}M$ generation might exist, especially in the case of E_d^T (Scheme 4CSM).

3.2.4. Study of the transition of E_d^R to E_d^T with sequential addition of substrates: first O_2 and then monophenol

Fig. 9 shows the results obtained. These are similar to the results in Fig. 3 with *o*-diphenol but also show the values of the lag phase, τ. The explanation is also similar to that given for Fig. 3. At short pre-incubation times (1 min) with O_2, the form E_d^R changes to E_{ox} and enzymatic activity is favoured. The formation of $E_{ox}M$ would follow a normal pathway (Scheme 4BSM), K_m^M is lower and so the τ is greater [34]. However, at longer times, there is more enzyme in the form E_d^T, and its binding with O_2 makes it follow the slow route, hindering enzymatic activity (Schemes 1ESM and 4CSM). The lag period in the tyrosinase mechanism increases when the concentration of enzyme decreases and when the enzyme affinity for the substrate increases (smaller K_m). These two situations are reflected in Fig. 9: at short times more enzyme exists in the E_d^R form (smaller K_m for L-tyrosine), and the lag is longer. At long times, more enzyme exists in the slow oxygenation pathway, less enzyme is totally active and so τ increases. These effects are amplified at short pre-incubation times with oxygen.

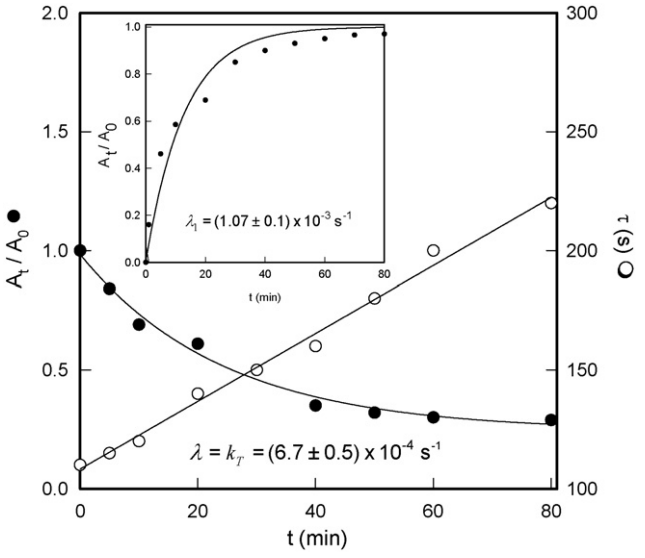

Fig. 8. Variation of the A_t/A_0-values *vs.* time obtained from a kinetic study of the transition of E_d^R to E_d^T followed by measuring monophenolase activity. The experimental conditions were: 30 mM sodium phosphate buffer (pH 7.0), 25 °C and O_2 (225 μM). The method was the same as in Fig. 1 but the instantaneous activities were measured with L-tyrosine (0.5 mM), spectrophotometrically measuring the increase in absorbance at 475 nm (●). Lag phase of monophenolase activity (○). Inset: Re-oxygenation of E_d^T followed by monophenolase activity. Procedure as in Fig. 3, but activity followed as in above case (●).

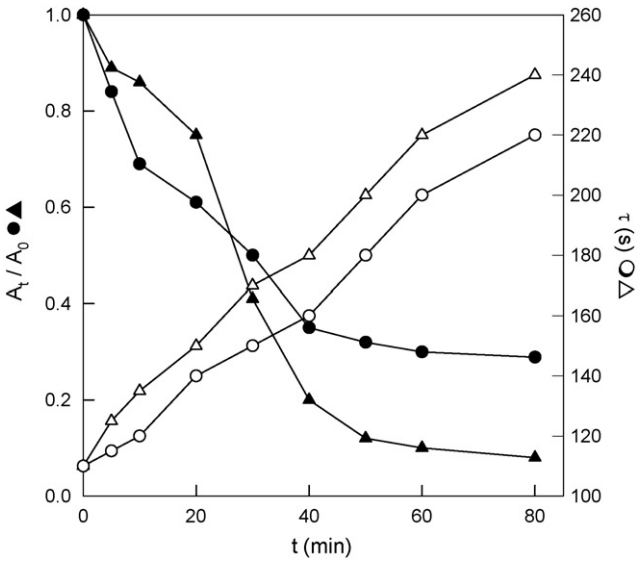

Fig. 9. Dependence of the A_t/A_0-values *vs.* time obtained from a kinetic study of the transition of E_d^R to E_d^T with sequential addition of substrates and followed through monophenolase activity. The method was the same as in Fig. 4 but the instantaneous activities were measured with L-tyrosine (0.5 mM), spectrophotometrically measuring the increase in absorbance at 475 nm. ● Instantaneous monophenolase activities without pre-incubating with O_2, ○ lag period (τ) of the monophenolase activity without pre-incubating with O_2 ▲ Monophenolase activity, pre-incubating 1 min with O_2 (0.26 mM), △ lag phase (τ) of monophenolase activity, pre-incubating 1 min with O_2 (0.26 mM).

3.2.5. Pre-incubation of the forms E_d^R and E_d^T with monophenols

When E_d^R and E_d^T are pre-incubated with small quantities of monophenol and the activity with *o*-diphenol is registered, no inactivation is detected (result not shown), although the monophenol binds to the enzyme, as can be seen from the fact that monophenol protects it from inactivation by *o*-diphenol (Fig. 7 for E_d^R; in the case of E_d^T, the results were similar) (Scheme 4A for E_d^R and Scheme 4B

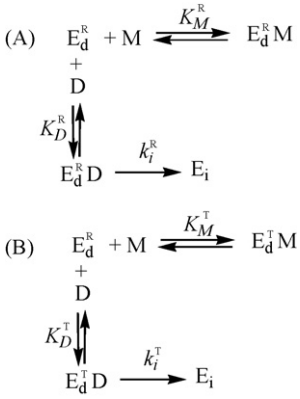

Scheme 4. (A) Kinetic mechanism to explain inactivation of E_d^R by *o*-diphenol and its protection by monophenol. (B) Kinetic mechanism to explain inactivation of E_d^T by *o*-diphenol and its protection by monophenol.

Author's personal copy

for E_d^T). A study of enzyme inactivation at different concentrations of *o*-diphenol in the presence of L-tyrosine (20 μM), provides the value of the apparent inactivation constant ($\lambda_{E_d^R}^{D(M)}$ or $\lambda_{E_d^T}^{D(M)}$, respectively) (result not shown), and an analysis by non-linear regression to Eqs. (10) and (11) provides the values of $K_{E_d^R}^{D(M)}$ and $K_{E_d^T}^{(M)}$ for E_d^R and E_d^R, respectively.

$$\lambda_{E_d^R}^{D(M)} = \frac{k_{i_{D(M)}}^R [D]_0}{K_{E_d^R}^{D(M)} + [D]_0} \quad (10)$$

$$\lambda_{E_d^T}^{D(M)} = \frac{k_{i_{D(M)}}^T [D]_0}{K_{E_d^T}^{D(M)} + [D]_0} \quad (11)$$

where $\lambda_{E_d^R}^{D(M)}$ is the apparent inactivation constant of E_d^R for L-dopa in the presence of L-tyrosine (see Fig. 7 Inset), $\lambda_{E_d^T}^{D(M)}$ is the apparent inactivation constant of E_d^T for L-dopa in the presence of L-tyrosine, $k_{i_{D(M)}}^R$ is maximum value of $\lambda_{E_d^R}^{D(M)}$ for saturating substrate and $k_{i_{D(M)}}^T$ is maximum value of $\lambda_{E_d^T}^{D(M)}$ for saturating substrate (result not shown for E_d^T). From $K_{E_d^R}^{D(M)}$ and $K_{E_d^T}^{(M)}$ and according to Eqs. (12) and (13), we can calculate $K_{E_d^R}^{M}$ and $K_{E_d^T}^{M}$, the binding constants of L-tyrosine for E_d^R and E_d^T, respectively.

$$K_{E_d^R}^{D(M)} = K_{E_d^R}^{D} \left(1 + \frac{[M]_0}{K_{E_d^R}^{M}}\right) \quad (12)$$

$$K_{E_d^T}^{D(M)} = K_{E_d^T}^{D} \left(1 + \frac{[M]_0}{K_{E_d^T}^{M}}\right) \quad (13)$$

When the transition of E_d^R to E_d^T was studied in the presence of 30 μM L-tyrosine, the kinetics was the same as in its absence (Fig. 8). Under anaerobic conditions, the most probable binding way of the monophenol to the Cu^A would be through previous transfer the proton of OH in *para*-position to His^{54}, followed by the reversible attack of the phenolate on this Cu^A (Schemes 5CMS and 5DMS for E_d^R and E_d^T, respectively).

4. Conclusions

We have carried out a kinetic study of the *deoxy*-tyrosinase (intermediate in the tyrosinase catalytic cycle) obtained under anaerobic conditions from E_{ox}. The results obtained can be explained by the structural and energetic aspects demonstrated with *deoxy*-hemocyanin [8]. *Deoxy*-tyrosinase exists in two forms, E_d^R (relaxed) and E_d^T (tense), the latter being more stable. The pH affects the transition of E_d^R to E_d^T: at values other than pH 6.5, the generation of two positive or negative charges may initiate the transition process, which will be slow both in the transition of E_d^R to E_d^T and in the re-oxygenation of E_d^T. However, at pH 6.5 the transition step, while being less pronounced, occurs more rapidly, and the properties of E_d^T and of the native enzyme are practically the same. The kinetic properties of these enzymatic forms differ, especially as regards their binding affinity for their substrates, but not as regards their catalytic capacity. Under anaerobic conditions, the *o*-diphenols irreversibly inactivate the enzyme in both E_d^R and E_d^T forms, but the monophenols protect it from inactivation. This inactivation process may have industrial applications in, for example, the food industry since a nitrogen stream could be passed through a juice extract to obtain *deoxy*-tyrosinase. Since different *o*-diphenols would exist in this extract (mainly chlorogenic acid), this tyrosinase could be inactivated, thus diminishing considerably the enzymatic browning that normally occurs.

Acknowledgements

This paper was partially supported by grants from the Ministerio de Educación y Ciencia (Madrid, Spain) Projects BIO2006-15363 and SAF2006-07040-C02-01, from the Fundación Séneca (CARM, Murcia, Spain) Project 00672/PI/04, from the Consejería de Educación (CARM, Murcia, Spain) BIO-BMC 06/01-0004, and from FISCAM PI-2007/53. JLMM has a fellowship from the Ministerio de Educación y Ciencia (Madrid, Spain) Reference AP2005-4721. FGM has a fellowship from Fundación Caja Murcia (Murcia, Spain).

Appendix A.

Expression of the variation in enzymatic activity with time during the transition of E_d^R to E_d^T according to the following Scheme.$E_d^R \xrightarrow{k_T} E_d^T$

Variation of E_d^R and E_d^T with time:

$$[E_d^R]_t = [E_d^R]_0 \, e^{-k_T t} \quad (1A)$$

$$[E_d^T]_t = [E_d^R]_0 \, (1 - e^{-k_T t}) \quad (2A)$$

Variation in activity with time:

$$A_t = A_t^{E_d^R} + A_t^{E_d^T} \quad (3A)$$

or

$$V_0^t = V_0^{t(E_d^R)} + V_0^{t(E_d^T)} \quad (4A)$$

As regards initial activity:

$$\frac{A_t}{A_0} = \frac{A_t^{E_d^R} + A_t^{E_d^T}}{A_0} = \frac{V_0^t}{V_0} = \frac{V_0^{t(E_d^R)} + V_0^{t(E_d^T)}}{V_0} \quad (5A)$$

The expressions of $V_0^{t(E_d^R)}$, $V_0^{t(E_d^T)}$ and V_0 are:

$$V_0^{t(E_d^D)} = \frac{k_{cat}^R [E]_0 \, e^{-k_T t} [D]_0}{K_{m_D}^R + [D]_0} \quad (6A)$$

$$V_0^{t(E_d^T)} = \frac{k_{cat}^T [E]_0 (1 - e^{-k_T t}) [O_2]_0 [D]_0}{K_{O_2}^T K_{m_D}^T + K_{m_D}^T [O_2]_0 + K_{m_{O_2}}^T [D]_0 + [O_2]_0 [D]_0} \quad (7A)$$

$$V^{E_d^R} = \frac{k_{cat}^R [E]_0 [D]_0}{K_{m_D}^R + [D]_0} \quad (8A)$$

In agreement with Eq. (5A):

$$\frac{A_t}{A_0} = \frac{V_0^t}{V_0} = \alpha + \beta e^{-\lambda t} = \alpha + \beta e^{-k_T t} \quad (9A)$$

with

$$\alpha = \frac{k_{cat}^T (K_{m_D}^R + [D]_0)[O_2]_0}{k_{cat}^R (K_{O_2}^T K_{m_D}^T + K_{m_D}^T [O_2]_0 + K_{m_{O_2}}^T [D]_0 + [O_2]_0 [D]_0)} \quad (10A)$$

$$\beta = 1 - \alpha = 1 - \frac{k_{cat}^T (K_{m_D}^R + [D]_0)[O_2]_0}{k_{cat}^R (K_{O_2}^T K_{m_D}^T + K_{m_D}^T [O_2]_0 + K_{m_{O_2}}^T [D]_0 + [O_2]_0 [D]_0)} \quad (11A)$$

where k_{cat}^R and k_{cat}^T are the catalytic constant for E_d^R and E_d^T forms of tyrosinase, respectively; $K_{m_D}^R$ and $K_{m_D}^T$ are the Michaelis constants for the *o*-diphenol of the E_d^R and E_d^T forms of tyrosinase, respectively; $K_{O_2}^T$ is the dissociation constant for the oxygen of the E_d^T form of

Author's personal copy

tyrosinase and $K^T_{m_{O_2}}$ is the Michaelis constant for the oxygen of the E^T_d form of tyrosinase.

Appendix B.

The E^T_d oxygenation mechanism can be depicted as:

$$E^T_d + O_2 \underset{k_r}{\overset{k_b}{\rightleftarrows}} E^T_d O_2 \xrightarrow{k*} (E^T_d O_2)^* \xrightarrow{k_{ox}} E_{ox}$$

Variation in concentration of E_{ox} with time, considering that the binding of O_2 in rapid equilibrium is:

$$[E_{ox}] = [E^T_d]_0 + A_1\, e^{-\lambda_1 t} + A_2\, e^{-\lambda_2 t} \tag{1B}$$

with

$$\lambda_1 = \frac{k^*[O_2]_0}{K^T_{O_2} + [O_2]_0} \tag{2B}$$

$$\lambda_2 = k_{ox} \tag{3B}$$

$$A_1 = \frac{k_{ox}(K^T_{O_2} + [O_2]_0)[E^T_d]_0}{k^*[O_2]_0 - k_{ox}(K^T_{O_2} + [O_2]_0)} \tag{4B}$$

$$A_2 = \frac{k^*[O_2]_0[E^T_d]_0}{k_{ox}(K^T_{O_2} + [O_2]_0) - k^*[O_2]_0} \tag{5B}$$

$$K^T_{O_2} = \frac{k_r}{k_b} \tag{6B}$$

If $\lambda_2 \gg \lambda_1$, then:

$$[E_{ox}] = [E^T_d]_0(1 - e^{-\lambda_1 t}) \tag{7B}$$

If $K^T_{O_2} \gg [O_2]_0$, then, from Eq. (2B):

$$\lambda_1 = \frac{k^*}{K^T_{O_2}}[O_2]_0 \tag{8B}$$

Appendix C. Supplementary data

Supplementary data associated with this article can be found, in the online version, at doi:10.1016/j.molcatb.2009.10.005.

References

[1] E.I. Solomon, U.M. Sundaram, T.E. Machonkin, Chem. Rev. 96 (1996) 2563–2606.
[2] A.C. Rosenzweig, M.H. Sazinsky, Curr. Opin. Struct. Biol. 16 (2006) 729–735.
[3] R.L. Jolley, L.H. Evans, N. Makino, H.S. Mason, J. Biol. Chem. 249 (1974) 335–345.
[4] M.E. Cuff, K.I. Miller, K.E. van Holde, W.A. Hendrickson, J. Mol. Biol. 278 (1998) 855–870.
[5] T. Klabunde, C. Eicken, J.C. Sacchettini, B. Krebs, Nat. Struct. Biol. 5 (1998) 1084–1090.
[6] Y. Matoba, T. Kumagai, A. Yamamoto, H. Yoshitsu, M. Sugiyama, J. Biol. Chem. 281 (2006) 8981–8990.
[7] M. Beltramini, L. Bubacco, B. Salvato, L. Casella, M. Gullotti, S. Garofani, Biochim. Biophys. Acta 1120 (1992) 24–32.
[8] M. Metz, E.I. Solomon, J. Am. Chem. Soc. 123 (2001) 4938–4950.
[9] E.I. Solomon, P. Chen, M. Metz, S.K. Lee, A.E. Palmer, Angew. Chem. Int. Ed. Engl. 40 (2001) 4570–4590.
[10] P. Chen, E.I. Solomon, Proc. Natl. Acad. Sci. U.S.A. 101 (2004) 13105–13110.
[11] W. Erker, R. Hübler, H. Decker, Biochim. Biophys. Acta 1780 (2008) 1143–1147.
[12] L. Ronda, S. Faggiano, S. Bettati, N. Hellmann, H. Decker, T. Weidenbach, A. Mozzarelli, Gene 398 (2007) 202–207.
[13] T.N. Sorrell, M. Beltramini, K. Lerch, J. Biol. Chem. 263 (1988) 9576–9577.
[14] S. Hirota, T. Kawahara, E. Lonardi, E. de Waal, N. Funasaki, G.W. Canters, J. Am. Chem. Soc. 127 (2005) 17966–17967.
[15] S. Della Longa, E.I. Ascone, A. Bianconi, A. Bonfigli, A. Castellano, O. Zarivi, M. Miranda, J. Biol. Chem. 271 (1996) 21025–21030.
[16] H. Decker, T. Schweikardt, D. Nillius, U. Salzbrunn, E. Jaenicke, F. Tuczek, Gene 398 (2007) 183–191.
[17] H. Decker, F. Tuczek, Trends Biochem. Sci. 25 (2000) 392–397.
[18] L. Bubacco, M. van Gastel, M. Benfatto, A.W. Tepper, G.W. Canters, Micron 35 (2004) 143–145.
[19] B. Salvato, M. Santamaria, M. Beltramini, G. Alzuet, L. Casella, Biochemistry 37 (1998) 14065–14077.
[20] E. Jaenicke, H. Decker, FEBS J. 275 (2008) 1518–1528.
[21] D. Nillius, E. Jaenicke, H. Decker, FEBS Lett. 582 (2008) 749–754.
[22] S. Baird, S.M. Kelly, N.C. Price, E. Jaenicke, C. Meesters, D. Nillius, H. Decker, J. Nairn, Biochim. Biophys. Acta 1774 (2007) 1380–1394.
[23] H. Decker, E. Jaenicke, Dev. Comp. Immunol. 28 (2004) 673–687.
[24] E. Jaenicke, H. Decker, Micron 35 (2004) 89–90.
[25] H. Decker, M. Ryan, E. Jaenicke, N. Terwilliger, J. Biol. Chem. 276 (2001) 17796–17799.
[26] H. Decker, T. Rimke, J. Biol. Chem. 273 (1998) 25889–25892.
[27] K. Suzuki, C. Shimokawa, C. Morioka, S. Itoh, Biochemistry 47 (2008) 7108–7115.
[28] L.M. Mirica, D.J. Rudd, M.A. Vance, E.I. Solomon, K.O. Hodgson, B. Hedman, T. Stack, J. Am. Chem. Soc. 128 (2006) 2654–2665.
[29] L.M. Mirica, M. Vance, D.J. Rudd, B. Hedman, K.O. Hodgson, E.I. Solomon, T.D. Stack, Science 308 (2005) 1890–1892.
[30] O. Sander, A. Henss, C. Näther, C. Würtele, M. Holthausen, S. Schindler, F. Tuczek, Chemistry 14 (2008) 9714–9729.
[31] J.N. Rodriguez-Lopez, J. Tudela, R. Varon, F. Garcia-Carmona, F. Garcia-Canovas, J. Biol. Chem. 267 (1992) 3801–3810.
[32] J.N. Rodriguez-Lopez, L.G. Fenoll, P.A. Garcia-Ruiz, R. Varon, J. Tudela, R.N. Thorneley, F. Garcia-Canovas, Biochemistry 39 (2000) 10497–10506.
[33] L.G. Fenoll, J.N. Rodriguez-Lopez, F. Garcia-Sevilla, P.A. Garcia-Ruiz, R. Varon, F. Garcia-Canovas, J. Tudela, Biochim. Biophys. Acta 1548 (2001) 1–22.
[34] F.G. Molina, J.L. Munoz, R. Varon, J.N. Rodriguez-Lopez, F.G. Canovas, J. Tudela, Int. J. Biochem. Cell Biol. 39 (2007) 238–252.
[35] J.L. Muñoz-Muñoz, F. Garcia-Molina, P.A. Garcia-Ruiz, M. Molina-Alarcón, J. Tudela, F. Garcia-Canovas, J.N. Rodriguez-Lopez, Biochem. J. 416 (2008) 431–440.
[36] J.L. Muñoz-Muñoz, F. Garcia-Molina, P.A. Garcia-Ruiz, R. Varon, J. Tudela, F. Garcia-Canovas, J.N. Rodriguez-Lopez, Biochim. Biophys. Acta 1794 (2009) 244–253.
[37] M.M. Bradford, Anal. Biochem. 7 (1976) 248–254.
[38] J.N. Rodriguez-Lopez, J.R. Ros-Martinez, R. Varon, F. Garcia-Canovas, Anal. Biochem. 202 (1992) 356–360.
[39] J.L. Munoz, F. Garcia-Molina, R. Varon, J.N. Rodriguez-Lopez, F. Garcia-Canovas, J. Tudela, Anal. Biochem. 351 (2006) 128–138.
[40] M. Jackman, M. Huber, A. Hajnal, K. Lerch, Biochem. J. 282 (1992) 915–918.
[41] R. Aasa, J. Deinum, K. Lerch, B. Reinhammar, Biochim. Biophys. Acta 535 (1978) 287–298.
[42] Jandel Scientific, Sigma Plot 9.0 for Windows™, Jandel Scientific, Core Madera, 2006.
[43] J.R. Ros, J.N. Rodriguez-Lopez, F. Garcia-Canovas, Biochim. Biophys. Acta 1204 (1994) 33–42.
[44] J.C. Espin, P.A. Garcia-Ruiz, J. Tudela, F. Garcia-Canovas, Biochem. J. 331 (1998) 547–551.
[45] J.C. Espin, R. Varon, L.G. Fenoll, M.A. Gilabert, P.A. Garcia-Ruiz, J. Tudela, F. Garcia-Canovas, Eur. J. Biochem. 267 (2000) 1270–1279.
[46] J. Yoon, S. Fujii, E.I. Solomon, Proc. Natl. Acad. Sci. U.S.A. 106 (2009) 6585–6590.
[47] J.N. Rodriguez-Lopez, L.G. Fenoll, M.J. Peñalver, P.A. Garcia-Ruiz, R. Varon, F. Martinez-Ortiz, F. Garcia-Canovas, J. Tudela, Biochim. Biophys. Acta 1548 (2001) 238–256.

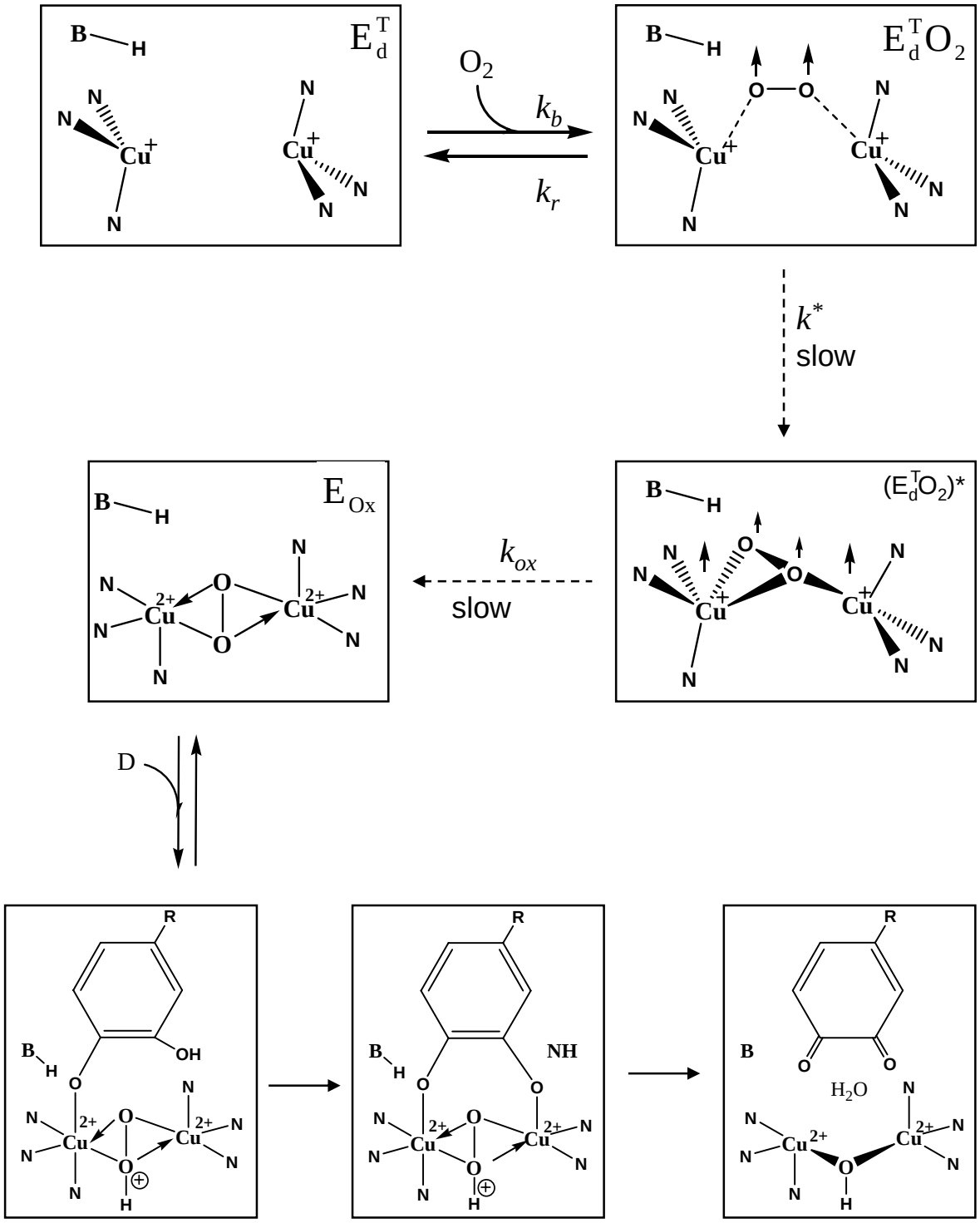

Scheme 1BSM

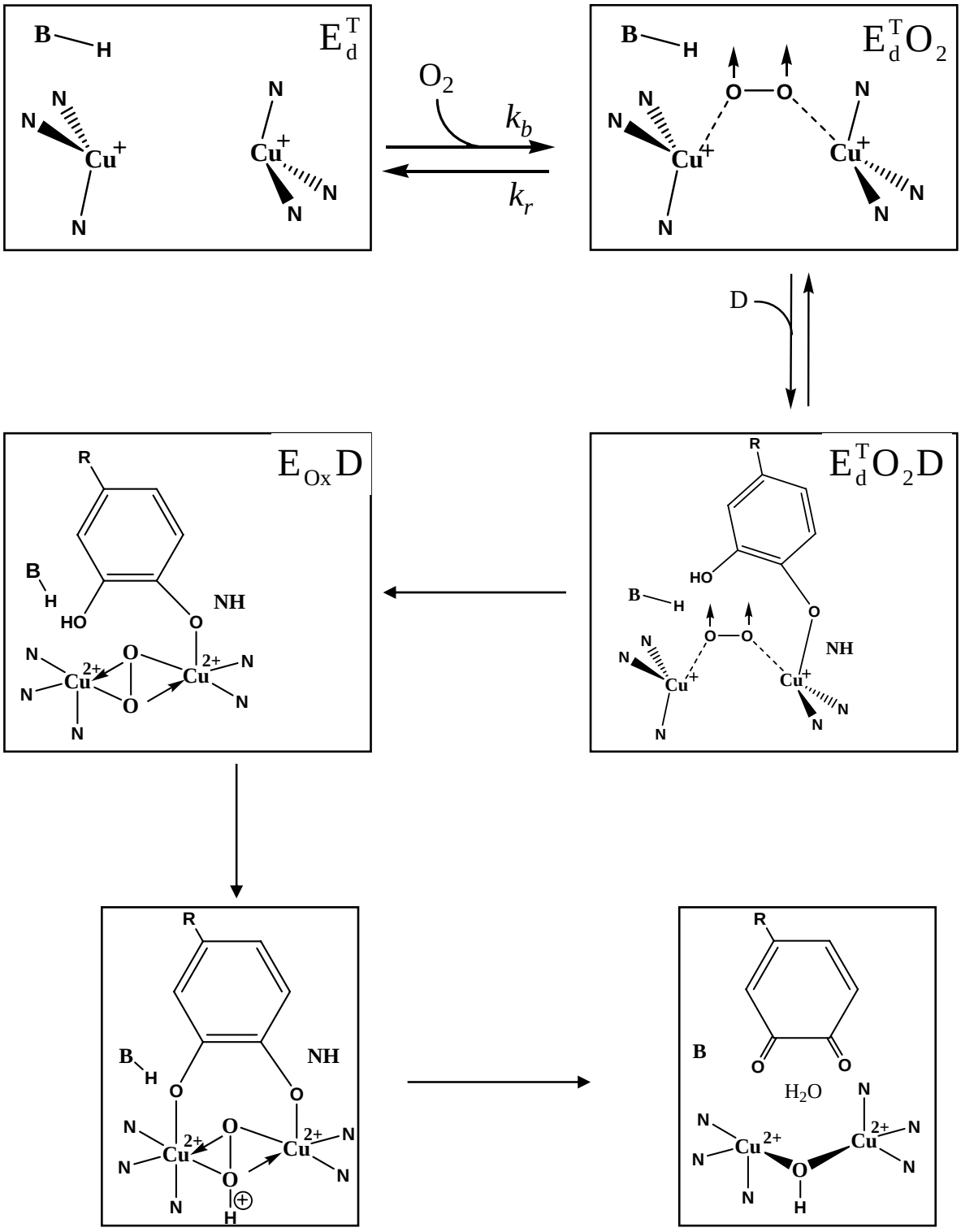

Scheme 1CSM

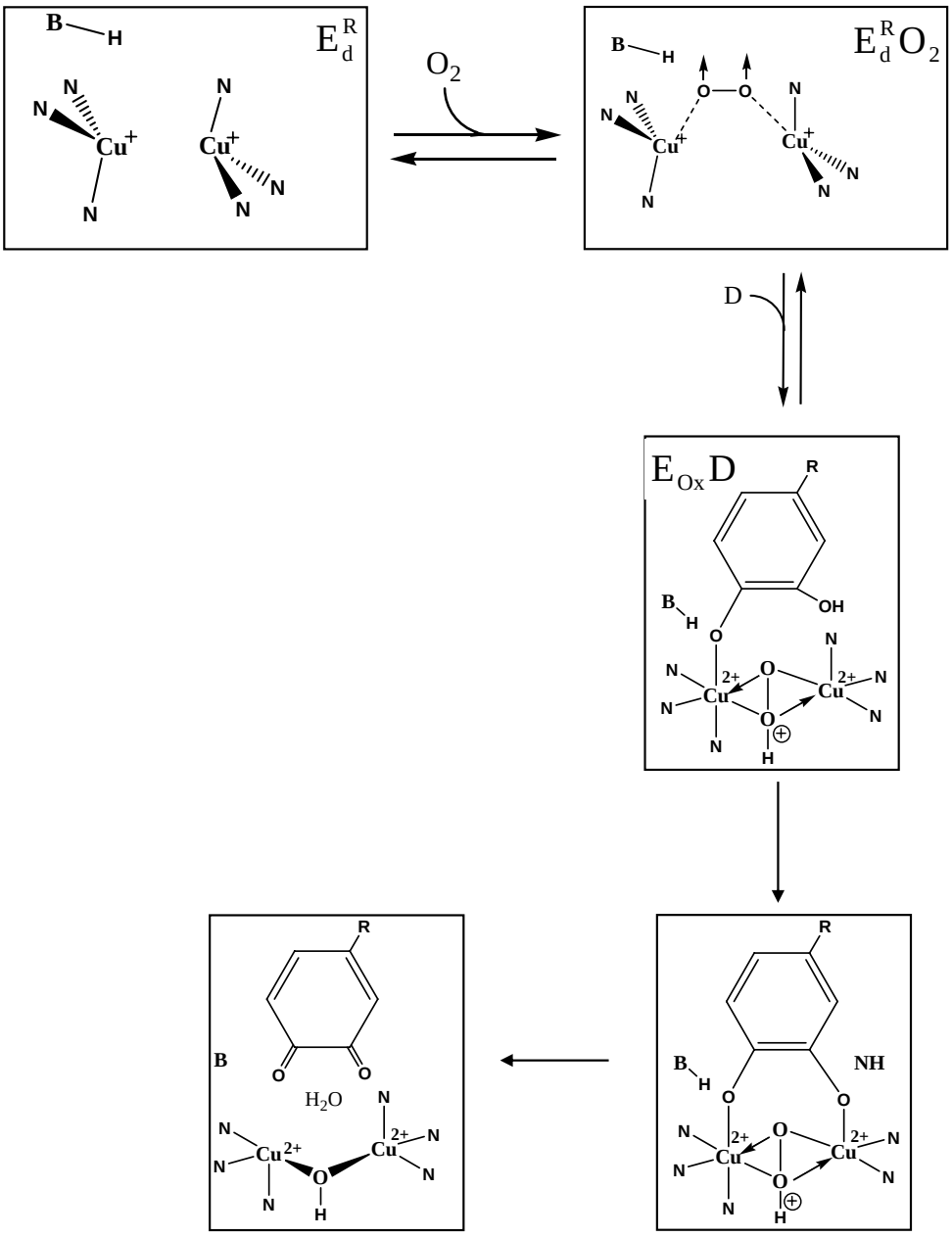

Scheme 1DSM

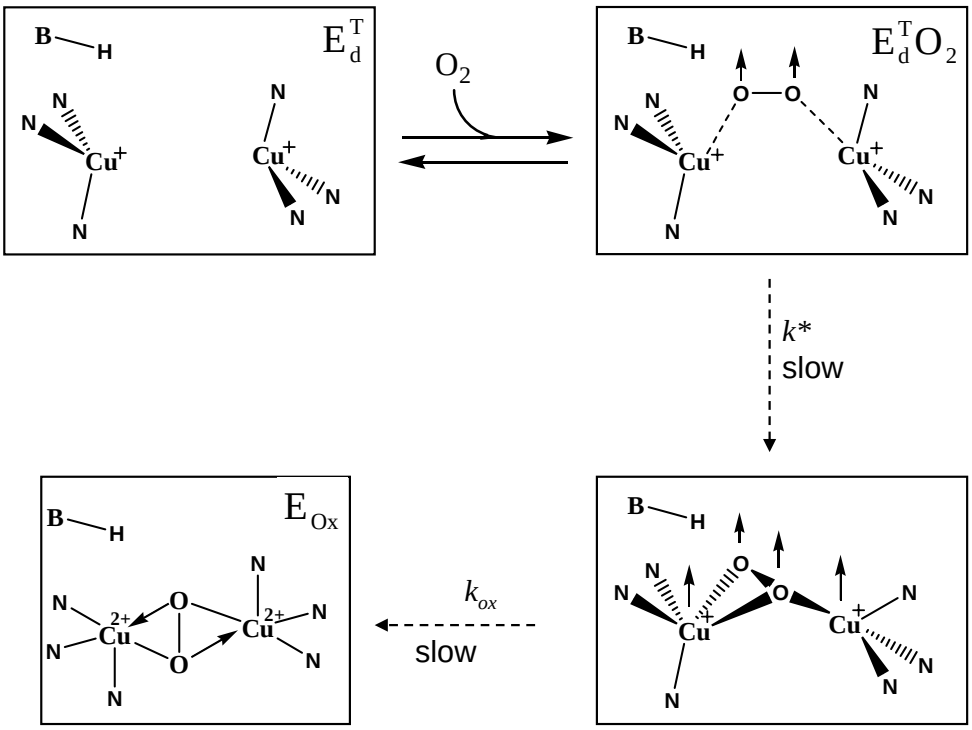

Scheme 1ESM

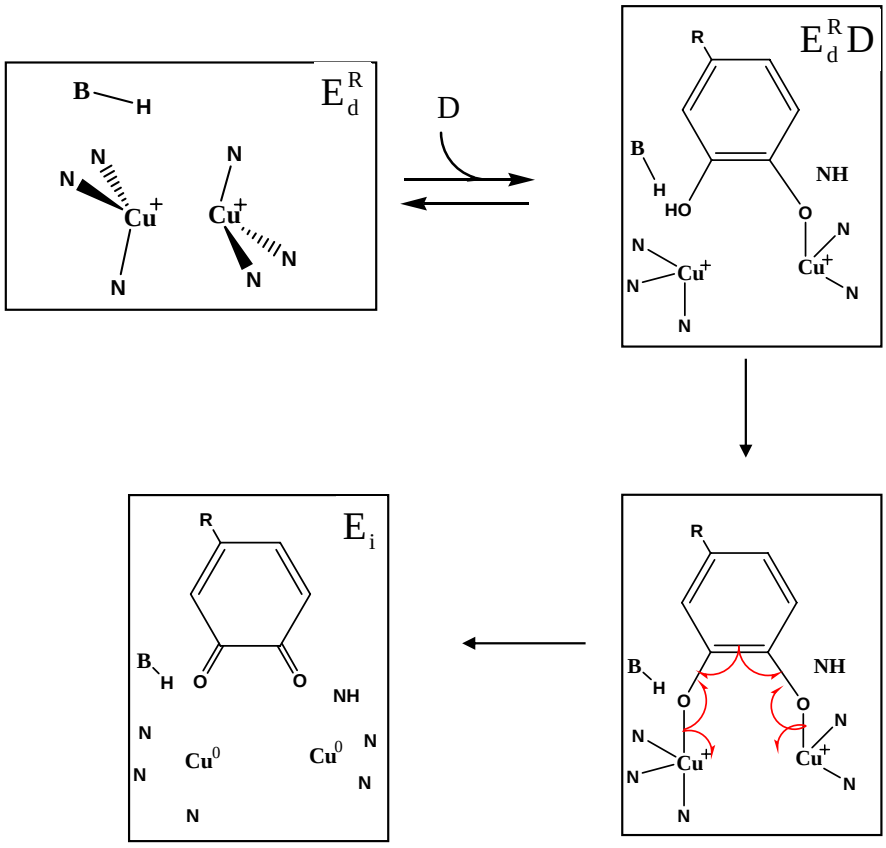

Scheme 3CSM

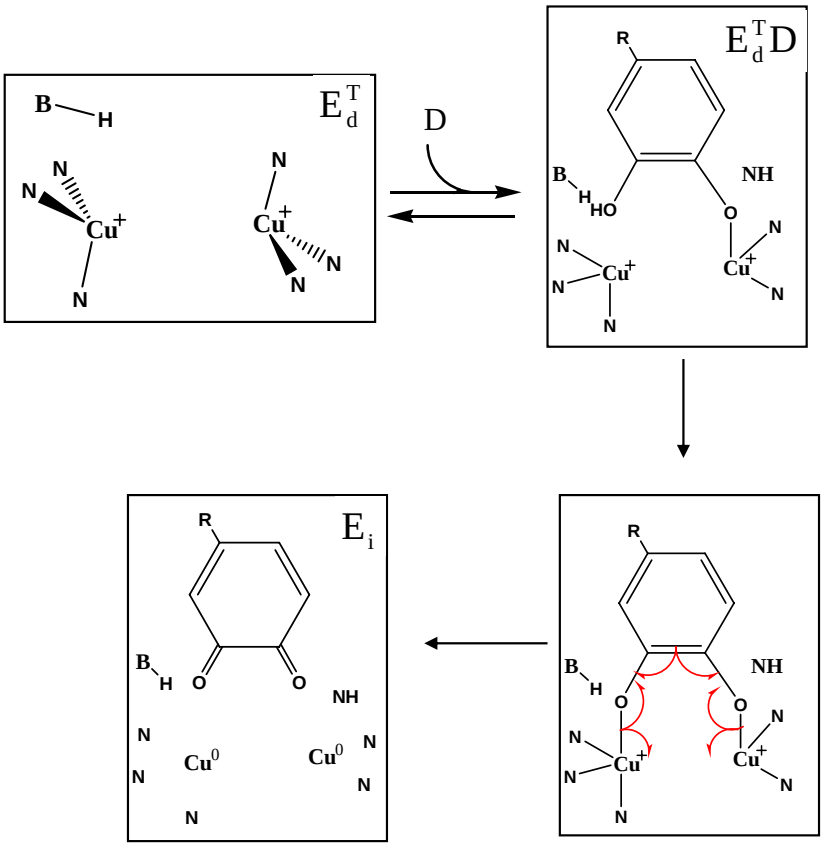

Scheme 3DSM

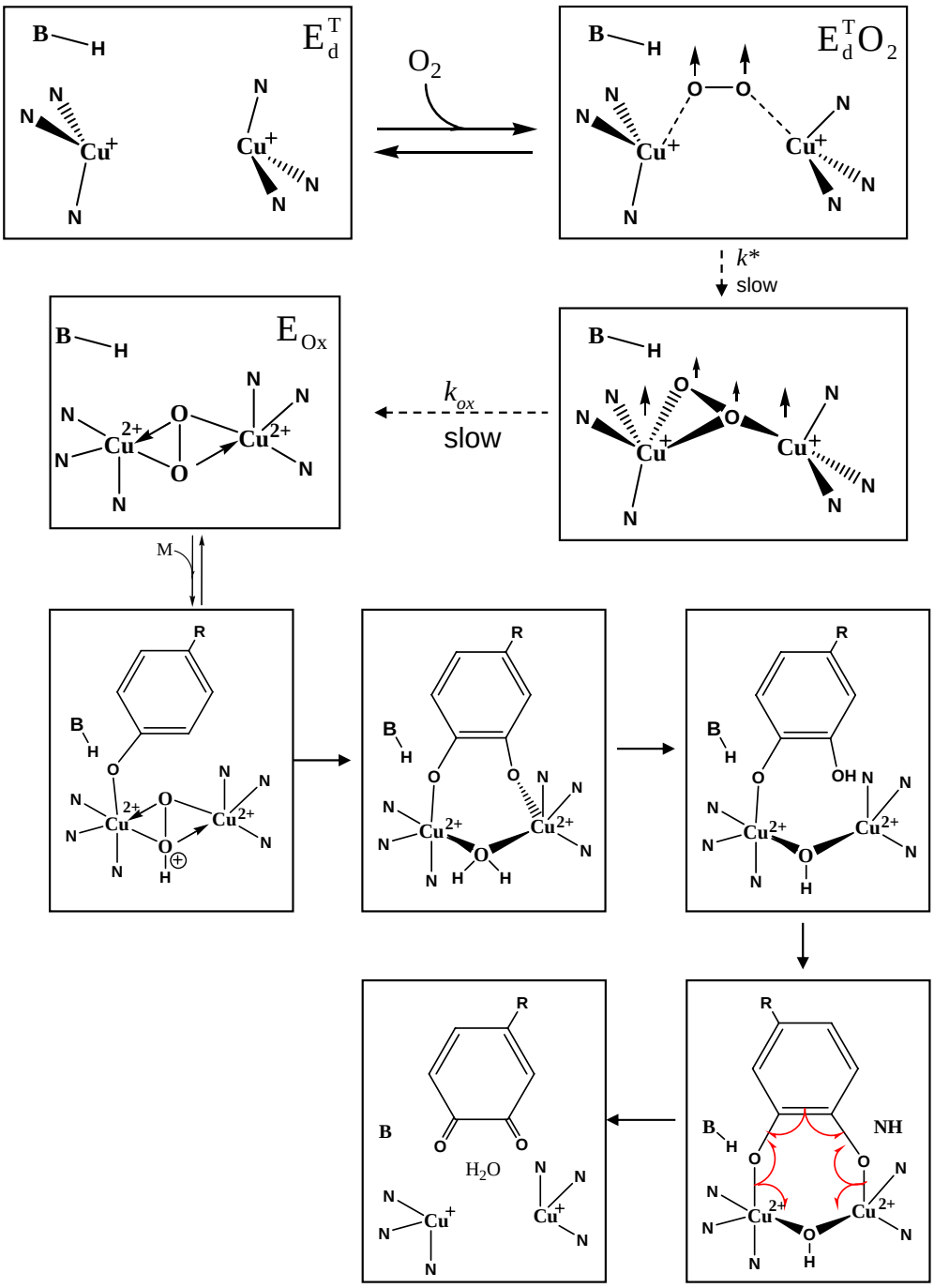

Scheme 4ASM

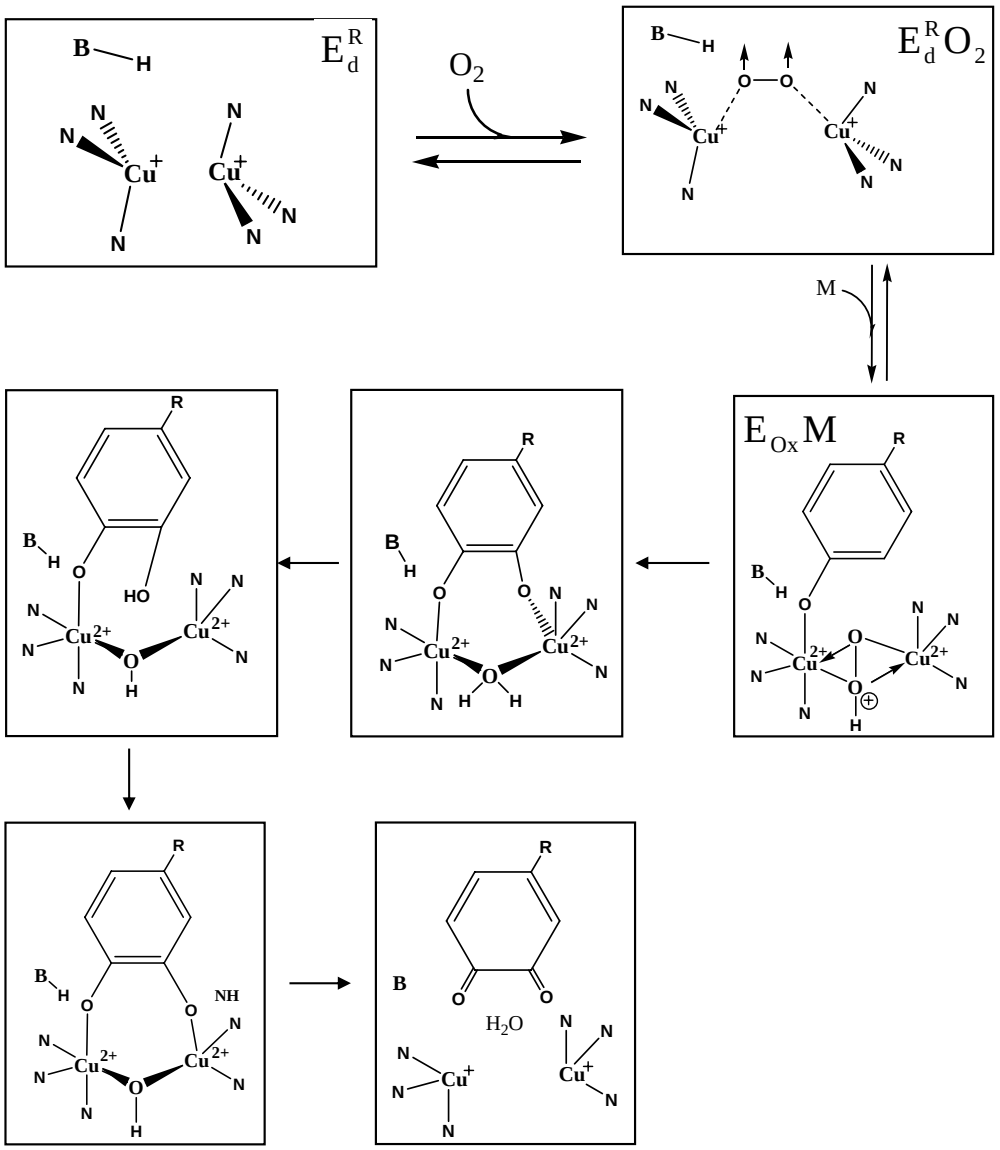

Scheme 4BSM

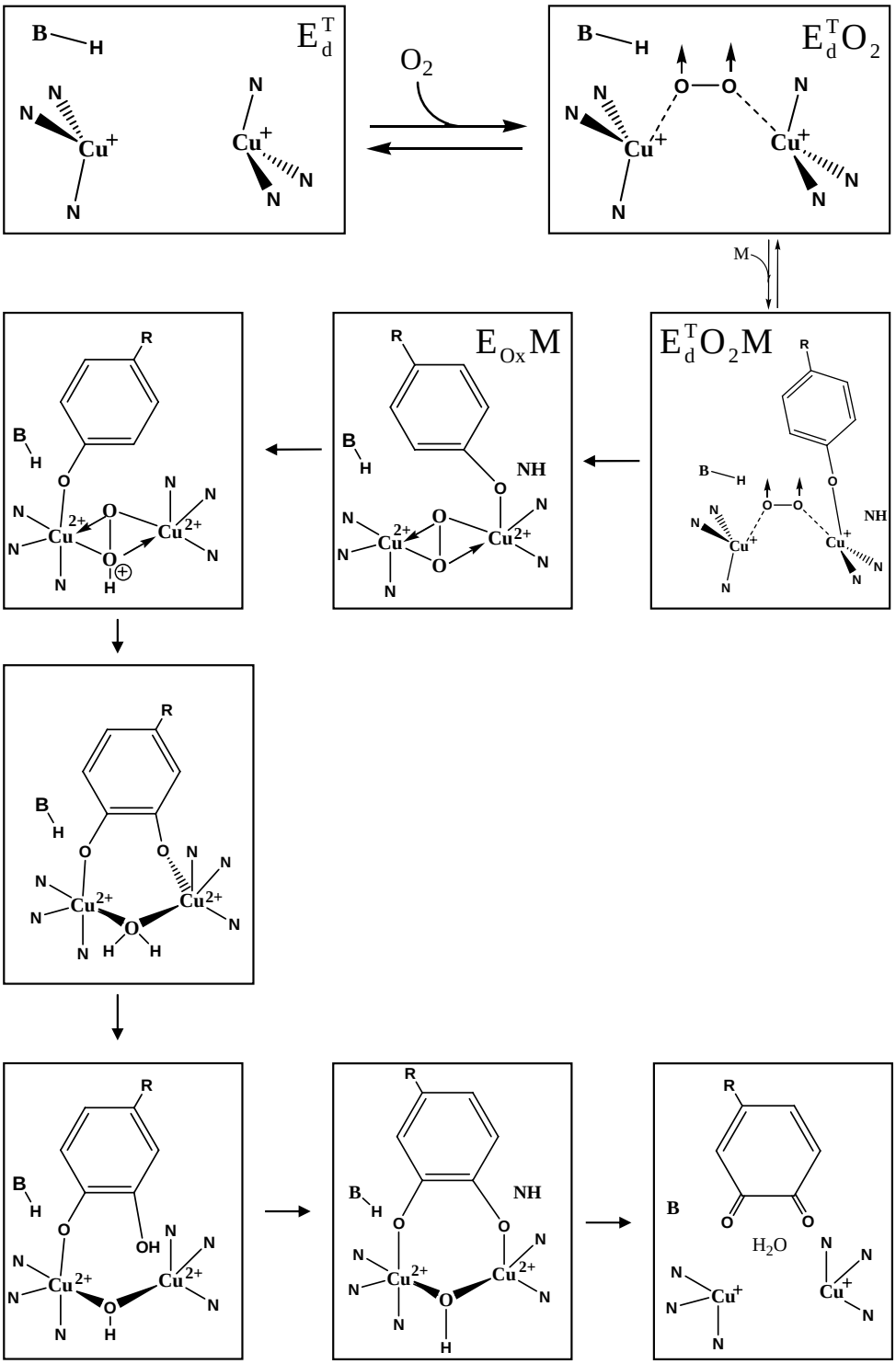

Scheme 4CSM

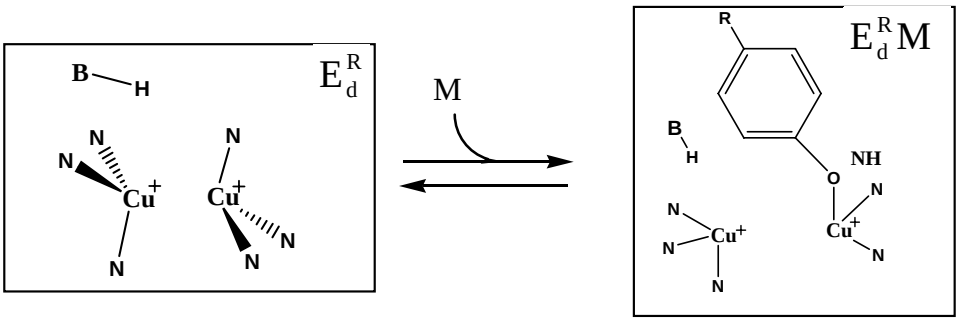

Scheme 5CSM

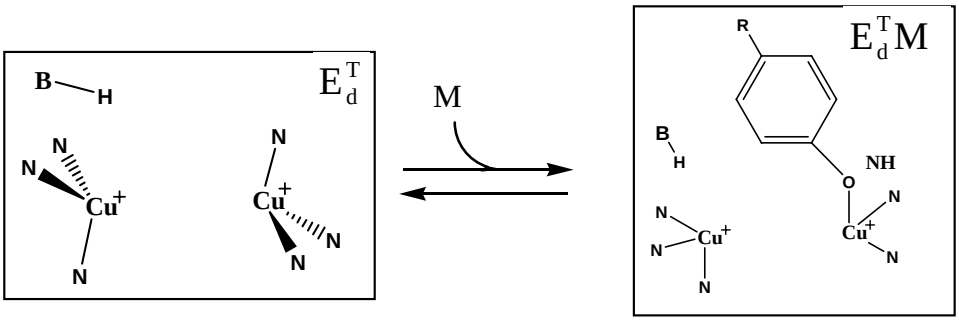

Scheme 5DSM

4.4. GENERACIÓN DE PERÓXIDO DE HIDRÓGENO EN LA RUTA DE BIOSÍNTESIS DE MELANINAS.

La demostración de la generación del peróxido de hidrógeno en la ruta de biosíntesis de melaninas ha dado lugar a la siguiente publicación adjunta.

4.4.1. Título

Generation of hydrogen peroxide in the melanin biosynthesis pathway.

4.4.2. Autores

Muñoz-Muñoz, J.L.; Garcia-Molina, F.; Varon, R.; Tudela, J.; Garcia-Cánovas, F. y Rodríguez-López, J.N.

4.4.3. Referencia

Biochimica et Biophysica Acta-Protein and Proteomics (2009) 1794, 1017-1029.

4.4.4. Resumen

La generación de H_2O_2 en la ruta de biosíntesis de melaninas es de gran importancia por el poder citotóxico de esta sustancia. Sin embargo, existe controversia en la literatura sobre la generación de H_2O_2 en esta ruta. En este trabajo se demuestra que la generación de este H_2O_2 se debe a la serie de reacciones químicas, acopladas a la formación enzimática de las *o*-quinonas por tirosinasa en su acción sobre monofenoles y *o*-difenoles y a su auto-oxidación. El uso de las enzimas catalasa, superóxido dismutasa y peroxidasa, ayudan a revelar el H_2O_2 generado. De los resultados obtenidos se propone un esquema de reacciones enzimáticas y no enzimáticas, que darían lugar a la biosíntesis de melaninas y que tiene en cuenta la formación de H_2O_2.

Biochimica et Biophysica Acta 1794 (2009) 1017–1029

Contents lists available at ScienceDirect

Biochimica et Biophysica Acta

journal homepage: www.elsevier.com/locate/bbapap

Generation of hydrogen peroxide in the melanin biosynthesis pathway

Jose Luis Munoz-Munoz [a], Francisco García-Molina [a], Ramón Varón [b], José Tudela [a], Francisco García-Cánovas [a,*], Jose Neptuno Rodríguez-López [a]

[a] GENZ: Grupo de Investigación de Enzimología, Departamento de Bioquímica y Biología Molecular-A, Facultad de Biología, Universidad de Murcia, E-30100, Espinardo, Murcia, Spain
[b] Departamento de Química-Física, Escuela Politécnica Superior, Universidad de Castilla la Mancha, Avda, España s/n, Campus Universitario, E-02071, Albacete, Spain

ARTICLE INFO

Article history:
Received 3 December 2008
Received in revised form 1 April 2009
Accepted 6 April 2009
Available online 15 April 2009

Keywords:
Hydrogen peroxide
Melanins
o-diphenols
Monophenols
Tyrosinase

ABSTRACT

The generation of H_2O_2 in the melanin biosynthesis pathway is of great importance because of its great cytotoxic capacity. However, there is controversy concerning the way in which H_2O_2 is generated in this pathway. In this work we demonstrate that it is generated in a series of chemical reactions coupled to the enzymatic formation of *o*-quinones by tyrosinase acting on monophenols and *o*-diphenols and during the auto-oxidation of the *o*-diphenols and other intermediates in the pathway. The use of the enzymes such as catalase, superoxide dismutase and peroxidase helps reveal the H_2O_2 generated. Based on the results obtained, we propose a scheme of enzymatic and non-enzymatic reactions that lead to the biosynthesis of melanins, which explains the formation of H_2O_2.

© 2009 Elsevier B.V. All rights reserved.

1. Introduction

The enzyme tyrosinase (TYR; monophenol, *o*-diphenol: oxygen oxidoreductase, E.C. 1.14.18.1) is of central importance in the melanin pigmentation of vertebrates and the browning of fruits and vegetables. This enzyme (Scheme 1A) catalyses monophenol hydroxylation (monophenolase activity) and *o*-diphenol oxidation to *o*-quinones (diphenolase activity). These *o*-quinones evolve non-enzymatically to generate several unstable intermediates, which polymerize to melanins [1].

The proximal phase, or phase I, of melanogenesis is started by the monophenolase and diphenolase activities of tyrosinase (Scheme 1A) [2]. While, in the distal phase, or phase II, of melanogenesis (Scheme 1B) the possible involvement of two additional enzymes, termed tyrosinase related protein-1 (TRP1) and tyrosinase related protein-2 (TRP2), should be taken into account [3,4].

The formation of H_2O_2 in the auto-oxidation of L-dopa and other *o*-diphenols has been described [5,6], reactions (1)–(3) of Scheme 2, henceforth "reactions". The enzymatic formation of H_2O_2 by tyrosinase has also been proposed [6–8]. Thus, in L-dopa photolysis studies, $O_2^{\bullet -}$ was produced, according to reaction (4), and it was proposed that the $O_2^{\bullet -}$ reacted with the *o*-diphenol according to reaction (3), generating H_2O_2. The SOD catalysing reaction (8) influences the formation of H_2O_2 in the photolysis experiments with L-dopa so that at high SOD concentrations, H_2O_2 production is halved [since, according to reaction (8), the ratio of $O_2^{\bullet -}$ to H_2O_2 is 2 $O_2^{\bullet -}$:1 H_2O_2 and, according to reaction (3) it is 1 $O_2^{\bullet -}$:1 H_2O_2]. These experiments were the starting points for these authors to study H_2O_2 production in the oxidation of L-dopa by tyrosinase [6] during which the addition of SOD did not halve H_2O_2 production as in the photolysis experiments. It was therefore proposed that the H_2O_2 accumulated during the enzymatic oxidation of L-dopa is produced via the superoxide anion (non-enzymatic reactions) and via the two-electron reduction of oxygen by the enzyme (enzymatic reaction), suggesting the reaction (6) along with the sequence of chemical reactions (1)–(3).

Using electrochemical methods, other authors have established the endogenous production of H_2O_2 in the action of tyrosinase on L-dopa and dopamine [7]. At the same time, it has been proposed that there is no evidence to suggest that H_2O_2 or any reactive oxygen intermediate (ROS) was produced during the tyrosinase-mediated conversion of L-tyrosine to L-dopa (monophenolase activity). To explain the production of H_2O_2, therefore, the same authors concluded that a univalent reduction of O_2 occurs, most probably at the enzyme's active copper site [7], which would agree with reaction (6).

Recently, another study has been published in which it is proposed that H_2O_2 is formed by TYR and oxidises the cofactor 5,6,7,8-tetrahydrobiopterin in the absence of substrate (L-tyrosine) [8]. Therefore several proposals exist for the enzymatic generation of H_2O_2, reaction (6) [6–8].

The oxidation of *o*-diphenols by oxygen generates H_2O_2 in the medium [5]. The consecutive reactions are described in reactions (1)–(3). However, in accordance with the stability of *o*-quinone, reaction (5) might occur but to a different extent. This would influence the formation of H_2O_2 and the effect of SOD, reaction (8).

* Corresponding author. Fax: +34 968 363963.
E-mail address: canovasf@um.es (F. García-Cánovas).
URL: http://www.um.es/genz (F. García-Cánovas).

1570-9639/$ – see front matter © 2009 Elsevier B.V. All rights reserved.
doi:10.1016/j.bbapap.2009.04.002

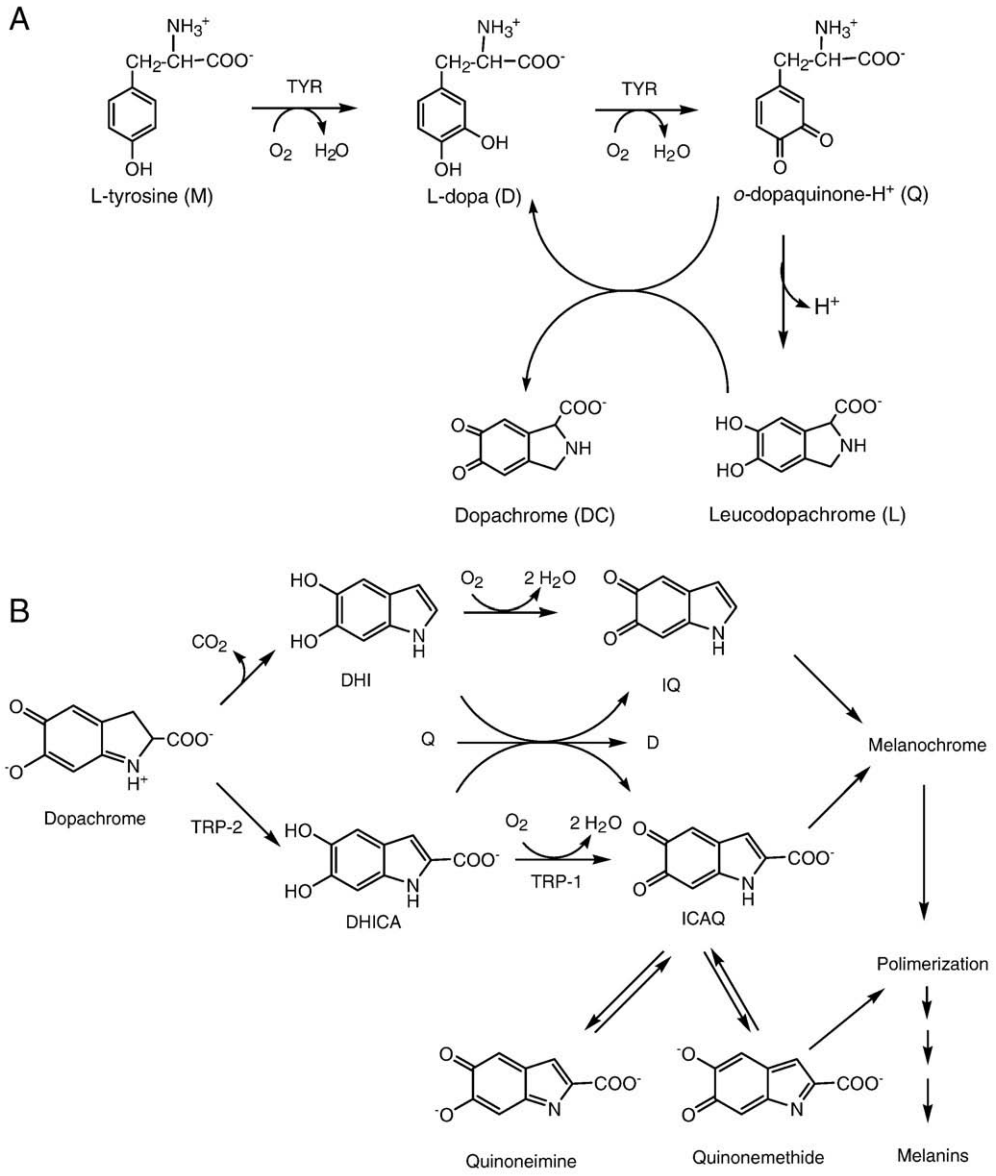

Scheme 1. (A) Proximal phase of the melanogenesis pathway, from L-tyrosine to dopachrome [1,2]. (B) Intermediate compounds in the distal phase of the melanin biosynthesis pathway [1,4].

The objective of this work is to demonstrate that in the melanin biosynthesis pathway, which begins with the action of tyrosinase on L-tyrosine, H_2O_2 is formed and accumulated in the medium through non-enzymatic reactions. Several types of substrate are considered, 4-*tert*-butylcatechol (TBC), 3,4-dihydroxymandelic acid (DOMA), L-dopa, dopamine, L-tyrosine and tyramine (Scheme 3A) each originating an *o*-quinone of a different degree of stability. In addition, we use superoxide dismutase (SOD), catalase (CAT) and peroxidase (POD) to confirm and quantify the formation of H_2O_2.

2. Materials and methods

2.1. Reagents

L-tyrosine, L-dopa, 4-*tert*-butylcatechol (TBC) and 3,4-dihydroxymandelic acid (DOMA) were purchased from Sigma (Madrid, Spain). Tyramine and dopamine were purchased from Fluka (Switzerland). Stock solutions of substrates were prepared in 0.15 mM phosphoric acid to prevent auto-oxidation. All other chemicals were of analytical grade and supplied by Merck (Germany). Milli-Q system (Millipore Corp.) ultrapure water was used throughout this research. H_2O_2 (30% v/v) was obtained from BDH-Merck (Poole, UK) and its concentration was determined using a molar absorptivity of 43.6 M^{-1} cm^{-1} at 340 nm [9].

2.2. Enzyme source

Mushroom tyrosinase (TYR; EC 1.14.18.1, 8300 U/mg), superoxide dismutase (SOD: EC 1.15.1.1, 4140 U/mg), horseradish peroxidase (POD: EC 1.11.1.7 297 U/mg) and catalase (CAT; EC 1.11.1.6, 9300 U/mg) were supplied by Sigma (St. Louis, MO). Tyrosinase was purified as previously described [10]. POD was purchased from Sigma (type VI; Rz = 3.2) and used without further purification. The concentration of POD was determined spectrophotometrically using a Soret molar absorptivity of 102 mM^{-1} cm^{-1} [9]. The protein concentration was determined by Bradford's method [11] and using bovine serum albumin as the standard.

2.3. Spectrophotometric assays

Absorption spectra were recorded in a visible–ultraviolet Perkin-Elmer Lambda-35 spectrophotometer interfaced on-line with a PC

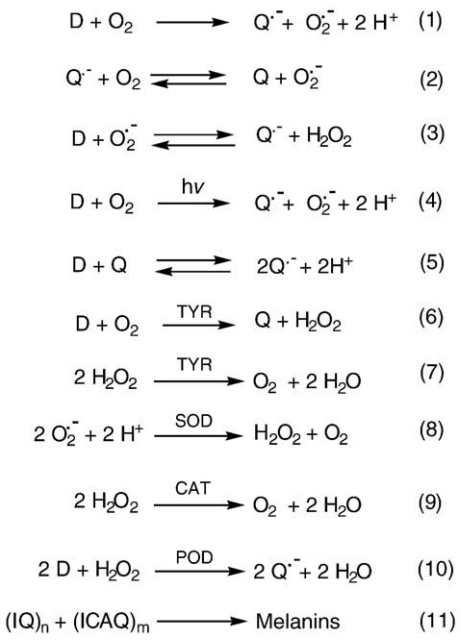

Scheme 2. Non-enzymatic reactions (1)–(3) and (5) proposed to explain H_2O_2 formation in the TYR reaction on *o*-diphenols. D is an *o*-diphenol; Q is an *o*-quinone; $Q^{\cdot -}$ is a semiquinone; $O_2^{\cdot -}$ is superoxide anion [5]. Enzymatic reactions (7)–(10) involved in the H_2O_2 metabolism. SOD generates H_2O_2, while POD, TYR and CAT consume it. Reaction (4), $O_2^{\cdot -}$ production in the L-dopa photolysis [6]. Reaction (6), proposed enzymatic production of H_2O_2 [6,7]. Melanin formation by polymerization, reaction (11) [4].

compatible microcomputer, at a scanning speed of 60 nm/s. The temperature was controlled at 25 °C using a Haake D1G circulating water bath with a heater/cooler, and checked using a Cole-Parmer digital thermometer with a precision of ±0.1 °C. Kinetic assays were also carried out with the above instruments, using a suitable wavelength to follow the reaction. In the case of TBC, the *o*-quinone was followed at 410 nm ($\varepsilon = 1100\ M^{-1}\ cm^{-1}$) [12]; in the case of DOMA, the formation of DOBA (3,4-dihydroxybenzaldehyde) was followed at a 350 nm ($\varepsilon = 9000\ M^{-1}\ cm^{-1}$) [13]; for L-dopa and L-tyrosine dopachrome formation was followed at 475 nm ($\varepsilon = 3600\ M^{-1}\ cm^{-1}$) [12]; finally, with dopamine and tyramine the formation of dopaminechrome (DMC) was followed at 480 nm ($\varepsilon = 3300\ M^{-1}\ cm^{-1}$) [12]. For tyrosinase, all the assays were carried out under saturating conditions of tyrosinase by molecular oxygen (0.26 mM oxygen in the assay medium) [10,14].

2.4. Oxymetric assays

Oxygen evolution was measured with a Clark-type electrode coupled to a Hansatech Oxygraph (King's Lynn, Norfolk, UK). The equipment was calibrated using the tyrosinase/4-*tert*-butylcatechol method [15]. Nitrogen was bubbled through the reaction medium to remove the oxygen when necessary. The reaction medium contained 0.18 M sodium phosphate buffer (pH 7.0) for DOMA and 30 mM sodium phosphate buffer (pH 7.0) for the rest of the substrates. The medium was stirred constantly and the temperature was kept at 25 ± 0.1 °C using a Haake D1G circulating water bath. Initial rate values ($V_0^{O_2}$) were determined from triplicate measurements at each substrate and enzyme concentration.

2.5. Hydrogen peroxide evaluation

The formation of H_2O_2 was measured detecting the production of O_2 after the addition of catalase (CAT) in an oxygraph, and taking into account the stoichiometry, reaction (9). The concentration of formed H_2O_2 was determined from triplicate measurements at each substrate and enzyme concentration.

2.6. Generation of *o*-quinones and aminochromes

Oxidation of the substrates (TBC and dopamine) in 30 mM sodium phosphate buffer (pH 7.0) was carried out with stoichiometric periodate [12,16]. TBC oxidation by periodate generates a stoichiometric amount of *o*-quinone, while the oxidation of dopamine by periodate generates a stoichiometric amount of *o*-dopaminequinone, which evolves to dopaminechrome [16,17]. The *o*-quinones and the aminochromes generated were extracted twice with ether to remove sodium iodate. In the case of TBC, the mixture was acidified to pH 4.5, after which the *o*-quinone was extracted with 30 mM sodium phosphate buffer (pH 7.0). The recovery was practically 100%, as demonstrated by the visible spectra ($\lambda_{max} = 410$ nm) as compared with the oxidation of TBC by TYR [12]. Dopaminechrome was extracted from a initial ether extract with 30 mM sodium phosphate buffer (pH 7.0). The recovery was 20% as demonstrated by quantification at its maximum wavelength ($\lambda_{max} = 480$ nm) and compared with the oxidation of dopamine by TYR [12,17].

2.7. Relation between the initial substrate consumption rates (O_2) and product formation in TYR-catalysed reactions

At short reaction times (Schemes 1A and 3B), the following stoichiometric relations were maintained between the initial chromophoric product formation rates (X, V_0^X) and oxygen consumption ($V_0^{O_2}$). TBC: $V_0^Q = 2\ V_0^{O_2}$, DOMA: $V_0^{DOBA} = 2\ V_0^{O_2}$, L-dopa; $V_0^{DC} = V_0^{O_2}$, dopamine: $V_0^{DMC} = V_0^{O_2}$, L-tyrosine: $V_0^{O_2} = 1.5\ V_0^{DC}$, tyramine: $V_0^{O_2} = 1.5\ V_0^{DMC}$. However, at longer reaction times, the *o*-quinones generated by the enzyme and by auto-oxidation of the substrates evolve, leading to the rupture of the above stoichiometric relations and the formation of H_2O_2, reactions (1)–(3) and (5).

3. Results and discussion

To understand the possible formation of H_2O_2 during the biosynthesis of melanin, it is first necessary to be aware of how exactly tyrosinase acts (Schemes 1A and 4) [2].

Besides the reactions described in Scheme 1A, a series of reactions should be added that arise from the *o*-quinones generated chemically through the auto-oxidation of *o*-diphenols, reactions (1)–(3) and (5), or enzymatically via TYR. Whatever the case, TYR, in its action on monophenols and *o*-diphenols (L-tyrosine and L-dopa), originates very unstable *o*-quinones which produce H_2O_2 and dopachrome. In turn, the dopachrome evolves, generating more H_2O_2 (Scheme 1B).

In what is termed the distal phase or phase II of melanogenesis, it has been suggested that dopachrome evolves to indoles (Scheme 1B) [1,3,4], followed by polymerisation of the indolquinones [the terminal phase or phase III of melanogenesis, reaction (11)] [4].

Therefore, all the processes that give rise to *o*-quinones may be a source of H_2O_2 and the following should be taken into account: (*i*) the auto-oxidation of *o*-diphenols and monophenols, (*ii*) the enzymatic oxidation of *o*-diphenols and monophenols and (*iii*) the evolution of *o*-quinones.

3.1. Auto-oxidation and enzymatic oxidation of *o*-diphenols and monophenols

Firstly, we shall consider the four types of *o*-diphenols chosen for this study (TBC, DOMA, L-dopa and dopamine) and then the monophenols, L-tyrosine and tyramine.

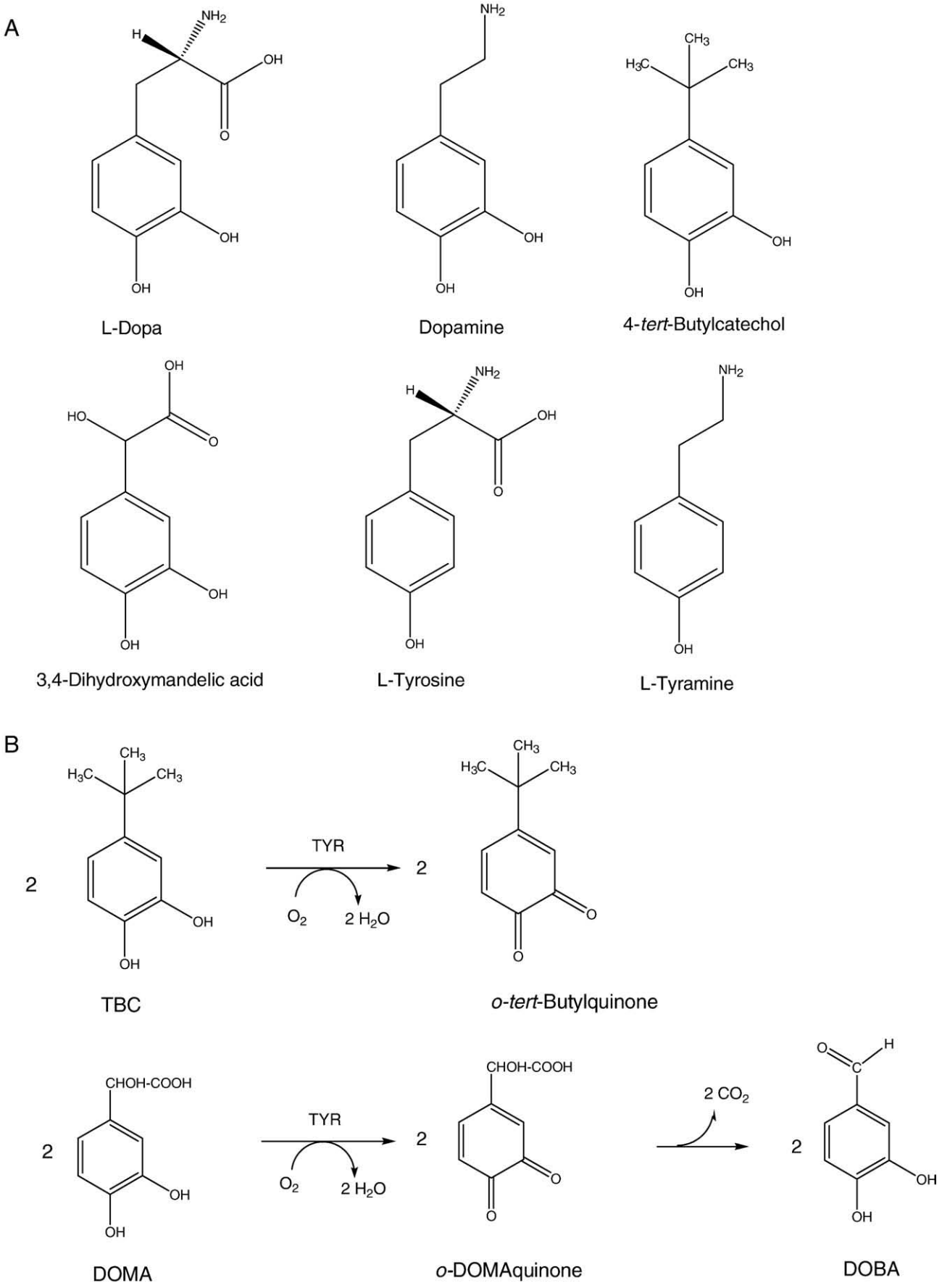

Scheme 3. (A) Chemical structures of the TYR substrates studied in this work. (B) Oxidation of TBC [12,18] and DOMA [13] by TYR.

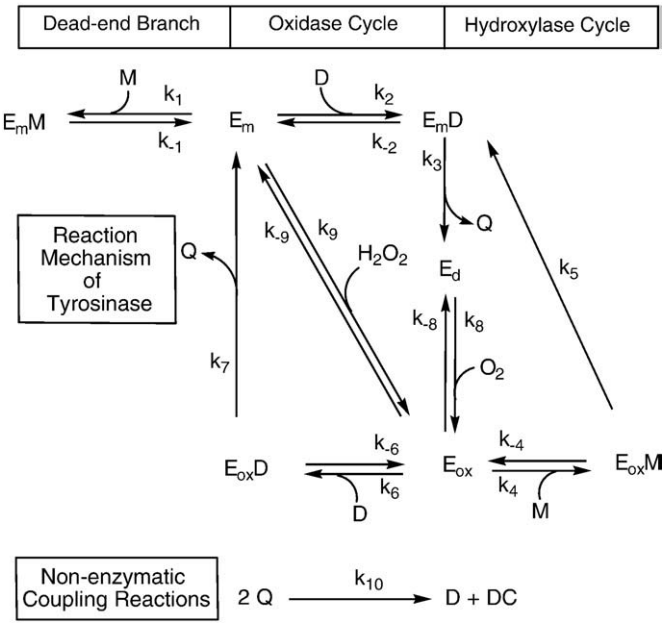

Scheme 4. Reaction mechanism of TYR acting on M and D with chemical reactions corresponding to Q evolution (Scheme 1A) [2].

3.1.1. *o*-Diphenols and monophenols auto-oxidation

3.1.1.1. 4-tert-Butylcatechol (TBC). The *o*-quinone of TBC is very stable (Scheme 3B) [12,18], which means that the auto-oxidation that begins with reaction (1), followed by (2) and (3), must take into account the oxidation of the *o*-diphenol by the *o*-quinone, reaction (5). Hence, at pH 7.0, a given initial O_2 consumption rate is reached, while H_2O_2 is gradually accumulated (see Table 1). In the presence of SOD, the reaction (8) is more intense, so that the equilibrium of the reaction (2) is displaced towards the right. Similarly, the reaction (1) is displaced towards the right because of the withdrawal of $O_2^{\cdot -}$. The consumption of $Q_2^{\cdot -}$ in reaction (2) will mean that the equilibrium in reaction (5) will be displaced towards the right, increasing the formation of $Q_2^{\cdot -}$ and so increasing the oxygen consumption rate of reaction (2) and the formation of $O_2^{\cdot -}$, leading to the accumulation of more H_2O_2 (Fig. 1A) (see Table 1). A study of other *o*-diphenols (catechol, 4-methylcatechol and 4-ethylcatechol), which originate stable *o*-quinones, provides similar results (Table 1).

3.1.1.2. 3,4-Dihydroxymandelic acid (DOMA). The auto-oxidation of DOMA at pH 7.0 occurs through reactions (1)–(3). The *o*-quinone of the DOMA is very unstable and undergoes oxidative decarboxylation and is transformed into 3,4-dihydroxybenzaldehyde (DOBA), (Scheme 3B) [13]. Because the *o*-quinone is unstable, reaction (5) does not occur and so there is no additional source of $Q_2^{\cdot -}$. In the presence of SOD, reactions (1) and (2) are more intense but reactions (3) and (5) do not occur (there being no additional source of $Q_2^{\cdot -}$), so the oxygen consumption rate decreases, as does the accumulation of H_2O_2 (Fig. 1B) (Table 1).

Table 1
Auto-oxidation of *o*-diphenols at pH 7.0.

$[o\text{-diphenol}]_0$ (5 mM)	Absence of SOD[a]		Presence of SOD[b]	
	$V_0^{O_2}$ (μM/min)	$[H_2O_2]^c$ (μM)	$V_0^{O_2}$ (μM/min)	$[H_2O_2]^c$ (μM)
TBC	1.12 ± 0.11	9 ± 1	2.51 ± 0.11	12 ± 2
Catechol	0.31 ± 0.01	4 ± 1	2.42 ± 0.13	9 ± 1
4-Methylcatechol	11.22 ± 1.53	8 ± 1	42.72 ± 3.12	14 ± 3
4-Ethylcatechol	13.22 ± 1.08	6 ± 1	26.61 ± 2.59	13 ± 2
DOMA[d]	0.61 ± 0.07	8 ± 1	0.41 ± 0.06	2 ± 1
L-dopa	1.51 ± 0.05	10 ± 2	0.53 ± 0.03	3 ± 1
Dopamine	1.12 ± 0.81	11 ± 2	2.42 ± 0.19	9 ± 1

[a] Assay conditions: 30 mM sodium phosphate buffer (pH 7.0).
[b] Conditions (a) with $[SOD]_0 = 414$ U/ml.
[c] Concentration of H_2O_2 accumulated after 15 min of reaction.
[d] Assay conditions: 0.18 M sodium phosphate buffer (pH 7.0).

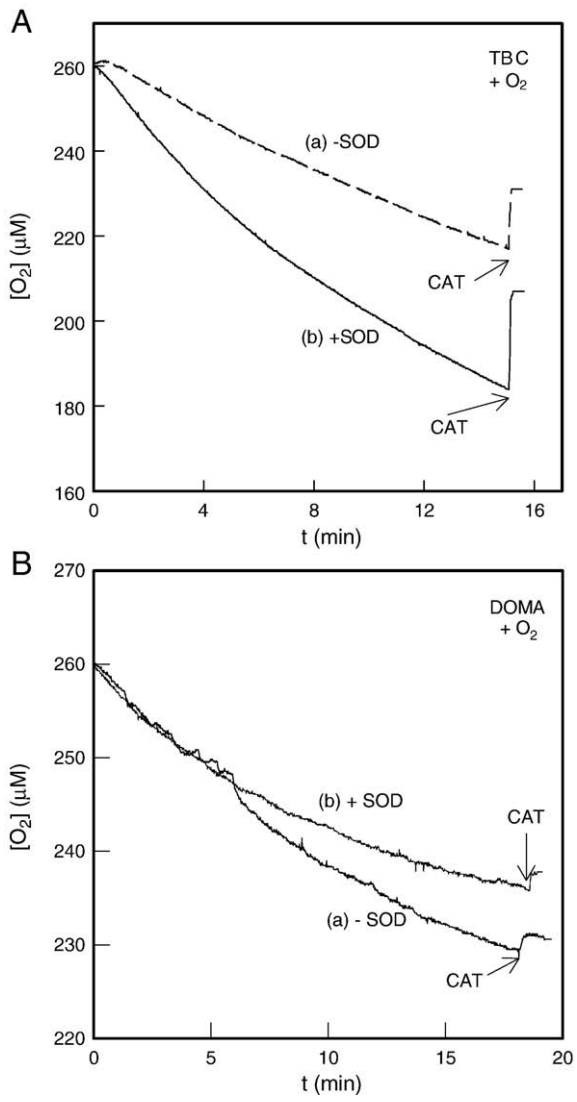

Fig. 1. (A) Oxygen consumption during the auto-oxidation of TBC in the absence (a) and the presence (b) of SOD. Evaluation of the H_2O_2 accumulated by the addition of CAT at the indicated time. The experimental conditions were 30 mM sodium phosphate buffer (pH 7.0), $[TBC]_0 = 15$ mM and $[SOD]_0 = 414$ U/ml. At the time indicated by the arrow, 930 U/ml of CAT were added. (B) Oxygen consumption during the auto-oxidation of DOMA in the absence (a) and the presence (b) of SOD. Evaluation at the time indicated of the H_2O_2 accumulated after the addition of catalase. The experimental conditions were 0.18 M sodium phosphate buffer (pH 7.0), $[DOMA]_0 = 14$ mM and $[SOD]_0 = 414$ U/ml. At the time indicated by the arrow, 930 U/ml of CAT were added.

3.1.1.3. L-Dopa and dopamine. Auto-oxidation at pH 7.0 begins through reaction (1) and continues through (2) and (3), while the reaction described by (5) does not occur (there is no additional source of $Q_2^{\cdot -}$ because the *o*-quinone is very unstable and evolves according to $2Q \rightarrow D + DC$). In the presence of SOD, the reactions (1) and (2) are favoured, but as reaction (5) does not take place the formation of H_2O_2 through (3) diminishes and occurs through (8). Therefore, the system slows down and the oxygen consumption rate falls, as does the quantity of H_2O_2 accumulated (Table 1). At long times, the evolution of aminochromes towards DHI and DHICA (Scheme 1B), intensifies

the formation of H_2O_2 due to reactions (1)–(3), but from DHI (in the case of L-dopa and dopamine) and DHICA (in the case of L-dopa).

3.1.1.4. L-Tyrosine and tyramine. The monophenols L-tyrosine and tyramine show no practically auto-oxidation and so do not consume oxygen, meaning that no H_2O_2 is generated in this way. For this reason, they do not appear in Table 1. The H_2O_2 generated during the melanogenesis pathway, therefore, must have a source other than the auto-oxidation of L-tyrosine. More specifically, it will be formed from *o*-diphenolic and quinonic intermediates such as quinones, semiquinones, *o*-diphenols, aminochromes, 5,6-dihydroxyindoles and indolequinones (see below).

3.1.2 Enzymatic oxidation of o-diphenols

The action of TYR on monophenols and *o*-diphenols originates *o*-quinones which, depending on their chemical nature, evolve, sometimes leading to the formation of H_2O_2. First, we shall consider the enzymatic oxidation of *o*-diphenols and then of monophenols. When tyrosinase acts on *o*-diphenols the mechanism is that described in Scheme 4, but each *o*-diphenol (because of its chemical nature) will give rise to a specific *o*-quinone that will evolve in its own way: L-tyrosine/L-dopa and tyramine/dopamine (Scheme 1), or TBC and DOMA (Scheme 3B). In the case of TBC and DOMA, the only source of H_2O_2 is that described in sections 3.1.1.1 and 3.1.1.2. However, in the case of L-tyrosine/L-dopa and tyramine/dopamine, the aminochromes formed from the *o*-quinones evolve towards 5,6-dihydroxyindoles (Scheme 1B) and, with time, generate more H_2O_2 [reactions (1)–(3)]. The oxidation of these substrates by tyrosinase was studied in two different experimental conditions: (A) oxidation at a constant enzyme concentration and variable substrate concentrations and (B) oxidation at a constant substrate concentration and variable enzyme concentrations.

3.1.2.1 Enzymatic oxidation of o-diphenols: effect of initial concentration of o-diphenol. Maintaining the initial enzyme concentration (constant $[E]_0$), the concentration of substrate was varied. Fig. 2A shows the variation in TBC and the accumulation of H_2O_2. As the concentration of substrate increased, so did the rate of the enzymatic formation of *o*-quinone and substrate auto-oxidation, leading to an increase in the formation of H_2O_2. The concentration of the H_2O_2 was determined by adding catalase to the oxygraph cell and by taking into consideration the stoichiometry of reaction (9). When the same experiments were carried out in the presence of SOD (Fig. 2A), the concentration of H_2O_2 accumulated increased as a result of the effect of the SOD on the auto-oxidation of TBC (see Table 1). Reaction (5) generates more $Q_2^{\bullet -}$ and this increases H_2O_2. The oxygen consumption rate increased with increasing substrate concentrations (Fig. 2A).

Fig. 2B shows experiments depicting the oxidation of DOMA by TYR: once again, H_2O_2 production increased with increasing initial concentrations of substrate. In accordance with Scheme 2, reactions (1)–(3) are reinforced but reaction (5) does not take place because the *o*-quinone is very unstable. The addition of SOD had the effect depicted in Fig. 2B, a decrease in the concentration of H_2O_2 as was observed in the auto-oxidation of the substrate (see section 3.1.2.) (Table 1). The oxygen consumption rate increases with increasing substrate concentrations (Fig. 2B).

The same effect is observed for the enzymatic oxidation of L-dopa and dopamine (Fig. 2C and D, respectively). In both cases the *o*-quinone is unstable and generates aminochrome; the reaction (5) does not occur but the aminochromes evolve towards 5,6-dihydroxyindoles in the used time scale, providing a new source of H_2O_2, reactions (1)–(3). In the presence of SOD the quantity of H_2O_2 diminishes, which agrees with the auto-oxidation experiments (see sections 3.1.1.3. and 3.1.1.4.) (Table 1). In both cases, as the substrate concentration increases, so the oxygen consumption rate increases (Fig. 2C and D).

3.1.2.2. Enzymatic oxidation of o-diphenols: effect of initial concentration of enzyme. When the initial concentration of *o*-diphenol is kept constant, the rate of auto-oxidation remains constant and so does the concentration of H_2O_2 originated by this pathway. In all cases the oxygen consumption rate increases with increasing enzyme concentration. When the enzyme concentration is varied in the case of TBC (Fig. 3A), the concentration of H_2O_2 does not vary, the increased Q affects the equilibrium shown in reaction (2), shifting it towards the left, and the reaction shown in (5) shifts it towards the right so that it reaches the steady-state and the concentration of H_2O_2 does not vary. In the presence of SOD the effect described in the auto-oxidation study occurs (Fig. 1A and Table 1) (see section 3.1.1.1.) and so H_2O_2 increases (Fig. 3A). The reactions (1) and (2) shift towards the right and the reaction (5) generates $Q_2^{\bullet -}$, increasing oxygen consumption, reaction (2), and the generation of H_2O_2.

In the case of DOMA oxidation, auto-oxidation (at constant substrate concentration) is constant (Fig. 3B), and the fact that the system reaches the steady-state, as in the above case, means that the concentration of H_2O_2 does not vary with the concentration of enzyme. As the product DOBA is stable there is no variation in H_2O_2. The addition of SOD has the same effect as indicated in the auto-oxidation (see section 3.1.1.2.) (Fig. 1B and Table 1) and the H_2O_2 diminishes (Fig. 3B).

When the substrate to be oxidised is L-dopa (at a constant concentration) it undergo auto-oxidation and the H_2O_2 produced is also constant. However, as the concentration of enzyme is increased, the dopachrome concentration also increases. This product evolves towards 5,6-dihydroxyindole, which, as it is oxidised, reactions (1)–(3), generate an additional source of H_2O_2 (Fig. 3C). The effect of adding SOD is the same as that seen when SOD was added during the auto-oxidation study (see section 3.1.1.3.) (Fig. 3D).

Similar behaviour is seen in the case of dopamine oxidation. As the enzyme concentration is increased, so the dopaminechrome concentration increases. This produces DHI, which is auto-oxidised [reactions (1)–(3)] to form H_2O_2, which increases with the concentration of enzyme (Fig. 3D). The effect of SOD on the enzymatic oxidation is identical to that it has on auto-oxidation (Fig. 3D) (see section 3.1.1.4.).

3.1.3. Enzymatic oxidation of monophenols

In this case, the oxidation was carried out with L-tyrosine and tyramine since they are monophenols which, due to the chemical evolution of their *o*-quinones, enable the system to reach the steady-state [19]. In the reaction of TYR with L-tyrosine, H_2O_2 is accumulated in the medium and its concentration increases as the concentration of substrate increases since *o*-quinone formation also increases. In the presence of SOD, the concentration of H_2O_2 diminishes, as described for the oxidation of L-dopa. L-tyrosine does not undergo significant auto-oxidation in the measuring time, but when the concentration of substrate is increased, the concentration of L-dopa accumulated in the medium also increases [19]. This does undergo auto-oxidation, as described previously, and so the concentration of dopachrome also increases, leading to an increase in 5,6-dihydroxyindoles (DHI and DHICA, Scheme 1B), indolequinones and, therefore, H_2O_2, reactions (1)–(3). The effect of SOD in the medium is a diminution in the concentration of H_2O_2 (Fig. 4A). Varying the concentration of enzyme has the same effect as varying the substrate concentration (Fig. 4C), the explanation being similar to the above. In both cases, a new *o*-quinone is produced, dopachrome, which, in turn, evolves towards 5,6-dihydroxyindole; and it must be kept in mind that dopachrome increases with increasing initial enzyme concentration or initial substrate concentration.

In the oxidation of tyramine, the same results are obtained when the concentration of substrate (Fig. 4B) and the concentration of enzyme (Fig. 4D) are varied. In this case, dopaminechrome is accumulated before it evolves to DHI (Scheme 1B).

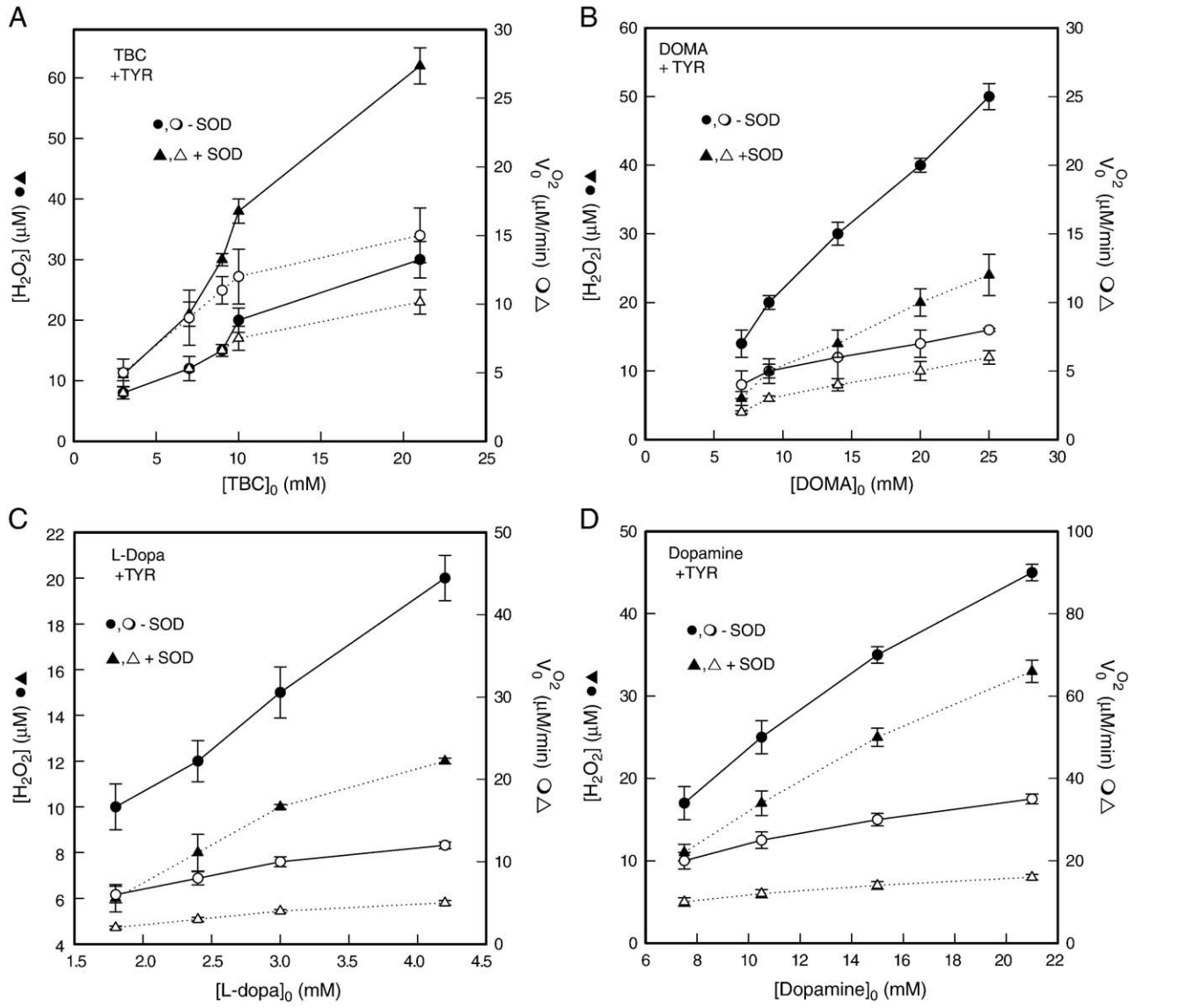

Fig. 2. (A) H_2O_2 accumulated during the oxidation of TBC by TYR. Variation of substrate concentration in the absence (●) and the presence (▲) of SOD (414 U/ml). Values obtained for $V_0^{O_2}$ in the absence (○) and the presence (△) of SOD. The experimental conditions were: 30 mM phosphate buffer (pH 7.0), $[TYR]_0$ (0.4 nM) and the substrate concentrations indicated in the figure. The reaction was begun by the addition of enzyme and after 15 min, CAT (930 U/ml) was added. (B) H_2O_2 accumulated during the enzymatic oxidation of DOMA by TYR (0.3 nM). Variation of substrate concentration in the absence (●) and the presence (▲) of SOD (414 U/ml). Values obtained for $V_0^{O_2}$ in the absence (○) and the presence (△) of SOD. The experimental conditions were the same as above but with 0.18 M phosphate buffer (pH 7.0). The substrate concentrations are indicated in the figure. (C) H_2O_2 accumulated during the enzymatic oxidation of L-dopa by TYR. Variation of substrate concentration in the absence (●) and the presence (▲) of SOD (414 U/ml). Values obtained for $V_0^{O_2}$ in the absence (○) and the presence (△) of SOD. The experimental conditions and methodology are those indicated in panel A, using 1.8 nM $[TYR]_0$. The substrate concentration is indicated in the figure. (D) H_2O_2 accumulated during the enzymatic oxidation of dopamine by TYR (1 nM). Variation of substrate concentration in the absence (●) and the presence (▲) of $[SOD]_0 = 414$ U/ml. Values obtained for $V_0^{O_2}$ in the absence (○) and the presence (△) of SOD. The experimental conditions and methodology are those indicated in panel B.

This series of experiments, then, demonstrates that H_2O_2 is accumulated in a purely chemical way in the melanin biosynthesis pathway. To confirm these results, the following series of spectrophotometric experiments was carried out, continuously monitoring the reactions. Additional enzymes: CAT, reaction (9), POD, reaction (10), and SOD, reaction (8), were used to help confirm the presence of H_2O_2.

3.2. Monitoring the formation of the o-diphenol oxidation products

The action of tyrosinase on *o*-diphenols generates *o*-quinones, which are normally unstable, except in the case of TBC. Furthermore, peroxidase also acts on *o*-diphenols giving rise to the formation of free radicals, semiquinones, which disproportionate to form *o*-quinone. CAT acts by discomposing the H_2O_2 [reaction (9)] while SOD forms it, reaction (8).

3.2.1. Oxidation of TBC

The oxidation of TBC by TYR is studied in Fig. 5A. Trace (a) shows the formation of *o*-quinone in the absence of enzyme (auto-oxidation), while the action of TYR on TBC corresponds to trace (b). The addition of catalase (930 U) hardly affects the activity (trace c) since it merely discomposes the H_2O_2 formed without therefore affecting the diphenolase activity. The presence of SOD (414 U) increases the velocity (curve d). Note in this case that the presence of SOD increases the O_2 consumption rate during the auto-oxidation, generating more *o*-quinone and increasing H_2O_2 formation (see section 3.1.1.1.).

The spectophotometric recording in the presence of SOD and CAT (trace e) shows little variations in the formation of *o*-quinone. The addition of CAT only leads to the discomposition of the H_2O_2 without affecting *o*-quinone formation. However, the addition of POD (trace f) shows how H_2O_2 is accumulated in the medium, which is used by the

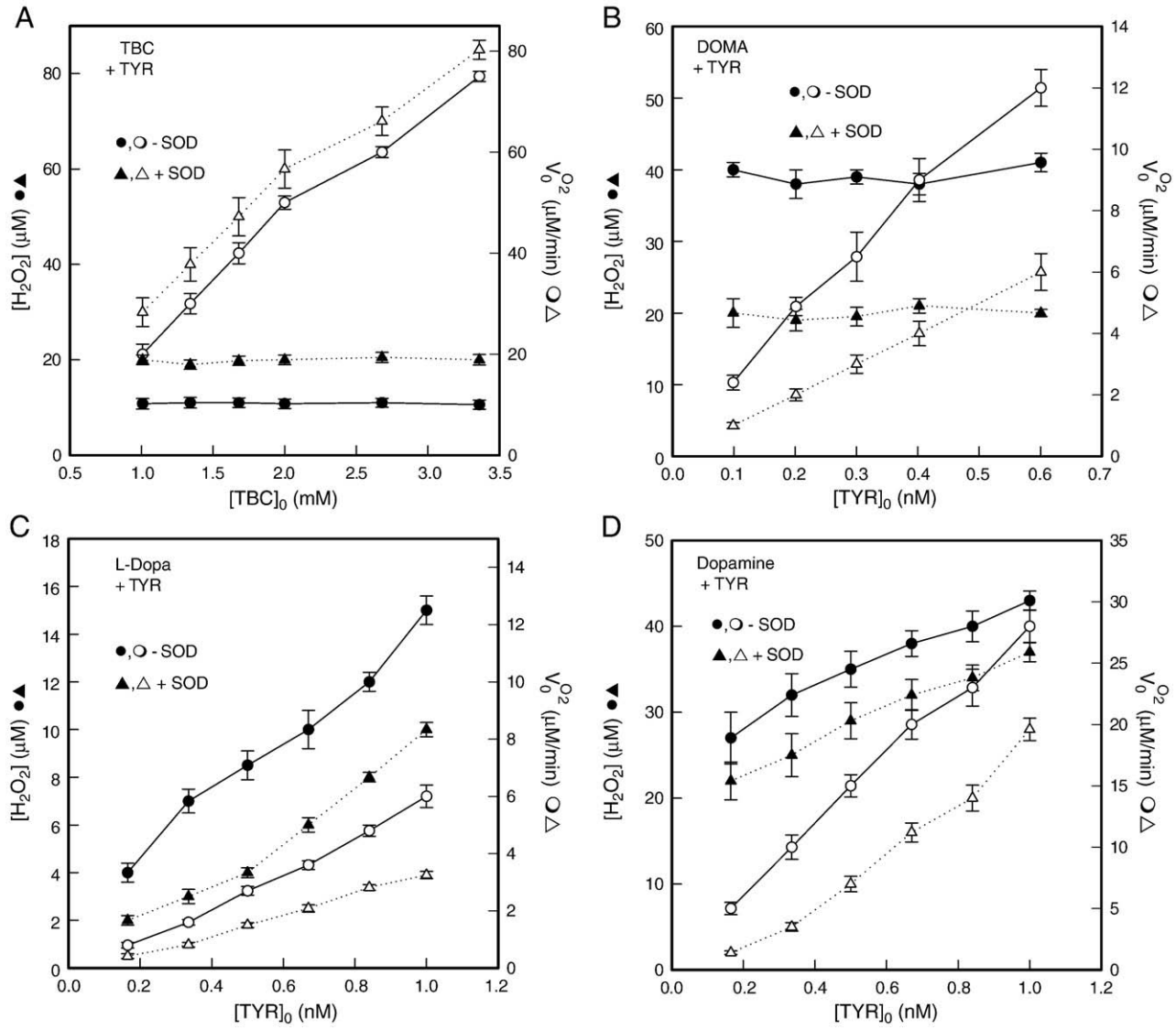

Fig. 3. (A) H_2O_2 accumulated during the oxidation of TBC by TYR. Variation of substrate concentration in the absence (●) and the presence (▲) of SOD (414 U/ml). Values obtained for $V_0^{O_2}$ in the absence (○) and the presence (△) of SOD. The experimental conditions were: 30 mM phosphate buffer (pH 7.0), $[TBC]_0$ (7.5 mM) and the TYR concentrations are indicated in the figure. The reaction was begun by the addition of TYR and after 15 min, CAT (930 U/ml) was added. (B) As in panel 3A but with 0.18 M phosphate buffer (pH 7.0) and $[DOMA]_0 = 20$ mM. (C) As in (A) but with [L-dopa]$_0 = 3$ mM. (D) As in (A) but with $[dopamine]_0 = 15$ mM.

enzyme to oxidise new molecules of TBC increasing the rate of *o*-quinone formation [9]. Trace (g) is the same as (f) but, with the addition of CAT, H_2O_2 decreases and so, therefore, does the accumulation of *o*-quinone. Trace (h) is the same as (f) after the addition of SOD. In this case, the increase in the auto-oxidation of TBC and the increased accumulation of H_2O_2 (see section 3.1.1.1.) is evident from the maximum accumulation of *o*-quinone during the reaction of POD. To summarise, in the action of TYR on TBC, *o*-quinone is formed and this evolves chemically to form H_2O_2. This reaction is stronger in the presence of SOD, when H_2O_2 is detected by the presence of POD, reactions (1)–(3), (5), (8) and (10).

3.2.2. Oxidation of DOMA

The experiments involving DOMA oxidation by TYR are depicted in Fig. 5B. Trace (a) corresponds to the formation of DOBA, which results from the auto-oxidation of DOMA [13]. The action of TYR on DOMA is shown by trace (b), monitoring the formation of DOBA. As in the case of TBC, the addition of CAT does not modify the formation of DOBA (trace c). When SOD is added to the medium (section 3.1.1.2), the withdrawing effect of $O_2^{\cdot -}$ and the decrease in the oxygen consumption rate can be appreciated from the decrease in the rate of DOBA formation (trace d). In this case, the CAT has hardly any effect on the rate of DOBA formation, although, as CAT prevents the accumulation of H_2O_2, it may also prevent additional auto-oxidation (curve e). Trace (f), obtained in the presence of POD, depicts the accumulation of H_2O_2, since this enzyme uses it as substrate to oxidase DOMA to semiquinone and finally DOBA [13]. Trace (g) is identical to (f) after the addition of CAT; this enzyme eliminates the H_2O_2 and so hinders the action of POD, decreasing the spectrophotometric signal. Lastly, trace (h) is the same as (f) after the addition of SOD and, as explained above, oxygen consumption decreases during auto-oxidation, as does the formation of H_2O_2 and therefore the activity of POD [reactions (1)–(3), (8) and (10)], leading to a decreased spectrophotometric signal [(h)<(f)), but ((h)>(g)].

3.2.3. L-Dopa oxidation

The oxidation of L-dopa by TYR is depicted in Fig. 5C, where the accumulation of dopachrome is measured at 475 nm [2]. Trace (a) points to the low degree of L-dopa auto-oxidation. The action of tyrosinase is depicted in trace (b), while the addition of CAT has no

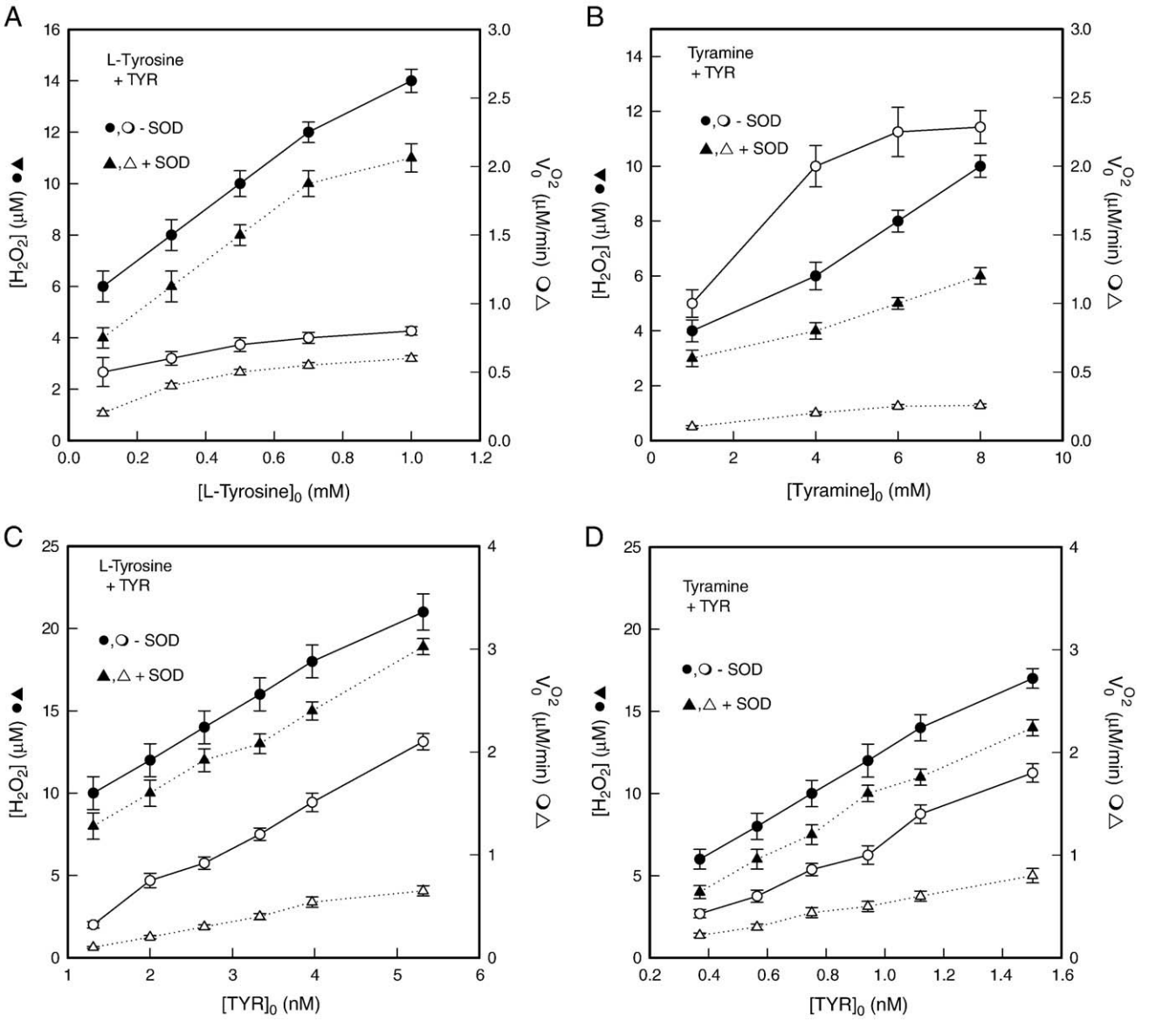

Fig. 4. (A) H_2O_2 accumulated during the oxidation of L-tyrosine by TYR. Variation of substrate concentration in the absence (●) and the presence (▲) of SOD (414 U/ml). Values obtained for $V_0^{O_2}$ in the absence (○) and the presence (△) of SOD. The experimental conditions were 30 mM phosphate buffer (pH 7.0), $[TYR]_0$ (2 nM) and the substrate concentrations indicated in the figure. The reaction was begun by the addition of TYR and after 15 min CAT (930 U/ml) was added. (B) Oxidation of tyramine by TYR in the same conditions as in (A) but $[TYR]_0$ was 1.5 nM. The tyramine concentrations are indicated in the figure. (C) Oxidation of tyramine by TYR. The experimental conditions were as in (A) but the substrate concentration was kept constant and the enzyme concentration was varied as indicated in the figure. $[L\text{-tyrosine}]_0 = 0.7$ mM. (D) Oxidation of tyramine by TYR in the same conditions as in (B), but $[Tyramine]_0 = 4$ mM.

effect on the kinetics (trace c). However, the addition of SOD (section 3.1.1.3) leads to a diminution of dopachrome accumulation and oxygen consumption (trace d). The addition of CAT (trace e) eliminates the H_2O_2, but has little effect on the dopachrome accumulation kinetics. The presence of POD (trace f) points to the accumulation of H_2O_2 in the medium, producing the maximum signal. When CAT is added to the experiment depicted in trace (f) the result is trace (g), which demonstrates the decomposition of H_2O_2; POD activity is weaker and so the signal is also weak. However, if SOD is added to experiment (f), we obtain trace (h) [(h)<(f), (h)>(g)], pointing to a diminution in the formation and accumulation of H_2O_2 [reactions (1)–(3), (8) and (10)] and in POD activity, resulting in a weaker signal compared with trace (f).

3.2.4. Dopamine oxidation

The oxidation of dopamine by TYR is shown in Fig. 5D. Trace (a) corresponds to the auto-oxidation of dopamine which is monitored at 480 nm [12,17]. Traces (b) and (c) correspond to enzymatic oxidation by TYR in the absence and presence of CAT, respectively. The action of SOD is reflected in trace (d), where it decreases the dopaminechrome formation rate, in agreement with section 3.1.1.4. Note how traces (b), (c) and (d) run parallel to the time axis, basically as a result of dopaminechrome evolving to DHI. In this case, the action of CAT (trace e) can be appreciated as a result of the lower oxidation of dopamine and DHI by H_2O_2. In trace (f), the addition of POD reveals the accumulation of H_2O_2 since it is used by the enzyme to oxidise more molecules of dopamine to dopaminechrome (maximum signal). Trace (g) corresponds to the addition of CAT to the experiment depicted in (f), while the destruction of H_2O_2 is evident from the decrease in the signal with respect to trace (f). However, trace (h), which corresponds to an experiment such as depicted in (f) to which SOD is added, leads to a diminution in H_2O_2 accumulation (decreased signal) and lower POD activity than in trace (f), but (h>g), reactions (1)–(3), (8) and (10).

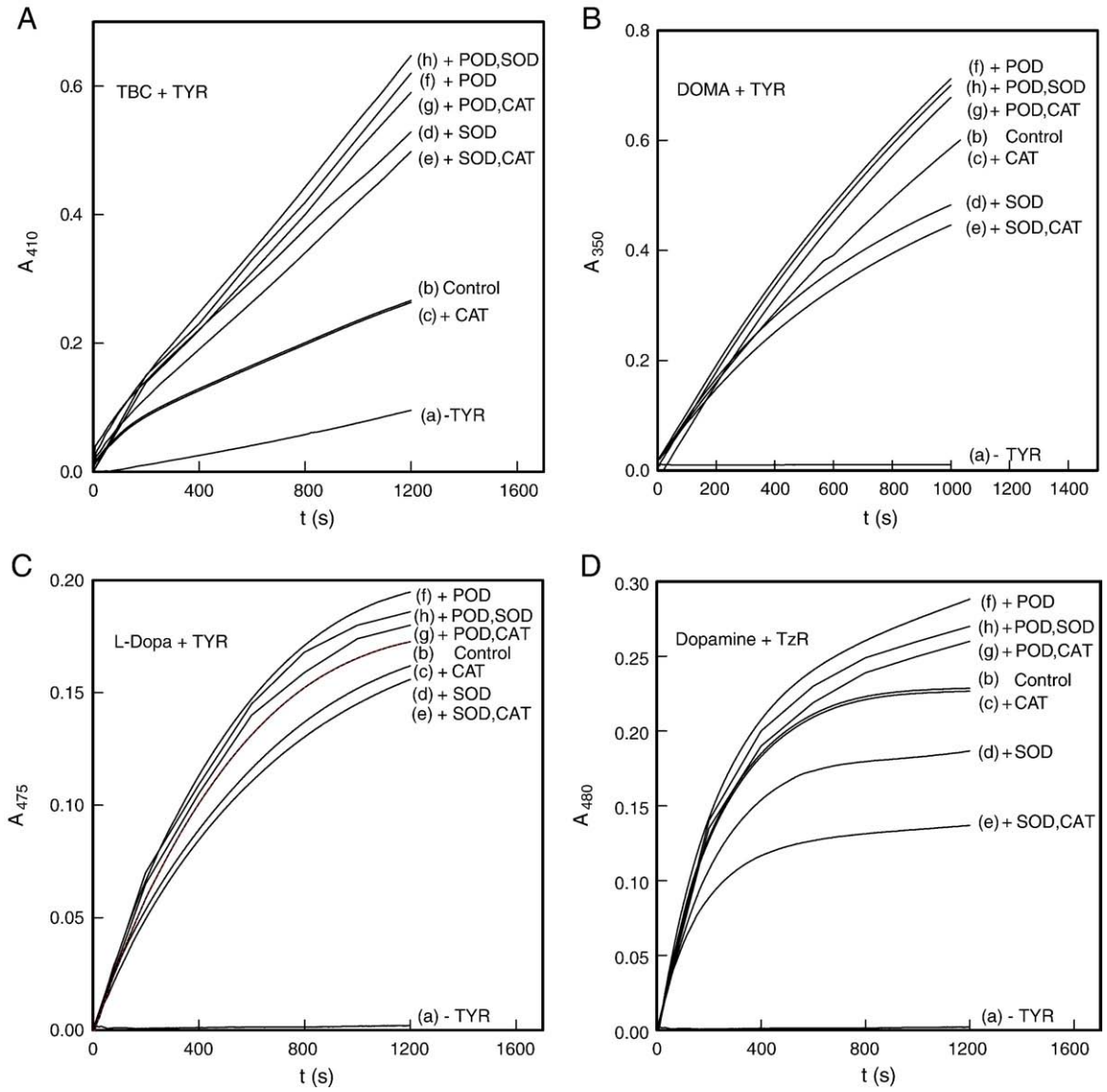

Fig. 5. Spectrophotometric recordings of the oxidation of the different *o*-diphenols by TYR in different experimental conditions. The fixed experimental conditions in all cases were: 30 mM phosphate buffer (pH 7.0), 25 °C. Recording (b) is the control (TYR + substrate). The other recordings [(c)–(h)] are those of the experiment with TYR plus the indicated enzyme. Auto-oxidation is always trace (a), which is the same as (b), but without TYR. (A) Oxidation of TBC. (a) Auto-oxidation of $[TBC]_0$ at 15 mM recorded at λ 410 nm. (b) Oxidation by $[TYR]_0$ (0.4 nM). (c) $[CAT]_0 = 930$ U/ml. (d) $[SOD]_0 = 414$ U/ml. (e) $[SOD]_0 = 414$ U/ml and $[CAT]_0 = 930$ U/ml. (f) $[POD]_0 = 30$ U/ml. (g) $[CAT]_0 = 930$ U/ml. (h) $[SOD]_0 = 414$ U/ml. (B) The same conditions as in (A) but with 0.18 M sodium phosphate buffer (pH 7.0), $[DOMA]_0 = 10$ mM, λ 350 nm and $[TYR]_0 = 0.1$ nM. (C) The same conditions as in (A), but with $[L\text{-dopa}]_0 = 3$ mM, λ 475 nm and $[TYR]_0 = 0.8$ nM. (D) The same conditions as in (A), but with $[dopamine]_0 = 6$ mM, λ 480 nm and $[TYR]_0 = 0.80$ nM.

The case of dopamine is similar to that of L-dopa, the dopamine-chrome formed evolving to a 5,6-dihydroxyindole (DHI, Scheme 1B). DHI also generates H_2O_2, through reactions (1)–(3).

3.3. Monitoring product formation during the oxidation of monophenols

The effects are slight because the monophenols hardly undergo auto-oxidation, as indicated in section 3.1.1.4. Instead, H_2O_2 is formed during the evolution of the *o*-quinones generated from the *o*-diphenol accumulated in the medium (proximal phase of melanogenesis, Scheme 1A) and during the evolution of the aminochrome towards DHI and DHICA and their subsequent evolution to indolequinones (distal phase of melanogenesis, Scheme 1B) and to melanins [terminal phase of melanogenesis, reaction (11)]. As a consequence the effects for the same quantity of enzyme are not as pronounced as in the action of TYR on *o*-diphenols, and long reaction times would be necessary.

The action of TYR on the monophenols L-tyrosine and tyramine was monitored in the following experimental conditions.

(A) The reaction is begun by mixing the enzyme with the monophenol [20]. (B) The reaction is begun by adding the enzyme to a mixture of monophenol and the corresponding quantity of *o*-diphenol for the system to reach the steady-state instantaneously, according to $[o\text{-diphenol}]_{ss}/[monophenol]_{ss} = R$ [19,21].

3.3.1. Absence of initial o-diphenol concentration

In this case, the action of TYR on tyramine, recording (b) Fig. 6A, suffers a lag phase, τ, which is the time necessary for the enzyme to generate (as a result of the evolution of the *o*-quinones) the quantity of *o*-diphenol necessary to reach the steady-state [2]. Note that the reaction time (Fig. 6A and B) is longer than in the case of diphenolase activity (Fig. 5A–D).

In Fig. 6A the effect on the lag phase, τ, corresponding to each case can be appreciated. First, auto-oxidation hardly occurs (trace a). In the presence of TYR, recording (b), the $\tau = 200$ s (Fig. 6A and A inset). The presence of CAT, recording (c) (Fig. 6A), has hardly any effect on τ except for lengthening it very slightly due to the consumption of H_2O_2,

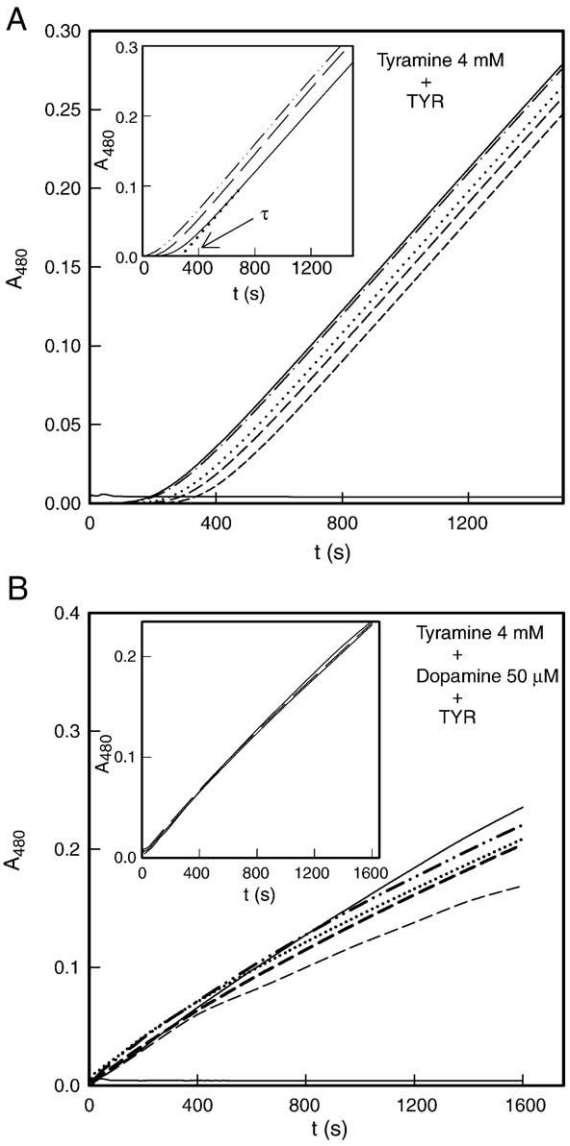

Fig. 6. Spectrophotometric registers of the action of TYR on tyramine in different experimental conditions. The fixed experimental conditions in all cases were: 30 mM phosphate buffer (pH 7.0), 25 °C and $[tyramine]_0 = 4$ mM. Recording (b) is the control (TYR + substrate). The other recordings (c–h) are those of experiment with TYR plus the indicated enzyme. Auto-oxidation is always trace (a), which is the same as (b), but without TYR. (A) The system does not start from the steady-state, $[dopamine]_0 = 0$. (a) Auto-oxidation of tyramine at λ 480 nm. (b) Control. Oxidation by $[TYR]_0 = 3$ nM. (c) $[CAT]_0 = 930$ U/ml. (f) $[POD]_0 = 30$ U/ml. (g) $[CAT]_0 = 930$ U/ml. (h) $[SOD]_0 = 414$ U/ml. Inset. (b) Oxidation of Tyramine by TYR (3 nM). (d) $[SOD]_0 = 414$ U/ml. (e) $[SOD]_0 = 414$ U/ml and $[CAT]_0 = 930$ U/ml. (B) The system starts from the steady-state, $[dopamine]_0 = 50$ μM. (a) Auto-oxidation of tyramine and dopamine. (b) Control. Oxidation of tyramine and dopamine by TYR (1.5 nM). (d) $[SOD]_0 = 414$ U/ml. (f) $[POD]_0 = 30$ U/ml. (g) $[CAT]_0 = 930$ U/ml. (h) $[SOD]_0 = 414$ U/ml. Inset. (b) Oxidation of tyramine and dopamine by TYR (1.5 nM). (c) $[CAT]_0 = 930$ U/ml. (e) $[SOD]_0 = 414$ U/ml and $[CAT]_0 = 930$ U/ml.

since this probably inhibits the reaction $E_m + H_2O_2 \rightleftarrows E_{ox}$ (Scheme 4). In the presence of SOD, recording (d) (Fig. 6A inset), the lag is shortened to 50 s due to the withdrawal of the anion $O_2^{\cdot -}$ and so the anion cannot react with the accumulated *o*-diphenol, in accordance with reaction (3). However, SOD withdraws the $O_2^{\cdot -}$ and generates H_2O_2 through another pathway, reaction (8). This peroxide causes E_m to become E_{ox} (Scheme 4) at the same time preventing the accumulated *o*-diphenol from diminishing; all this leads to a shorter τ. In trace (e) (Fig. 6A inset), the presence of CAT and SOD means that the lag is shortened less. SOD turns the $O_2^{\cdot -}$ towards H_2O_2, reaction (8), thus preventing the accumulation of *o*-diphenol the same effect as in (d) although in this case the CAT partially consumes the H_2O_2 formed. In this way, less enzyme is activated from E_m to E_{ox} and so the lag phase is longer than in (d) (Fig. 6A inset). When experiment (b) is carried out in the presence of POD, trace (f) (Fig. 6A), τ shows its maximum increase. In this case POD would use the H_2O_2 as it is being formed to attack the *o*-diphenol which is being accumulated (reducing its concentration). Alternatively, POD attacks the tyramine, which is more concentrated, originating a radical tyraminil which, in turn, attacks the *o*-diphenol, preventing it from accumulating and so the system finds it more difficult to reach the steady-state, longer τ. Trace (g) of Fig. 6A corresponds to an experiment (f) to which CAT is added. In this case, CAT reduces the level of the H_2O_2 accumulated and, to a certain extent, competes with POD. As a result the POD has a lower effect on the accumulated *o*-diphenol and the τ shorter than in recording (f) (Fig. 6A). Trace (h) (Fig. 6A) corresponds to the addition of SOD to the experiment described in (f). SOD diminishes the formation of H_2O_2, and so POD has less substrate available to act on the *o*-diphenol which is necessary to reach the steady-state, consequently τ is shortened (Fig. 6A).

At long times, dopaminechrome evolves to DHI (Scheme 1B), whose oxidation, due to its *o*-diphenolic structure, would lead to the formation of additional H_2O_2, reactions (1)–(3).

3.3.2. Presence of initial o-diphenol concentration

The system reaches the steady-state at $t \rightarrow 0$ when the corresponding quantity of *o*-diphenol is added, so that $[o\text{-diphenol}]_{ss}/[monophenol]_{ss} = R$, where R is for mushroom tyrosinase and the pair $[dopamine]_{ss}/[tyramine]_{ss}$ takes the value of 0.032 [21]. As the system starts from the steady-state rate $V_{ss}^{M_2}$ [19], the product is accumulated more rapidly than in the case of (A) (Fig. 6B and B inset).

In this case, the auto-oxidation corresponds to the mixture 4 mM tyramine + 50 μM dopamine (trace a) of Fig. 6B. In the presence of TYR, the steady-state is reached immediately see recording (b) of Fig. 6B and B inset. The presence of CAT in a type (b) experiment (trace c of Fig. 6B inset) hardly affects the steady-state since this is maintained because of the *o*-diphenol (dopamine). When SOD is added to the control assay (b), $O_2^{\cdot -}$ is withdrawn, reaction (8), O_2 consumption and H_2O_2 formation are reduced, and the steady-state rate begins to diminish, trace (d) (Fig. 6B). In trace (e) of Fig. 6B inset, the presence of CAT and SOD (with their opposite effects) means that the steady-state remains unaltered. However, POD, when added to a control assay (see trace f of Fig. 6B), acts on dopamine directly using the H_2O_2 accumulated over long times. In this way, the level of *o*-diphenol in the steady-state diminishes and the rate falls. The same effect may be produced if POD acts on tyramine, generating the free radical that attacks dopamine. If CAT [Fig. 6B trace (g)] is added to a type (f) experiment, the level of H_2O_2 falls and POD weakens its attack on *o*-diphenol (dopamine) or the monophenol (tyramine), and so the steady-state rate remains high. After the addition of SOD, Fig. 6B trace (h), to a type (f) experiment the H_2O_2 decay and, therefore POD acts less efficiently and the steady-state rate is higher than in (f) since less H_2O_2 is formed at long times. At longer times, the concentration of H_2O_2 would increase due to the production of DHI, reactions (1)–(3). In conclusion, both the experiments of Fig. 6A and B support the generation of H_2O_2 in non-enzymatic reactions after the reaction of tyrosinase on monophenols.

3.4. Generation of H_2O_2 in the evolution of o-quinones and aminochromes

Two cases should now be distinguished: (A) the evolution of *o*-quinones that are slightly unstable [12,18], (B) the evolution of moderately unstable *o*-quinones such as aminechromes [4,19]. As regards the melanin biosynthesis pathway, case (B) is of particular interest, although case (A) will also be studied for comparative purposes.

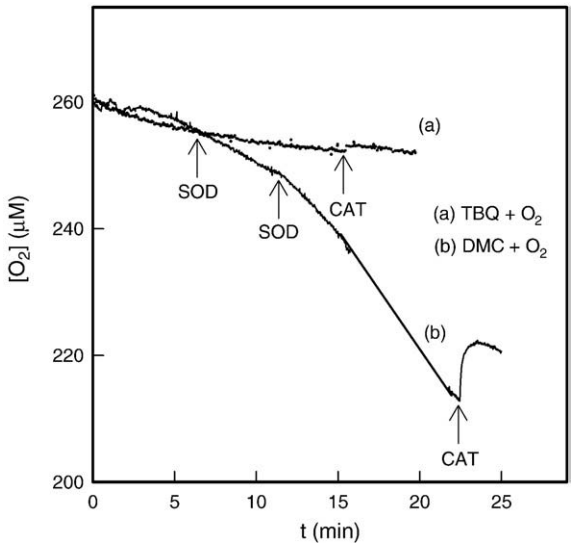

Fig. 7. Oxygen consumption during the evolution of a slightly unstable (a) and moderately unstable (b) *o*-quinone such as *o*-*tert*-butylquinone and dopaminechrome, respectively. The experimental conditions for these experiments were 30 mM phosphate buffer (pH 7.0), 25 °C and 0.1 mM of the *o*-quinones. At the time indicated, 414 U/ml of SOD was added and at the end of the reaction 930 U/ml of CAT was added.

3.4.1. Slightly unstable o-quinones

TBC was oxidised with stoichiometric sodium periodate and the *o*-quinone was extracted with ether. The mixture was acidified to pH 4.5 and, finally, the *o*-quinone was extracted with 30 mM sodium phosphate buffer (pH 7.0). The spectrum of the visible region (λ_{max} = 410 nm) was the same as that obtained by TYR or sodium periodate oxidation (see Materials and methods section). As the *o*-quinone evolves it consumes a small amount of O_2, Fig. 7 (a). Water is added slowly to the *o*-quinone, generating a trihydroxylated compound, which, in turn, may be oxidised by another molecule of *o*-quinone, generating TBC in the medium. In turn, this may be oxidised by reactions (1)–(3) and (5), generating H_2O_2 and consuming O_2. In fact, this process is minimal since the addition of water takes place very slowly. The addition of SOD should lead to increased oxygen consumption in agreement with section 3.1.1.1. However, the slowness with which water is added means that the process on the experimental time scale hardly occurs [Fig. 7 (a)].

3.4.2. Moderately unstable o-quinones

Dopamine was oxidised with stoichiometric sodium periodate, and the resulting dopaminechrome was partially extracted with ether and finally with 30 mM sodium phosphate buffer (pH 7.0). The spectrum of the visible region (λ_{max} = 480 nm) was the same as that obtained by oxidation of dopamine with periodate or TYR (see Materials and methods section), its evolution being followed by measuring the oxygen consumed, Fig. 7 (b). However, the addition of SOD led to a different behaviour from that observed when the auto-oxidation of dopamine was studied, oxygen consumption increasing due to reaction (5) between indolequinone and DHI, while the generation of $IQ^{\bullet -}$ involved the consumption of O_2. As a consequence, H_2O_2 formation increased [Fig. 7 (b)].

3.5. Non-enzymatic generation of H_2O_2 and melanogenesis

The above experiments confirm the non-enzymatic formation of H_2O_2 in the melanin biosynthesis pathway, which throws into doubt the reaction (6) proposed by other authors [6,7], and the mechanism suggested for H_2O_2 generation by TYR in [8].

The toxicity of the melanogenesis intermediates has been widely studied [22]. Experiments on melanoma cells and non-melanocytic cells have revealed that the dopachrome derivates, DHI and DHICA, have cytotoxic effects, which increase with the time of incubation and are markedly reduced by the addition of catalase to the medium, suggesting that H_2O_2 is formed during the auto-oxidation of these intermediates. In the case of DHI, it has been suggested that it may be oxidised to indolequinone and H_2O_2 [4].

The enzyme TYR can respond to oxidative stress by accumulating H_2O_2 through a variety of mechanisms. For example, in the presence of reducing substrates like L-dopa the enzyme may show a pseudoperoxidase activity [23], which would involve the consumption of H_2O_2 and the formation of dopachrome. In the presence of monophenols such as L-tyrosine, the enzyme may show a peroxygenase activity that hydroxylate L-tyrosine to L-dopa [24–26]. In both cases the H_2O_2 binds to *met*-tyrosinase to give *oxy*tyrosinase which is active towards monophenols and *o*-diphenols [2]. This occurs at low concentrations of H_2O_2 since the K_s of *met*-tyrosinase towards H_2O_2 is small [27]. In the absence of reducing substrates, TYR can consume H_2O_2 through its catalase activity, reaction (7) [24,28], but the K_m is very high (for mushroom tyrosinase K_m = 20 mM [28]); furthermore this process would lead to suicide inactivation [28]. In the case of low concentrations of H_2O_2, these processes may contribute to eliminating the H_2O_2 present in the medium.

In the case of high concentrations of H_2O_2 (10^{-3} M has been described in the literature [29]), tyrosinase cannot control the oxidative stress. Consequently, the H_2O_2 attacks a series of enzymes and coenzymes that are necessary for the melanosome (and so the melanocyte) to function. This manifests itself in diseases such as vitiligo, with its characteristic depigmented zones.

High concentrations of H_2O_2 affect the epidermal anti-oxidant defence machine and its repair mechanism. More specifically, it inactivates catalase [30–32], and oxidises the active site of thioredoxin reductase [32] and methionine sulfoxide reductase A [33–35]. It affects the enzymes tyrosine hydroxylase, phenylalanine hydroxylase and tryptophan hydroxylase, and the nitric oxide synthases [36]. High concentrations of H_2O_2 also oxidise essential cofactor [6R]-L-erythro-5,6,7,8-tetrahydrobiopterin ($6BH_4$) [37,38]. The main modifications carried out by the H_2O_2 involve the oxidation of methionine and tryptophan residues [39,40].

4. Conclusions

This work, therefore, shows that tyrosinase, which is the principal enzyme involved in the melanogenesis pathway, originates *o*-quinones from L-tyrosine and L-dopa. These *o*-quinones evolve through a series of steps (which may or may not be catalysed enzymatically) and generate melanins, which play a protective role against ultraviolet radiation. At the same time, this pathway acts as a source of H_2O_2 by means of purely chemical reactions [reactions (1)–(3) and (5)] which increase the oxidative stress. Of the three phases of melanogenesis, the results of this study suggest that highly unstable *o*-quinones (*o*-dopaquinone), which generate H_2O_2 and moderately unstable *o*-quinones (dopachrome), are formed in the proximal phase (Scheme 1A). The evolution of dopachrome towards indolequinones in the distal phase (Scheme 1B) would be responsible for the greatest accumulation of H_2O_2 in the melanosome. The polymerisation of indolequinones towards melanins [terminal phase, reaction (11)] would occur at longer times, although this phase is not studied in this work.

Acknowledgements

This paper was partially supported by grants from the Ministerio de Educación y Ciencia (Madrid, Spain) Projects BIO2006-15363 and SAF2006-07040-C02-01, from the Fundación Séneca (CARM, Murcia, Spain) Project 00672/PI/04, from the Consejería de Educación (CARM, Murcia, Spain) BIO-BMC 06/01-0004, and from FISCAM PI-2007/53. JLMM has a fellowship from the Ministerio de Educación y Ciencia

(Madrid, Spain) Reference AP2005-4721. FGM has a fellowship from Fundación Caja Murcia (Murcia, Spain).

References

[1] G. Prota, M. d'Ischia, A. Napolitano, The chemistry of melanins and related metabolites, in: J.J. Nordlund, R.E. Boissy, V.J. Hearing, R.A. King, J.P. Ortonne (Eds.), The Pigmentary System, Physiology and Pathology, Oxford University Press, Oxford, 1998, pp. 307–332.

[2] J.N. Rodriguez-Lopez, J. Tudela, R. Varon, F. Garcia-Carmona, F. Garcia-Canovas, Analysis of a kinetic model for melanin biosynthesis pathway, J. Biol. Chem. 267 (1992) 3801–3810.

[3] F. Solano, J.H. Martinez-Liarte, C. Jimenez-Cervantes, J.C. Garcia-Borron, J.A. Lozano, Dopachrome tautomerase is a zinc-containing enzyme, Biochem. Biophys. Res. Commun. 204 (1994) 1243–1250.

[4] N.P.M. Smith, S. Pavel, P.A. Riley, Mechanisms of control of the cytotoxicity of orthoquinone intermediates of melanogenesis, in: C.R. Creveling (Ed.), Role of Catechol Quinone Species in Cellular Toxicity, Tenesee, 2000, pp. 191–246.

[5] V. Roginsky, A. Alegria, Oxidation of tea extracts and tea catechins by molecular oxygen, J. Agric. Food Chem. 53 (2005) 4529–4535.

[6] D. Komarov, I. Slepneva, V. Glupov, V. Khramtsov, Superoxide and hydrogen peroxide formation during enzymatic oxidation of DOPA by phenoloxidase, Free Rad. Res. 39 (2005) 853–858.

[7] M. Mastore, L. Kholer, A.J. Nappi, Production and utilization of hydrogen peroxide associated with melanogenesis and tyrosinase-mediated oxidations of DOPA and dopamine, FEBS J. 272 (2005) 2407–2425.

[8] J.M. Wood, B. Chavan, I. Hafeez, K.U. Schallreuter, Regulation of tyrosinase by tetrahydropteridines and H_2O_2, Biochem. Biophys. Res. Commum. 325 (2004) 1412–1417.

[9] J.N. Rodríguez-López, M.A. Gilabert, J. Tudela, R.N.F. Thorneley, F. García-Cánovas, Reactivity of horseradish peroxidase compound II toward substrates: kinetic evidence for a two-step mechanism, Biochemistry 39 (2000) 13201–13209.

[10] J.N. Rodriguez-Lopez, L.G. Fenoll, P.A. Garcia-Ruiz, R. Varon, J. Tudela, R.N.F. Thorneley, F. Garcia-Canovas, Stopped-flow and steady-state study of the diphenolase activity of mushroom tyrosinase, Biochemistry 39 (2000) 10497–10506.

[11] M.M. Bradford, A rapid and sensitive method for the quantification of microgram quantities of proteins utilising the principle of protein–dye binding, Anal. Biochem. 72 (1976) 248–254.

[12] J.L. Muñoz, F. Garcia-Molina, R. Varon, J.N. Rodríguez-Lopez, F. Garcia-Canovas, J. Tudela, Calculating molar absortivities for quinones: application to the measurements of tyrosinase activity, Anal. Biochem. 351 (2006) 128–138.

[13] J.N. Rodriguez-Lopez, P. Serna-Rodriguez, J. Tudela, R. Varon, F. Garcia-Canovas, A continuous spectrophotometric method for the determination of the diphenolase activity of tyrosinase using 3,4-dihydroxymandelic acid, Anal. Biochem. 195 (1991) 369–374.

[14] J.N. Rodriguez-Lopez, J.R. Ros, R. Varon, F. Garcia-Canovas, Oxygen Michaelis constants for tyrosinase, Biochem. J. 293 (1993) 859–866.

[15] J.N. Rodriguez-Lopez, J.R. Ros, R. Varon, F. Garcia-Canovas, Calibration of a Clark-type oxygen electrode by tyrosinase-catalyzed oxidation of 4-*tert*-butylcatechol, Anal. Biochem. 202 (1992) 356–360.

[16] S.W. Weidman, E.T. Kaiser, The mechanism of the periodate oxidation of aromatic systems. a kinetic study of the periodate oxidation of catechol, J. Amer. Chem. Soc. 435 (1966) 5820–5826.

[17] M. Jimenez, F. Garcia-Carmona, F. Garcia-Canovas, J.L. Iborra, J.A. Lozano, F. Martinez, Chemical intermediates in dopamine oxidation by tyrosinase and kinetic-studies of the process, Archiv. Biochem. Biophys. 235 (1984) 438–448.

[18] L.G. Fenoll, J.N. Rodríguez-Lopez, F. Garcia-Sevilla, J. Tudela, P.A. Garcia-Ruiz, R. Varon, F. Garcia-Canovas, Oxidation by mushroom tyrosinase of monophenols generating slightly unstable *o*-quinones, Eur. J. Biochem. 267 (2000) 5864–5878.

[19] L.G. Fenoll, J.N. Rodriguez-Lopez, F. Garcia-Sevilla, P.A. Garcia-Ruiz, R. Varon, F. Garcia-Canovas, J. Tudela, Analysis and interpretation of the action mechanism of mushroom tyrosinase on monophenols and diphenols generating highly unstable *o*-quinones, Biochim. Biophys. Acta 1548 (2001) 1–22.

[20] F. Garcia-Molina, J.L. Muñoz, R. Varon, J.N. Rodriguez-Lopez, F. Garcia-Canovas, J. Tudela, An approximate analytical solution to the lag period of monophenolase activity of tyrosinase, Int. J. Biochem. Cell Biol. 39 (2007) 238–252.

[21] J.R. Ros, J.N. Rodriguez-Lopez, F. Garcia-Canovas, Tyrosinase: kinetic analysis of the transient phase and the steady-state, Biochim. Biophys. Acta 1204 (1994) 33–42.

[22] K. Urabe, P. Aroca, K. Tsukamoto, D. Mascagna, A. Palumbo, G. Prota, V. Hearing, The inherent cytotoxicity of melanin precursors: a revision, Biochim. Biophys. Acta 1221 (1994) 272–278.

[23] K.G. Strothkamp, H.S. Mason, Pseudoperoxidase activity of mushroom tyrosinase, Biochem. Biophys. Res. Commum. 61 (1974) 827–832.

[24] S. Yamazaki, C. Morioka, S. Itoh, Kinetic evaluation of catalase and peroxygenase activities of tyrosinase, Biochemistry 43 (2004) 11546–11553.

[25] M. Jimenez, F. Garcia-Carmona, Hydrogen peroxide dependent-4-*t*-butylphenol hydroxylation by tyrosinase. A new catalytic activity, Biochim. Biophys. Acta 1297 (1996) 33–39.

[26] M. Jimenez, F. Garcia-Carmona, Hydroxylating activity of tyrosinase and its dependence on hydrogen peroxide, Arch. Biochem. Biophys. 373 (2000) 255–260.

[27] R.L. Jolley, L.H. Evans, L. Makino, H.S. Mason, Oxytyrosinase, J. Biol. Chem. 249 (1974) 335–345.

[28] F. Garcia-Molina, A.N. Hiner, L.G. Fenoll, J.N. Rodriguez-Lopez, P.A. Garcia-Ruiz, F. Garcia-Canovas, J. Tudela, Mushroom tyrosinase: catalase activity, inhibition, and suicide inactivation, J. Agric. Food Chem. 53 (2005) 3702–3709.

[29] K.U. Schallreuter, Controversies in experimental dermatology, Experimen. Dermatol. 17 (2008) 141–144.

[30] J.M. Wood, K.U. Schallreuter, UVA-irradiated pheomelanin alters the structure of catalase and decrease its activity in human skin, J. Invest. Dermatol. 126 (2006) 13–14.

[31] V. Maresca, E. Flori, S. Briganti, E. Camera, M. Cario-André, A. Taieb, M. Picardo, UVA-induced modification of catalase charge properties in the epidermis is correlated with the skin phenotype, J. Invest. Dermatol. 126 (2006) 182–190.

[32] N.C. Gibbons, J.M. Wood, H. Rokos, K.U. Schallreuter, Computer simulation of native epidermal enzymes structures in the presence and absence of hydrogen peroxide (H_2O_2): potential and pitfalls, J. Invest. Dermatol. 126 (2006) 2576–2582.

[33] K.U. Schallreuter, K. Rubsan, N.C. Gibbons, D.J. Maitland, B. Chavan, C. Zothner, H. Rokos, J.M. Wood, Methionine sulfoxide reductases A and B are deactivated by hydrogen peroxide (H_2O_2) in the epidermis of patients with vitiligo, J. Invest. Dermatol. 128 (2008) 808–815.

[34] K.U. Schallreuter, K. Rubsan, B. Chavan, C. Zothner, J.M. Gillbro, J.D. Spencer, J.M. Wood, Functioning methionine sulfoxide reductases A and B are present in human epidermal melanocytes in the cytosol and in the nucleus, Biochem. Biophys. Res. Commum. 342 (2006) 145–152.

[35] K.U. Schallreuter, Functioning methionine sulfoxide reductases A and B are present in human skin, J. Invest. Dermatol. 126 (2006) 947–949.

[36] B. Thony, G. Auerbach, N. Blau, Tetrahydrobiopterin biosynthesis, regeneration and functions, Biochem. J. 347 (2000) 1–16.

[37] K.U. Schallreuter, J.M. Wood, I. Ziegler, K.R. Lemke, M.R. Pittelkow, N.J. Lindsey, M. Gutlich, Defective tetrahydrobiopterin and catecholamine biosynthesis in the depigmentation disorder vitiligo, Biochim. Biophys. Acta 1226 (1994) 181–192.

[38] K.U. Schallreuter, J.M. Wood, M.R. Pittelkow, M. Gutlich, K.R. Lemke, W. Rodl, N.N. Swanson, K. Hitzemann, I. Ziegler, Regulation of melanin biosynthesis in the human epidermis by tetrahydrobiopterin, Science 263 (1994) 1444–1446.

[39] K.U. Schallreuter, J. Moore, J.M. Wood, W.D. Beazley, E.M. Peters, L.K. Marles, S.C. Behrens-Williams, R. Dummer, N. Blau, B. Thony, Epidermal H_2O_2 accumulation alters tetrahydrobiopterin ($6BH_4$) recycling in vitiligo: identification of a general mechanism in regulation of all $6BH_4$-dependent processes? J. Invest. Dermatol. 116 (2001) 167–174.

[40] S. Hasse, N.C. Gibbons, K. Roko, L.K. Marles, K.U. Schallreuter, Perturbed 6-tetrahydrobiopterin recycling via decreased dihydriobiopterine reductase in vitiligo: more evidence for H_2O_2 stress, J. Invest. Dermatol. 122 (2004) 307–313.

4.5. CÁLCULO DE LAS ABSORTIVIDADES MOLARES DE QUINONAS: APLICACIÓN A LA MEDIDA DE LA ACTIVIDAD DE TIROSINASA.

El cálculo de los coeficientes de absortividad molar de diferentes quinonas y su aplicación a la medida de la actividad tirosinasa ha dado lugar a la siguiente publicación adjunta.

4.5.1. Título

Calculating molar absorptivities for quinones: Application to the measurement of tyrosinase activity.

4.5.2. Autores

Muñoz, J.L.; Garcia-Molina, F.; Varon, R.; Rodríguez-López, J.N.; Garcia-Cánovas, F. y Tudela, J.

4.5.3. Referencia

Analytical Biochemistry (2006) 351, 128-138.

4.5.4. Resumen

Se han calculado los coeficientes de asbortividad molar de las quinonas producidas a partir de diferentes *o*-difenoles, trifenoles y flavonoides por oxidación con periodato en exceso. La oxidación de estos sustratos por este reactivo es análoga a la que realiza tirosinasa con oxigeno molecular. El procedimiento tiene algunas ventajas respecto al método enzimático, puesto que la oxidación es prácticamente instantánea y, al no existir sustrato remanente, la estabilidad de la *o*-quinona se favorece. Los *o*-difenoles estudiados han sido: pirocatecol, 4-metilcatecol, 4-*terc*-butilcatecol, 3,4-dihidroxifenilalanina, 3,4-dihidroxifeniletilamina, ácido 3,4-dihidroxifenilacetico, ácido 3,4-dihidroxifenilpropiónico y ácido cafeico, los trifenoles han sido: pirogalol, 1,2,4-trihidroxibenceno, 6-hidroxidopa y 6-hidroxidopamina y los flavonoides: (+) catequina, (-) epicatequina y quercetina. Además, se ha estudiado la estabilidad de las *o*-quinonas generadas por oxidación de estos compuestos con periodato en defecto. Teniendo en cuenta los estudios anteriores, la actividad de tirosinasa podría medirse siguiendo la formación de la *o*-quinona en estudios de cinética rápida usando un método de flujo detenido. Sin embargo, la medida de la formación de *o*-quinona podría no ser válida para estudios de estado estacionario. Entonces, se proponen varios

métodos para seguir la actividad de tirosinasa y proceder a la caracterización cinética de la actuación de la enzima sobre estos sustratos.

Available online at www.sciencedirect.com
SCIENCE DIRECT
Analytical Biochemistry 351 (2006) 128–138
ANALYTICAL BIOCHEMISTRY
www.elsevier.com/locate/yabio

Calculating molar absorptivities for quinones: Application to the measurement of tyrosinase activity

J.L. Muñoz [a], F. García-Molina [a], R. Varón [b], J.N. Rodriguez-Lopez [a], F. García-Cánovas [a,*], J. Tudela [a]

[a] *Grupo de Investigación de Enzimología (GENZ), Departamento de Bioquímica y Biología Molecular-A, Facultad de Biología, Universidad de Murcia, E-30100 Espinardo, Murcia, Spain*

[b] *Departamento de Química-Física, Escuela Politécnica Superior, Universidad de Castilla–La Mancha, Campus Universitario, E-02071 Albacete, Spain*

Received 21 October 2005
Available online 26 January 2006

Abstract

The molar absorptivities of the quinones produced from different *o*-diphenols, triphenols, and flavonoids were calculated by generating the respective quinones through oxidation with an excess of periodate. Oxidation of these substrates by this reagent was analogous to oxidation by tyrosinase with molecular oxygen, although the procedure showed several advantages over the enzymatic method in that oxidation took place almost immediately and quinone stability was favored because no substrate remained. The *o*-diphenols studied were pyrocatechol, 4-methylcatechol, 4-*tert*-butylcatechol, 3,4-dihydroxyphenylalanine, 3,4-dihydroxyphenylethylamine, 3,4-dihydroxyphenylacetic acid, 3,4-dihydroxyphenylpropionic acid, and caffeic acid; the triphenols studied were pyrogallol, 1,2,4-benzenetriol, 6-hydroxydopa, and 6-hydroxydopamine; and the flavonoids studied were (+)catechin, (−)epicatechin, and quercetin. In addition, the stability of the quinones generated by oxidation of the compounds by $[\text{periodate}]_0/[\text{substrate}]_0 \ll 1$ was studied. Taking the findings into account, tyrosinase could be measured by following *o*-quinone formation in rapid kinetic studies using the stopped-flow method. However, measuring *o*-quinone formation could not be useful for steady-state studies. Therefore, several methods for following tyrosinase activity are proposed, and a kinetic characterization of the enzyme's action on these substrates is made.
© 2006 Elsevier Inc. All rights reserved.

Keywords: Molar absorptivities; *o*-Quinones; *o*-Diphenols; Triphenols; Flavonoids; Tyrosinase

Quinones are catalytically produced from *o*-diphenols, triphenols, and flavonoids by polyphenol oxidase (tyrosinase) (monophenol, *o*-diphenol; oxygen-oxidoreductase; EC 1.14.18.1), a binuclear copper cluster containing monooxygenase ubiquitously present in biological systems [1,2]. Tyrosinase catalyzes the oxidation of *o*-diphenols (*o*-diphenolase or catecholase activity) to the corresponding *o*-quinones by the consumption of molecular oxygen. It may also catalyze the regioselective orthohydroxylation of monophenols to catechols (monophenolase or cresolase activity) and their subsequent oxidation to *o*-quinones. Periodate, like tyrosinase, oxidizes *o*-diphenols to *o*-quinones but does not hydroxylate monophenols to *o*-diphenols [3]. This reagent has been used in several studies for comparison with tyrosinase and to characterize the *o*-diphenol oxidation products [4]. In all cases, The resulting quinones may undergo nonenzymatic autopolymerization to produce colored compounds [5–7]. Browning in plant materials is associated with the enzymatic oxidation of phenolic compounds [9,10].

Several methods have been used to measure tyrosinase activity, including (i) measuring the consumption of oxygen [11]; (ii) using nucleophilic reagents that trap the *o*-quinones and generate chromophoric adducts [12–15]; (iii) using

* Corresponding author. Fax: +34 968 363 963.
E-mail address: canovasf@um.es (F. García-Cánovas).

0003-2697/$ - see front matter © 2006 Elsevier Inc. All rights reserved.
doi:10.1016/j.ab.2006.01.011

reducing agents such as ascorbic acid (AH_2)[1] [16] and NADH + H^+ [17], measuring their disappearance as a result of oxidation by the quinones; and (iv) directly measuring the formation of *o*-quinones or their products as they evolve to form aminochromes [18–20].

In a classic work, Waite [21] established an enzymatic method using tyrosinase to calculate the *o*-quinone molar absorptivities of several *o*-diphenols. The method consists of using large quantities of enzyme and very small quantities of substrate for the enzyme to work with a first-order kinetic and high-rate constant V^D_{max}/K^D_m. In this way, the *o*-diphenol can be completely transformed into *o*-quinone in a time scale of minutes, a transformation that is taken to have occurred when the variation of absorbance with time becomes zero.

However, this method has two disadvantages: (i) the long time period (minutes) needed to transform all of the *o*-diphenol into *o*-quinone and (ii) the large quantity of enzyme needed to ensure the highest possible first-order constant (V^D_{max}/K^D_m) and for t_{99} (i.e., the time needed for 99% of the substrate to be consumed) not to be too great.

In this work, we propose an alternative method based on the oxidation of the substrate by an excess of sodium periodate, conditions under which the reaction is instantaneous and the molar absorptivity can be determined more reliably. An additional advantage is the lower cost of the method.

We also studied the stability of quinones and the possibility of measuring tyrosinase activity. Furthermore, in the case of substrates with unstable quinones, one can use AH_2, which reduces the quinones instantaneously; therefore, the initial rate of the enzyme action can be calculated in some cases from the rate at which AH_2 disappears [16]. To characterize a wide range of substrates to be able to study structure–activity, two new measuring methods, both of which use AH_2, are proposed. Both methods are chronometric and measure the time taken for a given quantity of AH_2 to be consumed. A kinetic study is carried out permitting the initial rate values (V_{ss}) to be calculated, making it possible to kinetically characterize the substrates.

Materials and methods

Reagents

The substrates used were pyrocatechol (CAT), 4-methylcatechol (4-MeCAT), 4-*tert*-butylcatechol (TBC), 3,4-dihydroxyphenylalanine, 3,4-dihydroxyphenylethylamine, 3,4-dihydroxyphenylacetic acid (DHPAA), 3,4-dihydroxyphenylpropionic acid (DHPPA), pyrogallol, 1,2,4-benzenetriol, 6-hydroxydopa, 6-hydroxydopamine, (+)catechin [(+)CQ], (−)epicatechin [(−)EQ], and quercetin, all of which were obtained from Sigma (USA) or Fluka (Switzerland). The sodium periodate was obtained from Scharlau (Spain). Stock solutions of the reducing substrates were prepared in 0.15 mM phosphoric acid to prevent autooxidation. The buffer used was sodium phosphate (pH 7.0, 30 mM).

Enzyme source

Mushroom tyrosinase (8300 U mg^{-1}) was purified by Duckworth and Coleman's procedure [22], but with two additional chromatographic steps [23]. Enzyme solution was passed through a column (2.0 × 30 cm) of Sephadex G-100 (Pharmacia) equilibrated on 0.01 M sodium phosphate (pH 7.0). Samples showing tyrosinase activity were further purified by fast performance liquid chromatography (FPLC) anion exchange chromatography on a Mono-Q HR 5/5 column (Pharmacia) equilibrated with 0.01 M sodium phosphate buffer (pH 7.0) and eluted with sodium chloride (0–0.5 M gradient). Purified enzyme was desalted with Sephadex G-25 (Pharmacia) into ultrapure water and stored in liquid nitrogen. Protein concentration was determined by Bradford's method [24] using bovine serum albumin as standard.

Spectrophotometric assays

Absorption spectra were recorded in a UV–visible PerkinElmer Lambda 2 spectrophotometer interfaced on-line with a PC-compatible 486DX microcomputer with a scanning speed of 60 nm/s. The temperature was controlled at 25 °C using a Haake D16 circulating water bath with a heater/cooler and was checked using a Cole–Parmer digital thermometer with a precision of ±0.1 °C. Kinetic assays were also carried out with the above instruments by measuring the appearance of the products in the reaction medium. Reference cuvettes contained all of the components, except the substrate, with a final volume of 1 ml. All of the assays were carried out under saturating conditions of tyrosinase by molecular oxygen (0.26 mM oxygen in the assay medium) [25].

Determination of the initial rate

Spectrophotometric recording of quinone

When the reaction product was measured, the V_{ss} values were determined at short reaction times from triplicate measurements at each $[S]_0$. From experiments studying the dependence on $[S]_0$, V_{max} and K_m were obtained by nonlinear regression to a plot of V_{ss} against $[S]_0$ by using the SigmaPlot program for Windows (version 8.0) [26]. The only substrate monitored using this method was TBC at 400 nm.

Measurement of the AH_2

If the AH_2 and substrate spectra do not totally overlap, it is possible to follow the enzyme activity at a wavelength

[1] *Abbreviations used:* AH_2, ascorbic acid; CAT, pyrocatechol; 4-MeCAT, 4-methylcatechol; TBC, 4-*tert*-butylcatechol; DHPAA, 3,4-dihydroxyphenylacetic acid; DHPPA, 3,4-dihydroxyphenylpropionic acid; (+)CQ, (+)catechin; (−)EQ, (−)epicatechin; FPLC, fast performance liquid chromatography; *o*-TBC, *o*-*tert*-butylquinone.

corresponding to the UV region at which AH_2 absorbs by monitoring the time course of its disappearance [16].

Chronometric methods

Enzymatic activity was determined spectrophotometrically using the methods described subsequently in Results and discussion. The only condition is that there must be a measurable increase in absorbance (due to product formation) once the AH_2 is consumed. Preliminary experiments were carried out in the absence of AH_2 in a tyrosinase/O_2-reducing substrate system, making a spectrophotometric scan to identify in which zone of the spectrum, particularly the visible zone, the greatest changes in absorbance occurred. The wavelengths used were 480 nm for dopamine, 400 nm for DHPAA, and 440 for (−)EQ. In other cases, the spectrophotometric recording was followed at a wavelength of the UV region, measuring the absorbance decrease of the AH_2 and the sharp increase in the product absorbance. The wavelengths used were 265 nm for 4-MeCAT, 270 nm for (+)CQ, and 260 nm for DHPPA. In the case of phosphate buffer, the pH was 7.0 at 25 °C. The concentrations of $[AH_2]_0$ and $[E]_0$ were 15 μM and 2 nM, respectively. The concentrations of the substrates varied in the rank (K_m/5 to 5 K_m).

The absorbance data were analyzed according to Beer's law using the standard least-squares linear regression program. Molar absorptivities at various λ_{max} values were estimated for a known pathlength of 1 cm. The minimal acceptable coefficient of determination (r^2) was taken as 0.995. Data yielding coefficients less than this were due to pipetting errors and redone. With this precaution, the 95% confidence limits for the molar absorptivity estimates were $\leqslant$5%.

Results and discussion

To determine the molar absorptivities of the quinones obtained from the tyrosinase substrates studied, the substrates were oxidized by using the following ratios: $[\text{periodate}]_0/[\text{substrate}]_0 \gg 1$ and $[\text{periodate}]_0/[\text{substrate}]_0 \ll 1$. The quinones generated were scanned several times to determine their λ_{max} and stability.

Oxidation of the substrates by an excess of periodate

The substrates were oxidized instantaneously by a 10- to 100-fold excess of sodium periodate [3] so that all of the quinone corresponding to a given concentration of reagent was generated. This allowed the molar absorptivity to be calculated with little error because, with no nucleophiles in the medium, the quinone can react only (i) with the H_2O that acts as weak nucleophile, (ii) with itself, or (iii) with the product resulting from adding water [6]. Whatever the case, reaction with the originating substrate is avoided [3,27].

In this work, we distinguish among three types of quinones: (i) quinones that are very stable, *o-tert*-butylquinone (*o*-TBC), those that tautomerize rapidly to stable *p*-quinones (6-hydroxydopaminoquinone to 4-hydroxy *p*-dopaminequinone and 6-hydroxydopaquinone to 4-hydroxy *p*-dopaquinone) [8,28] or that evolve very rapidly to generate very stable compounds (e.g., *o*-dopaquinone to dopachrome and *o*-dopaminequinone to dopaminechrome) [5,29]; (ii) unstable quinones that evolve slowly with a clear stoichiometry, generating an isosbestic point (e.g., CAT); and (iii) unstable quinones that evolve according to a nondefined stoichiometry and that therefore do not generate an isosbestic point [e.g., (−)EQ)].

Fig. 1 shows the evolution spectra of quinones generated by oxidation with an excess of periodate. Note how in the figure the successive scans of the *o*-TBC hardly vary and show great stability. The left inset shows the evolution of the catechol quinone by means of a defined stoichiometry, generating an isosbestic point. The right inset depicts the quinone generated by the oxidation of (−)EQ, with the absence of an isosbestic point indicating a nondefined stoichiometry.

Based on the recordings of Fig. 1, an experimental design can be carried out to determine the molar absorptivities of the different quinones. The design consists of the following steps:

Step 1: Choosing the measurement wavelength (λ). In the case of the stable quinones, this is obviously their λ_{max} (Fig. 1). In the case of those that evolve and generate an isosbestic point, it is the λ_i (isosbestic wavelength) or their λ_{max} (Fig. 1, left inset). When no isosbestic point is generated (Fig. 1, right inset), λ_{max} is selected, in which case special care must be taken to use low substrate concentrations so as to minimize the second-order reaction between the quinones and to make short time measurements.

Step 2: Carrying out a series of experiments with different substrate concentrations and recording the variations in absorbance at the chosen λ.

Step 3: Fitting the data obtained in step 2 to a Beer–Lambert equation by linear regression:

$$A = \varepsilon c l, \tag{1}$$

where A is the estimate of absorbance at a given wavelength, ε is the molar absorptivity (M^{-1} cm^{-1}), c is the concentration (in M), and l is the pathlength of light through the cuvette (1 cm).

Fig. 2 shows the variations in absorbance using different concentrations of substrate, with one example for each type of quinone. Fig. 2, the left inset, and the right inset show oxidation of TBC, CAT, and (−)EQ, respectively. From the absorbance values obtained for the different substrate concentrations, we can construct Fig. 3 to calculate the molar absorptivity (Table 1).

Although the method used in this study for this purpose is rigorous and reliable, it cannot be ensured that the measurement of tyrosinase activity is accurate given that in the

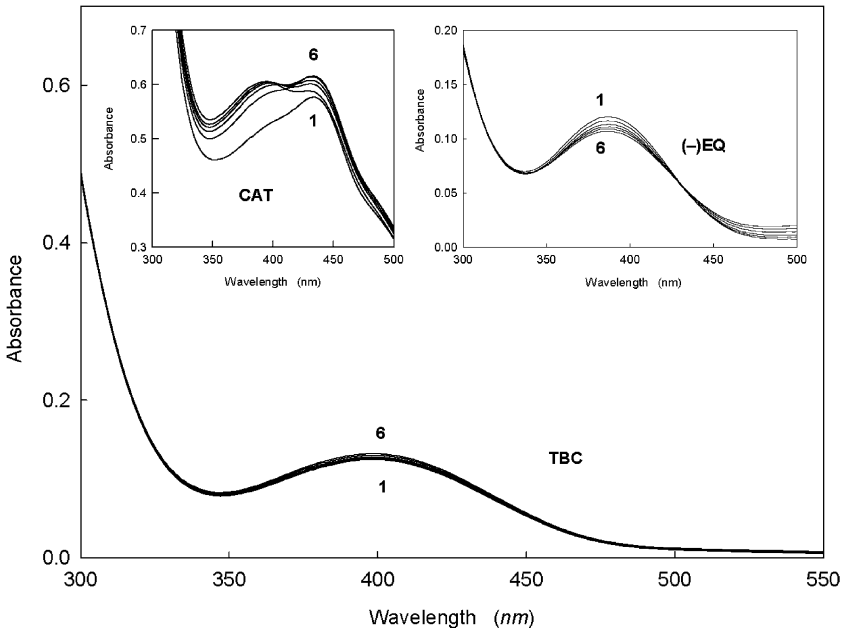

Fig. 1. Spectrophotometric plots of the oxidation of several substrates by an excess of sodium periodate. The lower part of the figure shows a plot of the oxidation of 110 μM TBC by 2.5 mM $NaIO_4$. In all cases, the experimental conditions were 30 mM phosphate buffer (pH 7.0) at 25 °C, and the plots were made every 50 s, starting at 1 and finishing at 6. The left inset shows spectrophotometric plots of the oxidation of 75 μM CAT by 1 mM $NaIO_4$. The left inset shows spectrophotometric plots of the oxidation of 125 μM (−)EQ by 1 mM $NaIO_4$.

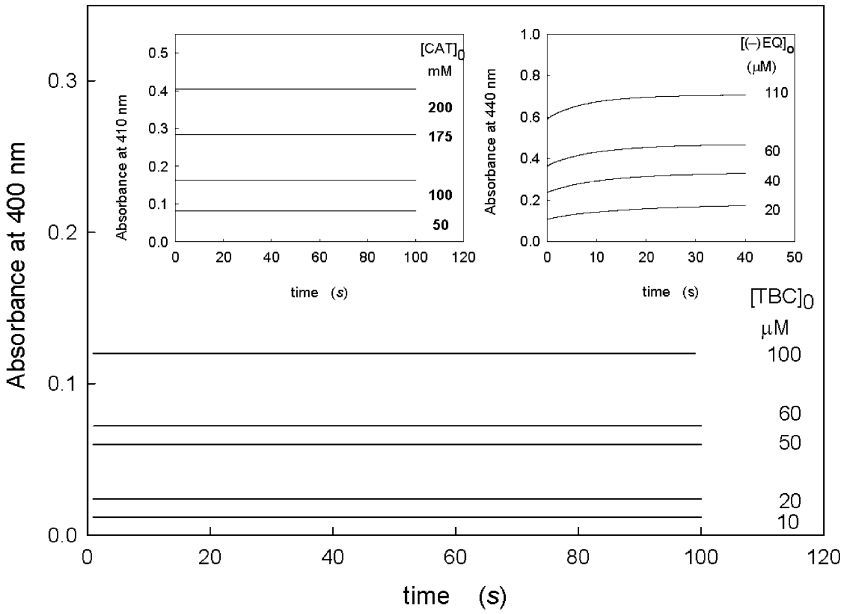

Fig. 2. Variation of absorbance with time during the oxidation of different substrates by excess of sodium periodate. The lower part of the figure shows plots at $\lambda_{max} = 400$ nm of the evolution of quinone at different concentrations of TBC oxidized by 2.5 mM $NaIO_4$. The left inset shows plots of the evolution of quinone at $\lambda_i = 410$ nm of the isosbestic point during the oxidation of CAT by 2.5 mM $NaIO_4$. The right inset shows plots of the evolution of quinone at $\lambda_{max} = 440$ nm during the oxidation of (−)EQ by 1.9 mM $NaIO_4$.

enzymatic assay conditions $[S]_0 \gg [E]_0$, and substrate variations are small when initial steady-state rates (V_{ss}) are measured, so that whenever the enzymatic activity is measured, $[S]_0 \gg [\text{quinone}]_0$. Because of this, the quinone stability should be studied under these conditions by studying how the different substrates are oxidized with a deficiency of periodate (10- to 100-fold less).

Oxidation with deficiency of periodate

Fig. 4 shows the spectrophotometric records of the quinones formed in the medium with $[\text{periodate}]_0 \ll [S]_0$. In these conditions, three types of quinones are formed: (i) quinones that are stable in the presence of substrate, as in the case of TBC (Fig. 4A, right inset); (ii) quinones that

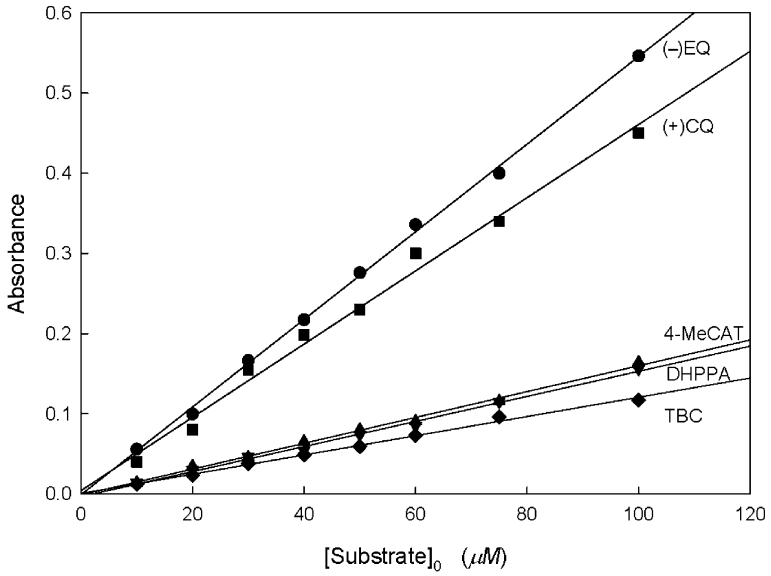

Fig. 3. Representation of the absorbances obtained in the experiments of Fig. 2 with some of the substrates studied. In all cases, the experimental conditions were 2.5 mM $NaIO_4$ and 30 mM phosphate buffer (pH 7.0) at 25 °C. The substrate concentrations are indicated in the figure, and the wavelengths for the substrates were as follows: (−)EQ, $\lambda = 440$ nm; (+)CQ, $\lambda = 350$ nm; $[NaIO_4]_0/[(+)CQ]_0 = 40/1$; 4-MeCAT, $\lambda = 400$ nm; DHPPA, $\lambda = 400$ nm; TBC, $\lambda = 400$ nm.

Table 1
Molar absorptivities of quinones generated during the oxidation of different substrates of tyrosinase by excess of periodate

Substrate	λ_{max} (nm)	$\varepsilon_{\lambda max}$ (M^{-1} cm^{-1})	λ_i (nm)	ε_i (M^{-1} cm^{-1})
Caffeic acid	495	2062		
CAT	410	1623	430	560
(+)CQ	436	4800	350	3125
DHPAA	395	1601		
DHPPA	400	1462	420	1137
Dopamine	480	3300		
(−)EQ	440	5482		
3,4-Dihydroxyphenylalanine	475	3600		
	310	9750		
4-MeCAT	400	1638	356	635
Pyrogallol	446	3000	473	2383
TBC	400	1200		
6-Hydroxydopa	270	9900		
	485	2500		
6-Hydroxydopamine	490	1742	360	200
1,2,4-Benzenetriol	480	1387	388	388
Quercetin	330	8187		

Note. The isosbestic points (λ_i) correspond to experiments using an excess of sodium periodate with respect to substrate.

evolve and generate an isosbestic point, as in the cases of DHPPA (Fig. 4A) and 4-MeCAT (Fig. 4B); and (iii) quinones that evolve but that show no isosbestic point, as in the case of DHPAA (Fig. 4B, right inset).

By means of these experiments, it can be deduced that the molar absorptivities when $[\text{periodate}]_0 \gg [S]_0$ are valid for determining tyrosinase activity on substrates that generate group (i) quinones. However, in the case of substrates that generate group (ii) quinones, the wavelength (λ) should be displaced toward the isosbestic point and the absorptivity should be calculated at this wavelength (λ_i). The values obtained are shown in Table 1 (note that the molar absorptivity values are very small near the isosbestic point). It is not possible to correctly measure V_{ss} for the action of tyrosinase on the substrates of group (iii) because when the substrate concentration is increased (as is necessary for the kinetic characterization) the quinone evolves more rapidly (Fig. 4B, right inset).

Application to the measurement of tyrosinase activity

The kinetic reaction mechanism of tyrosinase on different types of substrate is very complex [30], and because the reaction products are quinones (most of which are unstable), the experimental studies are difficult to design. Reliable measurement methods are a prerequisite for such studies, and it is very important to study the stability of the product (quinone), as we describe below.

Fig. 5 shows the stability of the TBC quinone generated by a deficiency of periodate. In the case of TBC, measurements are made at λ_{max} (400 nm), whereas in the case of 4-MeCAT, they are made at the isosbestic point (Fig. 5, left inset). Tyrosinase activity can be followed quantitatively in the case of substrates that produce stable quinones (TBC). The representation of V_{ss} versus $[S]_0$ is hyperbolic, and the parameters that characterize the action of the enzyme on this substrate ($V_{max} = 3.20 \pm 0.21$ μM s^{-1} and $K_m = 1.60 \pm 0.19$ mM) can be obtained by nonlinear regression (Table 2).

In the case of 4-MeCAT, the left inset of Fig. 5 shows the recordings of absorbance versus time at the λ of the isosbestic point (λ_i). In this case, the isosbestic point should be maintained at all concentrations of the substrate used. However, this does not occur, as can be seen in Fig. 4B and the left inset of Fig. 4B. A similar effect happens with

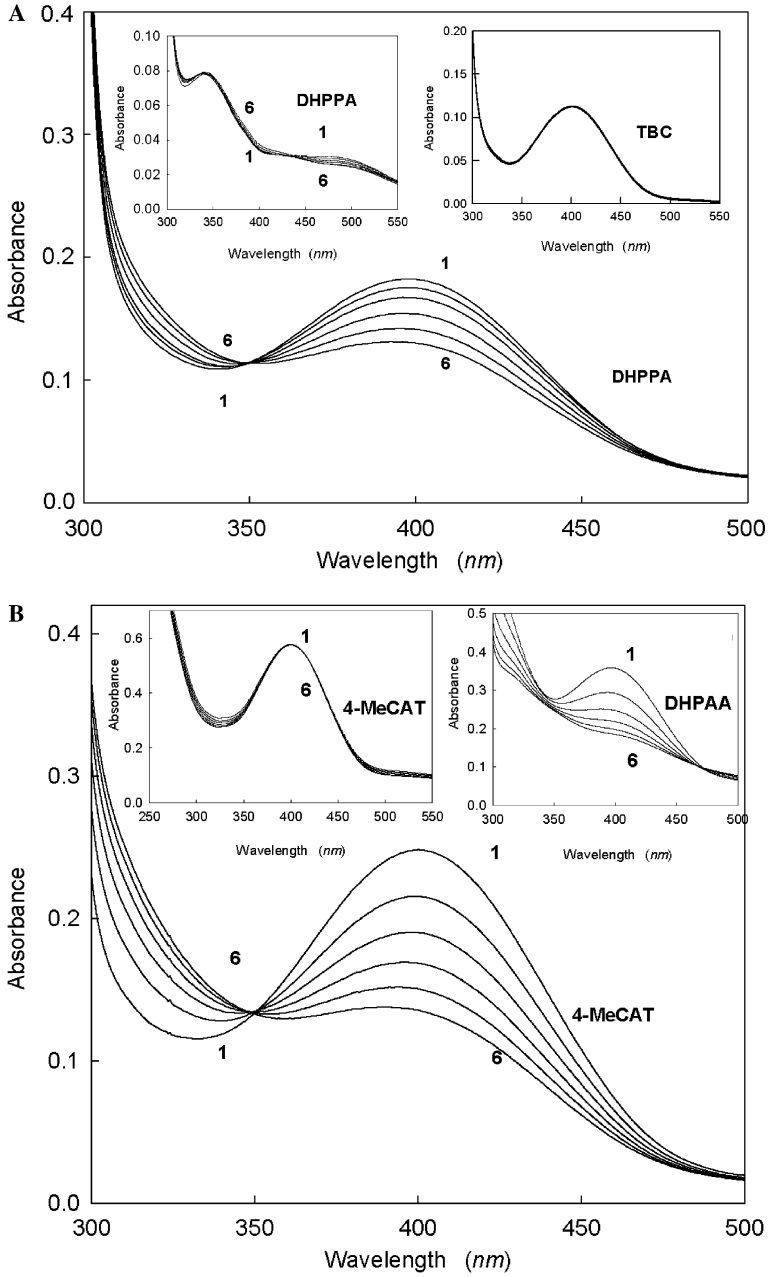

Fig. 4. Spectrophotometric plots of the oxidation of different substrates by a deficiency of periodate. The experimental conditions were 30 mM phosphate buffer (pH 7.0) at 25 °C. In all cases, the plots were made every 50 s, starting at 1 and finishing at 6. The lower parts of panels A and B show unstable quinones generating an isosbestic point. (A) Plots of the oxidation of 5 mM DHPPA by 120 μM $NaIO_4$. The left inset shows plots of the oxidation of 0.2 mM DHPPA by 27 μM $NaIO_4$. The right inset shows plots of the oxidation of 1 mM TBC by 95 μM $NaIO_4$ (stable quinones). (B) Plots of the oxidation of 5 mM 4-MeCAT by 150 μM $NaIO_4$. The left inset shows plots of the oxidation of 0.4 mM 4-MeCAT by 225 μM $NaIO_4$. The right inset shows plots of the oxidation of 5 mM DHPAA by 215 μM $NaIO_4$ (unstable quinones not generating an isosbestic point).

DHPPA (Fig. 4A and left inset of Fig. 4A) because, at low substrate concentrations, the quinone follows other reactions besides the one with the substrate (e.g., the addition of water and subsequent oxidation by another molecule of quinone).

In the case of substrates giving rise to quinones that do not generate an isosbestic point, the formation of quinone cannot be used as a reliable measurement. This is clear in the right inset of Fig. 5, which corresponds to DHPAA. An apparent inhibition by excess of substrate is observed when V_{ss} is represented versus $[S]_0$ due to the destabilizing effect of the substrate on the quinone (Fig. 6). A similar effect is observed when 4-MeCAT (Fig. 6 inset) is studied. This has led some authors to propose kinetic mechanisms, which imply an inhibition by excess of substrate [31–33]. In general, for all of the substrates that originate unstable quinones or that do not stabilize through reactions with a defined stoichiometry, other methods should be used.

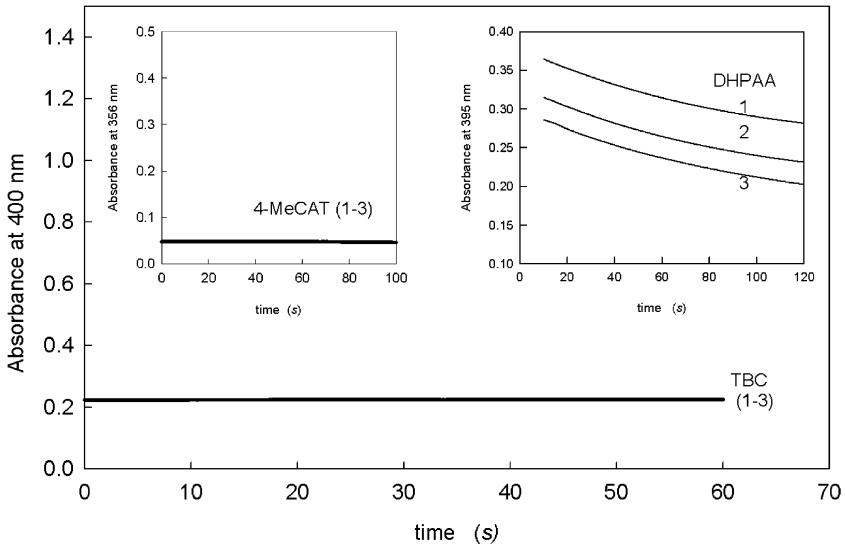

Fig. 5. Variations in absorbance during the oxidation of different substrates by a deficiency of periodate. The lower part of the figure shows plots at the λ_{max} of the evolution of the quinone at different concentrations of TBC (200, 500, and 700 μM) that is oxidized by 180 μM $NaIO_4$ (plots 1–3). The left inset shows plots at the λ_i of the quinone generated during the oxidation of 4-MeCAT (8, 10, and 12 mM) by 80 μM $NaIO_4$ (plots 1–3). The right inset shows plots at the λ_{max} of the quinone generated during the oxidation of DHPAA (1, 1.25, and 2 mM) by 235 μM $NaIO_4$ (plots 1, 2, and 3, respectively). The experimental conditions were 30 mM phosphate buffer (pH 7.0) at 25 °C.

Table 2
Kinetic constants characterizing the reaction of tyrosinase on different substrates

Substrate	Method used	λ (nm)	K_m (mM)	k_{cat} (s^{-1})
CAT	AH_2 disappearance	262	0.10 ± 0.04	878 ± 75
4-MeCAT	Alternative chronometric	265	0.15 ± 0.03	842 ± 25
(−)EQ	Chronometric	440	0.51 ± 0.14	706 ± 150
TBC	Quinone formation	400	1.60 ± 0.19	641 ± 42
DHPPA	Alternative chronometric	260	0.70 ± 0.11	622 ± 25
DHPAA	Chronometric	400	1.20 ± 0.11	445 ± 25
Dopamine	Chronometric	480	0.62 ± 0.19	439 ± 75
(+)CQ	Alternative chronometric	270	0.38 ± 0.11	355 ± 90

Note. The experimental data were done in 30 mM phosphate buffer (pH 7.0) at 25 °C.

For example, a reductant (in our case AH_2) can be used in the medium to prevent the evolution of the quinone that is the product of the enzyme's action on the substrate. Such assays must be carried out bearing the following three things in mind, depending on the spectra of the substrate and of the AH_2, as is shown in Figs. 7B–D.

Case 1

If the substrate and AH_2spectra differ (i.e., there is a zone where they do not overlap), the reaction is followed by measuring the disappearance of the AH_2. In the AH_2 and CAT spectra shown in the left inset of Fig. 7B, $\lambda = 262$ nm is chosen because this is where there is no overlap. Fig. 7B shows some recordings that are useful for determining V_{ss}, measuring at a wavelength (λ) where the substrate does not absorb to prevent saturation of the photomultiplier. This method has been described previously [16], and because the stoichiometry of the reaction (o-quinone + $AH_2 \rightarrow D + A$) is already known, this is adequate for the kinetic characterization ($V_{max} = 0.26 \pm 0.02$ μM s^{-1} and $K_m = 0.10 \pm 0.04$ mM) (Fig. 7B, right inset, and Table 2).

Chronometric method

For substrates whose spectra overlap that of AH_2, we suggest a chronometric method consisting of calculating the time needed by the enzyme to consume a given amount of AH_2 in its action on the substrate. The spectrophotometric recording can be made in two ways, depending on the extent to which the substrate and AH_2 spectra overlap. However, the underlying theory is the same in both cases, as we see below.

Case 2a

In this case, the substrate and AH_2 spectra overlap totally and the substrate molar absorptivity is very high. The appearance of product (quinone) is measured at a wavelength (λ) of the visible region where neither the substrate nor the AH_2 absorbs. A clear example of this is DHPAA (Fig. 7C. left inset), in which case it is necessary to determine the time taken for a given amount of AH_2 to be consumed during its reaction with the quinone generated as the enzyme acts on the substrate. For this, a wavelength (λ) where the quinone absorbs is chosen (Fig. 7C). This time corresponds to the point at which two straight lines intersect: one of the constant absorbance corresponding to the consumption of AH_2 and the other corresponding to the spectrophotometric signal produced when all of the AH_2 is consumed. This time, τ, is related to V_{ss}, the initial rate of the enzyme, and the concentration of the AH_2 according to

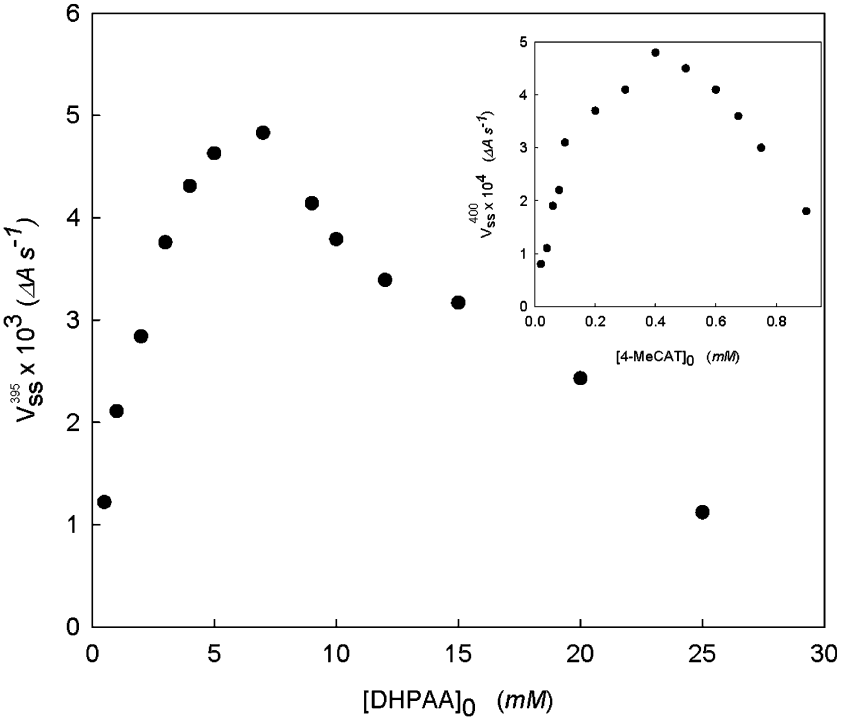

Fig. 6. Representation of the steady-state rates versus substrate concentration during the oxidation of DHPPA by tyrosinase. The inset shows a representation of the steady-state rates during the oxidation of 4-MeCAT by tyrosinase. In both cases, the experimental conditions were 30 mM phosphate buffer (pH 7.0) at 25 °C and $\lambda = 400$ nm.

$$V_{ss} = [AH_2]/\tau. \quad (2)$$

Eq. (2) is easily demonstrated if the following mass balance is taken into account. The quantity of matter, Q, generated by the enzyme acting on the substrate in time t is

$$Q = V_{ss}\ t, \quad (3)$$

where V_{ss} is the steady-state rate:

$$D + O_2 \xrightarrow[\text{tyrosinase}]{V_{ss}} Q + H_2O. \quad (4)$$

Then in the presence of AH_2 and through the reaction

$$Q + AH_2 \rightarrow D + A, \quad (5)$$

Q is reduced, D is regenerated, and AH_2 is consumed so that at any reaction time the following relationship is fulfilled:

$$V_{ss}\ t = [AH_2]_0 + [Q]. \quad (6)$$

Because at $t = \tau$ (the lag time) it is observed that $[Q] = 0$, from Eq. (6) we obtain Eq. (2).

From the values of τ and $[AH_2]_0$, the V_{ss} at different substrate concentrations can be calculated and the values can be fitted by nonlinear regression to give $V_{max} = 1.02 \pm 0.06\ \mu M\ s^{-1}$ and $K_m = 1.20 \pm 0.11$ mM (Fig. 7C, right inset, and Table 2). A similar method has been proposed for characterizing the action of HRPC on monophenols, *o*-diphenols, and anilines [34–36].

Case 2b

The overlap of the substrate and AH_2 spectra is not total, and so an alternative chronometric method is proposed. This consists of following the disappearance of the AH_2 at a wavelength (λ) of the UV region far from the maximum. When the AH_2 is consumed, there is a sharp change in the absorbance because the appearance of quinone shows increased absorbance. In this way, two straight lines are recorded—one decreasing and the other increasing, with the intersection corresponding to $t = \tau$. In this time, a given $[AH_2]_0$ is consumed, thereby fulfilling Eq. (2). This method can be illustrated by the characterization of the flavonoid (+)CQ (Fig. 7D). Note how the spectra of (+)CQ and AH_2 do not overlap totally (Fig. 7D, left inset), and so a λ at 270 nm is chosen. From the intersection of the two lines (Fig. 7D), τ can be determined, and because $[AH_2]_0$ is known, the values of V_{ss} can also be calculated according to Eq. (2). The values of V_{ss},when fitted to $[S]_0$ (as shown in Fig. 7D, right inset), provide the kinetic parameters $V_{max} = 1.60 \pm 0.18\ \mu M\ s^{-1}$ and $K_m = 0.38 \pm 0.11$ mM (Table 2). In general, the results obtained by using these methods are similar to those obtained by measuring the oxygen consumption [23].

Advantages and disadvantages

The advantages and disadvantages of the different measuring methods in the presence of AH_2 and the most suitable method to choose are detailed below:

(i) When the substrate and AH_2 spectra are separate, the best method is that which follows the disappearance of AH_2 because to determine V_{ss} it is not necessary

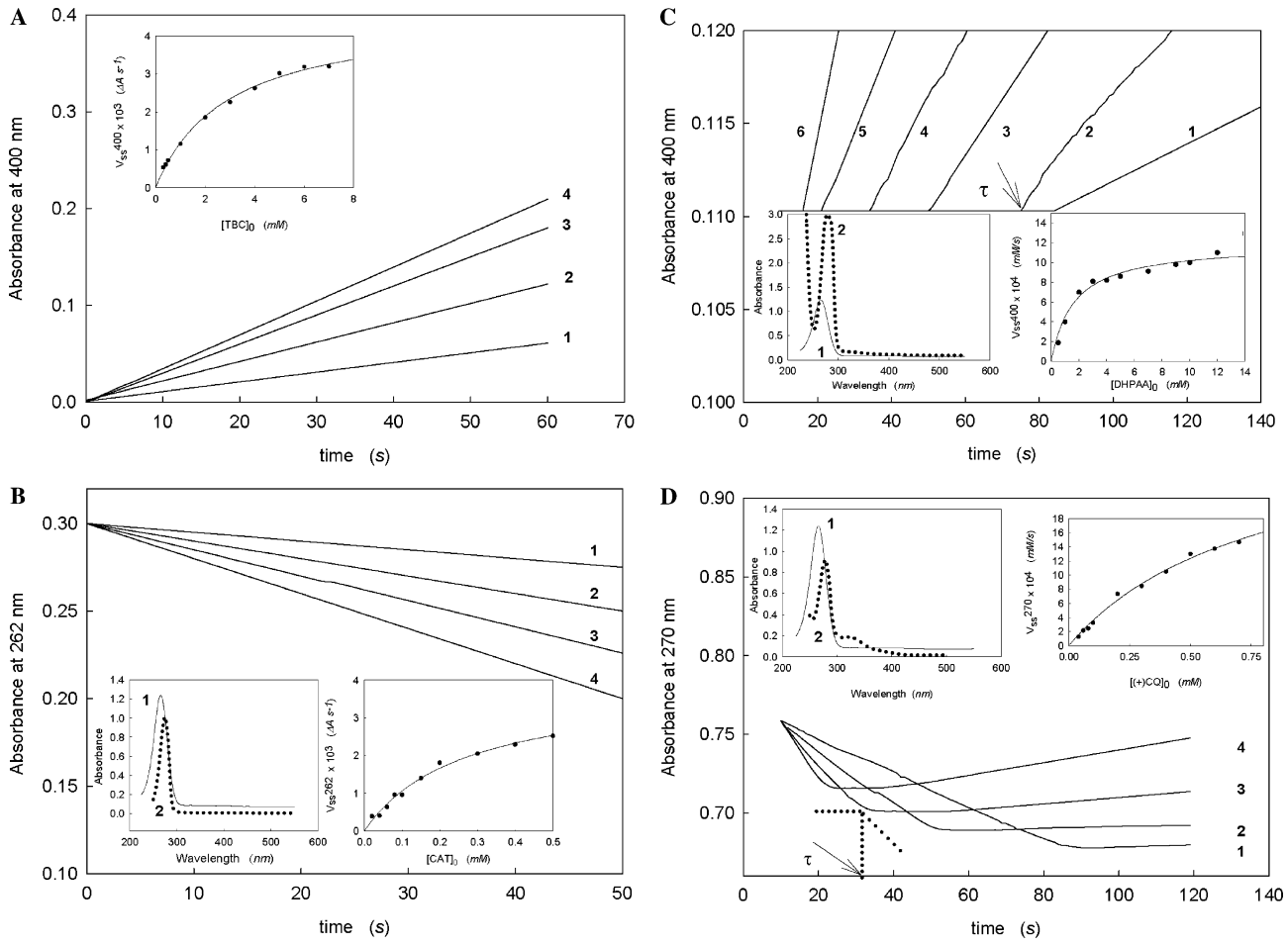

Fig. 7. Tyrosinase measuring methods. (A) Characterization of an *o*-diphenol (TBC) whose oxidation gives rise to a stable quinone, with spectrophotometric plots at $\lambda = 400$ nm of the formation of quinone. The experimental conditions were 30 mM phosphate buffer (pH 7.0) at 25 °C, and the concentrations of TBC were 1 mM (1), 2 mM (2), 4.5 mM (3), and 6 mM (4). The concentration of enzyme was 2.5 nM. The inset shows a representation of V_{ss} versus $[TBC]_0$. (B) Characterization of an *o*-diphenol (CAT) whose spectrum does not overlap that of AH_2, with spectrophotometric plots at $\lambda = 262$ nm of the disappearance of AH_2. The experimental conditions were pH 7.0 at 25 °C, $[AH_2]_0 = 27$ μM, and $[E]_0 = 0.15$ nM, and the concentrations of CAT were 0.05 mM (1), 0.1 mM (2), 0.15 mM (3), and 0.3 mM (4). The left inset shows spectra of AH_2 (1) and CAT (2). The concentrations were 0.11 and 0.62 mM, respectively. The right inset shows a representation of V_{ss} versus $[CAT]_0$. (C) Characterization of an *o*-diphenol (DHPAA) by the chronometric method, with spectrophotometric plots at $\lambda = 400$ nm for the formation of quinone after the consumption of AH_2 and determination of τ. The experimental conditions were pH 7.0 at 25 °C, $[AH_2]_0 = 15$ μM, and $[E]_0 = 1.15$ nM, and the concentrations of DHPAA were 0.2 mM (1), 0.25 mM (2), 0.75 mM (3), 1.25 mM (4), 2 mM (5), and 2.5 mM (6). The left inset shows spectra of AH_2 (1) and DHPAA (2). The concentrations were 0.11 and 1 mM, respectively. The right inset shows a representation of V_{ss} versus $[DHPAA]_0$. (D) Characterization of an *o*-diphenol [(+)CQ] by the alternative chronometric method, with spectrophotometric plots at $\lambda = 270$ nm of the formation of quinone after the consumption of AH_2. The absorbance increases as a result of the presence of quinone, and the intersection of the straight lines gives τ. The experimental conditions were pH 7.0 at 25 °C, $[AH_2]_0 = 7.75$ μM, and $[E]_0 = 2.25$ nM, and the concentrations of (+)CQ were 0.05 mM (1), 0.075 mM (2), 0.1 mM (3), and 0.12 mM (4). The left inset shows spectra of AH_2 (1) and (+)CQ (2). The concentrations were 0.11 and 0.19 mM, respectively. The right inset shows a representation of V_{ss} versus $[(+)CQ]_0$.

to know the absolute concentration of AH_2; it is only necessary to know the molar absorptivity ($\lambda =$ 265 nm, pH 7.0, and $\varepsilon = 11{,}170\ M^{-1}\ cm^{-1}$).

(ii) When the substrate and AH_2 spectra overlap completely, it is necessary to use the chronometric method.

(iii) When the spectra do not overlap completely, the alternative chronometric method should be used.

(iv) In both methods (ii) and (iii), the absolute concentration of the AH_2 must be known.

(v) In all three methods, care must be taken with the blanks originated by the spontaneous oxidation of the substrates and the AH_2. To minimize this effect, the substrates should be prepared in dilute phosphoric acid and the assays should be carried out quickly (40–120 s).

To summarize, we have proposed a rapid method for determining the molar absorptivities of the quinones formed from tyrosinase substrates based on oxidation by an excess of periodate. The method is inexpensive because it does not use enzyme. In addition, the stability of the quinones generated by oxidation with a deficiency of perio-

date was studied in the presence of substrate. Based on the above studies, we propose measuring *o*-quinones in rapid kinetic studies using the stopped-flow method and three different spectrophotometric methods not involving *o*-quinone measurement to measure tyrosinase activity in the steady state: (i) measurement of the variation in absorbance of AH_2 with time, (ii) measurement of the time necessary for a given quantity of AH_2 to be consumed (chronometric method), and (iii) measurement of the time when the sharp change in absorbance occurs (alternative chronometric method).

Acknowledgments

This work was supported in part by grants from the MCYT (Spain) (project AGL 2002-01255 ALI), from the Fundación Séneca, and from the Fundación Séneca/Consejería de Educación y Universidades (Murcia) (project 00672/PI/04). F. García-Molina has a fellowship from the MEC (Spain) (reference AP2003-0891).

References

[1] E.I. Solomon, U.M. Sundaram, T.E. Machonkin, Multicopper oxidases and oxygenases, Chem. Rev. 96 (1996) 2563–2606.
[2] T. Klabunde, C. Eicken, J.C. Sacchettini, B. Krebs, Crystal structure of a plant catechol oxidase containing a dicopper center, Nat. Struct. Biol. 5 (1998) 1084–1090.
[3] S.W. Weidman, E.T. Kaiser, The mechanism of the periodate oxidation of aromatic systems: III. A kinetic study of the periodate oxidation of catechol, J. Am. Chem. Soc. 88 (1966) 5820–5827.
[4] L.M. Rzepecki, T. Nagafuchi, J.H. Waite, α,β-Dehydro-3,4-dihydroxyphenylalanine derivatives: Potential schlerotization intermediates in natural composite materials, Arch. Biochem. Biophys. 285 (1991) 17–26.
[5] F. García-Carmona, F. García-Canovas, J.L. Iborra, J.A. Lozano, Kinetic study of the pathway of melanization between L-dopa and dopachrome, Biochim. Biophys. Acta 717 (1982) 124–131.
[6] F. Garcia-Cánovas, F. Garcia-Carmona, J. Vera-Sanchez, J.L. Iborra, J.A. Lozano, The role of pH in the melanin biosynthesis pathway, J. Biol. Chem. 257 (1982) 8738–8744.
[7] J.N. Rodriguez-Lopez, J. Tudela, R. Varón, F. Garcia-Canovas, Kinetic study on the effect of pH on the melanin biosynthesis pathway, Biochim. Biophys. Acta 1076 (1991) 379–386.
[8] J.N. Rodriguez-Lopez, M. Arnao, F. Martinez-Ortiz, J. Tudela, R. Varón, F. Garcia-Canovas, Catalytic oxidation of 2,4,5-thihydroxyphenylalanine by tyrosinase: identification and evolution of intermediates, Biochim. Biophys. Acta 1160 (1992) 221–228.
[9] J.R. Whitaker, C.Y. Lee, in: J.R. Whitaker, C.Y. Lee (Eds.), Enzymatic Browning and Its Prevention, American Chemical Society, Washington, DC, 1995.
[10] J.R.L. Walker, in: J.R. Whitaker, C.Y. Lee (Eds.), Enzymatic Browning and Its Prevention, American Chemical Society, Washington, DC, 1995.
[11] J.N. Rodriguez-Lopez, J.R. Ros-Martínez, R. Varón, F. Garcia-Canovas, Calibration of a Clark-type oxygen electrode by tyrosinase-catalyzed oxidation of 4-*tert*-butylcatechol, Anal. Biochem. 202 (1992) 356–360.
[12] L.M. Rzepecki, H. Waite, A chromogenic assay for catechol oxidases based on the addition of L-proline to quinones, Anal. Biochem. 179 (1989) 375–381.
[13] A.J. Winder, H. Harris, New assays for the tyrosine hydroxylase and dopa oxidase activities of tyrosinase, Eur. J. Biochem. 198 (1991) 317–326.
[14] J.N. Rodriguez-Lopez, J. Escribano, F. García-Canovas, A continuous spectrophotometric method for the determination of monophenolase activity of tyrosinase using 3-methyl-benzothiazolinone hydrazone, Anal. Biochem. 216 (1994) 205–212.
[15] J.J. Nicolas, F. Richard-Forget, P.M. Goupy, M.J. Amiot, S. Aubert, Enzymatic browning reactions in apple products, Crit. Rev. Food Sci. 34 (1994) 109–157.
[16] M.A. El-Bayoumi, E. Frieden, A spectrophotometric method for the determination of the catecholase activity of tyrosinase and some of its applications, J. Am. Chem. Soc. 79 (1957) 4854–4858.
[17] F. García-Cánovas, J. Tudela, C. Martinez, R. Varón, F. Garcia-Carmona, J.A. Lozano, Kinetic study on the suicide inactivation of tyrosinase induced by catechol, Biochim. Biophys. Acta 912 (1987) 417–423.
[18] F. García-Molina, M.J. Peñalver, J.N. Rodriguez-López, F. García-Cánovas, J. Tudela, Enzymatic method with polyphenol oxidase for the determination of cysteine and *N*-acetylcysteine, J. Agric. Food Chem. 53 (2005) 6183–6189.
[19] L.G. Fenoll, J.N. Rodriguez-Lopez, F. García-Sevilla, F. García-Cánovas, J. Tudela, P.A. Ruiz, R. Varón, F. García-Cánovas, Oxidation by mushroom tyrosinase of monophenols generating slightly unstable *o*-quinones, Eur. J. Biochem. 267 (2000) 5865–5878.
[20] J.R. Ros, J.N. Rodriguez-López, R. Varón, F. García-Cánovas, Kinetics study of the oxidation of 4-*tert*-butylphenol by tyrosinase, Eur. J. Biochem. 222 (1994) 449–452.
[21] J.H. Waite, Calculating molar absorptivities for enzymatically produced *o*-quinones, Anal. Biochem. 75 (1976) 211–218.
[22] H.W. Duckworth, J.E. Coleman, Physicochemical and kinetic properties of mushroom tyrosinase, J. Biol. Chem. 245 (1970) 1613–1625.
[23] J.N. Rodriguez-Lopez, L.G. Fenoll, P.A. García-Ruiz, R. Varón, J. Tudela, R.N. Thorneley, F. García-Cánovas, Stopped-flow and steady-state study of the diphenolase activity of mushroom tyrosinase, Biochemistry 39 (2000) 10497–10506.
[24] M.M. Bradford, A rapid and sensitive method for the quantitation of microgram quantities of protein utilizing the principle of protein–dye binding, Anal. Biochem. 72 (1976) 248–254.
[25] J.N. Rodriguez-Lopez, J.R. Ros, R. Varón, F. García-Cánovas, Oxygen Michaelis constants for tyrosinase, Biochem. J. 293 (1993) 859–866.
[26] Jandel Scientific, SigmaPlot 2.01 for Windows, Jandel Scientific, Core Madera, CA, 1994.
[27] M. Jimenez-Atienzar, J. Cabanes, F. Gandia-Herrero, F. Garcia-Carmona, Kinetic analysis of catechin oxidation by polyphenol oxidase at neutral pH, Biochem. Biophys. Res. Commun. 319 (2004) 902–910.
[28] S. Guyot, V. Cheynier, M. Moutounet, Influence of pH on the enzymic oxidation of (+)-catechin in model systems, J. Agric. Food Chem. 43 (1995) 2458–2462.
[29] J.N. Rodriguez-Lopez, R. Varón, F. García-Cánovas, Oxidation of 6-hydroxydopamine catalyzed by tyrosinase, Intl. J. Biochem. 25 (1993) 1175–1182.
[30] M. García-Moreno, J.N. Rodriguez-López, F. Martinez-Ortíz, J. Tudela, R. Varón, F. García-Cánovas, Effect of pH on the oxidation pathway of dopamine catalyzed by tyrosinase, Arch. Biochem. Biophys. 288 (1991) 427–434.
[31] A. Sanchez-Ferrer, J.N. Rodriguez-López, F. García-Cánovas, F. García-Carmona, Tyrosinase: a comprehensive review of its mechanism, Biochim. Biophys. Acta 1247 (1995) 1–11.
[32] J. Zawistowski, C.G. Biliaderis, N.A. Michael Eskin, in: D.S. Robinson, N.A.M. Eskin (Eds.), Oxidative Enzymes in Foods, Elsevier Science, London, 1991, pp. 217–273.

[33] D.A. Abukarma, H.W. Woolhouse, The preparation and properties of diphenol: oxygen oxidoreductase from potato tubers, New Phytol. 65 (1966) 477–478.
[34] P. Beena, R.G. Latitha, Purification and characterization of polyphenol oxidase from the seeds of field bean (*Dolichos lablab*), J. Agric. Food Chem. 48 (2000) 3839–3846.
[35] J.N. Rodriguez-López, M.A. Gilabert, J. Tudela, R.N. Thorneley, F. García-Cánovas, Reactivity of horseradish peroxidase compound II toward substrates: kinetic evidence for a two-step mechanism, Biochemistry 39 (2000) 13201–13209.
[36] M.A. Gilabert, A.N. Hiner, P.A. García-Ruiz, J. Tudela, F. García-Molina, M. Acosta, F. García-Cánovas, J.N. Rodriguez-López, Differential substrate behaviour of phenol and aniline derivatives during oxidation by horseradish peroxidase: kinetic evidence for a two-step mechanism, Biochim. Biophys. Acta 1699 (2004) 235–243.

4.6. CARACTERIZACIÓN CINÉTICA DE LA OXIDACIÓN DE ESCULETINA POR POLIFENOL OXIDASA Y PEROXIDASA.

La caracterización cinética de la oxidación de esculetina por polifenol oxidasa y peroxidasa ha dado lugar a la siguiente publicación adjunta.

4.6.1. Título

Kinetic characterization of the oxidation of esculetin by polyphenol oxidase and peroxidase.

4.6.2. Autores

Munoz-Munoz, J.L.; Garcia-Molina, F.; Varon, R.; Rodríguez-López, J.N.; Garcia-Cánovas, F. y Tudela, J.

4.6.3. Referencia

Bioscience Biotechnology and Biochemistry (2007) 71, 390-396.

4.6.4. Resumen

La esculetina ha sido descrita como un inhibidor de polifenol oxidasa y por tanto, de la melanogénesis. En este trabajo, se demuestra que esculetina no es un inhibidor sino un sustrato de polifenol oxidasa de champiñón (PPO) y de peroxidasa de rábano picante (POD), enzimas que oxidan a la esculetina generando su *o*-quinona. Debido a que las *o*-quinonas son muy inestables, la forma natural de determinar la actividad enzimática (pendiente de cada registro de formación de producto) es dificultosa. Por esta razón, desarrollamos un método cronométrico para caracterizar la cinética de este sustrato, basado en las medidas del periodo de retardo en presencia de concentraciones micromolares de ácido ascórbico. La constante catalítica determinada fue del mismo orden de magnitud para ambas enzimas. Sin embargo, polifenol oxidasa mostró mayor afinidad (menor constante de Michaelis) que peroxidasa para la esculetina. La afinidad de PPO y POD hacia el oxigeno y el peróxido de hidrógeno es muy alta, sugiriendo la posible catálisis de ambas enzimas en presencia de bajas concentraciones fisiológicas de estos sustratos oxidantes. Tomando en consideración los pHs óptimos de 4.5 y 7.0 para POD y PPO respectivamente, y el pH ácido de los melanosomas, los estudios se llevaron a cabo a pH 4.5 y 7.0.

Biosci. Biotechnol. Biochem., **71** (2), 390–396, 2007

Kinetic Characterization of the Oxidation of Esculetin by Polyphenol Oxidase and Peroxidase

Joseph Louis MUNOZ-MUNOZ,[1] Francis GARCIA-MOLINA,[1] Raymond VARON,[2] Joseph Neptune RODRIGUEZ-LOPEZ,[1] Francis GARCIA-CANOVAS,[1,†] and Joseph TUDELA[1]

[1]*GENZ: Investigation Group of Enzymology, Department of Biochemistry and Molecular Biology A, Faculty of Biology, University of Murcia, E-30100, Espinardo, Murcia, Spain*
[2]*Department of Physical Chemistry, Upper Polytechnic School, University of Castilla la Mancha, Spain Avenue s/n, University Campus, E-02071, Albacete, Spain*

Received August 1, 2006; Accepted November 7, 2006; Online Publication, February 7, 2007
[doi:10.1271/bbb.60431]

Esculetin has been described as an inhibitor of tyrosinase and polyphenol oxidase and, therefore, of melanogenesis. In this work, we demonstrate that esculetin is not an inhibitor but a substrate of mushroom polyphenol oxidase (PPO) and horseradish peroxidase (POD), enzymes which oxidize esculetin, generating its *o*-quinone. Since *o*-quinones are very unstable, the usual way of determining the enzymatic activity (slope of recordings) is difficult. For this reason, we developed a chronometric method to characterize the kinetics of this substrate, based on measurements of the lag period in the presence of micromolar concentrations of ascorbic acid. The catalytic constant determined was of the same order for both enzymes. However, polyphenol oxidase showed greater affinity (a lower Michaelis constant) than peroxidase for esculetin. The affinity of PPO and POD towards oxygen and hydrogen peroxide was very high, suggesting the possible catalysis of both enzymes in the presence of low physiological concentrations of these oxidizing substrates. Taking into consideration optimum pHs of 4.5 and 7 for POD and PPO respectively, and the acidic pHs of melanosomes, the studies were carried out at pH 4.5 and 7. The *in vivo* pH might be responsible for the stronger effect of these enzymes on L-tyrosine and L-3,4-dihydroxyphenylanaline (L-DOPA) (towards melanogenesis) and on cumarins such as esculetin towards an alternative oxidative pathway.

Key words: esculetin; polyphenol oxidase; peroxidase; ascorbic acid; molar absorption coefficient

Polyphenol oxidase (EC 1.14.18.1; PPO) is a binuclear copper cluster containing monooxygenase activity ubiquitously present in biological systems.[1,2] It catalyzes the oxidation of *o*-diphenols (*o*-diphenolase and catecholase activity) to the corresponding *o*-quinones by the consumption of molecular oxygen. It might also catalyze the regioselective orthohydroxylation of monophenols to catechols (monophenolase and cresolase activity) and their subsequent oxidation to *o*-quinones. This is shown in Scheme 1. Periodate, like PPO, oxidizes *o*-diphenols to *o*-quinones, but does not hydroxylate monophenols to *o*-diphenols.[3] This reagent has been used in several studies for comparison with PPO and to characterize the *o*-diphenol oxidation products.[4]

Peroxidases are ubiquitous in the plant and animal kingdoms.[5] The cationic isoenzyme from horseradish peroxidase (EC 1.11.1.7; POD) has been studied intensively because of its commercial use in diagnostic assays and potential application in bioremediation.[6] The oxidation of phenols by POD produces extremely reactive free radical intermediates which, following release from the enzyme, readily condense to yield polymeric products of variable stoichiometry. The kinetics of these reactions is not described by classical Michaelis–Menten equations, and saturation kinetics are often not observed because of the limited solubility of many of these substrates.

Cumarins are widely distributed in plants and are especially abundant in the bark, leaves, and roots of *Umbelliferae*, *Rutaceae*, and *Euphorbiaceae* plants.[7] They are made of fused benzene and α-pyrone rings. To date, more than 1,300 cumarins have been described, principally as secondary metabolites not only in green

† To whom correspondence should be addressed. Fax: +34-968-363963; E-mail: canovasf@um.es

Abbreviations: PPO, polyphenol oxidase; POD, peroxidase; ESC, esculetin; Q, quinone of esculetin; AH_2, ascorbic acid; A, dehydroascorbic acid; L-DOPA, L-3,4 dihydroxyphenyl alanine; V_0, initial rate of PPO and POD; V_{ss}, steady-state rate of PPO and POD; τ, lag period; $[AH_2]_0$, initial concentration of AH_2; E_m, *met*tyrosinase; E_d, *deoxy*tyrosinase; E_{ox}, *oxy*tyrosinase; $[O_2]_0$, initial oxygen concentration; K_m^{ESC}, Michaelis constant of PPO for esculetin; $K_s^{O_2}$, dissociation constant of O_2 of E_{ox}; $K_m^{O_2}$, Michaelis constant for O_2 in presence of ESC; k_{cat}, catalytic constant; $[E]_0$, initial enzyme concentration; V_{max}, maximum rate for PPO and POD

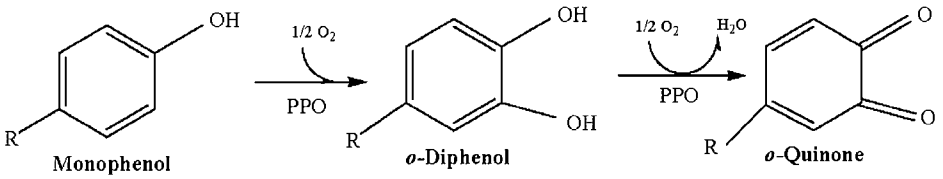

Scheme 1.

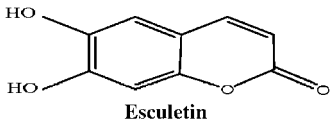

Esculetin

Scheme 2.

plants but also in fungi and bacteria.[8,9] From their structure, we can see that many permutations are possible by substitution and conjugation, which is why so many of these substances exist in nature. They have recently been reported to have interesting pharmacological and biochemical properties, such as anti-oxidative, anti-inflamatory, and anti-allergic effects,[10,11] and are capable of inducing apoptosis,[12] *etc*. Besides cumarin and its metabolites, there are the other related compounds, such as the isocumarins. Warfarin, an antagonist of vitamin K, also derives from cumarins, and aflatoxins are also based on their structure.

Esculetin (Scheme 2) is a cumarin derivative contained in many plants, such as *Citrus limonia* and *Euphorbia lathyris*. It has multiple biological activities, including the inhibition of xantine oxidase activity,[13] platelet aggregation,[14] and the induction of apoptosis. In addition, esculetin shows antioxidative activity,[15,16] an inhibitory effect on the growth of human breast cancer cells,[17] and a synergistic effect with retinoic acid on the differentiation of human leukemia cells.[12] The antitumor mechanism of esculetin is not well understood, although it appears to work as a result of the increased cytosolic translocation of cytochrome c from the mitochondrial inner membrane to cellular cytosol. This signal triggers programmed cell death.

Recently,[7,18] considerable attention has been focused on possible inhibition displayed by the cumarins, especially by esculetin on melanin biosynthesis. In particular, esculetin appears to act on PPO, playing a key role in the regulation of this biosynthetic route. Of all cumarins studied, esculetin is the one the displays the greatest potential to inhibit this enzyme.[18]

Since esculetin has a diphenolic structure, however, it can be oxidized by PPO and POD. In this work, we propose to characterize kinetically the oxidation of esculetin, as a possible PPO and POD substrate rather than an inhibitor. In addition, due to the instability of the *o*-quinones generated by these enzymes and the resulting difficulty in measuring their activity,[19] we propose an alternative chronometric method, based on the measurement of the lag period involved in the consumption of a small quantity of ascorbic acid (AH_2), to determine accurately the initial rate (V_{ss}) of their action on this substrate.

Material and Methods

Reagents. Mushroom tyrosinase (1,530 U mg^{-1}) and horseradish POD (297 U mg^{-1}) were obtained from Sigma Chemical (St. Louis, MO). Dimethylformamide was obtained from J. T. Baker (Amsterdam, Holland). Esculetin was obtained from Flucka (Bem, Switzerland), and sodium periodate was obtained from Scharlau (Malaga, Spain). Stock solutions of the reducing substrates were prepared in 0.15 mM phosphoric acid to prevent autooxidation. The buffers used were 30 mM sodium phosphate buffer (pH 7) and 30 mM sodium acetate (pH 4.5) for PPO and POD, repectively.

Enzyme source. Mushroom tyrosinase (1,530 U mg^{-1}) was purified by Duckworth and Coleman's procedure,[20] but with two additional chromatographic steps.[21] The enzyme solution was passed through a column (2.0 × 30 cm) of Sephadex G-100 (Pharmacia, Upsala, Sweden) equilibrated on 0.01 M sodium phosphate buffer (pH 7). Samples showing tyrosinase activity were further purified by FPLC anion-exchange chromatography on a Mono-Q HR 5/5 column (2.0 × 30 cm) (Pharmacia, Upsala, Sweden) equilibrated with 0.01 M sodium phosphate (pH 7) and eluted with sodium chloride (0–0.5 M gradient). Purified enzyme was desalted with Sephadex G-25 (Pharmacia, Upsala, Sweden) into ultrapure water and stored in liquid nitrogen. The protein concentration was determinated by Bradford's method,[22] using bovine serum albumin as the standard.

Spectrophotometric assays. Absorption spectra were recorded in a visible-ultraviolet Perkin-Elmer Lambda 2-spectrophotometer interfaced on-line with a PC compatible 486DX microcomputer, at a scanning speed of 60 nm/s. The temperature was controlled at 25 °C using a Haake D16 circulating water bath with a heater/cooler, and checked using a Cole-Parmer digital thermometer with a precision of ±0.1 °C. Kinetic assays were also carried out with the above instruments following a chronometric method by measuring the appearance of the products in the reaction medium. Reference cuvettes contained all the components, except the substrate, in a final volume of 1 ml. All the assays

were carried out under saturating conditions of PPO by molecular oxygen (0.26 mM oxygen in the assay medium),[23]

Chronometric method. Enzymatic activity was determined spectrophotometrically using the chronometric method described in "Results and Discussion."[19] The only condition was that there had to be an absorbance increase (due to the product formation) measurable once the ascorbic acid (AH_2) was consumed, to be able to determine the time necessary, τ, to consume the quantity of AH_2 called $[AH_2]_0$. From these values, the initial, V_0, rate can be determined (see "Results and Discussion"). Preliminary experiments were carried out in the absence of ascorbic acid with the tyrosinase/O_2/esculetin system by recording spectrophotometric scans to identify in which zone of the spectrum, particularly the visible zone, the greatest changes in absorbance occurred. The wavelength chosen at acid and neutral pH was 460 nm. The activity of POD was continued using the same methodology, but with the POD/H_2O_2/escueltin system. Dimethylformamide (DMF) (2% v/v) was added to the cuvettes to increase the concentration of ESC due to the low solubility of the substrate.

Determination of molar absorption coefficients. The absorbance data were analyzed according to Beer's law using the standard least-squares linear regression program. Molar absorption coefficients were estimated for a known path length of 1 cm. The minimal acceptable coefficient of determination (r^2) was taken to be 0.995. Data yielding coefficients less than this were due to pipetting errors and rounding up/down of the values. With this precaution, the 95% confidence limits for the molar absorption coefficient estimates were $\leq$5%.

Kinetic data analysis.

Polyphenol oxidase (PPO). Initial rate values (V_0) were calculated from triplicate measurements at each reducing substrate concentration. The reciprocals of the variances of V_0 were used as weighting factors in the non-linear regression fitting of V_0 *versus* $[ESC]_0$ data to the Michaelis–Menten equation (Eq. 9). The fitting was carried out using Marquardt's algorithm,[24] implemented in the Sigma Plot 9.0 program for Windows,[25] obtaining V_{max} and K_m^{ESC}. From these values and according to Eq. (5) and Eq. (8), one can calculate k_{cat} and k_6. Knowing the value of k_8, the value of $K_m^{O_2}$ can be obtained following Eq. (7).[21]

Horseradish peroxidase (POD). Initial rate values (V_0) were calculated from triplicate measurements at each reducing substrate concentration. The reciprocals of the variances of V_0 were used as weighting factors in the non-linear regression fitting of V_0 *versus* $[ESC]_0$ data to the Michaelis–Menten equation (Eq. 11). The fitting was carried out using Marquardt's algorithm,[24] implemented in the Sigma Plot 9.0 program for Windows,[25] obtaining $V_{max}^{app,ESC}$ and $K_m^{app,ESC}$. From these values and according to Eqs. (12) and (13), and knowing k_1,[6] and $[H_2O_2]_0$, one can calculate k_{cat} (Eq. 12) and k_5 (Eq. 13). Taking Eqs. (15) and (16) into account, one obtains K_m^{ESC} and $K_m^{H_2O_2}$.

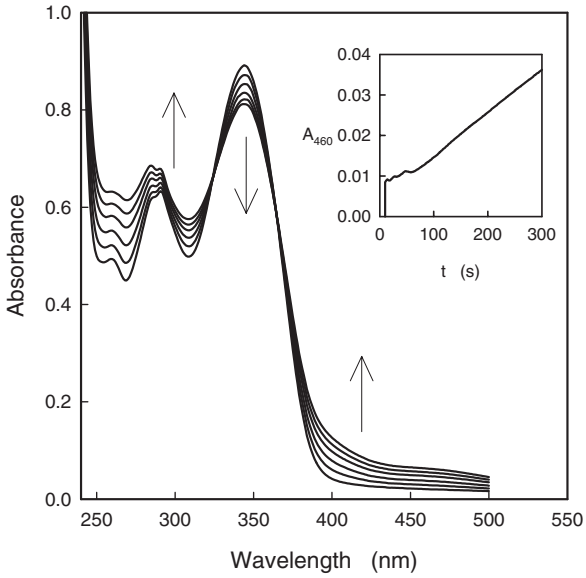

Fig. 1. Spectrophotometric Scans of the Evolution of Q Generated with High Concentration of PPO.

The experimental conditions were 30 mM acetate buffer pH 4.5, $[ESC]_0 = 0.1$ mM, $[E]_0 = 1.6\,\mu$M; scans were made every 60 s. Inset: Kinetics of the evolution of Q generated with a high concentration of PPO recorded at $\lambda = 460$ nm. Experimental conditions are described in "Materials and Methods."

Results and Discussion

Oxidation of esculetin by high concentrations of PPO

The possible enzymatic oxidation of esculetin (ESC) by PPO/O_2 and POD/H_2O_2 was studied at both pH 7 and pH 4.5, taking into account the pH optimum of both enzymes,[1,5] and the acidic pH of melanosomes.[7] The enzymatic oxidation of ESC by PPO at pH 4.5 generates *o*-quinone (Q), which is unstable, with a very clear stoichiometry, as revealed by the formation of two isosbestic points, at 330 and 360 nm (Fig. 1 and inset). In similar experiments carried out at pH 7, isosbestic points were produced at $\lambda = 350$ nm and $\lambda = 410$ nm, which also implies the instability of Q with a clear stoichiometry.

The characterisation of ESC as a substrate of PPO and POD requires assays with $[ESC]_0$ of around 1 mM. However, at such high concentrations, the absorbance of Q at the isobestic points is very high (Fig. 1), and it saturates the photomultiplicator of the spectrophotometers, for which reason 460 nm was chosen as the wavelength for Q detection.

Oxidation of esculetin by excess of periodate

Periodate oxidizes *o*-diphenols in a way similar to PPO, but, when an excess of periodate is used for the

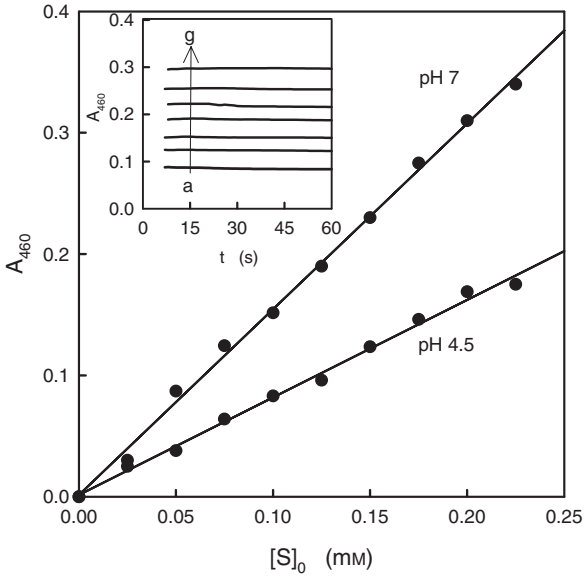

Fig. 2. Representation of Absorbance *Versus* Concentration of Q.
Absorbance values at $\lambda = 460$ nm obtained by oxidation with excess periodate. The experimental conditions were 30 mM sodium acetate (pH 4.5) and 30 mM sodium phosphate (pH 7). The concentration of de $[IO_4^-]_0$ was 5 mM. Inset: Kinetics of the evolution of Q generated with excess periodate. The experimental conditions were 30 mM sodium phosphate (pH 7), $\lambda = 460$ nm, $[IO_4^-]_0 = 5$ mM and $[ESC]_0$ was (a) 0.05 mM, (b) 0.075 mM, (c) 0.1 mM, (d) 0.125 mM, (e) 0.150 mM, (f) 0.175 mM, and (g) 0.2 mM.

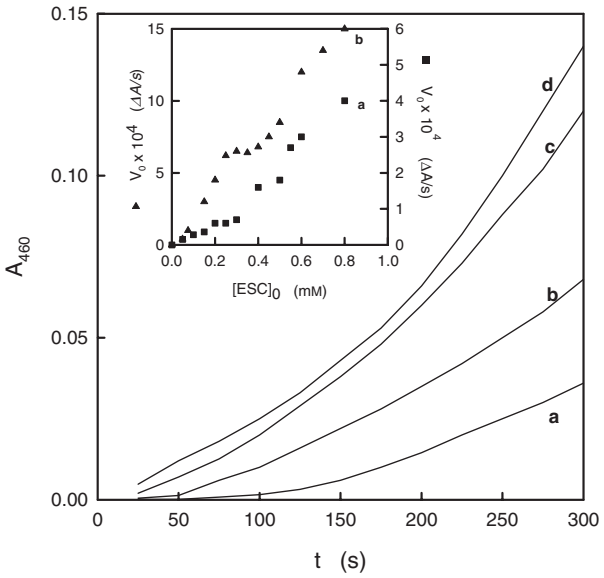

Fig. 3. Spectrophotometric Recordings of Q Generated in the Action of PPO on ESC.
The experimental conditions were 30 mM sodium phosphate (pH 7), $\lambda = 460$ nm, $[E]_0 = 1.25$ nM. The substrate concentrations were (a) 0.2 mM, (b) 0.4 mM, (c) 0.6 mM, and (d) 0.8 mM. Inset: Initial slope of V_0 *versus* $[ESC]_0$, directly measuring the appearance of Q. The experimental conditions were 30 mM sodium acetate (pH 4.5), 30 mM sodium phosphate (pH 7), $\lambda = 460$ nm, $[E]_0 = 1.25$ nM, (a) pH 4.5, (b) pH 7.

oxidation, the reaction is instantaneous, and this allows the molar absorption coefficients,[3] to be calculated for Q at both pH values (Fig. 2 and inset). These coefficients, at $\lambda = 460$ nm, are 803 M^{-1} cm^{-1} at pH 4.5 and 1,503 M^{-1} cm^{-1} at pH 7 (and when ESC is oxidized with a defect of periodate, similar values are obtained). This physical characteristic of Q is important in several types of study, such as those involving HPLC.

Kinetic characterization of the oxidation of esculetin by PPO and POD

To characterize ESC, the initial slope of the appearance of Q (V_0) can be measured directly at 460 nm, but the recordings are parabolics, without linear zones, and thus a true steady-state is not reached (Fig. 3). Furthermore, this gives rise to false results due to the instability of Q, which involves a curve V_0 *versus* $[ESC]_0$ (Fig. 3 inset) that does not resemble the hyperbola necessary to estimate k_{cat} and K_m.

In some cases where the *o*-quinones generated by PPO and POD are unstable, the use of a reductant such as AH_2, which instantaneously reduces to Q, has been proposed to follow the enzymatic activity; the disappearance of the AH_2 can then be followed spectrophotometrically.[19] However, it was not possible follow the disappearance of AH_2 by referring to the overlapping spectra for ESC or AH_2 at the different pH values used.

Hence we propose a chronometric method, based on measurement of the time required for the consumption of a small quantity of ascorbic acid (AH_2), which

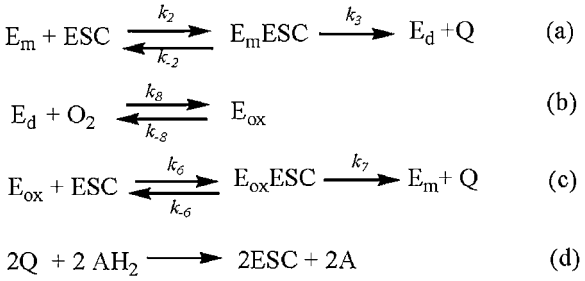

Scheme 3.

prevents Q from evolving, according to the following Scheme for PPO:[26] where E_m, E_d, and E_{ox} represent the oxidized and deoxygenated forms and that with a peroxide group of the enzyme, respectively.

This method uses the reduction by AH_2 of Q (Scheme 3d), which is generated by the enzyme (Scheme 3a–c).[19] The true steady-state rate, V_{ss}, is rapidly reached when $[O_2]_0$ and $[ESC]_0 \gg [E]_0$ in the case of PPO, or $[H_2O_2]_0$ and $[ESC]_0 \gg [E]_0$ in the case of POD, according to the following mass balance:

$$V_{ss}t - [AH_2]_0 = Q \qquad (1)$$

The total quantity of material entering the system is $V_{ss}t$, where t is the time during which the enzyme acts. In the presence of AH_2, Q is reduced to ESC and while AH_2 remains, ESC is not consumed. The intersection of the increase in absorbance of the recording Q *versus* t and the time axis, corresponds to $Q = 0$

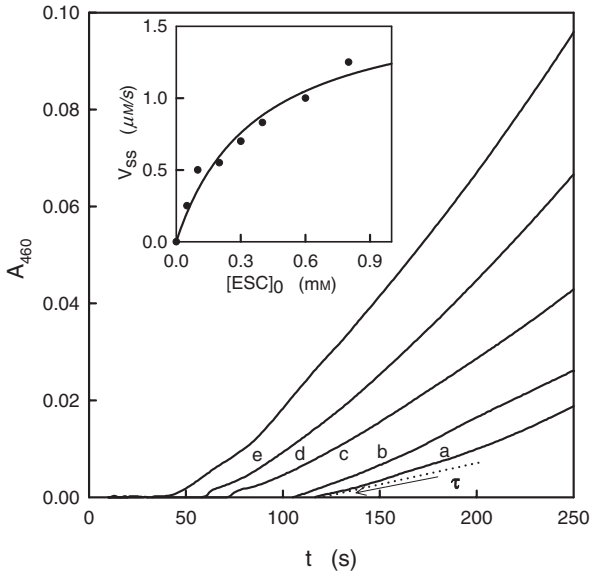

Fig. 4. Chronometric Method for Characterizing the Enzymatic Activity of PPO on ESC.

The experimental conditions were 30 mM sodium acetate (pH 7), $\lambda = 460$ nm, $[E]_0 = 1.25$ nM, $[AH_2]_0 = 50$ μM, and $[DMF]_0 = 2\%$ (v/v). Substrate centrations were (a) 0.1 mM, (b) 0.2 mM, (c) 0.3 mM, (d) 0.4 mM, and (e) 0.6 mM. Inset: Representation of true steady-state rate *versus* $[ESC]_0$, pH 7.

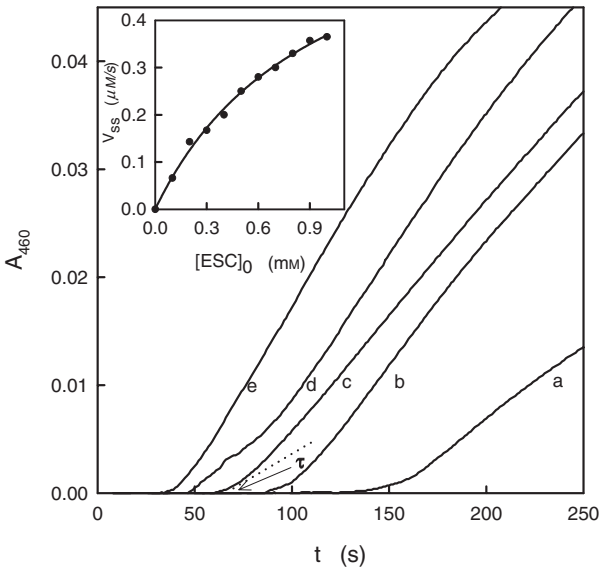

Fig. 5. Chronometric Method for Characterizing the Enzymatic Activity of POD.

The experimental conditions were 30 mM sodium phosphate (pH 4.5), $\lambda = 460$ nm, $[E]_0 = 0.4$ nM, $[AH_2]_0 = 10$ μM, $[H_2O_2]_0 = 100$ μM, and $[DMF]_0 = 2\%$ (v/v). Substrate concentrations were (a) 0.1 mM, (b) 0.2 mM, (c) 0.3 mM, (d) 0.4 mM, and (e) 0.5 mM. Inset: Representation of true steady-state rate *versus* $[ESC]_0$, pH 4.5.

and $t = \tau$ (lag period, Figs. 4 and 5). Thus, Eq. (1) is transformed into

$$V_{ss}\tau - [AH_2]_0 = 0 \tag{2}$$

Therefore, the experimental measurement of τ, in assays with a known value of $[AH_2]_0$, lead to the calculation of the true V_{ss} value:

$$V_{ss} = \frac{[AH_2]_0}{\tau} \tag{3}$$

Taking into consideration the kinetic mechanisms of PPO and POD, described below, some restrictions can be established so that this chronometric method provides suitable values for the parameter V_{ss}, so that the enzymes can be characterized kinetically.

The expression of V_{ss} is given by:

$$V_{ss} = \frac{V_{max}[ESC]_0[O_2]_0}{K_m^{ESC}K_s^{O_2} + K_m^{O_2}[ESC]_0 + K_m^{ESC}[O_2]_0 + [ESC]_0[O_2]_0} \tag{4}$$

where

$$V_{max} = 2k_{cat}[E]_0 = 2\frac{k_3k_7}{k_3 + k_7}[E]_0 \tag{5}$$

$$K_s^{O_2} = \frac{k_{-8}}{k_8} \tag{6}$$

$$K_m^{O_2} = \frac{k_{cat}}{k_8} \tag{7}$$

$$K_m^{ESC} = \frac{k_{cat}}{k_6} \tag{8}$$

Since at this value of k_8 ($(2.3 \pm 0.4) \times 10^7$ M^{-1} s^{-1}),[21] PPO is saturated by oxygen,[23] and if $[O_2]_0 \rightarrow \infty$ in Eq. (4), then

$$V_{ss} = \frac{V_{max}[ESC]_0}{K_m^{ESC} + [ESC]_0} \tag{9}$$

The action of POD on reducing substrates (ESC) in the presence of H_2O_2 is described by Scheme 4[6] where POD indicates that free enzyme POD-I is compound I, POD-II is compound II, and SQ-ESC is the semiquinone radical corresponding to ESC.

The following expression is obtained for the rate of radical formation:

$$V_{ss} = \frac{2k_{cat}[H_2O_2]_0[ESC]_0[E]_0}{\frac{k_{cat}}{k_5}[H_2O_2]_0 + \frac{k_{cat}}{k_1}[ESC]_0 + [H_2O_2]_0[ESC]_0} \tag{10}$$

This equation can be rearranged as follows:

$$V_{ss} = \frac{V_{max}^{app,ESC}[ESC]_0}{K_m^{app,ESC} + [ESC]_0} \tag{11}$$

where

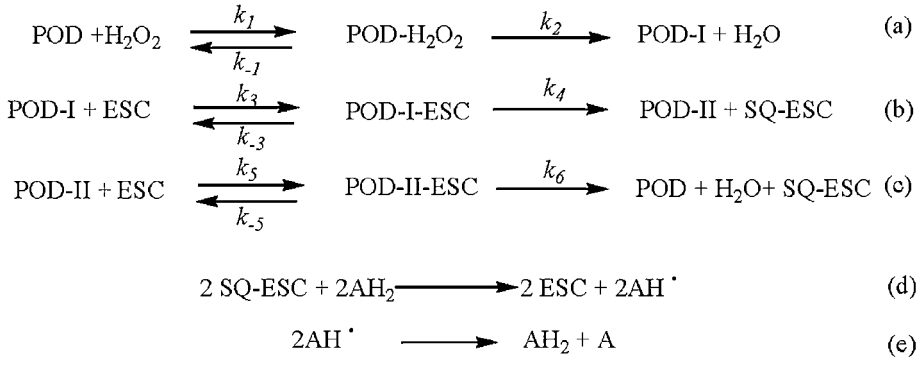

Scheme 4.

Table 1. Kinetic Constants of the PPO/O_2/ESC and POD/H_2O_2/ESC Systems for Their Action on Esculetin

	pH	k_{cat} (s^{-1})	k_{+5} ($M^{-1}\,s^{-1}$)	k_2* (s^{-1})	k_6** (s^{-1})	k_6*** ($M^{-1}\,s^{-1}$)	K_m^{ESC} (mM)	$K_m^{H_2O_2}$ (μM)	$K_m^{O_2}$ (μM)
PPO	4.5	551 ± 95				$(6.12 \pm 0.16) \times 10^5$	0.90 ± 0.16		41 ± 4.10
	7	928 ± 92				$(14.73 \pm 0.31) \times 10^5$	0.63 ± 0.13		40 ± 4.00
POD	4.5	890 ± 56	$(4.26 \pm 0.25) \times 10^5$	2000	1613		2.00 ± 0.12	52.0 ± 0.31	
	7	871 ± 52	$(6.10 \pm 0.36) \times 10^5$	2000	1542		1.40 ± 0.10	5.2 ± 0.28	

* Taken from Ref. 6.
** Transformation constant of ESC in SQ-ESC for POD-II (Scheme 4).
*** Binding constant of ESC to E_{ox} (Scheme 3).

$$V_{max}^{app,ESC} = \frac{2k_{cat}[H_2O_2]_0[E]_0}{\frac{k_{cat}}{k_1} + [H_2O_2]_0} \quad (12)$$

$$K_m^{app,ESC} = \frac{\frac{k_{cat}}{k_5}[H_2O_2]_0}{\frac{k_{cat}}{k_1} + [H_2O_2]_0} \quad (13)$$

and

$$k_{cat} = \frac{k_2 k_6}{k_2 + k_6} \quad (14)$$

$$K_m^{ESC} = \frac{k_{cat}}{k_5} \quad (15)$$

$$K_m^{H_2O_2} = \frac{k_{cat}}{k_1} \quad (16)$$

In order to apply the method, it is necessary to take into account the following:

(a) Limitation of consumption: As mentioned above, the concentration of O_2 determines the suitable concentration of AH_2. Thus, $[AH_2]_0 \leq [O_2]_0$ should be used.
(b) Length of the lag period: The minimum length of the lag period must be greater than the "dead-time" of the measurement, τ_d (10 s). We opted for $\tau \geq 3\tau_d$, which was achieved by varying $[E]_0$ (see Eq. 6). However, τ should not be so long that changes in the blank samples (due to the chemical reaction of O_2 with AH_2) become significant.
(c) The quantity of AH_2 used in the assays. This quantity is limited by O_2 consumption (see above).

In assays with POD, the same restrictions are applied, except that since this enzyme consumes H_2O_2, the concentration of AH_2 must fulfill $[AH_2]_0 \leq 0.1\,[H_2O_2]_0$.

Furthermore, in agreement with the stoichiometry of Scheme 4, the expression of V_{ss} is

$$V_{ss} = \frac{2[AH_2]_0}{\tau} \quad (17)$$

Evaluation of kinetic constants

When the chronometric method described above was applied to the characterization of the substrate (ESC), a hyperbolic dependence of V_{ss} *vs* $[ESC]_0$ was obtained (Fig. 4 and inset for PPO, and Fig. 5 and inset for POD). Analysis of the data, as described in Material and Methods, provided the information summarized in Table 1 for PPO and POD.

From these results (Table 1), it can be concluded that ESC is a good substrate for PPO and POD. The catalytic constant, k_{cat}, is of the same order of magnitude as those obtained for PPO acting on *o*-diphenols,[21] and for POD.[6] The Michaelis constant values increase slightly at lower pH values, and the same constants for hydrogen peroxide and oxygen are very low, which implies that both enzymes can act with low physiological concentrations of these oxidizing substrates.

In conclusion, the use of a chronometric method to determine the enzymatic activity of PPO and POD acting on ESC enabled the kinetic characterization of this compound, which acts as substrate for both enzymes. From the results obtained, we conclude that ESC is not a true inhibitor of PPO, as has been

claimed.[7] Rather, ESC acts as an alternative to the physiological substrates L-tyrosine and L-DOPA. Therefore, ESC probably directs the melanogenesis pathway towards quinonic derivatives other than *o*-dopaquinone and dopachrome, which are intermediates of the melanogenesis pathway.

Acknowledgments

This work was supported in part by grants from the Ministry of Education and Culture of Spain, Project BIO 2006-15363, and from the Séneca Foundation/Department of Education (Murcia) Project 00672/PI/04. Francis Garcia-Molina has a fellowship from the Ministry of Education and Culture, reference AP2003-0891. Joseph Louis Munoz Munoz has a fellowship from the Ministry of Education and Culture, reference AP2005-4721.

References

1) Solomon, E. I., Sundaram, U. M., and Machonkin, T. E., Multicooper oxidases and oxygenases. *Chem. Rev.*, **96**, 2563–2606 (1996).
2) Klabunde, T., Eicken, C., Sacchettini, J. C., and Krebs, B., Crystal structure of a plant catechol oxidase containing a dicooper center. *Nat. Struct. Biol.*, **5**, 1084–1090 (1998).
3) Weidman, S. W., and Kaiser, E. T., The mechanism of the periodate oxidation of aromatic systems III. A kinetic study of the periodate oxidation of catechol. *J. Am. Chem. Soc.*, **88**, 5820–5827 (1966).
4) Rzepecki, L. M., Nagafuchi, T., and Waite, J. H., α,β-Dehydro-3,4-dihydroxyphenylalanine derivatives: potential schlerotization intermediates in natural composite materials. *Arch. Biochem. Biophys.*, **285**, 17–26 (1991).
5) Dunford, H. B., "Heme Peroxidases," Wiley-VHC, New York, pp. 92–97 (1999).
6) Rodríguez-López, J. N., Gilabert, M. A., Tudela, J., Thorneley, R. N. F., and García-Cánovas, F., Reactivity of horseradish peroxidase compound II toward substrates: kinetic evidence for a two-step mechanism. *Biochemistry*, **39**, 13201–13209 (2000).
7) Masamoto, Y., Murata, Y., Baba, K., Shimoishi, Y., Tada, M., and Takahata, K., Inhibitory effects of esculetin on melanin biosynthesis. *Biol. Pharm. Bull.*, **27**, 422–425 (2004).
8) Murray, R. D. H., Cumarins. *Nat. Prod. Rep.*, **8**, 591–594 (1989).
9) Murray, R. D. H., "Progress in the Chemistry of Organic Natural Products," Springer-Verlag, New York, pp. 84–316 (1991).
10) Muschietti, L., Gorzalczany, S., Ferraro, G., Acevedo, C., and Marino, V., Phenolic compounds with anti-inflammatory activity from Eupatorium buniifolium. *Planta Med.*, **67**, 743–744 (2001).
11) Neichi, T., Koshihara, S., and Murota, S., Inhibitory effect of esculetin on 5-lipoxygenase and leukotriene biosynthesis. *Biochim. Biophys. Acta*, **753**, 130–132 (1983).
12) Chu, C. Y., Tsai, Y. Y., Wang, C. J., Lin, W. L., and Tseng, T. H., Induction of apoptosis by esculetin in human leukemia cells. *Eur. J. Pharmacol.*, **23**, 25–32 (2001).
13) Egan, D., O'Kennedy, R., Moran, E., Cox, D., Prosser, E., and Thornes, R. D., The pharmacology, metabolism, analysis and applications of cumarin and cumarin-related compounds. *Drug Metab. Rev.*, **22**, 503–529 (1990).
14) Okada, Y., Miyauchi, N., Suzuki, K., Kobayasashi, T., Tsutsui, C., Mayuzumi, K., Nishibe, S., and Okuyama, T., Search for naturally occurring substances to prevent the complications of diabetes. II. Inhibitory effects of cumarin and flavonoid derivatives on bovine lens aldose reductase and rabbit platelet aggregation. *Chem. Pharm. Bull.*, **43**, 1385–1387 (1995).
15) Paya, M., Halliwell, B., and Hoult, J. R. S., Interactions of a series of cumarins with reactions oxygen species: scavenging of superoxide, hypochlorous acid and hydroxyl radicals. *Biochem. Pharmacol.*, **44**, 205–214 (1992).
16) Lin, W. L., Wang, C. J., Tsai, Y. Y., Liu, C. L., Hwang, J. M., and Tseng, T. H., Inhibitory effect of esculetin on oxidative damage induced by t-buthyl hydroperoxide in rat liver. *Arch. Toxicol.*, **74**, 467–472 (2000).
17) Noguchi, M., Arashi, M., Minami, M., Miyazaki, I., Tanaka, M., and Sasaki, T., Effects of piroxicam and esculetin on the MDA-MB-231 human, prostaglandins, leukotrienes essentials. *Fatty Acids*, **53**, 325–329 (1995).
18) Masamoto, Y., Ando, H., Murata, Y., Shimoishi, Y., Tada, M., and Takahata, K., Mushroom tyrosinase inhibitory activity of esculetin isolated from seeds of *Euphorbia lathyris L. Biosci. Biotechnol. Biochem.*, **67**, 631–634 (2003).
19) Muñoz, J. L., Garcia-Molina, F., Varon, F., Rodríguez-Lopez, J. N., Garcia-Canovas, F., and Tudela, J., Calculating molar absortivities for quinones: application to the measurements of tyrosinase activity. *Anal. Biochem.*, **351**, 128–138 (2006).
20) Duckworth, H. W., and Coleman, J. E., Physicochemical and kinetic properties of mushroom tyrosinase. *J. Biol. Chem.*, **245**, 1613–1625 (1970).
21) Rodríguez-Lopez, J. N., Fenoll, L. G., Garcia-Ruiz, P. A., Varon, R., Tudela, J., Thorneley, R. N., and Garcia-Canovas, F., Stopped-flow and steady-state study of the diphenolase activity of mushroom tyrosinase. *Biochemistry*, **39**, 10497–10506 (2000).
22) Bradford, M. M., A rapid and sensitive method for the quantitation of microgram quantities of protein utilizing the principle of protein-dye binding. *Anal. Biochem.*, **72**, 248–254 (1976).
23) Rodríguez-Lopez, J. N., Ros, J. R., Varon, R., and Garcia-Canovas, F., Oxygen Michaelis constant for tyrosinase. *Biochem. J.*, **293**, 859–866 (1993).
24) Marquart, D. W., An algorithm lest-squares estimation of non-linear parameters. *J. Soc. Ind. Appl. Math.*, **11**, 431–441 (1963).
25) Jandel Scientific, SigmaPlot 2.01 for Windows®, Jandel Scientific, Core Madera, CA, 1994.
26) García-Cánovas, F., Tudela, J., Martínez Madrid, C., Varón, R., García-Carmona, F., and Lozano, J. A., Kinetic study on the suicide inactivation of tyrosinase induced by catechol. *Biochim. Biophys. Acta*, **912**, 417–423 (1987).

4.7. CARACTERIZACIÓN CINÉTICA DE LA OXIDACIÓN DE CARBIDOPA Y BENSERAZIDA POR TIROSINASA Y PEROXIDASA.

La caracterización cinética de la oxidación de carbidopa y benserazida por tirosinasa y peroxidasa ha dado lugar a la siguiente publicación adjunta.

4.7.1. Título

Kinetic characterization of the oxidation of carbidopa and benserazide by tyrosinase and peroxidase.

4.7.2. Autores

Munoz-Munoz, J.L.; Garcia-Molina, F.; Garcia-Molina, M..; Tudela, J.; Garcia-Cánovas, F. y Rodríguez-López, J.N.

4.7.3. Referencia

Bioscience, Biotechnology and Biochemistry (2009) 73, 1308-1313.

4.7.4. Resumen

Carbidopa y benserazida son inhibidores de dopa descarboxilasa y ambos son utilizados en el tratamiento de la enfermedad del Parkinson. Debido a su estructura química como polifenoles, estos compuestos pueden actuar como sustratos de tirosinasa y peroxidasa. En este trabajo, se demuestra que estas enzimas oxidan ambos sustratos. Debido a que las *o*-quinonas son muy inestables, se utilizó un método cronométrico para caracterizar cinéticamente estos sustratos. En el caso de tirosinasa, los valores de la constante de Michaelis para ambos sustratos son mayores que los descritos para el L-dopa, aunque las constantes catalíticas son menores, probablemente debido al mayor tamaño del grupo sustituyente del carbono 1 del anillo benzénico. Con respecto a peroxidasa, es posible la saturación de la enzima por ambos sustratos, al contrario de lo que ocurre con los isómeros del dopa. Quizás el alejamiento de las cargas respecto al anillo bencénico, posibilita el acercamiento al hierro del sitio activo de la enzima y, por lo tanto, la catálisis.

Biosci. Biotechnol. Biochem., **73** (6), 1308–1313, 2009

Kinetic Characterization of the Oxidation of Carbidopa and Benserazide by Tyrosinase and Peroxidase

Joseph Louis MUNOZ-MUNOZ, Francis GARCIA-MOLINA, Mary GARCIA-MOLINA, Joseph TUDELA, Francis GARCÍA-CÁNOVAS,† and Joseph Neptune RODRIGUEZ-LOPEZ

GENZ: Investigation Group of Enzymology, Department of Biochemistry and Molecular Biology A, Faculty of Biology, University of Murcia, Espinardo, Murcia, E-30100, Spain

Received November 20, 2008; Accepted December 16, 2008; Online Publication, June 7, 2009
[doi:10.1271/bbb.80820]

Carbidopa and benserazide have been described as inhibitors of dopa decarboxylase and both have been used in the treatment of Parkinson's disease. Because of their chemical structure as polyphenols, these compounds can behave as substrates of tyrosinase and peroxidase. We demonstrate that these enzymes oxidize both substrates. Since *o*-quinones are unstable, a chronometric method for enzymatic initial rate determinations was used based on measurements of the lag period in the presence of micromolar concentrations of ascorbic acid to kinetically characterize these substrates. In the case of tyrosinase, the values of the Michaelis constant for both substrates were greater than those described for dopa, although the catalytic constants were lower, probably due to the greater size of the substitute group in carbon 1. As regards peroxidase, the saturation of the enzyme by both substrates is possible, however this effect does not occur with the isomers of dopa. The distance of the charges from the benzene ring may enable the ring to approach the iron of the active site and, therefore, act.

Key words: carbidopa; benserazide; tyrosinase; peroxidase; dopa decarboxylase

Tyrosinase (TYR; EC 1.14.18.1) is a type-3 copper protein, which contains a binuclear copper cluster consisting of two copper atoms coordinated by 3 histidines, and is ubiquitously present in biological systems.[1,2] It catalyzes the regioselective orthohydroxylation of monophenols to catechols (monophenolase or cresolase activity). It also catalyzes the oxidation of *o*-diphenols to the corresponding *o*-quinones by the consumption of molecular oxygen (*o*-diphenolase or catecholase activity).

Peroxidases are ubiquitous in the plant and animal kingdoms.[3] The cationic isoenzyme from horseradish peroxidase (EC 1.11.1.7; POD) has been studied intensively because of its commercial use in diagnostic assays and its potential application in bioremediation.[4] The oxidation of phenols by POD produces extremely reactive free radical intermediates which, following release from the enzyme, readily condense to yield polymeric products of variable stoichiometry. Because of this, the kinetics of these reactions was not described by classical Michaelis-Menten equations for a long time. However, when a suitable method was found, it became possible to establish the typical Michaelis-Menten kinetics with a series of *o*-diphenols, monophenols, and anilines.[4]

L-DOPA is central in the melanin synthetic pathway and *in vivo* studies have suggested that L-DOPA may be cytotoxic to melanoma cells through the intracellular accumulation of toxic melanin intermediates.[5] L-DOPA is used to treat Parkinson's disease but it must first cross the hematocephalic barrier. However, in the peripheral system, l-dopa is decarboxylated and transformed into dopamine, which cannot cross the above barrier. To diminish the quantity of L-DOPA that is transformed into dopamine in the peripheral system, and thereby increase the quantity that crosses the blood-brain barrier and which decarboxylates inside the central system, a series of inhibitors of dopa decarboxylase (which is the key enzyme in L-DOPA decarboxylation and other amino acids), such as cardidopa or benserazide, is added along with L-DOPA. This is done by means of drugs such as madopar® (dopa/benserazide) or sinemet® (dopa/carbidopa) respectively. Since both cardidopa and benserazide increase plasma levels of L-DOPA, they have also been used to treat malignant melanoma.[5,6] However, these drugs may also have secondary effects such as activating malignant melanoma in people with a history of melanoma, or causing skin lesions which might well be malignant due to the dose of L-DOPA they contain. They may also cause respiratory alterations (arrhythmias), increased depression, or psychosis due to the increased concentration of dopamine in the organism, arterial hypertension, renal insufficiency, *etc*.

Dopa decarboxylase or aromatic L-amino acid decarboxylase (EC 4.1.1.28) is the enzyme which catalyzes the rate-limiting step in the decarboxylation of aromatic L-amino acids, such as L-DOPA to dopamine (neuro-

† To whom correspondence should be addressed. Fax: +34-968-363963; E-mail: canovasf@um.es

Abbreviations: TYR, tyrosinase; POD, peroxidase; S, substrate, carbidopa or benserazide; Q, quinone of S; AH_2, ascorbic acid; A, dehydroascorbic acid; L-DOPA, L-3,4 dihydroxyphenyl alanine; V_0^{TYR}, initial rate of TYR; V_0^{POD}, initial rate of POD; τ, lag period; $[AH_2]_0$, initial concentration of AH_2; E_m, *met*-tyrosinase; E_d, *deoxy*-tyrosinase; E_{ox}, *oxy*-tyrosinase; $[O_2]_0$, initial oxygen concentration; $K_m^{S,TYR}$, Michaelis constant of TYR for S; $K_m^{S,POD}$, Michaelis constant of POD for S; $K_s^{O_2}$, dissociation constant for O_2 of E_{ox}; $K_m^{O_2}$, Michaelis constant for O_2 in presence of S; k_{cat}^{TYR}, catalytic constant of TYR for S; k_{cat}^{POD}, catalytic constant of POD for S; $[E]_0$, initial enzyme concentration; V_{max}^{TYR}, maximum rate for TYR; V_{max}^{POD}, maximum rate for POD

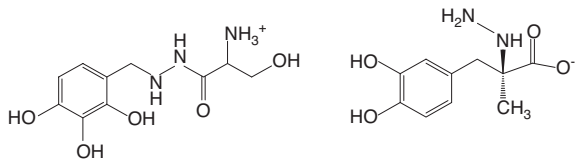

Scheme 1. Structures of the Compounds Used in This Work.

transmitter), 5-hydroxytryptamine to serotonine (neurotransmitter), or tryptophan to tryptamine (a precursor to many alkaloids found in plants and animals).

Since benserazide and carbidopa have a diphenolic structure (Scheme 1), they can be oxidized by tyrosinase and peroxidase. In this work, we proposed to kinetically characterize the oxidation of these compounds as possible substrates of these enzymes, commonly used as model enzymes in processes such as melanin biosynthesis.[7–9)]

Material and Methods

Reagents. Mushroom tyrosinase (1,530 U mg^{-1}), horseradish peroxidase (297 U mg^{-1}), benserazide, and carbidopa were obtained from Sigma Chemical (St. Louis, MO). Stock solutions of the reducing substrates were prepared in 0.15 mM phosphoric acid to prevent autooxidation. The structures of benserazide and carbidopa are depicted in Scheme 1. The buffers used were 30 mM (pH 7.0) sodium phosphate buffer at °C 25 for benserazide, and 30 mM (pH 6.0) sodium phosphate buffer at °C 25 for carbidopa, due to its instability and rapid cyclation at pH 7.0.

Enzyme source. Mushroom tyrosinase (1,530 U mg^{-1}; TYR) was purified by Duckworth and Coleman's procedure, but with two additional chromatographic steps.[10)] The enzyme solution was passed through a column (2.0 × 30 cm) of Sephadex G-100 (Pharmacia, Upsala, Sweden) equilibrated on 0.01 M sodium phosphate buffer (pH 7). Samples showing tyrosinase activity were further purified by FPLC anion-exchange chromatography on a Mono-Q HR 5/5 column (2.0 × 30 cm) (Pharmacia) equilibrated with 0.01 M sodium phosphate (pH 7) and eluted with sodium chloride (0–0.5 M gradient). Purified enzyme was desalted with Sephadex G-25 (Pharmacia) into ultrapure water and stored in liquid nitrogen. Horseradish peroxidase (297 U mg^{-1}; POD) was purchased from Sigma (type VI; Rz = 3.2) and used without further purification. The concentration of POD was determined spectrophotometrically using a Soret molar absorptivity of 102 $mM^{-1}\,cm^{-1}$.[4)] The protein concentration was determined (for TYR and POD) by Bradford's method,[11)] using bovine serum albumin as the standard.

Spectrophotometric assays. Absorption spectra were recorded in a visible-ultraviolet Perkin-Elmer Lambda 35-spectrophotometer interfaced on-line with a PC compatible microcomputer, at a scanning speed of 60 nm/s. The temperature was controlled at °C 25 using a Haake D16 circulating water bath with a heater/cooler, and checked using a Cole-Parmer digital thermometer with a precision of ±0.1 °C. Kinetic assays were also carried out with the above instruments following a chronometric method by measuring the appearance of the products in the reaction medium. Reference cuvettes contained all the components, except the substrate, in a final volume of 1 ml. For TYR, all the assays were carried out under saturating conditions of TYR by molecular oxygen (0.26 mM oxygen in the assay medium).[10,12)] In the case of POD, the H_2O_2 concentration was saturating (1 mM) (see Table 1).

Chronometric method. Enzymatic activity was determined spectrophotometrically using the chronometric method described in refs. 4 and 13. Briefly, the method uses ascorbic acid (AH_2), which is capable of reducing the products of both enzymes (*o*-quinones in the case of tyrosinase (TYR) and free radicals, semiquinones, in the case of POD). Once the AH_2 has been consumed, an absorbance signal should appear due to the presence of the above products, from which the time necessary, τ, to consume the quantity of AH_2 called $[AH_2]_0$ can be determined. From these values, the initial rate, V_0, can be determined (see "Results and Discussion"). Preliminary experiments were carried out in the absence of ascorbic acid with the TYR/O_2/S system by recording spectrophotometric scans to identify in which zone of the spectrum, particularly the visible zone, the greatest changes in absorbance occurred. The wavelength chosen at both pH was 360 nm. The activity of horseradish peroxidase (POD) was continued using the same methodology, but with the POD/H_2O_2/S system.

Kinetic data analysis.

Tyrosinase (TYR). Initial rate values (V_0^{TYR}) were calculated from triplicate measurements at each reducing substrate concentration. The fitting of V_0^{TYR} *versus* the $[S]_0$ data to the Michaelis-Menten equation (Eq. (5)) was carried out using the Sigma Plot 9.0 program for Windows,[14)] giving V_{max}^{TYR} and $K_m^{S,TYR}$. From these values and according to Eq. (6) and Eq. (7), one can calculate k_{cat}^{TYR} and k_6 (see Scheme 2). Knowing the value of k_8,[10)] the value of $K_m^{O_2}$ can be obtained following Eq. (9).

Horseradish peroxidase (POD). Initial rate values (V_0^{POD}) were calculated from triplicate measurements at each reducing substrate concentration. V_0^{POD} *versus* $[S]_0$ data was fitted to the Michaelis-Menten equation (Eq. (10)) using the Sigma Plot 9.0 program for Windows,[14)] providing V_{max}^{POD} and $K_m^{S,POD}$. From these values and according to Eqs. (11) and (12), the values of k_{cat}^{POD} (Eq. (11)) and k_5 (Eq. (12)) can be calculated (see Scheme 3). Taking Eq. (14) into account, and knowing k_1,[4)] one can obtain $K_m^{H_2O_2}$.

Results and Discussion

Kinetic characterization of the oxidation of carbidopa and benserazide by TYR and POD

To characterize carbidopa and benserazide as substrates of TYR and POD, the initial slope of the appearance of Product *vs.* t (V_0) was measured directly at 360 nm (Figs. 1 and 2). However, these recordings did not provide the hyperbolas necessary to estimate V_{max} and K_m when V_0 is represented *vs.* $[S]_0$ (Fig. 1 Inset and Fig. 2 Inset). As can be appreciated from these graphs, false activations may become apparent at high substrate concentrations and due to the instability of the products generated both with TYR (Fig. 1) and POD (Fig. 2) for carbidopa and benserazide, respectively.

In some cases where the *o*-quinones generated by TYR and POD are unstable, the use of a reductant, such as AH_2, which instantaneously reduces to Q, has been proposed to follow the enzymatic activity; this enables the disappearance of the AH_2 to be followed spectrophotometrically.[13)] However, it was not possible to follow the disappearance of AH_2 by referring to the overlapping spectra of S and AH_2 at the different pH values used, for which reason we used a chronometric method, which was previously described to determine the enzymatic activity on substrates producing unstable *o*-quinones,[4,13)] based on measurement of the time required for the consumption of a small quantity of AH_2, sufficient to prevent Q from evolving, according to the following Scheme for TYR:[10)] where E_m, E_d and E_{ox} represent the oxidized and deoxygenated forms and a form with a peroxide group of the enzyme, respectively. Substrate is represented as S (Scheme 2).

This method uses the reduction by AH_2 of the product (Scheme 2d), which is generated by the enzyme (Scheme 2a–c).[10)] The true steady-state initial rate,

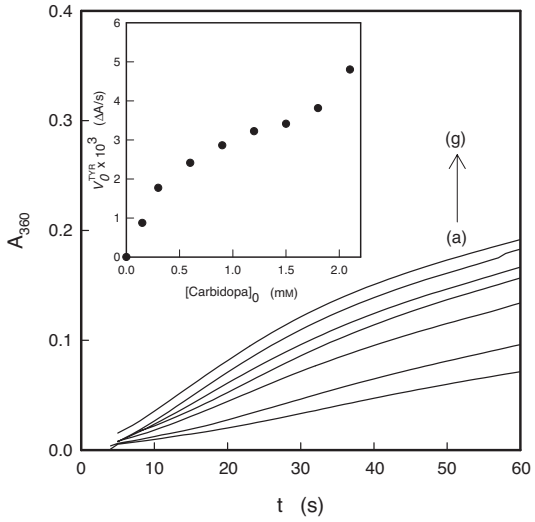

Fig. 1. Spectrophotometric Recordings of Product Generated in the Action of TYR on Carbidopa.

The experimental conditions were 30 mM sodium phosphate buffer (pH 6.0) at °C 25, λ 360 nm, 55 nM TYR. The substrate concentrations (mM) were (a) 0.15, (b) 0.3, (c) 0.6, (d) 0.9, (e) 1.2, (f) 1.5, and (g) 1.8. Inset. (●) Initial slope of V_0^{TYR} *vs.* [carbidopa]$_0$, directly measuring the appearance of product for TYR.

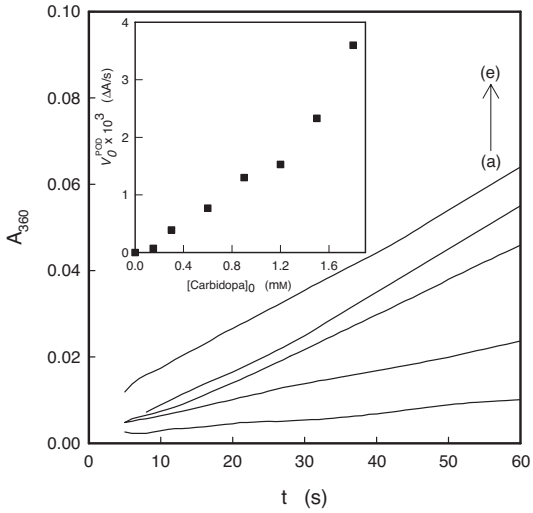

Fig. 2. Spectrophotometric Recordings of Product Generated in the Action of POD on Carbidopa.

The experimental conditions were 30 mM sodium phosphate buffer (pH 6.0) at °C 25, λ 360 nm, 1.35 nM POD, and 1 mM H_2O_2. The substrate concentrations (mM) were (a) 0.15, (b) 0.3, (c) 0.6, (d) 0.9, (e) 1.2, and (f) 1.5. Inset. (■) Initial slope of V_0^{POD} *vs.* [carbidopa]$_0$, directly measuring the appearance of product for POD.

V_0^{TYR}, is rapidly reached when $[O_2]_0$ and $[S]_0 \gg [E]_0$ in the case of TYR, or $[H_2O_2]_0$ and $[S]_0 \gg [E]_0$ in the case of POD, according to the following mass balance:

$$[AH_2]_t = [AH_2]_0 - V_0^{TYR} t \tag{1}$$

The term $V_0 t$ means the matter generated by the enzyme in the form of *o*-quinone or semiquinone in its action on substrate (TYR or POD). The intersection of the increase in absorbance of the recording Q *vs.* t and the time axis corresponds to $Q = 0$ and $t = \tau$ (lag period, Figs. 3 and 4). Thus, Eq. (1) is transformed into:

$$0 = [AH_2]_0 - V_0 \tau \tag{2}$$

and so, in the case of TYR:

$$V_0^{TYR} = \frac{[AH_2]_0}{\tau} \tag{3}$$

Therefore, if we can experimentally determine τ, and it $[AH_2]_0$ is known, V_0^{TYR} can be calculated according to Eq. (3). The value of τ can be experimentally determined if a spectrophotometric signal indicates that AH_2 has been consumed (see Fig. 3).

In the case of POD, in agreement with the stoichiometry of Scheme 3, the expression of V_0^{POD} is

$$V_0^{POD} = \frac{2[AH_2]_0}{\tau} \tag{4}$$

TYR is saturated by oxygen,[12] and, if $[O_2]_0 \to \infty$, the expression of V_0^{TYR}, in agreement with Scheme 2, is given by:

$$V_0^{TYR} = \frac{V_{\max}^{TYR}[S]_0}{K_m^{S,TYR} + [S]_0} \tag{5}$$

where

$$V_{\max}^{TYR} = 2k_{cat}^{TYR}[E]_0 = 2\frac{k_3 k_7}{k_3 + k_7}[E]_0 \tag{6}$$

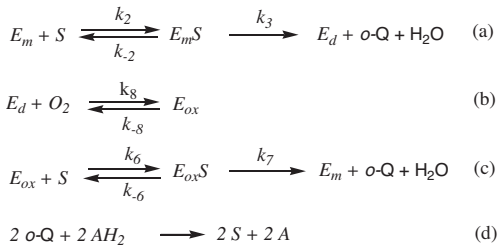

Scheme 2. Kinetic Mechanism of the Action of TYR.

$$K_m^{S,TYR} = \frac{k_2 k_3 (k_{-6} + k_7) + k_6 k_7 (k_{-2} + k_3)}{k_2 k_6 (k_3 + k_7)} \tag{7}$$

Due to the absence of rapid equilibrium in the oxidation of *o*-diphenols by *met*-tyrosinase and *oxy*-tyrosinase, $k_7 \gg k_{-6}$ and $k_3 \gg k_{-2}$.[10] From a pre-steady-state experiment, was determined that $k_2 \gg k_6$,[10] and therefore, from Eq. (7):

$$K_m^{S,TYR} = \frac{k_{cat}^{TYR}}{k_6} \tag{8}$$

When the enzyme is saturated by the substrate S and not by O_2, the expression of V_0^{TYR} is:

$$V_0^{TYR} = \frac{V_{\max}^{TYR}[O_2]_0}{K_m^{O_2} + [O_2]_0} \tag{9}$$

where

$$K_m^{O_2} = \frac{k_{cat}^{TYR}}{k_8} \tag{10}$$

Knowing k_{cat}^{TYR} for the reaction of TYR with a substrate and since k_8 is $((2.3 \pm 0.4) \times 10^7\ M^{-1}\ s^{-1})$,[10] the value of $K_m^{O_2}$ can be obtained (see Table 1).

From Eq. (8) for TYR, it is possible to calculate k_6, the binding rate constant of the substrate to the form E_{ox} (see Table 1).

The action of POD on reducing substrates (S) in the presence of H_2O_2 is described by Scheme 3:[4] where

Table 1. Kinetic Constants of the TYR/O_2/S and POD/H_2O_2/S Systems in Their Action on Carbidopa and Benserazide

TYR/O_2 S	k_{cat} (s^{-1})	K_m^S (mM)	$K_m^{O_2}$ (μM)	$k_6 \times 10^{-5}$ ($M^{-1}\,s^{-1}$)
Carbidopa	89 ± 3	0.79 ± 0.07	3.87 ± 0.69	$1.13 \pm 0.11^{\blacktriangle}$
Benserazide	35 ± 4	5.11 ± 0.51	$1.52 \pm 0.31^{\S}$	$0.68 \pm 0.01^{\blacktriangle}$
L-DOPA*	108 ± 9	0.38 ± 0.04	$6.51 \pm 3.01^{\S}$	$2.82 \pm 0.51^{\blacktriangle}$
POD/H_2O_2 S	k_{cat} (s^{-1})	K_m^S (mM)	$K_m^{H_2O_2}$ (μM)	$k_5 \times 10^{-3}$ ($M^{-1}\,s^{-1}$)
Carbidopa	1642 ± 98	0.96 ± 0.09	$96.58 \pm 11.58^{\ddagger}$	$1710.3 \pm 190.2^{\diamond}$
Benserazide	760 ± 34	4.26 ± 0.44	$44.71 \pm 6.03^{\ddagger}$	$180.2 \pm 20.1^{\diamond}$
L-DOPA#	—	—	—	$1.1 \pm 0.2^{\diamond}$

*Reference 10 and #Reference 4. §Data calculated from Eq. (10). ▲Data calculated from Eq. (8). ‡Data calculated from Eq. (17). ◇Data calculated from Eq. (18).

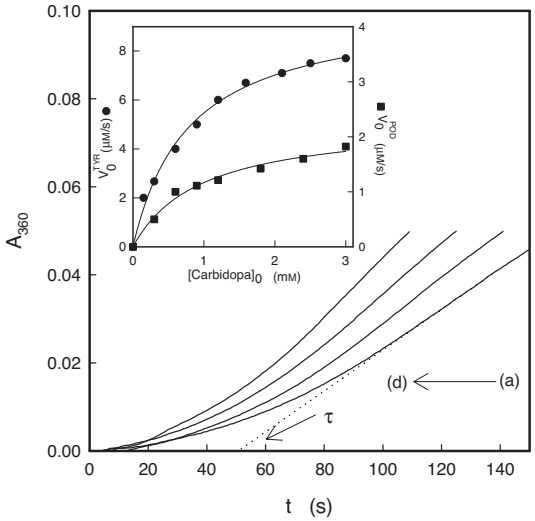

Fig. 3. Application of the Chronometric Method for Characterizing the Enzymatic Activity of TYR and POD on Carbidopa.

The experimental conditions were 30 mM sodium phosphate buffer (pH 6.0) at °C 25, λ 360 nm, 55 nM TYR, and 0.2 mM AH_2. Substrate concentrations (mM) were (a) 0.15, (b) 0.3, (c) 0.6, and (d) 0.9. Inset. (●) Representation of V_0^{TYR} *vs.* [carbidopa]$_0$ (■) Representation of V_0^{POD} *vs.* [carbidopa]$_0$. The experimental conditions were 30 mM sodium phosphate buffer (pH 6.0) at °C 25, λ 360 nm, 1.35 nM POD, 1 mM H_2O_2, and 0.1 mM AH_2.

POD indicates that free enzyme, POD-I, is compound I, POD-II, is compound II, and SQ-S is the semiquinone radical corresponding to *S*.

The kinetic analysis of the mechanism shown in Scheme 3,[4] results at saturating concentrations of H_2O_2 in:

$$V_0^{POD} = \frac{V_{\max}^{POD}[S]_0}{K_m^{S,POD} + [S]_0} \tag{11}$$

where

$$V_{\max}^{POD} = \frac{2k_2k_4k_6[E]_0}{k_2k_4 + k_4k_6 + k_2k_6} \tag{12}$$

and

$$K_m^{S,POD} = \frac{k_2k_5k_6(k_{-3} + k_4) + k_2k_3k_4(k_{-5} + k_6)}{k_3k_4k_5k_6 + k_2k_3k_5k_6 + k_2k_3k_4k_5} \tag{13}$$

When POD is saturated by the substrate *S*, the V_0^{POD} expression is:

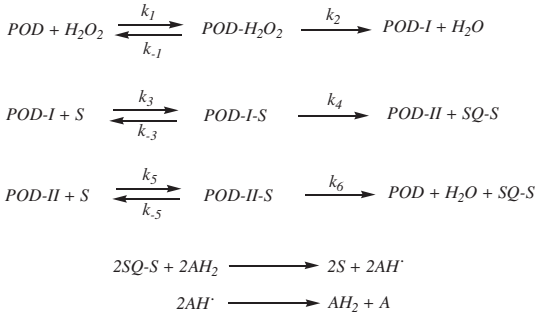

Scheme 3. Kinetic Mechanism of the Action of POD.

$$V_0^{POD} = \frac{V_{\max}^{POD}[H_2O_2]_0}{K_m^{H_2O_2} + [H_2O_2]_0} \tag{14}$$

where

$$K_m^{H_2O_2} = \frac{k_4k_6(k_{-1} + k_2)}{k_1k_4k_6 + k_1k_2k_6 + k_1k_2k_4} \tag{15}$$

If in the mechanism shown in Scheme 3, and from data found in the literature,[4] $k_2 \gg k_{-1}$, $k_4 \gg k_{-3}$, $k_6 \gg k_{-5}$, $k_3 \gg k_5$ and $k_4 \gg k_2$, k_6, the analytical expression for $V_{\max}^{POD}$, $K_m^{H_2O_2}$ and $K_m^{S,POD}$ are given after rearrangement by:

$$V_{\max}^{POD} = \frac{2k_2k_6[E]_0}{k_2 + k_6} = 2k_{cat}^{POD}[E]_0 \tag{16}$$

$$K_m^{H_2O_2} = \frac{k_2k_6}{k_1(k_2 + k_6)} = \frac{k_{cat}^{POD}}{k_1} \tag{17}$$

$$K_m^{S,POD} = \frac{k_2k_6}{k_5(k_2 + k_6)} = \frac{k_{cat}^{POD}}{k_5} \tag{18}$$

The value of k_1 is $1.7 \times 10^7\ M^{-1}\,s^{-1}$.[4] From Eq. (16), we can calculate k_{cat}^{POD} and from Eq. (17), $K_m^{H_2O_2}$. The binding rate constant of the substrate to compound II, k_5, can be calculated from Eq. (18) (Table 1). Therefore, the analysis of the data according to Eqs. (11)–(18) provides the kinetic information shown in Table 1 (Fig. 4 and Inset).

Calculation of $K_m^{O_2}$ *for TYR*

The Michaelis constant for the O_2 is given by Eq. (10). For tyrosinase substrates presenting a high value of K_m for oxygen (and, therefore, high k_{cat}^{TYR}) (*i.e.*, L-DOPA; see Table 1), $K_m^{O_2}$ can be calculated by the initial-rate method (obtained from initial rate determi-

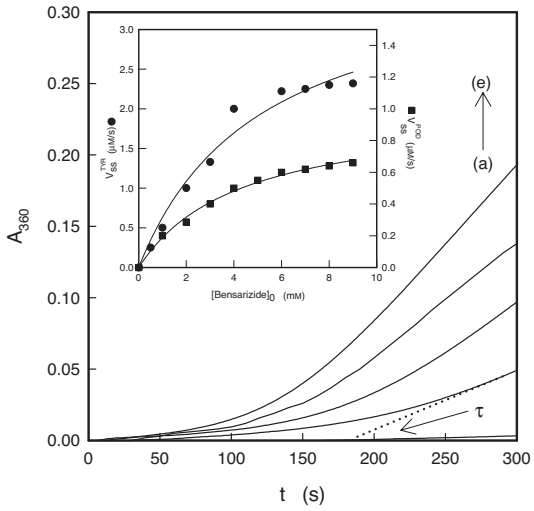

Fig. 4. Application of the Chronometric Method for Characterizing the Enzymatic Activity of TYR and POD on Benserazide.

The experimental conditions were 30 mM sodium phosphate buffer (pH 7.0) at °C 25, λ 360 nm, 1.35 nM POD, 1 mM H_2O_2, and 0.1 mM AH_2. Substrate concentrations (mM) were (a) 0.15, (b) 1, (c) 2, (d) 3, and (e) 6. Inset. (■) Representation of V_0^{POD} *vs.* [Benserazide]$_0$ (●) Representation of V_0^{TYR} *vs.* [benserazide]$_0$.

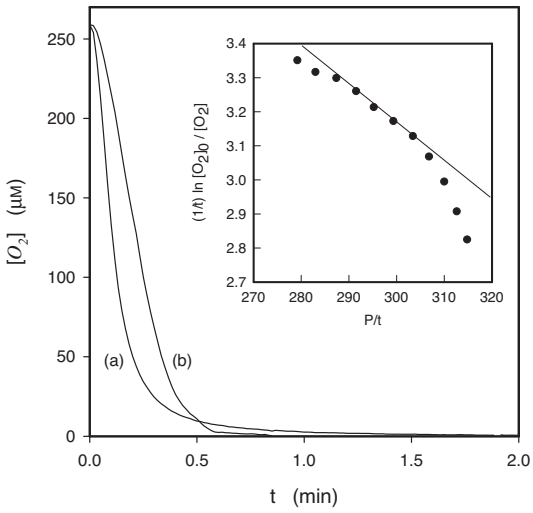

Fig. 5. Experimental Recording of the Disappearance of O_2 as a Result of TYR Oxidation of Carbidopa (a) and Benserazide (b).

The experimental conditions were 30 mM sodium phosphate buffer (pH 6.0) at °C 25, 0.35 µM TYR, 4 mM carbidopa (a), and 20 mM benserazide (b). Inset. Analysis according to Eq. (15) of the oxymetric recording of carbidopa oxidation (a) to calculate $K_m^{O_2}$.

nations). However, the values obtained for k_{cat}^{TYR} for carbidopa and benserazide (Table 1) predict low values of $K_m^{O_2}$ and, therefore, they should be determined experimentally by applying the integrated Michaelis equation:

$$\frac{1}{t}\ln\frac{[O_2]_0}{[O_2]} = -\frac{1}{K_m^{O_2}}\frac{[O_2]_0 - [O_2]}{t} + \frac{V_{\max}^{TYR}}{K_m^{O_2}} \quad (19)$$

For the oxidation of cabidopa by TYR/O_2, O_2 consumption curves can be obtained (Fig. 5a), which can be analyzed with Eq. (19) (Fig. 5 Inset). In the oxidation of benserazide by TYR/O_2, the O_2 consumption recordings are predominantly linear (Fig. 5b), and Eq. (19) could not be applied, probably because of the low value of k_{cat}^{TYR}, meaning that the $K_m^{O_2}$ could be very low and must be calculated with Eq. (10).

Comments on the kinetic constants

When the chronometric method described above was applied to the kinetic characterization of these substrates (carbidopa or benserazide), a hyperbolic dependence of V_0 *vs.* [S]$_0$ was obtained (Fig. 3 inset for TYR and Fig. 4 inset for POD).[13] Analysis of the data, as described in [66]Materials, and Methods[99], provided the information summarized in Table 1 for TYR and POD.

From these results (Table 1), it can be concluded that both substrates (carbidopa and benserazide) are worse substrates than L-DOPA for TYR.[10] The catalytic constant for TYR, k_{cat}^{TYR} was lower than that of the physiological substrate L-DOPA. The Michaelis constant values were higher than for L-DOPA, while the Michaelis constants for oxygen were very low, in agreement with Eq. (10). These data as a whole (Table 1) may be explained by the steric hindrance caused by the large size of the group in C-1.

The kinetic constants of POD with respect to these substrates are good and even better than those determined for L-DOPA.[4] Note how L-DOPA could not saturate the enzyme and so only the attack constant of the substrate on POD-II, k_5 could be calculated.[4] However, due to the chain in C-1, these substrates could have charges far from the benzene ring, which may favour access to the active site and so enable them to saturate the enzyme since there is a hydrophobic channel, with several phenylanalines, in the active site of this enzyme (Phe[68], Phe[179] and Phe[142]) (see Table 1).

In conclusion, the kinetic characterization of carbidopa and benserazide (dopa decarboxylase inhibitors) shows them to better substrates of peroxidase than L-DOPA, while the opposite is true in the case of tyrosinase.

Acknowledgments

This paper has been partially supported by grants from the Ministerio de Educación y Ciencia (Madrid, Spain) Project BIO2006-15363 and SAF2006-07040-C02-01, from the Fundación Séneca (CARM, Murcia, Spain) Project 00672/PI/04, and from the Consejería de Educación (CARM, Murcia, Spain) BIO-BMC 06/01-0004. JLMM has a fellowship from the Ministerio de Educación y Ciencia (Madrid, Spain) Reference AP2005-4721. FGM has a fellowship from Fundación Caja Murcia (Murcia, Spain).

References

1) Halaouli S, Asther M, Sigoillot JC, Hamdi M, and Lomascolo A, *J. Appl. Microbiol.*, **100**, 219–232 (2006).
2) Decker H, Schweikardt T, and Tuczek F, *Angew. Chem. Int. Ed. Engl.*, **45**, 4546–4550 (2006).
3) Dunford HB, "Heme Peroxidases," Wiley-VHC, New York, pp. 92–97 (1999).
4) Rodríguez-López JN, Gilabert MA, Tudela J, Thorneley RNF, and García-Cánovas F, *Biochemistry*, **39**, 13201–13209 (2000).
5) Gurney H, Coates A, and Kefford R, *J. Invest. Dermatol.*, **96**, 85–87 (1990).
6) Wick MM, *J. Invest. Dermatol.*, **88**, 535–537 (1987).
7) Palumbo A, d'Ischia M, Misuraca G, and Prota G, *Biochim.*

Biophys. Acta, **1073**, 85–90 (1991).
8) Palumbo A, Napolitano A, De Martino L, Vieira W, and Hearing V, *Biochim. Biophys. Acta*, **1200**, 271–276 (1994).
9) Borovanski J, Edge R, Land EJ, Navaratnam S, Pavel S, Ramsden CA, Riley PA, and Smith N, *Pigment Cell Res.*, **19**, 170–178 (2006).
10) Rodríguez-Lopez JN, Fenoll LG, Garcia-Ruiz PA, Varon R, Tudela J, Thorneley RN, and Garcia-Canovas F, *Biochemistry*, **39**, 10497–10506 (2000).
11) Bradford MM, *Anal. Biochem.*, **72**, 248–254 (1976).
12) Rodríguez-Lopez JN, Ros JR, Varon R, and Garcia-Canovas F, *Biochem. J.*, **293**, 859–866 (1993).
13) Muñoz JL, Garcia-Molina F, Varon F, Rodríguez-Lopez JN, Garcia-Canovas F, and Tudela J, *Anal. Biochem.*, **351**, 128–138 (2006).
14) Jandel Scientific. 2007 SigmaPlot 9.0 for Windows®, Jandel Scientific, Core Madera, CA.

4.8. CARACTERIZACIÓN CINÉTICA DE LA OXIDACIÓN DEL ÁCIDO CLOROGÉNICO POR POLIFENOL OXIDASA Y PEROXIDASA. CARACTERÍSTICAS DE LA *o*-QUINONA.

La caracterización cinética de la oxidación del ácido clorogénico por polifenol oxidasa y peroxidasa y la determinación de algunas características de su o-quinona ha dado lugar a la siguiente publicación adjunta.

4.8.1. Título

Kinetic characterization of the oxidation of chlorogenic acid by polyphenol oxidase and peroxidase. Characteristics of the *o*-quinone.

4.8.2. Autores

Muñoz, J.L.; Garcia-Molina, F.; Varon, R.; Rodríguez-López, J.N.; Garcia-Cánovas, F. y Tudela, J.

4.8.3. Referencia

Journal of Agricultural and Food Chemistry (2007) 55, 920-928.

4.8.4. Resumen

El ácido clorogénico es el difenol mayoritario en muchas frutas, donde es oxidado enzimáticamente por polifenol oxidasa (PPO) o peroxidasa (POD) a su *o*-quinona. En estudios espectrofotométricos de la oxidación de ácido clorogénico con una ratio de periodato $[CGA]_0/[IO_4^-]_0 < 1$ y $[CGA]_0/[IO_4^-]_0 > 1$, la *o*-quinona se caracterizó como sigue: λ_{max} a 400 nm y $\varepsilon = 2000\ M^{-1}\ cm^{-1}$ y $2200\ M^{-1}\ cm^{-1}$ a pH = 4.5 y 7.0 respectivamente. En estudios de la *o*-quinona generada por la oxidación de ácido clorogénico usando una ratio de $[CGA]_0/[IO_4^-]_0 > 1$, se detectó una reacción con el sustrato en exceso, mostrando unas constantes de velocidad $k = 2.73 \pm 0.17\ M^{-1}\ s^{-1}$ y $k' = 0.05 \pm 0.01\ M^{-1}\ s^{-1}$ a pH 4.5 y 7.0 respectivamente. Se propone un método espectrofotométrico cronométrico para caracterizar cinéticamente la acción de polifenol oxidasa y peroxidasa, basado en medir el tiempo que tarda en consumirse una determinada cantidad de ácido ascórbico a través de su reacción con la *o*-quinona. Se calculan las constantes cinéticas de polifenol oxidasa de champiñón y peroxidasa de rábano picante.

JOURNAL OF AGRICULTURAL AND FOOD CHEMISTRY

Kinetic Characterization of the Oxidation of Chlorogenic Acid by Polyphenol Oxidase and Peroxidase. Characteristics of the *o*-Quinone

J. MUÑOZ,† F. GARCIA-MOLINA,† R. VARON,§ J. N. RODRIGUEZ-LOPEZ,† P. A. GARCÍA-RUIZ,# F. GARCÍA-CÁNOVAS,*,† AND J. TUDELA†

GENZ: Grupo de Investigación de Enzimología, Departamento de Bioquímica y Biología Molecular-A, Facultad de Biología, Universidad de Murcia, E-30100 Espinardo, Murcia, Spain; Departamento de Química-Física, Escuela Politécnica Superior, Universidad de Castilla la Mancha, Avenida España s/n, Campus Universitario, E-02071 Albacete, Spain; and Departamento de Quimica Orgánica, Facultad de Quimica, Universidad de Murcia, E-30100 Espinardo, Murcia, Spain

Chlorogenic acid is the major diphenol of many fruits, where it is oxidized enzymatically by polyphenol oxidase (PPO) or peroxidase (POD) to its *o*-quinone. In spectrophotometric studies of chlorogenic acid oxidation with a periodate ratio of $[CGA]_0/[IO_4^-]_0 < 1$ and $[CGA]_0/[IO_4^-]_0 > 1$, the *o*-quinone was characterized as follows: λ_{max} at 400 nm and $\epsilon = 2000$ and 2200 M^{-1} cm^{-1} at pH 4.5 and 7.0, respectively. In studies of *o*-quinone generated by the oxidation of chlorogenic acid using a periodate at ratio of $[CGA]_0/[IO_4^-]_0 > 1$, a reaction with the remaining substrate was detected, showing rate constants of $k = 2.73 \pm 0.17$ M^{-1} s^{-1} and $K' = 0.05 \pm 0.01$ M^{-1} s^{-1} at the above pH values. A chronometric spectrophotometric method is proposed to kinetically characterize the action of the PPO or POD on the basis of measuring the time it takes for a given amount of ascorbic acid to be consumed in the reaction with the *o*-quinone. The kinetic constants of mushroom PPO and horseradish POD are determined.

KEYWORDS: Chlorogenic acid; polyphenol oxidase; peroxidase; ascorbic acid; *o*-quinone; molar absorptivity

INTRODUCTION

Chlorogenic acid (CGA) is the major phenolic compound found in many fruits, including apples, pears, cherries, and apricots (*1*). The product resulting from the enzymatic oxidation of CGA, the *o*-quinone (CGA-Q), has been reported to oxidize other polyphenols, such as flavans, by a coupled oxidation reaction (*1*). The enzymatic oxidation of polyphenols is important because polyphenols are the precursors of several biosynthetic pathways, including those of tannins, lignins, and melanins (*2*).

The browning damage caused to the tissues of fruits and vegetables during postharvest handling and processing is one of the main causes of quality loss (*3*). The main enzymes involved in these processes are polyphenol oxidase (EC 1.14.18.1; PPO) and peroxidase (EC 1.11.1.7; POD) (*4*).

Because CGA is the major component of many fruits, its enzymatic oxidation has attracted much attention. For example, it has been demonstrated that tobacco leaf and mushroom PPOs oxidize CGA at different velocities of catalysis and with different affinities (*5*).

The product formed by the enzymatic oxidation of CGA by PPO and POD is CGA-Q, directly in the case of PPO (*6*) and through the disproportion reaction of the semiquinone in the case of POD (*7*).

The evolution of CGA-Q has been studied by several authors (*6*−*9*). For example, it has been shown that CGA-Q generates H_2O_2 in the medium and CGA (*7*, *8*), which suggests that POD may be involved in the process of enzymatic browning, the enzyme working at the expense of the H_2O_2 generated by PPO in its action on CGA (*7*). The production of H_2O_2 in the melanogenesis pathway associated with L-dopa and dopamine oxidation has also been revealed (*10*).

However, the great instability of the CGA-Q has hindered its characterization. Very low absorptivity coefficients on the order of 970 M^{-1} cm^{-1} have been proposed (*8*), as have several pathways for CGA-Q evolution from the addition of water to generate a trihydroxylated compound, which would be oxidized by another molecule of CGA-Q (*6*, *9*), to the reaction of CGA-Q with molecules of substrate to generate polymers (*9*).

Spectrophotometric measurements of PPO or POD enzymatic activity on CGA may give erroneous results, precisely because of the instability of the CGA-Q, for which reason several authors

* Corresponding author (fax +34 968 363963; e-mail canovasf@um.es).
† Departamento de Bioquímica y Biología Molecular-A, Universidad de Murcia.
§ Departamento de Química-Física, Universidad de Castilla la Mancha.
# Departamento de Quimica Orgánica, Universidad ded Murcia.

10.1021/jf062081+ CCC: $37.00 © 2007 American Chemical Society
Published on Web 01/17/2007

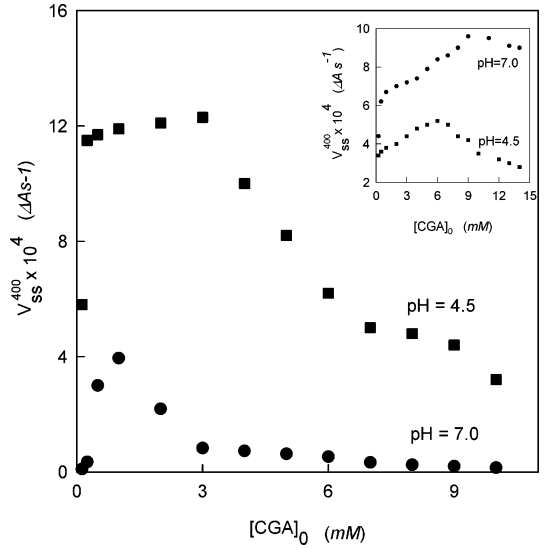

Figure 1. Representation of the rate of oxidation of CGA by PPO and POD. The velocity was monitored by measuring the variation in absorbance at 400 nm. Experimental conditions: phosphate buffer, 30 mM, pH 7.0; acetate buffer, 30 mM, pH 4.5, at 25 °C; [POD] = 2 nM; $[H_2O_2]_0 = 0.25$ mM. (Inset) To measure the rate of oxidation of CGA by PPO at the same pH values, the experimental conditions were the same except $[PPO]_0 = 35$ nM.

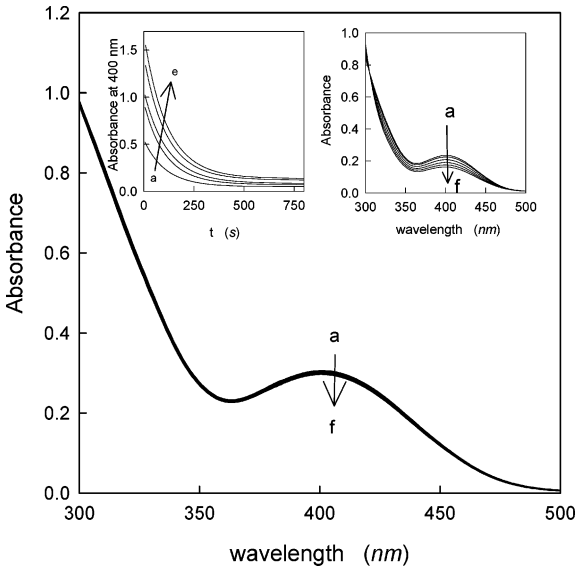

Figure 2. Oxidation of CGA by periodate at ratios of $[CGA]_0/[IO_4^-]_0 < 1$. Experimental conditions: $[CGA]_0 = 0.15$ mM; $[IO_4^-]_0 = 2.25$ mM; acetate buffer, 30 mM, pH 4.5. (Right inset) Oxidation in phosphate buffer, 30 mM, pH 7.0, $[CGA]_0 = 0.11$ mM; $[IO_4^-]_0 = 2.25$ mM. The measurements were made every 60 s. (Left inset) To measure the evolution of the CGA-Q generated by oxidation with periodate at ratios of $[CGA]_0/[IO_4^-]_0 < 1$, the experimental conditions were as follows: phosphate buffer, 30 mM, pH 7.0; $[IO_4^-]_0 = 7.5$ mM; and $[CGA]_0$ was varied [(a) 0.3 mM; (b) 0.45 mM; (c) 0.6 mM; (d) 0.75 mM; (e) 0.9 mM].

have proposed kinetic mechanisms of inhibition by excess of substrate (*1*, *2*, *11*−*14*). In the same way, studies involving the inhibition of mushroom PPO using CGA as substrate have concluded that the type and degree of inhibition depend not only on the inhibitor but also, and especially, on the method used to measure the enzymatic activity, which may be spectrophotometric (following the increase in absorbance at 420 nm)

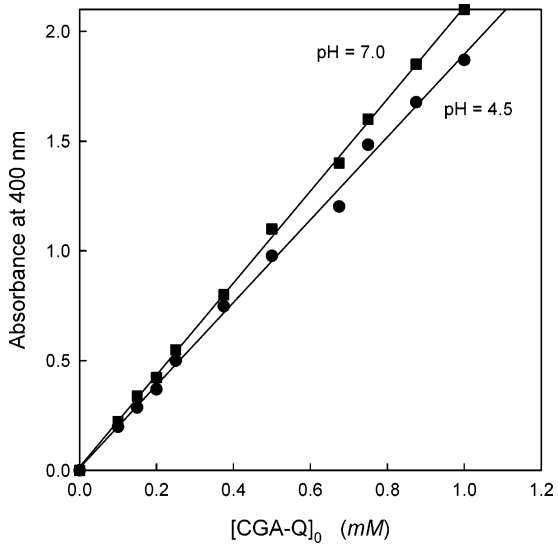

Figure 3. Representation of absorbance versus concentration of CGA-Q. Values of absorbance $\lambda = 400$ nm were obtained by oxidation with periodate at ratios of $[CGA]_0/[IO_4^-]_0 < 1$. Experimental conditions: acetate buffer, 30 mM, pH 4.5; phosphate buffer, 30 mM, pH 7.0. The concentration of $[IO_4^-]_0$ was 1.5 mM, and CGA concentration was the same as CGA-Q.

Scheme 1

$$\text{CGA-Q+CGA} \xrightarrow{k} \text{P}$$

or polarographic (monitoring oxygen consumption using a Wilson oxygraph equipped with a Clark electrode) (*15*). The results described above can be explained by the instability of the CGA-Q.

Because CGA is the major compound in many fruits, several methods have been designed to monitor PPO activity, sometimes termed chlorogenic acid oxidase, measuring the disappearance of chlorogenic acid at 325 nm (*1*). A method based on differential spectrophotometry has been designed for PPO, whereby the reaction is followed in the ultraviolet wavelength range during enzymatic polyphenol oxidation (*16*). Although measurements obtained in this way closely agree with the measurements of oxygen uptake done with the manometric method, the method can be applied only at low concentrations of CGA (*16*).

The study of CGA and its products is important because of the abundance of this compound: for example, 3.4−14 mg/100 mg of fresh weight in potatoes, 12−31 mg/100 mL in apple juice, 89 mg /100 mg in dry tea shorts, and 250 mg per cup of coffee (*17*, *18*). Furthermore, it has been attributed anticarcinogenic (*19*, *20*), antimutagenic (*21*), and antiinflammatory (*22*) properties. Recently, too, the antinitrosating properties of CGA, which serves as an efficient nitrite scavenger and a suppresser of nitrosamine formation in the gastric compartment (*23*−*25*), have also been emphasized. The formation of CGA adducts with glutathiones has also been characterized (*26*).

In this work, we study some of the properties of CGA-Q and some kinetic characteristics of its evolution; we also propose a chronometric spectrophotometric measurement method that kinetically characterizes the enzymes responsible for its oxidation, including PPO and POD.

MATERIALS AND METHODS

Materials. Chlorogenic acid, mushroom tyrosinase (3320 units/mg), and horseradish peroxidase (HRP isoenzyme C type IV, 280 units/mg)

were obtained from Sigma Chemical Co. H_2O_2 was obtained from Scharlau (Madrid, Spain). The substrate was prepared in dilute phosphoric acid.

Other Methods. Protein was determined according to Bradford's method using bovine serum albumin as standard (*27*).

Determination of Enzymatic Activity. Enzymatic activity was determined spectrophotometrically using the method described under Results and Discussion. The only condition is that there must be an absorbance increase (due to product formation) that can be measured once the ascorbic acid is consumed. Preliminary experiments were carried out in the absence of ascorbic acid with the PPO/O_2/CGA and POD/H_2O_2/CGA systems, recording spectrophotometric scans to identify in which zone of the spectrum, particularly the visible zone, the greatest changes in absorbance occurred. The wavelength chosen at both acid and neutral pH was 400 nm. Peroxidase activity was followed in the same way.

Kinetic Data Analysis. Initial rate values (V_0) were calculated from triplicate measurements at each reducing substrate concentration. The reciprocals of the variances of V_0 were used as weighting factors in the nonlinear regression fitting of V_0 versus $[CGA]_0$ data to the Michaelis−Menten equation. The fitting was carried out using Marquardt's algorithm (*28*) implemented in the Sigma Plot 9.0 program for Windows (*29*).

NMR Assays. ^{13}C NMR spectra of chlorogenic acid were recorded at pH 4.5 and 7.0 on a Varian Unity spectrometer (300 MHz) using ^2H_2O as solvent. Chemical shift values (δ) were determined relative to those of tetramethylsilane ($\delta = 0$). The maximum accepted error for each peak was ± 0.1 ppm.

RESULTS AND DISCUSSION

Enzymatic Oxidation of Chlorogenic Acid. CGA is the main acid found in fruits, including apples and pears (*1*). Peroxidase catalyzes the oxidation of the *o*-diphenols to semiquinones, which disproportionate to generate the corresponding *o*-quinone, regenerating substrate at the same time (*30*). The enzymatic oxidation of CGA by POD/H_2O_2 and PPO/O_2 transforms the substrate into one product with a maximum at 400 nm. CGA is oxidized by PPO to its corresponding *o*-quinone (CGA-Q), which shows a maximum at 400 nm (*8*). When the enzymatic reaction is followed at this wavelength, during the oxidation of CGA both with POD/H_2O_2 and with PPO/O_2, the results shown in **Figure 1** and its inset are obtained. The explanation of the results shown in **Figure 1** has been given as an inhibition by excess of substrate (*1*, *2*, *11*−*14*). However, the characteristics of *o*-quinones described in other works (*31*) led us to look at the instability of the CGA-Q and its possible control to enable the kinetic characterization of this important substrate. For this, we carried out the following series of experiments.

Oxidation of CGA by Sodium Periodate. It is known that sodium periodate oxidizes different *o*-diphenols in a way similar to that followed by PPO (*32*). Because our aim was to characterize POD and PPO, which can show pH maxima running from acidic (pH 4.5), in the case of POD, to close to neutrality (pH 7.0) for mushroom PPO (*33*), oxidations were carried out using sodium periodate at both pH values to characterize CGA-Q.

Oxidation of CGA with Periodate at a Ratio of $[CGA]_0/[IO_4^-]_0 < 1$. When oxidation was carried out at pH 4.5 with $[CGA]_0/[IO_4^-]_0 < 1$, the spectra of CGA-Q showed a maximum at $\lambda = 400$ nm. Successive scans indicated that in these conditions CGA-Q is stable during the measurement time. However, at pH 7.0, the CGA-Q evolves to generate two isosbestic points, indicating stoichiometric evolution (**Figure 2**, right inset). This behavior might be the result of attack by a hydroxyl or by another *o*-quinone (*6*), and the adduct would be freshly oxidized by periodate (**Figure 3**).

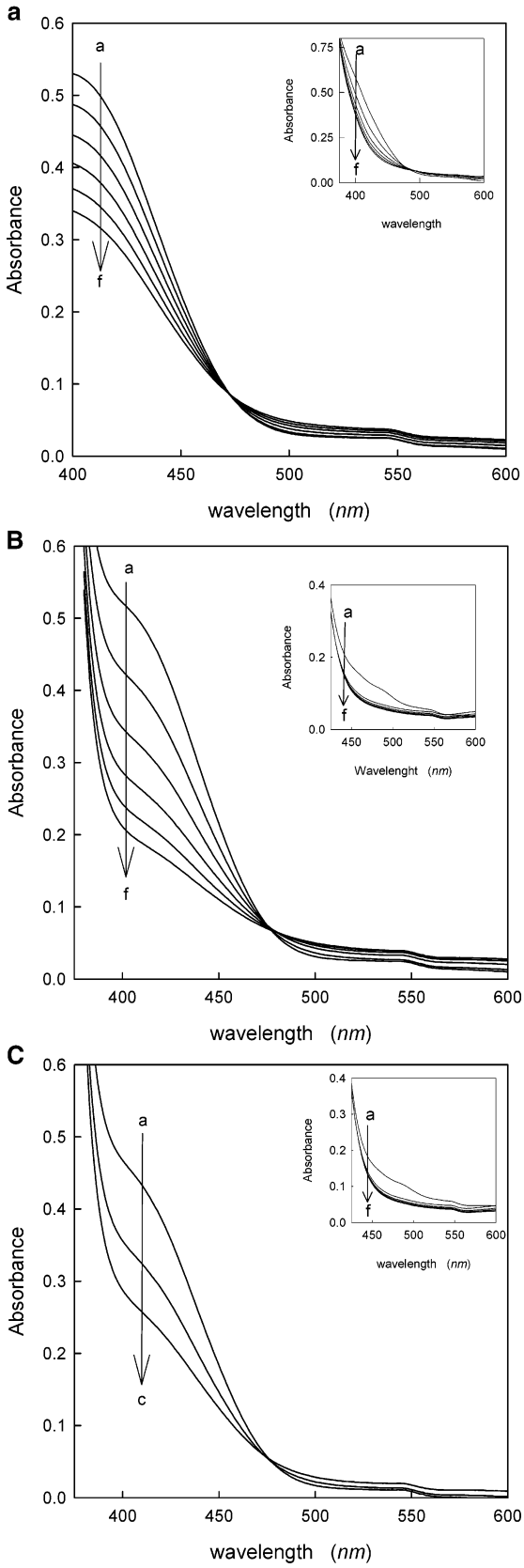

Figure 4. Spectrophotometric scans of CGA-Q generated with periodate at different $[CGA]_0/[IO_4^-]_0$ ratios: (**A**) $[CGA]_0/[IO_4^-]_0$ ratio = 2, $[CGA]_0 = 0.5$ mM, pH 4.5, acetate buffer, 30 mM [(inset) pH 7.0, phosphate buffer, 30 mM]; (**B**) $[CGA]_0/[IO_4^-]_0$ ratio = 6, $[CGA]_0 = 1.5$, pH 4.5 [(inset) pH 7.0]; (**C**) $[CGA]_0/[IO_4^-]_0$ ratio = 8, $[CGA]_0 = 2$ mM, pH 4.5 [(inset) pH 7.0].

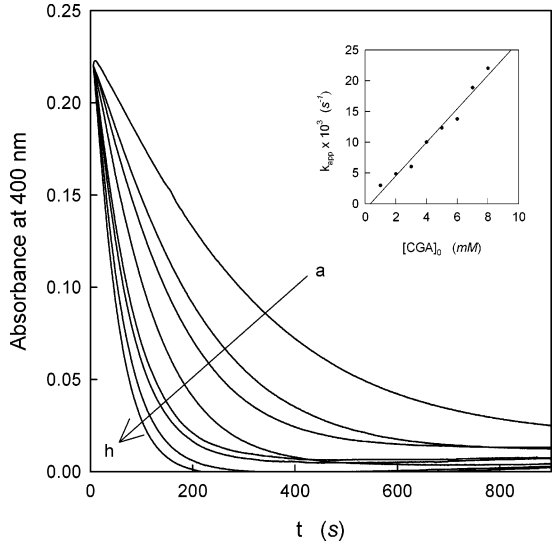

Figure 5. Kinetic of evolution of CGA-Q generated by oxidation with periodate at ratios of $[CGA]_0/[IO_4^-]_0 > 1$. Experimental conditions: acetate buffer, 30 mM, pH 4.5, $[IO_4^-]_0 = 0.12$ mM. Concentrations of $[CGA]_0$: (a) 1 mM; (b) 2 mM; (c) 3 mM; (d) 4 mM; (e) 5 mM; (f) 6 mM; (g) 7 mM; (h) 8 mM. (Inset) Representation of apparent constant with respect to CGA concentration.

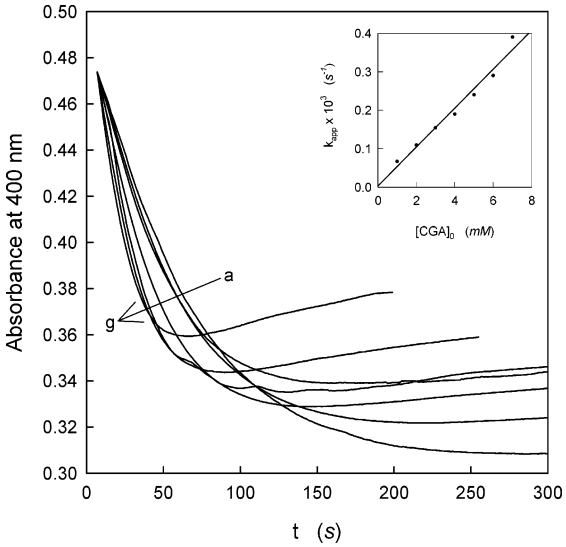

Figure 6. Kinetic of evolution of CGA-Q generated by oxidation with periodate at ratios of $[CGA]_0/[IO_4^-]_0 > 1$. Experimental conditions: phosphate buffer, 30 mM, pH 7.0, $[IO_4^-]_0 = 0.2$ mM. Concentrations of CGA: (a) 0.5 mM; (b) 1 mM; (c) 1.10 mM; (d) 1.5 mM; (e) 2 mM; (f) 2.25 mM; (g) 3 mM. (Inset) Representation of apparent constant with respect to CGA concentration.

Experiments were carried out at different concentrations of CGA at pH 7.0, and the evolution of CGA-Q with time was recorded at $\lambda = 400$ nm. The kinetic of this reaction was complex (**Figure 2**, left Inset).

The above experimental approach with periodate at ratios of $[CGA]_0/[IO_4^-]_0 < 1$ allowed us to calculate the molar absorptivity coefficient of the CGA-Q at the different pH values studied (**Figure 3**), the values at 400 nm being 2000 and 2200 M^{-1} cm^{-1} at pH 4.5 and 7.0, respectively. When CGA was oxidized at a ratio of $[CGA]_0/[IO_4^-]_0 > 1$, similar values were obtained.

Oxidation of CGA with Periodate at a Ratio of $[CGA]_0/[IO_4^-]_0 > 1$. Although the above experimental conditions of oxidation periodate at ratios of $[CGA]_0/[IO_4^-]_0 < 1$ are suitable for calculating the molar absorptivity coefficient, neither PPO nor POD works in these conditions. For any kinetic characterization $[CGA]_0 \gg [E]_0$ must be accomplished, and, because to maintain the steady state the substrate concentration should not vary much, then $[CGA\text{-}Q] \ll [CGA]_0$. These are conditions similar to those obtained by oxidation at ratios of $[CGA]_0/[IO_4^-]_0 > 1$.

Several oxidations of CGA with periodate were carried out with different $[CGA]_0/[IO_4^-]_0$ ratios of 2−8. **Figure 4A** (ratio 2), **Figure 4B** (ratio 6), and **Figure 4C** (ratio 8) show the scans obtained for oxidation by periodate. Note the isosbestic point

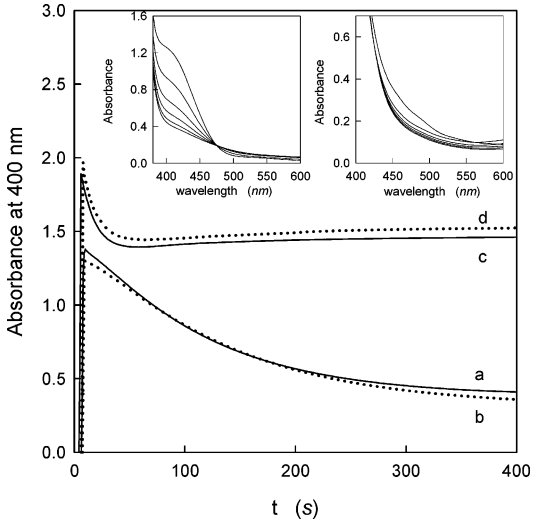

Figure 7. Enzymatic oxidation of CGA: (a) oxidation of CGA with PPO 0.2 μM at pH 4.5;(b) oxidation of CGA with POD 20 nM at pH 4.5 and $[H_2O_2]_0 = 0.5$ mM; (c) oxidation of CGA with PPO 0.2 μM at pH 7.0; (d) oxidation of CGA with POD 20 nM, at pH 7.0 and $[H_2O_2]_0 = 0.5$ mM. In curves a–d, $[CGA]_0 = 3$ mM. (Left inset) Spectrophotometric scans of evolution of CGA-Q generated enzymatically at pH 4.5. (Right inset) Spectrophotometric scans of evolution of CGA-Q generated enzymatically at pH 7.0.

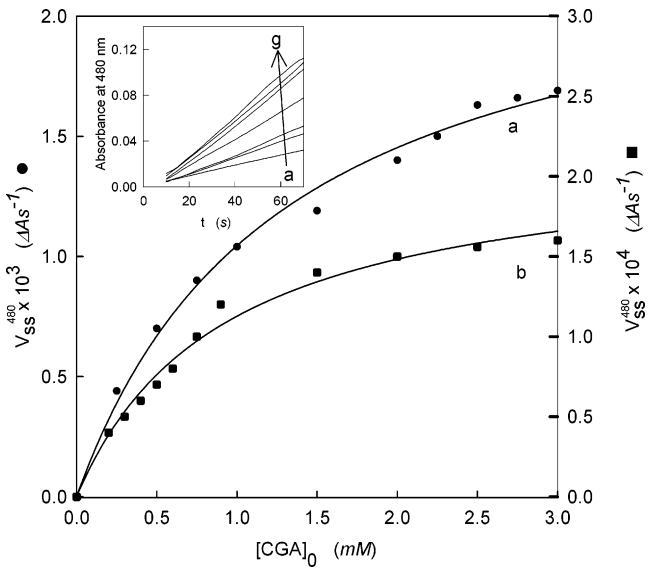

Figure 8. Measurement of PPO and POD activity at pH 4.5; representation of V_0 versus $[CGA]_0$: (a) PPO 25 nM; (b) POD 2 nM at $[H_2O_2]_0 = 0.1$ mM. (Inset) Experimental recordings of isosbestic point $\lambda = 480$ nm, of CGA-Q generation at pH 4.5. Substrate concentration: (a) 0.25 mM; (b) 0.5 mM; (c) 0.75 mM; (d) 1.5 mM; (e) 2.5 mM; (f) 2.75 mM; (g) 3 mM.

Table 1. Kinetic Constants That Characterize the Action of PPO on CGA

substrate[a]	pH	method	k_{cat} (s^{-1})	K_m (mM)	k_6[b] (M^{-1} s^{-1})	$K_m^{O_2}$ (μM)	δ_3	δ_5	reference
CGA	4.5	isosbestic point	135 ± 12	1.30 ± 0.10	$(1.04 \pm 0.8) \times 10^5$	5.8 ± 0.12	145.9	148.8	this paper
	4.5	chronometric	121 ± 7	1.38 ± 0.11	$(8.77 \pm 1.0) \times 10^4$	5.3 ± 0.10			this paper
	7.0	chronometric	176 ± 10	0.87 ± 0.08	$(2.03 \pm 0.5) \times 10^5$	7.6 ± 0.08	146.4	149.3	this paper
MeCAT	7.0	O_2 consumption	842 ± 25	0.12 ± 0.02	$(7.02 \pm 1.5) \times 10^6$	35.8 ± 3.20	146.4	144.1	*34*
TBC	7.0	O_2 consumption	641 ± 20	1.41 ± 0.20	$(4.55 \pm 0.8) \times 10^5$	28.0 ± 3.10	146.2	144.1	*34*
CAT	7.0	O_2 consumption	878 ± 50	0.10 ± 0.01	$(8.78 \pm 1.2) \times 10^6$	40.5 ± 4.00	146.6	146.6	*34*
dopamine	7.0	O_2 consumption	439 ± 25	0.72 ± 0.01	$(6.10 \pm 1.1) \times 10^5$	21.5 ± 3.10	146.9	145.7	*34*

[a] CGA, chlorogenic acid; MeCAT, 1-methylcatechol; TBC, 1-*tert*-butylcatechol; CAT, pyrocatechol. [b] Binding constant of CGA to E_{ox} (**Scheme 3**).

Table 2. Kinetic Constants That Characterize the Action of POD on CGA

substrate	pH	method	k_{cat} (s^{-1})	K_m^S (mM)	$K_m^{H_2O_2}$ (μM)	k_{+5} (M^{-1} s^{-1})	k_{+6}[a] (s^{-1})	k_2[b] (s^{-1})	δ_3	δ_4	reference
CGA	4.5	isosbestic point chronometric	880 ± 40	0.30 ± 0.05	25 ± 1	$(3.00 \pm 1.32) \times 10^4$	1.57×10^3	2000	145.9	148.8	this paper
	4.5	chronometric	910 ± 22	0.52 ± 0.05	26 ± 1	$(3.80 \pm 1.52) \times 10^4$	1.67×10^3	2000			this paper
	7.0		674 ± 13	0.48 ± 0.05	20 ± 1	$(2.60 \pm 1.02) \times 10^4$	1.02×10^3	2000	146.4	149.3	this paper
MeCAT	7.0	chronometric	2155 ± 105	1.30 ± 0.10	128 ± 8	$(1.66 \pm 0.20) \times 10^6$	$>2.00 \times 10^4$	2000	146.4	144.1	*31*
TBC	7.0	chronometric	2146 ± 100	2.60 ± 0.20	125 ± 7	$(8.25 \pm 1.02) \times 10^5$	$>2.00 \times 10^4$	2000	146.2	144.1	*31*
CAT	7.0	chronometric	2200 ± 150	2.30 ± 0.10	129 ± 8	$(9.56 \pm 1.06) \times 10^5$	$>2.00 \times 10^4$	2000	146.6	146.6	*31*
dopamine	7.0	chronometric	447 ± 42	16.80 ± 1.30	27 ± 4	$(2.66 \pm 0.45) \times 10^4$	5.36×10^2	2000	146.9	145.7	*31*

[a] Transformation constant of CGA in CGA-SQ for POD-II (**Scheme 4**). [b] Data taken from ref *31*.

is maintained at 475 nm and pH 4.5, with clear stoichiometry in the evolution of CGA-Q. When oxidation was carried out at pH 7.0, there was an isosbestic point at low concentrations of CGA, but this was broken when concentrations were raised (**Figure 4A−C**, inset). In theory, these experiments show that CGA-Q does not evolve with a clear stoichiometry at pH 7.0.

Kinetic Evolution of the *o*-Quinone. Oxidation of CGA with periodate at a ratio of $[CGA]_0/[IO_4^-]_0 > 1$ at acid pH (4.5) generates CGA-Q, which evolves with a clear stoichiometry (**Figure 4**). The kinetic of this evolution is shown in **Figure 5**. In these experiments, different initial concentrations of CGA were oxidized with the same concentration of sodium periodate and the evolution of the CGA-Q was monitored at $\lambda = 400$ nm. The apparent constant of the evolution of CGA-Q increased with increasing concentrations of CGA, suggesting that the quinone reacted with the substrate according to the mechanism shown in **Scheme 1**, where P may be a dimer.

The rate of disappearance of CGA-Q is

$$\frac{-\mathrm{d[CGA\text{-}Q]}}{\mathrm{d}t} = k_{app}[\mathrm{CGA\text{-}Q}] \quad (1)$$

and so

$$[\mathrm{CGA\text{-}Q}]_t = [\mathrm{CGA\text{-}Q}]_0 \, \mathrm{e}^{-k_{app}t} \quad (2)$$

with

$$k_{app} = k[\mathrm{CGA}]_0 \quad (3)$$

Analysis of the experimental recordings (**Figure 5**) according to eq 2 provides k_{app}, and its dependence on $[CGA]_0$ is shown in the inset of **Figure 5**, giving a second-order rate constant (k) of 2.73 ± 0.17 M^{-1} s^{-1}.

When CGA is oxidized in conditions by periodate at a ratio of $[CGA]_0/[IO_4^-]_0 > 1$ but at pH 7.0, the recordings shown in **Figure 6** are obtained, and the disappearance of CGA-Q can be followed as in **Figure 5**. Analysis of the data using eq 2 gives us the value of k'_{app}, which increases with increasing concentrations of CGA. The inset of **Figure 6** depicts k'_{app} versus $[CGA]_0$, giving a second-order rate constant (k') of 0.05 ± 0.01 M^{-1} s^{-1}. Note that at longer times the absorbance at 400 nm increases, perhaps because the adduct is oxidized by the CGA-Q, to give a new quinone, in agreement with ref *9*. These results would be in agreement with a rupture of the isosbestic point in **Figure 4A−C** (inset), because several reactions would overlap in time.

Enzymatic Oxidation of Chlorogenic Acid. When the CGA is oxidized at pH 4.5 with high enzyme concentrations, the recordings of **Figure 7** are obtained. With PPO, **Figure 7**, trace a, the absorbance at 400 nm increases until all of the oxygen is used up, after which the CGA-Q disappears as a result of the reaction with the substrate, giving a kinetic similar to that shown in **Figure 5**. How the CGA-Q evolves is shown in **Figure 7** (left inset); the isosbestic point is similar to that obtained for the oxidations with sodium periodate at a ratio of $[CGA]_0/[IO_4^-]_0 > 1$ (**Figure 4A−C**). Similar results were obtained with POD [**Figure 7** (trace b and left inset)].

If oxidation is carried out at pH 7.0, we obtain trace c with PPO and trace d with POD, again similar to that obtained with oxidation using sodium periodate at a ratio of $[CGA]_0/[IO_4^-]_0 > 1$. The absence of an isosbestic point (**Figure 7**, right inset) confirms the nonstoichiometric evolution of the CGA-Q during the oxidation with both enzymes at this pH.

In light of the above results, the kinetic characterization of CGA with enzymes such as mushroom PPO at its optimum pH (7.0) is difficult, and the results have been interpreted as an inhibition through excess of substrate (*1*, *2*, *11−14*). Something similar occurs with POD/H_2O_2 (**Figure 1**).

In this work we propose two methods for kinetically characterizing CGA as a substrate for PPO and POD, which have different pH optima. Both methods are based on the monitoring of the evolution of the quinone, but two cases can be distinguished.

(a) Kinetic Characterization at Acid pH. In this case, the isosbestic point obtained for the evolution of CGA-Q is selected as measurement wavelength (**Figure 8**). The wavelength of 480 nm is obtained in **Figure 7** (right inset), and once the molar absorptivity coefficient has been obtained ($\epsilon_i = 360$ M^{-1} cm^{-1}),

the recordings of **Figure 8** (inset) and their analysis give the values of k_{cat} and K_m, which are shown in **Table 1** for PPO and in **Table 2** for POD.

(b) Kinetic Characterization at Acid or Neutral pH. This spectrophotometric method does not involve measuring CGA-Q because of its instability. However, it may be prevented by using ascorbic acid (AH_2), according to **Scheme 2** for PPO.

However, it is not possible to follow the disappearance of AH_2 because the spectra of CGA and AH_2 overlap at the different pH values assayed (results not shown), and so we propose the following chronometric method.

The method uses the antioxidant power of AH_2, which reacts rapidly with the CGA-Q generated by the enzyme (*31*) (**Scheme 2**). The steady-state rate is V_0, which is rapidly reached when $[O_2]_0$ and $[CGA]_0 \gg [E]_0$ in the case of PPO or when $[H_2O_2]_0$ and $[CGA]_0 \gg [E]_0$ in the case of POD, fulfilling the following mass balance:

$$V_0 t - [AH_2] = \text{CGA-Q} \tag{4}$$

The total quantity of material entering the system is $V_0 t$, where t is the time during which the enzyme acts. In the presence of ascorbic acid, the CGA-Q is reduced to CGA, until no AH_2 remains. The straight line absorbance versus t cuts axis X at CGA-Q = 0, and so eq 4 is transformed into

$$V_0 \tau - [AH_2] = 0 \tag{5}$$

Reorganising eq 5 gives

$$V_0 = \frac{[AH_2]_0}{\tau} \tag{6}$$

Taking into account the kinetic mechanisms of PPO and POD described below, some conditions can be established so that this chronometric method provides suitable values for parameter V_0, thus permitting these enzymes to be characterized.

The diphenolase activity of PPO is described in **Scheme 3** (*33*), where E_m, E_d, and E_{oxy} represent the oxygenated and deoxygenated forms and another with a peroxide group, respectively. V_0 is given by (*33*)

$$V_0 = \frac{V_{max}[CGA]_0[O_2]_0}{K_m^{CGA} k_s^{O_2} + K_m^{O_2}[CGA]_0 + K_m^{CGA}[O_2]_0 + [CGA]_0[O_2]_0} \tag{7}$$

where

$$V_{max} = 2k_{cat}[E]_0 = \frac{2k_3 k_7}{k_3 + k_7}[E]_0 \tag{8}$$

$$K_s^{O_2} = \frac{k_{-8}}{k_8} \tag{9}$$

$$K_m^{O_2} = \frac{k_{cat}}{k_8} \tag{10}$$

$$K_m^{CGA} = \frac{k_{cat}}{k_6} \tag{11}$$

POD activity on the reducing substrates (CGA) in the presence of H_2O_2 is described by **Scheme 4** (*30*), where POD stands for the free enzyme, POD-I is compound **I**, POD-II is compound **II**, and CGA-SQ is the semiquinone radical corresponding to the CGA.

The following expression is obtained for the rate of radical formation:

$$V_0 = \frac{2k_{cat}[H_2O_2]_0[CGA]_0[E]_0}{\frac{k_{cat}}{k_5}[H_2O_2]_0 + \frac{k_{cat}}{k_1}[CGA]_0 + [H_2O_2]_0[CGA]} \tag{12}$$

This equation can be rearranged as follows:

$$V_0 = \frac{V_{max}^{app,CGA}[CGA]_0}{K_m^{app,CGA} + [CGA]_0} \tag{13}$$

where

$$V_{max}^{app,CGA} = \frac{2k_{cat}[H_2O_2]_0[E]_0}{\frac{k_{cat}}{k_1} + [H_2O_2]_0} \tag{14}$$

$$K_m^{app,CGA} = \frac{\frac{k_{cat}}{k_5}[H_2O_2]_0}{\frac{k_{cat}}{k_1} + [H_2O_2]_0} \tag{15}$$

and

$$k_{cat} = \frac{k_2 k_6}{k_2 + k_6} \tag{16}$$

$$K_m^{CGA} = \frac{k_{cat}}{k_5} \tag{17}$$

$$K_m^{H_2O_2} = \frac{k_{cat}}{k_1} \tag{18}$$

Characterization of PPO. The experimental conditions in the presence of AH_2 imply that the concentration of reducing substrate (CGA) remains constant during the lag phase, although $[O_2]$ will vary with the stoichiometry $1O_2$:2CGA:$2AH_2$. Thus, the permitted concentration of AH_2 in the experiment will be $\leq 0.1[O_2]$, so that O_2 consumption will be <10% and V_0 will not vary, and the steady-state will be reached.

Kinetic Experiments To Accurately Estimate the Initial Rate. To apply the method, it is necessary to take into account the following points: (a) limitation of the consumption (as mentioned above, the concentration of O_2 determines the suitable concentration of AH_2; thus, $[AH_2]_0 \leq [O_2]_0$ should be used); (b) length of the lag period [the minimum length of the lag period must be greater than the "dead time" of the measurement, τ_d (12 s); we opted for $\tau \geq 3\,\tau_d$, which was achieved by varying $[E]_0$ (see eq 6); however, τ should not be so long that changes in the blank samples (due to the chemical reaction of O_2 with AH_2) become significant]; (c) quantity of AH_2 used in the assays [this quantity is limited by O_2 consumption (see above)].

Validation of Initial Rate Determination. *Effect of Enzyme Concentration.* At constant concentrations of both substrates and AH_2, the lag period diminishes as the enzyme concentration increases, resulting in an increase of V_0 (see eq 6) (results not shown).

Effect of Substrate Concentration. When the concentrations of the other reagents are kept constant and the concentration of substrate (CGA) is increased, the lag period becomes shorter because V_0 increases, according to eq 6 (**Figure 9**).

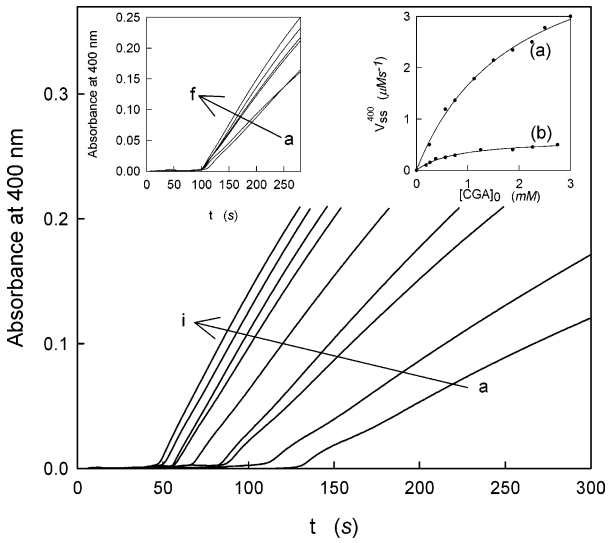

Figure 9. Chronometric method for characterizing enzymatic activity of PPO on CGA; effect of substrate concentration. Experimental conditions: acetate buffer, 30 mM, pH 4.5; $[E]_0 = 13.5$ nM; $[AH_2]_0 = 75$ μM. Substrate concentration: (a) 0.35 mM; (b) 0.55 mM; (c) 0.75 mM; (d) 1.10 mM; (e) 1.85 mM; (f) 2 mM; (g) 2.25 mM; (h) 3 mM; (i) 3.15 mM. (Left inset) Spectrophotometric recordings of chronometric method at constant $[CGA]_0 \times [E]_0$ value. Experimental conditions: acetate buffer, 30 mM, pH 4.5. The value of $[CGA]_0 \times [E]_0 = 6.5 \times 10^{-6}$ mM^2 and the concentrations of $[CGA]_0$ and $[E]_0$ were (a) 0.35 mM, (b) 0.55 mM, (c) 0.75 mM, (d) 0.95 mM, (e) 1.10 mM, (f) 2.25 mM and $[E]_0$ (a) 17.5 nM, (b) 11.5 nM, (c) 8.5 nM, (d) 7 nM, (e) 6 nM, and (f) 3 nM, respectively, and $[AH_2]_0 = 75$ μM. (Right inset) Representation of steady-state rate versus $[CGA]_0$; (a) pH 4.5; (b) pH 7.0.

Scheme 2

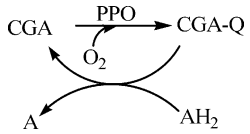

Scheme 3

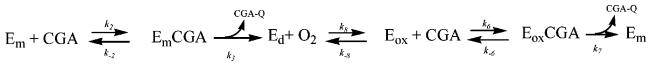

To avoid the effects of V_0 due to the blanks of the assays, we propose that in a kinetic characterization where the substrate varies and therefore V_0, too, the τ may be very different. To make the values of τ as similar as possible so that the oxidation of AH_2 by O_2 or H_2O_2 takes place at the same time, we suggest varying the enzyme and substrate concentrations at the same time in such a way that their product ($[CGA]_0 \times [E]_0$) is constant. In this way τ remains practically constant and the values of V_0 can be normalized in accordance with the corresponding factor (see **Figure 9**, left inset).

Kinetic Characterization of POD. In these experiments, the same restrictions as for PPO are applied, except that, because this enzyme consumes H_2O_2, the concentration of AH_2 must fulfill $[AH_2]_0 \leq 0.1\ [H_2O_2]_0$.

Furthermore, in agreement with the stoichiometry of **Scheme 4**, the expression of V_0 is

$$V_0 = \frac{2[AH_2]_0}{\tau} \qquad (19)$$

When the concentrations of the other reagents are kept constant and the concentration of substrate (CGA) is increased,

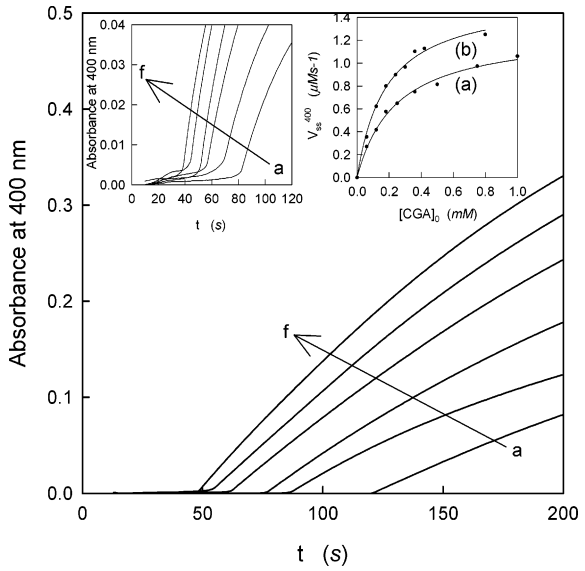

Figure 10. Chronometric method used for characterizing enzymatic activity of POD on CGA. The effect of the substrate concentration is presented. Experimental conditions: acetate buffer, 30 mM, pH 4.5; $[AH_2]_0 = 50$ μM; $[H_2O_2]_0 = 0.5$ mM; $[E]_0 = 2$ nM. Substrate concentrations: (a) 0.12 mM; (b) 0.20 mM; (c) 0.25 mM; (d) 0.5 mM; (e) 0.75 mM; (f) 1 mM. (Left inset) Results obtained in phosphate buffer, 30 mM, pH 7.0, $[AH_2]_0 = 50$ μM, $[H_2O_2]_0 = 0.50$ mM, $[E]_0 = 2$ nM. Substrate concentrations: (a) 0.05 mM; (b) 0.10 mM; (c) 0.20 mM; (d) 0.25 mM; (e) 0.30 mM; (f) 0.35 mM; (g) 0.40 mM. (Right inset) Representation of steady-state rate versus $[CGA]_0$: (a) pH 4.5; (b) pH 7.0.

Scheme 4

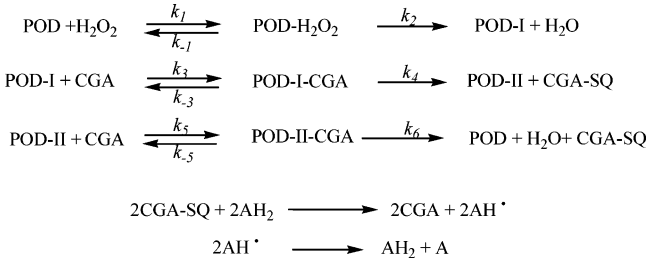

the lag period becomes shorter because V_0 increased, according to eq 19 (**Figure 10** and its left inset) at pH 4.5 and 7.0, respectively.

Kinetic Constants. When the methods described above are applied to the kinetic characterization of the substrate CGA, a hyperbolic dependence is obtained for V_0 versus $[CGA]_0$ (**Figure 9**, right inset, and **Figure 10**, right inset). Analysis of the data, as described under Materials and Methods, provided the information described in **Table 1** for PPO and in **Table 2** for POD.

The kinetic constants determined for the action of PPO on CGA are compared with the values obtained for other *o*-diphenols in **Table 1** (*33*). The CGA, with its higher δ_4, has a lower V_0, which reflects electronic effects. With regard to the values of k_{cat}, the presence of a voluminous group in C-1 (in the case of TBC) provokes a great increase in K_m, as discussed in other studies (*33*). However, in the case of CGA, although the volume of substituent is greater in C-1, perhaps the length of the acid chain does not hinder the attack of the OH of C-4 on the copper of the active center. Note that the K_m increases as the pH falls, as in the case of mushroom PPO, with other substrates (*34*), whereas K_m hardly varies.

With regard to the other PPO substrate, O_2, its k_{cat} in the presence of CGA depends on the nature of the substrate and, according to eq 10 and the value determined for $K_m^{O_2}$ (*34*), its value is very small, which facilitates the enzyme's action at low concentrations of O_2.

In **Table 2**, the values of the constants determined for the action of POD on CGA are compared with those obtained for other *o*-diphenols (*30*).

The value of the δ_4 of CGA compared with the other *o*-diphenols considered in **Table 2** is very high, which implies that the electron density of the oxygen of the OH in C-4 is less and therefore more difficult to oxidize by POD, meaning that the value of k_{+8} will be less than that of MeCat, CAT, and TBC. The carbonyl group of CGA, with its ester bond, may favor the union in the active center of the enzyme, as occurs with benzhydroxamic acid (BHA), whose NH−CO group means that this compound reacts with a constant of 7.8×10^5 M^{-1} s^{-1} (*35*). The Michaelis constant, k_{cat}, is lower than in the case of dopamine, reflecting the effect of a positive charge near the ring.

The Michaelis constant for H_2O_2, calculated according to eq 18, reflects the great affinity for the H_2O_2. The value of K_m^S, the constant of oxidation by compound **II**, is low, in accordance with the high value of δ_4.

In conclusion, this work has characterized the CGA-Q corresponding to the CGA (k_6 and λ_{max}) and studied the kinetics of its evolution, describing its reaction with the substrate. A chronometric spectrophotometric method for measuring the enzymatic activities of PPO and POD is established, enabling the characterization of their action on CGA. The values of the δ_3 and δ_4 obtained by NMR are discussed in relation with other *o*-diphenolic substrates of these enzymes.

LITERATURE CITED

(1) Murata, M.; Kurokami, C.; Homma, S. Purification and some properties of chlorogenic acid oxidase from apple (*Malus pumila*). *Biosci., Biotechnol., Biochem.* **1992**, *56*, 1705−1710.

(2) Zawistowski, J.; Biliaderis, C. G.; Eskin, N. A. M. Polyphenol oxidase. In *Oxidative Enzymes in Foods*; Robinson, D. S., Eskin, N. M. A., Eds.; Elsevier Science: London, U.K., 1991.

(3) Mathew, A. G.; Parpia, H. A. B. Food browning as a polyphenol reaction. *Adv. Food Res.* **1971**, *19*, 74−145.

(4) Nicholas, J. J.; Richard-Forget, F.; Goupy, P.; Amito, M. J.; Aubert, S. Enzymatic browning reactions in apple and apple products. *CRC Crit. Rev. Food Sci. Nutr.* **1994**, *34*, 109−157.

(5) Sisler, F. C.; Evans, H. J. A comparison of chlorogenic acid and catechol as substrates for the polyphenol oxidase from tobacco and mushroom. *Plant Physiol.* **1958**, 255−257.

(6) Pierpoint, W. S. The enzymic oxidation of chlorogenic acid and some reactions of the quinone produced. *Biochem. J.* **1966**, *98*, 567−580.

(7) Richard-Forget, F.; Gaulliard, F. Oxidation of chlorogenic acid, catechins, and 4-methylcatechol in model solutions by combinations of pear (*Pyrus communis* Cv. Williams) polyphenol oxidase and peroxidase: a posible involvement of peroxidase in enzymatic browning. *J. Agric. Food Chem.* **1997**, *45*, 2472−2476.

(8) Murata, M.; Sugiera, M.; Sonokawa, Y.; Shimamura, T.; Homma, S. Properties of chlorogenic acid quinone: relationship between browning and the formation of hydrogen peroxide from a quinone solution. *Biosci., Biotechnol., Biochem.* **2002**, *66*, 2525−2530.

(9) Richard-Forget, F.; Amiot, M. J.; Goupy, P.; Nicolas, J. Evolution of chlorogenic acid *o*-quinones in model solutions. In *Enzymatic Browning and Its Prevention*; Lee, C. Y., Whitaker, J. R., Eds.; American Chemical Society: Washington, DC, 1995; pp 145−158.

(10) Mastore, M.; Kolher, L.; Nappi, A. J. Production and utilization of hydrogen peroxide associated with melanogenesis and tyrosinase-mediated oxidations of DOPA and dopamine. *FEBS J.* **2005**, *272*, 2407−2415.

(11) Abukharma, D. A.; Woolhouse, H. W. The preparation and properties of o-diphenol:oxygen oxidoreductase from potatoes tubers. *New Phytol.* **1966**, *65*, 477−478.

(12) Zawistowski, J.; Biliaderis, C. G.; Murria, E. D. Isolation and some properties of an acidic fraction of polyphenol oxidase from Jerusalem artichoke (*Helianthus tuberosus* L.). *J. Food Biochem.* **1988**, *12*, 23−25.

(13) Interesse, F. S.; Ruggiero, P.; D'Avella, G.; Lamparelli, F. Characterization of wheat o-diphenolase isoenzyme. *Phytochemistry* **1983**, *22*, 1885−1889.

(14) Koller, A.; Neukom, H. Untersuchungen ubre den abbaumechanismus einer gereinigten polygalakturonase aus *Aspergillus niger*. *Eur. J. Biochem.* **1969**, *7*, 485−489.

(15) Kermasha, S.; Goetghebeur, M.; Monfette, A. Studies on inhibition of mushroom polyphenol oxidase using chlorogenic acid as substrate. *J. Agric. Food Chem.* **1993**, *41*, 526−531.

(16) Tono, T.; Fujita, S. Difference spectra spectrophotometry for polyphenol oxidase assay. In *Enzymatic Browning and Its Prevention*; Lee, C. Y., Whitaker, J. R., Eds.; American Chemical Society: Washington, DC, 1995; pp 188−199.

(17) Kono, Y.; Shibata, H.; Kodama, Y.; Sawa, Y. The suppression of the N-nitrosating reaction by chlorogenic acid. *Biochem. J.* **1995**, *312*, 947−953.

(18) Clifford, M. N. Chlorogenic acid and the other cinnamates—nature, occurrence and dietary burden. *J. Sci. Food Agric.* **1999**, *79*, 362−372.

(19) Yagasaki, K.; Miura, Y.; Okauchi, R.; Furuse, T. Inhibitory effects of chlorogenic acid and its related compounds on the invasion of the hepatoma cells in culture. *Cytotechnology* **2000**, *33*, 229−235.

(20) Shimizu, M.; Yoshimi, N.; Yamada, Y.; Matsunaga, K.; Kawabata, K.; Hara, A.; Morikawa, H.; Mori, H. Suppressive effects of chlorogenic acid on *N*-methyl-*N*-nitrosourea-induced glandular stomach carcinogenesis in male F344 rats. *J. Toxicol. Sci.* **1999**, *24*, 433−439.

(21) Yamada, J.; Tomita, Y. Antimutagenic activity of caffeic acid and related compounds. *Biosci., Biotechnol., Biochem.* **1996**, *60*, 328−329.

(22) Krakauer, T. The polyphenol chlorogenic acid inhibits staphylococcal exotoxin-induced inflammatory cytokines and chemokines. *Inmunopharmacol. Inmunotoxicol.* **2002**, *24*, 113−119.

(23) Stich, H. F. Teas and tea components as inhibitors of carcinogen formation in model systems and man. *Prev. Med.* **1992**, *21*, 377−384.

(24) Li, P.; Wang, H. Z.; Wang, X. Q.; Zu, Y. N. The blocking effect of phenolic acid on *N*-nitrosomorpholine formation in vitro. *Biomed. Environ. Sci.* **1994**, *7*, 68−78.

(25) Torres y Torres, J. L.; Rosazza, J. P. N. Reactions of *p*-coumaric acid with nitrite: product isolation and mechanism studies. *J. Agric. Food Chem.* **2001**, *49*, 1486−1492.

(26) Panzella, L.; Napolitano, A.; d'Ischia, M. Oxidative conjugation of chlorogenic acid with glutathione: structural characterization of addition products and a new nitrite-promoted pathway. *Bioorg. Med. Chem.* **2003**, *11*, 4797−4805.

(27) Bradford, M. M. A rapid and sensitive method for the quantification of microgram quantities of proteins utilising the principle of protein−dye binding. *Anal. Biochem.* **1976**, *72*, 248−254.

(28) Marquart, D. W. An algorithm least-squares estimation of nonlinear parameters. *J. Soc. Ind. Appl. Math.* **1963**, *11*, 431−441.

(29) Jandel Scientific. *Sigma Plot 9.0 for Windows*; Jandel Scientific: Core Madera, CA, 2006.

(30) Rodriguez-Lopez, J. N.; Gilabert, M. A.; Tudela, J.; Thorneley, R. N.; Garcia-Canovas, F. Reactivity of horseradish peroxidase compound II toward substrates: kinetic evidence for a two-step mechanism. *Biochemistry* **2000**, *39*, 13201−13209.

(31) Muñoz, J. L.; Garcia-Molina, F.; Varon, R.; Rodriguez-Lopez, J. N.; Garcia-Canovas, F.; Tudela, J. Calculating molar absorptivities for quinones: application to the measurement of tyrosinase activity. *Anal. Biochem.* **2006**, *351*, 128−138.

(32) Weidman, S. W.; Kaiser, E. T. The mechanism of the periodate oxidation of aromatic systems. A kinetic study of the periodate oxidation of catechol. *J. Am. Chem. Soc.* **1966**, *88*, 5820−5826.

(33) Rodríguez-López, J. N.; Fenoll, L. G.; García-Ruiz, P. A.; Varón, R.; Tudela, J.; Thorneley, R. N.; García-Canovas, F. Stopped-flow and steady-state study of the diphenolase activity of mushroom tyrosinase. *Biochemistry* **2000**, *39*, 10497−10506.

(34) García-Cánovas, F.; Tudela, J.; Martínez Madrid, C.; Varón, R.; García-Carmona, F.; Lozano, J. A. Kinetic study on the suicide inactivation of tyrosinase induced by catechol. *Biochim. Biophys. Acta* **1987**, *912*, 417−423.

(35) Aviram, I. The interaction of benzhydroxamic acid with horseradish peroxidase and its fluorescent analogs. *Arch. Biochem. Biophys.* **1981**, *212*, 483−490.

Received for review July 24, 2006. Revised manuscript received November 28, 2006. Accepted December 1, 2006. This work was supported in part by grants from the MCYT (Spain) Project AGL 2002-01255 ALI, from the Fundación Séneca, and from the Fundación Séneca/Consejería de Educación y Universidades (Murcia) Project 00672/PI/04. F.G.-M. has a fellowship from the MEC (Spain), Reference AP2003-0891. J.M. has a fellowship from the MEC (Spain) Reference AP2005-4721.

JF062081+

4.9. CARACTERIZACIÓN CINÉTICA DE LA OXIDACIÓN ENZIMÁTICA Y QUÍMICA DE LAS CATEQUINAS DEL TÉ VERDE.

La caracterización cinética de la oxidación enzimática y química de las catequinas del té verde ha dado lugar a la siguiente publicación adjunta.

4.9.1. Título

Kinetic characterization of the enzymatic and chemical oxidation of the catechins in green tea.

4.9.2. Autores

Muñoz-Muñoz, J.L.; Garcia-Molina, F.; Molina-Alarcón, M.; Tudela, J.; Garcia-Cánovas, F. y Rodríguez-López, J.N.

4.9.3. Referencia

Journal of Agricultural and Food Chemistry (2008) 56, 9215-9224.

4.9.4. Resumen

La oxidación de las catequinas del té verde mediante polifenoloxidasa/O_2 y peroxidasa/H_2O_2 da lugar a *o*-quinonas y semiquinonas respectivamente, esto ha hecho difícil la caracterización cinética de estos compuestos. En este trabajo, se ha utilizado ácido ascórbico como reactivo acoplado, bien con un método de medida basado en la desaparición de ácido ascórbico o bien con un método cronométrico. Así, se han podido determinar las constantes cinéticas que caracterizan la actuación de polifenoloxidasa y peroxidasa hacia estos sustratos. A partir de los resultados obtenidos, se desprende que el mejor sustrato es (-)epicatequina para ambas enzimas con el grupo OH del anillo C, en posición *cis* respecto al anillo B. Posteriormente, estaría (+)catequina con el grupo OH del anillo C en posición *trans* respecto al anillo B. Sin embargo, epigalocatequina que debería ser el primero debido a la presencia de tres hidroxilos vecinales en su estructura (anillo B), no lo es por el impedimento estérico del hidroxilo en *cis* del anillo C. Las epicatequina galato y epigalocatequina galato son muy malos sustratos debido a la presencia de ácido gálico esterificando el grupo hidroxilo del anillo C. Por otra parte, se ha mostrado que la producción de H_2O_2 en la autooxidación de catequinas por O_2, es muy baja para (-)epicatequina y (+)catequina. Sin embargo, la producción de H_2O_2 a partir de las *o*-quinonas, generadas por oxidación con periodato aumenta, poniendo de manifiesto la importancia de la evolución de las *o*-quinonas en la producción de H_2O_2. Cuando la

relación $[sustrato]_0/[IO_4^-]_0 = 1$ o bien $[sustrato]_0/[IO_4^-]_0 >> 1$, la formación de H_2O_2 aumenta de forma muy clara en los casos de (-)epicatequina y (+)catequina y prácticamente no afecta a epicatequina galato, epigalocatequina y epigalocatequina galato. Además, el poder antioxidante es mayor para los galatos del té verde, probablemente debido al mayor número de grupos hidroxilos en su estructura capaces de atrapar neutralizar radicales libres. Por tanto, en este trabajo se caracteriza la acción de polifenoloxidasa y peroxidasa sobre las catequinas del té verde. Además, se estudia la formación de H_2O_2 durante la autooxidación de estos compuestos y durante la evolución de sus *o*-quinonas.

JOURNAL OF AGRICULTURAL AND FOOD CHEMISTRY

Kinetic Characterization of the Enzymatic and Chemical Oxidation of the Catechins in Green Tea

J. L. MUNOZ-MUNOZ,[†] F. GARCÍA-MOLINA,[†] M. MOLINA-ALARCÓN,[‡] J. TUDELA,[†] F. GARCÍA-CÁNOVAS,*[,†] AND J. N. RODRÍGUEZ-LÓPEZ[†]

GENZ, Grupo de Investigación de Enzimología, Departamento de Bioquímica y Biología Molecular-A, Facultad de Biología, Universidad de Murcia, E-30100 Espinardo, Murcia, Spain; and Departamento de Enfermería, Escuela Universitaria de Enfermería, Universidad de Castilla la Mancha, E-02071, Albacete, Spain

The oxidation of green tea catechins by polyphenol oxidase/O_2 and peroxidase/H_2O_2 gives rise to *o*-quinones and semiquinones, respectively, which inestability, until now, have hindered the kinetic characterization of enzymatic oxidation of the catechins. To overcome this problem, ascorbic acid (AH_2) was used as a coupled reagent, either measuring the disappearance of AH_2 or using a chronometric method in which the time necessary for a fixed quantity of AH_2 to be consumed was measured. In this way, it was possible to determine the kinetic constants characterizing the action of polyphenol oxidase and peroxidase toward these substrates. From the results obtained, (−) epicatechin was seen to be the best substrate for both enzymes with the OH group of the C ring in the cis position with respect to the B ring. The next best was (+) catechin with the OH group of the C ring in the trans position with respect to the B ring. Epigallocatechin, which should be in first place because of the presence of three vecinal hydroxyls in its structure (B ring), is not because of the steric hindrance resulting from the hydroxyl in the cis position in the C ring. The epicatechin gallate and epigallocatechin gallate are very poor substrates due to the presence of sterified gallic acid in the OH group of the C ring. In addition, the production of H_2O_2 in the auto-oxidation of the catechins by O_2 was seen to be very low for (−) epicatechin and (+) catechin. However, its production from the *o*-quinones generated by oxidation with periodate was greater, underlining the importance of the evolution of the *o*-quinones in this process. When the $[substrate]_0/[IO_4^-]_0$ ratio = 1 or ≫1, H_2O_2 formation increases in cases of (−) epicatechin and (+) catechin and practically is not affected in cases involving epicatechin gallate, epigallocatechin, or epigallocatechin gallate. Moreover, the antioxidant power is greater for the gallates of green tea, probably because of the greater number of hydroxyl groups in its structure capable of sequestering and neutralizing free radicals. Therefore, we kinetically characterized the action of polyphenol oxidase and peroxidase on green tea catechins. Furthermore, the formation of H_2O_2 during the auto-oxidation of these compounds and during the evolution of their *o*-quinones is studied.

KEYWORDS: Polyphenol oxidase; peroxidase; catechins; green tea; hydrogen peroxide

INTRODUCTION

Polyphenol oxidase (tyrosinase) (monophenol, *o*-diphenol; oxygen-oxidoreductase; EC 1.14.18.1; PPO) is a binuclear copper-cluster ubiquituously present in biological systems (*1, 2*). It catalyzes the oxidation of *o*-diphenols (*o*-diphenolase or catecholase activity) to the corresponding *o*-quinones, through the consumption of molecular oxygen. It may also catalyze the regioselective ortho-hydroxylation of monophenols to catechols (monophenolase or cresolase activity) and their subsequent oxidation to *o*-quinones. The resulting *o*-quinones may undergo nonenzymatic autopolymerisation to produce colored compounds (*3–5*). Browning in plant materials is associated with the enzymatic oxidation of phenolic compounds (*6, 7*).

Peroxidases are ubiquituous in the fungi, plant, and animal kingdoms (*8*).The cationic isoenzyme from horseradish peroxidase (EC 1.11.1.7; POD) has been studied intensively because of its commercial use in diagnostic assays and potential application in bioremediation (*9*). The oxidation of phenols by POD produces extremely reactive free radical intermediates, which following release from the enzyme, readily condense to yield polymeric products of variable stoichiometry. Because of this, the kinetics of these reactions were not described by classical Michaelis−Menten equations for a long time before a suitable method was found, which permitted the typical

* To whom correspondence should be addressed. Fax: +34 968 364147. E-mail: canovasf@um.es.
[†] Universidad de Murcia.
[‡] Universidad de Castilla la Mancha.

10.1021/jf8012162 CCC: $40.75 © 2008 American Chemical Society
Published on Web 09/13/2008

Scheme 1

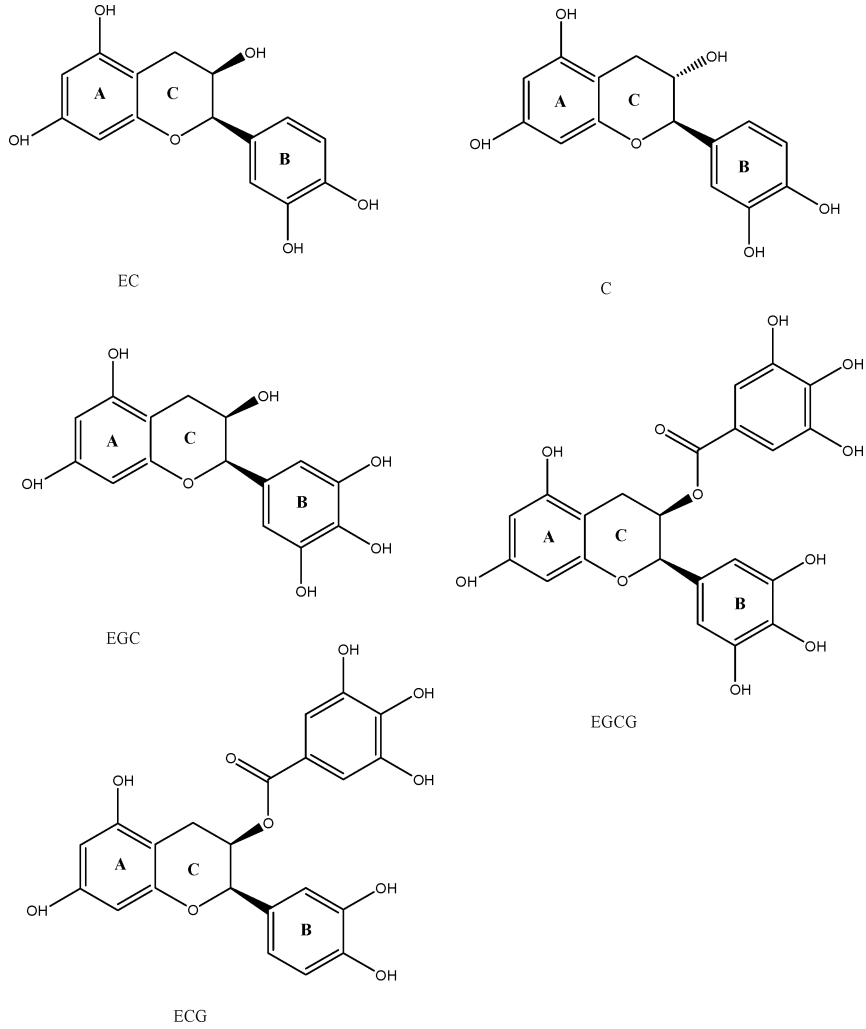

Michaelis−Menten kinetics to be established with a series of *o*-diphenols, monophenols, and anilines (*9–11*).

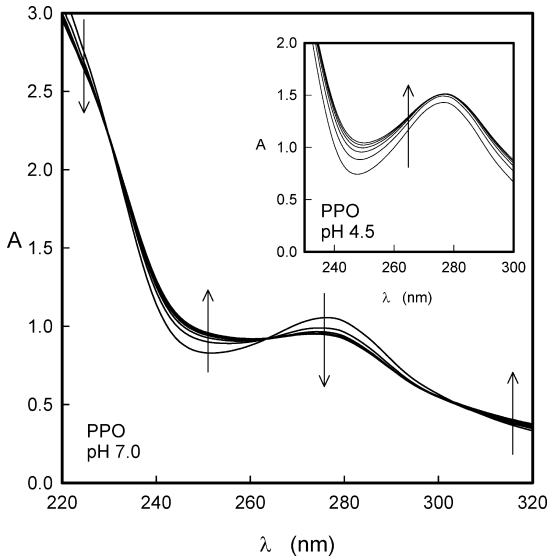

Figure 1. Spectrophotometric scans of the evolution of *o*-quinone, Q, generated with a high concentration of PPO. Experimental conditions were 30 mM phosphate buffer pH 7.0, $[ECG]_0 = 0.1$ mM, $[E]_0 = 60$ nM; scans were made every 60 s. **Inset**: Experimental conditions were 30 mM acetate buffer pH 4.5, $[ECG]_0 = 0.1$ mM, $[E]_0 = 60$ nM; scans were made every 60 s.

Tea is a popular beverage all over the world. The growing evidence of the potential health benefits of tea has prompted a large number of investigations into tea, its major components, and their biological activities. The overall results indicate that every type of tea (green, black, white, dark, yellow, and oolong) have significant antimutagenic and anticlastogenic effects (*12*). Additionally, tea catechins and their gallate esters possess antioxidant properties that prevent lipid peroxidation in erythrocyte membranes and microsomes and suppress the mutagenic effects induced by H_2O_2 (*12*). Tea extracts and individual tea polyphenols display both antioxidant and pro-oxidant effects (*13*). On the one hand, tea has been known for a long time to help prevent many diseases including cardiovascular diseases and cancer. The last claim is commonly attributed to the pronounced antioxidant activity of tea polyphenols. On the other hand, tea polyphenols have been reported as cytotoxic and mutagenic agents. This may be associated with the pro-oxidant activity of tea polyphenols as a result of their tendency to autoxidation accompanied by the formation of active forms of oxygen (reactive oxygen species, ROS) (*13*). We have recently demonstrated the inhibition of the dihydrofolate reductase enzyme, by the components of green tea (*14–16*).

Although the autoxidation of tea polyphenols has received substantial attention in the literature (*17*), the kinetic characterization of the enzymes involved in the transformation of these polyphenols, PPO and POD, is rather limited. It has been proposed that both enzymes participate in the browning and

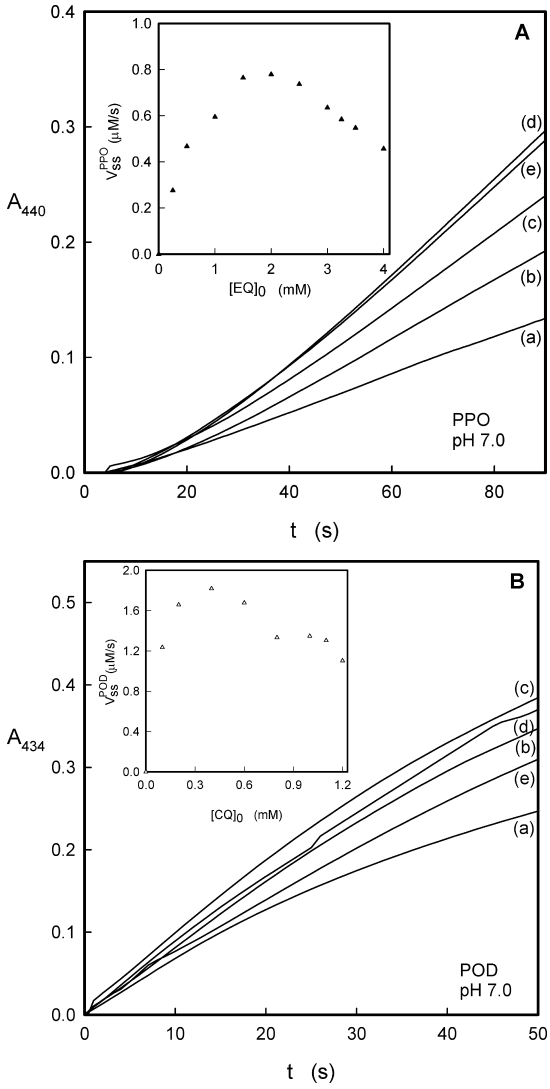

Figure 2. Spectrophotometric recordings of Q generated in the action of PPO and POD on (**A**) EC and (**B**) C. (**A**) Experimental conditions were 30 mM sodium phosphate pH 7.0, $\lambda = 440$ nm, $[PPO]_0 = 0.56$ nM. The substrate concentrations were (a) 0.5 mM, (b) 1 mM, (c) 1.5 mM, (d) 2 mM, and (e) 2.5 mM. **Inset**: Initial slope, V_0 vs $[EC]_0$, directly measuring the appearance of Q. (**B**) Experimental conditions were 30 mM sodium phosphate buffer pH 7.0, $\lambda = 440$ nm, $[POD]_0 = 9.1$ nM, and $[H_2O_2]_0 = 150$ μM. The substrate concentrations were (a) 0.1 mM, (b) 0.2 mM, (c) 0.4 mM, (d) 0.6 mM, and (e) 0.8 mM. **Inset**: Initial slope, V_0 vs $[C]_0$, directly measuring the appearance of Q.

spoilage of fruits and vegetables (*18, 19*). The formation of products resulting from the evolution of the *o*-quinones and semiquinones originated by the action of purified strawberry PPO and POD has been studied (*18*). Recently, considerable attention has been given to the possible inhibition displayed by green tea catechins, especially on melanin biosynthesis (*20*). It has been suggested that they act on PPO, thus playing a role in the regulation of this biosynthetic route (*20*). In addition, the formation of H_2O_2 in green tea as a result of autoxidation of its components has been studied (*21–25*), and its possible physiological function in plant tissues has been discussed (*23*).

The instability of the products originated by the action of PPO and POD (*o*-quinones and semiquinones, respectively) is responsible for the formation of H_2O_2 and at the same time hinders the kinetic characterization of these substrates (*9, 26*). For this reason, we used ascorbic acid (AH_2) to prevent the evolution of these products and characterized the enzymes by two spectrophotometric

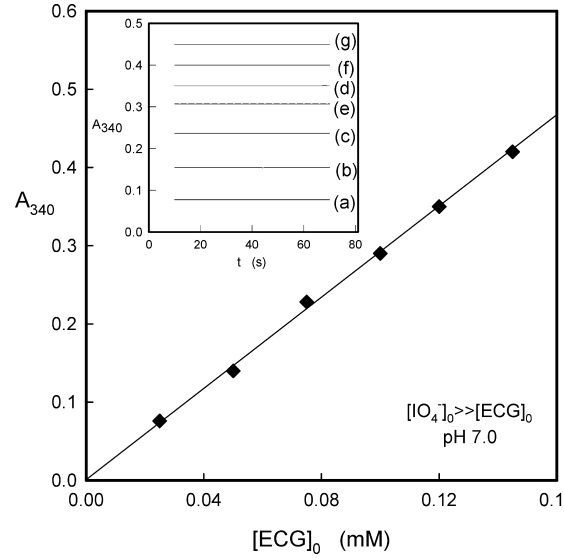

Figure 3. Determination of the molar absorptivity of the *o*-quinone of EGC. Plot of Absorbance vs $[S]_0$. Absorbance values at $\lambda = 340$ nm obtained by oxidation with excess periodate. The experimental conditions were 30 mM sodium phosphate buffer pH 7.0. The concentration of IO_4^- was 0.5 mM, and $[EGC]_0$ was (a) 0.025 mM, (b) 0.05 mM, (c) 0.075 mM, (d) 0.1 mM, (e) 0.12 mM, (f) 0.145 mM, and (g) 0.17 mM. **Inset**: Kinetics of the evolution of Q generated with excess of periodate.

Table 1. Molar Absorptivities of the *o*-Quinones of the Catechins[a]

	$\varepsilon^{4.5}$ (M^{-1} cm^{-1})		$\varepsilon^{7.0}$ (M^{-1} cm^{-1})	
substrate	λ_{max}	λ_i	λ_{max}	λ_i
C	4184 ± 210		4800 ± 288	3125 ± 125
EC	4900 ± 340		5482 ± 250	
EGCG	8800 ± 440	450 ± 22	8995 ± 360	650 ± 30
EGC	32000 ± 1600	4500 ± 325	3829 ± 153	21000 ± 1050
ECG	13357 ± 800	15100 ± 906	9300 ± 370	5102 ± 200

[a] The oxidation was carried out at ratios $[IO_4^-]_0/[\text{catechins}]_0 \gg 1$ at pHs 4.5 and 7.0. The maximum wavelengths (λ_{max}) for the *o*-quinones were determined. Some *o*-quinones showed a constant absorbance at a determined wavelength, isosbestic point (λ_i). The molar absorptivities at a specified pH value ($\varepsilon^{4.5}$ and $\varepsilon^{7.0}$) were determined at the corresponding λ_{max} and λ_i, as described in **Figure 3**.

methods, either measuring the disappearance of AH_2 or using a chronometric method in which the time necessary for a fixed quantity of AH_2 to be consumed was measured. At the same time, H_2O_2 formation (pro-oxidant capacity) was studied from two different viewpoints along with the antioxidant potential of the products. Particular attention was paid to green tea and its major constituents, (−) epicatechin (EC), (+) catechin (C), epigallocatechin (EGC), epicatechin gallate (ECG), and epigallocatechin gallate (EGCG) (**Scheme 1**).

MATERIALS AND METHODS

Reagents. Mushroom polyphenol oxidase (PPO; 1530 U mg^{-1}), horseradish peroxidase (POD; 251 U mg^{-1}), catalase (9300 U mg^{-1}), and superoxide dismutase (SOD; 4140 U mg^{-1}) were obtained from Sigma Chemical (St. Louis, MO). PPO was purified as described elsewhere (*26*). POD was purchased from Sigma (type VI; Rz = 3.2) and used without further purification. The concentration of POD was determined spectrophotometrically using a Soret molar absorptivity of 102 mM^{-1} cm^{-1} (*9*). The protein concentration was determined by the Bradford's method (*27*) and using bovine serum albumin as the standard. (−) Epicatechin (EC), (+) catechin (C), (−) epicatechin gallate (ECG), (−) epigallocatechin (EGC), (−) epigallocatechin gallate (EGCG), and 2,2′-azino-bis(3-ethylbenzothiazoline-6-sulfonic acid) (ABTS) were obtained from Sigma Chemical (St. Louis, MO), and sodium periodate was obtained from Scharlau (Malaga, Spain). Stock solutions of the reducing substrates were

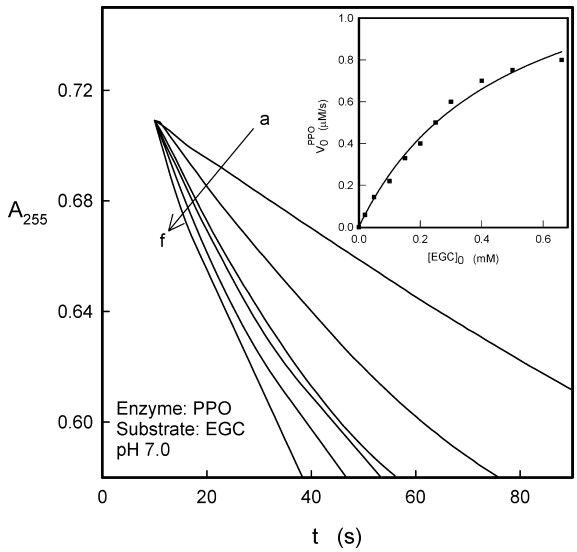

Figure 4. AH_2 disappearance method for characterizing the enzymatic activity of PPO on EGC. Experimental conditions were 30 mM sodium phosphate buffer pH 7.0, $\lambda = 255$ nm, $[E]_0 = 2$ nM, and $[AH_2]_0 = 20$ μM. Substrate concentrations were (a) 0.05 mM, (b) 0.075 mM, (c) 0.1 mM, (d) 0.15 mM, (e) 0.2 mM, and (f) 0.3 mM. **Inset**: Plot of V_0^{PPO} true steady-state rate vs $[EGC]_0$.

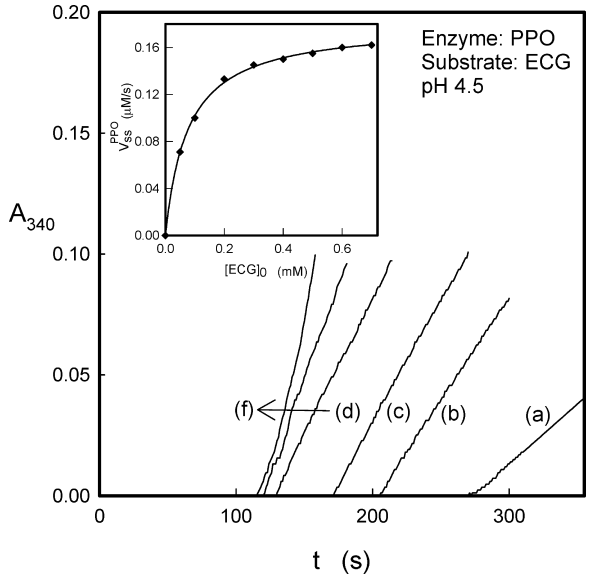

Figure 5. Chronometric method for characterizing the enzymatic activity of PPO on ECG. Experimental conditions were 30 mM sodium acetate buffer pH 4.5, $\lambda = 340$ nm, $[E]_0 = 4.2$ nM, and $[AH_2]_0 = 20$ μM. Substrate concentrations were (a) 0.05 mM, (b) 0.1 mM, (c) 0.2 mM, (d) 0.3 mM, (e) 0.4 mM, and (f) 0.6 mM. **Inset**: Plot of V_0^{PPO} vs $[ECG]_0$.

Scheme 2

$$E_m + S \underset{k_{-2}}{\overset{k_2}{\rightleftharpoons}} E_mS \xrightarrow{k_3} E_d + Q \quad (a)$$

$$E_d + O_2 \underset{k_{-8}}{\overset{k_8}{\rightleftharpoons}} E_{ox} \quad (b)$$

$$E_{ox} + S \underset{k_{-6}}{\overset{k_6}{\rightleftharpoons}} E_{ox}S \xrightarrow{k_7} E_m + Q \quad (c)$$

$$2\,Q + 2\,AH_2 \longrightarrow 2\,S + 2\,A \quad (d)$$

prepared in 0.15 mM phosphoric acid to prevent auto-oxidation. The buffers used were 30 mM sodium phosphate buffer (pH 7.0) and 30 mM sodium acetate (pH 4.5).

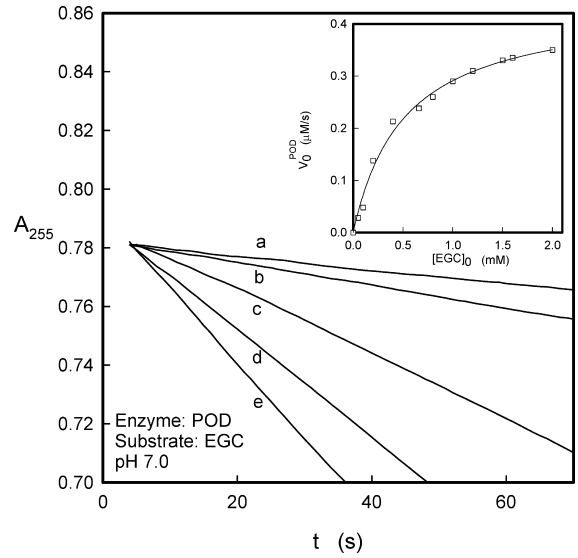

Figure 6. AH_2 disappearance method for characterizing the enzymatic activity of POD on EGC. Experimental conditions were 30 mM sodium phosphate buffer pH 7.0, $\lambda = 255$ nm, $[E]_0 = 1.76$ nM, $[AH_2]_0 = 20$ μM, and $[H_2O_2]_0 = 200$ μM. Substrate concentrations were (a) 0.05 mM, (b) 0.1 mM, (c) 0.2 mM, (d) 0.4 mM, and (e) 0.66 mM. **Inset**: Plot of V_0^{POD} vs $[EGC]_0$.

Scheme 3

$$POD + H_2O_2 \underset{k_{-1}}{\overset{k_1}{\rightleftharpoons}} POD\text{-}H_2O_2 \xrightarrow{k_2} POD\text{-}I + H_2O \quad (a)$$

$$POD\text{-}I + S \underset{k_{-3}}{\overset{k_3}{\rightleftharpoons}} POD\text{-}I\text{-}S \xrightarrow{k_4} POD\text{-}II + sQ\text{-}S \quad (b)$$

$$POD\text{-}II + S \underset{k_{-5}}{\overset{k_5}{\rightleftharpoons}} POD\text{-}I\text{-}S \xrightarrow{k_6} POD + H_2O + sQ\text{-}S \quad (c)$$

$$2\,sQ\text{-}S + 2\,AH_2 \longrightarrow 2\,S + AH^{\cdot} \quad (d)$$

$$2\,AH^{\cdot} \longrightarrow AH_2 + A \quad (e)$$

Spectrophotometric Assays. Absorption spectra were recorded in a visible−ultraviolet Perkin-Elmer Lambda 35 spectrophotometer interfaced online with a PC compatible Intel-Pentium microcomputer, at a scanning speed of 60 nm/s controlled by the UV-Winlab software. The temperature was maintained at 25 °C using a Haake D16 circulating water bath with a heater/cooler and checked using a Cole-Parmer digital thermometer with a precision of 0.1 °C. Kinetic assays were also carried out with the above instruments following the disappearance of AH_2 at $\lambda = 255$ nm ($\varepsilon = 7970$ M^{-1} cm^{-1}) or using a chronometric method (detailed below). Reference cuvettes contained all the components, except the substrate and AH_2, in a final volume of 1 mL. All the assays were carried out with PPO saturated by molecular oxygen (0.26 mM in the assay medium) (*28*) or with POD saturated by H_2O_2 (*9*).

Oxymetric Assays. Oxygen evolution was measured with a Clark-type electrode coupled to a Hansatech Oxygraph (King's Lynn, Norfolk, U.K.). The equipment was calibrated using the tyrosinase/4-*tert*-butylcatechol method (*29*). Nitrogen was bubbled through the reaction medium to remove the oxygen when necessary. The reaction medium contained 30 mM sodium phosphate buffer, pH 7.0. The medium was stirred constantly, and the temperature was kept at 25 ± 0.1 °C using a Haake D1G circulating water-bath.

Chronometric Method. Enzymatic activity was determined spectrophotometrically using the chronometric method described in the Results and Discussion section (*9, 30, 31*). The only condition was that there had to be an absorbance increase (due to the product formation) measurable once the ascorbic acid (AH_2) was consumed to be able to determine the time necessary, τ, to consume the quantity of AH_2 called $[AH_2]_0$. From these values, the initial rate, V_0, can be

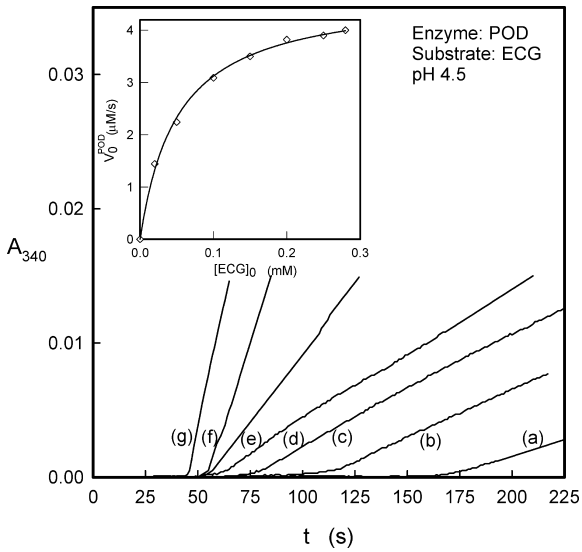

Figure 7. Chronometric method for characterizing the enzymatic activity of POD on ECG. Experimental conditions were 30 mM sodium acetate buffer pH 4.5, $\lambda = 340$ nm, $[E]_0 = 52$ nM, $[AH_2]_0 = 65$ μM, and $[H_2O_2]_0 = 200$ μM. Substrate concentrations were (a) 0.025 mM, (b) 0.05 mM, (c) 0.1 mM, (d) 0.15 mM, (e) 0.2 mM, (f) 0.25 mM, and (g) 0.28 mM. **Inset**: Plot of V_0^{POD} vs $[ECG]_0$.

Scheme 4

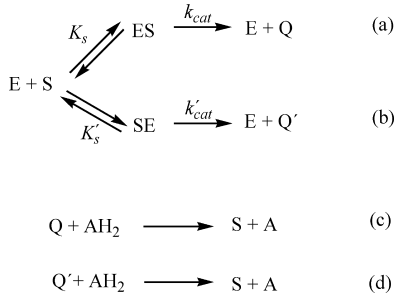

determined (see the Results and Discussion section). Preliminary experiments were carried out in the absence of ascorbic acid with the tyrosinase/O_2/catechin system by recording spectrophotometric scans to identify in which zone of the spectrum, particularly the visible zone, the greatest changes in absorbance occurred. The wavelength chosen at acid and neutral pH was 330 nm. The activity of POD was continued using the same methodology but with the POD/H_2O_2/catechin system.

Determination of the *o*-Quinone Molar Absorptivities. The absorbance data were analyzed according to Beer's law using the standard least-squares linear regression program. Molar absorptivities were estimated for a known path length of 1 cm. The minimal acceptable coefficient of correlation (R) was taken to be 0.995. Data yielding coefficients less than this were due to pipetting errors and rounding up/down of the values. With this precaution, the 95% confidence limits for the molar absorptivity estimates were ≤5%.

Determination of H_2O_2 Generated. *1. Auto-oxidation of Catechins.* (a) Oxymetric experiment. The auto-oxidation of each of the catechins of green tea was followed by measuring oxygen consumption in an oxygraph in 30 mM phosphate buffer, pH 7.0. After 60 min, 0.2 μM of catalase was added, and the instantaneous appearance of oxygen was measured according to the following stoichiometry: $2\ H_2O_2 \rightarrow O_2 + 2\ H_2O$.

(b) Spectrophotometric experiments. The catechins were preincubated in 30 mM phosphate buffer, pH 7.0. After 60 min, the unoxidised catechins and the quinones were extracted twice with ether at pH 4.5. The H_2O_2 generated was evaluated in an aliquot of aqueous extract using the POD/ABTS system at $\lambda = 414$ nm, measuring the $ABTS^{\bullet+}$ radical ($\varepsilon = 31\ 100\ M^{-1}\ cm^{-1}$) in 0.1 M acetate buffer, pH 4.5 (*9*).

Table 2. Kinetic Constants for PPO and POD at Both pH Values[a]

PPO					
substrate	method	k_{cat}^{PPO} (s^{-1})	K_m^{PPO} (mM)	K_m^{O2} (μM)	$k_6 \times 10^5$ ($M^{-1}\ s^{-1}$)
			pH 4.5		
C	τ_{440}	335 ± 32.1	0.41 ± 0.13	14.50 ± 0.13	8.2 ± 0.40
EC	τ_{440}	696 ± 68.5	0.55 ± 0.17	30.20 ± 0.41	12.6 ± 0.50
EGCG	τ_{320}	33 ± 3.3	0.50 ± 0.06	1.43 ± 0.13	0.6 ± 0.03
EGC	A_{255}	18 ± 2.1	0.30 ± 0.04	0.78 ± 0.09	0.6 ± 0.04
ECG	τ_{340}	15 ± 0.8	0.16 ± 0.02	0.65 ± 0.03	0.9 ± 0.05
			pH 7.0		
C	τ_{440}	355 ± 31.2	0.38 ± 0.11	15.40 ± 0.15	9.34 ± 0.40
EC	τ_{440}	706 ± 70.2	0.51 ± 0.14	30.70 ± 0.50	14.01 ± 0.50
EGCG	τ_{320}	40 ± 3.9	0.45 ± 0.05	1.73 ± 0.13	0.88 ± 0.03
EGC	A_{255}	23 ± 2.8	0.50 ± 0.02	1.00 ± 0.10	0.46 ± 0.04
ECG	τ_{340}	21 ± 1.9	0.11 ± 0.03	0.91 ± 0.11	1.91 ± 0.05

POD					
substrate	method	k_{cat}^{POD} (s^{-1})	K_m^{POD} (mM)	K_m^{H2O2} (μM)	$k_5 \times 10^6$ ($M^{-1}\ s^{-1}$)
			pH 4.5		
C	τ_{440}	1995 ± 120	0.71 ± 0.11	117 ± 7.02	2.81 ± 0.27
EC	τ_{440}	2080 ± 153	0.23 ± 0.04	122 ± 8.54	9.04 ± 0.61
EGCG	τ_{320}	1900 ± 76	0.16 ± 0.03	112 ± 7.84	11.87 ± 0.59
EGC	A_{255}	430 ± 25	0.53 ± 0.08	25 ± 1.02	0.81 ± 0.06
ECG	τ_{340}	680 ± 70	0.05 ± 0.01	40 ± 2.27	13.60 ± 0.65
			pH 7.0		
C	τ_{440}	2065 ± 103	0.75 ± 0.15	122 ± 6.10	2.75 ± 0.15
EC	τ_{440}	2166 ± 160	0.25 ± 0.05	127 ± 7.62	8.66 ± 0.41
EGCG	τ_{320}	1963 ± 137	0.21 ± 0.02	115 ± 8.05	9.35 ± 0.69
EGC	A_{255}	425 ± 21	0.51 ± 0.06	25 ± 1.47	0.83 ± 0.07
ECG	τ_{340}	700 ± 49	0.07 ± 0.01	41 ± 2.81	10.00 ± 0.86

[a] τ_λ = Chronometric method at wavelength λ. A_λ = Disappearance of AH2 at wavelength λ.

Table 3. Rate of Oxygen Consumption and Production of Oxygen during the Oxidation of Catechins by Molecular Oxygen[a]

	$V_0^{O2} \times 10^3$ (μM/min)		$[H_2O_2]$ (μM)	
	−SOD[b]	+SOD[c]	catalase[d]	POD/ABTS[e]
EC	5.1 ± 0.2	1.1 ± 0.1		1.82 ± 0.12
C	5.3 ± 0.2	1.2 ± 0.1		1.33 ± 0.06
ECG	253.1 ± 7.6	124.2 ± 6.2	16 ± 1	17.51 ± 0.71
EGCG	375.3 ± 9.8	301.3 ± 9.9	14 ± 1	15.82 ± 0.47
EGC	492.2 ± 9.9	159.1 ± 6.5	16 ± 1	16.11 ± 0.64

[a] Substrate concentration was always 0.1 mM at pH 7.0. [b] Absence of superoxide dismutase. [c] Presence of superoxide dismutase (414 units). [d] $[H_2O_2]$ determination with the addition of catalase (930 units). [e] $[H_2O_2]$ determination with the POD/ABTS method.

2. Oxidation of Catechins with Periodate. (a) Stoichiometric oxidation of catechins with periodate. Oxidation of the catechins in 30 mM phosphate buffer pH 7.0 was carried out with stoichiometric periodate. The mixture was acidified to pH 4.5, and the *o*-quinones generated were extracted twice with ether. Then, the *o*-quinones were extracted from the ether phase with 30 mM phosphate buffer pH 7.0 and allowed to evolve for 60 min, after which following acidification to pH 4.5, the *o*-quinones, dimers, and trimers formed were extracted with ether. The H_2O_2 generated in an aliquot of the aqueous extract was evaluated by the POD/ABTS system at $\lambda = 414$ nm, measuring the $ABTS^{\bullet+}$ radical in acetate buffer 0.1 M, pH 4.5.

(b) Oxidation of catechins by periodate in defect. The catechins were oxidized in a 5/1 defect ratio, following the same procedure as in section 2 (a).

Kinetic Data Analysis. For PPO, the initial rate values (V_0^{PPO}) were calculated from triplicate measurements at each reducing substrate concentration $[S]_0$, and V_0^{PPO} versus $[S]_0$ data were adjusted to the Michaelis−Menten equation (eq 6) through the Sigma Plot 9.0 program

Table 4. Production of H_2O_2 during Evolution of the *o*-Quinones Generated by Oxidation with Periodate

	$[S]_0/[IO_4^-]_0$[a] (mM/mM)	$[H_2O_2]$[c] (μM)	$[S]_0/[IO_4^-]_0$[b] (mM/mM)	$[H_2O_2]$[c] (μM)	EC50[d]	ARP[e]	n[f]
EC	0.1/0.1	80 ± 4	0.5/0.1	200.1 ± 10	0.16	6.25	3.12
C	0.1/0.1	78 ± 3	0.5/0.1	180.1 ± 9	0.18	5.55	2.77
ECG	0.1/0.1	20 ± 1	0.5/0.1	40.2 ± 2	0.03	32.26	16.67
EGCG	0.1/0.1	19 ± 1	0.5/0.1	38.1 ± 2	0.06	16.67	8.33
EGC	0.1/0.1	18 ± 1	0.5/0.1	36.5 ± 2	0.11	9.09	4.54

[a] $[S]_0/[IO_4^-]_0 = 1$. [b] $[S]_0/[IO_4^-]_0 = 5$. [c] $[H_2O_2]$ was determined using the POD/ABTS method. [d] EC50 = ratio of the antioxidant concentration necessary to decrease the initial concentration of $ABTS^{\bullet-}$ to 50%. [e] ARP = antiradical power (1/EC50). [f] n = stoichiometric number of electrons of $ABTS^{\bullet-}$ involved in the reaction with each antioxidant (1/(2EC50)).

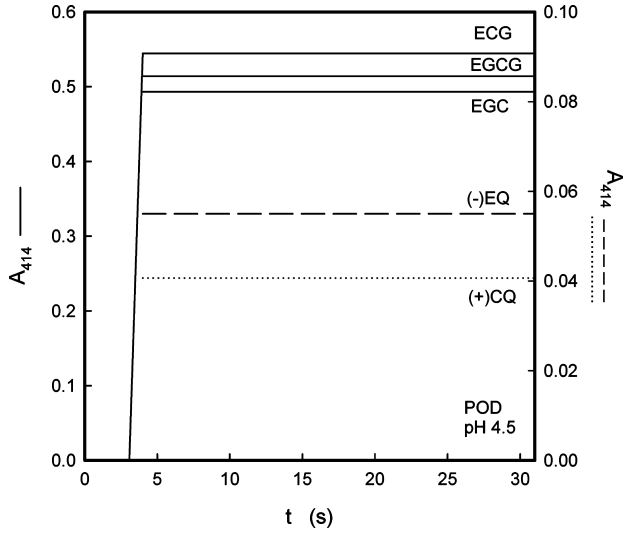

Figure 8. Spectrophotometric quantification of H_2O_2 generated during the auto-oxidation of different green tea catechins. The method described in the Materials and Methods section was followed. Initial concentration of all the substrates was 0.1 mM, and the experimental conditions were $[ABTS]_0 = 5$ mM, $[POD]_0 = 0.22$ μM, and 30 mM sodium acetate buffer pH 4.5. The increase in absorbance due to the formation of $ABTS^{\bullet+}$ was measured at 414 nm for (a) C, (b) EC, (c) EGC, (d) EGCG, and (e) ECG.

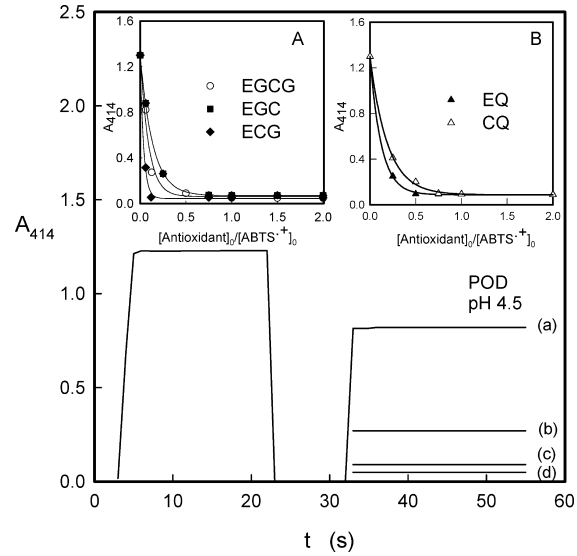

Figure 9. Evaluation of antioxidant activity. Disappearance of absorbance of $ABTS^{\bullet+}$ with time at 414 nm when different quantities of EGCG were added to pregenerated quantities of $ABTS^{\bullet+}$ (40 μM). Experimental conditions were 30 mM sodium acetate buffer pH 4.5, $\lambda = 414$ nm, $[POD]_0 = 0.22$ μM, $[ABTS]_0 = 5$ mM, and $[H_2O_2]_0 = 20$ μM, and the substrate concentrations were (a) 2.4 μM, (b) 5 μM, (c) 30 μM, and (d) 80 μM. The substrates were (a) EGC, (b) ECG, (c) EGCG, (d) EC, and (e) C. **Insets**: (**A**) The disappearance of $ABTS^{\bullet+}$ as a function of the $[antioxidant]_0/[ABTS^{\bullet+}]_0$ at 414 nm; the substrates were (○) EGCG, (■) EGC, and (◆) ECG. (**B**) The disappearance of $ABTS^{\bullet+}$ as a function of the $[antioxidant]_0/[ABTS^{\bullet+}]_0$ at 414 nm; the substrates were (▲) EC and (△) C.

for Windows (*32*), obtaining the maximum rate (V_{max}^{PPO}) and Michaelis constant for the substrate (K_m^{PPO}). From these values and according to eq 7, one can calculate the catalytic constant (k_{cat}^{PPO}). Knowing the value of k_8 (the binding constant of oxygen to the *deoxy*-tyrosinase form (E_d)), the value of the Michaelis constant for O_2 (K_m^{O2}) can be obtained following eq 9 (*26*). For POD, the initial rate values (V_0^{POD}) were calculated from triplicate measurements at each reducing substrate concentration, and V_0^{POD} versus $[S]_0$ data were fitted to the Michaelis−Menten equation (eq 11) through the Sigma Plot 9.0 program for Windows (*32*), obtaining V_{max}^{POD} and K_m^{POD}. From these values and according to eqs 12 and 14, and knowing k_1 (*9*), one can calculate k_{cat}^{POD} (eq 12) and the Michaelis constant for H_2O_2 ($K_m^{H2}O2$) (eq 14).

RESULTS AND DISCUSSION

Oxidation of Green Tea Catechins by High Concentrations of PPO. To characterize the green tea catechins as substrates of PPO and POD, the stability of the *o*-quinones generated in the oxidation step was first studied, by carrying out oxidation experiments using PPO (**Figure 1**). The enzymatic oxidation of EGC by PPO at pH 7.0 generates *o*-quinone (Q), which is unstable and evolves with a very clear stoichiometry, as revealed by the formation of three isosbestic points at 230, 265, and 310 nm (**Figure 1**), which are not maintained at high substrate concentrations. In similar experiments carried out at pH 4.5, no isosbestic points were produced because the *o*-quinone did not follow a clearly defined stoichiometry (**Figure 1**, **inset**). The instability of the *o*-quinones means that these measurements could not be considered reliable for kinetically characterizing the enzymes. This was confirmed in the experiments depicted in **Figure 2A** and **B** showing the oxidation of catechin by PPO/O_2 and POD/H_2O_2. The representations of V_0 versus $[S]_0$ point to an apparent inhibition caused by the excess of substrate, so that this method is of no use for the kinetic characterization of these enzymes and other experimental methods must be used (see below).

Oxidation of Green Tea Catechins by Excess of Periodate. Periodate oxidizes *o*-diphenols in a way similar to PPO, but when an excess of periodate is used for the oxidation, the reaction is instantaneous. The *o*-quinone generated is more stable, and this allowed the molar absorptivities to be calculated for Q at pH 7.0 and pH 4.5 (**Figure 3**) (*33*). These values are shown in **Table 1**. This physical characteristic of Q is important in several types of study, such as those involving HPLC or for determining the concentration of Q.

Kinetic Characterization of the Oxidation of Green Tea Catechins by PPO and POD. As mentioned above, the kinetic characterization of green tea catechins cannot be carried out by measuring the formation of *o*-quinones due to their instability.

However, a spectrophotometric method using a reductant such as AH_2, which instantaneously reduces Q to S, thus preventing its chemical evolution, can be used by following the disappearance of AH_2 (**Figure 4** and **Figure 4**, **inset**) or by measuring the time necessary for a fixed quantity of the reductant to be consumed (chronometric method) (*9, 30, 31*) (**Figure 5**, **inset**).

In the case of PPO, reactions **a**−**c** of **Scheme 2** correspond to the enzymatic catalysis (*34*) and reaction **d** to the reduction of Q to S by AH_2. V_0^{PPO}, the steady-state rate, corresponds to the disappearance rate of AH_2 (**Figure 4**). Nonlinear regression fitting of V_0^{PPO} versus $[S]_0$ according to eq 6 (**Figure 4**, **inset**) gives K_m^{PPO} and V_{max}^{PPO}. In **Scheme 2**, E_m, E_d, and E_{ox} represent the oxidized and deoxygenated forms and that with a peroxide group of the enzyme, respectively.

In the case of POD, the activity can also be followed by measuring the disappearance of AH_2 (**Figure 6** and **Figure 6**, **inset**). The action of POD on reducing substrates (S) in the presence of AH_2 is described by **Scheme 3** (*9*), where POD corresponds to free enzyme, POD-I to compound I, POD-II to compound II, and sQ-S is the semiquinone radical corresponding to S.

Figure 6 depicts the action of POD on EGC, measuring the disappearance of AH_2. Note the difference in the reduction stoichiometry of the products of both enzymes. In PPO reaction **d** (**Scheme 2**), the reduction is $1AH_2/1Q$. However, in POD reactions **d** and **e** (**Scheme 3**), the stoichiometry is $1AH_2/2SQ$-S. In the first case, then, the real steady-state rate V_0^{PPO} is measured and in the second $V_0^{POD}/2$.

The spectrophotometric method described above does not serve to characterize all substrates because the spectra of AH_2 and some catechins overlap, so that a chronometric method is necessary based on measuring the time needed for a small quantity of AH_2 to be consumed (*9, 30, 31*).

Deduction of the Steady-State Rate Expression by the Chronometric Method. The expression of V_0 as a function of AH_2 is derived by applying the material balance method. It is assumed that enzymatic reactions rapidly reach the steady state (when $t \rightarrow 0$), so that the steady-state rate of the enzyme is V_0. The products of both reactions (**Schemes 2** and **3**) react with AH_2, consuming it at the same time, so that the concentration remaining at time t is

$$[AH_2]_t = [AH_2]_0 - V_0 t \tag{1}$$

where the term $V_0 t$ is the matter generated by the enzyme (PPO or POD).

When no AH_2 remains, the following will be true at time $t = \tau$:

$$0 = [AH_2]_0 - V_0 \tau \tag{2}$$

and so

$$V_0^{PPO} = \frac{[AH_2]_0}{\tau} \tag{3}$$

Therefore, if we can experimentally determine τ, then, knowing $[AH_2]_0$, V_0^{PPO} can be calculated according to eq 3; τ can be experimentally determined if a spectrophotometric signal indicates that AH_2 has been consumed (see **Figures 5** and **7**).

In the case of POD (**Scheme 4**), the expression of V_0 (eq 3) must be modified by taking into consideration the stoichiometry (steps **d** and **e**):

$$V_0^{POD} = \frac{2[AH_2]_0}{\tau} \tag{4}$$

This method was used to kinetically characterize EC, C, EGCG, and ECG as substrates of PPO and POD (**Table 2** and **Figures 5** and **7**).

The values of V_0 obtained by both of these methods were analyzed by nonlinear regression to the Michaelis equation.

The analytical expression of V_0^{PPO} in the case of PPO is (*34*)

$$V_0^{PPO} = \frac{V_{max}^{PPO}[S]_0[O_2]_0}{K_m^{PPO}K_S^{O_2} + K_m^{O_2}[S]_0 + K_m^{PPO}[O_2]_0 + [S]_0[O_2]_0} \tag{5}$$

The values of K_m^{O2} for PPO are very small (*35*), so that at the concentration of O_2 in the solution (0.26 mM), the enzyme is saturated and eq 5 is transformed into

$$V_0^{PPO} = \frac{V_{max}^{PPO}[S]_0}{K_m^{PPO} + [S]_0} \tag{6}$$

The values of K_m^{PPO} and V_{max}^{PPO} can be obtained from eq 6 and taking into account (*28*) that

$$V_{max}^{PPO} = 2k_{cat}^{PPO}[E]_0 \tag{7}$$

$$K_m^{PPO} = \frac{k_{cat}^{PPO}}{k_6} \tag{8}$$

$$K_m^{O_2} = \frac{k_{cat}^{PPO}}{k_8} \tag{9}$$

we can calculate k_{cat}^{PPO} and K_m^{O2} from eqs 7 and 9, respectively, since $k_8 = (2.3 \pm 0.4) \times 10^7\ M^{-1}\ s^{-1}$ (*28*). From eq 8, the kinetic constant for the binding of the substrate to E_{ox} (*28*) can be determinated. The values are shown in **Table 2**.

As regards POD, the kinetic analysis of the mechanism shown in **Scheme 3** (*9*), results in

$$V_0^{POD} = \frac{V_{max}^{POD}[S]_0[H_2O_2]_0}{K_m^{POD}[H_2O_2]_0 + K_m^{H_2O_2}[S]_0 + [S]_0[H_2O_2]_0} \tag{10}$$

at saturating concentrations of H_2O_2:

$$V_0^{POD} = \frac{V_{max}^{POD}[S]_0}{K_m^{POD} + [S]_0} \tag{11}$$

$$V_{max}^{POD} = 2k_{cat}^{POD}[E]_0 \tag{12}$$

$$K_m^{POD} = \frac{k_{cat}^{POD}}{k_5} \tag{13}$$

$$K_m^{H_2O_2} = \frac{k_{cat}^{POD}}{k_1} \tag{14}$$

The value of k_1 is $1.7 \times 10^7\ M^{-1}\ s^{-1}$ (*9*). From eq 12, we can calculate k_{cat}^{POD} and from eq 14, $K_m^{H2}O2$. The constant for the binding of the substrate to compound II can be calculated from eq 13. Therefore, the analysis of the data according to eqs 11 and 14 provides the kinetic information shown in **Table 2**.

For the substrates indicated in **Scheme 1**, the data obtained for the enzymatic oxidation are shown in **Table 2**, and they indicate that both enzymes show similar behavior. As regards C, similar values of K_m^{PPO} have been described for PPO from Indian tea leaves (*36*) and marula fruit (*37*) but much higher values in mushroom PPO in organic solvents (*38*). Note that the studies that describe the K_m^{PPO} for C do not provide the k_{cat}^{PPO} because the *o*-quinones evolve although it would be possible to obtain by measuring the consumption of oxygen. The best

substrate for both enzymes is EC, which has a diphenolic structure and between the B ring and the OH of the C ring is in the cis position; the values of K_m^{PPO} are within the same order of magnitude (**Table 2**). The order of catalysis of the different catechins with respect to PPO k_{cat}^{PPO} is EC > C > EGCG > EGC > ECG. However, in the case of POD, the order is EC > EGC > EGCG > C > ECG. The values of K_m^{O2} and K_m^{H2O2}, which depend on k_{cat}, (eqs 9 and 14), follow the same order as k_{cat} and are very low in all cases. In physiological conditions, then, these enzymes can catalyze the transformation of catechins at low concentrations of O_2 and H_2O_2.

As regards the data shown in **Table 2**, the low values of k_{cat} obtained for both enzymes with EGCG and ECG. In the gallate derivates (ECG and EGCG), the enzyme may act on the B ring, *o*-diphenol in ECG or pyrogallol in EGCG, or even on the gallate bound to the C ring. In the first case, k_{cat} should be high (particularly with EGCG) due to the three hydroxyls vecinal with respect to the *o*-diphenol of ECG (*26*). However, if the enzyme binds to the substrate through the gallate portion, the electron withdrawing effect will make k_{cat} much lower, as can be seen in **Scheme 4**.

In **Scheme 4**, S represents ECG or EGCG, the complex ES represents the binding to the B ring and the complex SE the binding to the gallate portion of the same molecule of substrate.

As the product in both cases is reduced by AH_2, the total activity is measured by the chronometric method (**Figures 5** and **7**), giving

$$V_{ss} = \frac{\left(\frac{k_{cat}K'_S + K'_{cat}K_S}{K_S + K'_S}\right)[S]_0[E]_0}{\frac{K_S K'_S}{K_S + K'_S}} \quad (15)$$

The Michaelis constant of PPO for free pyrogallol is high (*26*), $K_S = 1.96$ mM, while for gallic acid $K'_S = 0.20$ mM (unpublished data). Therefore, $K_S \gg K'_S$, $K'_S/K_S \ll 1$, and eq 15 can be expressed as

$$V_{ss} = \frac{\left(\frac{k_{cat}K'_S}{K_s} + K'_{cat}\right)[S]_0[E]_0}{K'_S + [S]_0} \quad (16)$$

with

$$K_m^{app} = K'_S \quad (17)$$

and

$$k_{cat}^{app} = \frac{k_{cat}K'_S}{K_S} + K'_{cat} \quad (18)$$

From eq. 16, it should be noted that these substrates, kinetically, should have a low K_m^{app} (K'_S) and low k_{cat}^{app} ($k_{cat} > k'_{cat}$). Data obtained experimentally with PPO support the reaction mechanism described in **Scheme 4**, since when the enzyme acts on free pyrogallol $k_{cat}^{PPO} = 1263\ s^{-1}$ (*28*) and on free gallic acid $k_{cat}^{PPO} = 27\ s^{-1}$ (unpublished data). Moreover, there should be steric hindrance because of the cis position between the gallate of the C ring and B ring. However, this is not reflected in the values of K_m^{app}, since k_{cat}^{app} in **Table 2** is low. K_m^{app} represents K_m (PPO) or (POD), respectively. k_{cat}^{app} represents k_{cat} (PPO) or (POD), respectively.

Production of H_2O_2. Catechins have been described as both antioxidants and pro-oxidants due to their capacity to scavenger free radicals and to form H_2O_2 (*13, 17*). In this work, we study the autoxidation of the catechins by measuring the oxygen consumption rate during the oxidation of the reduced substrates using an oxygraph. In these experiments, the effect of the enzyme superoxide dismutase (SOD) was observed, and the formation of H_2O_2 was followed by adding catalase (in the oxygraph) or spectrophotometrically at $\lambda = 414$ nm, using POD/ABTS.

(a) Oxygen consumption rate. The oxygen consumption rate increased with the concentration of both substrates, catechin and O_2 (results not shown). This result agrees with the findings of other authors (*13, 17*) and confirms that oxidation begins with the substrate reacting with O_2 (*5*). Thus, the oxygen consumption rate is very low for EC and C and higher for EGC, EGCG, and ECG (**Table 3**).

(b) Inhibition of oxygen consumption by superoxide dismutase. In all the substrates studied, SOD inhibited oxygen consumption, in agreement with (*13, 17*) (**Table 3**), indicating the formation of $O_2^{\bullet-}$ and its sequestering:

$$2O_2^{\bullet-} + 2H^+ \rightarrow O_2 + H_2O_2 \quad (19)$$

Furthermore, the presence of SOD diminishes H_2O_2 formation, since according to (*17*), the stoichiometry is $2O_2^{\bullet-}/1H_2O_2$, although the $O_2^{\bullet-}$ can also provoke the reaction of the reduced substrate with the superoxide anion and generating H_2O_2, where the stoichiometry is $1O_2^{\bullet-}/1H_2O_2$.

(c) Formation of H_2O_2. The formation of H_2O_2 in the autoxidation of some catechins has been demonstrated by several authors (*13, 17, 39, 40*). Here, we compare the formation of H_2O_2 during the autoxidation of C, EC, EGC, ECG, and EGCG at pH = 7.0. Its formation was measured by oxygraph from the activity of the enzyme catalase or after twice extracting the remaining substrate with ether and evaluating the H_2O_2 (**Figure 8**). Three situations have been considered: (*i*) Direct autoxidation. We refer to the formation of H_2O_2, which is accumulated in the medium through the direct oxidation by O_2 and by the $O_2^{\bullet-}$ generated. As can be seen in **Table 3**, the values of C and EC are low, while those obtained with ECG, EGC, and EGCG are relatively high; (*ii*) Oxidation with stoichiometric periodate. When the different catechins are oxidized with stoichiometric periodate, the results shown in **Table 4** point to the slight evolution of the *o*-quinones corresponding to ECG, EGC, and EGCG, while the *o*-quinones corresponding to C and EC lead to the formation of large quantities of H_2O_2. These results show how the *o*-quinones in C, EC, and ECG evolve to generate the highest values of H_2O_2 and also confirm that the limiting step is the reaction described in eq 19; (*iii*) Oxidation of catechins by defect periodate. These conditions are equivalent to those in the action of PPO on its substrates, during which *o*-quinones are generated that can react with the substrate again, as indicated in (*41–43*). **Table 4**shows the results obtained, evaluating H_2O_2 as described in the Materials and Methods. The evolution of the *o*-quinones of C and EC, as they react with the substrate and oxygen, leads to the formation of large quantities of H_2O_2. However, the *o*-quinones of ECG, EGC, and EGCG produce less H_2O_2.

Antioxidant Power. Besides quantifying the H_2O_2 formed during the autoxidation of each substrate, we assessed their antioxidant power using the POD/ABTS/ H_2O_2 system (*44, 45*). For this, the radical $ABTS^{\bullet+}$ is generated with a limiting hydrogen peroxide, while keeping the concentration of the radical constant. By varying the antioxidant, we calculate the EC50 (the concentration of antioxidant that lowers the concentration of radical by 50%) (see **Figure 9**) (*45*). In addition, we calculate the number of electrons of the radical involved in its reaction with each particular oxidant (n_{ABTS}). As can be seen, the gallates of green tea have a lower EC50 and therefore higher antiradical or antioxidant power

(ARP), defined as the inverse of the EC50 (*46, 47*). The catechins have a lower ARP; of the gallates, ECG has the highest antioxidant power. This work therefore demonstrates the dual effect of catechins and gallates from green tea as regards their pro- and antioxidant power in biological systems.

In conclusion, the use of a chronometric method with AH_2 and the measurement of the variation in absorbance of AH_2 with time, to determine the enzymatic activity of PPO and POD acting on green tea catechins, enabled the kinetic characterization of these compounds, which act as substrates for both enzymes. The catechins with a diphenolic structure, C and EC, are better substrates than the epigallocatechins, while among the catechins, the best is EC because of the cis position of the OH in the C ring. From the results obtained, we conclude that green tea catechins do not inhibit the melanogenesis pathway by acting on PPO, as has been claimed (*20*). Rather, these compounds act as an alternative to the physiological substrates L-tyrosine and L-DOPA. It seems therefore that catechins direct the melanogenesis pathway toward quinonic derivatives other than *o*-dopaquinone and dopachrome, which are intermediates of the melanogenesis pathway. However, their oxidation by PPO and POD contributes to the browning of tea and other vegetables that contain catechins (*19*). On the other hand, there has been extensive investigation into the ways by which tea catechins might act in cancer prevention. The observed pro-oxidant nature of these catechins appears to conflict with the generally recognized concept that tea polyphenolics act as antioxidants. Here, we demonstrate that tea catechins possess both antioxidant and pro-oxidant properties. However, and despite these properties, several investigations have suggested that tea polyphenols might act on different cellular targets such as the proteasome (*48*), 5-cytosine DNA methyltransferase (*49*), and dihydrofolate reductase (*14–16*), among others. Deciphering the mechanisms by which tea catechins affect several molecular and cellular pathways would be of importance for the rational use of these compounds in the prevention and treatment of cancer and other physiological disorders.

LITERATURE CITED

(1) Solomon, E. I.; Sundaran, U. M.; Machonkin, T. E. Multicopper oxidases and oxygenases. *Chem. Rev.* **1996**, *96*, 2563–2606.

(2) Klabunde, T.; Eicken, C.; Sacchettini, J. C.; Krebs, B. Crystal structure of a plant catechol oxidase containing a dicopper center. *Nat. Struct. Biol.* **1998**, *5*, 1084–1090.

(3) García-Carmona, F.; García-Canovas, F.; Iborra, J. L.; Lozano, J. A. Kinetic study of the pathway of melanization between L-dopa and dopachrome. *Biochim. Biophys. Acta* **1982**, *717*, 124–131.

(4) Garcia-Cánovas, F.; Garcia-Carmona, F.; Vera-Sanchez, J.; Iborra, J. L.; Lozano, J. A. The role of pH in the melanin biosynthesis pathway. *J. Biol. Chem.* **1982**, *257*, 8738–8744.

(5) Rodriguez-Lopez, J. N.; Tudela, J.; Varón, R.; Garcia-Canovas, F. Kinetic study on the effect of pH on the melanin biosynthesis pathway. *Biochim. Biophys. Acta* **1991**, *1076*, 379–386.

(6) Whitaker, C. Y.; Lee, Y. In *Enzymatic Browning and Its Prevention*; Whitaker, J. R., Lee C. Y., Eds.; American Chemical Society: Washington, DC, 1995.

(7) Walker J. R. L. In *Enzymatic Browning and Its Prevention*; Whitaker, J. R., Lee, C. Y., Eds.; American Chemical Society: Washington, DC, 1995.

(8) Dunford H. B. *Heme Peroxidases*; Wiley-VHC: New York, 1999; pp 92−97.

(9) Rodríguez-López, J. N.; Gilabert, M. A.; Tudela, J.; Thorneley, R. N. F.; García-Cánovas, F. Reactivity of horseradish peroxidase compound II toward substrates: kinetic evidence for a two-step mechanism. *Biochemistry* **2000**, *39*, 13201–13209.

(10) Gilabert, M. A.; Fenoll, L. G.; Garcia-Molina, F.; Tudela, J.; Garcia-Canovas, F.; Rodríguez-López, J. N. Kinetic characterization of phenol and anilines derivates as substrate of peroxidase. *Biol. Chem.* **2004**, *385*, 795800.

(11) Gilabert, M. A.; Hiner, A. N.; Garcia-Ruiz, P. A.; Tudela, J.; Garcia-Molina, F.; Acosta, M.; Garcia-Canovas, F.; Rodríguez-López, J. N. Differential substrate behaviour of phenol and aniline derivatives during oxidation by horseradish peroxidise: kinetic evidence for a two-step mechanism. *Biochim. Biophys. Acta* **2004**, *1699*, 235–243.

(12) You-Ying, T.; Xin-Qing, X.; Hui-Long, X.; Naoharu, W. Optimization of theaflavin biosynthesis from tea polyphenols using an inmobilized enzyme system and response surface methodology. *Biotechnol. Lett.* **2005**, *27*, 269–274.

(13) Roginsky, V.; Alegria, A. E. Oxidation of tea extracts and tea catechins by molecular oxygen. *J. Agric. Food Chem.* **2005**, *53*, 4529–4535.

(14) Navarro-Martinez, M. D.; Navarro-Peran, E.; Cabezas-Herrera, J.; Ruiz-Gomez, J.; Garcia-Canovas, F.; Rodriguez-Lopez, J. N. Antifolate activity of epigallocatechin gallate against *Stenophomonas maltophilia*. *Antimicrob. Agents Chemother.* **2005**, *49*, 2914–2920.

(15) Navarro-Peran, E.; Cabezas-Herrera, J.; Hiner, A. N. P.; Sadunishvili, T.; Garcia-Canovas, F.; Rodriguez-Lopez, J. N. Kinetics of the inhibition of bovine liver dihydrofolate reductase by tea catechins: origin of sowl-binding inhibition and pH studies. *Biochemistry* **2005**, *44*, 7512–7525.

(16) Navarro-Peran, E.; Cabezas-Herrera, J.; Garcia-Canovas, F.; Durrant, M. C.; Thorneley, R. N. F.; Rodriguez-Lopez, J. N. The antifolate activity of tea catechins. *Cancer Res.* **2005**, *65*, 2059–2064.

(17) Mochizuki, M.; Yamazaki, S. I.; Kano, K.; Ikeda, T. Kinetic analysis and mechanistic aspects of autooxidation of catechins. *Biochim. Biophys. Acta* **2002**, *1569*, 35–44.

(18) Lopez-Serrano, M.; Ros-Barcelo, A. Kinetic properties of (+)catechin oxidation by a basic peroxidase isoenzyme from strawberries. *J. Food Chem.* **1997**, *62*, 676–723.

(19) Lopez-Serrano, M.; Ros-Barcelo, A. Comparative study of the products of the peroxidase-catalyzed and the polyphenol oxidase-catalyzed (+)-catechin oxidation. Their possible implications in strawberry (*Fragaria* × *ananassa*) browning reactions. *J. Agric. Food Chem.* **2002**, *50*, 1218–1224.

(20) No, J. K.; Soung, D. Y.; Kim, Y. J.; Shim, K. H.; Jun, Y. S.; Rhee, S. H.; Yokozawa, T.; Chung, H. Y. Inhibition of tyrosinase by green tea components. *Pharmacol. Lett.* **1999**, *65*, 241–246.

(21) Chung, F. L.; Schwartz, J.; Herzog, C. R.; Yang, Y. M. Tea and cancer prevention: studies in animals and humans. *J. Nutr.* **2003**, *133*, 3268–3274.

(22) Chen, Z. Y.; Zhu, Q. Y.; Wong, Y. F.; Zhang, Z.; Chung, H. Y. Stabilizing effect of ascorbic acid on green tea catechins. *J. Agric. Food Chem.* **1998**, *46*, 2512–2516.

(23) Long, L. H.; Lan, A. N. B.; Hsuan, P. Y. Y.; Halliwell, B. Generation of hydrogen peroxide by "antioxidant" beverages and the effect of milk addition. Is cocoa the best beverage. *Free Radical Res.* **1999**, *31*, 65–71.

(24) Peng, M.; Kuc, J. Peroxidase-generated hydrogen-peroxide as a source of antifungal activity in vitro and on tobacco leaf-disks. *Phytopathology* **1992**, *82*, 696–699.

(25) Murray, R. D. H. *Progress in the Chemistry of Organic Natural Products*; Springer-Verlag: New York, 1999; pp 84−316.

(26) Rodríguez-Lopez, J. N.; Fenoll, L. G.; Garcia-Ruiz, P. A.; Varon, R.; Tudela, J.; Thorneley, R. N.; Garcia-Canovas, F. Stopped-flow and steady-state study of the diphenolase activity of mushroom tyrosinase. *Biochemistry* **2000**, *39*, 10497–10506.

(27) Bradford, M. M. A rapid and sensitive method for the quantitation of microgram quantities of protein utilizing the principle of protein-dye binding. *Anal. Biochem.* **1976**, *72*, 248–254.

(28) Rodríguez-Lopez, J. N.; Ros, J. R.; Varon, R.; GarciaCanovas, F. Oxygen Michaelis constant for tyrosinase. *Biochem. J.* **1993**, *293*, 859–866.

(29) Rodriguez-Lopez, J. N.; Ros-Martinez, J. R.; Varon, R.; Garcia-Canovas, F. Calibration of a Clark-type oxygen electrode by tyrosinase-catalyzed oxidation of a 4-*tert*-butylcatechol. *Anal. Biochem.* **1992**, *202*, 356–360.

(30) Muñoz, J. L.; Garcia-Molina, F.; Varon, R.; Rodríguez-Lopez, J. N.; Garcia-Canovas, F.; Tudela, J. Calculating molar absortivities for quinones: application to the measurements of tyrosinase activity. *Anal. Biochem.* **2006**, *351*, 128–138.

(31) Garcia-Molina, F.; Munoz, J. L.; Varon, R.; Rodríguez-Lopez, J. N.; Garcia-Canovas, F.; Tudela, J. A review on spectrophotometric methods for a measuring the monophenolase and diphenolase activities of tyrosinase. *J. Agric. Food Chem.* **2007**, *55*, 9739–9749.

(32) Jandel Scientific. SigmaPlot 9 for Windows; Jandel Scientific: Core Madera, CA, 2007.

(33) Weidman, S. W. A kinetic study of the periodate oxidation of catechol. *J. Am. Chem. Soc.* **1966**, *88*, 5820–5827.

(34) Sanchez-Ferrer, A.; Rodriguez-Lopez, J. N.; Garcia-Canovas, F.; Garcia- Carmona, F. Tyrosinase: A conprehensive review of its mechanism. *Biochim. Biophys. Acta* **1995**, *1247*, 1–11.

(35) Fenoll, L. G.; Rodrigez-Lopez, J. N.; Garcia-Molina, F.; Garcia-Canovas, F.; Tudela, J. Michaelis constant of mushroom tyrosinase with respect to oxygen in the presence of monophenols and diphenols. *Int. J. Biochem. Cell Biol.* **2002**, *34*, 332–336.

(36) Halder, J.; Tamuli, P.; Bhaduri, A. N. Isolation and characterization of polyphenol oxidase from Indian tea leaf (*Camellia sinensis*). *J. Nutr. Biochem.* **1998**, *9*, 75–80.

(37) Mdluli, K. M. Partial purification and characterisation of polyphenol oxidase and peroxidase from marula fruit (*Sclerocarya birrea* subsp. *Caffra*). *Food Chem.* **2005**, *92*, 311–323.

(38) Kermasha, S.; Bao, H.; Bisakowski, B. Biocatalysis of tyrosinase using catechin assubstrate in selected organic solvent media. *J. Mol. Catal. B: Enzym.* **2001**, *11*, 292–238.

(39) Jiang, Y.; Miles, P. W. Generation of H_2O_2 during enzymic oxidation of catechin. *Phytochemistry* **1993**, *33*, 29–34.

(40) Akagawa, M.; Shigemitsu, T.; Suyama, K. Production of hydrogen peroxide by polyphenols and polyphenol-rich beverages under quasi-physiological conditions. *Biosci. Biotechnol. Biochem.* **2003**, *67*, 2632–2640.

(41) Jimenez-Atiénzar, M.; Cabanes, J.; GandiaHerrero, F.; Garcia-Carmona, F. Kinetic analysis of catechin oxidation by polyphenol oxidase at neutral pH. *Biochem. Biophys. Res. Commun.* **2004**, *319*, 902–910.

(42) Guyot, S.; Vercauteren, J.; Cheynier, V. Structural determination of colourless and Bellow Diners resulting from (+)-catechin coupling catalysed by grape polyphenol oxidase. *Phytochemistry* **1996**, *42*, 1279–1288.

(43) Guyot, S.; Cheynier, V.; Souquet, J. M.; Moutounet, M. Influence of pH on the enzymatic oxidation of (+)-catechin in model systems. *J. Agric. Food Chem.* **1995**, *43*, 2458–2462.

(44) Cano, A.; Hernandez-Ruiz, J.; Garcia-Canovas, F.; Acosta, M.; Arnao, M. B. An end-point method for estimation of the total antioxidant activity in plant material. *Phytochem. Anal.* **1998**, *9*, 196–202.

(45) Hotta, H.; Nagano, S.; Ueda, M.; Tsujino, Y.; Koyama, J.; Osakai, T. Higher radical scavenging activities of polyphenolic antioxidants can be ascribed to chemicals reactions following their oxidation. *Biochem. Biophys. Acta* **2002**, *1572*, 123–132.

(46) Torres, J. L.; Lozano, C.; Maher, P. Conjugation of catechins with cysteine generates antioxidant compounds with enhanced neuroprotective activity. *Phytochemistry* **2005**, *66*, 2032–2037.

(47) Brand-Williams, W.; Cuvelier, M. E.; Berset, C. Use of a free radical method to evaluate antioxidant activity. *Lebensm.−Wiss. Technol.* **1995**, *28*, 25–30.

(48) Nam, S.; Smith, D. M.; Dou, Q. P. Ester bond-containing tea polyphenols potently inhibit proteasome activity in vitro and in vivo. *J. Biol. Chem.* **2001**, *276*, 13322–13330.

(49) Fang, M. Z.; Wang, Y.; Ai, N.; Hou, Z.; Sun, Y.; Lu, H.; Welsh, W.; Yang, C. S. Tea polyphenol (−)-epigallocatechin-3-gallate inhibits DNA methyltransferase and reactivates methylation-silenced genes in cancer cell lines. *Cancer Res.* **2003**, *63*, 7563–7570.

Received for review April 17, 2008. Revised manuscript received July 1, 2008. Accepted July 2, 2008. This paper has been partially supported by grants from the Ministerio de Educación y Ciencia (Madrid, Spain) Project BIO2006-15363 and SAF2006-07040-C02-01, from the Fundación Séneca (CARM, Murcia, Spain) Project 00672/PI/04, and from the Consejería de Educación (CARM, Murcia, Spain) BIO-BMC 06/01-0004. J.L.M.-M. has a fellowship from the Ministerio de Educación y Ciencia (Madrid, Spain) Reference AP2005-4721. F.G.-M. has a fellowship from Fundación Caja Murcia (Murcia, Spain).

JF8012162

4.10. OXIDACIÓN ENZIMÁTICA Y QUÍMICA DE FENOLES TRIDROXILADOS.

La oxidación enzimática y química de distintos fenoles trihidroxilados ha dado lugar a la siguiente publicación adjunta.

4.10.1. Título

Enzymatic and chemical oxidation of tridydroxylated phenols.

4.10.2. Autores

Muñoz-Muñoz, J.L.; Garcia-Molina, F.; Garcia-Ruiz, P.A.; Arribas, E.; Tudela, J.; Garcia-Cánovas, F. y Rodríguez-López, J.N.

4.10.3. Referencia

Food Chemistry (2009) 113, 435-444.

4.10.4. Resumen

Se han caracterizado cinéticamente el ácido gálico, pirogalol y ácido gálico metil ester como sustratos de polifenoloxidasa (PPO) y peroxidasa (POD) y se han estudiado las propiedades pro- y antioxidantes. Los datos obtenidos se correlacionan con los desplazamientos químicos, obtenidos por ^{13}C-RMN, de los átomos de carbono que soportan los grupos hidroxilos. Pirogalol mostró la mayor constante catalítica tanto para PPO como para POD, de acuerdo con su bajo valor de δ_2. Esto también implica que ambas enzimas tengan una alta constante de Michaelis para el pirogalol.

Food Chemistry 113 (2009) 435–444

Contents lists available at ScienceDirect

Food Chemistry

journal homepage: www.elsevier.com/locate/foodchem

Enzymatic and chemical oxidation of trihydroxylated phenols

J.L. Muñoz-Muñoz [a], F. García-Molina [a], P.A. García-Ruiz [b], E. Arribas [c], J. Tudela [a], F. García-Cánovas [a,*], J.N. Rodríguez-López [a]

[a] GENZ, Grupo de Investigación de Enzimología, Departamento de Bioquímica y Biología Molecular-A, Facultad de Biología, Universidad de Murcia, E-30100 Espinardo, Murcia, Spain
[b] QCBA, Grupo de Química de Carbohidratos y Biotecnología de Alimentos, Departamento de Química Orgánica, Facultad de Química, Universidad de Murcia, E-30100 Espinardo, Murcia, Spain
[c] Departamento de Física Aplicada, Escuela Politécnica Superior, Universidad de Castilla la Mancha, Avda, España s/n, Campus Universitario, E-02071 Albacete, Spain

ARTICLE INFO

Article history:
Received 29 April 2008
Received in revised form 10 June 2008
Accepted 23 July 2008

Keywords:
Tyrosinase
Peroxidase
Trihydroxylated compounds
Hydrogen peroxide
Pro-oxidant
Anti-oxidant

ABSTRACT

Gallic acid, pyrogallol and gallic acid methyl ester were kinetically characterised as substrates of polyphenoloxidase (PPO) and peroxidase (POD) and their pro- and anti-oxidant capacities were studied. The data obtained are correlated with the chemical shifts of the carbons supporting the vicinal hydroxyls obtained by ^{13}C NMR. Pyrogallol showed the highest catalytic constant for both PPO and POD, reflecting its low δ_2 value. This also implies that both enzymes have a high Michaelis constant for pyrogallol.

Pyrogallol also showed higher pro- and anti-oxidant activity (generating H_2O_2) than did gallic acid and gallic acid methyl esters. However, gallic acid inhibited the formation of H_2O_2, due to the peroxidation reaction with its carboxylic group, which generated O_2.

© 2008 Elsevier Ltd. All rights reserved.

1. Introduction

Melanin production is the phenomenon responsible for skin, hair and eye pigmentation in mammals (Tomita, Hariu, Mizuno, & Seiji, 1980) and the undesirable browning of fruits and vegetables (Vámos-Vigázó, 1995). Both its accumulation and deficiency can lead to illnesses such as melanoma, melasma and albinism (Briganti, Camera, & Picardo, 2003; Hearing, 2005). Consequently, modulators of melanogenesis have assumed great importance in recent years for the prevention of hypo- and hyper-pigmentary disorders, for both therapeutic (Seo, Sharma, & Sharma, 2003) and cosmetic (Funasaka, Komoto, & Ichihashi, 2000) purposes.

Tyrosinase or polyphenoloxidase (monophenol, *o*-diphenol; oxygen-oxidoreductase; EC 1.14.18.1; PPO) is a key enzyme in regulating the melanogenesis pathway (Kim & Uyama, 2005). It has two copper atoms in its active site, capable of catalysing two types of reactions in which molecular oxygen takes part: (a) the hydroxylation of monophenols to *o*-diphenols (monophenolase activity) and (b) the oxidation of *o*-diphenols to their corresponding *o*-quinones (diphenolase activity). These *o*-quinones are highly reactive species that evolve through chemical reactions to form polymers, in the process of which free radicals may be generated. Indeed, it is the oxidative stress caused by an excess of free radicals, together with ultraviolet light, that causes pigment disorders, which is why anti-oxidants have beneficial effects for skin health (Yasui & Sakurai, 2003).

Peroxidase (EC 1.11.1.7; POD) is widely distributed in the animal, plant and fungal kingdoms (Dunford, 1999). The cationic isoenzyme of horseradish has been widely studied due to its use in analysis kits and for potential application for bioremediation purposes (Rodríguez-López, Gilabert, Tudela, Thorneley, & García-Cánovas, 2000). The oxidation of polyphenols by this enzyme gives rise to highly reactive intermediate species (free radicals), which rapidly polymerise to give polymeric products of diverse stoichiometries. Because of these reactions, it was very difficult to study the steady-state kinetically and it was suggested that these enzymes do not follow classical Michaelis–Menten kinetics. However, the development of a chronometric method established the existence of typical Michaelis–Menten kinetic schemes for a series of *o*-diphenols, monophenols and anilines (Gilabert, Fenoll, et al., 2004; Gilabert, Hiner, et al., 2004; Muñoz et al., 2006; Rodríguez-López, Gilabert, et al., 2000).

Many phenolic compounds have been shown to act as potent anti-oxidants and many are tyrosinase substrates. Among these, gallic acid (3,4,5-trihydroxybenzoic acid), gallic acid methyl ester (methyl 3,4,5-trihydroxybenzoic acid, GME) and pyrogallol (1,2,3-trihydroxybenzene) are natural trihydroxylated compounds. Gallic acid has been proposed as a potent inhibitor of tyrosinase (Kim,

* Corresponding author. Fax: +34 968 364147.
E-mail address: canovasf@um.es (F. García-Cánovas).
URL: http://www.um.es/genz (F. García-Cánovas).

0308-8146/$ - see front matter © 2008 Elsevier Ltd. All rights reserved.
doi:10.1016/j.foodchem.2008.07.076

2007), and potent anti-oxidant and neuroprotector (Lu, Nie, Belton, Tang, & Zhao, 2006). It has been suggested that pyrogallol can generate superoxide anions and act as a powerful anti-carcinogen since it destroys HeLa cells of human cervical adenocarcinoma by a mechanism that breaks the cell cycle and leads to apoptosis (Kim et al., 2008). A similar anti-carcinogenic role for pyrogallol has been described for human prostate cancer (Noguchi, Yokoyama, & Watanabe, 2006) and breast cancer cells (Zhao, Tian, Ma, & Li, 2006). This same anti-carcinogenic effect has been demonstrated, in recent publications, for gallic acid and GME which induce the apoptosis of leukaemia cells (Locatelli et al., 2008). The structures of these triphenols are depicted in Scheme 1.

As mentioned, the anti-oxidant role of phenols and polyphenols has been much discussed, as has their pro-oxidant effect, due to its auto-oxidation, which generates reactive oxygen species (ROS). It now seems clear that superoxide anion and hydrogen peroxide are formed by an auto-catalytic mechanism (see below). Several years ago it was demonstrated that the H_2O_2 formed by the auto-oxidation of pyrogallol reacts with the pool of cellular DNA to produce great structural damage on genes (Lee, Liang, & Lin, 1995), and it interacts with cell proteins, provoking irreversible damage (Lee & Lin, 1994; Lin & Lee, 1992).

Recently, it has been proposed that gallic acid acts as an inhibitor of melanogenesis (Kim, 2007). However, the polyphenolic structure of these compounds (Scheme 1) suggests that they are substrates of tyrosinase. This work, therefore, examines gallic acid and its trihydroxylated homologues, gallic acid methyl ester and pyrogallol, as alternative tyrosinase substrates, to prevent the enzyme forming eumelanins. At the same time, we characterise the pro- and anti-oxidant properties of these triphenols.

2. Materials and methods

2.1. Reagents

Mushroom tyrosinase or polyphenoloxidase (1530 U mg^{-1}, PPO) and horseradish peroxidase (297 U mg^{-1}, POD) were obtained from Sigma Chemical (St. Louis, MO). Ascorbic acid (AH_2), gallic acid, gallic acid methyl ester (GME), pyrogallol, glutathione (GSH) and 5,5′-dithiobis(2-nitrobenzoic acid) (DTNB) were obtained from Sigma Chemical (St. Louis, MO), and sodium periodate was obtained from Scharlau (Malaga, Spain). Stock solutions of the reducing substrates were prepared in 0.15 mM phosphoric acid to prevent auto-oxidation. The buffers used were 30 mM sodium phosphate buffer (pH 7.0) and 30 mM sodium acetate (pH 4.5) for PPO and POD. The chemical structures of the substrates studied are shown in Scheme 1.

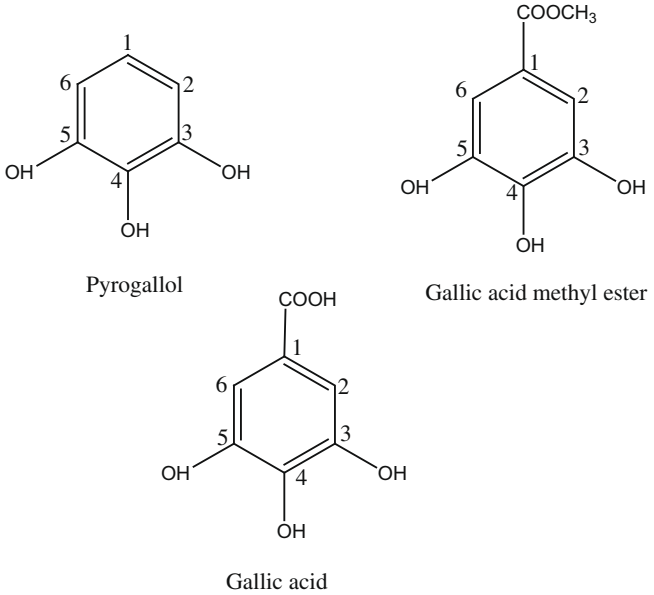

Scheme 1. Structures of the compounds used in this work.

2.2. Enzyme source

PPO (1530 U mg^{-1}) was purified according to (Rodríguez-López, Fenoll, et al., 2000). POD was purchased from Sigma (type VI; Rz = 3.2) and used without further purification. The concentration of POD was determined spectrophotometrically using a Soret extinction coefficient of 102 mM^{-1} cm^{-1} (Rodríguez-López, Gilabert, et al., 2000). The protein concentration was determined by Bradford's method (Bradford, 1976), using bovine serum albumin as the standard.

2.3. Spectrophotometric assays

Absorption spectra were recorded in a visible–ultraviolet Perkin–Elmer Lambda 35-spectrophotometer interfaced on-line with a PC-compatible microcomputer, at a scanning speed of 60 nm/s. The temperature was controlled at 25 °C using a Haake D16 circulating water-bath with a heater/cooler, and checked using a Cole–Parmer digital thermometer with a precision of ±0.1 °C. Kinetic assays were also carried out with the above instruments following the disappearance of AH_2 at λ = 280 nm (ε = 6507 M^{-1} cm^{-1}) or using a chronometric method that involved measuring the appearance of the products in the reaction medium once the AH_2 had been consumed (λ = 340 nm). Reference cuvettes contained all the components, except the substrate and AH_2, in a final volume of 1 ml. All the assays for PPO were carried out under saturating conditions of molecular oxygen (0.26 mM oxygen in the assay medium) (Rodríguez-López, Ros, Varon, & Garcia-Canovas, 1993).

2.4. Oxymetric assays

Oxygen evolution was measured with a Clark-type electrode coupled to a Hansatech Oxygraph (King's Lynn, Norfolk, UK). The equipment was calibrated using the tyrosinase/4-*tert*-butylcatechol method (Rodríguez-López, Ros-Martinez, Varon, & Garcia-Canovas, 1992). Nitrogen was bubbled through the reaction medium to remove the oxygen when necessary. The reaction medium contained 30 mM sodium phosphate buffer, pH 7.0. The medium was stirred constantly and temperature was kept at 25 ± 0.1 °C using a Haake D1G circulating water-bath.

2.5. Chronometric method

Enzymatic activity was determined spectrophotometrically using the chronometric method described in Section 3 (Muñoz et al., 2006; Rodríguez-López, Gilabert, et al., 2000). The only condition was that there had to be an absorbance increase (due to the product formation) measurable once the AH_2 was consumed, to be able to determine the time, τ, necessary to consume the quantity of AH_2 called $[AH_2]_0$. From these values, the initial, V_0, rate can be determined (see Section 3). Preliminary experiments were carried out in the absence of AH_2 with the tyrosinase/O_2/triphenol system by recording spectrophotometric scans to identify in which zone of the spectrum, particularly the visible zone, the greatest changes in absorbance occurred. The wavelength chosen at acid and neutral pH was 340 nm. The activity of POD was continued using the same methodology, but with the POD/H_2O_2/triphenol system.

2.6. Determination of molar absorption coefficients

The absorbance data were analysed according to Beer's law, using the standard least-squares linear regression programme. Molar absorption coefficients were estimated for a known path length of 1 cm. The minimal acceptable coefficient of determination (r^2) was taken to be 0.995. Data yielding coefficients less than this were due to pipetting errors and rounding up/down of the values. With this precaution, the 95% confidence limits for the molar absorption coefficient estimates were $\leqslant 5\%$.

2.7. Kinetic data analysis

2.7.1. Polyphenoloxidase (PPO)

Initial rate values (V_0^{PPO}) were calculated from triplicate measurements at each reducing substrate concentration and V_0^{PPO} vs. $[S]_0$ data were fitted to the Michaelis–Menten equation (Eq. (6)) with the Sigma Plot 9.0 program for Windows (Jandel Scientific, 2007), giving V_{max}^{PPO} and K_m^{PPO}. From these values, and according to Eq. (7), one can calculate k_{cat}^{PPO}. Knowing the value of k_8 (the binding constant of oxygen to desoxytyrosinase (E_d)), the value of $K_m^{O_2}$ can be obtained following Eq. (10) (Rodríguez-López, Fenoll, et al., 2000) and, from Eq. (9), the binding constant of the substrate to *oxy*tyrosinase (k_6) can be calculated.

2.7.2. Horseradish peroxidase (POD)

Initial rate values (V_0^{POD}) were calculated from triplicate measurements at each reducing substrate concentration and V_0^{POD} vs. $[S]_0$ data were fitted to the Michaelis–Menten equation (Eq. (18)) through the Sigma Plot 9.0 program for Windows (Jandel Scientific, 2007), giving V_{max}^{POD} and K_m^{POD}. From these values, and according to Eq. (12), one can calculate k_{cat}^{POD}. The value of $K_m^{H_2O_2}$ can be determined from Eq. (17) and knowing k_1 (Rodríguez-López, Gilabert, et al., 2000). Taking into account Eq. (16), it is possible to obtain k_5, the binding constant of the substrate to compound II (Rodríguez-López, Gilabert, et al., 2000).

2.8. Determination of GSH formation

The thiol solutions were prepared immediately before being used. The total thiol content was measured using 5,5′-dithiobis(2-nitrobenzoic acid) (DTNB) reagent and a slight modification of the method previously described (Garcia-Molina, Peñalver, Rodríguez-Lopez, Garcia-Canovas, & Tudela, 2005; Habebb, 1972).

2.9. ^{13}C NMR

The ^{13}C NMR spectra were obtained for all the substrates used in deuterated water, pH 7.0, the shifts of the C-1 (δ_1^7) and C-2 (δ_2^7) carbons being measured for the different *o*-diphenols. The ^{13}C NMR spectra of the different *o*-diphenols considered here were obtained in a Varian unity spectrometer of 300 MHz. The δ values were measured relative to those for tetramethylsilane ($\delta = 0$). The maximum line breadth accepted in the ^{13}C NMR spectra was 0.06 Hz. Therefore, the maximum accepted error for each peak was ±0.03 ppm. Moreover, the electron-donating capacity of the oxygen atom from different phenolic compounds (nucleophilic power) was correlated with the experimental δ values in ^{13}C NMR for the carbon atom that supports the hydroxyl group (Tomiyama, Sakai, Nihiyama, & Yasmada, 1993). Taking all the above into account, low values of δ_1^7 and δ_2^7 in ^{13}C NMR for *o*-diphenols indicate high nucleophilic power at pH 7.0 (Espin et al., 2000).

3. Results and discussion

3.1. Oxidation of trihydroxylated compounds by PPO and POD

The enzymatic oxidation of these substrates (gallic acid, pyrogallol and GME) by PPO/O_2 and POD/H_2O_2 was studied at both pH 7.0 and 4.5, taking into account the pH optimum of both enzymes (Dunford, 1999; Solomon, Sundaran, & Machonkin, 1996). The enzymatic oxidation of gallic acid by PPO and POD at both pH values with high concentrations of these enzymes generates

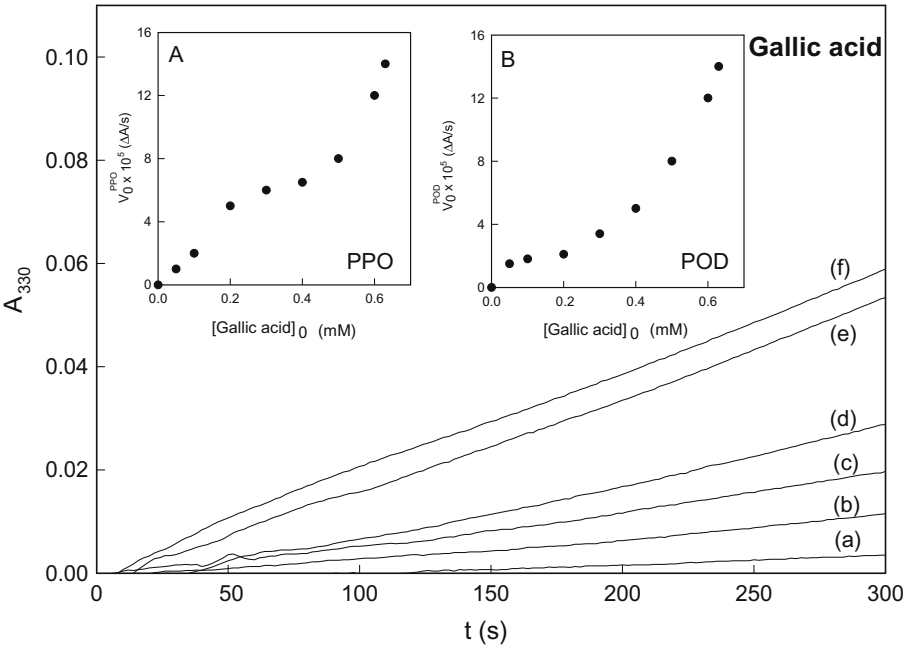

Fig. 1. Spectrophotometric recordings of the products generated in the action of PPO and POD on gallic acid. The experimental conditions were 30 mM sodium phosphate buffer, pH 7.0, λ = 330 nm, $[PPO]_0$ = 0.22 μM. The gallic acid concentrations were (a) 0.05 mM, (b) 0.1 mM, (c) 0.2 mM, (d) 0.4 mM, (e) 0.6 mM and (f) 0.63 mM. (Inset A) Representation of V_0^{PPO} vs. $[gallic\ acid]_0$, directly measuring the appearance of product in the PPO reaction. (Inset B) Representation of V_0^{POD} vs. $[gallic\ acid]_0$, directly measuring the appearance of product in the POD reaction. The experimental conditions were 30 mM sodium phosphate buffer, pH 7.0, λ = 330 nm, $[POD]_0$ = 10 nM and $[H_2O_2]_0$ = 150 μM.

o-quinones (Q), which are unstable. Due to the instability of the *o*-quinones, these measurements cannot be taken as accurate for the kinetic characterisation of the enzymes (Muñoz et al., 2006). Thus, for the oxidation of gallic acid by PPO/O_2 (Fig. 1, inset A) and POD/H_2O_2 (Fig. 1, inset B), respectively, the plots of V_0^{PPO} vs. $[S]_0$ and V_0^{POD} vs. $[S]_0$ show apparent activation by excess of substrate, meaning that this method is of no use for the kinetic characterisation of these enzymes and that other experimental measurement methods are needed (Garcia-Molina et al., 2007).

3.2. Oxidation of trihydroxylated phenols by periodate at a high periodate/triphenol ratio

Periodate oxidises *o*-diphenols and triphenols to *o*-quinones (Q) in a way similar to PPO, but, when an excess of periodate is used for the oxidation, the reaction is instantaneous and the *o*-quinone is more stable, which allows the molar absorption coefficients (Weidman & Kaiser, 1966) to be calculated for Q at pH 7.0 and 4.5. These coefficients are shown in Table 1. This physical characteristic of Q is important in several types of study, such as those involving HPLC or for determining the concentration of Q.

3.3. Kinetic characterisation of the oxidation of trihydroxylated compounds by PPO and POD

As mentioned above, the appearance of the *o*-quinones of these triphenols cannot be measured by spectrophotometry with any degree of reliance because of their great instability. However, another spectrophotometric method, involving a reductant such as AH_2, can be used to measure the disappearance of AH_2, which instantaneously reduces Q to S and prevents its chemical evolution (Fig. 2, inset). Alternatively, the time necessary to consume a fixed quantity of AH_2 can be measured (chronometric method) (Fig. 3, inset) (Muñoz et al., 2006; Rodríguez-López, Gilabert, et al., 2000).

In the case of POD, the activity can be followed by measuring the disappearance of AH_2 (Fig. 2, inset). The action of POD on reducing substrates (S) in the presence of AH_2 is described in Scheme 3 (Rodríguez-López, Gilabert, et al., 2000) where POD indicates the free enzyme, POD-I is compound I, POD-II is compound II, and sQ-S is the semiquinone radical corresponding to S.

In the case of PPO, reactions (a–c) of Scheme 3, correspond to the enzymatic catalysis and reaction (d) to the reduction of Q to S by AH_2. The disappearance rate of AH_2 corresponds to V_0^{PPO}, the steady-state rate where E_m, E_d, and E_{ox} represent the oxidised and deoxygenated forms and that with a peroxide group of the enzyme, respectively.

The spectrophotometric method described above does not permit all the substrates to be characterised because the spectra of AH_2 and of some of the trihydroxylated phenols overlap. This means that the chronometric method, based on measuring the time necessary to consume a small quantity of AH_2, must be used (Muñoz et al., 2006; Rodríguez-López, Gilabert, et al., 2000).

3.4. Steady-state expression using the chronometric method

The expression V_0, as a function of $[AH_2]$, can be easily deduced using the material balance method. It is considered that the enzymatic reactions rapidly reach the steady-state (when $t \to 0$), so that the rate of enzyme activity is V_0. The products of both reactions (Schemes 2 and 3) react with AH_2, consuming it, so that the concentration of AH_2 remaining at time t, is

$$[AH_2]_t = [AH_2]_0 - V_0 t \quad (1)$$

The term V_0t is the matter generated by the enzyme (PPO or POD). When no AH_2 remains at time $t = \tau$, the following is fulfilled:

Table 1
Molar absorptivity coefficients of the *o*-quinones of the trihydroxylated phenols

	$\varepsilon^{4.5}$ (M^{-1} cm^{-1})		$\varepsilon^{7.0}$ (M^{-1} cm^{-1})	
	λ_{max}	λ_i	λ_{max}	λ_i
Gallic acid	7400 ± 370	1800 ± 90	3825 ± 230	2750 ± 137
Pyrogallol	18,000 ± 540	11,900 ± 357	3000 ± 140	3700 ± 222
GME	2000 ± 60	985 ± 20	1000 ± 30	600 ± 36

λ_i, isosbestic point for each substrate.

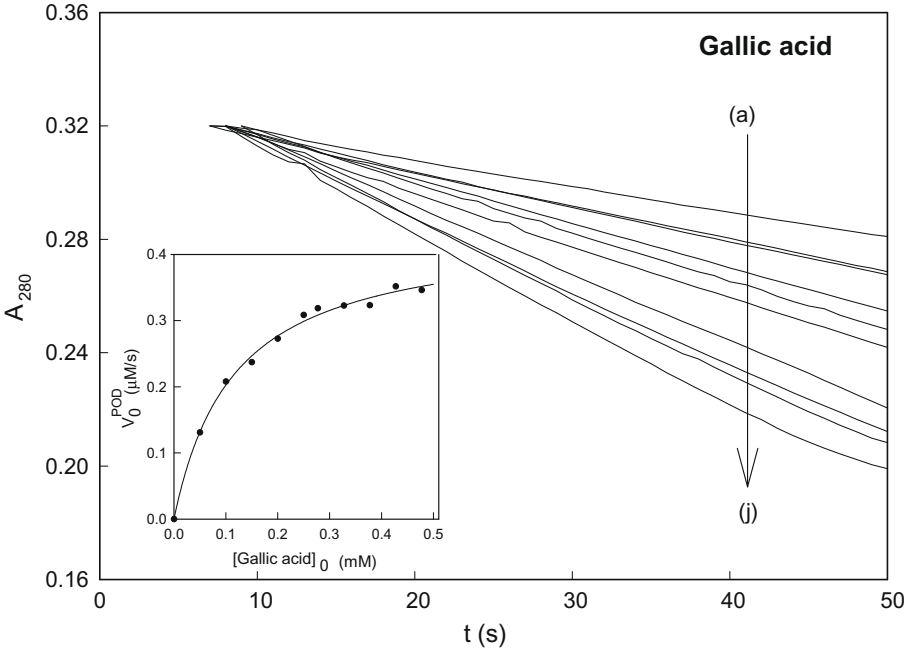

Fig. 2. Spectrophotometric recordings of AH_2 disappearance for measuring the enzymatic activity of POD on gallic acid. The experimental conditions were 30 mM sodium phosphate buffer, pH 7.0, λ = 280 nm, $[E]_0$ = 4 nM, $[AH_2]_0$ = 20 μM, $[H_2O_2]_0$ = 150 μM and $[SOD]_0$ = 1.2 μM. Substrate concentrations were (a) 0.05 mM, (b) 0.1 mM, (c) 0.15 mM, (d) 0.2 mM, (e) 0.25 mM, (f) 0.3 mM, (g) 0.35 mM, (h) 0.4 mM, (i) 0.45 mM and (j) 0.5 mM. (Inset) Representation of V_0^{POD} vs. $[gallic\ acid]_0$.

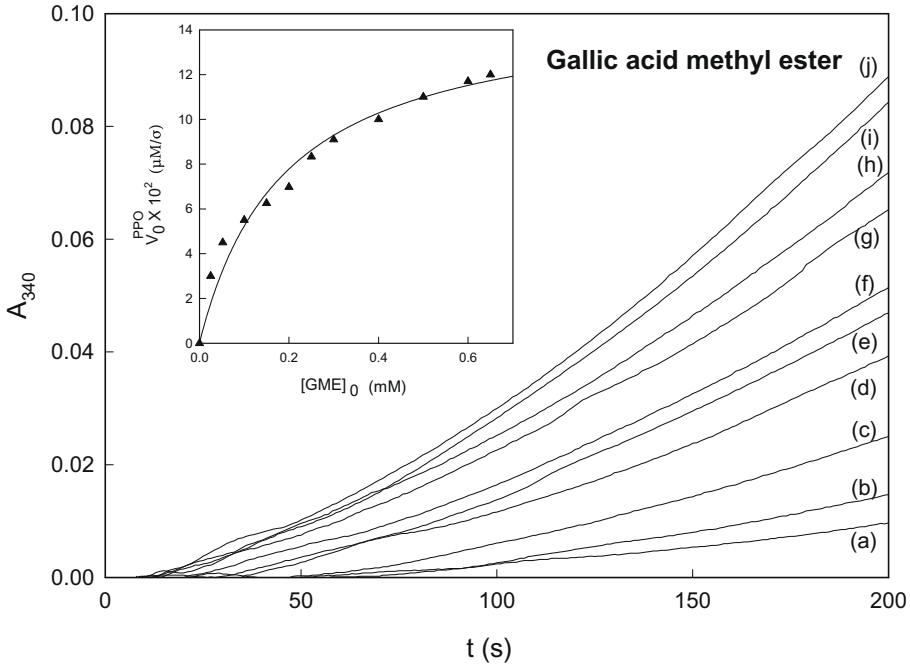

Fig. 3. Chronometric method for measuring the enzymatic activity of PPO on GME. The experimental conditions were 30 mM sodium phosphate buffer, pH 7.0, λ = 340 nm, $[E]_0$ = 0.95 nM, $[AH_2]_0$ = 20 μM and $[SOD]_0$ = 1.2 μM. Substrate concentrations were (a) 0.05 mM, (b) 0.1 mM, (c) 0.15 mM, (d) 0.2 mM, (e) 0.25 mM, (f) 0.3 mM, (g) 0.4 mM, (h) 0.5 mM, (i) 0.6 mM and (j) 0.65 mM. (Inset) Representation of V_0^{PPO} vs. $[GME]_0$.

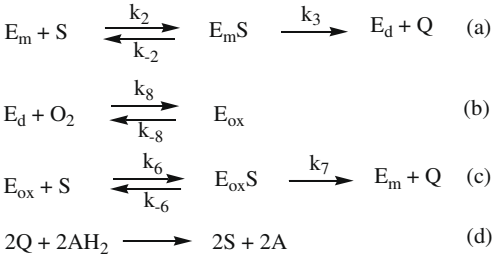

Scheme 3. Kinetic mechanism of the action of PPO.

$$0 = [AH_2]_0 - V_0\tau \quad (2)$$

Furthermore, in the case of PPO (Scheme 3):

$$V_0^{PPO} = \frac{[AH_2]_0}{\tau} \quad (3)$$

Therefore, if we can experimentally determine τ, knowing $[AH_2]_0$, it will be possible to determine V_0^{PPO} according to Eq. (3). The experimental determination of τ is only possible if there is a spectrophotometric signal that indicates that the AH_2 has been consumed (see Fig. 3).

In the case of POD, Scheme 2, the expression of V_0^{POD}, Eq. (3), must be modified by taking into account the stoichiometry (steps d and e), giving

$$V_0^{POD} = \frac{2[AH_2]_0}{\tau} \quad (4)$$

By applying this method, GME was kinetically characterised as substrate of PPO and POD, Table 3 and Fig. 3. The V_0 values obtained by either of these methods were fitted by nonlinear regression to the Michaelis equation for PPO, Eq. (6), and POD, Eq. (18). The rest of the kinetic information will be discussed below.

The analytic expression V_0^{PPO} in the case of PPO is (Rodríguez-López, Fenoll, et al., 2000)

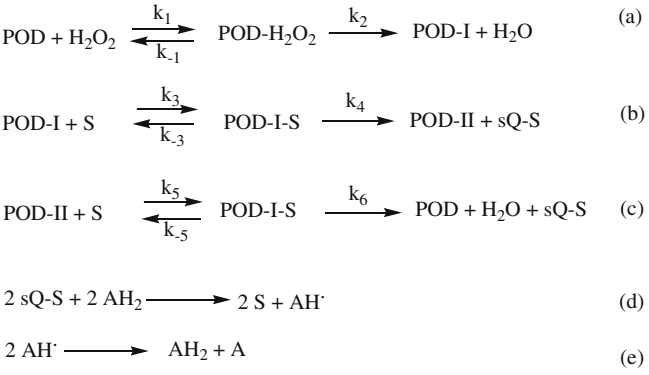

Scheme 2. Kinetic mechanism of the action of POD.

$$V_0^{PPO} = \frac{V_{max}^{PPO}[S]_0[O_2]_0}{K_m^{PPO}K_S^{O_2} + K_m^{O_2}[S]_0 + K_m^{PPO}[O_2]_0 + [S]_0[O_2]_0} \quad (5)$$

The $K_m^{O_2}$ values of PPO are very low (Fenoll, Rodriquez-Lopez, Garcia-Molina, Garcia-Canovas, & Tudela, 2002), so that, at the concentration of O_2 in the solution (0.26 mM), the enzyme is saturated and Eq. (5) is transformed into

$$V_0^{PPO} = \frac{V_{max}^{PPO}[S]_0}{K_m^{PPO} + [S]_0} \quad (6)$$

The values of K_m^{PPO} and V_{max}^{PPO} can be obtained from Eq. (6) and, taking into account (Rodríguez-López, Fenoll, et al., 2000) that

$$V_{max}^{PPO} = 2k_{cat}^{PPO}[E]_0 \quad (7)$$

$$k_{cat}^{PPO} = k_3k_7/k_3 + k_7 \quad (8)$$

$$K_m^{PPO} = k_{cat}^{PPO}/k_6 \quad (9)$$

$$K_m^{O_2} = k_{cat}^{PPO}/k_8 \quad (10)$$

it is possible to calculate k_{cat}^{PPO} (Eq. (7)) and $K_m^{O_2}$ (Eq. (10)), since $k_8 = (2.3 \pm 0.4) \times 10^7\ M^{-1}\ s^{-1}$ (Rodríguez-López, Fenoll, et al.,

2000). The values are specified in Table 3. The binding of the substrates to E_{ox} is controlled by k_6 (Eq. (9), Table 3).

As regards POD, kinetic analysis of the mechanism shown in Scheme 2 (Rodríguez-López, Gilabert, et al., 2000) gives

$$V_0^{POD} = \frac{V_{max}^{POD}[S]_0[H_2O_2]_0}{K_m^{POD}[H_2O_2]_0 + K_m^{H_2O_2}[S]_0 + [S]_0[H_2O_2]_0} \quad (11)$$

with

$$V_{max}^{POD} = 2k_{cat}^{POD}[E]_0 \quad (12)$$

$$k_{cat}^{POD} = \frac{k_2k_4k_6}{k_2k_4 + k_2k_6 + k_4k_6} \quad (13)$$

If k_6 (Scheme 2) is the rate limiting step, Eq. (13) leads to

$$k_{cat}^{POD} = k_6 \quad (14)$$

However, if k_2 (Scheme 2) is the rate limiting step, Eq. (13) leads to

$$k_{cat}^{POD} = k_2 \quad (15)$$

The Michaelis constants are (Rodríguez-López, Gilabert, et al., 2000)

$$K_m^{POD} = \frac{k_{cat}^{POD}}{k_5} \quad (16)$$

and

$$K_m^{H_2O_2} = \frac{k_{cat}^{POD}}{k_1} \quad (17)$$

The value of k_1 is $1.7 \times 10^7\ M^{-1}\ s^{-1}$ (Rodríguez-López, Gilabert, et al., 2000). In agreement with Eq. (17), if k_{cat}^{POD} is low, $K_m^{H_2O_2}$ will be low and Eq. (11) will become

$$V_0^{POD} = \frac{V_{max}^{POD}[S]_0}{K_m^{POD} + [S]_0} \quad (18)$$

Eq. (11) is also transformed into Eq. (18) in the case of pyrogallol, whose k_{cat}^{POD} is high (Table 3), working at a 1 mM concentration of H_2O_2. Analysis of the data from Eqs. (12), (16), (17), and (18) provides the kinetic information shown in Table 3.

The values of the chemical shifts, δ, obtained by ^{13}C NMR are related to the values of k_{cat}^{PPO} (Eq. (8)) for the three substrates studied with PPO. Hence, pyrogallol with its low δ_2 (greater nucleophilic attack potential) and with two equivalent positions at C-1 and C-2, is oxidised more easily by PPO (higher k_{cat}^{PPO}). However, gallic acid, with a COOH group (withdrawer at C-1) has a much lower k_{cat}^{PPO} whilst GME shows a slightly higher value but of the same order of magnitude as that of gallic acid.

The values of K_m^{PPO} (Table 3) do not follow the order of the chemical shift values, δ, obtained by ^{13}C NMR (Table 2), because its analytical expression includes another rate constant, k_6, the substrate binding constant to the E_{ox} form (Eq. (9)). Due to the vicinal position of the three hydroxyls, the hydroxyl of C-4 is partially deprotonated (pK_a = 9.03 and 11.6 for pyrogallol, 4.26, 8.70 and 11.5 for gallic acid and 7.92 and 8.03 for GME) (Deorkar & Tavlarides, 1997; Erdemgil et al., 2007; Muzolf, Szymusiak, Gliszczynska-Swiglo, Rietjens, & Tyrakowska, 2008), which means that it does not bind very rapidly to the enzyme (low k_6). However, in the case of pyrogallol, once it is bound, its transformation is rapid (high k_{cat}^{PPO}), and K_m^{PPO} is more than one order of magnitude higher than those of the other trihydroxylated phenols. The values of K_m^{PPO} for gallic acid and GME reflect the very low k_{cat}^{PPO} values (Eq. (8)) due to the withdrawing effect at C-1, of the –COOH or $–COOCH_3$ groups, respectively.

As regards the values of $K_m^{O_2}$, since they are directly related to k_{cat}^{PPO}, they can be determined analytically from Eq. (10). As can be seen from Table 3, they are very low for gallic acid and GME, but higher for pyrogallol. The values of k_6 (Table 3) are not related to those of δ_1, since k_6 corresponds to a binding constant. With respect to the kinetic constants of POD, the k_{cat}^{POD} values follow the chemical shift values obtained by ^{13}C NMR. Hence, pyrogallol has the highest k_{cat}^{POD} value, followed by GME and gallic acid. In the case of pyrogallol, according to Eq. (13), if the rate limiting step corresponds to k_2, Eq. (13) is transformed in Eq. (15) (Rodríguez-López, Gilabert, et al., 2000). In this case, there is no nucleophilic attack on the iron atom and the distance of the hydroxyl group of the substrate from iron is more important (Fenoll et al., 2005). The lower δ_1 and higher k_{cat}^{POD} values for pyrogallol result in higher K_m^{POD} and $K_m^{H_2O_2}$ values (Eq. (17)). For gallic acid and GME, whose δ_4 values are higher due to the withdrawing group at C-1, the k_{cat}^{POD} values (Table 3) are lower, and in this case the limiting step is k_6 (Eq. (14)). The values of K_m^{POD} and $K_m^{H_2O_2}$ (Eqs. (16) and (17)) are lower (Table 3). The binding of substrates to compound II, which is controlled by k_5 and obtained from Eq. (16), is shown in Table 3. In accordance with the values of δ_1, k_5 is higher for pyrogallol and lower for gallic acid and GME.

Table 2
Values of the chemical shifts of the different trihydroxylated phenols obtained by ^{13}C NMR for the C-1 and C-2 carbons at pH 7.0 and the parameters defining the anti-oxidant potential of the compounds

	EC_{50}[a]	ARP[b]	n[c]	δ_1	δ_2
Pyrogallol	0.05	20.0	10.0	135	148
Gallic acid	0.11	9.09	4.54	141	147
GME	0.16	6.25	3.12	141	147

[a] EC_{50}, ratio of the anti-oxidant concentration necessary to decrease the initial concentration of $ABTS^{\cdot-}$ by 50%.
[b] ARP, antiradical power.
[c] n, mean stoichiometric number of $ABTS^{\cdot-}$ electrons involved in the reaction with each anti-oxidant.

Table 3
Kinetic constants for PPO and POD at both pH values

PPO		pH 4.5			
Substrate	Measurement method	k_{cat}^{PPO} (s^{-1})	K_m^{PPO} (mM)	$K_m^{O_2}$ (μM)	$k_6 \times 10^{-5}$ ($M^{-1}\ s^{-1}$)
Gallic acid	AH_2 disappearance	25 ± 1	0.26 ± 0.01	1.02 ± 0.04	0.96 ± 0.07
Pyrogallol	AH_2 disappearance	1205 ± 40	2.02 ± 0.08	35.0 ± 1.05	5.96 ± 0.41
GME	Chronometric	78 ± 4	0.13 ± 0.01	3.40 ± 0.13	0.58 ± 0.04
		pH 7.0			
Gallic acid	AH_2 disappearance	27 ± 1	0.20 ± 0.01	1.17 ± 0.04	1.35 ± 0.08
Pyrogallol	AH_2 disappearance	1227 ± 73	1.99 ± 0.10	44.7 ± 1.78	6.16 ± 0.49
GME	Chronometric	80 ± 4	0.10 ± 0.01	3.50 ± 0.10	8.00 ± 0.51
POD		pH 4.5			
Substrate	Measurement method	k_{cat}^{POD} (s^{-1})	K_m^{POD} (mM)	$K_m^{H_2O_2}$ (μM)	$k_5 \times 10^{-5}$ ($M^{-1}s^{-1}$)
Gallic acid	AH_2 disappearance	52 ± 2	0.10 ± 0.01	3.06 ± 0.08	0.52±0.02
Pyrogallol	AH_2 disappearance	2040 ± 98	5.08 ± 0.51	120 ± 6.24	4.01±0.21
GME	Chronometric	65 ± 4	0.71 ± 0.03	3.82 ± 0.17	0.91±0.06
		pH 7.0			
Gallic acid	AH_2 disappearance	55 ± 2	0.11 ± 0.01	3.23 ± 0.08	0.55±0.03
Pyrogallol	AH_2 disappearance	2100 ± 126	5.05 ± 0.53	123 ± 7.38	4.15±0.25
GME	Chronometric	70 ± 5	0.68 ± 0.03	4.12 ± 0.11	1.02±0.08

3.5. Production of H_2O_2

3.5.1. General

Trihydroxylated phenols have been described as both anti- and pro-oxidants because of their capacity to trap free radicals and form H_2O_2 during their auto-oxidation by oxygen (Lee et al., 1995; Lu et al., 2006; Roth & Gilbert, 1984). In this work, we study this auto-oxidation using an oxymetric technique to measure the rate of oxygen consumption during the oxidation of the reduced substrates and spectrometry to follow the appearance of the quinonic products formed. The effect of the enzyme superoxide dismutase on the formation of H_2O_2 was observed and the H_2O_2 formed was evaluated by (a) measuring the action of catalase ($2H_2O_2 \rightarrow O_2 + 2H_2O$) and (b) spectrophotometrically at $\lambda = 414$ nm, measuring the formation of $ABTS^{\cdot+}$ radical with the POD/ABTS system, according to the stoichiometry $1H_2O_2 \rightarrow 2ABTS^{\cdot-}$ (Fig. 4).

3.5.2. Rate of oxygen consumption in the reaction: trihydroxylated phenol with oxygen

The oxygen consumption rate increased with increasing concentrations of both substrates gallic acid and O_2 (Fig. 5, inset A, Table 4), a result also found by other authors (Lee et al., 1995; Roth & Gilbert, 1984). This confirms that the reaction is initiated by the interaction of the reduced substrate with O_2, according to

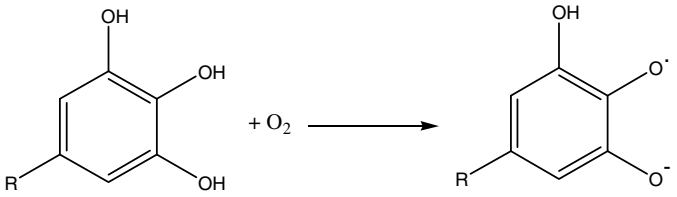

(19)

The oxygen consumption rate was very low for gallic acid and GME, and higher for pyrogallol (Table 4). A similar result was obtained by spectrophotometrically measuring the appearance of quinonic compounds during the auto-oxidation of gallic acid (Fig. 5, inset A). However, the increase in the oxygen consumption rate was directly proportional to the concentration of reduced substrate in the case of pyrogallol (Fig. 5, inset C) and GME (results not shown), whilst excess substrate induced inhibition phenomena with gallic acid (Fig. 5, insets A and B).

3.5.3. Inhibition of the oxygen consumption rate by superoxide dismutase

With all the substrates studied, SOD inhibited O_2 consumption, as mentioned by Lee et al. (1995) and Roth and Gilbert (1984) (Table 4), pointing to the formation of $O_2^{\cdot-}$ according to Eq. (19) and its entrapment according to

$$2O_2^{\cdot-} + 2H^+ \rightarrow O_2 + H_2O_2 \quad (20)$$

Moreover, the presence of SOD decreased H_2O_2 formation since, according to Roth and Gilbert (1984) the stoichiometry is $2O_2^{\cdot-}/1H_2O_2$, although the $O_2^{\cdot-}$ may also bring about the reaction:

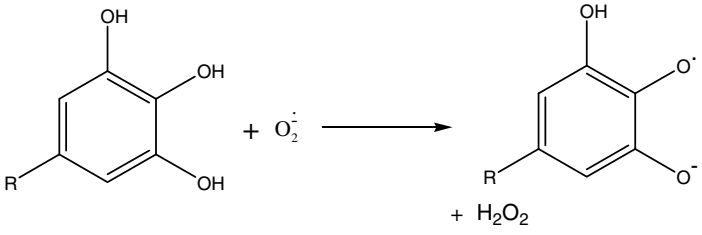

(21)

where the stoichiometry is $1O_2^{\cdot-}/1H_2O_2$.

3.5.4. Formation of H_2O_2

The anti-oxidant effect of some trihydroxylated phenols has been demonstrated (Kim, 2007). However, in this work we

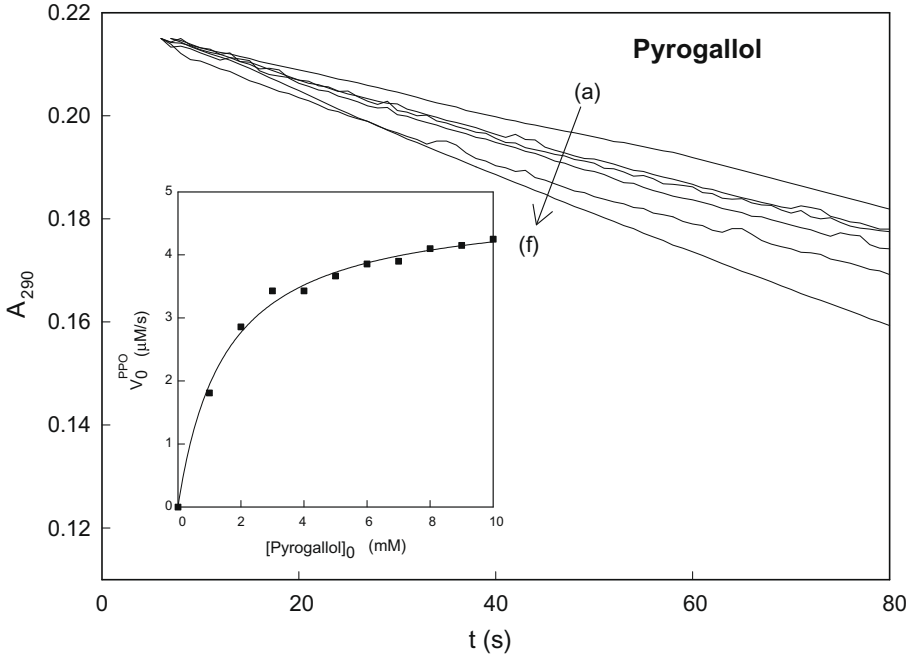

Fig. 4. AH_2 disappearance method for characterising the enzymatic activity of PPO on pyrogallol. The experimental conditions were 30 mM sodium phosphate buffer, pH 7.0, $\lambda = 290$ nm, $[E]_0 = 4$ nM, $[AH_2]_0 = 0.1$ mM and $[SOD]_0 = 1.2$ μM. Substrate concentrations were (a) 1 mM, (b) 2 mM, (c) 3 mM, (d) 4 mM, (e) 5 mM and (f) 6 mM. (Inset) Representation of V_0^{PPO} vs. $[pyrogallol]_0$.

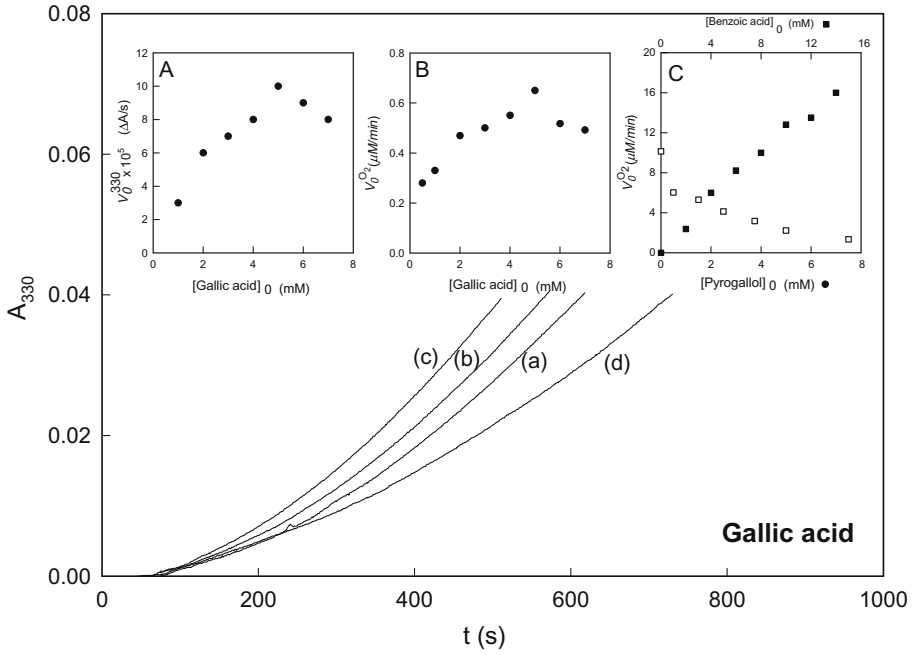

Fig. 5. Spectrophotometric recordings of gallic acid auto-oxidation. The experimental conditions were 30 mM sodium phosphate buffer, pH 7.0, λ = 330 nm, and the substrate concentrations were: (a) 1 mM, (b) 2 mM, (c) 4 mM and (d) 7 mM. (Inset A) Representation of the rate of quinonic product formation *vs.* [gallic acid]$_0$. (Inset B) Representation of the oxygen consumption rate for the auto-oxidation of gallic acid $V_0^{O_2}$ vs. [gallic acid]$_0$. The experimental conditions were 30 mM sodium phosphate buffer, pH 7.0. (Inset C) ■, representation of the oxygen consumption rate for the auto-oxidation of pyrogallol $V_0^{O_2}$ vs. [pyrogallol]$_0$ and □, effect of adding different concentrations of benzoic acid on oxygen consumption rate for the auto-oxidation of a fixed concentration of pyrogallol. The experimental conditions were 30 mM sodium phosphate buffer, pH 7.0, [pyrogallol]$_0$ = 5 mM and the concentrations of benzoic acid are shown in the figure.

Table 4
H_2O_2 production during the oxidation of trihydroxylated phenols by molecular oxygen

	[S]$_0$ (mM)	[H_2O_2] (μM)		$V_0^{O_2} \times 10^3$ (μM/min)[a]	
		Catalase	POD/ABTS	−SOD	+SOD
Gallic acid	2	65 ± 2	67 ± 3	30 ± 1	19 ± 1
Pyrogallol	2	71 ± 2	69 ± 3	411 ± 16	262 ± 7
GME	2	62 ± 2	65 ± 3	35 ± 2	29 ± 1

[a] $V_0^{O_2}$, initial oxygen consumption rate.

compare the formation of H_2O_2 during auto-oxidation of pyrogallol, gallic acid and GME at pH 7.0. The formation of H_2O_2 was measured electrochemically by measuring catalase activity in an oxygraph or after extracting the remaining substrate twice with ether and measuring the H_2O_2 spectrophotometrically with the POD/ABTS system (Fig. 6). Three different situations were considered:

(1) *Direct auto-oxidation:* This refers to the formation of H_2O_2 by the direct oxidation of by O_2 and by the $O_2^{\cdot-}$ generated (Fig. 6). As can be seen from Table 4, the values were relatively high, both with gallic acid and GME.
(2) *The oxidation of trihydroxylated phenols with stoichiometric periodate:* When the different substrates were oxidised with stoichiometric periodate, there was an increase in the H_2O_2 generated as the corresponding *o*-quinones evolved (Table 5), which confirms that the limiting step is the reaction described in Eq. (19).
(3) *Oxidation of trihydroxylated phenols by periodate at a low periodate/triphenol ratio:* This oxidation condition is equivalent to the action of PPO on their substrates: [Q] << [S]$_0$. The formation of H_2O_2 increases as a result of the *o*-quinone interacting with oxygen to generate $O_2^{\cdot-}$ which can interact with the substrates, producing H_2O_2, Eq. (21), whilst the *o*-quinone interacts with the substrate to generate semiquinones, which, in turn, produce more $O_2^{\cdot-}$ (Li, Tanaka, & Kouno, 2007; Matsuo, Yamada, Tanaka, & Kouno, in press). Table 5 shows the results obtained by measuring the H_2O_2 as described in Section 2. The evolution of the *o*-quinones of each substrate studied as they react with the substrates and oxygen, points to the great formation of H_2O_2, especially in the case of pyrogallol.

3.6. Hydrogen peroxide-scavenging activity

The H_2O_2-scavenging activity of phenolic acids has been described (Sroka & Cisowski, 2003). The experiments described in Fig. 5 (insets A and B) demonstrate the inhibition of oxidation by excess substrate at high concentrations of gallic acid, whether measured spectrophotometrically (inset A) or from the amount of oxygen consumed (inset B). This effect does not occur with pyrogallol (Fig. 5, inset C) or with GME (results not shown).

The oxymetric experiments (Fig. 5, inset B) provide a clear explanation for this scavenging phenomenon (Davis, Lovelace, Martinez, & Millar, 1995) in the reaction

$$\text{R-COOH} + H_2O_2 \rightleftharpoons \text{R-COOOH} + H_2O$$
$$\text{R-COOOH} \xrightarrow{\text{R-COOOH}} 2\,\text{R-COOH} + O_2 \qquad (22)$$

Gallic acid, which shows the greatest scavenging activity, underlines this effect, in agreement with Sroka and Cisowski (2003). Fig. 5 (inset C) shows how an increase in the concentration of pyrogallol leads to an increase in the oxygen consumption rate, whilst the rate diminishes when benzoic acid is added at different concentrations, lending weight to the mechanism proposed in Eq. (22).

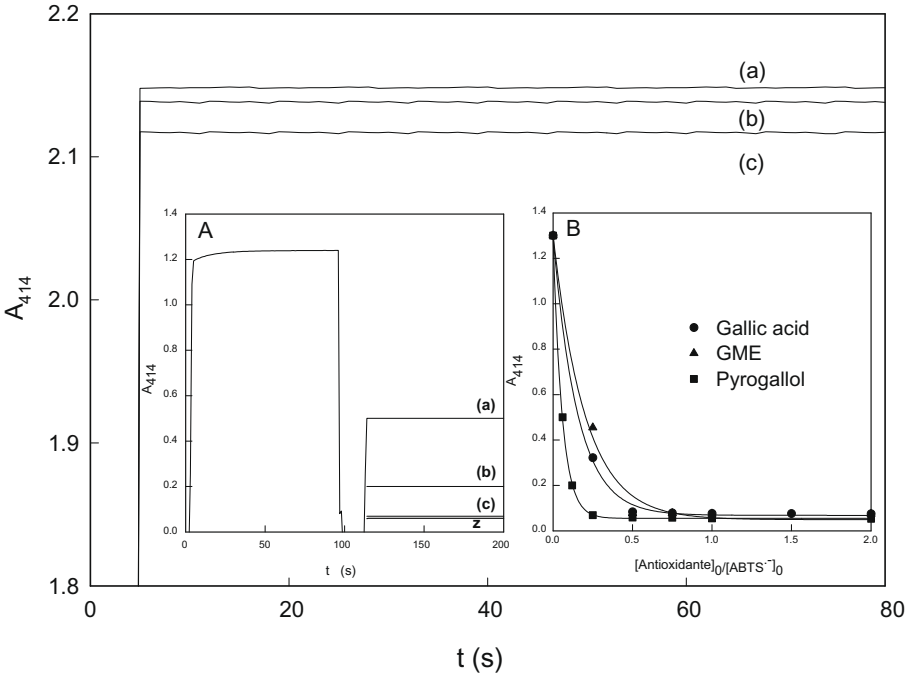

Fig. 6. Spectrophotometric determination of H_2O_2 generated during the auto-oxidation of different trihydroxylated phenols. H_2O_2 extraction is described in Section 2 and an aliquot is evaluated using the POD/ABTS system. The experimental conditions were: $[ABTS]_0$ = 5 mM, $[POD]_0$ = 0.22 μM and the buffer was 30 mM sodium acetate, pH 4.5. After 20 min of the auto-oxidation process, the increase in absorbance was measured at λ = 414 nm. (a) Pyrogallol, (b) gallic acid and (c) GME. The substrate concentrations were 0.1 mM each. (Inset A) Evaluation of anti-oxidant activity. Disappearance of absorbance of $ABTS^{\cdot+}$ with time at 414 nm when different concentrations of GME were added to pregenerated concentrations of $ABTS^{\cdot+}$ (40 μM). The experimental conditions were 30 mM sodium acetate buffer pH 4.5, λ = 414 nm, $[POD]_0$ = 0.22 μM, $[ABTS]_0$ = 5 mM, $[H_2O_2]_0$ = 20 μM and the substrate concentrations were (a) 2.4 μM, (b) 5 μM, (c) 30 μM and (d) 80 μM. (Inset B) The disappearance of $ABTS^{\cdot+}$ (40 μM) as a function of the $[anti\text{-}oxidant]_0/[ABTS^{\cdot+}]_0$ at 414 nm, the substrates are: (a) pyrogallol ■, (b) gallic acid ● and (c) GME ▲.

3.7. Anti-oxidant potential

Besides quantifying the H_2O_2 formed during the auto-oxidation of each substrate, we evaluate the anti-oxidant potential of the same substrates by means of the POD/ABTS/H_2O_2 system (Cano, Hernandez-Ruiz, Garcia-Canovas, Acosta, & Arnao, 1998; Hotta et al., 2002). The decrease in absorbance of the $ABTS^{\cdot+}$ radical after adding the anti-oxidant is manifest in Fig. 6 (inset A). As can be seen from Fig. 6 (inset B), pyrogallol has the greatest anti-oxidant potential since it captures more free radicals, probably because it has no electron-withdrawing group in its structure (see Scheme 1), unlike gallic acid and GME, both of which have such a group at their carbon 1. In addition, it should be pointed out that GME has the lowest anti-oxidant potential, probably because its carboxylic group is esterified by a methyl group, meaning that it captures a smaller number of free radicals. This work, therefore, reveals the dual effect, pro- and anti-oxidant potentials, of trihydroxylated phenols in biological systems. As revealed in Table 2, the anti-oxidant effect is related to the values of δ_1 obtained by ^{13}C NMR.

Table 5
H_2O_2 production during the evolution of the *o*-quinones generated by oxidation of triphenols with periodate (5 min)

	$[S]_0/[IO_4^-]_0$ (mM/mM)	$[H_2O_2]$ (μM)	$[S]_0/[IO_4^-]_0$ (mM/mM)	$[H_2O_2]$ (μM)
Gallic acid	0.3/0.3	91 ± 3	0.5/0.1	109 ± 3
Pyrogallol	0.3/0.3	100 ± 5	0.5/0.1	120 ± 7
GME	0.3/0.3	87 ± 3	0.5/0.1	99 ± 5

Conditions $[S]_0/[IO_4^-]_0$ = 1 and $[S]_0/[IO_4^-]_0$ = 5.

3.8. Effect on the GSH/GSSG ratio

As described previously (Kim, 2007), gallic acid increases the GSH/GSSG ratio, thereby increasing its intracellular reducing power and providing it with a crucial role in the regulation of the melanogenesis pathway. This increase in the GSH/GSSG ratio is also demonstrated in this work and may be explained by the oxidised gallic acid (in the form of a semiquinone) reacting with the oxidised glutathione through a nucleophilic attack. As a result, the disulphide bond (–S–S–) is broken and reduced glutathione is released, along with a glutathione–gallic acid adduct, thus increasing GSH. This attack mechanism would be time-dependent up to the moment at which the reduction and formation of oxidised glutathione balance each other (Table 6).

In conclusion, the use of a chronometric method with AH_2 and the measurement of the variation in absorbance of AH_2 with time to determine the enzymatic activity of PPO and POD acting on trihydroxylated phenols enabled the kinetic characterisation of these compounds, which act as substrates for both enzymes. The inhibition of PPO described by other authors is apparent and is shown

Table 6
Formation of GSH from GSSG[a]

t (min)	GSH (μM)
0	0
180	1.47 ± 0.04
300	35.3 ± 1.05
385	41.8 ± 1.67
520	43.8 ± 1.75
580	45.7 ± 2.28

[a] The experimental conditions were 0.1 M phosphate buffer, pH 7.0, [gallic acid]$_0$ = 2 mM, $[GSSG]_0$ = 1 mM and $[DTNB]_0$ = 0.3 mM. The wavelength used was 412 nm.

with respect to the oxidation of the physiological substrate, L-tyrosine. The compounds studied in this work are not inhibitors but alternative substrates of the enzyme, diminishing the formation of the *o*-quinones typical of the main eumelanine pathway (*o*-dopaquinone) (Rodríguez-López, Tudela, Varon, Garcia-Carmona, & Garcia-Canovas, 1991). However, as these results show, it must be born in mind that these triphenols (gallic acid, GME and pyrogallol) generate other *o*-quinones through enzymatic oxidation. The anti- and pro-oxidant properties of these triphenols are confirmed and the hydrogen peroxide-scavenging activity of gallic acid is explained. Pyrogallol is seen to be the best substrate for both PPO and POD; it also has the greatest anti-oxidant power (measured as antiradical activity) and, at the same time, the greatest pro-oxidant power (measured from the formation of H_2O_2).

Acknowledgements

This paper has been partially supported by grants from the Ministerio de Educación y Ciencia (Madrid, Spain) Project BIO2006-15363, from the Fundación Séneca (CARM, Murcia, Spain) Project 00672/PI/04, and from the Consejería de Educación (CARM, Murcia, Spain) BIO-BMC 06/01-0004. J.L.M.M. has a fellowship from the Ministerio de Educación y Ciencia (Madrid, Spain) Reference AP2005-4721. F.G.M. has a fellowship from Fundación Caja Murcia (Murcia, Spain).

References

Bradford, M. M. (1976). A rapid and sensitive method for the quantitation of microgram quantities of protein utilizing the principle of protein–dye binding. *Analytical Biochemistry, 72*, 248–254.

Briganti, S., Camera, E., & Picardo, M. (2003). Chemical and instrumental approaches to treat hyperpigmentation. *Pigment Cell Research, 16*, 101–110.

Cano, A., Hernandez-Ruiz, J., Garcia-Canovas, F., Acosta, M., & Arnao, M. B. (1998). An end-point method for estimation of the total anti-oxidant activity in plant material. *Phytochemical Analysis, 9*, 196–202.

Davis, R., Lovelace, T. C., Martinez, N. J., & Millar, A. (1995). Decomposition of peracids and their salts with activated carbon. *Catalysis Letters, 31*, 307–311.

Deorkar, N. V., & Tavlarides, L. L. (1997). A chemically bonded adsorbent for separation of antimony, cooper and lead. *Hydrometallurgy, 46*, 121–135.

Dunford, H. B. (1999). In *Heme peroxidases* (pp. 92–97). New York: Wiley-VHC.

Erdemgil, F. Z., Sanli, S., Sanli, N., Ozkan, G., Barbosa, J., Guiteras, J., et al. (2007). Determination of pK_a values of some hydroxylated benzoic acids in methanol–water binary mixtures by LC methodology and potentiometry. *Talanta, 72*, 489–496.

Espin, J. C., Varon, R., Fenoll, L. G., Gilabert, M. A., Garcia-Ruiz, P. A., Tudela, J., et al. (2000). Kinetic characterization of the substrate specificity and mechanism of mushroom tyrosinase. *European Journal of Biochemistry, 267*, 1270–1279.

Fenoll, L. G., Rodriguez-Lopez, J. N., Garcia-Molina, F., Garcia-Canovas, F., & Tudela, J. (2002). Michaelis constant of mushroom tyrosinase with respect to oxygen in the presence of monophenols and diphenols. *International Journal of Biochemistry and Cell Biology, 34*, 332–336.

Fenoll, L. G., Garcia-Molina, F., Gilabert, M. A., Varon, R., Garcia-Ruiz, P. A., Tudela, J., et al. (2005). Interpretation of the reactivity of peroxidase compound II with phenols and anilines using the Marcus equation. *Biological Chemistry, 386*, 351–360.

Funasaka, Y., Komoto, M., & Ichihashi, M. (2000). Depigmenting effect of alpha-tocopheryl ferulate on normal human melanocytes. *Pigment Cell Research, 8*, 170–174.

Garcia-Molina, F., Munoz, J. L., Varon, R., Rodríguez-Lopez, J. N., Garcia-Canovas, F., & Tudela, J. (2007). A review on spectrophotometric methods for measuring the monophenolase and diphenolase activities of tyrosinase. *Journal of Agricultural and Food Chemistry, 55*, 9739–9749.

Garcia-Molina, F., Peñalver, M. J., Rodríguez-Lopez, J. N., Garcia-Canovas, F., & Tudela, J. (2005). Enzymatic method with polyphenoloxidase for the determination of cysteine and *N*-acetylcysteine. *Journal of Agricultural and Food Chemistry, 53*, 6183–6189.

Gilabert, M. A., Fenoll, L. G., Garcia-Molina, F., Tudela, J., Garcia-Canovas, F., & Rodríguez-López, J. N. (2004). Kinetic characterization of phenol and anilines derivates as substrates of peroxidase. *Biological Chemistry, 385*, 795–800.

Gilabert, M. A., Hiner, A. N., Garcia-Ruiz, P. A., Tudela, J., Garcia-Molina, F., Acosta, M., et al. (2004). Differential substrate behaviour of phenol and aniline derivatives during oxidation by horseradish peroxidise: Kinetic evidence for a two-step mechanism. *Biochimica Biophysica Acta, 1699*, 235–243.

Habebb, A. F. S. A. (1972). Reaction of protein sulfhydryl groups with reagent Ellman's. *Methods Enzymology, 25*, 457–464.

Hearing, V. (2005). Biogenesis of pigment granules: A sensitive way to regulate melanocyte function. *Journal of Dermatological Science, 37*, 3–14.

Hotta, H., Nagano, S., Ueda, M., Tsujino, Y., Koyama, J., & Osakai, T. (2002). Higher radical scavenging activities of polyphenolic anti-oxidants can be ascribed to chemicals reactions following their oxidation. *Biochimica et Biophysica Acta, 1572*, 123–132.

Jandel Scientific (2007). SigmaPlot 9 for Windows®. Core Madera, CA: Jandel Scientific.

Kim, Y. (2007). Antimelanogenic and anti-oxidant properties of gallic acid. *Biological and Pharmaceutical Bulletin, 30*, 1052–1055.

Kim, S. W., Han, Y. W., Lee, S. T., Jeong, H. J., Kim, S. H., Kim, I. H., et al. (2008). A superoxide anion generator, pyrogallol, inhibits the growth of HeLa cells via cell cycle arrest and apoptosis. *Molecular Carcinogenesis, 47*, 114–125.

Kim, Y. J., & Uyama, H. (2005). Tyrosinase inhibitors from natural and synthetic sources: Structure, inhibition mechanism and perspective for the future. *Cellular and Molecular Life Sciences, 62*, 1707–1723.

Lee, S. F., Liang, Y. C., & Lin, J. K. (1995). Inhibition of 1,2,4-benzenetriol-generated active oxygen species and induction of phase II enzymes by green tea polyphenols. *Chemico-Biological Interactions, 98*, 283–301.

Lee, S. F., & Lin, J. K. (1994). Generation of hydrogen peroxide, superoxide anion and the hydroxyl free radical from polyphenols and active benzene metabolites: Their possible role in mutagenesis. *Journal of Biomedical Science, 1*, 125–130.

Li, Y., Tanaka, T., & Kouno, I. (2007). Oxidative coupling of the pyrogallol B-ring with a galloyl group during enzymatic oxidation of epigallocatechin 3-*O*-gallate. *Phytochemistry, 68*, 1081–1088.

Lin, J. K., & Lee, S. F. (1992). Enhancement of the mutagenicity of polyphenols by chlorination and nitrosation in *Salmonella typhimurium*. *Mutation Research, 269*, 217–224.

Locatelli, C., Rosso, R., Santos-Silva, M. C., de Souza, C. A., Licinio, M. A., Leal, P., et al. (2008). Ester derivatives of gallic acid with potential toxicity toward L1210 leukemia cells. *Bioorganic and Medicinal Chemistry, 16*, 3791–3799.

Lu, Z., Nie, G., Belton, P. S., Tang, H., & Zhao, B. (2006). Structure–activity relationship analysis of anti-oxidant ability effect of gallic acid derivatives. *Neurochemistry International, 48*, 263–274.

Matsuo, Y., Yamada, Y., Tanaka, T., Kouno, I. (in press). Enzymatic oxidation of gallocatechin and epigallocatechin: Effects of C-ring configuration on the reaction products. *Phytochemistry*.

Muñoz, J. L., Garcia-Molina, F., Varon, R., Rodríguez-Lopez, J. N., Garcia-Canovas, F., & Tudela, J. (2006). Calculating molar absorptivities for quinones: Application to the measurements of tyrosinase activity. *Analytical Biochemistry, 351*, 128–138.

Muzolf, M., Szymusiak, H., Gliszczynska-Swiglo, A., Rietjens, I. M. C. M., & Tyrakowska, B. (2008). pH-dependent radical scavenging capacity of green tea catechins. *Journal of Agricultural and Food Chemistry, 56*, 816–823.

Noguchi, M., Yokoyama, M., & Watanabe, S. (2006). Inhibitory effect of the tea polyphenol, (−)-epigallocatechin gallate, on growth of cervical adenocarcinoma cell lines. *Cancer Letters, 234*, 135–142.

Rodríguez-López, J. N., Fenoll, L. G., Garcia-Ruiz, P. A., Varon, R., Tudela, J., Thorneley, R. N., et al. (2000). Stopped-flow and steady-state study of the diphenolase activity of mushroom tyrosinase. *Biochemistry, 39*, 10497–10506.

Rodríguez-López, J. N., Gilabert, M. A., Tudela, J., Thorneley, R. N. F., & García-Cánovas, F. (2000). Reactivity of horseradish peroxidase compound II toward substrates: Kinetic evidence for a two-step mechanism. *Biochemistry, 39*, 13201–13209.

Rodríguez-López, J. N., Ros, J. R., Varon, R., & Garcia-Canovas, F. (1993). Oxygen Michaelis constant for tyrosinase. *Biochemical Journal, 293*, 859–866.

Rodríguez-López, J. N., Ros-Martinez, J. R., Varon, R., & Garcia-Canovas, F. (1992). Calibration of a Clark-type oxygen electrode by tyrosinase-catalyzed oxidation of a 4-*tert*-butylcatechol. *Analytical Biochemistry, 202*, 356–360.

Rodríguez-López, J. N., Tudela, J., Varon, R., Garcia-Carmona, F., & Garcia-Canovas, F. (1991). Kinetic study on the effect of pH on the melanin biosynthesis pathway. *Biochimica Biophysica Acta, 1076*, 379–386.

Roth, E. F., & Gilbert, H. (1984). The pyrogallol assay for superoxide dismutase: Absence of a glutathione artifact. *Analytical Biochemistry, 137*, 50–53.

Seo, S. Y., Sharma, V. K., & Sharma, N. (2003). Mushroom tyrosinase: A recent prospects. *Journal of Agricultural and Food Chemistry, 51*, 2837–2853.

Solomon, E. I., Sundaran, U. M., & Machonkin, T. E. (1996). Multicopper oxidases and oxygenases. *Chemical Reviews, 96*, 2563–2606.

Sroka, Z., & Cisowski, W. (2003). Hydrogen peroxide scavenging, anti-oxidant and anti-radical activity of some phenolic acids. *Food and Chemical Toxicology, 41*, 753–758.

Tomita, Y., Hariu, A., Mizuno, C., & Seiji, M. (1980). Inactivation of tyrosinase by dopa. *Journal of Investigative Dermatology, 75*, 379–382.

Tomiyama, S., Sakai, S., Nihiyama, T., & Yasmada, F. (1993). Factors influencing the anti-oxidant activities of phenols by an ab initio study. *Bulletin of the Chemical Society of Japan, 66*, 293–304.

Vámos-Vigázó, L. (1995). In C. Y. Lee & J. R. Whitacker (Eds.), *Enzymatic browning and its prevention*. Washington, DC: American Chemical Society.

Weidman, S. W., & Kaiser, E. T. (1966). The mechanism of the periodate oxidation of aromatic systems III. A kinetic study of the periodate oxidation of catechol. *Journal of the American Chemical Society, 88*, 5820–5827.

Yasui, H., & Sakurai, H. (2003). Age-dependent generation of reactive oxygen species in the skin of live hairless rats exposed to UVA light. *Experimental Dermatology, 12*, 655–661.

Zhao, X., Tian, H., Ma, X., & Li, L. (2006). Epigallocatechin gallate, the main ingredient of green tea induces apoptosis in breast cancer cell. *Frontiers in Bioscience, 11*, 2428–2433.

4.11. ÁCIDO ELÁGICO: CARACTERIZACIÓN COMO SUSTRATO DE POLIFENOL OXIDASA.

La caracterización del ácido elágico como sustrato de polifenol oxidasa ha dado lugar a la siguiente publicación adjunta.

4.11.1. Título

Ellagic acid: Characterization as substrate of polyphenol oxidase.

4.11.2. Autores

Muñoz-Muñoz, J.L.; Garcia-Molina, F.; Garcia-Molina, M.; Tudela, J.; Garcia-Cánovas, F. y Rodríguez-López, J.N.

4.11.3. Referencia

International Union of Biochemistry and Molecular Biology Life (IUBMB Life) (2009) 61, 171-177.

4.11.4. Resumen

Se ha descrito al ácido elágico como un inhibidor de tirosinasa o polifenol oxidasa y, por tanto, de la melanogénesis. En este trabajo, se demuestra que el ácido elágico no es un inhibidor sino un sustrato de polifenol oxidasa de champiñón (PPO), enzima que oxida a este sustrato generando su *o*-quinona. Debido a que las o-quinonas son muy inestables, se utiliza un método oximétrico para caracterizar la cinética de este sustrato, basado en las medidas del consumo de oxigeno en la reacción de tirosinasa. La constante catalítica es muy baja a los pH utilizados en este trabajo (4.5 y 7.0) lo que significa que la constante de Michaelis para el oxigeno es también muy baja. En cambio, la afinidad de la enzima por el sustrato es alta (baja K_m^S) probablemente debido a la doble posibilidad de unión que tiene el sustrato sobre la enzima. Por otra parte, el ácido elágico muestra una gran actividad antioxidante (EC50 = 0.05 y el número de electrones consumidos por una molécula de antioxidante n = 10), probablemente debido al elevado número de grupos hidroxilos que existen en su estructura química capaces de secuestrar y neutralizar radicales libres.

IUBMB *Life*, 61(2): 171–177, February 2009

Research Communication

Ellagic Acid: Characterization as Substrate of Polyphenol Oxidase

Jose Luis Muñoz-Muñoz, Francisco Garcia-Molina, Maria Garcia-Molina, Jose Tudela, Francisco García-Cánovas and Jose Neptuno Rodriguez-Lopez

GENZ: Grupo de Investigación de Enzimología, Departamento de Bioquímica y Biología Molecular-A, Facultad de Biología, Universidad de Murcia, Espinardo, Murcia, Spain

Summary

Ellagic acid has been described as an inhibitor of tyrosinase or polyphenol oxidase and, therefore, of melanogenesis. In this work, we demonstrate that ellagic acid is not an inhibitor, but a substrate of mushroom polyphenol oxidase, an enzyme which oxidizes ellagic acid, generating its *o*-quinone. Because *o*-quinones are very unstable, we used an oxymetric method to characterize the kinetics of this substrate, based on measurements of the oxygen consumed in the tyrosinase reaction. The catalytic constant is very low at both pH values used in this work (4.5 and 7.0), which means that the Michaelis constant for the oxygen is low. The affinity of the enzyme for the substrate is high (low K_m^S), showing the double possibility of binding the substrate. Moreover, a new enzymatic method is applied for determining the antioxidant activity. Ellagic acid shows high antioxidant activity (EC50 = 0.05; number of electrons consumed by molecule of antioxidant = 10), probably because of the greater number of hydroxyl groups in its structure capable of sequestering and neutralizing free radicals. © 2008 IUBMB

IUBMB *Life*, 61(2): 171–177, 2009

Keywords ellagic acid; polyphenol oxidase; tyrosinase; ABTS; antioxidant activity; peroxidase.

INTRODUCTION

Tyrosinase or polyphenol oxidase (EC 1.14.18.1; PPO) is a binuclear copper cluster ubiquitously present in biological systems (*1, 2*). It catalyzes two types of reactions in which molecular oxygen participates: (*a*) the orthohydroxylation of monophenols to *o*-diphenols (monophenolase activity) and (*b*) the oxidation of *o*-diphenols to the corresponding *o*-quinones (diphenolase activity).

Received 21 July 2008; accepted 9 September 2008

Address correspondence to: F. García-Cánovas, GENZ: Grupo de Investigación de Enzimología, Departamento de Bioquímica y Biología Molecular-A, Facultad de Biologia, Universidad de Murcia, E-30100 Espinardo, Murcia, Spain. Tel: +34 968 364782. Fax: +34 968 363963. E-mail: canovasf@um.es

ISSN 1521-6543 print/ISSN 1521-6551 online
DOI: 10.1002/iub.143

Tyrosinase catalyzes the rate limiting step in the melanin biosynthetic pathway. Control of this enzyme is important in processes such as pigmentation (*3*). Thus, several natural and synthetic inhibitors have been described (*4*). It is frequent to find substrates that are described as inhibitors of tyrosinase in the bibliography due to the decrease in eumelanin formation (*5–7*).

Ellagic acid (Scheme 1) is a natural compound that is very abundant in vegetables in the form of ellagitannins. Only a small portion of the ellagic acid store is found in the free form (*8*). Several applications have been found for this acid in the pharmaceutical, chemical, and food industries (*9*). For example, antioxidant (*10*), chemopreventive, antiviral (*8*), or anticarcinogenic activities (*7*) have been attributed to ellagitannins.

Recently, too, ellagic acid has been attributed the capacity to regulate the biosynthetic pathway of melanins through the inhibition of tyrosinase (*7*). However, despite its polyphenolic structure, the possible role of ellagic acid as alternative tyrosinase substrate and, therefore, its indirect inhibition of this compound in the melanin biosynthesis pathway have not previously been described.

In this work, we propose to kinetically characterize the oxidation of ellagic acid in its role as a possible PPO substrate. Because of the instability of the *o*-quinone generated by this enzyme, we follow the enzymatic activity, measuring oxygen consumption by means of an oxymetric method. In addition, a kinetic enzymatic method is applied to determine the number of electrons consumed and the antioxidant power of this compound.

MATERIAL AND METHODS

Reagents

Mushroom tyrosinase (PPO; 1530 U mg^{-1}) and horseradish peroxidase (POD; 297 U mg^{-1}) were obtained from Sigma Chemical (St. Louis, MO). Ellagic acid (Scheme 1) was obtained from Fluka (Switzerland). Hydrogen peroxide and 2,2′-azino-bis(3-ethylbenzothiazoline-6-sulfonic acid) (ABTS) were

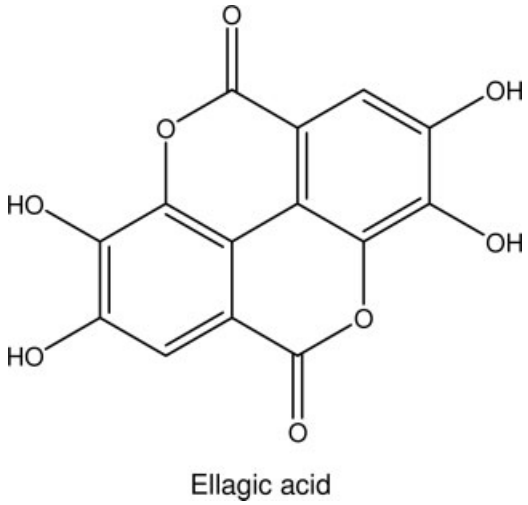

Scheme 1. Chemical structure of ellagic acid.

obtained from Sigma Chemical (St. Louis, MO). Stock solutions of the reducing substrates were prepared in 0.15 mM phosphoric acid to prevent auto-oxidation. The buffers used were 30 mM sodium phosphate buffer (pH 7.0) and 30 mM sodium acetate buffer (pH 4.5).

Enzyme Source

PPO (1530 U mg^{-1}) was purified according to ref. (*11*). POD was purchased from Sigma (type VI; Rz = 3.2) and used without further purification (*12*). The protein concentration was determined by Bradford's method (*13*), using bovine serum albumin as the standard.

Spectrophotometric Assays

Absorption spectra were recorded in a visible-ultraviolet Perkin–Elmer Lambda-35 spectrophotometer interfaced on-line with a PC compatible microcomputer, at a scanning speed of 60 nm s^{-1}. The temperature was controlled at 25°C using a Haake D16 circulating water bath with a heater/cooler and checked using a Cole-Parmer digital thermometer with a precision of ±0.1°C. Reference cuvettes contained all the components, except the substrate, in a final volume of 1 mL. For PPO, all the assays were carried out under saturating conditions of PPO by molecular oxygen (0.26 mM oxygen in the assay medium) (*11, 14*). TBC was measured as described in reference (*15*). In the case of POD, the concentration of H_2O_2 was 0.1 mM (see Results and Discussion).

Oxymetric Assays

Oxygen evolution was measured with a Clark-type electrode coupled to a Hansatech Oxygraph (King's Lynn, Norfolk, UK). The equipment was calibrated using the tyrosinase/4-*tert*-butylcatechol method (*16*). Nitrogen was bubbled through the reaction medium to remove the oxygen when necessary. The reaction medium contained 30 mM sodium phosphate buffer, pH 7.0. The medium was stirred constantly and temperature was kept at 25°C ± 0.1°C using a Haake D1G circulating waterbath.

$$E_m + S \underset{k_{-2}}{\overset{k_2}{\rightleftharpoons}} E_mS \xrightarrow{k_3} E_d + \text{Product} \quad \text{(a)}$$

$$E_d + O_2 \underset{k_{-8}}{\overset{k_8}{\rightleftharpoons}} E_{ox} \quad \text{(b)}$$

$$E_{ox} + S \underset{k_{-6}}{\overset{k_6}{\rightleftharpoons}} E_{ox}S \xrightarrow{k_7} E_m + \text{Product} \quad \text{(c)}$$

Scheme 2. Kinetic mechanism of the action of polyphenol oxidase.

Kinetic Data Analysis

Polyphenol oxidase (PPO) initial rate ($V_0^{O_2}$) were calculated from triplicate measurements at each reducing substrate concentration. The data were analyzed by nonlinear regression fitting of $V_0^{O_2}$ versus $[S]_0$ data to the Michaelis-Menten equation [Eq. (6)]. The fitting was carried out using the Sigma Plot 9.0 program for Windows (*17*), obtaining $V_{max}^{O_2}$ and K_m^S. From these values and according to Eqs. (2) and (5), it is possible to calculate k_{cat} and k_6 (see Scheme 2). Knowing the value of k_8, the value of $K_m^{O_2}$ can be obtained following Eq. (4).

RESULTS AND DISCUSSION

Kinetic Characterization of the Oxidation of Ellagic Acid by PPO

To characterize ellagic acid as substrate of PPO, the initial slope of the appearance of Product versus $t(V_0)$, can be measured directly at 357 nm (data not shown), but these recordings do not provide the hyperboles necessary to estimate V_{max} and K_m when attempts a made to fitted V_0 versus $[S]_0$ as indicated in (*15*). Instead, the recordings shown false apparent activations because of the excess of substrate due to the instability of the products generated in the action of PPO on ellagic acid (data not shown). There is evidence that periodate generates *o*-quinones in its reaction on *o*-diphenols (*18*). Experiments of ellagic acid oxidation with periodate (high ellagic acid/periodate ratio) shown the same results to experiments of ellagic acid oxidation with PPO (result not shown), which indicate that the *o*-quinone is the first product of the enzyme action.

In some cases where the *o*-quinones generated by PPO are unstable, the use of an oxymetric method has been proposed to follow the enzymatic activity (Fig. 1). The action of PPO follows the next scheme, Scheme 2.

Where E_m, E_d, and E_{ox} represent the oxidized and deoxygenated forms and the form with a peroxide group of the enzyme, respectively. Ellagic acid is represented as S.

According to Scheme 2, the expression of $V_0^{O_2}$ is given by:

$$V_0^{O_2} = \frac{V_{max}^{O_2}[S]_0[O_2]_0}{K_m^S K_s^{O_2} + K_m^{O_2}[S]_0 + K_m^S[O_2]_0 + [S]_0[O_2]_0} \quad (1)$$

where

$$V_{max}^{O_2} = k_{cat}[E]_0 = \frac{k_3 k_7}{k_3 + k_7}[E]_0 \quad (2)$$

$$K_s^{O_2} = \frac{k_{-8}}{k_8} \quad (3)$$

$$K_m^{O_2} = \frac{k_{cat}}{k_8} \quad (4)$$

$$K_m^S = \frac{k_{cat}}{k_6}. \quad (5)$$

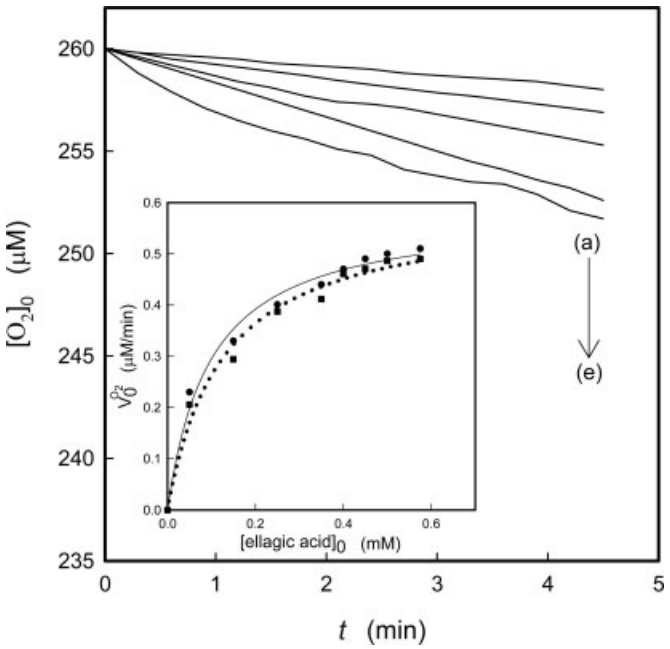

Figure 1. Oxymetric method for characterizing the enzymatic activity of PPO on ellagic acid. The experimental conditions were 30 mM sodium phosphate buffer pH 7.0 or sodium acetate buffer pH 4.5, $[O_2]_0$ 0.26 mM, and $[PPO]_0$ 27 nM. Substrate concentrations (mM) were (a) 0.35, (b) 0.4, (c) 0.45, (d) 0.5, and (e) 0.6. Inset: Representation of $V_0^{O_2}$ versus $[ellagic\ acid]_0$, pH 7.0 (●) and pH 4.5 (■).

The concentration of O_2 in the medium (0.26 mM) is saturating (*14*) and so Eq. (1) is transformed in:

$$V_0^{O_2} = \frac{V_{max}^{O_2}[S]_0}{K_m^S + [S]_0}. \quad (6)$$

The data analysis of $V_0^{O_2}$ versus $[S]_0$ (Materials and methods) provides $V_{max}^{O_2}$ and K_m^S. From Eq. (2), k_{cat} is obtained (Fig. 1 inset). Taking into consideration Eq. (5), the substrate binding constant to the form oxytyrosinase (k_6) can be obtained (Table 1).

Calculation of $K_m^{O_2}$ for PPO in Its Action on Ellagic Acid

The Michaelis constant of tyrosinase for O_2 is given Eq. (4), where it can be seen that it depends on the nature of the phenolic substrate. The value obtained for k_{cat} in the action of PPO on ellagic acid (see Table 1) predicts a low $K_m^{O_2}$ value, which, however, could not be determined experimentally. Linear recordings of oxygen consumption were obtained for the oxidation of ellagic acid (data not shown), meaning that $K_m^{O_2}$ must be calculated from Eq. (4), considering k_8 as $(2.3 \pm 0.4) \times 10^7$ $M^{-1}\ s^{-1}$ (*11*) (see Table 1).

Effect of pH Variation

The kinetic mechanism of diphenolase activity of tyrosinase is described in Scheme 2. The enzyme shows a kinetically significant p*K*a. The substrate, ellagic acid, has four p*K*as corresponding to the different prototropic equilibria (Scheme 3).

A study of the effect of pH on the ionization of ellagic acid pointed to the existence of two kinetically significant p*K*a: $pKa_1 = 6.3$ and $pKa_2 = 11.2$ (*19*). This contrasts with the existence of four hydroxyl groups in each molecule of the same acid (Scheme 1). However, it should be remembered that ellagic acid is a symmetric dimer, a dilactone between two molecules of gallic acid whose benzene rings are linked by a carbon–carbon bond. As a consequence, it contains two hydroxyl equivalents in para-position and another two in meta-position with respect to the carbons that bind to each carbonyl group. This structural peculiarity would explain the existence of only two chemically distinguishable p*K*a, corresponding to the ionization of both *p*-OH (K^p) and both *m*-OH (K^m), respectively (Scheme 3).

The most acidic p*K*as would correspond to the OH in para-position with respect to the carboxylic portion of the gallic acid structure, K_1^p in Scheme 3 corresponding to SH_4. Based on its symmetry, K_2^p would have approximately the same value as K_1^p corresponding to SH_3^-. At higher pH values, deprotonations cor-

Table 1
Kinetic constants of PPO in its action on ellagic acid

pH	k_{cat} (s^{-1})	K_m^S (mM)	$K_m^{O_2}$ (μM)	$k_6 \times 10^{-3}$ ($M^{-1}\ s^{-1}$)
4.5	0.36 ± 0.01	0.12 ± 0.02	0.015 ± 0.001	3.00 ± 0.51
7.0	0.37 ± 0.01	0.10 ± 0.01	0.016 ± 0.001	3.60 ± 0.38

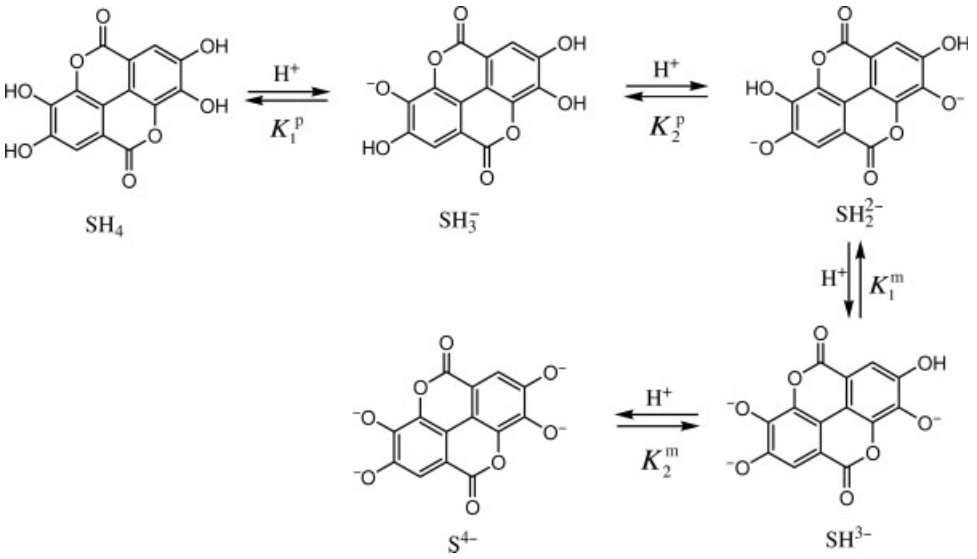

Scheme 3. Kinetic representation of the ellagic acid's p*K*a.

responding to the OH in meta position, K_1^m in SH_2^{2-} and K_2^m in SH^{3-}, which would be more or less similar, would be fulfilled (Scheme 3). All the above would imply that the predominant forms at the work pH values are SH_4 and SH_2^{2-}.

From the low value of the catalytic constant (see Table 1), $K_m^{O_2}$ is deduced to be very small, so that the enzyme, at an oxygen concentration of 0.26 mM, would be saturated (*14*).

Taking all these into consideration, the simplest mechanism to explain the effect of pH on tyrosinase's effect on ellagic acid would consider the p*K*a of the free enzyme and the first two p*K*as of the ellagic acid:

$$EA(OH)_4 \underset{K_{1,2}^p}{\rightleftharpoons} EA(OH)_2(O^-)_2 + 2\,H^+ \underset{K_{3,4}^m}{\rightleftharpoons} EA(O^-)_4 + 2\,H^+ \tag{7}$$

Tyrosinase only shows one p*K*a = 5.3 when it acts on a noncharged substrate such as 4-*tert*-butylcatechol (Fig. 2, ■). The tyrosinase-catalyzed oxidation of ellagic has two kinetically significant p*K*as, $pKa_1 = 5.5$ and $pKa_2 = 7.0$ (Fig. 2, ●). These values are very close to the p*K*a of tyrosinase and the first pKa_1 ($K_{1,2}^p$) of ellagic acid. The second pKa_2 of ellagic acid ($K_{3,4}^m$) would only make any noticeable contribution at pH values of ≥10, much higher than the pH 8.5 studied in this article (Fig. 2).

These experimental results (Fig. 2) and taking all above into consideration, the simplest mechanism to explain the experimental results obtained would be as shown in Scheme 4.

Where E represents the deprotonated free enzyme, EH is the protonated enzyme, SH_4 is the protonated ellagic acid, SH_3^- is the ellagic acid with one deprotonation, and SH_2^{2-} is the ellagic acid that has donated two protons. The forms SH_3^-, SH_2^{2-}, SH^{3-}, and S^{-4} are considered inactive and do not bind to the enzyme. Therefore, to simplify the kinetic analysis we consider

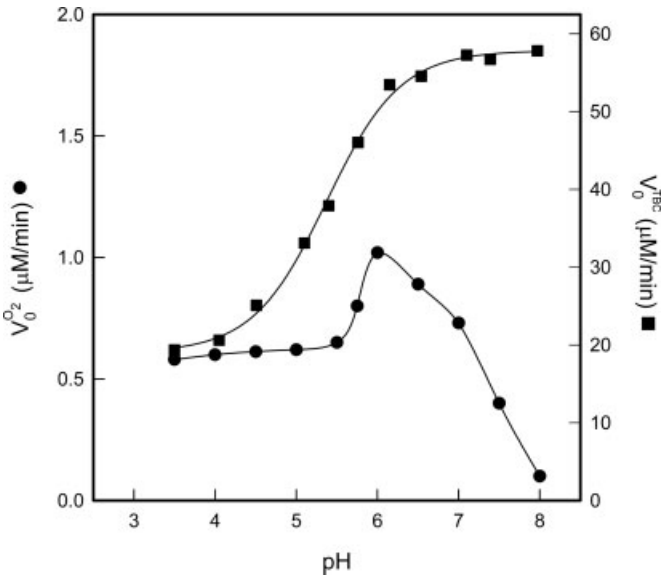

Figure 2. Effect of pH on the oxidation rate of ellagic acid by PPO. Corresponding values of $V_0^{O_2}$ versus pH for ellagic acid (●) and $V_0^{TBC_2}$ for TBC (■). Conditions were: $[O_2]_0$ 0.26 mM, and the buffer used: 30 mM acetate buffer pH 3.5, 4.0, and 5.0 and phosphate buffer pH 5.5, 5.75, 6.0, 6.5, 7.0, 7.5, and 8.0, respectively. (●) $[PPO]_0$ 30 nM and $[Ellagic\ acid]_0$ 0.45 mM. (■) $[PPO]_0$ 8.5 nM and $[TBC]_0$ 2 mM.

the system to be in rapid equilibrium. The experimental measurements (Fig. 2) are made by measuring the consumption of oxygen, so that:

$$V_0^{O_2} = k_{cat}[ESH_4]. \tag{8}$$

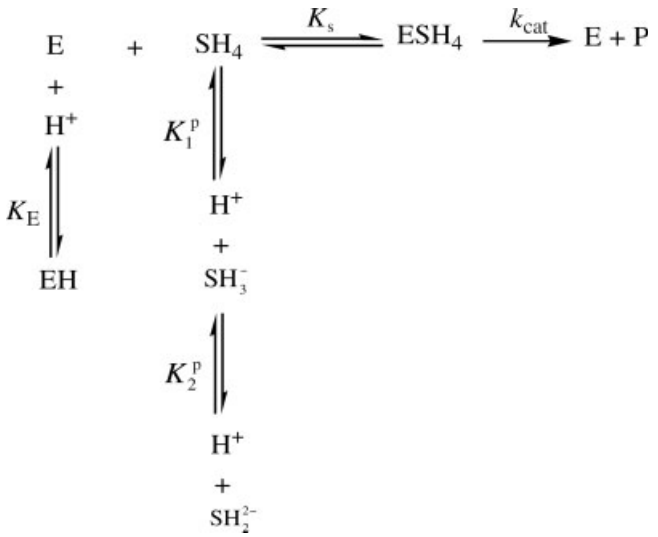

Scheme 4. Kinetic mechanism of the pH effect on the ellagic acid oxidation by polyphenol oxidase.

The matter balance of the enzyme is given by:

$$[E]_0 = [E] + [EH] + [ESH_4]. \quad (9)$$

The matter balance of the substrate is given by:

$$[SH_4]_0 = [SH_4] + [SH_3^-] + [SH_2^{2-}]. \quad (10)$$

Using the expressions K_E, K_s, K_1^p, and K_2^p gives:

$$V_0^{O_2} = \frac{V_{max}^{O_2}[SH_4]_0}{K_m^{app} + [SH_4]_0} \quad (11)$$

with

$$V_{max}^{O_2} = k_{cat}[E]_0 \quad (12)$$

and

$$K_m^{app} = \frac{K_s(K_E + [H^+])(K_1^pK_2^p + K_1^p[H^+] + [H^+]^2)}{K_E[H^+]^2}. \quad (13)$$

As a function of $[H^+]$, we obtain:

$$V_0^{O_2} = \frac{\alpha_0[H^+]^2}{\beta_0 + \beta_1[H^+] + \beta_2[H^+]^2 + \beta_3[H^+]^3} \quad (14)$$

where

$$\alpha_0 = k_{cat}K_E[SH_4]_0[E]_0 \quad (15)$$

$$\beta_0 = K_EK_sK_1^pK_2^p \quad (16)$$

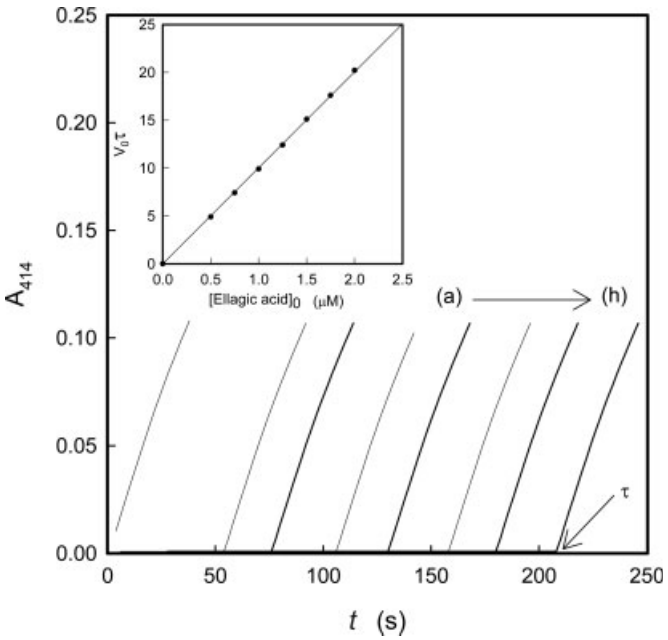

Figure 3. Evaluation of antioxidant activity. Time courses of radical accumulation in the presence of POD. The experimental conditions were sodium phosphate buffer pH 7.0, $[ABTS]_0$ 2.5 mM, $[H_2O_2]_0$ 100 μM, $[POD]_0$ 0.25 nM. The reaction was followed by measuring the ΔA_{414nm}. Trace (a), control. Traces (b)–(h), time courses of the same reaction as in (a) but with 0.5, 0.75, 1, 1.25, 1.5, 1.75, and 2 μM of ellagic acid, respectively. Inset: Representation of $V_0\tau$ versus $[ellagic\ acid]_0$ and determination of n according to Eq. (10).

$$\beta_1 = K_EK_sK_1^p + K_1^pK_2^pK_s \quad (17)$$

$$\beta_2 = K_EK_s + K_sK_1^p + K_E[SH_4]_0 \quad (18)$$

$$\beta_3 = K_s. \quad (19)$$

Equation (14) explains the appearance of a maximum, with ascending and descending branches, which agrees with the behavior observed experimentally (Fig. 2).

Data analysis of $V_0^{O_2}$ with respect to $[ellagic\ acid]_0$ at different pH, according to Eq. (11), provides the kinetic constants shown in Table 1. These results point to the independence of de $V_{max}^{O_2}$ and the increase in K_m^{app} with respect to pH, which agrees with Eqs. (12) and (13).

Antioxidant Power

To calculate the antioxidant power, we use an enzymatic method with the POD/ABTS/H_2O_2 system (*20*). In the absence of antioxidant, the system rapidly reaches the steady-state (see Fig. 3a). Maintaining all the substrates constant, different concentrations of antioxidant are added to the medium (curves b–h of Fig. 3). The parallel lines obtained indicate that the system

Table 2
Evaluation of antioxidant capacity of ellagic acid by the POD/ABTS/H_2O_2 system

Substrate	n[a]	EC50[b]	ARP[c]
Ellagic acid	10.0	0.05	20
Ellagic acid[d]	7.6	0.06	15
Ascorbic acid[e]	2.0	0.25	4

[a]n = stoichiometric number of electrons of $ABTS^-$ involved in the reaction with each antioxidant.
[b]EC50 = ratio of the antioxidant concentration necessary to decrease the initial concentration of $ABTS^-$ to 50%.
[c]ARP, Antiradical power.
[d]Data obtained from ref. (*17*).
[e]Data obtained from ref. (*20*).

reaches the same steady-state in all cases, fulfilling the matter balance.

The radical $R^\bullet$ is accumulated in the medium according to:

$$[R^\bullet] = V_0 t - n\,[\text{ellagic acid}]_0 \tag{20}$$

where V_0 is the steady-state rate, and n is the number of radical molecules ($R^\bullet$) that react with one molecule of ellagic acid. The representation of $[R^\bullet]$ versus t, corresponds to a straight line which cuts the axis t at $t = \tau$, then $[R^\bullet] = 0$ and we obtain:

$$n = \frac{V_0 \tau}{[\text{ellagic acid}]}. \tag{21}$$

Thus, we calculate the number of electrons (n) of the radical involved in its reaction with the antioxidant (Fig. 3, inset). In the case of ellagic acid, this value is 10 (see Table 2). Taking into consideration the value of n, we can calculate the EC50 (the ratio concentration of antioxidant that lowers the concentration of radical by 50%) (*21*), because n and EC50 are related by:

$$\text{EC50} = \frac{1}{2n} \tag{22}$$

In the case of ellagic acid, the value of EC50 is 0.05 (see Table 2). Using the 1,1-diphenyl-2-picrylhydrazyl (DPPH) radical assay, a value of 0.066 is obtained (*19*). In addition, we calculate the antiradical or antioxidant power (ARP), defined as the inverse of the EC50 (*22*). For ellagic acid, this parameter is 20 (see Table 2).

In conclusion, ellagic acid is kinetically characterized as a substrate of tyrosinase, explaining its inhibitory effect on the melanogenesis pathway. The kinetic constants obtained, k_{cat}, $K_m^{O_2}$ and K_m^S, point to a low k_{cat}, probably as a result of steric hindrance and the carbonyl withdrawing effect in para-position with respect to OH, which leads to a low $K_m^{O_2}$. However, the low values of K_m^S may correspond to the symmetry of the molecule and the double possibility of binding to the enzyme. The high antioxidant power of this compound is revealed by using an enzymatic method with peroxidase.

ACKNOWLEDGEMENTS

This paper has been partially supported by grants from the Ministerio de Educación y Ciencia (Madrid, Spain) Project BIO2006-15363 and SAF2006-07040-C02-01, from the Fundación Séneca (CARM, Murcia, Spain) Project 00672/PI/04, and from the Consejería de Educación (CARM, Murcia, Spain) BIO-BMC 06/01-0004. JLMM has a fellowship from the Ministerio de Educación y Ciencia (Madrid, Spain) Reference AP2005-4721. FGM has a fellowship from Fundación Caja Murcia (Murcia, Spain).

REFERENCES

1. Halaouli, S., Asther, M., Sigoillot, J. C., Hamdi, M., and Lomascolo, A. (2006) Fungal tyrosinases: new prospects in molecular characteristics, bioengineering and biotechnological applications. *J. Appl. Microbiol.* **100**, 219–232.
2. Decker, H., Schweikardt, T., and Tuczek, F. (2006) The first crystal structure of tyrosinase. All questions answered? *Angew. Chem. Int. Ed. Engl.* **45**, 4546–4550.
3. Prota, G. (1993) Regulatory mechanism of melanogenesis: beyond the tyrosinase concept. *J. Invest. Dermatol.* **100**, 156S–161S.
4. Kim, Y. J. and Uyama, H. (2005) Tyrosinase inhibitors from natural and synthetic sources: structure, inhibition mechanism and perspective for the future. *Cell Mol. Life Sci.* **62**, 1707–1723.
5. Masamoto, Y., Ando, H., Murata, Y., Shimoishi, Y., Tada, M., and Takahata, K. (2003) Mushroom tyrosinase inhibitory activity of esculetin isolated from seeds of *Euphorbia lathyris* L. *Biosci. Biotechnol. Biochem.* **67**, 631–634.
6. No, J. K., Soung, D. Y., Kim, Y. J., Shim, K. H., Jun, Y. S., Rhee, S. H., Yokozawa, T., and Chung, H. Y. (1999) Inhibition of tyrosinase by green tea components. *Life Sci.* **65**, 241–246.
7. Yoshimura, M., Watanabe, Y., Kasai, K., Yamakoshi, J., and Koga, T. (2005) Inhibitory effect of an ellagic acid-rich pomegranate extract on tyrosinase activity and ultraviolet–induced pigmentation. *Biosci. Biotechnol. Biochem.* **69**, 2368–2373.
8. Zafrilla, P., Ferreres, F., and Tomas-Barberan, F. A. (2001) Effect of processing and storage on the antioxidant ellagic acid derivatives and flavonoids of red raspberry (*Rubus idaeus*) jams. *J. Agric. Food Chem.* **49**, 3651–3655.
9. Huang, W., Niu, H., Li, Z., Li, L., and Wang, W. (2008) Ellagic acid from acorn fringe by enzymatic hydrolysis and combined effects of operational variables and enzymes on yield of the production. *Bioresour. Technol.* **99**, 1518–1525.
10. Rangkadilok, N., Sitthimonchai, S., Worasuttayangkurn, L., Mahidol, C., Ruchirawat, M., and Satayavivad, J. (2007) Evaluation of free radical scavenging and antityrosinase activities of standarized longan fruits extract. *Food Chem. Toxicol.* **45**, 328–336.
11. Rodríguez-López, J. N., Fenoll, L. G., García-Ruiz, P. A., Varón, R., Tudela, J., Thorneley, R. N., and García-Canovas, F. (2000) Stopped-flow and steady-state study of the diphenolase activity of mushroom tyrosinase. *Biochemistry* **39**, 10497–10506.
12. Rodríguez-López, J. N., Gilabert, M. A., Tudela, J., Thorneley, R. N. F., and García-Cánovas, F. (2000) Reactivity of horseradish peroxidase

compound II toward substrates: kinetic evidence for a two-step mechanism. *Biochemistry* **39**, 13201–13209.
13. Bradford, M. M. (1976) A rapid and sensitive method for the quantization of microgram quantities of protein utilizing the principle of protein-dye binding. *Anal. Biochem.* **72**, 248–254.
14. Rodríguez-López, J. N., Ros, J. R., Varón, R., and García-Canovas, F. (1993) Oxygen Michaelis constant for tyrosinase. *Biochem. J.* **293**, 859–866.
15. Muñoz, J. L., Garcia-Molina, F., Varon, F., Rodríguez-Lopez, J. N., Garcia-Canovas, F., and Tudela, J. (2006) Calculating molar absortivities for quinones: application to the measurements of tyrosinase activity. *Anal. Biochem.* **351**, 128–138.
16. Rodriguez-Lopez, J. N., Ros-Martinez, J. R., Varon, R., and Garcia-Canovas, F. (1992) Calibration of a Clark-type oxygen electrode by tyrosinase-catalyzed oxidation of a 4-*tert*-butylcatechol. *Anal. Biochem.* **202**, 356–360.
17. Jandel Scientific. (2007) *SigmaPlot 9.0 for Windows®*. Jandel Scientific, Core Madera, CA.
18. Weidman, S. W. and Kaiser, E. T. (1966) The mechanism of the periodate oxidation of aromatic systems. III. A kinetic study of the periodate oxidation of catechol. *J. Am. Chem. Soc.* **88**, 5820–5827.
19. Priyadarsini, K. I., Khopde, S. M., Kumar, S. S., and Mohan, H. (2002) Free radical studies of ellagic acid, a natural phenolic antioxidant. *J. Agric. Food Chem.* **50**, 2200–2206.
20. Arnao, M. B., Cano, A., Hernández-Ruiz, J., Garcia-Canovas, F., and Acosta, M. (1996) Inhibition of L-ascorbic acid and other antioxidant of the 2,2′-azino-bis(3-ethylbenzthiazoline-3-sulfonic acid) oxidation catalyzed by peroxidise: a new approach for determining total antioxidant status of foods. *Anal. Biochem.* **236**, 255–261.
21. Hotta, H., Nagano, S., Ueda, M., Tsujino, Y., Koyama, J., and Osakai, T. (2002) Higher radical scavenging activities of polyphenolic antioxidants can be ascribed to chemicals reactions following their oxidation. *Biochim. Biophys. Acta.* **1572**, 123–132.
22. Brand-Williams, W., Cuvelier, M. E., and Berset, C. (1995) Use of a free radical method to evaluate antioxidant activity. *Lebensm. Wiss. U-Technol.* **28**, 25–30.

SUPPLEMENTARY MATERIAL

The kinetic mechanism of diphenolase activity of tyrosinase is described in Scheme II of the main text. The enzyme shows a kinetically significant pKa. The substrate, ellagic acid, has 4 pKa's corresponding to the different prototropic equilibria (Scheme IS):

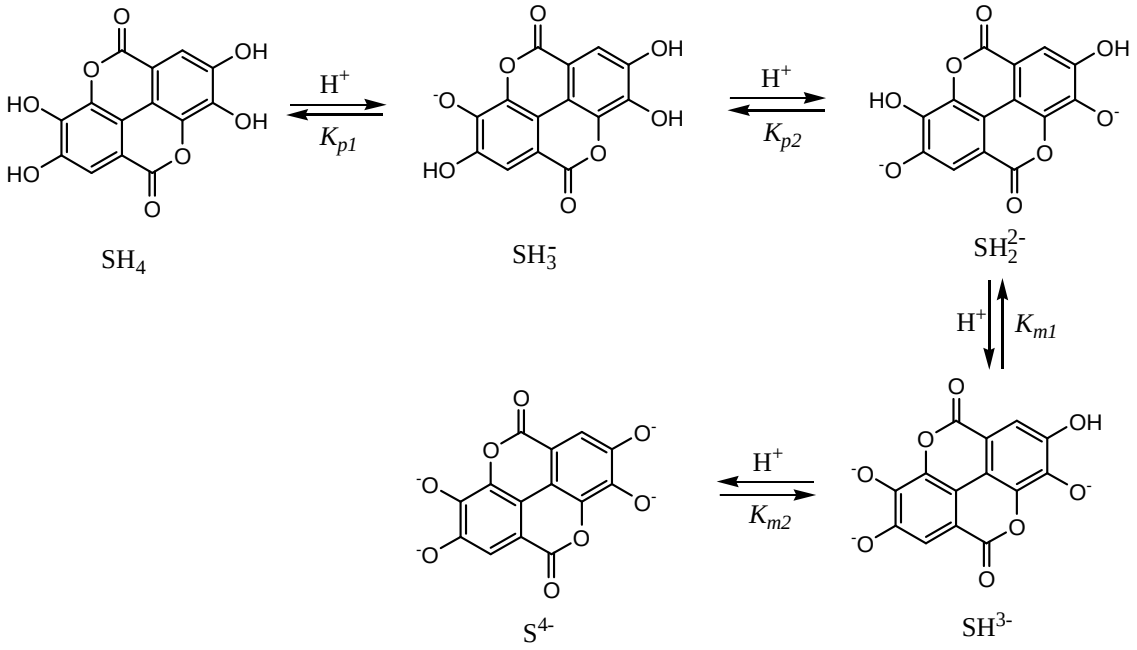

Scheme IS

From studies of changes in the absorption spectra with the pH, pKa values of 6.3 and 11.2 were evaluated, while other pKa values were probably irresolvable but are expected to be in this pH range (1S). The most acidic pKa's would correspond to the OH in para-position with respect to the carboxylic portion of the gallic acid strucutre, Kp_1 in Scheme IS corresponding to SH_4. Based on its symmetry, Kp_2 would have approximately the same value as Kp_1 corresponding to SH_3^-. At higher pH values, deprotonations corresponding to the OH in meta position, K_{m_1} in SH_2^{2-} and K_{m_2} in SH^{3-}, which would be more or less similar, would be fulfilled (Scheme IS). All the above would imply that the predominant forms at the work pH values are SH_4 and

SH_2^{2-}. Taking everything into consideration, the simplest mechanism to explain the effect of pH on tyrosinase's effect on ellagic acid would consider the pKa of the free enzyme and the first two pKa's of the ellagic acid.

From the low value of the catalytic constant (see Table 1 of the main text), $K_m^{O_2}$ is deduced to be very small, so that the enzyme, at an oxygen concentration of 0.26 mM, would be saturated (2S). Taking all the above into consideration, the simplest mechanism to explain the experimental results obtained would be:

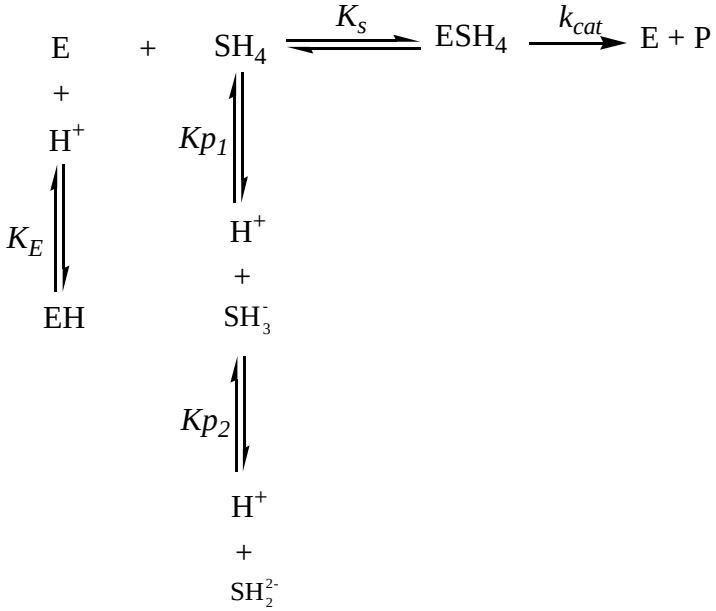

Scheme IIS

where E represents the deprotonated free enzyme; EH, the protonated enzyme; SH_4, protonated ellagic acid; SH_3^-, ellagic acid with one deprotonation; SH_2^{2-}, ellagic acid that has donated two protons. The forms SH_3^-, SH_2^{2-}, SH^{3-} and S^{-4} are considered inactive and do not bind to the enzyme. In short, we consider the system to be in rapid equilibrium. The experimental measurements (see main text) are made by measuring the consumption of oxygen, so that:

$$V_0^{O_2} = k_{cat}[\mathrm{ESH_4}] \quad (1S)$$

The matter balance of the enzyme is:

$$[\mathrm{E}]_0 = [\mathrm{E}] + [\mathrm{EH}] + [\mathrm{ESH_4}] \quad (2S)$$

The matter balance of the substrate is:

$$[\mathrm{SH_4}]_0 = [\mathrm{SH_4}] + [\mathrm{SH_3^-}] + [\mathrm{SH_2^{2-}}] \quad (3S)$$

Using the expressions K_E, K_s, K_{p1} and K_{p2} gives:

$$V_0^{O_2} = \frac{V_{\max}^{O_2}[\mathrm{SH_4}]_0}{K_m^{app} + [\mathrm{SH_4}]_0} \quad (4S)$$

with

$$V_{\max}^{O_2} = k_{cat}[\mathrm{E}]_0 \quad (5S)$$

and

$$K_m^{app} = \frac{K_s(K_E + [\mathrm{H^+}])(K_{p_1}K_{p_2} + K_{p_1}[\mathrm{H^+}] + [\mathrm{H^+}]^2)}{K_E[\mathrm{H^+}]^2} \quad (6S)$$

As a function of $[\mathrm{H^+}]$, we obtain:

$$V_0^{O_2} = \frac{\alpha_0[\mathrm{H^+}]^2}{\beta_0 + \beta_1[\mathrm{H^+}] + \beta_2[\mathrm{H^+}]^2 + \beta_3[\mathrm{H^+}]^3} \quad (7S)$$

where

$$\alpha_0 = k_{cat}K_E[\mathrm{SH_4}]_0[\mathrm{E}]_0 \quad (8S)$$

$$\beta_0 = K_E K_s K_{p_1} K_{p_2} \quad (9S)$$

$$\beta_1 = K_E K_s K_{p1} + K_{p1}K_{p2}K_s \quad (10S)$$

$$\beta_2 = K_E K_s + K_s K_{p1} + K_E\ [\mathrm{SH_4}]_0 \quad (10S)$$

$$\beta_3 = K_s \quad (11S)$$

REFERENCES

1S. Priyadarsini, K.I., Khopde, S.M., Kumar, S.S., and Mohan, H. (2002) Free radical studies of ellagic acid, a natural phenolic antioxidant. *J. Agric. Food Chem.* **50**, 2200-2206.

2S. Rodríguez-Lopez, J.N., Ros, J.R., Varon, R., and Garcia-Canovas, F. (1993) Oxygen Michaelis constant for tyrosinase. *Biochem. J.* **293**, 859-866.

4.12. ACTIVIDADES PROOXIDANTES Y ANTIOXIDANTES DEL ÁCIDO ROSMARÍNICO.

La determinación de las actividades prooxidantes y antioxidantes del ácido rosmarínico ha dado lugar a la siguiente publicación adjunta.

4.12.1. Título

Prooxidant and antioxidant activities of rosmarinic acid.

4.12.2. Autores

Muñoz-Muñoz, J.L.; Garcia-Molina, F.; Ros, E.; Tudela, J.; Garcia-Cánovas, F. y Rodríguez-López, J.N.

4.12.3. Referencia

Journal of Food Biochemistry (2011) En prensa.

4.12.4. Resumen

El ácido rosmarínico es un componente fundamental del *Rosmarinus officinalis*. En este trabajo, se han caracterizado las propiedades prooxidantes (generación de H_2O_2 y radicales libre por la acción de peroxidasa) y antioxidantes intrínsecas (consumo de H_2O_2 y radicales libres) del ácido rosmarínico. Además, se ha caracterizado su capacidad prooxidante melanogénica (al actuar como sustrato de polifenol oxidasa y generar *o*-quinonas) y su capacidad antimelanogénica y, por tanto, actividad antioxidante (produce la inactivación suicida de polifenol oxidasa). El balance entre sus actividades pro- y antioxidantes demuestra que el ácido rosmarínico puede ser considerado como un antioxidante neto.

-------- Mensaje original --------
Asunto: Journal of Food Biochemistry - Decision on Manuscript ID JFBC-03-11-0140.R2
Fecha: Mon, 26 Sep 2011 11:28:42 -0400 (EDT)
De: martym@ufl.edu
Para: canovasf@um.es
CC: ikeashie@aol.com

26-Sep-2011

Dear Prof. Garcia-Canovas:

It is a pleasure to accept your manuscript entitled "Prooxidant and antioxidant activities of rosmarinic acid" in its current form for publication in the Journal of Food Biochemistry. The comments of the reviewer(s) who reviewed your manuscript are included at the foot of this letter. Please complete and return the attached copyright form directly to me by email attachment. Be sure in the subject line to add the Manuscript Number. Acceptance of your paper is conditional upon receipt of the completed and signed Copyright Transfer Agreement (CTA) that can be found by clicking on the link below or with the attachment to this email.

http://media.wiley.com/assets/1540/87/ctaaus.pdf

All completed and signed CTAs should be faxed/mailed using the following fax number, address or email:

Fax: 352-392-1988

Maurice R. Marshall
Food Science and Human Nutrition Dept.
Food & Environmental Toxicology Lab
SW 23rd Dr., Bldg. 685
PO Box 110720
Gainesville, FL 32611-0720
martym@ufl.edu

Due to a backlog of accepted manuscripts publication may be delayed by as much as one year. We are working to reduce this backlog and the journal page numbers will increase in 2010.

Thank you for your fine contribution. On behalf of the Editors of the Journal of Food Biochemistry, we look forward to your continued contributions to the Journal.

Sincerely,
Prof. Maurice Marshall
Editor in Chief, Journal of Food Biochemistry
martym@ufl.edu
6700 Lakefront Drive
Magalia, CA 95954 USA

Reviewer(s)' Comments to Author:

Reviewer: 1
Comments to the Author
All my points of criticism have been sorted out. I have no problems with publishing this manuscript in its present form.

Reviewer: 2
Comments to the Author
The revision is satisfactory and the paper can now be accepted

Reviewer: 3
Comments to the Author
The manuscript and the new revised version is now acceptable for publication

---
avast! Antivirus: Mensaje saliente limpio.
Base de datos de Virus (VPS): 120329-0, 29/03/2012
Comprobado el: 29/03/2012 14:16:29
avast! - copyright (c) 1988-2012 ALWIL Software.
http://www.avast.com

Running head: Properties of rosmarinic acid.

Prooxidant and antioxidant activities of rosmarinic acid.

AUTHORS

J. L. Muñoz-Muñoz, F. Garcia-Molina, E. Ros, J. Tudela, F. García-Canovas*, J. N. Rodriguez-Lopez

ADDRESSES

GENZ: Grupo de Investigación Enzimología, Departamento de Bioquímica y Biología Molecular-A, Facultad de Biología, Universidad de Murcia, E-30100, Espinardo, Murcia, Spain.

*Corresponding author. Tel. +34 868 884764, Fax, +34 868 883963
E-mail address: canovasf@um.es

ABSTRACT

Rosmarinic acid is a fundamental compound of Rosmarinus officinalis. In this work, the intrinsic prooxidant (generation of H_2O_2 and free radicals by the action of peroxidase) and antioxidant (consumption of H_2O_2 and free radicals) properties of rosmarinic acid are characterized. In addition, its melanogenic prooxidant activity is characterized as it acts as a substrate of polyphenol oxidase to generate o-quinones, and its antimelanogenic and, so, antioxidant activity as it carries out the suicide inactivation of polyphenol oxidase. The balance between its pro- and antioxidant activities demonstrates that rosmarinic acid can be considered as a net antioxidant.

Key words: Rosmarinic acid, polyphenol oxidase, suicide inactivation, kinetics, antioxidant power.

PRACTICAL APPLICATIONS

Antioxidants prevent oxidative damage by modulating the oxidative status of cells. The present results indicated that rosmarinic acid is an antioxidant and can act as scavenger of free radicals in biological systems, and could therefore provide health benefits to consumers. Moreover, rosmarinic acid can act as a suicide substrate of polyphenol oxidase and can inhibit the enzymatic browning of vegetables and fruits and melanogenesis in mammals.

INTRODUCTION

Rosmarinic acid (S) is a water-soluble ester of 3,4-dihydroxycinnamic acid and 3,4-dihydroxyphenyllactate (Scheme 1) (Petersen & Simmonds, 2003). It is found mainly in the family of Lamiaceae, although it has also been described in other plant families such as Apiaceae (Petersen & Simmonds, 2003). In nature, the main source of rosmarinic acid is common rosemary (*Rosmarinus officinalis*).

-Scheme 1 here-

Rosmarinic acid has been reported to have anti-viral, antibacterial, anti-hepatitis, anti-mutagenic, anti-allergic, anti-carcinogenic and anti-inflammatory properties (Cao et al., 2005, Ito et al., 1998). Rosmarinic acid also inhibits HIV-1 and blood clotting (Pirker et al., 2009). Moreover, it has a therapeutic potential in the treatment or prevention of bronchial asthma, spasmogenic disorders, peptic ulcer, hepatoxicity, atherosclerosis, ischaemic heart disease, cataract, cancer and poor sperm counts (Al-Sereiti et al., 1999). In addition, rosmarinic acid inhibits seasonal allergic rhinoconjuctivitis (SAR) by two independent mechanisms: inhibition of the inflammatory response and scavenging of reactive oxygen species (ROS) (Osakabe et al., 2004). Furthermore, different concentrations of rosmarinic acid have been incorporated in the diet of ewes, thus improving the antioxidant status of the subsequent lamb meat (Moñino et al., 2008) and it is also used as a fragrant additive in soups and cosmetics (Martinez-Tome et al, 2001).

The polyphenolic structure of rosmarinic acid has been related with pro and antioxidant effects (Bors et al., 2004). As can be seen in Scheme 1, rosmarinic acid has two diphenolic rings, A and B, which can be oxidised to their respective *o*-quinones by autooxidation, generating ROS (Pirker, et al., 2009). It now seems clear that superoxide anion and hydrogen peroxide are formed by an auto-catalytic mechanism (Pirker, et al., 2009). Moreover, this compound is a substrate of peroxidase, leading to the formation of free radicals (Pirker, et al., 2009). On the other hand, the possible involvement of rosmarinic acid in the biosynthesis of melanins through the protein

kinase A signalling pathway has been described (Lee et al., 2007). A recent study described how polyphenol oxidase and, consequently, the melanin biosynthesis pathway are activated in melanoma cells by the presence of rosmarinic acid (Sanchez-Campillo et al., 2009).

Among the plants reported to present antioxidant activity, rosemary, *Rosmarinus officinalis* L., is the most widely used, not only as a culinary herb for flavouring (Zheng & Wang, 2001) but also as antioxidant in foods, in nutritional supplements and cosmetics (Calabrese et al., 2000). It is generally assumed that antioxidant molecules from *R. officinalis* act as free radical scavengers and might play a role by regulating the activity and/or expression of certain enzymatic systems involved in physiological processes like apoptosis, tumour promotion, intracellular signal, transduction or xenobiotic-metabolizing enzymes in the liver (Singletary, 1996a, Singletary, et al., 1996b, Perez-Fons et al., 2006).

The aim of this work was to quantitatively characterise the intrinsic prooxidant (production of H_2O_2 and its role as substrate of peroxidase) and antioxidant (elimination of H_2O_2 and free radicals) capacities of this compound. In addition, we quantitatively characterise its melanogenic prooxidant (as a substrate of polyphenol oxidase) and antimelanogenic and, so, antioxidant (suicide inactivation of polyphenol oxidase) activities. A balance of the pro- and antioxidant activities is made.

ABBREVIATIONS

Species and concentrations

ABTS, 2,2´-azino-bis(3-ethylbenzothiazoline-6-sulfonic acid); $ABTS^{\bullet+}$, 2,2´-azino-bis(3-ethylbenzothiazoline-6-sulfonic acid) radical cation; $[ABTS^{\bullet+}]$, Instantaneous concentration of $ABTS^{\bullet+}$; $[ABTS^{\bullet+}]_0$, Initial concentration of $ABTS^{\bullet+}$; $[ABTS^{\bullet+}]_\infty$, Remaining concentration of $ABTS^{\bullet+}$ at $t \to \infty$; AH_2, L-ascorbic acid; $B^{\bullet}$, Product of the reaction of $ABTS^{\bullet+}$ with S; $[B^{\bullet}]$, Instantaneous concentration of $B^{\bullet}$; C, Product of the reaction of $B^{\bullet}$ + $B^{\bullet}$ (second order); [C], Instantaneous concentration of C; D, Product of the reaction of C with $ABTS^{\bullet+}$; [D], Instantaneous concentration of D; NADH, Nicotinamide adenin dinucleotide; Phe-OH, Phenolic compound; POD, Peroxidase; S, Rosmarinic acid; PPO, polyphenol oxidase.

Kinetic constants

$\lambda_{E_{ox}}^{S}$, Apparent constant of suicide inactivation of PPO in the presence of S; τ, Lag period; K_m^S, Michaelis constant of PPO or POD for S; k_d^{app}, Apparent decomposition constant of the radical $ABTS^{\bullet+}$; k_2^{app}, Apparent rate constant of the limiting step of the coupled chemical reactions; k_{cat}^{POD}, Catalytic constant of POD for S; k_{cat}^{PPO}, Catalytic constant of PPO for S ; $t_{1/2}^{app}$, Half life of the reaction, $t_{1/2}^{app} = 1/(k_2^{app} \text{ x } [A]_0)$; *Kinetic parameters:* AE; Antiradical efficiency, $AE = 1/(EC50 \text{ x } T_{EC50})$; ARP, antioxidant or antiradical power; ARP_s^{app}, Apparent secondary antiradical power; ARP_p, Primary antiradical power; ARP_T^{app}, Apparent total antiradical power ($ARP = 2n$); EC50, Effective concentration, $EC50 = 1/(2n)$, defined as the concentration of antioxidant (S) leading to 50 % reduction of the initial radical concentration; EC_p50, Primary effective concentration; EC_s50_{app}, Apparent secondary effective concentration; EC_T50_{app}, Apparent total effective concentration; KAE_{app}, Apparent kinetic antiradical efficiency,

$KAE_{app} = 1/(EC_T50_{app} \times t_{1/2}^{app})$; n', Number of electrons yielded by the antioxidant (S), which coincides with the number of radical molecules consumed by electron-donating action by one molecule of C in the assay conditions; n_{app}, Number of electrons yielded by the antioxidant (S), which coincides with the number of radical molecules consumed by electron-donating action during the evolution of one molecule of the product of the reaction of $ABTS^{\bullet+}$ with S or its evolution in the assay conditions used; n, Number of electrons yielded by the antioxidant (S), which coincides with the number of radical molecules consumed by electron-donating action of one molecule of S; $n + n_{app}$, Total number of electrons yielded by the antioxidant (S), which coincides with the number of radical molecules consumed by electron-donating action of one molecule of S, during its evolution in the kinetic conditions described in the assay conditions used; r, partition ratio for the diphenolase activity of PPO $r = k_{7_2} / k_{7_2}^i = k_{cat}^{PPO} / \lambda_{E_{ox}(\max)}^{PPO}$; T_{EC50}, Time needed to reach the steady-state at the concentration corresponding to EC50; V_0^{POD}, Initial rate of POD acting on S; V_0^{PPO}, Initial rate of PPO acting on S.

MATERIAL AND METHODS

Reagents

The enzymes: mushroom polyphenol oxidase or tyrosinase (PPO, *o*-diphenol:O_2 oxidoreductase, EC 1.14.18.1) (1530 units/mg), horseradish peroxidase (POD; 251 U/mg) catalase (9300 U/mg) and superoxide dismutase (SOD; 4140 U/mg) were obtained from Sigma Chemical (St. Louis, MO). The substrates rosmarinic acid (S, Scheme 1), and 2,2´-azino-bis(3-ethylbenzothiazoline-6-sulfonic acid) (ABTS, Scheme 1) were obtained from Sigma Chemical (St. Louis, MO), and sodium periodate from Scharlau (Malaga, Spain). Stock solutions of the reducing substrates were prepared in 0.15 mM phosphoric acid to prevent auto-oxidation. Milli-Q system (Millipore Corp.) ultrapure water was used throughout this research. H_2O_2 (30 % v/v) was obtained from BDH-Merck (Poole, UK). The buffers used were 30 mM sodium phosphate buffer (pH 6.5-8.0) and 30 mM sodium acetate (pH 4.5).

Enzyme source

Horseradish peroxidase (251 U/mg; POD) was purchased from Sigma (type VI; Rz = 3.2) and used without further purification. The concentration of POD was determined spectrophotometrically using a Soret molar absorptivity of 102 mM^{-1} cm^{-1} (Rodriguez-Lopez et al., 2000a). Polyphenol oxidase (1,530 U/mg; PPO) was purified according to Rodriguez-Lopez et al., 2000b. The protein concentration was determined by Bradford's method using bovine serum albumin as the standard (Bradford, 1976).

Spectrophotometric assays

Absorption spectra were recorded in a visible-ultraviolet Perkin-Elmer Lambda 35-spectrophotometer interfaced on-line with a PC compatible Intel-Pentium microcomputer, at a scanning speed of 60 nm/s controlled by the UV-Winlab software. The temperature was maintained at 25 ºC using a Haake D16 circulating water bath

with a heater/cooler, and checked using a Cole-Parmer digital thermometer with a precision of 0.1 ºC. Kinetic assays were also carried out with the above instruments, monitoring NADH disappearance at λ = 340 nm (ε = 6230 M^{-1} cm^{-1}), or at λ = 400 nm (ε = 170 M^{-1} cm^{-1}) or using a chronometric method (detailed below). Cuvettes (final volume of 1 ml) contained 30 mM sodium phosphate buffer (pH indicated in each figure legend) and O_2 (PPO) (Fenoll et al., 2002) or H_2O_2 (POD) (Rodriguez-Lopez et al., 2000a) at a concentration which saturates their corresponding enzymes. Moreover, the substrate concentration was varied as indicated in each figure legend, and the reaction was started by addition of the enzyme (PPO or POD). The coupled reagent concentration (AH_2 or NADH) is indicated in each figure legend.

Oxymetric assays

Oxygen consumption was measured with a Clark-type electrode coupled to a Hansatech Oxygraph (King´s Lynn, Norfolk, UK). The cuvette (final volume 2 ml) contained 30 mM sodium phosphate buffer (pH 7.0) and the substrate concentration was varied (3 - 13.5 mM, see Results and discussion section). The reaction was started by the addition of rosmarinic acid. The medium was stirred constantly and the temperature was kept at 25 ± 0.1 ºC using a Haake D1G circulating water-bath.

Chronometric method

Enzymatic activity was determined spectrophotometrically using the chronometric method described in the Results and Discussion section (Rodriguez-Lopez et al., 2000a). The only condition was that there had to be an absorbance increase (due to product formation) measurable once the ascorbic acid (AH_2) had been consumed, to be able to determine the time, τ, necessary to consume a quantity of AH_2 - called $[AH_2]_0$. From these values, the initial rate, V_0, can be determined (see Results and Discussion section). The wavelength chosen at both acid and neutral pH

was 460 nm because the appearance of the *o*-quinone of rosmarinic acid can be appreciated at this wavelength.

Suicide inactivation of PPO by rosmarinic acid

The experimental recordings obtained were fitted to eq. (1B) (see Appendix B), from which the corresponding inactivation parameters, $[NADH]_\infty = [Q]_\infty$ and $\lambda_{E_{ox}}$, can be obtained by non-linear regression (Jandel Scientific, 2007). These are analyzed according to eqs. (3B) and (4B) of Appendix B. There is always a slow spontaneous oxidation of *o*-diphenol and NADH, which should be computer subtracted in subsequent NADH *vs*. time plots (in general this treatment is applied to all the kinetic recordings).

Determination of H_2O_2 generated. Autooxidation of rosmarinic acid

(a) Oxymetric experiments. The autooxidation of rosmarinic acid was followed by measuring oxygen consumption in an oxygraph in 30 mM sodium phosphate buffer (pH 7.0). After 60 min, catalase was added to reach a final concentration of 0.2 μM and the instantaneous appearance of oxygen was measured according to the stoichiometry: $2\ H_2O_2 \longrightarrow O_2 + 2\ H_2O$.

(b) Spectrophotometric experiments. Rosmarinic acid was preincubated in 30 mM sodium phosphate buffer (pH 7.0). After 60 minutes, the unoxidised substrate and the *o*-quinone were extracted twice with ether at pH 4.5. The H_2O_2 generated was evaluated in an aliquot of aqueous extract using the POD/ABTS system at λ = 734 nm, measuring the $ABTS^{\bullet+}$ radical (ε = 15000 $M^{-1}\ cm^{-1}$), in 0.1 M sodium acetate buffer (pH 4.5) (Rodriguez-Lopez et al., 2000a).

Kinetic data analysis

For POD, the initial rate values (V_0^{POD}) were calculated from triplicate measurements at each reducing substrate concentration and V_0^{POD} *vs.* $[S]_0$ data were fitted to the Michaelis-Menten equation [eq. (1)], obtaining V_{max}^{POD} and K_m^S. For PPO, the initial rate values (V_0^{PPO}) were calculated from triplicate measurements at each reducing substrate concentration, and V_0^{PPO} *vs.* $[S]_0$ data were adjusted to the Michaelis-Menten equation [eq. (6)] through the Sigma Plot 9.0 program for Windows (Jandel Scientific, 2007), giving the maximum rate (V_{max}^{PPO}) and Michaelis constant for the substrate (K_m^S).

RESULTS AND DISCUSSION

Intrinsic prooxidant and antioxidant activities of rosmarinic acid

Through its intrinsic prooxidant activity, rosmarinic acid (a) produces H_2O_2 during its autooxidation by molecular oxygen, and (b) generates free radicals since it acts as a substrate of POD. On the other hand, through its antioxidant activity, rosmarinic acid (c) eliminates H_2O_2 due to the free COOH group in its chemical structure and, at the same time, (d) eliminates free radicals through the –OH groups of its structure. These properties will be studied quantitatively below.

Generation of H_2O_2 due to the intrinsic prooxidant activity. Rosmarinic acid has been described as a prooxidant because of its capacity to generate free radical and H_2O_2 (Pirker et al., 2009), activity that is also expressed in the presence of transition metals (Murakami et al., 2007). In this work, we study this autooxidation, using an oxymetric technique to measure the rate of oxygen consumption during the oxidation of the reduced substrates by molecular oxygen, and the formation of H_2O_2 is determined. The effect of the enzyme superoxide dismutase on the formation of H_2O_2 was observed and the H_2O_2 was evaluated by (a) measuring the action of catalase ($2H_2O_2 \rightarrow O_2 + 2H_2O$) (Munoz-Munoz et al., 2009) and (b) measuring, spectrophotometrically at λ = 734 nm, the formation of $ABTS^{\bullet+}$ radical with the POD/ABTS system, according to the stoichiometry $1H_2O_2 \rightarrow 2ABTS^{\bullet+}$ (Munoz-Munoz et al., 2010). The extent of this autooxidation by O_2 is very high and in the same order of magnitude as observed with other compounds such as trihydroxylated phenols and gallic acid derivatives from green tea (Munoz-Munoz et al., 2009). Thus, when the rosmarinic acid concentration is 3 mM, 28 μM of H_2O_2 is generated in 1 hour. The concentration of H_2O_2 increases with the concentration of rosmarinic acid (at 5 mM, 30 of H_2O_2 is generated, at 10 mM, 43 μM of H_2O_2, while, at 13.5 mM, the resulting concentration begins to decrease (34 μM). See below for details.

Generation of free radicals due to the intrinsic prooxidant activity. In accordance with its chemical structure, rosmarinic acid (S) can act as a POD substrate. The activity can be followed by measuring the time necessary for a fixed quantity of the reductant (AH_2) to be consumed (chronometric method), Fig. 1 and Fig. 1, inset. The action of POD on reducing substrates (rosmarinic acid) in the presence of AH_2 is described in (Rodriguez-Lopez et al., 2000a).

The kinetic analysis of the reaction mechanism of POD (Rodriguez-Lopez et al., 2000a), at saturating concentrations of H_2O_2, results in:

$$V_0^{POD} = \frac{V_{\max}^{POD}[S]_0}{K_m^S + [S]_0} \qquad (1)$$

Fitting V_0^{POD} *vs.* $[S]_0$ by non-linear regression, according to eq. (1), K_m^S and $V_{\max}^{POD}$ can be obtained (810 ± 86 μM and 0.750 ± 0.036 μM/s respectively).

Elimination of H_2O_2 due to the intrinsic antioxidant activity. Due to its intrinsic prooxidant activity, the concentration of H_2O_2 increases with the concentration of rosmarinic acid until its formation is inhibited (in this case at 13.5 mM), as in the case of gallic acid (Munoz-Munoz et al., 2009). This means that at high concentrations, rosmarinic acid acts as a scavenger of H_2O_2. Such H_2O_2 scavenging activity of phenolic acids has been described previously (Munoz-Munoz et al., 2009).

Eq. (2) provides a clear explanation for this scavenging phenomenon in the reaction:

$$\begin{aligned} &\text{R-COOH} + H_2O_2 \rightleftharpoons \text{R-COOOH} + H_2O \\ &2\ \text{R-COOOH} \longrightarrow 2\ \text{R-COOH} + O_2 \end{aligned} \qquad (2)$$

This scavenging activity is not seen in other polyphenols such as pyrogallol or gallic methyl ester (Munoz-Munoz et al., 2009) because they have no free COOH group in their chemical structure. The enzyme superoxide dismutase (2 μM) reduces H_2O_2 generation by withdrawing superoxide anions from the reaction medium and

transforming $O_2^{-\bullet}$ into H_2O_2 with the result that the autocatalytic reaction generated by these anions does not occur, and the autooxidation of rosmarinic acid is reduced.

Elimination of free radicals due to the intrinsic antioxidant activity. The reaction of an antioxidant (phenolic or polyphenolic), in our case rosmarinic acid (S), with the free radical $ABTS^{\bullet+}$ produces a phenol radical (Scheme 2).

-Scheme 2 here-

This phenol radical may evolve following different pathways by (a) stabilizing through canonical structures; (b) forming dimers; (c) forming dimers-polymers with the generation of –OH groups that consume more free radical.

If $B^{\bullet}$ is stabilized through chemical reactions in which $ABTS^{\bullet+}$ does not participate, evolving to C, the limiting step may be of the second order (Scheme 2) (Munoz-Munoz et al., 2010). The compound formed (C) could act again with the radical $ABTS^{\bullet+}$, evolving to radical $C^{\bullet}$ (Scheme 2, reaction c), and this radical would evolve towards D.

To characterize the antioxidant capacity of a compound, the kinetic method described below is proposed:

1) Enzymatic kinetic method.

The enzymatic system POD/ABTS/H_2O_2 is used:

$$2\ ABTS + H_2O_2 \xrightarrow[V_0]{POD} 2\ H_2O + 2\ ABTS^{\bullet+} \qquad (3)$$

In the absence of antioxidant, eq. (3) rapidly reaches the steady-state with a velocity V_0 (Fig. 2). While maintaining the substrate concentrations constant, different concentrations of antioxidant are used in the assay medium. The parallel lines obtained indicate that the system reaches the same steady-state in all cases.

The radical $ABTS^{\bullet+}$ is accumulated in the medium according to:

$$[ABTS^{\bullet+}] = V_0 t - n[S]_0 \qquad (4)$$

where V_0 is the steady-state rate, and n is the number of radical molecules ($ABTS^{\bullet+}$) that react with one molecule of antioxidant. The representation of [$ABTS^{\bullet+}$] *vs.* t corresponds to a straight line which intercepts the axis t at $t = \tau$. When [$ABTS^{\bullet+}$] = 0, we obtain (Fig. 2, inset A):

$$n = \frac{V_0 \tau}{[S]_0} \qquad (5)$$

This value of n corresponds to the primary antioxidant capacity. The reaction of $ABTS^{\bullet+}$ with S is rapid and the system returns to the same initial steady-state. Taking into consideration the value of n, we can calculate the effective concentration EC50 [defined as the concentration of antioxidant (S) leading to 50 % reduction of the initial radical concentration] (Hotta et al., 2002), because n and EC50 are related by $EC50 = 1/2n$. In addition, we calculate the antiradical or antioxidant power (ARP), defined as the inverse of the EC50 (Brand-Williams et al., 1995).

When the action of the antioxidant corresponds to Scheme 2, in which the product of reaction $B^{\bullet}$ stabilizes with no additional consumption of $ABTS^{\bullet+}$ (Scheme 2, reaction b), the parameters n, EC50 and ARP define the behaviour of the antioxidant/radical pair under study.

As can be seen in Table 1, in the case of rosmarinic acid, n has a value of 4.1, which agrees with its chemical structure since rosmarinic acid possesses 4 hydroxyl groups (Scheme 1). Rosmarinic acid (Table 1) has a similar primary antioxidant power to (-)epicatechin (EQ), a molecule considered to have both a strong primary and secondary antioxidant power(Munoz-Munoz et al., 2010).

If the enzymatic kinetic method is applied and the reaction, after consuming the antioxidant, does not return to the same steady-state, it is because there is a greater consumption of electrons due to the subsequent production of reaction products, which may be dimers or even trimers (Scheme 2, reaction c). In this case, we will describe the reaction mechanism of S with free radical, according to Scheme 2, reactions a-c, in

which there is additional free radical consumption. In order to characterize this new antioxidant capacity, we propose a non-enzymatic kinetic test.

2) Non-enzymatic kinetic test.

The kinetic analysis of Scheme 2 (reactions a-c) has been described in Munoz-Munoz et al. (2010), and is summarized in the section of Appendix A. In the present case, in which a greater number of electrons are consumed due to chemical reactions following the enzymatic reaction, we propose a non-enzymatic kinetic test to calculate the number of electrons in the non-enzymatic steps (n_{app}), the kinetic constant controlling the process (k_2^{app}) [see eq. (1A) of Appendix A] and the parameters EC_s50_{app} (the effective concentration in these secondary non-enzymatic steps), ARP_S (antiradical power in the steps), EC_T50_{app} (total effective concentration efficient of the process), ARP_T^{app} (apparent total antiradical power) and a new kinetic parameter that we have already introduced, which relates the velocity of the process with the total number of electrons consumed in the process (apparent kinetic antiradical efficiency, KAE_{app}) [see eq. (2A) of Appendix A] (Munoz-Munoz et al., 2010). As in the case of the enzymatic kinetic method, a series of steps must be followed if this non-enzymatic kinetic test is to be valid.

When the secondary antioxidant power of the reaction of S with a free radical ($ABTS^{\bullet+}$) was studied [Fig. 2B according to eq. (1A) of Appendix A], the values of n_{app} obtained (6.8 electrons) were very similar to those of EQ (7.2 electrons), which illustrates the strong primary and secondary antioxidant power of S (Table 1). However, the value of k_2^{app} in the case of S is very small (13 M^{-1} s^{-1}), reflecting the slowness of the process. Note that EQ, on the other hand, has a very high k_2^{app} (2089 M^{-1} s^{-1}), indicating that the process in this case is very fast (Munoz-Munoz et al., 2010).

Study of the pH effect on the antioxidant capacity. The literature describes how the antioxidant capacity of different molecules varies with the pH (Zhen and Wang, 2001; Munoz-Munoz et al., 2010, Martinez-Tome et al., 2001). In this work, we study the effect of pH on the antioxidant capacity of rosmarinic acid. Note that the primary antioxidant capacity does not vary (see Table 1) and that at pH < 7 the chemical evolution of the coupled reactions is very slow. However, the secondary antioxidant capacity increases as the pH of the medium increases due to the increasingly strong coupled chemical reactions, which lead to an increasing k_2^{app} (the apparent second order constant that governs the process, Scheme 2, reaction b). This means that the KAE_{app} increases with pH (Table 1) [see eq. (2A) of Appendix A]. The result is that the balance between the pro- and antioxidant activities of rosmarinic acid tends towards a net intrinsic antioxidant role.

Melanogenic prooxidant and antioxidant activities of rosmarinic acid

The active site of PPO can be found in three forms in its catalytic cycle: *met*-PPO (E_m), *deoxy*-PPO (E_d) and *oxy*-PPO (E_{ox}) (Jackman et al., 1992). Under aerobic conditions, the enzyme can act on *o*-diphenols to transform them into *o*-quinones. Moreover, a process of suicide inactivation, localised in *oxy*-PPO, may occur. These processes are studied below with rosmarinic acid.

Melanogenic prooxidant activity. Substrate of PPO. The possible influence of rosmarinic acid in the biosynthesis of melanins has been indicated in Sanchez-Campillo et al. (2009). In addition, this compound may be oxidized by PPO to generate *o*-quinones, underlining its prooxidant power.

Kinetic characterization of the oxidation of rosmarinic acid by PPO. The kinetic characterisation of PPO in its action on rosmarinic acid cannot be carried out by measuring the formation of *o*-quinone due to its instability. However, a spectrophotometric method using a reductant, such as NADH (in the case of PPO, Fig.

3 and Fig. 3, inset) or AH_2 (in the case of POD), which instantaneously reduces *o*-quinone to rosmarinic acid, thus preventing its chemical evolution, can be used.

The kinetic mechanism of PPO in its action on *o*-diphenols is shown in Rodriguez-Lopez et al. 2000b. The steady-state rate, V_0^{PPO}, corresponds to the disappearance rate of NADH (Fig. 3). Non-linear regression fitting of V_0^{PPO} *vs.* $[S]_0$ according to eq. (6) (Fig. 3, inset) gives K_m^S and V_{max}^{PPO} (95 ± 8 μM and 2.69 ± 0.21 μM/s, respectively).

The analytical expression of V_0^{PPO} in the case of PPO is (Rodriguez-Lopez et al., 2000b):

$$V_0^{PPO} = \frac{V_{max}^{PPO}[S]_0}{K_m^S + [S]_0} \qquad (6)$$

Antimelanogenic and antioxidant activity: Suicide inactivation of PPO. The kinetic characterization of the suicide substrates of PPO has received a boost due to their possible clinical applications (Escribano et al., 1989; Chang T.S., 2007, Chang et al., 2010, Tai et al., 2009). The kinetic mechanism proposed to explain the suicide inactivation of PPO acting on rosmarinic acid is based on the structural mechanism proposed in (Munoz-Munoz et al., 2008), and can be outlined as follows in Scheme 3:

-Scheme 3-

When $[S]_0$, $[O_2]_0$ >> $[E]_0$ and $[Q]_\infty$ << $[S]_0$, $[O_2]_0$, a derivation of the analytical expression is possible, which establishes the accumulation of the product (*o*-quinone) or the disappearance of the coupled reactive NADH with time, as detailed in (Munoz-Munoz et al., 2008) (see Appendix B).

Experimental study of suicide inactivation. PPO inactivation by rosmarinic acid was studied experimentally with the following methodology:

(a) Variation in enzyme concentration. The $[E]_0$ value is varied while the substrate concentration is kept constant. The results obtained are shown in Fig. 4A.

The concentration of the substrate in these experiments does not change because the *o*-quinone is reduced by NADH. However, the concentrations of O_2 and NADH do change. In the case of PPO, $K_m^{O_2}$ is very small (Fenoll et al., 2002), which permits an oxygen consumption of more than 10%. The NADH must be in excess. Note how the values of $[NADH]_\infty$ are directly proportional to $[E]_0$ [see eq. (2B) of Appendix B], while $\lambda_{E_{ox}}^S$ does not vary with $[E]_0$ (Fig. 4A, inset) [see eq. (3B) of Appendix B].

Fig. 4A, inset shows the dependence of the values obtained for the product at the end of the reaction, $[NADH]_\infty$ *vs*. $[E]_0$, from whose slopes and, according to eq. (2B) of Appendix B, r can be determined (Table 2).

(b) Variation in substrate concentration. The experimental recordings for the disappearance of NADH during the action of PPO on rosmarinic acid obtained by varying the concentration of substrate are shown in Fig. 4B. Fitting by non-linear regression to eq. (1B) of Appendix B gives the apparent inactivation constant, $\lambda_{E_{ox}}^S$. The hyperbolic dependence of $\lambda_{E_{ox}}^S$ *vs.* $[S]_0$ is shown in Fig. 4B, inset. Fitting these data by non-linear regression according to eq. (3B) of Appendix B gives $\lambda_{E_{ox}(max)}^S$ and K_m^S (Table 2). $\lambda_{E_{ox}(max)}^S$ and r (Table 2) permit us to obtain k_{cat}^{PPO} (Table 2).

Kinetic reaction mechanism. In the mechanism described in Scheme 3, the critical process as regards the suicide inactivation would correspond to Step 7, in which the *o*-diphenol transfers the proton from the hydroxyl group in C-4 to the peroxide, a transfer similar to that proposed by other authors (Matoba et al., 2006; Inoue et al., 2008; Ismaya et al., 2011). In this way, the complex $(E_{ox}S)$ is transformed into $(E_{ox}-S)_1$, which through Step 8 governed by k_{7_2}, enters the catalytic pathway and, according to Step 10 governed by $k_{7_2}^i$, the enzyme undergoes inactivation. In Step 8, the substrate might transfer the proton from the hydroxyl group of C-3 to a histidine of the CuA and the oxygen would then attack the copper atom. This process is still

unclear and subject to controversy: for example, Matoba et al., 2006 and Inoue et al., 2008 suggest the proton is transferred to His54, which they consider to be axial to CuA. In contrast, Decker et al., 2006; Deeth and Diedrich, 2010 and Rolff et al., 2011 propose a mechanism in which no Cu-N bond is broken. Moreover, working with copper complexes, the tyrosinase activity has been mimicked, suggesting mechanisms similar to those described above (Koval et al., 2006; Rolff et al., 2010). Other authors suggest that the monophenol binds to the enzyme through the CuA, while the *o*-diphenol would bind through the CuB (Olivares et al., 2002),

The crystallisation of tyrosinase from *Bacillus megaterium* (Sendovski et al., 2011) has established His69 and His231 as axial in cis position to the copper atoms, although these authors propose that a histidine equatorial to the CuA (His60) may be flexible during the catalysis. If we accept the proposal of Deeth and Diedrich, 2010, concerning the rotation of the histidines coordinating CuA, this His60 could accept the proton on the part of the substrate. Then according to Step 9 *o*-quinone and H_2O are formed, and the *met*-tyrosinase form (E_m) is regenerated. The above could apply to the enzyme *Agaricus bisporus,* as suggested by Ismaya et al. (2011), authors who also propose protonation of the peroxide and the subsequent intervention of an equatorial histidine, since the axial His85 is covalently bound to Cys83 by means a thioether bond. Crystallising prophenoloxidase from *Manduca sexta*, Li et al. (2009) propose Glu395 as the base that may abstract a proton from the phenolic substrates.

The inactivation (Step 10) would occur through transfer of the proton from the hydroxyl group in C-3 to the peroxide, the subsequent oxidation/reduction leading to the formation of *o*-quinone and H_2O_2 and the release of the CuB.

This inactivation mechanism is consistent with the experimental observation that 50 % of the copper is lost from the active site during catechol inactivation (Dietler and Lerch, 1982) and also with the experiments carried out by Land et al. (2007) concerning the impossibility of reactivating the inactivated enzyme by adding Cu^{2+},

perhaps indicating the need for a “caddie” protein (Matoba et al., 2006). Although the environment of the CuB is better conserved than that of the CuA, it seems to bind more weakly since crystals of tyrosinase from *Bacillus megaterium* have been obtained without CuB (Sendovski et al., 2011). Matoba et al., 2006 suggested that the incorporation of copper in the tyrosinase of *Streptomyces castaneoglobisporus* may be mediated by a caddie protein (ORF378). This helping hand does not exist in the tyrosinase of *Bacillus megaterium* and the active centre is more exposed (Sendovski et al., 2011). The difference in the accumulation of copper may be the result of the different conditions in the medium to which the enzyme is secreted. Sendovski et al. (2011) suggested that a histidine (His60) bound equatorially to the CuA might be flexible in the tyrosinase of *Bacillus megaterium*, as the Val218 near CuA. In the mechanism proposed in Scheme 3, the copper atom released would correspond to CuB. However, this is only one of the possible explanations for the PPO suicide inactivation mechanism.

In the effect of rosmarinic acid on melanogenesis, there is also a balance between the pro- and antioxidant activity, which finally tends to a predominance of the antimelanogenic and, so, antioxidant activity due to the suicide inactivation of the enzyme.

CONCLUSIONS

Rosmarinic acid has been characterized with regards to its intrinsic prooxidant activity, through which it generates H_2O_2 and acts as substrate of POD, generating semiquinone/free radicals. Its intrinsic antioxidant activity was also characterized (an ability to eliminate H_2O_2 and sequester free radicals). In addition, the melanogenic prooxidant activity of rosmarinic acid as phenolic substrate of PPO has been studied, as well as its antimelanogenic and antioxidant activity as substrate, which results in the suicide inactivation of PPO. The overall balance between the prooxidant and antioxidant activities leads us to consider rosmarinic acid as a net antioxidant.

ACKNOWLEDGEMENTS

This paper was partially supported by grants from the Ministerio de Educación y Ciencia (Madrid, Spain) Projects BIO2009-12956 and SAF2009-12043-C02-01 and from the Fundación Séneca (CARM, Murcia, Spain) Projects 08856/PI/08 and 08595/PI/08. JLMM and FGM hold two fellowships from Fundación Caja Murcia (Murcia, Spain).

REFERENCES

AL-SEREITI, M.R., ABU-AMER, K.M. and SEN, P. 1999. Pharmacology of rosemary (*Rosmarinus officinalis Linn.*) and its therapeutic potentials. Indian J. Exp. Biol. *37*, 124-130.

BORS, W., MICHEL, C., STETTMAIER, K., LU, Y. and FOO, L.Y. 2004. Antioxidant mechanisms of polyphenolic caffeic acid oligomers, constituents of *Salvia officinalis*. Biol. Res. *37*, 301-311.

BRADFORD, M.M. 1976. A rapid and sensitive method for the quantitation of microgram quantities of protein utilizing the principle of protein-dye binding. Anal. Biochem. *72*, 248-254.

BRAND-WILLIAMS, W., CUVELIER, M.E. and BERSET, C. 1995. Use of a free radical method to evaluate antioxidant activity. Lebensm.-Wiss. Tecnol. *28*, 25-30.

CALABRESE, V., SCAPAGNINI, G., CATALANO, C., DINOTTA, F., GERACI, D. and MORGANTI, P. 2000. Biochemical studies of a natural antioxidant isolated from rosemary and its application in cosmetic dermatology. Int. J. Tiss. Reac. *22*, 5-13.

CAO, H., CHENG, W.-X., LI, C., PAN, X.-L., XIE, X.G. and LIE, T.H. 2005. DFT study on the antioxidant activity of rosmarinic acid. *J. Mol. Struct.-THEOCHEM*, *719*, 177-183.

CHANG T.S. 2007. Two potent suicide substrates of mushroom tyrosinase. J. Agric. Food Chem. *55,* 2010-2015.

CHANG T.S., LIN, M.Y. and LIN H.J. 2010. Indentifying 8-hydroxynaringenin as a suicide substrate of mushroom tyrosinase. J. Cosmet. Sci. *61,* 205-210.

DECKER, H., SCHWEIKARDT, T. and TUCZEK, F. 2006. The crystal structure of tyrosinase: All questions answered?. Angew. Chem. Int. Ed. *45*, 4546-4550.

DEETH, R.J. and DIEDRICH, C. 2010. Structural and mechanistic insights into the oxy form of tyrosinase from molecular dynamics simulations. J. Bio. Inorg. Chem. *15*, 117-129.

DIETLER, C. and LERCH, K. 1982. in *Oxidases and Related Redox Systems* (KING, T.E., MASON, H.S. and MORRISON, M., ed), pp. 305-317, Pergamon Press, New York.

ESCRIBANO, J., TUDELA, J., GARCIA-CARMONA, F. and GARCIA-CANOVAS, F. 1989. A kinetic study of the suicide inactivation of an enzyme measured through coupling reactions. Biochem. J. *262*, 597-603.

FENOLL, L.G., RODRÍGUEZ-LOPEZ, J.N., GARCIA-MOLINA, F., GARCIA-CANOVAS, F. and TUDELA, J. 2002. Michaelis constant of mushroom tyrosinase with respect to oxygen in the presence of monophenols and diphenols. Int. J. Biochem. and Cell Biol. *34*, 332-336.

HOTTA, H., NAGANO, S., UEDA, M., TSUJINO, Y., KOYAMA, J. and OSAKAI, T. 2002. Higher radical scavenging activities of polyphenolic antioxidants can be ascribed to chemicals reactions following their oxidation. Biochim. Biophys. Acta *1572*, 123-132.

INOUE, T., SHIOTA., Y. and YOSHIZAWA, K. 2008. Quantum chemical approach to the mechanism for the biological conversion of tyrosine to dopaquinone. J. Am. Chem. Soc. *130*, 16890-16897.

ISMAYA, W.T., ROZEBOOM, H.J., WEIJN, A., MES, J.J., FUSETTI, F., WICHERS, H.J. and DIJKSTRA, W.B. 2011. Crystal structure of *Agaricus bisporus* mushroom tyrosinase: identity of the tetramer subunits and interaction with tropolone. Biochemistry Epub ahead of print.

ITO, H., MIYAZAKI, T., ONO, M. and SAKURAI, H. 1998. Antiallergic activities of rabdosiin and its related compounds: chemical and biochemical evaluations. Bioorg. Med. Chem. *6*, 1051-1056.

JACKMAN, M., HUBER, M., HAJNAL, A. and LERCH, K. 1992. Stabilization of the oxy form of tyrosinase by a single conservative amino acid substitution. Biochem. J. *282*, 915-918.

Jandel Scientific, SigmaPlot 9 for Windows®, Jandel Scientific, Core Madera, CA, (2007).

KOVAL., I.A., GAMEZ, P., BELLE C., SELMECZI, K. and REEDIJK, J. 2006. Synthetic models of the active site of catechol oxidase: mechanistic studies. Chem. Soc. Rev. *35*, 814-840.

LAND, E.J., RAMSDEN, C.A. and RILEY, P.A. 2007. The mechanism of suicide-inactivation of tyrosinase: a substrate structure investigation. Tohoku J. Exp. Med. *212*, 341-348.

LEE, J., KIM, Y.S. and PARK, D. 2007. Rosmarinic acid induces melanogenesis through protein kinase A activation signalling. Biochem. Pharmacol. *74*, 960-968.

LI, Y., WANG, Y., JIANG, H. and DENG, J. 2009. Crystal structure of Manduca sexta prophenoloxidase provides insights into the mechanism of type 3 copper enzymes. Prc. Natl. Acad. Sci. USA *106*, 17002-17006.

MARTINEZ-TOME, M., JIMENEZ, A.M., RUGGIERI, S., FREGA, N., STRABBIOLI, R. and MURCIA, M.A. 2001. Antioxidant properties of Mediterranean spices compared with common food additives. J. Food Protec. *64*, 1412-1419.

MATOBA, Y., KUMAGAI, T., YAMAMOTO, A., YOSHITSU, H. and SUGIYAMA, M. 2006. Crystallographic evidence that the dinuclear copper center of tyrosinase is flexible during catalysis. J. Biol. Chem. *281*, 8981-8990.

MOÑINO, I., MARTINEZ, C., SOTOMAYOR, J.A., LAFUENTE, A. and JORDAN, M.J. 2008. Polyphenolic transmission to Segureño lamb meat from ewes´ diet supplemented with the distillate from rosemary (*Rosmarinus officinalis*) leaves. J. Agric. Food Chem. *26*, 3363-3367.

MUNOZ-MUNOZ, J.L., GARCIA-MOLINA, F., GARCIA-RUIZ, P.A., MOLINA-ALARCON, M., TUDELA, J., GARCIA-CANOVAS, F. and RODRÍGUEZ-LOPEZ, J.N. 2008. Phenolic substrates and suicide inactivation of tyrosinase: kinetics and mechanism. Biochem. J. *416*, 431-440.

MUNOZ-MUNOZ, J.L., GARCIA-MOLINA, F., GARCIA-RUIZ, P.A., ARRIBAS, E., TUDELA, J., GARCIA-CANOVAS, F. and RODRIGUEZ-LOPEZ, J.N. 2009.

Enzymatic and chemical reactions of trihydroxylated phenols. Food Chem. *113*, 435-444.

MUNOZ-MUNOZ, J.L., GARCIA-MOLINA, F., VARON, R., TUDELA, J., GARCIA-CANOVAS, F. and RODRIGUEZ-LOPEZ, J.N. 2010. Quantification of the antioxidant capacity of different molecules and their kinetic antioxidant efficiency. J. Agric. Food Chem. *58*, 2062-2070.

MURAKAMI, K., HANEDA, M., QIAO, S., NARUSE, M. and YOSHINO, M. 2007. Prooxidant action of rosmarinic acid: Transition metal-dependent generation of reactive oxygen species. Toxicol. in Vitro *21*, 613-617.

OLIVARES, C., GARCIA-BORRON, J.C. and SOLANO, F. 2002. Identification of active site residues involved in metal cofactor binding and stereospecific substrate recognition in mammalian tyrosinase. Implications to the catalytic cycle. Biochemistry *41*, 679-686.

OSAKABE, N., TAKANO, H., SANBONGI, C., YASUDA, A., YANAGISAWA, R., INOUE, K. and YOSHIKAWA, T. 2004. Anti-inflammatory and anti-allergic effect of rosmarinic acid (RA); inhibition of seasonal allergic rhinoconjunctivitis (SAR) and its mechanism. Biofactors *21*, 127-131.

PEREZ-FONS, F., ARANDA, F.J., GUILLEN, J., VILLALAIN, J. and MICOL, V. 2006. Rosemary (*Rosmarinus officinalis*) diterpenes affect lipid polymorphism and fluidity in phospholipids membranes. Arch. Biochem. Biophys. *453*, 224-236.

PETERSEN, M. and SIMMONDS, M.S.J. 2003. Rosmarinic acid. Phytochemistry *62*, 121-125.

PIRKER, K.F., KAY, C.W.M., SOLZE, K., TUNEGA, D., RECHENAUER, T.G. and GOODMAN, B.A. 2009. Free radical generation in rosmarinic acid investigated by electron paramagnetic resonance spectroscopy. Free Rad. Res. *43*, 47-57.

RODRÍGUEZ-LÓPEZ, J.N., GILABERT, M.A., TUDELA, J., THORNELEY, R.N.F. and GARCÍA-CÁNOVAS, F. 2000a. Reactivity of horseradish peroxidase compound II toward substrates: kinetic evidence for a two-step mechanism. Biochemistry *39*, 13201-13209.

RODRÍGUEZ-LOPEZ, J.N., FENOLL, L.G., GARCIA-RUIZ, P.A., VARON, R., TUDELA, J., THORNELEY, R.N. and GARCIA-CANOVAS, F. 2000b. Stopped-flow and steady-state study of the diphenolase activity of mushroom tyrosinase. Biochemistry *39*, 10497-10506.

ROLFF, M., SCHOTTENHEIM, J., PETERS, G. and TUCZEK, F. 2010. The first catalytic tyrosinase model system based on a mononuclear copper(I) complex: kinetics and mechanism. Angew. Chem. Int. Ed. *49*, 6438-6442.

ROLFF, M., SCHOTTENHEIM, J., DECKER, H. and TUCZEK, F. 2011. Copper-O_2 reactivity of tyrosinase models towards external monophenolic substrates: molecular mechanism and comparison with the enzyme. Chem. Soc. Rev. Epub ahead of print.

SANCHEZ-CAMPILLO, M., GABALON, J.A., CASTILLO, J., BENAVENTE-GARCIA, O., DEL BAÑO, M.J., ALCARAZ, M., VICENTE, V., ALVAREZ, N. and LOZANO, J.A. 2009. Rosmarinic acid, a photo-protective agent against UV and other ionizing radiations. Food Chem. Toxicol. *47*, 386-392.

SENDOVSKI, M., KANTEEV, M., SHUSTER BEN-YOSEF, V., ADIR, N. and FISHMAN A. 2011. First structures of an active bacterial tyrosinase reveal copper plasticity. J. Mol. Biol. *405*, 227-237.

SINGLETARY, K.W. 1996a. Rosemary extract and carnosol stimulate rat liver glutathione-S-transferase and quinone reductase activities. Cancer Lett. *100*, 139-144.

SINGLETARY, K., MACDONAL, C. and WALLIG, M. 1996b. Inhibition by rosemary and carnosol of 7,12-dimethylbenz-α-anthracene (DMBA)-induced rat mammary tumorigenesis and in vivo DMBA-DNA adduct formation. Cancer Lett. *104*, 43-48.

TAI S.S.-K., LIN C.-G., WU M.-H. and CHANG T.S. 2009. Evaluation of depigmenting activity by 8-hydroxydaidzein in mouse B16 melanoma cells and human volunteers. Int. J. Mol. Sci. 10:4257-4266.

ZHENG, W. and WANG, S.Y. 2001. Antioxidant activity and phenolics compounds in selected herbs. J. Agric. Food Chem. *49*, 5165-5170.

LEGENDS TO FIGURES AND SCHEMES

FIG. 1. CHRONOMETRIC METHOD USED FOR CHARACTERIZING THE ENZYMATIC ACTIVITY OF POD ON ROSMARINIC ACID. EFFECT OF SUBSTRATE CONCENTRATION. The experimental conditions were 30 mM sodium phosphate buffer (pH = 7.0), $[AH_2]_0$ = 40 μM, $[H_2O_2]_0$ = 0.1 mM, $[E]_0$ = 1 nM, wavelength = 460 nm and varying substrate concentrations (mM): (a) 0.2, (b) 0.4, (c) 0.5, (d) 0.6, (e) 0.8, (f) 1, (g) 1.5, (h) 2 and (i) 2.5. Inset. Representation of steady-state rate (V_0) *vs.* $[S]_0$.

FIG. 2. CHARACTERIZATION OF COMPOUNDS WITH MONOPHASIC ANTIOXIDANT ACTIVITY. Time course of $ABTS^{\bullet+}$ accumulation in the presence of POD (0.25 nM), ABTS (5 mM) and H_2O_2 (0.1 mM) in sodium phosphate buffer 30 mM (pH 7.0), at 25ºC. The reaction was followed by measuring the ΔA_{734}. Recording (a), control. Recordings (b) – (g), time courses of the same reaction as in (a) but with 1, 2, 3, 4, 5 and 7 μM of rosmarinic acid added, respectively. Inset A. Representation of $V_0\tau$ *vs.* $[S]_0$. Inset B. Characterization of compounds with biphasic antioxidant activity. Non-enzymatic kinetic test to calculate n_{app} and k_2^{app}. The buffer used was 30 mM sodium phosphate buffer (pH 7.0), 25 ºC. The radical $ABTS^{\bullet+}$ (R) was generated with the POD/ABTS/H_2O_2 system. The concentration of POD was 0.3 nM and the $[H_2O_2]_0$ = 70 μM. At t = 0, a 5 μM concentration of antioxidant was added and the changes in absorbance at 734 nm were recorded from the initial fall of R.

FIG. 3. NADH DISAPPEARANCE METHOD FOR CHARACTERIZING ENZYMATIC ACTIVITY OF PPO ON ROSMARINIC ACID. EFFECT OF SUBSTRATE CONCENTRATION. The experimental conditions were 30 mM sodium phosphate buffer (pH = 7.0), $[NADH]_0$ = 0.81 mM, $[E]_0$ = 30 nM, wavelength = 400 nm and varying substrate concentrations (mM): (a) 0.04, (b) 0.1, (c) 0.15, (d) 0.2, (e) 0.25, (f)

0.3, (g) 0.35, (h) 0.4, (i) 0.45, (j) 0.5, (k) 0.58 and (l) 0.7. Inset. Representation of steady-state rate *vs*. $[S]_0$.

FIG. 4. SPECTROPHOTOMETRIC RECORDINGS OF THE SUICIDE INACTIVATION OF PPO IN ITS ACTION ON ROSMARINIC ACID. A. Corrected recordings of the disappearance of NADH in the suicide inactivation of PPO in its action on rosmarinic acid for different enzyme concentrations. Conditions were: 30 mM sodium phosphate buffer (pH 7.0), wavelength = 400 nm, 0.81 mM NADH, 0.26 mM O_2, 0.2 mM rosmarinic acid and $[E]_0$ (nM): (a) 10, (b) 15, (c) 19, (d) 22, (e) 25, (f) 28, (g) 33, (h) 35 and (i) 45. Inset. Representation of the values of $[NADH]_\infty$ (●) and $\lambda^S_{E_{ox}}$ (O) *vs.* enzyme concentration. B. Corrected recordings of the disappearance of NADH in the suicide inactivation of PPO by different rosmarinic acid concentrations. Conditions were 30 mM sodium phosphate buffer (pH 7.0), 0.26 mM O_2, wavelength = 400 nm and the initial concentrations of NADH and PPO were: 0.81 mM and 35 nM. The substrate concentrations were (mM): (a) 0.02, (b) 0.04, (c) 0.06, (d) 0.08, (e) 0.12, (f) 0.15, (g) 0.2 and (h) 0.3. Inset. Values of $\lambda^S_{E_{ox}}$ *vs.* $[S]_0$.

SCHEME 1. CHEMICAL STRUCTURE OF ROSMARINIC ACID AND 2,2´-AZINO-BIS(3-ETHYLBENZOTHIAZOLINE-6-SULFONIC ACID) (ABTS).

SCHEME 2. SIMPLE KINETIC MECHANISM TO EXPLAIN THE PRIMARY AND SECONDARY ANTIOXIDANT CAPACITIES OF ROSMARINIC ACID.

SCHEME 3. STRUCTURAL MECHANISM TO EXPLAIN THE SUICIDE INACTIVATION AND CATALYTIC REACTIONS OF POLYPHENOL OXIDASE IN ITS ACTION ON ROSMARINIC ACID. *Diphenolase cycle:* E_m, *met*tyrosinase; E_mS,

interaction between E_m and S; $(E_m\text{-S})_1$, axial nucleophilic attack complex from OH of C-1 to E_m; $(E_m\text{-S})_2$, diaxial binding complex of S with E_m; E_d, *deoxy*tyrosinase; E_{ox}, *oxy*tyrosinase; E_{ox}S, interaction complex between E_{ox} with S; $(E_{ox}\text{-S})_1$, axial binding complex of protonated S with $\mathrm{E_{ox}}$; $(E_{ox}\text{-S})_2$, diaxial binding complex of S with E_{ox}. *Suicide inactivation:* $(E_{ox}\text{-S})_3$, Axial binding complex of deprotonated S with E_{ox}; E_i, inactive enzyme.

APPENDIX

Appendix A. Kinetic analysis of Scheme 2, reactions a-c

The kinetic analysis of Scheme 2 provides the following equation for determining n_{app} and k_2^{app} and is described in Muñoz-Muñoz et al., 2010.

$$[ABTS^{\bullet+}] = [ABTS^{\bullet+}]_\infty + \frac{ab}{b+t} \qquad (1A)$$

where $a = n_{app}[S]_0$ and $b = 1/(k_2^{app}[S]_0)$.

By means of non-linear regression of the experimental registers of $[ABTS^{\bullet+}]$ *vs.* *t* (Fig. 2, inset B) to eq. (1A), we can determine n_{app} and k_2^{app}.

KAE_{app} was calculated for rosmarinic acid and, for the sake of comparison, for EQ. This KAE_{app} value responds to the following equation:

$$KAE_{app} = \frac{1}{EC_T50_{app} \text{ x } t_{1/2}^{app}} = 2\,(n + n_{app})\,k_2^{app}\,[S]_0 \qquad (2A)$$

As already mentioned, KAE_{app} is a kinetic parameter that relates the velocity of the process (k_2^{app}) with the number of electrons consumed in the process (n_{app}). As can be seen from Table 1, the value of KAE_{app} is very small for S (200 electrons/s) compared with EQ ($5.1 \text{ x} 10^4$ electrons/s) (Munoz-Munoz et al., 2010).

Appendix B. Kinetic analysis of suicide inactivation of PPO

The experimental data of time-based assays for the disappearance of NADH follow eq. (1B):

$$[NADH] = [NADH]_f + [NADH]_\infty e^{-\lambda_{E_{ox}} t} \qquad (1B)$$

where [NADH] is the instantaneous concentration of NADH, $[NADH]_f$ is the NADH-value at $t \to \infty$, $[NADH]_\infty$, NADH consumed at the end of the reaction, $t \to \infty$,

i.e. $[NADH]_\infty = [NADH]_0 - [NADH]_f$ and $\lambda_{E_{ox}}$, the apparent constant of suicide inactivation of PPO in the presence of rosmarinic acid.

When $t \to \infty$, $[NADH] = [NADH]_\infty$ and, according to Munoz-Munoz et al., 2008:

$$[NADH]_\infty = \frac{2k_{7_2}}{k_{7_2}^{i}}[E]_0 \qquad (2B)$$

The velocity of the suicide inactivation is regulated by the apparent inactivation constant, $\lambda_{E_{ox}}^{S}$, whose expression is given by eq. (3B). Taking into account the saturation of PPO by oxygen, ($[O_2]_0 \to \infty$), result:

$$\lambda_{E_{ox}}^{S} = \frac{\lambda_{E_{ox}(\max)}^{S}[S]_0}{K_m^S + [S]_0} \qquad (3B)$$

The partition ratio, r, between the catalytic and suicide inactivation pathways is:

$$r = \frac{k_{7_2}}{k_{7_2}^{i}} = \frac{k_{cat}^{PPO}}{\lambda_{E_{ox}(\max)}^{S}} = \frac{[Q]_\infty}{2[E]_0} = \frac{[NADH]_\infty}{2[E]_0} \qquad (4B)$$

where k_{7_2} is the substrate binding constant to the copper atom through the C-3 hydroxyl (axial) and $k_{7_2}^{i}$ is the rate constant of transfer of a H^+ to the protonated peroxide from C-3 hydroxyl.

Therefore, from eq. (1B)-(4B), we can obtain the kinetic constants that characterize the kinetic behaviour of a suicide substrate: r, $\lambda_{E_{ox}(\max)}^{S}$, K_m^S and k_{cat}^{PPO}.

TABLE 1. EFFECT OF PH ON THE BIPHASIC ANTIOXIDANT CAPACITY OF ROSMARINIC ACID.

pH	Primary antioxidant capacity			Secondary antioxidant capacity			Total antioxidant capacity				
	n (electrons)	EC_p50	ARP_p	n_{app} (electrons)	EC_s50_{app}	ARP_s^{app}	$n + n_{app}$ (electrons)	EC_T50_{app}	ARP_T^{app}	k_2^{app} (M^{-1} s^{-1})	KAE_{app} (electrons/s)*
7.00	4.1 ± 0.3	0.12 ± 0.01	8.2 ± 0.83	6.8 ± 0.7	0.07 ± 0.01	13.6 ± 0.8	10.9 ± 1.3	0.05 ± 0.01	21.8 ± 2.8	13 ± 1	283 ± 30
7.50	4.1 ± 0.3	0.12 ± 0.01	8.2 ± 0.83	6.8 ± 0.7	0.07 ± 0.01	13.6 ± 0.8	10.9 ± 1.3	0.05 ± 0.01	21.8 ± 2.8	16 ± 2	348 ± 37
7.75	4.1 ± 0.3	0.12 ± 0.01	8.2 ± 0.83	6.8 ± 0.7	0.07 ± 0.01	13.6 ± 0.8	10.9 ± 1.3	0.05 ± 0.01	21.8 ± 2.8	43 ±3	937 ± 99
8.00	4.1 ± 0.3	0.12 ± 0.01	8.2 ± 0.83	6.8 ± 0.7	0.07 ± 0.01	13.6 ± 0.8	10.9 ± 1.3	0.05 ± 0.01	21.8 ± 2.8	66 ± 5	1438 ± 126
8.25	4.1 ± 0.3	0.12 ± 0.01	8.2 ± 0.83	6.8 ± 0.7	0.07 ± 0.01	13.6 ± 0.8	10.9 ± 1.3	0.05 ± 0.01	21.8 ± 2.8	83 ± 9	1810 ± 198
8.50	4.1 ± 0.3	0.12 ± 0.01	8.2 ± 0.83	6.8 ± 0.7	0.07 ± 0.01	13.6 ± 0.8	10.9 ± 1.3	0.05 ± 0.01	21.8 ± 2.8	103 ± 12	2245 ± 268

* For 1 M antioxidant solution.

TABLE 2. KINETIC CONSTANTS WHICH CHARACTERIZE THE SUICIDE INACTIVATION OF POLYPHENOL OXIDASE BY ROSMARINIC ACID

Substrate	$\lambda^{S}_{E_{ox}(max)}$ x 10^3 (s^{-1})	$r = k^{PPO}_{cat} / \lambda^{S}_{E_{ox}(max)}$	k^{PPO}_{cat} (s^{-1})	K^{S}_{m} (μM)
Rosmarinic acid	5.9 ± 0.3	21885 ± 2325	129 ± 15	89.9 ± 10.4

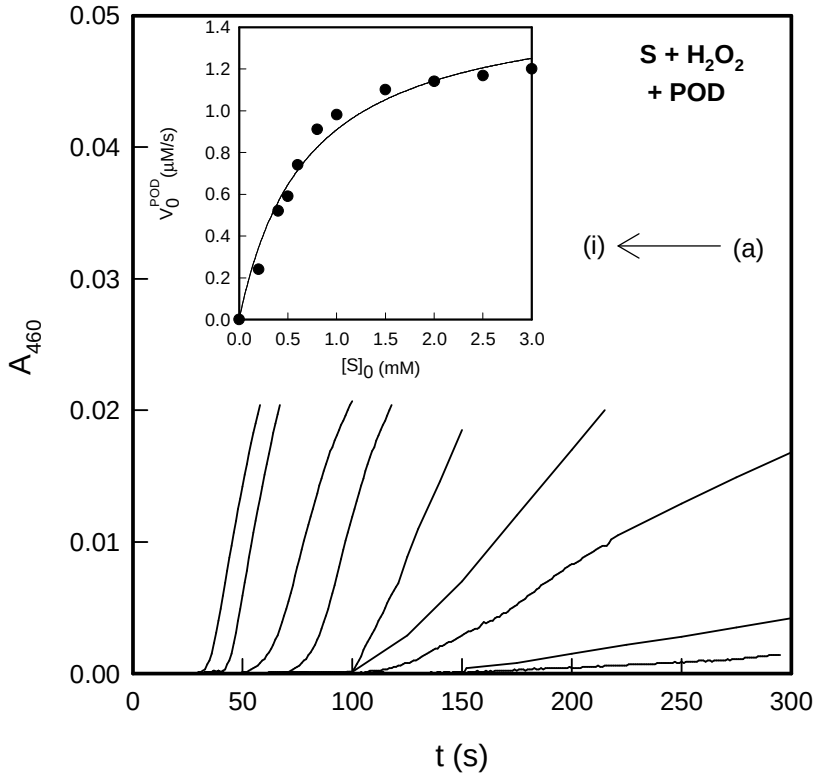

Fig. 1

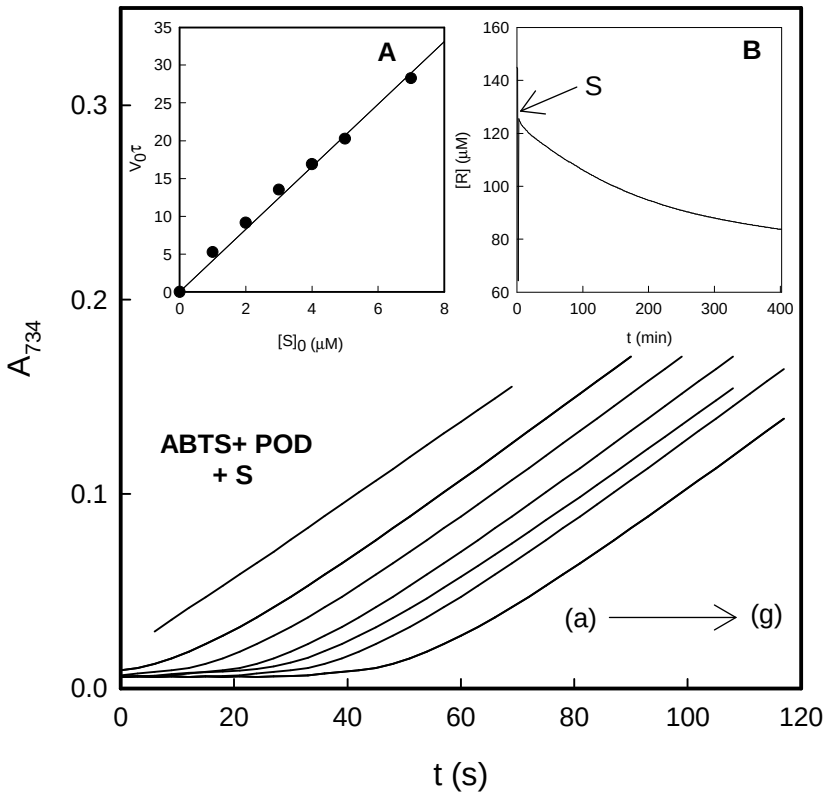

Fig. 2.

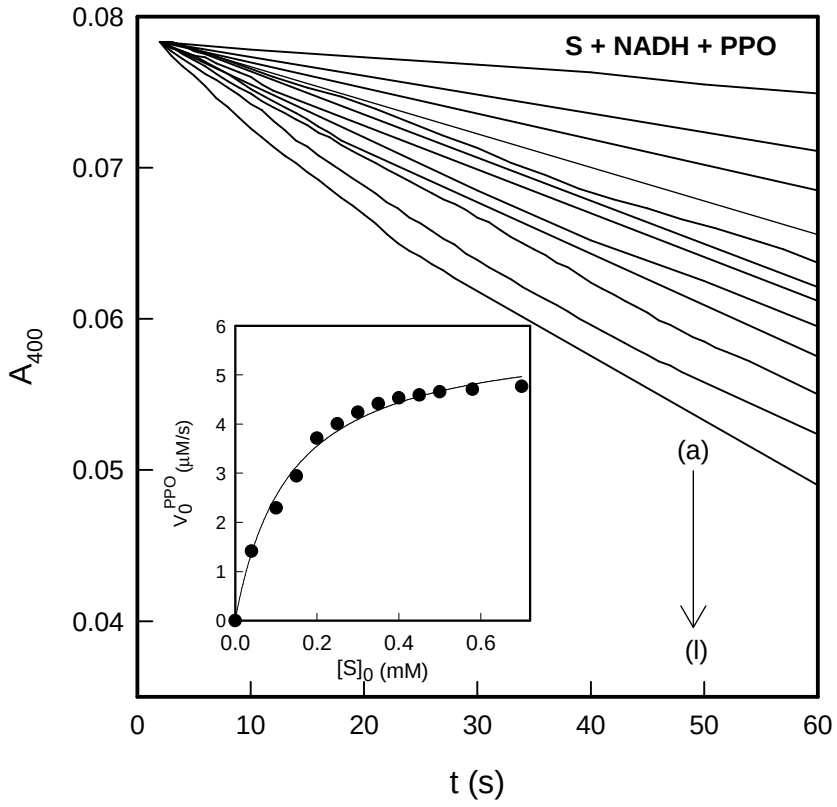

Fig. 3.

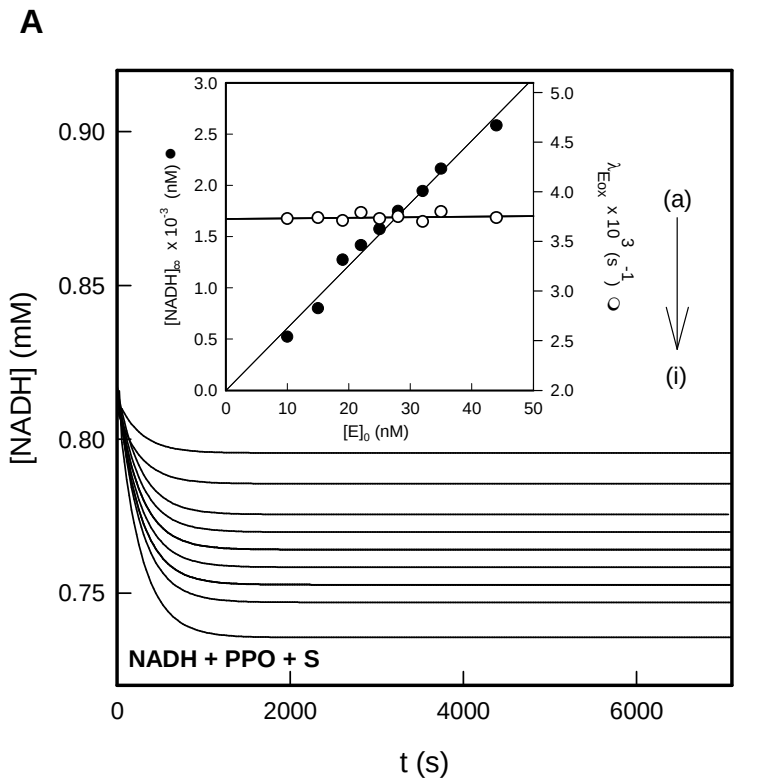

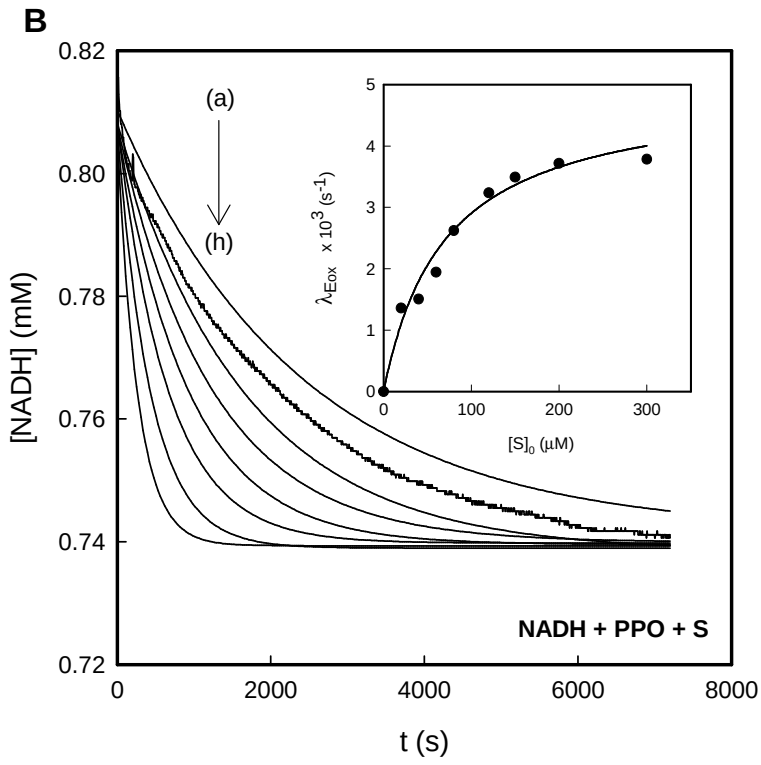

Figs. 4A and 4B

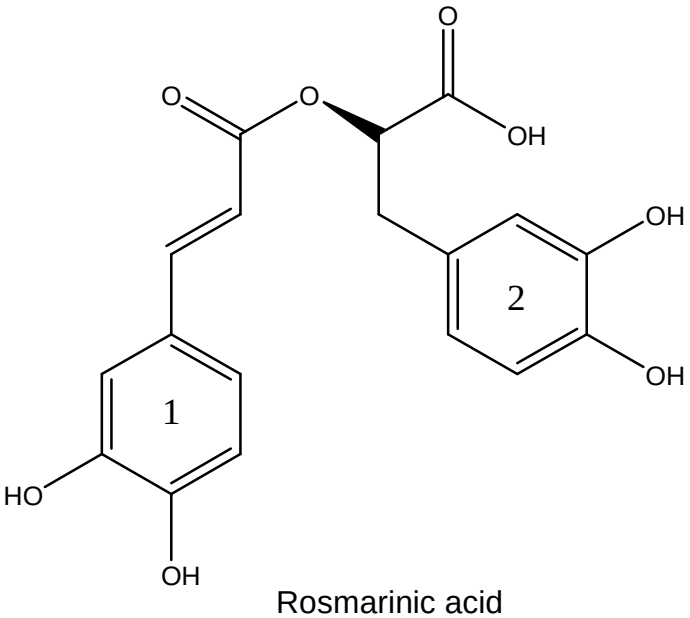

Rosmarinic acid

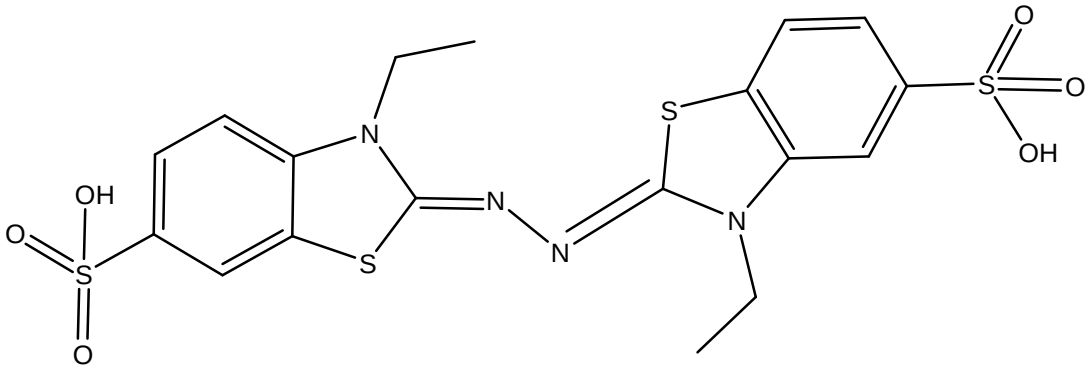

ABTS

-Scheme 1-

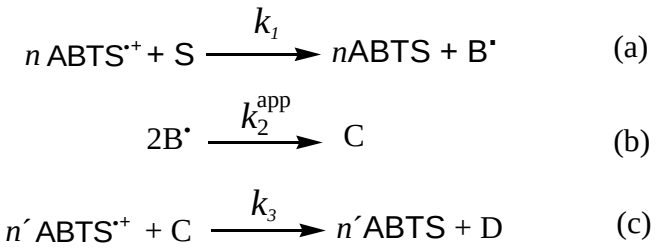

-Scheme 2-

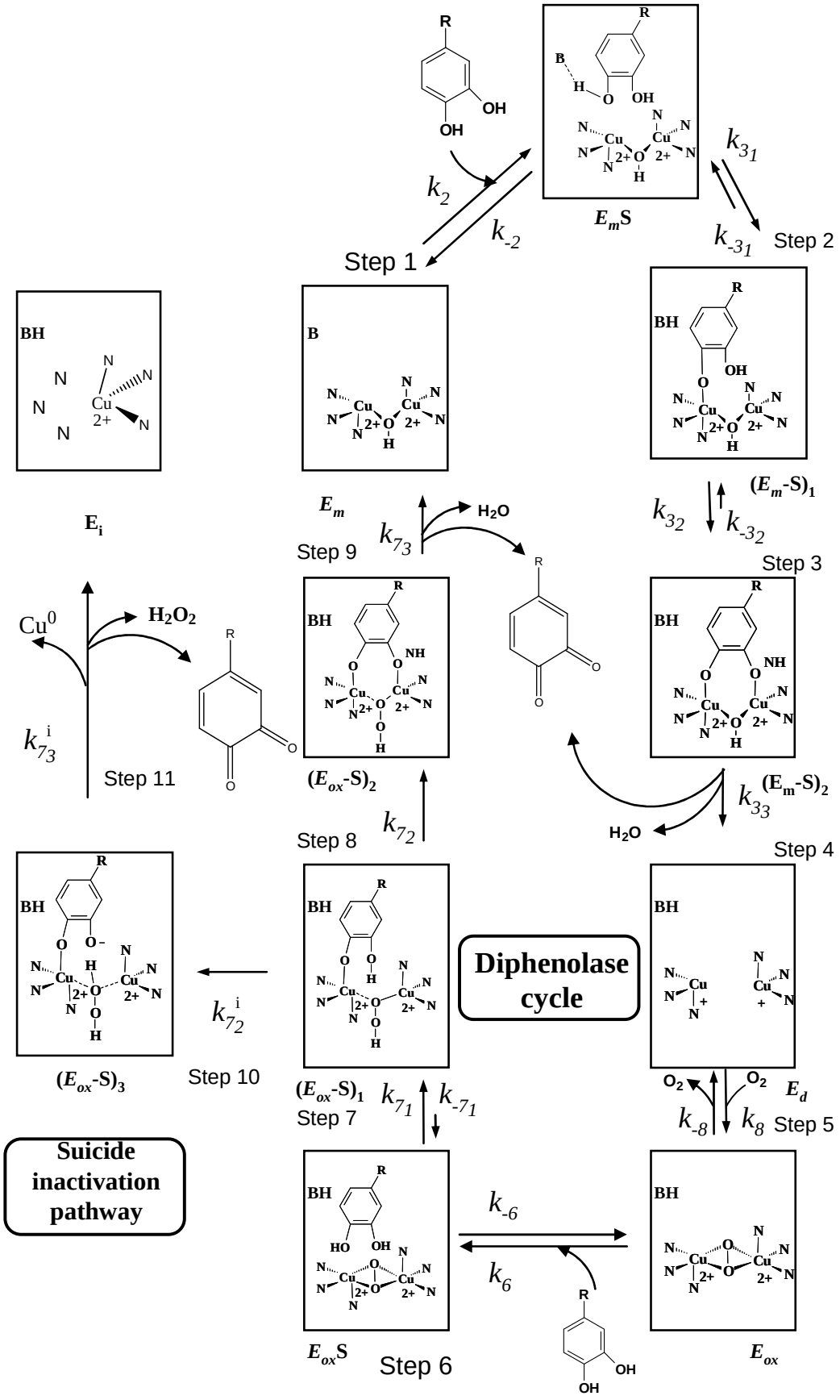
Step 1
Step 2
Step 3
Step 4
Step 5
Step 6
Step 7
Step 8
Step 9
Step 10
Step 11
E_mS
E_i
E_m
$(E_m\text{-S})_1$
$(E_m\text{-S})_2$
$(E_{ox}\text{-S})_1$
$(E_{ox}\text{-S})_2$
$(E_{ox}\text{-S})_3$
E_{ox}S
E_{ox}
E_d
k_2
k_{-2}
k_{3_1}
k_{-3_1}
k_{3_2}
k_{-3_2}
k_{3_3}
k_{7_3}
k_{7_2}
k_{7_1}
k_{-7_1}
$k_{7_3}^{i}$
$k_{7_2}^{i}$
k_{-8}
k_8
k_6
k_{-6}
H_2O
H_2O_2
O_2
Cu^0
Diphenolase cycle
Suicide inactivation pathway

-Scheme 3-

4.13. CUANTIFICACIÓN DE LA CAPACIDAD ANTIOXIDANTE DE DIFERENTES MOLÉCULAS Y SU EFICIENCIA ANTIOXIDANTE CINÉTICA.

La cuantificación de la capacidad antioxidante de diferentes moléculas y su eficiencia antioxidante cinética ha dado lugar a la siguiente publicación adjunta.

4.13.1. Título

Quantification of the antioxidant capacity of different molecules and their kinetic antioxidant efficiencies.

4.13.2. Autores

Muñoz-Muñoz, J.L.; Garcia-Molina, F.; Varon, R; Tudela, J.; Garcia-Cánovas, F. y Rodríguez-López, J.N.

4.13.3. Referencia

Journal of Agricultural and Food Chemistry (2010) 58, 2062-2070.

4.13.4. Resumen

Se ha diseñado un método cinético para la determinación de la capacidad antioxidante de distintos compuestos. En este método, denominado método enzimático cinético, se genera el radical libre del ABTS continuamente en el medio de reacción por el sistema peroxidasa/ABTS/H_2O_2. La presencia de un antioxidante en la disolución provoca la aparición de un periodo de retardo en la acumulación en el medio del radical libre, a partir del estudio de este periodo de retardo se puede calcular la capacidad antioxidante de la molécula en estudio. Esta capacidad antioxidante, llamada capacidad antioxidante primaria, está cuantificada por: n, número de electrones consumidos por molécula de antioxidante, la concentración efectiva, EC50, y el poder antioxidante o antiradical (ARP), (ARP = 1/EC50 = $2n$). Si los productos que se forman en la reacción entre el antioxidante y el radical libre evolucionan consumiendo más moléculas de radical, se genera una capacidad antioxidante secundaria. Para calcular ésta capacidad antioxidante secundaria, se propone un test no enzimático.

DOI:10.1021/jf9042024

JOURNAL OF AGRICULTURAL AND FOOD CHEMISTRY
ARTICLE

Quantification of the Antioxidant Capacity of Different Molecules and Their Kinetic Antioxidant Efficiencies

Jose Luis Munoz-Munoz,[†] Francisco Garcia-Molina,[†] Ramon Varon,[‡] Jose Tudela,[†] Francisco García-Cánovas,*[,†] and Jose Neptuno Rodriguez-Lopez[†]

[†]GENZ: Grupo de Investigación de Enzimología, Departamento de Bioquímica y Biología Molecular-A, Facultad de Biología, Universidad de Murcia, E-30100 Espinardo, Murcia, Spain, and [‡]Departamento de Química-Física, Escuela de Ingenieros Industriales de Albacete, Universidad de Castilla la Mancha, Avenida España s/n, Campus Universitario, E-02071 Albacete, Spain

A kinetic method has been developed to determine the antioxidant capacity of a variety of molecules. In this method, named the enzymatic kinetic method, the free radical of ABTS is generated continuously in the reaction medium by a peroxidase/ABTS/H_2O_2 system. The presence of an antioxidant in the solution provokes a lag period in the accumulation of the free radical in the medium, and by studying this lag period it is possible to calculate the antioxidant capacity of the molecule in question. This antioxidant capacity, named the primary antioxidant capacity, will be quantified by *n*, the number of electrons donated per molecule of antioxidant, the effective concentration, EC50, and the antioxidant or antiradical power (ARP) (ARP = 1/EC50 = 2*n*). If the products arising from the reaction between the antioxidant and the free radical evolve by consuming more radical, a secondary antioxidant capacity is generated. To calculate this, a nonenzymatic test is proposed.

KEYWORDS: Enzymatic kinetic method; antioxidant capacity; antiradical power

INTRODUCTION

Numerous antioxidants, including phenols, flavonoids, anthocyanins, tannins, vitamins, etc., are contained in fruits and vegetables, although their proportions vary from one food to another. Their composition can also be profoundly altered by processing, storage, or cooking practices. Polyphenols, which are widely distributed in plants, are known to act as antioxidants (*1*).

Several methods to determine free radical scavenging have been reported (*2*), and a comparative evaluation of various total antioxidant capability assays applied to phenolic compounds using the CUPRAC assay is the subject of a more recent review (*3*). Among the methods used to determine antioxidant power that have proved to be most successful are those that use two stable free radicals as indicators of the antioxidant activity: α,α′-diphenyl-β-picrylhydrazyl radical (DPPH$^{\bullet}$) (*4*) and 2,2′-azinobis(3-ethylbenzthiazoline-6-sulfonic acid) radical cation (ABTS$^{\bullet+}$) (*5*). ABTS$^{\bullet+}$ has been used in the determination of antioxidant activity of single compounds (*6*) and in various mixtures (e.g., body fluids (*7*) and foods (*8*)). Subsequently, improvements were made in the ABTS$^{\bullet+}$ decoloration assay (*9*). From electrochemical measurements, the redox potential of several antioxidants has been determined with the aim of correlating this with antioxidant capacity, for example, that determined for DPPH radical scavenging activity (*10*). No clear correlation was found between the oxidation potentials of flavonoids and their DPPH scavenging activities (*10*). Moreover, the number of electrons (*n*) involved in the redox reaction of polyphenols determined by means of continuous flow-column electrolysis has been related with the antioxidant activities of polyphenols (*11*−*13*). In such cases, the high number obtained for *n* has been related with the existence of dimerization and polymerization reactions of the reaction products. The correlation study of *n* values at a slow flow-column electrolysis rate with the DPPH radical scavenging activity has served to support the involvement of slow chemical reactions that follow the initial oxidation of polyphenols (*13*).

Kinetic studies have been published on antioxidant activity using the DPPH$^{\bullet}$ free radical methods (*4*, *14*, *15*). These studies point to the biphasic behavior of many antioxidants, leading to their classification into three groups (rapid, intermediate, and slow) depending on the time they take to reach the steady state (the free radical does not vary with time) (*4*, *14*). On the basis of these studies, three parameters have been proposed to characterize an antioxidant: effective concentration (EC50), which is defined by the ratio of the antioxidant concentration necessary for decreasing the initial DPPH$^{\bullet}$ concentration by 50% to the initial DPPH$^{\bullet}$ concentration; T_{EC50}, the time needed to reach the steady state at the concentration corresponding to EC50; and antiradical efficiency (AE), defined as AE = 1/(EC50 × T_{EC50}), which takes in both effects (concentration and time) (*14*, *15*).

Several investigators have examined the kinetics of the reaction of ABTS$^{\bullet+}$ with antioxidants (*16*). Most plant polyphenols studied have demonstrated a biphasic kinetic pattern, involving fast and slow steps (*16*). Evidence suggests that the ABTS$^{\bullet+}$ initially extracts an electron or hydrogen atom from polyphenols,

*Corresponding author (telephone +34 868 884764; fax +34 868 883963; e-mail canovasf@um.es).

 Published on Web 01/26/2010 © 2010 American Chemical Society

No.	Compound	Substituent	Structures
	Benzenes		
1	Catechol	1,2-OH	
2	*p*-Hydroquinone	1,4-OH	
3	Pyrogallol	1,2,3-OH	
4	Phenol	1-OH	
5	Guaiacol	3-OH,4-OCH_3	
6	Eugenol	1-CH_2-CH_2-CH_2,3-OCH_3,4-OH	
	Benzoic acids		
7	*p*-Hydroxybenzoic acid	4-OH	
8	Vanillin	3-OCH_3,4-OH	
9	Syringic acid	3,5-OCH_3,4-OH	
10	Protocatechuic acid	3,4-OH	
11	Gallic acid	3,4,5-OH	
	Cinnamic acids		
12	*p*-Coumaric acid	4-OH, R = H	
13	Ferulic acid	3-OCH_3,4-OH, R = H	
14	Sinapinic acid	3,5-OCH_3,4-OH, R = H	
15	Caffeic acid	3,4-OH, R = H	
16	Chlorogenic acid	3,4-OH, R = quinic acid	
	Flavans		
17	(+)-Catechin	3,5,7,3′,4′-OH	
18	(-)-Epicatechin	3,5,7,3′,4′-OH	
	Flavonols		
19	Quercetin	3,5,7,3′,4′-OH	
20	Rutin	5,7,3′,4′-OH, 3′-rutinoside	
	Tannin		
21	Ellagic acid		
	Others		
22	Trolox		
23	3-*tert*-butyl-4-hydroxyanisole		
	Non-polyphenols		
24	L-cysteine		
25	L-ascorbic acid		
26	D-ascorbic acid		

Figure 1. Structures of antioxidants.

resulting in the formation of a semiquinone (*16*). Evidence has been put forward to suggest that the semiquinone may dimerize upon reaction with $ABTS^{\bullet+}$ and that the resulting dimers may retain antioxidant activity. It has been demonstrated recently that dimerization may contribute to the biphasic pattern observed with some phenolics (*16*). Also, recent data demonstrate that some polyphenols react with $ABTS^{\bullet+}$ to form covalent adducts (*16*). In some cases, these adducts have been seen to retain antioxidant activity and may contribute to the complex kinetic behavior that has been observed.

The aim of the present study was to develop an enzymatic kinetic method that will permit the characterization of the antioxidant capacity of a compound. In cases when a secondary antioxidant activity exists, a nonenzymatic kinetic test is proposed, consisting of a kinetic analysis of how the concentration of the excess of free radical varies when it reacts with the initial product generated by the reaction of the antioxidant with the free radical.

MATERIALS AND METHODS

Enzyme Source. Horseradish peroxidase (POD; 251 U/mg) type VI, Rz ($A_{430\ nm}/A_{275\ nm}$) = 3.1, was obtained from Sigma Chemical (St. Louis, MO). The enzyme concentration was determined by measuring the absorbance at 403 nm using $\varepsilon_{403} = 100000/(M \times cm)$ (*17*).

Reagents. The compounds (**Figure 1**) *p*-hydroquinone (1,4-dihydroxybenzene), pyrogallol (1,2,3-trihydroxybenzene), *p*-hydroxybenzoic acid, protocatechuic acid (3,4-dihydroxybenzoic acid), *p*-coumaric acid (*trans*-4-hydroxycinnamic acid), ferulic acid (*trans*-4-hydroxy-3-methoxycinnamic acid), sinapinic acid (3,5-dimethoxy-4-hydroxycinnamic acid), quercetin (3,3′,4′,5,6-pentahydroxyflavone), rutin (quercetin-3-rutinoside), L-cysteine [(*R*)-2-amino-3-mercaptopropionic acid], L-ascorbic acid

(L-threoascorbic acid), D-ascorbic acid (D-threoascorbic acid), 3-*tert*-butyl-4-hydroxyanisole, phenol (hydroxybenzene), guaiacol (2-methoxyphenol), eugenol [2-methoxy-4-(2-propenyl)phenol], Trolox (6-hydroxy-2,5,7,8-tetramethylchrome-2-carboxylic acid), (+)-catechin (*trans*-3,3′,4′,5,7-pentahydroxyflavane), and ABTS [2,2′-azinobis(3-ethylbenzothiazoline-6-sulfonic acid)] were obtained from Sigma Chemical. Catechol (1,2-benzenediol), syringic acid (3,5-dimethoxy-4-hydroxybenzoic acid), chlorogenic acid [1,3,4,5-tetrahydroxycyclohexanecarboxylic acid 3-(3,4-dihydroxycinnamate)], (−)-epicatechin [(−)-*cis*-3,3′,4′,5,7-pentahydroxyflavane], gallic acid (3,4,5-trihydroxybenzoic acid), and ellagic acid (4,4′,5,5′,6,6′-hexahydroxydiphenic acid 2,6,2′,6′-dilactone) were obtained from Fluka, and caffeic acid (3,4-dihydroxycinnamic acid) was obtained from Aldrich. Stock solutions of the reducing substrates were prepared in 0.15 mM phosphoric acid to prevent autoxidation. The buffer used was 30 mM sodium phosphate buffer (pH 6.0−7.5).

Spectrophotometric Assays. Absorption spectra were recorded on a Perkin-Elmer Lambda 35 UV−vis spectrophotometer, at a scanning speed of 60 nm/s controlled by UV-Winlab software. The temperature was maintained at 25 °C using a Haake D16 circulating water bath with a heater/cooler and checked using a Cole-Parmer digital thermometer with a precision of 0.1 °C. Kinetic assays were also carried out with the above instruments following the appearance (kinetic enzymatic method) (*8*) or disappearance (nonenzymatic kinetic test) of $ABTS^{\bullet+}$ at $\lambda = 734$ nm [$\varepsilon = 15000/(M \times cm)$] (*18*). In the enzymatic kinetic method, the cuvette (final volume of 1 mL) contained 30 mM sodium phosphate buffer (pH 7.0), H_2O_2, and ABTS at a concentration at which POD is saturated by them (0.1 and 5 mM, respectively) (*17*), and the antioxidant was varied in the range specified in each figure. The reaction was started by adding enzyme (POD). In the nonenzymatic kinetic test, the cuvette (final volume of 1 mL) contained 30 mM sodium phosphate buffer (pH indicated in each figure) and ABTS at a concentration whereby POD is saturated (5 mM) (*17*). H_2O_2 was the limiting reagent and was totally consumed in each experiment after the addition of enzyme, generating the desired free radical. Once this free radical is generated, the reaction with the antioxidant (A) begins after the latter is added. Below, we describe in detail each of these methods.

Enzymatic Kinetic Method. The following six-step procedure is recommended to carry out this method.

Step 1. Select the experimental conditions. The initial concentration of ABTS, $[ABTS]_0$, should be high so that (i) there is a negligible variation of [ABTS] when ABTS evolves to $ABTS^{\bullet+}$ during the experiment (taking into consideration the value of K_m^{ABTS} (0.64 mM), a 5 mM concentration is suggested (*17*)) and (ii) the molecules of antioxidant (which could be substrates of the enzyme) should not have access to the enzyme (taking into account the low value of $K_m^{H_2O_2}$ (2.5 μM) (*17*), an initial concentration of H_2O_2, $[H_2O_2]_0$, of 0.1 mM should be chosen so that the enzyme is saturated by both substrates (ABTS and H_2O_2)). Note that the use of myoglobin has been reported (*19*); however, the ratio of the initial concentrations of ABTS and H_2O_2 was low, which led to deviations in the experimental measurements. The initial concentration of enzyme, $[E]_0$, should be such that, in the absence of antioxidant, it generates a quantity of radical acceptable with regard to its absorbance and which, in the presence of low concentrations of the same, gives rise to a measurable lag period outside the dead time of the measurement.

Step 2. Vary the initial concentration of antioxidant, A_0, so that it gives rise to short lag periods but well-defined with respect to the dead time of the measurement.

Step 3. Control the return to the steady state by referring to the parallelism of the straight lines. This is a fundamental test when using the enzymatic kinetic method.

Step 4. Analyze the lineal portion of the progress curves to determine V_0 (confirming the test) and τ, the lag period.

Step 5. Fit $V_0\tau$ versus $[A]_0$ by linear regression to determine the number of electrons (n, stoichiometric factor) (*13*, *15*, *20*).

Step 6. Calculate the effective concentration, EC50 [EC50 = 1/(2n)], and antioxidant capacity, ARP (ARP = 1/EC50), as shown in **Table 1**.

Nonenzymatic Kinetic Test. Step 1. Generate the free radical. First, radical $ABTS^{\bullet+}$ must be generated, for which several methods have been suggested: the chemical oxidation of ABTS with potassium persulfate solution (*12*, *13*) or enzymatically with POD/H_2O_2 (*17*). In this study, $ABTS^{\bullet+}$ is generated in the same reaction medium with POD/ABTS/H_2O_2, limiting H_2O_2, and a great excess of ABTS; the radical thus generated can be followed spectrophotometrically at $\lambda = 734$ nm [$\varepsilon = 15000/(M \times cm)$] or at $\lambda = 414$ nm [$\varepsilon = 30000/(M \times cm)$], the wavelength depending on any interferences that may exist.

Table 1. Characterization of Compounds with Monophasic Antioxidant Capacity

	primary antioxidant capacity		
substrate	n (electrons)	EC_p50	ARP_p
pyrogallol	5.81 ± 0.51	0.08 ± 0.01	12.51 ± 1.13
gallic acid	4.74 ± 0.42	0.11 ± 0.01	9.09 ± 1.01
catechol	2.91 ± 0.11	0.17 ± 0.01	5.88 ± 0.38
sinapinic acid	2.82 ± 0.11	0.18 ± 0.02	5.56 ± 0.21
BHA	2.82 ± 0.14	0.18 ± 0.02	5.56 ± 0.35
protocatechuic acid	2.26 ± 0.13	0.22 ± 0.02	4.55 ± 0.36
syringic acid	2.18 ± 0.12	0.23 ± 0.02	4.35 ± 0.21
L-ascorbic acid	2.01 ± 0.12	0.25 ± 0.03	4.00 ± 0.21
D-ascorbic acid	1.99 ± 0.16	0.25 ± 0.03	4.00 ± 0.25
Trolox	1.98 ± 0.12	0.25 ± 0.03	4.00 ± 0.24
ferulic acid	1.35 ± 0.09	0.37 ± 0.04	2.70 ± 0.10
p-hydroquinone	2.30 ± 0.11	0.38 ± 0.04	2.63 ± 0.19
vanillin	1.18 ± 0.06	0.42 ± 0.04	2.38 ± 0.21
L-cysteine	1.01 ± 0.05	0.49 ± 0.05	2.04 ± 0.12
phenol	0.95 ± 0.06	0.52 ± 0.05	1.92 ± 0.09
p-coumaric acid	0.66 ± 0.03	0.75 ± 0.08	1.33 ± 0.02
p-hydroxybenzoic acid	0.35 ± 0.02	1.42 ± 0.15	0.71 ± 0.01

Step 2. Choose the antioxidant concentration. The initial concentration of antioxidant should be such that a quantity of product (B) is generated, the evolution of which consumes a substantial quantity of free radical. Furthermore, the following must be fulfilled $n[A]_0 \ll [ABTS^{\bullet+}]_0$, so that free radical remains in excess. With regard to different antioxidants, the concentration of excess $ABTS^{\bullet+}$ must be the same.

Step 3. Select the initial concentration of free radical. The concentration of free radical ($[ABTS^{\bullet+}]_0$) generated must be greater than $n[A]_0$. For different antioxidants to be compared by the kinetic test, $[ABTS^{\bullet+}]_0 - n[A]_0 = [ABTS^{\bullet+}]$ should be equal in all cases; therefore, depending on the value of n, because $[A]_0$ is constant, $[ABTS^{\bullet+}]_0$ must be varied for each antioxidant studied.

Step 4. Generate the desired $[ABTS^{\bullet+}]_0$ value in the medium. Free radical is generated with the POD/H_2O_2/ABTS system. The H_2O_2 must be in defect with respect to ABTS and the stoichiometry should be $1H_2O_2$: $2ABTS^{\bullet+}$.

Step 5. React the free radical with the antioxidant. First, the desired concentration of $[ABTS^{\bullet+}]_0$ is generated, and then $[A]_0$ is added. The disappearance of free radical is measured spectrophotometrically.

Step 6. Analyze the progress curve by nonlinear fitting based on the initial fall (this corresponds to the primary antioxidant power) according to eq **4**. In this way, the parameters n_{app} and k_2^{app} are determined in the work conditions.

Step 7. Study the different antioxidants. Repeat steps 5 and 6 for each compound in the fixed experimental conditions, which are the same $[A]_0$ value and the same free radical in excess, that is, the same value of the difference $[ABTS^{\bullet+}]_0 - n[A]_0$.

RESULTS AND DISCUSSION

ABTS is a substrate of POD which, on oxidation, generates a quite stable radical cation, $ABTS^{\bullet+}$, a characteristic that has led to its use in kinetic studies of POD (*17*). In addition, we use ABTS to determine the total antioxidant status of foods, either generating it in situ with the POD/ABTS/H_2O_2 system and determining the lag period resulting from the presence of an antioxidant such as ascorbic acid (*8*) or applying a final point method, starting with a predetermined quantity of radical $ABTS^{\bullet+}$ (*18*). In both cases, at the working pH and with the compounds studied, the reaction was immediate and there was no subsequent evolution. However, two facts drew our attention: on the one hand, the appearance of a series of studies on the antioxidant capacity of polyphenols, together with the demonstration of the existence of slow chemical

Scheme 1

$$n\,\mathrm{ABTS}^{\bullet+} + \mathrm{A} \xrightarrow{k_1} n\,\mathrm{ABTS} + \mathrm{B}$$

reactions coupled to the process of initial oxidation (*15*, *20*−*22*), and, on the other, the consideration that many of these compounds are substrates of tyrosinase (catechins of green tea (*21*) or chlorogenic acid (*22*))). Taking these aspects into account, we consider that it is important to approach the characterization of the antioxidant capacity of polyphenols and related compounds using the POD/ABTS/H_2O_2 system.

Enzymatic Kinetic Method. The method is based on the accumulation of the radical ($ABTS^{\bullet+}$) generated by the POD/ABTS/H_2O_2 system according to

$$2\mathrm{ABTS} + \mathrm{H_2O_2} \xrightarrow[V_0]{\mathrm{POD}} 2\mathrm{H_2O} + 2\mathrm{ABTS}^{\bullet+} \qquad (1)$$

In these conditions, the system rapidly reaches the steady state with a velocity of V_0. If there is an antioxidant (A) in the medium, the free radical $ABTS^{\bullet+}$ could react with it according to **Scheme 1**. If the k_1 is high and the antioxidant concentration low, the velocity of accumulation of $ABTS^{\bullet+}$ returns to the steady state after a lag period to reach the same velocity V_0.

From eq **1** and **Scheme 1**, the balance of matter is

$$[\mathrm{ABTS}^{\bullet+}] = V_0 t - n[\mathrm{A}]_0 \qquad (2)$$

Figure 2A shows a series of assays of the activity of the POD/ABTS/H_2O_2 system in the presence of the antioxidant, Trolox. Recordings b−g of **Figure 2A** correspond to assays with increasing quantities of Trolox. Data analysis, according to eq **2**, gives the values of V_0 and τ, whereas the inset of **Figure 2A** confirms the linearity. From the slope the value of n, the stoichiometric factor, can be calculated. In this case, no chemical reactions coupled to the reaction of A with $ABTS^{\bullet+}$ exist, and so the parameters EC50 and the antioxidant capacity, ARP, can be calculated from the value of n (**Table 1**). The degree of parallelism between the straight lines is a test of the validity of the assay. **Figure 2B** shows the same experiments for L-ascorbic acid. **Table 1** shows a series of molecules characterized by this enzymatic method.

The following precautions should be taken in the application of the enzymatic kinetic method:

(a) Because the parallelism of the straight lines is the only way of validating the method, the velocity of the steady state must be the same, for which the substrates must vary as little as possible. In the case of ABTS, this is ensured because the radical $ABTS^{\bullet+}$ is reduced to ABTS. The other substrate, H_2O_2, can vary, but the POD/H_2O_2/ABTS system has the advantage that $K_m^{H_2O_2}$ is very small (*17*) and so the enzyme works at concentrations of H_2O_2 of 100 μM in zero-order kinetics. In this way, at low enzyme and antioxidant concentrations, curves like those shown in **Figure 2** are obtained.

(b) The antioxidant or its products are very powerful inhibitors of the enzyme, that is, they inhibit POD at very low concentrations; consequently, the parallelism shown in **Figure 2A** is not attained and the method cannot be applied.

(c) Due to possible competition of the antioxidant as substrate with the substrates of the enzyme, ABTS and H_2O_2, this situation is difficult because the enzyme is saturated by ABTS and H_2O_2. Moreover, using data from refs *17* and *23*, we can compare the pseudo-first-order rate constant of the attack of compound II on the ABTS and phenol. Bearing in mind that $k_5 = 7.82 \times 10^4$ 1/(M × s) and $k_5^* = 2.5 \times 10^5$ 1/(M × s) and because $[ABTS]_0 = 5 \times 10^{-3}$ M and $[phenol]_0 = 5 \times 10^{-6}$ M, the pseudo-first-order rate constant will be $k_5 \times [ABTS]_0$ and $k_5^* \times [phenol]_0$ for ABTS and phenol, respectively. The relation of the pseudo-first-order rate constants will be 200, so that the antioxidant probably does not interfere in these assays.

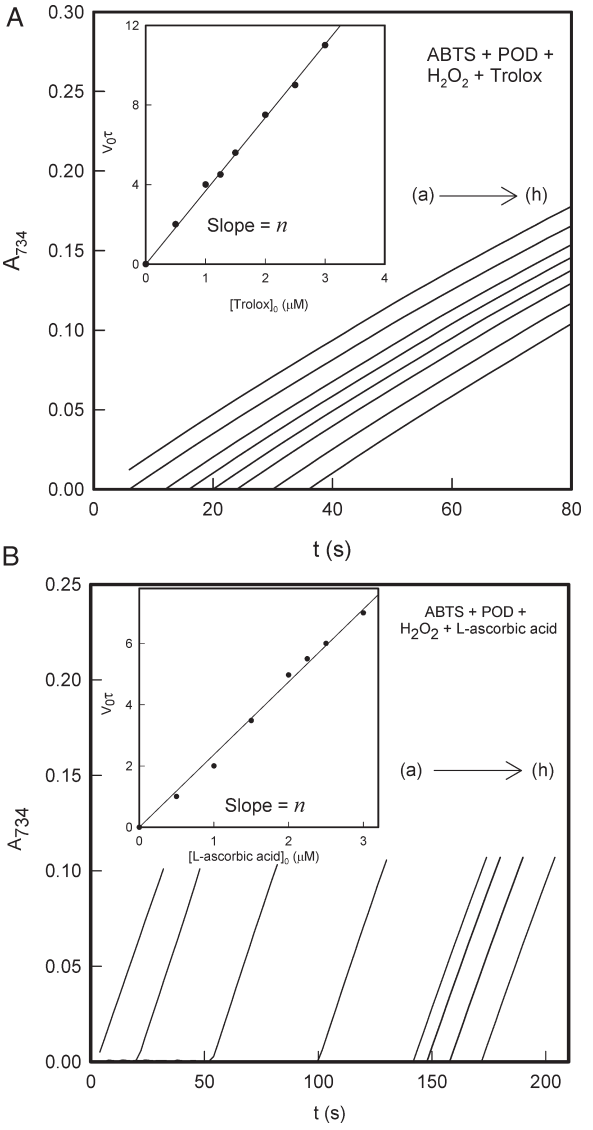

Figure 2. (**A**) Characterization of compounds with monophasic antioxidant activity. Time course of $ABTS^{\bullet+}$ accumulation in the presence of POD (0.25 nM), ABTS (5 mM). and H_2O_2 (0.1 mM) in sodium phosphate buffer 30 mM (pH 6.5), at 25 °C. The reaction was followed by measuring ΔA_{734}. Recording a, control; recordings b−h, time courses of the same reaction as in (a) but with 0.5, 1.0, 1.25, 1.5, 2.0, 2.5, and 3 μM Trolox added, respectively. (Inset) Representation of $V_0\tau$ versus $[Trolox]_0$. (**B**) Characterization of compounds with monophasic antioxidant activity. Time course of $ABTS^{\bullet+}$ accumulation in the presence of POD (0.25 nM), ABTS (5 mM), and H_2O_2 (0.1 mM) in sodium phosphate buffer 30 mM (pH 6.5), at 25 °C. The reaction was followed by measuring ΔA_{734}. Recording a, control; recordings b−h, time courses of the same reaction as in (a) but with 0.5, 1.0, 1.5, 2.0, 2.25, 2.5, and 3 μM L-ascorbic acid added, respectively. (Inset) Representation of $V_0\tau$ versus $[L\text{-ascorbic acid}]_0$.

(d) Deviations in the parallelism increase as the concentration of antioxidant in the medium increases. This is clear from **Figure 3A**, when quercetin acts as antioxidant, and indicates the secondary antioxidant capacity. Note that in this case the experiments at very low antioxidant concentrations fulfill the parallelism and, from the data analysis, a first estimation of the value of n, the stoichiometric factor, can be obtained **Figure 3A**, inset.

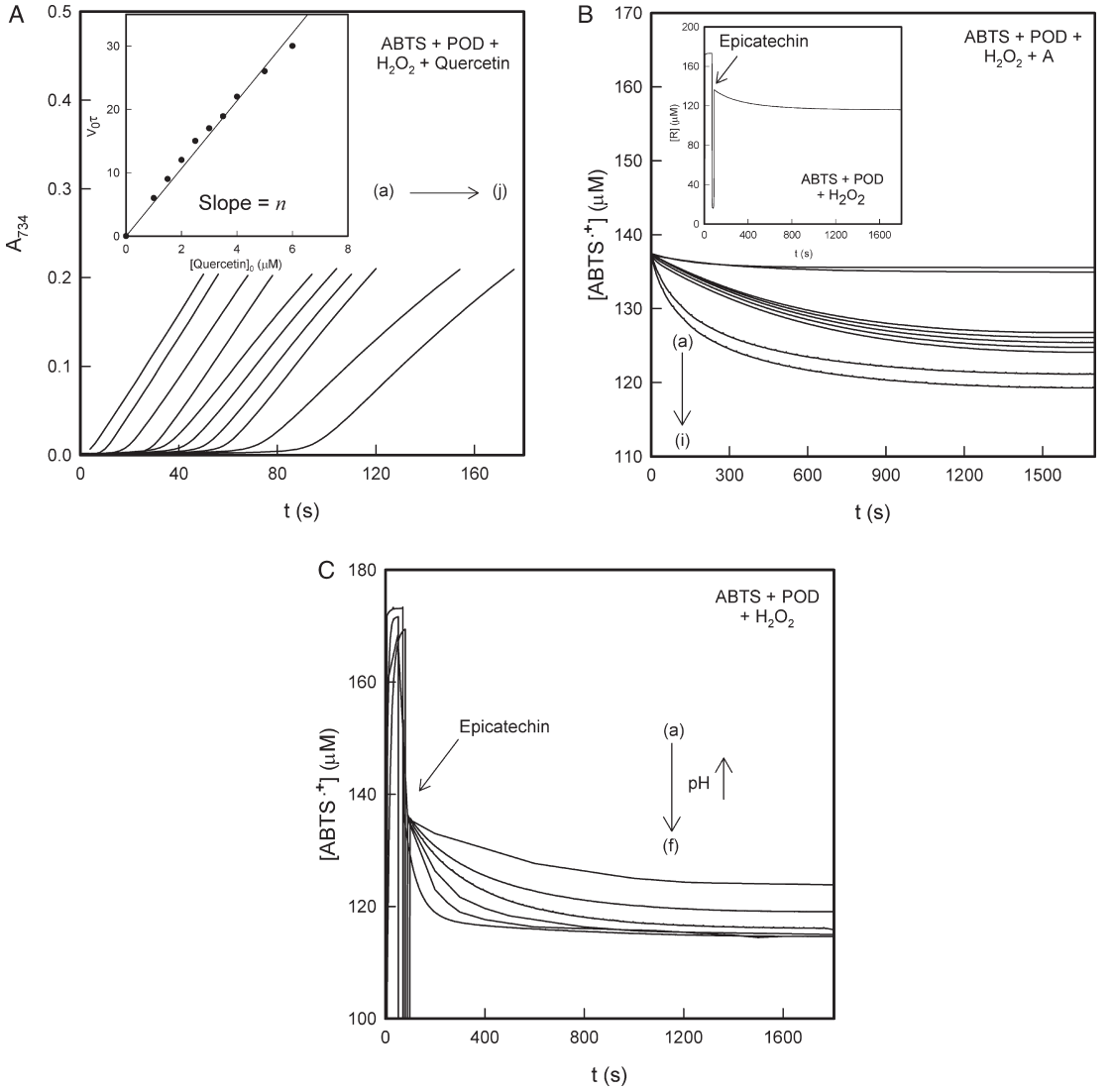

Figure 3. (**A**) Characterization of compounds with biphasic antioxidant activity: time course of $ABTS^{\bullet+}$ accumulation in the presence of POD (0.25 nM), ABTS (5 mM) and H_2O_2 (0.1 mM) in sodium phosphate buffer 30 mM (pH 6.5), at 25 °C. The reaction was followed by measuring ΔA_{734}. Recording a, control; recordings b−j, time courses of the same reaction as in (a) but with 1.0, 1.5, 2.0, 2.5, 3.0, 3.5, 4.0, 5.0, 6.0 μM quercetin added, respectively. (Inset) Representation of $V_0\tau$ versus $[quercetin]_0$. (**B**) Characterization of compounds with biphasic antioxidant activity: nonenzymatic kinetic test to calculate n_{app} and k_2^{app}. The buffer used was 30 mM sodium phosphate buffer (pH 7.0), at 25 °C. The radical $ABTS^{\bullet+}$ was generated with the POD/ABTS/H_2O_2 system. The concentration of POD was 0.3 nM, $[ABTS]_0$ = 5 mM, and the $[H_2O_2]_0$ values (μM) were (a) rutin, 71; (b) eugenol, 64; (c) chlorogenic acid, 67; (d) quercetin, 73; (e) guaiacol, 65; (f) ellagic acid, 75; (g) caffeic acid, 63; (h) catechin, 68; and (i) epicatechin, 70. At t = 0, a 5 μM concentration of antioxidant was added and the changes in absorbance at 734 nm were recorded from the initial fall. (Inset) Recording of the change in absorbance at 734 nm from the beginning of the reaction in the case of epicatechin. (**C**) Characterization of compounds with biphasic antioxidant activity: study of the pH effect on epicatechin antioxidant capability. The buffers used were 30 mM sodium phosphate buffer pH (a) 6.25, (b) 6.5, (c) 6.75, (d) 7.0, (e) 7.25, and (f) 7.5. The concentrations (μM) of epicatechin and $ABTS^{\bullet+}$ were 5 and 150, respectively. The radical $ABTS^{\bullet+}$ was generated with the POD/ABTS/H_2O_2 system. The concentrations of POD and H_2O_2 were 0.3 nM and 75 μM, respectively. At t = 0, the antioxidant epicatechin was added at 5 μM. The reaction was recorded at 734 nm from the initial fall.

Scheme 2

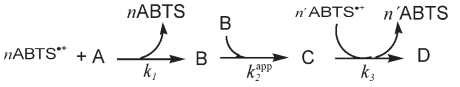

Scheme 3

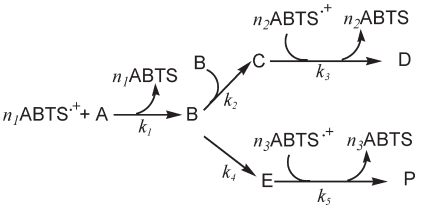

(e) The fact that the behavior of an antioxidant fits the enzymatic kinetic method does not mean that no chemical reactions exist subsequent to the formation of antioxidant radical, but that, if they do exist, they must be very rapid (see **Schemes 2** and **3**), the system returning in little time to the steady state (**Figure 2**).

The compounds described in **Table 1** fit the enzymatic kinetic method very well and should therefore reflect their antioxidant capacity because of their chemical structure. Such is the case with many of them, that is, the n obtained experimentally corresponds to what might be expected from their structure; for example, in the case of *p*-hydroquinone, protocatechuic acid, L-ascorbic acid,

D-ascorbic acid, L-cysteine, or phenol. Other compounds, such as *p*-hydroxybenzoic acid or *p*-coumaric acid, have much lower values also due to their chemical structures, in which withdrawing groups in para position diminish the capacity to be oxidized to the corresponding phenoxyl radicals. Finally, there are compounds that show high *n* values and therefore high ARP values (**Table 1**). For example, it has been proposed that the main oxidation mechanism for catechol involves donation of a single electron to the radical cation, resulting in the formation of a semiquinone, which can donate a further electron to form the quinone. In turn, this can suffer nucleophilic attack by the OH group, followed by a new oxidation before being polymerized (*24*); pyrogallol shows good antioxidant capacity but has also been used to form superoxide anions, meaning that it also acts as a pro-oxidant (*25*); gallic acid (as seen by NMR), when it reacts with DPPH radical, rapidly forms dimers from galloquinones, which explains its higher *n* value of 3 (*25*); in the case of ferulic, syringic, and sinapinic acids, which have been described as having a higher antioxidant capacity than *p*-coumaric acid, the presence of methoxyl groups in the ortho position means that the OH groups are more easily oxidizable and that they also stabilize the phenoxyl radical, which may react with another molecule of $ABTS^{\bullet+}$, explaining why the *n* value would be greater than 1 (*24*); BHA contains a methoxy group in the para position with respect to the OH group and a *tert*-butyl group on the ortho position; this renders it easily oxidizable, perhaps acting through a mechanism similar to that described for ferulic acid, and as may occur in Trolox due to the effect of the methyl groups. The interpretation of these results (compounds with a higher than expected value of *n*) should consider the possibility of rapid coupled chemical reactions (i.e., **Schemes 2** and **3**), in which free radical is consumed after an initial reaction of the compound with the free radical. This suggests that the chemical structure of a compound provides only an approximate idea of its antioxidant capacity toward a given free radical, as is the case with the oxidation/reduction potentials that, as has been seen, do not exactly correlate with the antioxidant capacity (*11*).

When an antioxidant is studied by the enzymatic kinetic method and deviations are observed such as those in **Figure 3A**, the compound has secondary antioxidant capacity and a nonenzymatic kinetic test is proposed, the basis of which consists of making the radical $ABTS^{\bullet+}$ be in excess with regard to the concentration of the antioxidant used and of following the decrease in absorbance of the free radical with time. This decrease in absorbance will have two phases: first, a very rapid one corresponding to the antioxidant reacting with the free radical (primary antioxidant capacity) and reflecting the *n* value, followed by coupled chemical reactions of the type indicated in **Schemes 2** and **3** (second order) as the radical continues reacting with the products until the reaction is exhausted.

The literature describes slow dimerization reactions during the reaction of the products of the antioxidant with the free radical (*11*−*13*). In our experiments with compounds showing a secondary antioxidant capacity, we demonstrated the second-order dependence of the disappearance of free radical mainly. However, the kinetics is complex, and only if the simplification of **Scheme 2** is accepted can an analytical expression be deduced to fit the experimental data. Although offering only apparent parameters and constants, this fit can be used for comparative purposes.

If the reactions of radical $ABTS^{\bullet+}$ with A and C are rapid, so that $k_2^{app} \ll k_1, k_3$, **Scheme 2** is kinetically equivalent to

$$2B \xrightarrow{k_2^{app}} D \qquad (3)$$

It can be demonstrated that the expression of the variation of free radical with time corresponds to the expression

$$[ABTS^{\bullet+}] = [ABTS^{\bullet+}]_\infty + \frac{ab}{b+t} \qquad (4)$$

with $a = n_{app}[A]_0$ and $b = 1/(k_2^{app}[A]_0)$.

A fit of the experimental $[ABTS^{\bullet+}]$ values to eq **4** gives $[ABTS^{\bullet+}]_\infty$, *a*, and *b*, which enables n_{app} and k_2^{app} (second-order rate constant) to be calculated. The velocity of the process is governed by k_2^{app}, but, in this case, being a second-order reaction (limiting), the $t_{1/2}^{app}$ can be defined, after reaction of the radical with the antioxidant, as the time necessary for the free radical (in excess) to fall to 50% of its total fall, at a fixed initial antioxidant concentration. The parameter $t_{1/2}^{app}$ depends on the concentration of antioxidant, according to $t_{1/2}^{app} = 1/(k_2^{app}[A]_0)$. Therefore, to characterize an antioxidant of this nature, the experiments to calculate the time factor should not be carried out with the particular EC_T50 value of each molecule as suggested in refs *15* and *16*, but at the same concentration of A, so that $t_{1/2}^{app} = 1/(k_2^{app} \times [A]_0)$ is a comparative parameter.

From the values obtained for n_{app} and k_2^{app}, the apparent kinetic antiradical efficiency (KAE_{app}) can be defined as $KAE_{app} = 1/(EC_T50_{app} \times t_{1/2}^{app})$, which includes both effects (concentration and time). Note that to compare the antioxidant capacity of different compounds in their reaction with the radical $ABTS^{\bullet+}$, the most interesting parameters for the primary antioxidant capacity and for the total antioxidant capacity are ARP_p and KAE_{app}, respectively.

The expression for the new parameter proposed in this study, the apparent kinetic antiradical efficiency (KAE_{app}), takes the form

$$KAE_{app} = \frac{1}{EC_T50_{app} \times t_{1/2}^{app}} = 2(n + n_{app})k_2^{app}[A]_0 \qquad (5)$$

This is equivalent to the number of electrons transferred per second by a 1 M antioxidant solution.

If the kinetic study points to second-order kinetic regardless of the concentration of free radical, analysis of the data provides the absolute values of n_{app} and k_2^{app}, which permits the real secondary antioxidant power to be characterized. In our case, in all of the compounds shown in **Table 2** there is a kinetic dependence on the concentration of free radical and, therefore, only the nonenzymatic kinetic test can be used to compare the different molecules, for which we propose the experimental design described under Material and Methods.

The enzymatic kinetic method was applied to the compounds shown in **Tables 1** and **2**. Those in **Table 2** deviate from linearity, as shown in **Figure 3A** for quercetin, meaning that they present a secondary antioxidant capacity. The nonenzymatic kinetic test was applied to this group of compounds, using the experimental conditions specified in **Figure 3B**. The same figure shows the spectrophotometric recordings for the disappearance of free radical with time. Fitting, by nonlinear regression, of these curves to eq **4** gives the n_{app} and k_2^{app} (see **Table 2**). From the values obtained for n_{app} with respect to the secondary antioxidant, the parameters EC_s50_{app} and ARP_s^{app}, corresponding to the secondary effective concentration and secondary antiradical power, can be calculated by comparison with the primary antioxidant capacity and, by extension, the total antioxidant capability in these assay conditions can be characterized (see **Table 2**).

The data shown in **Table 2** for the primary and secondary antioxidant capacities are better reflected in the new parameter we propose in this study, the apparent antiradical kinetic efficiency (KAE_{app}), which includes the information referring to the

Table 2. Characterization of Compounds with Biphasic Antioxidant Capacity

	primary antioxidant capacity			secondary antioxidant capacity			total antioxidant capacity				
substrate	n (electrons)	EC_p50	ARP_p	n_{app} (electrons)	EC_s50_{app}	ARP_s^{app}	$n + n_{app}$ (electrons)	EC_T50_{app}	ARP_T^{app}	k_2^{app} (M^{-1} s^{-1})	$KAE_{app} \times 10^{-4}$ (electrons/s)[a]
epicatechin	5.2 ± 0.5	0.09 ± 0.01	11.1 ± 0.4	7.2 ± 0.8	0.07 ± 0.01	14.4 ± 0.7	12.3 ± 1.3	0.04 ± 0.01	24.6 ± 1.3	2089 ± 27	5.1 ± 0.4
catechin	4.7 ± 0.4	0.11 ± 0.01	9.1 ± 0.1	6.9 ± 0.8	0.07 ± 0.01	14.3 ± 0.8	11.6 ± 1.2	0.04 ± 0.01	25.0 ± 1.2	2025 ± 25	4.7 ± 0.5
quercetin	6.4 ± 0.5	0.08 ± 0.01	12.5 ± 0.9	5.6 ± 0.6	0.09 ± 0.01	11.1 ± 0.7	12.0 ± 1.1	0.04 ± 0.01	25.0 ± 1.5	1907 ± 21	4.6 ± 0.8
ellagic acid	7.6 ± 0.7	0.07 ± 0.01	14.3 ± 0.6	6.2 ± 0.7	0.08 ± 0.01	12.5 ± 0.7	13.8 ± 1.4	0.03 ± 0.01	33.3 ± 1.9	1348 ± 15	3.7 ± 0.5
guaiacol	3.1 ± 0.3	0.16 ± 0.01	6.3 ± 0.4	5.9 ± 0.6	0.08 ± 0.01	12.5 ± 0.6	9.0 ± 0.9	0.05 ± 0.01	20.0 ± 1.1	1997 ± 20	3.6 ± 0.4
chlorogenic acid	4.1 ± 0.3	0.12 ± 0.01	8.3 ± 0.4	5.3 ± 0.6	0.09 ± 0.01	11.1 ± 0.6	9.4 ± 0.9	0.05 ± 0.01	20.0 ± 1.2	1857 ± 29	3.5 ± 0.6
caffeic acid	2.5 ± 0.2	0.19 ± 0.02	5.3 ± 0.2	7.0 ± 0.7	0.07 ± 0.01	14.3 ± 0.8	9.5 ± 0.9	0.05 ± 0.01	20.0 ± 1.0	1359 ± 14	2.6 ± 0.3
rutin	5.6 ± 0.5	0.09 ± 0.01	11.1 ± 0.7	1.4 ± 0.2	0.35 ± 0.03	2.8 ± 0.1	7.0 ± 0.7	0.07 ± 0.01	14.3 ± 0.9	1150 ± 17	1.7 ± 0.3
eugenol	2.8 ± 0.2	0.17 ± 0.01	5.9 ± 0.1	1.5 ± 0.2	0.33 ± 0.03	3.03 ± 0.1	4.3 ± 0.4	0.11 ± 0.01	9.1 ± 0.6	1100 ± 19	0.9 ± 0.2

[a] For a 1 M antioxidant solution.

Table 3. Effect of pH on the Biphasic Antioxidant Capacity for Epicatechin

	primary antioxidant capacity			secondary antioxidant capacity			total antioxidant capacity				
pH	n (electrons)	EC_p50	ARP_p	n_{app} (electrons)	EC_s50_{app}	ARP_s^{app}	$n + n_{app}$ (electrons)	EC_T50_{app}	ARP_T^{app}	k_2^{app} (M^{-1} s^{-1})	$KAE_{app} \times 10^{-4}$ (electrons/s)[a]
6.25	5.2 ± 0.5	0.09 ± 0.01	11.1 ± 0.4	6.899 ± 0.324	0.07 ± 0.01	13.80 ± 0.97	12.10 ± 1.19	0.04 ± 0.01	24.20 ± 1.98	229 ± 11	5.52 ± 0.65
6.50	5.2 ± 0.5	0.09 ± 0.01	11.1 ± 0.4	7.082 ± 0.393	0.07 ± 0.01	14.16 ± 0.89	12.28 ± 1.02	0.04 ± 0.01	24.56 ± 1.58	709 ± 12	17.41 ± 1.84
6.75	5.2 ± 0.5	0.09 ± 0.01	11.1 ± 0.4	7.105 ± 0.593	0.08 ± 0.01	14.21 ± 0.89	12.30 ± 0.99	0.04 ± 0.01	24.60 ± 1.38	1910 ± 61	46.71 ± 4.10
7.00	5.1 ± 0.5	0.09 ± 0.01	11.1 ± 0.4	7.223 ± 0.810	0.07 ± 0.01	14.41 ± 0.71	12.31 ± 1.30	0.04 ± 0.01	24.62 ± 1.33	2089 ± 27	51.00 ± 4.03
7.25	5.2 ± 0.5	0.09 ± 0.01	11.1 ± 0.4	7.190 ± 0.726	0.07 ± 0.01	14.28 ± 1.12	12.39 ± 1.26	0.04 ± 0.01	24.68 ± 1.87	2250 ± 14	55.72 ± 4.58
7.50	5.2 ± 0.5	0.09 ± 0.01	11.1 ± 0.4	7.651 ± 0.798	0.06 ± 0.01	16.67 ± 0.87	12.85 ± 1.98	0.04 ± 0.01	25.70 ± 1.99	2502 ± 17	64.32 ± 6.99

[a] For a 1 M antioxidant solution.

effective concentration and the time the process takes, but through $t_{1/2}^{app}$ (see **Table 2**).

In the case of caffeic and chlorogenic acids, dimerizations (*12*, *13*) have been proposed, whereas dimerizations and reducing nucleophilic attacks have been proposed in the case of catechin and epicatechin (*26*), although in the latter cases the primary antioxidant capacity corresponds to their chemical structure. Furthermore, because the k_2^{app} is high, the KAE_{app} value is the highest of all those studied in this work, meaning that epicatechin is the strongest antioxidant. In the case of quercetin, several types of reactions have been described (*27*); for example, depending on the type of oxidant, quercetin has been demonstrated to originate different products, including heterodimers, which would explain the high number of electrons (*27*). For the polyphenol rutin, a slightly lower result than for quercetin is to be expected, as can be seen from the value of n described in **Table 2**, although the subsequent polymerization is presumably less favored because of the glycoside chain (*26*). The case of guaiacol and eugenol is of note because of the high n value, because they are monophenols, but both give rise to coupled reactions that increase their antioxidant capacity. With regard to guaiacol, tetraguaiacol is formed during its oxidation. Finally, the high antioxidant capacity shown by ellagic acid can be attributed to rapid dimerization reactions (*28*).

Considering the data of **Table 2** and in light of this new parameter, it can be appreciated how ellagic acid, which shows higher electron consumption, passes to fourth place, because its k_2^{app} is the lowest of all. However, although the number of electrons consumed is lower, catechin passes to second place because of its high k_2^{app}.

For the test to be comparable for different antioxidants, the initial concentration of free radical should be varied so that the difference between this initial value and that consumed in the primary antioxidant capacity by the reaction with the antioxidant remains constant. From this kinetic study, the apparent second-order rate constant k_2^{app} can be calculated along with the number of electrons consumed in this secondary antioxidant capacity n_{app} in the study conditions used. This additional information permits us to define a new parameter, the apparent kinetic antiradical efficiency (KAE_{app}), which provides information on the effective concentration (EC_T50_{app}) and $t_{1/2}^{app}$. Once the radical has reacted with the antioxidant, this $t_{1/2}^{app}$ may be defined as the time necessary for the free radical in excess to fall to 50% of its total decline, at a fixed initial antioxidant concentration. This new parameter serves to compare different antioxidants if the kinetic conditions described above are fulfilled.

Study of the pH Effect on the Antioxidant Capacity. The literature describes how the antioxidant capacity of different molecules varies with the pH (*11*). In this work, we have studied the effect of pH on the antioxidant capacity of epicatechin. The experimental recordings of the disappearance of free radical are shown in **Figure 3C**. Note that the primary antioxidant capacity does not vary (see **Table 3**) and that at pH < 5 the chemical evolution of the coupled reactions is very slow (data not shown). However, the secondary antioxidant capacity increases as the pH (pH values of 6.25−7.5) of the medium increases due to the increasingly strong coupled chemical reactions, which lead to an increasing k_2^{app} (the apparent second-order rate constant that governs the process). This means that the KAE_{app} increases with pH (**Table 3**). For comparison purposes, the antioxidant capacities of the different compounds should be studied at the same pH value.

On the other hand, the formal redox potential of $ABTS^{\bullet+}$/ABTS is 0.490 V (*29*), whereas for $DPPH^{\bullet}$/DPPH it is 0.340 V (*30*), when both redox pairs are studied in a glassy carbon electrode and are expressed versus Ag/AgCl reference electrode (pH 7.0), meaning that the former system is applicable to a much greater number of antioxidants. **Figure 4** shows the greater power of $ABTS^{\bullet+}$ because the number of electrons transferred is slightly higher with the series of molecules studied.

In conclusion, this study proposes a kinetic method for characterizing different antioxidants and a nonenzymatic kinetic

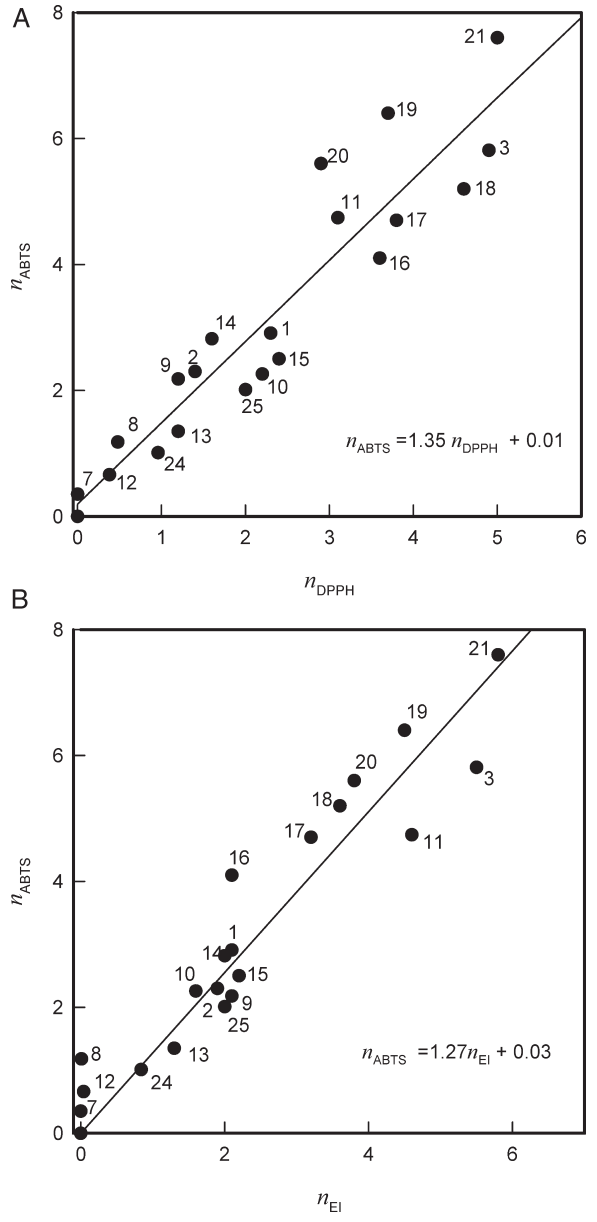

Figure 4. (**A**) Correlation of the number of electrons obtained by the ABTS method (n_{ABTS}) and by the DPPH method (n_{DPPH}), using data from ref *13*. (**B**) Correlation of the number of electrons yielded by different antioxidants obtained by the ABTS method (n_{ABTS}) with the number determined by flow-column electrolysis (n_{EI}) at a slower flow rate (0.05 mL min^{-1}), using data from ref *22*. The molecules were (1) catechol, (2) *p*-hydroxyquinone, (3) pyrogallol, (7) *p*-hydroxybencoic acid, (8) vanillin, (9) syringic acid, (10) protocatechuic acid, (11) gallic acid, (12) *p*-coumaric acid, (13) ferulic acid, (14) sinapinic acid, (15) caffeic acid, (16) chlorogenic acid, (17) catechin, (18) epicatechin, (19) quercetin, (20) rutin, (21) ellagic acid, (24) L-cysteine, and (25) L-ascorbic acid.

test. The enzymatic method uses POD, ABTS, and H_2O_2 to generate the radical ABTS$^{\bullet+}$ in situ. The kinetic test uses the ABTS$^{\bullet+}$ previously generated with POD. The combination of both can be used to characterize and compare the action of a series of antioxidants. We introduce the concept of primary antioxidant power (at short times) and secondary antioxidant power (at longer times) through the values of the number of electrons n and n_{app} for each process and the values EC_p50 and ARP_p for the first process and of EC_s50_{app} and ARP_s^{app} for the second process. From these values, the total values of the process, EC_T50_{app} and ARP_T^{app}, can be obtained. An experimental design is presented, which enables the value of the apparent second-order rate constant of the limiting step (k_2^{app}) to be obtained. Finally, all of the information obtained gives a new parameter, which we denominate the apparent kinetic antioxidant efficiency (KAE_{app}), which is the inverse of the product of the EC_T50_{app} and $t_{1/2}^{app}$ of the reaction and related directly with the total efficient concentration and time that the process takes. The parameter KAE_{app} is useful for comparing antioxidants.

ABBREVIATIONS USED

Species and Concentrations: ABTS, 2,2′-azinobis(3-ethylbenzothiazoline-6-sulfonic acid); ABTS$^{\bullet+}$, 2,2′-azinobis(3-ethylbenzothiazoline-6-sulfonic acid) radical cation; Phe-OH, phenolic compound; [ABTS$^{\bullet+}$], instantaneous concentration of ABTS$^{\bullet+}$; [ABTS$^{\bullet+}$]$_0$, initial concentration of ABTS$^{\bullet+}$; [ABTS$^{\bullet+}$]$_\infty$, remaining concentration of ABTS$^{\bullet+}$ at $t \rightarrow \infty$; A, antioxidant; [A]$_0$, initial concentration of A; B, product of the reaction of ABTS$^{\bullet+}$ with A; [B], instantaneous concentration of B; C, product of the reaction of B + B (second order); [C], instantaneous concentration of C; D, product of the reaction of C with ABTS$^{\bullet+}$; [D], instantaneous concentration of D; E, product of the evolution of B (first order); [E], instantaneous concentration of E; P, product of the reaction of E with ABTS$^{\bullet+}$; [P], instantaneous concentration of P.

Parameters and Kinetic Constants: n, number of electrons yielded by the antioxidant, which coincides with the number of radical molecules consumed by electron-donating action of one molecule of A; n', number of electrons yielded by the antioxidant, which coincides with the number of radical molecules consumed by electron-donating action by one molecule of C in the assay conditions; n_{app}, number of electrons yielded by the antioxidant, which coincides with the number of radical molecules consumed by electron-donating action during the evolution of one molecule of the product of the reaction of ABTS$^{\bullet+}$ with A or its evolution in the assay conditions used; τ, lag period; EC50, effective concentration, EC50 = 1/(2n), and is defined as the ratio between the concentration of antioxidant that decreases the concentration of radical by 50%; ARP, antioxidant or antiradical power, ARP = 2n; EC_p50, primary effective concentration; ARP_p, primary antiradical power; EC_s50_{app}, apparent secondary effective concentration; ARP_s^{app}, apparent secondary antiradical power; EC_T50_{app}, apparent total effective concentration; ARP_T^{app}, apparent total antiradical power; $n + n_{app}$, total number of electrons yielded by the antioxidant, which coincides with the number of radical molecules consumed by electron-donating action of one molecule of A, during its evolution in the kinetic conditions described in the assay conditions used; k_2^{app}, apparent rate constant of the limiting step of the coupled chemical reactions; $t_{1/2}^{app}$, half-life of the reaction, $t_{1/2}^{app} = 1/(k_2^{app}[A]_0)$; k_d^{app}, apparent decomposition constant of the radical ABTS$^{\bullet+}$; KAE_{app}, apparent kinetic antiradical efficiency, $KAE_{app} = 1/(EC_T50_{app}\ t_{1/2}^{app})$; T_{EC50}, time needed to reach steady state at the concentration corresponding to EC50; AE, antiradical efficiency, AE = 1/(EC50 × T_{EC50}).

Supporting Information Available: Kinetic analysis of the enzymatic kinetic method and description of the nonenzymatic kinetic test. This material is available free of charge via the Internet at http://pubs.acs.org.

LITERATURE CITED

(1) Rice-Evans, C. A.; Miller, N. J.; Paganga, G. Antioxidant properties of phenolic compounds. *Trends Plant Sci.* **1997**, *2*, 152–159.
(2) Huang, D.; Ou, B.; Prior, R. L. The chemistry behind antioxidant capacity assays. *J. Agric. Food Chem.* **2005**, *53*, 1841–1856.

(3) Apak, R.; Guclu, K.; Demirata, B.; Ozyurek, M.; Celik, S. E.; Bektasoglu, B.; Berker, K. I.; Ozyurt, D. Comparative evaluation of various total antioxidant capacity assays applied to phenolic compounds with the CUPRAC assay. *Molecules* **2007**, *12*, 1496–1547.
(4) Brand-Williams, W.; Cuvelier, M. E.; Berset, C. Use of a free radical method to evaluate antioxidant activity. *Lebensm.-Wiss. -Technol.* **1995**, *28*, 25–30.
(5) Miller, N. J.; Rice-Evans, C.; Davies, M. J.; Gopinethan, V.; Milner, A. A novel for measuring antioxidant capacity and its application to monitoring the antioxidant status in premature neonates. *Clin. Sci.* **1993**, *84*, 407–412.
(6) Rice-Evans, C. A.; Miler, N. J.; Badwell, P. G.; Bramley, P. M.; Pidham, J. B. The relative antioxidant activities of plant-derived polyphenolic flavonoids. *Free Radical Res.* **1995**, *22*, 375–383.
(7) Rice-Evans, C. A.; Miler, N. J. In *Methods in Enzymology*. *Oxygen Radicals in Biological Systems*; Packer, L., Ed.; Academic Press: New York,1994; Vol. 234, pp 279−293.
(8) Arnao, M. B.; Cano, A.; Hernandez-Ruiz, J.; Garcia-Canovas, F.; Acosta, M. Inihibition by L-ascorbic acid and others antioxidants of the 2,2′-azinobis(3-ethylbenzthiazoline-6-sulfonic acid) oxidation catalyzed by peroxidase: a new approach for determining total antioxidant status of foods. *Anal. Biochem.* **1996**, *236*, 255–261.
(9) Re, R.; Pellegrini, N.; Proteggete, A.; Pannala, A.; Yang, M.; Rice-Evans, C. Antioxidant activity applying an improved ABTS radical cation decolorization assay. *Free Radical Biol. Med.* **1999**, *26*, 1231–1237.
(10) Peyrat-Maillard, M. N.; Bonnely, S.; Berset, C. Determination of the antioxidant activity of phenolic compounds by coulometric detection. *Talanta* **2000**, *51*, 709–716.
(11) Hotta, H.; Sakamoto, H.; Nagano, S.; Tsujino, Y. Unusually large number of electrons for the oxidation of polyphenolic antioxidants. *Biochim. Biophys. Acta* **2001**, *1526*, 159–167.
(12) Hotta, H.; Ueda, M.; Nagano, S.; Tsujino, Y.; Kojama, J.; Osakai, T. Mechanistic study of the oxidation of caffeic acid by digital simulation of cyclic voltammograms. *Anal. Biochem.* **2002**, *303*, 66–72.
(13) Hotta, H.; Nagano, S.; Ueda, M.; Tsujino, Y.; Kojama, J.; Osakai, T. Higher radical scavenging activities of polyphenolic antioxidants can be ascribed to chemicals reactions following their oxidation. *Biochim. Biophys. Acta* **2002**, *1572*, 123–132.
(14) Sanchez-Moreno, C.; Larrauri, J. A.; Saura-Calixto, F. A procedure to measure the antiradical efficiency of polyphenols. *J. Sci. Food Agric.* **1998**, *76*, 270–276.
(15) Villaño, D.; Fernandez-Pachon, M. S.; Moyá, M. L.; Troncoso, A. M.; Garcia-Parrilla, M. C. Radical scavenging ability of polyphenolic compounds towards DPPH free radical. *Talanta* **2007**, *71*, 230–235.
(16) Oman, A. M.; Wong, K. K. Y.; Fernyhough, A. ABTS radical-driven oxidation of polyphenols: isolation and structural elucidation of covalent adducts. *Biochem. Biophys. Res. Commun.* **2006**, *346*, 321–329.
(17) Rodríguez-López, J. N.; Gilabert, M. A.; Tudela, J.; Thorneley, R. N. F.; García-Cánovas, F. Reactivity of horseradish peroxidase compound II toward substrates: kinetic evidence for a two-step mechanism. *Biochemistry* **2000**, *39*, 13201–13209.
(18) Cano, A.; Hernandez-Ruiz, J.; Garcia-Canovas, F.; Acosta, M.; Arnao, M. B. An end-point method for estimation of the total antioxidant activity in plant material. *Phytochem. Anal.* **1998**, *9*, 196–202.
(19) Yu, T. W.; Ong, C. N. Lag-time measurement of antioxidant capa-01wcity using myoglobin and 2,2′-azinobis(3-ethylbenzthiacoline-6-sulfonic acid): rationale, application and limitation. *Anal. Biochem.* **1999**, *275*, 217–223.
(20) Foti, M. C.; Daquino, C.; Geraci, C. Electron-transfer reaction of cinnamic acids and their methyl esters with the DPPH• radical in alcoholic solutions. *J. Org. Chem.* **2004**, *69*, 2309–2314.
(21) Munoz-Munoz, J. L.; Garcia-Molina, F.; Molina-Alarcon, M.; Tudela, J.; Garcia-Canovas, F.; Rodriguez-Lopez, J. N. Kinetic characterization of the enzymatic and chemical reactions of the catechins in green tea. *J. Agric. Food Chem.* **2009**, *56*, 435–444.
(22) Munoz, J.; Garcia-Molina, F.; Varon, R.; Rodriguez-Lopez, J. N.; Garcia-Ruiz, P. A.; Garcia-Canovas, F.; Tudela, J. Kinetic characterization of the oxidation of chlorogenic acid by polyphenol oxidase and peroxidase. Characteristics of the *o*-quinone. *J. Agric. Food Chem.* **2007**, *55*, 920–928.
(23) Gilabert, M. A.; Hiner, A. N.; Garcia-Ruiz, P. A.; Tudela, J.; Garcia-Molina, F.; Acosta, M.; Garcia-Canovas, F.; Rodríguez-Lopez, J. N. Differential substrate behaviour of phenol and anilines derivatives during oxidation by horseradish peroxidase: kinetic evidence for a two-step mechanism. *Biochim. Biophys. Acta* **2004**, *1699*, 235–243.
(24) Sekher Pannala, A.; Chan, T. S.; O'Brien, P. J.; Rice-Evans, C. A. Flavonoid B-ring chemistry and antioxidant activity: fast reaction kinetics. *Biochem. Biophys. Res. Commun.* **2001**, *282*, 1161–1168.
(25) Kawabata, J.; Okamoto, Y.; Kodama, A.; Makimoto, T.; Kasai, T. Oxidative dimers produced from protocatechuic and gallic esters in the DPPH radical scavenging reaction. *J. Agric. Food Chem.* **2002**, *50*, 5468–5471.
(26) Roginski, V. Chain-breaking antioxidant activity of natural polyphenols as determined during the chain oxidation by methyl linoleate in Triton X-100 micelles. *Arch. Biochem. Biophys.* **2003**, *414*, 261–270.
(27) Zhou, A.; Sadik, O. A. Comparative analysis of quercetin oxidation by electrochemical, enzymatic, autooxidation and free radical generation techniques: a mechanistic study. *J. Agric. Food Chem.* **2008**, *56*, 12081–12091.
(28) Viriot, C.; Scalbert, A.; Herve, D. U.; Penhoat, C.; Moutounet, M. Ellagitannins in woods of sessile oak and sweet chesnut dimerization and hydrolysis during wood ageing. *Phytochemistry* **1994**, *36*, 1253–1260.
(29) Otsuka, K.; Sugihara, T.; Tsujino, Y.; Osakai, T.; Tamiya, E. Electrochemical consideration on the optimum pH of bilirubin oxidase. *Anal. Biochem.* **2007**, *370*, 98–106.
(30) Zhuang, Q.-K.; Scholz, F.; Pragst, F. The voltammetric behaviour of solid 2,2′-diphenyl-1-picrylhydrazyl (DPPH) microparticules. *Electrochem. Commum.* **1999**, *1*, 406–410.

Received for review September 10, 2009. Revised manuscript received January 11, 2010. Accepted January 13, 2010. This paper was partially supported by grants from the Ministerio de Educación y Ciencia (Madrid, Spain) Projects BIO2006-15363 and SAF2006-07040-C02-01, from the Fundación Séneca (CARM, Murcia, Spain) Project 08856/PI/08, from the Consejería de Educación (CARM, Murcia, Spain) BIO-BMC 06/01-0004, and from FISCAM PI-2007/53 from the Consejería de Salud y Bienestar Social de la Junta de Comunidades de Castilla La Mancha. J.L.M.-M. has a fellowship from the Ministerio de Educación y Ciencia (Madrid, Spain) Reference AP2005-4721. F.G.-M. has a fellowship from Fundación Caja Murcia (Murcia, Spain).

Supplementary material

Kinetic analysis

The reaction of an antioxidant, A (phenolic or polyphenolic), with the free radical $ABTS^{\bullet+}$ produces a phenol radical according to $[ABTS^{\bullet+} + Phe\text{-}OH \rightarrow ABTS + Phe\text{-}O^{\bullet}]$ or, in general, $ABTS^{\bullet+} + A \rightarrow ABTS + A^{\bullet}$. This phenol radical may evolve following different pathways: a) stabilising through canonical structures; b) forming dimers; c) forming dimers-polymers with the regeneration of –OH groups that consume more free radical. These reactions may be summarised as follows.

a) $Phe\text{-}O^{\bullet}[I] \rightleftharpoons Phe\text{-}O^{\bullet}[II] \rightleftharpoons Phe\text{-}O^{\bullet}[III]$

where [I], [II], and [III] are canonical structures.

b) $Phe\text{-}O^{\bullet} + Phe\text{-}O^{\bullet} \rightleftharpoons PheO - PheO$

c) $Phe\text{-}O^{\cdot} \rightleftharpoons (Phe\text{-}O^{\cdot})' \xrightarrow{H_2O} Dimer \xrightarrow{ABTS^{\cdot+}} Products$

Bearing in mind that B is the free radical corresponding to A, the simplest scheme for the reaction of n molecules of radical with the antioxidant is **Scheme 1** of the main text (henceforth **Scheme 1**). On the other hand, B can be stabilize through chemical reactions (B+B) in which $ABTS^{\bullet+}$ does not participate, evolving to C, the rate limiting step may be of the second order, and if the compounds formed (C) can react again with the radical $ABTS^{\bullet+}$, evolving to product D, according to **Scheme 2** of the main text, henceforth **Scheme 2**.

To characterise the antioxidant capacity of a compound (**Schemes 1** and **2**), the kinetic method described below is proposed:

1) Enzymatic kinetic method.

The enzymatic system POD/ABTS/H_2O_2 is used *(1),* [see eq. (1) of the main text, henceforth eq. (1)]:

In the absence of antioxidant A, eq. (1), rapidly reaches the steady-state with a velocity V_0 (**Figures 1** and **2**). Maintaining the substrate concentrations constant, different concentrations of antioxidant are used in the assay medium. The parallel lines obtained indicate that the system reaches the same steady-state rate in all cases, fulfilling the matter balance expressed in eq. (2) of the main text [henceforth eq. (2)]. Thus, the radical $ABTS^{\bullet+}$ is accumulated in the medium according to eq. (2).

The representation of [$ABTS^{\bullet+}$] *vs.* t corresponds to a straight line which intercepts the axis t at $t = \tau$. When [$ABTS^{\bullet+}$] = 0, we obtain (see **Figure 1** and **Figure 2**):

$$n = \frac{V_0 \tau}{[A]_0} \qquad (1SM)$$

This value of n corresponds to the primary antioxidant capacity. The reaction of $ABTS^{\bullet+}$ with A is rapid and the system returns to the same initial steady-state. Taking into consideration the value of n, we can calculate the efficient concentration EC50 (the ratio between the concentration of antioxidant that decreases the concentration of radical by 50%) *(2,3)*, because n and EC50 are related by EC50 = 1/2 n.

In addition, we calculate the antiradical or antioxidant power (ARP), defined as the inverse of the EC50 *(4)*.

When the action of the antioxidant corresponds to **Scheme 1**, in which the product of reaction B is stabilised with no additional consumption of radical, the parameters n, EC50 and ARP define the behaviour of the antioxidant/radical under study.

However, note that this enzymatic kinetic method includes the information concerning the total number of electrons donated by the antioxidant, even in different chemical steps, assuming that product B (**Scheme 1**) is not stable, as long as these steps are rapid and the system can return to the initial steady-state. Hence, according to the mechanism described in **Schemes 2** and **3** of the main text [henceforth **Schemes 2** and **3**], the matter balance, taking into account eq. (1) and **Scheme 3**, is:

$$[\text{ABTS}^{\bullet+}] = V_0 t - n_1[\text{A}]_0 - n_2[\text{C}] - n_3[\text{E}] \quad \text{(2SM)}$$

From **Scheme 3**, it is observed that $[C] = f[B]_0 = f[A]_0$ and $[E] = f'[B]_0 = f'[A]_0$ where f is the fraction of A transformed in C and f' is the fraction of A transformed in E. Therefore, according to eq. (2SM):

$$[\text{ABTS}^{\bullet+}] = V_0 t - [n_1[\text{A}]_0 + n_2 f[\text{A}]_0 + n_3 f'[\text{A}]_0] \quad \text{(3SM)}$$

Hence,

$$[\text{ABTS}^{\bullet+}] = V_0 t - [n_1 + n_2 f + n_3 f'][\text{A}]_0 \quad \text{(4SM)}$$

and, taking into account that, according to the stoichiometry, $n = n_1 + n_2 f + n_3 f'$,

$$[\text{ABTS}^{\bullet+}] = V_0 t - n[\text{A}]_0 \quad \text{(5SM)}$$

Eq. (5SM) is identical to eq. (2), and so the enzymatic kinetic method permits the total consumption of electrons and the primary antioxidant power to be obtained, as long as, kinetically, the system returns to the initial steady-state, regardless of the pathway followed by the reaction and the different stoichiometries possible in the steps (**Scheme 3**).

However, it may occur that the coupled chemical reactions are slow and, if the product of this slow reaction consumes radical, the system does not reach the same initial steady-state, until these steps are fulfilled kinetically. This means the enzyme must act at long times, consuming large quantities of substrate and meaning that it cannot return to the initial steady-state (**Figure 3A**). This test (non-parallel straight lines) indicates that chemical reactions coupled to the reaction of $ABTS^{\bullet+}$ with A are occurring and are slow (for example **Schemes 2** and **3**). The bibliography describes mainly second order coupled reactions *(2)*. In general, when a set of parallel straight lines is obtained in the enzymatic kinetic method, we can calculate the antioxidant capacity, denominated primary capacity. If at higher antioxidant concentrations deviations from the parallel lines are obtained, this indicates that secondary antioxidant capacity exists. An estimated measurement of this secondary capacity can be obtained through the non-enzymatic kinetic test described below.

2) Non-enzymatic kinetic test.

In this test, an excess of free radical is set to react with the antioxidant until the radical concentration remains constant. The radicals generally used are $DPPH^{\bullet}$ *(4)* and $ABTS^{\bullet+}$ *(5,6)*. A typical spectrophotometric recording is shown in **Figure 3B, inset**, in which a sharp fall in absorbance can be seen, corresponding to the primary antioxidant capacity, also known as stoichiometric factor, n *(3,7)*, followed by a more gradual fall. $ABTS^{\bullet+}$ can be studied kinetically by following the variation in its absorbance with time.

The literature describes slow dimerisation reactions during the reaction of the products of the antioxidant with the free radical *(8-11)*. In our experiments with compounds showing a secondary antioxidant capacity, we demonstrated the second order dependence of the disappearance of free radical mainly. However, the kinetics is complex, and only if the simplification of **Scheme 2** is accepted can an analytical

expression be deduced to fit the experimental data. Although offering only apparent parameters and constants, this fit can be used for comparative purposes.

If the reactions of radical $ABTS^{\bullet+}$ with A and with C are rapid, so that $k_2^{app} << k_1, k_3$, **Scheme 2** is kinetically equivalent to eq. (3) of the main text, henceforth eq. (3):

From eq. (3), we can write:

$$\frac{d[D]}{dt} = \frac{1}{2} k_2^{app} [B]^2 \qquad (6SM)$$

If $[B]_0 = [A]_0$, the matter balance is:

$$[A]_0 = [B] + 2\,[D] \qquad (7SM)$$

From eq. (6SM) and taking into account eq. (7SM) and integrating, the variation of [D] with time is obtained:

$$[D] = \frac{k_2^{app}\,[A]_0^2\,t}{2\,(k_2^{app}\,[A]_0\,t + 1)} \qquad (8SM)$$

If the initial concentration of the radical $ABTS^{\bullet+}$ falls rapidly to reach $[ABTS^{\bullet+}]_0 - n[A]_0$, then the matter balance of the free radical is:

$$[ABTS^{\bullet+}] = [ABTS^{\bullet+}]_0 - n\,[A]_0 - n'\,[D] \qquad (9SM)$$

Inserting eq. (8SM) into eq. (9SM) gives:

$$[ABTS^{\bullet+}] = [ABTS^{\bullet+}]_0 - n\,[A]_0 - \frac{n'\,k_2^{app}\,[A]_0^2 t}{2\,(k_2^{app}[A]_0 t + 1)} \qquad (10SM)$$

If now in eq. (10SM) we set $t \to \infty$, then the corresponding [ABTS$^{\bullet+}$] value, i.e. $[ABTS^{\bullet+}]_{\infty}$, is given by:

$$[ABTS^{\bullet+}]_{\infty} = [ABTS^{\bullet+}]_0 - (n + \frac{n'}{2})\,[A]_0 = [ABTS^{\bullet+}]_0 - (n + n_{app})\,[A]_0 \quad (11SM)$$

From eq. (11SM), we have:

$$[ABTS^{\bullet+}]_0 = [ABTS^{\bullet+}]_{\infty} + (n + n_{app})[A]_0 \quad (12SM)$$

If eq. (12SM) is inserted in eq. (10SM), we obtain eq. (4) of the main text.

The expression for the new parameter proposed in this study, the apparent kinetic antiradical efficiency (KAE_{app}), takes the form expressed in eq. (5) of the main text.

References

(1) Arnao, M.B.; Cano, A.; Hernandez-Ruiz, J.; Garcia-Canovas, F.; Acosta, M. Inihibition by L-ascorbic acid and others antioxidants of the 2,2´-azino-bis(3-ethylbenzthiazoline-6-sulfonic acid) oxidation catalyzed by peroxidase: a new approach for determining total antioxidant status of foods. *Anal. Biochem.* **1996**, *236*, 255-261.

(2) Hotta, H.; Nagano, S.; Ueda, M.; Tsujino, Y.; Kojama, J.; Osakai, T. Higher radical scavenging activities of polyphenolic antioxidants can be ascribed to chemicals reactions following their oxidation. *Biochim. Biophys. Acta* **2002**, *1572*, 123-132.

(3) Villaño, D.; Fernandez-Pachon, M.S.; Moyá, M.L.; Troncoso, A.M.; Garcia-Parrilla, M.C. Radical scavenging ability of polyphenolic compounds towards DPPH free radical. *Talanta* **2007**, *71*, 230-235.

(4) Brand-Williams, W.; Cuvelier, M.E.; Berset, C. Use of a free radical method to evaluate antioxidant activity. *Lebensm.-Wiss. U-Technol.* **1995**, *28*, 25-30.

(5) Miller, N.J.; Rice-Evans, C.; Davies, M.J.; Gopinethan, V.; Milner, A. A novel for measuring antioxidant capacity and its application to monitoring the antioxidant status in premature neonates. *Clin. Sci.* **1993**, *84*, 407-412.

(6) Rice-Evans, C.A.; Miler, N.J.; Badwell, P.G.; Bramley, P.M.; Pidham, J.B. The relative antioxidant activities of plant-derived polyphenolic flavonoids. *Free Rad. Res.* **1995**, *22*, 375-383.

(7) Foti, M.C.; Daquino, C.; Geraci, C. Electron-transfer reaction of cinnamic acids and their methyl esters with the DPPH$^{\cdot}$ radical in alcoholic solutions. *J. Org. Chem.* **2004**, *69*, 2309-2314.

(8) Hotta, H.; Sakamoto, H.; Nagano, S.; Tsujino, Y. Unusually large number of electrons for the oxidation of polyphenolic antioxidants. *Biochim. Biophys. Acta* **2001**, *1526*, 159-167.

(9) Hotta, H.; Ueda, M.; Nagano, S.; Tsujino, Y.; Kojama, J.; Osakai, T. Mechanistic study of the oxidation of caffeic acid by digital simulation of cyclic voltammograms. *Anal. Biochem.* **2002**, *303*, 66-72.

(10) Hotta, H.; Nagano, S.; Ueda, M.; Tsujino, Y.; Kojama, J.; Osakai, T. Higher radical scavenging activities of polyphenolic antioxidants can be ascribed to chemicals reactions following their oxidation. *Biochim. Biophys. Acta* **2002**, *1572*, 123-132.

(11) Jimenez-Atienzar, M.; Cabanes, J.; Gandia-Herrero, F.; Garcia-Carmona, F. Kinetic analysis of catechin oxidation by polyphenol oxidase at neutral pH. *Biochem. Biophys. Res. Commun.* **2004**, *319*, 902-910.

4.14. OXIDACIÓN CATALÍTICA DE *o*-AMINOFENOLES Y AMINAS AROMÁTICAS POR TIROSINASA DE CHAMPIÑÓN.

El estudio de la oxidación catalítica de o-aminofenoles y aminas aromáticas por tirosinasa de champiñón ha dado lugar a la siguiente publicación adjunta.

4.14.1. Título

Catalytic oxidation of *o*-aminophenols and aromatic amines by mushroom tyrosinase.

4.14.2. Autores

Muñoz-Muñoz, J.L.; Garcia-Molina, F.; Garcia-Ruiz, P.A.; Varon, R; Tudela, J.; Rodríguez-López, J.N. y Garcia-Cánovas, F.

4.14.3. Referencia

Biochimica et Biophysica Acta-Protein and Porteomics (2011) 1814, 1974-1983.

4.14.4. Resumen

Se ha estudiado la caracterización cinética de *o*-aminofenoles y aminas aromáticas como sustratos de tirosinasa. Las constantes catalíticas de las monoaminas y diaminas aromáticas son muy semejantes y bajas, confirmando el mecanismo previamente descrito por nosotros, en el que la etapa lenta es la transferencia de un protón por parte de un hidroxilo al peróxido en oxitirosinasa (Fenoll et al., Biochem. J. 380 (2004) 643-650). En el caso de *o*-aminofenoles, la presencia de un grupo hidroxilo coopera indirectamente a la transferencia del protón y así los valores de las constantes catalíticas en la acción de tirosinasa sobre estos compuestos son más altos. En el caso de las monoaminas aromáticas, las constantes de Michaelis son del mismo orden de magnitud que para los monofenoles, lo que sugiere que éstos últimos se unen mejor (mayor constante de unión) a la enzima al facilitarse las interacciones π-π entre el anillo aromático y una posible histidina del sitio activo. En el caso de las *o*-diaminas aromáticas, tanto el valor de la constante catalítica como el de la constante de Michaelis son bajos. Los valores de las constantes catalíticas son menores que los de sus correspondientes *o*-difenoles. Los valores de las constantes de Michaelis de las *o*-diaminas aromáticas son ligeramente menores que los de su *o*-difenoles correspondientes, confirmando que las *o*-diaminas aromáticas se une peor a la enzima (menor constante de unión).

Author's personal copy

Biochimica et Biophysica Acta 1814 (2011) 1974–1983

Contents lists available at ScienceDirect

Biochimica et Biophysica Acta

journal homepage: www.elsevier.com/locate/bbapap

Catalytic oxidation of *o*-aminophenols and aromatic amines by mushroom tyrosinase

Jose Luis Muñoz-Muñoz [a], Francisco Garcia-Molina [a], Pedro Antonio Garcia-Ruiz [b], Ramon Varon [c], Jose Tudela [a], Jose N. Rodriguez-Lopez [a], Francisco Garcia-Canovas [a,*]

[a] GENZ: Grupo de Investigación Enzimología, Departamento de Bioquímica y Biología Molecular-A, Facultad de Biología, Universidad de Murcia, E-30100, Espinardo, Murcia, Spain
[b] QCPAI: Grupo de Química de Carbohidratos, Polímeros y Aditivos Industriales, Departamento de Química Orgánica, Facultad de Química, Universidad de Murcia, E-30100, Espinardo, Murcia, Spain
[c] Departamento de Química-Física, Escuela de Ingenieros Industriales de Albacete, Universidad de Castilla la Mancha, Avda, España s/n, Campus Universitario, E-02071, Albacete, Spain

ARTICLE INFO

Article history:
Received 11 May 2011
Received in revised form 12 July 2011
Accepted 13 July 2011
Available online 22 July 2011

Keywords:
Tyrosinase
Aromatic amine
Aromatic *o*-diamines
o-aminophenols
Catalytic constant
Michaelis constant

ABSTRACT

The kinetics of tyrosinase acting on *o*-aminophenols and aromatic amines as substrates was studied. The catalytic constants of aromatic monoamines and *o*-diamines were both low, these results are consistent with our previous mechanism in which the slow step is the transfer of a proton by a hydroxyl to the peroxide in oxy-tyrosinase (Fenoll et al., Biochem. J. 380 (2004) 643–650). In the case of *o*-aminophenols, the hydroxyl group indirectly cooperates in the transfer of the proton and consequently the catalytic constants in the action of tyrosinase on these compounds are higher. In the case of aromatic monoamines, the Michaelis constants are of the same order of magnitude than for monophenols, which suggests that the monophenols bind better (higher binding constant) to the enzyme to facilitate the π–π interactions between the aromatic ring and a possible histidine of the active site. In the case of aromatic *o*-diamines, both the catalytic and Michaelis constants are low, the values of the catalytic constants being lower than those of the corresponding *o*-diphenols. The values of the Michaelis constants of the aromatic *o*-diamines are slightly lower than those of their corresponding *o*-diphenols, confirming that the aromatic *o*-diamines bind less well (lower binding constant) to the enzyme.

© 2011 Elsevier B.V. All rights reserved.

1. Introduction

Tyrosinase (TYR, EC 1.14.18.1) is a copper-containing enzyme widely distributed in nature. It catalyses two types of reactions: (a) the *ortho*-hydroxylation of monophenols to *o*-diphenols (monophenolase activity) and (b) the oxidation of *o*-diphenols to *o*-quinones (diphenolase activity). Both types of reaction require molecular oxygen as the second substrate of the enzyme [2,3].

The catalytic centre of tyrosinase possesses a binuclear copper similar to that of hemocyanin and catechol oxidase [3]. The catalytic cycle of tyrosinase has three enzymatic forms: E_m (met-tyrosinase) with the copper as $Cu^{2+}Cu^{2+}$, E_d (deoxy-tyrosinase) with the copper as $Cu^{+}Cu^{+}$ and E_{ox} (oxy-tyrosinase) with copper in the form $Cu^{2+}Cu^{2+}O_2^{2-}$ [4]. In the structures of hemocyanin [3,5], catechol oxidase [6] and tyrosinase from *Streptomyces castaneoglobisporus*[7] and from *Bacillus megaterium*[8,9], each copper ion is coordinated by three histidines.

Apart from its natural substrates (monophenols and *o*-diphenols), tyrosinase is also capable of oxidising a variety of aromatic monoamines and *o*-aminophenols, such as 4-aminotoluene, or several aminophenolic derivatives of benzoic acid, such as 3-amino-4-hydroxybenzoic acid, 4-amino-3-hydroxybenzoic acid and 3,4-diaminobenzoic acid [10]. The source of tyrosinase used by these authors [10] was *Neurospora crassa*. Moreover, 3-hydroxyanthranilic acid has been shown to act as an activator of the monophenolase activity of mushroom tyrosinase [11], reducing the lag period for reactions with non-cyclising phenolic substrates (4-*tert*-butylphenol/4-*tert*-butylcatechol). In another report, the same authors described the oxidation of 3-hydroxykynurenine, a tryptophan catabolite, by mushroom tyrosinase [12]. On the other hand, 3-amino-L-tyrosine has been described as a potent competitive inhibitor of the monophenolase activity and does not serve as a substrate. It was proposed that this aminophenol acts as a complexing agent of the copper ions in the *oxy* form of tyrosinase [13].

In a recent work [14], the interaction of mushroom tyrosinase with several aromatic monoamines, *o*-diamines and *o*-aminophenols was described using different spectrophotometric and oxymetric techniques. Consequently, 3-amino-L-tyrosine was shown to be a real substrate of tyrosinase, contrary to the findings published by Maddaluno and Faull [13].

In all the works above [11–14], *o*-aminophenols and aromatic monoamines and *o*-diamines were seen to act as substrates of tyrosinase because they are all structural analogues of the natural substrates of the enzyme (*o*-diphenols and monophenols).

The kinetic characterisation of aromatic monoamines, *o*-diamines and *o*-aminophenols is difficult because the product of the reaction, *o*-quinoneimine, is unstable [10,11]. Kinetic studies have been carried out using oxymetric techniques, which have provided quantitative

* Corresponding author. Tel.: +34 868 884764; fax: +34 868 883963.
E-mail address: canovasf@um.es (F. Garcia-Canovas).

1570-9639/$ – see front matter © 2011 Elsevier B.V. All rights reserved.
doi:10.1016/j.bbapap.2011.07.015

Author's personal copy

information [10]. However, spectrophotometric techniques [10,14] do not provide such information because the product evolves. In a recent work [15], we presented a revision of the spectrophotometric techniques used for measuring tyrosinase activity. In the present work, we widen the use of these methods to the characterisation of the substrates above, applied especially to the case of *o*-aminophenols and aromatic *o*-diamines, using ascorbic acid, the concentration of which decays and is followed spectrophotometrically. We also study the possibility that some *o*-quinoneimines may give rise to an isosbestic point during their evolution. Oxymetric techniques have also been used [16], especially to characterise monophenols and aromatic amines, permitting kinetic parameters to be reliably obtained for this series of compounds.

Bearing in mind the above, the aim of this study was to take a deeper look at the tyrosinase mechanism, considering its action on several substrates: aromatic monoamines, *o*-diamines and *o*-aminophenols. The results obtained are compared to those obtained for *o*-diphenols and monophenols. Based on the findings, the mechanism of tyrosinase is discussed and the decisive steps of the catalysis are characterised.

2. Material and methods

2.1. Reagents

Mushroom tyrosinase (TYR, *o*-diphenol:O_2 oxidoreductase, EC 1.14.18.1) (1530 U/mg), was obtained from Sigma Chemical (St. Louis, MO). All substrates and L-ascorbic acid (AH_2) were obtained from Sigma Chemical (St. Louis, MO). Stock solutions of the reducing substrates were prepared in 0.15 mM phosphoric acid to prevent autooxidation. Milli-Q system (Millipore Corp.) ultrapure water was used throughout this research. The buffer used was 30 mM sodium phosphate (pH 7.0).

2.2. Enzyme source

Tyrosinase (1530 U/mg; TYR) was purified according to [17]. Protein concentration was determined by Bradford's method using bovine serum albumin as standard [18].

2.3. Spectrophotometric assays

Absorption spectra were recorded in a visible–ultraviolet Perkin-Elmer Lambda 35-spectrophotometer interfaced on-line with a PC compatible Intel-Pentium microcomputer, at a scanning speed of 60 nm/s controlled by the UV-Winlab software. The temperature was maintained at 25 °C using a Haake D16 circulating water bath with a heater/cooler, and checked using a Cole-Parmer digital thermometer with a precision of 0.1 °C. Kinetic assays were also carried out with the instruments above, monitoring AH_2 disappearance (2,3-diaminobenzoic acid, 3,4-diaminotoluene, 4-methoxy-1,2-phenylendiamine, 4-amino-3-hydroxybenzoic acid, 3-amino-L-tyrosine, 2-aminophenol and 3-methylcatechol), NADH disappearance (catechol), the formation of dopachrome (L-tyrosine and L-dopa), the appearance of an adduct between *o*-quinoneimine and substrate (2-aminobenzoic acid, 3-aminotoluene, 4-aminotoluene, 2,3-diaminotoluene, 1,2-diaminobenzene, 2-amino-3-hydroxybenozic acid, 3-amino-4-hydroxybenzoic acid, 3-amino-4-hydroxytoluene, 4-amino-3-hydroxytoluene, 3-hydroxytoluene, 2-hydroxyanisole, 4-methylcatechol and 3-methoxycatechol) or the appearance of an adduct between MBTH, a nucleophile reagent, and the substrate (4-aminoanisole, 4-aminophenylalanine and 4-hydroxyanisole). The measuring wavelength (λ) and the molar absorbtivity coefficient (ε) for each substrate are summarised in Table 1SM (Supplementary material). The cuvettes (final volume of 1 mL) contained 30 mM sodium phosphate buffer (pH 7.0) and O_2 at a concentration which saturates the corresponding enzymes [19]. The substrate concentration was varied as indicated in each figure legend, and the reaction was started by adding enzyme (TYR). The coupled reagent concentration (AH_2, NADH or MBTH) is indicated in each figure legend.

2.4. Oxymetric assays

Oxygen consumption was measured with a Clark-type electrode coupled to a Hansatech Oxygraph (King's Lynn, Norfolk, UK). The equipment was calibrated using the TYR/4-*tert*-butylcatechol method [16]. Nitrogen was bubbled through the reaction medium to remove the oxygen when necessary. The cuvette (final volume 2 mL) contained 30 mM sodium phosphate buffer (pH 7.0) and the substrate concentration was varied. In every case, AH_2 was added to the medium to maintain the substrate concentration constant. The reaction was started by adding substrate. The medium was stirred constantly and the temperature was kept at 25 ± 0.1 °C using a Haake D16 circulating water-bath. The substrates characterised by this method were: 3-aminobenzoic acid, 4-aminobenzoic acid, 2-aminotoluene, 2-aminoanisole, 3-aminoanisole, aniline, 3,4-diaminobenzoic acid, 3-amino-2-hydroxybenzoic acid, 2-hydroxybenzoic acid, 3-hydroxybenzoic acid, 4-hydroxybenzoic acid, 2-methylphenol (*o*-cresol), 4-methylphenol (*p*-cresol), 3-hydroxyanisole, phenol, 2,3-dihydroxybenzoic acid and 3,4-dihydroxybenzoic acid. In the cases of aromatic monoamines and monophenols, the corresponding *o*-diphenol or 4-*tert*-butylcatechol (when the corresponding *o*-aminophenols or *o*-diphenol was not available commercially, e.g. 2-aminotoluene, 2-aminoanisole and 3-aminoanisole) were added to the medium to avoid the lag phase of the monophenolase activity of tyrosinase ($[D]_{ss}/[M]_{ss} = R$) [20].

2.5. Kinetic analysis

For TYR, the initial rate values (V_0) were calculated from triplicate measurements at each reducing substrate concentration, and V_0*vs.* $[S]_0$ data were adjusted to the Michaelis–Menten equation [Eq. (1)] through the Sigma Plot 9.0 program for Windows [21], obtaining the maximum rate (V_{max}) and Michaelis constant for each substrate (K_m). From these values and according to Eq. (2), the catalytic constant (k_{cat}) can be calculated.

3. Results and discussion

In recent years much effort has been dedicated to the kinetics of the action mechanism of tyrosinase acting on its physiological substrates, monophenols and *o*-diphenols [2,3,22–24]. Besides these physiological substrates, other types of non-phenolic substrate, such as NADH [25], ascorbic acid [26], tetrahydropterines or tetrahydrofolic acid [27,28], have been characterised. Moreover, to characterise kinetically aromatic monoamines and *o*-diamines and *o*-aminophenols, several oxymetric and spectrophotometric measuring methods have been designed [15].

3.1. Oxymetric methods

Generally speaking, all substrates of tyrosinase can be characterised according to their consumption of oxygen, although, due to the low activity shown by the enzyme towards some of them, such as aromatic monoamines and *o*-diamines and *o*-aminophenols, spectrophotometric methods are preferred, especially when the disappearance of a coupled reagent with a high coefficient of molar absorptivity can be measured.

3.2. Spectrophotometric methods

When possible, ascorbic acid (AH_2) was used, since it reduces the *o*-quinoneimine or *o*-diimine to the corresponding *o*-aminophenol or aromatic *o*-diamine, respectively. When the spectrum of the substrate overlaps that of the AH_2, a problem arises with the saturation of the

Author's personal copy

phototube. In this case, the oxymetric method is used or, if possible, depending on the substrate, the visible zone is measured, taking advantage of the formation of adducts between the *o*-quinoneimine and the substrate (Scheme 1), or between the *o*-quinoneimine and a coupled/bound reagent, such as MBTH.

3.3. Oxidation of o-aminophenols and aromatic o-diamines by periodate in deficiency

The oxidation of *o*-aminophenols and aromatic *o*-diamines by periodate in deficiency gives rise to the formation of *o*-quinoneimine (Scheme 1), which suffers a nucleophilic attack on the part of the amino group of the substrate, originating an adduct which is oxidised again by another molecule of *o*-quinoneimine. The new quinone suffers a nucleophilic attack, giving rise to a new leuco compound, which, in turn, is oxidised by another molecule of *o*-quinoneimine to form a *p*-quinone. Fig. 1 depicts the appearance of an isosbestic point during the evolution of the *o*-quinoneimine as a result of the oxidation of 3-hydroxyantrhanilic acid by periodate in deficiency. Note that a stoichiometry of 3 *o*-quinoneimine/1 *p*-quinoneimine is accomplished. The existence of an isosbestic point permits the oxidation of 3-hydroxyanthranilic acid to be followed at this wavelength.

3.4. Formation of chromophoric adducts with MBTH

In order to study the characteristics of the MBTH-*o*-quinoneimine adducts, the oxidation of various aromatic monoamines by O_2 catalysed by tyrosinase was carried out in the presence of MBTH (Fig. 2). The pigment formed with 4-aminophenylalanine and 4-aminoanisole had an absorbance maximum which ranged from 497 to 498 nm (Table 1SM). The pH affected the solubility and stability of the adducts. The solubilisation of these compounds was achieved by adding 2% (v/v) dimethylformamide (DMF) to the reaction medium [29]. At pH 7.0, the adducts were unstable but showed an isosbestic point. The MBTH is a potent nucleophile through its amino group, which shows different degrees of protonation–deprotonation, depending on the pH. The ionisation constant for this group was determined by both potentiometric and spectrophotometric methods ($pK = 5.8 \pm 0.4$) [29]. Depending on its stability, each *o*-quinoneimine needs a different $[MBTH]_{sat}$ to complete the formation of the adduct (see the legends of the figures).

3.5. Oxidation of o-aminophenols by TYR and comparison with o-diphenols

We studied the oxidation of several *o*-aminophenols by mushroom tyrosinase using different measuring methods (see Supplementary material), which enabled us to characterise kinetically these substrates (Table 1).

Fig. 1 depicts the oxidation of 3-hydroxyanthranilic acid (2-amino-3-hydroxybenzoic acid) by periodate in deficiency measuring the gradual appearance of the product. An adduct is formed between the

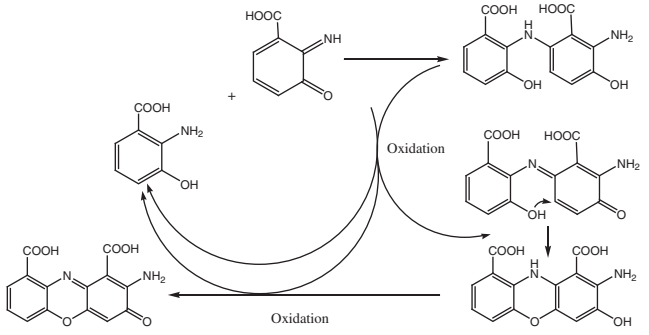

Scheme 1. Mechanism for evolution of 3-hydroxyanthranilic acid´s *o*-quinoneimine in the presence of an excess of *o*-aminophenol.

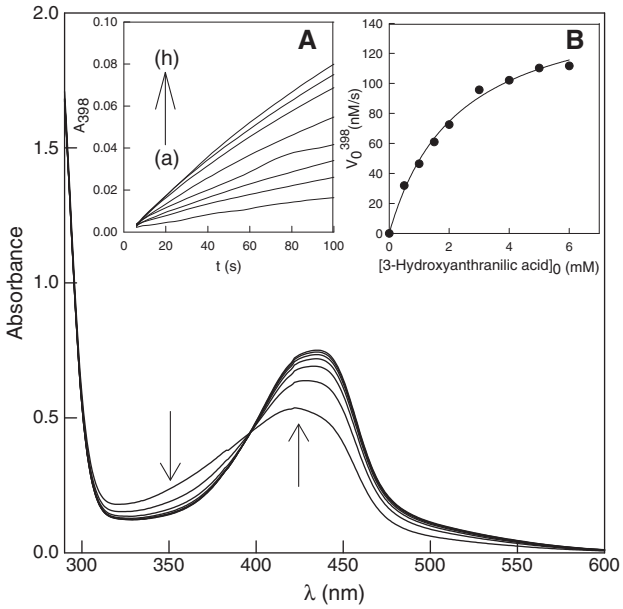

Fig. 1. Spectrophotometric scans of the 3-hydroxyanthranilic acid oxidation by periodate in deficiency. The experimental conditions were 30 mM sodium phosphate buffer (pH 7.0), 25 °C, initial concentrations of 3-hydroxyanthranilic acid and periodate, [3-hydroxyanthranilic acid]$_0$ and $[IO_4^-]_0$, were 0.6 mM and 60 μM, respectively. The spectrophotometric scans were made every 3 min. Inset A. Spectrophotometric recordings of the oxidation of 3-hydroxyanthranilic acid by TYR at a wavelength of 398 nm. The experimental conditions were 30 mM sodium phosphate buffer (pH 7.0), 25 °C, initial concentration of enzyme, $[E]_0$, was 0.61 μM and the initial substrate concentrations (mM) were: (a) 0.5, (b) 1, (c) 1.5, (d) 2, (e) 3, (f) 4, (g) 5 and (h) 6. Inset B. Representation of the steady-states rates (V_0) *vs.* [3-hydroxyanthranilic acid]$_0$.

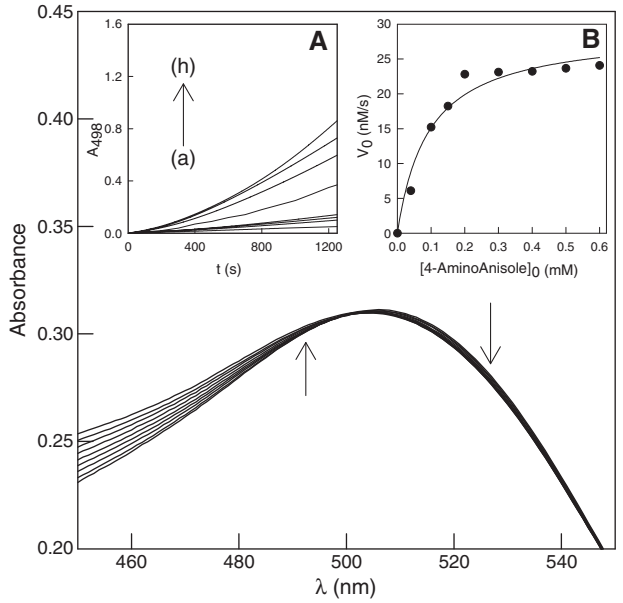

Fig. 2. Spectrophotometric scans of the 4-aminoanisole oxidation by TYR in the presence of MBTH. The experimental conditions were 30 mM sodium phosphate buffer (pH 7.0), 25 °C, [4-aminoanisole]$_0$ = 0.5 mM, $[E]_0$ = 0.9 μM, $[MBTH]_0$ = 2.5 mM and $[DMF]_0$ = 2%. The spectrophotometric scans were made every 15 min. Inset A. Spectrophotometric recordings of the oxidation of 4-aminoanisole by TYR at a wavelength of 498 nm. The experimental conditions were 30 mM sodium phosphate buffer (pH 7.0), 25 °C, $[E]_0$ = 10 nM, initial concentration of MBTH and DMF, $[MBTH]_0$ and $[DMF]_0$, were 2.5 mM and 2%, respectively and the initial substrate concentrations (mM) were (a) 0.05, (b) 0.1, (c) 0.15, (d) 0.2, (e)0.3, (f) 0.4, (g) 0.5 and (h) 0.6. Inset B. Representation of the initial steady-state rates (V_0) *vs.* [4-aminoanisole]$_0$. The experimental conditions are the same as in Fig. 2.

Author's personal copy

Table 1
Values of the kinetic constants characterising the oxidation of aminophenols and diphenols by TYR.

Aminophenols	k_{cat} (s^{-1})	K_m (mM)	Diphenols	k_{cat} (s^{-1})	K_m (mM)
2-amino-3-hydroxybenzoic acid	0.13 ± 0.01	2.27 ± 0.22	2,3-dihydroxybenzoic acid	0.37 ± 0.04	1.02 ± 0.12
3-amino-2-hydroxybenzoic acid	0.13 ± 0.01	0.36 ± 0.04			
3-amino-4-hydroxybenzoic acid	0.45 ± 0.01	0.11 ± 0.01	3,4-dihydroxybenzoic acid	8.11 ± 0.31	0.07 ± 0.01
4-amino-3-hydroxybenzoic acid	0.50 ± 0.01	0.15 ± 0.01			
3-amino-4-hydroxytoluene	29.42 ± 1.58	2.73 ± 0.56	4-methylcatechol	842.12 ± 26.11	0.10 ± 0.01
4-amino-3-hydroxytoluene	26.12 ± 2.13	2.36 ± 0.43			
3-amino-L-tyrosine	1.35 ± 0.15	0.90 ± 0.18	L-dopa	102.62 ± 19.21	0.55 ± 0.08
2-aminophenol	60.57 ± 2.84	0.78 ± 0.08	Catechol	874.10 ± 30.21	0.16 ± 0.01

substrate and product of the reaction. This adduct is rapidly oxidised to form cinnabarinic acid, giving rise to an isosbestic point at 398 nm [10,11]. Fig. 1 inset A shows the experimental recordings of the oxidation of different initial concentrations of 3-hydroxyanthranilic acid, $[S]_0$, by TYR. The initial rates of these oxidation processes with respect to $[S]_0$ are shown in Fig. 1 inset B. Non-linear regression gives V_{max} and K_m according to the equation:

$$V_0 = \frac{V_{max}[S]_0}{K_m + [S]_0} \quad (1)$$

where:

$$V_{max} = 2k_{cat}[E]_0 \quad (2)$$

and

$$K_m = \frac{k_{cat}}{k_6} \quad (3)$$

k_{cat} being the catalytic constant, $[E]_0$ the initial enzyme concentration and k_6 the substrate binding constant to the form oxy-tyrosinase.

In the case of 2-aminophenol, as shown in Fig. 3, ascorbic acid (AH_2) was used as reductant. In order to choose the most suitable wavelength for the measurement, we first obtained the absorption spectra of AH_2 (recording a, Fig. 3) and of 2-aminophenol (recording b, Fig. 3), choosing in this case 265 nm, which represents the absorption maximum of AH_2 ($\varepsilon = 11170\ M^{-1}\ cm^{-1}$) [30]. Fig. 3, Inset A depicts the experimental recordings of the gradual disappearance of AH_2. Fig. 3, Inset B shows the initial rates of TYR *vs.* $[2\text{-aminophenol}]_0$. Non-linear-fitting of the values of V_0, in accordance with Eq. (1), gives V_{max} and K_m (see Table 1). In the case of 3-amino-2-hydroxybenzoic acid (3-aminosalicylic acid), the consumption of oxygen was measured (see Table 1).

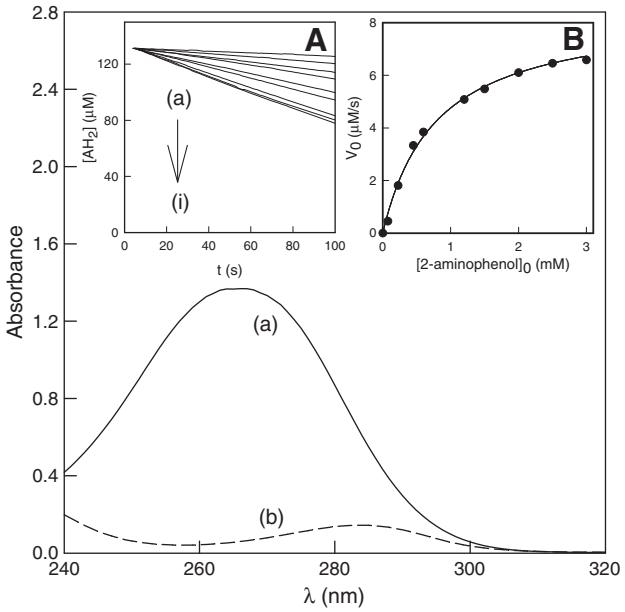

Fig. 3. Spectrophotometric scan of the 2-aminophenol and AH_2. The experimental conditions were 30 mM sodium phosphate buffer (pH 7.0), 25 °C, initial concentration of ascorbic acid and 2-aminophenol, $[AH_2]_0$ and $[2\text{-aminophenol}]_0$, were 0.12 mM (a) and 0.6 mM (b), respectively. Inset A. Spectrophotometric recordings of the 2-aminophenol oxidation by TYR at a wavelength of 265 nm. The experimental conditions were 30 mM sodium phosphate buffer (pH 7.0), 25 °C, $[AH_2]_0 = 0.13$ mM and $[E]_0 = 60$ nM and the initial substrate concentrations (mM) were: (a) 0.075, (b) 0.225, (c) 0.45, (d) 0.6, (e) 1.2, (f) 1.5, (g) 2, (h) 2.5 and (i) 3. Inset B. Representation of the initial steady-state rates (V_0) *vs.* $[2\text{-aminophenol}]_0$.

Table 1 shows the kinetic constants obtained for the different substrates and, where possible, these are compared with those obtained for the corresponding *o*-diphenols. Note how the *o*-aminophenols have the same or similar k_{cat} values when positions 2 and 3 or 3 and 4 are compared for the amino or hydroxyl group; for example, the value of k_{cat} for 2-amino-3-hydroxybenzoic acid is approximately the same as that of 2-hydroxy-3-aminobenzoic acid ($0.13 \pm 0.01\ s^{-1}$) and the k_{cat} of 3-amino-4-hydroxybenzoic acid is approximately the same as that of 3-hydroxy-4-aminobenzoic acid (Table 1). The catalytic constant increases from the *ortho*/*meta* position to the *meta*/*para* position and the same occurs if the substituent in C-1 is an electro-donating (—CH_3) or electrowithdrawing (—COOH) group. A similar situation exists for *o*-diphenols (see Table 1). The same applies when a chain exists in C-1, as in the case of 3-amino-L-tyrosine and L-dopa, while the values of k_{cat} are much lower than in the case of 2-aminophenol and catechol.

The Michaelis constants (see Table 1) and Eq. (3) are related with the catalytic constants and, in the case of *o*-aminophenols, which have low k_{cat} values, the K_m values are also low. Note that the *ortho* position of the amino group of 2-amino-3-hydroxybenzoic acid has a higher K_m, which, according to Eq. (3), indicates that its binding constant k_6 is lower than that of 3-amino-2-hydroxybenzoic acid, which might be explained by the steric hindrance of the amino group *ortho* position. The corresponding *o*-diphenol (2,3-dihydroxybenzoic acid) has a lower K_m value than 2-amino-3-hydroxybenzoic acid but it is three times higher than the value corresponding to 2-hydroxy-3-aminobenzoic acid, which agrees with the higher k_{cat}. In the case of 3-amino-4-hydroxybenzoic acid and 3-hydroxy-4-aminobenzoic acid, their values are similar to that of 3,4-dihydroxybenzoic acid (Table 1). The K_m values of 3-amino-4-hydroxytoluene and 3-hydroxy-4-aminotoluene (2.73 ± 0.56 and 2.36 ± 0.43 mM, respectively) are almost identical but, because the k_{cat} is higher than in the case above, the K_m is also higher. When these values are compared with those of their corresponding *o*-diphenols (Table 1), the values of k_{cat} are much lower in the case of *o*-aminophenols and the K_m values are in the same range, meaning that the *o*-diphenols bind better to the enzyme (higher k_6). The binding of the *o*-diphenols to the enzyme may be more favoured than in the case of the *o*-aminophenols because the π–π interaction between the substrate and a possible histidine of the active site is favoured in the case of *o*-diphenols and hindered in the case of aminophenols (Table 1).

If an electrodonating group exists on C-1, the benzene ring will be more electron-dense, binding will be less strong (due to the greater repulsion between the rings) and therefore, the k_6 value will be lower since the π–π interactions are hindered. If an electrowithdrawing

Author's personal copy

Table 2
Values of the kinetic constants characterising the oxidation of aromatic diamines and *o*-diphenols by TYR.

Aromatic diamines	k_{cat} (s^{-1})	K_m (mM)	Diphenols	k_{cat} (s^{-1})	K_m (mM)
2,3-diaminobenzoic acid	0.05 ± 0.01	0.28 ± 0.04	2,3-dihydroxybenzoic acid	0.37 ± 0.04	1.02 ± 0.12
3,4-diaminobenzoic acid	0.08 ± 0.01	0.15 ± 0.02	3,4-dihydroxybenzoic acid	8.11 ± 0.31	0.07 ± 0.01
2,3-diaminotoluene	0.11 ± 0.01	0.96 ± 0.11	3-methyl Catechol	104.2 ± 4.7	1.10 ± 0.14
3,4-diaminotoluene	0.51 ± 0.04	0.06 ± 0.01	4-methyl Catechol	842.12 ± 26.11	0.10 ± 0.01
4-methoxy-1,2-phenylendiamine	1.51 ± 0.13	0.36 ± 0.05	3-methoxycatechol	17.83 ± 0.53	1.26 ± 0.13
1,2-diaminobenzene	0.53 ± 0.05	0.46 ± 0.05	Catechol	874.10 ± 30.21	0.16 ± 0.01

group exists on C-1 the benzene ring will be of lower electron density, which will result in better substrate binding (higher k_6).

3.6. Oxidation of aromatic *o*-diamines by TYR and comparison with their respective *o*-diphenols

Table 2 shows the results obtained when the oxidation of aromatic *o*-diamines was studied. The values of the catalytic constants of the aromatic *o*-diamines are low, the 2,3-diamines having, as expected, a lower k_{cat} than the *o*-diamines substituted in 3,4. Furthermore, if the molecule in C-1 has an electrowithdrawing group, the values of k_{cat} are lower than when an electrodonating group is present. The same applies in the case of *o*-diphenols, although the catalytic constants are greater than in the case of the corresponding aromatic *o*-diamines.

The values of K_m are greater in the case of substrates with their substituents in *ortho* position with respect to C-1 and, in general, fulfil Eq. (3). Although the k_{cat} values of the *o*-diphenols are much greater than those of the aromatic *o*-diamines, the value of the binding constant (k_6) to the form E_{ox} must be high, so that, according to Eq. (3), the K_m values must be in the same range as those of the aromatic *o*-diamines. A possible explanation for this is that, in the case of *o*-diphenols, π–π interactions between the aromatic ring and a possible histidine of the active site are favoured.

Fig. 4 shows the recordings of the oxidation of 3,4-diaminobenzoic acid by TYR and Fig. 4 inset shows the values of V_0*vs.* the initial concentration of 3,4-diaminobenzoic acid, [3,4-diaminobenzoic acid]$_0$, which enables V_{max} and K_m to be calculated, by means of Eq. (1).

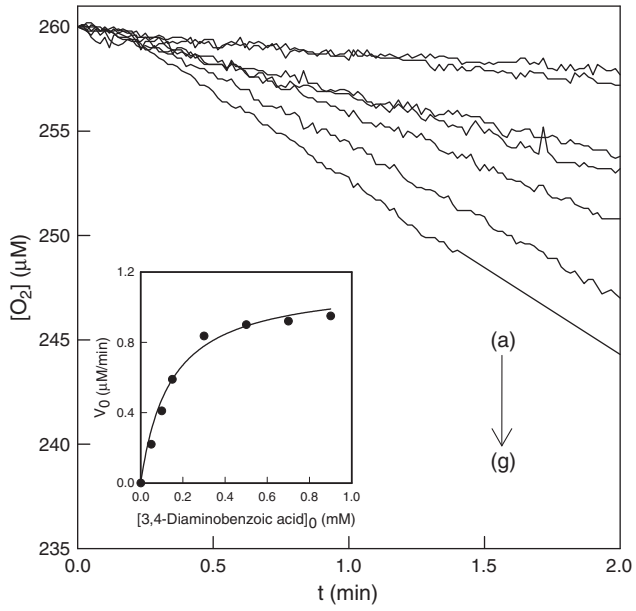

Fig. 4. Oxymetric recordings of the oxidation of 3,4-diaminobenzoic acid by TYR. The experimental conditions were 30 mM sodium phosphate buffer (pH 7.0), 25 °C, $[AH_2]_0 = 0.2$ mM, $[E]_0 = 0.25$ μM and the initial substrate concentrations (mM) were: (a) 0.05, (b) 0.1, (c) 0.15, (d) 0.3, (e) 10.5, (f) 0.7 and (g) 0.9. Inset. Representation of the initial steady-state rates (V_0) *vs.* [3,4-diaminobenzoic acid]$_0$.

3.7. Oxidation of aromatic monoamines by TYR and comparison with monophenols

TYR oxidises *o*-diphenols to *o*-quinones because of its diphenolase or catecholase activity. However, it also shows monophenolase or cresolase, whereby it hydroxylates monophenols to *o*-diphenols. In the same way as it oxidises *o*-aminophenols and aromatic *o*-diamines to their corresponding *o*-quinoneimine and diimines, TYR can also hydroxylate aromatic monoamines and convert them into *o*-aminophenols and *o*-quinoneimines. Using the measuring methods described in this study, the hydroxylation of several aromatic monoamines with different groups in their side chains (in C-1) was characterised.

Fig. 5 depicts how the oxidation of 3-amino-4-hydroxytoluene by periodate in deficiency gives rise to an isosbestic point at λ = 318 nm. Fig. 5 inset A shows the spectrophotometric recordings at 318 nm, obtained by measuring the appearance of oxidised adduct. Raising the initial concentration of 3-aminotoluene (the aromatic monoamine corresponding to 3-amino-4-hydroxytoluene) increases the reaction rate, and when these initial rates are represented with respect to $[S]_0$ and fitted by non-linear regression to Eq. (1), V_{max} and K_m can be obtained for this aromatic monoamine, as shown in Fig. 5 inset B (see Table 2).

The oxidation of 4-aminoanisole by tyrosinase in the presence of MBTH gives an isosbestic point at λ = 498 nm (Fig. 2), which permits the molar absorptivity (ε) to be calculated at this point. Fig. 2 inset A

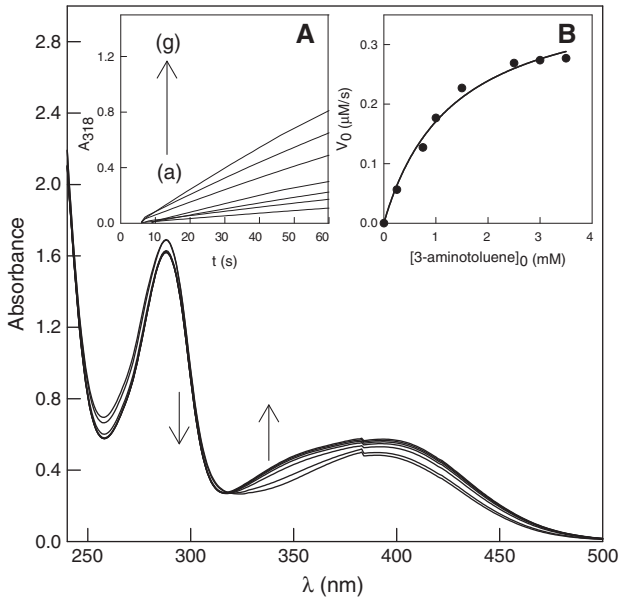

Fig. 5. Spectrophotometric scans of the 3-amino-4-hydroxytoluene oxidation by periodate in deficiency. The experimental conditions were 30 mM sodium phosphate buffer (pH 7.0), 25 °C, $[3\text{-amino-4-hydroxytoluene}]_0 = 0.6$ mM and $[IO_4^-]_0 = 60$ μM. The spectrophotometric scans were made every 3 min. Inset A. Spectrophotometric recordings of the oxidation of 3-aminotoluene by TYR at a wavelength of 318 nm. The experimental conditions were 30 mM sodium phosphate buffer (pH 7.0), 25 °C, $[E]_0 = 0.45$ μM and the initial substrate concentrations (mM) were: (a) 0.25, (b) 0.75, (c) 1.0, (d) 1.5, (e) 2.5, (f) 3 and (g) 3.5. Inset B. Representation of the initial steady-state rates (V_0) *vs.* [3-aminotoluene]$_0$.

Author's personal copy

Table 3
Values of the kinetic constants characterising the oxidation of aromatic monoamines and monophenols by TYR.

Aromatic monoamines	k_{cat} (s^{-1})	K_m (mM)	Phenols	k_{cat} (s^{-1})	K_m (mM)
Aniline	0.45 ± 0.03	0.64 ± 0.09	Phenol	10.81 ± 1.51	0.61 ± 0.04
2-aminobenzoic acid	$(0.13 \pm 0.01) \times 10^{-3}$	2.36 ± 0.34	2-hydroxybenzoic acid	0.046 ± 0.002	2.62 ± 0.18
3-aminobenzoic acid	$(0.33 \pm 0.01) \times 10^{-3}$	0.28 ± 0.02	3-hydroxybenzoic acid	0.64 ± 0.03	2.35 ± 0.32
4-aminobenzoic acid	$(5.04 \pm 0.32) \times 10^{-3}$	0.14 ± 0.01	4-hydroxybenzoic acid	1.70 ± 0.07	0.22 ± 0.03
2-aminotoluene	0.33 ± 0.02	2.93 ± 0.38	2-methylphenol	7.37 ± 0.40	1.48 ± 0.18
3-aminotoluene	0.46 ± 0.04	1.26 ± 0.07	3-methylphenol	7.51 ± 0.65	0.62 ± 0.09
4-aminotoluene	1.01 ± 0.03	1.04 ± 0.12	4-methylphenol	16.12 ± 1.53	0.38 ± 0.05
2-aminoanisole	0.09 ± 0.01	0.26 ± 0.03	2-hydroxyanisole	5.47 ± 0.21	5.40 ± 0.60
3-aminoanisole	0.12 ± 0.01	0.15 ± 0.02	3-hydroxyanisole	46.87 ± 2.06	2.53 ± 0.26
4-aminoanisole	1.24 ± 0.21	0.09 ± 0.01	4-hydroxyanisole	184.20 ± 6.10	0.08 ± 0.01
4-aminophenylalanine	0.01 ± 0.01	0.42 ± 0.05	4-hydroxyphenylalanine	8.12 ± 1.44	0.27 ± 0.03

depicts the oxidation of 4-aminoanisole by TYR, measuring the appearance of oxidised adduct formed between the *o*-quinoneimine and a powerful nucleophile like MBTH [15,29]. By representing V_0*vs.* $[S]_0$ (Fig. 2 inset B), V_{max} and K_m can be calculated by non-linear regression fitting with respect to Eq. (1) (Table 3).

As in the case of monophenols, the natural substrates of TYR, aromatic monoamines, have very low catalytic constants compared with *o*-aminophenols, although the constants are higher in aromatic monoamines with electrodonating groups or with H in their side chain on C-1 than in those with electrowithdrawing groups. When aromatic monoamines substituted in 2, 3 or 4 position of the benzene ring are compared, those with the amino group in 4 show a higher k_{cat}, suggesting that the enzyme hydroxylates substrates substituted in *para* position more readily than those substituted in *meta* and *ortho* positions because of the lower steric hindrance [31] (Table 3).

The Michaelis constants (K_m) follow the order *ortho*>*meta*>*para* for both aromatic monoamines and phenols and, moreover, fulfil Eq. (3). Note the very little difference that frequently exists between the Michaelis constants of the aromatic monoamines and *o*-diamines (Tables 2 and 3).

3.8. Proposed mechanisms for the oxidation of aromatic monoamines and o-diamines and aminophenols by TYR

Schemes 2 and 3 represent the proposed structural mechanism to explain the oxidation of aromatic monoamines and *o*-diamines and *o*-aminophenols by TYR. Scheme 2 refers to the oxidation of *o*-aminophenols (diphenolase activity) and aromatic monoamines (monophenolase activity). Starting with the enzymatic form E_m, its binding to the *o*-aminophenol in Step 1 is seen to form the complex $(E_m - S)_0$. Once bound to the substrate, a proton from the NH_2 group is transferred to a group of the enzyme, which acts as a base, and then the nitrogen of the substrate binds to the *CuB* of the active site of the enzyme, forming the complex $(E_m - S)_1$. The amino group of the substrate is always the first to bind because it has a greater nucleophilic power than the hydroxyl (Step 2). In Step 3, the hydroxyl group transfers a proton to a histidine of the *CuA* of the enzyme active site [7]. The *o*-aminophenol is thus bound diaxially to the enzyme and the concerted oxidation/reduction generates the quinoneimine and the deoxygenated form of the enzyme E_d (Step 4). In Step 5, this form, E_d, binds to O_2 to form E_{ox}, while in Step 6, another molecule of the substrate (*o*-aminophenol) binds to the enzyme $(E_{ox} - S)_0$. Then, the nitrogen from the substrate binds to *CuB* of the enzyme because it is a more potent nucleophile than the oxygen of the hydroxyl, giving $(E_{ox} - S)_1$; subsequently, the oxygen from the OH attacks the copper and the hydrogen is transferred to the histidine $(E_{ox} - S)_2$ (Step 7). The electrowithdrawing effect of the *CuB* may facilitate the transfer of the proton from the amino group to the peroxide group of the active site, since the base is already protonated $(E_{ox} - S)_3$. (Step 8). Since the *o*-aminophenol is bound diaxially to E_{ox}, a concerted oxidation/reduction action gives rise to E_m and *o*-quinoneimine (Step 9), and the cycle starts again.

As regards the hydroxylation of the aromatic monoamines, as occurs with monophenols, the system starts with the form E_{ox} (Step 10) since the E_m form is inactive towards monophenols (Steps 16 and 17) and aromatic monoamines, which is the reason for the characteristic lag period of TYR [2,32,33]. The NH_2 group cedes the H^+ to the peroxide group of the active site of E_{ox}, while the remaining NH binds to the *CuB* of the enzyme (Step 11). Now the peroxide attacks the benzene ring, forming the complex $(E_m - A)_4$ (Step 12), which may undergo one of two possible reactions: (*i*) the NH group is protonated to become NH_2^+ (Step 13) and the complex $(E_m - S)_5$ is formed, while the binding of the oxygen to the copper of $(E_m - S)_5$ is broken, producing the complex $(E_m - S)_1$ (Step 15). This complex can yield $(E_m - S)_0$, releasing *o*-aminophenol or initiates the diphenolase cycle or (*ii*) the substrate is released from the enzyme by the OH group, forming the complex $(E_m - S)_2$ (Step 14), the rest of the cycle continuing as normal.

Note that, as with the monophenolase activity of TYR, which needs an *o*-diphenol to act, in the case of aromatic monoamines the presence of the *o*-aminophenol is necessary for the enzyme to act. This is formed in Steps 1 and 15 of Scheme 1.

As regards the aromatic *o*-diamines, the structural mechanism proposed (Scheme 3) is the same as that proposed for the *o*-aminophenols (Scheme 2) but, in this case, since two NH_2 groups exist, the NH_2 which attacks first will be that with a lower chemical shift (δ)—which, with electrodonating groups in C-1, will be the amino group in carbon 4 (δ_4).

4. Discussion on the kinetic constants of Tables 1–3

As a general commentary concerning Tables 1–3, the *o*-aminophenols and aromatic *o*-diamines are oxidised, while the aromatic monoamines are hydroxylated with catalytic constants that are much lower than those of the corresponding *o*-diphenols or monophenols.

In the case of *o*-aminophenols and *o*-diphenols (Table 1), the difference between the molecules with the same structure is one order of magnitude ($k_{cat}^{o-diphenols} > k_{cat}^{aminophenols}$). The similarity of the K_m values indicates, according to Eq. (3), that the *o*-diphenols bind

Scheme 2. Structural mechanism to explain the oxidation of *o*-aminophenols and aromatic monoamines by TYR. *Em*, met-tyrosinase; $(E_mS)_0$, met-tyrosinase/*o*-aminophenol complex; $(E_m{-}S)_1$, met-tyrosinase/*o*-aminophenol complex axially bound to a Cu atom; $(E_m{-}S)_2$, met-tyrosinase/*o*-aminophenol complex axially bound to a Cu atom with the proton transferred to the base B; $(E_m{-}S)_3$, met-tyrosinase/*o*-aminophenol complex axially bound to the two Cu atoms with the proton of the OH group transferred to the histidine; E_d, deoxy-tyrosinase; E_{ox}, oxy-tyrosinase; $(E_{ox}S)_0$, oxy-tyrosinase/*o*-aminophenol complex; $(E_{ox}{-}S)_1$, oxy-tyrosinase/*o*-aminophenol complex axially bound to a Cu atom; $(E_{ox}{-}S)_2$, oxy-tyrosinase/*o*-aminophenol complex axially bound to the two Cu atoms; $(E_{ox}{-}S)_3$, oxy-tyrosinase/*o*-aminophenol complex axially bound to the two Cu atoms with the proton transferred to the peroxide; $(E_{ox}A)_0$, oxy-tyrosinase/aromatic monoamine complex; $(E_{ox}A)_1$, oxy-tyrosinase/aromatic monoamine complex axially bound to a Cu atom with the proton transferred to the peroxide; $(E_m{-}S)_4$, met-tyrosinase/*o*-aminophenol complex axial-equatorially bound to the two Cu atoms; $(E_m{-}S)_5$, met-tyrosinase/*o*-aminophenol complex axial-equatorially bound to the two Cu atoms, binding to the base BH through a hydrogen bond; $(E_mA)_0$, met-tyrosinase/aromatic monoamine complex; $(E_mA)_1$, met-tyrosinase/aromatic monoamine complex axially bound to a Cu atom.

Author's personal copy

better to the enzyme (higher k_6) than the *o*-aminophenols, probably because a π–π interaction with a possible histidine is favoured. Note that the substituent in C-1 affects the values of k_{cat} and K_m—when the substituent is a methyl group (electrodonating), the k_{cat} for 3-hydroxy-4-aminotoluene or 3-amino-4-hydroxytoluene are high (slightly higher in the latter) and the K_m values, in accordance with

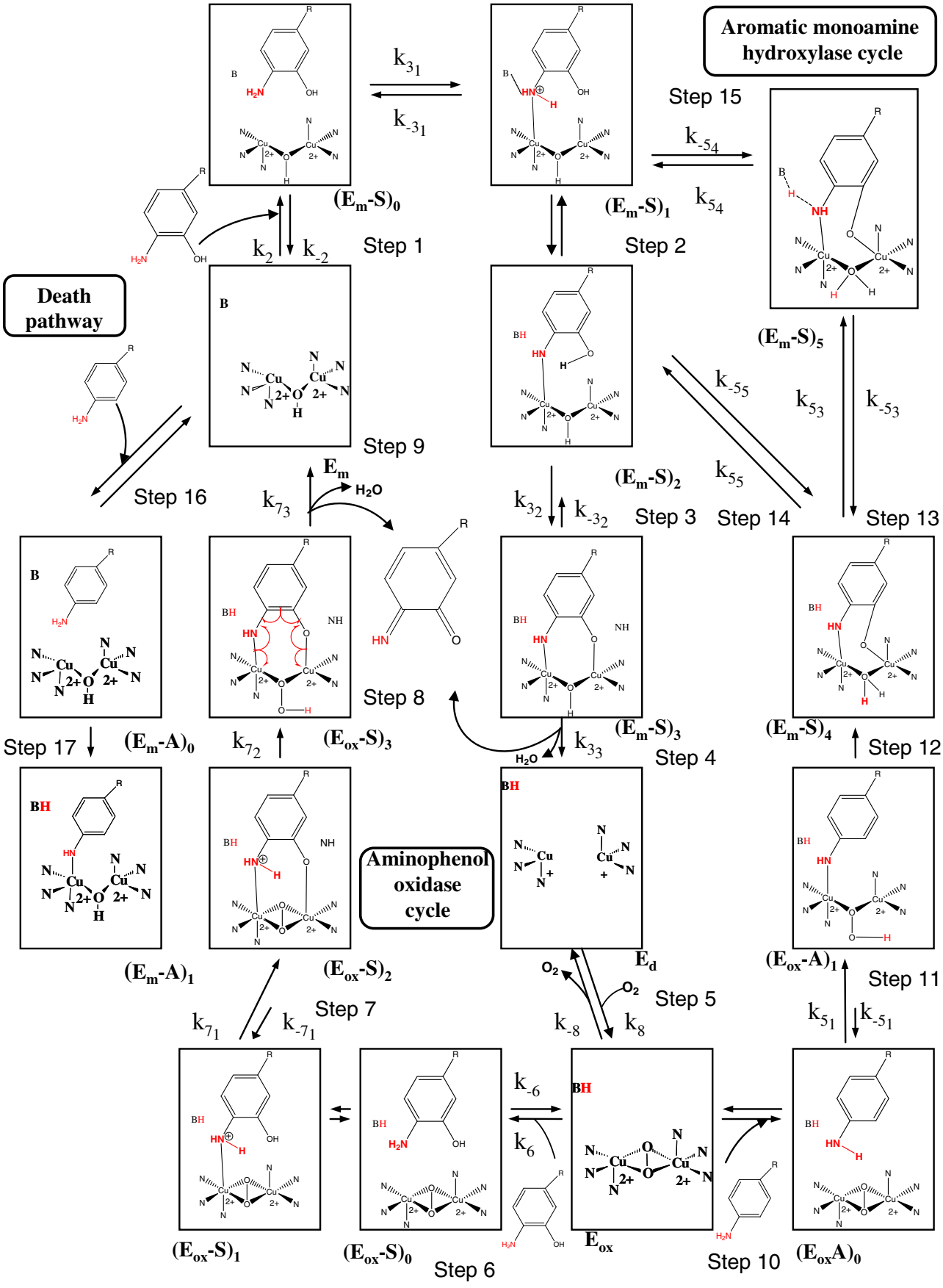

Author's personal copy

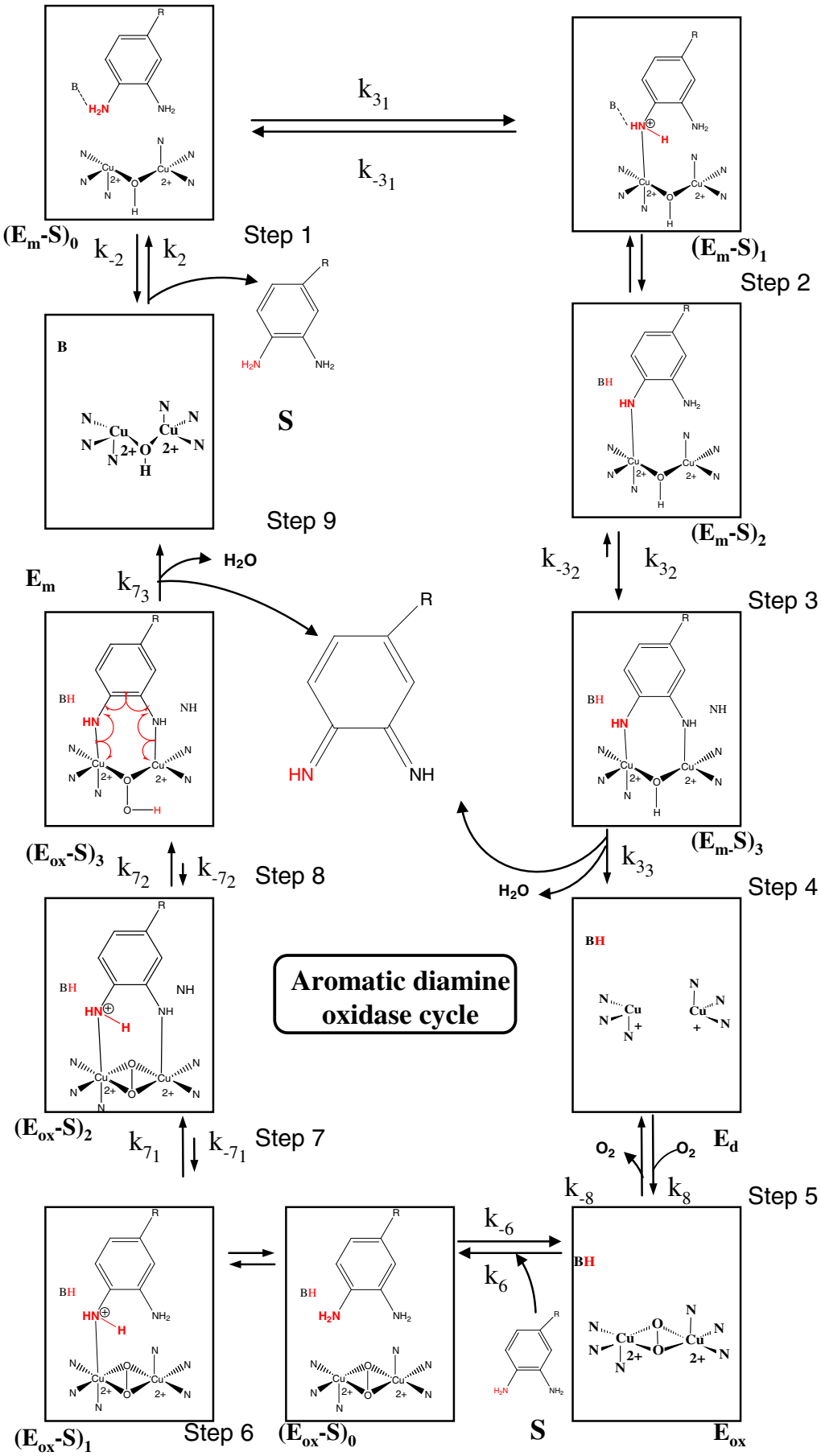

Author's personal copy

Eq. (3), increase (slightly more so in the case of 3-amino-4-hydroxytoluene). When an electrowithdrawing group exists on C-1 (such as a carboxyl group), the k_{cat} values fall (slightly more so for 3-amino-4-hydroxybenzoic acid), as do the K_m values (Table 2). Note that the k_{cat} is highest when there is no substituent in C-1 (see Table 2).

In the case of the aromatic *o*-diamines (Table 2), except 2,3-diaminobenzoic acid and 2,3-dihydroxybenzoic acid, in which steric hindrance phenomena dominate the process, the catalytic constants are two orders of magnitude lower than for their respective *o*-diphenols ($k_{cat}^{o-diphenols} \gg k_{cat}^{diamines}$). However, the K_m values are in the same range because the *o*-diphenols bind better to the enzyme than the aromatic *o*-diamines. When the amino group is in 2,3 position, the steric hindrance effect is greater than the electronic effect and the k_{cat} values fall, contrary to that which occurs with K_m.

Such behaviour is similar in the case of aromatic monoamines (Table 3). The values of the catalytic constants are two orders of magnitude greater than for the monophenols. Note that the k_{cat} values of the substrates with the group in *meta* position with respect to C-1 are always greater than those with the group in *ortho* position, since the steric hindrance is stronger than the electronic effect in *ortho*.

It has been demonstrated that TYR of *N. crassa* can oxidise several types of *o*-aminophenols and aromatic amines [10]. The same authors demonstrated the oxidation of these compounds using oxymetric methods, revealing also that the catalytic constants of TYR towards these compounds are three orders of magnitude lower than those of their phenolic analogues.

In a more recent work [11], mushroom TYR was demonstrated to oxidise an *o*-aminophenol substituted in 2 and 3 of the benzene ring, e.g. 3-hydroxy-2-aminobenzoic acid (3-hydroxyanthranilic acid, see Scheme 1), in the same way as *N. crassa* TYR. Similarly, the authors mention the influence of this compound on the monophenolase and diphenolase activities of mushroom TYR. A different type of effect was seen for *o*-aminophenol (3-hydroxykynurenine) on mushroom TYR, when it acted as a substrate/activator [12].

As in the case of *N. crassa* TYR, mushroom TYR shows catalytic constants that are two orders of magnitude lower for the oxidation of 2-aminobenzoic acid ($0.0001\ s^{-1}$) than for the oxidation of 2-hydroxybenzoic acid ($0.046\ s^{-1}$), the same being true for 4-aminoanisole ($1.24\ s^{-1}$) compared with 4-hydroxyanisole ($184.20\ s^{-1}$) (Table 3).

As regards the proposed reaction mechanism, regardless of the R group or the position that it occupies, the NH_2 group will always attack before the OH group in the case of *o*-aminophenols, while in the case of aromatic *o*-diamines, the amino group with the lowest chemical shift will attack first. In these mechanisms (Schemes 1 and 2), Steps 7 and 8 are the slowest since they involve a double migration of a proton.

Electrodonating groups such as methyl favour to the *para* position, and, as a consequence, the oxygen of the hydroxyl group in this position is more nucleophilic, while in electrowithdrawing groups (e.g. the carboxyl group), the *para* position is not favoured and so the oxygen of the hydroxyl group is less nucleophilic. Lastly, deprotonation of the aromatic *o*-diamines is much more difficult, which greatly slows down the oxidation process (Table 2).

We conclude therefore that deprotonation of the substrates in the action mechanism of tyrosinase is necessary, as we proposed previously [25,34,35], and that although the oxidation/reduction potentials are practically the same for both aromatic monoamines and phenols, the high *pK* of the amines slows down the reaction—data that agree with the results obtained for monophenols and *o*-diphenols [17,22,33].

In conclusion, we have demonstrated that mushroom TYR oxidises aromatic monoamines and *o*-diamines and *o*-aminophenols. For this oxidation process, we propose structural mechanisms that agree with the obtained experimental results and which show a certain parallelism to the mechanisms proposed for monophenolase and diphenolase activities of TYR [1,36,37]. In addition, we have kinetically characterised a wide number of substrates.

Acknowledgements

This paper was partially supported by grants from: Ministerio de Educación y Ciencia (Madrid, Spain) project BIO2009-12956, Fundación Séneca (CARM, Murcia, Spain) projects 08856/PI/08 and 08595/PI/08, andConsejería de Educación (CARM, Murcia, Spain) BIO-BMC 06/01-0004. JLMM and FGM hold two fellowships from Fundación Caja Murcia (Murcia, Spain).

Appendix A. Supplementary data

Supplementary data to this article can be found online at doi:10.1016/j.bbapap.2011.07.015.

References

[1] L. Fenoll, M.J. Peñalver, J.N. Rodriguez-Lopez, P.A. Garcia-Ruiz, F. Garcia-Canovas, J. Tudela, Deuterium isotope effect on the oxidation of monophenols and *o*-diphenols by tyrosinase, Biochem. J. 380 (2004) 643–650.
[2] A. Sanchez-Ferrer, J.N. Rodriguez-Lopez, F. Garcia-Canovas, F. Garcia-Carmona, Tyrosinase: a comprehensive review of its mechanism, Biochim. Biophys. Acta 1247 (1995) 1–11.
[3] E.I. Solomon, U.M. Sundaram, T.E. Machonkin, Multicopper oxidases and oxygenases, Chem. Rev. 96 (1996) 2563–2606.
[4] J.R. Jolley Jr., L.H. Evans, N. Makino, H.S. Mason, Oxytyrosinase, J. Biol. Chem. 249 (1974) 335–345.
[5] H. Decker, R. Dillinger, F. Tuczek, How does tyrosinase work? Recent insights from model chemistry and structural biology, Angew. Chem. Int. Ed. 39 (2000) 1591–1595.
[6] T. Klabunde, C. Eicken, J.C. Sacchettini, B. Krebs, Crystal structure of a plant catechol oxidase containing a dicopper center, Nat. Struct. Biol. 5 (1998) 1084–1090.
[7] Y. Matoba, T. Kumagai, A. Yamamoto, H. Yoshitsu, M. Sugiyama, Crystallographic evidence that the dinuclear copper center of tyrosinase is flexible during catalysis, J. Biol. Chem. 281 (2006) 8981–8990.
[8] M. Sendovski, M. Kanteev, V. Shuster Ben-Yosef, N. Adir, A. Fishman, Crystallization and preliminary X-ray crystallographic analysis of a bacterial tyrosinase from *Bacillus megaterium*, Acta Crystallogr. Sect. F Struct. Biol. Cryst. Commun. 66 (2010) 1101–1103.
[9] M. Sendovski, M. Kanteev, V. Shuster Ben-Yosef, N. Adir, A. Fishman, First structures of an active bacterial tyrosinase reveal copper plasticity, J. Mol. Biol. 405 (2011) 227–237.
[10] O. Toussaint, K. Lerch, Catalytic oxidation of 2-aminophenols and ortho hydroxylation of aromatic amines by tyrosinase, Biochemistry 26 (1987) 8567–8571.
[11] A. Rescigno, E. Sanjust, A.C. Rinaldi, F. Sollai, N. Curreli, A. Rinaldi, Effect of 3-hydroxyanthranilic acid on mushroom tyrosinase activity, Biochim. Biophys. Acta 1384 (1998) 268–276.
[12] E. Sanjust, G. Cecchini, F. Sollai, N. Curreli, A. Rescigno, 3-Hydroxykynureine as a substrate/activator for mushroom tyrosinase, Arch. Biochem. Biophys. 412 (2003) 272–278.
[13] F. Maddaluno, K.F. Faull, Inhibition of mushroom tyrosinase by 3-amino-L-tyrosine: molecular probing of the active site of the enzyme, Experientia 44 (1988) 885–887.
[14] B. Gasowska, P. Kafarski, H. Wojtasek, Interaction of mushroom tyrosinase with aromatic amines, *o*-diamines and *o*-aminophenols, Biochim. Biophys. Acta 1673 (2004) 170–177.
[15] F. Garcia-Molina, J.L. Muñoz, R. Varon, J.N. Rodriguez-Lopez, F. Garcia-Canovas, J. Tudela, A review on spectrophotometric methods for measuring the monophenolase and diphenolase activities of tyrosinase, J. Agric. Food Chem. 55 (2007) 9739–9749.
[16] J.N. Rodriguez-Lopez, J.R. Ros-Martinez, R. Varon, F. Garcia-Canovas, Calibration of a Clark-type oxygen electrode by tyrosinase-catalyzed oxidation of a 4-*tert*-butylcatechol, Anal. Biochem. 202 (1992) 356–360.
[17] J.N. Rodriguez-Lopez, L.G. Fenoll, P.A. Garcia-Ruiz, R. Varon, J. Tudela, R.N. Thorneley, F. Garcia-Canovas, Stopped-flow and steady-state study of the diphenolase activity of mushroom tyrosinase, Biochemistry 39 (2000) 10497–10506.

Scheme 3. Structural mechanism to explain the oxidation of aromatic *o*-diamines by TYR. E_m, met-tyrosinase; $(E_mS)_0$, met-tyrosinase/aromatic *o*-diamine complex; $(E_m\text{-}S)_1$, met-tyrosinase/aromatic *o*-diamine complex axially bound to a Cu atom with the base forming a hydrogen bridge; $(E_m\text{-}S)_2$, met-tyrosinase/aromatic *o*-diamine complex axially bound to a Cu atoms with protonated base; $(E_m\text{-}S)_3$, met-tyrosinase/aromatic *o*-diamine complex axially bound to the two Cu atoms; E_d, deoxy-tyrosinase; E_{ox}, oxy-tyrosinase; $(E_{ox}S)_0$, oxy-tyrosinase/aromatic *o*-diamine complex; $(E_{ox}\text{-}S)_1$, oxy-tyrosinase/aromatic *o*-diamine complex axially bound to a Cu atom; $(E_{ox}\text{-}S)_2$, oxy-tyrosinase/aromatic *o*-diamine complex axially bound to the two Cu atoms and with protonated base; $(E_{ox}\text{-}S)_3$, oxy-tyrosinase/aromatic o-diamine complex axially bound to the two Cu atoms with the proton transferred to the peroxide.

Author's personal copy

[18] M.M. Bradford, A rapid and sensitive method for the quantification of microgram quantities of proteins utilising the principle of protein–dye binding, Anal. Biochem. 72 (1976) 248–254.
[19] L.G. Fenoll, J.N. Rodriguez-Lopez, F. Garcia-Molina, F. Garcia-Canovas, J. Tudela, Michaelis constants of mushroom tyrosinase with respect to oxygen in the presence of monophenols and diphenols, Int. J. Biochem. Cell Biol. 34 (2002) 332–336.
[20] J.R. Ros, J.N. Rodriguez-Lopez, F. Garcia-Canovas, Tyrosinase: kinetics analysis of the transient phase and the steady state, Biochim. Biophys. Acta 1204 (1994) 33–42.
[21] Jandel Scientific., Sigma Plot 9.0 for Windows™, Jandel Scientific: Core Madera, 2006.
[22] J.L. Muñoz-Muñoz, F. Garcia-Molina, R. Varon, J. Tudela, F. Garcia-Canovas, J.N. Rodriguez-Lopez, New features of the steady-state rate related with the initial concentration of substrate in the diphenolase and monophenolase activities of tyrosinase, J. Math. Chem. 48 (2010) 347–362.
[23] K.D. Karlin, D.-H. Lee, H.V. Obias, K.J. Humphreys, Copper–dioxygen complexes: functional models of proteins, Pure Appl. Chem. 70 (1998) 855–862.
[24] L. Casella, E. Monzani, M. Gulloti, D. Cavagino, G. Cerina, L. Santagostini, R. Ugo, Functional modelling of tyrosinase. Mechanism of phenol ortho hydroxylation by dinuclear copper complexes, Inorg. Chem. 35 (1996) 7516–7625.
[25] F. García-Molina, J.L. Muñoz-Muñoz, M. Garcia-Molina, P.A. Garcia-Ruiz, J. Tudela, F. Garcia-Canovas, J.N. Rodriguez-Lopez, Melanogenesis inhibition due to NADH, Biosci. Biotechnol. Biochem. 74 (2010) 1777–1787.
[26] J.L. Muñoz-Muñoz, F. García-Molina, P.A. Garcia-Ruiz, R. Varon, J. Tudela, F. Garcia-Canovas, J.N. Rodriguez-Lopez, Stereospecific inactivation of tyrosinase by L- and D-ascorbic acid, Biochim. Biophys. Acta 1794 (2009) 244–253.
[27] F. García-Molina, J.L. Muñoz-Muñoz, J.R. Acosta, P.A. Garcia-Ruiz, J. Tudela, F. Garcia-Canovas, J.N. Rodriguez-Lopez, Melanogenesis inhibition by tetrahydropterines, Biochim. Biophys. Acta 1794 (2009) 1766–1774.
[28] F. García-Molina, J.L. Muñoz-Muñoz, F. Martinez-Ortiz, P.A. Garcia-Ruiz, J. Tudela, F. Garcia-Canovas, J.N. Rodriguez-Lopez, Tetrahydrofolic acid is a potent suicide substrate of mushroom tyrosinase, J. Agric. Food Chem. 59 (2011) 1383–1391.
[29] J.C. Espin, J. Tudela, F. Garcia-Canovas, 4-Hydroxyanisole: the most suitable monophenolic substrate for determining spectrophotometrically the monophenolase activity of polyphenol oxidase from fruits and vegetables, Anal. Biochem. 259 (1998) 118–126.
[30] J.L. Munoz, F. Garcia-Molina, R. Varon, J.N. Rodriguez-Lopez, F. Garcia-Canovas, J. Tudela, Calculating molar absorptivities for quinones: application to the measurement of tyrosinase activity, Anal. Biochem. 351 (2006) 128–138.
[31] L.G. Fenoll, J.N. Rodriguez-Lopez, R. Varon, P.A. Garcia-Ruiz, F. Garcia-Canovas, J. Tudela, Action mechanism of tyrosinase on meta- and para-hydroxylated monophenols, Biol. Chem. 381 (2000) 313–320.
[32] F.G. Molina, J.L. Munoz, R. Varon, J.N. Lopez, F.G. Canovas, J. Tudela, An approximate analytical solution to the lag period of monophenolase activity of tyrosinase, Int. J. Biochem. Cell Biol. 39 (2007) 238–252.
[33] D.E. Wilcox, A.G. Porras, Y.T. Hwang, K. Lerch, M.E. Winkler, E.I. Solomon, Substrate analogue binding to the coupled binuclear copper active site in tyrosinase, J. Am. Chem. Soc. 107 (1985) 4015–4027.
[34] J.L. Muñoz-Muñoz, F. Garcia-Molina, P.A. Garcia-Ruiz, M. Molina-Alarcon, J. Tudela, F. Garcia-Canovas, J.N. Rodriguez-Lopez, Phenolic substrates and suicide inactivation of tyrosinase: kinetics and mechanism, Biochem. J. 416 (2008) 413–440.
[35] J.L. Munoz-Munoz, F. Garcia-Molina, R. Varon, P.A. Garcia-Ruiz, J. Tudela, F. Garcia-Canovas, J.N. Rodriguez-Lopez, Suicide inactivation of the diphenolase and monophenolase activities of tyrosinase, IUBMB Life 62 (2010) 539–547.
[36] L. Fenoll, J.N. Rodriguez-Lopez, F. Garcia-Sevilla, P.A. Garcia-Ruiz, R. Varon, F. Garcia-Canovas, J. Tudela, Analysis and interpretation of the action mechanism of mushroom tyrosinase on monophenols and diphenols generating highly unstable *o*-quinones, Biochim. Biophys. Acta 1548 (2001) 1–22.
[37] M.J. Penalver, J.N. Rodriguez-Lopez, P.A. Garcia-Ruiz, F. Garcia-Canovas, J. Tudela, Solvent deuterium isotope effect on the oxidation of *o*-diphenols by tyrosinase, Biochim. Biophys. Acta 1650 (2003) 128–135.

Supplementary material.

Table 1SM

Measurement wavelength (λ) and molar absorptivities (ε) of the substrates used in this work.

Substrate	Method	λ (nm)	ε (M^{-1} cm^{-1})
2-Aminobenzoic acid	Adduct appearance	398	3450
3-aminobenzoic acid	O_2 disappearance	-	-
4-Aminobenzoic acid	O_2 disappearance	-	-
2-Aminotoluene (*o*-toluidine)	O_2 disappearance	-	-
3-Aminotoluene (*m*-toluidine)	Adduct appearance	318	3500
4-Aminotoluene (*p*-toluidine)	Adduct appearance	476	1583
2-Aminoanisole (*o*-anisidine)	O_2 disappearance	-	-
3-Aminoanisole (*m*-anisidine)	O_2 disappearance	-	-
4-Aminoanisole (*p*-anisidine)	Adduct MBTH-Quinoneimine	498	30700
4-Aminophenylalanine	Adduct MBTH-Quinoneimine	497	42000
Aniline	O_2 disappearance	-	-
2,3-Diaminobenzoic acid	AH_2 disappearance	277	8260
3,4-Diaminobenzoic acid	O_2 disappearance	-	-
2,3-Diaminotoluene	Adduct appearance	476	2800
3,4-Diaminotoluene	AH_2 disappearance	260	10810
4-Methoxy-1,2-phenylendiamine	AH_2 disappearance	265	11170
1,2-Diaminobenzene	Adduct appearance	397	6733
2-Amino-3-hydroxybenzoic acid	Adduct appearance	398	3450
3-Amino-2-hydroxybenzoic acid	O_2 disappearance	-	-

3-Amino-4-hydroxybenzoic acid	Adduct appearance	395	7273
4-Amino-3-hydroxybenzoic acid	AH_2 disappearance	280	7273
3-Amino-4-hydroxytoluene	Adduct appearance	318	3500
3-Hydroxy-4-aminotoluene	Adduct appearance	476	1583
3-Amino-L-tyrosine	AH_2 disappearance	265	11170
2-Aminophenol	AH_2 disappearance	265	11170
2-Hydroxybenzoic acid	O_2 disappearance	-	-
3-Hydroxybenzoic acid	O_2 disappearance	-	-
4-Hydroxybenzoic acid	O_2 disappearance	-	-
2-Methylphenol (*o*-cresol)	O_2 disappearance	-	-
3-Methylphenol (*m*-cresol)	Adduct appearance	351	667
4-Methylphenol (*p*-cresol)	O_2 disappearance	-	-
2-Hydroxyanisole	Adduct appearance	337	2150
3-Hydroxyanisole	O_2 disappearance	-	-
4-Hydroxyanisole	Adduct MBTH-Quinoneimine	492	31300
4-Hydroxyphenylalanine (L-tyrosine)	Appearance of dopachrome	475	3600
Phenol	O_2 disappearance	-	-
2,3-Dihydroxybenzoic acid	O_2 disappearance	-	-
3,4-Dihydroxybenzoic acid	O_2 disappearance	-	-
3-Methylcatechol	AH_2 disappearance	265	11170
4-Methylcatechol	Adduct appearance	351	667
3-Methoxycatechol	Adduct appearance	337	2150
L-dopa	Appearance of dopachrome	475	3600
Catechol	NADH disappearance	340	6230

Scheme ISM

Chemical structure of the substrates used in this work.

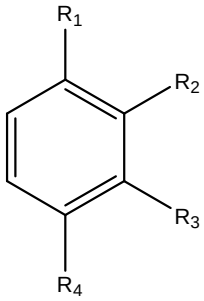

Substrate	R_1	R_2	R_3	R_4
2-Aminobenzoic acid	-COOH	NH_2	H	H
3-aminobenzoic acid	-COOH	H	NH_2	H
4-aminobenzoic acid	-COOH	H	H	NH_2
2-Aminotoluene (*o*-toluidine)	$-CH_3$	NH_2	H	H
3-Aminotoluene (*m*-toluidine)	$-CH_3$	H	NH_2	H
4-Aminotoluene (*p*-toluidine)	$-CH_3$	H	H	NH_2
2-aminoanisole (*o*-anisidine)	$-OCH_3$	NH_2	H	H
3-aminoanisole (*m*-anisidine)	$-OCH_3$	H	NH_2	H
4-Aminoanisole (*p*-anisidine)	$-OCH_3$	H	H	NH_2
4-Aminophenylalanine	$-CH_2-CH(NH_2)-COOH$	H	H	NH_2
Aniline	NH_2	H	H	H
2,3-Diaminobenzoic acid	-COOH	NH_2	NH_2	H
3,4-Diaminobenzoic acid	-COOH	H	NH_2	NH_2
2,3-Diaminotoluene	$-CH_3$	NH_2	NH_2	H
3,4-Diaminotoluene	$-CH_3$	H	NH_2	NH_2
4-Methoxy-1,2-phenylendiamine	$-OCH_3$	H	NH_2	NH_2
1,2-Diaminobenzene	NH_2	NH_2	H	H
2-Amino-3-hydroxybenzoic acid	-COOH	NH_2	OH	H
3-Amino-2-hydroxybenzoic acid	-COOH	OH	NH_2	H

3-Amino-4-hydroxybenzoic acid	-COOH	H	NH_2	OH
4-Amino-3-hydroxybenzoic acid	-COOH	H	OH	NH_2
3-Amino-4-hydroxytoluene	$-CH_3$	H	NH_2	OH
3-Hydroxy-4-aminotoluene	$-CH_3$	H	OH	NH_2
3-Amino-L-tyrosine	$-CH_2$-CH(NH_2)-COOH	H	NH_2	OH
2-Aminophenol	-OH	NH_2	H	H
2-Hydroxybenzoic acid	-COOH	OH	H	H
3-Hydroxybenzoic acid	-COOH	H	OH	H
4-Hydroxybenzoic acid	-COOH	H	H	OH
2-Methylphenol (*o*-cresol)	$-CH_3$	OH	H	H
3-Methylphenol (*m*-cresol)	$-CH_3$	H	OH	H
4-Methylphenol (*p*-cresol)	$-CH_3$	H	H	OH
2-Hydroxyanisole	$-OCH_3$	OH	H	H
3-Hydroxyanisole	$-OCH_3$	H	OH	H
4-Hydroxyanisole	$-OCH_3$	H	H	OH
4-Hydroxyphenylalanine (L-tyrosine)	$-CH_2$-CH(NH_2)-COOH	H	H	OH
Phenol	-OH	H	H	H
2,3-Dihydroxybenzoic acid	-COOH	OH	OH	H
3,4-Dihydroxybenzoic acid	-COOH	H	OH	OH
3-Methylcatechol	$-CH_3$	OH	OH	H
4-Methylcatechol	$-CH_3$	H	OH	OH
3-Methoxycatechol	$-OCH_3$	OH	OH	H
L-dopa	$-CH_2$-CH(NH_2)-COOH	H	OH	OH
Catechol	-OH	OH	H	H

4.15. SUSTRATOS FENÓLICOS E INACTIVACIÓN SUICIDA DE TIROSINASA: CINÉTICA Y MECANISMO.

El estudio de la cinética y el mecanismo de la inactivación suicida de tirosinasa en la actuación sobre sus sustratos fenólicos han dado lugar a la siguiente publicación adjunta.

4.15.1. Título

Phenolic substrates and suicide inactivation of tyrosinase: kinetics and mechanism.

4.15.2. Autores

Muñoz-Muñoz, J.L.; Garcia-Molina, F.; Garcia-Ruiz, P.A.; Molina-Alarcon, M.; Tudela, J.; Garcia-Cánovas, F. y Rodríguez-López, J.N.

4.15.3. Referencia

Biochemical Journal (2008) 416, 431-440.

4.15.4. Resumen

Se ha estudiado la inactivación suicida de tirosinasa en la actuación sobre sus sustratos. El análisis cinético en fase de transición del mecanismo propuesto, permite obtener soluciones analíticas explícitas de concentración de [Q] *vs.* t. Los efectos electrónicos, estéricos e hidrofóbicos de los sustratos influyen en la reacción enzimática aumentando la constante catalítica tres órdenes de magnitud y la de inactivación un orden de magnitud. Para explicar la inactivación suicida, proponemos un mecanismo en el que la forma enzimática E_{ox} (oxitirosinasa) es la responsable de la inactivación suicida. Una etapa clave podría consistir en la transferencia del protón del grupo hidroxilo de C-1 al peróxido, que actúa como una base generalizada. A partir de las soluciones analíticas obtenidas para este mecanismo, se propone un diseño experimental en distintas etapas, su aplicación consigue determinar las constantes cinéticas de las rutas de catálisis e inactivación suicida. La constante de velocidad de esta reacción está directamente relacionada con la potencia de ataque nucleofílico del grupo hidroxilo del átomo de carbono C-1, obtenido por ^{13}C-RMN (δ_1). La protonación del peróxido facilita el acercamiento de los dos átomos de cobre, y el ataque nucleofílico del grupo hidroxilo de C-2 en diaxial, la coplanaridad del anillo con los átomos de cobre y rápidamente la oxidación/reducción concertada, originando una *o*-quinona. La inactivación suicida tendría lugar, si el grupo hidroxilo de C-2 transfiere el

protón al peróxido protonado que volvería a actuar como una base generalizada. Si esto ocurre, la coplanaridad entre el átomo de cobre, el oxigeno de C-1 y el anillo, posibilitan la oxidación/reducción únicamente sobre un átomo de cobre, originando cobre(0), peróxido de hidrógeno y *o*-quinona que son liberados al medio, llevando consigo la inactivación de la enzima.

BJ www.biochemj.org

BJ Structure

Biochem. J. (2008) **416**, 431–440 (Printed in Great Britain) doi:10.1042/BJ20080892

online data

Phenolic substrates and suicide inactivation of tyrosinase: kinetics and mechanism

Jose L. MUÑOZ-MUÑOZ*, Francisco GARCÍA-MOLINA*, Pedro A. GARCÍA-RUIZ†, Milagros MOLINA-ALARCÓN‡, Jose TUDELA*, Francisco GARCÍA-CÁNOVAS*[1] and Jose N. RODRÍGUEZ-LÓPEZ*

*GENZ: Grupo de Investigación de Enzimología, Departamento de Bioquímica y Biología Molecular-A, Facultad de Química, Universidad de Murcia, E-30100 Espinardo, Murcia, Spain, †QCBA: Grupo de Química de Carbohidratos y Biotecnología de Alimentos, Departamento de Química Orgánica, Facultad de Química, Universidad de Murcia, E-30100 Espinardo, Murcia, Spain, and ‡Departamento de Enfermería, Escuela Universitaria de Enfermería, Universidad de Castilla la Mancha, E-02071, Albacete, Spain

The suicide inactivation mechanism of tyrosinase acting on its substrates has been studied. The kinetic analysis of the proposed mechanism during the transition phase provides explicit analytical expressions for the concentrations of *o*-quinone against time. The electronic, steric and hydrophobic effects of the substrates influence the enzymatic reaction, increasing the catalytic speed by three orders of magnitude and the inactivation by one order of magnitude. To explain the suicide inactivation, we propose a mechanism in which the enzymatic form E_{ox} (*oxy*-tyrosinase) is responsible for such inactivation. A key step might be the transfer of the C-1 hydroxyl group proton to the peroxide, which would act as a general base. Another essential step might be the axial attack of the *o*-diphenol on the copper atom. The rate constant of this reaction would be directly related to the strength of the nucleophilic attack of the C-1 hydroxyl group, which depends on the chemical shift of the carbon C-1 (δ_1) obtained by ^{13}C-NMR. Protonation of the peroxide would bring the copper atoms together and encourage the diaxial nucleophilic attack of the C-2 hydroxyl group, facilitating the co-planarity with the ring of the copper atoms and the concerted oxidation/reduction reaction, and giving rise to an *o*-quinone. The suicide inactivation would occur if the C-2 hydroxyl group transferred the proton to the protonated peroxide, which would again act as a general base. In this case, the co-planarity between the copper atom, the oxygen of the C-1 and the ring would only permit the oxidation/reduction reaction on one copper atom, giving rise to copper(0), hydrogen peroxide and an *o*-quinone, which would be released, thus inactivating the enzyme.

Key words: deprotonation, diaxial, equatorial, mechanism-based inhibitor, mushroom tyrosinase, suicide inactivation.

INTRODUCTION

Tyrosinase or polyphenol oxidase (EC 1.14.18.1) is a copper protein that uses molecular oxygen to catalyse the hydroxylation of monophenols to *o*-diphenols (monophenolase activity) and the oxidation of *o*-diphenols to *o*-quinones (diphenolase activity) [1,2]. Tyrosinase undergoes an inactivation process when it reacts with its substrate, a phenomenon that has long been known in the case of enzymes from a variety of natural sources, including fungi, plants and animals [3–9]. The study of enzymatic inactivation by suicide substrates or mechanism-based inhibitors is of growing importance because of possible pharmacological applications [10,11]. In the case of mammalian, viral, bacterial or parasitic proteases, a recent review looked at the design of mechanism-based enzyme inhibitors [10]. In addition, suicide substrates and mechanism-based enzyme inactivators may be useful for studying enzymatic mechanisms and designing new drugs [12]. Since tyrosinase participates in different physiological processes, such as fruit and vegetable browning and pigmentation in animals [2], the suicide inactivation of this enzyme is of even more interest.

We have made several kinetic studies of suicide inactivation mechanisms using mushroom tyrosinase [13], frog skin tyrosinase [14,15] and peroxidase from different sources [16,17]. We have also studied the suicide inactivation of an enzyme that can be measured from coupled reactions [18] and published a totally experimental study which used several experimental designs to kinetically study suicide inactivation [19].

The kinetics of the suicide inactivation of tyrosinase have been studied and characterized by determining the kinetic parameters that identify a suicide substrate: λ_{max} (maximum apparent inactivation constant), a partition ratio between the catalytic and the inactivation pathways, '*r*', and the Michaelis constant, K_m^S. However, the molecular processes that lead to the suicide inactivation of tyrosinase have not been fully clarified [13–15,18]. To date, three mechanisms have been proposed to explain this inactivation: (i) an attack by the *o*-quinone product on a sensitive nucleophilic group vicinal to the active site [5], (ii) free radical attack on the active site by the ROS (reactive oxygen species) generated during the catalytic oxidation [7], and (iii) a mechanism that involves the catechol substrate presenting itself at the active site as a cresol, 'cresolase presentation'. This leads to the catechol being oxidized to form a product able to undergo deprotonation and reductive elimination, resulting in inactivation of the enzyme through the formation of copper(0) at the active site [20].

Abbreviations used: **Species and concentrations**: AH_2, ascorbic acid; $[E]_0$, initial concentration of tyrosinase; E_d, *deoxy*-tyrosinase; E_i, inactive enzyme; E_m, *met*-tyrosinase; E_{ox}, *oxy*-tyrosinase; E_s, steady-state enzyme; DHPAA, 3,4-dihydroxyphenylacetic acid; DHPPA, 3,4-dihydroxyphenylpropionic acid; $[O_2]$, instantaneous concentration of oxygen; $[O_2]_0$, initial concentration of oxygen; *Q*, product of the enzymatic reaction; $[Q]$, instantaneous concentration of *Q*; *S*, *o*-diphenol acting as suicide substrate; $[S]_0$, initial concentration of *o*-diphenol substrate; SOD, superoxide dismutase. **Kinetic parameters**: λ, apparent inactivation constant; λ_{max}, maximum value of λ for saturating *S*; k_{cat}, catalytic constant of the catalytic pathway ($k_{cat} = \lambda_{max} r$); $K_m^{O_2}$, Michaelis constant for oxygen; K_m^S, Michaelis constant of tyrosinase for *S*; k_x, rate constants of the catalytic pathway; k_x^i, rate constants of the inactivation pathway; $[O_2]_\infty$, oxygen consumed at $t \to \infty$ ($[O_2]_\infty = [O_2]_0 - [O_2]_f$); $[O_2]_f$, oxygen remaining at $t \to \infty$; $[Q]_\infty$, concentration of product *Q* obtained at end of the reaction; V_0, initial rate of the catalytic pathway; *r*, partition ratio ($r = k_{7_2}/k_{7_2}^i = k_{cat}/\lambda_{max}$).

[1] To whom correspondence should be addressed (email canovasf@um.es).

© The Authors Journal compilation © 2008 Biochemical Society

Biochemical Journal

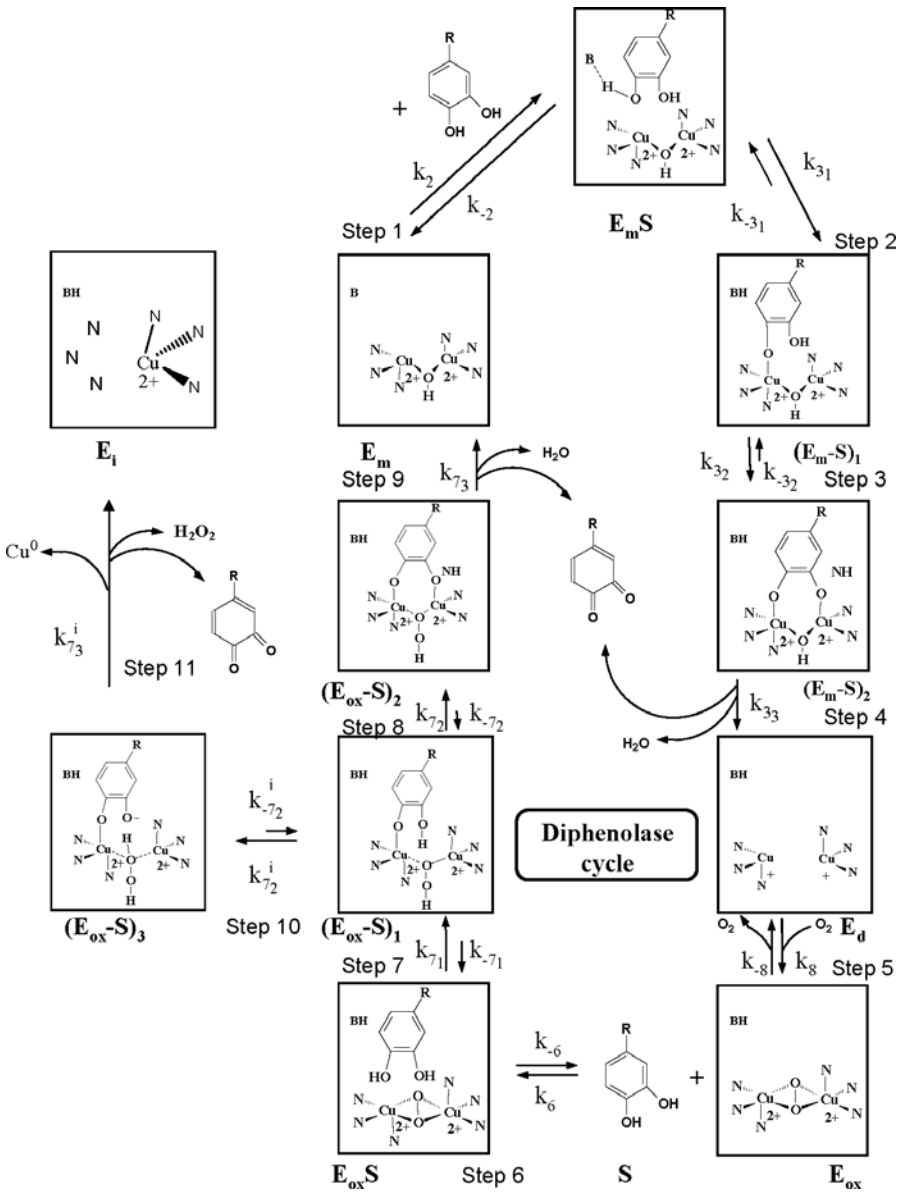

Scheme 1 Structural mechanism proposed to explain the diphenolase cycle and suicide inactivation of tyrosinase

Diphenolase cycle: E_m, *met*-tyrosinase; E_mS, interaction between E_m and S; $(E_m\text{-}S)_1$, axial nucleophilic attack complex from the OH of C-1 to E_m; $(E_m\text{-}S)_2$, diaxial binding complex of S with E_m; E_d, *deoxy*-tyrosinase; E_{ox}, *oxy*-tyrosinase; $E_{ox}S$, interaction complex between E_{ox} with S; $(E_{ox}\text{-}S)_1$, axial binding complex of protonated S with E_{ox}; $(E_{ox}\text{-}S)_2$, diaxial binding complex of S with E_{ox}. Suicide inactivation (steps 10 and 11): $(E_{ox}\text{-}S)_3$, axial binding complex of deprotonated S with E_{ox}; E_i, inactive enzyme. See text for further details.

With regard to the first two mechanisms proposed, in experiments where *o*-quinone binding was prevented, there was no influence on inactivation, and attempts to protect the enzyme with radical scavengers proved unsuccessful [8,21]. As regards to the third mechanism, the presentation of the *o*-diphenol as a monophenol (cresolase presentation) [20], the firmest evidence to support this, according to the authors, is the fact that trihydroxylated compounds such as pyrogallol do not produce inactivation.

Previously, we have taken a closer look at the tyrosinase catalysis mechanism, both as regards its monophenolase and diphenolase activities [1,22–27], and proposed a structural mechanism to explain the enzyme behaviour [28]. We have also studied the kinetics of the lag phase in monophenolase activity [29], although the structural mechanism of the suicide mechanism has been overlooked. To our mind, the study most directly related with suicide inactivation was one that considered the hydroxylation of monophenols to *o*-diphenols, whereby it was proposed that from the (enzyme–diphenol) complex generated, the *o*-diphenol may be oxidized to *o*-quinone, or be released to the medium as *o*-diphenol [28]. In this way, when E_{ox} (*oxy*-tyrosinase) binds to the monophenol, it is hydroxylated in the ortho position so that it remains in an axial-equatorial position. From this position, the enzyme releases the *o*-diphenol generated from the equatorial position, breaking the axial bond and giving rise to E_m (*met*-tyrosinase) + *o*-diphenol, or re-binding the *o*-diphenol in the diaxial position and oxidizing it, giving rise to E_d (*deoxy*-tyrosinase) + *o*-quinone. Hence, an explanation for the suicide inactivation (Scheme 1) would be that the binding of E_{ox} to the *o*-diphenol involves two possible alternatives: (i) diaxial binding with the copper atoms through the hydroxyl groups of C-1 and

© The Authors Journal compilation © 2008 Biochemical Society

Table 1 *o*-Diphenol structures used in the present study

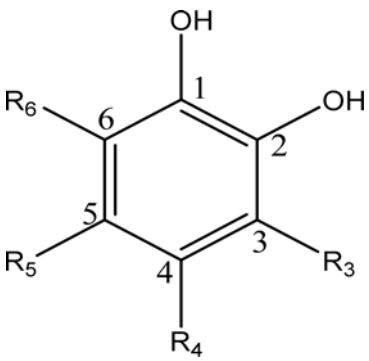

o-Diphenol	R_3	R_4	R_5	R_6
Pyrogallol	H	H	H	-OH
Catechol	H	H	H	H
4-Chlorocatechol	H	-Cl	H	H
4-Methylcatechol	H	$-CH_3$	H	H
4-Ethylcatechol	H	$-CH_2-CH_3$	H	H
4-*tert*-Butylcatechol	H	$-C-(CH_3)_3$	H	H
DHPPA	H	$-(CH_2)_2-COOH$	H	H
DHPAA	H	$-CH_2-COOH$	H	H
Gallic acid methyl ester	H	$-COOCH_3$	H	-OH
Gallic acid	H	-COOH	H	-OH
Protocatechuic acid	H	-COOH	H	H
Protocatechuic aldehyde	H	-CHO	H	H
4-Nitrocatechol	H	$-NO_2$	H	H

C-2, leading to the concerted oxidation/reduction of the *o*-diphenol to $E_m + o$-quinone (catalytic pathway), or (ii) axial binding with one copper atom through the hydroxyl group of C-1, while the hydroxyl group of C-2 transfers its proton to the peroxide. In the latter case, the concerted oxidation/reduction step could not occur, due to the lack of co-planarity. However, oxidation/reduction on one atom of copper could occur, the copper passing to copper(0) and forming *o*-quinone, hydrogen peroxide and inactive enzyme (inactivation pathway). We attempt to confirm this hypothesis (Scheme 1) by experimental data which can be correlated with the hydrophobic, steric and electronic effects. These effects are related to the catalysis and inactivation capacity of the enzyme by their substrates.

MATERIAL AND METHODS

Reagents

Mushroom tyrosinase or polyphenol oxidase (*o*-diphenol: O_2 oxidoreductase, EC 1.14.18.1, 8300 units/mg) and β-NADH were supplied by Sigma. The enzyme was purified as previously described in [25]. The substrates used, pyrogallol, catechol, 4-chlorocatechol, 4-methylcatechol, 4-ethylcatechol, 4-*tert*-butylcatechol, DHPPA (3,4-dihydroxyphenylpropionic acid), DHPAA (3,4-dihydroxyphenylacetic acid), gallic acid methyl esther, gallic acid, protocatechuic acid, protocatechuic aldehyde and 4-nitrocatechol, were all from Sigma. The corresponding structures are shown in Table 1. Other chemicals were of analytical grade.

The kinetic assays to study suicide inactivation use spectrophotometric and oxymetric methods, as described below and in [30,31].

Spectrophotometric assays

These assays were carried out with a PerkinElmer Lambda-35 spectrophotometer, on-line interfaced to a PC computer, where

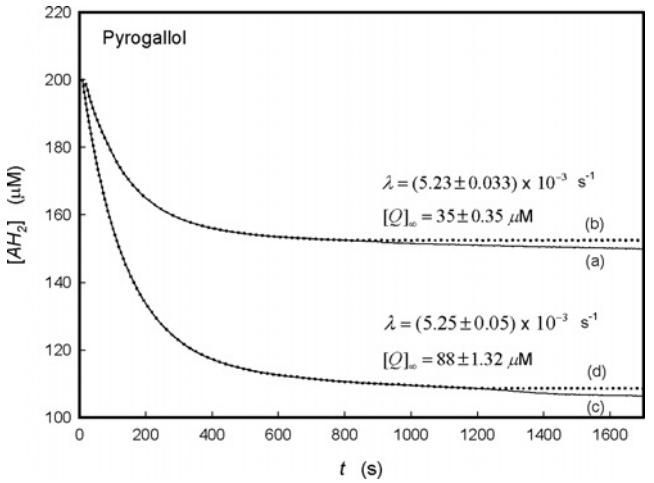

Figure 1 Experimental recordings of the disappearance of AH_2 in the suicide inactivation of tyrosinase by pyrogallol and corrected curves after applying the data analysis

Conditions were 30 mM phosphate buffer, pH 7.0, and the concentrations of AH_2, SOD, O_2 and pyrogallol at the start were 0.2 mM, 1.2 μM, 0.26 mM and 1.5 mM respectively. The enzyme concentration was 0.12 nM (a) or 0.30 nM (c). Curves (b) and (d) are the corrected recordings from (a) and (c) respectively.

the kinetic data were recorded, stored and later analysed. The product of the enzyme reaction, *o*-quinone, is not suitable for experimental detection at long assay times due to the instability of the *o*-quinones [32,33]. Depending on the spectrum of the substrate and oxidation potential of the corresponding *o*-quinone, the reaction was followed by measuring: (i) the disappearance of NADH at 340 nm, with $\varepsilon = 6230\ M^{-1} \cdot cm^{-1}$ (4-chlorocatechol, 4-methylcatechol, 4-ethylcatechol, 4-nitrocatechol, DHPPA, DHPAA, catechol, 4-*tert*-butyl-catechol, protocatechuic acid and protocatechuic aldehyde) or (ii) the disappearance of AH_2 (ascorbic acid) at 290 nm with $\varepsilon = 2175\ M^{-1} \cdot cm^{-1}$ (pyrogallol) [34].

Oxymetric assays

When the substrate and NADH (or AH_2) spectra overlapped, oxymetric assays were carried out [31]. Measurements of dissolved oxygen concentration were made with a Hansatech (Kings Lynn, Cambs, U.K.) oxygraph unit controlled by a PC. The oxygraph used a Clark-type silver/platinum electrode with a 12.5 μm Teflon membrane. The sample was continuously stirred during the experiments and its temperature was maintained at 25 °C. The zero oxygen level for calibration and the experiments was obtained by bubbling oxygen-free nitrogen through the sample for at least 10 min. The substrates gallic acid and gallic acid methyl ester were studied using this method.

The effects of various reagents were studied. Their concentrations are given in detail in the corresponding Figures of the Results section. In all assays, the following reagents were maintained constant: 0.26 mM O_2 (saturating), 30 mM phosphate buffer, pH 7.0, AH_2 or NADH. Protein concentration was determined by the Lowry method [35].

Data analysis

The experimental data for the disappearance of NADH or AH_2 with time (Figure 1) follow the equation:

$$[\text{NADH}] = [\text{NADH}]_0 - [Q]$$
$$= [\text{NADH}]_0 - [c_1(1 - e^{-c_2 t}) + c_3 + c_4 t] \quad (1)$$

© The Authors Journal compilation © 2008 Biochemical Society

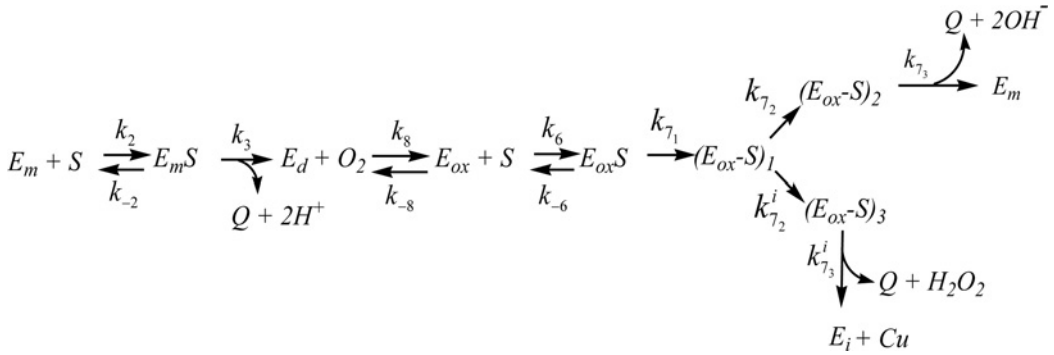

Scheme 2 The kinetic mechanism proposed to explain the suicide inactivation of tyrosinase acting on *o*-diphenols

See text and Scheme 1 for further details.

or

$$[AH_2] = [AH_2]_0 - [Q] = [AH_2]_0 - [c_1(1 - e^{-c_2 t}) + c_3 + c_4 t] \quad (2)$$

where [NADH] is the concentration of NADH, $[NADH]_0$ is the initial [NADH] ($[AH_2]$ and $[AH_2]_0$ are the equivalent for AH_2), $[Q]$ is the concentration of the product of the enzymatic reaction, t is time and in which $c_i (i = 1–4)$ can be obtained by non-linear regression (Sigma Plot 9.0 for Windows™; Jandel Scientific, Corte Madera, CA, U.S.A.).

The parameter c_1 is equal to $[Q]_\infty$ (concentration of product Q obtained at the end of the reaction) and c_2 to the corresponding λ. The coefficient c_3 represents the uncertainty at zero time absorbance caused by addition of the enzyme at the start of the reaction, while c_4 corresponds to the slow spontaneous oxidation of *o*-diphenol and NADH or AH_2. The effects of both experimental artefacts (Figure 1) should be computer subtracted in further NADH against time or AH_2 against time plots. The experimental recordings obtained in the following steps therefore fit eqns (1) or (2), from which the corresponding inactivation parameters, $[Q]_\infty$ and λ, can be determined.

The following equation is used to measure the disappearance of oxygen:

$$\begin{aligned}[O_2] &= [O_2]_0 - [c_1'(1 - e^{-c_2 t}) + c_3 + c_4 t] \\ &= [O_2]_\infty e^{-\lambda t} - c_4 t \end{aligned} \quad (3)$$

where $[O_2]$ is the instantaneous concentration of oxygen, $[O_2]_0$ is the initial concentration of oxygen and $[O_2]_\infty$ is the oxygen consumed at $t \to \infty$. Note that $[O_2]_\infty$ ($c_1' - c_{1/2}$) becomes $[Q]_\infty/2$, reflecting the stoichiometry of the reaction (Scheme 2), and the spontaneous oxidation rate of the substrate is represented by c_4.

Kinetic characteristics of the oxidation of trihydroxylated substrates

In the case of vicinal trihydroxylated phenolic substrates, the kinetic assays should be carried out in the presence of SOD (superoxide dismutase), since the spontaneous oxidation of these compounds is very strong and superoxide anion is formed, generating an autocatalytic oxidation mechanism. In the presence of SOD, however, this mechanism is inhibited and the inactivation kinetics can be followed spectrophotometrically or oxymetrically.

^{13}C-NMR

For all the substrates used, the ^{13}C-NMR spectra were obtained in deuterated water, pH 7.0, which provided the shifts of the C-1 (δ_1^7) and C-2 (δ_2^7) carbons for the different *o*-diphenols. The ^{13}C-NMR spectra of the different *o*-diphenols considered here were obtained in a 300 MHz Varian Unity spectrometer. The δ values were measured relative to those for tetramethylsilane ($\delta = 0$). The maximum line breadth accepted in the ^{13}C-NMR spectra was 0.06 Hz. Therefore, the maximum accepted error for each peak was ± 0.03 p.p.m. Moreover, the electron-donating capacity of the oxygen atom from different phenolic compounds (nucleophilic power) was correlated with the experimental δ values in ^{13}C-NMR for the carbon atom that supports the hydroxyl group. Taking all the above into account, low values of δ_1^7 and δ_2^7 in ^{13}C-NMR for *o*-diphenols indicate high nucleophilic power at pH 7.0 [22].

RESULTS

The kinetic mechanism proposed to explain the suicide inactivation of tyrosinase acting on *o*-diphenols is based on the structural mechanism proposed in Scheme 1 and can be outlined as shown in Scheme 2. The derivation of the analytical expression which establishes the accumulation of the product (Q) with time, when $[S]_0 \gg [E]_0$ (initial concentration of substrate $\gg$ initial concentration of tyrosinase), is described in detail in the Supplementary material section at http://www.BiochemJ.org/bj/416/bj4160431add.htm.

Previous kinetic studies on the suicide inactivation of tyrosinase from diverse sources indicated that the process follows first-order kinetics and has a much higher partition ratio (r) than 1 [5,9,13–15]. This implies that the species in the catalytic pathway of Scheme 2 are in a restricted steady-state, E_s, which overlaps in time with a transient phase due to the formation of inactive enzyme, E_i.

The variation of $[Q]$ with time is given by eqn (4) (see Supplementary material):

$$[Q] = [Q]_\infty(1 - e^{-\lambda t}) = \frac{V_0}{\lambda}(1 - e^{-\lambda t}) = \frac{V_{max}}{\lambda_{max}}(1 - e^{-\lambda t}) \quad (4)$$

when $t \to \infty$, this results in:

$$[Q]_\infty = \frac{2k_{cat}}{\lambda_{max}}[E]_0 = \frac{2k_{7_2}}{k_{7_2}^i}[E]_0 = 2r[E]_0 \quad (5)$$

© The Authors Journal compilation © 2008 Biochemical Society

where k_{7_2}, substrate binding constant to copper atom through C-1 hydroxyl (axial) and $k^{i}_{7_2}$, rate constant of transfer of a H^+ to the protonated peroxide. Bearing in mind that $K^{O_2}_m$ values are very low [37] and that the initial oxygen concentration is 0.26 mM, the enzyme is saturated with O_2 and, from supplementary eqns (S8) and (S9), we obtain:

$$\lambda = \frac{\lambda_{max}[S]_0}{K^S_m + [S]_0} \quad (6)$$

and:

$$V_0 = \frac{2k_{cat}[S]_0[E]_0}{K^S_m + [S]_0} \quad (7)$$

where K^S_m is the Michaelis constant of E for S.

Experimental design

The experimental study of the kinetics of suicide substrates or mechanism-based enzyme inhibitors is important for obtaining reliable kinetic parameters (λ_{max}, K^S_m and r) that will permit any *in vitro* information gained to be extrapolated to *in vivo* situations [11]. A recent revision of the inactivation of CYPs (cytochrome P450s) by metabolic products that form haem, protein adducts or a metabolic inhibitory complex, known as mechanism-based enzyme inhibitors, underlined the importance of kinetic studies, always making discontinuous measurements (preincubating the enzyme with the suicide substrate and taking aliquots to follow the diminution of enzymatic activity with time) [11].

In a previous study, we outlined the methodology necessary for kinetically characterizing a suicide substrate following the reaction continuously [19]. Two basic situations were described: (i) the suicide substrate gives rise to an easily measurable product, in which case the kinetics is studied by measuring this product, or (ii) when the suicide substrate gives rise to a product that cannot be measured easily, in which case a non-suicide auxiliary substrate is necessary to characterize the inactivation kinetics continuously. In the present work, we apply the experimental design described in [19] to the suicide inactivation of tyrosinase as it acts on *o*-diphenols, since although the products obtained, *o*-quinones, are unstable [32,33], they can be reduced by NADH or AH_2 and the disappearance of these coupled reagents can be measured. Alternatively, the consumption of oxygen can be measured in an oxygraph since oxygen is also a substrate of the enzyme. The experimental design can be described in three stages:

Step 1: preliminary assays, in which the experimental conditions are optimized and the design is detailed.

Step 2: study of the variation in enzyme concentration and determination of the parameter r.

Step 3: study of the variation of substrate concentration and determination of λ_{max} and K^S_m.

Experimental study of suicide inactivation

The following *o*-diphenols are used in the present study: catechol, 4-chlorocatechol, 4-methylcatechol, 4-ethylcatechol, 4-*tert*-butylcatechol, DHPPA, DHPAA, 4-nitrocatechol, protocatechuic acid and protocatechuic aldehyde (see Table 1).

For step 1, Figure 1 shows the spectrophotometric recordings of the disappearance of AH_2 [curves (a) and (c)] and their corrections after fitting according to eqn (2) and after subtracting the parameters c_3 and c_4t [curves (b) and (d)]. These corrected registers are analysed as described in the Data analysis section. By means of these preliminary studies, the concentration of enzyme is optimized so that $[Q]_\infty \ll [O_2]_0, [S]_0$.

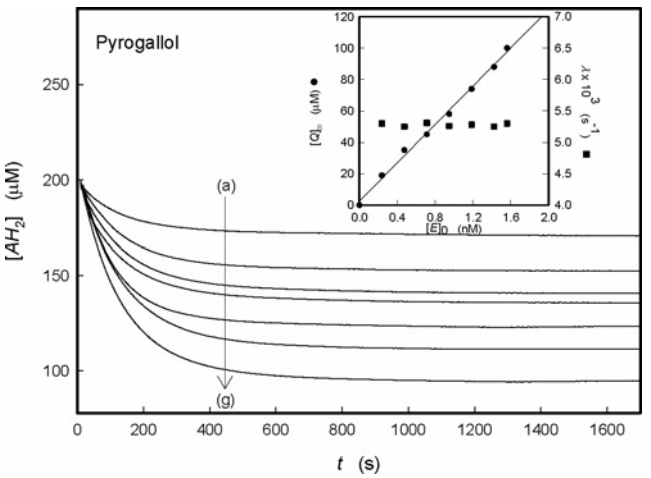

Figure 2 Corrected recordings of the disappearance of AH_2 in the suicide inactivation of tyrosinase by pyrogallol for different enzyme concentrations

Conditions were 30 mM phosphate buffer, pH 7.0, and the initial concentrations of SOD, AH_2 and Pyrogallol were 1.2 μM, 0.2 mM and 1.5 mM respectively, and enzyme concentrations were 0.06 nM (a), 0.12 nM (b), 0.17 nM (c), 0.24 nM (d), 0.3 nM (e), 0.35 nM (f) or 0.39 nM (g). Inset, corresponding values of $[Q]_\infty$ (●) and λ (■) for different concentrations of tyrosinase.

For step 2, variation in enzyme concentration, the concentration of $[E]_0$ was varied while the substrate concentration was kept constant. The results obtained in the presence of AH_2, in the case of a vicinal trihydroxylated substrate like pyrogallol, are shown in Figure 2. The concentration of the substrate in these experiments does not change because the *o*-quinone is reduced by AH_2. However, the concentrations of O_2, or AH_2 do change. In the case of the tyrosinase enzymatic system, there is the advantage that the $K^{O_2}_m$ values are very small [37], which permits an oxygen consumption of more than 10 %. The AH_2 must be in excess. The results obtained for catechol are shown in Supplementary Figure S1, at http://www.BiochemJ.org/bj/416/bj4160431add.htm.

To study substrates such as gallic acid methyl ester, whose suicide inactivation cannot be followed spectrophotometrically, an oxymetric method was employed which measures the consumption of oxygen with time (Supplementary Figure S2, at http://www.BiochemJ.org/bj/416/bj4160431add.htm). The inset of Supplementary Figure S2 shows $[O_2]_\infty$ against $[E]_0$ and the independence of λ plotted against $[E]_0$.

Figure 3 shows the dependence of the values obtained for the product at the end of the reaction, $[Q]_\infty$ against $[E]_0$, from whose slopes and according to eqn (5), the partition ratio r can be determined (see Table 2).

For step 3, variation of concentration of substrate (*o*-diphenol), after having fixed a concentration of enzyme sufficient to give $[Q]_\infty$ or $[O_2]_\infty \ll [O_2]_0$ for the lowest substrate concentration being assayed, the concentration of substrate is varied while the concentration of O_2 is kept constant at a saturating 0.26 mM. For the different types of substrate studied by the different methods, a hyperbolic dependence of the apparent inactivation constant is obtained in all cases with respect to the concentration of substrate (Figure 4, and Supplementary Figures S3 and S4 at http://www.BiochemJ.org/bj/416/bj4160431add.htm).

© The Authors Journal compilation © 2008 Biochemical Society

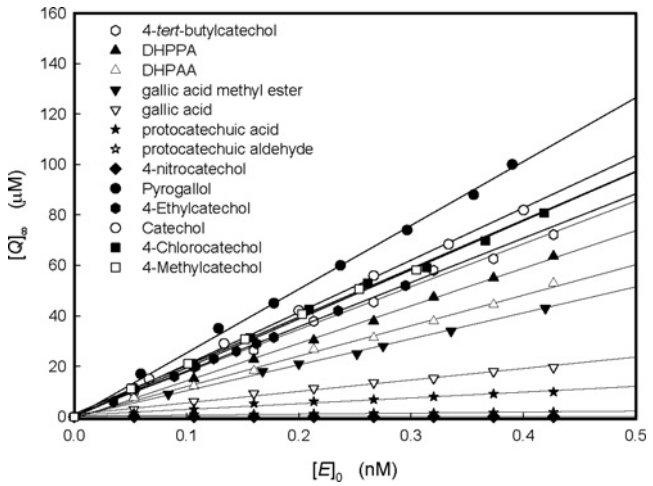

Figure 3 Representations of the values of $[Q]_\infty$ against enzyme concentration for the different substrates studied

Experimental conditions were 30 mM phosphate buffer, pH 7.0, 25 °C. Catechol, 4-methylcatechol, 4-ethylcatechol, 4-chlorocatechol, 4-*tert*-butyl-catechol, DHPPA, DHPAA, protocatechuic acid, protocatechuic aldehyde or 4-nitrocatechol were recorded from the disappearance of NADH, with an initial concentration of 0.2 mM, for every substrate. Pyrogallol and gallic acid were recorded from the disappearance of AH_2, and gallic acid methyl ester was recorded measuring oxygen consumption with AH_2 and SOD (with initial concentrations of 0.2 mM and 1.2 μM respectively for every substrate). Substrate concentration at the start: 2 mM 4-*tert*-butylcatechol, 3 mM DHPPA, 1.5 mM DHPAA, 0.3 mM gallic acid methyl ester, 0.1 mM gallic acid, 0.5 mM protocatechuic acid, 0.1 mM protocatechuic aldehyde, 0.1 mM 4-nitrocatechol, 1.5 mM pyrogallol, 0.3 mM catechol, 0.15 mM 4-chlorocatechol, 0.6 mM 4-methylcatechol, and 0.15 mM 4-ethylcatechol. For every substrate, the line represents a linear regression fitting of the experimental data points.

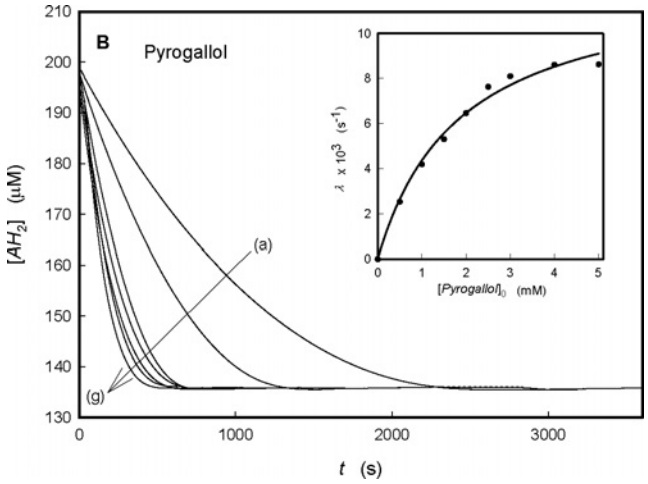

Figure 4 Corrected recordings of the disappearance of AH_2 in the suicide inactivation of tyrosinase by pyrogallol for different substrate concentrations

Conditions were 30 mM phosphate buffer, pH 7.0, and initial concentrations of 0.2 mM AH_2 and 1.2 μM SOD, $[E]_0 = 0.23$ nM, while substrate concentrations (mM) were 1 mM (a), 1.5 mM (b), 2 mM (c), 2.5 mM (d), 3 mM (e), 4 mM (f) and 5 mM (g). The inset shows corresponding values of λ for different pyrogallol concentrations.

Non-linear regression analysis of λ against $[S]_0$, according to eqn (6), gives the values of λ_{max}, the apparent maximum inactivation constant and K_m^S, the Michaelis constant of tyrosinase for the substrate being considered (Table 2). From these values and taking into consideration eqn (5), the catalytic constant k_{cat} can be obtained (see Table 2).

Figure 5, Supplementary Figures S5(A) and S5(B) (http://www.BiochemJ.org/bj/416/bj4160431add.htm) show the dependence of λ on $[S]_0$ for the different substrates studied. An analysis according to eqn (6) provides the apparent maximum inactivation constants (λ_{max}) and the Michaelis constant K_m^S (Table 2).

DISCUSSION

Pharmacological importance of suicide substrates

The study of suicide inactivation and irreversible inhibition is important in the functional design of synthetic inactivators for therapeutic applications. For example, irreversible inactivators (insecticides) have been designed against acetylcholinesterase and suicide substrates of β-lactamases (clavulanic acid) that help the action of antibiotics (amoxycilin) [12,38].

The process of tyrosinase inactivation has long been studied in plants and animals [3]. Later, tyrosinase was studied in *Neurospora crassa* [9,21], mammals [6–8], mushroom [13,39,40] and frog skin [14,15]. Recently, a possible mechanism to explain the suicide inactivation of mushroom tyrosinase has been proposed [20]. Based on kinetic studies with tyrosinases from several vegetal sources [41,42] and mushroom in steady state [22,24], we proposed a structural mechanism to explain the kinetic results obtained at short times, where the suicide inactivation process is not significant in practice. Studies with mushroom

Table 2 Kinetic constants which characterize the suicide inactivation of tyrosinase by different substrates and values of the chemical shifts of the different suicide substrates of tyrosinase obtained by ^{13}C-NMR for the C-1 and C-2 carbons at pH 7.0

Values are means (± S.D.).

o-Diphenol	$\lambda_{max} \times 10^3$ (s^{-1})	$r = k_{cat}/\lambda_{max}$	k_{cat} (s^{-1})	K_m^S (mM)	$K_m^{O_2}$ (μM)	δ_1^7 (p.p.m.)	δ_2^7 (p.p.m.)
Pyrogallol	12.01 ± 0.31	122093 ± 2740	1280.3 ± 47.1	1.96 ± 0.03	55.61 ± 2.81	135.19	148.22
Catechol	8.92 ± 0.27	99994 ± 1604	874.1 ± 30.2	0.16 ± 0.01	38.02 ± 2.61	146.59	146.59
4-Chlorocatechol	8.54 ± 0.25	99356 ± 1788	859.2 ± 28.3	0.60 ± 0.03	37.31 ± 1.62	145.04	147.35
4-Methylcatechol	8.21 ± 0.25	98366 ± 1377	842.1 ± 26.1	0.10 ± 0.01	36.62 ± 2.70	144.06	146.43
4-Ethylcatechol	7.95 ± 0.23	97562 ± 1951	802.3 ± 26.1	0.17 ± 0.01	34.83 ± 2.63	143.99	146.27
4-*tert*-Butylcatechol	7.28 ± 0.28	88788 ± 1864	640.1 ± 28.1	1.45 ± 0.12	27.82 ± 2.52	144.09	146.24
DHPPA	6.93 ± 0.27	87646 ± 1315	607.2 ± 25.1	0.70 ± 0.09	26.43 ± 2.13	144.96	146.43
DHPAA	6.89 ± 0.37	62838 ± 1187	433.1 ± 25.9	1.30 ± 0.10	18.82 ± 1.31	144.61	146.51
Gallic acid methyl ester	1.70 ± 0.09	47444 ± 501	80.2 ± 3.9	0.12 ± 0.01	3.41 ± 0.11	141.42	147.34
Gallic acid	1.57 ± 0.07	18666 ± 466	28.2 ± 0.9	0.18 ± 0.01	1.12 ± 0.11	140.64	147.29
Protocatechuic acid	0.85 ± 0.03	10186 ± 224	8.1 ± 0.3	0.07 ± 0.01	0.34 ± 0.02	150.00	146.04
Protocatechuic aldehyde	0.61 ± 0.02	2554 ± 40	1.5 ± 0.1	0.15 ± 0.02	0.06 ± 0.01	155.28	146.71
4-Nitrocatechol	0.45 ± 0.02	2254 ± 41	0.9 ± 0.1	0.10 ± 0.01	0.04 ± 0.01	155.87	148.07

© The Authors Journal compilation © 2008 Biochemical Society

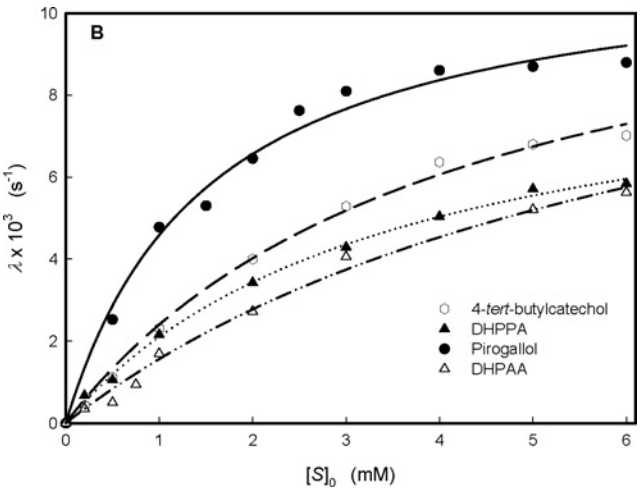

Figure 5 Representation of the values of the inactivation constant λ against $[S]_0$ for the different substrates studied

Conditions were 30 mM phosphate buffer, pH 7.0, 25 °C. 4-*tert*-butyl-catechol, DHPPA and DHPAA, were recorded from the disappearance of NADH, with an initial concentration of 0.2 mM, for every substrate and pyrogallol was recorded from the disappearance of AH_2, with SOD (initial concentrations of AH_2 and SOD were 0.2 mM and 1.2 μM respectively). The linear tracings show non-linear regression fitting to eqn (6) of the data analysis. Enzyme concentrations were: 0.23 nM pyrogallol, 0.09 nM 4-*tert*-butylcatechol, 0.09 nM DHPPA and 0.09 nM DHPAA.

tyrosinase in pre-steady-state permitted additional information to be obtained on the mechanism [25].

When an enzyme acts on a suicide substrate, the resulting transition phase permits us to look at the kinetics of the suicide inactivation process that coincides with enzymatic catalysis. When an enzyme acts on a suicide substrate, two pathways are set in action: the catalytic pathway, which gives rise to a product, and an inactivation pathway that gives rise to an inactive enzyme, the whole process taking place in a post-steady-state transition phase (the steady state is reached at $t \rightarrow 0$ and then evolves in transition phase until the reaction stops since the enzyme is inactivated, hence the name post-steady-state).

In our previous studies [13–15], we tried to obtain explicit solutions for product against time, since these are more useful for data analysis and make it easier to obtain the kinetic information that characterizes a suicide substrate: the partition coefficient, r; the maximum apparent inactivation constant, λ_{max}; and the Michaelis constant, K_m^S. In addition, information on the catalytic pathway (the catalytic constant k_{cat}) is also obtained. A pre-requisite for obtaining these explicit solutions is that the substrate concentrations should vary little, that is, be almost constant: $([Q]_\infty \ll [S]_0, [O_2]_0)$. With tyrosinase, such experimental conditions can be achieved by working with low enzyme concentrations and using a reductant such as NADH or AH_2. These reduce the *o*-quinones, with a given stoichiometry, which means the concentration of reducing substrate (*o*-diphenol) remains constant. As regards the other substrate, O_2, we determined the $K_m^{O_2}$ [37] and, at the concentration of oxygen in the solutions, 0.26 mM, the enzyme was saturated. These are the conditions used in the assays described here.

Another aspect to bear in mind is the spontaneous oxidation of the *o*-diphenol and triphenol substrates. In the case of vicinal triphenols, oxidation may become quite pronounced and can be stopped by adding SOD to the reaction medium. By following the steps of the experimental design described in the Results section, the kinetic information shown in Table 2 can be obtained.

From these data, the parallelism between the maximum apparent inactivation constant (λ_{max}) and the catalytic constant (k_{cat}) can be seen (Table 2), confirming the kinetic analysis, as both are related by eqn (5). In this way, the best substrates, such as pyrogallol, catechol, 4-chlorocatechol and 4-methylcatechol (with hydrogen or donating group in C-4), show higher catalytic (k_{cat}) and suicide inactivation (λ_{max}) constants, while the worst substrates, such as protocatechuic acid, protocatechuic aldehyde and 4-nitrocatechol (with electron withdrawing group in C-4), have a low k_{cat} and λ_{max}. Of note is the fact that the electronic, steric and hydrophobic effects on the substrate–enzyme binding and on the inactivation and catalysis processes affect the catalysis (constants around 10^3) and suicide inactivation (constants around 10) processes. Note how pyrogallol inactivates the enzyme in the same way as the *o*-diphenols; furthermore, as it is the best substrate of the enzyme (greater k_{cat}), the λ_{max} is also greater (Table 2).

The parameter $r = k_{7_2}/k_{7_2}^i$ indicates the probability that the hydroxyl group of C-2 will carry out a nucleophilic attack on the second copper (Cu^A), transferring the proton to the histidine and taking up a diaxial position (see Scheme l), an assumption derived from the flexible feature of the His[54] residue previously proposed for *Streptomyces castaneoglobisporus* tyrosinase [43], or transferring the proton to the protonated peroxide, remaining in position C-1 and axially bound to the copper and to C-2 as C-O^-, a step favoured by the charge density of the copper atom bound to the substrate. When this has an electron-donating group in C-4, the positive charge density in the copper will be lower and the proton will be transferred to the histidine. In this way, the hydroxyl group in C-2 will be better able to carry out the nucleophilic attack on the copper and the proton will be transferred to the histidine, binding to the substrate in a diaxial position. When the substrate has a withdrawing group in C-4, the positive charge density of the copper atom will be greater, influencing the hydroxyl group of C-2 and favouring deprotonation, the proton being transferred to the protonated peroxide (see Scheme 1). In addition, hydrophobic and esteric effects influence both process (catalysis and inactivation) (Table 2).

In the first case, the catalysis involves a concerted oxidation/reduction reaction, releasing *o*-quinone and E_m, as the oxygens are co-planar with the two copper atoms. However, in the second case, the oxidation/reduction may take place on the one copper atom, releasing *o*-quinone, copper(0), hydrogen peroxide and inactive enzyme.

Table 2 shows the values of k_{cat}, r, λ_{max} and of the chemical shifts of the different suicide substrates obtained by ^{13}C-NMR for the C-1 and C-2 carbons. The electronic, steric and hydrophobic effects are evident in the process of catalysis and inactivation. Note how the values of r decrease as the group in C-4 becomes more electron-withdrawing due to closer values of k_{7_2} and $k_{7_2}^i$ (the lowest corresponds to 4-nitrocatechol). It is important to note the high relation, in some cases, between the ^{13}C-NMR data compared with the values of k_{cat} and λ_{max} shown in Table 2. In the case of pyrogallol, which has the lowest δ_1 value, the electron density of the oxygen atom of the hydroxyl group of C-1 is very high and has the highest k_{cat} and λ_{max} values. However, the value of r is also at its maximum for all the substrates studied, which can be explained by the greater influence of the value of δ_1 on k_{cat} (10^3 range) than on λ_{max} (10 range). Furthermore, as this compound is vicinally trihydroxylated, the probability of catalysis taking place is doubled as there are two possible *o*-diphenol orientations. According to Scheme 1, in the complex $(E_{ox}\text{-}S)_1$, with the substrate bound axially to the copper by C-1 (which has a lower positive charge density), the adjacent hydroxyl group has a greater possibility to bind to the second copper, transferring its proton to the histidine.

© The Authors Journal compilation © 2008 Biochemical Society

Catechol is a good tyrosinase substrate (in this case, there are no steric or hydrophobic effects that hinder the process), even though the values of δ_1 and δ_2 are not good; however, since the OH groups are equivalent, the probability of catalysis and inactivation increases. The value of r is high, since, as in the previous case, the effect on k_{cat} is much higher than on λ_{max}, favouring the catalytic pathway. The group of substrates 4-chlorocatechol, 4-methylcatechol and 4-ethylcatechol, with very close δ_1 values, gives similar values of k_{cat}, λ_{max} and r (although, in the case of 4-ethylcatechol, steric effects exist). The effect of the donating group in C-4 is responsible for the powerful nucleophilic attack of the hydroxyl group in C-1. In the case of 4-*tert*-butylcatechol, although its δ_1 is similar to that of catechol, the size of the group in C-4, *tert*-butyl (steric effect), may cause steric hindrance, which decreases its k_{cat}, λ_{max} and r. That is, the *tert*-butyl group affects both routes through steric hindrance.

As regards DHPPA and DHPAA, although their δ_1 values are better than that of catechol, the effect of the negative charge of the carboxylic group decreases the k_{cat} and λ_{max} (decreased hydrophobicity). Gallic acid and gallic acid methyl ester are trihydroxylated compounds with low δ_1 values, although the withdrawing effect of the carboxyl group means that their k_{cat} and λ_{max} are low, as is their r (also decreased hydrophobicity). The withdrawing effect increases the possibility of the copper being bound to the substrate, bringing the second hydroxyl group in C-2 nearer, inducing deprotonation and proton transfer to the protonated peroxide, facilitating enzyme suicide and the release of copper(0) and hydrogen peroxide. Lastly, poor tyrosinase substrates, like protocatechuic acid, protocatechuic aldehyde and 4-nitrocatechol, whose δ_1 values are very high, order themselves in accordance with the values described in Table 2. Their very low values of k_{cat}, λ_{max} and r can be explained by the same withdrawing effect of the group in C-4.

Parameter *r*

The values of the parameter r (number of turnovers that 1 mol of enzyme makes before its suicide inactivation) is shown in Table 2. The values were obtained from the slopes shown in Figure 3 and using eqn (5). From the mechanism shown in Scheme 1 and eqn (5), it can be concluded that the second nucleophilic attack step of the oxygen of the hydroxyl group of C-2 (controlled by k_{7_2}) on the second copper atom in diaxial position is much faster than the deprotonation of the hydroxyl group in C-2 towards the protonated peroxide (controlled by $k^{i}_{7_2}$). Therefore, the values of r are high. Note how r is lower in substrates with a withdrawing group than in substrates with a donating group.

Values of K^S_m

The expression K^S_m is given by eqn (S15), which describes the attack constant of the oxygen of the hydroxyl group of C-1 on the copper, k_{7_2} and the binding constant of the substrate, k_6, to the enzyme (E_{ox}), which means that its correlation with the values of δ_1 is not similar to the correlation observed between this parameter and k_{cat} or λ_{max}. In the case of pyrogallol, whose hydroxyl group in C-1 is partially deprotonated at pH 7.0, the value of K^S_m will be much higher than that of catechol with its protonated hydroxyl groups. However, once the enzyme binds to pyrogallol, the latter is rapidly oxidized. Note that substrates such as 4-*tert*-butylcatechol (with a voluminous group in C-4), and DHPPA and DHPAA with a negative charge, have high K^S_m values. This implies that the catalytic efficiency ($\lambda_{max}r/K^S_m$) and inactivation (λ_{max}/K^S_m) are greater in substrates whose R group is H (catechol), -CH_3 (4-methylcatechol) or -CH_2-CH_3 (4-ethylcatechol) (Table 2).

Proposed structural mechanism to explain suicide inactivation

Three possible mechanisms have been proposed to explain the suicide inactivation of tyrosinase: (i) an attack by the *o*-quinone product of oxidation on a sensitive group vicinal to the active site [5], (ii) a free radical attack on the active site by reactive oxygen species generated during the catalytic oxidation [7], and, more recently, (iii) the processing of a catechol as though it was a monophenol ('cresolase'-type presentation) [20]. The first two hypotheses have been rejected because the inactivation takes place even in the presence of NADH or AH_2, whose presence prevents the *o*-quinone binding to the enzyme [13,21]. In addition, experiments that try to protect the enzyme from the action of free radicals were also unsuccessful [9,21]. Nor were we able to mark the enzyme in the process of suicide inactivation in experiments using [U-C^{14}]phenol [13]. As regards the third hypothesis, which implies the presentation of a catechol in the form of a 'cresolase', Land et al. [20] suggested that an intermediate product is formed that can undergo deprotonation and reductive elimination; this assumes that the orientation of the phenyl ring in the enzyme–substrate complex is approximately orthogonal to the plane defined by the copper and oxygen atoms [44–46]. The experiments carried out in the present study and previously [13–15] show that: (i) the enzyme undergoes inactivation in the presence of pyrogallol (see Table 2) with a very high inactivation constant; and (ii) the process of suicide inactivation does not depend on pH [13], although the K^S_m apparently increases at acid pH values, and so the apparent inactivation constant decreases with pH, although the maximum apparent inactivation constant (λ_{max}) remains constant, as does k_{cat} [13].

Therefore, none of the hypotheses proposed explain the experimental data. Based on previous results [13–15,19,22–28] and those of the present study, we propose an alternative mechanism to explain the diphenolase catalytic cycle and suicide inactivation. The catalytic cycle, Step 1, begins with the E_m form non-covalently binding to S to give E_mS, perhaps forming a hydrogen bridge between the base B (possibly a histidine) and the hydroxyl group of the substrate C-1. In Step 2, the enzyme with the help of base B withdraws the proton from the hydroxyl group of C-1 and so the substrate binds axially to the copper (by C-1) [25]. Then the hydroxyl group of C-2 of the substrate transfers a proton to the histidine [43], separating it from the copper atom and binding diaxially with both copper atoms in Step 3. Note that the distance between the copper atoms in the E_m form is 2.9 Å (1 Å = 0.1 nm). In this way, the substrate is co-planar with the copper atoms and the concerted redox reaction can occur, yielding *o*-quinone. Thus, the copper atoms change from Cu^{2+} Cu^{2+} in the *met* form to Cu^{1+} Cu^{1+} in the *deoxy* form, E_d (Step 4). Owing to the low $K^{O_2}_m$ and the high oxygen concentration in the medium, E_d becomes E_{ox} (Step 5), with Cu^{2+} Cu^{2+} and a peroxide group co-planar with the two atoms. Next, the E_{ox} form binds another molecule from the substrate (Step 6). In this case, the base is already protonated and cannot help the substrate bind to the copper. The proton of the hydroxyl group of C-1 must be transferred to the peroxide group, which acts as a base [27,43,47]. This would be the slow step of the turnover, controlled by k_{7_1} (Step 7) [27,43,47]. The fact that the peroxide acts as a base and is involved in the proton transfer from the hydroxyl group of C-1 and C-2 is important. Note that this step of peroxide group protonation has also been proposed in [43]. The protonated peroxide draws the copper atoms in the E_{ox} form

© The Authors Journal compilation © 2008 Biochemical Society

closer, since its distance in the unprotonated form, 3.6 Å, is too far for the molecule of substrate to bind diaxially. However, this would be possible in the protonated E_{ox} form. With the substrate axially bound to one copper atom, there are two possibilities (Step 8): (i) the oxygen of the hydroxyl group of C-2 may attack the other copper atom which is drawn closer following protonation of the peroxide, transferring the proton to the histidine [43], binding to the substrate diaxially and co-planar with the copper atoms. In this way, the concerted redox reaction (Step 9) can occur, releasing *o*-quinone and E_m. (ii) The hydroxyl group of C-2 may cede a proton to the protonated peroxide, remaining as C-O^- (Step 10). The co-planarity of the substrate ring, the oxygen of C-1 and the copper atom favour the simultaneous oxidation of the substrate to *o*-quinone and the reduction of one Cu^{2+} atom to copper(0) through the ring, while copper(0) and hydrogen peroxide are released, and the enzyme is inactivated as a consequence (Step 11). A more detailed representation of Steps 8–11 is provided in Supplementary Scheme S1 (http://www.BiochemJ.org/bj/416/bj4160431add.htm). Note that the observation concerning the possibility of a bidentated union of the *o*-diphenol with one copper atom may also lead to suicide inactivation [48]. Axial/equatorial-type bidentated structures have also been proposed for the binding of *o*-diphenols to copper (but only one copper) and have been seen by X-ray diffraction to be co-planar [49]. However, the axial/equatorial binding to one copper atom in tyrosinase is not co-planar and so the oxidation/reduction reaction cannot take place. For this reason, Steps 10 and 11 have been proposed in the mechanism of Scheme 1. The inactivation mechanism is consistent with the experimental observation that 50 % of the copper is lost from the active site during catechol inactivation [21] and also with the experiments carried out [20] concerning the impossibility of reactivating the inactivated enzyme by adding Cu^{2+}, perhaps indicating the need for a 'caddie' protein [43].

The physiological significance of the suicide inactivation of tyrosinase is not clear, although it could be taken as a limitation to the action of an enzyme that generates cytotoxic products, in this case *o*-quinones [20].

CONCLUSIONS

In this work, a kinetic study of the suicide inactivation of tyrosinase during its action on a variety of substrates has been described, and a mechanism has been proposed to explain the experimental kinetic results and to throw light on the suicide inactivation step of mushroom tyrosinase. Both processes, catalysis and inactivation, are affected by a series of factors related to the enzyme–substrate interaction. From the data obtained, it is clear that electronic, steric and hydrophobic effects play an important role in both processes. Substrates with R=H in C-4 (pyrogallol and catechol) are the best substrates for catalysis and inactivation, although the enzyme must undertake more turnovers (higher *r*). Other substrates, with a large group in C-4 or with negative charges in the C-4 chain, have a steric or hydrophobic effect on both processes. Lastly, substrates with an electron-withdrawing group in C-4 (4-nitrocatechol, protocatechuic acid and protocatechuic aldehyde) show the lowest values of k_{cat} and λ_{max}, and so the enzyme needs to undertake fewer turnovers before being inactivated.

This paper was partially supported by grants from the Ministerio de Educación y Ciencia (Madrid, Spain) Project BIO2006-15363 and SAF2006-07040-C02-01, from the Fundación Séneca (CARM, Murcia, Spain) Project 00672/PI/04, and from the Consejería de Educación (CARM, Murcia, Spain) BIO-BMC 06/01-0004. J. L. M.-M. has a fellowship from the Ministerio de Educación y Ciencia (Madrid, Spain) reference AP2005-4721. F. G.-M. has a fellowship from Fundación Caja Murcia (Murcia, Spain).

REFERENCES

1 Sanchez-Ferrer, A., Rodriguez-Lopez, J. N., Garcia-Canovas, F. and Garcia-Carmona, F. (1995) Tyrosinase: a comprehensive review of its mechanism. Biochim. Biophys. Acta **1247**, 1–11
2 Halaouli, S., Asther, M., Sigoillot, J. C., Hamdi, M. and Lomascolo, A. (2006) Fungal tyrosinases: new prospects in molecular characteristics, bioengineering and biotechnological applications. J. Appl. Microbiol. **100**, 219–232
3 Nelson, J. M. and Dawson, C. R. (1944) Tyrosinase. Adv. Enzymol. **4**, 99–152
4 Asimov, I. and Dawson, C. R. (1950) On the reaction inactivation of tyrosinase during the aerobic oxidation of catechol. J. Am. Chem. Soc. **72**, 820–828
5 Ingraham, L. L., Corse, J. and Makower, B. (1952) Enzymatic browning of fruits. 3. Kinetics of the reaction inactivation of polyphenol oxidase. J. Am. Chem. Soc. **74**, 2623–2626
6 Tomita, Y. and Seiji, M. (1977) Inactivation mechanism of tyrosinase in mouse melanoma. J. Dermatol. **4**, 245–249
7 Seiji, M., Sasaki, M. and Tomita, Y. (1978) Nature of tyrosinase inactivation in melanosomes. Tohoku J. Exp. Med. **125**, 233–245
8 Tomita, Y., Hariu, A., Mizuno, C. and Seiji, M. (1980) Inactivation of tyrosinase by dopa. J. Invest. Dermatol. **75**, 379–382
9 Lerch, K. (1983) Neurospora tyrosinase: structural, spectroscopic and catalytic properties. Mol. Cell. Biochem. **52**, 125–138
10 Zhong, J. Y. and Groutas, W. C. (2004) Recent developments in the design of mechanism-based and alternate substrate inhibitors of serine proteases. Curr. Top. Med. Chem. **4**, 1203–1216
11 Ghanbari, F., Rowland-Yeo, K., Bloomer, J. C., Clarke, S. E., Lennard, M. S., Tucker, G. T. and Rostami-Hodjegan, A. (2006) A critical evaluation of the experimental design of studies of mechanism based enzyme inhibition, with implications for *in vitro-in vivo* extrapolation. Curr. Drug Metab. **7**, 315–334
12 Silverman, R. B. (1995) Mechanism-based enzyme inactivators. Meth. Enzymol. **249**, 240–283
13 Garcia-Canovas, F., Tudela, J., Martinez-Madrid, C., Varon, R., Garcia-Carmona, F. and Lozano, J. A. (1987) Kinetic study on the suicide inactivation of tyrosinase induced by catechol. Biochim. Biophys. Acta **912**, 417–423
14 Tudela, J., Garcia-Canovas, F., Varon, R., Jimenez, M., Garcia-Carmona, F. and Lozano, J. A. (1987) Kinetic characterization of dopamine as a suicide substrate of tyrosinase. J. Enzyme Inhibition **2**, 47–56
15 Tudela, J., Garcia-Canovas, F., Varon, R., Jimenez, M., Garcia-Carmona, F. and Lozano, J. A. (1988) Kinetic study in the transient phase of the suicide inactivation of frog epidermis tyrosinase. Biophys. Chem. **30**, 303–310
16 Arnao, M. B., Acosta, M., del Rio, J. A., Varon, R. and Garcia-Canovas, F. (1990) A kinetic-study on the suicide inactivation of peroxidase by hydrogen-peroxide. Biochim. Biophys. Acta **1041**, 43–47
17 Hiner, A., Hernandez-Ruiz, J., Arnao, M. B., Garcia-Canovas, F. and Acosta, M. (1996) A comparative study of the purity, enzyme activity, and inactivation by hydrogen peroxide of commercially available horseradish peroxidase isoenzymes A and C. Biotechnol. Bioeng. **50**, 655–662
18 Escribano, J., Tudela, J., Garcia-Carmona, F. and Garcia-Canovas, F. (1989) A kinetic-study of the suicide inactivation of an enzyme measured through coupling reactions: application to the suicide inactivation of tyrosinase. Biochem. J. **262**, 597–603
19 Garcia-Canovas, F., Tudela, J., Varon, R. and Vazquez, A. M. (1989) Experimental methods for kinetic study of suicide substrates. J. Enzym. Inhib. **3**, 81–90
20 Land, E. J., Ramsden, C. A. and Riley, P. A. (2007) The mechanism of suicide-inactivation of tyrosinase: a substrate structure investigation. Tohoku J. Exp. Med. **212**, 341–348
21 Dietler, C. and Lerch, K. (1982) In Oxidases and Related Redox Systems (King, T. E., Mason, H. S. and Morrison, M., eds), pp. 305–317, Pergamon Press, New York
22 Espin, J. C., Varon, R., Fenoll, L. G., Gilarbert, M. A., Garcia-Ruiz, P. A., Tudela, J. and Garcia-Canovas, F., (2000) Kinetic characterization of the substrate specificity and mechanism of mushroom tyrosinase. Eur. J. Biochem. **267**, 1270–1279
23 Fenoll, L. G., Rodriguez-Lopez, J. N., Varon, R., Garcia-Ruiz, P. A., Garcia-Canovas, F. and Tudela, J. (2002) Kinetic characterisation of the reaction mechanism of mushroom tyrosinase on tyramine/dopamine and L-tyrosine methyl esther/L-dopa methyl esther. Int. J. Biochem. Cell Biol. **34**, 1594–1607
24 Fenoll, L. G., Rodriguez-Lopez, J. N., Garcia-Sevilla, F., Garcia-Ruiz, P. A., Varon, R., Garcia-Canovas, F. and Tudela, J. (2001) Analysis and interpretation of the action mechanism of mushroom tyrosinase on monophenols and diphenols generating highly unstable *o*-quinones. Biochim. Biophys. Acta **1548**, 1–22

© The Authors Journal compilation © 2008 Biochemical Society

25 Rodriguez-Lopez, J. N., Fenoll, L. G., Garcia-Ruiz, P. A., Varon, R., Tudela, J., Thorneley, R. N. and Garcia-Canovas, F. (2000) Stopped-flow and steady-state study of the diphenolase activity of mushroom tyrosinase. Biochemistry **39**, 10497–10506
26 Ros, J. R., Rodriguez-Lopez, J. N. and Garcia-Canovas, F. (1994) Tyrosinase kinetic analysis of the transient phase and the steady-state. Biochim. Biophys. Acta **1204**, 33–42
27 Fenoll, L. G., Penalver, M. J., Rodriguez-Lopez, J. N., Garcia-Ruiz, P. A., Garcia-Canovas, F. and Tudela, J. (2004) Deuterium isotope effect on the oxidation of monophenols and *o*-diphenols by tyrosinase. Biochem. J. **380**, 643–650
28 Rodriguez-Lopez, J. N., Fenoll, L. G., Penalver, M. J., Garcia-Ruiz, P. A., Varon, R., Martinez-Ortiz, F., Garcia-Canovas, F. and Tudela, J. (2001) Tyrosinase action on monophenols: evidence for direct enzymatic release of *o*-diphenol. Biochim. Biophys. Acta **1548**, 238–256
29 Garcia Molina, F., Munoz, J. L., Varon, R., Rodriguez Lopez, J. N., Garcia Canovas, F. and Tudela, J. (2007) An approximate analytical solution to the lag period of monophenolase activity of tyrosinase. Int. J. Biochem. Cell. Biol. **39**, 238–252
30 Garcia-Molina, F., Munoz, J. L., Varon, R., Rodriguez-Lopez, J. N., Garcia-Canovas, F. and Tudela, J. (2007) A review on spectrophotometric methods for measuring the monophenolase and diphenolase activities of tyrosinase. J. Agric. Food Chem. **55**, 9739–9749
31 Rodriguez-Lopez, J. N., Ros, J. R., Varon, R. and Garcia-Canovas, F. (1993) Oxygen Michaelis constants for tyrosinase. Biochem. J. **293**, 859–866
32 Garcia-Carmona, F., Garcia-Canovas, F., Iborra, J. L. and Lozano, J. A. (1982) Kinetic study of the pathway of melanization between L-dopa and dopachrome. Biochim. Biophys. Acta **717**, 124–131
33 Garcia-Canovas, F., Garcia-Carmona, F., Vera-Sanchez, J., Iborra, J. L. and Lozano, J. A. (1982) The role of pH in the melanin biosynthesis pathway. J. Biol. Chem. **257**, 8738–8744
34 Munoz, J. L., Garcia-Molina, F., Varon, R., Rodriguez-Lopez, J. N., Garcia-Canovas, F. and Tudela, J. (2006) Calculating molar absorptivities for quinones: application to the measurement of tyrosinase activity. Anal. Biochem. **351**, 128–138
35 Lowry, O. H., Rosebrough, N. J., Farr, A. L. and Randall, R. J. (1951) Protein measurement with the Folin phenol reagent. J. Biol. Chem. **193**, 265–275
36 Reference deleted
37 Fenoll, L. G., Rodriguez-Lopez, J. N., Garcia-Molina, F., Garcia-Canovas, F. and Tudela, J. (2002) Michaelis constants of mushroom tyrosinase with respect to oxygen in the presence of monophenols and diphenols. Int. J. Biochem. Cell Biol. **34**, 332–336
38 Walsh, C. T. (1984) Suicide substrates, mechanism-based enzyme inactivators: recent developments. Annu. Rev. Biochem. **53**, 493–535
39 Haghbeen, K., Saboury, A. A. and Karbassi, F. (2004) Substrate share in the suicide inactivation of mushroom tyrosinase. Biochim. Biophys. Acta **1675**, 139–146
40 Garcia-Molina, F., Hiner, A. N., Fenoll, L. G., Rodriguez-Lopez, J. N., Garcia-Canovas, F. and Tudela, J. (2005) Mushroom tyrosinase: Catalase activity, inhibition, and suicide inactivation. J. Agric. Food Chem. **53**, 3702–3709
41 Espin, J. C, Morales, M., Varon, R., Tudela, J. and Garcia-Canovas, F. (1995) A continuous spectrophotometric method for determining the monophenolase and diphenolase activities of apple polyphenol oxidase. Anal. Biochem. **231**, 237–246
42 Espin, J. C, Garcia-Ruiz, P. A., Tudela, J., Varon, R. and Garcia-Canovas, F. (1998) Monophenolase and diphenolase reaction mechanisms of apple and pear polyphenol oxidases. J. Agric. Food Chem. **46**, 2968–2975
43 Matoba, Y., Kumagai, T., Yamamoto, A., Yoshitsu, H. and Sugiyama, M. (2006) Crystallographic evidence that the dinuclear copper center of tyrosinase is flexible during catalysis. J. Biol. Chem. **281**, 8981–8990
44 Decker, H., Schweikardt, T. and Tuczek, F. (2006) The first crystal structure of tyrosinase: all questions answered? Angew. Chem. Int. Ed. **45**, 4546–4550
45 Van Gastel, M., Bubacco, L., Groenen, E. J. J., Vijgenboom, E. and Canters, G. W. (2000) EPR study of the dinuclear active copper site of tyrosinase from *Streptomyces antibioticus*. FEBS Lett. **474**, 228–232
46 Bubacco, L., Van Gastel, M., Groenen, E. J. J., Vijgenboom, E. and Canters, G. W. (2003) Spectroscopic characterization of the electronic changes in the active site of *Streptomyces antibioticus* tyrosinase upon binding of transition state analogue inhibitors. J. Biol. Chem. **278**, 7381–7389
47 Peñalver, M. J., Rodriguez-Lopez, J. N., Garcia-Ruiz, P. A., Garcia-Canovas, F. and and Tudela, J. (2003) Solvent deuterium isotope effect on the oxidation of the *o*-diphenols by tyrosinase, Biochim. Biophys. Acta **1650**, 128–135
48 Decker, H., Schweikardt, T., Nillius, Dd., Salzbrunn, U., Jaenicke, E. and Tuczek, F. (2007) Similar enzyme activation and catalysis in hemocyanins and tyrosinases. Gene **398**, 183–191
49 Speier, G., Tisza, S., Tyeklar, Z., Lange, C. W. and Pierpont, C. G. (1994) Coligand-dependent shifts in charge-distribution for copper-complexes containing 3,5-di-*tert*-butylcatecholate and 3,5-di-*tert*-butylsemiquinonate ligands. Inorg. Chem. **33**, 2041–2045

Received 2 May 2008/16 July 2008; accepted 23 July 2008
Published as BJ Immediate Publication 23 July 2008, doi:10.1042/BJ20080892

© The Authors Journal compilation © 2008 Biochemical Society

Biochem. J. (2008) **416**, 431–440 (Printed in Great Britain) doi:10.1042/BJ20080892

online data

SUPPLEMENTARY ONLINE DATA

Phenolic substrates and suicide inactivation of tyrosinase: kinetics and mechanism

Jose L. MUÑOZ-MUÑOZ*, Francisco GARCÍA-MOLINA*, Pedro A. GARCÍA-RUIZ†, Milagros MOLINA-ALARCÓN‡, Jose TUDELA*, Francisco GARCÍA-CÁNOVAS*[1] and Jose N. RODRÍGUEZ-LÓPEZ*

*GENZ: Grupo de Investigación de Enzimología, Departamento de Bioquímica y Biología Molecular-A, Facultad de Química, Universidad de Murcia, E-30100 Espinardo, Murcia, Spain, †QCBA: Grupo de Química de Carbohidratos y Biotecnología de Alimentos, Departamento de Química Orgánica, Facultad de Química, Universidad de Murcia, E-30100 Espinardo, Murcia, Spain, and ‡Departamento de Enfermería, Escuela Universitaria de Enfermería, Universidad de Castilla la Mancha, E-02071, Albacete, Spain

THEORY

Previous kinetic studies on the suicide inactivation of tyrosinase from diverse sources indicated that the process follows first-order kinetics and has a much higher partition ratio (r) than 1 [1–5]. This implies that the species of the catalytic pathway of Scheme 2 in the main paper are in a restricted steady-state, E_s, which overlaps in time with a transient phase due to the formation of inactive enzyme, E_i [6–12]. Taking into account these considerations, the mechanism described in Scheme 2 of the main paper can be schematized as in Scheme S1. All definitions for the equations below are given in the Supplementary abbreviations section.

The variation of $[E_s]$ and $[Q]$ on time is given by:

$$[\dot{E}_s] = -k^i_{7_2} f_{(E_{ox}-S)_1}[E_s] \quad \text{(S1)}$$

$$[\dot{Q}] = 2k_{7_2} f_{(E_{ox}-S)_1}[E_s] \quad \text{(S2)}$$

Integration of eqns (S1) and (S2), when considering $[E_s]=[E]_0$ and $[Q]=0$ at $t=0$, yields:

$$[Q] = [Q]_\infty(1-e^{-\lambda t}) = \frac{V_0}{\lambda}(1-e^{-\lambda t}) = \frac{V_{max}}{\lambda_{max}}(1-e^{-\lambda t}) \quad \text{(S3)}$$

when $t \to \infty$, this results in:

$$[Q]_\infty = \frac{2k_{cat}}{\lambda_{max}}[E]_0 = \frac{2k_{7_2}}{k^i_{7_2}}[E]_0 = 2r[E]_0 \quad \text{(S4)}$$

and

$$\lambda = k^i_{7_2} f_{(E_{ox}-S)_1} \quad \text{(S5)}$$

Note that eqns (S3) and (S4) are equivalent to eqns (4) and (5) of the main paper respectively.

The pseudo steady-state rate is:

$$V_0 = 2k_{7_2} f_{(E_{ox}-S)_1} \quad \text{(S6)}$$

The expression $f_{(E_{ox}-S)_1}$ can be obtained by applying the steady-state condition for all the enzymatic species in E_s, giving

$$f_{(E_{ox}-S)_1} = \frac{\frac{k_3k_{7_1}k_{7_3}[S]_0[O_2]_0[E]_0}{k_{7_1}k_{7_2}k_{7_3}+k_3k_{7_2}k_{7_3}+k_3k_{7_1}k_{7_3}+k_3k_{7_1}k_{7_2}}}{K^{O_2}K^S_{m_2}+K^{O_2}_m[S]_0+K^S_m[O_2]_0+[S]_0[O_2]_0} \quad \text{(S7)}$$

Taking into account eqn (S7), eqn (S5) gives

$$\lambda = \frac{\lambda_{max}[S]_0[O_2]_0}{K^{O_2}K^S_{m_2}+K^{O_2}_m[S]_0+K^S_m[O_2]_0+[S]_0[O_2]_0} \quad \text{(S8)}$$

and eqn (S6) gives

$$V_0 = \frac{2k_{cat}[S]_0[O_2]_0[E]_0}{K^{O_2}K^S_{m_2}+K^{O_2}_m[S]_0+K^S_m[O_2]_0+[S]_0[O_2]_0} \quad \text{(S9)}$$

where

$$\lambda_{max} = \frac{k^i_{7_2}k_3k_{7_1}k_{7_3}}{k_{7_1}k_{7_2}k_{7_3}+k_3k_{7_2}k_{7_3}+k_3k_{7_1}k_{7_3}+k_3k_{7_1}k_{7_2}} \quad \text{(S10)}$$

$$k_{cat} = \frac{k_3k_{7_1}k_{7_2}k_{7_3}}{k_{7_1}k_{7_2}k_{7_3}+k_3k_{7_2}k_{7_3}+k_3k_{7_1}k_{7_3}+k_3k_{7_1}k_{7_2}} \quad \text{(S11)}$$

and

$$K^{O_2} = \frac{k_{-8}}{k_8} \quad \text{(S12)}$$

$$K^S_{m_2} = \frac{k_2k_3k_{7_2}k_{7_3}(k_{-6}+k_{7_1})}{k_2k_6k_{7_2}k_{7_3}(k_{7_1}+k_3)+k_2k_6k_3k_{7_1}(k_{7_2}+k_{7_3})} \quad \text{(S13)}$$

Supplementary abbreviations used: **Species and concentrations:** $[E]_0$, initial concentration of tyrosinase; E_i, inactive enzyme; E_m, *met*-tyrosinase; E_d, *deoxy*-tyrosinase; E_{ox}, *oxy*-tyrosinase; E_mS, *met*-tyrosinase/substrate complex (diaxial); $E_{ox}S$, *oxy*-tyrosinase/substrate complex; $(E_{ox}$-$S)_1$, *oxy*-tyrosinase/substrate complex axially bound to a Cu atom; $(E_{ox}$-$S)_2$, *oxy*-tyrosinase/substrate complex axially bound to two Cu atoms; $(E_{ox}$-$S)_3$, *oxy*-tyrosinase/substrate complex axially bound to one Cu atom and the deprotonated hydroxyl group of C-2; E_s, set of enzyme species involved in a restricted steady-state, Scheme 2 of the main paper and Scheme S1 $\{[E_s]=[E_m]+[E_mS]+[E_d]+[E_{ox}]+[E_{ox}S]+[(E_{ox}$-$S)_1]+[(E_{ox}$-$S)_2]\}$; $[\dot{E}_S]$, instantaneous rate of the variation of $[E_s]$; $f_{(E_{ox}-S)_1}$, concentration factor corresponding to enzyme species $(E_{ox}$-$S)_1$ with regard to E_s: $f_{(E_{ox}-S)_1} = \frac{[(E_{ox}-S)_1]}{[E_s]}$; S, *o*-diphenol acting as suicide substrate; $[S]_0$, initial concentration of *o*-diphenol substrate; $[O_2]$, instantaneous concentration of oxygen; $[O_2]_0$, initial concentration of oxygen; $[O_2]_f$, oxygen remaining at $t \to \infty$; $[O_2]_\infty$, oxygen consumed at $t \to \infty$ $([O_2]_\infty = [O_2]_0 - [O_2]_f)$; Q, product of the enzymatic reaction; $[Q]$, instantaneous concentration of Q; $[\dot{Q}]$, instantaneous rate of the variation of $[Q]$. **Kinetic parameters:** λ, apparent inactivation constant; V_0, initial rate of the catalytic pathway; k_x, rate constants of the catalytic pathway; k_{7_1}, substrate binding constant to copper atom through C-1 hydroxyl (axial); k_{7_2}, substrate binding constant to copper atom through C-2 hydroxyl (axial); k^i_x, rate constants of the inactivation pathway; $k^i_{7_2}$, rate constant of transfer of a H^+ to the protonated peroxide; k_{7_3}, rate constant of substrate oxidation through complex $(E_{ox}-S)_2$; $k^i_{7_3}$, inactivation constant; r, partition ratio ($r = k_{7_2}/k^i_{7_2} = k_{cat}/\lambda_{max}$); K^{O_2}, dissociation constant for O_2; $K^{O_2}_m$, Michaelis constant for oxygen; $K^S_{m_1}$, Michaelis constant of *met*-tyrosinase for S; $K^S_{m_2}$, Michaelis constant of *oxy*-tyrosinase for S; K^S_m, Michaelis constant of tyrosinase for S; k_{cat}, catalytic constant of the catalytic pathway ($k_{cat} = \lambda_{max}r$); λ_{max}, maximum value of λ for saturating S; V_{max}, maximum value of V_0 for saturating S.

[1] To whom correspondence should be addressed (email canovasf@um.es).

© The Authors Journal compilation © 2008 Biochemical Society

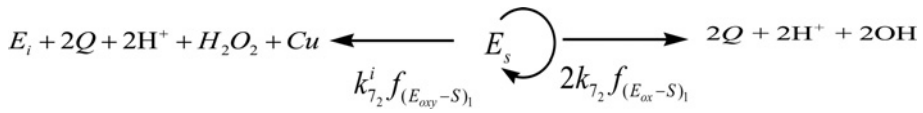

Scheme S1 **See Supplementory Theory for further details.**

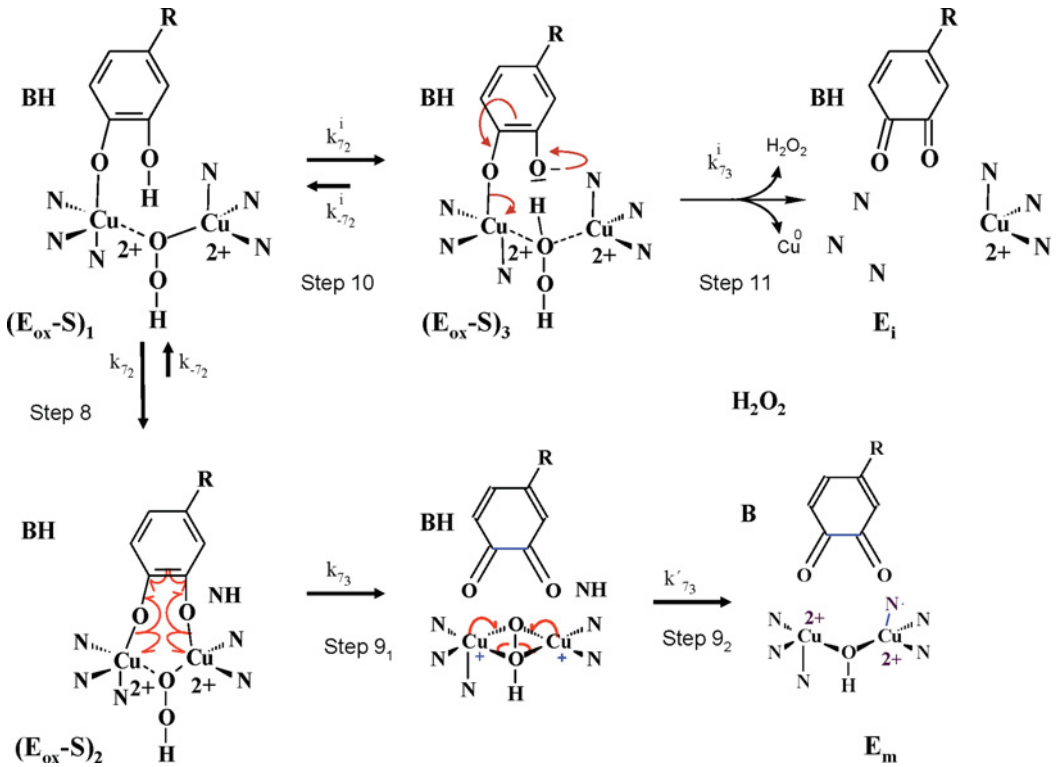

Scheme S2 **Detailed structural mechanism proposed for the suicide inactivation of tyrosinase**

The kinetic steps are explained in Scheme 1 of the main paper.

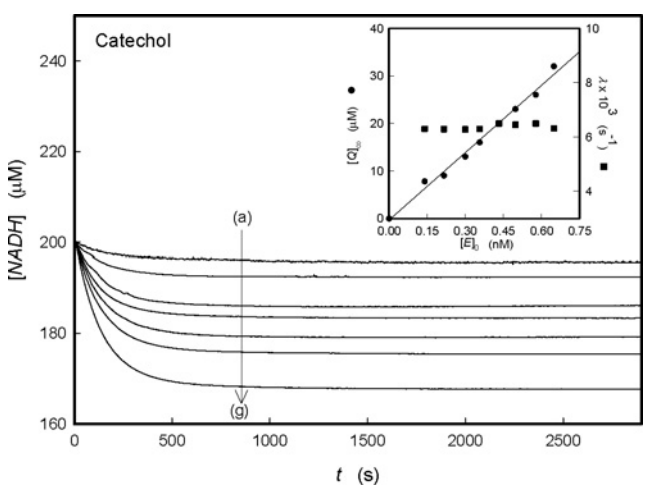

Figure S1 **Corrected recordings of the disappearance of NADH in the suicide inactivation of tyrosinase by catechol for different enzyme concentrations**

Conditions were 30 mM phosphate buffer, pH 7.0, with initial concentrations of NADH, catechol and O_2 of 0.2 mM, 0.3 mM and 0.26 mM respectively. Enzyme concentrations were 0.05 nM (a), 0.07 nM (b), 0.09 nM (c), 0.11 nM (d), 0.12 nM (e), 0.15 nM (f) and 0.16 nM (g). The inset shows corresponding values of $[Q]_\infty$ (●) and λ (■) for different concentrations of tyrosinase.

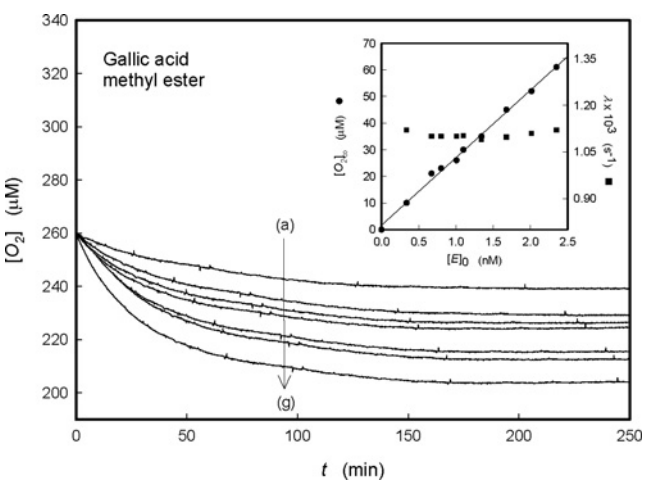

Figure S2 **Corrected recordings of the oxygen consumed in the suicide inactivation of tyrosinase by gallic acid methyl ester for different enzyme concentrations**

Conditions were 30 mM phosphate buffer, pH 7.0, and initial concentrations of SOD, AH_2, gallic acid methyl ester and O_2 were 1.2 μM, 0.2 mM, 0.3 mM and 0.26 mM respectively. Enzyme concentrations were 0.08 nM (a), 0.17 nM (b), 0.25 nM (c), 0.33 nM (d), 0.42 nM (e), 0.5 nM (f) or 0.58 nM (g). The inset shows corresponding values of $[O_2]_\infty$ (●) and λ (■) for different concentrations of tyrosinase.

© The Authors Journal compilation © 2008 Biochemical Society

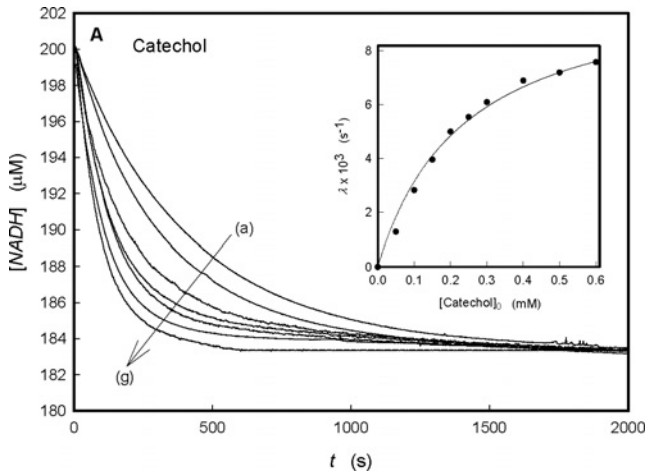

Figure S3 Corrected recordings of the disappearance of NADH in the suicide inactivation of tyrosinase by catechol for different substrate concentrations

Conditions were 30 mM phosphate buffer, pH 7.0, with initial concentrations of 0.2 mM NADH and $[E]_0 = 0.09$ nM. Substrate concentrations were 0.05 mM (a), 0.1 mM (b), 0.15 mM (c), 0.25 mM (d), 0.3 mM (e), 0.4 mM (f) or 0.6 mM (g). The inset shows corresponding values of λ for different catechol concentrations.

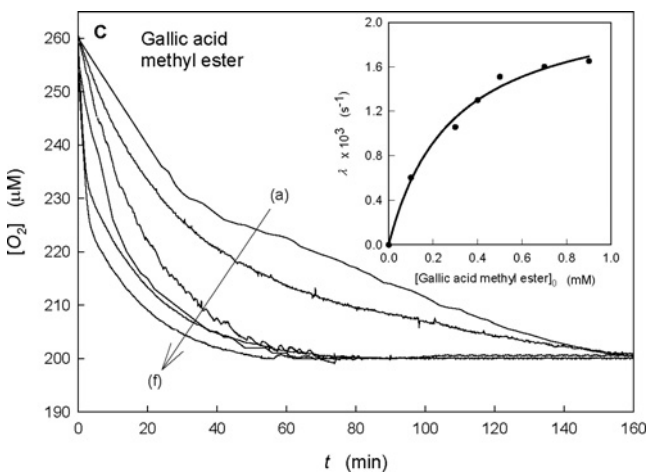

Figure S4 Corrected recordings of the disappearance of oxygen in the suicide inactivation of tyrosinase by gallic acid methyl ester for different substrate concentrations

Conditions were 30 mM phosphate buffer, pH 7.0, with initial concentrations of AH_2, SOD, O_2 at 0.1 mM, 1.2 μM and 0.26 mM respectively and $[E]_0 = 0.58$ nM. Substrate concentrations were 0.1 mM (a), 0.3 mM (b), 0.4 mM (c), 0.5 mM (d), 0.7 mM (e) or 0.9 mM (f). The inset shows the corresponding values of λ for different gallic acid methyl ester concentrations.

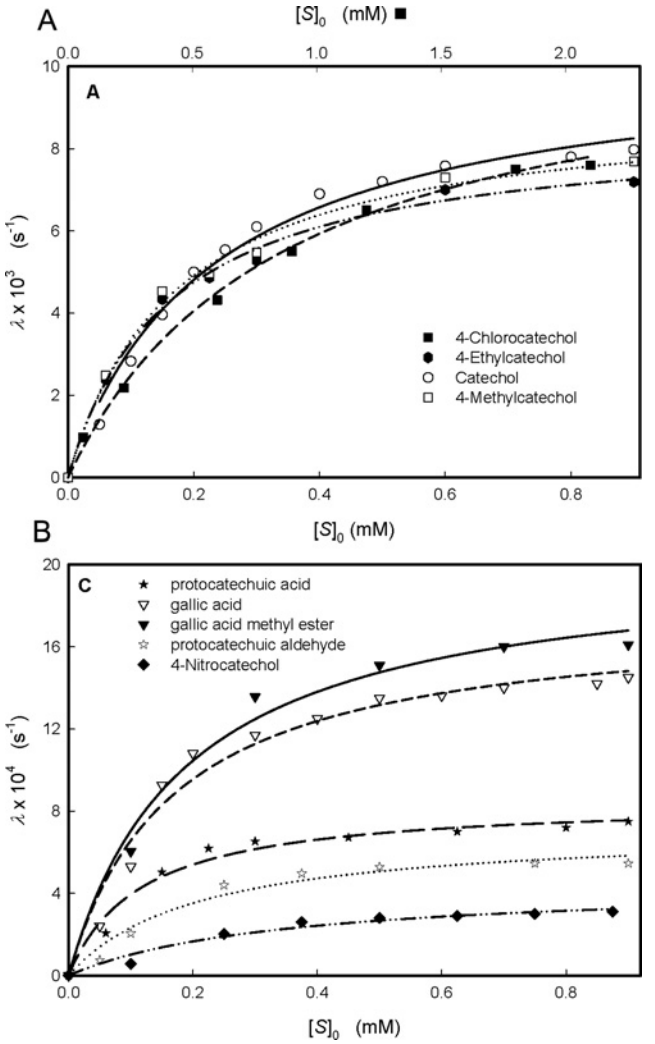

Figure S5 Representation of the values of the inactivation constant λ against $[S]_0$ for the different substrates studied

Conditions were 30 mM phosphate buffer, pH 7.0, 25 °C. Catechol, 4-methylcatechol, 4-ethylcatechol, 4-chlorocatechol, protocatechuic acid, protocatechuic aldehyde and 4-nitrocatechol were recorded from the disappearance of NADH (initial concentration 0.2 mM for every substrate). Gallic acid was recorded from the disappearance of AH_2 and gallic acid methyl ester was recorded by measuring oxygen consumption, with AH_2 and SOD (initial concentrations 0.2 mM and 1.2 μM respectively, for every substrate). Linear tracings are non-linear regression fitting to eqn (S16) of the data analysis. Enzyme concentrations were: (**A**) 0.09 nM catechol, 0.09 nM 4-methylcatechol, 0.09 nM 4-chlorocatechol and 0.09 nM 4-ethylcatechol; (**B**) 0.58 nM gallic acid methyl ester, 0.23 nM gallic acid, 2.25 nM protocatechuic acid, 2.25 nM protocatechuic aldehyde and 2.25 nM 4-nitrocatechol.

$$K_m^{O_2} = \frac{k_3 k_{7_1} k_{7_2} k_{7_3}}{k_8 k_{7_1} k_{7_2} k_{7_3} + k_3 k_8 k_{7_2} k_{7_3} + k_3 k_8 k_{7_1} k_{7_3} + k_3 k_8 k_{7_1} k_{7_2}} = \frac{k_{cat}}{k_8} \quad \text{(S14)}$$

$$K_m^S = \frac{k_6 k_{7_1} k_{7_2} k_{7_3} (k_{-2} + k_3) + k_2 k_3 k_{7_2} k_{7_3} (k_{-6} + k_{7_1})}{k_2 k_6 k_{7_2} k_{7_3} (k_{7_1} + k_3) + k_2 k_6 k_3 k_{7_1} (k_{7_2} + k_{7_3})} \quad \text{(S15)}$$

Bearing in mind that $K_m^{O_2}$ values are very low [13] and that the initial oxygen concentration is 0.26 mM, the enzyme is saturated with O_2 and, from eqns (S8) and (S9), we obtain

$$\lambda = \frac{\lambda_{max}[S]_0}{K_m^S + [S]_0} \quad \text{(S16)}$$

and

$$V_0 = \frac{2k_{cat}[S]_0[E]_0}{K_m^S + [S]_0} \quad \text{(S17)}$$

Note that eqns (S16) and (S17) are equivalent to eqns (6) and (7) of the main paper respectively.

© The Authors Journal compilation © 2008 Biochemical Society

The partition coefficient, r, between the catalytic and suicide inactivation pathways is

$$r = \frac{k_{7_2}}{k^i_{7_2}} \tag{S18}$$

So, considering eqns (S10) and (S11), eqn (S18) is transformed into

$$r = \frac{k_{cat}}{\lambda_{max}} \tag{S19}$$

Relation between the steady-state and suicide inactivation pathways

From eqns (S3), (S4) and (S19), we get

$$V_0 = \lambda[Q]_\infty \tag{S20}$$

$$V_{max} = \lambda_{max}[Q]_\infty \tag{S21}$$

The parallelism between the parameters and kinetic constants that characterize the catalytic pathway (V_0, V_{max} and k_{cat}) and the inactivation pathway ($[Q]_\infty$, λ and r), can be seen from eqns (S19), (S20) and (S21).

Therefore, from eqns (S4), (S16) and (S19), we can obtain the kinetic constants that define the behaviour of a suicide substrate: r, λ_{max}, and k_{cat}.

REFERENCES

1 Ingraham, L. L., Corse, J. and Makower, B. (1952) Enzymatic browning of fruits. 3. Kinetics of the reaction inactivation of polyphenol oxidase. J. Am. Chem. Soc. **74**, 2623–2626

2 Lerch, K. (1983) Neurospora tyrosinase: structural, spectroscopic and catalytic properties. Mol. Cell. Biochem. **52**, 125–138

3 Garcia-Canovas, F., Tudela, J., Martinez-Madrid, C., Varon, R., Garcia-Carmona, F. and Lozano, J. A. (1987) Kinetic study on the suicide inactivation of tyrosinase induced by catechol. Biochim. Biophys. Acta **912**, 417–423

4 Tudela, J., Garcia-Canovas, F., Varon, R., Jimenez, M., Garcia-Carmona, F. and Lozano, J. A. (1987) Kinetic characterization of dopamine as a suicide substrate of tyrosinase. J. Enzym. Inhib. **2**, 47–56

5 Tudela, J., Garcia-Canovas, F., Varon, R., Jimenez, M., Garcia-Carmona, F. and Lozano, J. A. (1988) Kinetic study in the transient phase of the suicide inactivation of frog epidermis tyrosinase. Biophys. Chem. **30**, 303–310

6 Waley, S. G. (1980) Kinetics of suicide substrates. Biochem. J. **185**, 771–773

7 Galvez, J. and Varon, R. (1981) Transient phase kinetics of enzyme reactions. J. Theor. Biol. **89**, 1–17

8 Galvez, J., Varon, R. and and Garcia-Carmona, F. (1981) Kinetics of enzyme reactions with inactivation steps. J. Theor. Biol. **89**, 37–44

9 Galvez, J., Varon, R. and and Garcia-Canovas, F. (1981) Transient phase of two-substrate enzyme systems. J. Theor. Biol. **89**, 19–35

10 Tudela, J., Garcia-Canovas, F., Varon, R., Garcia-Carmona, F. and Lozano, J. A. (1987) Transient-phase kinetics of enzyme inactivation induced by suicide substrates. Biochim. Biophys. Acta **912**, 408–416

11 Varon, R., Garrido-del Solo, C., Garcia-Moreno, M., Garcia-Canovas, F., Moya-Garcia, G., de Labra, J. V. and Havsteen, B. H. (1998) Kinetics of enzyme systems with unstable suicide substrates. Biosystems **47**, 177–192

12 Moruno-Davila, M. A., Garrido-del Solo, C., Garcia-Moreno, M., Havsteen, B. H., Garcia-Sevilla, F., Garcia-Canovas, F. and Varon, R. (2001) Kinetic analysis of enzyme systems with suicide substrate in the presence of a reversible competitive inhibitor, tested by simulated progress curves. Int. J. Biochem. Cell Biol. **33**, 181–191

13 Fenoll, L. G., Rodriguez-Lopez, J. N., Garcia-Molina, F., Garcia-Canovas, F. and Tudela, J. (2002) Michaelis constants of mushroom tyrosinase with respect to oxygen in the presence of monophenols and diphenols. Int. J. Biochem. Cell Biol. **34**, 332–336

Received 2 May 2008/16 July 2008; accepted 23 July 2008
Published as BJ Immediate Publication 23 July 2008, doi:10.1042/BJ20080892

© The Authors Journal compilation © 2008 Biochemical Society

4.16. INACTIVACIÓN DE TIROSINASA EN SU ACCIÓN SOBRE DOPA.

El estudio de la inactivación de tirosinasa en su acción sobre los isómeros del dopa ha dado lugar a la siguiente publicación adjunta.

4.16.1. Título

Tyrosinase inactivation in its action on dopa.

4.16.2. Autores

Muñoz-Muñoz, J.L.; Acosta-Motos, J.R.; Garcia-Molina, F.; Varon, R.; Garcia-Ruiz, P.A.; Tudela, J.; Garcia-Cánovas, F. y Rodríguez-López, J.N.

4.16.3. Referencia

Biochimica et Biophysica Acta-Protein and Proteomics (2010) 1804, 1467-1475.

4.16.4. Resumen

Bajo condiciones aerobias y anaerobias, tirosinasa sufre un proceso de inactivación irreversible inducido por su sustrato fisiológico L-dopa. En condiciones aerobias, la inactivación ocurre a través de un proceso de inactivación suicida que tiene lugar fundamentalmente en la forma oxitirosinasa. En condiciones anaerobias, tanto la forma metatirosinasa como la desoxitirosinasa, sufren un proceso de inactivación irreversible. La inactivación suicida es más lenta que la que ocurre en condiciones anaerobias. La enzima tiene menos afinidad por el isómero D-dopa, pero la rapidez de la inactivación es la misma. Se proponen mecanismos para explicar estos procesos de inactivación.

Author's personal copy

Biochimica et Biophysica Acta 1804 (2010) 1467–1475

Contents lists available at ScienceDirect

Biochimica et Biophysica Acta

journal homepage: www.elsevier.com/locate/bbapap

Tyrosinase inactivation in its action on dopa

J.L. Muñoz-Muñoz [a], J.R. Acosta-Motos [a], F. Garcia-Molina [a], R. Varon [b], P.A. Garcia-Ruíz [c], J. Tudela [a], F. Garcia-Cánovas [a,*], J.N. Rodríguez-López [a]

[a] GENZ: Grupo de Investigación Enzimología, Departamento de Bioquímica y Biología Molecular-A, Facultad de Biologia, Universidad de Murcia, E-30100, Espinardo, Murcia, Spain
[b] Departamento de Química-Física. Escuela de Ingenieros Industriales de Albacete. Universidad de Castilla la Mancha. Avda. España s/n. Campus Universitario, E-02071, Albacete, Spain
[c] QCBA: Grupo de Química de Carbohidratos y Biotecnología de Alimentos, Departamento de Química Orgánica. Facultad de Química, Universidad de Murcia, E-30100, Espinardo, Murcia, Spain

ARTICLE INFO

Article history:
Received 10 November 2009
Received in revised form 1 February 2010
Accepted 23 February 2010
Available online 6 March 2010

Keywords:
o-Diphenol
Stereospecificity
Inactivation
Suicide
Tyrosinase

ABSTRACT

Under aerobic or anaerobic conditions, tyrosinase undergoes a process of irreversible inactivation induced by its physiological substrate L-dopa. Under aerobic conditions, this inactivation occurs through a process of suicide inactivation involving the form *oxy*-tyrosinase. Under anaerobic conditions, both the *met*- and *deoxy*-tyrosinase forms undergo irreversible inactivation. Suicide inactivation in aerobic conditions is slower than the irreversible inactivation under anaerobic conditions. The enzyme has less affinity for the isomer D-dopa than for L-dopa but the velocity of inactivation is the same. We propose mechanisms to explain these processes.

© 2010 Elsevier B.V. All rights reserved.

1. Introduction

Tyrosinase or polyphenol oxidase (EC 1.14.18.1, *o*-diphenol:O_2 oxidoreductase) is a copper protein that uses molecular oxygen to catalyse the hydroxylation of monophenols to *o*-diphenols (monophenolase activity) and the oxidation of *o*-diphenols to *o*-quinones (diphenolase activity) [1,2]. Tyrosinase from a variety of sources undergoes an inactivation process when it reacts with its substrate under aerobic conditions [3–5]. The study of enzymatic inactivation by suicide substrates or mechanism-based inhibitors has grown in importance because of possible pharmacological applications [6,7]. Furthermore, these compounds may be useful for studying enzymatic mechanisms and for designing new pharmacological drugs [8].

The suicide inactivation of enzymes has been studied in several works since Waley in 1980 [9]. Our own group has made several kinetic studies of the suicide inactivation mechanism from a theoretical point of view [10,11] and using mushroom tyrosinase [12,13], frog skin tyrosinase [14,15] and peroxidase from different sources [16,17]. We have also studied the suicide inactivation of an enzyme that can be measured from coupled reactions [18] and published a review on the experimental designs for a kinetic study of suicide inactivation [19].

Several monophenols and *o*-diphenols are chiral tyrosinase substrates (L- and D-enantiomers). Some papers have reported the stereoselective action of several tyrosinases on these enantiomers, although the results have been unequal and even contradictory [20–22]. The use of a suitable measuring method to characterize monophenolase and diphenolase activities, using the chromogenic nucleophile 3-methyl-2-benzothiazolinone hydrazone (MBTH) [23,24], demonstrated that tyrosinase shows stereospecificity in its affinity towards its substrate and has a higher Michaelis constant for the isomers D (D-tyrosine and D-dopa) than for the L (L-tyrosine and L-dopa). However, it demonstrates the same velocity of catalysis for both isomers (L- and D-dopa and L- and D-tyrosine), confirming that the velocity is related with the charge density of the oxygen atoms of the hydroxyl groups of the benzene ring, which, in turn, is related with the chemical shifts δ_3 and δ_4. The same conclusion was reached using the immobilised enzyme [25].

The suicide inactivation of tyrosinase from different sources has been studied and many attempts have been made to find a mechanism that explains the phenomenon [26,27]. Recently, our group published a possible explication for this process [28]. In our mechanism (Scheme ISM), the E_{ox} form binds one molecule of substrate (*o*-diphenol) (Step 6). In this case, the base (B), possibly a histidine, is already protonated and cannot help the substrate bind to the copper. The proton of the hydroxyl group of C-4 must be transferred to the peroxide group, which acts as a base [29,30]. This would be the slow step of the turnover, controlled by k_{7_1} (Step 7) [30]. The fact that the peroxide acts as a base and is involved in the proton transfer from the hydroxyl group of C-4 and C-3 is important. The protonated peroxide draws the copper atoms in the E_{ox} form closer together, since the distance in the unprotonated form, 3.6 Å, is too great for the molecule of substrate to bind diaxially to them. However,

* Corresponding author. Tel.: +34 868 884764; fax: +34 868 883963.
E-mail address: canovasf@um.es (F. Garcia-Cánovas).

1570-9639/$ – see front matter © 2010 Elsevier B.V. All rights reserved.
doi:10.1016/j.bbapap.2010.02.015

Author's personal copy

this would be possible in the protonated E_{ox} form. With the substrate axially bound to one copper atom, there are two possibilities in Step 8: (a) the oxygen of the hydroxyl group of C-3 may attack the other copper atom, which is drawn closer following protonation of the peroxide group, transferring the proton to the histidine, binding to the substrate diaxially and co-planar with the copper atoms. In this way, the concerted redox reaction in Step 9 can occur, releasing *o*-quinone and E_m. (b) The hydroxyl group of C-3 may donate a proton to the protonated peroxide, remaining as $C–O^-$ in Step 10. The co-planarity of the substrate ring, the oxygen of C-4 and the copper atom favor the simultaneous oxidation of the substrate to *o*-quinone and the reduction of one Cu^{2+} atom to copper (0) through the ring, while copper (0) and hydrogen peroxide are released, and the enzyme is inactivated as a consequence (Step 11) (Scheme ISM).

For its part, under anaerobic conditions it has been demonstrated that a reductant like ascorbic acid inactivates the enzyme in its *met*-tyrosinase and *deoxy*-tyrosinase forms [31]. The capacity to inactivate the enzyme under both aerobic and anaerobic conditions may have an industrial application for protecting juices and other preparations from enzymatic browning: hence the interest in its study and characterisation.

The aims of this study were: to analyse the inactivation of tyrosinase by its physiological substrate L-dopa under aerobic conditions (suicide inactivation of *oxy*-tyrosinase form) and under anaerobic conditions (irreversible inactivation of *met*-tyrosinase and *deoxy*-tyrosinase) and to study the effect of the stereospecificity, using the isomers L- and D-dopa.

1.1. Notation

For clarity and for the sake of brevity, the following additional notations will be used in the text.

1.1.1. Species and concentrations

$[E]_0$	initial concentration of tyrosinase
E_a	active enzyme
$[E_a]$	instantaneous concentration of E_a
$[E_m]$	instantaneous concentration of *met*-tyrosinase
$[E_m]_0$	initial concentration of *met*-tyrosinase
$[E_d]$	instantaneous concentration of *deoxy*-tyrosinase
$[E_d]_0$	initial concentration of *deoxy*-tyrosinase
E_d^*	*deoxy*-tyrosinase after of E_d to E_d^* transition
$[E_d^*]$	instantaneous concentration of E_d^*
$[E_d^*]_0$	initial concentration of E_d^*
E_i	inactive enzyme
$[E_i]$	instantaneous concentration of E_i
D	L- or D-*o*-diphenol
$[D]_0$	initial concentration of D
Q	*o*-quinone product of the enzymatic reaction
[Q]	instantaneous concentration of Q
$[Q]_\infty$	*o*-quinone concentration at $t \to \infty$
NADH	nicotinamin adenin dinucleotide
$[NADH]_0$	initial concentration of NADH
[NADH]	instantaneous concentration of NADH
$[NADH]_f$	NADH-value at $t \to \infty$
$[NADH]_\infty$	NADH consumed at the end of the reaction, $t \to \infty$, i.e. $[NADH]_\infty = [NADH]_0 - [NADH]_f$

1.1.2. Kinetic parameters

$V_0^{D(NADH)}$	initial rate of tyrosinase acting on D in the presence of NADH.
$V_0^{D(Q)}$	initial rate of tyrosinase acting on D, $V_0^{D(Q)} = V_0^{D(NADH)}$.
$\lambda_{E_{ox}}^{D(L\text{ or }D)}$	apparent constant of suicide inactivation of tyrosinase in the presence of L- or D-dopa.
$\lambda_{E_{ox(max)}}^{D(L\text{ or }D)}$	maximum value of $\lambda_{E_{ox}}^{D(L\text{ or }D)}$ for saturating substrate.
$\lambda_{E_d}^{D(L\text{ or }D)}$	apparent constant of irreversible inhibition of E_d by L- or D-dopa.
$\lambda_{E_d^*}^{D(L\text{ or }D)}$	apparent constant of irreversible inhibition of E_d^* by L- or D-dopa.
$k_{i_{D(L\text{ or }D)}}$	maximum value of $\lambda_{E_d}^{D(L\text{ or }D)}$ for saturating substrate.
$k_{i_{D(L\text{ or }D)}}^*$	maximum value of $\lambda_{E_d^*}^{D(L\text{ or }D)}$ for saturating substrate.
k_T	rate constant of the transition E_d to E_d^*.
r_D	partition ratio for the diphenolase activity, $r_D = k_{7_2} k_{7_2}^i = k_{cat}^D / \lambda_{E_{ox}(max)}^D$.
$K_m^{O_2}$	Michaelis constant of oxygen.
$K_m^{D(L\text{ or }D)}$	Michaelis constant of tyrosinase for L- or D-dopa.
$k_{cat}^{D(L\text{ or }D)}$	catalytic constant of the diphenolase activity for L- or D-dopa.
$K_{E_d^*}^{D(L\text{ or }D)}$	dissociation constant of the complex E_d^*D, where D is L- or D-dopa.
$K_{E_d}^{D(L\text{ or }D)}$	dissociation constant of the complex E_dD, where D is L- or D-dopa.

2. Experimental

2.1. Materials

Mushroom tyrosinase or polyphenol oxidase (*o*-diphenol: O_2 oxidoreductase, EC 1.14.18.1) (8300 U/mg) and β-NADH were supplied by Sigma (Madrid, Spain). The enzyme was purified as previously described in [32]. Protein concentration was determined by the Lowry method [33]. The substrates used L- and D-dopa were purchased from Sigma (Madrid, Spain). All other chemicals were of analytical grade. Stock solutions of the diphenolic substrates were prepared in 0.15 mM phosphoric acid to prevent autooxidation. Milli-Q system (Millipore corp.) ultrapure water was used throughout.

2.2. Methods

2.2.1. Spectrophotometric assays

These assays were carried out with a Perkin-Elmer Lambda-35 spectrophotometer, on line interfaced to a PC-computer, where the kinetic data were recorded, stored and later analysed. The product of the enzyme reaction *o*-dopaquinone is unstable and evolves towards dopachrome, which is not stable at long assay times [34,35]. For this reason, the reaction was followed by measuring the disappearance of NADH at 340 nm, with $\varepsilon = 6230\ M^{-1}\ cm^{-1}$, which reduces *o*-dopaquinone to L-dopa [36]. The inactivation kinetics was studied in 30 mM sodium phosphate buffer (pH 6.0), since *o*-dopaquinone evolves rapidly to dopachrome at pH 7.0, while at lower pH the reaction slows down and *o*-dopaquinone is reduced by NADH [34].

2.2.2. Kinetic data analysis

2.2.2.1. Diphenolase activity. The experimental data of time-based assays for the disappearance of NADH (Fig. 1) follow the Eq. (1):

$$[NADH] = [NADH]_f + [NADH]_\infty e^{-\lambda_{E_{ox}}^D t} \quad (1)$$

$[NADH]_f$,$[NADH]_\infty = [Q]_\infty$ and $\lambda_{E_{ox}}^D$ can be obtained by non-linear regression [37]. There is always a slow spontaneous oxidation of *o*-diphenol and NADH (Fig. 1), which should be computer corrected in further NADH *vs.* time plots (in general this treatment is applied to all the kinetic recordings). The experimental recordings obtained in the following steps, therefore, fit Eq. (1), from which the corresponding inactivation parameters, $[NADH]_\infty = [Q]_\infty$ and $\lambda_{E_{ox}}^D$, can be determined.

2.2.3. Generation of E_{ox} and E_d

To kinetically characterize the inactivation of the E_d form of tyrosinase, E_d was generated from the native enzyme, adding

Author's personal copy

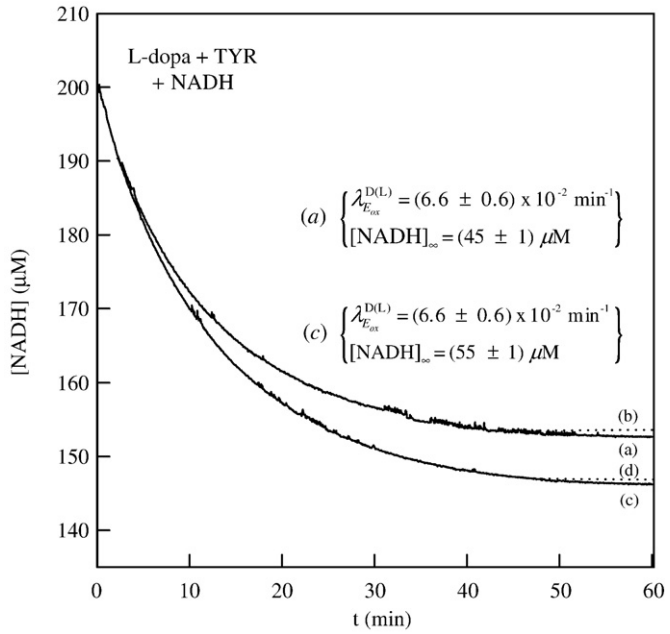

Fig. 1. Experimental recordings of the disappearance of NADH in the suicide inactivation of tyrosinase by L-dopa and curves corrected after applying the kinetic data analysis. Conditions were 30 mM sodium phosphate buffer (pH 6.0), 0.2 mM NADH, 0.26 mM O_2, 1 mM L-dopa and enzyme concentrations were: (a) 0.7 nM and (c) 0.85 nM. Curves (b) and (d) are the corrected recordings from (a) and (c), respectively, subtracting the L-dopa and NADH spontaneous oxidation.

micromolar concentrations (2 μM) of H_2O_2, so that, the E_m form passed to E_{ox}. Then, nitrogen was bubbled through the solution transforming all the E_{ox} to E_d ($E_{ox} \rightleftarrows E_d + O_2$) [38,39].

2.2.4. Generation of E_m

The inactivation of E_m was characterized by first generating it from the native enzyme in two ways: (a) adding catalase 2 μM, so that $E_{ox} \rightleftarrows E_m + H_2O_2$; the catalase acts on the H_2O_2 displacing the above equilibrium, $2H_2O_2 + \text{catalase} \rightarrow O_2 + 2H_2O$, so that all E_{ox} is transformed into E_m at the end of the reaction. (b) Adding 2 μM of H_2O_2, so that all the enzyme passes to E_{ox} and then adding 2 μM catalase [38,39].

2.2.5. Evaluation of enzymatic species E_m, E_d and E_{ox} in an enzymatic preparation of tyrosinase

It is known that in an enzymatic preparation of tyrosinase from any source is found in three forms, E_m, E_d and E_{ox} [39]. Several authors have proposed spectrophotometric methods for evaluating these forms [39–41]. Here, we propose a kinetic method based on the fact that the inactivation of these forms by 2-mercaptoethanol [42] occurs over a wide time range: inactivation constants of 0.014 s^{-1}, 4×10^{-5} s^{-1} and 1×10^{-5} s^{-1} for E_{ox}, E_m and E_d, respectively. Under aerobic conditions at oxygen concentrations of 0.26 mM, practically the only forms existing are E_{ox} and E_m [32]. Note that the difference between k_i^{ox} and k_i^m is three orders of magnitude, a difference that can be used to evaluate these enzymatic forms. The experimental method was described in [31].

2.2.6. ^{13}C-NMR assays

^{13}C-NMR spectra of several substrates were obtained in a Varian Unity spectrometer at 300 MHz. The spectra were obtained at pH = 6.0 by using ^2H_2O as solvent for the substrates. Chemical displacement (δ) values were measured relative to those for tetramethylsilane ($\delta = 0$). The maximum line breadth accepted in the ^{13}C-NMR spectra was 0.06 Hz. Therefore, the maximum accepted error for each peak of the spectrum was ±0.03 p.p.m.

3. Results

The active site of tyrosinase is found in three forms in the catalytic cycle: *met*-tyrosinase ($Cu^{2+}Cu^{2+}$), *deoxy*-tyrosinase ($Cu^{+}Cu^{+}$) and *oxy*-tyrosinase ($Cu^{2+}Cu^{2+}O_2^{2-}$) [39]. These enzymatic forms may undergo a substrate-induced irreversible inactivation. Under aerobic conditions, the enzyme undergoes a process of suicide inactivation, localised in *oxy*-tyrosinase, while under anaerobic conditions the *met*-tyrosinase and *deoxy*-tyrosinase forms undergo irreversible inactivation. These processes are studied below with *o*-diphenols (L- and D-dopa), under both aerobic and anaerobic conditions.

3.1. Tyrosinase action on o-diphenols

3.1.1. Inactivation of tyrosinase in its action on o-diphenols under aerobic conditions: suicide inactivation

The kinetic mechanism proposed to explain the suicide inactivation of tyrosinase acting on *o*-diphenols is based on the structural mechanism proposed in Scheme ISM and can be outlined as follows in Scheme I.

When $[D]_0$, $[O_2]_0 >> [E]_0$ and $[Q]_\infty << [D]_0$, $[O_2]_0$, it is possible a derivation of the analytical expression which establishes the accumulation of the product (*o*-quinone) with time, as is detailed in reference [28].

The variation of [Q] with time is given by Eq. (2) [28].

$$[Q] = [Q]_\infty \left(1 - e^{-\lambda^D_{E_{ox}} t}\right) \quad (2)$$

When $t \rightarrow \infty$, $[Q] = [Q]_\infty$ and, according to [28]:

$$[Q]_\infty = \frac{2k_{7_2}}{k^i_{7_2}} [E]_0 \quad (3)$$

The velocity of the suicide inactivation is regulated by the apparent inactivation constant, $\lambda^D_{E_{ox}}$, whose expression is given by Eq. (4). Taking into account the saturation of tyrosinase by oxygen ($[O_2]_0 \rightarrow \infty$), thus according to [28]:

$$\lambda^D_{E_{ox}} = \frac{\lambda^D_{E_{ox}(max)} [D]_0}{K^D_m + [D]_0} \quad (4)$$

The partition ratio, r_D, between the catalytic and suicide inactivation pathways is:

$$r_D = \frac{k_{7_2}}{k^i_{7_2}} = \frac{k^D_{cat}}{\lambda^D_{E_{ox}(max)}} = \frac{[Q]_\infty}{2[E]_0} = \frac{[NADH]_\infty}{2[E]_0} \quad (5)$$

where k_{7_2} is the substrate binding constant to the copper atom through the C-3 hydroxyl (axial) and $k^i_{7_2}$ is the rate constant of transfer of a H^+ to the protonated peroxide (see Scheme ISM).

Therefore, from Eq. (1–5), we can obtain the kinetic constants that characterize the kinetic behaviour of a suicide substrate: r_D, $\lambda^D_{E_{ox}(max)}$, K^D_m and k^D_{cat}. Note that if dopachrome or oxygen consumption is being measured, Eqs. (1–5) are totally applicable and it is only necessary to take into account the stoichiometric relations: 2Q:1 DC:1O_2 and that Q and DC are originated in the medium by the action of the enzyme, while the oxygen concentration falls.

3.1.1.1. Experimental study of suicide inactivation. The study of the suicide inactivation of tyrosinase was developed in three steps and the *o*-diphenols used in this work were L-dopa and D-dopa.

Step 1. Fig. 1 shows the spectrophotometric recordings of the disappearance of NADH, curves (a) and (c), and their corrections by fitting to Eq. (1), after subtracting the NADH and *o*-diphenol spontaneous oxidation, Fig. 1, curves (b) and (d). These corrected recordings are analysed as described in the Kinetic Data Analysis section. By means

Author's personal copy

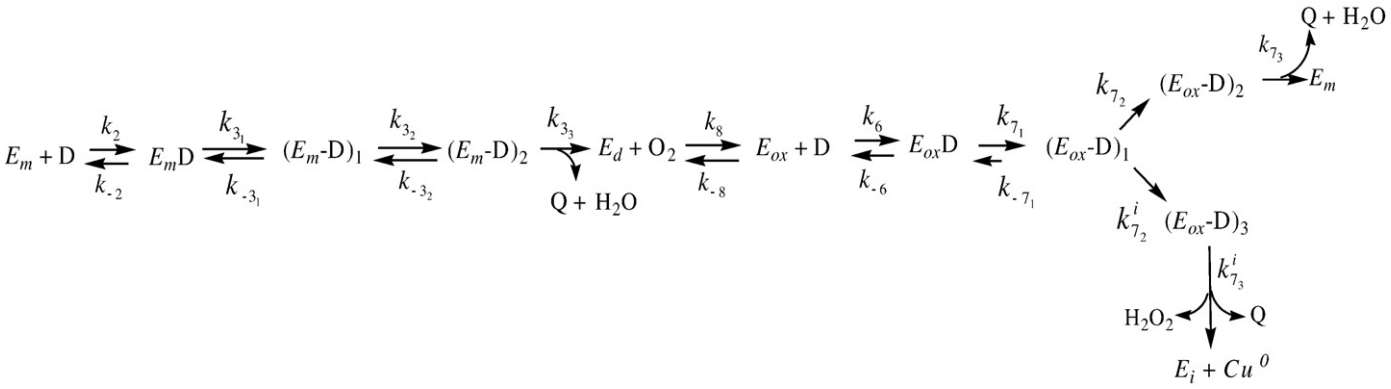

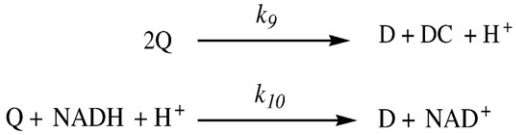

Scheme I. Kinetic mechanism proposed to explain the suicide inactivation of tyrosinase acting on dopa enantiomers (see text and Scheme ISM for further details).

of these preliminary studies, the concentration of enzyme is optimised so that $[Q]_\infty << [O_2]_0, [D]_0$.

Step 2. Variation in enzyme concentration. The $[E]_0$-value is varied while the substrate concentration is kept constant. The results obtained are shown in Fig. 2A and B. The concentration of the substrate in these experiments does not change because the *o*-quinone is reduced by NADH. However, the concentrations of O_2 and NADH do change. In the case of tyrosinase, $K_m^{O_2}$ is very small [43], which permits an oxygen consumption of more than 10%. The NADH must be in excess. Note how the values of $[NADH]_\infty$ are directly proportional to $[E]_0$, while $\lambda_{E_{ox}}^{D(L\text{ or }D)}$ does not vary with $[E]_0$ (Fig. 2A Inset and B Inset).

Fig. 2A Inset and B Inset show the dependence of the values obtained for the product at the end of the reaction, $[NADH]_\infty$ *vs.* $[E]_0$, from whose slopes and, according to Eq. (5), r_D can be determined (Table 1).

Step 3. Variation in substrate concentration. The experimental recordings for the disappearance of NADH during the action of tyrosinase on L-dopa and D-dopa obtained by varying the concentration of substrate are shown in Fig. 3A and B, respectively. Fitting by non-linear regression to Eq. (1) gives the apparent inactivation constant $\lambda_{E_{ox}}^{D(L\text{ or }D)}$. The hyperbolic dependence of $\lambda_{E_{ox}}^{D(L\text{ or }D)}$ *vs.* $[D]_0$ is shown in Fig. 3A Inset and B Inset. Fitting these data by non-linear regression according to Eq. (4) gives $\lambda_{E_{ox}(max)}^{D(L\text{ or }D)}$ and $K_m^{D(L\text{ or }D)}$ for each of the isomers (Table 1). These values of $\lambda_{E_{ox}(max)}^{D(L\text{ or }D)}$ and r_D (Table 1) permit us to obtain $k_{cat}^{D(LorD)}$ (Table 1).

3.1.2. Tyrosinase inactivation under anaerobic conditions: irreversible inactivation

The three enzymatic forms of the turnover of tyrosinase are in equilibrium, as shown by the following scheme (Scheme II).

In the presence of oxygen (0.26 mM), the principal forms are E_m and E_{ox}, whose concentration in an enzymatic preparation was determined by measuring the inactivation of the native enzyme by irreversible inhibition with 2-mercaptoethanol, as described in [31].

3.1.2.1. Inactivation of deoxy-tyrosinase by o-diphenols. The form *deoxy*-tyrosinase was generated as described in Materials and Methods sections [31]. Maintaining anaerobic conditions, E_d evolves slowly towards another enzymatic form that we denominate E_d^* [44], as described in the Scheme III.

Through analogy with that observed in hemocyanin, it has been proposed that the copper atoms in the enzymatic form E_d^* are more separated than in E_d [44,45].

The forms E_d and E_d^* show different affinities for *o*-diphenols and hence different activities ($K_{m,E_d}^{D(L)} = 0.52$ mM and $K_{m,E_d^*}^{D(L)} = 0.99$ mM in the case of L-dopa, and $K_{m,E_d}^{D(D)} = 3.95$ mM and $K_{m,E_d^*}^{D(D)} = 5.36$ mM in the case of D-dopa), so that the transition of E_d and E_d^* can be followed by measuring the initial rate with L-dopa, as shown in Fig. 4. Analysis of the data of Fig. 4 according to Eq. (6)

$$\frac{A}{A_0} = \frac{[E_a]}{[E_d]_0} = \alpha + \beta e^{-k_T t} \tag{6}$$

gives the apparent constant of the transition in the conditions described in Fig. 4 ($k_T = (3.9 \pm 0.4) \times 10^{-2}$ min^{-1}) and where A is the instantaneous enzymatic activity.

3.1.2.1.1. E_d^* inactivation by L-dopa and D-dopa. From the form E_{ox}, the form E_d was generated by passing a nitrogen stream. After 90 min, the form E_d is transformed into E_d^*, which is stable under anaerobic conditions. In this section, we shall study the reaction of E_d^* with L-dopa and D-dopa.

At t = 0, a given concentration of L-dopa was added as indicated in Fig. 5A. Aliquots were taken and, when the activity was followed with time, an irreversible inactivation, which can be described kinetically by Scheme IV and whose structural interpretation is depicted in Scheme IISM, was observed.

The monoexponential behaviour observed in Fig. 5A (gradual loss of activity) can be fitted to Eq. (7):

$$\left[E_d^*\right] = \left[E_d^*\right]_0 e^{-\lambda_{E_d^*}^{D(L)} t} \tag{7}$$

where D(L) corresponds to L-dopa. The values of $\lambda_{E_d^*}^{D(L)}$ vary with the concentration of substrate used in the assays, according to Eq. (8):

$$\lambda_{E_d^*}^{D(L)} = \frac{k_{i_{D(L)}}^* [D]_0}{K_{E_d^*}^{D(L)} + [D]_0}. \tag{8}$$

The data analysis by non-linear regression shown in Fig. 5A Inset according to Eq. (8) gives the values of $k_{i_{D(L)}}^*$ and $K_{E_d^*}^{D(L)}$ shown in Table 2. When the same experiments were carried out with D-dopa, Fig. 5B and B Inset, the data shown in Table 2 were obtained.

Author's personal copy

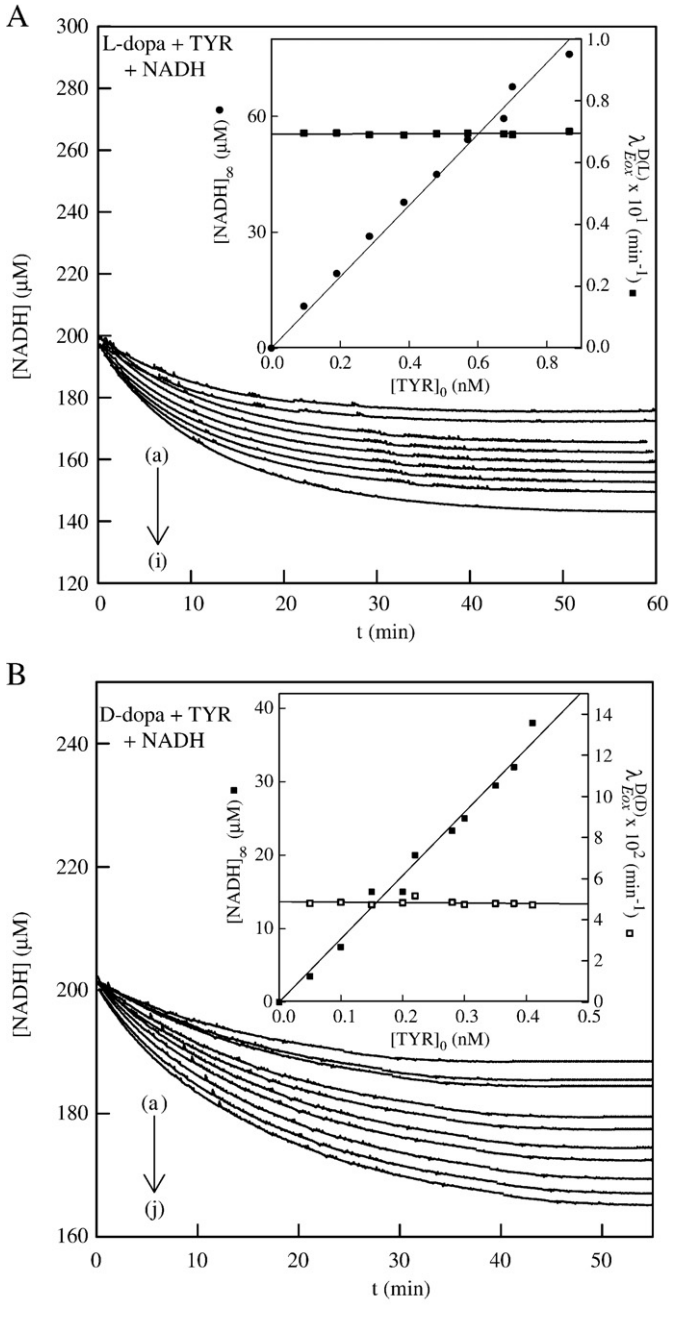

Fig. 2. Corrected recordings of the disappearance of NADH in the suicide inactivation of tyrosinase by *o*-diphenol for different enzyme concentrations. (A) L-dopa, (B) D-dopa. Conditions were: 30 mM sodium phosphate buffer (pH 6.0), 0.2 mM NADH, 0.26 mM O_2. (A). 1 mM L-dopa and $[E]_0$ (nM): (a) 0.09, (b) 0.19, (c) 0.28, (d) 0.38, (e) 0.48, (f) 0.57, (g) 0.67, (h) 0.70 and (i) 0.85. Inset. Representation of the values of $[NADH]_\infty$ (●) and $\lambda^{D(L)}_{E_{ox}}$ (■) *vs.* enzyme concentration for L-dopa. (B). 4 mM D-dopa and $[E]_0$ (nM): (a) 0.05, (b) 0.10, (c) 0.15, (d) 0.20, (e) 0.22, (f) 0.28, (g) 0.30, (h) 0.35, (i) 0.38 and (j) 0.41. Inset. Representation of the values of $[NADH]_\infty$ (●) and $\lambda^{D(D)}_{E_{ox}}$ (■) *vs.* enzyme concentration for D-dopa.

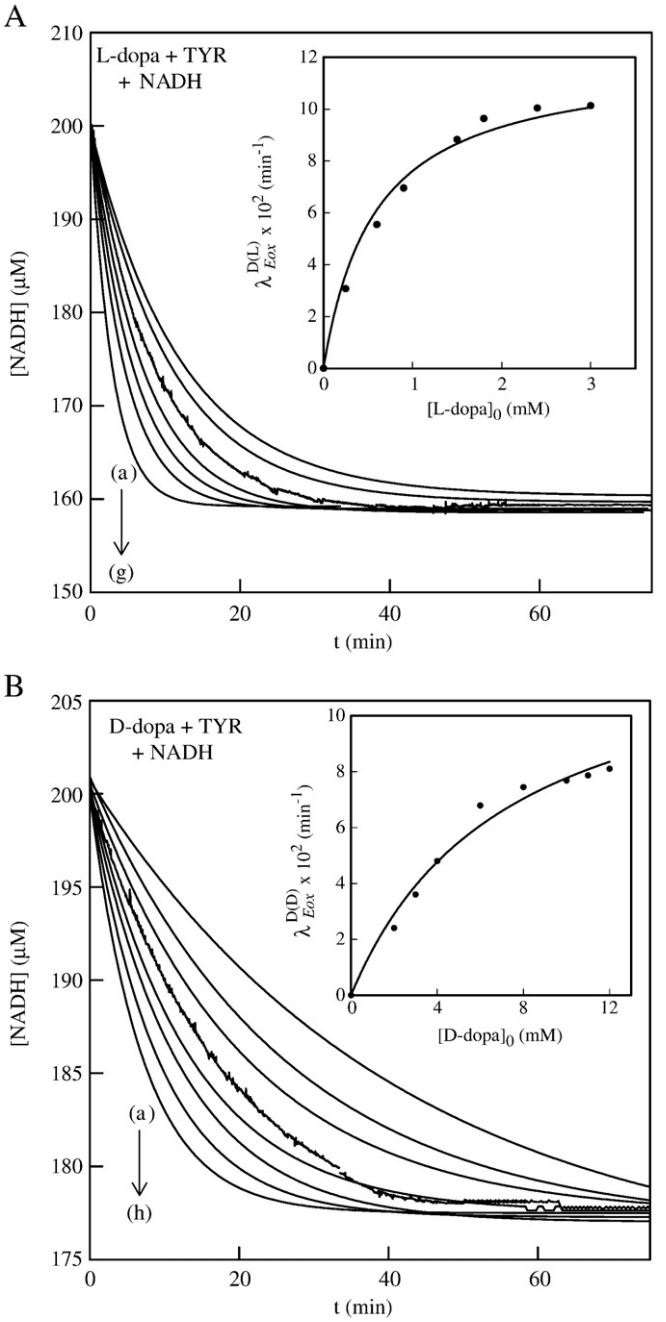

Fig. 3. Corrected recordings of the disappearance of NADH in the suicide inactivation of tyrosinase by different substrate concentrations. (A) L-dopa, (B) D-dopa. Conditions were 30 mM sodium phosphate buffer (pH 6.0), 0.26 mM O_2 and the initial concentrations of NADH and tyrosinase were: 0.2 mM and 0.6 nM for L-dopa and 0.2 mM and 0.2 nM for D-dopa, respectively. (A) L-dopa, the substrate concentrations were (mM): (a) 0.25, (b) 0.6, (c) 0.9, (d) 1.5, (e) 1.8, (f) 2.4 and (g) 3. Inset. Values of $\lambda^{D(L)}_{E_{ox}}$ for different L-dopa concentrations. (B) D-dopa, the substrate concentrations were (mM): (a) 2, (b) 3, (c) 4, (d) 6, (e) 8, (f) 10, (g) 11 and (h) 12. Inset. Values of $\lambda^{D(D)}_{E_{ox}}$ for different D-dopa concentrations.

Table 1
Kinetic constants which characterize the suicide inactivation of tyrosinase by the dopa isomers and values of the chemical shifts of these compounds obtained by ^{13}C-NMR for the C-3 and C-4 carbons at pH 6.0.

o-Diphenol	$\lambda^{D}_{E_{ox(max)}} \times 10^2$ (min^{-1})	$r = k^{D}_{cat}/\lambda^{D}_{E_{ox(max)}}$	k^{D}_{cat} (min^{-1})	K^{D}_{m} (mM)	$K^{O_2}_{m}$ (μM)	δ_3 (p.p.m.)	δ_4 (p.p.m.)
L-dopa	13.3 ± 0.6	46133 ± 2306	6156 ± 1152	0.55 ± 0.08	4.46 ± 0.89	146.92	146.06
D-dopa	12.9 ± 0.9	44895 ± 2573	5910 ± 1014	3.98 ± 0.57	4.28 ± 0.86	146.92	146.06

Author's personal copy

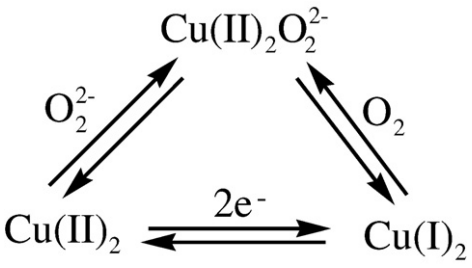

Scheme II. Equilibrium between E_{ox}, E_m and E_d forms of tyrosinase.

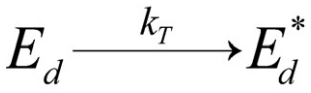

Scheme III. Kinetic mechanism of the transition of E_d to E_d^*.

3.1.2.1.2. E_d inactivation by L-dopa and D-dopa. The form E_d generated from E_{ox} under the nitrogen stream was made to react rapidly with different concentrations of L-dopa. The results (Fig. 6A) can be explained kinetically by Scheme V and, structurally, by a Scheme similar to Scheme IISM, although the distance between the coppers in E_d may be smaller, as occurs in [45]. Once again, monoexponential behaviour was observed, which can be fitted to Eq. (1SM), which is similar to Eq. (7), but for E_d , while the inactivation constant values better fit an equation similar to Eq. (8), but for E_d [Eq. (2SM)].

A fit, by non-linear regression, of the values of $\lambda_{E_d}^{D(L)}$ to Eq. (2SM), Fig. 6A Inset, gives $k_{i_{D(L)}}$ and $K_{E_d}^{D(L)}$ (Table 2). When the same experiments are carried out with D-dopa, Fig. 6B and B Inset, the values shown in Table 2 are obtained for $k_{i_{D(D)}}$ and $K_{E_d}^{D(D)}$.

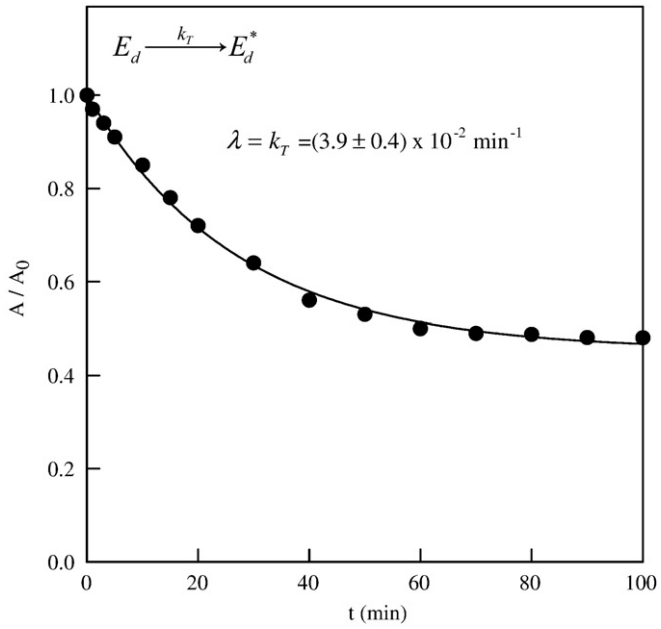

Fig. 4. Kinetic study of the transition of E_d to E_d^*. The enzyme form E_d was generated by passing a stream of nitrogen through a preparation of E_{ox}, $[E]_0 = 0.1$ μM (see Materials and Methods sections) and $[H_2O_2]_0 = 2$ μM. Aliquots were taken at different times and enzymatic activity was detected with 1 mM L-dopa ($\lambda = 475$ nm). The values obtained were fitted by non-linear regression to Eq. (6).

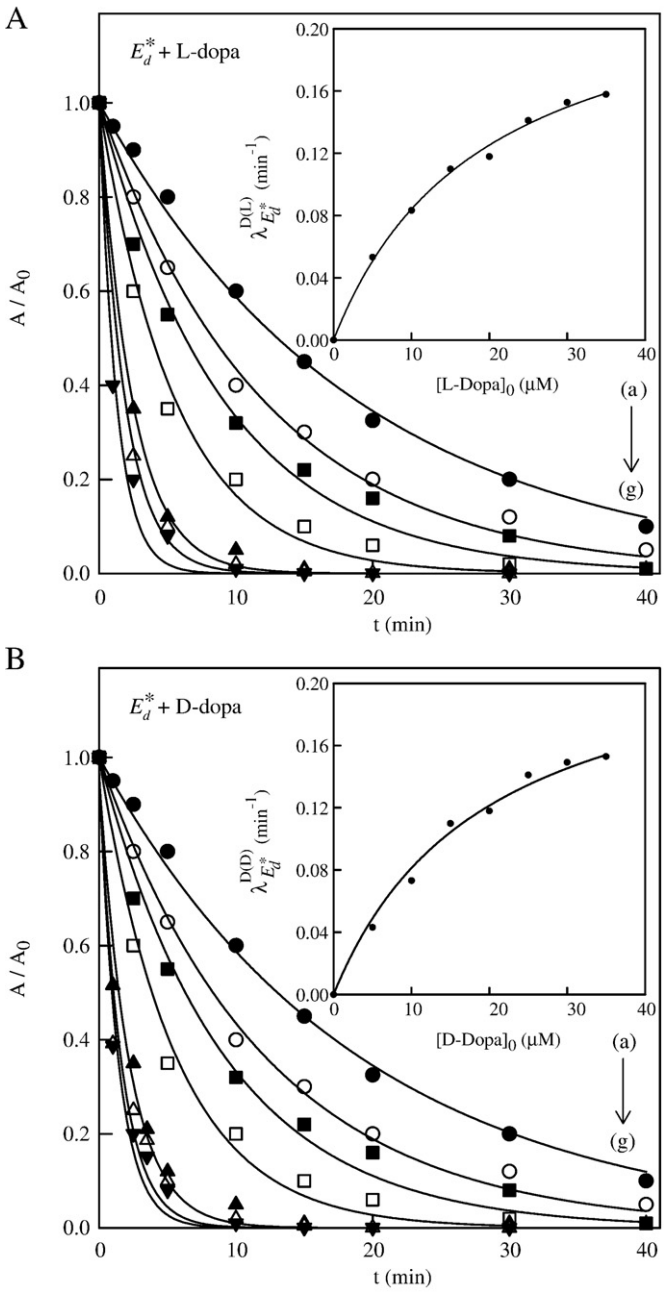

Fig. 5. Inactivation of the E_d^* form of tyrosinase by *o*-diphenols. The form E_d^* was obtained by allowing the form E_d obtained as described in Fig. 4 to evolve under anaerobic conditions for 90 min to obtain E_d^*. The *o*-diphenol was added at t = 0 and aliquots were taken at different times to measure the residual activity with 2.5 mM L-dopa ($\lambda = 475$ nm). The values obtained were fitted to Eq. (1SM) and the apparent inactivation constant was obtained at each substrate concentration. (A) L-dopa. The experimental conditions were: 30 mM sodium phosphate buffer (pH 6.0), 25 °C, $[E]_0 = 0.1$ μM (see Materials and Methods sections), $[H_2O_2]_0 = 2$ μM and L-dopa (μM): (a) 5 (●), (b) 10 (○), (c) 15 (■), (d) 20 (□), (e) 25 (▲), (f) 30 (△) and (g) 35 (▼). Inset. Representation of $\lambda_{E_d^*}^{D(L)}$ *vs.* $[L\text{-dopa}]_0$. (B) D-dopa. The experimental conditions were the same as in (A) but D-dopa (μM): (a) 5 (●), (b) 10 (○), (c) 15 (■), (d) 20 (□), (e) 25 (▲), (f) 30 (△) and (g) 35 (▼). Inset. Representation of $\lambda_{E_d^*}^{D(L)}$ *vs.* $[D\text{-dopa}]_0$.

3.1.2.1.3. E_m inactivation by L-dopa and D-dopa. E_m was generated from the native enzyme, as described in Materials and Methods sections [31]. Under anaerobic conditions, this form is stable, but in the presence of *o*-diphenols, it is inactivated, as described in kinetic form in Scheme VI and structurally in Scheme IIISM.

E_m was incubated with L-dopa and aliquots were taken at different times and revealed with L-dopa, the results being similar to those

Author's personal copy

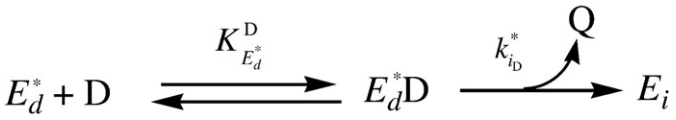

Scheme IV. Kinetic mechanism of E_d^* inactivation by *o*-diphenols.

obtained with the E_d. According to the mechanism described in Scheme VI, the enzyme E_m rapidly passes to E_d and is inactivated (Scheme VI and Scheme IIISM). The values of the constants are shown in Table 2.

4. Discussion

This study reveals that the physiological substrate of tyrosinase, L-dopa, and its iosomer, D-dopa, act as tyrosinase inactivators both in aerobic and anaerobic conditions. Under aerobic conditions, L- or D-dopa act as a suicide substrate of the enzyme basically through the enzymatic species E_{ox} and, under anaerobic conditions, they act as irreversible inactivators of the enzyme in the enzymatic species E_m, E_d and E_d^*.

4.1. Aerobic conditions: suicide inactivation

Kinetic characterisation of an enzyme acting on a suicide substrate is determined from *r* (partition ratio), λ (apparent constant of suicide inactivation) and K_m (Michaelis constant). In the action of tyrosinase on L- or D-dopa these parameters are determined according to Eqs. (4) and (5).

From an analysis of the data shown in Fig. 2A Inset and B Inset and, according to Eq. (5), r_D can be determined, giving practically the same value for the two isomers (Table 1). From Eq. (5) and taking into account that $k_{cat}^{D(D)} \approx k_{cat}^{D(L)}$ [23], it is deduced that the inactivation constant is approximately equal in both isomers (Table 1).

When the effect of substrate concentration is studied by analysing the results shown in Fig. 3A and B, the corresponding apparent inactivation constants ($\lambda_{E_{ox}}^{D(L\text{ or }D)}$) are obtained, and their analysis according to Eq. (4) (Fig. 3A Inset and B Inset) enables us to obtain $\lambda_{E_{ox(max)}}^{D}$ and K_m^D (Table 1). Note that the values of $\lambda_{E_{ox(max)}}^{D}$ are practically the same for L and D. However, $K_m^{D(L)} < K_m^{D(D)}$, thus, the enzyme shows stereospecificity in its substrate binding. These results agree with the values of k_{cat}^D obtained from a study of the steady state, $k_{cat}^{D(D)} \cong k_{cat}^{D(L)}$ [23], since these values and those of $\lambda_{E_{ox(max)}}^{D}$ are related with the strength of the nucleophilic attack of the oxygens of the hydroxyls of C-3 and C-4, which, in turn, depends on δ_3 and δ_4 (Table 1).

The inactivation mechanism described here agree with the experimental result obtained by other authors [27], regarding to the loss of a 50% of copper during the oxidation of catechol, and with others [26] regarding to the impossibility of inactive enzyme reactivation after Cu^{2+} addition, perhaps indicating the need for a "caddie" protein [29].

Table 2
Kinetic constants which characterize the inactivation of E_d, E_m and E_d^* by the dopa isomers.

Enzymatic form	Substrate	$K_E^{D(a)}$ (μM)	$k_{i_D} \times 10^3$ (min^{-1})	$k^*_{i_D} \times 10^3$ (min^{-1})
E_d^*	L-dopa	19.24 ± 2.12	–	0.25 ± 0.01
	D-dopa	28.88 ± 2.93	–	0.26 ± 0.02
E_d	L-dopa	10.77 ± 1.12	0.37 ± 0.01	–
	D-dopa	25.34 ± 2.24	0.37 ± 0.03	–
E_m	L-dopa	10.77 ± 1.12	0.37 ± 0.01	–
	D-dopa	25.34 ± 2.24	0.37 ± 0.03	–

(a) In K_E^D, *E* corresponds to the enzymatic forms E_d^* or E_d. When the reaction is begun with E_m, the data obtained correspond to E_d, because of the rapid transformation of E_m into E_d (Scheme VI).

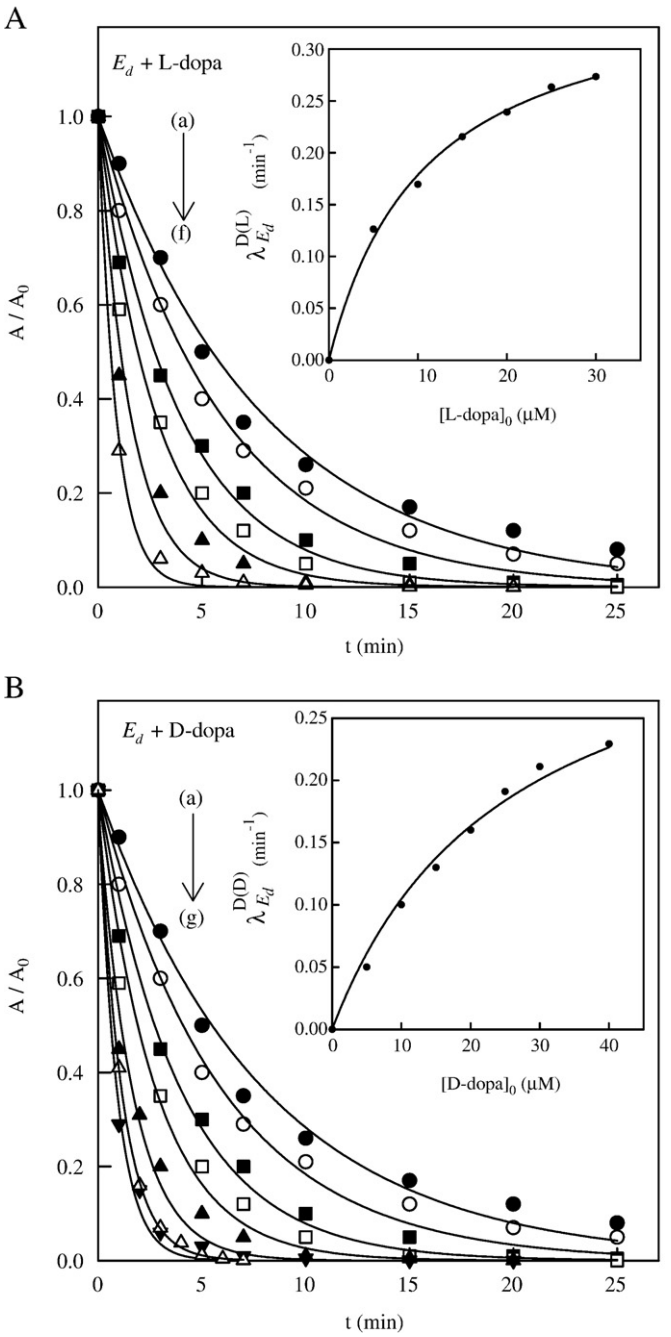

Fig. 6. Inactivation of the E_d form of tyrosinase by *o*-diphenols. The form E_d was obtained as is described in Fig. 4 and immediately incubated with *o*-diphenol, taking aliquots at different times to measure the residual activity with 2.5 mM L-dopa (λ = 475 nm). The values obtained were fitted to Eq. (2SM) and the apparent inactivation constant was obtained at each concentration of *o*-diphenol. (A) L-dopa. The experimental conditions were: 30 mM sodium phosphate buffer (pH 6.0), 25 °C, $[E]_0 = 0.1$ μM (see Materials and Methods sections), $[H_2O_2]_0 = 2$ μM and L-dopa (μM): (a) 5 (●), (b) 10 (○), (c) 15 (■), (d) 20 (□), (e) 25 (▲) and (f) 30 (△). Inset. Representation of $\lambda_{E_d}^{D(L)}$ *vs.* $[L\text{-dopa}]_0$. (B) D-dopa. The experimental conditions were the same as in (A) but D-dopa (μM): (a) 5 (●), (b) 10 (○), (c) 15 (■), (d) 20 (□), (e) 25 (▲), (f) 30 (△) and (g) 40 (▼). Inset. Representation of $\lambda_{E_d}^{D(L)}$ *vs.* $[D\text{-dopa}]_0$. In the case of E_m, the same procedure was followed as with E_d.

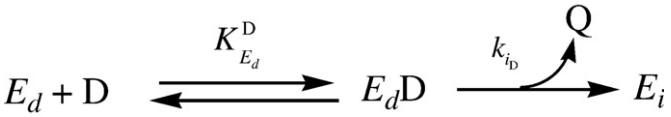

Scheme V. Kinetic mechanism of E_d inactivation by *o*-diphenols.

Author's personal copy

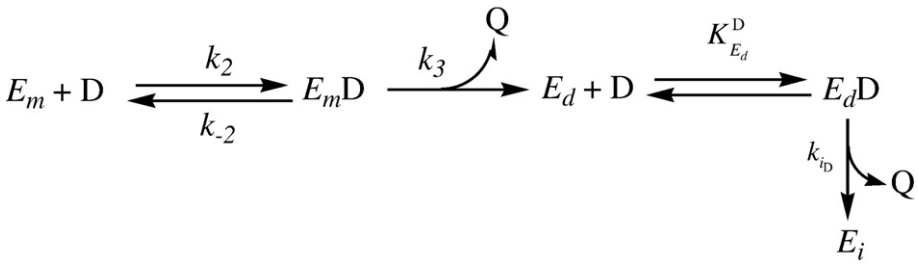

Scheme VI. Kinetic mechanism of E_m inactivation by *o*-diphenols.

On the other hand, the physiological implication of the suicide inactivation of tyrosinase by its physiological substrate (L-dopa) is not still clear, although it would result in a stop of action of the enzyme, since the products of its reaction are highly cytotoxic for the cell [46,47].

4.2. Inactivation of deoxy-tyrosinase by o-diphenols

The inactivation of E_d^*, E_d and E_m was studied in anaerobic conditions.

4.2.1. E_d^* inactivation by L-dopa and D-dopa

Analysis of the data of Fig. 5A and B according to Eq. (7) provides the apparent inactivation constant of E_d^* and its analysis according to Eq. (8) provides the values of k_i^* and $K_{E_d^*}$. The values of $k^*_{i_{D(L)}}$ and $k^*_{i_{D(D)}}$ are approximately equal (Table 2), which agrees with the values of δ_3 and δ_4 of the isomers (Table 1). However, the values of $K^{D(L)}_{E_d^*}$ and $K^{D(D)}_{E_d^*}$ are not the same (Table 2), ($K^{D(L)}_{E_d^*} < K^{D(D)}_{E_d^*}$), which indicates that this enzymatic form has more affinity for the L isomers.

4.2.2. E_d inactivation by L-dopa and D-dopa

When we study the inactivation of E_d by L- or D-dopa, analysis of the data in Fig. 6A and B according to Eq. (1SM) provides the apparent inactivation constant, and its analysis according to Eq. (2SM) gives the values k_i and K_{E_d}. The values of $k_{i_{D(L)}}$ and $k_{i_{D(D)}}$ are, approximately, equal (Table 2), since these values are directly related with the values of δ_3 and δ_4 of both isomers, which are equal (Table 1). However, $K^{D(L)}_{E_d} < K^{D}_{E_d}{}^{(D)}$, which demonstrates the stereospecificity of the substrate binding. Furthermore, the values of $k_{i_{D(L)}}$ and $k_{i_{D(D)}}$ are greater than those of $k^*_{i_{D(L)}}$ and $k^*_{i_{D(D)}}$, respectively (Table 2), indicating that the structure of the enzyme in the form E_d^* transforms the substrate less efficiently than the form E_d, perhaps because the Cu^+ atoms in E_d^* are more separated [44]. As regards the affinity of these forms for the substrates, the E_d form shows greater affinity (lower $K^{D(L)}_{E_d}$ and $K^{D(D)}_{E_d}$) than E_d^* (Table 2).

4.3. E_m inactivation by L- or D-dopa

When the inactivation of E_m by L- or D-dopa is studied, the results are similar to those obtained in the study of the inactivation of E_d and E_d^* by the same *o*-diphenols. According to the kinetic mechanism described in Scheme VI and the structural mechanism described in Scheme IIISM, the enzyme E_m rapidly passes to E_d and is inactivated (Scheme VI and Scheme IIISM). The values of the constants are shown in Table 2.

4.4. Oxygen protects against the inactivation of tyrosinase

From the results obtained in this study and, especially, taking into account the inactivation processes, suicide inactivation (under aerobic conditions) occurs through E_{ox} and irreversible inactivation (under anaerobic conditions) occurs through E_m, E_d and E_d^*, both with *o*-diphenols. It is clear that the oxygen protects the enzyme from inactivation, since the value of $\lambda^D_{E_{ox(max)}}$ (maximum apparent inactivation constant) in suicide inactivation (Table 1) is lower than the inactivation constants of *Em*, *Ed* and E_d^* under anaerobic conditions (Table 2). This observation may have industrial applications since a nitrogen stream passed quickly through a solution of a fruit extract would prevent the enzyme from acting, the presence of *o*-diphenols provoking its inactivation. In this way, browning would be avoided. Besides, irreversible inactivation has the advantage over suicide inactivation because there is no turnover, so the product would be stoichiometric with the enzyme.

4.5. Conclusions

From a kinetic study of the inactivation of tyrosinase in the different forms involved in the catalytic cycle, E_{ox} (aerobic conditions), *Em*, *Ed* and E_d^* (anaerobic conditions), it can be deduced that the enzyme shows stereospecificity in the binding of isomers but not in catalysis or inactivation, since both processes are related with the nucleophilic power of the oxygens of the hydroxyls in C-3 and C-4 of the benzene ring. *o*-Diphenols inactivate the enzyme both under aerobic conditions (suicide inactivation through the form E_{ox}) and under anaerobic conditions (irreversible inactivation through the forms E_m, E_d and E_d^*).

Acknowledgements

This paper was partially supported by grants from the Ministerio de Educación y Ciencia (Madrid, Spain) Project BIO2006-15363 and, from the Fundación Séneca (CARM, Murcia, Spain) Projects 08856/PI/08 and 08595/PI/08, from the Consejería de Educación (CARM, Murcia, Spain) BIO-BMC 06/01-0004 and from FISCAM PI-2007/53 from the Consejería de Salud y Bienestar Social de la Junta de Comunidades de Castilla La Mancha. JLMM has a fellowship from the Ministerio de Educación y Ciencia (Madrid, Spain) Reference AP2005-4721. FGM has a fellowship from Fundación Caja Murcia (Murcia, Spain).

Appendix A. Supplementary data

Supplementary data associated with this article can be found, in the online version, at doi:10.1016/j.bbapap.2010.02.015.

References

[1] A. Sanchez-Ferrer, J.N. Rodriguez-Lopez, F. Garcia-Canovas, F. Garcia-Carmona, Tyrosinase: a comprehensive review of its mechanism, Biochim. Biophys. Acta 1247 (1995) 1–11.
[2] S. Halaouli, M. Asther, J.C. Sigoillot, M. Hamdi, A. Lomascolo, Fungal tyrosinases: new prospects in molecular characteristics, bioengineering and biotechnological applications, J. Appl. Microbiol. 100 (2006) 219–232.
[3] L.L. Ingraham, J. Corse, B. Makower, Enzymatic browning of fruits. 3. Kinetics of the reaction inactivation of polyphenol oxidase, J. Am. Chem. Soc. 74 (1952) 2623–2626.
[4] Y. Tomita, A. Hariu, C. Mizuno, M. Seiji, Inactivation of tyrosinase by dopa, J. Invest. Dermatol. 75 (1980) 379–382.

Author's personal copy

[5] K. Lerch, Neurospora tyrosinase: structural, spectroscopic and catalytic properties, Mol. Cell. Biochem. 52 (1983) 125–138.
[6] J. Zhong, W.C. Groutas, Recent developments in the design of mechanism-based and alternate substrate inhibitors of serine proteases, Curr. Top. Med. Chem. 4 (2004) 1203–1216.
[7] F. Ghanbari, K. Rowland-Yeo, J.C. Bloomer, S.E. Clarke, M.S. Lennard, G. Tucker, A. Rostami-Hodjegan, A critical evaluation of the experimental design of studies of mechanism based enzyme inhibition, with implications for in vitro–in vivo extrapolation, Curr. Drug Metab. 7 (2006) 315–334.
[8] R.B. Silverman, Mechanism-based enzyme inactivators, Meth. Enzymol. 249 (1995) 240–283.
[9] S.G. Waley, Kinetics of suicide substrates, Biochem. J. 185 (1980) 771–773.
[10] J. Tudela, F. Garcia Canovas, R. Varon, F. Garcia Carmona, J. Galvez, J.A. Lozano, Transient-phase kinetics of enzyme inactivation induced by suicide substrates, Biochim. Biophys. Acta 912 (1987) 408–416.
[11] M.A. Moruno-Davila, C. Garrido-del Solo, M. Garcia-Moreno, B.H. Havsteen, F. Garcia-Sevilla, F. Garcia-Canovas, R. Varon, Kinetic analysis of enzyme systems with suicide substrate in the presence of a reversible competitive inhibitor, tested by simulator progress curves, Int. J. Biochem. Cell Biol. 33 (2001) 181–191.
[12] F. Garcia-Canovas, J. Tudela, C. Martinez-Madrid, R. Varon, F. Garcia-Carmona, J.A. Lozano, Kinetic study on the suicide inactivation of tyrosinase induced by catechol, Biochim. Biophys. Acta 912 (1987) 417–423.
[13] J. Tudela, F. Garcia-Canovas, R. Varon, M. Jimenez, F. Garcia-Carmona, J.A. Lozano, Kinetic characterization of dopamine as a suicide substrate of tyrosinase, J. Enzyme Inhib. 2 (1987) 47–56.
[14] J. Tudela, F. Garcia-Canovas, R. Varon, M. Jimenez, F. Garcia-Carmona, J.A. Lozano, Kinetic study in the transient phase of the suicide inactivation of frog epidermis tyrosinase, Biophys. Chem. 30 (1988) 303–310.
[15] M. Garcia-Moreno, R. Varon, A. Sanchez-Gracia, J. Tudela, F. Garcia-Canovas, The effect of pH on the suicide inactivation of frog epidermis tyrosinase, Biochim. Biophys. Acta 1205 (1994) 282–288.
[16] M.B. Arnao, M. Acosta, J.A. del Rio, R. Varon, F. Garcia-Canovas, A kinetic-study on the suicide inactivation of peroxidase by hydrogen-peroxide, Biochim. Biophys. Acta 1041 (1990) 43–47.
[17] A.N. Hiner, J. Hernandez-Ruiz, M.B. Arnao, F. Garcia-Canovas, M. Acosta, A comparative study of the purity, enzyme activity, and inactivation by hydrogen peroxide of commercially available horseradish peroxidase isoenzymes A and C, Biotechnol. Bioeng. 50 (1996) 655–662.
[18] J. Escribano, J. Tudela, F. Garcia-Carmona, F. Garcia-Canovas, A kinetic-study of the suicide inactivation of an enzyme measured through coupling reactions: application to the suicide inactivation of tyrosinase, Biochem. J. 262 (1989) 597–603.
[19] F. Garcia-Canovas, J. Tudela, R. Varon, A.M. Vazquez, Experimental methods for kinetic study of suicide substrates, J. Enzyme Inhib. 3 (1989) 81–90.
[20] A.J. Winder, H. Harris, New assays for the tyrosine hydroxilase and dopa oxidase activities of tyrosinase, Eur. J. Biochem. 198 (1991) 317–326.
[21] D.E. Wilcox, A.G. Porras, Y.T. Hwang, K. Lerch, M.E. Winkler, E.I. Solomon, Substrate analog binding to the coupled binuclear copper active site in tyrosinase, J. Am. Chem. Soc. 107 (1985) 4015–4027.
[22] V. Kahn, S.H. Pomerantz, Monophenolase activity of avocado polyphenol oxidase, Phytochemistry 19 (1980) 379–385.
[23] J.C. Espin, P.A. Garcia-Ruiz, J. Tudela, F. Garcia-Canovas, Study of the stereospecificity in mushroom tyrosinase, Biochem. J. 331 (1998) 547–551.
[24] J.C. Espin, P.A. Garcia-Ruiz, J. Tudela, F. Garcia-Canovas, Study of stereospecificity in pear and strawberry polyphenol oxidase, J. Agric. Food Chem. 46 (1998) 2469–2473.
[25] M.E. Marin-Zamora, F. Rojas-Melgarejo, F. Garcia-Canovas, P.A. Garcia-Ruiz, Stereospecificity of mushroom tyrosinase immobilized on a chiral and a nonchiral support, J. Agric. Food Chem. 55 (2007) 4569–4575.
[26] E.J. Land, C.A. Ramsden, P.A. Riley, The mechanism of suicide-inactivation of tyrosinase: a substrate structure investigation, Tohoku J. Exp. Med. 212 (2007) 341–348.
[27] C. Dietler, K. Lerch, Reaction inactivation of tyrosinase, in: T.E. King, H.S. Mason, M. Morrison (Eds.), Oxidases and Related Redox Systems, Pergamon Press, NY, 1982, pp. 305–317.
[28] J.L. Muñoz-Muñoz, F. Garcia-Molina, P.A. Garcia-Ruiz, M. Molina-Alarcon, J. Tudela, F. Garcia-Canovas, J.N. Rodriguez-Lopez, Phenolic substrates and suicide inactivation of tyrosinase: kinetics and mechanism, Biochem. J. 416 (2008) 413–440.
[29] Y. Matoba, T. Kumagai, A. Yamamoto, H. Yoshitsu, M. Sugiyama, Crystallographic evidence that the dinuclear copper center of tyrosinase is flexible during catalysis, J. Biol. Chem. 281 (2006) 8981–8990.
[30] L.G. Fenoll, M.J. Peñalver, J.N. Rodriguez-Lopez, P.A. Garcia-Ruiz, F. Garcia-Canovas, J. Tudela, Deuterium isotope effect on the oxidation of monophenols and *o*-diphenols by tyrosinase, Biochem. J. 380 (2004) 643–650.
[31] J.L. Munoz-Munoz, F. Garcia-Molina, P.A. Garcia-Ruiz, R. Varon, J. Tudela, F. Garcia-Canovas, J.N. Rodriguez-Lopez, Stereospecific inactivation of tyrosinase by L- and D-ascorbic acid, Biochim. Biophys. Acta 1794 (2009) 244–253.
[32] J.N. Rodriguez-Lopez, L.G. Fenoll, P.A. Garcia-Ruiz, R. Varon, J. Tudela, R.N. Thorneley, F. Garcia-Canovas, Stopped-flow and steady-state study of the diphenolase activity of mushroom tyrosinase, Biochemistry 39 (2000) 10497–10506.
[33] O.H. Lowry, N.J. Rosebrough, A.L. Farr, R.J. Randall, Protein measurement with the Folin phenol reagent, J. Biol. Chem. 193 (1951) 265–275.
[34] F. Garcia-Carmona, F. Garcia-Canovas, J.L. Iborra, J.A. Lozano, Kinetic study of the pathway of melanization between L-dopa and dopachrome, Biochim. Biophys. Acta 717 (1982) 124–131.
[35] F. Garcia-Canovas, F. Garcia-Carmona, J. Vera-Sanchez, J.L. Iborra-Pastor, J.A. Lozano-Teruel, The role of pH in the melanin biosynthesis pathway, J. Biol. Chem. 257 (1982) 8738–8744.
[36] F. Garcia-Molina, J.L. Muñoz, R. Varon, J.N. Rodriguez-Lopez, F. Garcia-Canovas, J. Tudela, A review on spectrophotometric methods for measuring the monophenolase and diphenolase activities of tyrosinase, J. Agric. Food Chem. 55 (2007) 9739–9749.
[37] Jandel scientific. Sigma Plot 9.0 for Windows™; Jandel scientific: Core Madera 2006.
[38] R.L. Jolley Jr., L.H. Evans, N. Makino, H.S. Mason, Oxytyrosinase, J. Biol. Chem. 249 (1974) 335–345.
[39] M. Jackman, M. Huber, A. Hajnal, K. Lerch, Stabilization of the oxy form of tyrosinase by a single conservative amino acid substitution, Biochem. J. 282 (1992) 915–918.
[40] M. Beltramini, K. Lerch, Fluorescence properties of Neurospora tyrosinase, Biochem. J. 205 (1982) 173–180.
[41] J. Deinum, K. Lerch, B. Reinhammar, An EPR study of Neurospora tyrosinase, FEBS Lett. 69 (1976) 161–164.
[42] R. Aasa, J. Deinum, K. Lerch, B. Reinhammar, The reaction of mercaptans with tyrosinases and hemocyanins, Biochim. Biophys. Acta 535 (1978) 287–298.
[43] L.G. Fenoll, J.N. Rodriguez-Lopez, F. Garcia-Molina, F. Garcia-Canovas, J. Tudela, Michaelis constants of mushroom tyrosinase with respect to oxygen in the presence of monophenols and diphenols, Int. J. Biochem. Cell Biol. 34 (2002) 332–336.
[44] J.L. Munoz-Munoz, F. Garcia-Molina, P.A. Garcia-Ruiz, R. Varon, J. Tudela, F. Garcia-Canovas, J.N. Rodríguez-Lopez, Some kinetic properties of deoxytyrosinase, J. Mol. Cat. B: Enzymatic 62 (2010) 173–182.
[45] M. Metz, E.I. Solomon, Dioxygen binding to deoxyhemocyanin: electronic structure and mechanism of the spin-forbidden two-electron reduction of O_2, J. Am. Chem. Soc. 123 (2001) 4938–4950.
[46] K. Urabe, P. Aroca, K. Tsukamoto, D. Mascagna, A. Palumbo, G. Prota, V. Hearing, The inherent toxicity of melanin precursors: a revision, Biochim. Biophys. Acta 1221 (1994) 272–278.
[47] J.L. Munoz-Munoz, F. Garcia-Molina, R. Varon, J. Tudela, F. Garcia-Canovas, J.N. Rodriguez-Lopez, Generation of hydrogen peroxide in the melanin biosynthesis pathway, Biochim. Biophys. Acta 1794 (2009) 1017–1029.

Supplementary Material

Kinetic analysis:

The experimental data of the E_d inactivation by L- and D-dopa follow monoexponential behavior and can be fitted to Eq. (1SM):

$$[E_d] = [E_d]_0 \, e^{-\lambda_{E_d}^{\mathrm{D(L)}} t} \qquad \text{(1SM)}$$

where

$$\lambda_{E_d}^{\mathrm{D(L)}} = \frac{k_{i_{\mathrm{D(L)}}}[\mathrm{D}]_0}{K_{E_d}^{\mathrm{D(L)}} + [\mathrm{D}]_0} \qquad \text{(2SM)}$$

Legends to Schemes:

Scheme ISM. Structural mechanism proposed to explain the diphenolase activity and the suicide inactivation of tyrosinase acting on dopa enantiomers. E_m, *met*-tyrosinase; E_d, *deoxy*-tyrosinase; E_{ox}, *oxy*-tyrosinase; $E_{ox}\mathrm{D}$, *oxy*-tyrosinase/*o*-diphenol complex; $(E_{ox}\text{-D})_1$, *oxy*-tyrosinase/*o*-diphenol complex axially bound to a Cu atom; $(E_{ox}\text{-D})_2$, *oxy*-tyrosinase/*o*-diphenol complex axially bound to the two Cu atoms; $(E_{ox}\text{-D})_3$, *oxy*-tyrosinase/*o*-diphenol complex axially bound to one Cu atom and the deprotonated hydroxyl group of C-3; $E_m\mathrm{D}$, *met*-tyrosinase/*o*-diphenol complex; $(E_m\text{-D})_1$, *met*-tyrosinase/*o*-diphenol complex axially bound to a Cu atom; $(E_m\text{-D})_2$, *met*-tyrosinase/*o*-diphenol complex axially bound to the two Cu atoms.

R = $-CH_2-CH-(NH_3^+)-COO^-$

Scheme IISM. Structural mechanism of E_d^* inactivation by *o*-diphenols.

Scheme IIISM. Structural mechanism of E_m inactivation by *o*-diphenols.

Schemes:

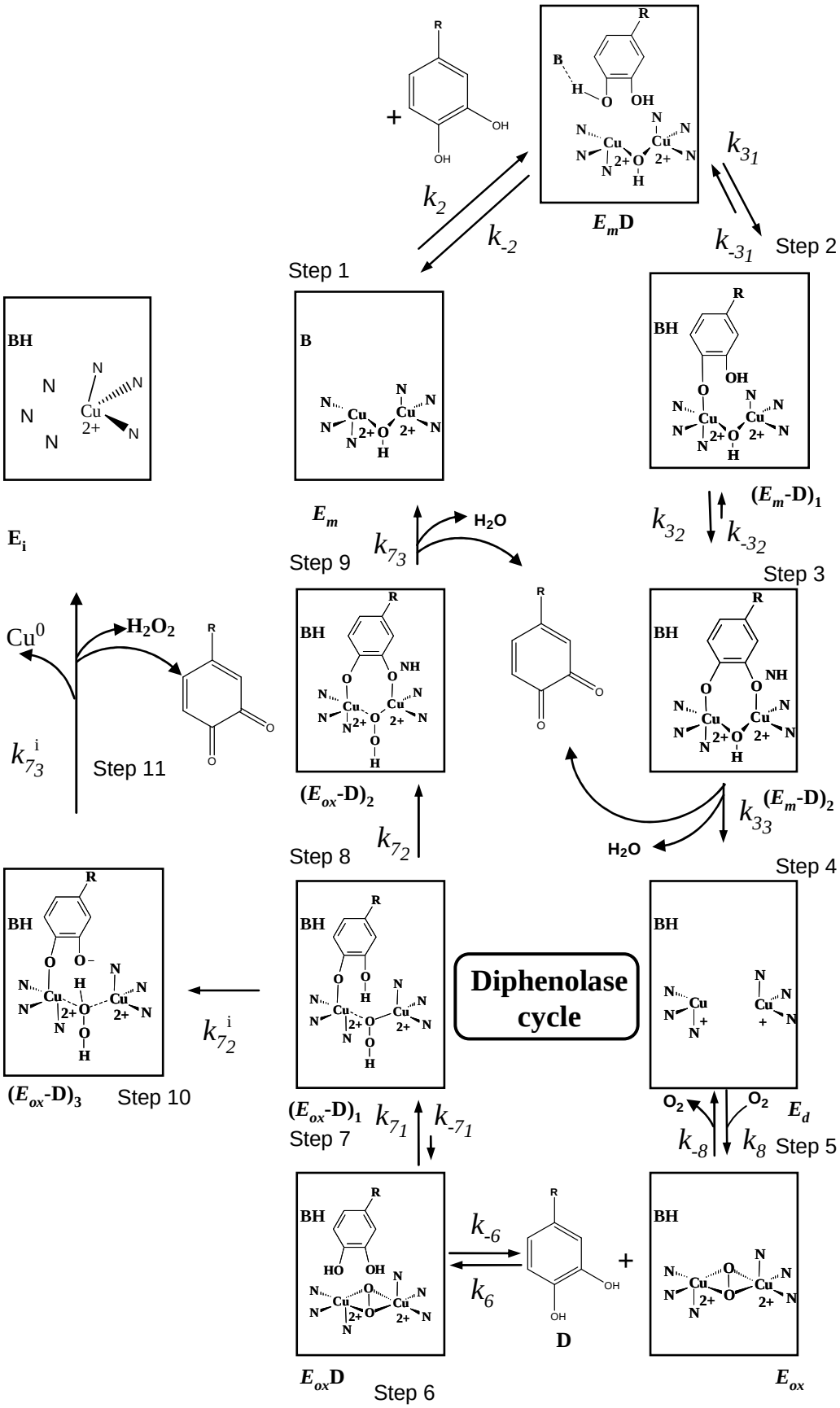

-Scheme ISM-

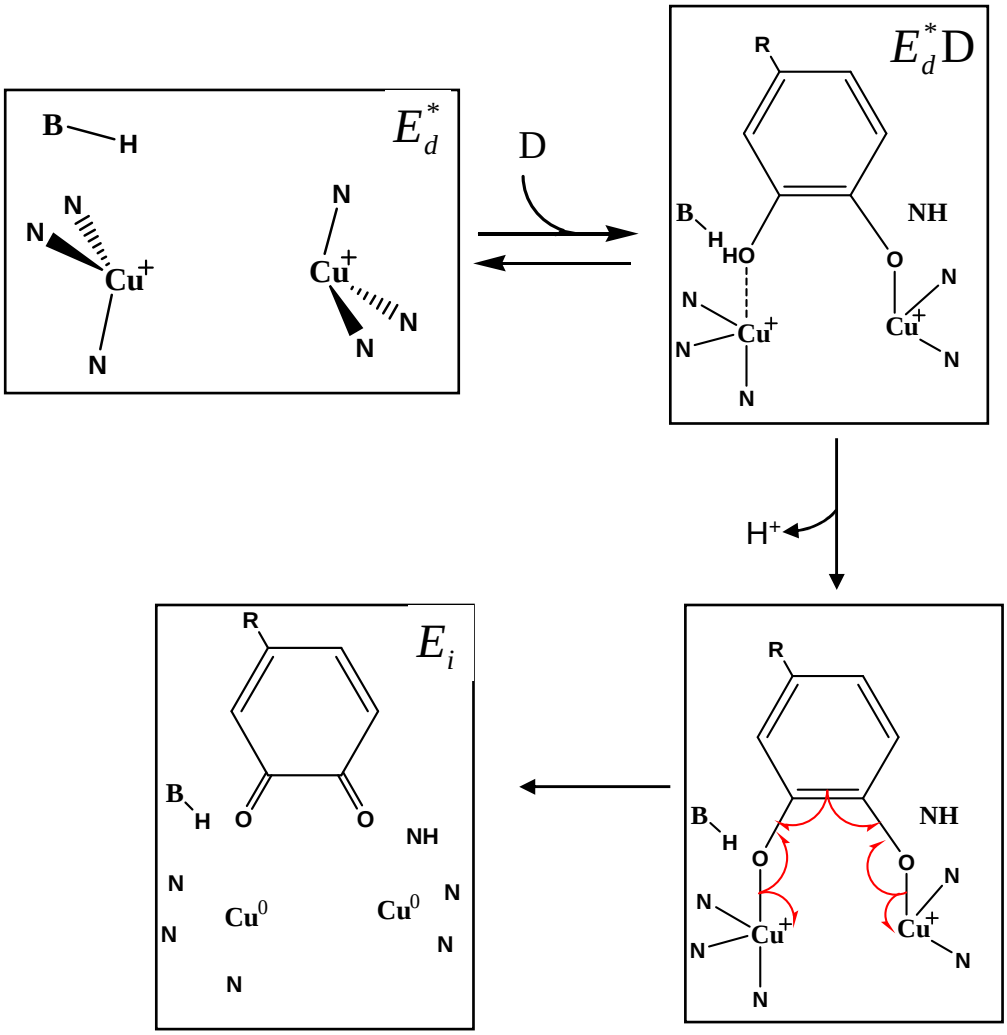

-Scheme IISM-

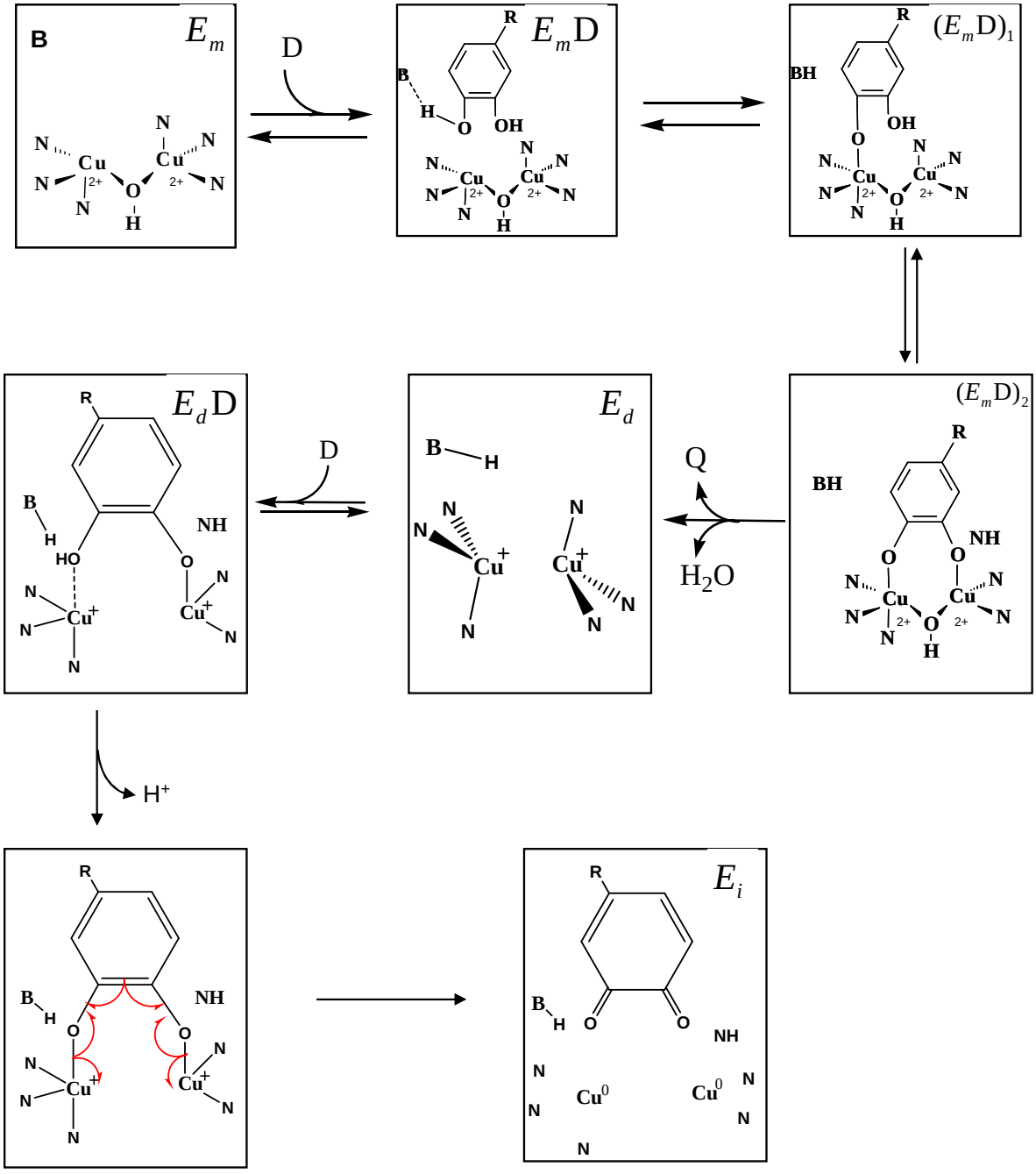

-Scheme IIISM-

4.17. INACTIVACIÓN INDIRECTA DE TIROSINASA EN SU ACCIÓN SOBRE TIROSINA.

El estudio de la inactivación indirecta de tirosinasa en su acción sobre tirosina ha dado lugar a la siguiente publicación adjunta.

4.17.1. Título

Indirect inactivation of tyrosinase in its action on tyrosine.

4.17.2. Autores

Muñoz-Muñoz, J.L.; Garcia-Molina, F.; Acosta-Motos, J.R.; Arribas, E.; Garcia-Ruiz, P.A.; Tudela, J.; Garcia-Cánovas, F. y Rodríguez-López, J.N.

4.17.3. Referencia

Acta Biochimica Polonica (2011) 58, 477-488.

4.17.4. Resumen

Bajo condiciones aerobias, tirosinasa se inactiva por dopa como consecuencia de una inactivación suicida y, bajo condiciones anaerobias, como consecuencia de una inactivación irreversible. Sin embargo, tirosina protege a la enzima de su inactivación por dopa bajo condiciones anaerobias. Este trabajo describe como, bajo condiciones aerobias, la enzima no es inactivada directamente cuando actúa sobre tirosina pero sí sufre un proceso de inactivación suicida indirecta provocado por la reacción con el *o*-difenol originado de la evolución de la *o*-dopaquinona y acumulado en el medio de reacción.

ACTA ABP BIOCHIMICA POLONICA

Vol. 58, No 4/2011
477–488
on-line at: www.actabp.pl

Regular paper

Indirect inactivation of tyrosinase in its action on tyrosine

Jose Luis Muñoz-Muñoz[1], Francisco Garcia-Molina[1], Jose Ramon Acosta-Motos[1], Enrique Arribas[2], Pedro Antonio Garcia-Ruíz[3], Jose Tudela[1], Francisco Garcia-Cánovas[1]✉ and Jose Neptuno Rodríguez-López[1]

[1]GENZ: Grupo de Investigación Enzimología, Departamento de Bioquímica y Biología Molecular-A, Facultad de Biología, Universidad de Murcia, Espinardo, Murcia, Spain; [2]Departamento de Física Aplicada, Escuela Politécnica Superior de Albacete, Universidad de Castilla la Mancha, Albacete, Spain; [3]QCBA: Grupo de Química de Carbohidratos y Biotecnología de Alimentos, Departamento de Química Orgánica, Facultad de Química, Universidad de Murcia, Espinardo, Murcia, Spain

Under aerobic conditions, tyrosinase is inactivated by dopa as a result of suicide inactivation, and, under anaerobic conditions, as a result of irreversible inactivation. However, tyrosine protects the enzyme from being inactivated by dopa under anaerobic conditions. This paper describes how under aerobic conditions the enzyme acting on tyrosine is not directly inactivated but undergoes a process of indirect suicide inactivation provoked by reaction with the o-diphenol originated from the evolution of o-dopaquinone and accumulated in the reaction medium.

Keywords: *o*-diphenol, monophenol, inactivation, suicide, tyrosinase.

Received: 09 December, 2010; revised: 09 November, 2011; accepted: 02 December, 2011; available on-line: 20 December, 2011

INTRODUCTION

Tyrosinase is a widespread dinuclear copper enzyme present in microorganisms as well as in plants and mammals. It is able to catalyse the hydroxylation of monophenols to *o*-diphenols and the oxidation of the latter to *o*-quinones (Battaini *et al.*, 2002; Solomon *et al.*, 2006; Rolff *et al.*, 2011; Marino *et al.*, 2011). It has long been known that the enzyme is inactivated when it acts on *o*-diphenols (Nelson & Dawson, 1944; Asimov & Dawson, 1950; Ingraham *et al.*, 1952; Tomita & Seiji, 1977; Seiji *et al.*, 1978; Tomita *et al.*, 1980; Lerch, 1983).

In general, the kinetics of the suicide inactivation of tyrosinase in its action on *o*-diphenols has been studied extensively (Ingraham *et al.*, 1952; Dietler & Lerch, 1982;

✉e-mail address: canovasf@um.es

Abbreviations: For clarity and for the sake of brevity, we will use the following notations in the text.

Species and concentrations. $[E]_0$, initial concentration of tyrosinase; E_a, active enzyme; $[E_a]$, instantaneous concentration of E_a; $[E_m]$, instantaneous concentration of *met*-tyrosinase; $[E_m]_0$, initial concentration of *met*-tyrosinase; $[E_d]$, instantaneous concentration of *deoxy*-tyrosinase; $[E_d]_0$, initial concentration of *deoxy*-tyrosinase; E_d^*, *deoxy*-tyrosinase after of E_d to E_d^* transition; $[E_d^*]$, instantaneous concentration of E_d^*; $[E_d^*]_0$, initial concentration of E_d^*; E_i, inactive enzyme; $[E]_i$, instantaneous concentration of E_i ; D, L- or D-*o*-diphenol (dopa); $[D]_0$, initial concentration of D; $[D]_{ss}$, *o*-diphenol concentration in the steady-state; Q, *o*-quinone product of the enzymatic reaction; $[Q]$, instantaneous concentration of Q; $[Q]_\infty$, *o*-quinone concentration at $t\rightarrow\infty$; $[NADH]_0$, initial concentration of NADH; [NADH], instantaneous concentration of NADH; $[NADH]_f$, NADH concentration at $t\rightarrow\infty$; $[NADH]_\infty$, NADH consumed at the end of the reaction, $t\rightarrow\infty$, i.e. $[NADH]_\infty = [NADH]_0-[NADH]_f$; M, L- or D-monophenol (tyrosine); $[M]_0$, initial concentration of monophenol; $[M]_{ss}$, monophenol concentration in the steady-state; C, relationship between *o*-diphenol and monophenol concentrations in the steady-state, $C=[D]_{ss}/[M]_{ss}$; *DC*, dopachrome; [DC], instantaneous concentration of DC; $[DC]_\infty$, dopachrome concentration at $t\rightarrow\infty$; $[O_2]_0$, initial concentration of oxygen; $[O_2]$, instantaneous concentration of oxygen; $[O_2]_f$, oxygen concentration at $t\rightarrow\infty$; $[O_2]_\infty$, oxygen consumed at $t\rightarrow\infty$, i.e. $[O_2]_\infty = [O_2]_0 - [O_2]_f$; R, reductant; $[R]_0$, initial concentration of R; [R], instantaneous concentration of R; $[R]_f$, [R] concentration at $t\rightarrow\infty$; $[R]_\infty$, [R] concentration at $t\rightarrow\infty$, i.e. $[R]_\infty = [R]_0-[R]_f$.

Kinetic parameters. $V_0^{D(Q)}$, initial rate of tyrosinase acting on D, measuring Q; $V_0^{D(Q)}$, initial rate of tyrosinase acting on D, measuring DC; $V_0^{D(DC)} = 0.5\ V_0^{D(Q)}$; $V_0^{D(O_2)}$, initial rate of tyrosinase acting on D, measuring O_2 $V_0^{D(O_2)} = V_0^{D(DC)}$; $\lambda_{E_{ox}}^{M}$, apparent suicide inactivation constant of tyrosinase in the presence of monophenol; $\lambda_{E_{ox}(max)}^{M}$, maximum value of $\lambda_{E_{ox}}^{M}$ for saturating substrate; $\lambda_{E_d}^{D(L\text{ or }D)(M)}$, apparent constant of irreversible inhibition of E_d by L- or D-dopa, in the presence of the monophenol L- or D-tyrosine; $\lambda_{E_d^*}^{D(L\text{ or }D)(M)}$, apparent constant of irreversible inhibition of E_d^* by L- or D-dopa, in the presence of the monophenol L- or D-tyrosine; $k_{i_{D(L\text{ or }D)(M)}}$, maximum value of $\lambda_{E_d}^{D(L\text{ or }D)(M)}$ for saturating substrate; $k_{i^*_{D(L\text{ or }D)(M)}}$, maximum value of $\lambda_{E_d^*}^{D(L\text{ or }D)(M)}$ for saturating substrate; r_D^{DC} partition ratio for the diphenolase activity measuring DC; $r_D^{O_2}$, partition ratio for the diphenolase activity measuring O_2, $r_D^{NADH} = r_D^{DC} = r_D^{Q} = r_D^{O_2}$ with $[NADH]_\infty = 2[DC]_\infty = [Q]_\infty$ and $[DC]_\infty = [O_2]_\infty$; $r_M^{O_2}$ number of total turnovers (in both cycles, hydroxylase and oxidase) made by one molecule of enzyme acting on L-tyrosine before its suicide inactivation, measuring oxygen consumed; $r_{M(O)}^{O_2}$, number of turnovers in the oxidase cycle made by one molecule of enzyme acting on L-tyrosine before its suicide inactivation, measuring oxygen consumed; $r_{M(H)}^{O_2}$, number of turnovers in the hydroxylase cycle made by one molecule of enzyme acting on L-tyrosine before its suicide inactivation, measuring oxygen consumed; r_M^{DC}, number of total turnovers (in both cycles) made by one molecule of enzyme acting on L-tyrosine before its suicide inactivation, measuring dopachrome formed; $r_{M(O)}^{DC}$, number of turnovers in the oxidase cycle made by one molecule of enzyme acting on L-tyrosine before its suicide inactivation, measuring dopachrome formed; $r_{M(H)}^{DC}$, number of turnovers in the hydroxylase cycle made by one molecule of enzyme acting on L-tyrosine before its suicide inactivation, measuring the dopachrome formed; $K_m^{M(L\text{ or }D)}$, Michaelis constant of tyrosinase for L- or D-tyrosine; $K_{cat}^{M(L\text{ or }D)}$, catalytic constant of the monophenolase activity for L- or D-tyrosine; $K_{E_d^*}^{D(L)M(L\text{ or }D)}$, dissociation constant of the complex E_d^*D, where D is L-dopa, in the presence of the monophenol L- or D-tyrosine; $K_{E_d^*}^{M(L\text{ or }D)}$, dissociation constant of the complex E_d^*M, where M is L- or D-tyrosine; $K_{E_d}^{D(L)M(L\text{ or }D)}$, dissociation constant of the complex E_dD, where D is L-dopa in the presence of the monophenol L- or D-tyrosine; $K_{E_d}^{M(L\text{ or }D)}$, dissociation constant of the complex E_dM, where M is L- or D-tyrosine.

Waley, 1980; 1985; Garcia-Canovas *et al*., 1987; Tudela *et al*., 1987). These studies have enabled the critical parameters of the suicide inactivation of the enzyme to be determined: k_{cat}, the catalytic constant; K_m, the Michaelis constant; *r*, number of turnovers made by one mole of enzyme before its suicide inactivation and λ_{max} (maximum apparent inactivation constant).

The progress made in the study of the tyrosinase structure, with the crystallization of the enzyme from *Streptomyces castaneoglobisporus* (Matoba *et al*., 2006), *Bacillus megaterium* (Sendovski *et al*., 2010; 2011), and *Agaricus bisporus* (Ismaya *et al*., 2011) has provided better insight into the underlying mechanisms of the suicide inactivation of tyrosinase (Muñoz-Muñoz *et al*., 2008; 2010a; 2010b; Chazarra *et al*., 1997; Chang, 2007; 2009; 2010; Tai *et al*., 2009; Land *et al*., 2007; 2008; Ramsden *et al*., 2009; Ramsden & Riley, 2010a; 2010b).

The suicide inactivation of tyrosinase acting on L-tyrosine (as an example of monophenols) is difficult to study because the enzyme shows a lag period (Rodriguez-Lopez *et al*., 1992a; Molina *et al*., 2007). Furthermore, the enzyme transforms L-tyrosine into L-dopa and this, in turn, into *o*-dopaquinone, which evolves towards dopachrome and L-dopa (Cabanes *et al*., 1987). This series of chemical reactions leads to the accumulation of L-dopa in the medium and, in this way, tyrosinase reaches the steady state (Rodriguez-Lopez *et al*., 1992a and Ros *et al*., 1994). In this situation, tyrosinase carries out two turnovers in the monophenolase pathway but only one in the diphenolase pathway (Rodriguez-Lopez *et al*., 1992a).

Although the action mechanism of tyrosinase on L-tyrosine is complex (Sanchez-Ferrer *et al*., 1995), some important aspects are known about it; for example, for the oxidation to occur there must be an electrophilic attack on the benzene ring (Karlin *et al*., 1998; Itoh & Fukuzumi, 2007) and the substrate must be deprotonated before it can be oxidised (Casella *et al*., 1996; Monzani *et al*., 1998).

Two models, which share certain aspects and diverge considerably in others (Schemes I–III and IV), have been proposed to explain the suicide inactivation of tyrosinase in its action on *o*-diphenolic substrates (Land *et al*., 2007; Muñoz-Muñoz *et al*., 2008). In both cases, it is suggested that one of the copper atoms at the active centre is reduced to Cu^0 and is released, thus inactivating the enzyme (Dietler & Lerch, 1982). Other authors (Land *et al*., 2007) suggest (Scheme IV) that the enzyme hydroxylates the *o*-diphenols because it considers them as another form of monophenol. According to this model, a compound like pyrogallol (1,2,3-trihydroxybenzene) would not lead to suicide inactivation of the enzyme. In a previous work, our group showed that all *o*-diphenols and triphenols are suicide substrates of tyrosinase, the most potent being pyrogallol (Muñoz-Muñoz *et al*., 2008). The mechanism proposed in Schemes I–III covers the possibility of suicide inactivation during the oxidation of *o*-diphenols and triphenols like gallic acid or pyrogallol since it is the way in which one proton of the substrate is transferred to the active centre of the enzyme which triggers its suicide inactivation.

In the structural mechanism described in Scheme ISM (Supplementary Material), and in its kinetic form (Scheme I), we propose that the enzyme does not suffer inactivation in its hydroxylase activity, but that this inactivation occurs in its action on the diphenol accumulated in the reaction medium (Munoz-Munoz *et al*., 2008; 2010a; 2010b). Scheme ISM proposes the transfer of a proton from monophenols or diphenols to the peroxide of the oxy-tyrosinase form of the enzyme. Such a transfer step was previously proposed by Tyeklar and Karlin (1989) working with copper complexes and by Miller and Klinman (1985) to explain the action of dopamine β-hydroxylase. More recently, the transfer of a proton from the monophenol to the peroxide, which acts as a catalytic base, has been proposed (Matoba *et al*., 2006). The transfer of this critical proton to the oxy-tyrosinase form has been considered in studies on the isotopic effect as the slow step of the process both in *o*-diphenols and monophenols (Peñalver *et al*., 2003; Fenoll *et al*., 2004). There is controversy as to whether the initial step of the substrate oxidation occurs on the CuA (Decker *et al*., 2006) or CuB (Matoba *et al*., 2006). We suggest that in the case of *o*-diphenols it occurs in the second transfer of a proton to the hydroperoxide, when it forms H_2O_2, reducing the copper to Cu^0 and inactivating the enzyme (see Scheme ISM).

Taking into consideration the mechanisms proposed to explain this suicide inactivation (Land *et al*., 2007; Munoz-Munoz *et al*., 2008), the aim of the present study was to establish the criteria necessary to be able to discriminate between the two models (Scheme III, inactivation through the diphenolase activity and Scheme IV, inactivation through the monophenolase activity).

MATERIAL AND METHODS

Materials. Mushroom tyrosinase or polyphenol oxidase (Tyr; *o*-diphenol:O_2 oxidoreductase, EC 1.14.18.1) (8300 units/mg) and β-NADH were supplied by Sigma (Madrid, Spain). The enzyme was purified as previously described in (Rodriguez-Lopez *et al*., 2000). Protein concentration was determined by the Lowry method (Lowry *et al*., 1951). The substrates used, L-dopa, D-dopa, L-tyrosine and D-tyrosine were purchased from Sigma. All other chemicals were of analytical grade. Stock solutions of the diphenolic substrates were prepared in 0.15 mM phosphoric acid to prevent autooxidation. Milli-Q system (Millipore Corp.) ultrapure water was used throughout the experiments.

Spectrophotometric assays. Diphenolase activity. These assays were carried out with a Perkin-Elmer Lambda-35 spectrophotometer, interfaced to a PC-computer, where the kinetic data were recorded, stored and later analyzed. The product of the enzyme reaction, *o*-dopaquinone, is unstable and evolves towards dopachrome, which is not stable at long assay times (Garcia-Carmona *et al*., 1982; Garcia-Canovas *et al*., 1982). For this reason, the reaction was followed by measuring the disappearance of NADH at 340 nm, with ε=6230 $M^{-1}\cdot cm^{-1}$, which reduces *o*-dopaquinone to L-dopa (Garcia-Molina *et al*., 2007). The inactivation kinetics was studied in 30 mM sodium phosphate buffer (pH 6.0), since *o*-dopaquinone evolves rapidly to dopachrome at pH 7.0, while at lower pH the reaction slows down and *o*-dopaquinone is reduced by NADH (Garcia-Canovas *et al*., 1982).

Monophenolase activity. These assays were carried out with the same apparatus as used in the diphenolase activity assays. The reaction was followed by measuring dopachrome accumulation in the reaction medium at λ=475 nm (ε=3600 $M^{-1}\cdot cm^{-1}$) (Garcia-Molina *et al*., 2007). The inactivation kinetics was studied in 30 mM sodium phosphate buffer (pH 7.0). A given quantity of *o*-diphenol was always added at t=0, $C=[D]_{ss}/[M]_{ss}=0.046$,

so that the steady-state was reached immediately (Ros *et al.*, 1994).

Oxymetric assays. Measurements of dissolved oxygen concentration were made with a Hansatech (Kings Lynn, Cambs, UK) oxygraph unit controlled by a PC. The oxygraph used a Clark-type silver/platinum electrode with a 12.5 mm Teflon membrane. The sample was continuously stirred during experiments and its temperature was maintained at 25°C. The zero oxygen level for calibration and experiments was obtained by bubbling oxygen-free nitrogen through the sample for 10 min (Rodriguez-Lopez *et al.*, 1992b). The substrates L-tyrosine and D-tyrosine were studied by means of this method, adding (at t=0) the quantity of *o*-diphenol necessary for the steady-state to be attained immediately (Ros *et al.*, 1994).

Kinetic data analysis of monophenolase activity. The experimental recordings of oxygen consumption in the action of tyrosinase on monophenol fit Eqn. (1):

$$[O_2]=[O_2]_f+[O_2]_\infty e^{-\lambda^{M}_{E_{ox}} t} \quad (1)$$

whose parameters can be obtained by non-linear regression (Jandel, 2006). Thus, the experimental recordings obtained fit Eqn. (1), from which the corresponding inactivation parameters, $[O_2]_\infty$ and $\lambda^{M}_{E_{ox}}$, can be determined.

Simulation assays. The simulation reveals the kinetic behavior of the concentrations of the ligand and enzymatic species involved in the reaction mechanism here proposed for tyrosinase. The respective systems of differential equations have been solved numerically for particular sets of values of the rate constants and of initial concentrations of the reaction mechanism species. The numerical integration is based on the Runge–Kuta–Fehlberg algorithm, implemented on a PC-compatible computer program (WES) (Garcia-Sevilla *et al.*, 2000).

Simulated data of time based assays for the accumulation of dopachrome, or for the disappearance of the coupled reductant R, were fitted to Eqns. (2) and (3), respectively (see Supplementary material):

$$[DC]=[DC]_\infty(1-e^{-\lambda^{D\text{ or }M}_{E_{ox}} t}) \quad (2)$$

$$[R]=[R]_f+[R]_\infty e^{-\lambda^{D\text{ or }M}_{E_{ox}} t} \quad (3)$$

Generation of E_{ox} and E_d. To kinetically characterize the inactivation of the E_d form of tyrosinase, this enzymatic form was generated from the native enzyme by adding micromolar concentrations (2 μM) of H_2O_2, so that the E_m form passed to E_{ox}. Then, nitrogen was bubbled through the solution transforming all the E_{ox} to E_d ($E_{ox} \leftrightarrows E_d+O_2$) (Jolley *et al.*, 1974; Beltramini & Lerch, 1982; Jackman *et al.*, 1992; Munoz-Munoz *et al.*, 2009).

Generation of E_d. To kinetically characterize the inactivation of the E_d^* form of tyrosinase, this enzymatic form was generated from the E_d^* form and, maintaining anaerobic conditions, E_d^* was allowed to evolve slowly towards the enzymatic form that we denominate E_d^* (Munoz-Munoz *et al.*, 2010c).

Generation of E_m. The inactivation of E_m was characterized by first generating it from the native enzyme in two ways: (a) Adding 2 μM catalase, so that $E_{ox} \leftrightarrows E_m+H_2O_2$; the catalase acts on the H_2O_2 displacing the above equilibrium $2H_2O_2$+catalase$\rightarrow O_2+2H_2O$, so that all E_{ox} is transformed into E_m by the end of the reaction. (b) Adding 2 μM of H_2O_2, so that the entire enzyme passes to E_{ox} and then adding 2 μM catalase (Munoz-Munoz *et al.*, 2009). E_m was generated to study its possible inactivation by monophenols.

Evaluation of enzymatic species E_m, E_d, and E_{ox} in an enzymatic preparation of tyrosinase. It is known that an enzymatic preparation of tyrosinase from any source is found in three forms, E_m, E_d and E_{ox} (Jackman *et al.*, 1992). Several authors have proposed spectrophotometric methods for evaluating these forms (Jolley *et al.*, 1974; Deinum *et al.*, 1976; Jackman *et al.*, 1992). Here, we propose a kinetic method based on the fact that their inactivation by 2-mercaptoethanol (Aasa *et al.*, 1978) occurs over a wide time range: inactivation constants of 0.014 s^{-1}, 4×10^{-5} s^{-1} and 1×10^{-5} s^{-1} for E_{ox}, E_m and E_d, respectively. Under aerobic conditions at oxygen concentrations of 0.26 mM, practically the only forms existing are E_{ox} and E_{om} (Rodriguez-Lopez *et al.*, 2000). Note that the difference between k_i^{ox} and k_i^{m} is three orders of magnitude, a difference that can be used to evaluate these enzymatic forms. The experimental method used was described in (Munoz-Munoz *et al.*, 2009).

^{13}C-NMR assays. ^{13}C-NMR spectra of several substrates were obtained at pH=6.0 in a Varian Unity spectrometer at 300 MHz, using ^2H_2O as solvent for the substrates. Chemical displacement (δ) values were measured relative to those for tetramethylsilane (δ=0). The maximum line breadth accepted in the ^{13}C-NMR spectra was 0.06 Hz. Therefore, the maximum accepted error for each peak of the spectrum was ±0.03 p.p.m.

RESULTS AND DISCUSSION

In this work, we study the reaction of the different enzymatic forms that exist in the turnover of tyrosinase with L- and D-tyrosine, that is, the form *oxy*-tyrosinase, under aerobic conditions, and the forms *met*-tyrosinase and *deoxy*-tyrosinase, under anaerobic conditions

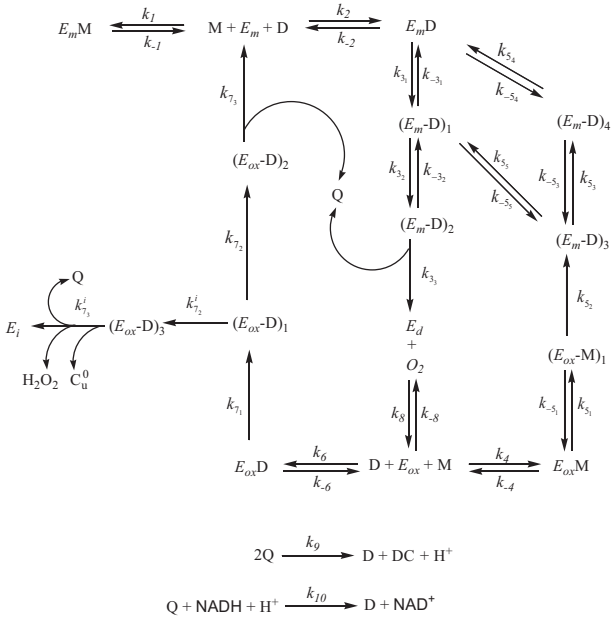

Scheme I. Kinetic mechanism proposed to explain the monophenolase together with diphenolase and suicide inactivation pathways of tyrosinase action on tyrosine enantiomers (see Scheme ISM for further details).

(Scheme I in the kinetic form and Scheme ISM in the structural form) (Sanchez-Ferrer *et al.*, 1995).

Inactivation of tyrosinase in its action on monophenols under aerobic conditions: suicide inactivation

As mentioned above, the model we proposed to explain the suicide inactivation of tyrosinase involves the enzymatic form *oxy*-tyrosinase reacting with an *o*-diphenol in the diphenolase activity (Scheme I and in its simplified form Scheme II) and is based on the structural mechanism proposed in Scheme ISM. It can be outlined as follows:

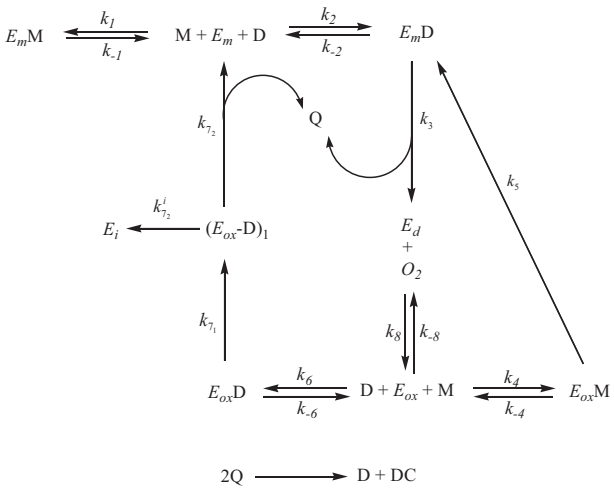

Scheme II. Simplified kinetic mechanism to explain the monophenolase and diphenolase activities of tyrosinase and the suicide inactivation process.

The kinetic mechanisms described in Schemes I and II and in the structural mechanisms of Scheme ISM suggest that the enzyme is not inactivated in the hydroxylase cycle. For the hydroxylase reaction to take place, the monophenol must transfer a proton to the peroxide, which represents the slow step of the process (Peñalver *et al.*, 2003; Fenoll *et al.*, 2004). The formation of a hydroperoxide has been proposed in copper complexes (Tyeklar & Karlin, 1989), for the hydroxylation of dopamine β-hydroxylase (Miller & Klinman, 1985) and, more recently, in the action of tyrosinase of *Streptomyces castaneoglobisporus* on monophenols (Matoba *et al.*, 2006). Subsequently the electrophilic attack of the oxygen of the peroxide group of the oxy-tyrosinase form takes place in a *meta*-position of the benzene ring of the L-tyrosine (Karlin *et al.*, 1998; Itoh & Fukuzumi, 2007). However, in the diphenolase cycle (Schemes I and II), although the first step is also the transfer of a proton from the hydroxyl group on C-4 to the peroxide in the oxy-tyrosinase form (Peñalver *et al.*, 2003; Fenoll *et al.*, 2004), the following step (see Matoba *et al.*, 2006) is another transfer of a proton from the hydroxyl group on C-3 to the nitrogen atom of the histidine bound axially to the CuA (catalysis) or to the peroxide group, which acts as a base (inactivation) (Scheme III). Note that this step does not exist in the hydroxylase cycle. However, a kinetic study of the suicide inactivation process with monophenol cannot be carried out experimentally in a rigorous and systematic manner, as it has for *o*-diphenols (Munoz-Munoz *et al.*, 2008; 2010a), for the following reasons:

i) The instability of dopachrome. The dopachrome resulting from the rapid evolution of *o*-dopaquinone, is unstable, and evolves towards indoles (Riley, 1997) (data not shown), which make it impossible to follow the suicide inactivation kinetics of tyrosinase spectrophotomet-

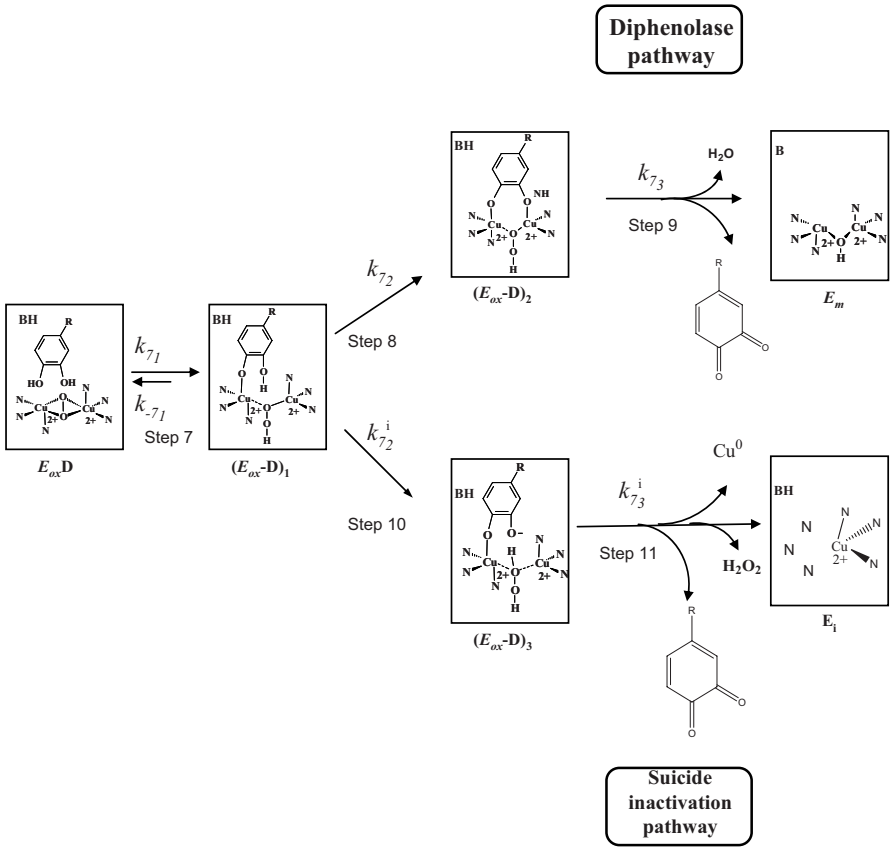

Scheme III. Proposed model to explain the suicide inactivation of tyrosinase during its diphenolase activity when it acts on *o*-diphenols (see Scheme ISM for further details).

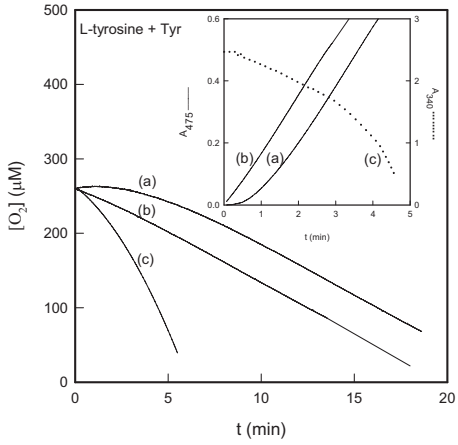

Figure 1. Monophenolase activity of tyrosinase.
Recordings of oxygen consumed in the monophenolase activity of tyrosinase. The experimental conditions were: 30 mM sodium phosphate buffer (pH 6.0), 25°C, $[O_2]_0$=0.26 mM, $[\text{L-tyrosine}]_0$=1 mM, $[Tyr]_0$=0.15 mM, curve (a) $[D]_0$=0; curve (b) $[D]_0$=46 μM and curve (c), $[D]_0$=46 μM and $[NADH]_0$=0.2 mM. **Inset**. Recordings of dopachrome accumulation at 475 nm, curves (a) ($[D]_0$=0) and (b) ($[D]_0$=46 μM), and of disappearance of NADH at 340 nm, curve (c), in the same experiment conditions as described in Fig. 1.

rically by measuring dopachrome. In the case of diphenolase activity, the *o*-quinone can be prevented from evolving by adding NADH to the medium to reduce the *o*-dopaquinone to L-dopa. However, when the enzyme acts on monophenols, the addition of NADH to the reaction medium leads to the continuous accumulation of *o*-diphenol in the medium and the system does not reach the initial steady-state from which the transition phase of the suicide inactivation would occur, Fig. 1, curve (c), and Fig. 1 Inset, curve (c). Note the difference from the kinetics depicted in Fig. 1, curves (a) and (b) and Fig. 1 Inset, curves (a) and (b), which were made in the absence of NADH.

ii) The concentration of monophenol cannot be maintained constant by the presence of the reductant (NADH). The reduction of the *o*-dopaquinone by NADH generates L-dopa, which constantly increases in the medium until the enzyme is inactivated. However, the concentration of monophenol decreases. Note that in the case of monophenolase activity, oxymetric and spectrophotometric short time measurements show that the velocity increases with time in the presence of reductant (parabolic behavior), Fig. 1, curve (c) and Fig. 1 Inset, curve (c), due to the accumulation of *o*-diphenol. Tyrosinase acts better (higher catalytic constant) with *o*-diphenols than with monophenols (Rodriguez-Lopez *et al*., 1992a).

iii) The inactivation kinetics of tyrosinase acting on monophenols is slower than when it acts on *o*-diphenols. In the case of diphenolase activity (Schemes I and II with $[M]_0$=0), all the enzyme participates in the catalytic cycle, which leads to suicide inactivation at long time-values. However, in the monophenolase activity (Schemes I and II), as was previously demonstrated (Rodriguez-Lopez *et al*., 1992a), the enzyme in the steady-state makes two turnovers in the hydroxylase cycle for every one in the oxidase cycle. Therefore, in agreement with our hypothesis, the hydroxylase activity does not inactivate the enzyme, but protects it from suicide inactivation. Moreover, much of the *met*-tyrosinase form is reversibly bound to the monophenol as *met*-tyrosinase/monophenol, which further slows the inactivation kinetics. All the above features (dopachrome instability, substrate variation and slowness of the process) means that the reaction cannot be followed by measuring the dopachrome at long times and that NADH cannot be added (Fig. 2, Inset B).

Taking into account all the experimental difficulties described, the only possibility to study the inactivation kinetics experimentally from the monophenolase activity is to measure the consumption of oxygen at high monophenol concentrations (Fig. 2). From these measurements of monophenolase activity and of diphenolase activity, a quantitative relation can be established between the experimentally measurable magnitudes, which give weight to our hypothesis that the enzyme is not inactivated in the hydroxylase cycle. The explanation for this is that the enzyme acting on the *o*-diphenol directly or on the *o*-diphenol accumulated in the steady-state when acting on monophenol, must undergo the same number of turnovers before inactivation. Below, we provide more details as a function of the parameters that can be measured experimentally: $[NADH]_\infty$, diphenolase activity and $[O_2]_\infty$, monophenolase activity.

If the diphenolase activity is followed spectrophotometrically by measuring the consumption of NADH, the number of turnovers that a molecule of enzyme must make before its suicide inactivation r_D^{NADH} (2 NADH molecules are consumed in each turnover) will be:

$$r_D^{NADH} = \frac{[NADH]_\infty/2}{[E]_0} \quad (4)$$

Since, according to our model, the enzyme acting on monophenols is only inactivated through its action on the *o*-diphenol accumulated in the steady-state, one of the difficulties involves the calculation of the number of turnovers made by the enzyme in the diphenolase cycle from the measurements of the monophenolase activity (oxygen consumption). This was done by taking into account: (*i*) the stoichiometric relation is $3O_2$:2DC, i.e., 3 molecules of oxygen generate 2 molecules of dopachrome, in the monophenolase activity, (*ii*) in the diphenolase cycle only one molecule of DC is formed, consuming one molecule of oxygen, and (*iii*) in the hydroxylase cycle two molecules of oxygen are consumed to form one molecule of DC (Rodriguez-Lopez *et al*., 1992a). The total number of turnovers made by one molecule of enzyme in the monophenolase activity before it is inactivated is:

$$r_M^{O_2} = \frac{[O_2]_\infty}{[E]_0} \quad (5)$$

These turnovers would be of two types, the first for the hydroxylase cycle ($r_{M(H)}^{O_2}$, non-inactivating) and the second for the oxidase cycle ($r_{M(O)}^{O_2}$, capable of provoking suicide inactivation) and, in turn, $r_{M(H)}^{O_2}=2r_{M(O)}^{O_2}$ (Rodriguez-Lopez *et al*., 1992a).

The formation of one molecule of DC in the oxidase cycle consumes one molecule of oxygen, and in the hydroxylase cycle two molecules of oxygen, so that:

$$r_M^{O_2} = r_{M(H)}^{O_2} + r_{M(O)}^{O_2} = \frac{\frac{2}{3}[O_2]_\infty}{[E]_0} + \frac{\frac{1}{3}[O_2]_\infty}{[E]_0} = \frac{[O_2]_\infty}{[E]_0} \quad (6)$$

To demonstrate that the suicide inactivation of tyrosinase acting on monophenols is indirect, and depending on the *o*-diphenol accumulated in the medium, the ratio of Eqn. (7) should be fulfilled. This equation shows the ratio between the number of turnovers of the enzyme acting on the *o*-diphenol (r_D^{NADH}) and the number

of turnovers of the enzyme acting on the *o*-diphenol accumulated by tyrosinase acting on monophenols and due to the *o*-quinone evolution ($r^{O_2}_{M(O)}$). Expressed as a function of the experimentally measurable parameters, $[NADH]_\infty$ and $[O_2]_\infty$:

$$\frac{r_D^{NADH}}{r_{M(O)}^{O_2}} = \frac{\frac{[NADH]_\infty/2}{[E]_0}}{\frac{[O_2]_\infty/3}{[E]_0}} = 1 \quad (7)$$

To check our model (Schemes I–III), two approaches were designed: numerical integration and experimental approach.

Numerical integration of the mechanisms proposed. The numerical integration of the mechanisms proposed in Scheme I in the presence and absence of monophenol ($[M]_0 = 0$) should confirm the predictions indicated in Eqn. (7). If the product of the evolution of *o*-dopaquinone (dopachrome) is considered stable in the numerical integration, the parameters r^{DC} should fulfil the following relations:

$$r_D^{DC} = \frac{[DC]_\infty^D}{[E]_0} \quad (8)$$

and

$$r_{M(O)}^{DC} = \frac{[DC]_\infty^M/2}{[E]_0} \quad (9)$$

The ratio between the r_D^{DC} and $r_{M(O)}^{DC}$ should be 1, according to:

$$\frac{r_D^{DC}}{r_{M(O)}^{DC}} = \frac{\frac{[DC]_\infty^D}{[E]_0}}{\frac{[DC]_\infty^M/2}{[E]_0}} = 1 \quad (10)$$

Therefore, the results for the time course of DC formation in the diphenolase and monophenolase activities (oxidase cycle) should fulfil Eqn. (10).

a) Diphenolase activity

i) Absence of reductant. Simulation of the mechanism proposed in Scheme I with $[M]_0=0$, and the analytical solution of the suicide inactivation process according to Scheme II, which is a simplified mechanism of Scheme I, are presented in Supplementary Material.

Variation of enzyme concentration. Figure 1SM depicts the effect of variations in enzyme concentration. The values of $\lambda^D_{E_{ox}}$ and $[DC]^D_\infty$ fulfil Eqns. (11) and (12) (Fig. 1SM Inset).

$$[DC]_\infty^D = r_D^{DC}[E]_0 \quad (11)$$

with

$$\lambda^D_{E_{ox}} = \frac{\lambda^D_{E_{ox}(max)}[D]_0}{K_m^D + [D]_0} \quad (12)$$

$$r_D^{DC} = \frac{k_{7_2}}{k^i_{7_2}} \quad (13)$$

$$\lambda^D_{E_{ox}(max)} = \frac{k^D_{cat}}{r_D^{DC}} \quad (14)$$

Variation of substrate concentration. Figure 2SM depicts the variation in substrate concentration and the Fig. 2SM Inset represents the apparent inactivation constant ($\lambda^D_{E_{ox}}$) *vs.* $[D]_0$, Eqn. (12).

ii) Presence of reductant. The suicide inactivation of tyrosinase acting on *o*-diphenols in the presence of reductant is simulated in Fig. 3SM. Note that the values of the apparent inactivation constant are equal to those obtained in the absence of reductant. The values of the reductant consumed at the end of the reaction, $[R]_\infty$, and the product formed in its absence, $[DC]_\infty$, have a ratio of 2 (Fig. 3SM), since the reductant is consumed with a stoichiometry of 1NADH:1Q, i.e. 1 NADH molecule consumes 1 *o*-quinone molecule, while, in its absence, the dopachrome is formed with a stoichiometry of 1DC:2Q, i.e., 1 dopachrome molecule is generated from 2 *o*-quinone molecules. Therefore, the suicide inactivation kinetics of tyrosinase in its diphenolase activity should be studied in the presence of reductant. This is not the situation with the monophenolase activity of tyrosinase, as we shall see below.

b) Monophenolase activity

i) Absence of reductant. The mechanism proposed in Scheme I was simulated by accepting that, at t=0, the *o*-diphenol concentration is such that $[D]_{ss}/[M]_{ss}=C$ (Ros *et al.*, 1994), thus avoiding a lag period (see Supplementary Material). The analytical solution of the suicide inactivation process is also described in the Supplementary Material according to Scheme II.

Varying enzyme concentration. Variations in enzyme concentration are shown in Fig. 4SM and Fig. 4SM Inset. The results agree with the kinetic analysis, Eqns. (15–16), and indicate that if experimental measurement were possible, similar results to those for diphenolase activity would be obtained.

According to Eqns. (8–10), the expressions for monophenolase activity are:

$$[DC]_\infty^D = 2r_D^{DC}[E]_0 \quad (15)$$

$$\lambda^M_{E_{ox}} = \frac{\lambda^M_{E_{ox}(max)}[M]_0}{K_m^M + [M]_0} \quad (16)$$

$$\lambda^M_{E_{ox}(max)} = \frac{k^M_{cat}}{r_D^{DC}} = \frac{k^M_{cat}}{r_{M(O)}^{DC}} \quad (17)$$

The experimental data of K^D_m and K^M_m (0.5 mM for L-dopa and 0.27 mM for L-tyrosine, respectively) are in the same range, and so the velocity of the process will depend, according to Eqn. (12) and Eqn. (16), on the value of the apparent inactivation constant. According to Eqn. (14) and Eqn. (17), the maximum apparent inactivation constant is related with the catalytic constant and, since $k_{cat}{}^D > k_{cat}{}^M$ (110 s^{-1} for L-dopa and 8 s^{-1} for L-tyrosine, respectively), $\lambda^D_{E_{ox}} > \lambda^M_{E_{ox}}$ for the same concentration of the substrate.

Varying the substrate concentration. Figure 5SM shows the variations in substrate concentration as tyrosinase acts on the monophenol, assuming that the product, dopachrome, is stable. Note that the kinetic test of suicide substrates is fulfilled: the product accumulated at the end of the reaction, $[DC]_\infty$, is constant and the apparent inactivation constant $\lambda^M_{E_{ox}}$ varies hyperbolically with the concentration of monophenol, Fig. 5SM Inset, Eqns. (15–17).

Table 1. Confirmation by computer simulation and experimentation of the relations described in Eqn. (7) and Eqn. (10)

Results	Substrate	$[E]_0$ (nM)	$[NADH]_\infty$ (μM)	$[O_2]_\infty$ (μM)	$[DC]_\infty$ (μM)	r_D^{NADH}	r_D^{DC}	$r_{M(O)}^{O_2}$	$r_{M(O)}^{DC}$	Eqn. (7)	Eqn. (10)	$\lambda_{E_{ox}}^{D}\times10^3$ (min^{-1})	$\lambda_{E_{ox}}^{M}\times10^3$ (min^{-1})
Simulated							53500		53500	–	1		
	$[M]_0$ (1 mM)	0.10	–	–	10.70	–	–	–	–	–	–	–	8.1 ± 0.06
	$[D]_{ss}$ (46 μM)	0.10	–	–	5.35	–	–	–	–	–	–	15.48 ± 0.06	–
	$[D]_0$ (1 mM)	0.10	–	–	5.35	–	–	–	–	–	–	73.26 ± 0.06	–
Experimental						46100 ± 4019		43975 ± 2938		1.05	–		
	$[M]_0$ (1 mM)	0.50	–	66.8 ± 0.1	–	–	–	–	–	–	–	–	5.76 ± 0.06
	$[D]_{ss}$ (46 μM)	0.50	43.7 ± 2.1*	–	–	–	–	–	–	–	–	10.86 ± 0.66**	–
	$[D]_0$ (1 mM)	0.50	44.9 ± 3.3	–	–	–	–	–	–	–	–	69.48 ± 6.12	–

$[D]_{ss}$=46 μM is the concentration of *o*-diphenol accumulated in the steady-state, when tyrosinase acts on 1 mM L-tyrosine. *Calculated from the *o*-diphenol accumulated in the steady-state of monophenolase activity, according to Eqn. (4). **Calculated from the *o*-diphenol accumulated in the steady-state of monophenolase activity, according to Eqn. (12).

ii) Presence of reductant. Simulation of the tyrosinase suicide inactivation as it acts on monophenols in the presence of reductant is shown in Fig. 6ASM, curve (a). In the same figure, curve (b) shows the inactivation in the same conditions but in the absence of reductant. Note the higher apparent inactivation constant in Fig. 6ASM, curve (a), than in Fig. 6ASM, curve (b). However, the value of the product accumulated at the end of the reaction in Fig. 6ASM, curve (a), is not double that shown in Fig. 6ASM, curve (b), as was the case for the diphenolase activity (Fig. 3SM), because, in the presence of reductant, the system is not in the steady-state and the relation between the turnovers of the oxidase and hydroxylase cycles is not maintained because *o*-diphenol is accumulated in the medium. The increased apparent inactivation constant can be explained by the result shown in Fig. 6BSM. Note that in Fig. 6BSM, curve (a), much more *o*-diphenol has been accumulated than in Fig. 6BSM, curve (b), so that the enzyme makes *r* turnovers (a fixed number) in the oxidase cycle more rapidly (in the presence of reductant). This acceleration of the inactivation is demonstrated in Fig. 6ASM, curve (a) and Fig. 6CSM, curve (a), which point to the accumulation of inactive enzyme with time. In Fig. 6CSM, curve (b), which represents the absence of reductant, the inactive enzyme, E_i, is accumulated in the medium with a smaller $\lambda_{E_{ox}}^{M}$ than in the presence of reductant, Fig. 6CSM, curve (a).

The results obtained by simulation, Fig. 1SM–Fig. 6SM, from the mechanism proposed in Scheme I with $[M]_0$=0 and Scheme I and the value of 1 taken by Eqn. (10) (see Table 1), reveal that if this test could be demonstrated experimentally, it would be sufficient to confirm our hypothesis that tyrosinase acting on monophenols is not inactivated in the hydroxylase cycle but only in the oxidase cycle. This cycle arises from the accumulation of *o*-diphenol from the *o*-quinones and also through its enzymatic release from (*met*-tyrosinase-D)$_3$, Scheme I (Rodriguez-Lopez *et al.*, 1992a), and is responsible for the enzyme's inactivation as it acts in the oxidase cycle.

Experimental approach. Following the suicide inactivation kinetics of tyrosinase in its action on *o*-diphenols spectrophotometrically measuring NADH disappearance and in its reaction on monophenols by measuring oxygen consumption. The experimental approach involved checking that Eqn. (7) was fulfilled by spectrophotometrically measuring the suicide inactivation kinetics with *o*-diphenols (disappearance of NADH) and measuring the suicide inactivation of the monophenolase activity according to the oxygen consumed during the enzyme's action on monophenols.

The suicide inactivation of tyrosinase acting on L-dopa in the presence of NADH is described in (Munoz-Munoz *et al.*, 2010a). When the action of tyrosinase on L-tyrosine is studied at t=0 in the absence of *o*-diphenol, tyrosinase shows the typical lag period both in oxymetric and spectrophotometric assays: Fig. 1, curve (a) and Fig. 1 Inset, curve (a). The addition of *o*-diphenol brings the system to the steady-state at t=0, Fig. 1, curve (b) and Fig. 1 Inset, curve (b). In Fig. 1, curve (c) and in Fig. 1 Inset, curve (c), it can be seen that when NADH is added to the reaction medium along with *o*-diphenol, the latter continues to accumulate. The velocity continues to increase constantly and the system never reaches the steady-state, meaning that these suicide inactivation experiments involving monophenolase activity should never be carried out in the presence of NADH.

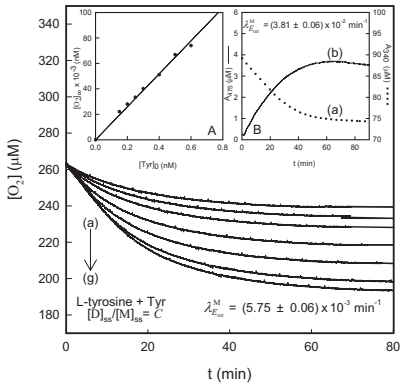

Figure 2. Indirect inactivation of tyrosinase in its action on L-tyrosine.
Oxymetric recordings of oxygen consumed in action of tyrosinase on L-tyrosine. The experimental conditions were 30 mM sodium phosphate buffer (pH 6.0), 25 ºC, $[O_2]_0$=0.26 mM, [L-tyrosine]0=1 mM, $[\text{L-dopa}]_0$=46 μM and the enzyme concentrations were (nM): (a) 0.15, (b) 0.20, (c) 0.25, (d) 0.30, (e) 0.40, (f) 0.50 and (g) 0.60. **Inset A.** Representation of the $[O_2]_\infty$-values vs. initial enzyme concentration. **Inset B.** Curve (a), disappearance of NADH (0.095 mM) in action of tyrosinase (0.1 nM) on L-tyrosine (1 mM). The experimental conditions were the same as in Fig. 2. Curve (b), accumulation of dopachrome in the action of Tyr (1.5 nM) on L-tyrosine (1 mM).

Figure 2 shows the recordings of oxygen consumption as tyrosinase acts on L-tyrosine at different enzyme concentrations. Figure 2 Inset A shows the representation of the $[O_2]_\infty$ values *vs.* $[E]_0$ in the case of the suicide inactivation of tyrosinase in the monophenolase activity observed by measuring the disappearance of O_2. Figure 2 Inset B, curve (a), depicts the inactivation of tyrosinase acting on L-tyrosine in the presence of NADH, while Fig. 2 Inset B, curve (b), depicts the inactivation observed by following dopachrome. Given the instability of dopachrome (data not shown) it is clear that its measurement, Fig. 2 Inset B, curve (b), cannot be used since it evolves towards 5,6-dihydroxyindol (DHI) and 5,6-dihydroxyindolcarboxylic acid (DICA) (Riley, 1997). Non-linear regression analysis of the results shown here, Fig. 2 and Fig, 2 Inset B, curve (a), enables us to obtain the value of $\lambda^{M}_{E_{ox}}$, $[O_2]_\infty$ and $[NADH]_\infty$. Note the difference between the values of $\lambda^{M}_{E_{ox}}$ (Fig. 2 and Fig. 2 Inset B), a result that agrees with the numerical integrations shown in Fig. 6ASM and Fig. 6CSM.

These findings support and even confirm our hypothesis that the enzyme is not inactivated in the hydroxylase cycle. The experimental recordings shown in Fig. 2 give the values of $\lambda_{E_{ox}}{}^{M}$ and $[O_2]_\infty$. These data, together with the values of $[NADH]_\infty=[Q]_\infty$ obtained spectrophotometrically in the inactivation experiments with L-dopa (Munoz-Munoz *et al.*, 2010a), confirm the closeness to the value 1 as predicted by Eqn. (7) (see Table 2). The data also confirm that the monophenol delays the process of suicide inactivation, as we hypothesized. Hence, from Table 1, both in the experimental and simulated results $\lambda^{D}_{E_{ox}}/\lambda^{M}_{E_{ox}} \cong 12$ and 9, respectively, for the same concentration of substrate. These results agree with Eqns. (12) and (14) for *o*-diphenols and Eqns. (16) and (17) for monophenols.

Comparison of our model with that proposed by other authors

Other authors (Land *et al.*, 2007) have proposed an alternative model to explain suicide inactivation (Scheme IV). This mechanism describes the binding of the enzyme to a diphenol as if it were a monophenol, while the suicide inactivation occurs through the hydroxylase activity. The model implies:

- The structure of the substrate may influence whether suicide inactivation takes place,

Table 2. Kinetic constants which characterize the inactivation of E_d, E_m and E_d^* by dopa isomers and their protection by isomers of tyrosine under anaerobic conditions

Enzymatic form	Substrate	$K_E^{D(a)}$ (μM)	$k_{iD}\times10^3$ (min^{-1})	$k_{iD}{}^*\times10^3$ (min^{-1})	$K_E^{M(a)}$ (μM)
E_d^*	L-dopa	19.24 ± 2.12	–	0.25 ± 0.01	–
	D-dopa	28.88 ± 2.93	–	0.26 ± 0.02	–
	L-tyrosine	–	–	–	22.32 ± 3.96
	D-tyrosine	–	–	–	28.04 ± 4.85
E_d	L-dopa	10.77 ± 1.12	0.37 ± 0.01	–	–
	D-dopa	25.34 ± 2.24	0.37 ± 0.03	–	–
	L-tyrosine	–	–	–	23.95 ± 2.99
	D-tyrosine	–	–	–	29.02 ± 3.11
E_m	L-dopa	10.77 ± 1.12	0.37 ± 0.01	–	–
	D-dopa	25.34 ± 2.24	0.37 ± 0.03	–	–
	L-tyrosine	–	–	–	23.15 ± 2.51
	D-tyrosine	–	–	–	29.92 ± 3.16

[(a)] In K_E^D and K_E^D, *E* corresponds to the enzymatic forms E_d^* or E_d. When the reaction is started with E_m, the data obtained correspond to E_d, because of the rapid transformation of E_m into E_d (Scheme VI).

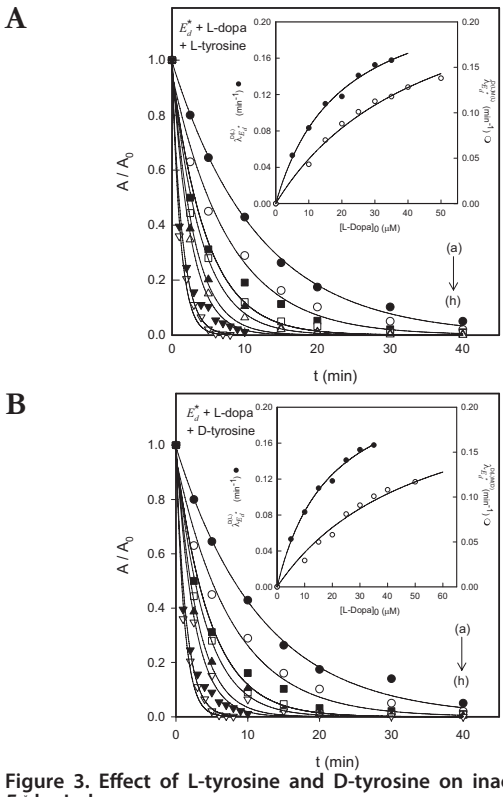

Figure 3. Effect of L-tyrosine and D-tyrosine on inactivation of E_d^* by L-dopa.
The inactivation of E_d^* by L-dopa was studied after generating it as described in Material and methods. **(A)** Effect of L-tyrosine. The *o*-diphenol and the monophenol (L-tyrosine) was added at t=0 and aliquots were taken at different times to measure the residual activity with 2.5 mM L-dopa (λ=475 nm). The experimental conditions were: 30 mM sodium phosphate buffer (pH 6.0), 25 ºC, $[E]_0$= 0.1 μM (see Material and Methods section), $[H_2O_2]_0$ = 2 μM and [L-tyrosine]$_0$ = 20 μM. The L-dopa concentrations were (μM): (a) 10 ●, (b) 15 ○, (c) 20 ■, (d) 25 □, (e) 30 ▲, (f) 35 △, (g) 40 ▼ and (h) 50 ▽. The experimental results were fitted to Eqn. (18) and the apparent inactivation constants to Eqn. (19). **Inset**. Representation of the values of $\lambda_{Ed^*}^{D(L)M(L)}$ *vs.* [L-dopa]$_0$ in the presence (○) of L-tyrosine and of $\lambda_{Ed^*}^{D(L)}$ *vs.* [L-dopa]$_0$ in its absence (●). **(B)** Effect of D-tyrosine. The experimental conditions were the same as in (A) but with 40 μM D-tyrosine. The experimental results were fitted to Eqn. (18) and the apparent inactivation constants to Eqn. (19). The L-dopa concentrations were (μM): (a) 10 ●, (b) 15 ○, (c) 20 ■, (d) 25 □, (e) 30 ▲, (f) 35 △, (g) 40 ▼ and (h) 50 ▽. **Inset**. Representation of the values of $\lambda_{Ed^*}^{D(L)M(D)}$ *vs.* [L-dopa]$_0$ in the presence (○) of D-tyrosine and of $\lambda_{Ed^*}^{D(L)}$ *vs.* [L-dopa]$_0$ in its absence (●).

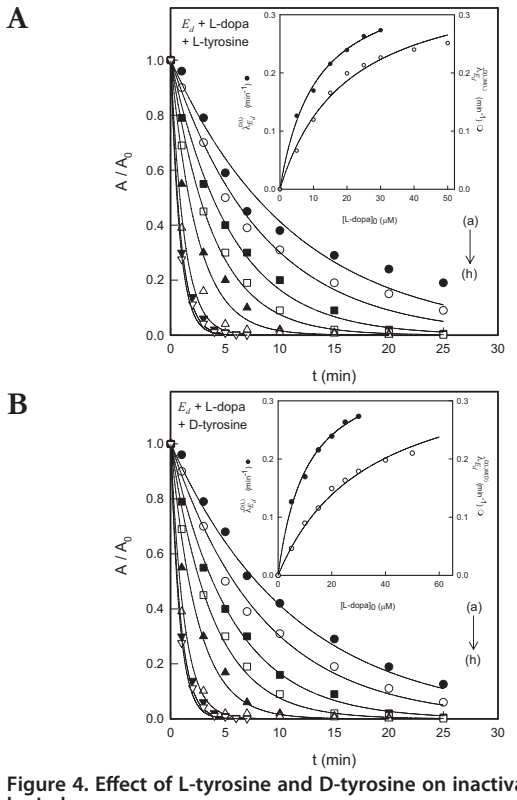

Figure 4. Effect of L-tyrosine and D-tyrosine on inactivation of E_d by L-dopa.
(A) Effect of L-tyrosine. The form E_d was obtained as described in Material and methods and immediately incubated with *o*-diphenol and monophenol (L-tyrosine), taking aliquots at different times to measure the residual activity with 2.5 mM L-dopa (λ=475 nm). The experimental conditions were: 30 mM sodium phosphate buffer (pH 6.0), 25 ºC, $[E]_0$=0.1 μM (see Material and Methods section), $[H_2O_2]_0$=2 μM and [L-tyrosine]$_0$=20 μM. The L-dopa concentrations were (μM): (a) 5 ●, (b) 10 ○, (c) 15 ■, (d) 20 □, (e) 25 ▲, (f) 30 △, (g) 40 ▼ and (h) 50 ▽. The experimental results were fitted to Eq. (21) and the apparent inactivation constants to Eqn. (22). **Inset**. Representation of the values of $\lambda_{E_d}^{D(L)M(L)}$ *vs.* [L-dopa]$_0$ in the presence (○) of L-tyrosine and of $\lambda_{E_d}^{D(L)}$ *vs.* [L-dopa]$_0$ in its absence (●). (**B**) Effect of D-tyrosine. The experimental conditions were the same as in (A) but with 40 μM D-tyrosine. The L-dopa concentrations were (μM): (a) 5 ●, (b) 10 ○, (c) 15 ■, (d) 20 □, (e) 25 ▲, (f) 30 △, (g) 40 ▼ and (h) 50 ▽. The experimental results were fitted to Eqn. (21) and the apparent inactivation constants to Eqn. (22). **Inset**. Representation of the values of $\lambda_{E_d}^{D(L)M(D)}$ *vs.* [L-dopa]$_0$ in the presence (○) of D-tyrosine and of $\lambda_{E_d}^{D(L)}$ *vs.* [L-dopa]$_0$ in its absence (●). In the case of E_m, the results are the same as those for E_d (see Table 2).

- The enzymes catechol oxidase should not suffer inactivation since they have no hydroxylase activity.

Let us look at these two implications below:

i) Scheme IV (Land *et al.*, 2007; 2008; Ramsden *et al.*, 2009) implies that the chemical structure of the substrate is of fundamental importance for suicide inactivation: the substrate must have at least two hydroxyl groups in *ortho* in the benzene ring. Hence, when the substrate is a trihydroxybenzene (e.g., pyrogallol), the proposed mechanism (Scheme IV) would indicate that this compound is not a suicide substrate (Land *et al.*, 2007), although our experimental results (Munoz-Munoz *et al.*, 2008) suggest that it is the most powerful suicide substrate of mushroom tyrosinase. The oxygen consumption that is observed is due to autooxidation (Munoz-Munoz *et al.*, 2008), not to the action of the enzyme. Indeed, the addition of superoxide dismutase and catalase to the medium inhibits this autooxidation process, underlining that pyrogallol is really a suicide substrate.

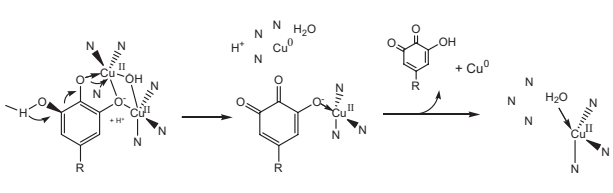

Scheme IV. Proposed model to explain the suicide inactivation of tyrosinase during its monophenolase activity when it acts on *o*-diphenols (Land *et al.*, 2007).

ii) The enzymes catechol oxidase should not suffer inactivation since they have no hydroxylase activity. The catechol oxidases studied to date in this respect are those of *Ipomoea batatas*, *Lycopus europaeus, Populus nigra* and *Aspergillus oryzae* (Klabunde *et al.*, 1998; Rompel *et al.*, 1999; Gasparetti *et al.*, 2010). The reason for choosing these oxidases is that these enzymes

have no monophenolase activity and so suicide inactivation will not occur. The authors (Land *et al.*, 2007; 2008; Ramsden *et al.*, 2009) chose banana enzyme (*Musa cavendishii*), but the experiments depicted in Fig. 1 of Land *et al.* (2008) are carried out at such a short time scale and with such a high concentration of the enzyme that practically all the oxygen is consumed. Moreover, this enzyme possesses monophenolase activity (Padron *et al.*, 1974) and suicide activation has been described when it acts on catechol (Padron *et al.*, 1975). However, in (Land *et al.*, 2008), differences in the mass spectra are seen depending on whether the experiments are carried out with mushroom or banana tyrosinase (Land *et al.*, 2008). The polyphenol oxidases studied to date – apple, pear, avocado and strawberry (Espin *et al.*, 1995; 1997a; 1997b; 1997c; 1997d) – show two activities, monophenolase and diphenolase, the first rather low. In short, the tests should have been carried out at long measuring times and with low enzyme concentrations.

The experimental results of the test proposed in the present study in relation to the model of Scheme I, see Table 1, give weight to the mechanism that we propose that only during the diphenolase activity of tyrosinase is the enzyme inactivated.

Effect of monophenols on tyrosinase under anaerobic conditions

Effect of monophenols on E_d E_d^* and E_m. When each of these enzymatic forms was generated anaerobically and preincubated with L-tyrosine or D-tyrosine, no inactivation was observed (result not shown). Under anaerobic conditions, therefore, tyrosinase is not inactivated by monophenols.

Effect of L-tyrosine and D-tyrosine on inactivation of E_d E_d^* and E_m by *o*-diphenols. When the experiments of inactivation by diphenols (Munoz-Munoz *et al.*, 2010a) were carried out in the presence of L-tyrosine, the results (Fig. 3A) showed that inactivation is delayed according to the mechanism depicted in Scheme VA.

The experimental results (Fig. 3A) were fitted to Eqn. (18).

$$[E_d^*] = [E_d^*]_0 \, e^{-\lambda_{E_d^*}^{\mathrm{D(L)M(L)}} t} \tag{18}$$

The values of $\lambda_{E_d^*}^{\mathrm{D(L)M(L)}}$ (Fig. 3A Inset) were fitted to Eqn. (19):

$$\lambda_{E_d^*}^{\mathrm{D(L)M(L\ or\ D)}} = \frac{k^*_{i_{\mathrm{D(L)M(L\ or\ D)}}}[\mathrm{D}]_0}{K_{E_d^*}^{\mathrm{D(L)M(L\ or\ D)}} + [\mathrm{D}]_0} \tag{19}$$

where $\lambda_{E_d^*}^{\mathrm{D(L)M(L)}}$ is the apparent inactivation constant of E_d^* for L-dopa in the presence of L-tyrosine. Note how $k^*_{i\,\mathrm{D(L)M(L)}}$ takes the same value as $k^*_{i\,\mathrm{D(L)}}$ (Munoz-Munoz *et al.*, 2010a), although $K_{E_d^*}^{\mathrm{D(L)}}$ is greater than $K_{E_d^*}^{\mathrm{D(L)}}$, according to Eqn. (20):

$$K_{E_d^*}^{\mathrm{D(L)M(L\ or\ D)}} = K_{E_d^*}^{\mathrm{D(L)}}\left(1 + \frac{[\mathrm{M}]_0}{K_{E_d^*}^{\mathrm{M(L\ or\ D)}}}\right) \tag{20}$$

where $K_{E_d^*}^{\mathrm{M(L)}}$ is the dissociation constant of the complex E_d^*M (Table 2). When D-tyrosine is used (Fig. 3B), the experimental data can be fitted to Eqn. (18) and subsequently the values of $\lambda_{E_d^*}^{\mathrm{D(L)M(L)}}$ (Fig. 3B Inset) to Eqn. (19), obtaining $k^*_{i\,\mathrm{D(L)M(D)}}$ and $K_{E_d^*}^{\mathrm{D(L)M(D)}}$. Note how $k^*_{i\,\mathrm{D(L)M(D)}}$ takes on the same value as $k^*_{i\,\mathrm{D(L)}}$ (Munoz-Munoz *et al.*, 2010a), although $K_{E_d^*}^{\mathrm{D(L)M(D)}}$ is greater than $K_{E_d^*}^{\mathrm{D(L)}}$. From Eqn. (20), one obtains the $K_{E_d^*}^{\mathrm{M(D)}}$ (Table 2), the value of which is only slightly greater than $K_{E_d^*}^{\mathrm{M(L)}}$, the E_d^* form of the enzyme showing stereospecificity for the binding of the isomers L- and D-tyrosine. As occurred with L- and D-dopa, although the values of δ_4 for L- and D-tyrosine are the same (δ_4=158.86 p.p.m.), stereospecific effects are originated in the binding. This effect is less pronounced than in the case of *o*-diphenols because the latter bind to two atoms of copper (Table 2).

The same experiments carried out with the E_d and E_m forms (Fig. 4A and Fig. 4B) can be fitted to Eqns. (21), (22) and (23) (Scheme VB and VI).

$$[E_d] = [E_d]_0 \, e^{-\lambda_{E_d}^{\mathrm{D(L)M(L)}} t} \tag{21}$$

$$\lambda_{E_d}^{\mathrm{D(L)M(L\ or\ D)}} = \frac{k_{i_{\mathrm{D(L)M(L\ or\ D)}}}[\mathrm{D}]_0}{K_{E_d}^{\mathrm{D(L)M(L\ or\ D)}} + [\mathrm{D}]_0} \tag{22}$$

and

$$K_{E_d}^{\mathrm{D(L)M(L\ or\ D)}} = K_{E_d}^{\mathrm{D(L)}}\left(1 + \frac{[\mathrm{M}]_0}{K_{E_d}^{\mathrm{M(L\ or\ D)}}}\right) \tag{23}$$

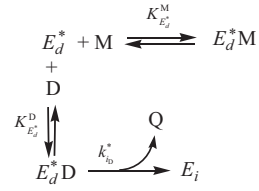

Scheme VA. Effect of monophenols on E_d^*, inactivation by *o*-diphenol.

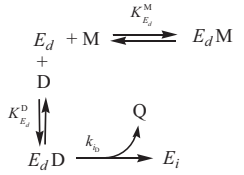

Scheme VB. Effect of monophenols on E_d, inactivation by *o*-diphenol.

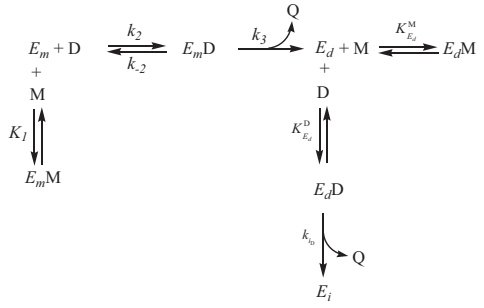

Scheme VI. Effect of monophenols on E_m, inactivation by o-diphenol.

Analysis of the data (Fig. 4A Inset and Fig. 4B Inset) provides the values of $k_{i_{\mathrm{D(L)M(L)}}}$ and $k^*_{i\,\mathrm{D(L)M(D)}}$ which are the same as $k_{i_{\mathrm{D(L)}}}$ (Munoz-Munoz *et al.*, 2010a), although, once again, the values of $K_{E_d}^{\mathrm{D(L)M(D)}}$ are greater than those

of $K_{E_d}^{D(L)}$ Eqn. (23) (Table 2). From the same equation $K_{E_d}^{M(L)}$ and $K_{E_d}^{M(D)}$ can be obtained for the binding of L-tyrosine and D-tyrosine to the form E_d and, once again, a stereospecific binding pattern can be observed, which is better for L than for D (Table 2). Since E_m is rapidly transformed into E_d (Scheme VI), any information gained in a kinetic study of the form E_m is the same as for the E_d (Table 2).

CONCLUSIONS

Monophenols protect the enzyme from inactivation by *o*-diphenols. However, under aerobic conditions, due to the accumulation of *o*-diphenol in the medium through the chemical evolution of the *o*-dopaquinone and its enzymatic release, the enzyme is inactivated. Therefore, it might be said that the monophenols inactivate the enzyme through an indirect process.

Acknowledgements

This paper was partially supported by grants from the Ministerio de Educación y Ciencia (Madrid, Spain) Project BIO2009-12956, from the Fundación Séneca (CARM, Murcia, Spain) Projects 08856/PI/08 and 08595/PI/08, from the Consejería de Educación (CARM, Murcia, Spain) BIO-BMC 06/01-0004 and from FISCAM PI-2007/53 from the Consejería de Salud y Bienestar Social de la Junta de Comunidades de Castilla La Mancha. F.G.M. and J.L.M.M. have two fellowships from Fundación Caja Murcia (Murcia, Spain).

REFERENCES

Aasa R, Deinum J, Lerch K, Reinhammar B (1978) The reaction of mercaptans with tyrosinases and hemocyanins. *Biochim Biophys Acta* **535:** 287–298.

Asimov I, Dawson CR (1950) On the reaction inactivation of tyrosinase during the aerobic oxidation of catechol, *J Am Chem Soc* **72:** 820–828.

Battaini G, Monzani E, Casella L, Lonardi L, Tepper AW, Canters GW, Bubacco L (2002) Tyrosinase-catalyzed oxidation of fluorophenols. *J Biol Chem* **277:** 44606–44612.

Beltramini M, Lerch K (1982) Fluorescence properties of Neurospora tyrosinase. *Biochem J* **205:** 173–180.

Cabanes J, Garcia-Canovas F, Lozano JA, Garcia-Carmona F (1987) A kinetic study of the melanization pathway between L-tyrosine and dopachrome. *Biochim Biophys Acta* **923:** 187–195.

Casella L, Monzani E, Gulloti M, Cavagnino D, Cerina G, Santagostini L, Ugo R (1996) Functional modeling of tyrosinase. Mechanism of phenol ortho-hydroxylation by dinuclear copper complexes. *Inorg Chem* **35:** 7516–7525.

Chang TS (2007) Two potent suicide substrates of mushroom tyrosinase: 7,8,4'-trihydroxyisoflavone and 5,7,8,4'-tetrahydroxyisoflavone. *J Agric Food Chem* **55:** 2010–2015.

Chang TS (2009) An updated review of tyrosinase inhibitors. *Int J Mol Sci* **16:** 2440–2475.

Chang TS, Lin, MY, Lin HJ (2010) Indentifying 8-hydroxynaringenin as a suicide substrate of mushroom tyrosinase. *J Cosmet Sci* **61:** 205–210.

Chazarra S, Cabanes J, Escribano J, Garcia-Carmona F (1997) Kinetic study of the suicide inactivation of latent polyphenoloxidase from iceberg lettuce (*Lactuca sativa*) induced by 4-tert-butylcatechol in the presence of SDS. *Biochim Biophys Acta* **1339:** 297–303.

Decker H, Schweikardt T, Tuczek F (2006) The first crystal structure of tyrosinase: All questions answered?. *Angew Chem Int Ed* **45:** 4546–4550.

Deinum J, Lerch K, Reinhammar B (1976) An EPR study of Neurospora tyrosinase. *FEBS Lett* **69:** 161–164.

Dietler C, Lerch K (1982) In *Oxidases and Related Redox Systems*. King TE, Mason HS, Morrison M, eds, pp 305–317. Pergamon Press, New York.

Espin JC, Morales M, Varon R, Tudela J, Garcia-Canovas F (1995) Monophenolase activity of polyphenol oxidase from verdedoncella apple. *J Agric Food Chem* **43:** 2807–2812.

Espin JC, Morales M, Varon R, Tudela J, Garcia-Canovas F (1997a) Monophenolase activity of polyphenol oxidase from Blanquilla pear. *Phytochemistry* **44:** 17–22.

Espin JC, Ochoa M, Tudela J, Garcia-Canovas F (1997b) Monophenolase activity of strawberry polyphenol oxidase. *Phytochemistry* **45:** 667–670.

Espin JC, Tudela J, Garcia-Canovas F (1997c) Monophenolase activity of polyphenol oxidase from artichoke heads (*Cynara scolymus* L.). *Food Science Technology-Lebensmittel-Wissenschaft Technologie* **30:** 819–825.

Espin JC, Trujano MF, Tudela J, Garcia-Canovas F (1997d) Monophenolase activity of polyphenol oxidase from Haas avocado. *J Agric Food Chem* **45:** 1091–1096.

Fenoll L, Peñalver MJ, Rodriguez-Lopez JN, Garcia-Ruiz PA, Garcia-Canovas F, Tudela J (2004) Deuterium isotope effect on the oxidation of monophenols and *o*-diphenols by tyrosinase. *Biochem J* **380:** 643–650.

Garcia-Canovas F, Garcia-Carmona F, Vera-Sanchez J, Iborra-Pastor JL, Lozano-Teruel JA (1982) The role of pH in the melanin biosynthesis pathway. *J Biol Chem* **257:** 8738–8744.

Garcia-Canovas F, Tudela J, Martinez-Madrid C, Varon R. Garcia-Carmona F, Lozano JA (1987) Kinetic study on the suicide inactivation of tyrosinase induced by catechol. *Biochim Biophys Acta* **912:** 417–423.

Garcia-Carmona F, Garcia-Canovas F, Iborra JL, Lozano JA (1982) Kinetic study of the pathway of melanization between L-dopa and dopachrome. *Biochim Biophys Acta* **717:** 124–131.

Garcia-Molina F., Muñoz JL, Varon R, Rodriguez-Lopez JN, Garcia-Canovas F, Tudela J (2007) A review on spectrophotometric methods for measuring the monophenolase and diphenolase activities of tyrosinase. *J Agric Food Chem* **55:** 9739–9749.

Garcia-Sevilla F, Garrido del Solo C, Duggleby RG, Garcia-Canovas F, Peyro R, Varon R (2000) Use of a window program for simulation of the progress curves of reactants and intermediates involved in enzyme-catalyzed reactions. *Biosystems* **54:** 151–164.

Gasparetti C, Faccio G, Arvas M, Buchert J, Saloheimo M, Kruus K (2010) Discovery of a new tyrosinase-like enzyme family lacking a C-terminally processed domain: production and characterization of an *Aspergillus oryzae* catechol oxidase. *App Microbiol Biotechnol* **86:** 213–226.

Ingraham LL, Corse J, Makower B (1952) Enzymatic browning of fruits. 3. Kinetics of the reaction inactivation of polyphenol oxidase. *J Am Chem Soc* **74:** 2623–2626.

Ismaya WT, Rozeboom HJ, Schurink M, Boeriu CG, Wichers H, Dijkstra BW (2011) Crystallization and preliminary X-ray crystallographic analysis of tyrosinase from the mushroom *Agaricus bisporus*. *Acta Crystallogr Sect F, Struct Biol Cryst Commun* **67:** 575–578.

Itoh S, Fukuzumi S (2007) Monooxygenase activity of type 3 copper proteins. *Acc Chem Res* **40:** 592–600.

Jackman M, Huber M, Hajnal A, Lerch K (1992) Stabilization of the oxy form of tyrosinase by a single conservative amino acid substitution. *Biochem J* **282:** 915–918.

Jandel scientific. *Sigma Plot 9.0 for Windows™*; Jandel scientific: Core Madera 2006.

Jolley Jr RL, Evans LH, Makino N, Mason HS (1974) Oxytyrosinase. *J Biol Chem* **249:** 335–345.

Karlin KD, Lee D-H, Obias HV, Humphreys KF (1998) Copper-dioxygen complexes: Functional models for proteins. *Pure Appl Chem* **70:** 855–862.

Klabunde T, Eicken C, Sachettini JC, Krebs B (1998) Cristal structure of a plant catechol oxidase containing a dicopper center. *Nat Struct Biol* **5:** 1084–1090.

Land EJ, Ramsden CA, Riley PA (2007) The mechanism of suicide-inactivation of tyrosinase: A substrate structure investigation. *Tohoku J Exp Med* **212:** 341–348.

Land EJ, Ramsden CA, Riley PA, Stratford MR (2008) Evidence consistent with the requirement of cresolase activity for suicide inactivation of tyrosinase. *Tohoku J Exp Med* **216:** 231–238.

Lerch K (1983) Neurospora tyrosinase: structural, spectroscopic and catalytic properties. *Mol Cell Biochem* **52:** 125–138.

Lowry OH, Rosebrough NJ, Farr AL, Randall RJ (1951) Protein measurement with the Folin phenol reagent. *J Biol Chem* **193:** 265–275.

Marino SM, Fogal S, Bisaglia M, Moro S, Scartabelli G, De Gioia L, Spada A, Monzani E, Casella L, Mammi S, Bubacco L (2011) Investigation of *Streptomyces antibioticus* tyrosinase reactivity towards chlorophenols. *Arch Biochem Biophys* **505:** 67–74.

Matoba Y, Kumagai T, Yamamoto A, Yoshitsu H, Sugiyama M (2006) Crystallogaphic evidence that the dinuclear copper center of tyrosinase is flexible Turing catalysis. *J Biol Chem* **281:** 8981–8990.

Miller SM, Klinman JP (1985) Secondary isotope effects and structure-reactivity correlations in the dopamine β-monooxygenase reaction: Evidence for a chemical mechanism. *Biochemistry* **24:** 2114–2127.

Molina FG, Munoz JL, Varon R, Rodriguez Lopez JN, Garcia Canovas F, Tudela J (2007) An approximate analytical solution to the lag period of the monophenolase activity of tyrosinase. *Int J Biochem Cell Biol* **39:** 238–252.

Monzani E, Quinti L, Perotti A, Casella L, Gulloti M, Randaccio L, Geremia S, Nardin G, Faleschini P, Tabbi G (1998) Tyrosinase

models. Synthesis, structure, catechol oxidase activity, and phenol monooxygenase activity of a dinuclear copper complex derived from a triamino pentabenzimidazole ligand. *Inorg Chem* **37:** 553–562.
Muñoz-Muñoz JL, Garcia-Molina F, Garcia-Ruiz PA, Molina-Alarcon M, Tudela J, Garcia-Canovas F, Rodriguez-Lopez JN (2008) Phenolic substrates and suicide inactivation of tyrosinase: kinetics and mechanism. *Biochem J* **416:** 413–440.
Munoz-Munoz JL, Garcia-Molina F, Garcia-Ruiz PA, Varon R, Tudela J, Garcia-Canovas F, Rodriguez-Lopez JN (2009) Stereospecific inactivation of tyrosinase by L-and D-ascorbic acid. *Biochim Biophys Acta* **1794:** 244–253.
Muñoz-Muñoz JL, Acosta-Motos JR, Garcia-Molina F, Varon R, Garcia-Ruiz PA, Tudela J, Garcia-Canovas F, Rodriguez-Lopez JN (2010a) Tyrosinase inactivation in its action on L-dopa. *Biochim Biophys Acta* **1804:** 1467–1475.
Munoz-Munoz JL, Garcia-Molina F, Varon R, Garcia-Ruiz PA, Tudela J, Garcia-Canovas F, Rodriguez-Lopez JN (2010b) Suicide inactivation of the diphenolase and monophenolase activities of tyrosinase. *IUBMB Life* **62:** 539–547.
Munoz-Munoz JL, Garcia-Molina F, Garcia-Ruiz PA, Varon R, Tudela J, Garcia-Canovas F, Rodríguez-Lopez JN (2010c) Some kinetic properties of deoxytyrosinase. *J Mol Cat B: Enzymatic* **62:** 173–182.
Nelson JM, Dawson CR (1944) Tyrosinase. *Adv Enzymol* **4:** 99–152.
Padron MP, Gonzalez AG, Lozano JA (1974) O-diphenol:oxygen-oxidoreductase from *Musa cavendishii*. *Rev Esp Fisiol* **30:** 167–176.
Padron MP, Lozano JA, Gonzalez AG (1975) Properties of *o*-diphenol:O_2 oxidoreductase from *Musa cavendishii*. *Phytochemistry* **14:** 1959–1963.
Peñalver MA, Rodriguez-Lopez JN, Garcia-Ruiz PA, Garcia-Canovas F, Tudela J (2003) Solvent deuterium isotope effect on the oxidation of *o*-diphenols by tyrosinase. *Biochim Biophys Acta* **1650:** 128–135.
Ramsden CA, Stratford MRL, Riley PA (2009) The influence of catechol structure on the suicide-inactivation of tyrosinase. *Org Biomol Chem* **7:** 3388–3390.
Riley PA (1997) Melanin. *Int J Biochem Cell Biol* **29:** 1235–1239.
Ramsden CA, Riley PA (2010a) Mechanistic studies of tyrosinase suicide inactivation. *ARKIVOC* **(i):** 260–274.
Ramsden CA, Riley PA (2010b) Studies of the competing rates of catechol oxidation and suicide inactivation of tyrosinase. *ARKIVOC* **(x):** 248–254.
Rodriguez-Lopez JN, Tudela J, Varon R, Garcia-Carmona F, Garcia-Canovas F (1992a) Analysis of a kinetic model for melanin biosynthesis pathway. *J Biol Chem* **267:** 3801–3810.
Rodríguez-Lopez JN, Ros-Martinez JR, Varon R, Garcia-Canovas F (1992b) Calibration of a Clark-type oxygen electrode by tyrosinase catalyzed-oxidation of 4-tert-butylcatechol. *Anal Biochem* **202:** 356–360.
Rodriguez-Lopez JN, Fenoll LG, Garcia-Ruiz PA, Varon R, Tudela J, Thorneley RN, Garcia-Canovas F (2000) Stopped-flow and steady-state study of the diphenolase activity of mushroom tyrosinase. *Biochemistry* **39:** 10497–10506.
Rolff M, Schottenheim J, Decker H, Tuczek F (2011) Copper-O_2 reactivity of tyrosinase models towards external monophenolic substrates: molecular mechanism and comparison with the enzyme. *Chem Soc Rev* **40:** 4077–4098.
Rompel A, Fisher H, Meiwes D, Buldt-Karentzopoulos K, Dillinger R, Tuczek F, Witzel H, Krebs B (1999) Purification and spectroscopic studies on catechol oxidase from *Lycopus europaeus* and *Populus nigra*: Evidence for a dinuclear copper center of type and spectroscopic similarities to tyrosinase and hemocyanin. *J Biol Inorg Chem* **4:** 56–63.
Ros JR, Rodriguez-Lopez JN, Garcia-Canovas F (1994) Tyrosinase: kinetic analysis of the transient phase and the steady state. *Biochim Biophys Acta* **1204:** 33–42.
Sanchez-Ferrer A, Rodriguez-Lopez JN, Garcia-Canovas F, Garcia-Carmona F (1995) Tyrosinase: a comprehensive review of its mechanism. *Biochim Biophys Acta* **1247:** 1–11.
Seiji M, Sasaki M, Tomita Y (1978) Nature of tyrosinase inactivation in melanosomes. *Tohoku J Exp Med* **125:** 233–245.
Sendovski M, Kanteev M, Shuster Ben-Yosef V, Adir N, Fishman A (2010) Crystallization and preliminary X-ray crystallographic analysis of a bacterial tyrosinase from *Bacillus megaterium*. *Acta Crystallog. Sect F, Struct Biol Cryst Commun* **66:** 1101–1103.
Sendovski M, Kanteev M, Shuster Ben-Yosef V, Adir N, Fishman A (2011) First structures of an active bacterial tyrosinase reveal copper plasticity. *J Mol Biol* **405:** 227–237.
Solomon EI, Sundaram UM, Machonkin TE (1996) Multicopper oxidases and oxygenases. *Chem Rev* **96:** 2563–2606.
Tai SS-K, Lin C-G, Wu M-H, Chang TS (2009) Evaluation of depigmenting activity by 8-hydroxydaidzein in mouse B16 melanoma cells and human volunteers. *Int J Mol Sci* **10:** 4257–4266.
Tomita Y, Seiji M (1977) Inactivation mechanism of tyrosinase in mouse melanoma. *J Dermatol* **4:** 245–249.
Tomita Y, Hariu A, Mizuno C, Seiji M (1980) Inactivation of tyrosinase by dopa. *J Invest Dermatol* **75:** 379–382.
Tudela J, Garcia Canovas F, Varon R, Garcia Carmona F, Galvez J, Lozano JA (1987) Transient-phase kinetics of enzyme inactivation induced by suicide substrates. *Biochim Biophys Acta* **912:** 408–416.
Tyeklar Z, Karlin KD (1989) Copper-dioxygen complexes: A bioionargic challenge. *Acc Chem Res* **22:** 241–248.
Waley S (1980) Kinetics of suicide substrates. *Biochem J* **185:** 771–773.
Waley SG (1985) Kinetics of suicide substrates. Practical procedures for determining parameters. *Biochem J* **227:** 843–849.

SUPPLEMENTARY MATERIAL

Conditions of simulation experiments.

1. Diphenolase activity.

The reaction mechanism of the diphenolase activity of TYR (Scheme I with $[M]_0 = 0$) involves the differential equations as follows:

(a) Formation of dopachrome. No reductant in the assay, $[R]_0 = [NADH]_0 = 0$. The substrate concentrations are considered constant during the assays.

$$[\dot{E}_m] = - k_2[E_m]\,[D] + k_{-2}[E_mD] + k_{7_3}[E_{ox}\text{-}D_1] \quad (1)$$

$$[\dot{E_m}D] = - (k_{3_1} + k_{-2})\,[E_mD] + k_2[E_m]\,[D] + k_{-3_1}[E_mD_1] \quad (2)$$

$$[\dot{E_m - D_1}] = k_{3_1}[E_mD] + k_{-3_2}[E_m\text{-}D_2] - (k_{3_2} + k_{-3_1})\,[E_m\text{-}D_1] \quad (3)$$

$$[\dot{E_m - D_2}] = k_{3_2}[E_m\text{-}D_1] - (k_{3_3} + k_{-3_2})\,[E_m\text{-}D_2] \quad (4)$$

$$[\dot{E}_d] = - k_8[O_2]\,[E_d] + k_{-8}[E_{ox}] + k_{3_3}[E_m\text{-}D_2] \quad (5)$$

$$[\dot{E}_{ox}] = - k_6[E_{ox}]\,[D] + k_8[O_2]\,[E_d] + k_{-6}[E_{ox}D] - k_{-8}[E_{ox}] \quad (6)$$

$$[\dot{E_{ox}}D] = - (k_{-6} + k_{7_1})\,[E_{ox}D] + k_6[E_{ox}]\,[D] + k_{-7_1}[E_{ox}\text{-}D_1] \quad (7)$$

$$[\dot{E_{ox} - D_1}] = k_{7_1}[E_{ox}D] - (k_{7_2} + k^i_{7_2} + k_{-7_1})\,[E_{ox}\text{-}D_1] \quad (8)$$

$$[\dot{E_{ox} - D_2}] = k_{7_2}[E_{ox}\text{-}D_1] - k^i_{7_3}[E_{ox}\text{-}D_2] \quad (9)$$

$$[\dot{E_{ox} - D_3}] = k^i_{7_2}[E_{ox}\text{-}D_1] - k^i_{7_3}[E_{ox}\text{-}D_3] \quad (10)$$

$$[\dot{E}_i] = k^i_{7_3}[E_{ox}\text{-}D_3] \quad (11)$$

$$[\dot{Q}] = k_{3_3}[E_mD] + k_{7_3}[E_{ox}\text{-}D_2] + k^i_{7_3}[E_{ox}\text{-}D_3] - k_9[Q] \quad (12)$$

$$[\dot{DC}] = 0.5\ k_9\,[Q] \quad (13)$$

$$[\dot{O}_2] = 0 \quad (14)$$

$$[\dot{D}] = 0 \quad (15)$$

(b) Disappearance of reductant. Reductant in the assay, $[R]_0 = [NADH]_0$. In the presence of reductant, it is assumed that the *o*-quinone does not evolve towards dopachrome. In addition, it is considered that the oxygen concentration is constant during the assays. The differential equations are the same as in case (a) with the following variations: Eq. (12) becomes Eq. (16), Eq. (15) is eliminated and Eqs. (17-19) are added.

$$[\dot{Q}] = k_{3_3}\,[E_m D] + k_{7_3}\,[E_{ox}\text{-}D_2] + k^i_{7_3}\,[E_{ox}\text{-}D_3] - k_{10}\,[Q]\,[R] \quad (16)$$

$$[\dot{D}] = k_{-2}[E_m D] + k_{-6}[E_{ox} D] - k_2[E_m]\,[D] - k_6[E_{ox}]\,[D] + k_{10}\,[Q]\,[R] \quad (17)$$

$$[\dot{R}] = -\,k_{10}\,[R]\,[Q] \quad (18)$$

$$[\dot{R}_{ox}] = k_{10}\,[R]\,[Q] \quad (19)$$

2. Monophenolase activity.

The reaction mechanism of the monophenolase activity of TYR (Scheme I) involves the differential equations as follows:

(a) Dopachrome formation. No reductant in the assay $[R]_0 = [NADH]_0 = 0$. The monophenol and oxygen concentrations are considered constant during the assays.

$$[\dot{E_m M}] = -\,k_{-1}[E_m M] + k_1[E_m]\,[M] \quad (20)$$

$$[\dot{E}_m] = -\,k_1[M]\,[E_m] - k_2[D]\,[E_m] + k_{-1}[E_m M] + k_{-2}[E_m D] + k_{7_3}\,[E_{ox} D_2] \quad (21)$$

$$[\dot{E_m}\mathrm{D}] = k_2[E_m]\,[\mathrm{D}] + k_{5_4}\,[E_m\text{-}\mathrm{D}_4] + k_{-3_1}\,[E_m\text{-}\mathrm{D}_1] - (k_{-2} + k_{-5_4} + k_{3_1})\,[E_m\mathrm{D}] \quad (22)$$

$$[\dot{E_m}\mathrm{D}_1] = k_{3_1}\,[E_m\mathrm{D}] + k_{5_5}\,[E_m\text{-}\mathrm{D}_3] + k_{-3_2}\,[E_m\text{-}\mathrm{D}_2] - (k_{-3_1} + k_{-5_5} + k_{3_2})\,[E_m\text{-}\mathrm{D}_1] \quad (23)$$

$$[\dot{E_m}\mathrm{D}_2] = k_{3_2}\,[E_m\text{-}\mathrm{D}_1] - (k_{-3_2} + k_{3_3})\,[E_m\text{-}\mathrm{D}_2] \quad (24)$$

$$[\dot{E_m}\mathrm{D}_3] = k_{-5_5}\,[E_m\text{-}\mathrm{D}_1] + k_{5_2}\,[E_{ox}\text{-}\mathrm{M}_1] + k_{-5_3}\,[E_m\text{-}\mathrm{D}_4] - (k_{5_3} + k_{5_5})\,[E_m\text{-}\mathrm{D}_3] \quad (25)$$

$$[\dot{E_m}\mathrm{D}_4] = k_{-5_4}\,[E_m\text{-}\mathrm{D}] + k_{5_3}\,[E_m\text{-}\mathrm{D}_3] - (k_{5_4} + k_{-5_3})\,[E_m\text{-}\mathrm{D}_4] \quad (26)$$

$$[\dot{E_d}] = k_{3_3}\,[E_m\text{-}\mathrm{D}_2] + k_{-8}[E_{ox}] - k_8[\mathrm{O}_2]\,[E_d] \quad (27)$$

$$[\dot{E_{ox}}] = k_8[\mathrm{O}_2]\,[E_d] + k_{-4}[E_{ox}\mathrm{M}] + k_{-6}[E_{ox}\mathrm{D}] - k_{-8}[E_{ox}] - k_4[\mathrm{M}]\,[E_{ox}] - k_6[\mathrm{D}]\,[E_{ox}] \quad (28)$$

$$[\dot{E_{ox}}\mathrm{M}] = k_4[\mathrm{M}]\,[E_{ox}] + k_{-5_1}\,[E_{ox}\text{-}\mathrm{M}_1] - (k_{-4} + k_{5_1})\,[E_{ox}\mathrm{M}] \quad (29)$$

$$[\dot{E_{ox}}\mathrm{M}_1] = k_{5_1}\,[E_{ox}\mathrm{M}] - (k_{-5_1} + k_{5_2})\,[E_{ox}\text{-}\mathrm{M}_1] \quad (30)$$

$$[\dot{E_{ox}}\mathrm{D}] = k_6[\mathrm{D}]\,[E_{ox}] - (k_{-6} + k_{7_1})\,[E_{ox}\mathrm{D}] + k_{-7_1}\,[E_{ox}\text{-}\mathrm{D}_1] \quad (31)$$

$$[\dot{E_{ox}}\mathrm{D}_1] = k_{7_1}\,[E_{ox}\mathrm{D}] - (k^i_{7_2} + k_{7_2} + k_{-7_1})\,[E_{ox}\text{-}\mathrm{D}_1] \quad (32)$$

$$[\dot{E_{ox}}\mathrm{D}_2] = k_{7_2}\,[E_{ox}\text{-}\mathrm{D}_1] - k_{7_3}\,[E_{ox}\text{-}\mathrm{D}_2] \quad (33)$$

$$[\dot{E_{ox}}\mathrm{D}_3] = k^i_{7_2}\,[E_{ox}\text{-}\mathrm{D}_1] - k^i_{7_3}\,[E_{ox}\text{-}\mathrm{D}_3] \quad (34)$$

$$[\dot{E_i}] = k^i_{7_3}\,[E_{ox}\text{-}\mathrm{D}_3] \quad (35)$$

$$[\dot{\mathrm{D}}] = k_{-2}[E_m\mathrm{D}] + k_{-6}[E_{ox}\mathrm{D}] - k_2[\mathrm{D}]\,[E_m] - k_6[\mathrm{D}]\,[E_{ox}] + 0.5\,k_9[\mathrm{Q}] \quad (36)$$

$$[\dot{\mathrm{Q}}] = k_{3_3}\,[E_m\text{-}\mathrm{D}_2] + k_{7_3}\,[E_{ox}\text{-}\mathrm{D}_2] - k_9[\mathrm{Q}] + k^i_{7_3}\,[E_{ox}\text{-}\mathrm{D}_3] \quad (37)$$

$$[\dot{\mathrm{DC}}] = 0.5\,k_9\,[\mathrm{Q}] \quad (38)$$

$$[\dot{\mathrm{M}}] = 0 \quad (39)$$

$$[\dot{O}_2] = 0 \quad (40)$$

(b) Disappearance of reductant. Reductant in the assay, $[R]_0 = [NADH]_0$. It is accepted that in the presence of the reductant, the *o*-quinone does not evolve towards dopachrome. Also, the concentrations of monophenol and oxygen are considered constant during the assays. The differential equations are the same as in case (a), with the following variations: Eq. (36) becomes Eq. (41) and Eq. (37) becomes Eq. (42); Eq. (38) is not considered and Eqs. (43) and (44) are added.

$$[\dot{D}] = k_{-2}[E_m D] + k_{-6}[E_{ox} D] - k_2[D]\,[E_m] - k_6[D]\,[E_{ox}] + k_{10}[Q]\,[R] \quad (41)$$

$$[\dot{Q}] = k_{3_3}[E_m\text{-}D_2] + k_{7_3}[E_{ox}\text{-}D_2] - k_{10}[Q]\,[R] + k^i_{7_3}[E_{ox}\text{-}D_3] \quad (42)$$

$$[\dot{R}] = - k_{10}[Q]\,[R] \quad (43)$$

$$[\dot{R}_{ox}] = k_{10}[Q]\,[R] \quad (44)$$

Kinetic analysis of suicide inactivation of monophenolase and diphenolase activities of tyrosinase.

According to Scheme II, which is the simplified Scheme of Scheme I, the analytical expression for the steady-state rate in the diphenolase activity is:

$$V_0^{DC(D)} = \frac{\alpha_1[O_2]_0[D]_0}{\beta_0 + \beta_1[D]_0 + \beta_2[O_2]_0 + [O_2]_0[D]_0}[E]_0 \quad (45)$$

with

$$\alpha_1 = k_{cat}^D = \frac{k_3 k_{7_1} k_{7_2}}{k_{7_1} k_{7_2} + k_3 k_{7_2} + k_3 k_{7_1}} \quad (46)$$

$$\beta_0 = K^D_{m(ox)} K_S^{O_2} = \frac{k_3 k_{7_2}(k_{-6} + k_{7_1})}{k_6(k_{7_1} k_{7_2} + k_3 k_{7_2} + k_3 k_{7_1})} \frac{k_8}{k_{-8}} \quad (47)$$

$$\beta_1 = K_m^{O_2} = \frac{k_3 k_{7_1} k_{7_2}}{k_8 (k_{7_1} k_{7_2} + k_3 k_{7_2} + k_3 k_{7_1})} \quad (48)$$

$$\beta_2 = K_m^{D} = \frac{k_6 k_{7_1} k_{7_2} (k_{-2} + k_3) + k_2 k_3 k_{7_2} (k_{-6} + k_{7_1})}{k_2 k_6 (k_{7_1} k_{7_2} + k_3 k_{7_2} + k_3 k_{7_1})} \quad (49)$$

When the enzyme is saturated by oxygen, $[O_2]_0 \to \infty$, Eq. (45) is simplified to:

$$V_0^{DC} = \frac{k_{cat}^D [D]_0}{K_m^D + [D]_0} \quad (50)$$

Tyrosinase suffers a suicide inactivation process when it acts on *o*-diphenols, while its reaction product, dopachrome (DC), is accumulated with time according to:

$$[DC]_t^D = [DC]_\infty^D (1 - e^{\lambda_{E_{ox}}^D t}) \quad (51)$$

$[DC]_\infty^D$ and $\lambda_{E_{ox}}^D$ are defined in Eqs. (11) and (12), respectively. At the same time, r_D^{DC} and $\lambda_{E_{ox}(\max)}^D$ are described by Eqs. (13) and (14), respectively.

From data published in the bibliography [11], it can be established that:

$$k_{cat}^D \cong k_{7_1} \quad (52)$$

and

$$K_m^D \cong \frac{k_{7_1}}{k_6} \quad (53)$$

In the same way as for diphenolase activity, the analytical expression for the steady-state rate in the monophenolase activity is:

$$V_0^{DC(M)} = \frac{\alpha_1 [O_2]_0 [D]_0 [M]_0 + \alpha_2 [O_2]_0 [D]_0^2}{\beta_1 [D]_0 + \beta_2 [D]_0 [M]_0 + \beta_3 [D]_0^2 + \beta_4 [O_2]_0 [M]_0 + \beta_5 [O_2]_0 [D]_0 + \\ + \beta_6 [O_2]_0 [M]_0^2 + \beta_7 [O_2]_0 [D]_0 [M]_0 + \beta_8 [O_2]_0 [D]_0^2} [E]_0 \quad (54)$$

with

$$\alpha_1 = k_2 k_3 k_8 k_{7_2} k_5 K_1 (k_{-6} + k_{7_1}) \quad (55)$$

$$\alpha_2 = 2k_2 k_3 k_8 k_6 k_{7_1} k_{7_2} K_4 K_1 \quad (56)$$

$$\beta_1 = k_2 k_3 k_{7_2} k_{-8} K_1 K_4 (k_{-6} + k_{7_1}) \quad (57)$$

$$\beta_2 = k_2 k_3 k_{7_2} k_5 K_1 (k_{-6} + k_{7_1}) \quad (58)$$

$$\beta_4 = k_{-2} k_8 k_{7_2} k_5 (k_{-6} + k_{7_1}) K_1 \quad (59)$$

$$\beta_5 = k_8 k_6 k_{7_1} k_{7_2} K_4 K_1 (k_{-2} + k_3) + k_3 k_2 k_8 k_{7_2} K_4 K_1 (k_{-6} + k_{7_1}) \quad (60)$$

$$\beta_6 = k_{-2} k_8 k_{7_2} k_5 (k_{-6} + k_{7_1}) \quad (61)$$

$$\beta_7 = (k_{-6} + k_{7_1})[(k_2 k_8 k_{7_2} k_5 K_1) + (k_2 k_3 k_8 k_{7_2} K_1)] + k_8 k_6 k_{7_1} k_{7_2} K_4 (k_{-2} + k_3) \quad (62)$$

$$\beta_8 = k_2 k_8 k_6 K_4 K_1 (k_{7_1} k_{7_2} + k_3 k_{7_2} + k_3 k_{7_1}) \quad (63)$$

$$\beta_3 = k_2 k_3 k_6 k_{7_1} k_{7_2} K_4 K_1 \quad (64)$$

When the enzyme is saturated by oxygen, $[\mathrm{O}_2]_0 \to \infty$, Eq. (54) is simplified to:

$$V_0^{\mathrm{DC(M)}} = \frac{\alpha_1 [\mathrm{D}]_0 [\mathrm{M}]_0 + \alpha_2 [\mathrm{D}]_0^2}{\beta_3 [\mathrm{M}]_0 + \beta_4 [\mathrm{D}]_0 + \beta_5 [\mathrm{M}]_0^2 + \beta_6 [\mathrm{D}]_0 [\mathrm{M}]_0 + \beta_7 [\mathrm{D}]_0^2} [E]_0 \quad (65)$$

According to [5], since $[\mathrm{D}]_0 / [\mathrm{M}]_0 = C = \frac{k_5 (k_{-6} + k_{7_1}) k_4}{2k_{7_1} (k_{-4} + k_5) k_6}$, result:

$$V_0^{\mathrm{DC(M)}} = \frac{\alpha_1 C [\mathrm{M}]_0^2 + \alpha_2 C^2 [\mathrm{M}]_0^2}{\beta_3 [\mathrm{M}]_0 + \beta_4 C [\mathrm{M}]_0 + \beta_5 [\mathrm{M}]_0^2 + \beta_6 C [\mathrm{M}]_0^2 + \beta_7 C^2 [\mathrm{M}]_0^2} [E]_0 \quad (66)$$

Thus:

$$V_0^{\mathrm{DC(M)}} = \frac{(\alpha_1 C + \alpha_2 C^2)[\mathrm{M}]_0}{\beta_3 + \beta_4 C + (\beta_5 + \beta_6 C + \beta_7 C^2)[\mathrm{M}]_0} [E]_0 \quad (67)$$

Consequently:

$$V_0^{\mathrm{DC(M)}} = \frac{k_{cat}^{\mathrm{M}} [\mathrm{M}]_0}{K_m^{\mathrm{M}} + [\mathrm{M}]_0} \quad (68)$$

with

$$k_{cat}^{\mathrm{M}} = \frac{\alpha_1 C + \alpha_2 C^2}{\beta_5 + \beta_6 C + \beta_7 C^2} \tag{69}$$

$$K_m^{\mathrm{M}} = \frac{\beta_3 + \beta_4 C}{\beta_5 + \beta_6 C + \beta_7 C^2} \tag{70}$$

Tyrosinase suffers the suicide inactivation process when it acts on monophenols while its reaction product, dopachrome (DC), is accumulated with time according to:

$$[\mathrm{DC}]_t^{\mathrm{M}} = [\mathrm{DC}]_\infty^{\mathrm{M}} (1 - e^{\lambda_{E_{ox}}^{\mathrm{M}} t}) \tag{71}$$

$[\mathrm{DC}]_\infty^{\mathrm{M}}$ and $\lambda_{E_{ox}}^{\mathrm{M}}$ are defined in Eqs. (15) and (16), respectively. At the same time, $r_{\mathrm{M(O)}}^{\mathrm{DC}}$ and $\lambda_{E_{ox}(\max)}^{\mathrm{M}}$ are described by Eqs. (9) and (17), respectively.

From data published in the literature (Fenoll et al., 2001), it can be established that:

$$k_{cat}^{\mathrm{M}} \cong k_5 \tag{72}$$

and

$$K_m^{\mathrm{M}} \cong K_4 \tag{73}$$

REFERENCES

Fenoll LG, Rodriguez-Lopez JN, Garcia-Sevilla F, Garcia-Ruiz PA, Varon R, Garcia-Canovas F, Tudela J. (2001) Analysis and interpretation of the action mechanism of mushroom tyrosinase on monophenols and diphenols generating highly unstable *o*-quinones *Biochim Biophys Acta* **1548:** 1-22.

Legends to figures

Figure 1SM. Simulation of the suicide inactivation of the mechanism proposed for diphenolase activity, Scheme I with $[M]_0 = 0$.

Variation of the enzyme concentration. Formation of DC with time. Inset. (●) Representation of the apparent inactivation constant ($\lambda_{E_{ox}}^{D}$) *vs.* initial enzyme concentration $[E]_0$. (○) Representation of the concentration of product at the end of the reaction, $[DC]_\infty$, *vs.* initial enzyme concentration $[E]_0$. The conditions were: $[O_2]_0$ = 0.26 mM, $[D]_0$ = 1 mM and the enzyme concentrations (nM) [$[E_{ox}]_0 = 0.3[E]_0$, $[E_m]_0 = 0.7[E]_0$] were: (a) 0.01, (b) 0.02, (c) 0.04, (d) 0.06, (e) 0.08, (f) 0.10, (g) 0.12, (h) 0.14, (i) 0.16, (j) 0.18 and (k) 0.2. The rate constants were: k_2 = 10^7 M^{-1} s^{-1}, k_{-2} = 90 s^{-1}, k_{3_1} = 900 s^{-1}, k_{-3_1} = 10 s^{-1}, k_{3_2} = 900 s^{-1}, k_{-3_2} = 10 s^{-1}, k_{3_3} = 900 s^{-1}, k_6 = 5 x 10^5 M^{-1} s^{-1}, k_{-6} = 90 s^{-1}, k_8 = 2.3 x 10^7 s^{-1}, k_{-8} = 1.07 x 10^3 s^{-1}, k_9 = 10 s^{-1}, k_{7_1} = 100 s^{-1}, k_{-7_1} = 1 s^{-1}, k_{7_2} = 107 s^{-1}, k_{7_3} = 1000 s^{-1}, $k_{7_2}^i$ = 2 x 10^{-3} s^{-1}, $k_{7_3}^i$ = 1000 s^{-1}, corresponding to the differential equations of the section A.1 Diphenolase activity. (a) Dopachrome formation. The rate constant values agree with the data given in the literature [37] and must fulfil the kinetic parameter (k_{cat} and K_m).

Figure 2SM. Simulation of suicide inactivation of the mechanism proposed for diphenolase activity, Scheme I with $[M]_0 = 0$.

Variation of the substrate concentration. Formation of DC with time. Inset. Representation of the apparent inactivation constant ($\lambda_{E_{ox}}^{D}$) *vs.* initial substrate concentration, $[D]_0$. Conditions were: $[E]_0$ = 0.2 nM, $[E_{ox}]_0 = 0.3[E]_0$, $[E_m]_0 = 0.7[E]_0$, $[O_2]_0$ = 0.26 mM and the initial concentrations of D (mM) were: (a) 0.1, (b) 0.2, (c) 0.3, (d) 0.4, (e) 0.5, (f) 0.6, (g) 0.8, (h) 1, (i) 1.2, (j) 1.4, (k) 1.6, (l) 1.8,

(m) 2.0, (n) 2.2, (o) 2.4 and (p) 2.6. The rate constants were the same as in Figure 1SM.

Figure 3SM. Simulation of the suicide inactivation of the mechanism proposed for diphenolase activity, Scheme I with $[M]_0 = 0$.

Curve (a), dopachrome DC formation with time in absence of reductant, curve (b), disappearance of reductant, [R], with time. Conditions were: (a) $[E]_0$ = 0.2 nM, $[E_{ox}]_0 = 0.3[E]_0$, $[E_m]_0 = 0.7[E]_0$, $[O_2]_0$ = 0.26 mM, $[D]_0$ = 1 mM. (b) The same as in (a) but with $[R]_0$ = 4 mM. Curve (a), the rate constants and the differential equations were the same as in Figure 1SM. Curve (b), the rate constants were the same as in Figure 1SM and the differential equations were the same as in section: A.1 Diphenolase activity, (b) disappearance of reductant with k_{10} = 5 X 10^5 M^{-1} s^{-1}.

Figure 4SM. Simulation of the suicide inactivation of the mechanism proposed for monophenolase activity, Scheme I.

Variation of enzyme concentration. Formation of dopachrome, DC, with time. Inset. (●) Representation of apparent inactivation constant ($\lambda^{M}_{E_{ox}}$) *vs.* initial enzyme concentration $[E]_0$. (○) representation of the concentration of the product accumulated at the end of the reaction $[DC]_\infty$ *vs.* to initial enzyme concentration, $[E]_0$.The conditions were: $[O_2]_0$ = 0.26 mM, $[D]_0$ = 46 μM, $[M]_0$ = 1.8 mM and the enzyme concentrations (nM) [$[E_{ox}]_0$ = $0.3[E]_0$, $[E_m]_0$ = $0.7[E]_0$] were: (a) 0.005, (b) 0.01, (c) 0.02, (d) 0.03, (e) 0.04, (f) 0.05, (g) 0.06, (h) 0.07, (i) 0.08, (j) 0.09 and (k) 0.1. The rate constants were: k_1 = 2.5 x 10^5 M^{-1} s^{-1}, k_{-1} = 20 s^{-1}, k_2 = 10^7 M^{-1} s^{-1}, k_{-2} = 90 s^{-1}, k_{3_1} = 900 s^{-1}, k_{-3_1} = 10 s^{-1}, k_{3_2} = 900 s^{-1}, k_{-3_2} = 10 s^{-1}, k_{3_3} = 900 s^{-1}, k_8 = 2.3 x 10^7 s^{-1}, k_{-8} = 1.07 x 10^3 s^{-1}, k_9 = 10 s^{-1}, k_6 = 5 x 10^5 M^{-1} s^{-1}, k_{-6} = 90 s^{-1}, k_{7_1} = 100 s^{-1}, k_{-7_1} = 1 s^{-1}, k_{7_2} = 107

s^{-1}, k_{7_3} = 1000 s^{-1}, $k^i_{7_2}$ = 2 x 10^{-3} s^{-1}, $k^i_{7_3}$ = 1000 s^{-1}, k_4 = 5 x 10^4 M^{-1} s^{-1}, k_{-4} = 10 s^{-1}, k_{5_1} = 60 s^{-1}, k_{-5_1} = 1 s^{-1}, k_{5_2} = 60 s^{-1}, k_{5_3} = 60 s^{-1}, k_{-5_3} = 1 s^{-1}, k_{5_4} = 40 s^{-1}, k_{-5_4} = 0.1 s^{-1}, k_{5_5} = 40 s^{-1}, k_{-5_5} = 0.1 s^{-1}. The differential equations were the same as in section: A.2 Monophenolase activity, (a) dopachrome formation. The rate constant values agree with the data given in the literature [37] and must fulfil the kinetic parameter (k_{cat} and K_m).

Figure 5SM. Simulation of the suicide inactivation of the mechanism proposed for monophenolase activity, Scheme I.

Variation of the substrate concentration. Formation of dopachrome with time. Inset. Representation of the apparent inactivation constant ($\lambda^{\mathrm{M}}_{E_{ox}}$) *vs.* initial substrate concentration, $[\mathrm{M}]_0$. The conditions were: $[E]_0$ = 0.1 nM, $[[E_{ox}]_0 = 0.3[E]_0$, $[E_m]_0 = 0.7[E]_0]$, $[\mathrm{O_2}]_0$ = 0.26 mM and the initial monophenol concentrations (mM) were: (a) 0.1, (b) 0.2, (c) 0.3, (d) 0.4, (e) 0.5, (f) 0.6, (g) 0.8, (h) 1.0, (i) 1.2, (j) 1.4, (k) 1.6, (l) 1.8, (m) 2.0, (n) 2.2, (o) 2.4 and (p) 2.6. *o*-Diphenol was added at t = 0 so that the *o*-diphenol concentration in the steady-state, $[\mathrm{D}]_{ss}$, *vs.* the monophenol concentration, $[\mathrm{M}]_{ss}$, fulfils the relation: $[\mathrm{D}]_{ss}/[\mathrm{M}]_{ss} = C$ = 0.046. The rate constants and the differential equations were the same as in Figure 4SM.

Figure 6SM. A. Simulation of the suicide inactivation of the mechanism proposed for monophenolase activity, Scheme I.

Curve (a), disappearance of reductant, [R], with time. The conditions were: $[E]_0$ = 10 nM, $[[E_{ox}]_0 = 0.3[E]_0$, $[E_m]_0 = 0.7[E]_0]$, $[\mathrm{O_2}]_0$ = 0.26 mM, $[\mathrm{M}]_0$ = 1.5 mM, $[\mathrm{D}]_0$ = 69 μM and $[\mathrm{R}]_0$ = 4 mM. The differential equations were the same as in section: A.2 Monophenolase activity. (b) disappearance of reductant but with k_{10} = 5 x 10^5 M^{-1} s^{-1}.

Curve (b), dopachrome formation, DC, with time in absence of reductant. The differential equations were the same as in section: A.2 Monophenolase activity. (a) dopachrome formation.

B. Simulation of the suicide inactivation of the mechanism proposed for monophenolase activity, Scheme I. Curve (a), accumulation of *o*-diphenol (D) with time in presence of reductant. The conditions were the same as in curve (a) in Figure 6ASM. Curve (b), accumulation of *o*-diphenol (D) with time in absence of reductant. Conditions were the same as in curve (b) in Figure 6ASM.

C. Simulation of the suicide inactivation of the mechanism proposed for monophenolase activity, Scheme I. Curve (a), accumulation of inactive enzyme with time in the presence of reductant. The conditions were the same as in curve (a) of Figure 6ASM. Curve (b), accumulation of inactive enzyme with time in the absence of reductant. The conditions were the same as in curve (b), of Figure 6ASM.

Scheme ISM. Structural mechanism proposed to explain the diphenolase, monophenolase and suicide inactivation pathways of tyrosinase during its action on dopa and tyrosine enantiomers.

E_m, *met*-tyrosinase; E_d, *deoxy*-tyrosinase; E_{ox}, *oxy*-tyrosinase; $E_{ox}\mathrm{D}$, *oxy*-tyrosinase/*o*-diphenol complex; $(E_{ox}\text{-}\mathrm{D})_1$, *oxy*-tyrosinase/*o*-diphenol complex axially bound to a Cu atom; $(E_{ox}\text{-}\mathrm{D})_2$, *oxy*-tyrosinase/*o*-diphenol complex axially bound to the two Cu atoms; $(E_{ox}\text{-}\mathrm{D})_3$, *oxy*-tyrosinase/*o*-diphenol complex axially bound to one Cu atom and the deprotonated hydroxyl group of C-2; $E_m\mathrm{D}$, *met*-tyrosinase/*o*-diphenol complex; $(E_m\text{-}\mathrm{D})_1$, *met*-tyrosinase/*o*-diphenol complex axially bound to a Cu atom; $(E_m\text{-}\mathrm{D})_2$, *met*-tyrosinase/*o*-diphenol complex axially bound to the two Cu atoms; $(E_m\text{-}\mathrm{D})_3$, *met*-tyrosinase/*o*-diphenol complex axial-equatorially bound to the two Cu

atoms; $(E_m\text{-D})_4$, *met*-tyrosinase/*o*-diphenol complex equatorially bound to a Cu atom; $E_m\text{M}$, *met*-tyrosinase/monophenol complex; $E_{ox}\text{M}$, *oxy*-tyrosinase/monophenol complex; $(E_{ox}\text{-M})_1$, *oxy*-tyrosinase/monophenol complex axially bound to a Cu atom.

$\text{R} = \text{-CH}_2\text{-CH-(NH}_3^+\text{)-COO}^-$

SCHEMES

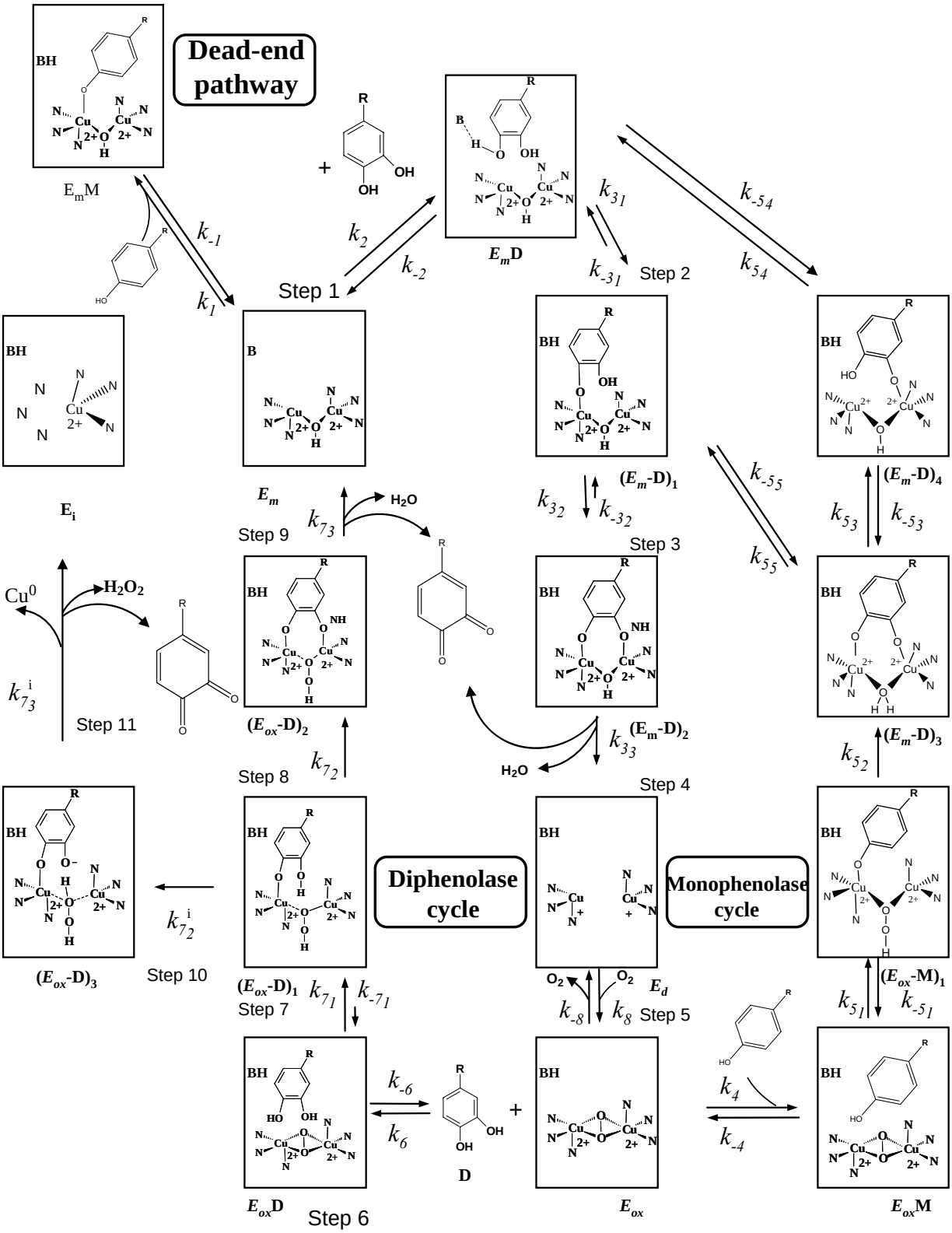

-Scheme ISM-

FIGURES

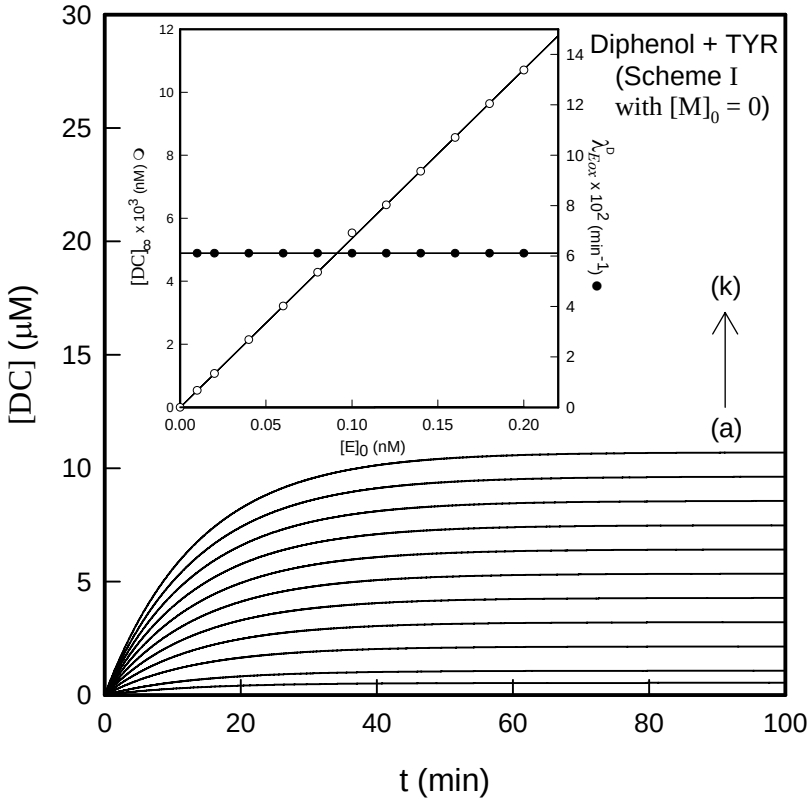

Fig. 1SM

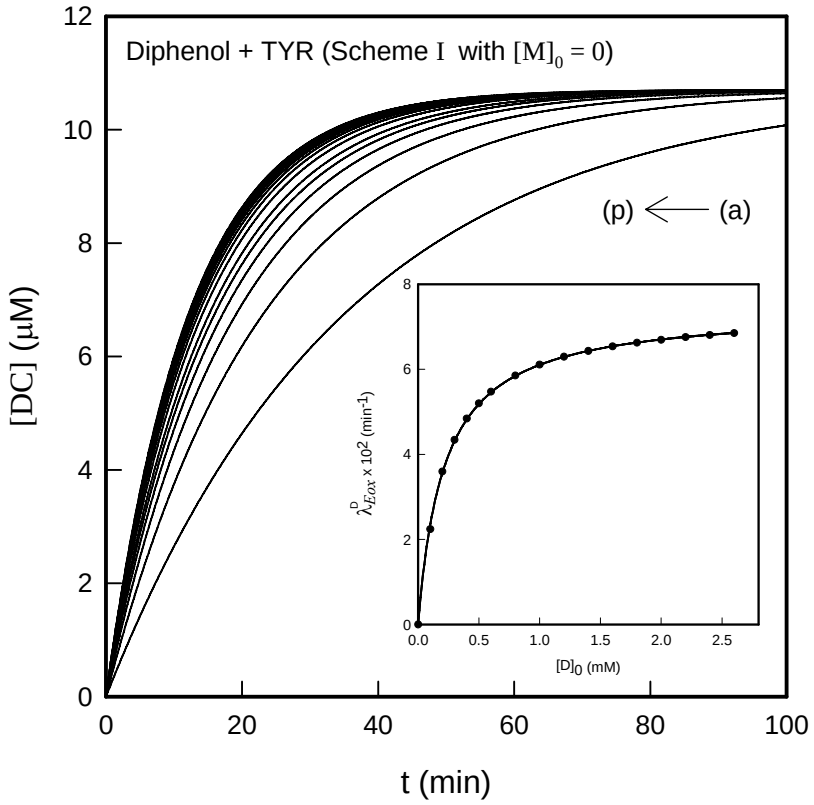
Diphenol + TYR (Scheme I with [M]0 = 0)
(p) ⟵ (a)
[DC] (μM)
t (min)
0
2
4
6
8
10
12
0
20
40
60
80
100
$\lambda^{D}_{Eox} \times 10^2$ (min^{-1})
[D]0 (mM)
0.0
0.5
1.0
1.5
2.0
2.5

Fig. 2SM

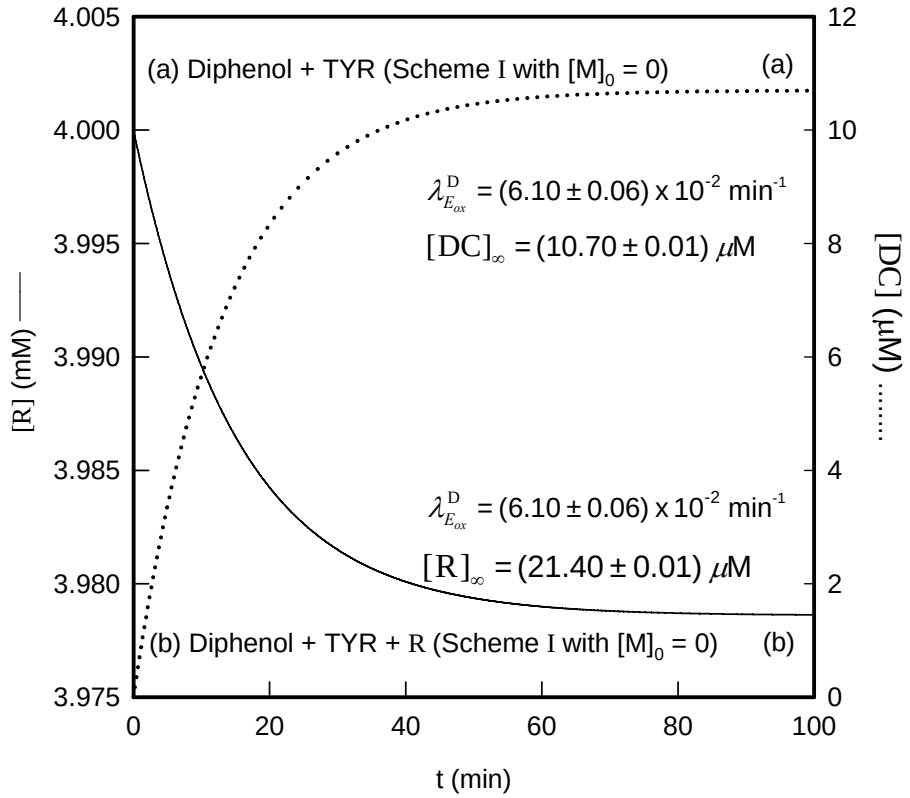
4.005
4.000
3.995
3.990
3.985
3.980
3.975
[R] (mM) ——
12
10
8
6
4
2
0
[DC] (μM) .....
0
20
40
60
80
100
t (min)
(a) Diphenol + TYR (Scheme I with [M]0 = 0)
(a)
$\lambda^{D}_{E_{ox}}$ = (6.10 ± 0.06) x 10-2 min-1
[DC]∞ = (10.70 ± 0.01) μM
$\lambda^{D}_{E_{ox}}$ = (6.10 ± 0.06) x 10-2 min-1
[R]∞ = (21.40 ± 0.01) μM
(b) Diphenol + TYR + R (Scheme I with [M]0 = 0)
(b)

Fig. 3SM

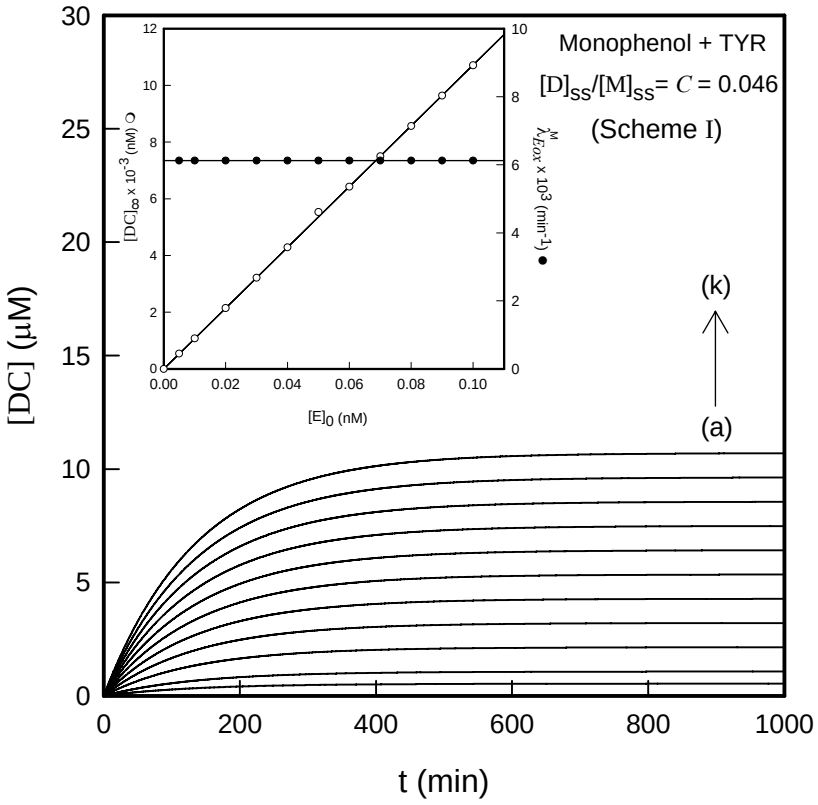
Monophenol + TYR
[D]SS/[M]SS= C = 0.046
(Scheme I)
(k)
(a)
[DC] (μM)
t (min)
[E]0 (nM)
[DC]∞ x 10-3 (nM) ○
λMEox x 10³ (min-1) ●

Fig. 4SM

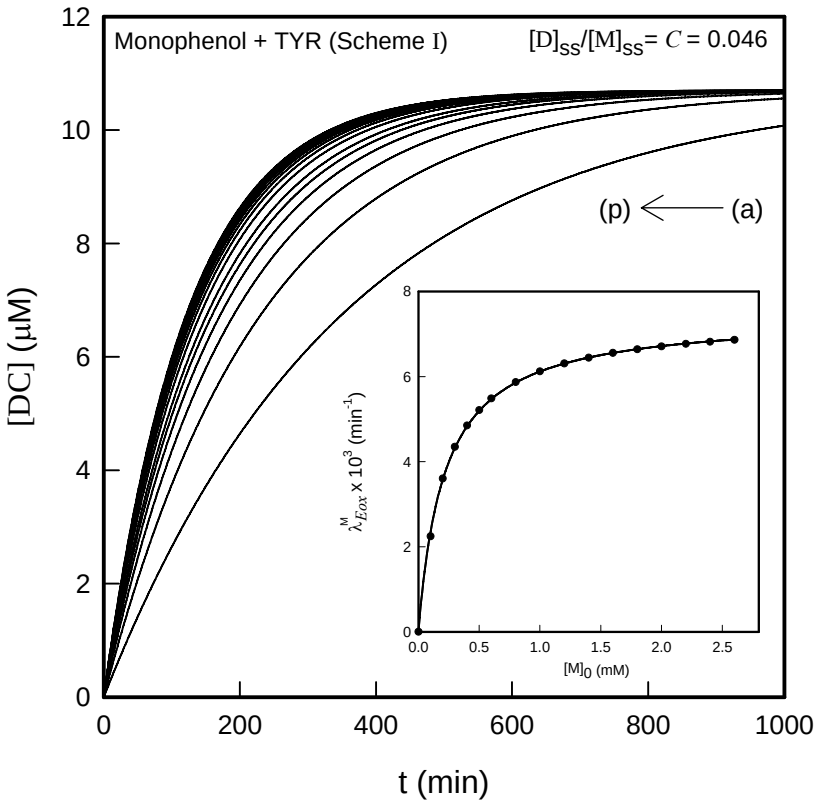
Monophenol + TYR (Scheme I)
[D]SS/[M]SS= C = 0.046
(p) ← (a)
[DC] (μM)
t (min)
0
2
4
6
8
10
12
0
200
400
600
800
1000
λ^{M}_{Eox} x 10^{3} (min^{-1})
[M]0 (mM)
0.0
0.5
1.0
1.5
2.0
2.5

Fig. 5SM

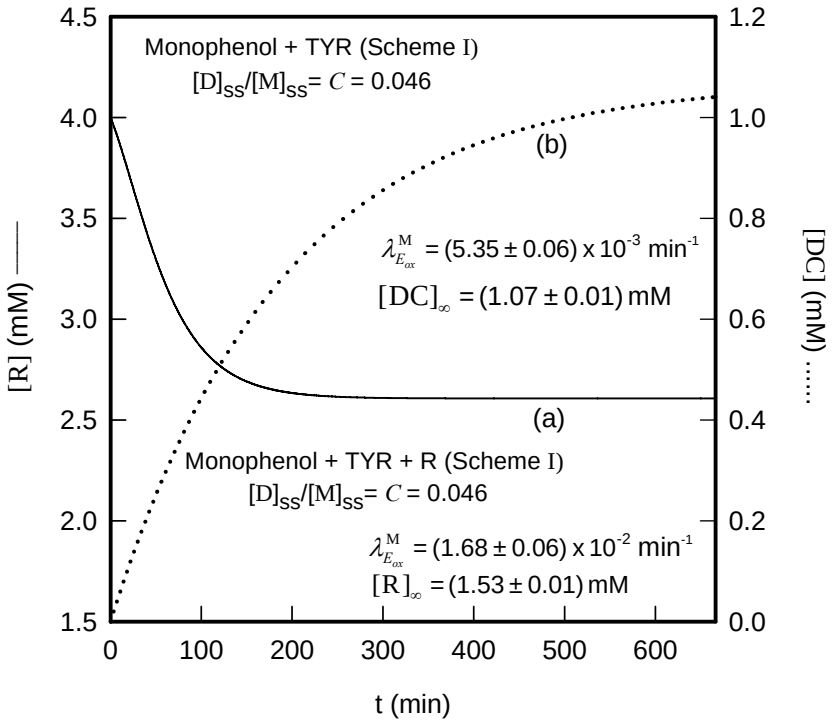
Monophenol + TYR (Scheme I)
[D]SS/[M]SS= C = 0.046
(b)
λ^M_Eox = (5.35 ± 0.06) x 10-3 min-1
[DC]∞ = (1.07 ± 0.01) mM
(a)
Monophenol + TYR + R (Scheme I)
[D]SS/[M]SS= C = 0.046
λ^M_Eox = (1.68 ± 0.06) x 10-2 min-1
[R]∞ = (1.53 ± 0.01) mM
[R] (mM) ——
..... [DC] (mM)
t (min)
4.5
4.0
3.5
3.0
2.5
2.0
1.5
1.2
1.0
0.8
0.6
0.4
0.2
0.0
0
100
200
300
400
500
600

Fig. 6ASM

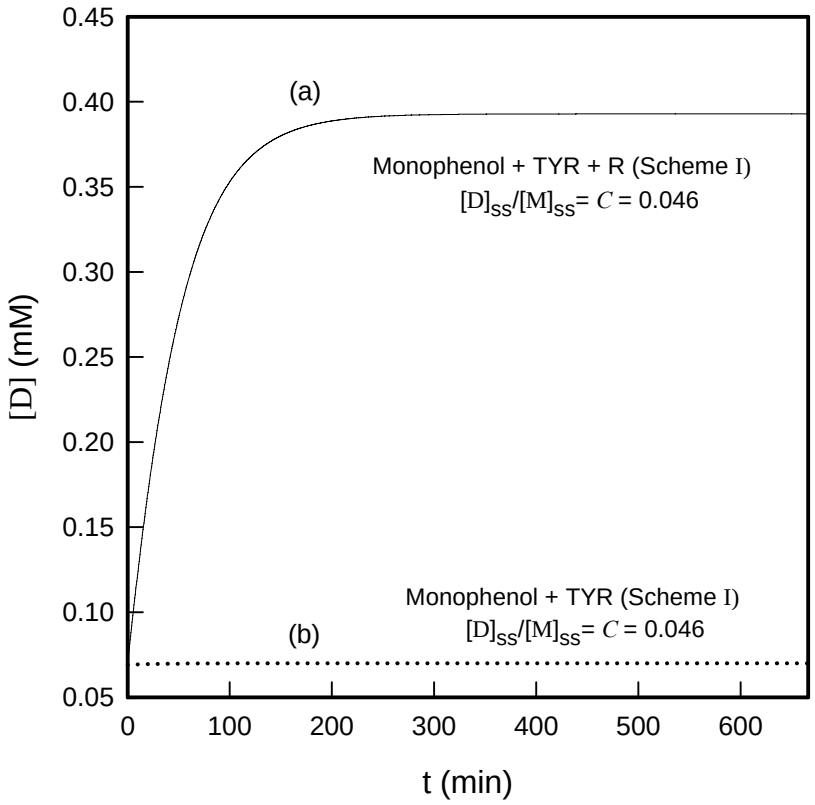
0.45
0.40
0.35
0.30
0.25
0.20
0.15
0.10
0.05
[D] (mM)
0
100
200
300
400
500
600
t (min)
(a)
Monophenol + TYR + R (Scheme I)
[D]SS/[M]SS= C = 0.046
(b)
Monophenol + TYR (Scheme I)
[D]SS/[M]SS= C = 0.046

Fig. 6BSM

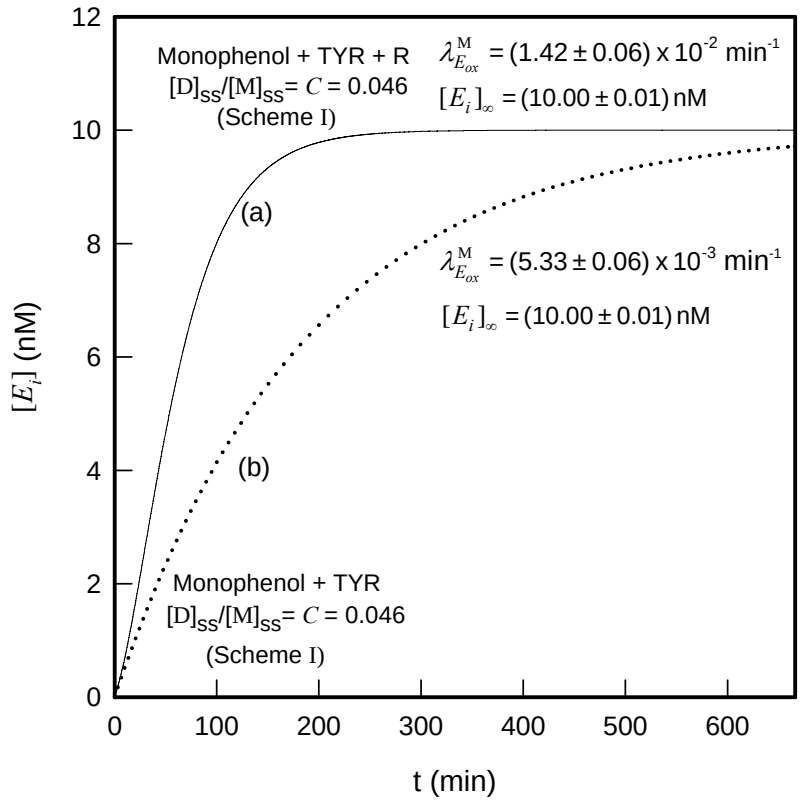
Monophenol + TYR + R
[D]SS/[M]SS= C = 0.046
(Scheme I)
$\lambda_{E_{ox}}^{M}$ = (1.42 ± 0.06) x 10-2 min-1
$[E_i]_\infty$ = (10.00 ± 0.01) nM
(a)
$\lambda_{E_{ox}}^{M}$ = (5.33 ± 0.06) x 10-3 min-1
$[E_i]_\infty$ = (10.00 ± 0.01) nM
(b)
Monophenol + TYR
[D]SS/[M]SS= C = 0.046
(Scheme I)
$[E_i]$ (nM)
t (min)
0
2
4
6
8
10
12
0
100
200
300
400
500
600

Fig. 6CSM

4.18. INACTIVACIÓN ESTEREOESPECÍFICA DE TIROSINASA POR ÁCIDO L- Y D-ASCÓRBICO.

El estudio de la inactivación estereoespecífica de tirosinasa por los ácidos L- y D-ascórbico ha dado lugar a la siguiente publicación adjunta.

4.18.1. Título

Stereospecific inactivation of tyrosinase by L- and D-ascorbic acid.

4.18.2. Autores

Muñoz-Muñoz, J.L.; Garcia-Molina, F.; Varon, R.; Garcia-Ruiz, P.A.; Tudela, J.; Garcia-Cánovas, F. y Rodríguez-López, J.N.

4.18.3. Referencia

Biochimica et Biophysica Acta-Protein and Proteomics (2009) 1794, 244-253.

4.18.4. Resumen

Se ha estudiado cinéticamente la inactivación de tirosinasa por los isómeros L y D del ácido ascórbico. En condiciones aerobias, ocurre un mecanismo de inactivación suicida, el cual fue atribuido a la forma enzimática oxitirosinasa. Esta inactivación suicida es estereoespecífica con respecto a la afinidad de la enzima por el sustrato pero no lo es respecto a la velocidad del proceso, el cual es el mismo para ambos isómeros, reflejando la influencia del desplazamiento químico del carbono C-2 (δ_2) y C-3 (δ_3) obtenidos por ^{13}C-RMN. La inactivación en condiciones anaeróbicas de las formas desoxitirosinasa y metatirosinasa, es una inhibición irreversible y más rápida que el proceso de inactivación suicida. Así, se pone de manifiesto que la presencia de oxigeno protege a la enzima de la inactivación.

Biochimica et Biophysica Acta 1794 (2009) 244–253

Contents lists available at ScienceDirect

Biochimica et Biophysica Acta

journal homepage: www.elsevier.com/locate/bbapap

Stereospecific inactivation of tyrosinase by L- and D-ascorbic acid

Jose Luis Munoz-Munoz [a], Francisco Garcia-Molina [a], Pedro Antonio García-Ruiz [b], Ramon Varon [c], Jose Tudela [a], Francisco García-Cánovas [a,*], Jose Neptuno Rodriguez-Lopez [a]

[a] GENZ: Grupo de Investigación de Enzimología, Departamento de Bioquímica y Biología Molecular-A, Facultad de Biología, Universidad de Murcia, E-30100, Espinardo, Murcia, Spain
[b] Departamento de Quimica Orgánica. Facultad de Quimica, E-0100, Universidad de Murcia, Espinardo, Murcia, Spain
[c] Departamento de Química-Física. Escuela Politécnica Superior. Universidad de Castilla la Mancha. Avda. España s/n. Campus Universitario, E-02071, Albacete, Spain

ARTICLE INFO

Article history:
Received 27 June 2008
Received in revised form 30 September 2008
Accepted 16 October 2008
Available online 29 October 2008

Keywords:
Ascorbic acid
Mushroom tyrosinase
Suicide
Irreversible
Inactivation

ABSTRACT

A kinetic study of the inactivation of tyrosinase by L- and D-ascorbic acid isomers has been carried out. In aerobic conditions, a suicide inactivation mechanism operates, which was attributed to the enzymatic form *oxy*tyrosinase. This suicide inactivation is stereospecific as regards the affinity of the enzyme for the substrate but not as regards the speed of the process, which is the same for both isomers, reflecting the influence of the chemical shift of the carbon C-2 (δ_2) and C-3 (δ_3) as seen by ^{13}C-NMR. The inactivation of *deoxy*tyrosinase and *met*tyrosinase observed in anaerobic conditions, is irreversible and faster than the suicide inactivation process, underlining the fact that the presence of oxygen protects the enzyme against inactivation.

© 2008 Elsevier B.V. All rights reserved.

1. Introduction

Enzymatic browning in fruits and vegetables is one of the most serious alteration processes for the food industry, where, it has been estimated, about 50% of economic losses are due to this phenomenon [1]. The control and prevention of this undesirable process is the key for minimising these losses and for prolonging the shelf life of these fresh products. The most important reactions intervening in browning are enzymatic processes catalysed mainly by peroxidases and, especially, polyphenol oxidases [2].

Polyphenol oxidase or tyrosinase (EC 1.14.18.1) is present in the tissues of plants and is widely distributed through the animal, vegetal and fungal kingdoms. tyrosinase has two coppers in its active site, which may be in three coordination states or forms: (*i*) Cu^{2+}–Cu^{2+}, *met*-tyrosinase, (*ii*) Cu^{2+}–O_2^{2-}–Cu^{2+} with a peroxide group in its active site, *oxy*-tyrosinase or (*iii*) Cu^{1+}–Cu^{1+}, *deoxy*-tyrosinase [3]. Tyrosinase catalyses two types of reaction in which molecular oxygen intervenes: (a) the hydroxylation of the monophenols to *o*-diphenols (monophenolase activity) and (b) the oxidation of *o*-diphenols to *o*-quinones (diphenolase activity) which, in turn, are polymerized to brown, red or black pigments [4,5]. Moreover, this enzyme is of central importance in vertebrate pigmentation. It is directly responsible for the conversion of the amino acid, L-tyrosine, to one of several types of melanin pigment [6].

Due to poor specificity of tyrosinase for phenolic substrates and for oxidisable compounds in general, several catalytic activities have been described for this enzyme, including catalase [7,8] or ascorbate oxidase [9–11].

Several strategies are being used to minimize or reduce tyrosinase-catalyzed browning in fruits and vegetables. For example, several inhibitors of this enzyme and/or antioxidants have been added [12]. Many inhibitors of enzymatic browning have been described, including 4-hexylresorcinol [13] and ascorbic acid itself (Scheme 1) [14]. However, the reaction mechanisms of these compounds still have to be elucidated. There has also been much discussion concerning the role of ascorbic acid as inhibitor/inactivator. For example, it has been suggested that it acts as an antioxidant, reducing the *o*-quinones generated by tyrosinase back to the initial *o*-diphenols, or that it interacts directly with the active site of the enzyme, thereby inactivating it [14,15]. Studies carried out in our laboratory several years ago pointed to the role of ascorbic acid as alternative substrate of tyrosinase, thus influencing melanogenesis [9,10].

In the present work, we attempt to ascertain whether ascorbic acid is a substrate that can inactivate tyrosinase. We propose mechanisms to explain the inactivation of the different enzymatic species of tyrosinase in both aerobic and anaerobic conditions. The kinetic analysis of the mechanism in aerobic conditions provides explicit equations for oxygen consumption with time, from which an experimental design can be described which permits the kinetic characterisation of the enzyme's action on the possible inactivating substrate. The mechanism is based on that previously proposed to

* Corresponding author. Fax: +34 968 363963.
E-mail address: canovasf@um.es (F. García-Cánovas).
URL: http://www.um.es/genz (F. García-Cánovas).

1570-9639/$ – see front matter © 2008 Elsevier B.V. All rights reserved.
doi:10.1016/j.bbapap.2008.10.002

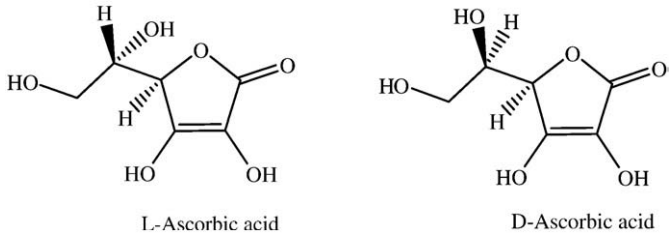

Scheme 1. Chemical structures of L- and D-ascorbic acid.

explain the suicide inactivation of tyrosinase as it acts on phenolic substrates [16]. Applying the same methodology, the stereospecificity of the enzyme in this process is studied, using the isomers L and D-ascorbic acid. The kinetic analysis of the mechanisms in anaerobic conditions provides explicit equations for the residual activity *vs.* time, from which the experimental design permits the kinetic characterisation of these inactivation processes.

1.1. Abbreviations

For clarity and for the sake of brevity, the following abbreviations will be used in the text.

Species and concentrations

E_m	*met*-tyrosinase.
$[E_m]_0$	initial concentration of *met*-tyrosinase
E_d	*deoxy*-tyrosinase.
$[E_d]$	instantaneous concentration of *deoxy*-tyrosinase.
$[E_d]_0$	initial concentration of *deoxy*-tyrosinase.
E_{ox}	*oxy*-tyrosinase.
E_mS	*met*-tyrosinase/substrate complex (diaxial).
$E_{ox}S$	*oxy*-tyrosinase/substrate complex.
$(E_{ox}-S)_1$	*oxy*-tyrosinase/substrate complex axially bound to a Cu atom.
$(E_{ox}-S)_2$	*oxy*-tyrosinase/substrate complex axially bound to two Cu atoms.
$(E_{ox}-S)_3$	*oxy*-tyrosinase/substrate complex axially bound to one Cu atom and the deprotonated hydroxyl group of C-3.
E_i	inactive enzyme originated by suicide inactivation.
E_{di}	inactive enzyme resulting from denaturalisation of E_d in anaerobic conditions.
E_{dSi}	inactive enzyme obtained by irreversible inhibition of E_d and E_m by L- and D-ascorbic acid.
$[E]_0$	initial concentration of tyrosinase.
E_a	active enzyme.
$[E_a]$	instantaneous concentration of E_a.
$L\text{-}AH_2$	L-ascorbic acid.
$D\text{-}AH_2$	D-ascorbic acid.
S	L-ascorbic acid ($L\text{-}AH_2$) or D-ascorbic acid ($D\text{-}AH_2$) acting as suicide substrate.
$[S]_0$	initial concentration of substrate.
P	Product of the enzymatic reaction, dehydroascorbic acid (*L-A*, *D-A*).
$[P]_\infty$	Product concentration at $t \to \infty$.
PPO	tyrosinase or polyphenol oxidase.
$[O_2]$	instantaneous concentration of oxygen.
$[O_2]_0$	initial concentration of oxygen.
$[\dot{O}_2]$	instantaneous rate of the variation of $[O_2]$.
$[O_2]_f$	Oxygen remaining at $t \to \infty$.
$[O_2]_\infty$	Oxygen consumed at $t \to \infty$. $[O_2]_\infty = [O_2]_0 - [O_2]_f$
$[E_S]$	total concentration of set of enzyme species involved in a restricted steady–state, Schemes 2 and 3, i.e.: $[E_S]=[E_m]+[E_mS]+[E_d]+[E_{ox}]+[E_{ox}S]+[(E_{ox}-S)_1]+[(E_{ox}-S)_2]$.
$[\dot{E}_s]$	instantaneous rate of the variation of $[Es]$.
$f_{(E_{ox}-S)_1}$	concentration factor corresponding to enzyme species $(E_{ox}-S)_1$ with regard to E_s : $f_{(E_{ox}-S)_1} = \frac{[(E_{ox}-S)_1]}{[E_s]}$.

Kinetic parameters

λ	apparent inactivation constant.
λ^d	apparent inactivation constant of E_d.
λ^m	apparent inactivation constant of E_m.
λ^{ox}	apparent inactivation constant of E_{ox}.
k_d^d	inactivation constant of E_d in anaerobic conditions.
k_i^d	inactivation constant of E_dS.
K_9	dissociation constant of E_dS complex.
$V_0^{O_2}$	initial rate of the catalytic pathway.
k_x	rate constants of the catalytic pathway (Scheme 2).
k_{7_1}	substrate binding constant to copper atom through C-2 hydroxyl (axial).
k_{7_2}	substrate binding constant to copper atom through C-3 hydroxyl (axial).
k_x^i	rate constants of the inactivation pathway (Scheme 2).
$k_{7_2}^i$	rate constant of transfer of a H^+ to the protonated peroxide.
k_{7_3}	rate constant of substrate oxidation through complex $(E_{ox}-S)_2$.
$k_{7_3}^i$	inactivation constant.
r	partition ratio $r=k_{7_2}/k_{7_2}^i=k_{cat}/\lambda_{max}^{ox}$.
K^{O_2}	dissociation constant of E_{ox}.
$K_m^{O_2}$	Michaelis constant of oxygen.
$K_{m_1}^S$	Michaelis constant of *met*–tyrosinase for *S*.
$K_{m_2}^S$	Michaelis constant of *oxy*–tyrosinase for *S*.
K_m^S	Michaelis constant of tyrosinase for *S*.
k_{cat}	catalytic constant of the catalytic pathway ($k_{cat}=\lambda_{max}^{ox}r$).
λ_{max}^{ox}	maximum value of λ^{ox} for saturating *S*.
$V_{max}^{O_2}$	maximum value of $V_0^{O_2}$ for saturating *S*.

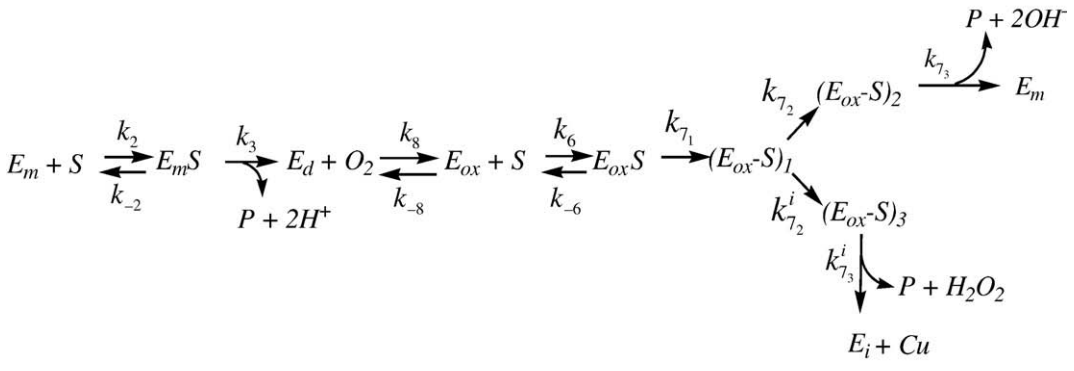

Scheme 2. Kinetic mechanism proposed to explain the suicide inactivation of tyrosinase acting on ascorbic acid.

$$E_i + 2P + 2H^+ + H_2O_2 + Cu \xleftarrow{k^i_{7_2} f_{(E_{ox}-S)_1}} E_s \xrightarrow{2k_{7_2} f_{(E_{ox}-S)_1}} 2P + 2H^+ + 2OH$$

Scheme 3. Simplified scheme of the mechanism described in Scheme 2.

$\frac{\lambda^{ox}_{max}}{K^S_m}$ inactivation efficiency induced by the substrate *S*.

$\frac{k_{cat}}{K^S_m}$ catalytic efficiency induced by the substrate *S*.

2. Materials and methods

2.1. Reagents

Mushroom tyrosinase or polyphenoloxidase (PPO; *o*-diphenol: O_2 oxidorreductase, EC 1.14.18.1, 8300 units/mg), superoxide dismutase (SOD: EC 1.15.1.1, 4140 units/mg) and catalase (EC 1.11.1.6, 9300 units/mg) were supplied by Sigma Chemical (St. Louis, MO). Tyrosinase was purified as previously described [17]. The protein concentration was determined by the Bradford's method [18] and using bovine serum albumin as the standard. The substrates used were: L-ascorbic acid (*L-AH*$_2$), D-ascorbic acid (*D-AH*$_2$) (the corresponding structures are shown in Scheme 1) and hydrogen peroxide, all supplied by Scharlau (Madrid, Spain). 4-*tert*-butylcatechol (*TBC*) was supplied by Acros Co. (Madrid, Spain), and tropolone by Aldrich (Switzerland). Other chemicals were of analytical grade and supplied by Merck (Dardmstadt, Germany).

2.2. Oxymetric assays

Measurements of dissolved oxygen concentration were made with a Hansatech (Kings Lynn, Cambs, U.K.) oxygraph unit controlled by a PC. The oxygraph used a Clark-type silver/platinum electrode with a 12.5 μm Teflon membrane. The sample was continuously stirred during the experiments and its temperature was maintained at 25 °C. The zero oxygen level for calibration and experiments was obtained by bubbling oxygen-free nitrogen through the sample for at least 10 min. The kinetic assays to study suicide inactivation used an oxymetric method. The oxygraph was calibrated as described in [19].

The effects of various ascorbic acid concentrations were studied. Their concentrations are given in detail in the corresponding figures of the Results and discussion section. In all suicide inactivation assays, the following reagents were maintained constant: 0.26 mM O_2 (saturating) and 1.2 μM SOD.

2.3. Data analysis

Since the reaction catalyzed by tyrosinase is bisubstrate (O_2 and *L-AH*$_2$ or *D-AH*$_2$), the disappearance of O_2 can be followed experimentally. The experimental data for the disappearance of O_2 with time follow the equation:

$$[O_2] = c_1 + c_2 e^{-e_3 t} - c_4 t = [O_2]_f + [O_2]_\infty e^{-\lambda^{ox} t} - c_4 t \quad (1)$$

which parameters can be obtained by non-linear regression [20].

The parameter c_4 corresponds to the slow spontaneous oxidation of *AH*$_2$. The effects of this experimental artefact (Fig. 1) should be computer subtracted in further O_2 *vs.* time plots. The introduction of a second exponential term in Eq. (1) does not significantly improve fitting, as revealed by the good discrimination criterion between alternative models [21]. The experimental recording obtained in the following steps therefore fit Eq. (1), from which the corresponding inactivation parameters, $[O_2]_\infty$ and λ^{ox}, can be determined.

2.4. ^{13}C-NMR

For the substrates used, the ^{13}C-NMR spectra were obtained in deuterated water pH 7.0, providing the shifts of the C-2 (δ^7_2) and C-3 (δ^7_3) carbons for the different isomers. The ^{13}C-NMR spectra of the different isomers considered here were obtained in a 300 MHz Varian Unity spectrometer. The δ values were measured relative to those for tetramethylsilane (δ=0). The maximum line breadth accepted in the ^{13}C-NMR spectra was 0.06 Hz. Therefore, the maximum accepted error for each peak was ±0.03 ppm. Moreover, the electron-donating capacity of the oxygen atom from different phenolic compounds (nucleophilic power) was correlated with the experimental δ values in ^{13}C-NMR for the carbon atom that supports the hydroxyl group [22]. Taking all the above into account, low values of δ^7_2 and δ^7_3 in ^{13}C-NMR indicate high nucleophilic power at pH 7.0 [23].

2.5. Generation of E_{ox} and E_d

As in the case of E_{ox}, we set out to kinetically characterise the inactivation of the E_d form of tyrosinase. E_d was generated from the native enzyme, adding micromolar concentrations (2 μM) of H_2O_2 so that the E_m form passed to E_{ox}. Then nitrogen was bubbled through the solution transforming all the E_{ox} to E_d ($E_{ox} \rightleftarrows E_d + O_2$) [24,25].

2.6. Generation of E_m

The inactivation of E_m was characterised by first generating it from the native enzyme in two ways: (a) adding 2 μM catalase, so that $E_{ox} \rightleftarrows E_m + H_2O_2$; catalase acts on the H_2O_2 displacing the equilibrium, $2H_2O_2$ + catalase → $O_2 + 2H_2O$, so that E_{ox} is transformed into E_m. (b) Adding 2 μM of H_2O_2, so that all the enzyme passes to E_{ox} and then adding 2 μM catalase [24,25].

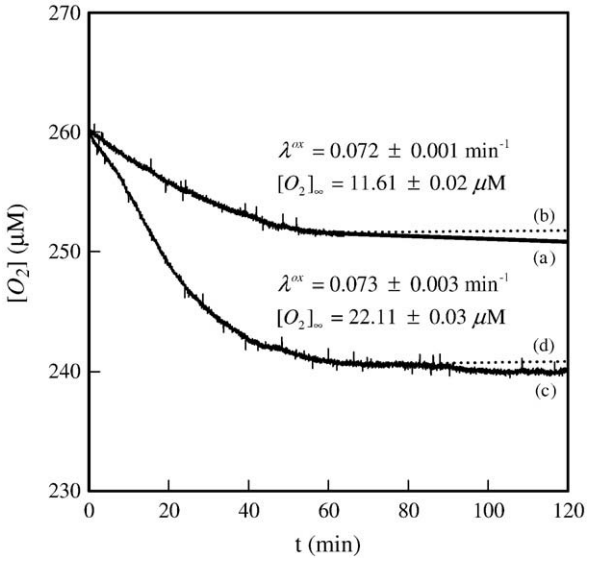

Fig. 1. Experimental recordings of the disappearance of O_2 in the suicide inactivation of tyrosinase by *L-AH*$_2$ and curves corrected after applying the data analysis. Conditions were 30 mM phosphate buffer pH 7.0, $[O_2]_0$ 0.26 mM, $[SOD]_0$ 1.2 μM and $[L\text{-}AH_2]_0$ 14 mM. The enzyme concentrations were: (a) 40 nM and (c) 60 nM. Curves (b) and (d) are the corrected recordings from (a) and (c), respectively.

2.7. Evaluation of enzymatic species E_m, E_d and E_{ox} in an enzymatic preparation of tyrosinase

It is known that in an enzymatic preparation of tyrosinase from any source is found in three forms, E_m, E_d and E_{ox} [24]. Several authors have proposed spectrophotometric methods for evaluating these forms [24–27]. Here, we propose a kinetic method based on the fact that the inactivation of these forms by 2-mercaptoethanol [28] occurs over a wide time range: inactivation constants of 0.014 s^{-1}, 4×10^{-5} s^{-1} and 1×10^{-5} s^{-1} for E_{ox}, E_m and E_d, respectively. In aerobic conditions at oxygen concentrations of 0.26 mM, practically the only forms existing are E_{ox} and E_m [17]. Note that the difference between k_i^{ox} and k_i^m is three orders of magnitude, a difference that can be used to evaluate these enzymatic forms.

The experimental method consists of preincubating the enzyme in aerobic conditions with 2-mercaptoethanol at a concentration of 10 μM. Aliquots are taken at different reaction times and the residual activity corresponding to *TBC* is measured. In this way, at sufficiently long times, a situation is reached in which the activity tends asymptotically to a constant value. The decrease in the initial activity to reach this approximately constant final value would correspond to the concentration of E_{ox} in the medium. In this way, inactivation assays of the enzyme sample previously incubated with different concentrations of H_2O_2 in the μM order are made with 2-mercaptoethanol. This gives rise to different concentrations of E_{ox} and therefore different levels of activity in the linear zone (see Results and discussion). The representation of the decrease in activity corresponding to E_{ox} versus residual activity (corresponding to E_m) shows a linear variation.

Analysis by non-linear regression fitting of the experimental data to the uniexponential equation (see Results and discussion)

$$\frac{A_t}{A_t} = \frac{A_{m_0}}{A_0} + \frac{A_{ox_0}}{A_0} e^{-k_{app}^{ox} t} \tag{2}$$

gives the values of $\frac{A_{m_0}}{A_0}\times100$, which is the percentage of E_m, $\frac{A_{ox_0}}{A_0}\times100$ which is the percentage of E_{ox} and k_{app}^{ox}, the apparent inactivation constant. In Eq. (2), A_t, is the residual activity at time t, A_0 is the initial activity, A_{m_0} is the activity corresponding to E_{m_0} and A_{ox_0} is the activity corresponding to E_{ox_0}.

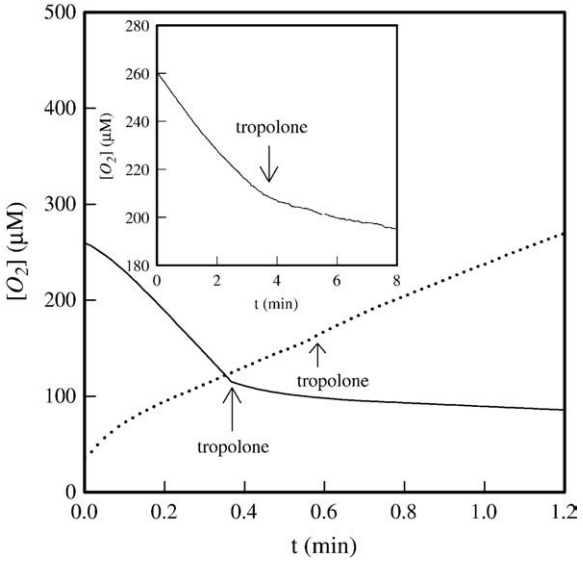

Fig. 2. Action of tropolone in the turnover of the diphenolase, catalase and ascorbate oxidase activities of tyrosinase. (—), oxygen consumption during the oxidation of *TBC* by tyrosinase in the following experimental conditions: phosphate buffer 30 mM, pH 7.0, $[TBC]_0$ 1.6 mM, $[O_2]_0$ 0.26 mM and $[E]_0$ 20 nM. Tropolone (2 μM) was added at the point indicated. (·····) Recording of oxygen formation during the catalase activity of tyrosinase in the following experimental conditions: phosphate buffer 30 mM, pH 7.0, $[H_2O_2]_0$ 20 mM and $[E]_0$ 0.55 μM. Tropolone (2 μM) was added at the point indicated. Inset. Recording of oxygen consumption during the oxidation of *L-AH*$_2$ by tyrosinase in the following experimental conditions: phosphate buffer 30 mM, pH 7.0, $[L\text{-}AH_2]_0$ 2.5 mM, $[O_2]_0$ 0.26 mM and $[E]_0$ 0.55 μM. Tropolone (2 μM) was added at the point indicated.

3. Results and discussion

We studied the inactivation of the different enzymatic forms of tyrosinase that are present in the turnover of the enzyme acting on substrate *S* (Scheme 2). In the case of the E_{ox} form, the inactivation was of the suicide type, or base-inhibitor mechanism, since the enzyme undergoes catalytic cycles in such conditions. In the case of forms E_d and E_m, the inactivation is irreversible since anaerobic conditions are necessary to maintain these forms and, in this case, there is no turnover.

3.1. Suicide inactivation of tyrosinase induced by L- and D-AH_2

The inactivation of the different enzymatic forms was studied by generating them in the medium.

3.1.1. Inactivation of E_{ox}

During the action of the native form of the enzyme on AH_2, all the enzymatic forms are present in the turnover (see Scheme 2): E_m, E_mS, E_d, E_{ox} and $E_{ox}S$. However, since the concentration of oxygen is 0.26 mM, E_d is saturated and kinetically does not exist in the free form. The binding constant of the substrate to the E_m form, k_2, is much higher than k_6, the binding constant to E_{ox} [17]. Therefore, the major forming the turnover is E_{ox}. This is confirmed by inhibition by tropolone (Fig. 2), which has been demonstrated to bind to E_{ox} [29,30]. Note that when tropolone is added, the diphenolase activity of tyrosinase on *TBC* is reduced by 93% and ascorbate oxidase activity by 86% (Fig. 2 Inset). However, there is hardly any inhibition of the catalase activity of tyrosinase, suggesting that another form, E_d, is accumulated in the turnover [7]. Hence, the kinetic study of the suicide inactivation of the enzyme in the turnover mainly concerns to E_{ox}.

3.1.2. Kinetic analysis

The kinetic mechanism proposed to explain the suicide inactivation of tyrosinase acting on AH_2 (*S*) is based on the structural mechanism proposed previously to explain the suicide inactivation of tyrosinase acting on phenolic substrates [16] and can be outlined as follows (see Scheme 2):

In this section, the derivation of the analytical expression which establishes the disappearance of oxygen with time, when $[S]_0 \gg [E]_0$, is described. For more details see reference [16].

Previous kinetic studies on the suicide inactivation of tyrosinase from diverse sources indicated that the process follows a first-order kinetics and has a much higher partition ratio (r) than 1 [31–33]. This implies that the species of the catalytic pathway of Scheme 2 are in a restricted steady-state, E_s, which overlaps in time with a transient phase due to the formation of inactive enzyme, E_i.

Taking into account these considerations, the mechanism described in Scheme 2 can be schematized as follows (see Scheme 3):

The dependence of $[E_s]$ and $[O_2]$ on time can be described by the following differential equations:

$$\left[\dot{E}_S\right] = -k_{7_2}^{i} f_{(E_{ox}-S)_1} [E_s] \tag{3}$$

$$\left[\dot{O}_2\right] = -k_{7_2} f_{(E_{ox}-S)_1} [E_s] \tag{4}$$

Integrating Eqs. (3) and (4), taking into account that $t=0$ is $[E_s]=[E]_0$ and $[O_2]=[O_2]_0$, yields:

$$[O_2] = [O_2]_f + \left([O_2]_0 - [O_2]_f\right) e^{-\lambda^{ox} t} = [O_2]_f + [O_2]_\infty e^{-\lambda^{ox} t} \tag{5}$$

with

$$[O_2]_\infty = \frac{k_{7_2}}{k^i_{7_2}}[E]_0 = r[E]_0 \quad (6)$$

and

$$\lambda^{ox} = k^i_{7_2} f_{(E_{ox}-S)_1} \quad (7)$$

The pseudo steady-state rate is:

$$V_0^{O_2} = k_{7_2} f_{(E_{ox}-S)_1} \quad (8)$$

The expression $f_{(E_{ox}-S)_1}$ can be obtained by applying the steady-state condition for all the enzymatic species in E_s [16]. Substituting this expression into Eq. (7) gives:

$$\lambda^{ox} = \frac{\lambda^{ox}_{max}[S]_0[O_2]_0}{K^{O_2}K^S_{m_2} + K^{O_2}_m[S]_0 + K^S_m[O_2]_0 + [S]_0[O_2]_0} \quad (9)$$

where

$$\lambda^{ox}_{max} = \frac{k^i_{7_2}k_3k_{7_1}k_{7_3}}{k_{7_1}k_{7_2}k_{7_3} + k_3k_{7_2}k_{7_3} + k_3k_{7_1}k_{7_3} + k_3k_{7_1}k_{7_2}} \quad (10)$$

Similarly, inserting the expression $f_{(E_{ox}-S)_1}$ in Eq. (8) gives:

$$V_0^{O_2} = \frac{k_{cat}[S]_0[O_2]_0[E]_0}{K^{O_2}K^S_{m_2} + K^{O_2}_m[S]_0 + K^S_m[O_2]_0 + [S]_0[O_2]_0} \quad (11)$$

where

$$k_{cat} = \frac{k_3k_{7_1}k_{7_2}k_{7_3}}{k_{7_1}k_{7_2}k_{7_3} + k_3k_{7_2}k_{7_3} + k_3k_{7_1}k_{7_3} + k_3k_{7_1}k_{7_2}} \quad (12)$$

The expressions for the kinetic parameters K^{O_2}, $K^S_{m_2}$, $K^{O_2}_m$ and K^S_m included in Eqs. (9) and (11), are given in reference [16].

Due to $K^{O_2}_m$ is very low [34] and that the initial oxygen concentration is 0.26 mM, the enzyme is saturated with O_2 and then, from Eqs. (9) and (10), we obtain:

$$\lambda^{ox} = \frac{\lambda^{ox}_{max}[S]_0}{K^S_m[S]_0} \quad (13)$$

and

$$V_0^{O_2} = \frac{k_{cat}[S]_0[E]_0}{K^S_m + [S]_0} \quad (14)$$

The partition coefficient, r, between the catalytic and suicide inactivation pathways is:

$$r = \frac{k_{7_2}}{k^i_{7_2}} = \frac{k_{cat}}{\lambda^{ox}_{max}} \quad (15)$$

Therefore, from Eqs. (6), (13) and (15), we can obtain the kinetic constants that define the behaviour of a suicide substrate: r, λ^{ox}_{max}, K^S_m, k_{cat}, λ^{ox}_{max}/K^S_m and $\lambda^{ox}_{max}r/K^S_m$.

3.1.3. Experimental design. The experimental study of the kinetics of suicide substrates or mechanism-based enzyme inhibitors is important for obtaining reliable kinetic parameters (λ^{ox}_{max}, K^S_m and r) that will permit any *in vitro* information gained to be extrapolated to *in vivo* situations [35]. Our method for measuring the suicide inactivation is continuous and therefore it is easier to obtain and treat experimental data than when using the discontinuous method, which consists of preincubating the enzyme with the suicide substrate and taking aliquots to follow the diminution of enzymatic activity with time [35].

In a previous work, we outlined the methodology necessary for kinetically characterising a suicide substrate following the reaction continuously [36]. An alternative consists of following the disappearance of the substrate experimentally. This is the method we use here, following the consumption of oxygen by means of an oxygraph, since this is also a substrate of tyrosinase. The design of this method can be described in three stages:

Step 1: Preliminary assays, in which the experimental conditions are optimised and the experimental design is detailed.

Step 2: Study of the variation in enzyme concentration and determination of the parameter r.

Step 3: Study of the variation of substrate concentration and determination of λ^{ox}_{max}, K^S_m and other parameters such as k_{cat}, λ^{ox}_{max}/K^S_m and $\lambda^{ox}_{max}r/K^S_m$.

3.1.4. Experimental study of suicide inactivation

The substrates *L-AH*$_2$ and *D-AH*$_2$ are used in this work (see Scheme 1).

Step 1. Fig. 1 shows the oxymetric recordings for the disappearance of O_2 (curves (a) and (c)) and their corrections after fitting according to Eq. (1) and after subtracting the parameter c_4 (curves (b) and (d)). These corrected recordings are analysed as described in the Data analysis section. By means of these preliminary studies, the concentration of enzyme is optimised so that $[O_2]_\infty \prec\prec [O_2]_0, [S]_0$.

Step 2. Variation in enzyme concentration. The concentration of $[E]_0$ is varied while the substrate concentration (*L-AH*$_2$ and *D-AH*$_2$) is kept constant. In the case of the tyrosinase enzymatic system, there is the advantage that the $K^{O_2}_m$ are very small [34]. However, for the analytical solutions to be fulfilled, the substrate concentration must remain practically constant, $[P]_\infty \leq 0.10\ [S]_0$, which implies $[O_2]_\infty \leq 0.05\ [S]_0$ (Scheme 2). The results obtained for *L-AH*$_2$ are shown in Fig. 3. Note how the values of $[O_2]_\infty$ are directly proportional to $[E]_0$, while λ^{ox} does not vary with $[E]_0$ (Fig. 3 Inset). Fig. 3 inset shows the dependence of the values obtained for the substrate consumed at the end of the reaction, $[O_2]_\infty$ *vs.* $[E]_0$, from whose slopes and according to Eq. (5), the partition

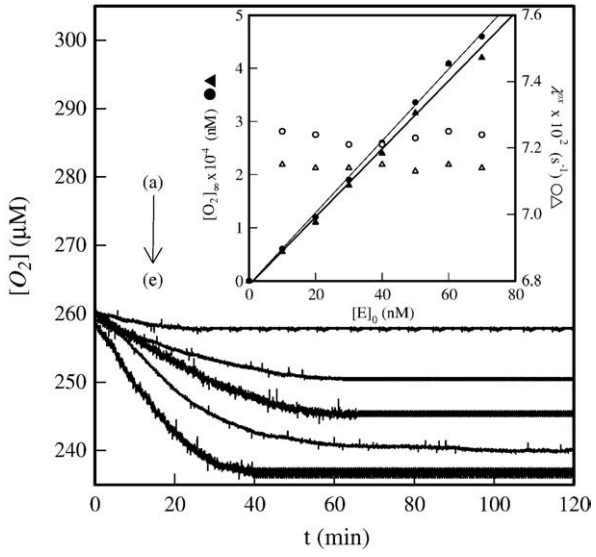

Fig. 3. Corrected recordings of the oxygen consumed in the suicide inactivation of tyrosinase by *L-AH*$_2$ for different enzyme concentrations. Conditions were 30 mM phosphate buffer pH 7.0, $[SOD]_0$ 1.2 μM, $[L\text{-}AH_2]_0$ 14 mM, $[O_2]_0$ 0.26 mM, while enzyme concentrations (nM) were (a) 10, (b) 40, (c) 50, (d) 60 and (e) 70. Inset. Corresponding values of $[O_2]_\infty$ (● *L-AH*$_2$, ▲ *D-AH*$_2$) and λ^{ox} (○ *L-AH*$_2$, △ *D-AH*$_2$) for different concentrations of tyrosinase.

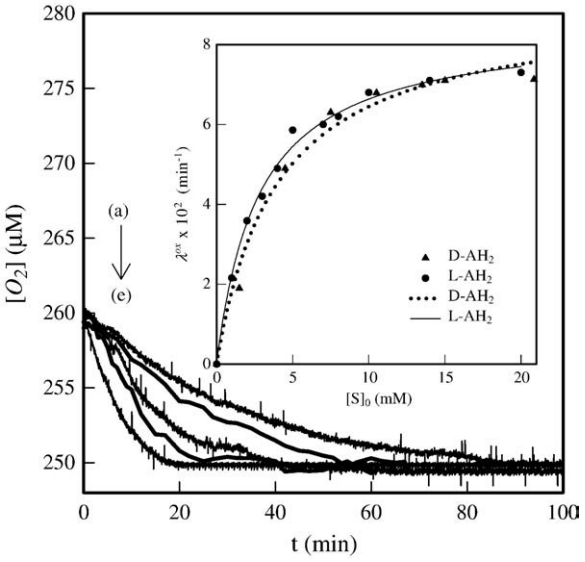

Fig. 4. Corrected recordings of the disappearance of oxygen in the suicide inactivation of tyrosinase by *L-AH*$_2$ for different substrate concentrations. Conditions were 30 mM phosphate buffer pH 7.0, $[SOD]_0$ 1.2 μM, $[O_2]_0$ 0.26 mM, $[E]_0$ 40 nM, while substrate concentrations (mM) were (a) 1, (b) 2, (c) 5, (d) 10 and (e) 14. Inset. Corresponding values of λ^{ox} for different *L-AH*$_2$ (●) and *D-AH*$_2$ (▲) concentrations.

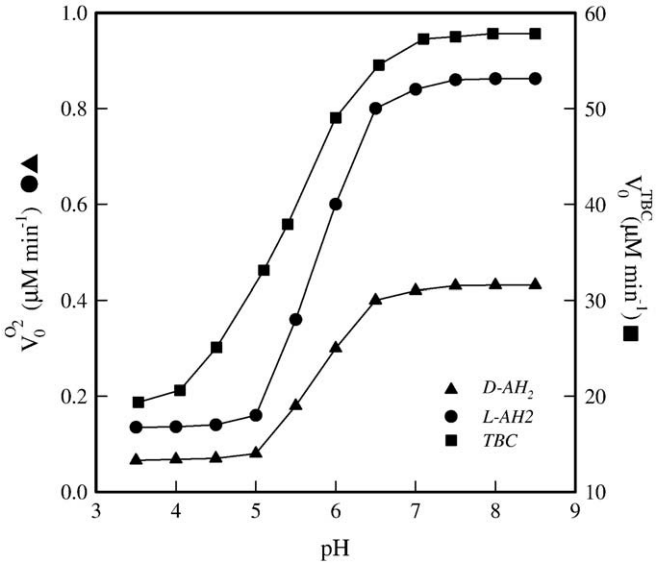

Fig. 5. Corresponding values of $V_0^{O_2}$ *vs.* pH for *L-AH*$_2$ (●) and *D-AH*$_2$ (▲) and V_0 *vs.* pH for *TBC* (■). Conditions were: $[SOD]_0$ 1.2 μM and $[O_2]_0$ 0.26 mM, (●) $[E]_0$ 40 nM and $[L\text{-}AH_2]_0$ 2.7 mM. (▲) $[E]_0$ 20 nM and $[D\text{-}AH_2]_0$ 4.3 mM. (■) $[TBC]_0$ 2 mM, $[E]_0$ 8.5 nM. In all cases, the buffers used were acetate buffer 30 mM, pH 3.5–5.0 and phosphate buffer 30 mM, pH 5.5–8.5.

ratio *r* can be determined (see Table 1). According to Eq. (15), the partition ratio "r" corresponds to the bifurcation depicted in Scheme 2. The step controlled by k_{7_2} could correspond to the attack of the hydroxyl group of C-3 on the copper atom and the transfer of the proton to the nitrogen of the histidine. This would be favoured by the flexibility of the active centre [37] and would lead the enzyme towards the catalytic pathway. The other alternative, represented by our proposal, would be that the step controlled by $k^i_{7_2}$ is responsible for the transfer of the proton of the hydroxyl group of C-3 to the protonated peroxide group that acts as a base, which would lead the enzyme to follow the suicide inactivation pathway. The initial protonation of the peroxide group (O_2^{2-}) controlled by k_{7_1} was proposed in [37]. For a more detailed explanation see [16].

Step 3. Variation of substrate concentration. Having fixed a concentration of enzyme sufficient to give $[O_2]_\infty \leq 0.05\ [S]_0$ for the lowest substrate concentration being assayed, the concentration of substrate is varied while O_2 is kept constant at a saturating 0.26 mM. An hyperbolic dependence of the apparent inactivation constant is obtained in all cases with respect to the concentration of substrate (Fig. 4). Non-linear regression analysis of λ^{ox} vs. $[S]_0$ according to Eq. (13) (Fig. 4 Inset), gives the values of λ^{ox}_{max}, the apparent constant of maximum inactivation and K^S_m, the Michaelis constant of tyrosinase for *L-AH*$_2$ and *D-AH*$_2$ (Table 1). From these values and taking into consideration Eq. (15), the catalytic constant, k_{cat}, can be obtained (Table 1). The inactivation efficiency λ^{ox}_{max}/K^S_m can be calculated from the above data, as can be the catalytic efficiency $\lambda^{ox}_{max} r/K^S_m$ (Table 1).

3.1.5. Stereospecificity of tyrosinase towards isomers L- and D-AH$_2$

As demonstrated in the case of the *o*-diphenolic substrates [38,39], tyrosinase shows greater affinity for the L isomers, followed by DL and lastly D, ($K^L_m < K^{DL}_m < K^D_m$). Similarly, tyrosinase shows greater affinity towards the L-isomer of ascorbic acid (see Table 1).

In the same way as an *o*-diphenol [38,39], the differing affinity that tyrosinase shows towards different isomers does not affect the catalytic constant k_{cat}, since it is similar in all cases (Table 1). This agrees with the ^{13}C-NMR values, since, as the values of *e* δ_2 and δ_3 are equal, the rate of nucleophilic attack on the copper atoms is the same and the catalytic constant depends on this attack process [23].

The dependence of the $V_0^{O_2}$ on pH is similar for both isomers and identical to that obtained with the *o*-diphenol *TBC* (Fig. 5 Inset B). The values of $V^{O_2}_{max}$ do not vary with the pH, while those of K^S_m do, increasing as the pH decreases (results not shown). This behaviour was observed with catechol [33]. From the results shown in Fig. 5, it can be seen that pK_a is kinetically significant, as occurs with *o*-diphenols and monophenols [40,41].

3.2. Evaluation of enzymatic species E_m and E_{ox} in an enzymatic preparation of tyrosinase

*Oxy*hemocianine and *oxy*tyrosinase are in equilibrium with both the E_m and E_{ox} forms [24,42], as illustrated in Scheme 4.

In the presence of oxygen (0.26 mM) and absence of H_2O_2, the principal forms are E_m ($Cu(II)_2$) and E_{ox} ($Cu(II)_2O_2^{2-}$). Inactivation of the native enzyme (1 μM) by irreversible inactivation with 2-mercaptoethanol (10 μM) begins rapidly and follows a process that fits the exponential curve depicted in recording (a) of Fig. 6. Aliquots were taken at the indicated times and diphenolase activity was determined with *TBC*.

The enzyme balance is:

$$[E]_0 = [E_m]_0 + [E_{ox}]_0 \quad (16)$$

Table 1
Kinetic constants which characterise the suicide inactivation of tyrosinase by L and D-ascorbic acid

	$\lambda^{ox}_{max} \times 10^3$ (s^{-1})	*r*	k_{cat} (s^{-1})	K^S_m (mM)	$(\lambda^{ox}_{max}/K^S_m) \times 10^4$ ($mM^{-1}\ s^{-1}$)	$(k_{cat}/K^S_m) \times 10^3$ ($mM^{-1}\ s^{-1}$)	$K^{O_2}_m \times 10^2$ (μM)
L-AH$_2$	1.41 ± 0.01	674 ± 13	0.97 ± 0.05	2.79 ± 0.11	5.01 ± 0.11	0.34 ± 0.02	4.21 ± 0.71
D-AH$_2$	1.46 ± 0.01	626 ± 35	0.92 ± 0.04	4.28 ± 0.21	3.04 ± .21	0.21 ± 0.01	3.93 ± 0.72

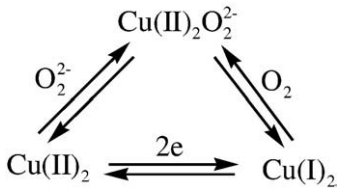

Scheme 4. Equilibrium between E_m, E_{ox} and E_d forms of tyrosinase [24].

The reaction of E_{ox} with 2-mercaptoethanol (I) is described in [28]:

$$E_{ox} + I \overset{k_1}{\rightleftarrows} E_{ox}I \overset{k_{inact}}{\longrightarrow} E_i \quad (17)$$

and so

$$[E_{ox}]_t = [E_{ox}]_0 e^{-k_{app}^{ox} t} \quad (18)$$

where k_{app}^{ox} is the apparent inactivation constant. The concentration of active enzyme evolves with time according to:

$$[E]_t = [E_m]_0 + [E_{ox}]_0 e^{-k_{app}^{ox} t} \quad (19)$$

or

$$\frac{[E]_t}{[E]_0} = \frac{[E_m]_0}{[E]_0} + \frac{[E_{ox}]_0}{[E]_0} e^{-k_{app}^{ox} t} \quad (20)$$

which, in terms of enzymatic activity, can be expressed as Eq. (2) of Materials and methods.

As indicated in Materials and methods, non-linear regression fitting of curve (a) of Fig. 6 to Eq. (2) provides the values of $\frac{A_{m_0}}{A_0}$, $\frac{A_{ox_0}}{A_0}$ and k_{app}^{ox} from which it is possible to know the proportions of E_m and E_{ox}.

Fig. 6 shows the inactivation kinetics involving 2-mercaptoethanol obtained starting with the same enzyme concentration but with different proportions of E_m and E_{ox} and treating the enzyme with

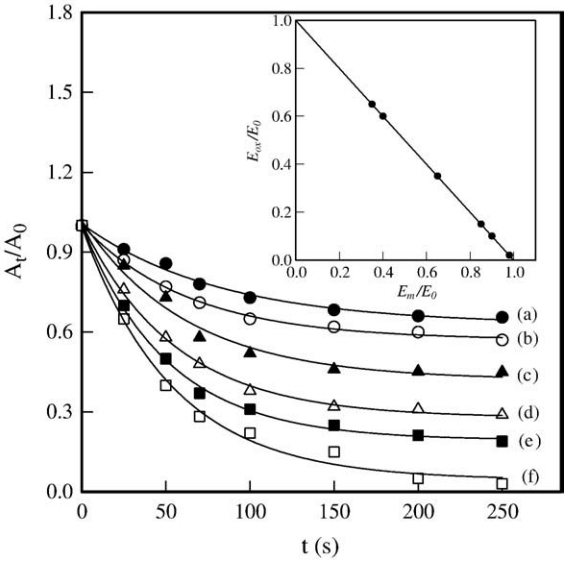

Fig. 6. Evaluation of the enzyme forms E_{ox} and E_m in an enzymatic preparation of tyrosinase. The enzyme at a concentration of 1 μM was incubated in aerobic conditions with 10 μM 2-mercaptoethanol. At the times indicated in the figure 100 μl aliquots were taken and the residual activity was determined in 30 mM phosphate buffer pH 7.0 with 10 mM. *TBC* The formation of *o*-quinone was followed at 410 nm. The residual activity values were fitted to Eq. (2), providing the concentrations of E_{ox} and E_m in the original sample (curve (a)). In experiments (b)–(f) the same concentration of enzyme was used but adding 0.25 μM (b), 0.5 μM (c), 0.75 μM (d), 1 μM (e) or 1.5 μM (f) hydrogen peroxide before its reaction with 2-mercaptoethanol and proceeding as in curve (a). Inset. Percentage of activity lost *vs.* remaining activity at long times.

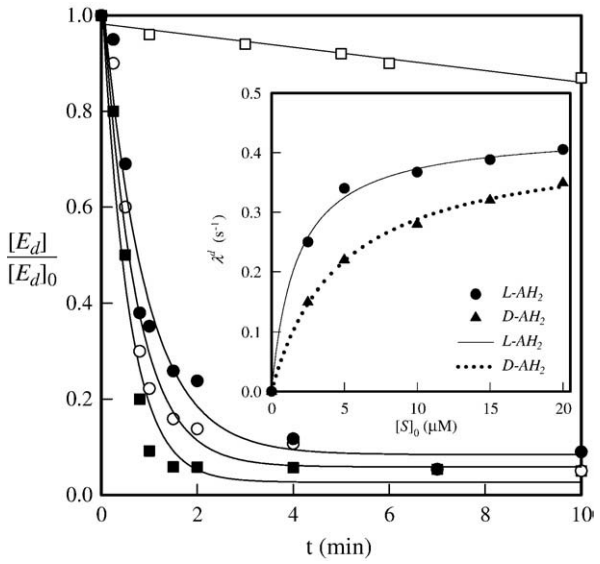

Fig. 7. Inactivation of the E_d form of tyrosinase. The experimental conditions were: phosphate buffer, 30 mM pH 7.0, $[E]_0$ 1 μM (see Materials and methods), $[H_2O_2]_0$ 5 μM and *L-AH*$_2$ concentrations (μM) of 0 □, 5 ●, 10 ○ and 20 ■. Aliquots were analyzed with 1 mM *TBC*. Inset. Representation of λ^d *vs.* $[L\text{-}AH_2]_0$ (●) and λ^d *vs.* $[D\text{-}AH_2]_0$ (▲).

different μM concentrations of H_2O_2. The variation in the E_{ox}/E_m ratio in an enzymatic preparation is shown in Fig. 6 inset.

From Scheme 4, it can be seen that by adding H_2O_2 in aerobic conditions to a sample of enzyme, it can be totally transformed into E_{ox} ($CU(II)_2O_2^{2-}$), which can be confirmed from the inactivation kinetics such as depicted in Fig. 6. Once E_{ox} has been formed, a stream of nitrogen is passed over the sample. Since all the enzyme is now in the E_{ox} form, this is now converted into E_d ($Cu(I)_2$), Scheme 4. In this way we achieve anaerobic conditions to obtain the enzyme in the form of E_d for subsequent experiments. The complete conversion of the enzyme into E_d is also confirmed by inactivation with 2-mercaptoethanol since in the timescale of Fig. 6 the enzyme is not inactivated ($k_{inact}^d = 1 \times 10^{-5}\ s^{-1}$).

The treatment of an enzymatic sample with catalase in aerobic conditions, in accordance with Scheme 4, would eliminate the H_2O_2 from the reaction medium and so the form E_{ox} would pass to E_m, so

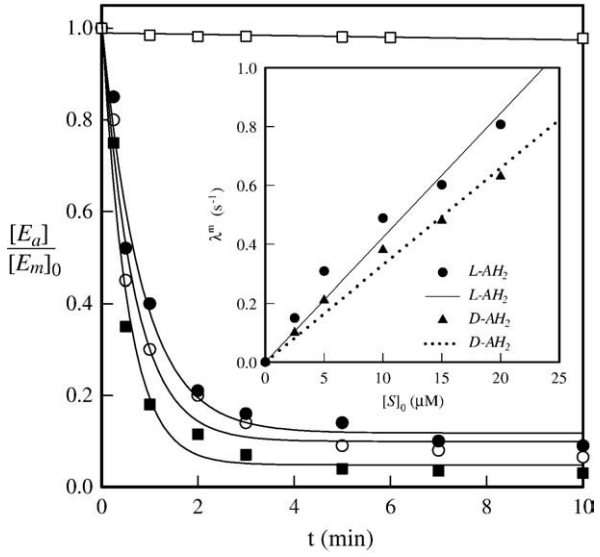

Fig. 8. Inactivation of the E_m form of tyrosinase. The experimental conditions were: phosphate buffer, 30 mM pH 7.0, $[E]_0$ 1 μM (see Materials and methods), $[H_2O_2]_0$ 5 μM and *L-AH*$_2$ concentrations (μM) of 0 □, 5 ●, 10 ○ and 20 ■. Aliquots were analyzed with 1 mM *TBC*. Inset. Representation of λ^m *vs.* $[L\text{-}AH_2]_0$ (●) and λ^d *vs.* $[D\text{-}AH_2]_0$ (▲).

Table 2
Kinetic constants which characterize the instability of E_d, in anaerobic conditions, controlled by k_d^d (Scheme 5) and, on the other hand, irreversible inactivation of E_d in the presence of *L-AH*$_2^d$ *and D-AH*$_2^b$, *controlled by* K_9 *and* k_i^d *(Scheme 6)*

$k_d^d \times 10^2$ (s^{-1})	K_9 (μM)	k_i^d (s^{-1})
1.13 ± 0.07	1.74 ± 0.19[a]	0.43 ± 0.01[a]
	4.70 ± 0.33[b]	0.42 ± 0.01[b]

that all the enzyme would be in the E_m form. This transformation can also be confirmed by the inactivation study with 2-mercaptoethanol, since in the timescale of Fig. 6 the enzyme is not inactivated ($k_{inact}^m = 4 \times 10^{-5}$ s^{-1}) (Fig. 6).

Therefore, in agreement with Scheme 4 and from the inactivation kinetic, the E_{ox}/E_m ratio can be ascertained in an enzyme sample of known concentration. Moreover, the proportions can be varied to obtain all the enzyme in the form of E_{ox} or E_m in aerobic conditions. By passing a nitrogen stream over a preparation of E_{ox} or E_m obtained in the above conditions it is possible to obtain E_d or E_m, respectively, in an anaerobic medium, which can be used to study the effect of AH_2 (Figs. 7 and 8).

3.3. Inactivation of E_d by L- and D-AH_2

The enzymatic species E_d was generated as described in Materials and methods and was studied in two stages:

Step 1. First the stability of E_d was studied in an anaerobic medium with nitrogen bubbled through it, taking aliquots occasionally and measuring the residual activity. From these experiments it was revealed that this enzymatic form is unstable and is inactivated:

The first order inactivation kinetic of E_d can be described as:

$$[E_d] = [E_d]_0 e^{-k_d^d t} \tag{21}$$

The values of the residual activity *vs.* time (Fig. 7) fit Eq. (21), giving the value of the instability constant k_d^d (Table 2).

Step 2. Inactivation of E_d in the presence of substrate. The addition of substrate in anaerobic conditions to a preparation of E_d (anaerobic conditions too) and monitoring the residual activity *vs.* time shows the inactivation of the enzyme (Scheme 6) as following the kinetic mechanism:

The kinetic analysis of the mechanism of Scheme 6 can be described as:

$$[E_d] = [E_d]_0 e^{-\lambda^d t} \tag{22}$$

with

$$\lambda^d = \frac{k_d^d K_9 + k_i^d [S]_0}{K_9 + [S]_0} \tag{23}$$

The values obtained for the residual activity vs. time (Fig. 7) fit Eq. (22), and provide the apparent inactivation constant λ^d.

Step 3. Varying the substrate concentration. The kinetic study of the irreversible inactivation when the substrate concentration is varied (Fig. 7) and its analysis according to Eq. (23) provides us with k_i^d and K_9 (Fig. 7 inset) (see Table 2). Note that $k_i^d \gg k_d^d$ and the value of K_9 are in the micromolar range (Table 2).

3.4. Inactivation of E_m by L- and D-AH_2

The form E_m is stable in anaerobic conditions (Fig. 8) but, in the presence of *L-* and *D-*AH_2, undergoes an inactivation (Scheme 7) which can be kinetically characterised in the following way:

$$E_d \xrightarrow{k_d^d} E_{di}$$

Scheme 5. *Deoxy*-tyrosinase instability.

$$E_d + S \underset{k_{-9}}{\overset{k_9}{\rightleftharpoons}} E_dS \qquad E_d \xrightarrow{k_d^d} E_{di} \qquad E_dS \xrightarrow{k_i^d} P + E_{dSi}$$

Scheme 6. *Deoxy*-tyrosinase inactivation in the presence of substrate.

Step 1. The E_m form, generated as described in Materials and methods, is preincubated anaerobically with *L-* or *D-*AH_2. Aliquots are taken at different times to determine residual activity. To explain the irreversible inactivation, Scheme 7 is proposed:

The enzymatic system indicated in Scheme 7 can be regarded as a linear system of five compartments, where each compartment represents one of the following enzyme species: E_m, E_mS, E_d, E_dS and enzyme inactive ($E_{di}+E_{dSi}$). The equation for the residual activity can be obtained by applying the software implemented in [43]. A tetraexponential equation is obtained (result not shown), which can be simplified to a uniexponential equation using a method for reducing exponential terms as described by our group in [43]. The result is:

$$[E_a] = [E_m]_0 e^{-\lambda^m t} \tag{24}$$

where $[E_a]$ represents the active enzyme concentration at time *t*. Furthermore, taking into account that k_d^d is much lower than k_i^d ($k_d^d \prec\prec k_i^d$) (see Table 2), the resulting expression for λ^m is:

$$\lambda^m = \frac{\frac{k_3 k_i^d}{k_3 + k_i^d}[S]_0}{\frac{k_2 k_3 (k_{-9} + k_i^d) + k_9 k_i^d (k_{-2} + k_3)}{k_2 k_9 (k_3 + k_i^d)} + [S]_0} \tag{25}$$

Furthermore, taking into account that there is no rapid equilibrium in the binding of *S* to E_m [17] due to $k_3 \gg k_{-2}$, Eq. (25) is simplified to:

$$\lambda^m = \frac{k_i^d [S]_0}{K_9 + \frac{k_i^d}{k_2} + [S]_0} \tag{26}$$

Fitting the experimental data of residual activity vs. time (Fig. 8), according to Eq. (24), permits λ^m to be obtained (Scheme 7).

Step 2. Variation of substrate concentration. Varying the substrate concentration (Fig. 8 inset), according to Eq. (26), provides the value of k_2 (Table 3), since k_i^d and K_9 are determined in Eq. (21) and (23).

3.5. Combination of steady state and inactivation studies

The values of K_m^S and k_{cat} are related as follows [17]:

$$K_m = \frac{k_{cat}}{k_6} \tag{28}$$

and therefore the binding constant of the substrate to E_{ox} (k_6) can be obtained. Table 3 shows these results, demonstrating, from the value

Table 3
Kinetic constants which characterize the binding of *L-*AH_2 and *D-*AH_2 to E_m and E_{ox}, respectively

	k_2 (M^{-1} s^{-1})	k_6 (M^{-1} s^{-1})	δ_2 (ppm)	δ_3 (ppm)
L-AH_2	15,619 ± 712	346 ± 13	118.6	156.4
D-AH_2	10,852 ± 553	214 ± 10	118.6	156.4

Values of δ in carbons C-2 and C-3 of *L-*AH_2 and *D-*AH_2.

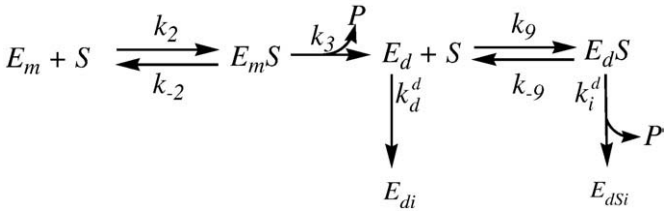

Scheme 7. Kinetic mechanism proposed for *met*-tyrosinase inactivation by ascorbic acid.

of k_2 obtained in Eq. (26) that $k_2 \succ\succ k_6$. This is confirmed by transient phase kinetics of the E_{ox} form in the case of *TBC* [17].

3.6. Oxygen protects against the inactivation of tyrosinase

Tyrosinase catalyses a bisubstrate reaction with O_2 and a reductant, in this case, *L-AH*$_2$ or *D-AH*$_2$. The most instable form in the enzyme's turnover, Scheme 2, is E_d. However, this form is practically non-existent in the turnover since it binds to the O_2 with a low constant [17]. The $K_m^{O_2}$ values are also small [34], and, at the oxygen concentration of the solutions (0.26 mM), the enzyme is saturated by O_2. The other substrate, *L-AH*$_2$ or *D-AH*$_2$, and, generally speaking, most of the *o*-diphenols and triphenols are true suicide substrates, this process occurring during electron transfer to the copper atoms.

4. Conclusions

In conclusion, AH_2 behaves like a suicide substrate when tyrosinase acts on it in aerobic conditions. Furthermore, the enzyme shows stereospecificicity in binding to the substrate ($K_m^L < K_m^D$). However, the rapidness of both steps, catalysis (k_{cat}) and inactivation (λ_{max}), which are related with the chemical shifts of C-2 and C-3, are equal. This implies that the partition ratio "r" is the same for both isomers. In anaerobic conditions, the forms E_d and E_m undergo an irreversible inactivation which is rapid compared with the suicide inactivation. That is due to the enzyme's protection afforded by the catalytic steps during the branched reaction mechanism of the suicide inactivation of tyrosinase (Scheme 2).

Acknowledgements

This paper was partially supported by grants from the Ministerio de Educación y Ciencia (Madrid, Spain) Projects BIO2006-15363 and SAF2006-07040-C02-01, from the Fundación Séneca (CARM, Murcia, Spain) Project 00672/PI/04, from the Consejería de Educación (CARM, Murcia, Spain) BIO-BMC 06/01-0004, and from FISCAM PI-2007/53. JLMM has a fellowship from the Ministerio de Educación y Ciencia (Madrid, Spain) Reference AP2005-4721. FGM has a fellowship from Fundación Caja Murcia (Murcia, Spain).

References

[1] C.Y. Lee, J.R. Whitaker, Enzymatic Browning and its prevention, ACS Symposium series 600, Washington DC, 1994.
[2] E. Arias, J. Gonzalez, R. Oria, P. Lopez-Buesa, Ascorbic acid and 4-hexylresorcinol effects on pear PPO and POD catalyzed browning reaction, J. Food Sci. 72 (2007) 422–429.
[3] A. Sanchez-Ferrer, J.N. Rodriguez-Lopez, F. Garcia-Canovas, F. Garcia-Carmona, Tyrosinase: a comprehensive review of its mechanism, Biochim. Biophys. Acta 1247 (1995) 1–11.
[4] S. Halaouli, M. Asther, J.C. Sigoillot, M. Handi, A. Lomascolo, Fungal tyrosinases: new prospects in molecular characteristics, bioengineering and biotechnological applications, J. App. Microbiol. 100 (2006) 219–232.
[5] G. Protta, Progress in the chemistry of melanin and related metabolites, Med. Res. Rev. 8 (1988) 525–556.
[6] H. Claus, H. Decker, Bacterial tyrosinases, Syst. and Appl. Microbiol. 29 (2006) 3–14.
[7] F. Garcia-Molina, A.N. Hiner, L.G. Fenoll, J.N. Rodriguez-Lopez, P.A. Garcia-Ruiz, F. Garcia-Canovas, J. Tudela, Mushroom tyrosinase: catalase activity, inhibition, and suicide inactivation, J. Agric. Food Chem. 53 (2005) 3702–3709.
[8] S. Yamazaki, C. Morioka, S. Itoh, Kinetic evaluation of catalase and peroxygenase activities of tyrosinase, Biochemistry 43 (2004) 11546–11553.
[9] J.R. Ros, J.N. Rodriguez-Lopez, R. Varon, F. Garcia-Canovas, Mushroom tyrosinase has an ascorbate oxidase activity, Biochem. Mol. Biol. Int. 36 (1995) 301–309.
[10] J.R. Ros, J.N. Rodriguez-Lopez, J.C. Espin, R. Varon, F. Garcia-Canovas, Oxymetric and spectrophotometric study of the ascorbate oxidase activity shown in frog epidermis tyrosinase, Int. J. Biochem. Cell Biol. 28 (1996) 917–923.
[11] J.C. Espin, R. Veltman, H. Wichers, The oxidation of L-ascorbic acid catalyzed by pear polyphenol oxidase, Physiologia Plantarum 109 (2000) 1–6.
[12] J. Buta, J. Abbott, Browning inhibition of fresh-cut Anjou, Barlett and Bosc pears, HortSciencie 35 (2000) 1111–1113.
[13] E. Arias, J. Gonzalez, J.M. Peiro, R. Oria, P. Lopez-Buesa, Browning prevention by ascorbic acid and 4-hexylresorcinol: different mechanism of action on polyphenol oxidase in the presence and in the absence of substrates, J. Food Sci. 72 (2007) 464–470.
[14] A. Golan-Goldhirsh, D.T. Osuga, A.O. Chen, J.R. Whitaker, The Bioorganic Chemistry of Enzymatic Catalysis; An Homage to Myron, CRC Press, Boca Raton, Florida, 1992.
[15] A. Golan-Goldhirsh, J.R. Whitaker, k_{cat} inactivation of mushroom polyphenol oxidase, J. Mol. Catal. 32 (1985) 141–147.
[16] J.L. Muñoz-Muñoz, F. Garcia-Molina, P. Garcia-Ruiz, M. Molina-Alarcón, J. Tudela, F. Garcia-Canovas, J.N. Rodriguez-Lopez, Phenolic substrates and suicide inactivation of tyrosinase: kinetics and mechanism, Biochem. J. (2008 In press).
[17] J.N. Rodriguez-Lopez, L.G. Fenoll, P.A. Garcia-Ruiz, R. Varon, J. Tudela, R.N. Thorneley, F. Garcia-Canovas, Stopped-flow and steady-state study of the diphenolase activity of mushroom tyrosinase, Biochemistry 39 (2000) 10497–10506.
[18] M.M. Bradford, A rapid and sensitive method for the quantification of microgram quantities of proteins utilising the principle of protein-dye binding, Anal. Biochem. 72 (1976) 248–254.
[19] J.N. Rodriguez-Lopez, J.R. Ros-Martinez, R. Varon, F. Garcia-Canovas, Calibration of a Clark-type oxygen electrode by tyrosinase-catalyzed oxidation of a 4-tert-butylcatechol, Anal. Biochem. 202 (1992) 356–360.
[20] Jandel Scientific. Sigma Plot 9.0 for Windows™; Jandel Scientific: Core Madera 2006.
[21] B. Mannervik, Kinetic Data Analysis, Plennum Press, New York, 1981.
[22] S. Tomiyama, S. Sakai, T. Nishiyama, F. Yamada, Factors influencing the antioxidant activities of phenols by an ab initio study, Bull. Chem. Soc. Jpn. 66 (1993) 299–304.
[23] J.C. Espin, R. Varon, L.G. Fenoll, M.A. Gilabert, P.A. Garcia-Ruiz, J. Tudela, F. Garcia-Canovas, Kinetic characterization of the substrate specificity and mechanism of mushroom tyrosinase, Eur. J. Biochem. 267 (2000) 1270–1279.
[24] M. Jackman, M. Huber, A. Hajnal, K. Lerch, Stabilization of the oxy form of tyrosinase by a single conservative amino acid substitution, Biochem. J. 282 (1982) 915–918.
[25] R. Jolley, L. Evans, N. Makino, H. Mason, Oxytyrosinase, J. Biol. Chem. 249 (1974) 335–345.
[26] M. Beltramini, K. Lerch, Fluorescence properties of Neurospora tyrosinase, Biochem. J. 205 (1982) 173–180.
[27] J. Deinum, K. Lerch, B. Reinhammar, An EPR study of Neurospora tyrosinase, FEBS Lett. 69 (1976) 161–164.
[28] R. Aasa, J. Deinum, K. Lerch, B. Reinhammar, The reaction of mercaptans with tyrosinases and hemocyanins, Biochim. Biophys. Acta 535 (1978) 287–298.
[29] J.C. Espin, H.J. Wichers, Slow-binding inhibition of mushroom (*Agaricus bisporus*) tyrosinase isoforms by tropolone, J. Agric. Food Chem. 47 (1999) 2638–2644.
[30] E. Valero, M. Garcia-Moreno, R. Varon, F. Garcia-Carmona, Time-dependent inhibition of grape polyphenol oxidase by tropolone, J. Agric. Food Chem. 39 (1991) 1043–1046.
[31] L.L. Ingraham, J. Corse, B. Makower, Enzymatic browning of fruits.3. Kinetics of the reaction inactivation of polyphenoloxidase, J. Am. Chem. Soc. 74 (1952) 2623–2626.
[32] K. Lerch, Neurospora tyrosinase: structural, spectroscopic and catalytic properties, Mol. Cell Biochem. 52 (1983) 125–138.
[33] F.G. Canovas, J. Tudela, C.M. Madrid, R. Varon, F.G. Carmona, J.A. Lozano, Kinetic study on the suicide inactivation of tyrosinase induced by catechol, Biochim. Biophys. Acta 912 (1987) 417–423.
[34] L.G. Fenoll, J.N. Rodriguez-Lopez, F. Garcia-Molina, F. Garcia-Canovas, J. Tudela, Michaelis constants of mushroom tyrosinase with respect to oxygen in the presence of monophenols and diphenols, Int. J. Biochem. Cell Biol. 34 (2002) 332–336.
[35] F. Ghanbari, K. Rowland-Yeo, J.C. Bloomer, S.E. Clarke, M.S. Lennard, G.T. Tucker, A. Rostami-Hodjegan, A critical evaluation of the experimental design of studies of mechanism based enzyme inhibition, with implications for in vitro–in vivo extrapolation, Curr. Drug Metab. 7 (2006) 315–334.
[36] F. Garcia-Canovas, J. Tudela, R. Varon, A.M. Vazquez, Experimental methods for kinetic study of suicide substrates, J. Enzyme Inhib. 3 (1989) 81–90.
[37] Y. Matoba, T. Kumagai, A. Yamamoto, H. Yoshitsu, M. Sugiyama, Crystallographic evidence that the dinuclear copper center of tyrosinase is flexible during catalysis, J. Biol. Chem. 281 (2006) 8981–8990.
[38] J.C. Espin, P.A. Garcia-Ruiz, J. Tudela, F. Garcia-Canovas, Study of the stereo-specificity in mushroom tyrosinase, Biochem. J. 331 (1998) 547–551.

[39] J.C. Espin, P.A. Garcia-Ruiz, J. Tudela, F. Garcia-Canovas, Study of stereospecificity in pear and strawberry polyphenol oxidase, J. Agric. Food Chem. 46 (1998) 2469–2473.
[40] J.N. Rodriguez-Lopez, J. Tudela, R. Varon, F. Garcia-Canovas, Kinetic study on the effect of pH on the melanin biosynthesis pathway, Biochim. Biophys. Acta 1076 (1991) 379–386.
[41] J.C. Espin, R. Varon, J. Tudela, F. Garcia-Canovas, Kinetic study of the oxidation of 4-hydroxyanisole catalyzed by tyrosinase, Biochem. Mol. Biol. Int. 41 (1997) 1265–1276.
[42] B. Linzen, N.M. Soeter, A.F. Riggs, H.J. Schneider, W. Schartau, M.D. Moore, E.A. Yotota, P.Q. Behrens, I. Nakashima, T. Tagaki, T. Nemoto, J.M. Vereijken, H.J. Bak, J.J. Bientema, A. Volbeda, W.P.J. Gaykema, W.G.J. Hol, The structure of arthropod hemocyanins, Sciencie 229 (1985) 519–524.
[43] M.J. Garcia-Meseguer, J.A. Vidal de Labra, F. Garcia-Canovas, B.H. Havsteen, M. Garcia-Moreno, R. Varon, Time course equations of the amount of substance in a linear compartimental system and their computerised derivation, Biosystems 59 (2001) 197–220.

4.19. INACTIVACIÓN SUICIDA DE TIROSINASA EN SU ACCIÓN SOBRE TETRAHIDROPTERINAS.

El estudio de la inactivación suicida de tirosinasa en su acción sobre diferentes tetrahidropterinas ha dado lugar a la siguiente publicación adjunta.

4.19.1. Título

Suicide inactivation of tyrosinase in its action on tetrahydropterines.

4.19.2. Autores

Muñoz-Muñoz, J.L.; Garcia-Molina, F.; Arribas, E.; Garcia-Ruiz, P.A.; Tudela, J.; Garcia-Cánovas, F. y Rodríguez-López, J.N.

4.19.3. Referencia

Journal of Enzyme Inhibition and Medicinal Chemistry (2011) 26, 728-733.

4.19.4. Resumen

Tetrahidrobiopterina (BH_4), metil-tetrahidropterina (MBH_4) and dimetil-tetrahidropterina ($DMBH_4$) son oxidadas por tirosinasa. En este proceso de oxidación, puede ocurrir la inactivación suicida de tirosinasa. Del estudio cinético de éste proceso de inactivación se puede obtener: $\lambda_{E_{ox}(\max)}^{S_R}$ (constante aparente máxima para la inactivación suicida), $K_m^{S_R}$ (constante de Michaelis para el sustrato) y r (número de ciclos catalíticos que realiza un mol de enzima antes de su inactivación). De la información obtenida, puede deducirse que la rapidez de la inactivación ($\lambda_{E_{ox}(\max)}^{S_R}$) y la potencia de inactivación ($\lambda_{E_{ox}(\max)}^{S_R} / K_m^{S_R}$) sigue el orden $BH_4 > MBH_4 > DMBH_4$.

Journal of Enzyme Inhibition and Medicinal Chemistry, 2011; 26(5): 728–733
© 2011 Informa UK, Ltd.
ISSN 1475-6366 print/ISSN 1475-6374 online
DOI: 10.3109/14756366.2010.548811

informa
healthcare

RESEARCH ARTICLE

Suicide inactivation of tyrosinase in its action on tetrahydropterines

Jose Luis Muñoz-Muñoz[1], Francisco Garcia-Molina[1], Enrique Arribas[2], Pedro Antonio Garcia-Ruíz[3], Jose Tudela[1], Francisco Garcia-Cánovas[1], and Jose Neptuno Rodríguez-López[1]

1Grupo de Investigación Enzimología, Departamento de Bioquímica y Biología Molecular-A, Facultad de Biología, Universidad de Murcia, E-30100, Espinardo, Murcia, Spain, 2Departamento de Física Aplicada, Escuela Politécnica Superior de Albacete, Universidad de Castilla la Mancha, Avda, España s/n, Campus Universitario, E-02071, Albacete, Spain, and 3QCBA: Grupo de Química de Carbohidratos y Biotecnología de Alimentos, Departamento de Química Orgánica, Facultad de Química, Universidad de Murcia, E-30100, Espinardo, Murcia, Spain

Abstract

Tetrahydrobiopterin (BH_4), methyl-tetrahydropterin (MBH_4) and dimethyl-tetrahydropterin ($DMBH_4$) are oxidized by tyrosinase in a process during which the suicide inactivation of tyrosinase may occur. From the kinetic study of this process, $\lambda^{S_R}_{E_{ox}(max)}$ (apparent maximum constant for the suicide inactivation), $K^{S_R}_m$ (Michaelis constant for the substrate) and *r* (number of turnovers that the enzyme makes before the inactivation) can be obtained. From the results obtained, it can be deduced that the velocity of the inactivation governed by ($\lambda^{S_R}_{E_{ox}(max)}$) and the potency of the same ($\lambda^{S_R}_{E_{ox}(max)}/K^{S_R}_m$) follow the order: $BH_4 > MBH_4 > DMBH_4$.

Keywords: Tyrosinase, suicide inactivation, tetrahydropterines

Introduction

Tyrosinase or polyphenol oxidase (TYR; EC 1.14.18.1) is a widely distributed enzyme through the animal, vegetal, bacterial and fungal kingdoms[1].

In a recent work[2], we studied the effect of tetrahydropterines at micromolar concentrations on the monophenolase and diphenolase activities of tyrosinase and demonstrated that they are oxidized by *o*-dopaquinone and that the systems reach the steady state when all the tetrahydropterines have been exhausted[2]. Subsequently, we demonstrated that the effect of tetrahydropterines on the catalytic activities of tyrosinase can occur at three levels: (i) through non-enzymatic inhibition, the tetrahydropterines acting as reductants of *o*-dopaquinone, (ii) by acting as competitive substrates of TYR and (iii) by acting as irreversible inhibitors of the enzymatic forms deoxy- and met-tyrosinase[3].

Tyrosinase undergoes an inactivation process when it reacts with its phenolic substrates, a phenomenon that has long been known[4]. The study of enzymatic inactivation by suicide substrates or mechanism-based inhibitors is of growing importance because of possible pharmacological applications, for studying enzymatic mechanisms and for designing new drugs[4,5,6]. As regards the possible applications of the suicide substrates of tyrosinase, some of the substrates, such as 7,8,4´-trihydroxyisoflavone and 8-hydroxydaidzein, have been studied for their depigmenting activity, the latter in both mouse melanoma cells and in human volunteers[7].

Several mechanisms have been proposed to explain the suicide inactivation of tyrosinase [4,8,9].

The objective of this work was the kinetic characterisation of the suicide inactivation of tyrosinase as it acts on tetrahydrobiopterin (BH_4), methyl-tetrahydropterin (MBH_4) and dimethyl-tetrahydropterin ($DMBH_4$), and we propose a structural mechanism to explain the results.

Address for Correspondence: Francisco Garcia-Cánovas, Grupo de Investigación Enzimología, Departamento de Bioquímica y Biología Molecular-A, Facultad de Biología, Universidad de Murcia, E-30100, Espinardo, Murcia, Spain. Tel.: +34 868 884764; Fax: +34 868 883963. E-mail: canovasf@um.es

(Received 05 October 2010; revised 10 December 2010; accepted 13 December 2010)

Journal of Enzyme Inhibition and Medicinal Chemistry Downloaded from informahealthcare.com by Prof. Jose Tudela on 03/27/12
For personal use only.

RIGHTSLINK

Journal of Enzyme Inhibition and Medicinal Chemistry Downloaded from informahealthcare.com by Prof. Jose Tudela on 03/27/12
For personal use only.

Material and methods

Reagents

L-tyrosine, 4-*tert*-butylcatechol (TBC), (6-R)-L-erythro-5,6,7,8-tetrahydro-biopterin dihydrochloride (BH_4), 6-(R,S)-methyl 5,6,7,8-tetrahydropterin monohydrochloride (MBH_4) and 6,7-(R,S)-dimethyl 5,6,7,8-tetrahydropterin monohydrochloride ($DMBH_4$) were purchased from Sigma (Madrid, Spain; Scheme 1). Stock solutions of the phenolic substrate were prepared in 0.15 mM phosphoric acid to prevent autooxidation. $6BH_4$, MBH_4 and $DMBH_4$ were prepared in 0.15 mM phosphoric acid, eliminating the oxygen by passing a current of nitrogen.

Enzyme source

Mushroom tyrosinase (TYR, 3300 U/mg) was purchased from Sigma (Madrid, Spain) and purified according to ref. (10). The enzyme concentration was calculated taking the value of M_r as 120,000. Protein content was determined by Bradford's method[11] using bovine serum albumin as standard. Superoxide dismutase (SOD, 4140 U/mg) was purchased from Sigma (Madrid, Spain).

Monophenolase activity of TYR

The monophenolase activity of TYR was followed spectrophotometrically, measuring the accumulation of dopachrome at a wavelength of 475 nm ($\varepsilon = 3500\ M^{-1}\ cm^{-1}$)[2] during the oxidation of L-tyrosine, using a Perkin-Elmer Lambda-35 spectrophotometer connected to a PC (Perkin-Elmer, North Billerica, MA). The conditions of the assay are specified in the corresponding figure legends.

Diphenolase activity of TYR

The diphenolase activity of TYR was followed spectrophotometrically, measuring the accumulation of dopachrome at a wavelength of 475 nm ($\varepsilon = 3500\ M^{-1}\ cm^{-1}$)[12] during the oxidation of L-dopa using the mentioned apparatus. The conditions of the assay are specified in the corresponding figure legends.

Kinetics of the suicide inactivation

The kinetics of the suicide inactivation of TYR in its action on tetrahydropterines, S_R, (BH_4, MBH_4 and $DMBH_4$) can be followed by measuring the formation of S_{ox} (BH_2, MBH_2 and $DMBH_2$), in a spectrophotometer. The assays were carried out in triplicate for each concentration of S_R and enzyme. These spectrophotometric assays were carried out as described above. The experimental data for the formation of S_{ox} (in the other cases is the same) with time follow the equation,

$$[S_{ox}] = [S_{ox}]_\infty (1 - e^{-\lambda^{S_R}_{E_{ox}} t}) \quad (1)$$

where $[S_{ox}]$ is the instantaneous concentration of S_{ox}, $[S_{ox}]_\infty$ is the S_{ox} formed at the end of the reaction, $t \mapsto \infty$, and $\lambda^{S_R}_{E_{ox}}$ the apparent inactivation constant for E_{ox} in the suicide inactivation of TYR under aerobic conditions.

Results and discussion

Under aerobic conditions, tetrahydropterines act as alternative substrates to the physiological substrates of the enzyme (L-tyrosine and L-dopa)[3]. Under such conditions, the tetrahydropterines may act as inactivators of TYR as a result of the enzyme's suicide inactivation as it acts on the substrates[4–8]. This suicide inactivation process is studied below during the action of TYR on BH_4, MBH_4 and $DMBH_4$.

Tyrosinase inactivation in its action on tetrahydropterines under aerobic conditions: suicide inactivation

The kinetic mechanism proposed to explain the suicide inactivation of tyrosinase acting on tetrahydropterines is described in Scheme 2:

When $[S_R]_0$, $[O_2]_0 >> [E]_o$ and $<< [S_{ox}]_\infty$ $[S_R]_0$, $[O_2]_0$, derivation of the analytical expression establishes the accumulation of the product (S_{Ox}) with time, as is detailed in ref. (4).

The variation of $[S_{ox}]$ with time is given by Eq. (2)[4].

$$[S_{ox}] = [S_{ox}]_\infty (1 - e^{-\lambda^{SR}_{E_{ox}} t}) \quad (2)$$

When $t \to \infty$, $[S_{ox}] = [S_{ox}]_\infty$ and according to (4),

$$[S_{ox}]_\infty = \frac{2k_{7_2}}{k^{i}_{7_2}}[E]_0 \quad (3)$$

The velocity of the suicide inactivation is regulated by the apparent inactivation constant, $\lambda^{S_R}_{E_{ox}}$, whose expression is given by Eq. (4). Taking into account the saturation of tyrosinase by oxygen ($[O_2]_0 \to \infty$), thus according to (4),

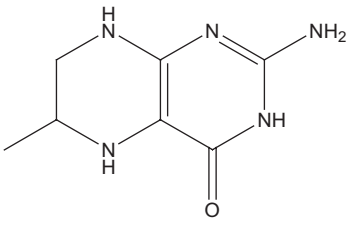

(±)-6-Methyl-5,6,7,8-tetrahydropterine

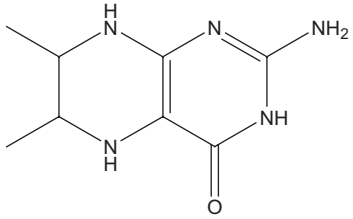

6,7-Dimethyl-5,6,7,8-tetrahydropterine

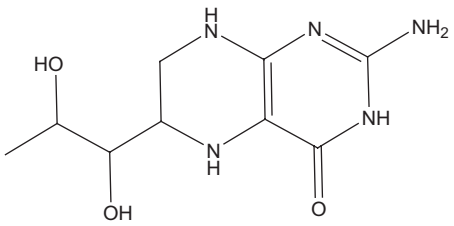

(6R)-5,6,7,8-Tetrahydrobiopterin

Scheme 1. Chemical structures of the tetrahydropterines used in this work.

© 2011 Informa UK, Ltd.

RIGHTSLINK

$$\lambda_{E_{ox}}^{S_R} = \frac{\lambda_{E_{ox}(max)}^{S_R}[S_R]_0}{K_m^{S_R} + [S_R]_0} \quad (4)$$

The partition ratio, r, between the catalytic and suicide inactivation pathways is,

$$r = \frac{k_{12_2}}{k_{12_2}^i} = \frac{k_{cat}^{S_R}}{\lambda_{E_{ox}(max)}^{S_R}} = \frac{[S_{ox}]_\infty}{2[E]_0} \quad (5)$$

where k_{12_2} is the substrate binding constant to the copper atom through the C-3 hydroxyl (axial) and $k_{12_2}^i$ is the rate constant of transfer of a H^+ to the protonated peroxide (see Scheme 2 and supplementary Scheme 1SM).

Therefore, from Eq. (1–5), we can obtain the kinetic constants that characterise the kinetic behaviour of a suicide substrate: r, $\lambda_{E_{ox}(max)}^{S_R}$, $K_m^{S_R}$ and $K_{cat}^{S_R}$.

Experimental study of the suicide inactivation

The study of the suicide inactivation has been developed in three steps using BH_4, MBH_4 and $DMBH_4$ as substrates of TYR.

Step 1. The suicide inactivation kinetics is corrected when fitting to Eq. (1) so that the non-enzymatic oxidation of the substrates, BH_4, MBH_4 and $DMBH_4$ is eliminated (results not shown). These corrected recordings were analysed as described in the Kinetic Analysis section. By

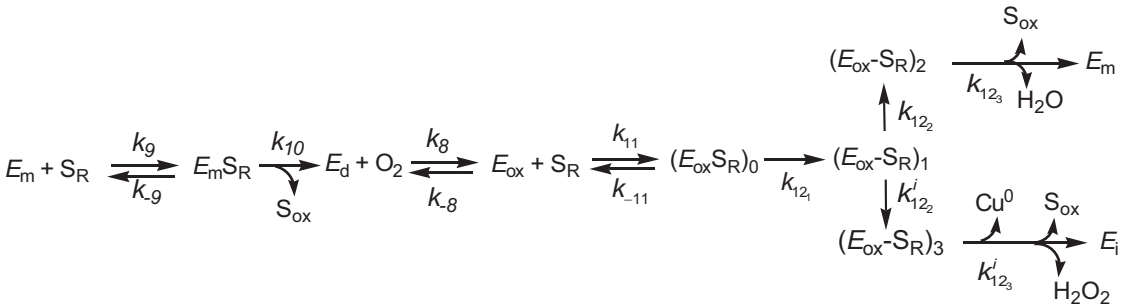

Scheme 2. Kinetic mechanism to explain the pterin oxidase pathway and suicide inactivation pathway of tyrosinase in its action on tetrahydropterines.

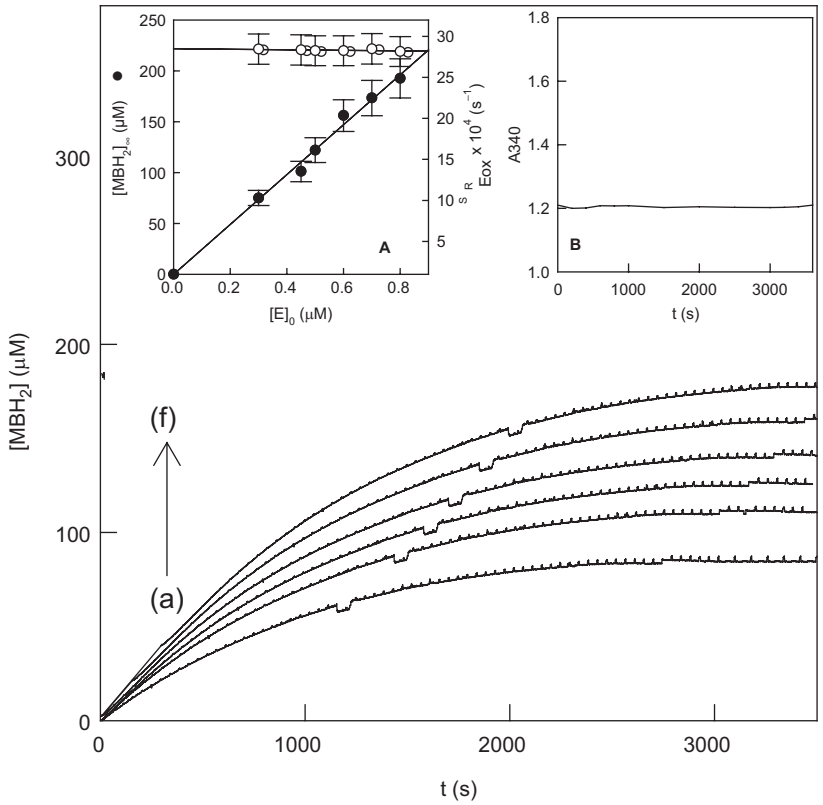

Figure 1. Corrected recordings of the appearance of MBH_2 in the suicide inactivation of tyrosinase (TYR) by MBH_4 for different enzyme concentrations. Conditions were 30 mM sodium phosphate buffer (pH 7.0), λ = 340 nm, 0.26 mM O_2, 0.5 mM $[MBH_4]_0$, 414 UI/m $[SOD]_0$, and $[E]_0$ (μM): (a) 0.3, (b) 0.45, (c) 0.5, (d) 0.6, (e) 0.7, and (f) 0.8. Inset A. Representation of the values of $[MBH_2]_\infty$ (•) and $\lambda_{E_{ox}}^{S_R}$ (O) vs. enzyme concentration. Inset B. Representation of absorbance at λ = 340 nm with time in the reaction of TYR on BH_2. The experimental conditions were 30 mM sodium phosphate buffer (pH = 7.0), 25°C, $[BH_2]_0$ = 0.2 mM and $[E]_0$ = 0.1 μM.

Journal of Enzyme Inhibition and Medicinal Chemistry Downloaded from informahealthcare.com by Prof. Jose Tudela on 03/27/12
For personal use only.

RIGHTSLINK

Table 1. Kinetic constants which characterize the suicide inactivation of tyrosinase by tetrahydropterines.

Substrate	$\lambda^{S_R}_{E_{ox}(max)} \times 10^3$ (s^{-1})	$r = k^{S_R}_{cat}/\lambda^{S_R}_{E_{ox}(max)}$	$k^{S_R}_{cat}$ (s^{-1})	$K^{S_R}_m$ * (mM)	$\lambda^{S_R}_{E_{ox}(max)}/K^{S_R}_m \times 10^3$ ($s^{-1}\,mM^{-1}$)	$K^{O_2}_m$ (μM)
BH_4	0.035 ± 0.004	168 ± 19	5.98 ± 0.63	4.13 ± 0.87	8.51 ± 0.4	0.26 ± 0.03
MBH_4	0.026 ± 0.003	179 ± 22	4.29 ± 0.44	4.41 ± 0.91	5.47 ± 0.8	0.18 ± 0.02
$DMBH_4$	0.018 ± 0.003	199 ± 25	3.42 ± 0.32	5.01 ± 0.88	3.56 ± 0.7	0.14 ± 0.02

*Data taken from ref. (3).

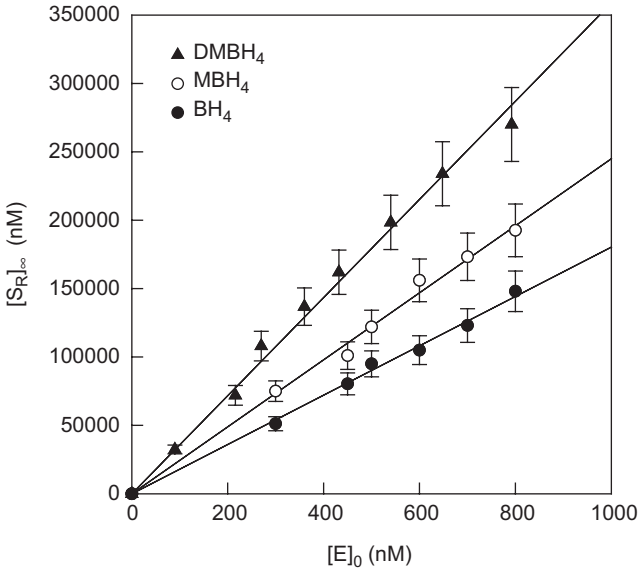

Figure 2. Representations of the values of $[S_{ox}]_\infty$ vs. enzyme concentration for the different substrates studied (BH4 •, MBH4 O and DMBH4 ▲). Experimental conditions were 30 mM sodium phosphate buffer (pH 7.0), 25°C and 414 UI/ml $[SOD]_0$. The substrates studied were recorded from the appearance of product. The initial concentration for every substrate was 0.8 mM. In every substrate, (—) linear regression fitting of the experimental data points.

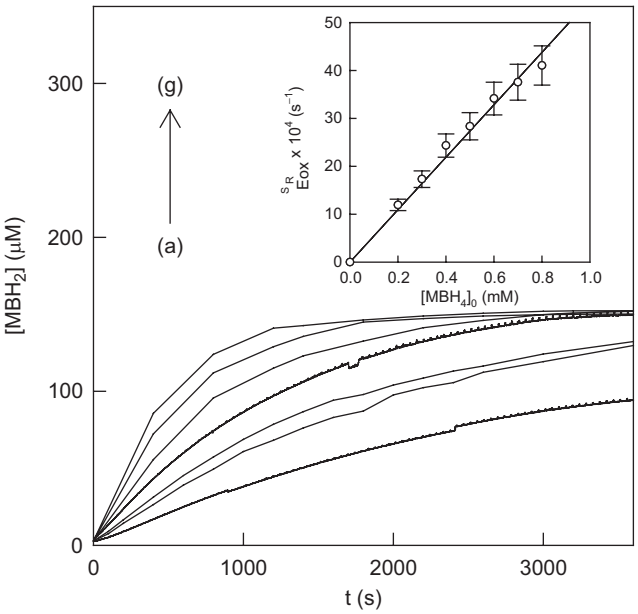

Figure 3. Corrected recordings of the appearance of MBH_2 in the suicide inactivation of TYR by different MBH_4 concentrations. Conditions were 30 mM sodium phosphate buffer (pH 7.0), 0.26 mM O_2, λ = 340 nm, 0.6 μM $[TYR]_0$, and 414 UI/ml $[SOD]_0$. The substrate concentrations were (mM): (a) 0.2, (b) 0.3, (c) 0.4, (d) 0.5, (e) 0.6, (f) 0.7, and (g) 0.8. Inset. Values of $\lambda^{S_R}_{E_{ox}}$ vs. $[MBH_2]_0$.

means of these preliminary studies, the concentration of enzyme was optimised so that $[S_{ox}]_\infty << [O_2]_0, [S_R]_0$.

Step 2. Variation in enzyme concentration. The $[E]_0$ -value is varied while the substrate concentration is kept constant. The results obtained are shown in Figure 1. The concentration of the substrate does not change significantly in these experiments so that $[S_{ox}]_\infty < 10\%\ [S_R]_0$. However, the concentration of O_2 does change. In the case of tyrosinase, $K^{O_2}_m$ is very small (Table 1), which permits an oxygen consumption of more than 10%. Note how the values of $[MBH_2]_\infty$ are directly proportional to $[E]_0$, while $\lambda^{S_R}_{E_{ox}}$ does not vary with $[E]_0$ (Figure 1 Inset A). Figure 1 Inset B shows the stability of BH_2 with time, which demonstrates that the product of the reaction of TYR with BH_4 during the time that the suicide inactivation kinetics is being measured is stable.

Figure 2 shows the dependence of the values obtained for the product at the end of the reaction, $[S_{ox}]_\infty$ vs. $[E]_0$, from whose slopes, and according to Eq. (5), r can be determined for BH_4, MBH_4 and $DMBH_4$ (Table 1). Note that the value of r is greater in the case of $DMBH_4$ than in that of MBH_4 or BH_4, indicating that the enzyme needs to undergo a greater number of turnovers before inactivation when it acts on $DMBH_4$ than it does in the case of MBH_4 or BH_4.

Step 3. Variation in substrate concentration. The experimental recordings for the appearance of MBH_2 during the action of tyrosinase on MBH_4 obtained by varying the concentration of substrate are shown in Figure 3. Fitting by non-linear regression to Eq. (1) gives the apparent inactivation constant $\lambda^{S_R}_{E_{ox}}$. The dependence of $\lambda^{S_R}_{E_{ox}}$ vs. $[S_R]_0$ is shown in Figure 3 Inset. Due to the high degree of autooxidation of the tetrahydropterines and the long measuring times involved, it is not convenient to increase the substrate concentration by much, so that we shall work in the linear dependence zone, Figure 3 Inset. Fitting these data by linear regression according to Eq. (4) gives the relation $\lambda^{S_R}_{E_{ox}(max)}/K^{S_R}_m$ for each of the isomers (Figure 4 and Table 1). Bearing in mind the values of $K^{S_R}_m$ calculated from the initial velocity measurements obtained at short times[3], we can obtain the values of $\lambda^{S_R}_{E_{ox}(max)}$ and r (Table 1). Figure 4 represents the values of $\lambda^{S_R}_{E_{ox}}$ vs. $[S_R]_0$ for the substrates BH_4, MBH_4 and $DMBH_4$. Note how TYR is not saturated during its action on any tetrahydropterine (Figure 4). The value of the ratio $\lambda^{S_R}_{E_{ox}(max)}/K^{S_R}_m$ is $BH_4 > MBH_4 > DMBH_4$.

Journal of Enzyme Inhibition and Medicinal Chemistry Downloaded from informahealthcare.com by Prof. Jose Tudela on 03/27/12
For personal use only.

© 2011 Informa UK, Ltd.

RIGHTSLINK

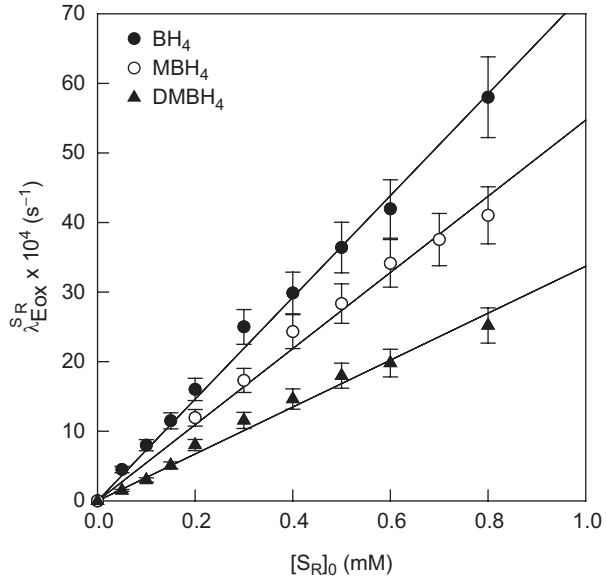

Figure 4. Representation of the values of the inactivation constant $\lambda^{S_R}_{E_{ox}}$ vs. $[S_R]_0$ for the different substrates studied. Conditions were 30 mM sodium phosphate buffer (pH 7.0), 25°C. Every substrates were recorded from the appearance of product (BH_2, MBH_2, and $DMBH_2$ for BH_4 •, MBH_4 O and $DMBH_4$ ▲, respectively). (—), Non-linear regression fitting to Eq. (4) of the data analysis. Enzyme concentration was, in each case, 0.6 μM. The initial concentration of superoxide dismutase (SOD) was 414 UI/ml.

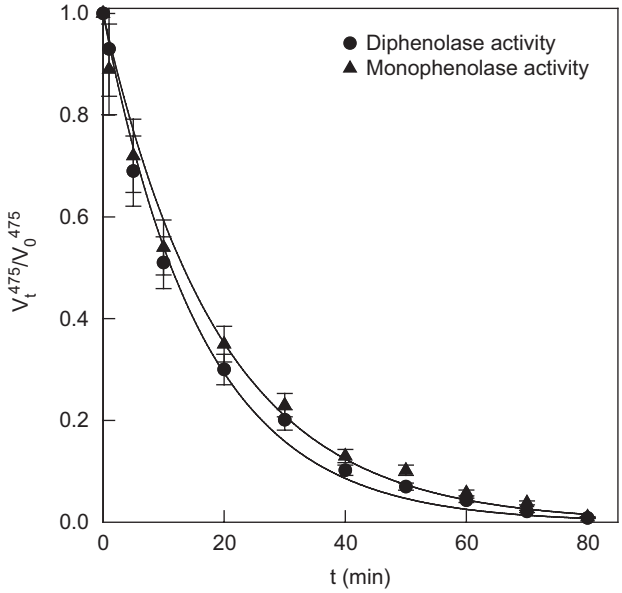

Figure 5. •Suicide inactivation kinetics of TYR in its action on $DMBH_4$. The process was followed by measuring the residual diphenolase activity of the enzyme with time. The experimental conditions were 30 mM sodium phosphate buffer (pH 7.0), $[O_2]_0 = 0.26$ mM, $[TYR]_0 = 0.61$ μM, $[SOD]_0 = 414$ UI/ml, and $[DMBH_4] = 0.8$ mM. Aliquots were taken at various times to measure the residual activity with 2.5 mM L-dopa (wavelength 475 nm). ▲Suicide inactivation kinetics of TYR in its action on $DMBH_2$. The process was followed by measurement of the residual monophenolase activity of the enzyme with time. The experimental conditions were 30 mM phosphate buffer (pH 7.0), $[O_2]_0 = 0.26$ mM, $[TYR]_0 = 0.61$ μM, $[SOD]_0 = 414$ UI/ml, and $[DMBH_4] = 0.8$ mM. Aliquots were taken at various times to measure the residual activity with 1 mM L-tyrosine and 46 μM L-DOPA (wavelength 475 nm). L-DOPA was added to eliminate the lag phase of the monophenolase activity of TYR.

In confirmation of the inactivation of tyrosinase as it acts on tetrahydropterines, Figure 5 shows the experimental values obtained for the residual diphenolase activity on TBC of the enzyme during the suicide inactivation of TYR with BH_4. This figure shows similar results obtained for monophenolase activity in its action on L-tyrosine. Note that the same value for the apparent inactivation constant, $\lambda^{S_R}_{E_{ox}}$, was obtained in both cases and the same as that in Figure 4 obtained with the same concentration of BH_4.

The inactivation mechanism, Scheme 2 and supplementary Scheme 1SM, is consistent with the experimental observation that 50% of the copper is lost from the active site during catechol inactivation[13], in the form of copper (0), and also with experiments carried out[8], concerning the impossibility of reactivating the inactivated enzyme by adding Cu^{2+}, which, in turn, suggests the need for a 'caddie' protein[14]. BH_4, MBH_4 and $DMBH_4$, therefore, are capable of irreversibly inactivating tyrosinase and may be useful as depigmenting agents or, at least, for designing the same.

Conclusions

In this article, the suicide inactivation process of tyrosinase acting on tetrahydropterines has been kinetically characterized. From the kinetic constants obtained, it can be deduced that the velocity of the inactivation governed by ($\lambda^{S_R}_{E_{ox}(max)}$) and its potency ($\lambda^{S_R}_{E_{ox}(max)}/K_m^{S_R}$) follow the order: $BH_4 > MBH_4 > DMBH_4$.

Acknowledgements

This article was partially supported by grants from the Ministerio de Educación y Ciencia (Madrid, Spain) Project BIO2009–12956, from the Fundación Séneca (CARM, Murcia, Spain) Projects 08856/PI/08 and 08595/PI/08 and from the Consejería de Educación (CARM, Murcia, Spain) BIO-BMC 06/01-0004. F.G.M. and J.L.M.M. have fellowships from Fundación Caja Murcia (Murcia, Spain).

References

1. Solomon EI, Sundaram UM, Machonkin TE. Multicopper Oxidases and Oxygenases. Chem Rev 1996;96:2563–2606.
2. García-Molina F, Muñoz JL, Varón R, Rodríguez-López JN, García-Cánovas F, Tudela J. Effect of tetrahydropteridines on the monophenolase and diphenolase activities of tyrosinase. J Enzyme Inhib Med Chem 2007;22:383–394.
3. García-Molina F, Munoz-Munoz JL, Acosta JR, García-Ruiz PA, Tudela J, García-Cánovas F et al. Melanogenesis inhibition by tetrahydropterines. Biochim Biophys Acta 2009;1794:1766–1774.
4. Muñoz-Muñoz JL, García-Molina F, García-Ruiz PA, Molina-Alarcón M, Tudela J, García-Cánovas F et al. Phenolic substrates and suicide inactivation of tyrosinase: kinetics and mechanism. Biochem J 2008;416:431–440.

Journal of Enzyme Inhibition and Medicinal Chemistry Downloaded from informahealthcare.com by Prof. Jose Tudela on 03/27/12
For personal use only.

RIGHTSLINK

5. Chang TS. Two potent suicide substrates of mushroom tyrosinase: 7,8,4′-trihydroxyisoflavone and 5,7,8,4′-tetrahydroxyisoflavone. J Agric Food Chem 2007;55:2010–2015.
6. Chang TS, Lin MY, Lin HJ. Identifying 8-hydroxynaringenin as a suicide substrate of mushroom tyrosinase. J Cosmet Sci 2010;61:205–210.
7. Tai SS, Lin CG, Wu MH, Chang TS. Evaluation of depigmenting activity by 8-hydroxydaidzein in mouse B16 melanoma cells and human volunteers. Int J Mol Sci 2009;10:4257–4266.
8. Land EJ, Ramsden CA, Riley PA. The mechanism of suicide-inactivation of tyrosinase: a substrate structure investigation. Tohoku J Exp Med 2007;212:341–348.
9. Muñoz-Muñoz JL, Garcia-Molina F, Varon R, Garcia-Ruíz PA, Tudela J, Garcia-Cánovas F et al. Suicide inactivation of the diphenolase and monophenolase activities of tyrosinase. IUBMB Life 2010;62:539–547.
10. Rodríguez-López JN, Fenoll LG, García-Ruiz PA, Varón R, Tudela J, Thorneley RN et al. Stopped-flow and steady-state study of the diphenolase activity of mushroom tyrosinase. Biochemistry 2000;39:10497–10506.
11. Bradford MM. A rapid and sensitive method for the quantitation of microgram quantities of protein utilizing the principle of protein-dye binding. Anal Biochem 1976;72:248–254.
12. García-Molina F, Muñoz JL, Varón R, Rodríguez-López JN, García-Cánovas F, Tudela J. A review on spectrophotometric methods for measuring the monophenolase and diphenolase activities of tyrosinase. J Agric Food Chem 2007;55:9739–9749.
13. Dietler C, Lerch, K. Oxidases and Related Redox Systems. In King TE, Mason HS, Morrison, M, ed. New York, Pergamon Press, 1982:305–317.
14. Matoba Y, Kumagai T, Yamamoto A, Yoshitsu H, Sugiyama M. Crystallographic evidence that the dinuclear copper center of tyrosinase is flexible during catalysis. J Biol Chem 2006;281:8981–8990.

Journal of Enzyme Inhibition and Medicinal Chemistry Downloaded from informahealthcare.com by Prof. Jose Tudela on 03/27/12
For personal use only.

© 2011 Informa UK, Ltd.

RIGHTSLINK

Supplementary material:

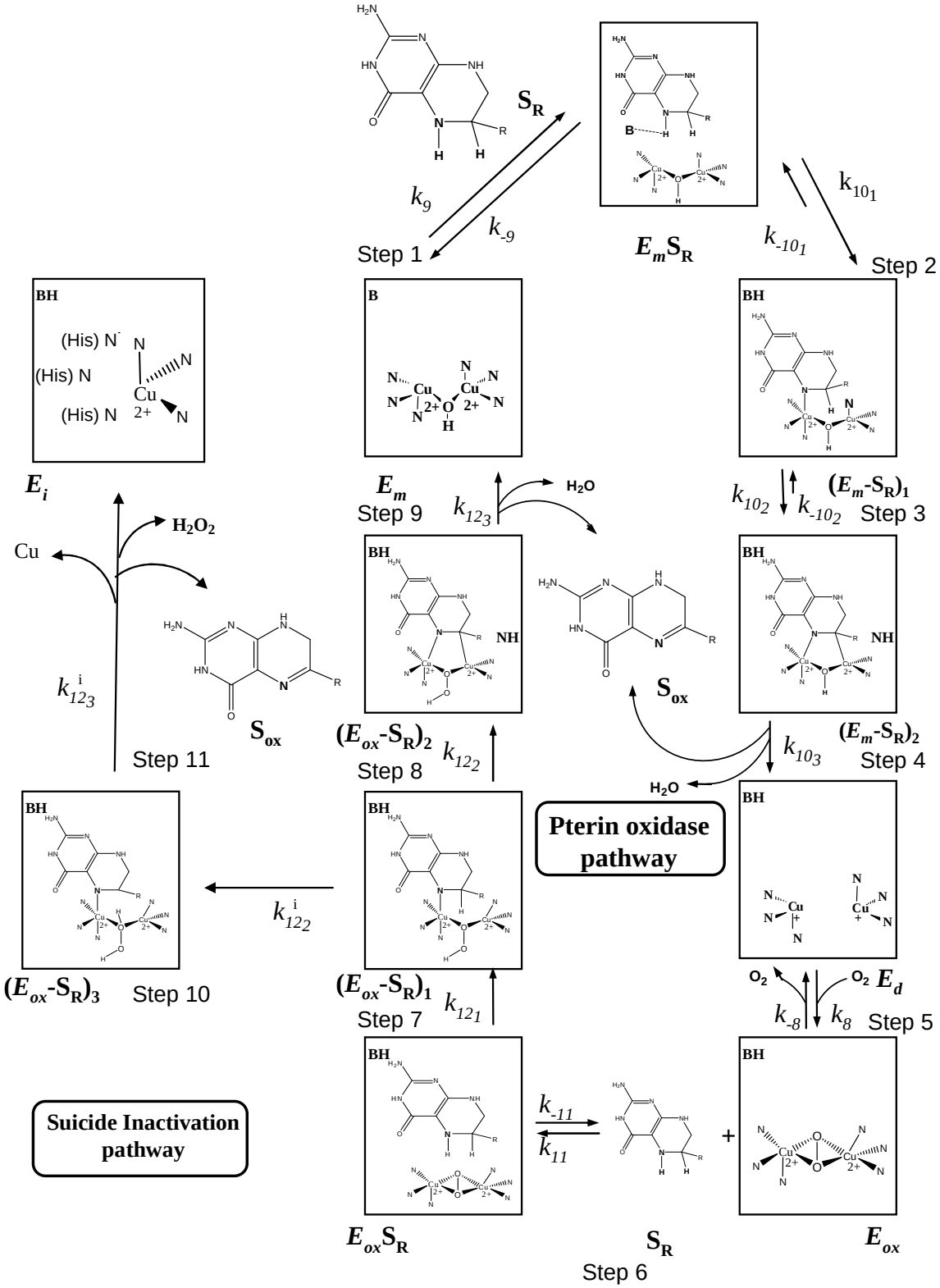

-Scheme 1SM-

Scheme 1SM. Structural mechanism proposed to explain the pterin oxidase and suicide inactivation pathways of tyrosinase during its tetrahydropterines (S_R). E_m, *met*-tyrosinase; E_d, *deoxy*-tyrosinase; E_{ox}, *oxy*-tyrosinase; $E_{ox}S_R$, *oxy*-tyrosinase/*o*-diphenol complex; $(E_{ox}\text{-}S_R)_1$, *oxy*-tyrosinase/*o*-diphenol complex axially bound to a Cu atom; $(E_{ox}\text{-}S_R)_2$, *oxy*-tyrosinase/*o*-diphenol complex axially bound to the two Cu atoms; $(E_{ox}\text{-}S_R)_3$, *oxy*-tyrosinase/*o*-diphenol complex axially bound to one Cu atom and the deprotonated hydroxyl group of C-2; E_mS_R, *met*-tyrosinase/*o*-diphenol complex; $(E_m\text{-}S_R)_1$, *met*-tyrosinase/*o*-diphenol complex axially bound to a Cu atom; $(E_m\text{-}S_R)_2$, *met*-tyrosinase/*o*-diphenol complex axially bound to the two Cu atoms. E_i, enzyme inactive.

4.20. CARACTERIZACIÓN CINÉTICA DE *o*-AMINOFENOLES Y *o*-DIAMINAS AROMÁTICAS COMO SUSTRATOS SUICIDAS DE TIROSINASA.

El estudio de la caracterización cinética de la o-aminofenoles y o-diaminas aromáticas como sustratos suicidas de tirosinasa ha dado lugar a la siguiente publicación adjunta.

4.20.1. Título

Kinetic characterizationn of *o*-aminophenols and aromatic *o*-diamines as suicide substrates of tyrosinase.

4.20.2. Autores

Muñoz-Muñoz, J.L.; Garcia-Molina, F.; Berna, J.; Garcia-Ruiz, P.A.; Varon, R.; Tudela, J.; Rodríguez-López, J.N. y Garcia-Cánovas, F.

4.20.3. Referencia

Biochimica et Biophysica Acta-Protein and Protemics (2012) 1824, 647-655.

4.20.4. Resumen

Se ha estudiado la cinética de la inactivación suicida de tirosinasa en su reacción sobre *o*-aminofenoles y *o*-diaminas aromáticas y se comparan los resultados con los obtenidos para los *o*-difenoles correspondientes. Las constantes catalíticas siguen el orden: *o*-diaminas aromáticas < *o*-aminofenoles < *o*-difenoles, lo que estaría de acuerdo con que la transferencia del protón al grupo peróxido de la forma oxi-tirosinasa es la etapa lenta del ciclo catalítico. Con respecto a la constante aparente de inactivación, esta se mantiene dentro del mismo orden de magnitud, siendo ligeramente menores para *o*-diaminas aromáticas y *o*-aminofenoles con relación a *o*-difenoles: *o*-diaminas < *o*-aminofenoles < *o*-difenoles. La eficiencia del segundo ataque nucleofílico del sustrato hacia el CuA, parece ser el determinante de la bifurcación entre la ruta de inactivación y la catalítica. Este ataque es más eficiente en *o*-diaminas (ataca un átomo de nitrógeno) que en *o*-aminofenoles y *o*-difenoles (en ambos casos ataca un átomo de oxigeno) favoreciendo la ruta catalítica y ralentizando la ruta de inactivación. La etapa de inactivación es la más lenta en todo el proceso. Los valores del parámetro r, número de ciclos catalíticos que realiza un mol de enzima antes de su inactivación, sigue el orden: *o*-diaminas aromáticas < *o*-aminofenoles < *o*-difenoles. Las constantes de Michaelis siguen el orden: *o*-diaminas aromáticas ligeramente menor que *o*-difenoles y *o*-aminofenoles ligeramente mayor que *o*-difenoles. Como

consecuencia de lo anterior, la potencia de inactivación, λ_{max} / K_m^S, sigue la relación: *o*-difenoles > *o*-aminofenoles > *o*-diaminas aromáticas.

Biochimica et Biophysica Acta 1824 (2012) 647–655

Contents lists available at SciVerse ScienceDirect

Biochimica et Biophysica Acta

journal homepage: www.elsevier.com/locate/bbapap

Kinetic characterisation of *o*-aminophenols and aromatic *o*-diamines as suicide substrates of tyrosinase

Jose Luis Muñoz-Muñoz [a], Francisco Garcia-Molina [a], Jose Berna [b], Pedro Antonio Garcia-Ruiz [c], Ramon Varon [d], Jose Tudela [a], Jose N. Rodriguez-Lopez [a], Francisco Garcia-Canovas [a,*]

[a] GENZ: Grupo de Investigación Enzimología, Departamento de Bioquímica y Biología Molecular-A, Facultad de Biología, Universidad de Murcia, E-30100, Espinardo, Murcia, Spain
[b] Departamento de Química Orgánica, Facultad de Química, Universidad de Murcia, E-30100, Espinardo, Murcia, Spain
[c] QCPAI: Grupo de Química de Carbohidratos, Polímeros y Aditivos Industriales, Departamento de Química Orgánica, Facultad de Química, Universidad de Murcia, E-30100, Espinardo, Murcia, Spain
[d] Departamento de Química-Física, Escuela de Ingenieros Industriales de Albacete, Universidad de Castilla la Mancha, Avda. España s/n. Campus Universitario, E-02071, Albacete, Spain

ARTICLE INFO

Article history:
Received 9 November 2011
Received in revised form 31 January 2012
Accepted 1 February 2012
Available online 10 February 2012

Keywords:
Tyrosinase
Aromatic *o*-diamine
o-Aminophenol
Suicide inactivation
o-Diphenol

ABSTRACT

We study the suicide inactivation of tyrosinase acting on *o*-aminophenols and aromatic *o*-diamines and compare the results with those obtained for the corresponding *o*-diphenols. The catalytic constants follow the order aromatic *o*-diamines<*o*-aminophenols<*o*-diphenols, which agrees with the view that the transfer of the proton to the peroxide group of the oxy-tyrosinase form is the slowest step in the catalytic cycle. As regards the apparent inactivation constant, it remains within the same order of magnitude, although slightly lower in the case of the aromatic *o*-diamines and *o*-aminophenols than *o*-diphenols: *o*-diamines<*o*-aminophenols<*o*-diphenols. The efficiency of the second nucleophilic attack of substrate on CuA seems to be the determining factor in the bifurcation of the inactivation and catalytic pathways. This attack is more efficient in *o*-diamines (where it attacks a nitrogen atom) than in *o*-aminophenols and *o*-diphenols (where it attacks an oxygen atom), favouring the catalytic pathway and slowing down the inactivation pathway. The inactivation step is the slowest of the whole process. The values of *r*, the number of turnovers that 1 mol of enzyme carries out before being inactivated, follows the order aromatic *o*-diamines<*o*-aminophenols<*o*-diphenols. As regards the Michaelis constants, that of the *o*-diamines is slightly lower than that of the *o*-diphenols, while that of the *o*-aminophenols is slightly greater than that observed for the *o*-diphenols. As a consequence of the above, the inactivation efficiency, λ_{max}/K_m^S, follows this order: *o*-diphenols > *o*-aminophenols > aromatic *o*-diamines.

© 2012 Elsevier B.V. All rights reserved.

1. Introduction

Tyrosinase is a cuproprotein that catalyses the hydroxylation of monophenols to *o*-diphenols (monophenolase activity) and the oxidation of the latter to *o*-quinones (diphenolase activity), using molecular oxygen [1–3].

Tyrosinase suffers inactivation when it reacts with its *o*-diphenolic and triphenolic substrates [4–11]. The catalytic process is related with the nucleophilic power of the oxygen atom of the hydroxyl group bound to the carbon atom in *para* position with respect to the R group (C-4). However, the inactivation process has no such direct relation, and substrates with low chemical shift (δ) values in C-4 have a high catalytic constant but low inactivation constant. The relation between these constants is given by the parameter *r*, the number of turnovers that 1 mol of enzyme carries out before being inactivated.

The crystallisation of tyrosinase from different sources, *Streptomyces castaneoglobisporus* [12], *Bacillus megaterium* [13,14] and *Agaricus bisporus* [15], has increased our knowledge of the structure of the enzyme. In addition, it has been described that mushroom tyrosinase has an active centre close to the surface [15], which would explain the low substrate specificity shown by this enzyme [16–20].

Kinetic studies in the transition phase and the steady state have shown that the *o*-diphenols bind to the form met-tyrosinase (E_m) more rapidly than to the form oxy-tyrosinase (E_{ox}) [21]. Furthermore, studies on the isotopic effect in the presence of deuterated water have suggested that the transfer of a proton from the hydroxyl group of C-4 to the peroxide group of E_{ox} is the rate-limiting step in both diphenolase and monophenolase activities [22,23].

Experiments using aromatic monoamines, aromatic *o*-diamines and *o*-aminophenols as substrates [20,24–27] point to the low values of the catalytic constant of these processes, lending support to the suggestion that the transfer of the critical proton to the oxy-tyrosinase form is the limiting step in the catalytic cycle [20,24,25]. In an earlier publication, we studied the catalytic action of tyrosinase

* Corresponding author. Tel.: +34 868 884764; fax: +34 868 883963.
E-mail address: canovasf@um.es (F. Garcia-Canovas).

1570-9639/$ – see front matter © 2012 Elsevier B.V. All rights reserved.
doi:10.1016/j.bbapap.2012.02.001

on aromatic monoamines, aromatic *o*-diamines and *o*-aminophenols, which were found to be substrates of the enzyme [20]. When the reactions above were followed at long measurement times, the suicide inactivation of tyrosinase was evident [5–7]. The wide variety of aromatic *o*-diamines and *o*-aminophenols that are available commercially has enabled us to look more deeply at this suicide inactivation process by studying their corresponding structure/reactivity relationships.

2. Material and methods

2.1. Materials

Mushroom tyrosinase or polyphenol oxidase (TYR, *o*-diphenol: O_2 oxidoreductase, EC 1.14.18.1) (8300 units/mg) and L-ascorbic acid (AH_2) were supplied by Sigma (Madrid, Spain). The enzyme was purified as previously described in Ref. [21]. Protein concentration was determined by the Lowry method [28]. All the substrates used in this work were purchased from Sigma (Madrid, Spain) (Table 1SM). All other chemicals were of analytical grade. Stock solutions of the *o*-diphenolic substrates, aromatic *o*-diamines and *o*-aminophenols were prepared in 0.15 mM phosphoric acid to prevent autooxidation. Milli-Q system (Millipore Corp.) ultrapure water was used throughout.

2.2. Methods

2.2.1. Spectrophotometric assays

These assays were carried out with a Perkin-Elmer Lambda-35 (Perkin-Elmer, Massachusetts, USA) spectrophotometer, on line interfaced to a PC-computer, where the kinetic data were recorded, stored and later analysed. The products of the enzyme reaction (*o*-quinoneimine or *o*-diimine) are unstable and evolve towards other products [24,29]. For this reason, the reaction was followed by measuring the disappearance of AH_2 at the wavelength and molar absorptivity coefficient specified for each substrate (Table 2SM). This coupled reagent reduces *o*-quinone to *o*-diphenol, *o*-quinoneimine to *o*-aminophenol and *o*-diimines to *o*-diamines, respectively [20,30,31]. The substrates used in this method were 2-aminophenol, 3-amino-4-hydroxybenzoic acid, 4-amino-3-hydroxybenzoic acid, 3-amino-L-tyrosine, 1,2-diaminobenzene, 3,4-diaminotoluene, 4-methoxy-1,2-phenylenediamine and 2,3-diaminobenzoic acid.

2.2.2. Oxymetric assays

When the substrate and ascorbic acid spectra overlapped, oxymetric assays were carried out [32]. Measurements of dissolved oxygen concentration were made with a Hansatech (Kings Lynn, Cambs, U.K.) oxygraph unit controlled by a PC. The oxygraph used a Clark-type silver/platinum electrode with a 12.5 μm Teflon membrane. The sample was continuously stirred during the experiments and its temperature was maintained at 25 °C. The zero oxygen level for calibration and the experiments was obtained by bubbling oxygen-free nitrogen through the sample for at least 10 min. The substrates 3-amino-4-hydroxytoluene, 4-amino-3-hydroxytoluene, 2-amino-3-hydroxybenzoic acid, 3-amino-2-hydroxybenzoic acid, 3,4-diaminobenzoic acid, 2,3-dihydroxybenzoic acid, 4-fluor-1,2-phenylenediamine, 4-chloro-1,2-phenylenediamine and 4-bromo-1,2-phenylenediamine were studied by means of this method.

The effect of various reagents, whose concentrations are given in detail in the corresponding figures of Section 3, was studied. In all the assays, the following reagents were maintained constant: 0.26 mM O_2 (saturating), 30 mM phosphate buffer pH 7.0 and the concentration of AH_2 that is indicated in the corresponding figure legend.

2.2.3. Data analysis

The experimental data of time-based assays for the disappearance of AH_2 follow Eq. (1):

$$[AH_2] = [AH_2]_f + [AH_2]_\infty e^{-\lambda^S_{E_{ox}} t} \quad (1)$$

where $[AH_2]_f$ is the AH_2-value at $t \to \infty$, $[AH_2]_\infty = [Q]_\infty$ is the AH_2 consumed at the end of the reaction and $\lambda^S_{E_{ox}}$ is the apparent constant of suicide inactivation of tyrosinase in the presence of the corresponding

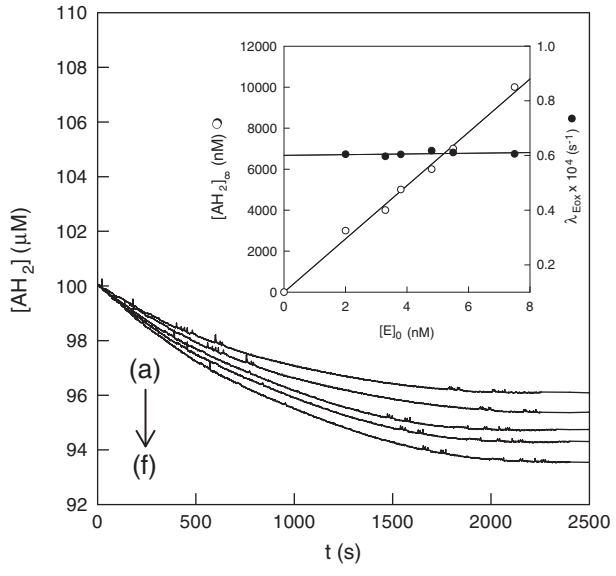

Fig. 1. Corrected recordings of the disappearance of AH_2 in the suicide inactivation of tyrosinase by the oxidation of 3,4-diaminotoluene for different enzyme concentrations. The experimental conditions were 30 mM sodium phosphate buffer (pH 7.0), 0.1 mM AH_2, 0.26 mM O_2, wavelength = 265 nm, the initial substrate concentration, $[S]_0 = 0.1$ mM, and the initial enzyme concentration, $[E]_0$, (nM): (a) 2, (b) 3.3, (c) 3.8, (d) 4.8, (e) 5.5 and (f) 7.5. Inset. Representation of the values of $[AH_2]_\infty$ (○) and $\lambda^S_{E_{ox}}$ (•) *vs.* enzyme concentration.

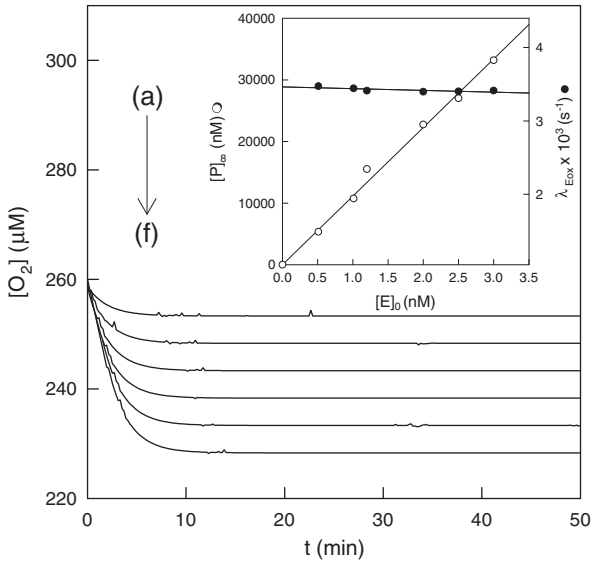

Fig. 2. Corrected recordings of the disappearance of oxygen in the suicide inactivation of tyrosinase by the oxidation of 3-amino-4-hydroxytoluene for different enzyme concentrations. The experimental conditions were 30 mM sodium phosphate buffer (pH 7.0), 0.15 mM AH_2, 0.26 mM O_2, $[S]_0 = 5$ mM and $[E]_0$ (nM): (a) 0.5, (b) 1, (c) 1.2, (d) 2, (e) 2.5 and (f) 3. Inset. Representation of the values of $[O_2]_\infty$ (○) and $\lambda^S_{E_{ox}}$ (•) *vs.* enzyme concentration.

Table 1
Kinetic constants characterising the suicide inactivation of tyrosinase acting on aromatic *o*-diamines.

Aromatic *o*-diamine	$\lambda_{E_{ox}(max)}{}^{S}$ x 10^3 (s^{-1})	*r*	k^S_{cat} (s^{-1})	K^S_m (mM)	k_6 (M^{-1} s^{-1})	δ_1 (ppm)	δ_2 (ppm)	δ_3 (ppm)	δ_4 (ppm)	$\Sigma\delta$ (ppm)
4-Fluor-1,2-phenylenediamine	3.87 ± 0.32	31 ± 3	0.12 ± 0.01	0.24 ± 0.03	500 ± 58	128.9	134.9	–	–	263.8
4-Bromo-1,2-phenylenediamine	3.75 ± 0.35	16 ± 2	0.06 ± 0.01	0.73 ± 0.10	82 ± 11	132.3	135.5	–	–	267.8
4-Chloro-1,2-phenylenediamine	2.57 ± 0.18	35 ± 3	0.09 ± 0.01	0.52 ± 0.07	173 ± 19	131.4	134.7	–	–	266.1
4-Methoxy-1,2-phenylenediamine	1.77 ± 0.12	852 ± 89	1.48 ± 0.15	0.38 ± 0.06	3894 ± 416	125.6	134.3	–	–	259.9
1,2-Diaminobenzene	1.47 ± 0.09	360 ± 31	0.51 ± 0.06	0.44 ± 0.04	1159 ± 132	133.3	133.3	–	–	266.6
3,4-Diaminotoluene	0.85 ± 0.09	599 ± 51	0.54 ± 0.05	0.07 ± 0.01	7714 ± 892	–	–	133.2	130.3	263.5
3,4-Diaminobenzoic acid	0.81 ± 0.07	98 ± 9	0.07 ± 0.01	0.13 ± 0.02	538 ± 58	–	–	127.2	132.4	259.6
2,3-Diaminobenzoic acid	0.57 ± 0.05	88 ± 7	0.04 ± 0.01	0.30 ± 0.04	133 ± 11	–	134.3	135.9	–	270.2

Table 2
Kinetic constants characterising the suicide inactivation of tyrosinase acting on *o*-aminophenols.

o-Aminophenol	$\lambda_{E_{ox}(max)}{}^{S} \times 10^3$ (s^{-1})	*r*	k^S_{cat} (s^{-1})	K^S_m (mM)	k_6 (M^{-1} s^{-1})	δ_1 (ppm)	δ_2 (ppm)	δ_3 (ppm)	δ_4 (ppm)	$\Sigma\delta$ (ppm)
2-Aminophenol	7.90 ± 0.09	7666 ± 815	58.12 ± 2.84	0.82 ± 0.09	70,878 ± 7502	143.9	133.9	–	–	277.8
3-Amino-4-hydroxytoluene	5.34 ± 0.39	5503 ± 502	25.02 ± 1.58	2.77 ± 0.59	9032 ± 918	–	–	133.8	140.9	274.7
4-Amino-3-hydroxytoluene	4.43 ± 0.41	5884 ± 510	21.72 ± 2.13	2.33 ± 0.41	9322 ± 950	–	–	143.8	130.9	274.7
3-Amino-L-tyrosine	2.01 ± 0.17	701 ± 65	1.21 ± 0.15	0.96 ± 0.20	1260 ± 121	–	–	133.8	141.1	274.9
4-Amino-3-hydroxybenzoic acid	0.62 ± 0.04	810 ± 76	0.48 ± 0.01	0.14 ± 0.01	3429 ± 315	–	–	144.1	139.1	283.2
3-Amino-4-hydroxybenzoic acid	0.37 ± 0.02	1230 ± 101	0.43 ± 0.01	0.13 ± 0.01	3308 ± 295	–	–	132.8	147.7	280.5
3-Amino-2-hydroxybenzoic acid	0.93 ± 0.07	140 ± 8	0.15 ± 0.01	0.39 ± 0.05	384 ± 39	–	150.6	134.7	–	285.3
2-Amino-3-hydroxybenzoic acid	1.38 ± 0.11	94 ± 7	0.15 ± 0.01	2.20 ± 0.24	68 ± 7	–	137.4	145.4	–	282.8

o-diphenol, *o*-aminophenol or aromatic *o*-diamine. These parameters can be obtained by non-linear regression [33]. There is always a slow spontaneous oxidation of *o*-diphenol, *o*-aminophenol, aromatic *o*-diamine and AH_2 (result not shown), which should be computer corrected in further [AH_2] *vs*. time plots (in general this treatment is applied to all the kinetic recordings). Fig. 1 shows the recordings for the oxidation of 3,4-diaminotoluene. Kinetic analysis of these recordings according to Eq. (1) provides the values of $[AH_2]_\infty$ and $\lambda_{E_{ox}}{}^{S}$. The inset of Fig. 1 reveals the dependence of these parameters on the enzyme concentration.

When the disappearance of oxygen is measured, the experimental data of time-based assays for the disappearance follow Eq. (2):

$$[O_2] = [O_2]_f + [O_2]_\infty e^{-\lambda^S_{Eox} t} \quad (2)$$

where $[O_2]_f$ is the O_2-value at $t \to \infty$, $[O_2]_\infty$ is the O_2 consumed at the end of the reaction and $\lambda^S_{E_{ox}}$ is the apparent constant of suicide inactivation of tyrosinase in the presence of the corresponding substrate. These parameters can be obtained by non-linear regression [33]. Note that $[O_2]_\infty$ becomes $[Q]_\infty/2$, reflecting the stoichiometry of the reaction. Fig. 2 depicts the recordings for the disappearance of oxygen during the oxidation of 3-amino-4-hydroxytoluene. Fitting these data to Eq. (2) gives the values of $[O_2]_\infty$ and $\lambda^S_{E_{ox}}$. The dependence of these parameters on the enzyme concentration can be seen from Fig. 2 inset.

2.2.4. Determination of ^{13}C NMR chemical shifts

The carbon chemical shifts given in Tables 1–3 were obtained from the corresponding ^{13}C NMR spectra, which were recorded at 298 K on a Bruker Avance 400 MHz instrument employing buffered solutions (at pH = 7.0) of pure samples in D_2O. For those compounds that were insoluble in this medium (4-fluor-1,2-phenylenediamine, 4-chloro-1,2-phenylenediamine, 4-bromo-1,2-phenylenediamine, 4-methoxy-1,2-phenylenediamine, *o*-phenylenediamine, 3,4-diaminotoluene, 2-aminophenol, 3-amino-4-hydroxytoluene, 4-amino-3-hydroxytoluene and 3-amino-L-tyrosine), the respective chemical shifts were estimated with the ChemNMR module included in the ChemDraw v8.0, a CambridgeSoft Desktop Software and corrected with the chemical shifts of the corresponding head compound (*o*-phenylenediamine, 2-aminophenol, *o*-catechol).

3. Results and discussion

The suicide inactivation kinetic of tyrosinase acting on aromatic *o*-diamines and *o*-aminophenols was studied. From this study, the kinetic parameters that characterise the suicide inactivation process were obtained: the maximum apparent suicide constant ($\lambda_{E_{ox}(max)}{}^{S}$), the catalytic constant (k^S_{cat}) and the parameter *r* which represents the number of turnovers that 1 mol of enzyme makes before it is inactivated.

3.1. Oxidation of aromatic *o*-diamines

Scheme 1 represents a proposed mechanism to explain the catalytic oxidation of aromatic *o*-diamines, which takes into account (*i*) the suicide inactivation [6] and (*ii*) the studies carried out with 3,6-difluorocatechol, in which the existence of two kinetically significant pK's is evident [34]. Kinetic studies measuring the initial velocity

Table 3
Kinetic constants characterising the suicide inactivation of tyrosinase acting on *o*-diphenols.

o-Diphenol	$\lambda_{E_{ox}(max)}{}^{S} \times 10^3$ (s^{-1})	*r*	k^S_{cat} (s^{-1})	K^S_m (mM)	$k_6 \times 10^{-3}$ (M^{-1} s^{-1})	δ_1 (ppm)	δ_2 (ppm)	δ_3 (ppm)	δ_4 (ppm)	$\Sigma\delta$ (ppm)
Catechol	8.92 ± 0.27	99,994 ± 1604	874.1 ± 30.2	0.16 ± 0.01	5463.13 ± 568.21	146.59	146.59	–	–	293.18
4-Chlorocatechol	8.54 ± 0.25	99,356 ± 1377	859.2 ± 28.3	0.60 ± 0.03	1432.00 ± 148.02	145.04	147.35	–	–	292.39
4-Methylcatechol	8.21 ± 0.25	98,366 ± 1377	842.1 ± 26.1	0.10 ± 0.01	8421.00 ± 853.34	144.06	146.43	–	–	290.49
L-Dopa	2.21 ± 0.01	46,133 ± 2306	102.6 ± 19.2	0.55 ± 0.08	186.55 ± 19.36	–	–	146.92	146.06	292.98
2,3-Dihydroxybenzoic acid	0.96 ± 0.08	386 ± 40	0.39 ± 0.05	1.09 ± 0.14	0.36 ± 0.05	–	149.01	143.89	–	292.90
3,4-Dihydroxybenzoic acid	0.85 ± 0.03	10,186 ± 224	8.11 ± 0.30	0.07 ± 0.01	115.86 ± 13.62	–	–	146.04	150.00	296.04

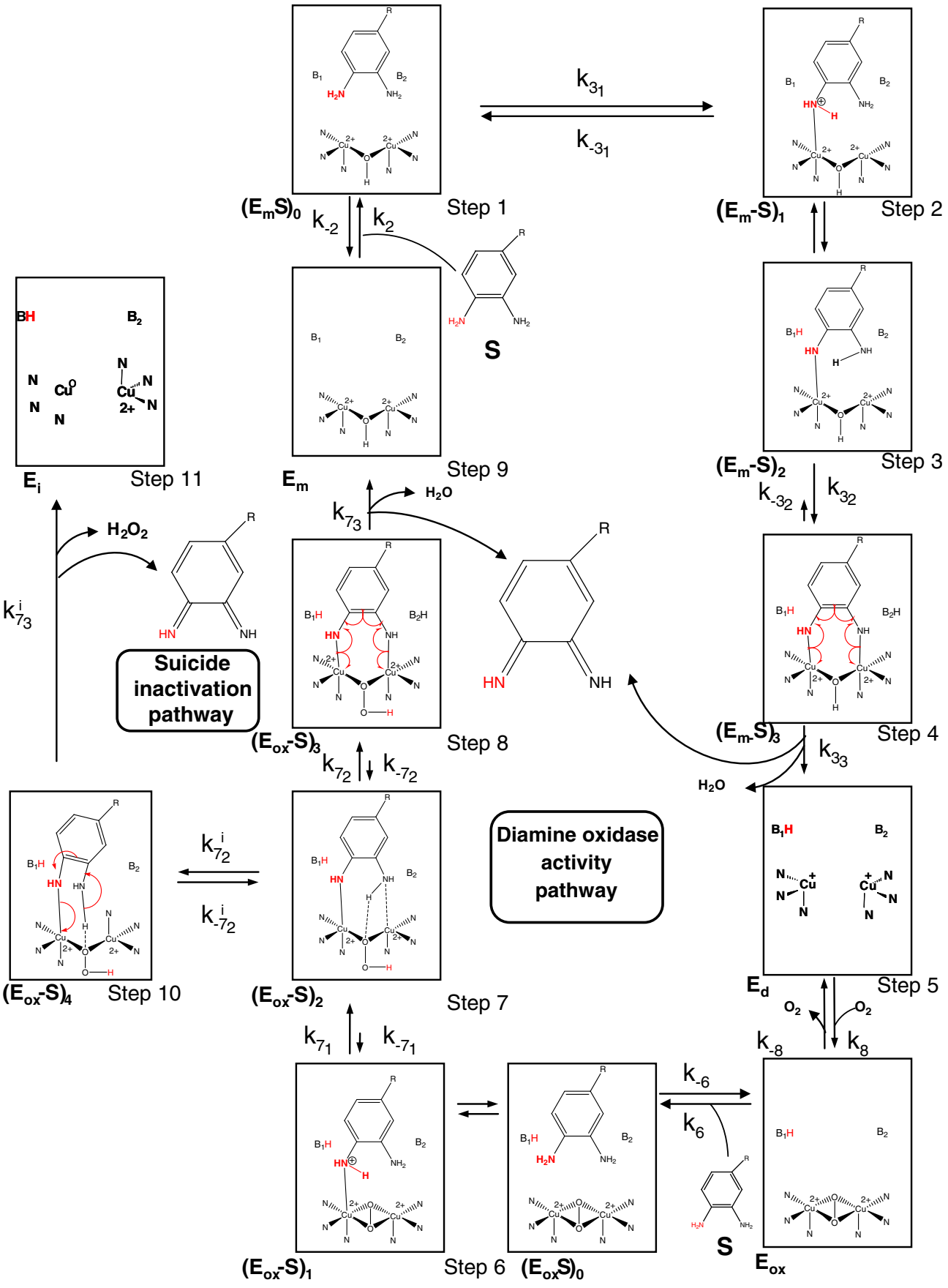

k_{3_1}
k_{-3_1}
$(E_mS)_0$
Step 1
k_{-2}
k_2
S
$(E_m\text{-}S)_1$
Step 2
$(E_m\text{-}S)_2$
Step 3
k_{-3_2}
k_{3_2}
E_i
Step 11
E_m
Step 9
H_2O
k_{7_3}
H_2O_2
$k^i_{7_3}$
Suicide inactivation pathway
$(E_{ox}\text{-}S)_3$
Step 8
$(E_m\text{-}S)_3$
Step 4
k_{3_3}
H_2O
k_{7_2}
k_{-7_2}
$k^i_{7_2}$
$k^i_{-7_2}$
Diamine oxidase activity pathway
$(E_{ox}\text{-}S)_4$
Step 10
$(E_{ox}\text{-}S)_2$
Step 7
E_d
Step 5
O_2
k_{-8}
k_8
k_{7_1}
k_{-7_1}
k_{-6}
k_6
$(E_{ox}\text{-}S)_1$
Step 6
$(E_{ox}S)_0$
S
E_{ox}

gave the catalytic constant (k^S_{cat}) and the Michaelis constant (K^S_m) (Table 1) [20]. Fig. 3 shows the recordings of the disappearance of AH_2 during the oxidation of 3,4-diaminotoluene, at long measuring times. Fig. 3 inset shows the values $\lambda^S_{E_{ox}}$ [obtained by means of Eq. (1)] for different concentrations of 3,4-diaminotoluene. Therefore, the hyperbolic behaviour observed in this representation allows us the calculation of $\lambda^S_{E_{ox}(max)}$ and K^S_m for this compound, according to Eq. (3) (Table 1) [6].

$$\lambda^S_{E_{ox}} = \frac{\lambda^S_{E_{ox}(max)}[S]_0}{K^S_m + [S]_0} \quad (3)$$

In the case of the oxidation of aromatic *o*-diamines, the velocity of catalysis reflected in the value of the catalytic constant (k^S_{cat}) is very low compared with those of the corresponding *o*-diphenols. This is because Step 7 in Scheme 1 is much slower due to the proton transfer from an amino group is less unlikely (compared when this transfer is produced from a hydroxyl group). This slowing down of the catalytic pathway has no effect on the suicide inactivation pathway because this process is limiting (Tables 1–3). From the values of $\lambda^S_{E_{ox}(max)}$ obtained for the aromatic *o*-diamines (Table 1) and bearing in mind the ^{13}C NMR values of these molecules (Table 1), it is deduced that (a) the substitution of oxygen by nitrogen slows down both the catalysis and suicide inactivation; (b) the first nucleophilic attack on CuB in Step 2 and Step 6 is always carried out by the nitrogen bound to the carbon atom with the lowest chemical shift (δ) in an attack that is facilitated by base 1 (B_1); (c) the second nitrogen atom can carry out a nucleophilic attack on the CuA, transferring the proton to the second base (B_2) or to the peroxide group of the oxy-tyrosinase form; (d) the lower the value of δ of the carbon atom that carries the NH_2 group responsible for the second attack on the CuA, the more nucleophilic the nature of the nitrogen, and so the catalytic pathway is preferred to the inactivation pathway and the apparent inactivation constant is lower; and (e) the sum of the chemical shifts of the carbon atoms that carry the diamine groups, will be responsible for the values of k^S_{cat}; hence, the lower the sum of the δ values, the greater the k^S_{cat}. Based on these predictions, the order of the aromatic *o*-diamines is given in Table 1.

The compounds 3,4-diaminobenzoic acid and 2,3-diaminobenzoic acid deserve additional comment. Taking into account its δ_3 and δ_4 values, 3,4-diaminobenzoic acid (Table 1) should have a low $\lambda^S_{E_{ox}(max)}$ and one of the highest k^S_{cat}. In the case of 2,3-diaminobenzoic acid, as the attack on the CuB is carried out by the C-2 group, a possible steric hindrance means that the behaviour of this compound could well differ from the predicted behaviour (see Table 1). The carboxylic group of 3,4-diaminobenzoic acid might inhibit tyrosinase, diminishing k^S_{cat}, $\lambda^S_{E_{ox}(max)}$ and K^S_m; in this case, 3,4-diaminobenzoic would be acting as a stoichiometric inhibitor with the substrate [35,36].

When the data shown in Table 1 for the aromatic *o*-diamines are compared with those obtained for *o*-diphenols (Table 3) k^S_{cat} can be seen to be smaller by three orders of magnitude, but the apparent inactivation constant ($\lambda^S_{E_{ox}(max)}$) remains in the same range, so that the value of *r* is much lower (by approximately three orders of magnitude) in the aromatic *o*-diamines (Tables 1 and 3).

The values of the Michaelis constants for the aromatic *o*-diamines are low (Table 1) and of a similar order of magnitude to those of the *o*-diphenols (Table 3), while the Michaelis constants of the *o*-aminophenols (Table 2) are greater, since

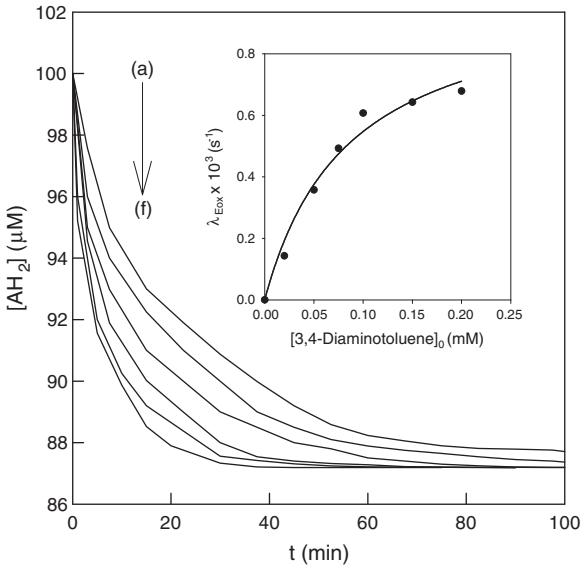

Fig. 3. Corrected recordings of the disappearance of AH_2 in the suicide inactivation of tyrosinase by the oxidation of different 3,4-diaminotoluene concentrations. The experimental conditions were 30 mM sodium phosphate buffer (pH 7.0), 0.26 mM O_2, wavelength = 265 nm and the initial concentrations of AH_2 and tyrosinase were 0.1 mM and 30 nM, respectively. The substrate concentrations were (mM) (a) 0.02, (b) 0.05, (c) 0.075, (d) 0.1, (e) 0.15 and (f) 0.2. Inset. Values of $\lambda^S_{E_{ox}}$ for different 3,4-diaminotoluene concentrations.

$$K^S_m = \frac{k^S_{cat}}{k_6} \quad (4)$$

The aromatic *o*-diamines have low k^S_{cat}, K^S_m and k_6 values (Table 1). We have postulated that it can be due that these compounds have an electron-rich ring and then repulsive π–π interactions with, probably, a histidine residue of the active site could established [37]. *o*-diphenols (Table 3) have high k^S_{cat} and k_6 values [21], and the ring of the substrate is less electron-rich and so there should be weaker repulsion at the active site. In the case of *o*-aminophenols (Table 2), the catalytic constant values, k^S_{cat}, are higher than those corresponding to the aromatic *o*-diamines and so K^S_m is slightly higher (see Eq. (4)). Thus, the k_6 values are lower in the case of aromatic *o*-diamines than in the case of *o*-diphenols (Tables 2 and 3).

3.2. Oxidation of o-aminophenols

The mechanism proposed to explain the catalytic oxidation and the suicide inactivation of *o*-aminophenols is described in Scheme 2. Fig. 4 shows the recordings obtained when varying the concentration of substrate in the oxidation of 3-amino-4-hydroxytoluene. Fig. 4 inset depicts the hyperbolic dependence of $\lambda^S_{E_{ox}}$ *vs.* $[S]_0$, while analysis using Eq. (3) permits us to obtain $\lambda^S_{E_{ox}(max)}$ and K^S_m. When the oxidation of the *o*-aminophenols is studied, the catalytic constants are greater than those obtained for the corresponding aromatic *o*-diamines (Tables 1 and 2) and lower than those of the *o*-diphenols (Table 3). The slowest step in the catalysis should be Step 7—the transfer of the proton to the peroxide group in oxy-tyrosinase. The

Scheme 1. Structural mechanism proposed to explain the catalytic and suicide inactivation pathways of tyrosinase in its action on aromatic *o*-diamines. E_m, met-tyrosinase; $(E_mS)_0$, met-tyrosinase/aromatic *o*-diamine complex; $(E_m–S)_1$, met-tyrosinase/aromatic *o*-diamine complex axially bound to a CuB atom with the base (B_1) forming a hydrogen bridge; $(E_m–S)_2$, met-tyrosinase/aromatic *o*-diamine complex axially bound to a CuB atom with protonated base (B_1H); $(E_m–S)_3$, met-tyrosinase/aromatic *o*-diamine complex axially bound to the two Cu atoms; E_d, deoxy-tyrosinase; E_{ox}, oxy-tyrosinase; $(E_{ox}S)_0$, oxy-tyrosinase/aromatic *o*-diamine complex; $(E_{ox}–S)_1$, oxy-tyrosinase/aromatic *o*-diamine complex axially bound to a CuB atom; $(E_{ox}–S)_2$, oxy-tyrosinase/aromatic *o*-diamine complex axially bound to the CuB atom and with the proton transferred to the peroxide group; $(E_{ox}–S)_3$, oxy-tyrosinase/aromatic *o*-diamine complex axially bound to the two Cu atoms with one proton transferred to the peroxide group and the other proton transferred to the base B_2 (B_2H); $(E_{ox}–S)_4$, oxy-tyrosinase/aromatic *o*-diamine complex axially bound to the CuB atom and with two protons transferred to the peroxide group; E_i, enzyme inactive.

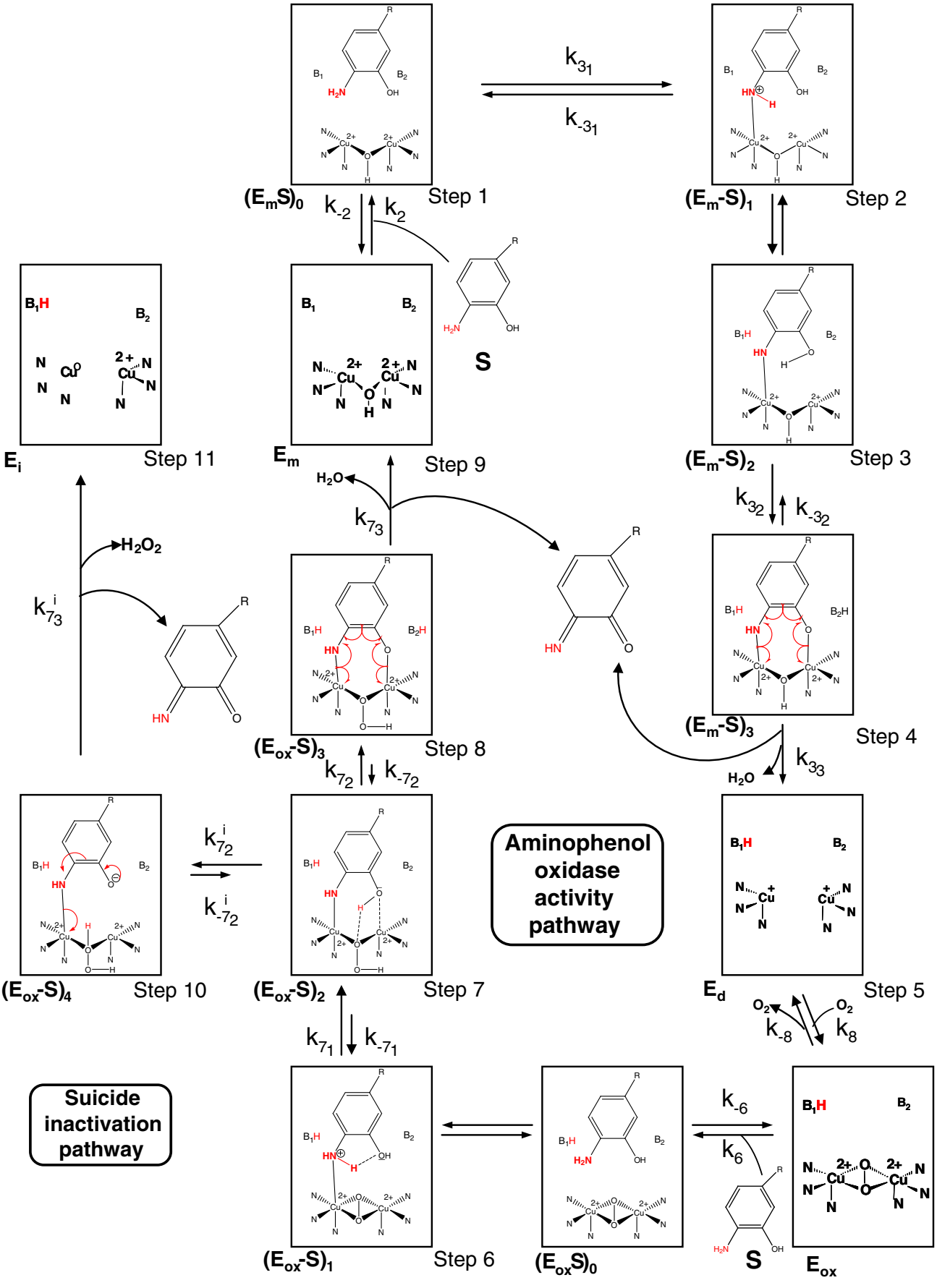
k_{31}
k_{-31}
$(E_mS)_0$
Step 1
$(E_m\text{-}S)_1$
Step 2
k_{-2}
k_2
S
E_i
Step 11
E_m
Step 9
$(E_m\text{-}S)_2$
Step 3
H_2O
k_{73}
k_{32}
k_{-32}
H_2O_2
k^i_{73}
$(E_{ox}\text{-}S)_3$
Step 8
$(E_m\text{-}S)_3$
Step 4
k_{72}
k_{-72}
H_2O
k_{33}
k^i_{72}
k^i_{-72}
Aminophenol oxidase activity pathway
$(E_{ox}\text{-}S)_4$
Step 10
$(E_{ox}\text{-}S)_2$
Step 7
E_d
Step 5
O_2
k_{-8}
O_2
k_8
k_{71}
k_{-71}
Suicide inactivation pathway
$(E_{ox}\text{-}S)_1$
Step 6
$(E_{ox}S)_0$
k_{-6}
k_6
S
E_{ox}

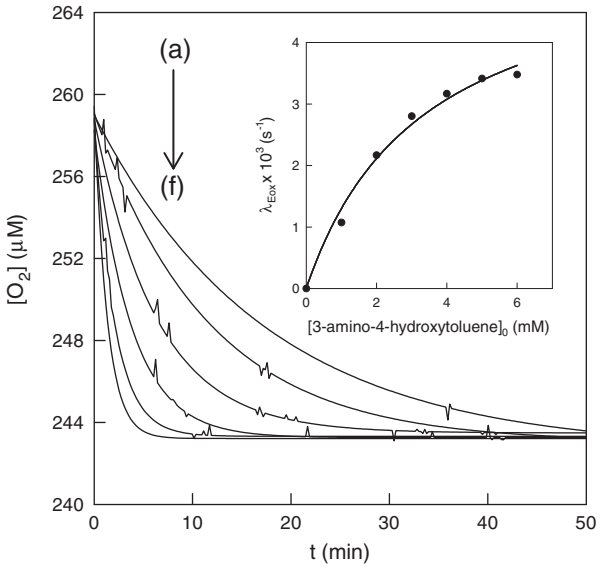

Fig. 4. Corrected recordings of the disappearance of oxygen in the suicide inactivation of tyrosinase by the oxidation of different 3-amino-4-hydroxytoluene concentrations. The experimental conditions were 30 mM sodium phosphate buffer (pH 7.0), 0.26 mM O_2 and the initial concentrations of AH_2 and tyrosinase were 0.15 mM and 2 nM, respectively. The substrate concentrations were (mM) (a) 1, (b) 2, (c) 3, (d) 4, (e) 5 and (f) 6. Inset. Values of $\lambda^S_{E_{ox}}$ for different 3-amino-4-hydroxytoluene concentrations.

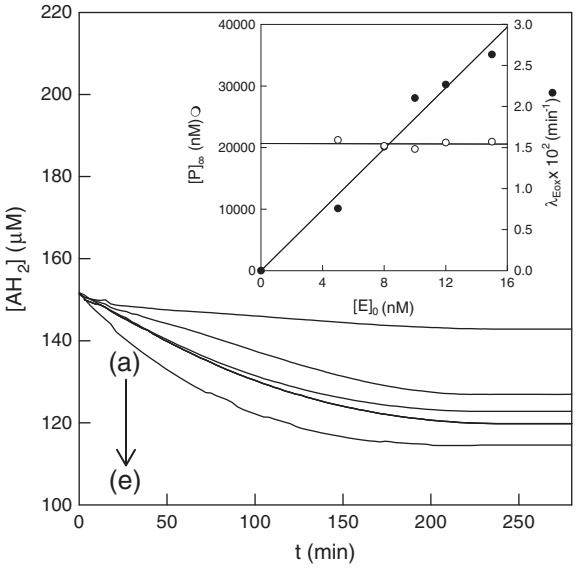

Fig. 5. Corrected recordings of the disappearance of AH_2 in the suicide inactivation of tyrosinase by the oxidation of 3-amino-4-hydroxybenzoic acid for different enzyme concentrations. The experimental conditions were 30 mM sodium phosphate buffer (pH 7.0), 0.15 mM AH_2, 0.26 mM O_2, wavelength = 280 nm, $[S]_0 = 0.37$ mM and $[E]_0$ (nM): (a) 5, (b) 8, (c) 10, (d) 12 and (e) 15. Inset. Representation of the values of $[AH_2]_\infty$ (○) and $\lambda^S_{E_{ox}}$ (•) *vs.* enzyme concentration.

speed of the suicide inactivation will depend on the efficiency of the nucleophilic attack of the oxygen atom of the hydroxyl group. In principle, the substrate attack will always occur through the amino group on the CuB and then of the oxygen atom of the hydroxyl group on CuA. Depending on the δ value of the carbon atom carrying the hydroxyl group, the catalytic or inactivation pathway will be favoured. When the δ value is low, the nucleophilic attack of the oxygen atom of the hydroxyl group on the copper atom (CuA) would be favoured and the proton transferred to base B_2 thereby favouring the catalytic pathway over the inactivation pathway. In this way, the value of $\lambda^S_{E_{ox}(max)}$ would be lower than in the case of *o*-diphenols. The results depicted in Table 2 agree with this reasoning. The catalytic constants are lower than for the *o*-diphenols, but, in this case, only by one order of magnitude (Tables 2 and 3). The apparent inactivation constants remain within the same order of magnitude as those corresponding to *o*-diphenols but are lower (Tables 2 and 3), which agrees with the behaviour of the aromatic *o*-diamines, suggesting that the slowest step of the whole process (inactivation pathway) is the transfer of a proton from the amine group (aromatic *o*-diamines) or the hydroxyl group (*o*-aminophenols and *o*-diphenols) to the peroxide group in the form E_{ox} (Tables 1–3).

Table 2 shows the compounds ordered by the decreasing value of $\lambda^S_{E_{ox}(max)}$, where, in addition, it is possible to distinguish between the compounds bearing -OH (2-aminophenol) or $-CH_3$ (3-amino-4-hydroxytoluene and 4-amino-3-hydroxytoluene) in C-1, and the group bearing $-CH_2-CHNH_2-COOH$ (3-amino-L-tyrosine). In this way, it is possible to distinguish the derivates of benzoic acid, which, as mentioned above, may inhibit the enzyme through carboxylic group. Such compounds would act as stoichiometric inhibitors, and so k^S_{cat}, K^S_m and $\lambda^S_{E_{ox}(max)}$ would decay. Figs. 5 and 6 show the recordings for the oxidation of 3-amino-4-hydroxybenzoic acid obtained byz varying the concentrations of enzyme and substrate, respectively. Fig. 5 inset and Fig. 6 inset show the dependence of $[AH_2]_\infty$ and $\lambda^S_{E_{ox}}$ on these concentrations. As can be seen, the concentration of $[AH_2]_\infty$ is

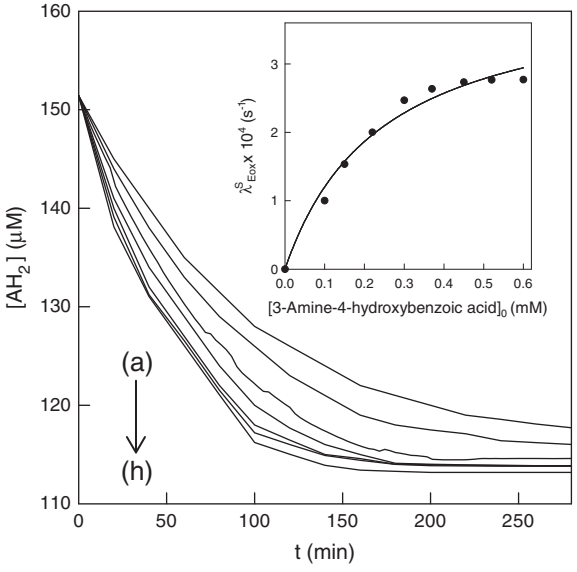

Fig. 6. Corrected recordings of the disappearance of AH_2 in the suicide inactivation of tyrosinase by the oxidation of different 3-amino-4-hydroxybenzoic acid concentrations. The experimental conditions were 30 mM sodium phosphate buffer (pH 7.0), 0.26 mM O_2, wavelength = 280 nm and the initial concentrations of AH_2 and tyrosinase were 0.15 mM and 15 nM, respectively. The substrate concentrations were (mM) (a) 0.1, (b) 0.15, (c) 0.22, (d) 0.3, (e) 0.37, (f) 0.45, (g) 0.52 and (h) 0.6. Inset. Values of $\lambda^S_{E_{ox}}$ for different 3-amino-4-hydroxybenzoic acid concentrations.

Scheme 2. Structural mechanism proposed to explain the catalytic and suicide inactivation pathways of tyrosinase in its action on *o*-aminophenols. E_m, met-tyrosinase; $(E_mS)_0$, met-tyrosinase/*o*-aminophenol complex; $(E_m–S)_1$, met-tyrosinase/*o*-aminophenol complex axially bound to a CuB atom; $(E_m–S)_2$, met-tyrosinase/*o*-aminophenol complex axially bound to a CuB atom with the proton transferred to the base B_1 (B_1H); $(E_m–S)_3$, met-tyrosinase/*o*-aminophenol complex axially bound to the two Cu atoms with the proton of the OH group transferred to the base B_2 (B_2H); E_d, deoxy-tyrosinase; E_{ox}, oxy-tyrosinase; $(E_{ox}S)_0$, oxy-tyrosinase/*o*-aminophenol complex; $(E_{ox}–S)_1$, oxy-tyrosinase/*o*-aminophenol complex axially bound to a CuB atom; $(E_{ox}–S)_2$, oxy-tyrosinase/*o*-aminophenol complex axially bound to the CuB atom and with the proton transferred to the peroxide group; $(E_{ox}–S)_3$, oxy-tyrosinase/*o*-aminophenol complex axially bound to the two Cu atoms with one proton transferred to the peroxide group and the other proton transferred to the base B_2 (B_2H); $(E_{ox}–S)_4$, oxy-tyrosinase/*o*-aminophenol complex axially bound to the CuB atom with two protons transferred to the peroxide group; E_i, inactive enzyme.

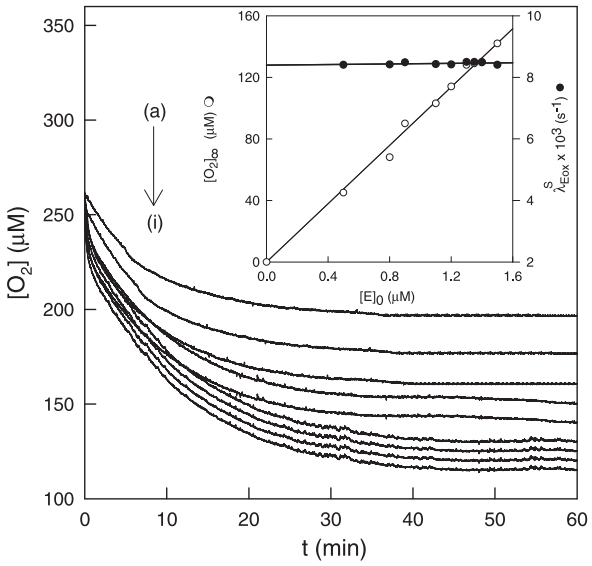

Fig. 7. Corrected recordings of the disappearance of oxygen in the suicide inactivation of tyrosinase by the oxidation of 2-amino-3-hydroxybenzoic acid for different enzyme concentrations. The experimental conditions were 30 mM sodium phosphate buffer (pH 7.0), 0.15 mM AH_2, 0.26 mM O_2, $[S]_0 = 3$ mM and $[E]_0$ (nM): (a) 0.5, (b) 0.8, (c) 0.9, (d) 1.1, (e) 1.2, (f) 1.3, (g) 1.35, (h) 1.4 and (i) 1.5. Inset. Representation of the values of $[O_2]_\infty$ (○) and $\lambda_{E_{ox}}{}^S$ (•) *vs.* enzyme concentration.

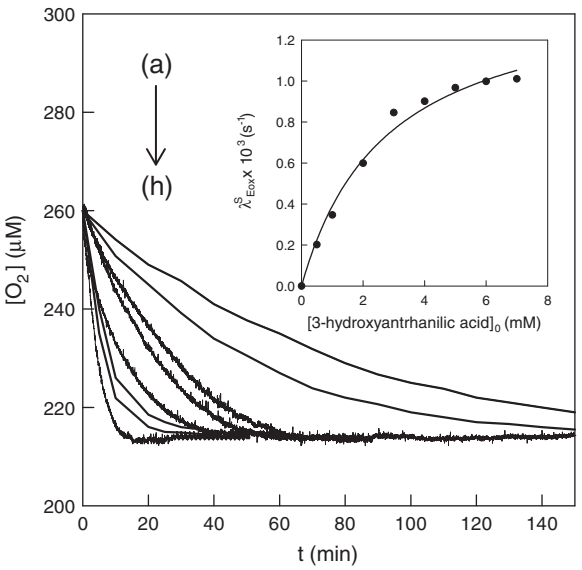

Fig. 8. Corrected recordings of the disappearance of oxygen in the suicide inactivation of tyrosinase by the oxidation of different 2-amino-3-hydroxybenzoic acid concentrations. The experimental conditions were 30 mM sodium phosphate buffer (pH 7.0), 0.26 mM O_2 and the initial concentrations of AH_2 and tyrosinase were 0.15 mM and 0.5 μM, respectively. The substrate concentrations were (mM) (a) 0.5, (b) 1, (c) 2, (d) 3, (e) 4, (f) 5, (g) 6 and (h) 7. Inset. Values of $\lambda_{E_{ox}}{}^S$ for different 2-amino-3-hydroxybenzoic acid concentrations.

directly proportional to the enzyme concentration, while $\lambda^S_{E_{ox}}$ is independent (Fig. 5 inset). However, $\lambda^S_{E_{ox}}$ shows a hyperbolic behaviour *vs.* the substrate concentration, while $[AH_2]_\infty$ is independent (Fig. 6 inset). By means of Eq. (3) it is possible to obtain $\lambda^S_{E_{ox}(max)}$ and K^S_m (Table 2). Figs. 7 and 8 depict the recordings of the disappearance of oxygen during the oxidation of 2-amino-3-hydroxybenzoic acid by tyrosinase, varying the enzyme and substrate concentrations, respectively. Fig. 7 inset depicts the values of $[O_2]_\infty$ and $\lambda^S_{E_{ox}}$ *vs.* enzyme concentration. Fig. 8 inset represents $\lambda^S_{E_{ox}}$ vs. the substrate concentration. From Eq. (3), it is possible to obtain $\lambda^S_{E_{ox}(max)}$ and K^S_m (Table 2). The results are similar to those obtained in the insets of Figs. 5 inset and 6.

Table 2 shows that the compound 2-aminophenol has the highest k^S_{cat} and, as the δ value of the carbon atom carrying the hydroxyl group is high, its $\lambda^S_{E_{ox}(max)}$ is also high and the *r* is the highest in Table 2. Its K^S_m is higher than that of catechol, possibly because the binding constant to the enzyme (k_6) is hindered by the repulsion involved in the π–π interactions (Table 2). As can be seen, the derivates of toluene show similar values of k^S_{cat} and $\lambda^S_{E_{ox}(max)}$ and, therefore, of *r*. Note that the Michaelis constants are one order of magnitude higher than that corresponding to 4-methylcatechol even though the k^S_{cat} is one order of magnitude less, probably because the lower binding constant (k_6) resulting from the greater electron density of the aromatic ring would hinder the binding (see Table 2). In the case of 3-amino-L-tyrosine, the nitrogen in C-3 would be responsible for the binding in CuB; the δ_4 value is very high and so the catalytic constant falls to 1.41 s^{-1}; furthermore, the first attack on CuB occurs through the amino group bound to C-3, and the Michaelis constant increases with respect to L-dopa, pointing to steric hindrances, as has been described previously for the compounds 2-amino-3-hydroxybenzenesulphonamide and 3-amino-2-hydroxybenzenesulphonamide [38].

In the case of the benzoic acid derivates, as in the case of aromatic *o*-diamines, the carboxylic group may react with the copper atoms, inhibiting the enzyme and resulting in an apparent diminution of k^S_{cat}, $\lambda^S_{E_{ox}(max)}$ and K^S_m [35,36]. Note the low values of these parameters in Table 2 and how the carbon atoms that support the NH_2 group have a lower δ value. In the same way, the withdrawing effect of the carboxylic group is stronger if the substituent in C-4 is a hydroxyl group. This is confirmed by comparing the 3-amino-4-hydroxybenzoic acid and 3-hydroxy-4-aminobenzoic acid, which have similar k^S_{cat}, $\lambda^S_{Eox}(max)$, K^S_m and *r* values. In the case of ortho derivates, the results are practically identical to those obtained for the dihydroxylated derivates (Tables 2 and 3) except that the K^S_m is higher in 2-amino-3-hydroxybenzoic acid (3-hydroxyanthranilic acid). The attack carried out by C-2 (CuB) points to the steric hindrance involved in the increase in K^S_m [38].

The results described above highlight the importance of proton transfer from the aromatic *o*-diamines and *o*-aminophenols to the peroxide group in the oxy-tyrosinase. During the catalysis, two transfers may occur to the oxy-tyrosinase, one to base B_2 and the other to the peroxide group in what is probably the limiting step (Step 7 in Schemes 1 and 2). The transfer of two protons probably occurs during suicide inactivation as well, but, in this case, both are transferred to the peroxide group of the oxy-tyrosinase. The first nucleophilic attack of the oxygen atom from the hydroxyl group involving the transfer of the first proton to the peroxide group is the limiting step of the catalysis, while the deprotonation involving no nucleophilic attack of the oxygen atom of the second hydroxyl group is the limiting step in the inactivation (Step 10 en Schemes 1 and 2). As regards Schemes 1 and 2, the first proton to the peroxide group corresponds to Step 7 in both cases (limiting step of the catalysis). The catalytic pathway continues in both Schemes with Step 8, in which the proton is transferred to base B_2. The inactivation pathway in both Schemes continues with Step 10, both for aromatic *o*-diamines (Scheme 1) and *o*-aminophenols (Scheme 2). This step would be limiting for the suicide inactivation.

Supplementary materials related to this article can be found online at doi:10.1016/j.bbapap.2012.02.001.

Acknowledgements

This paper was partially supported by grants from Ministerio de Educación y Ciencia (Madrid, Spain) Project BIO2009-12956, Fundación Séneca (CARM, Murcia, Spain) Projects 08856/PI/08 and 08595/PI/08, and Consejería de Educación (CARM, Murcia, Spain) BIO-BMC 06/01-0004. JLMM and FGM hold two fellowships from Fundación Caja Murcia

(Murcia, Spain). J.B. thanks the MICINN for a Ramon y Cajal Fellowship, co-financed by the European Social Fund.

References

[1] E.I. Solomon, U.M. Sundaram, T.E. Machonkin, Multicopper oxidases and oxygenases, Chem. Rev. 96 (1996) 2563–2606.

[2] M. Rolff, J. Schottenheim, H. Decker, F. Tuczek, Copper-O_2 reactivity of tyrosinase models towards external monophenolic substrates: molecular mechanism and comparison with the enzyme, Chem. Soc. Rev. 40 (2011) 4077–4098.

[3] L. Casella, E. Monzani, M. Gulloti, D. Cavagino, G. Cerina, L. Santagostini, R. Ugo, Functional modelling of tyrosinase. Mechanism of phenol ortho hydroxylation by dinuclear copper complexes, Inorg. Chem. 35 (1996) 7516–7625.

[4] J. Escribano, J. Tudela, F. Garcia-Carmona, F. Garcia-Canovas, A kinetic study of the suicide inactivation of an enzyme measured through coupling reactions, Biochem. J. 262 (1989) 597–603.

[5] J.L. Munoz-Munoz, F. Garcia-Molina, R. Varon, P.A. Garcia-Ruiz, J. Tudela, F. Garcia-Canovas, J.N. Rodriguez-Lopez, Suicide inactivation of the diphenolase and monophenolase activities of tyrosinase, IUBMB Life 62 (2010) 539–547.

[6] J.L. Muñoz-Muñoz, F. Garcia-Molina, P.A. Garcia-Ruiz, M. Molina-Alarcon, J. Tudela, F. Garcia-Canovas, J.N. Rodriguez-Lopez, Phenolic substrates and suicide inactivation of tyrosinase: kinetics and mechanism, Biochem. J. 416 (2008) 413–440.

[7] J.L. Muñoz-Muñoz, J.R. Acosta-Motos, F. Garcia-Molina, R. Varon, P.A. Garcia-Ruíz, J. Tudela, F. Garcia-Cánovas, J.N. Rodríguez-López, Tyrosinase inactivation in its action on L-dopa, Biochim. Biophys. Acta 1804 (2010) 1467–1475.

[8] T.S. Chang, Two potent suicide substrates of mushroom tyrosinase, J. Agric. Food Chem. 55 (2007) 2010–2015.

[9] T.S. Chang, M.Y. Lin, H.J. Lin, Indentifying 8-hydroxynaringenin as a suicide substrate of mushroom tyrosinase, J. Cosmet. Sci. 61 (2010) 205–210.

[10] S.S.-K. Tai, C.-G. Lin, M.-H. Wu, T.S. Chang, Evaluation of depigmenting activity by 8-hydroxydaidzein in mouse B16 melanoma cells and human volunteers, Int. J. Mol. Sci. 10 (2009) 4257–4266.

[11] E.J. Land, C.A. Ramsden, P.A. Riley, The mechanism of suicide-inactivation of tyrosinase: a substrate structure investigation, Tohoku J. Exp. Med. 212 (2007) 341–348.

[12] Y. Matoba, T. Kumagai, A. Yamamoto, H. Yoshitsu, M. Sugiyama, Crystallographic evidence that the dinuclear copper center of tyrosinase is flexible during catalysis, J. Biol. Chem. 281 (2006) 8981–8990.

[13] M. Sendovski, M. Kanteev, V. Shuster Ben-Yosef, N. Adir, A. Fishman, Crystallization and preliminary X-ray crystallographic analysis of a bacterial tyrosinase from *Bacillus megaterium*, Acta Crystallogr. Sect. F Struct. Biol. Cryst. Commun. 66 (2010) 1101–1103.

[14] M. Sendovski, M. Kanteev, V. Shuster Ben-Yosef, N. Adir, A. Fishman, First structures of an active bacterial tyrosinase reveal copper plasticity, J. Mol. Biol. 405 (2011) 227–237.

[15] W.T. Ismaya, H.J. Rozeboom, A. Weijn, J.J. Mes, F. Fusetti, H.J. Wichers, W.B. Dijkstra, Crystal structure of *Agaricus bisporus* mushroom tyrosinase: identity of the tetramer subunits and interaction with tropolone, Biochemistry 50 (2011) 5477–5486.

[16] F. García-Molina, J.L. Muñoz-Muñoz, M. Garcia-Molina, P.A. Garcia-Ruiz, J. Tudela, F. Garcia-Canovas, J.N. Rodriguez-Lopez, Melanogenesis inhibition due to NADH, Biosci. Biotechnol. Biochem. 74 (2010) 1777–1787.

[17] F. García-Molina, J.L. Muñoz-Muñoz, J.R. Acosta, P.A. Garcia-Ruiz, J. Tudela, F. Garcia-Canovas, J.N. Rodriguez-Lopez, Melanogenesis inhibition by tetrahydropterines, Biochim. Biophys. Acta 1794 (2009) 1766–1774.

[18] F. García-Molina, J.L. Muñoz-Muñoz, F. Martinez-Ortiz, P.A. Garcia-Ruiz, J. Tudela, F. Garcia-Canovas, J.N. Rodriguez-Lopez, Tetrahydrofolic acid is a potent suicide substrate of mushroom tyrosinase, J. Agric. Food Chem. 59 (2011) 1383–1391.

[19] F. Garcia-Molina, A.N. Hiner, L.G. Fenoll, J.N. Rodriguez-Lopez, P.A. Garcia-Ruiz, F. Garcia-Canovas, J. Tudela, Mushroom tyrosinase: catalase activity, inhibition and suicide inactivation, J. Agric. Food Chem. 53 (2005) 3702–3709.

[20] J.L. Munoz-Munoz, F. Garcia-Molina, P.A. Garcia-Ruiz, R. Varon, J. Tudela, J.N. Rodriguez-Lopez, F. Garcia-Canovas, Catalytic oxidation of aminophenols and aromatic amines by mushroom tyrosinase, Biochim. Biophys. Acta 1814 (2011) 1974–1983.

[21] J.N. Rodriguez-Lopez, L.G. Fenoll, P.A. Garcia-Ruiz, R. Varon, J. Tudela, R.N. Thorneley, F. Garcia-Canovas, Stopped-flow and steady-state study of the diphenolase activity of mushroom tyrosinase, Biochemistry 39 (2000) 10497–10506.

[22] L. Fenoll, M.J. Peñalver, J.N. Rodriguez-Lopez, P.A. Garcia-Ruiz, F. Garcia-Canovas, J. Tudela, Deuterium isotope effect on the oxidation of monophenols and *o*-diphenols by tyrosinase, Biochem. J. 380 (2004) 643–650.

[23] M.J. Penalver, J.N. Rodriguez-Lopez, P.A. Garcia-Ruiz, F. Garcia-Canovas, J. Tudela, Solvent deuterium isotope effect on the oxidation of *o*-diphenols by tyrosinase, Biochim. Biophys. Acta 1650 (2003) 128–135.

[24] O. Toussaint, K. Lerch, Catalytic oxidation of 2-aminophenols and ortho hydroxylation of aromatic amines by tyrosinase, Biochemistry 26 (1987) 8567–8571.

[25] B. Gasowska, P. Kafarski, H. Wojtasek, Interaction of mushroom tyrosinase with aromatic amines, *o*-diamines and *o*-aminophenols, Biochim. Biophys. Acta 1673 (2004) 170–177.

[26] F. Maddaluno, K.F. Faull, Inhibition of mushroom tyrosinase by 3-amino-L-tyrosine: molecular probing of the active site of the enzyme, Experientia 44 (1988) 885–887.

[27] A. Rescigno, E. Sanjust, A.C. Rinaldi, F. Sollai, N. Curreli, A. Rinaldi, Effect of 3-hydroxyanthranilic acid on mushroom tyrosinase activity, Biochim. Biophys. Acta 1384 (1998) 268–276.

[28] O.H. Lowry, N.J. Rosebrough, A.L. Farr, R.J. Randall, Protein measurement with the folin phenol reagent, J. Biol. Chem. 193 (1951) 265–275.

[29] J.N. Rodriguez-Lopez, M. Banon-Arnao, F. Martinez-Ortiz, J. Tudela, M. Acosta, R. Varon, F. Garcia-Canovas, Catalytic-oxidation of 2,4,5-trihydroxyphenylalanine by tyrosinase-identification and evolution of intermediates, Biochem. Biophys. Acta 1160 (1992) 221–228.

[30] F. Garcia-Molina, J.L. Muñoz, R. Varon, J.N. Rodriguez-Lopez, F. Garcia-Canovas, J. Tudela, A review on spectrophotometric methods for measuring the monophenolase and diphenolase activities of tyrosinase, J. Agric. Food Chem. 55 (2007) 9739–9749.

[31] J.L. Munoz, F. Garcia-Molina, R. Varon, J.N. Rodriguez-Lopez, F. Garcia-Canovas, J. Tudela, Calculating molar absorptivities for quinones: application to the measurement of tyrosinase activity, Anal. Biochem. 351 (2006) 128–138.

[32] J.N. Rodriguez-Lopez, J.R. Ros-Martinez, R. Varon, F. Garcia-Canovas, Calibration of a Clark-type oxygen electrode by tyrosinase-catalyzed oxidation of a 4-*tert*-butylcatechol, Anal. Biochem. 202 (1992) 356–360.

[33] Jandel Scientific, Sigma Plot 9.0 for Windows™, Jandel Scientific, Core Madera, 2006.

[34] J.L. Muñoz-Muñoz, J. Berna, F. Garcia-Molina, P.A. Garcia-Ruiz, J. Tudela, J.N. Rodriguez-Lopez, F. Garcia-Canovas, Unravelling the suicide inactivation of tyrosinase: a discrimination between mechanisms. J. Mol. Catal. B Enzym. (2011), Doi: 10.1016/j.molcatb.2011.11.001.

[35] S. Menon, R.W. Fleck, G. Yong, K.G. Strothkamp, Benzoic acid inhibition of the α, β, and γ isoenzymes of *Agaricus bisporus* tyrosinase, Arch. Biochem. Biophys. 280 (1990) 27–32.

[36] J.S. Conrad, S.R. Dawso, E.R. Hubbard, T.E. Meyers, K.G. Strothkamp, Inhibitor binding to the binuclear active site of tyrosinase: temperature, pH and solvent deuterium isotope effects, Biochemistry 33 (1994) 5739–5744.

[37] H. Decker, R. Dillinger, F. Tuczek, How does tyrosinase work? Recent insights from model chemistry and structural biology, Angew. Chem. Int. Ed. 39 (2000) 1591–1595.

[38] A. Rescigno, F. Bruyneel, A. Padiglia, F. sollai, A. Salis, J. Marchand-Brynaert, E. Sanjust, Structure-activity relationships of various amino-hydroxy-benzenesulphonic acids and sulphonamides as tyrosinase substrates, Biochim. Biophys. Acta 1810 (2011) 799–807.

Supplementary material.

Table 1SM

Chemical structure of the substrates used in this work.

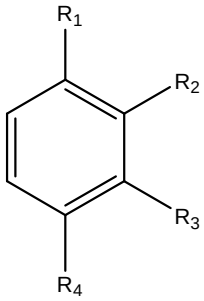

Substrate	R_1	R_2	R_3	R_4
2,3-Diaminobenzoic acid	COOH	NH_2	NH_2	H
3,4-Diaminobenzoic acid	COOH	H	NH_2	NH_2
3,4-Diaminotoluene	CH_3	H	NH_2	NH_2
4-Fluor-1,2-phenylendiamine	NH_2	NH_2	H	-F
4-Chloro-1,2-phenylendiamine	NH_2	NH_2	H	-Cl
4-Bromo-1,2-phenylendiamine	NH_2	NH_2	H	-Br
4-Methoxy-1,2-phenylendiamine	NH_2	NH_2	H	$-OCH_3$
1,2-Diaminobenzene	NH_2	NH_2	H	H
2-Amino-3-hydroxybenzoic acid	COOH	NH_2	OH	H
3-Amino-2-hydroxybenzoic acid	COOH	OH	NH_2	H
3-Amino-4-hydroxybenzoic acid	COOH	H	NH_2	OH
4-Amino-3-hydroxybenzoic acid	COOH	H	OH	NH_2
3-Amino-4-hydroxytoluene	CH_3	H	NH_2	OH
4-Amino-3-hydroxytoluene	CH_3	H	OH	NH_2
3-Amino-L-tyrosine	CH_2-CH(NH_2)-COOH	H	NH_2	OH
2-Aminophenol	OH	NH_2	H	H
2,3-Dihydroxybenzoic acid	COOH	OH	OH	H

3,4-Dihydroxybenzoic acid	COOH	H	OH	OH
4-Methylcatechol	OH	OH	H	CH_3
4-Chlorocatechol	OH	OH	H	Cl
L-dopa	CH_2-CH(NH_2)-COOH	H	OH	OH
Catechol	OH	OH	H	H

Table 2SM

Measurement wavelength (λ) and molar absorptivities (ε) of the substrates used in this work.

Substrate	Method	λ (nm)	ε (M^{-1} cm^{-1})
2,3-Diaminobenzoic acid	AH_2 disappearance	277	8260
3,4-Diaminobenzoic acid	O_2 disappearance	-	-
3,4-Diaminotoluene	AH_2 disappearance	260	10810
4-Methoxy-1,2-phenylendiamine	AH_2 disappearance	265	11170
4-Fluor-1,2-phenylendiamine	O_2 disappearance	-	-
4-Chloro-1,2-phenylendiamine	O_2 disappearance	-	-
4-Bromo-1,2-phenylendiamine	O_2 disappearance	-	-
1,2-Diaminobenzene	AH_2 disappearance	265	11170
2-Amino-3-hydroxybenzoic acid	O_2 disappearance	-	-
3-Amino-2-hydroxybenzoic acid	O_2 disappearance	-	-
3-Amino-4-hydroxybenzoic acid	AH_2 disappearance	280	7273
4-Amino-3-hydroxybenzoic acid	AH_2 disappearance	280	7273
3-Amino-4-hydroxytoluene	O_2 disappearance	-	-
3-Hydroxy-4-aminotoluene	O_2 disappearance	-	-
3-Amino-L-tyrosine	AH_2 disappearance	265	11170
2-Aminophenol	AH_2 disappearance	265	11170
2,3-Dihydroxybenzoic acid	O_2 disappearance	-	-
3,4-dihydroxybenzoic acid	O_2 disappearance	-	-
4-Methylcatechol	NADH disappearance	340	6230
4-Chlorocatechol	NADH disappearance	340	6230
L-dopa	Appearance of dopachrome	475	3600
Catechol	NADH disappearance	340	6230

4.21. INACTIVACIÓN SUICIDA DE LAS ACTIVIDADES DIFENOLASA Y MONOFENOLASA DE TIROSINASA.

El estudio de la inactivación suicida de las actividades difenolasa y monofenolasa de tirosinasa ha dado lugar a la siguiente publicación adjunta.

4.21.1. Título

Suicide inactivation of the diphenolase and monophenolase activitites of tyrosinase.

4.21.2. Autores

Muñoz-Muñoz, J.L.; Garcia-Molina, F.; Varon, R.; Garcia-Ruiz, P.A.; Tudela, J.; Garcia-Cánovas, F. y Rodríguez-López, J.N.

4.21.3. Referencia

International Union of Biochemistry and Molecular Biology (IUBMB Life) (2010) 62, 539-547.

4.21.4. Resumen

Se ha estudiado el mecanismo de inactivación suicida de tirosinasa al actuar sobre sus sustratos fenólicos. El análisis cinético del mecanismo propuesto durante la fase de transición permite obtener expresiones analíticas válidas para las concentraciones de *o*-quinonas *vs.* tiempo. Los efectos electrónicos, estéricos e hidrofóbicos de los sustratos fenólicos influyen en la reacción enzimática, aumentando la velocidad de catálisis tres órdenes de magnitud y la de inactivación un orden de magnitud. Para explicar esta inactivación suicida, proponemos un mecanismo donde la forma enzimática oxitirosinasa es la responsable de cada inactivación. En este mecanismo, la constante de velocidad estaría directamente relacionada con la fuerza del ataque nucleofílico del grupo hidroxilo presente en el átomo de carbono C-1. Este poder nucleofílico depende del desplazamiento químico del carbono C-1 (δ_1) obtenido por ^{13}C-RMN. La inactivación suicida ocurriría si el grupo hidroxilo en C-2 transfiere el protón al peróxido protonado, el cual actuaría de nuevo como una base generalizada. En este caso, la coplanaridad entre el átomo de cobre, el oxigeno de C-1 y el anillo permitiría solo la reacción de oxidación/reducción de un átomo de cobre, dando lugar a cobre (0), peróxido de hidrógeno y *o*-quinona, los cuales serían liberados, inactivando por tanto a la enzima. Una posible aplicación de esta propiedad podría ser el uso de estos sustratos suicidas como agentes despigmentantes de la piel.

IUBMB *Life*, 62(7): 539–547, July 2010

Critical Review

Suicide Inactivation of the Diphenolase and Monophenolase Activities of Tyrosinase

Jose Luis Muñoz-Muñoz[1], Francisco Garcia-Molina[1], Ramon Varon[2], Pedro A. Garcia-Ruíz[3], Jose Tudela[1], Francisco Garcia-Cánovas[1] and Jose Neptuno Rodríguez-López[1]

[1]*GENZ: Grupo de Investigación Enzimología, Departamento de Bioquímica y Biología Molecular-A, Facultad de Biologia, Universidad de Murcia, Espinardo, Murcia, Spain*

[2]*Departamento de Química-Física, Escuela de Ingenieros Industriales de Albacete, Universidad de Castilla la Mancha, Avda. España s/n, Campus Universitario, Albacete, Spain*

[3]*QCBA: Grupo de Química de Carbohidratos y Biotecnología de Alimentos, Departamento de Química Orgánica, Facultad de Química, Universidad de Murcia, Espinardo, Murcia, Spain*

Summary

The suicide inactivation mechanism of tyrosinase acting on its phenolic substrates has been studied. Kinetic analysis of the proposed mechanism during the transition phase provides explicit analytical expressions for the concentrations of *o*-quinone *versus* time. The electronic, steric, and hydrophobic effects of the phenolic substrates influence the enzymatic reaction, increasing the catalytic speed by three orders of magnitude and the inactivation by one order of magnitude. To explain this suicide inactivation, we propose a mechanism in which the enzymatic form oxy-tyrosinase is responsible for the inactivation. In this mechanism, the rate constant of the reaction would be directly related with the strength of the nucleophilic attack of the C-1 hydroxyl group, which depends on the chemical shift of the carbon C-1 (δ_1) obtained by ^{13}C-NMR. The suicide inactivation would occur if the C-2 hydroxyl group transferred the proton to the protonated peroxide, which would again act as a general base. In this case, the coplanarity between the copper atom, the oxygen of the C-1 and the ring would only permit the oxidation/reduction of one copper atom, giving rise to copper (0), hydrogen peroxide, and an *o*-quinone, which would be released, thus inactivating the enzyme. One possible application of this property could be the use of these suicide substrates as skin depigmenting agents. © 2010 IUBMB

IUBMB *Life*, 62(7): 539–547, 2010

Keywords mechanism-based inhibitors; suicide; inactivation; polyphenol oxidase; *o*-diphenols.

Received 2 March 2010; accepted 23 April 2010

Address correspondence to: Francisco Garcia-Cánovas, Facultad de Biologia, Campus de Espinardo, E-30100 Espinardo, Murcia, Spain. Tel: +34-968-364782. Fax: +34-968-363963. E-mail: canovasf@um.es

ISSN 1521-6543 print/ISSN 1521-6551 online
DOI: 10.1002/iub.00348

INTRODUCTION

Skin, hair, and eye pigmentation has been long and widely studied (*1*). The process is caused by melanins, heterogeneous polymers with a complex molecular structure, whose color ranges from yellow to black (*1*). Melanins are formed and accumulated in specialized organelles called melanosomes, which are to be found in cells known as melanocytes (*2*). Melanins are polymers that are formed in a series of enzymatic and non-enzymatic reactions from L-tyrosine and L-dopa. The melanin formation pathway (melanogenesis) includes chemical and enzymatic reactions (*1*).

Tyrosinase or polyphenol oxidase (EC 1.14.18.1) is widely distributed through the animal, vegetal, bacterial, and fungal kingdoms (*3, 4*). Tyrosinase catalyses two types of reactions on phenolic substrates, in which molecular oxygen intervenes: (*a*) the *ortho*-hydroxylation of the monophenols to *o*-diphenols (monophenolase activity) and (*b*) the oxidation of *o*-diphenols to *o*-quinones (diphenolase activity), which, in turn, are polymerized to brown, red, or black pigments (*1*).

Besides oxidizing their natural substrates (L-tyrosine and L-dopa), tyrosinase has a wide substrate specificity on monophenols (α-methyl-L-tyrosine, L-tyrosine methyl ester, etc.) and *o*-diphenols (dopamine, catechol, etc.) (*5*).

Tyrosinase undergoes an inactivation process when it reacts with their phenolic substrates, a phenomenon that has long been known in the case of enzymes from a variety of natural sources, including fungi, plant, and animals (*5–11*). The refining of spectrophotometric methods has allowed a kinetic study of the suicide inactivation of tyrosinase during its action on *o*-diphenols and triphenols (*7, 12, 13*). The study of enzymatic inactivation by suicide substrates or mechanism-based inhibitors is of

growing importance, because of possible pharmacological applications, for studying enzymatic mechanisms and designing new drugs (*14*). As tyrosinase participates in different physiological processes, such as fruit and vegetable browning and pigmentation in animals (*1*), the suicide inactivation process of this enzyme is of even more interest.

The main aim of kinetic studies of suicide substrates is their kinetic characterization through the parameters λ_{max} (maximum apparent inactivation constant), r (a partition ratio between the catalytic and the inactivation pathways), and K_m^S (Michaelis constant for the substrate) (*7–9*).

The kinetic mechanism of tyrosinase acting on monophenols and *o*-diphenols has been the object of several studies and has been reviewed (*15*). However, the suicide inactivation process of the enzyme is less well known, and so the purpose of this review is to summarize the kinetic studies on the suicide inactivation of tyrosinase acting on their different kinds of substrates, to propose reaction mechanism and look at possible physiological implications and applications.

KINETIC ANALYSIS OF THE SUICIDE INACTIVATION OF TYROSINASE

The kinetic mechanism proposed to explain the suicide inactivation of tyrosinase acting on *o*-diphenols is based on the structural mechanism proposed in Scheme 1 (*7*).

The derivation of the analytical expression, which establishes the accumulation of the product (Q) with time, when the initial substrate concentration $[S]_0$, is much higher than the initial concentration of enzyme $[E]_0$ and is described in detail in Supplementary material section of (*7*) (http://www.biochemj.org/bj/416/bj4160431add.htm).

The variation of $[Q]$ with time is given by Eq. (1) [see Supplementary material of (*7*)]:

$$[Q] = [Q]_\infty(1 - e^{-\lambda_{E_{ox}}t}) = \frac{V_0}{\lambda_{E_{ox}}}(1 - e^{-\lambda_{E_{ox}}t}) = \frac{V_{max}}{\lambda_{E_{ox}(max)}}(1 - e^{-\lambda_{E_{ox}}t}), \quad (1)$$

where $[Q]_\infty$ is the concentration of product accumulated at the end of the reaction, $\lambda_{E_{ox}}$ is the apparent inactivation constant of the E_{ox} form, $\lambda_{E_{ox}}(max)$ is the maximum value of the apparent inactivation constant, V_0 is the initial velocity, and V_{max} is the maximum velocity. When $t \to \infty$:

$$[Q]_\infty = \frac{2k_{cat}}{\lambda_{E_{ox}(max)}}[E]_0 = 2r[E_0], \quad (2)$$

where k_{cat} is the catalytic constant.

Bearing in mind that $K_m^{O_2}$ values are very low (*16*), and that the initial oxygen concentration is 0.26 mM, the enzyme is saturated with O_2, and from Eqs. (S8) and (S9) of (*7*), we obtain:

$$\lambda_{E_{ox}} = \frac{\lambda_{E_{ox}(max)}[S]_0}{K_m^S + [S]_0} \quad (3)$$

and

$$V_0 = \frac{2k_{cat}[S]_0[E]_0}{K_m^S + [S]_0} \quad (4)$$

When the disappearance of oxygen is measured:

$$[O_2] = [O_2]_f + [O_2]_\infty e^{-\lambda_{E_{ox}}t}, \quad (5)$$

where $[O_2]$ is the instantaneous concentration of oxygen, $[O_2]_f$ is the oxygen remaining at $t \to \infty$, and $[O_2]_\infty$ is the concentration of O_2 consumed at end of the reaction.

As *o*-quinones are unstable, reducing agents, such as nicotinamide adenine dinucleotide (NADH) or ascorbic acid (AH_2), can be used, and the corresponding equations for measuring the disappearance of NADH or AH_2 are as follows:

$$[NADH] = [NADH]_f + [NADH]_\infty e^{-\lambda_{E_{ox}}t}, \quad (6)$$

where [NADH] is the instantaneous concentration of NADH, $[NADH]_f$ is the NADH value at $t \to \infty$, and $[NADH]_\infty$ is the NADH consumed at the end of the reaction ($t \to \infty$). If the disappearance of AH_2 is measured, we obtain:

$$[AH_2] = [AH_2]_f + [AH_2]_\infty e^{-\lambda_{E_{ox}}t}, \quad (7)$$

where $[AH_2]$ is the instantaneous concentration of AH_2, $[AH_2]_f$ is the AH_2 value at $t \to \infty$, and $[AH_2]_\infty$ is the AH_2 consumed at the end of the reaction ($t \to \infty$).

Experimental Design

The experimental study of the kinetics of suicide substrates or mechanism-based enzyme inhibitors is important for obtaining reliable kinetic parameters ($\lambda_{E_{ox}(max)}$, K_m^S, and r) that will permit any *in vitro* information gained to be extrapolated to *in vivo* situations (*17*).

In a previous study, we outlined the methodology necessary for kinetically characterizing a suicide substrate following the reaction continuously (*9*). In this work, we apply the experimental design described in (*9*) to the suicide inactivation of tyrosinase as it acts on *o*-diphenols since, although the products obtained, *o*-quinones, are unstable, they can be reduced by NADH or AH_2 and the disappearance of these coupled reagents can be measured. Alternatively, the consumption of oxygen can be measured in an oxygraph because oxygen is also a substrate of the enzyme.

SUICIDE INACTIVATION OF TYROSINASE ACTING ON DIPHENOLIC SUBSTRATES

Numerous models on the tyrosinase reaction mechanism have appeared over the last 3 decades to explain the characteris-

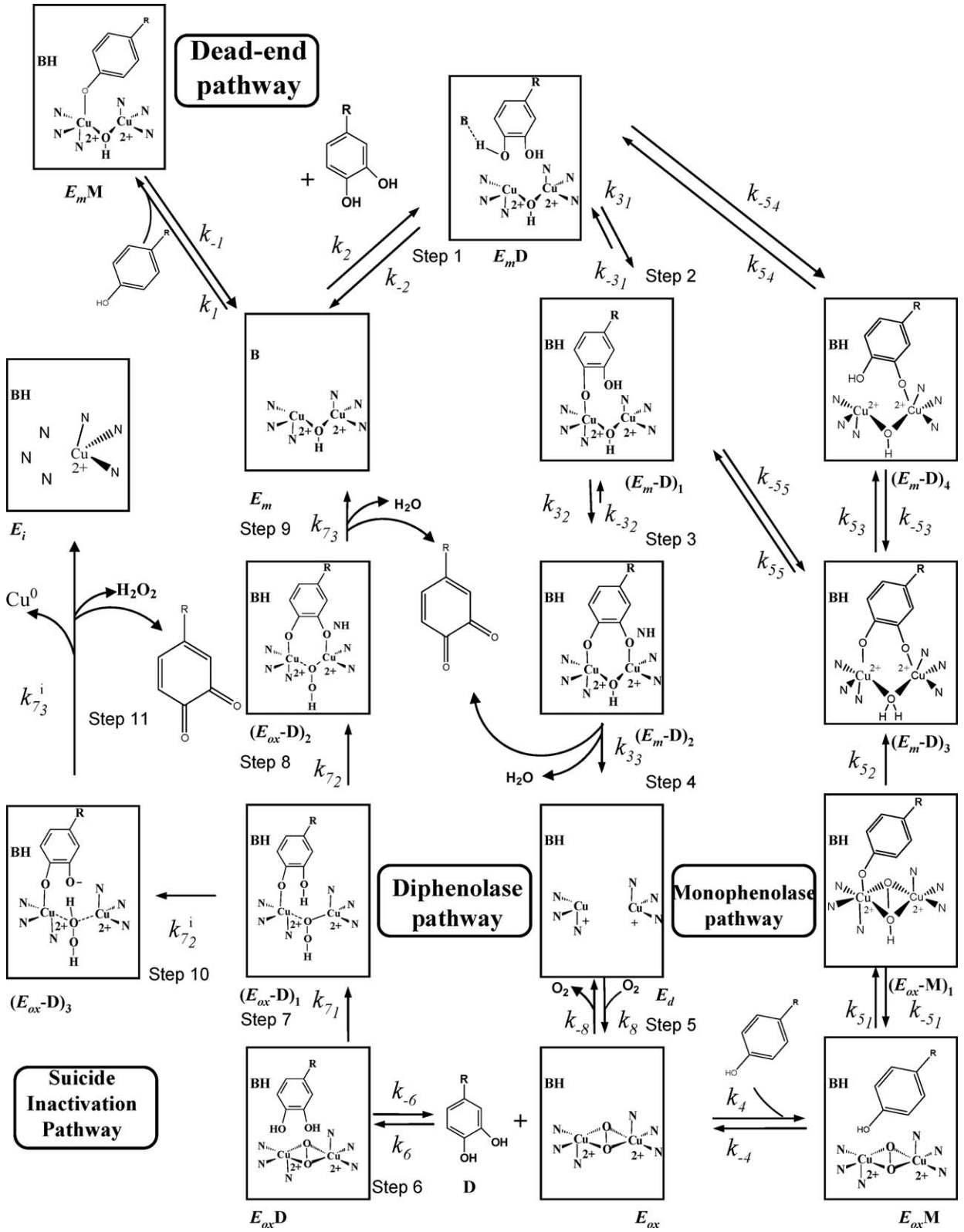

Scheme 1. Structural mechanism proposed to explain the diphenolase, monophenolase, and suicide inactivation pathways of tyrosinase acting on monophenols and *o*-diphenols. E_m, met-tyrosinase; E_d, deoxy-tyrosinase; E_{ox}, oxy-tyrosinase; E_{ox}D, oxy-tyrosinase/*o*-diphenol complex; $(E_{ox}\text{-D})_1$, oxy-tyrosinase/*o*-diphenol complex axially bound to a Cu atom; $(E_{ox}\text{-D})_2$, oxy-tyrosinase/*o*-diphenol complex axially bound to the two Cu atoms; E_mD, met-tyrosinase/*o*-diphenol complex; $(E_m\text{-D})_1$, met-tyrosinase/*o*-diphenol complex axially bound to a Cu atom; $(E_m\text{-D})_2$, met-tyrosinase/*o*-diphenol complex axially bound to the two Cu atoms; $(E_m\text{-D})_3$, met-tyrosinase/*o*-diphenol complex axial-equatorially bound to the two Cu atoms; $(E_m\text{-D})_4$, met-tyrosinase/*o*-diphenol complex equatorially bound to a Cu atom; E_mM, met-tyrosinase/monophenol complex; E_{ox}M, oxy-tyrosinase/monophenol complex; $(E_{ox}\text{-M})_1$, oxy-tyrosinase/monophenol complex axially bound to a Cu atom. $(E_{ox}\text{-D})_3$, oxy-tyrosinase/*o*-diphenol complex axially bound to one Cu atom and the deprotonated hydroxyl group of C-3; E_i, inactive form of tyrosinase.

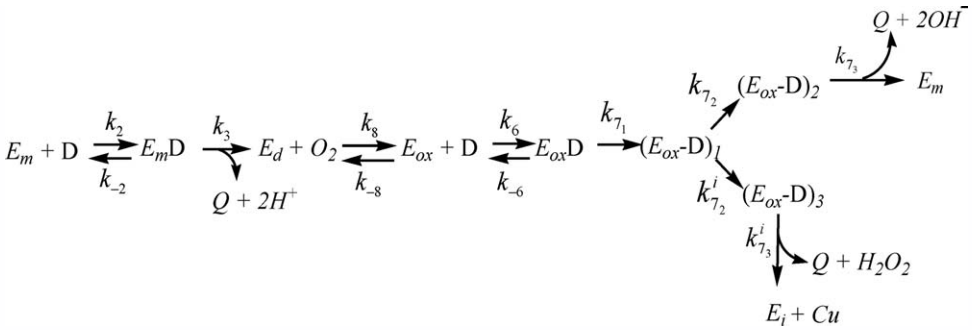

Scheme 2. Kinetic mechanism proposed to explain the suicide inactivation of tyrosinase acting on *o*-diphenols (see Scheme 1 for further details).

tics of monophenolase and diphenolase activities of tyrosinase, and, in particular, to clarify the presence of the lag period in its monophenolase activity (*15*). Our group has published a revision of the kinetic mechanism of tyrosinase activity (*15*) based on the structural aspects of the enzyme described by Dietler and Lerch (*4*) and Solomon et al. (*3*).

The catalytic cycle of tyrosinase acting on monophenols and *o*-diphenols is described in Scheme 1 (*15, 18*). The process of tyrosinase suicide inactivation has long been known, and we recently proposed a kinetic and structural mechanism to explain it (*7*).

When the enzyme acts on *o*-diphenols (Schemes 2 and 3), the suicide inactivation process is evident. The binding of the *o*-diphenol to the oxy form of the enzyme may begin with the transfer of an H^+ of the OH group in C-1 to the peroxide, while the phenolate attacks the copper (CuB) (*19*) (E_{ox}D). From this complex, two possibilities can exist: (*a*) the oxygen of the hydroxyl group of C-2 may attack the other copper atom (CuA), which is drawn closer following protonation of the peroxide, transferring the proton to the histidine (*19*), binding to the substrate diaxially and coplanar with the copper atoms. In this way, the concerted redox reaction (Step 9) can occur, releasing *o*-quinone and E_m. (*b*) The hydroxyl group of C-2 may cede a proton to the protonated peroxide, remaining as $C—O^-$ (Step 10). The coplanarity of the substrate ring, the oxygen of C-1 and the copper atom favor the simultaneous oxidation of the substrate to *o*-quinone and the reduction of one Cu^{2+} atom to copper (0) through the ring, while copper (0) and hydrogen peroxide are released, and the enzyme is inactivated as a consequence (Step 11). Note that the observation concerning the possibility of a bidentated union of the *o*-diphenol with one copper atom may also lead to suicide inactivation (*20*). Axial/equatorial-type bidentated structures have also been proposed for the binding of *o*-diphenols to copper (but only one copper) and have been seen by X-ray diffraction to be coplanar (*21*). However, the axial/equatorial binding to one copper atom in tyrosinase is not coplanar, and so the oxidation/reduction reaction cannot take place. For this reason, Steps 10 and 11 have been proposed in the mechanism of Schemes 2 and 3. The inactivation mechanism is consistent with the experimental observation that 50% of the copper is lost from the active site during catechol inactivation (*4*) and also with the experiments carried out (*22*) concerning the impossibility of reactivating the inactivated enzyme by adding Cu^{2+}, perhaps indicating the need for a "caddie" protein (*19*).

From the data shown in Table 1, the parallelism between the maximum apparent inactivation constant ($\lambda_{E_{ox}}$(max)) and the catalytic constant (k_{cat}) can be seen (Table 1), confirming the kinetic analysis as both are related by Eqs. (5)–(7). In this way, the best substrates, such as pyrogallol, catechol, 4-chlorocatechol, and 4-methylcatechol (with hydrogen or donating group in C-4), show higher catalytic (k_{cat}) and suicide inactivation ($\lambda_{E_{ox}(max)}$) constants, whereas the worst substrates, such as protocatechuic acid, protocatechuic aldehyde, and 4-nitrocatechol (with an electron-withdrawing group in C-4), have a low k_{cat} and $\lambda_{E_{ox}(max)}$. It should be noted that the electronic, steric, and hydrophobic effects on substrate–enzyme binding and on the inactivation and catalysis processes affect the catalysis (constants around 10^3) and suicide inactivation (constants around 10) processes. Note how pyrogallol inactivates the enzyme in the same way as the *o*-diphenols; furthermore, as it is the best substrate of the enzyme (greater k_{cat}), the $\lambda_{E_{ox}(max)}$ is also greater (Table 1).

The parameter $r = k_{7_2}/k^i_{7_2}$ (k_{7_2} and $k^i_{7_2}$ are the rate constants indicated in Scheme 2) indicates the probability that the hydroxyl group of C-2 will carry out a nucleophilic attack on the second copper (CuA), transferring the proton to the histidine and taking up a diaxial position (see Scheme 3). This assumption is derived from the flexible feature of the residue histidine previously proposed for *Streptomyces castaneoglobisporus* tyrosinase (*19*). Initially, it was proposed that the histidine bound axially to the E_{ox} form was His^{54}, although, subsequently, this axial position was attributed to His^{63} (*23, 24*). Another alternative, perhaps, is that it transfers the proton to the protonated peroxide, remaining in position C-1 and axially bound to the copper and to C-2 as $C—O^-$, a step favored by the charge density of the copper atom bound to the substrate. When this has a C-4 electron-donating group, the positive charge density in the

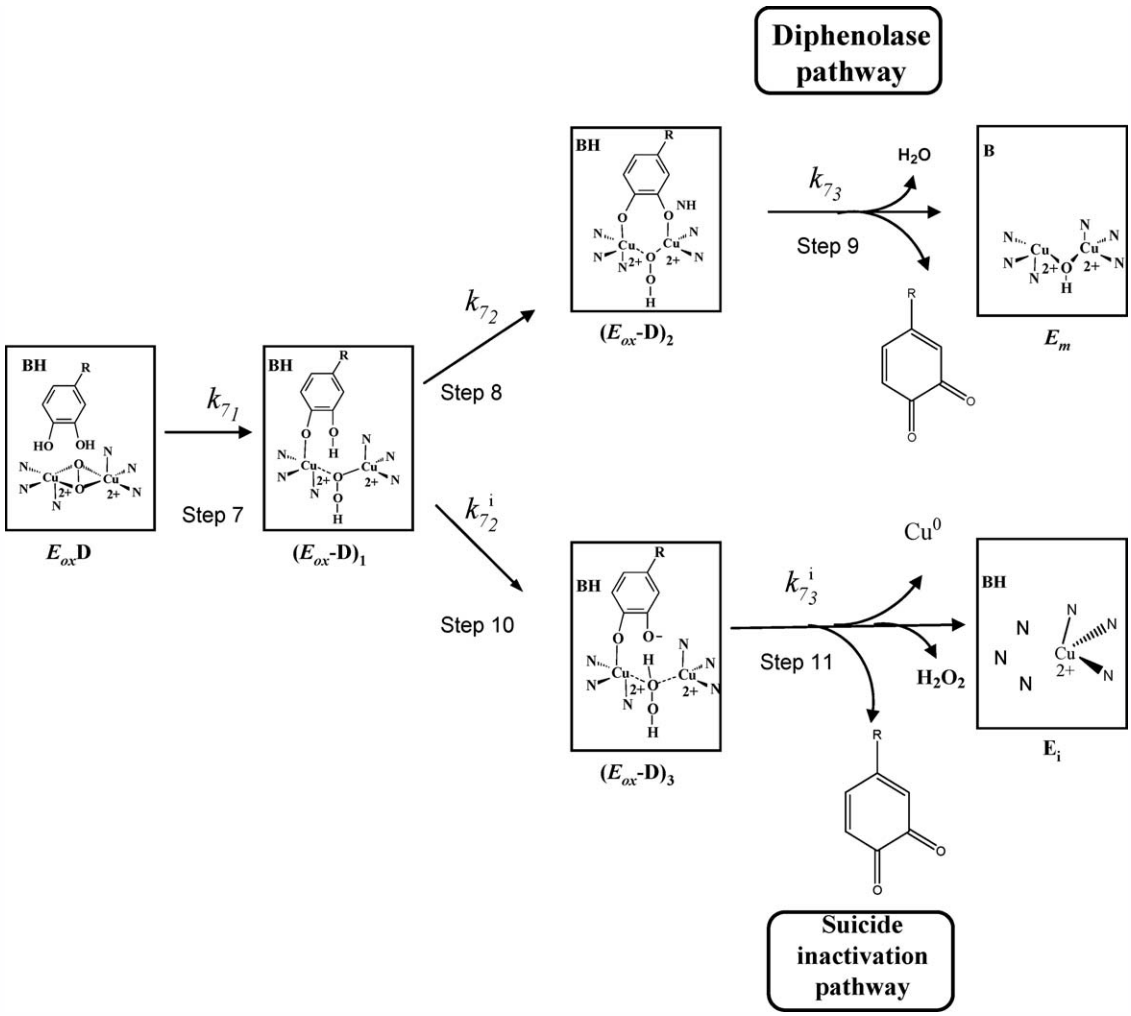

Scheme 3. Detail of the structural mechanism proposed to explain the suicide inactivation of tyrosinase during its action on *o*-diphenols (see Scheme 1 for further details).

copper will be lower, and the proton will be transferred to the histidine. In this way, the hydroxyl group in C-2 will be better able to carry out the nucleophilic attack on the copper, and the proton will be transferred to the histidine, binding to the substrate in a diaxial position. When the substrate has a withdrawing group in C-4, the positive charge density of the copper atom will be greater, influencing the hydroxyl group of C-2 and favoring deprotonation, the proton being transferred to the protonated peroxide (see Scheme 3). In addition, hydrophobic and esteric effects influence both process (catalysis and inactivation) (Table 1).

In the first case, the catalysis involves a concerted oxidation/reduction reaction, releasing *o*-quinone and E_m as the oxygens are coplanar with the two copper atoms. However, in the second case, the oxidation/reduction may take place on the one copper atom, releasing *o*-quinone, copper (0), hydrogen peroxide, and inactive enzyme.

Table 1 shows the values of k_{cat}, r, $\lambda_{E_{ox}(max)}$, and of the chemical shifts of the different suicide substrates obtained by ^{13}C-NMR for the C-1 and C-2 carbons. Note how the values of r decrease as the group in C-4 becomes more electron-withdrawing because of closer values of k_{7_2} and $k^i_{7_2}$ (the lower corresponds to 4-nitrocatechol). It is important to note the high relation, in some cases, between the ^{13}C-NMR data compared with the values of k_{cat} and $\lambda_{E_{ox}(max)}$ shown in Table 1. In the case of pyrogallol, the electron density of the oxygen atom of the hydroxyl group of C-1 is very high and has the highest k_{cat} and $\lambda_{E_{ox}(max)}$ values. However, the value of r is also at its maximum for all the substrates studied, which can be explained by the greater influence of the value of δ_1 on k_{cat} (10^3 range) than on $\lambda_{E_{ox}(max)}$ (10 range). Furthermore, as this compound is vicinal trihydroxylated, the probability of catalysis taking place is doubled as there are two possible *o*-diphenol orientations. According to Scheme 3, in the complex $(E_{ox}\text{-D})_r$, with the sub-

Table 1
Kinetic constants which characterize the suicide inactivation of tyrosinase by different substrates and values of the chemical shifts of the different suicide substrates of tyrosinase obtained by ^{13}C-NMR for the C-1 and C-2 carbons

o-Diphenol	$\lambda_{E_{ox}(max)} \times 10^3$ (s^{-1})	$r = k^S_{cat}/\lambda_{E_{ox}(max)}$	k^S_{cat} (s^{-1})	K^S_m (mM)	$K^{O_2}_m$ (μM)	δ^7_1 (ppm)	δ^7_2 (ppm)
Pyrogallol	12.01 ± 0.31	122,093 ± 2,740	1280.3 ± 47.1	1.96 ± 0.03	55.61 ± 2.81	135.19	148.22
Catechol	8.92 ± 0.27	99,994 ± 1,604	874.1 ± 30.2	0.16 ± 0.01	38.02 ± 2.61	146.59	146.59
4-Chlorocatechol	8.54 ± 0.25	99,356 ± 1,788	859.2 ± 28.3	0.60 ± 0.03	37.31 ± 1.62	145.04	147.35
4-Methylcatechol	8.21 ± 0.25	98,366 ± 1,377	842.1 ± 26.1	0.10 ± 0.01	36.62 ± 2.70	144.06	146.43
4-Ethylcatechol	7.95 ± 0.23	97,562 ± 1,951	802.3 ± 26.1	0.17 ± 0.01	34.83 ± 2.63	143.99	146.27
4-*tert*-Butylcatechol	7.28 ± 0.28	88,788 ± 1,864	640.1 ± 28.1	1.45 ± 0.12	27.82 ± 2.52	144.09	146.24
DHPPA	6.93 ± 0.27	87,646 ± 1,315	607.2 ± 25.1	0.70 ± 0.09	26.43 ± 2.13	144.96	146.43
DHPAA	6.89 ± 0.37	62,838 ± 1,187	433.1 ± 25.9	1.30 ± 0.10	18.82 ± 1.31	144.61	146.51
L-Dopa	2.21 ± 0.11	46,133 ± 2,306	102.6 ± 20.1	0.55 ± 0.08	4.46 ± 0.89	146.92	146.06
D-Dopa	2.15 ± 0.15	44,895 ± 2,573	98.5 ± 17.0	3.98 ± 0.57	4.28 ± 0.86	146.92	146.06
Gallic acid methyl ester	1.70 ± 0.09	47,444 ± 501	80.2 ± 3.9	0.12 ± 0.01	3.41 ± 0.11	141.42	147.34
Gallic acid	1.57 ± 0.07	18,666 ± 466	28.2 ± 0.9	0.18 ± 0.01	1.12 ± 0.11	140.64	147.29
Protocatechuic acid	0.85 ± 0.03	10,186 ± 224	8.1 ± 0.3	0.07 ± 0.01	0.34 ± 0.02	150.00	146.04
Protocatechuic aldehyde	0.61 ± 0.02	2,554 ± 40	1.5 ± 0.1	0.15 ± 0.02	0.06 ± 0.01	155.28	146.71
4-Nitrocatechol	0.45 ± 0.02	2,254 ± 41	0.9 ± 0.1	0.10 ± 0.01	0.04 ± 0.01	155.87	148.07

strate bound axially to the copper by C-1 (which has a lower positive charge density), the adjacent hydroxyl group has a greater possibility to bind to the second copper, transferring its proton to the histidine (*7*).

Catechol has no steric or hydrophobic effects that hinder the process, even though the values of δ_1 and δ_2 are not good; however, as the OH groups are equivalent, the probability of catalysis and inactivation increases. The value of r is high, since, as in the previous case, the effect on k_{cat} is much higher than on $\lambda_{E_{ox}(max)}$, favoring the catalytic pathway. The group of substrates, 4-chlorocatechol, 4-methylcatechol, and 4-ethylcatechol, with their very close δ_1 values, gives similar values of k_{cat}, $\lambda_{E_{ox}(max)}$, and r (although in the case of 4-ethylcatechol, steric effects exist). The effect of the donating group in C-4 is responsible for the powerful nucleophilic attack of the hydroxyl group in C-1. In the case of 4-*tert*-butylcatechol, although its δ_1 is similar to that of catechol, the size of the group in C-4 may cause steric hindrance, which decreases its k_{cat}, $\lambda_{E_{ox}(max)}$, and r.

As regards 3,4-dihydroxyphenylpropionic acid (DHPPA) and 3,4-dihydroxyphenylacetic acid (DHPAA), although their δ_1 are better than that of catechol, the effect of the negative charge of the carboxylic group decreases the k_{cat} and $\lambda_{E_{ox}(max)}$. Gallic acid and gallic acid methyl ester are trihydroxylated compounds with low δ_1 values, although the withdrawing effect of the carboxyl group means that their k_{cat} and $\lambda_{E_{ox}(max)}$ are low, as is their r. The withdrawing effect increases the possibility of the copper being bound to the substrate, bringing the second hydroxyl group in C-2 nearer, inducing deprotonation and proton transfer to the protonated peroxide, facilitating enzyme suicide. Lastly, poor tyrosinase substrates, such as protocatechuic acid, protocatechuic aldehyde, and 4-nitrocatechol, whose δ_1 are very high, order themselves in accordance with the values described in Table 1. Their very low values of k_{cat}, $\lambda_{E_{ox}(max)}$, and r can be explained by the same withdrawing effect of the group in C-4 (*7*).

Similarly, several studies have compared the stereospecific effects of the isomers, L- and D-dopa, and calculated their respective suicide inactivation parameters (*8*). From Table 1, it can be seen that the suicide inactivation process shows no specificity as regards $\lambda_{E_{ox}(max)}$, but does so with respect to K^S_m. This agrees with studies published on the substrate stereospecificity of tyrosinase in its action on monophenols and *o*-diphenols (*12*), as both L- and D-dopa show the same δ_1 and δ_2 (Table 1).

SUICIDE INACTIVATION OF TYROSINASE ACTING ON MONOPHENOLS

As regards the monophenolase activity, the enzymatic forms E_m and E_{ox} can bind to the monophenol, giving rise to the complexes E_m-M (inactive) and E_{ox}-M (active), respectively. The kinetic mechanism for the monophenolase activity is described in (*15, 18*).

The suicide inactivation kinetic of tyrosinase in its action on monophenols such as L-tyrosine has not been studied in depth for two reasons: (*a*) the presence of a lag period in the monophenolase activity, and (*b*) experimentally, there is no possibility that the phenolic substrate will remain constant through the reaction time.

The suicide inactivation kinetic of tyrosinase has been studied in the presence of L-tyrosine (results not published) from an experimental point of view and through simulation of the set of differential equations that make up the mechanism of Scheme 1. The overall results of the study show that the enzyme is not inactivated when it acts on monophenols (L-tyrosine), a hydrox-

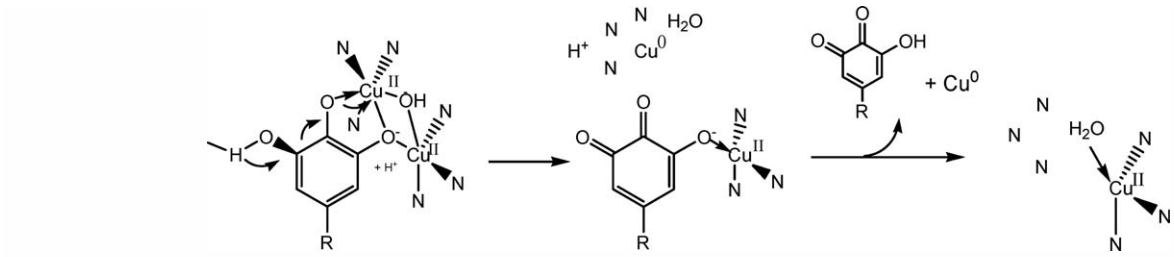

Scheme 4. Proposed model to explain the suicide inactivation of tyrosinase during its monophenolase activity when it acts on *o*-diphenols (*22*).

ylation reaction, but is inactivated as it acts on the L-dopa accumulated in the medium as a result of the chemical evolution of *o*-dopaquinone (Scheme 2). Thus, L-tyrosine does not directly inactivate the enzyme (suicide inactivation).

PROPOSED MECHANISMS TO EXPLAIN THE SUICIDE INACTIVATION OF TYROSINASE ACTING ON MONOPHENOLIC AND DIPHENOLIC SUBSTRATES

To date, three types of mechanism have been proposed to explain the suicide inactivation of tyrosinase:

(a) an attack by the *o*-quinone product on a sensitive nucleophilic group vicinal to the active site (*25*),
(b) a free radical attack on the active site by the reactive oxygen species generated during the catalytic oxidation (*10*), and, more recently,
(c) the processing of a catechol as though it was a monophenol ("cresolase"-type presentation) (*22, 26, 27*) (Scheme 4).

The first two hypotheses have been rejected because the inactivation takes place even in the presence of NADH or ascorbic acid whose presence prevents the *o*-quinone binding to the enzyme (*4*). Experiments that try to protect the enzyme from the action of free radicals were also unsuccessful (*4, 28*). Neither was it possible to mark the enzyme in the process of suicide inactivation in experiments using [U-C^{14}]phenol (*5*).

As regards the third hypothesis, which implies the hydroxylation of a catechol as though it was a monophenol ("cresolase"-type presentation), the authors (*22, 26, 27*) suggested that an intermediate product is formed that undergoes deprotonation and reductive elimination; this assumes that the orientation of the phenyl ring in the enzyme–substrate complex is approximately orthogonal to the plane defined by the copper and oxygen atoms (*23*).

Moreover, the inactivation mechanism proposed in (*22, 26, 27*) indicates that the chemical structure of the substrates is very important in the suicide inactivation process. Therefore, the substrate must have at least two hydroxyl groups in ortho in the benzene ring. Hence, when the substrate is a trihydroxybenzene (*e.g.*, pyrogallol), the proposed mechanism (Scheme 4) would indicate that this compound is not a suicide substrate (*22*), although our experimental results (*7*) suggest that it is the most powerful suicide substrate of mushroom tyrosinase. The oxygen consumption that is observed is due to autooxidation (*7*), not to the action of the enzyme. Indeed, the addition of superoxide dismutase and catalase to the medium inhibits this autooxidation process, underlining that pyrogallol is really a suicide substrate.

In a more recent work, Ramsden et al. (*26*), to support its suicide inactivation mechanism, used the compound 3,6-difluorocatechol. As this has positions 3 and 6 occupied, this compound would prevent the presentation of the *o*-diphenol as a monophenol and so, in the absence of hydroxylation, the enzyme is not inactivated. The experiments depicted in Fig. 1 of reference (*26*) compare, by means of oxymetric measurements, the inactivation of the enzyme acting on 3,6-difluorocatechol with the inactivation of 4-fluorocatechol (which has positions 3 and 6 free and could present itself to the enzyme as a monophenol). According to the model of these authors, 3,6-difluorocatechol would not produce suicide inactivation. If the experiments with 4-fluorocatechol and 3,6-difluorocatechol are fitted on the same time scale, it seems that 3,6-difluorocatechol does not inactivate the enzyme. We studied the suicide inactivation of the enzyme acting on 3-isopropyl-6-methylcatechol, which is available commercially and has a chemical structure which is similar to 3,6-difluorocatechol. According to the mechanism proposed in (*22*), 3-isopropyl-6-methylcatechol should not inactivate the enzyme, but we have showed that this substrate does indeed inactivate tyrosinase (results not published), although the inactivation constant ($\lambda^{D}_{E_{ox}}$) is 3×10^{-4} s^{-1} when the substrate concentration is 4 mM, indicating that the suicide inactivation provoked by the substrate is very slow (results not published). The experimental observation of this process would require a longer reaction time than that recorded (15 min) by other authors (*22, 26, 27*) to study inactivation by 3,6-difluorocatechol, Fig. 1 of reference (*26*). Note the smaller value of the suicide inactivation constant, which agrees with the chemical structure of the substrate, since, having groups in positions 3 and 6, the value of K^{D}_{m} is very high (4.9 mM). However, the suicide inactivation of tyrosinase by this compound (3-isopropyl-6-methylcatechol) has been studied (results not published).

From these data, it can be concluded that positions 3 and 6 of a diphenol do not necessarily have to be free for suicide inactivation to occur.

It is well known that some enzymes exist, named catechol oxidases, that do not have hydroxylase activity, and these would in principle be suitable for confirming or rejecting the mechanism proposed in (*22*) to explain the suicide inactivation of tyrosinase. The catechol oxidases studied to date in this respect are those of *Ipomoea batatas*, *Lycopus europaeus, Populus nigra*, and *Aspergyllus orizae* (*29–31*). In a recent work (*27*), the banana enzyme (*Musa cavendishii*) was used to confirm the mechanism proposed in (*22*), because it was claimed that it had no monophenolase activity. However, hydroxylase activity has been observed in this enzyme (*32*) along with its suicide inactivation acting on catechol (*11*). These results show that the mechanism proposed in (c) (*22*) does not explain the experimental results, but that the mechanism described in (*7*) would. Furthermore, this mechanism (*7*) would explain the suicide inactivation described in other activities of tyrosinase, such as ascorbate oxidase (*33*).

PHARMACOLOGICAL IMPORTANCE OF SUICIDE SUBSTRATES

The study of suicide inactivation and irreversible inhibition is important in the functional design of synthetic inactivators for therapeutic application. For example, irreversible inactivators (insecticides) have been designed against acetylcholinesterase and suicide substrates of β-lactamases (clavulanic acid) that help the action of antibiotics (amoxycilin) (*14*).

In mammals, the suicide inactivation of tyrosinase by L-dopa is significant when there is a considerable decrease in the concentration of L-tyrosine. This may be due to the decreased biosynthesis of L-tyrosine in situations of melanocyte dysfunction, such as in tissue lesions of the skin. In such cases, the melanosomes may have deteriorated, so that they release oxidizing melanogens, which are cytotoxic for the melanocyte (*34, 35*). Suicide inactivation of tyrosinase by L-dopa would protect the skin from the damage caused by the melanogens outside their physiological compartment.

As regards the application of the suicide substrates of tyrosinase, the depigmenting activity of some suicide substrates has been studied. More specifically, 8-hydroxydaidzein, which has been described as a powerful suicide substrate of tyrosinase (*36*), has demonstrated its depigmenting activity in both mouse melanoma cells and in human volunteers (*37*).

In conclusion, we have reviewed the mechanism and kinetic of the suicide inactivation of tyrosinase as it acts on different types of substrate. From the kinetic analysis, an experimental design is proposed that enables the calculation of the kinetic parameters and constants that characterize a suicide substrate of tyrosinase. This information can be used in an attempt to inhibit browning of fruits and vegetables and to evaluate the depigmenting activity of these compounds.

ACKNOWLEDGEMENTS

This article was partially supported by grants from: Ministerio de Educación y Ciencia (Madrid, Spain) Project BIO2009-12956, Fundación Séneca (CARM, Murcia, Spain) Projects 08856/PI/08 and 08595/PI/08, Consejería de Educación (CARM, Murcia, Spain) BIO-BMC 06/01-0004, and the Consejería de Salud y Bienestar Social de la Junta de Comunidades de Castilla La Mancha, project FISCAM PI-2007/53. JLMM has a fellowship from the Ministerio de Educación y Ciencia (Madrid, Spain) Reference AP2005-4721. FGM has a fellowship from Fundación Caja Murcia (Murcia, Spain).

REFERENCES

1. Prota, G., d'Ischia, M., and Napolitano, A. (1998) The chemistry of melanins and related metabolites. In *The Pigmentary System, Physiology and Pathology*. (Nordlund, J. J.,Boissy, R. E.,Hearing, V. J.,King, R. A., and Ortonne, J. P., eds.). pp. 307–332, Oxford University Press, Oxford.
2. Yamaguchi, Y. and Hearing, V. J. (2009) Physiological factors that regulate skin pigmentation. *Biofactors* **35**, 193–199.
3. Solomon, E. I., Sundaram, U. M., and Machonkin, T. E. (1996) Multicopper oxidases and oxygenases. *Chem. Rev.* **96**, 2563–2606.
4. Dietler, C. and Lerch, K. (1982) Reaction inactivation of tyrosinase. In *Oxidases and Related Redox Systems*. (King, T. E.,Mason, H. S., and Morrison, M., eds.). pp. 305–317, Pergamon Press, New York.
5. Canovas, F. G., Tudela, J., Madrid, C. M., Varon, R., Carmona, F. G., and Lozano, J. A. (1987) Kinetic study on the suicide inactivation of tyrosinase induced by catechol. *Biochim. Biophys. Acta* **912**, 417–423.
6. Tudela, J., Garcia-Canovas, F., Varon, R., Jimenez, M., Garcia-Carmona, F., and Lozano, J. A. (1987) Kinetic characterization of dopamine as a suicide substrate of tyrosinase. *J. Enzyme Inhib.* **2**, 47–56.
7. Muñoz-Muñoz, J. L., Garcia-Molina, F., Garcia-Ruiz, P. A., Molina-Alarcon, M., Tudela, J., Garcia-Canovas, F., and Rodriguez-Lopez, J. N. (2008) Phenolic substrates and suicide inactivation of tyrosinase: kinetics and mechanism. *Biochem. J.* **416**, 413–440.
8. Muñoz-Muñoz, J. L., Acosta-Motos, J. R., Garcia-Molina, F., Varon, R., Garcia-Ruíz, P. A., Tudela, J., Garcia-Cánovas, F., and Rodríguez-López, J. N. Tyrosinase inactivation in its action on L-dopa. *Biochim. Biophys. Acta* **1804**, 1467–1475.
9. Garcia-Canovas, F., Tudela, J., Varon, R., and Vazquez, A. M. (1989) Experimental methods for kinetic study of suicide substrates. *J. Enzyme Inhib.* **3**, 81–90.
10. Seiji, M., Sasaki, M., and Tomita, Y. (1978) Nature of tyrosinase inactivation in melanosomes. *Tohoku J. Exp. Med.* **125**, 233–245.
11. Padron, M. P., Lozano, J. A., and Gonzalez, A. G. (1975) Properties of o-diphenol:O_2 oxidoreductase from *Musa cavendishii*. *Phytochemistry* **14**, 1959–1963.
12. Espin, J. C., Garcia-Ruiz, P. A., Tudela, J., and Garcia-Canovas, F. (2000) Study of stereospecificity in mushroom tyrosinase. *Biochem. J.* **331**, 547–551.
13. Garcia-Molina, F., Muñoz, J. L., Varon, R., Rodriguez-Lopez, J. N., Garcia-Canovas, F., and Tudela, J. (2007) A review on spectrophotometric methods for measuring the monophenolase and diphenolase activities of tyrosinase. *J. Agric. Food Chem.* **55**, 9739–9749.
14. Silverman, R. B. (1995) Mechanism-based enzyme inactivators. *Methods Enzymol.* **249**, 240–283.
15. Sanchez-Ferrer, A., Rodriguez-López, J. N., García-Cánovas, F., and García-Carmona, F. (1995) Tyrosinase: a comprehensive review of its mechanism. *Biochim. Biophys. Acta* **1247**, 1–11.
16. Fenoll, L. G., Rodriguez-Lopez, J. N., Garcia-Molina, F., Garcia-Canovas, F., and Tudela, J. (2002) Michaelis constants of mushroom tyrosin-

ase with respect to oxygen in the presence of monophenols and diphenols. *Int. J. Biochem. Cell Biol.* **34**, 332–336.
17. Ghanbari, F., Rowland-Yeo, K., Bloomer, J. C., Clarke, S. E., Lennard, M. S., Tucker, G. T., and Rostami-Hodjegan, A. (2006) A critical evaluation of the experimental design of studies of mechanism based enzyme inhibition with implications for in vitro-in vivo extrapolation. *Curr. Drug Metab.* **7**, 315–334.
18. Rodriguez-Lopez, J. N., Fenoll, L. G., Peñalver, M. J., Garcia-Ruiz, P. A., Varon, R., Martinez-Ortiz, F., Garcia-Canovas, F., and Tudela, J. (2001) Tyrosinase action on monophenols: evidence for direct enzymatic release of o-diphenol. *Biochim. Biophys. Acta* **1548**, 238–256.
19. Matoba, Y., Kumagai, T., Yamamoto, A., Yoshitsu, H., and Sugiyama, M. (2006) Crystallographic evidence that the dinuclear copper center of tyrosinase is flexible during catalysis. *J. Biol. Chem.* **281**, 8981–8990.
20. Decker, H., Schweikardt, T., Nillius, Dd., Salzbrunn, U., Jaenicke, E., and Tuczek, F. (2007) Similar enzyme activation and catalysis in hemocyanins and tyrosinases. *Gene* **398**, 183–191.
21. Speier, G., Tisza, S., Tyeklar, Z., Lange, C. W., and Pierpont, C. G. (1994) Coligand-dependent shifts in charge-distribution for copper-complexes containing 3,5-di-tert-butylcatecholate and 3,5-di-tert-butylsemiquinonate ligands. *Inorg. Chem.* **33**, 2041–2045.
22. Land, E. J., Ramsden, C. A., and Riley, P. A. (2007) The mechanism of suicide-inactivation of tyrosinase: a substrate structure investigation. *Tohoku J. Exp. Med.* **212**, 341–348.
23. Decker, H., Schweikardt, T., and Tuczek, F. (2006) The first crystal structure of tyrosinase: all questions answered? *Angew. Chem. Int. Ed.* **45**, 4546–4550.
24. Deeth, R. J. and Diedrich, C. (2010) Structural and mechanistic insights into the oxy form of tyrosinase from molecular dynamics simulations. *J. Biol. Inorg. Chem.* **15**, 117–129.
25. Ingraham, L. L., Corse, J., and Makower, B. (1952) Enzymatic browning of fruits. III. Kinetics of the reaction inactivation of polyphenol oxidase. *J. Am. Chem. Soc.* **74**, 2623–2626.
26. Ramsden, C. A., Stratford, M. R. L., and Riley, P. A. (2009) The influence of catechol structure on the suicide-inactivation of tyrosinase. *Org. Biomol. Chem.* **7**, 3388–3390.
27. Land, E. J., Ramsden, C. A., Riley, P. A., and Stratford, M. R. (2008) Evidence consistent with the requirement of cresolase activity for suicide inactivation of tyrosinase. *Tohoku J. Exp. Med.* **216**, 231–238.
28. Lerch, K. (1983) Neurospora tyrosinase: structural, spectroscopic and catalytic properties. *Mol. Cell. Biochem.* **52**, 125–138.
29. Klabunde, T., Eicken, C., Sachettini, J. C., and Krebs, B. (1998) Crystal structure of a plant catechol oxidase containing a dicopper center. *Nat. Struct. Biol.* **5**, 1084–1090.
30. Rompel, A., Fisher, H., Meiwes, D., Buldt-Karentzopoulos, K., Dillinger, R., Tuczek, F., Witzel, H., and Krebs, B. (1999) Purification and spectroscopic studies on catechol oxidase from *Lycopus europaeus* and *Populus nigra*: evidence for a dinuclear copper center of type and spectroscopic similarities to tyrosinase and hemocyanin. *J. Biol. Inorg. Chem.* **4**, 56–63.
31. Gasparetti, C., Faccio, G., Arvas, M., Buchert, J., Saloheimo, M., and Kruus, K. (2010) Discovery of a new tyrosinase-like enzyme family lacking a C-terminally processed domain: production and characterization of an *Aspergillus oryzae* catechol oxidase. *Appl. Microbiol. Biotechnol.* **86**, 213–226.
32. Padron, M. P., Gonzalez, A. G., and Lozano, J. A. (1974) O-diphenol:oxygen-oxidoreductase from *Musa cavendishii*. *Rev. Esp. Fisiol.* **30**, 167–176.
33. Munoz-Munoz, J. L., Garcia-Molina, F., Garcia-Ruiz, P. A., Varon, R., Tudela, J., Garcia-Canovas, F., and Rodriguez-Lopez, J. N. (2009) Stereospecific inactivation of tyrosinase by L- and D-ascorbic acid. *Biochim. Biophys. Acta* **1794**, 244–253.
34. Urabe, K., Aroca, P., Tsukamoto, K., Mascagna, D., Palumbo, A., Prota, G., and Hearing, V. (1994) The inherent toxicity of melanin precursors: a revision. *Biochim. Biophys. Acta* **1221**, 272–278.
35. Munoz-Munoz, J. L., Garcia-Molina, F., Varon, R., Tudela, J., Garcia-Canovas, F., and Rodriguez-Lopez, J. N. (2009) Generation of hydrogen peroxide in the melanin biosynthesis pathway. *Biochim. Biophys. Acta* **1794**, 1017–1029.
36. Chang, T. S. (2007) Two potent suicide substrates of mushroom tyrosinase. *J. Agric. Food Chem.* **55**, 2010–2015.
37. Tai, S. S.-K., Lin, C.-G., Wu, M.-H., Chang, T. S. (2009) Evaluation of depigmenting activity by 8-hydroxydaidzein in mouse B16 melanoma cells and human volunteers. *Int. J. Mol. Sci.* **10**, 4257–4266.

4.22. ACLARANDO LA INACTIVACIÓN SUICIDA DE TIROSINASA: UNA DISCRIMINACIÓN ENTRE MECANISMOS.

La discriminación entre mecanismos propuestos para explicar la inactivación suicida de tirosinasa ha dado lugar a la siguiente publicación adjunta.

4.22.1. Título

Unravelling the suicide inactivation of tyrosinase: a discrimination between mechanisms.

4.22.2. Autores

Muñoz-Muñoz, J.L.; Berna, J.; Garcia-Molina, F.; Garcia-Ruiz, P.A.; Tudela, J.; Rodríguez-López, J.N. y Garcia-Cánovas, F.

4.22.3. Referencia

Journal of Molecular Catalysis B: Enzymatic (2012) 75, 11-19.

4.22.4. Resumen

Se ha estudiado la cinética de inactivación suicida en la actuación de tirosinasa sobre 3-isopropil-6-metilcatecol, 3-*terc*-butil-6-metilcatecol y 3,6-difluorocatecol. Los tres sustratos se comportan como sustratos suicidas a pesar de tener ocupadas las posiciones 3 y 6 confirmando la validez del mecanismo propuesto en Biochem. J. 416, 413-440. El sustrato suicida más potente de estos tres es el 3,6-difluorocatecol, sin embargo, su eficiencia de inactivación es mucho más pequeña que la del catecol utilizado como referencia. Para el 3,6-difluorocatecol, el parámetro r, número de ciclos catalíticos que realiza un mol de enzima antes de su inactivación, es el más alto de los descritos en la bibliografía correspondiendo a una mayor diferencia entre la constante catalítica y la de inactivación. A partir del estudio del efecto del pH sobre la actividad enzimática de tirosinasa sobre estos tres sustratos, se deduce que tanto el 3-isopropil-6-metilcatecol como el 3-*terc*-butil-6-metilcatecol se comportan como sustratos típicos de tirosinasa, sin embargo el 3,6-difluorocatecol tiene un comportamiento distinto. El comportamiento singular que muestra el 3,6-difluorocatecol al reaccionar con tirosinasa, podría deberse a que los dos grupos hidroxilos tienen valores muy bajos de pKa debido al efecto retirador de los átomos de flúor en la posición *orto*, de tal manera que, a pH 7.0, el sustrato estaría cargado negativamente. La constante de Michaelis aparente tiene un mínimo a pH 6.0, aumentado su valor a valores de pH altos y bajos. Sin embargo, los valores de la constante catalítica y de la

constante aparente de inactivación máxima no varían con el pH, de tal manera que el parámetro "r" permanece prácticamente constante. En condiciones anaerobias, 3,6-difluorocatecol se comporta como un inhibidor irreversible de las formas desoxitirosinasa y metatirosinasa.

Journal of Molecular Catalysis B: Enzymatic 75 (2012) 11–19

Contents lists available at SciVerse ScienceDirect

Journal of Molecular Catalysis B: Enzymatic

journal homepage: www.elsevier.com/locate/molcatb

Unravelling the suicide inactivation of tyrosinase: A discrimination between mechanisms

Jose Luis Muñoz-Muñoz[a], Jose Berna[b], Francisco Garcia-Molina[a], Pedro Antonio Garcia-Ruiz[c], Jose Tudela[a], Jose N. Rodriguez-Lopez[a], Francisco Garcia-Canovas[a,*]

[a] *GENZ: Grupo de Investigación Enzimología, Departamento de Bioquímica y Biología Molecular-A, Facultad de Biología, Universidad de Murcia, E-30100 Espinardo, Murcia, Spain*
[b] *Departamento de Química Orgánica, Facultad de Química, Universidad de Murcia, E-30100 Espinardo, Murcia, Spain*
[c] *QCPAI: Grupo de Química de Carbohidratos, Polímeros y Aditivos Industriales, Departamento de Química Orgánica, Facultad de Química, Universidad de Murcia, E-3010 Espinardo, Murcia, Spain*

ARTICLE INFO

Article history:
Received 5 May 2011
Received in revised form 5 October 2011
Accepted 1 November 2011
Available online 15 November 2011

Keywords:
Tyrosinase
Suicide inactivation
3,6-Difluorocatechol
3-Isopropyl-6-methylcatechol
3-*tert*-Butyl-6-methylcatechol
Irreversible inhibition

ABSTRACT

The suicide inactivation kinetics of tyrosinase acting on 3-isopropyl-6-methylcatechol, 3-*tert*-butyl-6-methylcatechol and 3,6-difluorocatechol was studied. All three substrates act as suicide substrates despite the fact that their 3 and 6 positions are occupied, confirming the mechanism proposed in Biochem. J. (2008) 416, 431–440. Although the most active substrate for the suicide inactivation was 3,6-difluorocatechol, its efficiency was much lower than that of the catechol used as reference. Its *r* value, the number of turnovers made by one mol of enzyme before its inactivation, is the highest described in the bibliography, highlighting the great difference between the catalytic and inactivation constants. A study of the effect of the pH on the enzymatic activity of tyrosinase showed that both 3-isopropyl-6-methylcatechol and 3-*tert*-butyl-6-methylcatechol behave as typical substrates of tyrosinase, while 3,6-difluorocatechol behaves differently. The remarkable behavior of 3,6-difluorocatechol when reacts with tyrosinase may be due to the fact that its two hydroxyl groups have very low p*K* values as a result of the strong electron-withdrawing effect of the fluorine atoms in the *ortho* positions, so that, at pH 7.0, the substrate would be mainly negatively charged. The apparent Michaelis constant shows a minimum value at pH 6.0, but increases at both high and low pH. However, the values of the catalytic constant and maximum apparent inactivation constant do not vary with the pH, so that the *r* remains practically constant. Under anaerobic conditions, 3,6-difluorocatechol acts as an irreversible inhibitor of the deoxy- and met-tyrosinase forms.

© 2011 Elsevier B.V. All rights reserved.

1. Introduction

Tyrosinase is a cuproprotein that catalyses the hydroxylation of monophenols to *o*-diphenols and the oxidation of the latter to *o*-quinones [1–5]. It has long been known that the enzyme is inactivated when it acts on *o*-diphenols [6–12]. This property of tyrosinase has been studied from several perspectives and the most relevant aspects can be summarized as follows: (i) the process does not occur by means of free radicals; (ii) it does not occur through an attack on the part of the *o*-quinone generated or any aminoacid from the active centre; (iii) during the process half of the copper content of the enzyme is released [13,14].

As indicated above, the *o*-diphenols inactivate the enzyme but only alter many catalytic cycles, in agreement with parameter, "*r*" (the number of turnovers made by one mol of enzyme before being inactivated). However, the *o*-diphenols in only one catalytic cycle manage to convert the met-tyrosinase form, which is inactive towards monophenols, to deoxy-tyrosinase, which, with O_2, is converted to *oxy*-tyrosinase, a form that acts on the monophenols [3,15,16].

The kinetics of the suicide inactivation of tyrosinase was studied some time ago [8], while a more systematic study on the kinetics of the steady-state and transition phase was carried out later [17–21]. The progress made in the study of the tyrosinase structure [22–26] has enabled greater insight into the underlying mechanisms of the suicide inactivation of tyrosinase [1,14,27–37].

Two models, which share certain aspects and diverge considerably in others (Schemes 1 and 2) have been proposed to explain the suicide inactivation of tyrosinase in its action on *o*-diphenolic substrates [14,33]. In both cases, it is suggested that one of the copper atoms at the active centre is reduced to Cu^0 and is released, thus inactivating the enzyme [13]. Other authors [33], suggest that the enzyme hydroxylates the *o*-diphenols because it considers them as another form of monophenol. According to this model, a compound

* Corresponding author. Tel.: +34 868 884764; fax: +34 868 883963.
E-mail address: canovasf@um.es (F. Garcia-Canovas).

1381-1177/$ – see front matter © 2011 Elsevier B.V. All rights reserved.
doi:10.1016/j.molcatb.2011.11.001

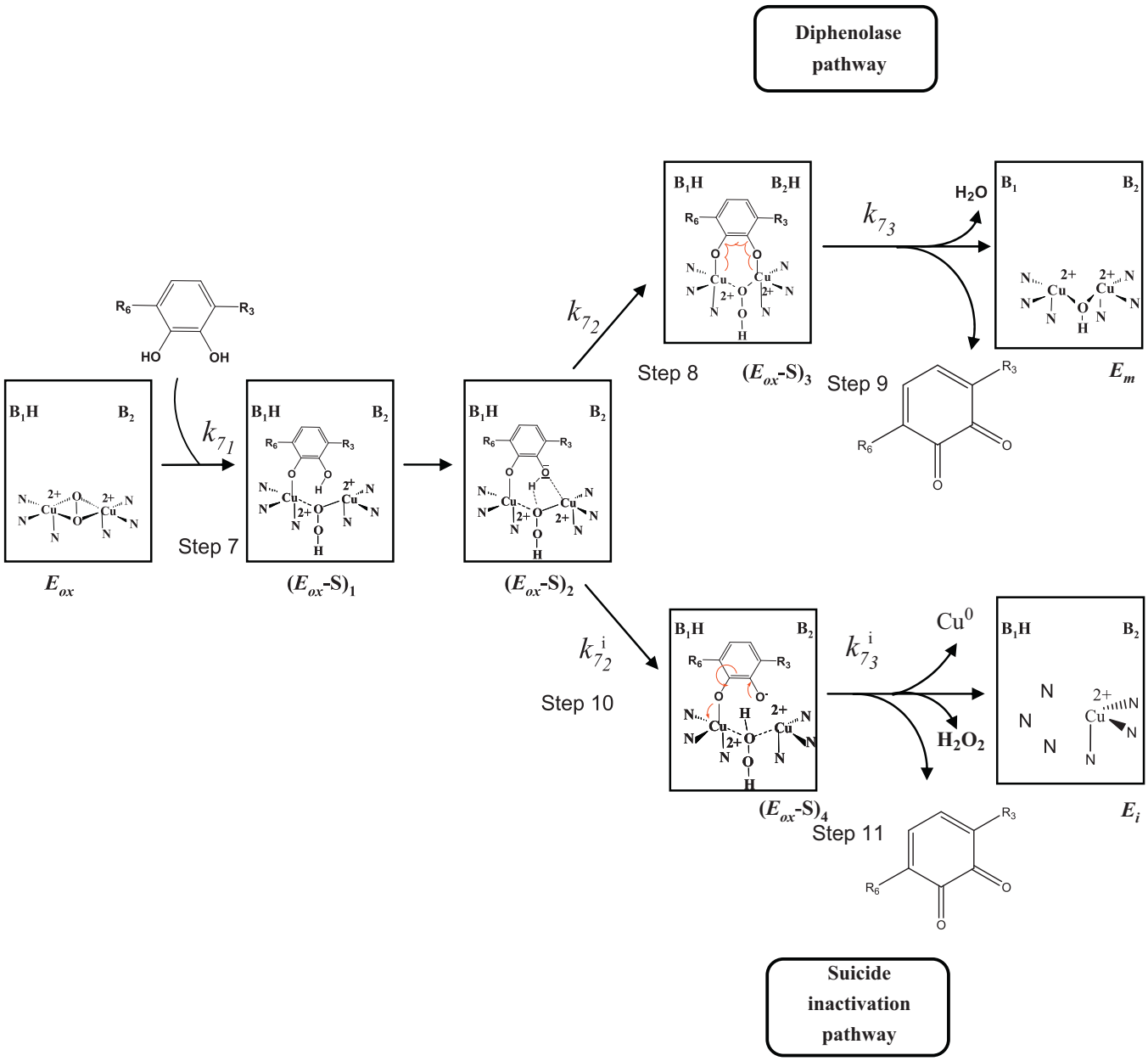

Scheme 1. Kinetic mechanism proposed to explain the diphenolase and suicide inactivation pathways of tyrosinase action on *o*-diphenols. E_{ox}, *oxy*-tyrosinase; $(E_{ox}\text{-S})_1$, *oxy*-tyrosinase/substrate complex axially bound to a Cu atom and with the proton of hydroxyl group transferred to the peroxide group; $(E_{ox}\text{-S})_2$, *oxy*-tyrosinase/substrate complex forming a hydrogen bond; $(E_{ox}\text{-S})_3$, *oxy*-tyrosinase/substrate complex axially bound to the two Cu atoms; $(E_{ox}\text{-S})_4$, *oxy*-tyrosinase/substrate complex axially bound to one Cu atom and the deprotonated hydroxyl group of C-2; E_m, *met*-tyrosinase; E_i, enzyme inactive.

like pyrogallol (1,2,3-trihydroxybenzene) would not lead to suicide inactivation of the enzyme. In a previous work, our group showed that all *o*-diphenols and triphenols are suicide substrates of tyrosinase, the most potent being pyrogallol [14]. The mechanism proposed in Scheme 1 covers the possibility of suicide inactivation during the oxidation of *o*-diphenols and triphenols like gallic acid or pyrogallol since it is the way in which one proton of substrate is transferred to the active centre of the enzyme which triggers its suicide inactivation mechanism. The mechanism of Scheme 1 predicts that the suicide inactivation of the enzyme would occur regardless of what R_3, R_4 and R_6 are. However, according to the mechanism proposed in Scheme 2, if the substituents in 3 and 6 positions are different from hydrogen, that is R_3 and $R_6 \neq H$, suicide inactivation would not occur.

In a subsequent series of studies, different authors [33–37] claim to have experimentally demonstrated the validity of the mechanism proposed in Scheme 2. For our part, we have demonstrated that compounds like ascorbic acid [38], tetrahydropterines [39], NADH [40] and tetrahydrofolic acid [41] behave as suicide substrates. According to our mechanism (Scheme 1), any of the substrates of tyrosinase studied – *o*-diphenols, triphenols, ascorbic acid or such different molecules as NADH, tetrahydropterines or tetrahydrofolic acid – may inactivate the enzyme, since this process would occur as long as there was the possibility of a proton being transferred from the substrate to a base B_2 (perhaps glutamic acid [26] or a histidine not bound to the copper) or to the peroxide group. Note that this possibility would exist in all substrates of tyrosinase in which suicide inactivation has been described [14,38–41].

In an attempt to differentiate the two mechanisms, Quintox' Group [35,36] synthesized 3,6-difluorocatechol, a compound which, according to the model proposed by these authors (Scheme 2), should not induce suicide inactivation because the 3

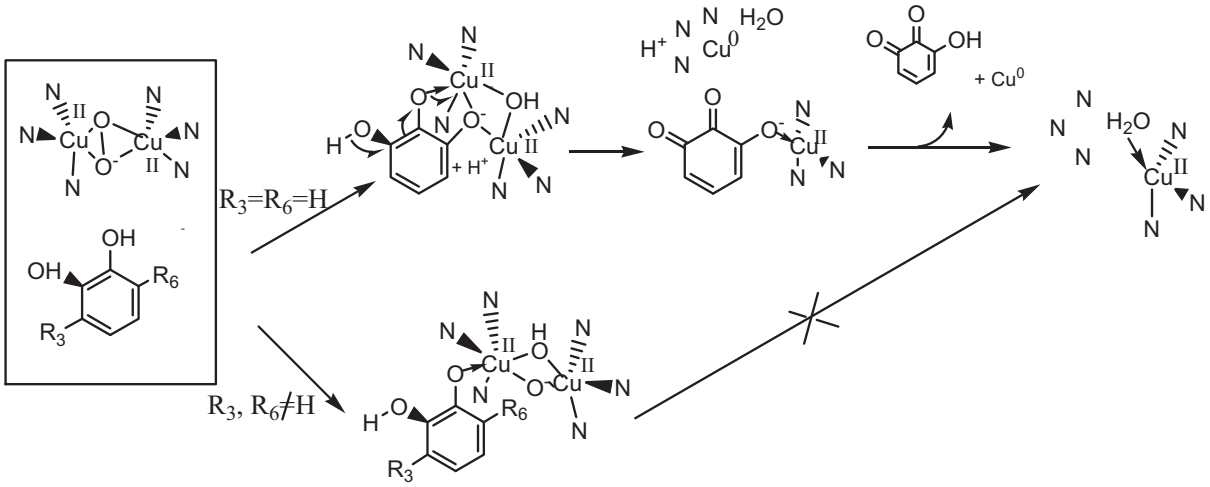

Scheme 2. Proposed model to explain the suicide inactivation of tyrosinase during its monophenolase activity when it acts on *o*-diphenols [33].

and 6 positions are occupied by fluorine atoms, and then it cannot be hydroxylated by the enzyme.

With the aim to discriminate between the proposed models, our group has studied the inactivation kinetics of tyrosinase by the catechol-derived compounds with their 3 and 6 positions substituted, in this case 3-isopropyl-6-methylcatechol (3I6MCat) and 3-*tert*-butyl-6-methylcatechol (3T6MCat). Furthermore, we synthesized 3,6-difluorocatechol (3,6DFCat). The results show that all three 3,6-disubstituted substrates studied behave as suicide substrates of tyrosinase, confirming Scheme 1.

2. Experimental

2.1. Materials

Mushroom tyrosinase or polyphenol oxidase (TYR, *o*-diphenol: O_2 oxidoreductase, EC 1.14.18.1) (8300 units/mg) and β-NADH were supplied by Sigma (Madrid, Spain). The enzyme was purified as previously described in [42]. Protein concentration was determined by the Lowry method [43]. The substrates used 3-isopropyl-6-methylcatechol (3I6MCat) and 3-*tert*-butyl-6-methylcatechol (3T6MCat) (Fig. 1) were purchased from Sigma (Madrid, Spain). All other chemicals were of analytical grade. Stock solutions of the diphenolic substrates were prepared in 0.15 mM phosphoric acid to prevent autooxidation. Milli-Q system (Millipore corp.) ultrapure water was used throughout.

2.2. Methods

2.2.1. Preparation of 3,6-difluorocatechol (3,6DFCat)

3,6-Difluorocatechol (3,6DFCat, Fig. 1) was synthesized from the commercially available 1,2,3,4-tetrafluorobenzene (CAS: 551-62-2) following the three-step methodology reported by Ladd et al. [44].

2.2.2. Characterization of 3,6-difluorocatechol (3,6DFCat)

^{1}H- and ^{13}C NMR spectra were recorded at 298 K on a Bruker Avance 400 MHz instrument. ^{1}H NMR chemical shifts are reported relative to Me_4Si and were referenced via residual proton resonances of the corresponding deuterated solvent whereas ^{13}C NMR spectra are reported relative to Me_4Si using the carbon signals of the deuterated solvent. Detailed physical data for 3,6DFCat are listed in the supplementary material and are complementary to those reported in the literature [44].

2.2.3. Dialysis

To know whether TYR was irreversibly inactivated by 3,6DFCat, the residual enzyme activity of TYR/3,6DFCat mixtures was measured before and after dialysis. The effect of dialysis on TYR/3,6DFCat mixture was tested as follows: TYR (2 nM) in 30 mM sodium phosphate buffer (pH 6.0) was preincubated with 12 mM of 3,6DFCat (in the case of the suicide inactivation reaction, aerobic conditions) and 0.5 mM of 3,6DFCat (in the case of E_d inhibition, anaerobic conditions) for 2 h, in both cases at room temperature. Each sample was placed into the dialysis membrane (Sigma, Madrid, Spain) with a molecular weight cut-off of 6000–8000 Da and then dialyzed overnight against two changes of 30 mM sodium phosphate buffer (pH 6.0) to remove the 3,6DFCat. Enzyme activity before and after dialysis was measured in a spectrophotometer by adding 100 μL of the dialyzed solution to the cuvette containing 900 μL of 9 mM TBC, 30 mM sodium phosphate buffer (pH 6.0) and 0.2 mM NADH.

2.2.4. Spectrophotometric assays

These assays were carried out with a Perkin-Elmer Lambda-35 (Perkin-Elmer, Massachusetts, USA) spectrophotometer, on line interfaced to a PC-computer, where the kinetic data were recorded, stored and later analyzed. The product of the enzyme reaction *o*-quinone is unstable and evolves towards melanins [45]. For this reason, the reaction was followed by measuring the disappearance

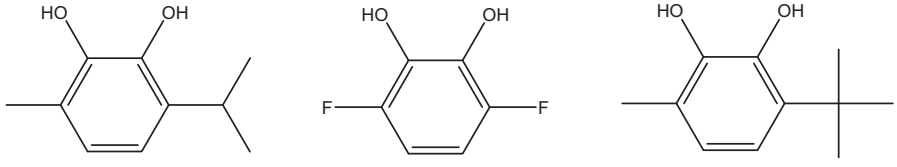

Fig. 1. Chemical structures of the substrates used in this work.

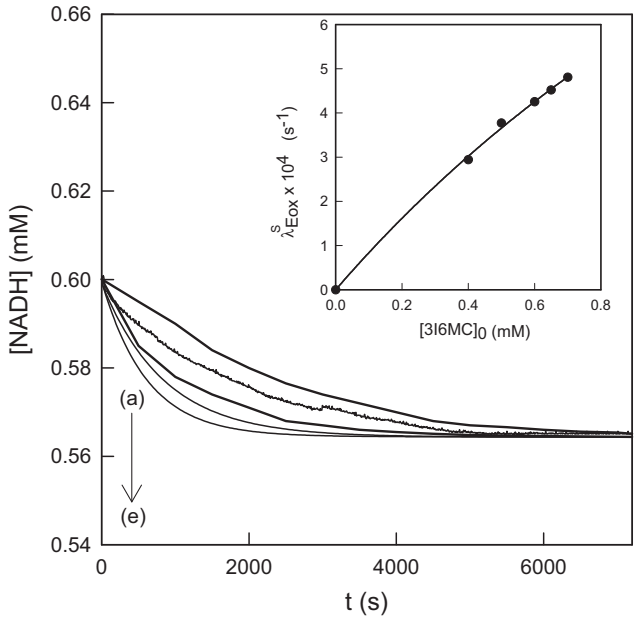

Fig. 2. Corrected recordings of the disappearance of NADH in the suicide inactivation of tyrosinase by different 3-isopropyl-6-methylcatechol concentrations. The experimental conditions were 30 mM sodium phosphate buffer (pH 7.0), 0.26 mM O_2, wavelength = 380 nm, and the initial concentrations of NADH and tyrosinase were 0.6 mM and 2.2 nM, respectively. The substrate concentrations were (mM): (a) 4, (b) 5, (c) 6, (d) 6.5 and (e) 7. Inset. Values of $\lambda^S_{E_{ox}}$ for different 3-isopropyl-6-methylcatechol concentrations.

of NADH at 340 nm, with $\varepsilon = 6230\,M^{-1}\,cm^{-1}$, which reduces *o*-quinone to *o*-diphenol or measuring the AH_2 disappearance at 262 nm, with $\varepsilon = 11{,}100\,M^{-1}\,cm^{-1}$ [46].

2.2.5. Kinetic data analysis

The experimental data of time-based assays for the disappearance of NADH (Fig. 2) follow Eq. (1):

$$[NADH] = [NADH]_f + [NADH]_\infty e^{-\lambda^S_{Eox} t} \quad (1)$$

where $[NADH]_f$ is the NADH-value at $t \to \infty$, $[NADH]_\infty = [Q]_\infty$ is the NADH consumed at the end of the reaction and $\lambda^S_{E_{ox}}$ is the apparent constant of suicide inactivation of tyrosinase in the presence of *o*-diphenol. These parameters can be obtained by non-linear regression [47]. There is always a slow spontaneous oxidation of *o*-diphenol and NADH (result not shown), which should be computer corrected in further NADH *vs*. time plots (in general this treatment is applied to all the kinetic recordings).

2.2.6. Generation of E_{ox} and E^R_d

We set out to kinetically characterize the inactivation of E^R_d (relaxed form of deoxy-tyrosinase). For this, E^R_d was generated from the native enzyme, adding micromolar concentrations (5 μM) of H_2O_2 so that the E_m form passed to E_{ox}. Then nitrogen was bubbled through the solution transforming all the E_{ox} to E^R_d ($E_{ox} \rightleftarrows E^R_d + O_2$) [42,48,49]. This enzyme sample was used to study the reaction of E^R_d with 3,6DFCat.

2.2.7. Generation of E^T_d

To generate the enzyme form E^T_d (tense form of deoxy-tyrosinase), E^R_d was allowed to evolve to E^T_d under anaerobic conditions for 90 min [42,48,49].

2.2.8. Generation of E_m

The inactivation of E_m was characterized by first generating it from the native enzyme in two ways: (a) adding 2 μM catalase, so that $E_{ox} \rightleftarrows E_m + H_2O_2$; catalase acts on the H_2O_2 displacing the equilibrium, $2H_2O_2 + \text{catalase} \rightarrow O_2 + 2H_2O$, so that E_{ox} is transformed into E_m. (b) Adding 5 μM of H_2O_2, so that all the enzyme passes to E_{ox} and then adding 2 μM catalase [48,49]. This enzyme sample was used to study the reaction of E_m with 3,6DFCat.

3. Results and discussion

In order to distinguish the mechanisms proposed to explain the suicide inactivation of tyrosinase (Schemes 1 and 2), three *o*-diphenolic substrates (derivatives of catechol) were studied, all with positions 3 and 6 occupied: 3-isopropyl-6-methylcatechol (3I6MCat), 3-*tert*-butyl-6-methylcatechol (3T6MCat) and 3,6-difluorocatechol (3,6DFCat) (Fig. 1).

3.1. Kinetic characterization of 3I6MCat as suicide substrate of tyrosinase

Fig. 2 shows the experimental recordings of the suicide inactivation of tyrosinase acting on 3I6MCat at pH 7.0, where the disappearance of NADH as coupled reagent is shown as it reduces the *o*-quinone to *o*-diphenol. The two-stage experimental design studied variations in substrate and enzyme concentrations.

3.1.1. Effect of substrate concentration

Fig. 2 shows the effect of varying the substrate concentration (at pH 7.0) while keeping the enzyme concentration constant. Non-linear regression analysis of these records in accordance with Eq. (1) gives the values of $\lambda^S_{E_{ox}}$ and $[NADH]_\infty$. Fig. 2 inset shows the variation of $\lambda^S_{E_{ox}}$ with regard to substrate concentration. The lineal behavior reflects the fact that the enzyme cannot be saturated by the substrate due to its molecular size. In agreement with Eq. (2), the slope of the straight line gives the value of the inactivation efficiency ($\lambda^S_{E_{ox}(max)}/K^S_m$), whose value is shown in Table 1 [14]:

$$\lambda^S_{E_{ox}} = \frac{\lambda^S_{E_{ox}\,(max)}[S]_0}{K^S_m + [S]_0} \quad (2)$$

3.1.2. Varying the enzyme concentration

The recordings of the suicide inactivation of tyrosinase acting on 3I6MCat at pH 7.0 are shown in Fig. 1SM, keeping the substrate concentration constant and varying the initial concentration of enzyme. Non-linear regression analysis of these records in accordance with Eq. (1) gives the values of $\lambda^S_{E_{ox}}$ and $[NADH]_\infty$. The Inset shows how the values of $\lambda^S_{E_{ox}}$ and $[NADH]_\infty$ vary with respect to the initial enzyme concentration. As can be seen, the apparent inactivation constant is independent of enzyme concentration (●). The slope of the straight line has a value of 2*r*, as determined from the linear dependence of $[NADH]_\infty$ on $[E]_0$ (○) (Fig. 1SM inset). The values of *r*, the number of turnovers made by one mol of enzyme before its inactivation, and of $\lambda^S_{E_{ox}(max)}/K^S_m$, the inactivation efficiency, are shown in Table 1.

3.2. Kinetic characterization of 3T6MCat as suicide substrate of tyrosinase

Following the same procedure as in the case of 3I6MCat, the inactivation efficiency ($\lambda^S_{E_{ox}(max)}/K^S_m$) and *r*, the partition ratio or the turnover numbers made by one mol of enzyme before its inactivation, can be obtained (see Figs. 2SM and 3SM and Table 1). Considering the data from Table 1, while the *r* values are of the same order of magnitude, the inactivation efficiency of 3I6MCat

Table 1
Kinetic constants characterizing the suicide inactivation of tyrosinase acting on 3,6-disubstituted *o*-diphenols.

	pH	$\lambda^S_{E_{ox}(max)} \times 10^4$ (s^{-1})	r[b]	k^S_{cat} (s^{-1})	K^S_m (mM)	k^S_{cat}/K^S_m ($s^{-1}\,M^{-1}$)	$\lambda^S_{E_{ox}(max)}/K^S_m \times 10^2$ ($s^{-1}\,M^{-1}$)	δ_1 (ppm.)	δ_2 (ppm)
3,6DFCat	4.0	5.55 ± 0.29	190156 ± 8211	105 ± 14	2.57 ± 0.29	(40 ± 5) × 10^3	21.6 ± 2.4		
	5.0	5.76 ± 0.35	194840 ± 8050	112 ± 13	2.19 ± 0.27	(51 ± 6) × 10^3	26.3 ± 3.5		
	5.5	5.83 ± 0.21	190010 ± 8888	110 ± 11	1.42 ± 0.15	(77 ± 9) × 10^3	41.1 ± 4.6		
	6.0	5.92 ± 0.25	182222 ± 7996	107 ± 10	0.77 ± 0.08	(139 ± 16) × 10^3	76.9 ± 8.3		
	7.0	5.81 ± 0.29	198744 ± 8902	115 ± 11	1.66 ± 0.18	(69 ± 8) × 10^3	35.0 ± 3.9	133.48	133.48
	8.0	5.99 ± 0.31	188848 ± 8137	113 ± 14	2.93 ± 0.33	(38 ± 4) × 10^3	20.4 ± 2.1		
3I6MCat	7.0	–	6890 ± 214	–	–	(38 ± 2) × 10^1	6 ± 0.5	146.70	144.00
3T6MCat	7.0	–	1613 ± 73	–	–	148 ± 6	7.7 ± 0.4	146.60	142.90
Cat[a]	7.0	89.20 ± 2.70	99994 ± 1604	874 ± 30	0.16 ± 0.01	(5463 ± 589) × 10^3	5575.0 ± 61.8	146.59	146.59

[a] Data taken from Ref. [14].
[b] Obtained from transition phase kinetic studies.

is one order of magnitude greater than that of 3T6MCat. Dialysis experiments, as described in Section 2, showed that the inactivated enzyme had no activity.

3.3. Kinetic characterization of 3,6DFCat as suicide substrate of tyrosinase

When the kinetic experiments were carried out with 3,6DFCat at pH 7.0, apparently no inactivation of tyrosinase was observed, at least on the time scale depicted in Fig. 4SM. However, inactivation was more apparent when the pH was lowered (Fig. 4SM). Table 1 shows the carbon-13 NMR chemical shifts (δ values) of the investigated substrates. It is noteworthy the low δ values of the carbons that support the hydroxyl groups of 3,6DFCat which is indicative the low p*K* values (≅7.2) of these groups. At pH 7.0, more than half of this fluorinated catechol is deprotonated and, consequently, the substrate is negatively charged which might explain the results obtained, as we shall see later. Note the wide difference from the δ values of the other compounds (Table 1), indicating that at pH 7.0 the hydroxyl groups of the other substrates are completely protonated.

3.4. Some considerations on the kinetic parameters of 3I6MCat and 3T6MCat

As mentioned above, the size and low solubility of these substrates mean that the enzyme cannot be saturated. From the experimental data obtained (Fig. 2 and Figs. 1SM–4SM), it is only possible to obtain the parameter "*r*" (the number of turnovers that one mol of enzyme makes before being inactivated) and the inactivation efficiency, $\lambda^S_{E_{ox}(max)}/K^S_m$. Note that the substrates have practically the same steric hindrance since the isopropyl group behaves like the *tert*-butyl group, which is equivalent to saying that the K^S_m should be practically the same, so that the maximum apparent inactivation constant, ($\lambda^S_{E_{ox}(max)}$) for 3T6MCat may be one order of magnitude higher than that for 3I6MCat (see Table 1).

The value of r ($k^S_{cat}/\lambda^S_{E_{ox}(max)}$) is greater for 3I6MCat than for 3T6MCat, which is in agreement with the higher value of $\lambda^S_{E_{ox}(max)}$ predicted for 3T6MCat (Table 1). However, although the catalytic constant for 3T6MCat should be greater than for 3I6MCat according to the values of δ_1 and δ_2 (Table 1), this increase is less than the increase in $\lambda^S_{E_{ox}(max)}$.

From measurements of the steady-state, V_0 can be obtained for each of the substrates, while a graph of $V_0/[E]_0$ *vs.* $[S]_0$, provides the catalytic efficiency (k^S_{cat}/K^S_m) (Fig. 5SM). The relation between k^S_{cat}/K^S_m and the inactivation efficiency $\lambda^S_{E_{ox}(max)}/K^S_m$ (Fig. 5SM inset) provides the value of r (Table 1). Therefore, a study of the transition phase and the steady-state with respect to initial substrate concentration provides r-values (6333 ± 621 for 3I6MCat and 1922 ± 203 for 3T6MCat), which practically coincide with those obtained from the analysis of the transition phase data with respect to variations in the initial enzyme concentration (Figs. 1SM and 3SM and Table 1).

3.5. Effect of pH on the oxidation of 3,6DFCat, 3I6MCat and 3T6MCat by tyrosinase

From the measurements of the initial velocity at different pH values, the dependence of V_0 *vs.* pH can be obtained. Fig. 3 shows these values – it can be seen that both 3I6MCat and 3T6MCat behave as typical tyrosinase substrates, with a sigmoidal dependence of V_0 *vs.* pH (indicating the existence of an apparent kinetically significant p*K*), while 3,6DFCat shows a bell shape, suggesting the existence of two apparents significant p*K*s. A sigmoidal curve is typical when the effect of pH on the kinetic of the oxidation of *o*-diphenols is studied, as can be seen in the case of catechol (Cat) (Fig. 3 inset A). This curve is of the same type although the substrates have charges in their R group of carbon 4 [48,50].

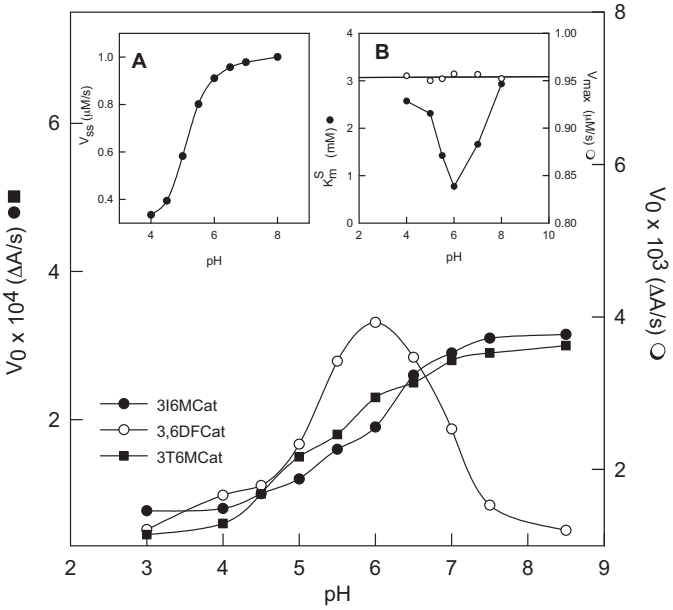

Fig. 3. Representation of the values of V_0 *vs.* pH for every substrates, (○) 3,6DFCat, (●) 3I6MCat and (■) 3T6MCat. The experimental conditions were 30 mM sodium acetate buffer (pH 3.0–5.5) or 30 mM sodium phosphate buffer (pH 6.0–8.5), 0.15 mM NADH, 0.26 mM O_2, wavelength = 340 nm (3T6MCat and 3,6DFCat) and 380 nm (3I6MCat), $[3,6DFCat]_0$ = 12 mM, $[3I6MCat]_0$ = 5 mM, $[3T6MCat]_0$ = 0.5 mM and $[E]_0$ = 0.05 nM for 3,6DFCat and 0.1 nM for 3I6MCat and 3T6MCat. Inset A. Representation of the ascorbic acid disappearance rates in the oxidation of Cat by tyrosinase rate at wavelength = 262 nm (V^{262}_{ss}) *vs.* pH, $[AH_2]_0$ = 50 μM, $[Cat]_0$ = 0.2 mM and $[E]_0$ = 1 nM. Inset B. Representation of K^S_m (●) and V^S_{max} (○) *vs.* pH for 3,6DFCat.

$$(E_d^R)^{2-} + 2H^+ \rightleftharpoons (E_d^R)^{-+} + 2H^+ \rightleftharpoons (E_d^R)^{2+}$$

$$(E_{ox})^{2-} + 2H^+ \rightleftharpoons (E_{ox})^{-+} + 2H^+ \rightleftharpoons (E_{ox})^{2+}$$

$$(E_m)^{2-} + 2H^+ \rightleftharpoons (E_m)^{-+} + 2H^+ \rightleftharpoons (E_m)^{2+}$$

Scheme 3. Kinetic mechanism to explain the effect of pH on the different enzymatic forms of tyrosinase in its catalytic cycle.

The substrate 3,6DFCat may have two negative charges at high pH, which may explain its behavior with respect to the steady-state data shown in Fig. 3 (○) and to the suicide inactivation seen in the experimental registers of Fig. 4SM. The existence of two apparents critical p*K* in the enzyme was revealed in a previous work on deoxytyrosinase based on a study of the transition of the deoxy form (relaxed) to another form (tense) with the copper atoms more separated [49]. Scheme 3 reflects the existence of two apparents p*K* in each of the enzymatic forms that exist in the catalytic cycle of tyrosinase.

An *o*-diphenolic substrate of tyrosinase with no charge, as is the case of Cat, provides V_0 *vs.* pH curve as seen in Fig. 3 inset A, with an apparent kinetically significant p*K*. This behavior can be explained if the form $(E)^{2+}$ is not active on the substrate since for its binding it would be necessary form a hydrogen bond with the hydroxyl group, accept a proton and therefore generate a nucleophilic reagent (like O^-) to attack the copper. The proton may be captured by the forms $(E)^{2-}$ and $(E)^{+-}$ and so the apparent p*K* involved in the step $(E)^{2-} + 2H^+ \rightleftarrows (E)^{-+}$ will not be kinetically significant; therefore, apparently only one significant p*K* exists since the form $(E)^{2+}$ is inactive. However, since the p*K* of the hydroxyl groups is low, the substrate 3,6DFCat may have two negative charges at pH 7.0 and thus demonstrate the two apparent p*K*s of the enzymatic forms (Scheme 3). Thus, at high pH values, the enzyme is in the form $(E)^{2-}$ and the substrate in the form $(S)^{2-}$; consequently, the enzyme will show low affinity for the substrate, the initial velocity will decrease substantially and the suicide inactivation will be very slow (very low apparent inactivation constant $\lambda^S_{E_{ox}}$). As the pH of the medium falls, enzyme activity will increase (greater affinity for the substrate) and the process of suicide inactivation now becomes evident (higher $\lambda^S_{E_{ox}}$, Fig. 4SM). Therefore, at low pH values, the suicide inactivation by 3,6DFCat can be studied (time scale of around 6000 s), the enzyme is in the form $(E)^{+-}$ and the substrate $(S)^0$. As the pH fallen further, the enzyme will be in the form $(E)^{2+}$ and the substrate $(S)^0$, so that the enzymatic activity falls (Fig. 3) and the suicide inactivation apparently becomes slower (Fig. 4SM).

3.6. Effect of pH on the steady-state parameters, V_{max} and K^S_m

We studied the effect of pH on the enzymatic activity and determined the values of the kinetic parameters at each pH value assayed. The non-dependence of V_{max} (○) *vs.* pH and the parabolic dependence of K^S_m (●) are evident in Fig. 3 inset B. The behavior of V_{max} is typical of tyrosinase substrates since this parameter depends on the nucleophilic power of the oxygens of the phenolic hydroxyls. However, the value of K^S_m shows a parabolic dependence, indicating that the enzyme shows maximum affinity for the substrate when it occurs as $(E)^{+-}$ and the substrate with protonated hydroxyl groups as $(S)^0$.

3.7. Kinetic characterization of 3,6DFCat as suicide substrate of tyrosinase

3.7.1. Effect of substrate concentration

The experimental registers of the suicide inactivation of tyrosinase acting on 3,6DFCat are shown in Fig. 4A (at pH 5.0). The

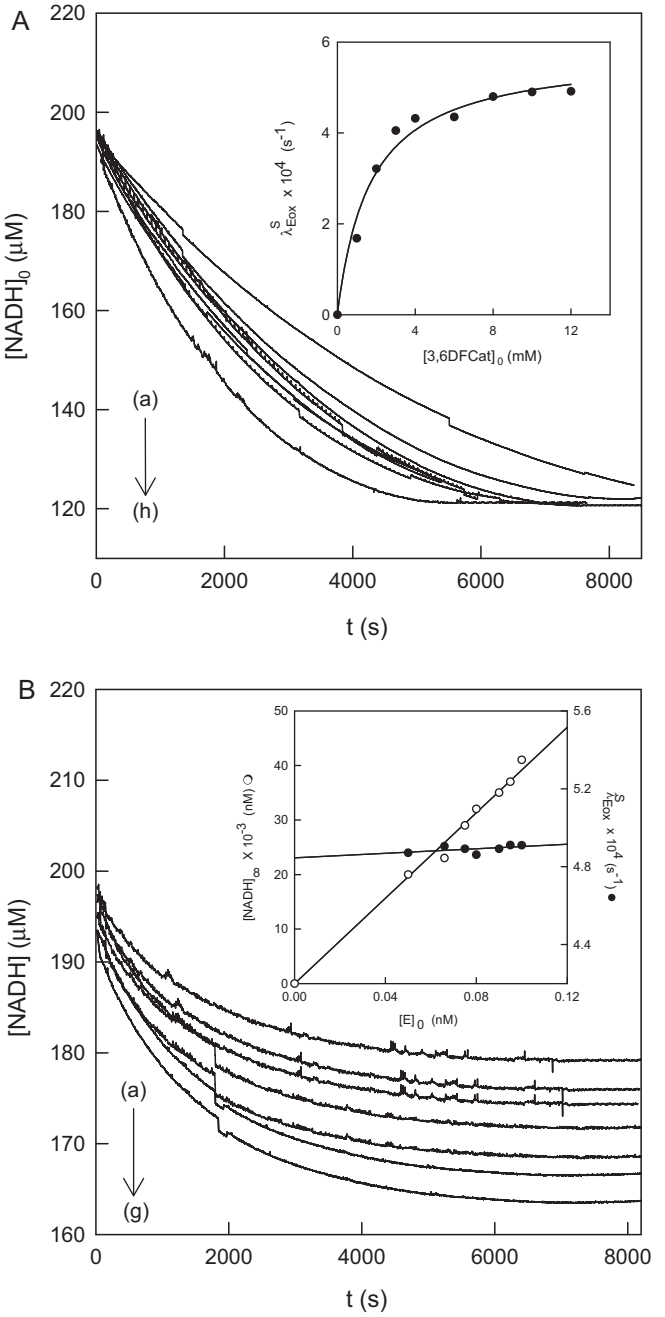

Fig. 4. (A) Corrected recordings of the disappearance of NADH in the suicide inactivation of tyrosinase by different 3,6DFCat concentrations. The experimental conditions were 30 mM sodium phosphate buffer (pH 5.0), 0.26 mM O_2, wavelength = 340 nm and the initial concentrations of NADH and tyrosinase were: 0.2 mM and 0.2 nM, respectively. The substrate concentrations were (mM): (a) 1, (b) 2, (c) 3, (d) 4, (e) 6, (f) 8, (g) 10 and (h) 12. Inset. Values of $\lambda^S_{E_{ox}}$ for different 3,6DFCat concentrations. (B) Corrected recordings of the disappearance of NADH in the suicide inactivation of tyrosinase by 3,6DFCat for different enzyme concentrations. The experimental conditions were 30 mM sodium phosphate buffer (pH 5.0), 0.2 mM NADH, 0.26 mM O_2, wavelength = 340 nm, $[3,6DFCat]_0$ = 12 mM and $[E]_0$ (nM): (a) 0.05, (b) 0.06, (c) 0.075, (d) 0.08, (e) 0.09, (f) 0.095 and (g) 0.1. Inset. Representation of the values of $[NADH]_\infty$ (○) and $\lambda^S_{E_{ox}}$ (●) *vs.* enzyme concentration.

non-linear regression analysis of these registers in accordance with Eq. (1) provides the parameters $\lambda^S_{E_{ox}}$ and $[NADH]_\infty$ [14]. In this case, as can be seen from Fig. 4A inset, the enzyme is saturated and $\lambda^S_{E_{ox}(max)}$ and K^S_m can be calculated (see Table 1). The inactivation efficiency $\lambda^S_{E_{ox}(max)}/K^S_m$, which is shown in Table 1, is higher than those obtained with the other two 3,6-disubstituted

catechols studied, but much lower than the catechol used as reference (Table 1).

3.7.2. Effect of enzyme concentration

Fig. 4B shows the effect of enzyme concentration when working at a constant substrate concentration at pH 5.0. Fig. 4B inset depicts the values obtained for $[NADH]_\infty$ *vs.* $[E]_0$. The slope has a value of 2*r*, giving a value of $r = k^S_{cat}/\lambda^S_{E_{ox}(max)} = 194,840 \pm 8050$. Note that this *r* is the highest described in the literature, meaning that the lower the value of the chemical shift of δ in C-1 and C-2 (see Table 1), the greater the nucleophilic power of the hydroxyl group's oxygen. This will facilitate the attack of the oxygen on the copper centre of tyrosinase and, subsequently, the transfer of the proton of the hydroxyl group to the base B_2 or the transfer of the proton of the hydroxyl group to the oxygen of the peroxide group, thus provoking inactivation. So, the kinetic and inactivation constants will be more separated and so the value of *r* will be higher.

3.8. Effect of pH on the kinetic of the suicide inactivation of tyrosinase by 3,6DFCat

As mentioned above, in a study of the effect of pH on the steady-state parameters, the apparent Michaelis constant is lowest at pH 6.0, and, in agreement with Eq. (2), the apparent inactivation constant will vary with the pH. A study of the effect of pH on the kinetics of suicide inactivation pointed to a hyperbolic dependence on substrate concentration (Fig. 4A inset). At both high and low pH values, $\lambda^S_{E_{ox}}$ decreases because K^S_m increases, and registers must be made on a greater time scale. However, the results obtained from fitting $\lambda^S_{E_{ox}}$ *vs.* $[S]_0$ provides the values of K^S_m and $\lambda^S_{E_{ox}(max)}$. Table 1 shows these values, which reflect the fact that the two processes of catalysis (k^S_{cat}) and inactivation ($\lambda^S_{E_{ox}(max)}$) are pH-independent, which means that the "*r*" is also pH-independent (Table 1). It should be noted that 3,6DFCat has the highest *r* described in the literature (maximum difference between k^S_{cat} and $\lambda^S_{E_{ox}(max)}$), although the catalytic (k^S_{cat}/K^S_m) and inactivation ($\lambda^S_{E_{ox}(max)}/K^S_m$) efficiencies, while higher than for 3I6MCat and 3T6MCat, are much lower than for catechol (Cat, Table 1).

In Table 1 it is possible to compare 3,6DFCat with catechol at pH 7.0. As can be seen, the K^S_m for 3,6DFCat is higher, although the catalytic efficiency is lower despite the lower values of δ. This may be due to the presence of fluorine groups in 3 and 6 positions, which would hamper the binding of the substrate to the enzyme and so lead to a lower k^S_{cat} and higher K^S_m. Note how the k^S_{cat} and the *r* values of 3,6DFCat do not agree with the results obtained for *o*-diphenols with hydrogen atoms at the 3 and 6 positions [14].

Therefore 3,6DFCat behaves as a suicide substrate according to the mechanism depicted in Scheme 1, and in turn confirms the reliability of this model. According to recent publications [3,51–53], the mechanism proposed to explain the suicide inactivation of tyrosinase takes into account the existence of two p*K*s for the enzyme acting on 3,6-DFCat (Fig. 3). The complete mechanism is depicted in Supplementary material. Scheme 1 shows the most important steps in the inactivation. One molecule of substrate 3,6DFCat interacts with the form E_{ox} of the enzyme. Since base B_1 is protonated, the oxygen of the hydroxyl group bound to the carbon atom with the lowest value of δ, can carry out a nucleophilic attack on the copper atom (*CuB*) and transfer the proton of the same hydroxyl group to the peroxide group of the form E_{ox}, this being the slowest catalytic step. Subsequently, the oxygen atom of the second hydroxyl group bound to the carbon atom with the highest δ carries out the nucleophilic attack on the other copper atom (*CuA*) and base B_2 accepts the proton. Another possibility is that the proton of the second hydroxyl group is transferred to the peroxide group that is already protonated, in which case the suicide inactivation of the enzyme will occur in what would be the slowest step of the process (see Tables 1 and 2).

Table 2
Kinetic constants characterizing the inactivation of E^R_d, E_m and E^T_d by 3,6DFCat under anaerobic conditions.

Enzymatic form	K_S (mM)	k_{i_S} (min^{-1})	k_{i_S}/K_S ($min^{-1}\,mM^{-1}$)
E^T_d	0.14 ± 0.02	0.093 ± 0.008	0.66 ± 0.09
E^R_d	0.11 ± 0.02	0.345 ± 0.034	3.13 ± 0.49
E_m	0.11 ± 0.02	0.345 ± 0.034	3.13 ± 0.49

Above, it has demonstrated that under aerobic conditions, 3,6DFCat acts as a suicide substrate of tyrosinase, while below we disclose the study of the irreversible inhibition of tyrosinase by the same substrate, but under anaerobic conditions.

3.9. Inactivation of tyrosinase by 3,6DFCat under anaerobic conditions

Under anaerobic conditions, the enzyme is irreversibly inactivated in the presence of 3,6DFCat. The enzymatic forms present under anaerobic conditions are: deoxy-tyrosinase (E_d) and met-tyrosinase (E_m). Furthermore, the form E_d undergoes a transition in such conditions to another form, as described in [49]. By analogy with hemocyanin [54], these forms are denominated E^R_d (relaxed) and E^T_d (tense). Fig. 6SM depicts the transition of E^R_d to E^T_d and, again by analogy with hemocyanin [54], the copper atoms are considered to be more separated in E^T_d (Scheme ISM). Note that the forms E_m and E_{ox} do not undergo transition (Fig. 6SM), probably because the binding between the copper atoms in these forms precludes their separation. In the case of E_m it is a hydroxyl group and in E_{ox} a peroxide group (Scheme ISM) [2,49].

The enzymatic form E^R_d is inactivated by 3,6DFCat with a first order kinetics that depends on the pH (Fig. 5). Data analysis according to:

$$[E^R_d]_t = [E^R_d]_0 e^{-\lambda^S_{E^R_d} t} \quad (3)$$

gives the value of $\lambda^S_{E^R_d}$. The apparent inactivation constant varies with the pH (Fig. 5 inset), data which are in agreement with those of Fig. 3 inset B. The apparent inactivation constant is maximum at pH 6.0, at which value the Michaelis constant is minimal.

Fig. 7SM depicts the variation of 3,6DFCat concentration, at optimal pH. Analysis according to Eq. (3) gives the values of $\lambda^S_{E^R_d}$. The values of this constant ($\lambda^S_{E^R_d}$) is represented *vs.* the initial concentration of 3,6DFCat and the analysis of Eq. (4) enables us to obtain the values of $k^R_{i_S}$ and K^R_S (Table 2):

$$\lambda^S_{E^R_d} = \frac{k^R_{i_S}[S]_0}{K^R_S + [S]_0} \quad (4)$$

When E^R_d is allowed to evolve for 90 min under anaerobic conditions, it is converted into the form E^T_d (Scheme ISM). A similar study of the inactivation of E^T_d (Figs. 8SM and 9SM) provides the data contained in Table 2. When the inactivation of the form E_m is studied, its transformation into E^R_d first occurs and then is inactivated according to Scheme 4 (Table 2).

The forms E^R_d and E_m show greater substrate affinity and higher inactivation constants. This may be due to the greater distance between the copper atoms at the active centre of the E^T_d form of tyrosinase, as occurs with hemocyanin [54]. Both in experiments carried out under aerobic conditions (suicide inactivation) and under anaerobic conditions (that lead to irreversible inactivation), dialysis of the samples and the determination of enzymatic activity reveal that the enzyme is irreversibly inactivated.

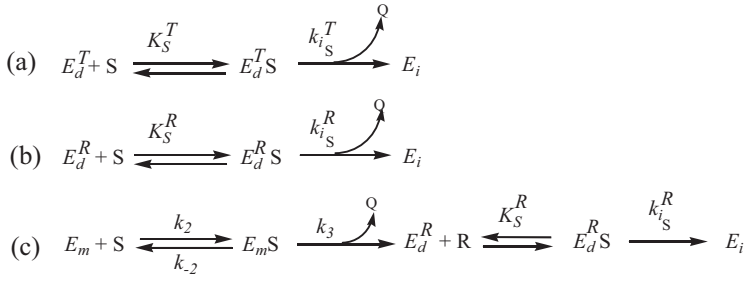

Scheme 4. Kinetic mechanism showing the inhibition of E_d^T, E_d^R and E_m by 3,6DFCat.

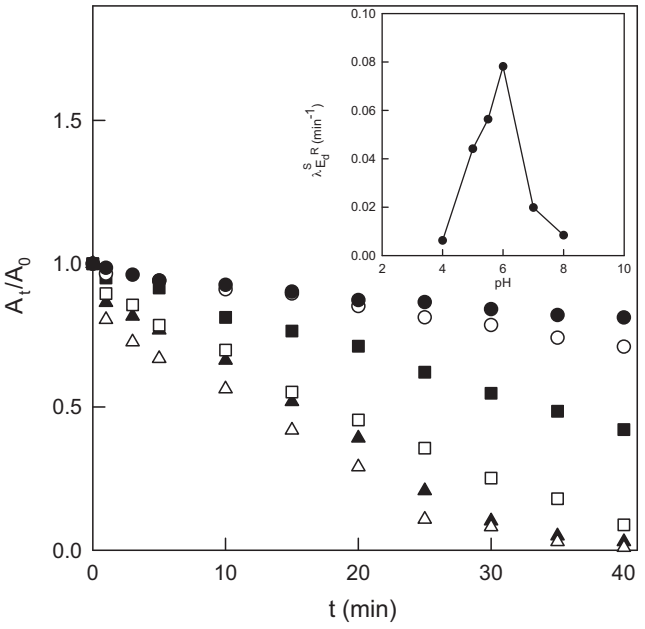

Fig. 5. Inactivation of the E_d^R form of TYR by 3,6DFCat at different pH. The form E_d^R was generated (see Section 2) and immediately incubated with 3,6DFCat, taking aliquots at different times to measure the residual activity with 9 mM TBC (wavelength = 410 nm). The values obtained were fitted to Eq. (3), and the apparent inactivation constant ($\lambda^S_{E_d^R}$) was obtained at each pH. The experimental conditions were: 30 mM sodium acetate buffer (pH 4.0–5.5) or 30 mM sodium phosphate buffer (pH 6.0–8.0) at 25 °C, $[E]_0$ 0.2 μM (see Section 2), $[H_2O_2]_0$ 5 μM [3,6DFCat]$_0$ = 50 μM and the pH-values used were: 4.0 (●), 8.0 (○), 7.0 (■), 5.0 (□), 5.5 (▲) and 6.0 (△). Inset. Representation of $\lambda^S_{E_d^R}$ *vs.* pH.

4. Conclusions

The compounds derived from catechol, 3,6-disubstituted, behave as suicide substrates of tyrosinase under aerobic conditions, confirming the validity of the mechanism proposed in Scheme 1. 3,6-Difluorocatechol shows a different kinetic behavior from all the *o*-diphenols studied for this enzyme [14]: (i) the K_m^S *vs.* pH follows a parabolic behavior, (ii) its action mechanism points to the existence of two critical apparent p*K*s in the enzyme, (iii) the *r*-value is the highest described in the literature, which explains the great difference between the catalytic and inactivation constants. Under anaerobic conditions, 3,6-difluorocatechol irreversibly inactivates the enzyme.

Acknowledgements

This paper was partially supported by grants from the Ministerio de Educación y Ciencia (Madrid, Spain) Project BIO2009-12956, from the Fundación Séneca (CARM, Murcia, Spain) Projects 08856/PI/08 and 08595/PI/08 and from the Consejería de Educación (CARM, Murcia, Spain) BIO-BMC 06/01-0004. FGM and JLMM have fellowships from Fundación Caja Murcia (Murcia, Spain). J.B. thanks the MICINN for a Ramón y Cajal Fellowship, cofinanced by the European Social Fund.

Appendix A. Supplementary data

Supplementary data associated with this article can be found, in the online version, at doi:10.1016/j.molcatb.2011.11.001.

References

[1] J.L. Muñoz-Muñoz, F. Garcia-Molina, R. Varon, P.A. Garcia-Ruiz, J. Tudela, F. Garcia-Canovas, J.N. Rodriguez-Lopez, IUBMB Life 62 (2010) 539–547.
[2] E.I. Solomon, U.M. Sundaram, T.E. Machonkin, Chem. Rev. 96 (1996) 2563–2606.
[3] M. Rolff, J. Schottenheim, H. Decker, F. Tuczek, Chem. Soc. Rev. 40 (2011) 4077–4098.
[4] S.M. Marino, S. Fogal, M. Bisaglia, S. Moro, G. Scartabelli, L. De Gioia, A. Spada, E. Monzani, L. Casella, S. Mammi, L. Bubacco, Arch. Biochem. Biophys. 505 (2011) 67–74.
[5] G. Battaini, E. Monzani, L. Casella, L. Lonardi, A.W. Tepper, G.W. Canters, L. Bubacco, J. Biol. Chem. 277 (2002) 44606–44612.
[6] J.M. Nelson, C.R. Dawson, Adv. Enzymol. 4 (1944) 99–152.
[7] I. Asimov, C.R. Dawson, J. Am. Chem. Soc. 72 (1950) 820–828.
[8] L.L. Ingraham, J. Corse, B. Makower, J. Am. Chem. Soc. 74 (1952) 2623–2626.
[9] Y. Tomita, M. Seiji, J. Dermatol. 4 (1977) 245–249.
[10] M. Seiji, M. Sasaki, Y. Tomita, Tohoku J. Exp. Med. 125 (1978) 233–245.
[11] Y. Tomita, A. Hariu, C. Mizuno, M. Seiji, J. Invest. Dermatol. 75 (1980) 379–382.
[12] K. Lerch, Mol. Cell. Biochem. 52 (1983) 125–138.
[13] C. Dietler, K. Lerch, in: T.E. King, H.S. Mason, M. Morrison (Eds.), Oxidases and Related Redox Systems, Pergamon Press, New York, 1982, pp. 305–317.
[14] J.L. Muñoz-Muñoz, F. Garcia-Molina, P.A. Garcia-Ruiz, M. Molina-Alarcon, J. Tudela, F. Garcia-Canovas, J.N. Rodriguez-Lopez, Biochem. J. 416 (2008) 431–440.
[15] A. Sanchez-Ferrer, J.N. Rodriguez-Lopez, F. Garcia-Canovas, F. Garcia-Carmona, Biochim. Biophys. Acta 1247 (1995) 1–11.
[16] J.R. Ros, J.N. Rodriguez-Lopez, F. Garcia-Canovas, Biochim. Biophys. Acta 1204 (1994) 33–42.
[17] F. Garcia-Canovas, J. Tudela, C. Martinez-Madrid, R. Varon, F. Garcia-Carmona, J.A. Lozano, Biochim. Biophys. Acta 912 (1987) 417–423.
[18] J. Tudela, F. Garcia Canovas, R. Varon, F. Garcia Carmona, J. Galvez, J.A. Lozano, Biochim. Biophys. Acta 912 (1987) 408–416.
[19] J. Escribano, J. Tudela, F. Garcia-Carmona, F. Garcia-Canovas, Biochem. J. 262 (1989) 597–603.
[20] S.G. Waley, Biochem. J. 185 (1980) 771–773.
[21] S.G. Waley, Biochem. J. 227 (1985) 843–849.
[22] Y. Matoba, T. Kumagai, A. Yamamoto, H. Yoshitsu, M. Sugiyama, J. Biol. Chem. 281 (2006) 8981–8990.
[23] M. Sendovski, M. Kanteev, V. Shuster Ben-Yosef, N. Adir, A. Fishman, Acta Crystallogr. Sect. F, Struct. Biol. Cryst. Commun. 66 (2010) 1101–1103.
[24] M. Sendovski, M. Kanteev, V. Shuster Ben-Yosef, N. Adir, A. Fishman, J. Mol. Biol. 405 (2011) 227–237.
[25] W.T. Ismaya, H.J. Rozeboom, A. Weijn, J.J. Mes, F. Fusetti, H.J. Wichers, W.B. Dijkstra, Biochemistry 50 (2011) 5477–5486.
[26] Y. Li, Y. Wang, H. Jiang, J. Deng, Proc. Natl. Acad. Sci. U.S.A. 106 (2009) 17002–17006.
[27] S. Chazarra, J. Cabanes, J. Escribano, F. Garcia-Carmona, Biochim. Biophys. Acta 1339 (1997) 297–303.
[28] T.S. Chang, J. Agric. Food Chem. 55 (2007) 2010–2015.
[29] T.S. Chang, Int. J. Mol. Sci. 16 (2009) 2440–2475.
[30] T.S. Chang, M.Y. Lin, H.J. Lin, J. Cosmet. Sci. 61 (2010) 205–210.
[31] S.S.-K. Tai, C.-G. Lin, M.-H. Wu, T.S. Chang, Int. J. Mol. Sci. 10 (2009) 4257–4266.

[32] J.L. Muñoz-Muñoz, J.R. Acosta-Motos, F. Garcia-Molina, R. Varon, P.A. Garcia-Ruíz, J. Tudela, F. Garcia-Cánovas, J.N. Rodríguez-López, Biochim. Biophys. Acta 1804 (2010) 1467–1475.
[33] E.J. Land, C.A. Ramsden, P.A. Riley, Tohoku J. Exp. Med. 212 (2007) 341–348.
[34] E.J. Land, C.A. Ramsden, P.A. Riley, M.R. Stratford, Tohoku J. Exp. Med. 216 (2008) 231–238.
[35] C.A. Ramsden, M.R.L. Stratford, P.A. Riley, Org. Biomol. Chem. 7 (2009) 3388–3390.
[36] C.A. Ramsden, P.A. Riley, ARKIVOC (i) (2010) 260–274.
[37] C.A. Ramsden, P.A. Riley, ARKIVOC (x) (2010) 248–254.
[38] J.L. Munoz-Munoz, F. Garcia-Molina, P.A. Garcia-Ruiz, R. Varon, J. Tudela, F. Garcia-Canovas, J.N. Rodriguez-Lopez, Biochim. Biophys. Acta 1794 (2009) 244–253.
[39] J.L. Munoz-Munoz, F. Garcia-Molina, E. Arribas, P.A. Garcia-Ruiz, J. Tudela, F. Garcia-Canovas, J.N. Rodriguez-Lopez, J. Enzyme Inhib. Med. Chem. 26 (2011) 728–733.
[40] F. Garcia-Molina, J.L. Munoz-Munoz, M. Garcia-Molina, P.A. Garcia-Ruiz, J. Tudela, F. Garcia-Canovas, J.N. Rodriguez-Lopez, Biosci. Biotechnol. Biochem. 74 (2010) 1777–1787.
[41] F. Garcia-Molina, J.L. Munoz-Munoz, F. Martinez-Ortiz, P.A. Garcia-Ruiz, J. Tudela, F. Garcia-Canovas, J.N. Rodriguez-Lopez, J. Agric. Food Chem. 59 (2011) 1383–1391.
[42] J.N. Rodriguez-Lopez, L.G. Fenoll, P.A. Garcia-Ruiz, R. Varon, J. Tudela, R.N. Thorneley, F. Garcia-Canovas, Biochemistry 39 (2000) 10497–10506.
[43] O.H. Lowry, N.J. Rosebrough, A.L. Farr, R.J. Randall, J. Biol. Chem. 19 (1951) 265–275.
[44] D.L. Ladd, J. Weinstock, J. Org. Chem. 46 (1981) 203–206.
[45] F. Garcia-Carmona, F. Garcia-Canovas, J.L. Iborra, J.A. Lozano, Biochim. Biophys. Acta 717 (1982) 124–131.
[46] F. Garcia-Molina, J.L. Muñoz, R. Varon, J.N. Rodriguez-Lopez, F. Garcia-Canovas, J. Tudela, J. Agric. Food Chem. 55 (2007) 9739–9749.
[47] Jandel scientific, Sigma Plot 9.0 for Windows™, Jandel scientific, Core Madera, 2006.
[48] F. Garcia-Molina, A.N. Hiner, L.G. Fenoll, J.N. Rodriguez-Lopez, F. Garcia-Canovas, J. Tudela, J. Agric. Food Chem. 53 (2005) 3702–3709.
[49] J.L. Munoz-Munoz, F. Garcia-Molina, P.A. Garcia-Ruiz, R. Varon, J. Tudela, F. Garcia-Canovas, J.N. Rodríguez-Lopez, J. Mol. Catal. B: Enzymatic 62 (2010) 173–182.
[50] M. Garcia-Moreno, R. Varon, A. Sanchez Gracia, J. Tudela, F. Garcia Canovas, Biochim. Biophys. Acta 1205 (1994) 282–288.
[51] I. Koval, P. Gamez, C. Belle, K. Selmeczi, J. Reedijk, Chem. Soc. Rev. 35 (2006) 814–840.
[52] A.W.J.W. Tepper, L. Bubacco, G.W. Canters, J. Biol. Chem. 277 (2002) 30436–30444.
[53] A.W.J.W. Tepper, L. Bubacco, G.W. Canters, J. Biol. Chem. 279 (2004) 13425–13434.
[54] M. Metz, E.I. Solomon, J. Am. Chem. Soc. 123 (2001) 4938–4950.

SUPPLEMENTARY Data:

Selected Data for 3,6DFCat

^{1}H- and ^{13}C-NMR spectra were recorded at 298 K on a Bruker Avance 400 MHz instrument. ^{1}H-NMR chemical shifts are reported relative to Me_4Si and were referenced via residual proton resonances of the corresponding deuterated solvent, whereas ^{13}C-NMR spectra are reported relative to Me_4Si using the carbon signals of the deuterated solvent. ^{19}F-NMR spectrum was measured at 298 K on a Bruker Avance 300 instrument at 282 MHz. ^{19}F chemical shifts are given relative to trifluorotoluene. Mass spectra were recorded with an HPLC/MS TOF 6220 mass spectrometer.

(3,6DFC): ^{1}H NMR (400 MHz, $CDCl_3$) δ = 6.62 (m, 2H, CH), 5.33 (br s, 2H, OH); ^{13}C NMR (100 MHz, $CDCl_3$) δ = 147.81 (dd, *J* = 236.5, 3.5 Hz, CF), 133.48 (dd, *J*=14.0, 8.2 Hz, COH), δ = 106.31 (dd, *J* = 17.1, 12.0 Hz, CH); ^{19}F NMR (282 MHz, $CDCl_3$) δ = - 142.19 (t, *J* = 7.1 Hz) p.p.m.; HRMS (ESI^-) calculated for $C_6H_3F_2O_2$ $[M - H]^-$ 145.0107, found 145.0110.

Schemes

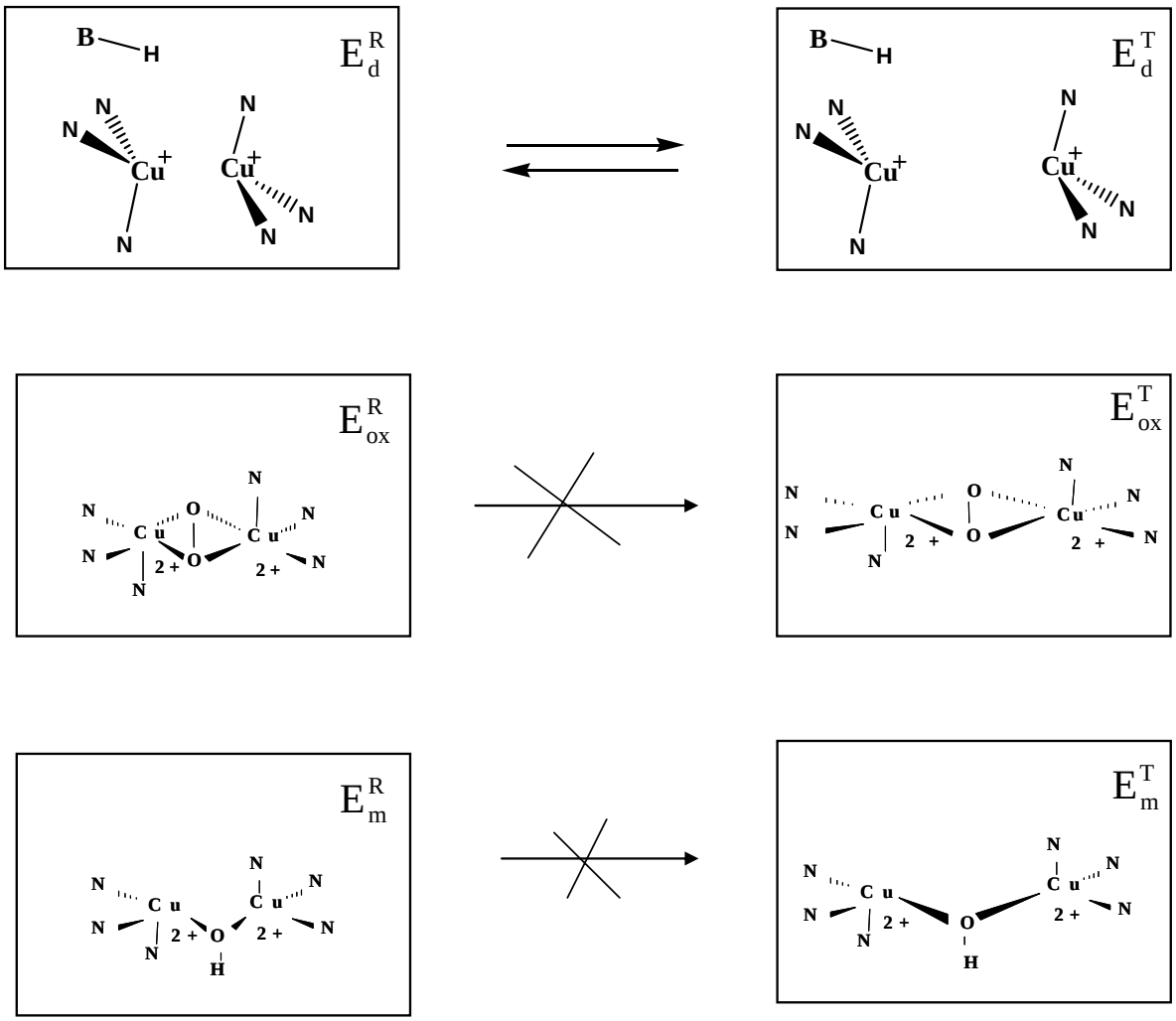

Scheme 1SM. Structural mechanism to explain the transition of relaxed deoxy-tyrosinase to tense deoxy-tyrosinase and the non-transition of met-tyrosinase and oxy-tyrosinase.

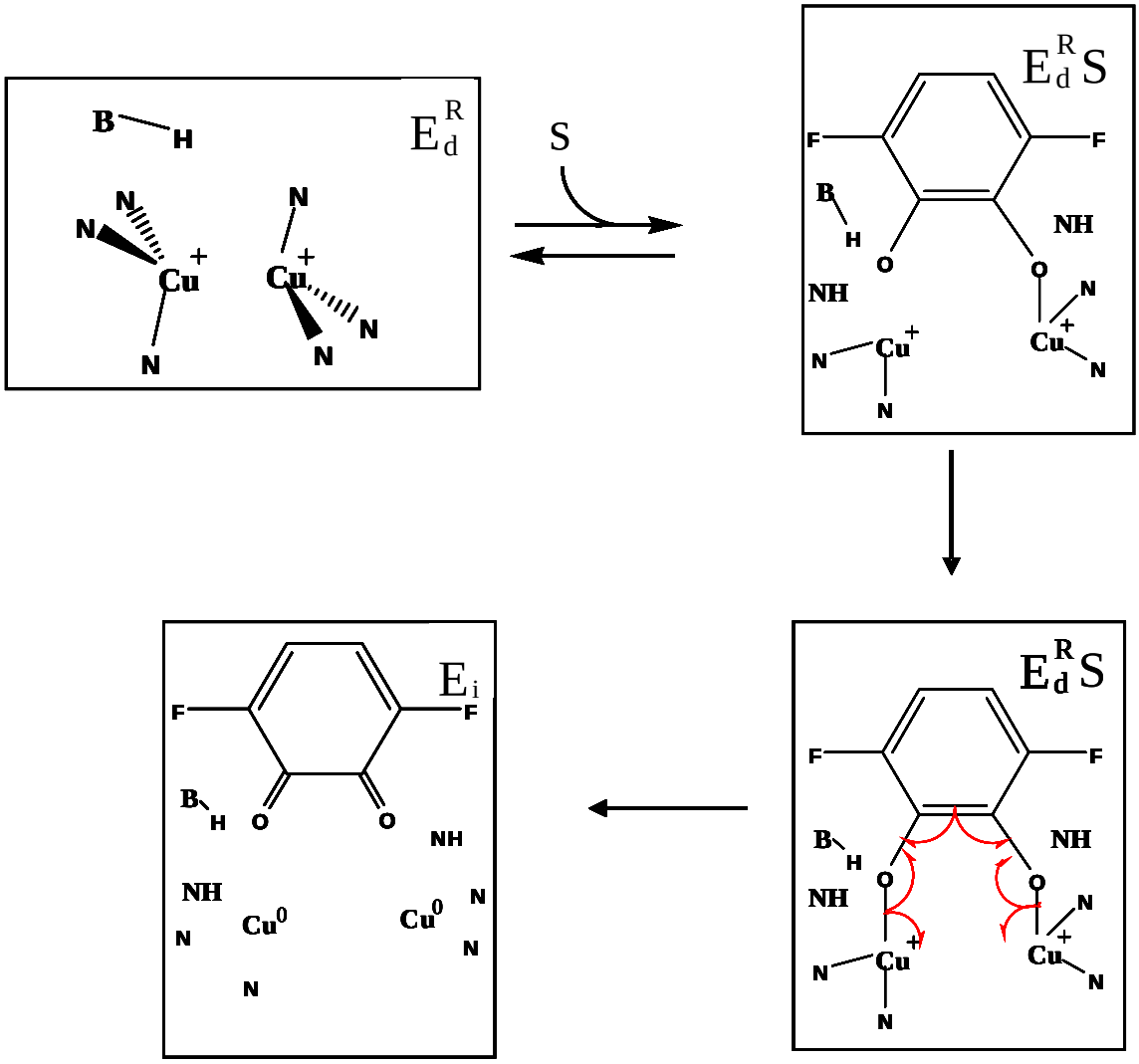

Scheme 2ASM. Structural mechanism to explain the irreversible inhibition of relaxed deoxy-tyrosinase by 3,6-DFCat.

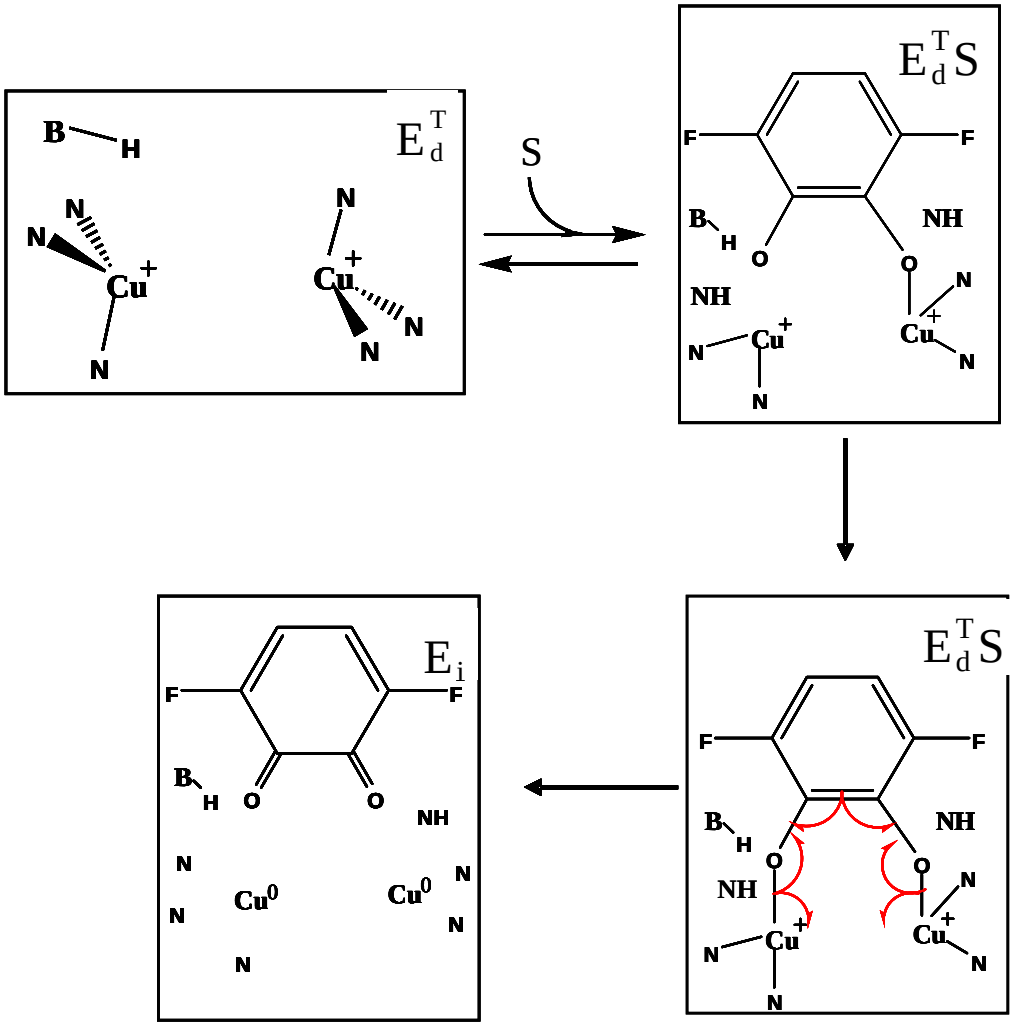

Scheme 2BSM. Structural mechanism to explain the irreversible inhibition of tense deoxy-tyrosinase by 3,6-DFCat.

Figures

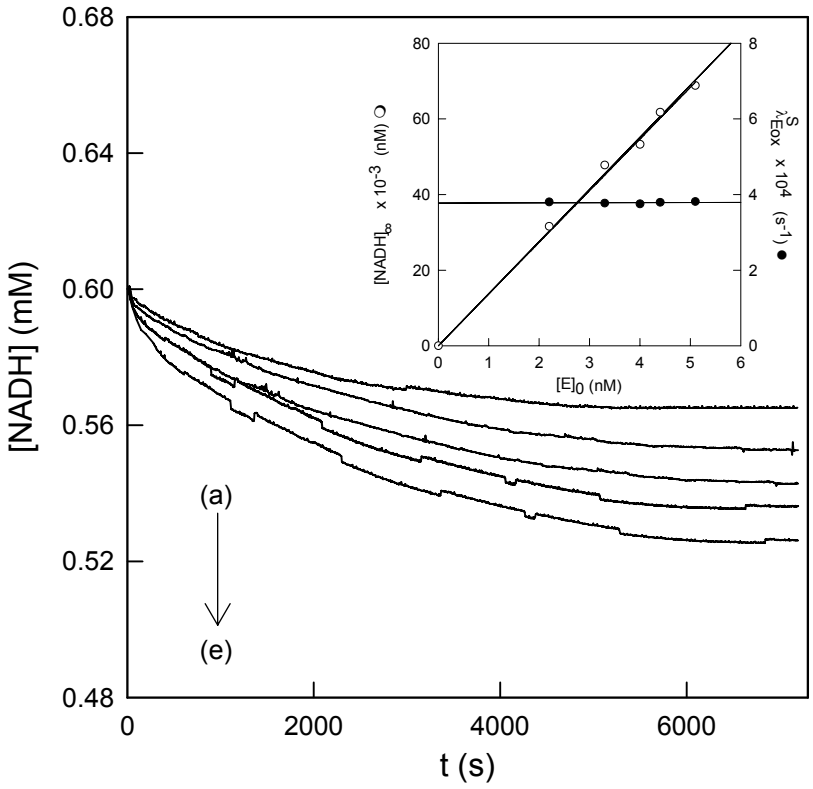

Fig. 1SM

Fig. 1SM. Corrected recordings of the disappearance of NADH in the suicide inactivation of tyrosinase by 3-isopropyl-6-methylcatechol for different enzyme concentrations. The experimental conditions were 30 mM sodium phosphate buffer (pH 7.0), 0.6 mM NADH, 0.26 mM O_2, wavelength = 380 nm, $[3I6MCat]_0$ = 5 mM and $[E]_0$ (nM): (a) 2.2, (b) 3.3, (c) 4.0, (d) 4.4 and (e) 5.1. **Inset.** Representation of the values of $[NADH]_\infty$ (○) and $\lambda^S_{E_{ox}}$ (●) *vs.* enzyme concentration.

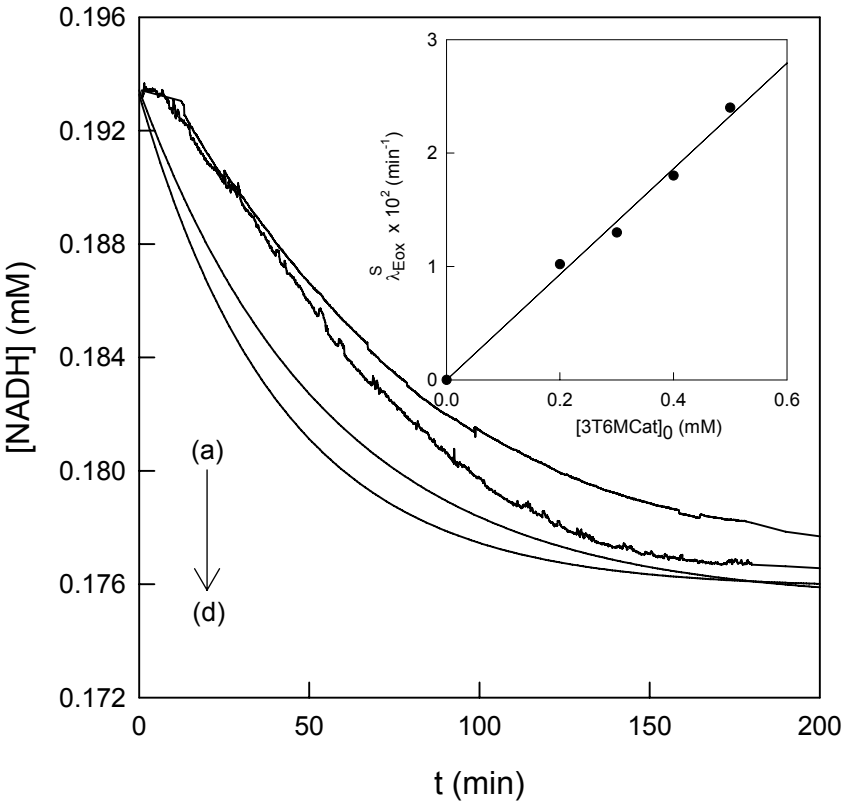

Fig. 2SM

Fig. 2SM. Corrected recordings of the disappearance of NADH in the suicide inactivation of tyrosinase by different 3-*tert*-butyl-6-methylcatechol concentrations. The experimental conditions were 30 mM sodium phosphate buffer (pH 7.0), 0.26 mM O_2, wavelength = 340 nm and the initial concentrations of NADH and tyrosinase were 0.19 mM and 6 nM, respectively. The substrate concentrations were (mM): (a) 0.2, (b) 0.3, (c) 0.4 and (d) 0.5. **Inset.** Values of $\lambda^S_{E_{ox}}$ for different 3-*tert*-butyl-6-methylcatechol concentrations.

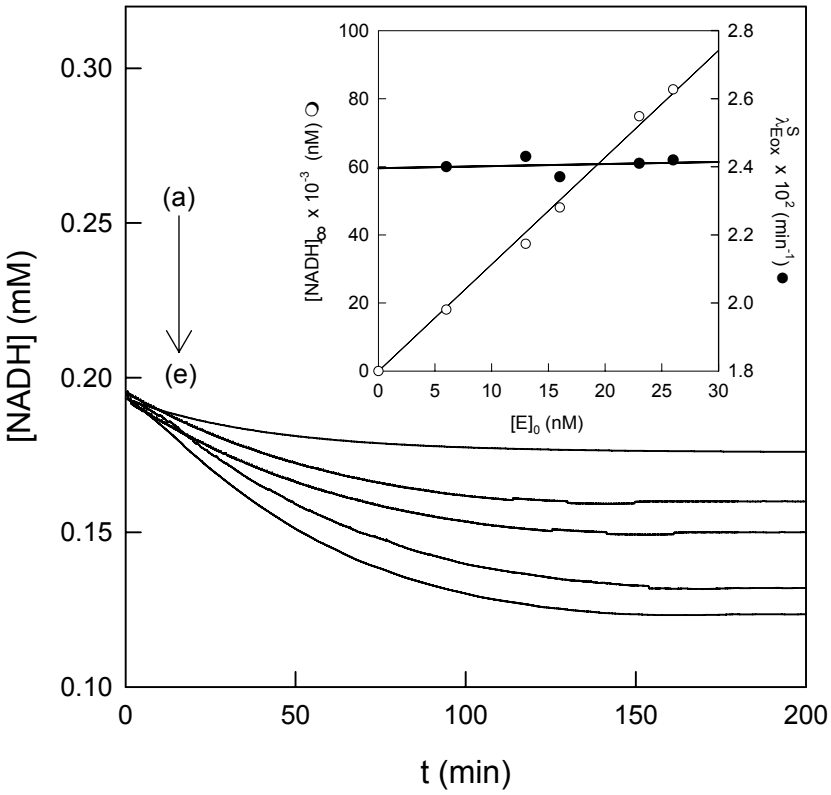

Fig. 3SM

Fig. 3SM. Corrected recordings of the disappearance of NADH in the suicide inactivation of tyrosinase by 3-*tert*-butyl-6-methylcatechol for different enzyme concentrations. The experimental conditions were 30 mM sodium phosphate buffer (pH 7.0), 0.2 mM NADH, 0.26 mM O_2, wavelength = 340 nm, $[3T6MCat]_0$ = 0.5 mM and $[E]_0$ (nM): (a) 6, (b) 13, (c) 16, (d) 23 and (e) 26. **Inset.** Representation of the values of $[NADH]_\infty$ (○) and $\lambda^S_{E_{ox}}$ (●) *vs.* enzyme concentration.

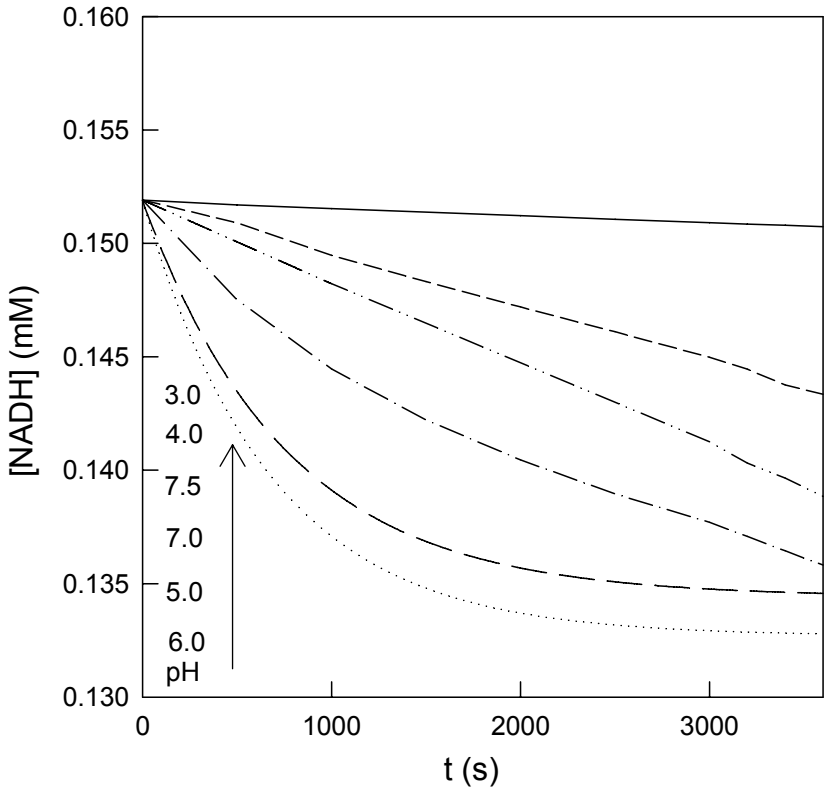

Fig. 4SM

Fig. 4SM. Corrected recordings of the disappearance of NADH in the suicide inactivation of tyrosinase by 3,6DFCat for different pH. The experimental conditions are the same as in Fig. 3 but the initial concentration of 3,6DFCat was 6 mM.

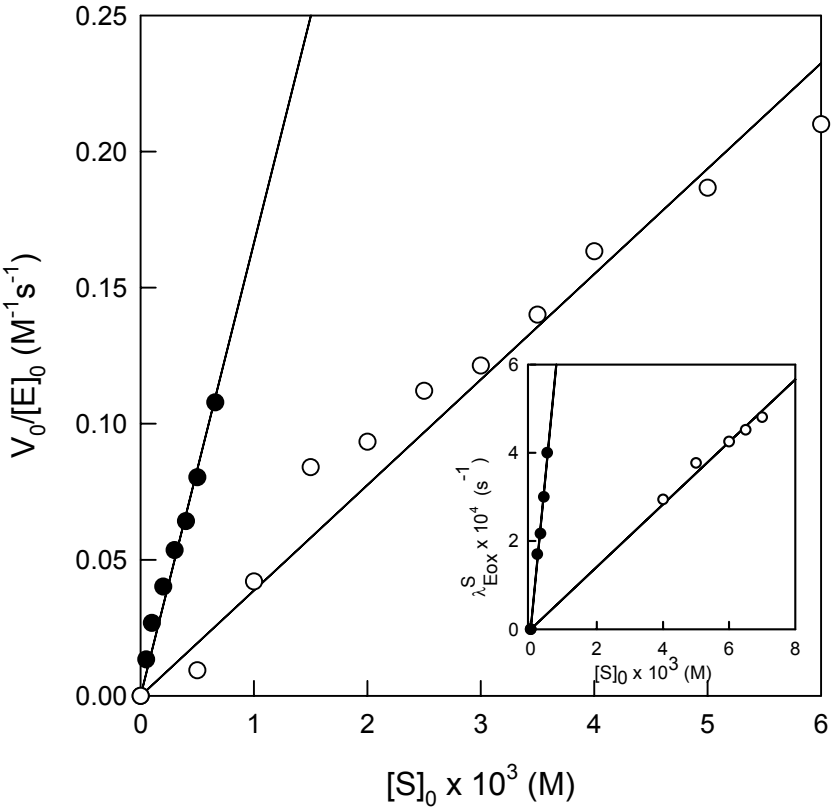

Fig. 5SM

Fig. 5SM. Representation of $V_0/[E]_0$ *vs.* $[S]_0$ for 3I6MCat and 3T6MCat. The experimental conditions were 30 mM sodium phosphate buffer (pH 7.0), 0.6 mM NADH, wavelength = 380 nm (3I6MCat) and 340 nm (3T6MCat and 3,6DFCat), $[E]_0$ = 0.2 μM for 3I6MCat (O) and 30 mM sodium phosphate buffer (pH 7.0), 0.2 mM NADH, λ = 340 nm, $[E]_0$ = 0.6 μM for 3T6MCat (●). **Inset.** Representation of $\lambda^S_{E_{ox}}$ *vs.* $[S]_0$ for 3I6MCat (O) and 3T6MCat (●). The experimental conditions are the same as in Fig. 5SM but the enzyme concentrations were 2.2 nM (3I6MCat) and 6 nM (3T6MCat).

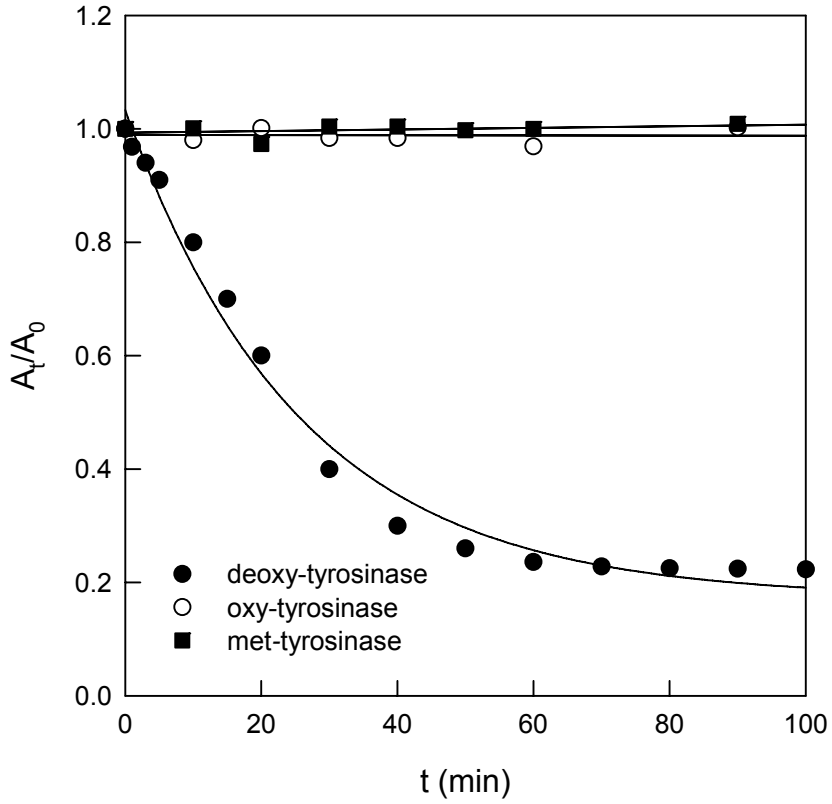

Figure 6SM

Fig. 6SM. Variation of the A_t/A_0-values *vs.* time obtained from a kinetic study of transition of E_d^R to E_d^T followed through the diphenolase activity. The experimental conditions were as follows: deoxy-tyrosinase (●): 30 mM sodium phosphate buffer (pH 7.0), 25 ºC. A nitrogen stream was first passed through the buffer and then 100 nM enzyme (previously treated with 5 μM H_2O_2) was added; still passing the nitrogen stream, aliquots were taken at the indicated times and the activity was followed using TBC, measuring the increase in absorbance at λ = 410 nm with a TBC concentration of 1 mM. Oxy-tyrosinase (○) and met-tyrosinase (■) were generated as indicated in the Material and Methods section and, then, the residual activity was measured taking aliquots and measuring the increase in absorbance at λ = 410 nm with a TBC concentration of 1 mM.

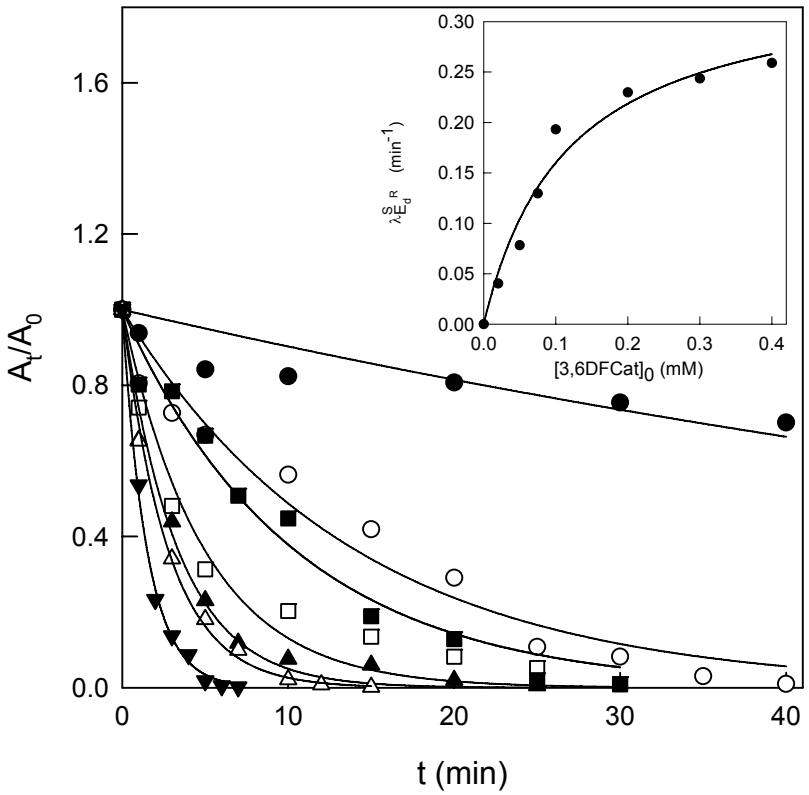

Fig. 7SM

Fig. 7SM. Inactivation of the E_d^R form of TYR by 3,6DFCat. The form E_d^R was generated (see Material and Methods) and immediately incubated with 3,6DFCat, taking aliquots at different times to measure the residual activity with 9 mM TBC (wavelength = 410 nm). The values obtained were fitted to eqn (3), and the apparent inactivation constant ($\lambda^S_{E_d^R}$) was obtained for each concentration of 3,6DFCat. The experimental conditions were 30 mM sodium phosphate buffer (pH 6.0) at 25 ºC, $[E]_0$ 0.2 μM (see Materials and Methods), $[H_2O_2]_0$ 5 μM and [3,6DFCat]$_0$ (μM) of 20 •, 50 ○, 75 ■, 100 □, 200 ▲, 300 △ and 400 ▼. **Inset.** Representation of $\lambda^S_{E_d^R}$ *vs.* [3,6DFCat]$_0$.

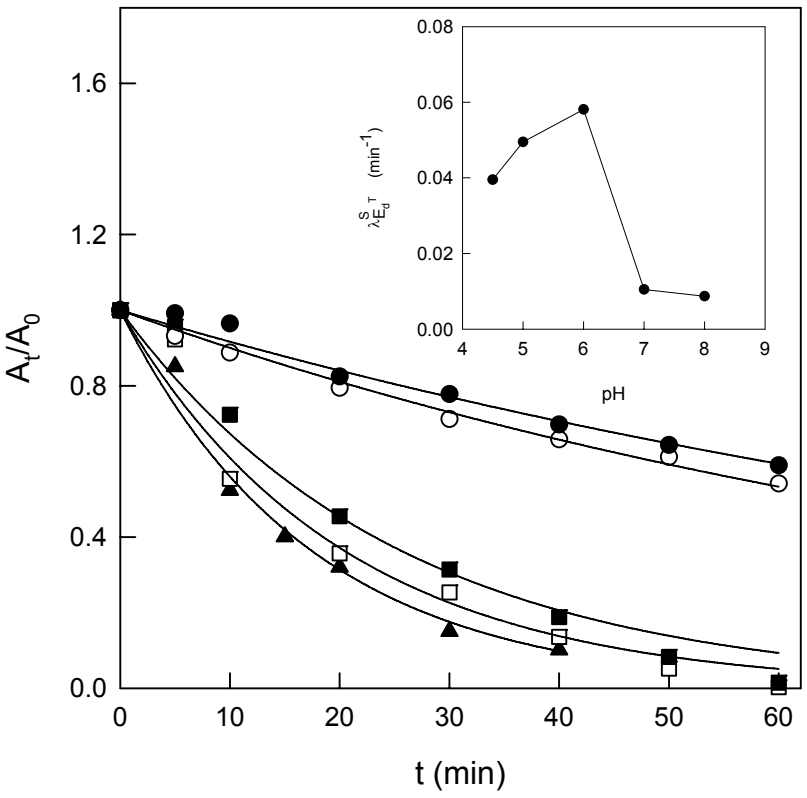

Fig. 8SM

Fig. 8SM. Inactivation of the E_d^T form of TYR by 3,6DFCat at different pH. The form E_d^R, obtained as indicated in Material and methods section, was allowed to stand for 90 min to obtain E_d^T. 3,6DFCat was added at t = 0 and aliquots were taken at different times to measure the residual activity with 9 mM TBC (wavelength = 410 nm). The values obtained were fitted to eqn (3) but referring to E_d^T, and the apparent inactivation constant ($\lambda^S_{E_d^T}$) was obtained at each pH. The experimental conditions were 30 mM sodium acetate buffer (pH 4.5 and 5.0) or 30 mM sodium phosphate buffer (pH-values 6.0, 7.0 and 8.0) at 25 ºC, $[E]_0$ 0.2 μM (see Materials and Methods), $[H_2O_2]_0$ 5 μM and $[3,6DFCat]_0$ 200 μM. The pH-values used were: ● 8.0, ○ 7.0, ■ 4.0, □ 5.0 and ▲ 6.0. **Inset.** Representation of $\lambda^S_{E_d^T}$ *vs.* pH.

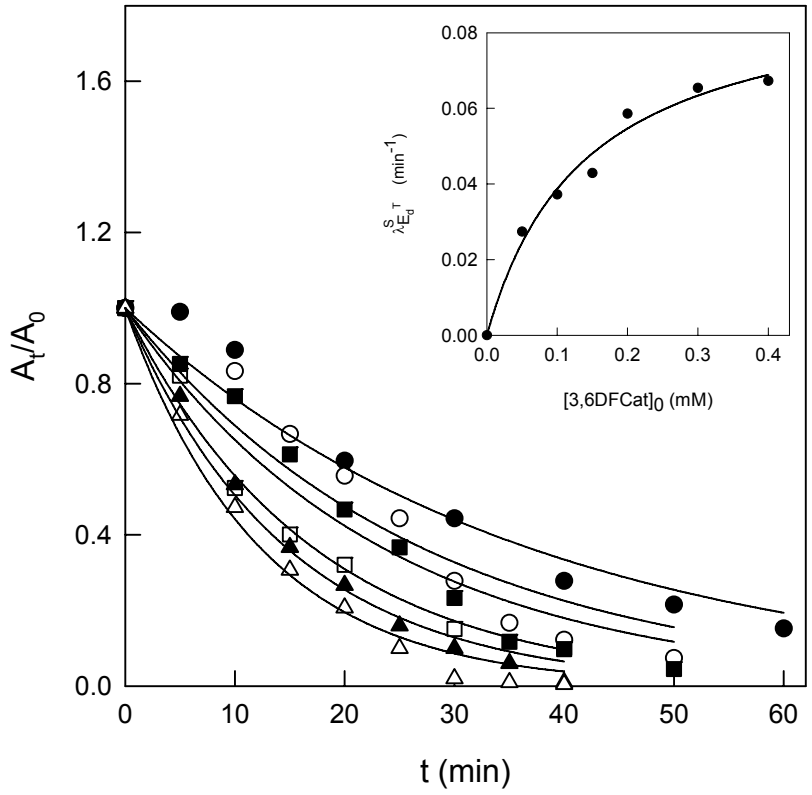

Fig. 9SM

Fig. 9SM. Inactivation of the E_d^T form of TYR by 3,6DFCat. The form E_d^R, obtained as indicated in Material and methods section, was allowed to stand for 90 min to obtain E_d^T. 3,6DFCat was added at t = 0 and aliquots were taken at different times to measure the residual activity with 9 mM TBC (λ = 410 nm). The values obtained were fitted to eqn (4) but referring to E_d^T, and the apparent inactivation constant ($\lambda^S_{E_d^T}$) was obtained at each substrate concentration. The experimental conditions were 30 mM sodium phosphate buffer (pH 6.0) at 25 ºC, $[E]_0$ 0.2 μM (see Materials and Methods), $[H_2O_2]_0$ 5 μM and 3,6DFCat initial concentration (mM) of 0.05 ●, 0.1 ○, 0.15 ■, 0.2 □, 0.3 ▲ and 0.4 △. **Inset.** Representation of $\lambda^S_{E_d^T}$ *vs.* $[3,6DFCat]_0$.

Conclusiones

5. CONCLUSIONES

El desarrollo de esta memoria ha conducido al establecimiento de un conjunto de conclusiones específicas y generales sobre el tema de estudio.

5.1. CONCLUSIONES ESPECÍFICAS

Las conclusiones detalladas en los distintos capítulos pueden resumirse en varias conclusiones específicas.

1. Se ha profundizado en el mecanismo cinético de actuación de tirosinasa sobre distintas parejas monofenol/*o*-difenol. Se ha demostrado que la enzima expresa cooperatividad cinética (mecanismo de ruta favorecida) cuando actúa sobre *o*-difenoles, confirmando la hipótesis previa en la que se proponía que todas las etapas del ciclo catalítico de la actividad difenolasa estaban en estado estacionario. Por otra parte, se ha demostrado que la enzima no muestra cooperatividad cinética cuando actúa sobre monofenoles, confirmando la existencia de una etapa crítica en el nuevo ciclo catalítico que transcurre en equilibrio rápido, esta etapa podría corresponder a la hidroxilación de monofenoles a *o*-difenoles.
2. Se han caracterizado cinéticamente diez parejas monofenol/*o*-difenol. A partir de los resultados obtenidos, se puso de manifiesto que la afinidad de la enzima por oxigeno es mayor en la ruta favorecida que en la ruta lenta.
3. Se han descrito propiedades cinéticas nuevas de la especie enzimática desoxitirosinasa, demostrando cinéticamente que desoxitirosinasa existe en dos formas: relajada (menos distancia entre átomos de cobre) y tensa (mayor distancia entre átomos de cobre), con propiedades cinéticas distintas.
4. Se ha estudiado el efecto del pH en la cinética de la transición de la forma relajada de desoxitirosinasa a la forma tensa y se han obtenido los parámetros

cinéticos que caracterizan cada una de estas formas. Se demuestra la existencia de dos pKas críticos en la enzima.

5. Se caracterizó cinéticamente la inactivación irreversible bajo condiciones anaerobias de cada una de estas especies enzimáticas (relajada y tensa) por *o*-difenoles.
6. Se ha profundizado en el origen no enzimático del peróxido de hidrógeno en la ruta de biosíntesis de melaninas, demostrando que se produce por autooxidación de sustratos e intermedios de la ruta.
7. Se han calculado los coeficientes de absortividad molar de las *o*-quinonas correspondientes a una serie de *o*-difenoles, trifenoles y flavonoides, generándolas mediante oxidación con periodato sódico en exceso.
8. Se ha estudiado la estabilidad de las *o*-quinonas generadas mediante oxidación del sustrato (*o*-difenol, trifenol o flavonoide) mediante periodato sódico en defecto. Atendiendo a esta propiedad, se diseñan métodos espectrofotométricos para medir la actividad de tirosinasa, evitando el seguimiento de las *o*-quinonas mediante su reducción con ácido ascórbico. Estos métodos pueden resumirse en: (*i*) seguimiento de la disminución de la absorbancia del ácido ascórbico con el tiempo, (*ii*) medida del tiempo necesario para consumir una cantidad fija de ácido ascórbico (método cronométrico) y (*iii*) medida del tiempo necesario para que cambie la pendiente del consumo de ácido ascórbico por la de formación de *o*-quinona.
9. En base a los métodos descritos anteriormente, se caracterizó cinéticamente a esculetina como un sustrato de tirosinasa, explicando su aparente inhibición en la melanogenesis.
10. Se han caracterizado cinéticamente a carbidopa y benserazida (inhibidores de dopa descarboxilasa) como sustratos de tirosinasa.

11. Se ha aplicado el método cronométrico a la caracterización cinética del ácido clorogénico (sustrato mayoritario en frutas) como sustrato de tirosinasa.
12. Mediante la aplicación de los métodos cronométrico y el basado en la medida de desaparición de ácido ascórbico, se han caracterizado cinéticamente las catequinas del té verde.
13. Se han estudiado las propiedades prooxidantes y antioxidantes de las catequinas del té verde, resultando que: (+)-catequina y (-)-epicatequina son más prooxidantes y menos antioxidantes que EGC, EGCG y ECG.
14. Se han caracterizado cinéticamente compuestos trihidroxilados (ácido gálico, pirogalol y ácido gálico metil ester) como sustratos de tirosinasa.
15. Se han estudiado las propiedades prooxidantes y antioxidantes de algunos compuestos trihidroxilados. Pirogalol muestra el mayor poder prooxidante y antioxidante. El ácido gálico inhibe la formación de peróxido de hidrógeno y el consumo de oxigeno debido a la reacción de peroxidación con su grupo carboxilo.
16. Se ha llevado a cabo la caracterización cinética del ácido elágico como sustrato de tirosinasa y se ha cuantificado su gran poder antioxidante.
17. El estudio del ácido rosmarínico permitió su caracterización cinética como sustrato de tirosinasa y se pudieron establecer sus propiedades prooxidantes y antioxidantes.
18. Se ha propuesto una metodología general para el estudio del poder antioxidante de un compuesto, ésta consta de dos partes: (i) un método enzimático cinético y (ii) un test cinético no enzimático.
19. La metodología propuesta se ha aplicado a la determinación del poder antioxidante primario y secundario de un conjunto de fenoles, polifenoles y flavonoides.

20. Se ha propuesto un nuevo parámetro que compara a distintas moléculas antioxidantes. El parámetro se denomina: eficiencia cinética antiradical aparente que incluye el efecto de la concentración y del tiempo.

21. Se ha demostrado que tirosinasa tiene una amplia especificidad de sustrato, hidroxila a aminas aromáticas y oxida a orto-diaminas aromáticas y orto-aminofenoles. Se proponen mecanismos estructurales para explicar estas actividades enzimáticas.

22. Se ha realizado un estudio cinético sobre la inactivación suicida de tirosinasa al actuar sobre sus sustratos difenólicos y trifenólicos. Los datos cinéticos: $\lambda_{\max}$ (constante aparente de inactivación máxima), k_{cat} (constante catalítica), K_m (constante de Michaelis) y r (razón de partición o número de ciclos catalíticos que realiza un mol de enzima antes de su inactivación), están relacionados con efectos electrónicos, estéricos e hidrofóbicos. Se propone un mecanismo estructural que explica los resultados experimentales.

23. Se ha profundizado en el estudio de la inactivación de tirosinasa por su sustrato fisiológico L-dopa, tanto en condiciones aerobias como anaerobias. En condiciones aerobias, se produce la inactivación suicida y en condiciones anaerobias ocurre el proceso de inhibición irreversible. La constante de velocidad aparente de la inactivación suicida es mucho menor que la de la inhibición irreversible, de donde se concluye que la presencia de oxigeno protege a la enzima. Además, el proceso es estereoespecífico en cuanto a la afinidad de la enzima por el sustrato.

24. A partir del estudio de la actividad monofenolasa de tirosinasa, se ha demostrado que los monofenoles no inactivan a tirosinasa en presencia o en ausencia de oxigeno. Así pues, la inactivación suicida que se origina en presencia de L-tirosina se debe al L-dopa acumulado en el medio a partir de la evolución de la *o*-dopaquinona.

25. El ácido ascórbico es un inactivador de tirosinasa, tanto en condiciones aerobias como en condiciones anaerobias. El proceso es estereoespecífico, pero únicamente respecto a la afinidad de unión del sustrato, no interviene en la rapidez. En condiciones aerobias, el sistema muestra inactivación suicida. Sin embargo, en condiciones anaerobias se da la inhibición irreversible. La rapidez de la inhibición irreversible es mayor que la de la inactivación suicida.
26. Se ha estudiado la inactivación suicida de tirosinasa en su acción sobre tetrahidropterinas. La potencia de inactivación siguió el orden: BH_4>MBH_4>$DMBH_4$.
27. Se ha caracterizado cinéticamente la inactivación suicida de tirosinasa en su acción sobre *o*-diaminas aromáticas y *o*-aminofenoles. La constante aparente de inactivación sigue la secuencia: *o*-diaminas<*o*-aminofenoles<*o*-difenoles. Los valores de r siguen el mismo orden, confirmando el mecanismo cinético propuesto para explicar la actuación de la enzima. La etapa más lenta del proceso corresponde a la inactivación.
28. Estudiando la inactivación suicida con sustratos *o*-difenólicos sustituidos en las posiciones 3 y 6 y teniendo en cuenta los trabajos publicados sobre estructura de distintas tirosinasas, se ha propuesto un mecanismo estructural que explica los resultados experimentales. A partir del estudio del efecto del pH y utilizando 3,6-difluorocatecol como sustrato, se ha puesto de manifiesto un segundo pKa crítico de la enzima, que se ajusta al mecanismo estructural.

5.2. CONCLUSIONES GENERALES

Las conclusiones específicas previas permiten establecer las siguientes conclusiones generales:

1. El estudio cinético de distintas parejas monofenol/*o*-difenol ha permitido demostrar la existencia de cooperatividad cinética en la actividad difenolasa de

tirosinasa pero no en la actividad monofenolasa. Se ha propuesto un mecanismo al azar que contempla una ruta favorecida.

2. Se ha estudiado la transición de desoxitirosinasa desde la forma relajada a la forma tensa y su dependencia del pH. Se demuestra la existencia de dos pKas críticos en la enzima.
3. Se ha demostrado el origen no enzimático de la acumulación de peróxido de hidrógeno en la ruta de biosíntesis de melaninas.
4. Se ha diseñado un método rápido para el cálculo de las absortividades molares de las *o*-quinonas originadas mediante oxidación con periodato sódico en exceso de *o*-difenoles, trifenoles y flavonoides.
5. Se han diseñado distintos métodos de medida de la actividad de tirosinasa basados en la reducción de las *o*-quinonas por ácido ascórbico, estos métodos son: seguir espectrofotométricamente la desaparición de ácido ascórbico o bien medir el tiempo que tarda en consumirse una cantidad de ácido ascórbico determinada, dando lugar al método cronométrico y al método cronométrico alternativo.
6. Utilizando los métodos descritos anteriormente, se han caracterizado cinéticamente distintos sustratos de tirosinasa que tras su oxidación por la enzima originan *o*-quinonas muy inestables, entre estos se encuentran: esculetina, carbidopa, benserazida, ácido clorogénico, catequinas del té, ácido elágico, ácido gálico, pirogalol, ácido gálico metil ester y ácido rosmarínico. Además, se han estudiado sus propiedades prooxidantes y antioxidantes.
7. Se ha propuesto una metodología para el estudio del poder antioxidante de un compuesto. Esta consta de dos partes: (*i*) un método enzimático cinético y (*ii*) un test cinético no enzimático. Esta metodología permite calcular el poder antioxidante primario y secundario de cualquier compuesto. Además, se ha definido un parámetro cinético nuevo que se denomina eficiencia cinética

antiradical aparente que incluye el efecto de la concentración y el tiempo y compara a distintas moléculas antioxidantes.

8. Se ha realizado un estudio sistemático del proceso de inactivación suicida de tirosinasa en su actuación sobre *o*-difenoles, trifenoles y otras moléculas como ácido ascórbico y tetrahidropterinas. Los parámetros cinéticos $\lambda_{\max}$ (constante aparente de inactivación máxima), k_{cat} (constante catalítica), K_m (constante de Michaelis) y r (razón de partición o número de ciclos catalíticos que realiza un mol de enzima antes de su inactivación) están relacionados con efectos electrónicos, estéricos e hidrofóbicos.

9. Se ha profundizado en el estudio del proceso de inactivación suicida con los sustratos fisiológicos L-tirosina, L-dopa y sus isómeros correspondientes. Puede concluirse que los monofenoles no inactivan a la enzima bajo condiciones aerobias o anaerobias. Sin embargo, los *o*-difenoles, en condiciones aerobias, dan lugar a la inactivación suicida de la enzima y, en condiciones anaerobias, inducen la inhibición irreversible. Además, se ha demostrado que estos procesos son estereoespecíficos en cuanto a la unión de los sustratos a la enzima pero no en la rapidez de inactivación.

10. Se ha demostrado que tirosinasa es capaz de atacar a aminas aromáticas y *o*-aminofenoles, este aspecto puede ser interesante en la descontaminación de aguas residuales. Se han caracterizado cinéticamente estos compuestos como sustratos y, en concreto, las *o*-diaminas aromáticas y los *o*-aminofenoles como sustratos suicidas de la enzima.

11. A partir del estudio cinético del proceso de inactivación suicida con distintos sustratos y en especial con sustratos *o*-difenólicos sustituidos en las posiciones 3 y 6, y teniendo en cuenta la bibliografía actual sobre la estructura de tirosinasa de distintas fuentes, se ha propuesto un mecanismo estructural que explica los resultados experimentales. Además, a partir del estudio del efecto

del pH, se ha puesto de manifiesto la existencia de un segundo pKa crítico de la enzima.

Biobliografía

6. BIBLIOGRAFÍA

Aasa,R., Deinum,J., Lerch,K. y Reinhammar,B. (1978) The reaction of mercaptans with tyrosinse and hemocyanins. *Biochim. Biophys. Acta* 535, 287-298.

Abede,A., Zheng,D., Evans,J. y Sugumaran,M. (2010) Reexamination of the mechanisms of oxidative transformation for the insect cuticular sclerotizing precursor, 1,2-dehydro-N-acetyldopamine. *Insect Biochem. Mol. Biol.* 40, 650-659.

Abdel-Malek,Z., Swope,V.B., Pallas,J., Krug,K. y Nordlund,J.J. (1992) Mitogenic, melanogenic, and cAMP responses of cultured neonatal human melanocytes to commonly used mitogens. *J. Cell Physiol.* 150, 416-425.

Aberg,C.M., Chen,T., Olumide,A., Raghavan,S.R. y Payne,G.F. (2004) Enzymatic grafting of peptides from casein hydrolysates to chitosan. Potential for value-added byproducts from food-processing wastes. *J. Agric. Food Chem.* 52, 788-793.

Alique,R. y de la Plaza.J.L. (1995) Tecnologías postcosecha del champiñón cultivado, en I Jornadas técnicas del champiñón y otros hongos comestibles en Castilla La Mancha, pgs. 85-94. Motilla del Palancar, Cuenca (Pardo,J., Ed.). CIES-Consejería de Agricultura y Medio Ambiente de Castilla La Mancha/Diputación Provincial de Cuenca.

Allan,A.E., Archambault,M., Messana,E. y Gilchrest,B.A. (1995) Topically applied diacylglycerols increase pigmentation in guinea pigs skin. *J. Invest. Dermatol.* 105, 687-692.

Andersen,S.O. (2010) Insect cuticular sclerotization: a review. *Insect Biochem. Mol Biol.* 40, 166-178.

Andreescu,S., Avramescu,A., Bala,C., Magearu,V. y Marty,J.L. (2002) Detection of organophosphorus insecticides with immobilized acetylcholinesterase-comparative study of two enzyme sensors. *Anal. Bioanal. Chem.* 374, 39-45.

Anghileri,A., Lantto,R., Kruus,K., Arosio,C. y Freddi,G. (2007) Tyrosinase-catalyzed grafting of sericin peptides onto chitosan and production of protein-polysaccharide bioconjugates. *J. Biotechnol.* 127, 508-519.

Arnao,M.B., Acosta,M., del Rio,J.A., Varon,R. y Garcia-Canovas,F. (1990) A kinetic study on the suicide inactivation of peroxidase by hydrogen peroxide. *Biochim. Biophys. Acta* 1041, 43-47.

Aroca,P., García-Borrón,J.C., Solano,F. y Lozano,J.A. (1990) Regulation of mammalian melanogenesis. I: Partial purification and characterization of a dopachrome converting factor: dopachrome tautomerase. *Biochim. Biophys. Acta* 1035, 266-275.

Arslan,O., Erzengin,M., Sinan,S. y Ozensoy,O. (2004) Purification of mulberry (*Morus alba L.*) polyphenol oxidase by affinity chromatography and investigation of its kinetic and electrophoretic properties. *Food Chem.* 88, 479-484.

Asano,T. y Ashida,M. (2001) Cuticular pro-phenoloxidase of the silkworm, *Bombyx mori*. Purification and demonstration of its transport from hemolymph. *J. Biol. Chem.* 276, 11100-11112.

Ates,S., Cortenlioglu,E., Bayraktar,E. y Mehmetoglu,U. (2007) Production of L-DOPA using Cu-alginate gel immobilized tyrosinase in a batch and packed bed reactor. *Enzyme Microb. Technol.* 40, 683-687.

Autier,P., Doré,J.F., Renard,F., Luther,H., Cattaruzza,M.S., Gefeller,O. y Grivegnée,A. (1997) Melanoma and sunscreen use: need for studies representative of actual behaviours. *Melanoma Res.* Suppl 2, S115-120.

Averbeck,D. (1989) Recent advances in psoralen phototoxicity mechanism. *Photochem. Photobiol.* 50, 859-882.

Azcón-Bieto,J. y Talón,M (1993) Fisiología y Bioquímica Vegetal. McGraw-Hill- Interamericana, Madrid.

Baharav,E., Merimski,O., Shoenfeld,Y., Zigelman,R., Gilbrud,B., Yecheskel,G., Youinou,P. y Fishman,P. (1996) Tyrosinase as an autoantigen in patients with vitiligo. *Clin. Exp. Immunol.* 105, 84-88.

Baird,S., Kelly,S.M., Price,N.C., Jaenicke,E., Meesters,C., Nillius,D., Decker,H. y Nairn,J.(2007) Hemocyanin conformational changes associated with SDS-induced phenol oxidase activation. *Biochim. Biophys. Acta* 1774, 1380-1394.

Bao,K., Dai,Y., Zhu,Z.B., Tu,F.J., Zhang,W.G. y Yao,X.S. (2010) Design and synthesis of biphenyl derivatives as mushroom tyrosinase inhibitors. *Bioorg. Med. Chem.* 18, 6708-6714.

Barber,J.L., Townsend,D., Olds,D.P. y King,R.A. (1984) Dopachrome oxidoreductase: a new enzyme in the pigment pathway. *J. Invest. Dermatol.* 83, 145-149.

Bécherel,P.A., Mossalayi,M.D., Ouaaz,F., Le Goff,L., Dugas,B., Paul-Eugène,N., Frances,C., Chosidow,O., Kilchherr,E., Guillosson,J.J., Debré,P. y Arock,M. (1994) Involvement of cyclic AMP and nitric oxide in immunoglobulin E-dependent activation of Fc epsilon RII/CD23+ normal human keratinocytes. *J. Clin. Invest.* 93, 2275-2279.

Bell,A.A. y Wheeler,M.H. (1986) Biosynthesis and functions of fungal melanins. *Ann. Rev. Phytopathol.* 24, 411-451.

Beltramini,M., Bubacco,L., Salvato,B., Casella,L., Gullotti,M. y Garofani,S. (1992) The aromatic circular dichroism spectrum as a probe for conformational changes in the active site environment of hemocyanins. *Biochim. Biophys. Acta* 1120, 24-32.

Bertolotto,C., Abbe,P., Hemesath,T.J., Bille,K., Fisher,D.E., Ortonne,J.P. y Balotti,R. (1998) Microphtalmia gene product as a signal transducer in cAMP-induced differentiation of melanocytes. *J. Cell. Biol.* 142, 827-835.

Bertolotto,C., Bille,K., Ortonne,J.P. y Ballotti,R. (1996) Regulation of tyrosinase gene expression by cAMP in B16 melanoma cells involves two CATGTG motifs surrounding the TATA box: implication of the microphthalmiagene product. *Cell Sci.* 134, 747-755.

Bevilaqua,J.V., Cammarota,M.C., Freire,D.M.G. y Sant-Anna,G.L. (2002) Phenol removal through combined biological and enzymatic treatments. *Braz. J. Chem. Eng.* 19, 151-158.

Boissy,R.E. y Nordlund,J.J. (1997) Molecular basis of congenital hypopigmentary disorders in humans: a review. *Pigment Cell Res.* 10, 12-24.

Boekelheide,K., Graham,D.G., Mize,P.D. y Jeffs, P.W. (1980) The metabolic pathway catalyzed by the tyrosinase of *Agaricus bisporus*. *J. Biol. Chem*. 255, 4766-4771.

Bordell,F.G. y Hughes,D.L. (1984) S_N2 Reactions of nitranions with benzyl chlorides. *J. Am. Chem. Soc.* 106, 3234-3240.

Botchkarev,V.A., Yaar,M., Peters,E.M., Raychaudhuri,S.P., Botchkareva,N.V., Marconi,A., Raychaudhuri,S.K., Paus,R. y Pincelli,C. (2006) Neurotrophins in skin biology and pathology. *J Invest. Dermatol.* 126, 1719-1727.

Bouchilloux,S., McMahill,P. y Mason,M.S. (1963) The multiple forms of mushroom tyrosinase. Purification and molecular properties of the enzymes. *J. Biol. Chem.* 238, 1699-1707.

Bradford,M.M. (1976) A rapid and sensitive method for the quatification of microgram quatities of proteins utilizing the principle of protein-dye binding. *Anal. Biochem*. 72, 248-256.

Briganti,S., Camera,E. y Picardo,M. (2003) Chemical and instrumental approaches to treat hyperpigmentation. *Pigment Cell Res.* 16, 101-110.

Brown,D.A., Ren,W.Y., Khorlinl,A., Lesiak,K., Conkin,D., Watanabe,K.A., Seidman,M.M. y George,J. (1998) Aliphatic and alicyclic diols induce melanogenesis in cultured cells and guinea pig skin. *J. Invest. Dermatol*. 110, 428-437.

Bubacco,L., Salgado,J., Tepper,A.W., Vijgenboom,E. y Canters,G.W. (1999) ^{1}H NMR spectroscopy of the binuclear Cu(II) active site of *Streptomyces antibioticus* tyrosinase. *FEBS Lett.* 442, 215-220.

Bubacco,L., van Gastel,M., Benfatto,M., Tepper,A.W. y Canters,G.W. (2004) What are the structural features of the active site that define binuclear copper proteins function? *Micron* 35, 143-145.

Burnett,J.B. (1971) The tyrosinases of mouse melanoma. Isolation and molecular properties. *J. Biol. Chem.* 246, 3079-3091.

Burton,K.S., Love,M.E. y Smith,J.F. (1993) Biochemical changes associated with mushroom quality in *Agaricus* spp. *Enzyme Microb. Technol*. 15, 736-741.

Burton, S.G. (2003) Oxidizing enzymes as biocatalysts. *Trends Biotechnol.* 21, 543-549.

Bustamante,J., Bredeston,L., Malanga,G. y Mordoh,J. (1993) Role of melanin as a scavenger of active oxygen species. *Pigment Cell Res.* 6, 348-353.

Cabanes,J., Escribano,J., Gandía-Herrero,F., García-Carmona,F. y Jiménez-Atiénzar,M. (2007) Partial purification of lantent polyphenol oxidase from peach (*Prunus persica* L. Cv. Catherina). Molecular properties and kinetic characterization of soluble and membrane-bound forms. *J. Agric. Food Chem*. 55, 10446-10451.

Cabanes,J., García-Cánovas,F., Lozano,J.A. y García-Carmona,F. (1987a) A kinetic study of the melanization pathway between L-tyrosine and dopachrome. *Biochim. Biophys. Acta* 923, 187-195.

Cabanes,J., García-Cánovas,F., Tudela,J., Lozano,J.A. y García-Carmona,F. (1987b) L-mimosine a slow-binding inhibitor of mushroom tyrosinase. *Phytochemistry* 26, 917-919.

Cabanes,J., Chazarra,S. y Garcia-Carmona,F. (1994) Kojic acid, a cosmetic skin whitening agent, is a slow-binding inhibitor of catecholase activity of tyrosinase. *J. Pharm. Pharmacol.* 46, 982-985.

Camand,O., Marchant,D., Boutboul,S., Péquignot,M., Odent,S., Dollfus,H., Sutherland,J., Levin,A., Menasche,M., Marsac,C., Dufier,J.L., Heon,E. y Abitbol, M. (2001) Mutation analysis of the tyrosinase gene in oculocutaneous albinism. *Hum. Mutat.* 17, 352.

Campbell,P.M. y Der,C.J. (2004) Oncogenic Ras and its role in tumor cell invasion and metastasis. *Semin. Cancer Biol*. 14, 105-114.

Candille,S.I., Kaelin.C.B., Cattanach,B.M., Yu,B., Thompson,D.A., Nix,M.A., Kerns,J.A., Schmutz,S.M., Millhauser,G.L. y Barsh,G.S. (2007) A-defensin mutation causes black coat color in domestic dogs. *Science* 318, 1418-1423.

Cardinali,G., Ceccarelli,S., Kovacs,D., Aspite,N., Lotti,L.V., Torrisi,M.R. y Picardo,M. (2005) Keratinocyte growth factor promotes melanosome transfer to keratinocytes. *J. Invest. Dermatol.* 125, 1190-1199.

Carreira,S., Goodall,J., Aksan,I., La Rocca,S.A., Galibert,M.D., Denat.,L., Larue,L. y Goding,C.R. (2005) Mitf cooperates with Rbl and activates p21Cipl expression to regulate cell cycle progression. *Natur*e 433,764-769.

Carvalho,G.M., Alves,T.L. y Freire,D.M. (2000) L-DOPA production by immobilized tyrosinase, *Appl. Biochem. Biotechnol.* 84, 791-800.

Casañola-Martín,G.M., Marrero-Ponce,Y., Tareq-Hassan-Khan,M., Torrens,F., Pérez-Gimenez,F. y Rescigno,A. (2008) Atom-and bond-based 2D TOMOCOMD-CARDD approach and ligand-based virtual screening for the drug discovery of new tyrosinase inhibitors. *J. Biomol. Screen.* 13, 1014-1024.

Casañola-Martín,G.M., Marrero-Ponce,Y., Khan,M.T., Khan,S.B., Torrens,F., Perez-Jiménez,F., Rescigno,A. y Abad,C. (2010) Bond-based 2D quadratic fingerprints in QSAR studies: virtual and in vitro tyrosinase inhibitory activity elucidation. *Chem. Biol. Drug Des.* 76, 538-545.

Casella,L., Monzani,E., Gullotti,M., Cavagino,D., Cerina,G., Santagostini,L. y Ugo,R. (1996) Functional Modeling of Tyrosinase. Mechanism of Phenol *ortho*-Hydroxylation by Dinuclear Copper Complexes *Inorg. Chem.* 35, 7516-7525.

Chakraborty,A.K., Mishima,Y., Inazu,M., Hatta,S. y Ichiashi,M. (1989) Melanogenic regulatory factors in coated vesicles from melanoma cells. *J. Invest. Dermatol.* 93, 616-620.

Chang,T.S. (2007) Two potent suicide substrates of mushroom tyrosinase: 7,8,4´-trihydroxyisoflavone and 5,7,8,4´-tetrahydroxyisoflavone. *J. Agric. Food Chem.* 55, 2010-2015.

Chang,T.S. (2009) An update review of Tyrosinase Inhibitors. *Int. J. Mol. Sci.* 10, 2440-2475.

Chang,T.S., Ding,H.Y.y Lin,H.C. (2005) Identifying 6,7,4´-trihydroxyisoflavone as a potent tyrosinase inhibitor. *Biosci. Biotechnol. Biochem.* 69, 1999-2001.

Chang,T.S., Lin,M.Y. y Lin,H.C. (2010) Identifying 8-hydroxynaringenin as a suicide substrate of musroom tyrosinase. *J. Cosmet. Sci.* 61, 205-210.

Chang,T.S. y Wu,C.Y. (2008) Suicide substrate of tyrosinase and use thereof Patente N. US2008/0317692 A1.

Chazarra,S., García-Carmona,F. y Cabanes,J. (2001) Hysteresis and positive cooperativity of iceberg lettuce polyphenol oxidase. *Biochem. Biophys. Res. Commun.* 289, 769-775.

Chen,J.S., Wei,C. y Marshall,M.R. (1991) Inhibition mechanism of kojic acid on polyphenol oxidase. *J. Agric. Food. Chem.* 39, 1897-1901.

Chen,L.Y., Chen,M.Y., Leu,W.M., Tsai,T.Y. y Lee,Y.H. (1993) Mutational study of Streptomyces tyrosinase trans-activator MelC1. MelC1 is likely a chaperone for apotyrosinase. *J. Biol. Chem.* 268, 18710-18716.

Chen,P. y Solomon,E.I. (2004) O_2 activation by binuclear Cu sites: noncoupled versus exchange coupled reaction mechanisms. *Proc. Natl. Acad. Sci. USA* 101, 13105-13110.

Chen,T., Embree,H.D., Wu,L.Q. y Payne,G.F. (2002) In vitro protein-polysaccharide conjugation: tyrosinase-catalyzed conjugation of gelatine and chitosan. *Biopolymers* 64, 292-302.

Claus,H. y Decker,H. (2006) Bacterial tyrosinases. *Syst. Appl. Microbiol*. 29, 3-14.

Conrad,J.S., Dawso,S.R., Hubbard,E.R., Meyers,T.E. y Strothkamp,K.G. (1994) Inhibitor binding to the binuclear active site of tyrosinase: temperature, pH, and solvent deuterium isotope effects. *Biochemistry* 33, 5739-5744.

Dahl,C. y Guldberg,P. (2007) The genome and epigenome of malignant melanoma. *APMIS* 115, 1161-1176.

Dawson,C.R. y Tarpley,W.B. (1963) On the pathway of the catecholtyrosinase reaction. *Ann. N. Y. Acad. Sci.* 100¸937-950.

Decareau,R.V. (1985) *Microwaves in the Food Procesing Industry*. Academic Press: London.

Decker,H., Ryan,M., Jaenicke,E. y Terwiliiger,N. (2001) SDS-induced phenoloxidase activity of hemocyanins from *Limulus polyphemus*, *Eurypelma californicum* and Cancer magister. *J. Biol.Chem.* 276, 17796-17799.

Decker,H., Schwelkardt,T., Nillius,D., Salzbrunn,U., Jaenicke,E. y Tuczek,F. (2007) Similar enzyme activation and catalysis in hemocyanins and tyrosinases. *Gene* 398, 183-191.

Decker,H., Schweikardt,T. y Tuczek,F. (2006) The first crystal structure of tyrosinase: all questions answered? *Angew. Chem. Int. Ed. Engl.* 45, 4546-4550.

Decker,H. y Jaenicke,E. (2004) Recent findings on phenoloxidase activity and antimicrobial activity of hemocyanis. *Dev. Comp. Immunol.* 28, 673-687.

Decker,H. y Tuczek,F. (2000) Tyrosinase/catecholoxidase activity of hemocyanins: structural basis and molecular mechanism. *Trends Biochem Sci.* 25,392-397.

Deeth,J.D. y Diecrich,C. (2010) Structural and mechanistic insights into the oxy form of tyrosinase from molecular dynamics simulations. *J. Biol. Inorg. Chem.* 15, 117-129.

del Marmol,V. y Beerman,F. (1996) Tyrosinase and related proteins in mammalian pigmentation. *FEBS Lett*. 381, 161-168.

Della Longa,S., Ascone,I., Bianconi,A., Bonfigli,A., Castellano,A.C., Zaviri,O. y Miranda,M. (1996) The dinuclear copper site structure of *Agaricus bisporus* tyrosinase in solution probed by X-ray absorption spectroscopy. *J. Biol. Chem.* 271, 21025-21030.

Dessinioti,C., Stratigos,A.J., Rigopoulos,D. y Katsambas,A.D. (2009) A review of genetic disorders of hypopigmentation: lessons learned from the biology of melanociytes. *Exp. Dermatol.* 18, 741-749.

Devi,C.C., Tripathi,R.K. y Ramaiah,A. (1987) pH-dependent interconvertible allosteric forms of murine melanoma tyrosinase. Physiological implications. *Eur. J. Biochem.* 166, 705-711.

Dietler,C. y Lerch,K. (1982) Oxidases and related redox systems (King, T.E., Mason, H.S. y Morrison,M., Eds), Pergamon Press, New York. pp. 305-317.

Draper,N.R. y Smith,H. (1981) *Applied Regression Analysis.* Wiley, New York.

Du,J., Widlund,H.R., Horstmann,M.A., Ramaswamy,S., Ross,K., Huber,W.E., Nishimura,E.K., Golub,T.R. y Fisher,D.E. (2004) Critical role of CDK2 for melanoma growth linked to its melanocytespecific transcriptional regulation by MITF. *Cancer Cell* 6, 565-576.

Du,J.Y., Miller,A.J., Widlund,H.R., Horstmann,M.A., Ramaswamy,S. y Fischer,D.E. (2003) MLANA/ MART1 and SILV/PMEL17/GP100 are transcriptionally regulated by MITF in melanocytes and melanoma. *Am. J. Pathol.* 163, 333-343.

Dubois.C., Haudecoeur,R., Orio,M., Belle,C., Bochot,C., Boumendjel,A., Hardré,R., Jamet,H. y Réglier,M. (2012) Versatile effects of aurone structure on mushroom tyrosinase activity. *ChemBioChem* 13, 559-565.

Duckworth,H.W. y Coleman,J.E. (1970) Physicochemical and kinetic properties of mushroom tyrosinase. *J. Biol. Chem.* 245, 1613-1625.

Dudley,E.D. y Hotchkiss,J.H. (1989) Cysteine as an inhibitor of polyphenol oxidase. *J. Food Biochem.* 13, 65-75.

Durán,N. y Espósito,E. (2000) Potential applications of oxidative enzymes and phenoloxidase-like compounds in *wastewater* and soil treatment: a review. *Appl. Catal. B-Environ*. 28, 83-99.

Eicken,C., Krebs,B. y Sacchettini,J.C. (1999) Catechol oxidase-structure and activity. *Curr. Opin. Struct. Biol*. 9, 677-683.

Eller,M.S., Yaar,M. y Gilchrest,B.A. (1994) DNA damage and melanogenesis. *Nature* 372, 413-414.

Endrenyi,L. (Ed.) (1981) *Kinetic Data Analysis: Design and Analysis of Enzyme and Pharmacokinetics Experiments.* Plenum Press, New York.

Erker,W., Hübler,R y Decker,H. (2008) Tryptophan quenching as linear sensor for oxygen binding of arthropod hemocyanins. *Biochim. Biophys. Acta* 1780, 1143-1147.

Escribano,J., Tudela,J., Garcia-Carmona,F. y García-Cánovas,F. (1989) A kinetic study of the suicide inactivation of an enzyme measured through coupling reactions. Application to the suicide inactivation of tyrosinase. *Biochem. J.* 262, 597-603.

Espín,J.C., Morales,M., Varón,R., Tudela,J. y García-Cánovas,F. (1995) A continuous spectrophotometric method for determining the monophenolase and diphenolase activities of apple polyphenol oxidase. *Anal. Biochem.* 231, 237-246.

Espín,J.C., Morales,M., Varón,R., Tudela,J. y García-Cánovas,F. (1996) Continuous spectrophotometric method for determining the monophenolase and diphenolase activities of pear polyphenoloxidase. *J. Food. Sci.* 61, 1177-1182.

Espín,J.C., Varón,R., Tudela,J. y García-Cánovas,F. (1997) Kinetic study of the oxidation of 4-hydroxyanisole catalyzed by tyrosinase. *Biochem. Mol. Biol. Int*. 41, 1265-1276.

Espín,J.C., García-Ruiz,P.A., Tudela,J. y García-Cánovas, F. (1998a) Study of stereospecifity in pear and strawberry polyphenol oxidases. *J. Agric. Food Chem.* 46, 2469-2473.

Espín,J.C., García-Ruiz,P.A.,Tudela,J. y García-Cánovas,F. (1998b) Study of stereospecifity in mushroom tyrosinase. *Biochem. J.* 331, 547-551.

Espin,J.C. y Wichers,H.J. (1999a) Kinetics of activation of latent mushroom (*Agaricus bisporus)* tyrosinase by benzyl alcohol. *J. Agric. Food Chem.* 47, 3503-3508.

Espín,J.C. y Wichers,H.J. (1999b) Slow-binding inhibition of mushroom (*Agaricus bisporus*) tyrosinase isoforms by tropolone. *J. Agric. Food Chem.* 47, 2638-2644.

Espín,J.C. y Wichers,H.J. (2001) Effect of captopril on mushroom tyrosinase activity in vitro. *Biochim. Biophys. Acta* 1544, 289-300.

Espín,J.C., Veltman,R.H. y Wichers, H.J. (2000a) The oxidation of L-ascorbic acid catalysed by pear tyrosinase. *Physiol. Plant.* 109,1-6.

Espín,J.C., Varón,R., Fenoll,L.G., Gilabert,M.A., García-Ruiz,P.A., Tudela,J. y García-Cánovas,F. (2000b) Kinetic characterization of the substrate specificity and mechanism of mushromm tyrosinase. *Eur. J. Biochem.* 267, 1270-1279.

Fairhead,M., y Thony-Meyer,L. (2010) Role of the C-terminal extension in a bacterial tyrosinase. *FEBS J.* 277, 2083-2095.

Farihead,M. y Thony-Meyer,L. (2012) Bacterial tyrosinases: old enzymes with new relevance to biotechnology. *N. Biotechnol.* 29, 183-191.

Fan,Y. y Flurkey,W.H. (2004) Purification and characterization of tyrosinase from gill tissue of Portabella mushrooms. *Phytochemistry* 65, 671-678.

Fang,S., Jensen,J.P., Ludwing,R.L., Voudsen,K.H. y Weissman,A.M. (2000) MDM2 is a RING finger-dependent ubiquitin protein ligase for itself and p53. *J. Biol.Chem.* 275, 8945-8951.

Farnun,D.G. (1975) Charge density-NMR chemical shift correlations in organic Ions En: *Advances in Physical Organic Chemistry,* pp. 123-173.

Fecker,L.F., Eberle,J., Orfanos,C.E. y Geilen,C.C. (2002) Inducible nitric oxide synthase is expressed in normal human melanocytes but not in melanoma cells in response to tumor necrosis factor-alpha, interferon-gamma, and lipopolysaccharide. *J. Invest. Dermatol.* 118, 1019-1025.

Fenoll,L.G., Peñalver,M.J., Rodríguez-López,J.N., García-Ruiz,P.A., García-Cánovas,F y Tudela,J. (2004) Deuterium isotope effect an the oxidation of monophenols and *o*-diphenols by tyrosinase.*Biochem. J.* 380, 643-650.

Fenoll,L.G., Rodriguez-Lopez,J.N., García-Sevilla,F., García-Ruiz.,P.A., Varón,R., García-Cánovas,F. y Tudela,J. (2001) Analysis and interpretation of the action mechanism of mushroom tyrosinase on monophenols and diphenols generating highly instable o-quinones. *Biochim. Biophys. Acta* 1548, 1-22.

Ferrini,U., Mileo,A.M. y Hearing,V.J. (1987) Microheterogeneity of melanosome-bound tyrosinase from the Harding-Passey murine melanoma. *Int. J. Biochem.* 19, 227-234.

Fistarol,S.K. e Itin,P.H. (2010) Disorders of pigmentation. *J Dtsch. Dermatol. Ges.* 8, 187-201.

Frankos,V.H., Schmidtt,D.F., Haws,L.C. McEvely,A.J., Iyengar,R. y Miller, S.A. (1991) Generally recognised as safe (GRAS) evaluation of 4-hexylresorcinal for use for processing aid for prevention of melanosis in shrimp. *Regul. Toxicol. Pharmacol.* 14, 202-212.

Fu,B., Li,H., Wang,X., Lee,F.S. y Cui,S. (2005) Isolation and identification of flavonoids in licorice and a study of their inhibitory effects on tyrosinase. *J. Agric. Food Chem.* 53, 7408-7414.

Fujieda,N., Murata,M., Yabuta,S., Ikeda,T., Shimokawa,C., Nakamura,Y., Hata,Y. e Itoh,S. (2012) Multifunctions of MelB, a fungal tyrosinase from *Aspergillus oryzae*. *ChemBioChem* 13, 193-201.

Fujimoto,K., Okino,N., Kawabata,S., Iwanaga,S. y Ohnishi,E. (1995) Nucleotide-sequence of the cDNA-encoding the proenzyme of phenol oxidase A (1) of *Drosophila melanogaster*. *Proc. Natl. Acad. Sci. USA* 92, 7769-7773.

Fuller,B.B., Niekrasz,I. y Hoganson,G.E. (1990) Down regulation of tyrosinase mRNA levels in melanoma cells by tumor promoters and by insulin. *Mol. Cell Endocrinol.* 72, 81-87.

Funasaka,Y., Chakraborty,A.K., Hayashi,Y., Komoto,M., Ohashi,A., Nagahama,M., Inoue,Y., Pawelek,J. y Ichihashi,M. (1998) Modulation of melanocyte-stimulating hormone receptor expression on normal human melanocytes: evidence for a regulatory role of ultraviolet B, interleukin-1alpha, interleukin-1beta, endothelin-1 and tumour necrosis factor-alpha. *Br. J. Dermatol.* 139, 216-224.

Fusaro,R.M. y Johnson,J.A. (1975) Protection against long ultraviolet and/or visible light with topical dihydroxyacetone. Implications for the mechanism of action of the sunscreen combination, dihydroxyacetone/naphtoquinone. *Dermatologica* 150, 346-351.

Fusaro,R.M. y Lynch,H.T. (2000) The FAMMM syndrome: epidemiology and surveillance strategies, *Cancer Invest.* 18, 670-680.

Fuse,N., Yasumoto,K., Suzuki,H., Takahashi,K. y Shibahara,S. (1996) Identification of a melanocyte-type promoter of the microphtalmia-associated transcription factor gene. *Biochem. Biophys. Res. Commun.* 219, 702-707.

Galindo,J.D., Pedreño,E., García-Carmona,F., García-Cánovas,F., Solano-Muñoz,F. y Lozano,J.A. (1983) Steady-state study of the mechanism of dopa-oxidase activity of tyrosinase. *Int. J. Biochem.* 15, 1455-1461.

Gálvez,J. y Varón,R. (1981) Transient phase kinetics of enzyme reactions*. J. Theor. Biol*. 89, 1-17.

Gandia-Herrero,F., Escribano,J. y Garcia-Carmona,F. (2005) Characterization of the monophenolase activity of tyrosinase on betaxhantins: the tyramine-betaxanthin/dopamine-betaxanthin pair. *Planta* 222, 307-316.

Gandia-Herrero,F., García-Carmona,F. y Escribano,J. (2004) Purification and characterization of a latent polyphenol oxidase from beet root (*Beta vulgaris* L.). *J. Agric. Food Chem.* 52, 609-615.

Gantz,I., Munzert,G., Tashiro,T., Schäffer,M., Wang,L., DelValle,J. y Yamada,T. (1991) Molecular cloning of the human histamine H_2 receptor. *Biochem. Biophys. Res. Commun*. 178, 1386-1392.

García-Borron,J.C. y Solano,F. (2002) Molecular anatomy of tyrosinase and its related proteins: beyond the histidine-bound metal catalytic center. *Pigment Cell Res.* 15, 162-173.

Garcia-Canovas,F., Garcia-Carmona,F., Vera-Sanchez,J., Iborra,J.L. y Lozano,J.A. (1982) The role pf pH in the melanin biosynthesis pathway. *J. Biol. Chem.* 257, 8738-8744.

Garcia-Cánovas,F., Tudela,J., Martinez-Madrid,C., Varon,R., García-Carmona,F. y Lozano,J.A. (1987) Kinetic study on the suicide inactivation of tyrosinase induced by catechol. *Biochim. Biophys. Acta.* 912, 417-423.

García-Cánovas,F., Tudela,J., Varón,R. y Vazquez,A.M. (1989) Experimental methods for kinetic study of suicide substrates.*J. Enzyme Inhib.* 3, 81-90.

García-Carmona,F., García-Cánovas,F., Iborra,J.L. y Lozano,J.A. (1982) Kinetic study of the pathway of melanization between L-dopa and dopachrome. *Biochim. Biophys. Acta.* 717, 124-131.

Garcia-Molina,F., Hiner,A.N.P., Fenoll,L.G., Rodríguez-López,J.N., García-Ruiz,P.A., García-Cánovas,F. y Tudela,J. (2005) Mushroom tyrosinase: Catalase activity, inhibition, and suicide inactivation, *J. Agric. Food Chem.* 53, 3702-3709.

Garcia-Molina,F., Muñoz,J.L., Varón,R., Rodriguez-Lopez,J.N., García-Cánovas,F. y Tudela,J. (2007a) A review on spectrophotometric methods for measuring the monophenolase and diphenolase activities of tyrosinase. *J. Agric. Food Chem.* 55, 9739-9749.

García-Molina.F., Muñoz,J.L., Varón,R., Rodríguez-López,J.N., García-Cánovas,F. y Tudela,J. (2007b) Effect of tetrahydropteridines on the monophenolase and diphenolase activities of tyrosinase. *J. Enzyme Inhib. Med. Chem*. 22, 383-94.

García-Molina,F., Muñoz-Muñoz,J.L., Acosta,J.R., Garcia-Ruiz,P.A., Tudela,J., García-Cánovas,F. y Rodríguez-López, J.N. (2009) Melanogenesis inhibition by tetrahydropterines. *Biochim. Biophys. Acta* 1794, 1766-1774.

García-Molina,F., Muñoz-Muñoz,J.L., Martinez-Ortiz,F., Tudela,J., García-Cánovas,F. y Rodríguez-López,J.N. (2010a) Effects of tetrahydropterines on the generation of quinones catalyzed by tyrosinase. *Biosci. Biotechnol. Biochem.* 74, 1108-1109.

Garcia-Molina,F., Muñoz-Muñoz,J.L., García-Molina,M., García-Ruiz,P.A., Tudela,J., García-Cánovas,F. y Rodríguez-López,J.N. (2010b) Melanogenesis inhibition due to NADH. *Biosci. Biotechnol. Biochem*. 74, 1777-1787.

García-Molina,F., Muñoz-Muñoz,J.L., Martinez-Ortiz,F., García-Ruiz.,P.A., Tudela,J., García-Cánovas,F. y Rodríguez-López,J.N. (2011) Tetrahydrofolic acid is a potent suicide substrate of mushroom tyrosinase. *J. Agric. Food Chem.* 59, 1383-1391.

Garcia-Ruiz,P.A., García-Cánovas,F. y Marín Zamora,M.E. (2008) Procedimiento de obtención de *o*-difenoles. Patente número 2301453.

Garcia-Sevilla,F., Garrido-del Solo,C., Duggleby,R.G., Garcia-Cánovas,F., Peyro,R. y Varon,R. (2000) Use of a windows program for simulation of the progress curves of reactants and intermediates involved in enzyme-catalyzed reactions. *BioSystems* 54, 151-164.

Gasowska,B., Kafarski,P. y Wojtasek,H. (2004) Interaction of mushroom tyrosinase with aromatic amines, *o*-diamines and *o*-aminophenols. *Biochim. Biophys. Acta* 1673, 170-177.

Gates,R.R. y Zimmermann,A.A. (1953) Comparison of skin color with melanin content. *J. Invest. Dermatol.* 21, 339-348.

Gerald,C.F. y Wheatley, P.O. (1989) *Applied numerical analysis. Fourth edition.* Addison Wesley P. C., New York.

Gerdemann,C., Eicken,C. y Krebs,B. (2002) The crystal structure of catechol oxidase: new insight into the function of type-3 copper proteins. *Acc. Chem. Res.* 35, 183-191.

Gerritsen,Y.A.M., Chapelon,C.G.J. y Wichers,H.J. (1994) The low-isoelectric point tyrosinase of *Agaricus bisporus* may be a glycoprotein. *Phytochemistry* 35, 573-577.

Ghanbari,F., Rowland-Yeo,K., Bloomer,J.C., Clarke,S.E., Lennard,M.S., Tucker,G.T. y Rostami-Hodjegan,A. (2006) A critical evaluation of the experimental design of studies of mechanism based enzyme inhibition, with implications for in vitro-in vivo extrapolation. *Curr. Drug Metab.* 7, 315-334.

Gheibi,N., Saboury,A.A. y Haghbeen,K. (2006) Substrate construes the copper and nickel ions impacts on the mushroom tyrosinase activities. *Bull. Korean Chem. Soc.* 27, 642-648.

Gheibi,N., Saboury,A.A. y Sarreshtehdari,M. (2011) Non-esential activation of Co(2+) and Zn(2+) on mushroom tyrosinase: kinetic and structural stability. *Bull. Korean Chem. Soc.* 32, 1500-1506.

Giebel,L.B., Tripathi,R.K., Strunk,K.M., Hanifin,J.M., Jackson,C.E., King,R.A. y Spritz,R.A. (1991) Tyrosinase gene mutations associated with type IB ("yellow") oculocutaneous albinism. *Am. J. Hum. Genet.* 48, 1159-1167.

Giehl,K. (2005) Oncogenic Ras in tumor progression and metastasis. *Biol. Chem.* 386, 193-205.

Gillbro,J.M., Marles,L.K., Hibberts,N.A. y Schallreuter,K.U. (2004) Autocrine catecholamine biosynthesis and the beta-adrenoceptor signal promote pigmentation in human epidermal melanocytes. *J. Invest. Dermatol.* 123, 346-353.

Gillbro,J.M. y Olsson,M.J. (2011) The melanogenesis and mechanisms of skin-lightening agents-existing and new approaches. *Int. J. Cosmet. Sci*. 33, 210-221.

Goding,C.R. (2000) Mitf from neural crest to melanoma: signal transduction and transcription in the melanocyte lineage. *Genes Dev.* 14, 1712-1728.

Gómez-López,V.M. (2002) Some biochemical properties of polyphenol oxidase from two varieties of avocado. *Food Chem.* 77, 163-169.

Goulart,P.D.P., Alves,J.D., Magalhaes,M.M., Lima,L.C.D. y Meyer,L.E. (2003) Purification of polyphenoloxidase from coffee fruits. *Food Chem.* 83, 7-11.

Graham,D.G. y Jeffs,P.W. (1977) The role of 2,4,5-trihydroxyphenylalanine in melanin biosynthesis. *J. Biol. Chem.* 252, 5729-5734.

Grando,S.A., Pittelkow,M.R. y Schallreuter,K.U. (2006) Adrenergic and cholinergic control in the biology of epidermis: physiological and clinical significance. *J. Invest. Dermatol*. 126, 1948-1965.

Gray-Schopfer,V., Wellbrock,C. y Marais,R. (2007) Melanoma biology and new targeted therapy. *Nature* 22, 851-857.

Greco,G., Wakamatsu,K., Panzella,L., Ito,S., Napolitano,A. y d´Ischia,M. (2009) Isomeric cysteinildopas provide a (photo) degradable bulk componen and a robust structural element in red human hair pheomelanin. *Pigment Cell Melanoma Res.* 22, 319-327.

Griffith,O.W. (1982) Mechanism of action, metabolism, and toxicity of buthionine sulfoximine and its higher homologs, potent inhibitors of glutathione synthesis. *J. Biol. Chem.* 257, 13704-13712.

Griffith,O.W. y Meister,A. (1979) Potent and specific inhibition of glutathione synthesis by buthione sulfoximine (S-n-butyl homocysteine solfoximine). *J. Biol. Chem.* 254, 7558-7560.

Guazzaroni,M., Pasqualini,M., Botta,G. Y Saladino,R. (2012a) A novel synthesis of bioactive catechols by layer-by-layer immbolized tyrosinase in an organic solvent medium. *ChemCatChem* 4, 89-99.

Guazzaroni,M., Crestini,C. y Saladino,R. (2012b) Layer-by-layer coated tyrosinase: An efficient and selective synthesis of catechols. *Bioorg. Med. Chem.* 20, 157-166.

Günther,H. (1980) Nuclear magnetic resonance of fluorine-19 and carbon-13 En: *NMR Spectroscopy*, pp. 364-374.

Gutteridge,S. y Robb,D. (1975) The catecholase activity of Neurospora tyrosinase. *Eur. J. Biochem.* 54, 107-116.

Ha,M.H., Park,Y.J., Lee,J.Y., Park,D., Choi,Y.J., Lee,E.K., Kim,J.M., Kim,J.A., Park,J.Y., Lee,H.J., Moon,H.R. y Chung,H.Y. (2012a) Design, synthesis and biological evaluation of 2-(substituted phenyl)thiazolidine-4-carboxylic acid derivatives as novel tyrosinase inhibitors. *Biochimie* 94, 533-540.

Ha,M.H., Park,Y.J., Kim,J.A., Park,D., Park,J.Y., Lee,H.J., Lee,J.Y., Moon,H.R. y Chung,H.Y. (2012b) Design and synthesis of 5-(substituted benzylidene)thiazolidine-2,4-dione derivatives as novel tyrosinase inhibitors. *Eur. J. Med. Chem.* 49, 245-252.

Ha,T., Naysmith,L., Waterston,K., Oh,C., Weller,R. y Rees,J.L. (2003) Defining the quantitative contribution of the malanocortin 1 receptor (MC1R) to variation in pigmentary phenotype. *Ann. N. Y. Acad. Sci.* 994, 339-347.

Halaban,R., Langdon,R., Birchall,N., Cuono,C., Baird,A., Scott,G., Moellmann,G. y McGuire,J. (1988) Basic fibroblast growth factor from human keratinocytes is a natural mitogen for melanocytes. *J. Cell Biol.* 107, 1611-1619.

Halaban,R., Ghosh,S. y Baird,A. (1987) bFGF is the putative natural growth factor for human melanocytes. *In Vitro Cell Dev. Biol.* 23, 47-52.

Halaouli,S., Asther,M., Kruus,K., Guo,L., Hamdi,M., Sigoillot,J.C., Asther,M. y Lomascolo,A. (2005) Characterization of a new tyrosinase from *Pycnoporus* species with high potential for food technological applications. *J. Appl. Microbiol.* 98, 332-343.

Halaouli,S., Asther,M., Sigoillot,J.C., Hamdi,M. y Lomascolo,A. (2006) Fungal tyrosinases: new prospects in molecular characteristics, bioengineering and biotechnological applications. *J. Appl. Microbiol.* 100, 219-232.

Hall,M., Scott,T., Sugumaran,M., Söderhäll,K. y Law,J.H. (1995) Proenzyme of *Manduca sexta* phenol oxidase: purification, activation, substrate specificity of the active enzyme, and molecular cloning.*Proc. Natl. Acad. Sci. USA* 92, 7764-7768.

Hara,M., Yaar,M. y Gilchrest,B.A. (1995) Endothelin-1 of keratinocyte origin is a mediator of melanocyte dendricity. *J. Invest. Dermatol.* 105, 744-748.

Harbone,J.B. y Williams,C.A. (2000) Advances in flavonoid research since 1992. Phytochemistry 55, 481-504.

Hayaishi,O. (1962) Oxygenases. Academic Press. New York.

Hayaishi,O. (1974) Molecular mechanism of oxygen activation. Academic Press, New York.

Hearing,V.J. (1999) Biochemical control of melanogenesis and melanosomal organization. *J. Investig. Dermatol. Symp. Proc.* 4, 24-48.

Hearing,V.J. (2005) Biogenesis of pigment granules: a sensitive way to regulate melanocyte function. *J. Dermatol. Sci.* 37, 3-14.

Hearing,V.J., Ekel,T.M. y Montague,P.M. (1981) Mammalian tyrosinase: isozymic forms of the enzyme. *Int. J. Biochem.* 13, 99-103.

Hearing,V.J. y Ekel,T.M. (1976) Mammalian tyrosinase. A comparison of tyrosine hydroxylation and melanin formation. *Biochem. J.* 157, 549-557.

Hearing,V.J. y Jiménez,M. (1987) Mammalian tyrosinase-the critical regulatory control point in melanocyte pigmentation. *Int. J. Biochem.* 19, 1141-1147.

Hearing,V.J. y Tsukamoto,K. (1991) Enzymatic control of pigmentation in mammals. *FASEB J.* 5, 2902-2909.

Heck,D.E., Laskin,D.L., Gardner,C.R. y Laskin,J.D. (1992) Epidermal growth factor suppresses nitric oxide and hydrogen peroxide production by keratinocytes. Potential role for nitric oxide in the regulation of wound healing. *J. Biol. Chem.* 267, 21277-21280.

Heinrich,M.C., Rubin,B.P., Longley,B.J. y Fletcher,J.A. (2002) Biology and genetic aspects of gastrointestinal stromal tumors: KIT activation and cytogenetic alterations. *Hum. Pathol.* 33, 484-495.

Hemesath,T.J., Price,E.R., Takemoto,C., Badalian,T. y Fisher,D.E. (1998) MAP kinase links the transcription factor Microphtalmia to c-Kit signalling in melanocytes. *Nature* 391, 298-301.

Herráiz,C., Sánchez-Laorden,B.L., Jiménez-Cervantes,C. y García-Borrón,J.C. (2011a) N-glycosylation of the human melanocortin 1 receptor: occupancy of glycosylation sequons and functional role. *Pigment. Cell Melanoma Res.* 24, 479-489.

Herráiz,C., Journé,F., Abdel-Malek,Z., Ghanem,G, Jiménez-Cervantes,C. y García-Borrón,J.C. (2011b) Signaling from the human melanocortin 1 receptor to ERK1 and ERK2 mitogen-activated proteín kinases involves transactivation of cKIT. *Mol. Endocrinol.* 25, 138-156.

Hernández-Romero,D., Sanchez-Amat,A. y Solano,F. (2006) A tyrosinase with an abnormally high tyrosine hydroxylase/dopa oxidase ratio. *FEBS J.* 273, 257-270.

Hida,T, Wakamatsu,K, Sviderskaya,E.V., Donkin,A.J., Montoliu,L., Lamoreux,M., Yu,B., Millhauser,G.L., Ito,S., Barsh,G.S., Jimbow,K. y Bennett,D.C. (2009) Agouti protein, mahogunin, and attractin in pheomelanogenesis and melanoblast-like alteration of melanocytes: a cAMP-independent pathway. *Pigment Cell Melanoma Res.* 22, 623-634.

Hiner,A.N., Hernandez-Ruiz,J., Arnao,M.B., Garcia-Canovas,F. y Acosta,M. (1996) A comparative study of the purity, enzyme activity, and inactivation by hydrogen peroxide of commercially available horseradish peroxidase isoenzymes A and C. *Biotechnol. Bioeng.* 50, 655-662.

Hirota,S., Kawahara,T., Lonardi,E., de Waal,E., Funasaki,N. y Canters,G.W. (2005) Oxygen binding to tyrosinase *streptomyces antibioticus* studied by laser flash photolysis. *J. Am. Chem. Soc.* 127, 17966-17967.

Hirsch,J.A. (1972) Concepts en: *Theoretical Organic Chemistry*, Vol. 11, Allyn and Bacon Inc. Boston. pp. 184-189.

Ho,P.Y., Chiou,M.S. y Chao,A.C. (2003) Production of L-DOPA by tyrosinase immobilized on modified polystyrene. *Appl. Biochem. Biotechnol.* 111, 139-152.

Hoek,K.S., Eichoff,O.M., Schlegel,N.C., Döbbeling,U., Kobert,N., Schaerer,L., Hemmi,S. y Dummer,R. (2008) In vivo switching of human melanoma cells between proliferative and invasive states. *Cancer Res*. 68, 650-656.

Hoganson,G.E., Ledwitz-Rigby,F., Davidson,R.L. y Fuller,B.B. (1989) Regulation of tyrosinase mRNA levels in mouse melanoma cell clones by melanocyte-stimulating hormone and cylic AMP. *Somat. Cell Mol. Genet.* 15, 255-263.

Hohn,A., Leibrock,J., Bailey,K. y Barde,Y.A. (1990) Identification and characterization of a novel member of the nerve growth factor/brain-derived neurotrophic factor familiy. *Nature* 344, 339-341.

Holm,R.H., Kennepohl,P. y Solomon,E.I. (1996) Structural and functional aspects of metal sites in Biology. *Chem. Rev.* 96, 2239-2314.

Hughes,A.E., Newton,V.E., Liu,X.Z. y Read,A.P. (1994) A gene for Waardenburg syndrome type 2 maps close to the human homologue of the microphtalmia gene at chromosome 3p12-pI4.I. *Nat. Genet*. 7, 509-512.

Hurrell,R.F., Finot,P.A. y Cuq,J.L. (1982) Protein-polyphenol reactions.1. Nutritional and metabolic consequences of the reaction between oxidized caffeic acid and the lysine residues of casein. *Br. J. Nutr.* 47, 191-211.

Imokawa,G., Yada,Y. y Miyagishi,M. (1992) Endothelins secreted from human keratinocytes are intrisic mitogens for human melanocytes. *J. Biol. Chem.* 267, 24675-24680.

Ingraham,L.L., Corse,J. y Makower,B. (1952) Enzymatic browning of fruits. III. Kinetics of the reaction inactivation of polyphenoloxidase. *J. Am. Chem. Soc*. 74, 2623-2626.

Inlow,J.K. (2012) Homology models of four Agaricus bisporus tyrosinases. *Int. J. Biol. Macromol.* 50, 283-293.

Inoue,T., Shiota,Y. y Yoshizawa,K. (2008) Quantum chemical approach to the mechanism for the biological conversion of tyrosine to dopaquinone. *J. Am. Chem. Soc.* 130, 16890-16897.

Ishida,H., Matsumura,K., Hata,Y., Kawato,A., Suginami,K., Abe,Y., Imayasu,S. e Ichishima,E. (2001) Establishment of a hyper-protein production system in submerged *Aspergillus oryzae* culture under tyrosinase-encoding gene (meIO) promoter control. *Appl. Microbiol. Biotecnol.* 57, 131-137.

Ismaya,W., Rozeboom,H.J., Wejin,A., Mes,J.J., Fusetti,F., Wichers,H.J. y Dijkstra,B.W. (2011a) Crystal structure of *Agaricus bisporus* mushroom tyrosinase: identity of the tetramer subunits and interaction with tropolone. Biochemistry 50, 5477-5486.

Ismaya,W.T., Rozeboom,H.J., Schrink,M., Boering,C.G., Wichers,H.J. y Dijkstra,B.W. (2011b) Crystallization and preliminary X-ray crystallographic analysis of tyrosinase from the mushroom Agaricus bisporus. *Acta Crystallogra. Sect. F Struct. Biol. Cryst. Commun.* 67, 575-578.

Ito,S. y Wakamatsu,K. (2008) Chemistry of mixed melanogénesis-pivotal roles of dopaquinone. *Photochem. Photobiol.* 84, 582-592.

Jackman,M.P., Huber,M., Hajnal,A. y Lerch,K. (1992) Stabilization of the oxy form of tyrosinase by a single conservative amino acid substitution. *Biochem. J.* 282, 915-918.

Jackson,I.J. (1994) Evolution and expression of tyrosinase-related proteins. *Pigment Cell Res.*7, 241-242.

Jaenicke,E. y Decker,H. (2004) Conversion of crustacean hemocyanin to catecholoxidase. *Micron* 35, 89-90.

Jahangiri,E., Agharafeie,R., Kaiser,H.J., Tahmasbi,Y., Legge,R.L. y Haghbeen,K. (2012) Medium engineering to enhance mushroom tyrosinase stability. *Biochem. Eng. J.* 60, 99-105.

Jeon,H.J., Noda,M., Maruyama,M., Matoba,Y., Kumagai,T. y Sugiyama,M. (2006) Identification and kinetic study of tyrosinase inhibitors found in sake less. *J Agric. Food. Chem.* 54, 9827-9833.

Jimbow,K., Fitzpatrick,T.B. y Wick,M.M. (1991) Biochemistry and physiology of melanin pigmentation, En: *Physiology, biochemistry, and molecular biology of the skin*, Goldsmith L.A. (Ed.) Oxford University Pess, New York, pp 873-909.

Jimbow,K., Quevedo,W.C.Jr., Fitzpatrick,T.B. y Szabo,G. (1993) Biology of melanocytes. En: *Dermatology in general medicine*. Fiztpatrick,T.B., Eisen,A.Z., Wolff,K., Fredberg,I.M. y Austen,K.F. (Eds), Mc Graw-Hill, New York, pp. 261-289.

Jimbow,K., Gómez,P.F., Toyofuku,K., Chang,D., Miura,S., Tsujiya,H. y Park,J.S. (1997) Biological role of tyrosinase related protein and its biosynthesis and transport from TGN to stage I melanosoma, late endosome, through gene transfection study. *Pigment Cell Res.* 10, 206-213.

Jiménez-Atienzar,M., Pedreño,M.A. y García-Carmona,F. (1991) Activation of polyphenol oxidase by polyamines. *Biochem. Int.* 25, 861-868.

Jimenez-Cervantes,C., Germer,S., Gonzalez,P., Sanchez,J. Sanchez,C.O. y Garcia-Borron,J.C. (2001) Thr 40 and Met122 are new partial loss-of-function natural mutations of the human melanocortin 1 receptor. *FEBS lett.* 508, 44-48.

Jiménez-Cervantes,C., Solano,F., Kobayashi,T., Urabe,K., Hearing,V.J., Lozano,J.A. y García-Borrón,J.C. (1994) A new enzymatic function in the melanogenic pathway. The 5,6-dihydroxyindole-2-carboxylic acid oxidase activity of tyrosinase-related protein-1 (TRP-1). *J. Biol. Chem.* 269, 17993-18000.

Jin,Y.H., Lee,S.J., Chung,M.H., Park,J.H., Park,Y.I., Cho,T.H. y Lee,S.K. (1999) Aloesin and arbutin inhibit tyrosinase activity in a synergistic manner via a different action mechanism. *Arch. Pharm. Res.* 22, 232-236.

Jolivet,J., Arpin,N., Wichers,H.J. y Pellon,G. (1998) *Agaricus bisporus* browning: a review. *Mycol. Res.* 102, 1459-1483.

Jolley,R.L.Jr., Evans,L.H., Makino,N. y Mason,H.S. (1974) Oxytyrosinase. *J.Biol.Chem.* 249, 335-345.

Jordan,A.M., Khan,T.H., Malkin,H., Osborn,H.M.I., Photiou,A. y Riley,P.A. (2001) Melanocyte-directed enzyme prodrug therapy (MDEPT): development of second generation prodrugs for targeted treatment of malignant melanoma. *Bioorg. Med. Chem.* 9, 1549-1558.

Jordan,A.M., Khan,T.H., Osborn,H.M.I., Photiou,A. y Riley, P.A. (1999) Melanocyte-directed enzyme prodrug therapy (MDEPT): development of a targeted treatment for malignant melanoma. *Bioorg. Med. Chem.* 7, 1775-1780.

Joshi,M., Strandhoy,J. y White,W.L. (1996) Nitric oxide synthase activity is up-regulated in melanoma cell lines: a potential mechanism for metastasis formation. *Melanoma Res.* 6, 121-126.

Joy,R.W., Sugiyama,M., Fukuda,H. y Komamine,A. (1995) Cloning and characterization of polyphenol oxidase cDNAs of *Phytolacca americana*. *Plant Physiol*. 107, 1083-1089.

Kadekaro,A.L., Kanto,H., Kavanagh,R. y Abdel-Malek,Z.A. (2003) Significance of the melanocortin 1 receptor in regulating human melanocyte pigmentation, proliferation, and survival. *Ann. N. Y. Acad. Sci.* 994,359-365.

Kaljunen,H., Gasparetti,C., Kruus,K., Rouvinen,J. y Hakulinen,N. (2011) Crystalization and preliminary X-ray analysis of Aspergillus oryzae catechol oxidase. *Acta Crystallogr. Sect. F Struct. Biol. Cryst. Commun.* 67, 672-674.

Kalka,K., Mukhatar,H., Turowski-Wanke,A. y Merk,H. (2000) Biomelanin antioxidants in cosmetics: assessment based on inhibition of lipid peroxidation. *Skin Pharmacol. Appl. Skin Physiol.* 13, 143-149.

Karlin,K.D., Lee,D.H., Obias,H.V. y Humphreys,K.J. (1998) Copper-dioxygen complexes: Functional models for proteins. *Pure Appl. Chem.* 70, 855-862.

Kauser,S., Schallreuter,K.U., Thody,A.J., Gummer,C. y Tobin,D.J. (2003) Regulation of human epidermal melanocyte biology by beta-endorphin. *J. Invest. Dermatol.* 120, 1073-1080.

Kavrayan,D. y Aydemir,T. (2001) Partial purification and characterization of polyphenoloxidase from peppermint *(Mentha piperita)*. *Food Chem.* 74, 147-154.

Kane,J.B., Tompkins,R.G., Yarmush,M.L. y Burke,I.F. (1996) Burn dressins. En: *Biomaterials science an introduction to materials in medicine*. Ratner,B.D., Hoffman,A.S., Schoen,F.J. y Lemons J.E. (Eds). San Diego, Academic Press. pp. 360-370.

Kertesz,D. y Zito,H.Z. (1962) Oxygenases. *Academic Press*. New York.

Khan,S.B., Azhar-Ul,H., Afza,N., Malik,A., Khan,M.T., Shah,M.R. y Choudhary,M. (2005) Tyrosinase-inhibitory long-chain esters from *Amberboa ramosa*. *Chem. Pharm. Bull.* 53, 86-89.

Khlgatian,M.K., Hadshiew,I.M., Asawanonda,P., Yaar,M., Eller,M.S., Fujita,M., Norris,D.A. y Gilchrest,B.A. (2002) Tyrosinase gene expression is regulated by p53. *J. Invest. Dermatol.* 118, 126-132.

Kim,H., Choi,H.R., Kim,D.S. y Park,K.C. (2012) Topical hypopigmentating agents for pigmentary disorders and their mechanisms of action. *Ann. Dermatol.* 24, 1-6.

Kim,Y.J. y Uyama,H. (2005) Tyrosinase inhibitors from natural and synthetic sources: structure, inhibition, mechanism and perspective for the future. *Cell Mol. Life. Sci.* 62, 1707-1723.

Kimura,E.T., Nikiforova,M.N., Zhu,Z., Knauf,J.A., Nikiforov,Y.E. y Fagin,J.A. (2003) High prevalence of BRAF mutations in papillary thyroid cancer: genetic evidence for constitutive activation of the RET/PTC-RAS-BRAF signalling pathway in papillary carcinoma. *Cancer Res.* 63, 1454-1457.

King,D.B. (1999) Parkinson´s disease—levodopa complications. *Can. J. Neurol. Sci.* 26 (Suppl. 2) S13-S20.

Klabunde,T., Eicken,C., Sacchettini,J.C. y Krebs,B. (1998) Crystal structure of a plant catechol oxidase containing a dicopper center. *Nat. Struct. Biol*. 5, 1084-1090.

Knaggs,S., Malkin,H., Osborn,H.M.I., Williams,N.A.O. y Yaqoob,P. (2005) New prodrugs derived from 6-aminodopamine and 4-aminophenol as candidates for melanocyte-directed enzyme prodrug therapy. *Org. Biomol. Chem*. 3, 4002-4010.

Kobayashi,T., Imokawa,G., Bennett,D.C. y Hearing,V.J. (1998a) Tyrosinase stabilization by Tyrp1 (the brown locus protein) *J. Biol. Chem*. 273, 31801-31805.

Kobayashi,N., Nakagawa,A., Muramatsu,T., Yamashina,Y., Shirai,T., Hashimoto,M.W., Ishigaki,Y., Ohnishi,T. y Mori,T. (1998b) Supranuclear melanin caps reduce ultraviolet induced DNA photoproducts in human epidermis. *J. Invest. Dermatol.* 110, 806-810.

Kohashi,P.Y., Kumagai,T., Matoba,Y., Yamamoto,A., Maruyama,M. y Sugiyama,M. (2004) An efficient method for the overexpression and purification of active tyrosinase from *Streptomyces castaneoglobisporus*. *Protein. Expr. Purif.* 34, 202-207.

Konanayakam,M. y Sastry,S.K. (1988) Kinetics and shrinkage of mushroom during blanching. J. Food Sci. 53, 1406-1411.

Kondo,T. y Hearing,V.J. (2011) Update on the regulation of mammalian melanocyte function and skin pigmentation. Expert Rev. Dermatol. 6, 97-108.

Kong,K.H., Hong,M.P., Choi,S.S., Kim,Y.T. y Cho,S.H. (2000) Purification and characterization of a higly stable tyrosinase from *Thermomicrobium roseum*. *Biotechnol. Appl. Biochem.* 31, 113-118.

Körner,A.M. y Pawelek,J. (1980) Dopachrome conversion: a possible control point in melanin biosynthesis. *J. Invest. Dermatol.* 75, 192-195.

Körner,A.M. y Pawelek,J. (1982) Mammalian tyrosinase catalyzes three reactions in the biosynthesis of melanin. *Science* 217, 1163-1165.

Kruzmane,D., Jankevica,L., Ievinsh,G. (2002) Effect of regurgitant from *Leptinotarsa decemlineata* on wound responses in *Solanum tuberosum* and *Phaseolus vulgaris*. *Physiol. Plant.* 115, 577-584.

Kubo,I., Kinst-Hori,I., Kubo,Y., Yamagiwa,Y., Kamikawa,T. y Haraguchi,H. (2000) Molecular design of antibrowning agents. *J. Agric. Food Chem.* 48, 1393-1399.

Kubowitz,F. (1938) Spaltung und resynthese der polyphenoloxydase und des hemocyanins. *Biochem. Z.* 299, 32-57.

Kuo,M.J. y Alexander,M. (1967) Inhibition of the lysis of fungi by melanins. *J. Bacteriol.* 94, 624-629.

Kupper,U., Niedermann,D.M., Travaglini,G. y Lerch,K. (1989) Isolation and characterization of the tyrosinase gene from *Neurospora crassa*. *J. Biol. Chem.* 264, 17250-17258.

Kushimoto,T., Basrur,V., Valencia,J., Matsunaga,J., Vieira,W.D., Ferrans,V.J., Muller,J., Appella,E. y Hearing,V.J. (2001) A model for melanosome biogenesis based on the purification and analysis of early melanosomes. *Proc. Natl. Acad. Sci. USA* 98, 10698-10703.

Ladd,D. y Weistock,J. (1981) Improved synthesis of fluoroveratroles and fluorophenethylamines via organolithium reagents. *J. Org. Chem.* 46, 203-206.

Lambert,C., Chacon,J.N., Chedekel,M.R., Land,E.J., Riley,P.A., Thompson,A. y Truscott,T.G. (1989) A pulse radiolysis investigation of the oxidation of indolic melanin precursors: evidence for indolequinones and subsequent intermediates. *Biochim. Biophys. Acta* 993, 12-20.

Lamoreux,M.L., Wakamatsu,K. e Ito,S. (2001) Interaction of major coat color gene functions in mice as studied by chemical analysis of eumelanin and pheomelanin. *Pigment Cell Res.* 14, 23-31.

Land,E.J., Ramsden,C.A. y Riley,P.A. (2003) Tyrosinase autoactivation and the chemistry of ortho-quinone amines. *Acc. Chem. Res.* 36, 300-308.

Land,E.J., Ramsden,C.A. y Riley,P.A. (2007) The mechanism of suicide-inactivation of tyrosinase: a substrate structure investigation. *Tohoku J. Exp. Med.* 212, 341-348.

Land,E.J., Ramsden,C.A., Riley,P.A. y Stratford,M.R. (2008) Evidence consistent with the requirement of cresolase activity for suicide inactivation of tyrosinase. *Tohoku J. Exp. Med.* 216, 231-138.

Laskin,J.D. y Piccinini,L.A. (1986) Tyrosinase isozyme heterogeneity in differentiating B16/C3 melanoma. *J. Biol. Chem.* 261, 16626-16635.

Lassam,N. y Bickford,S. (1992) Loss of c-kit expression in cultured melanoma cells. *Oncogene* 7, 51-56.

Laveda,F., Nuñez-Delicado,E., García-Carmona,F. y Sánchez-Ferrer,A. (2000) Reversible sodium dodecyl sulfate activation of latent peach polyphenol oxidase by cyclodextrins. *Arch. Biochem. Biophys.* 379, 1-6.

Laveda,F., Nuñez-Delicado,E., García-Carmona,F. y Sánchez-Ferrer,A. (2001) Proteolytic activation of latent *Paraguaya peach* PPO. Characterization of monophenolase activity. *J. Agric. Food Chem*. 49, 1003-1008.

Lax,A.R. y Vaughn,K.C. (1991) Colocalization of polyphenol oxidase and photosystem II proteins. *Plant Physiol*. 96, 26-31.

Lee,B.P., Dalsin,J.L. y Messersmith,P.B. (2002) Synthesis and gelation of DOPA modified poly(ethylene glycol) hydrogels. *Biomacromolecules* 3, 1038-1047.

Lee,K.Y. y Mooney D.J. (2001) Hydrogels for tissue engineering. *Chem. Rev.* 101, 1869-1879.

Lee,S.G., Ro,H.S., Hong,S.P., Kim,E.H. y Sung,M.H. (1996) Production of L-dopa by thermostable tyrosinase phenol-lyase of thermophilic *Symbiobacterium* species overexpressed in recombinant *Escherichia Coli, J. Microbiol. Biotechnol.* 6, 98-102.

Lenhart,J.L., Chaubal,M.V., Payne,G.F. y Barbari,T.A. (1998) Enzymatic modification of chitosan by tyrosinase. En: *Enzymes in polymer synthesis*. Gross,R.A., Kaplan,D.I. y Swift,G. (Eds). Washington DC; American Chemical Society Symposium Series 684. pp. 188-198.

Leoni,O., Palmieri,S., Lattanzio,V. y Van Sumere,C.F. (1990) Polyphenol oxidase from artichoke (*Cynara scolymus L.*) *Food Chem.* 38, 27-39.

Lerch,K. (1976) Neurospora tyrosinase: molecular weight, copper content and spectral properties. *FEBS lett.* 69, 157-160.

Lerch,K. (1981) Copper monooxygenases: tyrosinase and dopamine β-hydroxilase. En: *Metal Ions in Biological Systems.* Sigel, H.Ed. Marcel Dekker, New York. pp. 143-186.

Lerch,K. (1982) Primary structure of tyrosinase from *Neurospora crassa* II. Complete amino acid sequence and chemical structure of a tripeptide containing an unusual thioether.*J. Biol. Chem.* 257, 6414-6419.

Lerch,K. (1983) Neurospora tyrosinase: structural, spectroscopic and catalytic properties. *Mol. Cell. Biochem.* 52, 125-138.

Lerch,K., y Ettinger,L. (1972) Purification and characterizacion of a tyrosinase from *Streptomyces glaucescens*. *Eur. J. Biochem.* 31, 427-437.

Lerner,A.B. y Fitzpatrick,T.B. (1949) Mammalian tyrosinase: preparation and properties. *J. Biol. Chem.* 178, 185-195.

Lerner,A.B. y Fitzpatrick,T.B. (1950) Biochemistry of melanin formation. *Physiol. Rev.* 30, 91-126.

Le-Thi-Thu,H., Casañola-Martín,G.M., Marrero-Ponce,Y., Rescigno,A., Saso,L., Parmar,V.S., Torrens,F. y Abad,C. (2011) Novel coumarin-based tyrosinase inhibitors discovered by OECD principles-validated QSAR approach from an enlarged, balanced database. *Mol. Divers.* 15, 507-520.

Levi-Montalcini,R. (1987) The nerve growth factor 35 years later. *Science* 237, 1154-1162.

Levy,G. y Nelson,G.L. (1976) *Resonancia Magnética Nuclear de Carbono 13 Para Químicos Orgánicos*, Ediciones Bellaterra S.A., Barcelona.

Levy,S.B. (2000) Tanning preparations, *Dermatol. Clin*. 18, 591-596.

Li.Y., Wang,Y., Jiang,H. y Deng,J. (2009) Crystal structure of *Manduca sexta* prophenoloxidase provides insights into the mechanism of type 3 copper enzymes *Proc. Natl. Acad. Sci. USA* 106, 17002-17006.

Libra,M., Malaponte,G., Navolanic,P.M., Gangemi,P., Bevelacqua,V., Proietti,L., Bruni,B., Stivala,F., Mazzarino,M.C., Travali,S. y McCubre,J.A. (2005) Analysis of BRAF mutation in primary and metastatic melanoma. *Cell cycle* 4, 1382-1384.

Liu,N., Zhang,T., Wang,Y.J., Huang,Y.P., Ou,J.H. y Shen,P. (2004) A heat inducible tyrosinase with distinct properties from *Bacillus thuringensis*. *Lett. Appl. Microbiol.* 39, 407-412.

Loercher,A.E., Tank,E.M., Delston,R.B. y Harbour,J.W. (2005) MITF links differentiation with cell cycle arrest in melanocytes by transcriptional activation of INK4A. *J. Cell Biol.* 168, 35-40.

Loh,K.C. y Tan,C.P. (2000) Effect of additional carbon sources on biodegradation of phenol, *Bull. Environ. Contam. Toxicol*. 64, 756-763.

Lopez-Serrano,D., Solano,F. y Sanchez-Amat,A. (2004) Identification of an operon involved in tyrosinase activity and melanin synthesis in *Marinomonas mediterranea*. *Gene* 342, 179-187.

Lowry,O.H., Rosenbrough,N.J., Farr,A.L. y Randall,R.J. (1951) Protein measurement with the Folin phenol reagent. *J. Biol. Chem.* 133, 265-275.

Lozano,J.A. y Solano,F. (1989) Bioquímica de la pigmentación en mamíferos. *Investigación y Ciencia* 157, 87-93.

Lozumi,K., Hoganson,G.E., Pennella,R., Everett,M.A. y Fuller,B.B. (1993) Role of tyrosinase as the determinant of pigmentation in cultured human melanocytes. *J. Invest. Dermatol.* 100, 806-811.

Lu,D., Willard,D., Patel,I.R., Kadwell,S., Overton,L., Kost,T., Luther,M., Chen,W., Woychik,R.P. y Wilkison,W.O. (1994) Agouti protein is an antagonist of the melanocyte stimulating-hormone receptor. *Nature* 371, 799-802.

Maeda,K. y Fukuda,M. (1991) In vitro effectiveness of several whitening cosmetic components in human melanocytes. *J. Soc. Cosmet. Chem.* 42, 361-368.

Makino,N., McMahill,P. y Mason,H.S. (1974) The oxidation state of copper in resting tyrosinase. *J. Biol. Chem.* 249, 6062-6066.

Makino,N. y Mason,H.S. (1973) Reactivity of oxytyrosinase toward substrates. *J. Biol. Chem.* 248, 5731-5735.

Mallapragada,S.K. y Narasimhan,B. (2008) Immunomodulatory biomaterials. *Int. J. Pharm.* 364, 265-271.

Marín-Zamora,M.E., Rojas-Melgarejo,F., García-Cánovas,F. y García-Ruiz,P.A. (2009) Production of *o*-diphenols by immobilized mushroom tyrosinase. *J. Biotechnol.* 139, 163-168.

Marquardt,D.W. (1963) An algorithm for least-squares estimation of nonlinear parameters. *J. Soc. Ind. Appl. Math.* 11, 431-441.

Marrero-Ponce,Y., Casañola-Martín,G.M., Khan,M.T., Torrens,F., Rescigno,A. y Abad,C. (2010) Ligand-based computer-aided discovery of tyrosinase inhibitors. Applications of the TOMOCOMD-CARDD method to the elucidation of new compounds. *Curr. Pharm. Des.* 16, 2601-2624.

Marri,C., Frazzoli,A., Hochkoeppler,A. y Poggi,V. (2003) Purification of a polyphenol oxidase isoform *from potato (Solanum tuberosum) tubers. Phytochemistry* 63, 745-752.

Marriott,S. y Topsom,R.D. (1985) A theorical scale of substituent resonance parameters (σ_R^0). *J. Chem. Soc. Perkin Trans II*. 7, 1045-1047.

Marusek,C.M., Trobaugh,N.M., Flurkey,W.H. y Inlow,J.K. (2006) Comparative analysis of polyphenol oxidase from plant and fungal species. *J. Inorg. Biochem.* 100, 108-123.

Martinez,M.V. y Whitaker J.R. (1995) The biochemistry and control of enzymatic browning. *Trends Food Sci. Technol.* 6, 195-200.

Mason,H.S. (1948) The chemistry of melanin; mechanism of the oxidation of dihydroxyphenylalanine by tyrosinase. *J. Biol. Chem*. 172, 83-99.

Mason,H.S. (1955) Comparative biochemistry of the phenolase complex. *Adv. Enzymol.* 16, 105-184.

Mason,H.S. (1956) Structures and functions of the phenolase complex. *Nature* 177, 79-81.

Mason,H.S., Spencer,E. y Yamazaki,I. (1961) Identification by electron spin resonance spectroscopy of the primary product of tyrosinase-catalyzed catechol oxidation. *Biochem. Biophys. Res. Commun.* 4, 236-238.

Masuda,T., Odaka,Y., Ogawa,N., Nakamoto,K. y Kuninaga,H. (2008) Identification of geranic acid, a tyrosinase inhibitor in lemongrass (*Cymbopogon citratus*). *J. Agric. Food Chem.* 56, 597-601.

Matheis,G. y Whitaker,J.R. (1984) Modification of proteins by polyphenol oxidase and peroxidase and their products. *J. Food Biochem.* 8, 137-162.

Matoba,Y., Kumagai,T., Yamamoto,A., Yoshitsu,H. y Sugiyama,M. (2006) Crystallographic evidence that the dinuclear copper center of tyrosinase is flexible during catalysis. *J. Biol. Chem.* 281, 8981-8990.

Matoba,Y., Bando,N., Oda,K., Noda,M., Higashikawa,F., Kumagai,T. y Sugiyama,M. (2011) A molecular mechanism for copper transportation to tyrosinase that is assisted by a metallochaperone, caddie protein. *J. Biol. Chem.* 286, 30219-30231.

Matsui,M.S., Wang,N., MacFarlane,D. y DeLeo,V.A. (1994) Long-wave ultraviolet radiation induces protein kinase C in normal human keratinocytes. *Photochem. Photobiol*. 59,53-57.

Mayer,A.M. (2006) Polyphenol oxidases in plants and fungi: Going places? A review. *Phytochemistry* 67, 2318-2331.

Mayer,A.M. y Harel,E. (1979) Polyphenol oxidases in plants. *Phytochemistry* 18, 193-215.

McMahon,A.M., Doyle,E.M., Brooks,S. y O´Connor,K.E. (2007) Biochemical characterisation of the coexisting tyrosinase and laccase in the soil bacterium *Pseudomonas putida* F6. *Enzyme Microb. Technol.* 40, 1435-1441.

McEvily,A.J., Iyengar,R. y Otwell,W.S. (1991) Sulfite alternative prevents shrimp melanosis. *Food Technol.* 45, 80-86.

McGill,C.G., Horstmann,M., Widlund,H.R., Du,J., Motyckova,G., Nishimura,E.K., Lin,Y.L., Ramaswamy,S., Avery,W., Ding,H.F., Jordan,S.A., Jackson,I.J., Korsmeyher,S.J., Golub,T.R. y Fisher,D.E. (2002) Bcl-2 regulation by the melanocyte master regulator Mitf modulates lineage survival and melanoma cell viability. *Cell* 109, 707-718.

Metz,M. y Solomon,E.I. (2001) Dioxygen binding to deoxyhemocyanin. Electronic structure and mechanism of the spinforbidden two-electron reduction of O_2. *J. Am. Chem. Soc.* 123, 4938-4950.

Messerschmidt,A. y Huber,R. (1990) The blue oxidases, ascorbate oxidase, laccase and ceruloplasmin. Modelling and structural relationships. *Eur. J. Biochem.* 187, 341-352.

Miller,A.J. y Mihm,M.C. (2006) Melanoma. *N. Engl. J. Med.* 355, 51-65.

Min,K., Park,D.H. y Yoo,Y.J. (2010) Electroenzymatic synthesis of L-Dopa. *J. Biotechnol.* 146, 40-44.

Miranda,M., Bonfigli,A., Zarivi,O., Manilla,A., Cimini,A. y Arcadi,A. (1987) Restriction patterns of model DNA trated with 5,6-dihydroxyindole, a potent cytotoxic intermediate of melanin synthesis-effect of UV irradiation. *Mutagenesis* 2, 45-50.

Mirica,L.M., Rudd,D.J., Vance,M.A., Solomon,E.I., Hodgson,K.O., Hedman,B. y Stadk,T.D. (2006) mu-eta2:eta2-peroxodicopper (II) complex with a secondary diamine ligand: a fuctional model of tyrosinase. *J. Am. Chem. Soc.* 128, 2654-2665.

Mirica,L.M., Vance,M., Rudd,D.J., Hedman,B., Hodgson,K.O., Solomon,E.I. y Stack,T.D. (2002) A stabilized mu-eta (2): eta (2) peroxodicopper(II) complex with a secondary diamine ligand and its tyrosinase-like reactivity. *J. Am. Chem. Soc.* 14, 9332-9333.

Misra,H.P. y Fridovich,I. (1972) The univalent reduction of oxygen by reduced flavins and quinones. *J. Biol. Chem.* 247, 188-192.

Miyamura,Y., Coelho,S., Wolber,R., Miller,S.A., Wakamatsu,K., Zmudska,B.Z., Ito,S., Smuda,C., Passeron,T., Choi,W., Batzer,J., Yamaguchi,Y., Beer,J.Z. y Hearing,V.J. (2007) Regulation of human skin pigmentation and responses to ultraviolet radiation. *Pigment Cell Res.* 20, 2-13.

Mochly-Rosen,D. (1995) Localization of protein kinases by anchoring proteins: a theme in signal transduction. *Science* 268, 247-251.

Molina,F.G., Muñoz,J.L., Varón,R., López,J.N., Cánovas,F.G. y Tudela,J. (2007) An approximate analytical solution to the lag period of monophenolase activity of tyrosinase. *Int. J. Biochem. Cell. Biol.* 39, 238-252.

Mountjoy,K.G., Robbins,L.S., Mortrud,M.T. y Cone,R.D. (1992) The cloning of a family of genes that encode the melanocortin receptors. *Science* 257,1248-1251.

Muñoz-Muñoz,J.L., García-Molina,F., García-Ruiz,P.A., Varón,R., Tudela,J., García Cánovas,F. y Rodriguez-Lopez,J.N. (2009a) Stereospecific inactivation of tyrosinase by L-and D-ascorbic acid. *Biochim. Biophys. Acta* 1794, 244-253.

Muñoz-Muñoz,J.L., García-Molina,F., Varón,R., Tudela,J., García-Cánovas,F. y Rodríguez-López,J.N. (2009b) Generation of hydrogen peroxide in the melanin biosíntesis pathway. *Biochim. Biophys. Acta* 1794, 1017-1029.

Muñoz-Muñoz,J.L., García-Molina,F., García-Ruíz,P.A., Varón,R., Tudela,J., García-Cánovas,F. y Rodriguez-Lopez,J.N. (2010a) Some kinetic properties of deoxytirosinase. *J. Mol. Catal.-B Enzymatic* 62, 173-182.

Muñoz-Muñoz,J.L., Acosta-Motos,J.R., Garcia-Molina,F., Varón,R., García-Ruiz,P.A., Tudela,J., García-Cánovas,F. y Rodriguez-López,J.N. (2010b) Tyrosinase inactivation in its action on dopa. *Biochim. Biophys. Acta* 1804, 1467-1475.

Muñoz-Muñoz, J.L.; Garcia-Molina, F.; Arribas, E.; Garcia-Ruiz, P.A.; Tudela, J.; García-Cánovas, F. y Rodriguez-López, J.N. (2011a) Suicide inactivation of tyrosinase in its action on tetrahydropterines. *J. Enzyme Inhib. Med. Chem.* 26, 728-733.

Muñoz-Muñoz,J.L., Garcia-Molina,F., Garcia-Ruiz,P.A., Varon,R., Tudela,J., Rodriguez-Lopez,J.N. y Garcia-Canovas,F. (2011b) Catalytic oxidation of *o*-aminophenols and aromatic amines by mushroom tyrosinase. *Biochim. Biophys. Acta* 1814, 1974-1983.

Muñoz-Muñoz,J.L., Berna,P., Garcia-Molina,F., Garcia-Ruiz,P.A., Tudela,J., Rodriguez-López,J.N. y García-Cánovas,F. (2012) Unravelling the suicide inactivation of tyrosinase: A discrimination between mechanisms. *J. Mol. Catal. B: Enzymatic* 75, 11-19.

Nagai,T. y Suzuki,N. (2001) Partial purification of polyphenol oxidase form Chinese cabbage *Brassica rapa* L. *J. Agric. Food Chem*. 49, 3922-3926.

Naish-Byfield,S. y Riley,P.A. (1992) Oxidation of monohydric phenol substrates by tyrosinase. An oximetric study. *Biochem. J.* 288, 63-67.

Nakayama,T., Sato,T., Fukui,Y., Yonekura-Sakakibara,K., Hayashi,H., Tanaka,Y., Kusumi,T. y Nishino,T. (2001) Specificity analysis and mechanism of aurone synthesis catalyzed by aureusidin synthase, a polyphenol oxidase homolog responsible for flower coloration. *FEBS lett.* 499, 107-111.

Nakayama,T., Yonekura-Sakakibara,K., Sato,T., Kikuchi,S., Fukui,Y., Fukuchi-Mizutani,M., Ueda,T., Nakao,M., Tanaka,Y., Kusumi,T. y Nishino,T. (2000) Aureusidin synthase: a polyphenol oxidase homolog responsible for flower coloration. *Science* 290, 1163-1166.

Nambudiri,A.M.D. y Bhat,J.V. (1972) Conversion of *p*-cumarate into caffeate by Streptomyces nigrifaciens. *Biochem. J.* 130, 425-433.

Nappi,A.J., Vass,E., Frey,F. y Carton,Y. (1995) Superoxide anion generation in Drosophila during melanotic encapsulation of parasites. *Eur. J. Cell Biol.* 68, 450-456.

Nappi,A.J. y Vass,E. (1996) Hyrogen peroxide generation associated with the oxidations of the eumelanin precursors 5,6-dihydroxyindole and 5,6-dihydroyindole-2-carboxylic acid. *Melanoma Res.* 6, 341-349.

Napolitano,A., Di Donato,P. y Prota,G. (2000) New regulatory mechanisms in the biosynthesis of pheomelanins: rearrangement vs. redox exchange reaction routes of a transient 2H-1,4-benzothiazine-*o*-quinonimine intermediate. *Biochim. Biophys. Acta* 1475, 47-54.

Nerya,O., Musa,R., Khatib,S., Tamir,S. y Vaya,J. (2004) Chalcones as potent tyrosinase inhibitors: the effect of hydroxyl positions and numbers. *Phytochemistry* 65, 1389-1395.

Nicolas,J.J., Richard-Forget,F.C., Goupy,P.M., Amiot,M.J. y Aubert,S.Y. (1994) Enzimatic browning reactions in apple and apple products. *CRC Crit. Rev. Food Sci. Nutr.* 34, 109-157.

Nillius,D., Jaenicke,E. y Decker,H. (2008) Switch between tyrosinase and catecholoxidase activity of scorpion hemocyanin by allosteric effectors. *FEBS Letters* 582, 749-754.

Noble,R., y Burton,K.S. (1993) Postharvest storage and handling of mushrooms: physiology and technology. *Postharvest news and information* 4, 125N-129N.

Norris,D.A., Morelli,J.G. y Fujita,M. (1998) Melanocytes interactions in skin. En: *The pigmentary system.* Nordlund,J.J., Boissy,R.E., Hearing,V.J., King, R.A. y Ortonne, J.P. (Eds.) Oxford Univ. Press, New York, pp. 123-133.

Nosanchuk,J.D. y Casadevall,A. (2003) The contribution of melanin to microbial pathogenesis. *Cell Microbiol.* 5, 203-223.

Novikoff,P.M., Novikoff,A.B., Quintana,N. y Hawn,J.J. (1971) Golgi apparatus, GERL, and lysosomes of neurons in rat dorsal root ganglia, studied by thick section and thin section cytochemistry. *J. Cell Biol.* 50, 859-886.

Núñez-Delicado,E., Sojo,M.M., García-Carmona,F. y Sánchez-Ferrer,A. (2003) Partial purification of latent persimmon fruit polyphenol oxidase. *J. Agric. Food Chem.* 51, 2058-2063.

Oberley,T.D. y Oberley,L.W. (1997) Antioxidant enzyme levels in cancer. *Histol. Histopathol.* 12, 525-535.

Oetting,W.S. (2000) The tyrosinase gene and oculocutaneous albinism type 1 (OCA1): A model for understanding the molecular biology of melanin formation. *Pigment Cell Res.* 13, 320-325.

Ohguchi,K., Tanaka,T., Iliya,I., Ito,T., Iinuma,M., Matsumoto,K., Akao,Y. y Nozawa,Y. (2003) Gnetol as a pontent tyrosinase inhibitor from genus *Gnetum*. *Biosci. Biotechnol. Biochem.* 67, 663-665.

Ohsie,S.J., Sarantopoulos,G.P., Cochran,A.J. y Binder,S.W. (2008) Immunohistochemical characteristics of melanoma. *J. Cutan. Pathol.* 35, 433-444.

Oikawa,A., Saeki,H., Akiyama,T. y Matsumoto,J. (1987) Electron microscopic evidence for stimulation of melanosomal maturation by lysomotropic agents and monensin in cultured B16 mouse melanoma cells. *Pigment Cell Res.* 1, 44-50.

Olivares,C., Jiménez-Cervantes,C., Lozano,J.A., Solano,F. y García-Borrón,J.C. (2001) The 5,6-dihydroxyindole-2-carboxylic acid (DHICA) oxidase activity of human tyrosinase. *Biochem. J.* 354, 131-139.

Olivares,C. y Solano,F. (2009) New insights into the active site structure and catalytic mechanism of tyrosinase and its related proteins. *Pigment Cell Melanoma Res.* 22, 750-760.

Ollmann,M.M., Wilson,B.D., Yang,Y.K., Kerns,J.A., Chen,Y., Gantz,I. y Barsh,G.S. (1997) Antagonism of central melanocortin receptors in vitro and in vivo by agouti-related protein. *Science* 278,135-138.

Onsa,G.H., bin Saari,N., Selamat,J. y Bakar,J. (2000) Latent polyphenol oxidases from sago log (Metroxylon sagu): partial purification, activation, and some properties. *J. Agric. Food Chem.* 48, 5041-5045.

Orlow,S.J., Osber,M.P. y Pawelek,J.M. (1992) Synthesis and characterization of melanins from dihydroxyindole-2-carboxylic acid and dihydroxyindole. *Pigment Cell Res.* 5, 113-121.

Osaki,S. (1963) The mechanism of tyrosine oxidation by mushroom tyrosinase. *Arch. Biochem. Biophys.* 100, 378-384.

Otávio de Faria,R., Moure,V.R., Lopes de Almeida,M.A., Krieger,N. y Mitchell,D.A. (2007) The biotechnological potencial of mushroom tyrosinases. *Food Tecnol. Biotechnol.* 45, 287-294.

Pacificio,A. y Leone,G. (2007) Role of p53 and CDKN2A inactivation in human squamous cell carcinomas. *J. Biomed. Biotechnol.* 2007. DOI: 10.1155/2007/43418.

Paice,M.G., Bourbonnais,R., Reid,I.D., Archibald,F.S. y Jurasek,L. (1995) Oxidative bleaching enzymes: a review. *J. Pulp. Paper Sci.* 21, 280-284.

Palmieri,G., Capone,M., Ascierto,M.L., Gentilcore,G., Stroncek,D.F., Casula,M., Sini,M.C., Palla,M., Mozzillo,N. y Ascierto,P.A. (2009) Main roads to melanoma. *J. Transl. Med.* 14, 86.

Palmieri,G., Casula,M., Sini,M.C., Ascierto,P.A. y Cossu,A. (2007) Issues affecting molecular staging in the management of patients with melanoma. *J. Cell Mol. Med.* 11, 1052-1068.

Palumbo,A., Misuraca,G., D´Ischia,M. y Prota,G. (1985) Effect of metal ions on the kinetics of tyrosine oxidation catalysed by tyrosinase. *Biochem. J.* 228, 647-651.

Papaparaskeva-Petrides,C., Ioannides,C. y Walker,R. (1993) Contribution of phenolic and quinonoid structures in the mutagenicity of the edible mushroom *Agaricus bisporus*. *Food Chem. Toxicol*. 31, 561-567.

Park,H.Y., Kosmadaki,M., Yaar,M. y Gilchrest.B.A. (2009) Cellular mechanisms regulating human melanogenesis. *Cell. Mol. Life Sci.* 66, 1493-1506.

Park,H.Y., Perez,J.M., Laursen,R., Hara,M. y Gilchrest,B.A. (1999) Protein kinase C-beta activates tyrosinase by phosphorylating serine residues in its cytoplasmic domain. *J. Biol. Chem*. 274,16470-16478.

Park,H.Y., Russakovsky,V., Ohno,S. y Gilchrest,B.A. (1993) The beta isoform of protein kinase C stimulates human melanogenesis by activating tyrosinase in pigment cells. *J. Biol. Chem*. 268, 11742-11749.

Park,H.Y., Wu,C., Yonemoto,L., Murphy-Smith,M., Wu,H., Stachur,C.M. y Gilchrest,B.A. (2006) MITF mediates cAMP-induced protein kinase C-beta expression in human melanocytes. *Biochem. J*. 395, 571-578.

Park,H.Y., Wu,H., Killoran,C.E. y Gilchrest,B.A. (2004) The receptor for activated C-kinase-I (RACK-I) anchors activated PKC-beta on melanosomes. *J. Cell Sci.* 117, 3659-3668.

Parvez,S., Kang,M., Chung,H.S. y Bae,H. (2007) Naturally occurring tyrosinase inhibitors: mechanism and applications in skin health cosmetics and agriculture industries. *Phytother. Res.* 21, 805-816.

Pathak,M.A. y Fitzpatrick,T.B. (1993) Protective treatment of sunburn, and skin cancer with sun-protective agents, En: *Dermatology in general medicine*. Fiztpatrick,T.B., Eisen,A.Z., Wolff,K., Fredberg,I.M. y Austen,K.F. (Eds), Mc Graw-Hill, New York, pp. 1689-1717.

Patton,E.E., Widlund,H.R., Kutok,J.L., Kopani,K.R., Amatruda,J.F., Murphey,R.D., Berghmans,S., Mayhall,E.A., Traver,D., Fletcher,CD., Aster,J.C., Granter,S.R., Look,A.T., Lee,C., Fisher,D.E. y Zon,LI (2005) BRAF mutations are sufficient to promote nevi formation and cooperate with p53 in the genesis of melanoma. *Curr. Biol.* 15, 249-254.

Pawelek,J., Korner,A., Bergstrom,A. y Bologna,J. (1980) New regulators of melanin biosynthesis and the auto-destruction of melanoma-cells. *Nature* 286, 617-619.

Pawelek,J.M. y Lerner,A.B. (1978) 5,6-dihydroxyindole is a melanin precursor showing potent cytotoxicity. *Nature* 276, 626-628.

Peacocke,M., Yaar,M., Mansur,C.P., Chao,M.V. y Gilchrest,B.A. (1988) Induction of nerve growth factor receptors on cultured human melanocytes. *Proc. Natl. Acad. Sci. USA* 85, 5282-5286.

Pedeux,R., Al-irani,N., Marteau,C., Pellicier,F., Branche,R., Ozturk,M., Franchi,J. y Doré,J.F. (1998) Thymidine dinucleotides induce S phase cell cycle arrest in addition to increased melanogenesis in human melanocytes. *J. Invest. Deramtol.* 111, 472-477.

Peñalver,M.J., Rodríguez-López,J.N., García-Ruiz,P.A., García-Cánovas,F. y Tudela,J. (2003) Solvent deuterium isotope effect on the oxidation of *o*-diphenols by tirosinase. *Biochim. Biophys. Acta* 1650¸128-135.

Peppas,N.A. y Sahlin,J.J. (1996) Hydrogels as mucoadhesive y bioadhesive materials: a review. *Biomaterials* 17, 1553-1561.

Perchellet,J.P. y Boutwell,R.K. (1981) Effects of 3 isobutyl-1-methylxanthine and cyclic nucleotides on the biochemical processes linked to skin tumor promotion by 12-O-tetradecanoylphorbol-13-acetate. *Cancer Res.* 41, 3927-3935.

Pérez-Oliva,A.B., Fernéndez,L.P., Detorre,C., Herráiz,C., Martínez-Escribano,J.A., Benítez,J., Lozano-Teruel,J.A., García-Borrón,J.C., Jiménez-Cervantes,C. y Ribas,G. (2009) Identification and functional analysis of novel variants of the human melanocortin 1 receptor found in melanoma patients. *Hum. Mutat*. 30, 811-822.

Perry,M.J., Mendes,E., Simplicio,A.L., Coelho,A., Soares,R.V., Lley,J., Moreira,R. y Francisco,A.P. (2009) Dopamine- and tyramine-based derivatives of triazenes: activation by tyrosinase and implications for prodrug design. *Eur. J. Med. Chem.* 44, 3228-3234.

Pialis,P., Jimenez-Hamann,M.C. y Saville.,B.A. (1996) L-DOPA production from tyrosinase immobilized on nylon 6,6. *Biotechnol. Bioeng.* 20, 141-147.

Pierpoint,W.S., Ireland,R.J. y Carpenter,J.M. (1977) Modification of proteins during the oxidation of leaf phenols: reaction of potato virus X with chlorogenoquinone. *Phytochemistry* 16, 29-34.

Piquemal,J.P., Maddaluno,J., Silvi,B. y Giessner-Prettre,C. (2003) Theoretical study of phenol and 2-aminopheol docking at a model of the tyrosinase active site. *New J. Chem.* 27, 909-913.

Platz,A., Ringborg,U. y Hansson,J. (2000) Hereditary cutaneous melanoma. *Semin. Cancer Biol.* 10, 319-326.

Pollock,P.M., Harper,U.L., Hansen,K.S., Yudt,L.M., Stark,M., Robbins,C.M., Moses,T.Y., Hostetter,G., Wagner,U., Kakareka,J., Salem,G., Pohida,T., Haenan,P., Duray,P., Kallioniemi,O., Hayward,N.K., Trent,J.M. y Meltzer,P.S. (2003) High frequency of BRAF mutations in nevi. *Nat. Genet.* 33,19-20.

Pomerantz,S.H. (1966) The tyrosine hydroxylase activity of mammalian tyrosinase. *J. Biol. Chem.* 241, 161-168.

Prota,G. (1988) Progress in the chemistry of melanins and related metabolites. *Med. Res. Rev.* 8, 525-556.

Prota,G. (2000) Melanins, melanogenesis and melanocytes: looking at their functional significance from the chemist's viewpoint. *Pigment Cell Res.* 13, 283-293.

Prota,G., d´Ischia,M. y Napolitano,A. (1998) The chemistry of melanins and related metabolites. En: *The pigmentary system.* Nordlund,J.J., Boissy,R., Hearing,V., King,R., y Ortonne,J.P. (Eds), Univ. Press., Oxford. pp. 307-332.

Pryor,M.G.M. (1940) On the hardening of the cuticle of insects. *Proc. R. Soc. London Ser. B.* 128, 393-407.

Ramsden,C.A., Stratford,M.R. y Riley,P.A. (2009) The influence of catechol structure on the suicide-inactivation of tyrosinase. *Org. Biomol. Chem.* 7, 3388-3390.

Ramsden,C.A. y Riley,P.A. (2010a) Mechanistic studies of tyrosinase suicide inactivation. *Arkivoc* SI, 260-274.

Ramsden,C.A. y Riley,P.A. (2010b) Studies of the competing rates of catechol oxidation and suicide inactivation of tyrosinase. *Arkivoc* SI, 248-254.

Raper,H.S. (1928) The aerobic oxidases. *Physiol. Rev.* 8, 245-258.

Rathjen,A.H. y Robinson,S.P. (1992) Aberrant processing of polyphenol oxidase in a variegated grapevine mutant. *Plant Physiol.* 99, 1619-1625.

Reinhold,D.F., Utne,T. y Abrason,N.L. (1987) Process for L-dopa. United States patent 4716246.

Rescigno,A., Bruyneel,F., Padiglia,A., Sollai,F., Salis,A., Marchand-Brynaert,J. y Sanjust,E. (2011) Structure-activity relationships of various amino-hydroxy-benzenesulfonic acids and sulfonamides as tyrosinase substrates. *Biochim. Biophys. Acta* 1810, 799-807.

Rescigno,A., Casañola-Martin,G.M., Sanjust,E., Zucca,P. y Marrero-Ponce,Y. (2011) Vanilloid derivatives as tyrosinase inhibitors driven by virtual screening-based QSAR models. *Drug Test Anal.* 3, 176-181.

Rescigno,A., Sanjust,E., Soddu,G., Rinaldi,A.C., Sollai,F., Curreli,N. y Rinaldi,A. (1998) Effect of 3-hydroxyanthranilic acid on mushroom tyrosinase activity. *Biochim. Biophys. Acta* 1384, 268-276.

Rescigno,A., Sollai,F., Sanjust,E., Rinaldi,A.C., Curreli,N. y Rinaldi,A. (1997) Diafiltration in the presence of ascorbate in the purification of mushroom tyrosinase. *Phytochemistry* 46, 21-22.

Rescigno,A., Sollai,F., Pisu,B., Rinaldi,A. y Sanjust,E. (2002) Tyrosinase inhibition: general and applied aspects. *J. Enzyme Inhib. Med. Chem.* 17, 207-218.

Robb,D.A. (1984) Tyrosinase. En: *Copper proteins and copper enzymes.* Lontie, R. Ed., CRC Press, Boca Ratón pp. 207-241.

Rodríguez-López,J.N., Fenoll,L.G., García-Ruiz,P.A., Varon,R., Tudela,J., Thorneley,R.N. y Garcia-Canovas,F. (2000) Stopped-flow and steady-state study of the diphenolase activity of mushroom tyrosinase. *Biochemistry* 39, 10497-10506.

Rodríguez-López,J.N., Tudela,J., Varón,R., García-Carmona,F. y García-Cánovas,F. (1992a) Analysis of a kinetic model for melanin biosynthesis pathway. *J. Biol. Chem.* 267, 3801-3810.

Rodriguez-López,J.N., Ros-Martinez,J.R., Varón,R. y García-Cánovas,F. (1992b) Calibration of a Clark-Type oxygen electrode by tyrosinase-catalyzed oxidation of 4-tert-butylcatechol. *Anal. Biochem.* 202, 356-360.

Rodriguez-Lopez,J.N., Tudela,J., Varon,R. y Garcia-Canovas,F. (1991) Kinetic study on the effect of pH on the melanin biosynthesis pathway. *Biochim. Biophys. Acta* 1076, 379-386.

Rodríguez-López,J.N., Fenoll,L.G., Peñalver,M.J., García-Ruiz,P.A., Varón,R., Martinez-Ortiz,F. y Tudela,J. (2001) Tyrosinase action on monophenols: evidence for direct enzymatic relaease of *o*-diphenol. *Biochim. Bioophys. Acta.* 1548, 238-256.

Rolff,M., Schottenheim,J., Decker,H. y Tuczek,F. (2011) Copper-O_2 reactivity of tyrosinase models towards external monophenolic substrates: molecular mechanism and comparison with the enzyme. *Chem. Soc. Rev.* 40, 4077-4098.

Rolff,M., Schottenheim,J., Peters,G. y Tuczek,F. (2010) The first catalytic tyrosinase model system based on a mononuclear copper(I) complex: kinetics and mechanism. *Angew. Chem. Int. Ed. Engl.* 49, 6438-6442.

Romero-Graillet,C., Aberdam,E., Clément,M., Ortonne,J.P. y Ballotti,R. (1997) Nitric oxide produced by ultraviolet-irradiated keratinocytes stimulates melanogenesis. *J. Clin. Invest.* 99, 635-642.

Ronda,L., Faggiano,S., Bettati,S., Hellmann,N., Decker,H., Weidenbach,T. y Mozzarelli,A. (2007) Hemocyanin from *E. Californicum* encapsulated in silica gels: oxygen binding and conformational states. *Gene* 398, 202-207.

Rooseboom,M., Commandeur,J.N. y Vermeulen,N.P. (2004) Enzyme-catalyzed activation of anticáncer prodrugs. *Pharmacol. Rev.* 56, 53-102.

Ros,J.R., Rodriguez-Lopez,J.N., Varón,R. y Garcia-Cánovas,F. (1995) Mushroom tyrosinase has an ascorbate oxidase activity. *Biochem. Mol. Biol.* 36, 301-309.

Ros,J.R., Rodríguez-López,J.N., Espín,J.C., Varon,R. y Garcia-Cánovas,F. (1996) Oxymetric and spectrophotometric study of the ascorbate oxidase activity shown by frog epidermis tyrosinase. *Int. J. Biochem. Cell Biol.* 28, 917-923.

Ros,J.R., Rodríguez-López,J.N. y García-Cánovas,F. (1993a) Effect of L-ascorbic acid on the monophenolase activity of tyrosinase. *Biochem. J.* 295, 309-312.

Ros,J.R., Rodriguez-Lopez,J.N. y Garcia-Canovas,F. (1993b) Effect of ferrous ions on the monophenolase activity of tyrosinase. *Biochim. Biophys. Acta* 1163, 303-308.

Ros,J.R., Rodríguez-López,J.N. y García-Cánovas,F. (1994) Tyrosinase : Kinetic analysis of the transient phase and the steady-state. *Biochim. Biophys. Acta* 1204, 33-42.

Rosenzweig,A.C. y Sazinsky,M.H. (2006) Structural insights into dioxygen-activating copper enzymes. *Curr. Opin. Struct. Biol.* 16, 729-735.

Rouet-Mayer,M.A. y Philippon,J. (1986) Inhibition of catechol oxidases from apples by sodium chloride. *Phytochemistry* 25, 2717-2719.

Rouzaud,F., Kadekaro,A.L., Abdel-Malek,Z.A. y Hearing,V.J. (2005) MC1R and the response of melanocytes to ultraviolet radiation. *Mutant. Res*. 571,133-152.

Ruan,L., Yu,Z., Fang,B., He,W., Wang,Y. y Shen,P. (2004) Melanin pigment formation and increased UV resistance in *Bacillus thuringiensis* following high temperature induction. *Syst. Appl. Microbiol.* 27, 286-289.

Sakurai,T. y Kataoka,K. (2007) Basic and applied features of multicopper oxidases, CueO, bilirubin oxidase, and laccase. *Chem. Rec.* 7, 220-229.

Salti,G.I., Manougian,T., Farolan,M., Shilkaitis,A., Majundar,D. y Das Gupta,T.K. (2000) Microphtalmia transcription factor: a new prognostic marker in intermediate-thickness cutaneos malignant melanoma. *Cancer Res*. 60: 5012-5016.

Salvato,B., Santamaría,M., Beltramini,M., Alzuet,G. y Casella,L. (1998) The enzymatic properties of *Octopus vulgaris* hemocyanin: *o*-diphenol oxidase activity. *Biochemistry* 37, 14065-14077.

Sanchez-Amat,A., Lucas-Elío,P., Fernández,E., García-Borrón,J.C. y Solano,F. (2001) Molecular cloning and functional characterization of a unique multipotent polyphenol oxidase from *Marinomonas mediterranea*. *Biochim. Biophys. Acta* 1547, 104-116.

Sanchez-Amat,A., Solano,F. y Lucas-Elio,P. (2010) Finding new enzymes from bacterial physiology: a successful approach illustrated by the detection of novel oxidases in *Marinomonas mediterranea*. *Mar Drugs* 8, 519-541.

Sánchez-Ferrer,A., Rodríguez-López,J.N., García-Cánovas,F. y García-Carmona,F. (1995) Tyrosinase: a comprehensive review of its mechanism. *Biochim. Biophys. Acta* 1247, 1-11.

Sánchez-Hernandez,D., Devece,C., Catalá,J.M., Rodríguez-López,J.N., Tudela,J., García-Cánovas,F. y de los Reyes,E. (1999) Enzyme inactivation analyses for industrial blanching applications employing 2450 Mhz monomode microwave cavities. *J. Microw. Power Elctromagn. Energy* 34, 239-252.

Sander,O., Henss,A., Näther,C., Würtele,C., Holthausen,M.C., Scyhindler,S. y Tuczek,F. (2008) Aromatic hydroxylation in a copper bis (imine) complex mediated by a micro-eta2:eta2 peroxo dicopper core: a mechanistic scenario. *Chemistry* 14, 9714-9729.

Sanjust,E., Cecchini,G., Sollai,F., Curreli,N. y Rescigno,A. (2003) 3-Hydroxykynurenine as a substrate/activator for mushroom tyrosinase. *Arch. Biochem. Biophys.* 412, 272-278.

Santerre,C.R., Cash,J.N. y Vannorman,D.J. (1988) Ascorbic acid/citric acid combinations in the prozesing of frozen apple slices. *J. Food Sci.* 53, 1713-1716.

Sarna,T., Swarz,H.M. y Scout,G. (1993) Interactions of melanin with oxygen(and related species). En: *Atmospheric oxidation and antioxidants*, vol III. Sarna,T., Swarz,H.M. y Scout,G, (Eds) Oxford: Elsevier Science Publishers. pp. 129-165.

Sato,C., Ito,S. y Takeuchi,T. (1987) Enhancement of pheomelanogenesis by L-dopa in the mouse melanocyte cell line, TM10, in vitro. *J. Cell Sci.* 87, 507-512.

Sato,M. (1969) The conversion by phenolase of *p*-coumaric acid to caffeic acid with special reference to the role of ascorbic acid. *Phytochemistry* 8, 353-362.

Saul,S.J. y Sugumaran,M (1989) Characterization of a new enzyme system that desaturates the side chain of N-acetyldopamine. *FEBS lett.* 251, 69-73.

Saul,S.J. y Sugumaran,M (1990) Biosynthesis of dehydro-N-acetyldopamine by a soluble enzyme preparation from the larval cuticle of *Sarcophaga bullata* involves intermediary formation of N-acetyldopamine quinone and N-acetyldopamine quinone methyde. *Arch. Insect Biochem. Physiol.* 15, 237-254.

Schachtschabel,D.O., Leising,H.B., Schjeide,O.A. y Moisen,D.V. (1978) Uptake of melanosomes and increased melanin formation by cultured melanoma cells after treatment with isolated melanosomes. *Cytobios*. 21, 23-36.

Schachtschabel,D.O., Pfab,R., Paul,N. y Hess,F. (1988) Augmentation by L-dopa of growth inhibition and melanin formation of X-irradiated Harding-Passey melanoma cells in culture. *Strahlenther. Onkol*. 164, 419-424.

Schaerlaekens,K., Schierová,M., Lammertyn,E., Geukens,N., Anné,J. y Van Mellaert,L. (2001) Twin-arginine translocation pathway in *Streptomyces lividans*. *J. Bacterial.* 183, 6727-6732.

Schallreuter,K.U. (1999) A review of recent advances on the regulation of pigmentation in the human epidermis. *Cell Mol. Biol.* 45, 943-949.

Schallreuter,K.U., Kothari,S., Chavan,B. y Spencer,J.D. (2008) Regulation of melanogénesis-controversies and new concepts. *Exp. Dermatol*. 17, 395-404.

Schallreuter,K.U., Wood,J.M., Pittelkow,M.R., Gütlich,M., Lemke,K.R., Rödi,W., Swanson,N.H., Hitzemann,K. y Ziegler,I. (1994) Regulation of melanin biosynthesis in the human epidermis by tetrahydrobiopterin. *Science* 263, 1444-1446.

Scott,G., Jacobs,S., Leopardi,S., Anthony,F.A., Learn,D., Malaviya,R. y Pentland,A. (2005) Effects of PGF2alpha on human melanocytes and regulation of the FP receptor by ultraviolet radiation. *Exp. Cell Res.* 304, 407-416.

Scott,G., Leopardi,S., Printup,S., Malhi,N., Seiberg,M. y Lapoint,R. (2004) Proteinase-activated receptor-2 stimulates prostaglandin production in keratinocytes: analysis of prostaglandin receptors on human melanocytes and effects of PGE2 and PGF2alpha on melanocyte dendricity. *J. Invest. Dermatol*. 122, 1214-1224.

Sealy,R.C., Hyde,J.S., Felix,C.C., Menon,I.A. y Prota,G. (1982) Eumelanins and pheomelanins. Characterization by electron spin resonance spectroscopy. *Science* 217, 545-547.

Seiji,M., Sasaki,M. y Tomita,Y. (1978) Nature of tyrosinase inactivation in melanosomes. *Tohoku J. Exp. Med.* 125, 233-245.

Selinheimo,E., Nieidhin,D., Steffensen,C., Nielsen,J., Lomascolo,A., Halaouli,S., Record,E., O´Beirne,D., Buchert,J. y Kruus,K. (2007) Comparison of the characteristics of fungal and plant tyrosinases. *J. Biotechonol*. 130, 471-480.

Sendovski,M., Kanteev,M., Ben-Yosef,V.S., Adir,N. y Fishman,A. (2010) Crystallization and preliminary X-ray crystallographic analysis of a bacterial tyrosinase from *Bacillus megaterium*. *Acta Crystallogr. Sect. F Struct. Biol. Cryst. Commun.* 66, 1101-1103.

Sendovski,M., Kanteev,M., Ben-Yosef,V.S., Adir,N. y Fishman,A. (2011) First structures of an active bacterial tyrosinase reveal copper plasticity. *J. Mol. Biol.* 405. 227-237.

Seo,S.Y., Sharma,V.K. y Sharma,N. (2003) Mushroom tyrosinase: recent prospects. *J. Agric. Food Chem.* 51, 2837-2853.

Serra,B., Morales,M.D., Reviejo,A.J., Hall,E.H. y Pingarrón,J.M. (2005) Rapid and highly sensitive electrochemical determination of alkaline phosphatase using a composite tyrosinase biosensor. *Anal. Biochem.* 336, 289-294.

Shi,C., Dai,Y., Xu,X., Xie,Y. y Liu,Q. (2002) The purification of polyphenol oxidase from tobacco. *Protein Exp. Pur.* 24, 51-55.

Shin,N.H., Ryu,S.Y., Choi,E.J., Kang,S.H., Chang,I.M., Min,K.R. y Kim.Y. (1998) Oxyresveratrol as the potent inhibitor on dopa oxidase activity of mushroom tyrosinase. *Biochem. Biophys. Res. Commun.* 243, 801-803.

Shuster,V. y Fishman,A. (2009) Isolation, cloning and characterization of a tyrosinase with improved activity in organic solvents from *Bacillus megaterium*. *J. Mol. Microbiol. Biotechnol.* 17, 188-200.

Siegrist,W., Drozdz,R., Cotti,R., Willard,D.H., Wilkison,W.O. y Eberle,A.N. (1997) Interactions of alpha-melanotropin and agouti on B16 melanoma cells: evidence for inverse agonism of agouti. *J. Recept. Signal Transduct. Res.* 17, 75-98.

Sigolaeva,L., Makhaeva,G., Rudakova,E., Boltneva,N., Porus,M., Dubacheva, G., Eremenko,A., Kurochkin,I. y Richardson, R.J. (2010) Biosensor analysis of blood esterases for organophosporus compounds exposure assessment: approaches to simultaneous determination of several esterases. *Chem. Bio. Interact.* 187, 312-317.

Silverman,R.B. (1995) Mechanism-based enzyme inactivators. *Methods Enzymol*. 249, 240-283.

Sima,V.H., Patris,S., Aydogmus,Z., Sarakbi,A., Sandulescu,R. y Kauffmann,J.M. (2011) Tyrosinase immobilized magnetic nanobeads for the amperometric assay of enzyme inhibitors: application to the skin whitening agents. *Talanta* 83, 980-987.

Slominski,A., Moellmann,G., Kuklinska,E., Bormirski,A. y Pawelek,J. (1988) Positive regulation of melanin pigmentation by two key substrates of the melanogenic pathway, L-tyrosine and L-dopa. *J. Cell Sci.* 89, 287-296.

Slominski,A., Paus,R. y Mihm,M.C. (1998) Inhibition of melanogenesis as an adjuyant strategy in the treatment of melanotic melanomas: selective review and hypothesis. *Anticancer Res.* 18, 3709-3715.

Slominski,A., Tobin,D.J., Shibahara,S. y Wortsman,J. (2004) Melanin pigmentation in mammalian skin and its hormonal regulation. *Physiol. Rev.* 84, 1155-1228.

Söderhäll,K., Aspán,A. y Duvic,B. (1990) The proPO-system and associated proteins; role in cellular communication in arthropods. *Res. Immunol.* 141, 896-907.

Solano,F., Briganti,S., Picardo,M. y Ghanem,G. (2006) Hypopigmentating agents: an updated review on biological, chemical and clinical aspects. *Pigment Cell Res.* 19, 550-571.

Solomon,E.I., Chen,P., Metz,M., Lee,S.K. y Palmer,A.E. (2001) Oxygen binding, activation, and reduction to water by copper proteins. *Angew. Chem. Int. Ed. Engl.* 40,4570-4590.

Solomon,E.I., Sundaram,U.M. y Machonkin,T.E. (1996) Multicopper oxidases and oxygenases. *Chem. Rev.* 96, 2563-2606.

Sommer,A., Neeman,E., Steffens,J.C., Mayer,A.M. y Harel,E. (1994) Import, targeting and processing of a plant polyphenol oxidase. *Plant Physiol.* 105, 1301-1311.

Sorrell,T.N., Beltramini,M. y Lerch,K. (1988) Luminescence of deoxyhemocyanin and deoxytyrosinase. *J. Biol. Chem.* 263, 9576-9577.

Spritz,R.A., Chiang,P.W., Oiso,N. y Alkhateeb,A. (2003) Human and mouse disorders of pigmentation. *Curr. Opin. Genet. Dev.* 13, 284-289.

Stefanato,C.M., Yaar,M., Hawan,J., Phillips,T.J., Kosmadaki,M.G., Botchkarev,V. y Gilchrest,B.A. (2003) Modulations of nerve growth factor and Bcl-2 in ultraviolet-irradiated human epidermis. *J. Cutan. Pathol*. 30, 351-357.

Stone,S., Jiang,P., Dayananth,P., Tavtigian,S.V., Katcher,H., Parry,D., Peters,G. y Kamb,A. (1995) Complex structure and regulation of the P16 (MTSI) Locus. *Cancer Res.* 55, 2988-2994.

Stott,F.J., Bates,S., James,M.C., McConnell,B.B., Starborg,M., Brookes,S., Palmero,I., Ryan,K., Hara, E., Vousden,K.H. y Peters,G. (1998) The alternative product from the human CDKN2A locus, pI4(ARF), participates in a regulatory feedback loop with p53 and MDM2. *EMBO. J.* 17, 5001-5014.

Strothkamp,K.G., Jolley,R.L. y Mason,H.S. (1976) Quaternary structure of mushroom tyrosinase. *Biochem. Biophys. Res. Commun.* 70, 519-524.

Sugumaran,M. (2001) Control mechanisms of the prophenoloxidase cascade. *Adv. Exp. Med. Biol.* 484, 289-298.

Sugumaran,M. (2002) Comparative biochemistry of eumelanogenesis and the protective roles of phenoloxidase and melanin in insects. *Pigment Cell Res*. 15, 2-9.

Sugumaran,M. (2010) Chemistry of cuticular sclerotization. *Adv. In insect phys.* 39, Academic Press, Elsevier.

Sugumaran,M. y Lipke,H. (1983) Quinone methide formation from 4-alkylcatechols: a novel reaction catalyzed by cuticular polyphenol oxidase. *FEBS Lett.* 155, 65-68.

Suzuki,I., Cone,R.D., Im,S., Nordlund,J. y Abdel-Malek,Z.A. (1996) Binding of melanotropic hormones to the melanocortin receptor MC1R on human melanocytes stimulates proliferation and melanogenesis. *Endocrinology* 137, 1627-1633.

Suzuki,K., Shimokawa,C., Morioka,C. e Itoh,S. (2008) Monooxygenase activity of *Octopus vulgaris* hemocyanin. *Biochemistry* 47, 7108-7115.

Tada,A., Suzuki,I., Im,S., Davis,M.B., Cornelius,J., Babcock,G., Nordlund,J.J. y Abdel-Malek,Z.A. (1998) Endothelin-1 is a paracrine growth factor that modulates melanogenesis of human melanocytes and participates in their responses to ultraviolet radiation. *Cell Growth Differ.*9, 575-584.

Tai,S.S., Lin,C.G., Wu,M.H. y Chang,T.S. (2009) Evaluation of depigmenting activity by 8-hydroxydaidzein in mouse B16 melanoma cells and human volunteers. *Int. J. Mol. Sci.* 10, 4257-4266.

Tembe,S., Karve,M., Inamdar,S., Haram,S., Melo,J. y D´Souza,S.F. (2006) Development of electrochemical biosensor based on tyrosinase immobilized in composite biopolymeric film. *Anal. Biochem.* 349, 72-77.

Tamura,M., Gu,J., Matsumuto,K., Aota,S., Parsons,R. y Yamada,K.M. (1998) Inhibition of cell migration, spreading, and focal adhesions by tumour suppressor PTEN. *Science* 280, 1614-1617.

Terabayashi,Y., Sano,M., Yamane,N., Marui,J., Tamano,K., Segara,J., Dohmoto,M., Oda,K., Ohshima,E., Tachibana,K., Higa,Y., Ohashi,S., Koike,H. y Machida,M. (2010) Identification and characterization of genes reponsible for biosynthesis of kojic acid, and industrially important compound from *Aspergillus oryzae*. *Fungal Genet. Biol.* 47, 953-961.

Thalmann,C.R. y Lötzbeyer,T. (2002) Enzymatic cross-linking of proteins with tyrosinase. *Eur. Food Res. Technol.* 214, 276-281.

Thomson,J.A., Murphy,K., Baker,E., Sutherland,G.R., Parsons,P.G., Sturm,R.A. y Thomson, F. (1995) The *brn-2* gene regulates the melanocytic phenotype and tumorigenic potential of human melanoma cells. *Oncogene.* 11, 691-700.

Toda,K., Pathak,M.A., Fitzpatrick,T.B., Quevedo,W.C.Jr., Morikawa,F. y Nakayama,U. (1973) Pigment Cell (McGovern, Rusell, Riley, Eds), Basilea.

Tomita,Y., Takeda,A., Okinaga,S., Tagami,H. y Shibahara,S. (1989) Human oculocutaneous albinism caused by a single base insertion in the tyrosinase gene. *Biochem. Biophys. Res. Commun.* 164, 990-996.

Tomiyama,S., Sakai,S., Nihiyama,T. y Yasmada,F. (1993) Factors influencing the antioxidant activities of phenols by an ab initio study. *Bull. Chem. Soc. Jpn.* 66, 205-211.

Toscano,G., Colarieti,M.L. y Greco,G. (2003) Oxidative polymerisation of phenols by a phenol oxidase from green olives. *Enzyme Microb. Technol.* 33, 47-54.

Toussaint,O. y Lerch,K. (1987) Catalytic-oxidation of 2-aminophenols y ortho-hydroxylation of aromatic-amines by tyrosinase. *Biochemistry* 26, 8567-8571.

Tripathi,R.K., Devi,C.C. y Ramaiah,A. (1988) pH-dependent interconversion of two forms of tyrosinase in human skin. *Biochem. J.* 252, 481-487.

Tudela,J., García-Cánovas,F., Varón,R., Jimenez,M., García-Carmona,F. y Lozano,J.A. (1987) Kinetic characterization of dopamine as suicide substrate of tyrosinase. *J. Enzyme. Inhib.* 2, 47-56.

Tudela,J., García-Cánovas,F., Varón,R., Jimenez,M., García-Carmona,F. y Lozano,J.A. (1988) Kinetic study in the transient phase of the suicide inactivation of frog epidermis tyrosinase. *Biophys. Chem*. 30, 303-310.

Tyeklar,Z. y Karlin,K.D. (1989) Copper-Dioxygen chemistry: A bioinorganic challenge. *Acc. Chem. Res.* 22, 241-248.

Vámos-Vigyázó, L. (1981) Polyphenol oxidase and peroxidase in fruits and vegetables. *CRC Crit. Rev. Food Sci. Nutr.* 15, 49-127.

van Gelder,C.W., Flurkey,W.H. y Wichers,H.J. (1997) Sequence and structural features of plant and fungal tyrosinases. *Phytochemistry* 45, 1309-1323.

Vaughn,K.C. y Duke,S.O. (1984) Function of polyphenol oxidase in higher plants. *Physiol. Plant.* 60, 106-112.

Vijayan,E., Husain,I., Ramaiah,A. y Madan,N.C. (1982) Purification of human skin tyrosinase and its protein inhibitor: properties of the enzyme and the mechanism of inhibition by protein. *Arch. Biochem. Biophys.* 217, 738-747.

Virador,V.M., Grajeda,J.P.R., Blanco-Labra,A., Mendiola-Olaya,E., Smith,G.M., Moreno,A. y Whitaker,J.R. (2010a) Cloning, sequencing, purification, and cristal structure of grenache (*Vitis vinifera*) polyphenol oxidase. *J. Agric. Food Chem.* 58, 1189-1201.

Virador,V.M., Reyes-Grajeda,J.P., Blanco-Labra,A., Mendiola-Olaya,E., Smith,G.M., Moreno,A. y Whitaker,J.R. (2010b) Correction to cloning, sequencing, purification and cristal structure of Grenache (*Vitis vinifera*) polyphenol oxidase. *J. Agric. Food Chem.* 58, 1189.

Wakamatsu,K. Ohtara,K. e Ito,S. (2009) Chemical analysis of late stages of pheomelanogenesis: conversion of dihydrobenzothiazine to a benzothiazole structure. *Pigment Cell Melanoma Res.* 22, 474-486.

Walsh,C.T. (1984) Suicide substrates, mechanism-based enzyme inactivators: recent developments. *Annu. Rev. Biochem.* 53, 493-535.

Wan,P.T., Garnett,M.J., Roe,S.M., Lee,S., Niculescu-Duvaz,D., Good,V.M., Jones,C.M., Marshall,C.J., Springer,C.J., Barford,D. y Marais,R. (2004) Cancer Genome Project. Mechanism of activation of the RAF-ERK signalling pathway by oncogenic mutations on BRAF. *Cell* 116, 885-867.

Wang,C.L., Wei,L.Y., Yuan,C.J. y Hwang,K.C. (2012) Reusable amperometric biosensor for measuring protein tyrosine kinase activity. *Anal. Chem.* 84, 971-977.

Wang,J. y Constabel,C.P. (2003) Biochemical characterization of two differentially expressed polyphenol oxidases from hybrid poplar. *Phytochemistry* 64, 115-121.

Watts,D.G.(1981) An introduction to nonlinear least squares, En: *Kinetic Data Analysis. Design and Analysis of Enzyme and Pharmacokinetics Experiments.* Endrenyi (Ed.) Plenum Press, New York. pp. 1-24.

Weemaes,C.A., Ludikhuyze,L.R., Van den Broeck,I., Hendricks,M.E. y Tobback,P.P. (1998) Activity, electrophoretic characteristics and heat inactivation of polyphenoloxidases from apples, avocados, grapes, pears and plums. *Food Sci. Technol. Lebensm. Wiss.* 31, 44-49.

Wellbrock,C. y Marais,R. (2005) Elevated expression of MITF counteracts B-RAF stimulated melanocyte and melanoma cell proliferation. *J. Cell Biol.* 170, 703-708.

Wesche-Ebeling,P. y Montgomery,M.W. (1990a) Strawberry polyphenoloxidase: its role in anthocyanin degradation. *J. Food. Sci.* 55, 731-734.

Wesche-Ebeling,P. y Montgomery,M.W. (1990b) Strawberry polyphenoloxidase: extraction and partial characterization. *J. Food Sci.* 55, 1315-1319.

Westerdahl,J., Olsson,H., Mäsbäck,A., Ingvar,C. y Jonsson,N. (1995) Is the use of sunscreens a risk factor for malignant melanoma? *Melanoma Res*. 5, 59-65.Wichers,H.J., Gerritsen,Y.A.M. y Chapelon,C.G.J. (1996) Tyrosinase isoforms from the fuitbodies of *Agaricus bisporus*. *Phytochemistry* 43, 333-337.

Wichers,H.J., Recourt,K., Hendriks,M., Ebbelaar,C.E., Biancone,G., Hoeberichts,F.A., Mooibroek,H. y Soler-Rivas,C. (2003) Cloning, expression and characterisation of two tyrosinase cDNAs from *Agaricus bisporus*. *Appl. Microbiol. Biotechnol.* 61,336-341.

Wilcox,D.E., Porras,A.G., Hwang,Y.T., Lerch,K., Winkler,M.E. y Solomon,E.I. (1985) Substrate-analog binding to the coupled binuclear copper active-site in tyrosinase. *J. Am. Chem. Soc.* 107, 4015-4027.

Wititsuwannakul,D., Chareonthiphakorn,N., Pace,M. y Wititsuwannakul,R. (2002) Polyphenol oxidases from latex *Hevea brasiliensis*: purification and characterization. *Phytochemistry* 61, 115-121.

Wolchok,J.D. y Saenger,Y.M. (2007) Current topics in melanoma. *Curr. Opin. Oncol.* 19, 116-120.

Wu,J., Chen,H., Gao,J., Liu,X., Cheng,W. y Ma,X. (2010) Cloning, characterization and expression of two new polyphenol oxidase cDNAs from *Agaricus bisporus. Biotechnol. Lett.* 32, 1439-1447.

Wu,H. y Park,H.Y. (2003) Protein kinase C-beta mediated complex formation between tyrosinase and TRP-1. *Biochem. Biophys. Res. Commun*. 311, 948-953.

Xue,C.B., Luo,W.C., Ding,Q., Liu,S.Z. y Gao,X.X. (2008) Quantitative structure-activity relationship studies of mushroom tyrosinase inhibitors. *J. Comput. Aided Mol. Des.* 22, 299-309.

Yaar,M., Grossman,K., Eller,M. y Gillchrest,B.A. (1991) Evidence for nerve growth factor mediated paracrine effects in human epidermis. *J. Cell Biol.* 115, 821-828.

Yada,Y., Higuchi,K. y Imokawa,G (1991) Effects of endothelins on signal transduction and proliferation in human melanocytes. *J. Biol. Chem.* 266, 18352-18357.

Yamada,K., Akiba,Y., Shibuya,T., Kashiwada,A., Matsuda,K. y Hirata,M. (2005) Water purification through bioconversion of phenol compounds by tyrosinase and chemicals adsorption by chitosan beads. *Biotechnol. Progr.* 21,823-829.

Yamaguchi,Y., Brenner,M. y Hearing,V.J. (2007) The regulation of skin pigmentation. *J. Biol. Chem.* 282, 27557-27561.

Yamaguchi,Y. y Hearing,V.J. (2009) Physiological factors that regulate skin pigmentation. *Biofactors* 35, 193-199.

Yamazaki,S., Morioka,S. e Itoh,S. (2004) Kinetic evaluation of catalase and peroxygenase activities of tyrosinase. *Biochemistry* 43, 11546-11553.

Yamazaki,S. e Itoh,S. (2003) Kinetic evaluation of phenolase activity of tyrosinase using simplified catalytic reaction system. *J. Am. Chem. Soc.* 125, 13034-13035.

Yohn,J.J., Norris,D.A., Yrastorza,D.G., Buno,I.J., Leff,J.A., Hake,S.S. y Repine,J.E. (1991) Disparate antioxidant enzyme activities in cultured cutaneous fibroblasts, keratinocytes and melanocytes. *J. Invest. Dermatol.* 97, 405-409.

Yokota,T., Nishio,H., Kubota,Y. y Mizoguchi,M. (1998) The inhibitory effect of glabridin from licorice extracts on melanogenesis and inflammation. *Pigment Cell Res.* 11, 355-361.

Yokozawa,T. y Kim,Y.J. (2007) Piceatannol inhibits melanogenesis by its antioxidative actions. *Biol. Pharm. Bull.* 30, 2007-2011.

Yoshida,M., Takahashi,Y. e Inoue,S. (2000) Histamine induces melanogenesis and morphologic changes by protein kinase A activation via H_2 receptors in human normal melanocytes. *J. Invest. Dermatol.* 114, 334-342.

Young,A.R., Potten,C.S., Chadwick,C.A., Murphy,G.M. y Cohen,A.J. (1988) Inhibition of UV radiation-induced DNA damage by a 5-methoxypsoralen tan in human skin. *Pigment Cell Res.* 1, 350-354.

Yuan,C.J., Wang,C.L., Wu,T.Y., Hwang,K.C. y Chao,W.C. (2011) Fabrication of a carbon fiber paper as the electrode and its application toward developing a sensitive unmediated amperometric biosensor. *Biosens. Bioelectron.* 26, 2858-2863.

Zakut,R., Perlis,R., Eliyahu,S, Yarden,Y., Givol,D., Lyman,S.D. y Halaban,R. (1993) KIT ligand (mast cell growth factor) inhibits the growth of KIT-expressing melanoma cells. *Oncogene* 8, 2221-2229.

Zawistowski,J., Biliaderis,C.G. y Michael Eskin,N.A. (1991) Polyphenol Oxidase. En*: Oxidative Enzymes in Foods*. Robinson,D.S. y Eskin,N.A.M (Eds),. Elsevier Science, London. pp. 217-273.

Zehtab,T., Yazdanparast,R. y Rafieii,S. (2001) Inhibition of experimental autoimmune vitiligo by oral administration of mushroom tyrosinase. *Cytobios* 105, 27-34.

Zhai,S., Yaar,M., Doyle,S.M. y Gilchrest,B.A. (1996) Nerve growth factor rescues pigment cells from ultraviolet-induced apoptosis by upregulating Bcl-2 levels. *Exp. Cell Res.* 224, 335-343.

Zhang,X., Hu,X., Hou,A. y Wang, H. (2009) Inhibitory effect of 2,4,2´,4´-tetrahydroxy-3-(3-methyl-2-butenyl)-chalcone on tyrosinase activity and melanin biosinthesis. *Biol. Pharm. Bull.* 32, 86-90.

Zhang,X., van Leeuwen,J., Wichers,H.J. y Flurkey,W.H. (1999) Characterization of tyrosinase from the cap flesh of portabella mushrooms. *J. Agric. Food. Chem.* 47, 374-378.

Zhao,J.F., Zhang,Y.J., Jin,X.H., Athar,M., Santella,R.M., Bickers,D.R. y Wang,Z.Y. (1999) Green tea protects agisnt psoralen plus ultraviolet A-induced photochemical damage to skin. *J. Invest. Dermatol.* 113, 1070-1075.

Zhong,J. y Groutas,W.C. (2004) Recent developments in the design of mechanism-based and alternate substrate inhibitors of serine proteases. *Curr. Top. Med. Chem.* 4, 1203-1216.

Zhuang,J.X., Hu,Y.H., Yang,M.H., Liu,F.J., Qiu,L., Zhou,X.W. y Chen,Q.X. (2010) Irreversible competitive inhibition kinetics of cardol triene on mushroom tyrosinase. *J. Agric. Food Chem.* 58, 12993-12998.